

EARLY ANGLO-SAXON GLASS BEADS:
COMPOSITION AND ORIGINS BASED
ON THE FINDS FROM
RAF LAKENHEATH, SUFFOLK

by

James Robert Nicholas Peake

BSc (Hons), MSc

Volume I of II

Submitted in fulfilment of the requirements
for the degree of Doctor of Philosophy in the School
Archaeology

CARDIFF UNIVERSITY

June 2013

DECLARATION

This work has not been submitted in substance for any other degree or award at this or any other university or place of learning, nor is being submitted concurrently in candidature for any degree or other award.

Signed Date

STATEMENT 1

This thesis is being submitted in partial fulfilment of the requirements for the degree of PhD Archaeology.

Signed Date

STATEMENT 2

This thesis is the result of my own independent work/investigation, except where otherwise stated. Other sources are acknowledged by explicit references. The views expressed are my own.

Signed Date

STATEMENT 3

I hereby give consent for my thesis, if accepted, to be available for photocopying and for inter-library loan, and for the title and summary to be made available to outside organisations.

Signed Date

© The copyright of this thesis rests with the author. No quotation from it may be published without the author's prior written consent, and any information derived from it must be acknowledged.

ABSTRACT

This study reports upon the compositional analysis of early Anglo-Saxon (5th-7th centuries AD) glass beads from the cemetery complex at RAF Lakenheath (Eriswell), Suffolk. Major element analysis was undertaken using energy-dispersive x-ray spectrometry in the scanning electron microscope (SEM-EDS) on 537 samples from a total of 380 monochrome and polychrome beads. Trace element analysis was undertaken by laser ablation inductively coupled plasma mass spectrometry (LA-ICP-MS) on 75 different samples from 65 of these beads. SEM-EDS analyses are also reported for a small number of glass beads from the early Anglo-Saxon cemeteries at Spong Hill, Bergh Apton and Morning Thorpe in Norfolk.

The beads analysed were produced from soda-lime-silica glass, which was originally made in the Near East from a mixture of a natron and calcareous quartz-rich sand. They have been grouped and compared according to the base glass types represented and their colourant technology. These groups have been systematically compared to a well-established typology and chronology for these beads.

The results demonstrate that the Anglo-Saxon glass bead industry was dependent upon the recycling of Roman material during the 5th and 6th centuries, but there is no evidence to suggest continuity in the glass industry from the preceding Roman period. Imported bead types were probably manufactured using a fresh supply of raw glass imported from the Near East. At some point in the latter half of the 6th century there appears to have been a drastic and rapid change in beadmaking practices. The Anglo-Saxon beadmaking industry in England appears to have largely collapsed, except for the production of a few crude bead types produced in the 7th century. Imported bead types come to dominate, but natron glass appears to have been in short supply by this time; some it was adulterated with potassium-rich plant ash, probably as an extender.

TABLE OF CONTENTS

DECLARATION	ii
ABSTRACT.....	iii
TABLE OF CONTENTS.....	iv
LIST OF FIGURES	x
LIST OF TABLES	xxxvi
ACKNOWLEDGEMENTS	xxxviii
LIST OF ABBREVIATIONS	xli
CHRONOLOGY.....	xliii

VOLUME I

CHAPTER ONE

1. Introduction	1
1.1. Historical Context	6
1.2. Archaeological Context.....	12
1.2.1. RAF Lakenheath (Eriswell), Suffolk	13
1.2.1.1. The Beads.....	17
1.2.2. Spong Hill, Bergh Apton and Morning Thorpe, Norfolk	19
1.2.2.1. The Beads.....	21
1.3. Glass Chemistry	23
1.4. Early Glass	25
1.4.1. The Eastern Mediterranean	28
1.4.2. Britain and Northwestern Europe.....	34
1.5. Early Anglo-Saxon Beads and Bead Studies	40
1.6. Aims	44

CHAPTER TWO

2. Materials and Methods	49
2.1. Samples Analysed	50
2.1.1. RAF Lakenheath (Eriswell), Suffolk	50
2.1.2. Spong Hill, Bergh Apton and Morning Thorpe, Norfolk	51
2.2. Methods Tested	53
2.2.1. The DIAM Technique	55

2.2.1.1. Sample Preparation and Analytical Procedure.....	55
2.2.1.2. Evaluation of Method and Results	56
2.2.2. Environmental Scanning Electron Microscopy (ESEM)	61
2.2.2.1. Sample Preparation and Analytical Procedure.....	62
2.2.2.2. Evaluation of Method and Results	63
2.2.3. Summary	67
2.3. Analytical Techniques Employed	69
2.3.1. Scanning Electron Microscopy (SEM)	69
2.3.1.1. Sample Preparation	70
2.3.1.2. Analytical Procedure.....	73
2.3.1.3. Presentation of Data	77
2.3.2. Laser Ablation Inductively Coupled Plasma Mass Spectrometry (LA-ICP-MS)	79
2.3.2.1. Sample Preparation	81
2.3.2.2. Analytical Procedure.....	81
2.3.2.3. Presentation of Data	83
2.3.3. X-Radiography.....	86

CHAPTER THREE

3. Production Technology	89
3.1. Manufacturing Techniques.....	89
3.1.1. Applied Decoration	92
3.1.2. ‘Metal-in-Glass’ Beads	94
3.2. Manufacturing Techniques: New Insights	98
3.2.1. Iron Scale	99
3.2.2. Opaque Red Glass Cores.....	102
3.2.3. ‘Reticella’ Beads	109
3.3. Chemical Durability and Decay	111

CHAPTER FOUR

4. Results: Glass Technology	116
4.1. Base Glasses.....	116
4.1.1. Raw Materials	123
4.1.1.1. Alkali.....	123
4.1.1.2. Silica.....	125
4.1.1.3. Lime	126
4.1.1.4. Decolourants	128

4.2. The Compositional Groups	133
4.2.1. Trace Element Analyses.....	148
4.2.1.1. Rare Earth Elements (REE)	149
4.2.1.2. Sediment-Related Elements (SRE)	151
4.2.1.3. Colourant and Colourant-Related Elements.....	157
4.3. ‘Roman’ Glass.....	159
4.3.1. Trace Element Analyses.....	174
4.3.1.1. Rare Earth Elements (REE)	174
4.3.1.2. Sediment-Related Elements (SRE)	176
4.4. ‘Saxon’ Glass	178
4.4.1. Trace Element Analyses.....	204
4.4.1.1. Rare Earth Elements (REE)	204
4.4.1.2. Sediment-Related Elements (SRE)	210
4.5. ‘HIMT’ Glass	221
4.5.1. Trace Element Analyses.....	227
4.5.1.1. Rare Earth Elements (REE)	227
4.5.1.2. Sediment-Related Elements (SRE)	228
4.6. ‘Levantine I’ Glass.....	231
4.6.1. Trace Element Analyses.....	233
4.6.1.1. Rare Earth Elements (REE)	233
4.6.1.2. Sediment-Related Elements (SRE)	236
4.7. ‘A2b Blue’ Glass.....	239
4.7.1. Trace Element Analyses.....	240
4.7.1.1. Rare Earth Elements (REE)	241
4.7.1.2. Sediment-Related Elements (SRE)	242
4.8. Relationship to Brugmann’s Bead Chronology	243
4.9. Relationship to Opacity and Colour of the Glass.....	255
4.10. Relationship to Brugmann’s Bead Typology.....	267
4.10.1. Bead Type Chronology	269
4.10.2. Bead Type Production Zones	280
4.10.3. Individual Bead Type Definitions.....	291
4.10.3.1. 4 th Century Types (Roman).....	291
4.10.3.2. 5 th -6 th Century Types (Phases A1 and A2)	292
4.10.3.3. 6 th -7 th Century Types (Phases A2b, B and C).....	297
4.10.4. Blue Glass Beads: Cobalt Sources	304
4.11. Relationship to Bead Context	310
4.11.1. The Chronology of the Burials at Eriswell	310

4.11.2. The Homogeneity of Bead Strings	321
4.11.2. The Distribution of Glass Types	324

CHAPTER FIVE

5. Results: Colourant Technology	326
5.1. Translucent Glass	329
5.1.1. Uncoloured and Naturally Tinted Glass.....	329
5.1.1.1. Trace Element Analyses.....	336
5.1.2. Translucent Pink-Brown Glass	338
5.1.3. Translucent Blue Glass	340
5.1.3.1. Trace Element Analyses.....	346
5.1.4. Translucent Copper-Green and Turquoise Glass	357
5.1.4.1. Trace Element Analyses.....	368
5.1.5. 'Dark' Glass	370
5.1.5.1. Trace Element Analyses.....	377
5.2. Opaque Glass	379
5.2.1. Opaque White Glass.....	379
5.2.1.1. Trace Element Analyses.....	390
5.2.2. Opaque Yellow and Green Glass	392
5.2.2.1. Trace Element Analyses.....	409
5.2.3. Opaque Red Glass	412
5.2.3.1. Slag Additions	421
5.2.3.1.1. Fayalitic Slag.....	426
5.2.3.1.2. Kirschsteinitic Slag	439
5.2.3.1.3. Copper or Iron Smelting Slag?.....	444
5.2.3.2. Anomalies	446
5.2.3.3. Trace Element Analyses.....	451
5.2.4. Opaque Orange Glass.....	453
5.2.4.1. Trace Element Analyses.....	460
5.2.5. Opaque Blue Glass	461
5.2.5.1. Trace Element Analyses.....	464
5.2.6. Opaque Turquoise Glass	465
5.2.7. Opaque Blue-Green Glass.....	467
5.2.7.1. Trace Element Analyses.....	470
5.3. Colourant Sources	472
5.3.1. Cobalt	473
5.3.2. Copper	475

5.3.3. Tin	478
5.3.4. Lead.....	480
5.3.5. Manganese and Antimony.....	483
5.3.6. Iron	484

CHAPTER SIX

6. Later Anglo-Saxon Glass	485
----------------------------------	-----

CHAPTER SEVEN

7. Discussion and Conclusions.....	490
7.1. Comparison with Contemporary Beads	490
7.2. The Glass and its Raw Materials.....	496
7.2.1. Glass Types and Sources.....	496
7.2.2. Colourant Sources	502
7.3. The Trade in Glass	504
7.4. Where Were the Beadmaking Workshops?	507
7.5. The Question of Roman Continuity	509
7.6. The Rise and Fall of Anglo-Saxon Beadmaking	511
7.7. Further Work.....	516
7.7.1. Glass Studies in General	516
7.7.2. Anglo-Saxon Glass Bead Studies	518
7.7.3. Near Eastern Glass	520

CHAPTER EIGHT

8. References	521
---------------------	-----

VOLUME II

APPENDIX A

Eriswell Glass Bead Catalogue	550
-------------------------------------	-----

APPENDIX B

The Distribution of the Bead Types at Eriswell.....	669
---	-----

APPENDIX C

Images of the Glass Beads Sampled from Eriswell	680
---	-----

APPENDIX D

Sampling Request for Glass Beads from Spong Hill	728
--	-----

APPENDIX E

Diagrams of Sample Blocks	737
---------------------------------	-----

APPENDIX F

Digitised X-Rays of the Glass Beads from Eriswell	745
---	-----

APPENDIX G

Eriswell Compositional Analyses	778
---------------------------------------	-----

APPENDIX H

Spong Hill Compositional Analyses	843
---	-----

APPENDIX I

Bergh Apton Compositional Analyses	854
--	-----

APPENDIX J

Morning Thorpe Compositional Analyses	859
---	-----

APPENDIX K

The Compositional Distribution of Bead Types	862
--	-----

APPENDIX L

Cobalt-Rich Mineral Inclusion	866
-------------------------------------	-----

LIST OF FIGURES

VOLUME I

Figure 1.2.1 – Map of Britain showing the location of East Anglia, currently the modern-day counties of Norfolk and Suffolk (map adapted from that of 1995 county boundaries © Ordnance Survey).	12
Figure 1.2.2 – Map of East Anglia showing the location of the principal archaeological sites discussed in this thesis.	13
Figure 1.2.3 – Location of the excavation areas showing the three cemeteries at Eriswell: ERL 046, ERL 104 and ERL 114 (Caruth and Anderson 2005: 1).	14
Figure 1.2.4 – Phase plan for the three cemeteries at Eriswell. Early Anglo-Saxon features (including graves) are highlighted in black (Caruth and Anderson 2005: 30).	15
Figure 1.2.5 – Photograph of beads <i>in situ</i> in Grave 107, cemetery ERL 104, at Eriswell (© SCCAS).	18
Figure 1.2.6 – Photograph of beads <i>in situ</i> in Grave 266, cemetery ERL 104, at Eriswell (© SCCAS).	19
Figure 1.3.1 – Structure of a hypothetical two-dimensional crystalline compound, A_2O_3 ; (a) in crystalline form, (b) in vitreous form, (c) as a vitreous glass modified by the addition of network modifying ions (after Frank 1982: 9). Black circles represent atoms of ‘A’, white circles atoms of ‘O’ and shaded circles atoms of singly charged metallic ion ‘M’.	23
Figure 1.4.1 – The traditional division of production for natron-based glass (after Freestone <i>et al.</i> 2008: 30). Here natron is imported from Egypt to individual glass-making ‘workshops’, for example in Europe, which each exploit local sources of sand. Each of these therefore produces glass of a distinctive composition.	27
Figure 1.4.2 – A series of seventeen 8 th -9 th century furnace floors at Bet Eli’ezer, near Hadera, Israel (Foy and Nenna 2001: 37).	29
Figure 1.4.3 – Division of production for natron-based glass (after Freestone <i>et al.</i> 2008: 31). The primary glass-making ‘factories’ make glass from its primary raw materials (sand and natron). These produced glass of distinctive compositions relating to the source of sand used. The finished glass is broken up and distributed to a number of secondary glass-working ‘workshops’, for example in Europe. Each of these will have therefore produced objects of similar composition regardless of their proximity to one another. In principle, a workshop may be supplied by glass from more than one factory (<i>e.g.</i> Workshop 3).	30
Figure 1.4.4 – A plot of alumina versus lime for the five major groups of natron glass produced in the Eastern Mediterranean between the 4 th and 9 th centuries AD (after Freestone <i>et al.</i> 2000; 2002a; 2002b; see text for details).	31
Figure 2.2.1 – A plot of soda (DIAM) versus soda (SEM-EDS) for Early Byzantine tesserae from Caesarea (Israel).	59
Figure 2.2.2 – A plot of magnesia (DIAM) versus soda (SEM-EDS) for Early Byzantine tesserae from Caesarea (Israel).	59
Figure 2.2.3 – A plot of alumina (DIAM) versus soda (SEM-EDS) for Early Byzantine tesserae from Caesarea (Israel).	59
Figure 2.2.4 – A plot of silica (DIAM) versus soda (SEM-EDS) for Early Byzantine tesserae from Caesarea (Israel).	59
Figure 2.2.5 – A plot of lime (DIAM) versus soda (SEM-EDS) for Early Byzantine tesserae from Caesarea (Israel).	60
Figure 2.2.6 – A plot of iron oxide (DIAM) versus soda (SEM-EDS) for Early Byzantine tesserae from Caesarea (Israel).	60
Figure 2.2.7 – A photograph showing fragments of Early Byzantine glass tesserae from Caesarea, Israel, mounted on the SEM stage (approximately 6cm in diameter) for analysis by environmental scanning electron microscopy (ESEM-EDS).	62
Figure 2.2.8 – A plot of soda (ESEM-EDS) versus soda (SEM-EDS) for Early Byzantine tesserae from Caesarea (Israel).	66

Figure 2.2.9 – A plot of magnesia (ESEM-EDS) versus soda (SEM-EDS) for Early Byzantine tesserae from Caesarea (Israel).	66
Figure 2.2.10 – A plot of alumina (ESEM-EDS) versus soda (SEM-EDS) for Early Byzantine tesserae from Caesarea (Israel).	66
Figure 2.2.11 – A plot of silica (ESEM-EDS) versus soda (SEM-EDS) for Early Byzantine tesserae from Caesarea (Israel).	66
Figure 2.2.12 – A plot of lime (ESEM-EDS) versus soda (SEM-EDS) for Early Byzantine tesserae from Caesarea (Israel).	67
Figure 2.2.13 – A plot of iron oxide (ESEM-EDS) versus soda (SEM-EDS) for Early Byzantine tesserae from Caesarea (Israel).	67
Figure 2.3.1 – A photograph showing glass samples from Eriswell mounted on 3cm resin block mould bases using double-sided tape and Araldite™ 5-minute epoxy resin.	71
Figure 2.3.2 – A photograph showing glass samples from Eriswell mounted on a 3cm resin block mould base using double-sided tape and Araldite™ 5-minute epoxy resin. Note the larger dark blue glass standard (Corning A) at the top of the image, which is orientated so as to provide a ‘north point’.	72
Figure 2.3.3 – A photograph showing a polished sample block containing glass samples from Eriswell. Note the larger dark blue glass standard (Corning A) at the top of the image, which is orientated so as to provide a ‘north point’. Resin block is approximately 3cm in diameter.	73
Figure 2.3.4 – A photograph showing a sample block mounted in the sample holder (shown by the red arrow) in the chamber of the scanning electron microscope ready for analysis.	74
Figure 2.3.5 – A screenshot showing a laser ablation pass of a glass sample from Eriswell during LA-ICP-MS analysis. Note the heterogeneity of the sample.	82
Figure 3.1.1 – Digital microscope image of translucent blue bead ERL046:G05:1438, a wound <i>Blue</i> bead, showing a ‘circumferential’ structure. Image is approximately 7mm across (image courtesy of Rebecca Lumsden).	90
Figure 3.1.2 – Digital microscope image of ‘dark’ bead ERL104:G242:2142, a wound <i>DarkPoly2</i> bead, showing fine applied opaque white trails combed into a zigzag pattern. Image is approximately 6mm across (image courtesy of Helen Butler).	93
Figure 3.1.3 – Digital microscope image of opaque yellow bead ERL104:G195:1346, a wound <i>Koch34</i> bead, showing an applied opaque red circumferential narrow crossing trail marvered flush with the bead surface. Image is approximately 6mm across (image courtesy of Helen Butler).	93
Figure 3.1.4 – Digital microscope image of ‘light’ bead ERL104:G172:3098, a drawn <i>Constricted Segmented</i> ‘metal-in-glass’ bead. A layer of metallic foil (probably gold) is visible, sandwiched between two layers of glass. Much of the outer layer of glass is missing, revealing the foil beneath (image courtesy of Jenny Mathiasson).	95
Figure 3.2.1 – Bead ERL104:G305:1871, a <i>Melon Associated</i> bead, showing an opaque yellow circumferential zigzag trail on a ‘dark’ bead body (left) and a positive x-radiograph of the bead (right). The opaque yellow glass appears darker in the image as it is denser, due to a much higher lead content.	98
Figure 3.2.2 – Bead ERL046:G15:1740, a <i>DarkPoly1</i> bead, showing an opaque white circumferential zigzag trail on a ‘dark’ bead body (left) and a positive x-radiograph of the bead (right). The dark flecks visible in the x-radiograph are particles of a crystalline opacifying agent (tin oxide) present in the opaque white decoration.	98
Figure 3.2.3 – A section through bead ERL104:G367:3619 (a <i>WhitePoly3</i> bead) showing a layer of opaque red glass at the core (left). A slight taper to the perforation can be seen, indicating the use of a tapered mandrel. The black layer visible within the perforation is oxidised iron scale pulled from the mandrel around which the bead was formed. Also shown is a positive x-radiograph of the same bead prior to sectioning (right); the red glass appears darker because it is denser, due to its higher lead content. Note the absence of any visible crystalline opacifying agent in the bead body; the more ‘mottled’ appearance on the x-radiograph results from opacification by bubbles.	100
Figure 3.2.4 – BSE micrograph showing translucent blue-green tinted sample ERL104:G144:2595, a <i>Hourglass Variation</i> bead. A thick layer of iron oxide scale (pale grey) can be seen adhered to the surface of the soda-lime-silica glass matrix (dark grey). Several large voids and bubbles are also visible.	100

Figure 3.2.5 – BSE micrograph showing translucent green tinted sample ERL104:G263:1396, a <i>Cloak</i> bead. A thick layer of iron oxide scale (pale grey) can be seen adhered to the surface of the soda-lime-silica glass matrix (dark grey).	101
Figure 3.2.6 – BSE micrograph showing opaque red sample ERL046:G03:1271, a <i>RedPoly6</i> bead. Several thick layers of iron oxide scale (pale grey) can be seen adhered to the surface of the soda-lime-silica glass matrix (darker grey). Several fayalitic slag particles and large bubbles are also visible. The bright white particles immediately surrounding the iron scale are metallic copper; copper having been added as a colourant in this glass (see Chapter 5, section 5.2.3).	101
Figure 3.2.7 – Bead ERL104:G305:1875, a <i>Reticella</i> bead (left) produced from three twisted trails of opaque red, opaque yellow and translucent glass arranged in a herringbone pattern. The high-lead opaque yellow glass appears darker in positive x-radiograph (right), and highlights the way in which the glass is twisted.	110
Figure 3.2.8 – Bead ERL104:G305:1876, a <i>Reticella</i> bead (left) produced from three twisted trails of opaque red, opaque yellow and translucent glass arranged in a herringbone pattern. The high-lead opaque yellow glass appears darker in positive x-radiograph (right), and highlights the way in which the glass is twisted.	110
Figure 3.3.1 – Digital microscope image of bead ERL046:G03:1228, a wound <i>Green Globular</i> bead, showing a ‘circumferential’ structure. A filmy layer of patchy iridescent weathered glass is visible in places. Image is approximately 7mm across (image courtesy of Rebecca Lumsden).	113
Figure 3.3.2 – Digital microscope image of bead ERL114:G414:1535, a wound <i>DarkPoly3</i> sword bead, showing opaque white applied decoration on a ‘dark’ bead body. The opaque white glass is opacified by bubbles and has suffered from considerable deterioration by groundwater as a result of its porosity. Image is approximately 7mm across (image courtesy of Rebecca Lumsden).	113
Figure 3.3.3 – BSE micrograph of an opaque white bead from Spong Hill (grave 5.6c), opacified by a dispersion of tiny bubbles in a soda-lime-silica glass matrix. This glass is heavily corroded; numerous cracks, fissures and pits are visible. The darker grey areas of glass adjacent to these cracks and fissures are depleted in alkali, which has been leached out of the glass by groundwater. Compare the condition of this glass with the adjacent translucent turquoise glass (pale grey glass towards the top-left of the image).	114
Figure 3.3.4 – BSE micrograph showing opaque white sample ERL104:G367:3619, a <i>WhitePoly3</i> bead. Numerous tiny bubbles are visible heterogeneously dispersed throughout the soda-lime-silica glass matrix. Surrounding several of these bubbles a thin layer of slightly darker grey glass can be seen, where the alkali components of the glass have been leached out by groundwater.	114
Figure 4.1.1 – A plot of alumina versus iron oxide for the high-lead yellow, green, red, white, turquoise and ‘dark’ samples from Eriswell. The size of the bubbles is proportional to the lead content (the larger the bubble, the higher the lead content), taken from the raw data (<i>i.e.</i> not reduced). Note that * indicates reduced glass composition in this and all subsequent graphs and tables.	118
Figure 4.1.2 – A plot of raw (<i>i.e.</i> not reduced) lead oxide versus iron oxide for the high-lead yellow, green, red, white, turquoise and ‘dark’ samples from Eriswell. The dashed line represents the approximate detection limits for lead oxide.	119
Figure 4.1.3 – A plot of alumina versus iron oxide for the high-lead yellow, green, white and turquoise samples from Eriswell. The size of the bubbles is proportional to the lead content (the larger the bubble, the higher the lead content), taken from the raw data (<i>i.e.</i> not reduced).	119
Figure 4.1.4 – A plot of raw (<i>i.e.</i> not reduced) lead oxide versus alumina for the high-lead yellow, green, red, white, turquoise and ‘dark’ glasses from Eriswell. The dashed line represents the approximate detection limits for lead oxide.	120
Figure 4.1.5 – A plot of raw (<i>i.e.</i> not reduced) lead oxide versus iron oxide for the high-lead yellow, green, white and turquoise glasses from Eriswell. The dashed line represents the approximate detection limits for lead oxide.	120
Figure 4.1.6 – A plot of magnesia versus potash in the base glasses from Eriswell.	124
Figure 4.1.7 – A plot of phosphate versus potash in the base glasses from Eriswell. The dashed line represents the approximate detection limits for phosphate.	124

Figure 4.1.8 – A plot of manganese oxide versus antimony oxide for the reduced glasses from Eriswell. High-lead samples affected by contamination have been omitted (see text for details). The dashed lines represent the approximate detection limits for antimony oxide and manganese oxide.	131
Figure 4.1.9 – A plot of iron oxide versus antimony oxide for the reduced glasses from Eriswell. High-lead samples affected by contamination have been omitted (see text for details). The dashed line represents the detection limits antimony oxide.	131
Figure 4.1.10 – A plot of iron oxide versus manganese oxide for the reduced glasses from Eriswell. High-lead samples affected by contamination have been omitted (see text for details). The dashed line represents the approximate detection limits for manganese oxide.	132
Figure 4.2.1 – A plot of soda versus lime for the different base glass types identified at Eriswell.	136
Figure 4.2.2 – A plot of magnesia versus lime for the different base glass types identified at Eriswell.	136
Figure 4.2.3 – A plot of potash versus lime for the different base glass types identified at Eriswell.	137
Figure 4.2.4 – A plot of magnesia versus potash for the different base glass types identified at Eriswell.	137
Figure 4.2.5 – A plot of silica versus lime for the different base glass types identified at Eriswell.	138
Figure 4.2.6 – A plot of silica versus magnesia for the different base glass types identified at Eriswell.	138
Figure 4.2.7 – A plot of phosphate versus magnesia for the different base glass types identified at Eriswell. The dashed line represents the approximate detection limits for phosphate.	139
Figure 4.2.8 – A plot of alumina versus iron oxide for the different base glass types identified at Eriswell, omitting those samples which are likely to have been affected by iron and alumina contamination (see text for details).	139
Figure 4.2.9 – A plot of alumina versus lime for the different base glass types identified at Eriswell, omitting those samples which are likely to have been affected by alumina contamination (see text for details).	140
Figure 4.2.10 – A plot of iron oxide versus manganese oxide for the different base glass types identified at Eriswell, omitting those samples which are likely to have been affected by iron and alumina contamination (see text for details). The dashed line represents the approximate detection limits for manganese oxide.	140
Figure 4.2.11 – A plot of soda versus lime for the different base glass types identified at Eriswell, showing the ‘low-soda-lime’ and ‘high soda-lime’ samples. Compare to Figure 4.2.1.	142
Figure 4.2.12 – A plot of silica versus lime for the different base glass types identified at Eriswell, showing the ‘low-soda-lime’ and ‘high soda-lime’ samples. Compare to Figure 4.2.5.	143
Figure 4.2.13 – A plot of magnesia versus lime for the different base glass types identified at Eriswell, showing high-magnesia and low-magnesia samples in the ‘low-soda-lime’ and ‘high soda-lime’ glasses respectively. Compare to Figure 4.2.2.	143
Figure 4.2.14 – Dendrogram for selected samples from Eriswell using Ward’s method, showing the grouping of the different base glass types identified.	147
Figure 4.2.15 – Average rare earth element concentrations for the different base glass types identified at Eriswell, normalised to the weathered continental crust (see Chapter 2, section 2.3.2.3). Note the logarithmic scale.	149
Figure 4.2.16 – Average sediment-related element concentrations for the different base glass types identified at Eriswell, normalised to the weathered continental crust (see Chapter 2, section 2.3.2.3). Note the logarithmic scale.	152
Figure 4.2.17 – A plot of zirconium versus hafnium for the different base glass types identified at Eriswell.	154
Figure 4.2.18 – A plot of titanium versus zirconium for the different base glass types identified at Eriswell.	154
Figure 4.2.19 – A plot of lime versus strontium for the different base glass types identified at Eriswell.	155
Figure 4.2.20 – A plot of manganese versus barium for the different base glass types identified at Eriswell. ‘HIMT’ samples have been excluded due to Ba contents in excess of 2500 ppm.	155
Figure 4.2.21 – A plot of manganese versus antimony for the different base glass types identified at Eriswell. Note the logarithmic scale.	157

Figure 4.3.1 – A plot of manganese oxide versus antimony oxide in ‘Roman’ glass from Eriswell. The dashed lines represent the approximate detection limits for manganese oxide and antimony oxide.....	161
Figure 4.3.2 – A plot of soda versus lime for the different base glass types identified at Eriswell. The size of the bubbles is proportional to the antimony content (the larger the bubble, the higher the antimony content). The smallest bubbles represent samples containing <0.3% Sb ₂ O ₃ *. The 7 samples containing >1.0% Sb ₂ O ₃ * (all ‘Roman’) have been omitted due to the excessive size of the bubbles produced. Compare to Figure 4.2.1.....	163
Figure 4.3.3 – A plot of magnesia versus lime for the different base glass types identified at Eriswell. The size of the bubbles is proportional to the antimony content (the larger the bubble, the higher the antimony content). The smallest bubbles represent samples containing <0.3% Sb ₂ O ₃ *. The 7 samples containing >1.0% Sb ₂ O ₃ * (all ‘Roman’) have been omitted due to the excessive size of the bubbles produced. Compare to Figure 4.2.2.	164
Figure 4.3.4 – A plot of silica versus magnesia for the different base glass types identified at Eriswell. The size of the bubbles is proportional to the antimony content (the larger the bubble, the higher the antimony content). The smallest bubbles represent samples containing <0.3% Sb ₂ O ₃ *. The 7 samples containing >1.0% Sb ₂ O ₃ * (all ‘Roman’) have been omitted due to the excessive size of the bubbles produced. Compare to Figure 4.2.6.	164
Figure 4.3.5 – A plot of soda versus lime for published Roman blue-green glass from (see text for details) compared to the different base glass types identified at Eriswell. Compare to Figure 4.2.1.....	165
Figure 4.3.6 – A plot of magnesia versus lime for published Roman blue-green glass (see text for details) compared to the different base glass types identified at Eriswell. Compare to Figure 4.2.2.....	165
Figure 4.3.7 – A plot of silica versus magnesia for Roman blue-green glass from Basinghall Street (see text for details) compared to the different base glass types identified at Eriswell. Compare to Figure 4.2.6.	166
Figure 4.3.8 – A plot of soda versus lime for published Roman antimony-decolourised glass (see text for details) compared to the different base glass types identified at Eriswell. Compare to Figure 4.2.1.	166
Figure 4.3.9 – A plot of magnesia versus lime for published Roman antimony-decolourised glass (see text for details) compared to the different base glass types identified at Eriswell. Compare to Figure 4.2.2.	167
Figure 4.3.10 – A plot of silica versus magnesia for published Roman antimony-decolourised glass (see text for details) compared to the different base glass types identified at Eriswell. Compare to Figure 4.2.6.	167
Figure 4.3.11 – A plot of soda versus lime for published Roman manganese-decolourised glass (see text for details) compared to the different base glass types identified at Eriswell. Compare to Figure 4.2.1.	168
Figure 4.3.12 – A plot of magnesia versus lime for published Roman manganese-decolourised glass (see text for details) compared to the different base glass types identified at Eriswell. Compare to Figure 4.2.2.....	168
Figure 4.3.13 – A plot of silica versus lime for published Roman manganese-decolourised glass (see text for details) compared to the different base glass types identified at Eriswell. Compare to Figure 4.2.6.	169
Figure 4.3.14 – A plot of alumina versus iron oxide for the lightly tinted ‘Roman’ beads and vessel glass fragments from Eriswell, compared to published data for Roman blue-green, antimony-decolourised and manganese-decolourised glass (see text for details).	169
Figure 4.3.15 – Average rare earth element concentrations for ‘Roman’ glass from Eriswell, by colour, normalised to the weathered continental crust (see Chapter 2, section 2.3.2.3). Note the logarithmic scale.	175
Figure 4.3.16 – Average sediment-related element concentrations for ‘Roman’ glass from Eriswell, by colour, normalised to the weathered continental crust (see Chapter 2, section 2.3.2.3). Note the logarithmic scale.	176
Figure 4.4.1 – A plot of magnesia versus potash for ‘Saxon I’ and ‘Saxon II’ glass from Eriswell.	181
Figure 4.4.2 – A plot of phosphate versus potash for ‘Saxon I’ and ‘Saxon II’ glass from Eriswell.	181

Figure 4.4.3 – A plot of magnesia versus alumina for ‘Saxon I’ and ‘Saxon II’ glass from Eriswell, omitting samples which are likely to have suffered from contamination by alumina (see this chapter, section 4.1 for details).....	182
Figure 4.4.4 – A plot of potash versus alumina for ‘Saxon I’ and ‘Saxon II’ glass from Eriswell, omitting samples which are likely to have suffered from contamination by alumina (see this chapter, section 4.1 for details).....	182
Figure 4.4.5 – A plot of magnesia versus alumina for ‘Saxon I’ glass from Eriswell, compared to published data for Late Roman ‘HIMT 1’ and ‘HIMT 2’ glass from Britain (after Foster and Jackson 2009). Samples which are likely to have been affected by alumina contamination have been omitted (see this chapter, section 4.1 for details) ...	183
Figure 4.4.6 – A plot of manganese oxide versus magnesia for early Anglo-Saxon vessel glass (after Freestone <i>et al.</i> 2008).....	186
Figure 4.4.7 – A plot of manganese oxide versus magnesia for the ‘Saxon I’ and ‘Saxon II’ glass types from Eriswell.....	187
Figure 4.4.8 – A plot of manganese oxide versus potash for the ‘Saxon I’ and ‘Saxon II’ glass types from Eriswell. Opaque red sample ERL104:G193:1311 has been omitted due to its extraordinarily high concentration of potash (2.6% K ₂ O*).	187
Figure 4.4.9 – A plot of alumina versus magnesia for the ‘Saxon I’ and ‘Saxon II’ glass types from Eriswell. Samples which are likely to have suffered from contamination by alumina have been omitted (see this chapter, section 4.1 for details).....	190
Figure 4.4.10 – A plot of magnesia versus lime for the ‘Saxon I’ and ‘Saxon II’ glass types from Eriswell.....	190
Figure 4.4.11 – A plot of manganese oxide versus alumina for the ‘Saxon I’ and ‘Saxon II’ glass types from Eriswell. Samples which are likely to have suffered from contamination by alumina have been omitted (see this chapter, section 4.1 for details).....	191
Figure 4.4.12 – A plot of magnesia versus lime for Merovingian (5 th -7 th century) glass from Vicq (Yvelines, N. France) (Velde 1990: 110) and 5 th -8 th century glass from Italy (Silvestri <i>et al.</i> 2005: Group A2/1), compared to the ‘Saxon I’ and ‘Saxon II’ glass types from Eriswell.....	193
Figure 4.4.13 – A plot of manganese oxide versus magnesia for Merovingian (5 th -7 th century) glass from Vicq (Yvelines, N. France) (Velde 1990: 110) and 5 th -8 th century glass from Italy (Silvestri <i>et al.</i> 2005: Group A2/1), compared to the ‘Saxon I’ and ‘Saxon II’ glass types from Eriswell.....	193
Figure 4.4.14 – A plot of magnesia versus lime for Foy <i>et al.</i> ’s ‘Group 2.1’ (Foy <i>et al.</i> 2003: 84), 5 th -8 th century glass from Italy (Silvestri <i>et al.</i> 2005: Group A2/2) and mid-6 th to early 7 th century Celtic vessel glass from Wales (Campbell and Lane 1993: 48), compared to ‘Saxon I’ and ‘Saxon II’ glass types from Eriswell.	194
Figure 4.4.15 – A plot of manganese oxide versus magnesia for Foy <i>et al.</i> ’s ‘Group 2.1’ (Foy <i>et al.</i> 2003: 84), 5 th -8 th century glass from Italy (Silvestri <i>et al.</i> 2005: Group A2/2) and mid-6 th to early 7 th century Celtic vessel glass from Wales (Campbell and Lane 1993: 48), compared to the ‘Saxon I’ and ‘Saxon II’ glass types from Eriswell.	194
Figure 4.4.16 – A plot of magnesia versus potash for the ‘Saxon I’ and ‘Saxon II’ glass types from Eriswell.....	195
Figure 4.4.17 – A plot of magnesia versus phosphate for ‘Saxon II (high MgO, low MnO)’ and ‘Saxon II (high MnO, MnO)’ glass from Eriswell.....	196
Figure 4.4.18 – A plot of potash versus phosphate for ‘Saxon II (high MgO, low MnO)’ and ‘Saxon II (high MnO, MnO)’ glass from Eriswell.....	196
Figure 4.4.19 – A plot of alumina versus lime for ‘Saxon I’ and ‘Saxon II’ glass from Eriswell, compared to the five major groups of natron glass produced in the Eastern Mediterranean between the 4 th and 9 th centuries AD (see text for details). Samples which are likely to have been affected by alumina contamination have been omitted (see this chapter, section 4.1).....	202
Figure 4.4.20 – Average rare earth elements concentrations for ‘Saxon I’ and 11 ‘Saxon II’ glass from Eriswell, normalised to the weathered continental crust (see Chapter 2, section 2.3.2.3). Note the logarithmic scale.	205
Figure 4.4.21 – Rare earth element concentrations for ‘Saxon I (blue)’ glass from Eriswell, by colour, normalised to the weathered continental crust (see Chapter 2, section 2.3.2.3). Note the logarithmic scale.	207

Figure 4.4.22 – Rare earth element concentrations for ‘Saxon I (natron)’ glass from Eriswell, by colour, normalised to the weathered continental crust (see Chapter 2, section 2.3.2.3). Note the logarithmic scale.	207
Figure 4.4.23 – Rare earth element concentrations for ‘Saxon II (natron)’ glass from Eriswell, by colour, normalised to the weathered continental crust (see Chapter 2, section 2.3.2.3). Note the logarithmic scale.	208
Figure 4.4.24 – Rare earth element concentrations for ‘Saxon II (high MgO, MnO)’ glass from Eriswell, by colour, normalised to the weathered continental crust (see Chapter 2, section 2.3.2.3). Note the logarithmic scale.	209
Figure 4.4.25 – Rare earth element concentrations for ‘Saxon II (high MgO, low MnO)’ glass from Eriswell, by colour, normalised to the weathered continental crust (see Chapter 2, section 2.3.2.3). Note the logarithmic scale.	209
Figure 4.4.26 – Average sediment-related element concentrations for ‘Saxon I’ and ‘Saxon II’ glass from Eriswell, normalised to the weathered continental crust (see Chapter 2, section 2.3.2.3). Note the logarithmic scale.	210
Figure 4.4.27 – Sediment-related element concentrations for ‘Saxon I (blue)’ glass from Eriswell, by colour, normalised to the weathered continental crust (see Chapter 2, section 2.3.2.3). Note the logarithmic scale.	211
Figure 4.4.28 – Sediment-related element concentrations for ‘Saxon I (natron)’ glass from Eriswell, by colour, normalised to the weathered continental crust (see Chapter 2, section 2.3.2.3). Note the logarithmic scale.	213
Figure 4.4.29 – Sediment-related element concentrations for ‘Saxon II (natron)’ glass from Eriswell, by colour, normalised to the weathered continental crust (see Chapter 2, section 2.3.2.3). Note the logarithmic scale.	213
Figure 4.4.30 – Sediment-related element concentrations for ‘Saxon II (high MgO, MnO)’ glass from Eriswell, by colour, normalised to the weathered continental crust (see Chapter 2, section 2.3.2.3). Note the logarithmic scale.	214
Figure 4.4.31 – Sediment-related element concentrations for ‘Saxon II (high MgO, low MnO)’ glass from Eriswell, by colour, normalised to the weathered continental crust (see Chapter 2, section 2.3.2.3). Note the logarithmic scale.	214
Figure 4.4.32 – A plot of lime versus strontium for the ‘Saxon I’ and ‘Saxon II’ samples from Eriswell.	215
Figure 4.4.33 – A plot of alumina versus strontium for the ‘Saxon I’ and ‘Saxon II’ samples from Eriswell.	216
Figure 4.4.34 – A plot of magnesia versus strontium for the ‘Saxon I’ and ‘Saxon II’ samples from Eriswell.	216
Figure 4.4.35 – A plot of potash versus strontium for the ‘Saxon I’ and ‘Saxon II’ samples from Eriswell.	218
Figure 4.4.36 – A plot of phosphate versus strontium for the ‘Saxon I’ and ‘Saxon II’ samples from Eriswell.	218
Figure 4.4.37 – Average concentrations of selected trace elements for ‘Saxon I’ and ‘Saxon II’ glass from Eriswell (dashed lines), compared to those for early Anglo-Saxon ‘Period I’ vessel glass (after Freestone <i>et al.</i> 2008).	219
Figure 4.4.38 – Average concentrations of selected trace elements for ‘Saxon I’ and ‘Saxon II’ glass from Eriswell (dashed lines), compared to those for early Anglo-Saxon ‘Period II high MgO, MnO’ vessel glass (after Freestone <i>et al.</i> 2008).	220
Figure 4.4.39 – Average concentrations of selected trace elements for ‘Saxon I’ and ‘Saxon II’ glass from Eriswell (dashed lines), compared to those for early Anglo-Saxon ‘Period II high MgO, low MnO’ vessel glass (after Freestone <i>et al.</i> 2008).	220
Figure 4.5.1 – A plot of alumina versus lime for ‘HIMT’ glass from Eriswell, compared to the five major groups of natron glass produced in the Eastern Mediterranean between the 4 th and 9 th centuries AD (see text for details). Samples which are likely to have been affected by alumina contamination have been omitted (see this chapter, section 4.1 for details).	224
Figure 4.5.2 – A plot of magnesia versus manganese oxide for ‘HIMT’ glass from Eriswell, compared to published data for Late Roman ‘HIMT 1’ and ‘HIMT 2’ glass from Britain (after Foster and Jackson 2009).	224

Figure 4.5.3 – A plot of alumina versus iron oxide for ‘HIMT’ glass from Eriswell, compared to published data for Late Roman ‘HIMT 1’ and ‘HIMT 2’ glass from Britain (after Foster and Jackson 2009). Samples which are likely to have been affected by iron and alumina contamination have been omitted (see this chapter, section 4.1 for details).	225
Figure 4.5.4 – A plot of iron oxide versus manganese oxide for ‘HIMT’ glass from Eriswell, compared to published data for Late Roman ‘HIMT 1’ and ‘HIMT 2’ glass from Britain (after Foster and Jackson 2009). Samples which are likely to have been affected by iron contamination have been omitted (see this chapter, section 4.1 for details).	225
Figure 4.5.5 – Rare earth element concentrations for ‘HIMT’ glass from Eriswell, by colour, normalised to the weathered continental crust (see Chapter 2, section 2.3.2.3). All samples are from bead ERL104:G268:3260 (<i>Candy Variant</i>). Note the logarithmic scale.	228
Figure 4.5.6 – Sediment-related element concentrations for ‘HIMT’ glass from Eriswell, by colour, normalised to the weathered continental crust (see Chapter 2, section 2.3.2.3). All samples are from bead ERL104:G268:3260 (<i>Candy Variant</i>). Note the logarithmic scale.	229
Figure 4.5.7 – A plot of lime versus strontium for 123 published ‘HIMT 1’ glass samples (after Foster and Jackson 2009), compared to the different base glass types identified at Eriswell.	230
Figure 4.6.1 – A plot of alumina versus lime for ‘Levantine I’ glass from Eriswell, compared to the five major groups of natron glass produced in the Eastern Mediterranean between the 4 th and 9 th centuries AD (see text for details). Samples which are likely to have been affected by alumina contamination have been omitted (see this chapter, section 4.2 for details).	232
Figure 4.6.2 – Rare earth element concentrations for ‘Levantine I’ glass from Eriswell, by colour, normalised to the weathered continental crust (see Chapter, 2, section 2.3.2.3). Note the logarithmic scale.	234
Figure 4.6.3 – Average rare earth element concentrations for ‘Levantine I’ glass from Eriswell, compared to ‘Levantine’ glass from Apollonia-Arsuf and Bet Eli’ezer in Israel (unpublished LA-ICP-MS data courtesy of Ian Freestone). Data are normalised to the weathered continental crust (see Chapter 2, section 2.3.2.3). Note the logarithmic scale.	235
Figure 4.6.4 – Sediment-related element concentrations for ‘Levantine I’ glass from Eriswell, by colour, normalised to the weathered continental crust (see Chapter, 2, section 2.3.2.3). Note the logarithmic scale.	236
Figure 4.6.5 – Average concentrations of selected sediment-related elements for ‘Levantine I’ glass from Eriswell, compared to ‘Levantine’ glass from Apollonia-Arsuf and Bet Eli’ezer in Israel (unpublished LA-ICP-MS data courtesy of Ian Freestone). Data are normalised to the weathered continental crust (see Chapter 2, section 2.3.2.3). Note the logarithmic scale.	237
Figure 4.6.6 – A plot of lime versus strontium for 24 published 4 th century ‘Levantine I’ glass samples from Britain (after Foster and Jackson 2009), compared to the different base glass types identified at Eriswell.	238
Figure 4.7.1 – A plot of alumina versus lime for ‘A2b Blue’ glass from Eriswell, compared to the five major groups of natron glass produced in the Eastern Mediterranean between the 4 th and 9 th centuries AD (see text for details).	240
Figure 4.7.2 – Rare earth element concentrations for ‘A2b Blue’ glass form Eriswell, by colour, normalised to the weathered continental crust (see Chapter 2, section 2.3.2.3). Note the logarithmic scale.	241
Figure 4.7.3 – Sediment-related element concentrations for ‘A2b Blue’ glass from Eriswell, by colour, normalised to the weathered continental crust (see Chapter 2, section 2.3.2.3). Note the logarithmic scale.	242
Figure 4.8.1 – Stacked histogram showing the relationship between the base glass types used for the bodies of the beads from Eriswell and Brugmann’s chronological attributions.	248
Figure 4.8.2 – Stacked histogram showing the relationship between the base glass types used for the decoration on polychrome beads from Eriswell and Brugmann’s chronological attributions.	249

Figure 4.8.3 – An approximate chronology for the base glass types identified at Eriswell, based solely upon Brugmann’s chronology (see text for details). Note that ‘HIMT’ glass is likely to reflect recycled material from the preceding 4 th century, but this cannot be confirmed at present.	252
Figure 4.8.4 – An approximate chronology for the base glass types identified at Eriswell in use after the 5 th century AD, based upon the chronology proposed by Hines <i>et al.</i> (in press). The dashed areas reflect uncertainties in the date ranges provided by the radiocarbon dates and the use of certain glass types; the more widely spaced dashes reflect greater uncertainty. There are considerable uncertainties relating to the end of phase A, meaning that it is not entirely clear when glass types in use during this period ceased to be used; this uncertainty is indicated by the red dashed line. Note that ‘HIMT’ glass is likely to reflect recycled material from the preceding 4 th century, but this cannot be confirmed at present.	252
Figure 4.8.5 – An approximate chronology for the base glass types identified at Eriswell, based upon subjective judgements made from Brugmann’s chronology (Figure 4.8.3), Hines <i>et al.</i> ’s chronology (Figure 4.8.4), the compositional characteristics of the glass and published data (see text for details). The dashed areas reflect uncertainties in the use of certain glass types; the more widely spaced dashes reflect greater uncertainty. Note that ‘HIMT’ glass is likely to reflect recycled material from the preceding 4 th century, but this cannot be confirmed at present.	253
Figure 4.9.1 – Stacked histogram showing the relationship between the different base glass types used for the bodies of the beads from Eriswell and their translucency/opacity. Note that ‘dark’ glass is treated as translucent.	256
Figure 4.9.2 – Stacked histogram showing the relationship between the base glass types used for the decoration on polychrome beads from Eriswell and their translucency/opacity. Note that ‘dark’ glass is treated as translucent.	256
Figure 4.9.3 – Stacked histogram showing the relationship between the different base glass types used for the bodies of the translucent beads from Eriswell and their colour.	258
Figure 4.9.4 – Stacked histogram showing the relationship between the base glass types used for the translucent decoration on polychrome beads from Eriswell and its colour.	259
Figure 4.9.5 – Stacked histogram showing the relationship between the base glass types used for the bodies of the opaque beads from Eriswell and their colour.	261
Figure 4.9.6 – Stacked histogram showing the relationship between the base glass types used for the opaque decoration on polychrome beads from Eriswell and its colour.	262
Figure 4.10.1 – Stacked histogram showing the relationship between the base glass types used for the bodies of the polychrome and monochrome beads from Eriswell.	268
Figure 4.10.2 – Stacked histogram showing the base glass types used for the bodies of the different bead types from Eriswell, ordered by their phase attributions. These beads are covered by the typologies in Brugmann (2004) and Penn and Brugmann (2007).	270
Figure 4.10.3 – Stacked histogram showing the ‘Saxon’ base glass types used for the bodies of the different bead types from Eriswell, ordered by their phase attributions. These beads are covered by the typologies in Brugmann (2004) and Penn and Brugmann (2007).	271
Figure 4.10.4 – Stacked histogram showing the base glass types used for the applied decoration on the different polychrome bead types from Eriswell, ordered by their phase attributions. These beads are covered by the typologies in Brugmann (2004) and Penn and Brugmann (2007).	272
Figure 4.10.5 – Stacked histogram showing the ‘Saxon’ base glass types used for the applied decoration on the different polychrome bead types from Eriswell, ordered by their phase attributions. These beads are covered by the typologies in Brugmann (2004) and Penn and Brugmann (2007).	273
Figure 4.10.6 – Stacked histogram showing the base glass types used for the bodies of the different bead types from Eriswell, attributed to phases according to their compositional attributes. These beads are <i>not</i> covered by the typologies in Brugmann (2004) and Penn and Brugmann (2007). * denotes bead sub-types that have been grouped together.	276
Figure 4.10.7 – Stacked histogram showing the ‘Saxon’ base glass types used for the bodies of the different bead types from Eriswell, attributed to phases according to their compositional attributes. These beads are <i>not</i> covered by the typologies in Brugmann (2004) and Penn and Brugmann (2007). * denotes bead sub-types that have been grouped together.	277

- Figure 4.10.8 – Stacked histogram showing the base glass types used for the applied decoration on the different polychrome bead types from Eriswell, attributed to phases according to their compositional attributes. These beads are *not* covered by the typologies in Brugmann (2004) and Penn and Brugmann (2007). * denotes bead sub-types that have been grouped together.278
- Figure 4.10.9 – Stacked histogram showing the ‘Saxon’ base glass types used for the applied decoration on the different polychrome bead types from Eriswell, attributed to phases according to their compositional attributes. These beads are *not* covered by the typologies in Brugmann (2004) and Penn and Brugmann (2007). * denotes bead sub-types that have been grouped together.279
- Figure 4.10.10 – Stacked histogram showing the base glass types used for the bodies of the different bead types from Eriswell, ordered by their main distribution. These beads are covered by the typologies in Brugmann (2004) and Penn and Brugmann (2007). ..282
- Figure 4.10.11 – Stacked histogram showing the ‘Saxon’ base glass types used for the bodies of the different bead types from Eriswell, ordered by their main distribution. These beads are covered by the typologies in Brugmann (2004) and Penn and Brugmann (2007).283
- Figure 4.10.12 – Stacked histogram showing the base glass types used for applied decoration on the different polychrome bead types from Eriswell, ordered by their main distribution. These beads are covered by the typologies in Brugmann (2004) and Penn and Brugmann (2007).284
- Figure 4.10.13 – Stacked histogram showing the ‘Saxon’ base glass types used for applied decoration on the different polychrome bead types from Eriswell, ordered by their main distribution. These beads are covered by the typologies in Brugmann (2004) and Penn and Brugmann (2007).285
- Figure 4.10.14 – Stacked histogram showing the base glass types used for the bodies of the different bead types from Eriswell, ordered by their possible production zones based upon their compositional attributes. These beads are *not* covered by the typologies in Brugmann (2004) and Penn and Brugmann (2007). * denotes bead sub-types that have been grouped together.287
- Figure 4.10.15 – Stacked histogram showing the ‘Saxon’ base glass types used for the bodies of the different bead types from Eriswell, ordered by their possible production zones based upon their compositional attributes. These beads are *not* covered by the typologies in Brugmann (2004) and Penn and Brugmann (2007). * denotes bead sub-types that have been grouped together.288
- Figure 4.10.16 – Stacked histogram showing the base glass types used for applied decoration on the different polychrome bead types from Eriswell, ordered by their possible production zones based upon their compositional attributes. These beads are *not* covered by the typologies in Brugmann (2004) and Penn and Brugmann (2007). * denotes bead sub-types that have been grouped together.289
- Figure 4.10.17 – Stacked histogram showing the ‘Saxon’ base glass types used for applied decoration on the different polychrome bead types from Eriswell, ordered by their possible production zones based upon their compositional attributes. These beads are *not* covered by the typologies in Brugmann (2004) and Penn and Brugmann (2007). * denotes bead sub-types that have been grouped together.290
- Figure 4.10.18 – A plot of cobalt versus nickel in the translucent cobalt-blue bead types from Eriswell (LA-ICP-MS data). * denotes bead sub-types that have been grouped together.305
- Figure 4.10.19 – A plot of iron oxide versus lead oxide in the translucent cobalt-blue bead types from Eriswell covered by the typologies in Brugmann (2004) and Penn and Brugmann (2007). The dashed line represents the approximate detection limits for lead oxide. * denotes bead sub-types that have been grouped together.305
- Figure 4.10.20 – A plot of iron oxide versus lead oxide in the translucent cobalt-blue bead types from Eriswell covered by the typologies in Brugmann (2004) and Penn and Brugmann (2007). The dashed line represents the approximate detection limits for lead oxide. * denotes bead sub-types that have been grouped together.306
- Figure 4.10.21 – A translucent blue-green globular beaker from Wye Down, Kent (Evison 2008: 141). Six turns of a translucent blue trail are applied to the neck and shoulder, and another six vertical loops to the lower half of the vessel (Evison 2008: cat no. 148). ...308

Figure 4.11.1 – Stacked histogram showing the relationship between the composition of bead bodies and grave number in cemetery ERL 046 at Eriswell.	311
Figure 4.11.2 – Stacked histogram showing the relationship between the composition of ‘Saxon’ type bead bodies and grave number in cemetery ERL 046 at Eriswell.	311
Figure 4.11.3 – Stacked histogram showing the relationship between the composition of applied decoration on polychrome beads and grave number in cemetery ERL 046 at Eriswell.	312
Figure 4.11.4 – Stacked histogram showing the relationship between the composition of ‘Saxon’ type applied decoration on polychrome beads and grave number in cemetery ERL 046 at Eriswell.	312
Figure 4.11.5 – Stacked histogram showing the relationship between the composition of bead bodies and grave number in cemetery ERL 104 at Eriswell.	313
Figure 4.11.6 – Stacked histogram showing the relationship between the composition of ‘Saxon’ type bead bodies of and grave number in cemetery ERL 104 at Eriswell.	314
Figure 4.11.7 – Stacked histogram showing the relationship between the composition of applied decoration on polychrome beads and grave number in cemetery ERL 104 at Eriswell.	315
Figure 4.11.8 – Stacked histogram showing the relationship between the composition of ‘Saxon’ type applied decoration on polychrome beads and grave number in cemetery ERL 104 at Eriswell.	316
Figure 4.11.9 – Stacked histogram showing the relationship between the composition of bead body and grave number in cemetery ERL 114 at Eriswell.	317
Figure 4.11.10 – Stacked histogram showing the relationship between the composition of ‘Saxon’ type bead bodies and grave number in cemetery ERL 114 at Eriswell.	317
Figure 4.11.11 – Stacked histogram showing the relationship between the composition of applied decoration on polychrome beads and grave number in cemetery ERL 114 at Eriswell.	318
Figure 4.11.12 – Stacked histogram showing the relationship between the composition of ‘Saxon’ type applied decoration on polychrome beads and grave number in cemetery ERL 114 at Eriswell.	318
Figure 4.11.13 – The number of graves at Eriswell in which the different base glass types identified are represented.	325
Figure 5.1.1 – A plot of iron oxide versus manganese oxide for the naturally coloured samples from Eriswell, showing ‘light’ (‘metal-in-glass’), blue-green and yellow tints. Compare to Figure 5.1.2.	331
Figure 5.1.2 – A plot of iron oxide versus manganese oxide for the naturally coloured samples from Eriswell, showing the different tints identified. Compare to Figure 5.1.3.	332
Figure 5.1.3 – A plot of iron oxide versus manganese oxide for the naturally coloured samples from Eriswell, showing the different base glass types identified. Compare to Figure 5.1.2.	332
Figure 5.1.4 – A plot of antimony oxide versus manganese oxide in the naturally coloured samples from Eriswell, showing the different tints identified. Compare to Figure 5.1.5. The dashed line represents the approximate detection limits for antimony.	333
Figure 5.1.5 – A plot of antimony oxide versus manganese oxide in the naturally coloured samples from Eriswell, showing the different base glass types identified. Compare to Figure 5.1.4. The dashed line represents the approximate detection limits for antimony.	333
Figure 5.1.6 – BSE micrograph showing ‘light’ sample ERL104:G315:3244, a <i>Constricted Segmented</i> (‘metal-in-glass’) bead. A layer of gold foil (bright white) is visible sandwiched between two layers of soda-lime-silica glass (grey).	335
Figure 5.1.7 – BSE micrograph showing ‘light’ sample ERL104:G358:2762, a <i>Constricted Segmented</i> (‘metal-in-glass’) bead. A layer of silver foil (bright white) is visible sandwiched between two layers of soda-lime-silica glass (grey).	335
Figure 5.1.8 – Colourant and colourant-related element concentrations for translucent blue-green sample ERL104:G290:1721 and translucent green sample ERL104:G268:3260 from Eriswell. Note the logarithmic scale.	337
Figure 5.1.9 – A plot of iron oxide versus manganese oxide for the translucent pink-brown samples from Eriswell, compared to the naturally coloured samples (Figure 5.1.1).	339
Figure 5.1.10 – A plot of manganese oxide versus magnesia for the translucent pink-brown samples from Eriswell, compared to ‘Saxon I’ glass (see Chapter 4, section 4.4).	339

Figure 5.1.11 – A plot of iron oxide versus lead oxide for the translucent cobalt-blue samples from Eriswell, showing the different base glass types identified. The dashed line represents the approximate detection limits for lead.	342
Figure 5.1.12 – A plot of antimony oxide versus manganese oxide in the translucent cobalt-blue samples from Eriswell, showing the different base glass types identified. The dashed line represents the approximate detection limits for antimony.	342
Figure 5.1.13 – BSE micrograph showing translucent blue sample ERL114:G450:1590, a <i>Constricted Cylindrical variation</i> bead. An irregular particle of calcium phosphate (pale grey) is visible within a soda-lime-silica glass matrix (grey). The black areas represent bubbles and voids.	344
Figure 5.1.14 – BSE micrograph showing translucent blue sample ERL046:G44:1015, a <i>Constricted Cylindrical</i> bead. Three sub-angular grains of silica (dark grey) and numerous calcium-iron-aluminium-silicate crystals (pale grey) are visible in a soda-lime-silica glass matrix. The bright white particles are metallic copper, containing approximately 2% nickel.	344
Figure 5.1.15 – BSE micrograph showing translucent blue sample ERL104:G263:1411, a <i>Constricted Cylindrical</i> bead. A complex cobalt-rich inclusion is visible within a soda-lime-silica glass matrix. For a detailed analysis of the individual phases present, refer to Appendix L.	345
Figure 5.1.16 – Average colourant and colourant-related element concentrations for the translucent cobalt-blue samples from Eriswell, showing the different base glass types identified. Note the logarithmic scale.	347
Figure 5.1.17 – A plot of cobalt versus copper for the translucent cobalt-blue samples from Eriswell, showing the different base glass types identified.	349
Figure 5.1.18 – A plot of cobalt versus iron for the translucent cobalt-blue samples from Eriswell, showing the different base glass types identified.	349
Figure 5.1.19 – A plot of cobalt versus nickel for the translucent cobalt-blue samples from Eriswell, showing the different base glass types identified.	350
Figure 5.1.20 – A plot of cobalt versus zinc for the translucent cobalt-blue samples from Eriswell, showing the different base glass types identified.	350
Figure 5.1.21 – A plot of cobalt versus lead for the translucent cobalt-blue samples from Eriswell, showing the different base glass types identified.	352
Figure 5.1.22 – A plot of cobalt versus antimony for the translucent cobalt-blue samples from Eriswell, showing the different base glass types identified. ‘Roman’ samples have been omitted due to the introduction of antimony with the base glass.	352
Figure 5.1.23 – A plot of cobalt versus indium for the translucent cobalt-blue samples from Eriswell, showing the different base glass types identified.	353
Figure 5.1.24 – A plot of cobalt versus arsenic for the translucent cobalt-blue samples from Eriswell, showing the different base glass types identified.	353
Figure 5.1.25 – A plot of the ratios of Ni/Co versus Zn/Co for the translucent cobalt-blue samples from Eriswell, showing the different base glass types identified.	355
Figure 5.1.26 – A plot of the ratios of Ni/Co versus Cu/Co for the translucent cobalt-blue samples from Eriswell, showing the different base glass types identified.	355
Figure 5.1.27 – A plot of the ratios of Cu/Co versus Zn/Co for the translucent cobalt-blue samples from Eriswell, showing the different base glass types identified.	356
Figure 5.1.28 – A plot of copper oxide versus lead oxide for the translucent copper-green and turquoise glasses from Eriswell.	358
Figure 5.1.29 – BSE micrograph showing translucent copper-green sample ERL104:G242:2266, a <i>Green Cylindrical</i> bead. A lead-rich soda-lime-silica glass matrix is visible, relatively free of inclusions except for a few sparse bubbles and voids. The brighter areas of glass are richer in lead, and have resulted from poor mixing of the batch.	359
Figure 5.1.30 – BSE micrograph showing sample ERL104:G290:1721, a <i>Mosaic?</i> bead. Three different colours of soda-lime-silica glass can be seen. The pale grey glass to the left is a lead-rich opaque red glass, coloured and opacified by nanoparticles of metallic copper. The darker grey glass in the centre is opaque yellow, coloured and opacified by lead-tin oxide (white crystals). The pale grey glass to the right is a lead-rich translucent copper-green glass. The dark grey streak running down the centre of the sample is lower in lead, and has resulted from poor mixing of the batch. Numerous large bubbles and voids are visible, particularly in the red glass. Note how the three colours have mixed at their boundaries.	359

- Figure 5.1.31 – BSE micrograph showing sample ERL104:G144:2567, a *Traffic Light Twisted Trail* bead. The pale grey glass is a lead-rich opaque yellow soda-lime-silica glass, opacified by lead-tin oxide (white crystals). Heavily inter-mixed with this is a translucent green glass (dark grey) containing slightly less lead. The dark grey crystals visible in both colours correspond to the mineral wollastonite (CaSiO_3).360
- Figure 5.1.32 – A plot of copper oxide versus tin oxide for the translucent copper-green and turquoise samples from Eriswell. The dashed line represents the approximate detection limits for tin oxide.362
- Figure 5.1.33 – A plot of tin oxide versus lead oxide for the translucent copper-green samples from Eriswell, compared to opaque yellow samples (see this chapter, section 5.2.2). The dashed line represents the approximate detection limits for tin oxide.362
- Figure 5.1.34 – A plot of tin oxide versus lead oxide for the translucent copper-green samples from Eriswell, compared to opaque copper-green samples (see this chapter, section 5.2.2). The dashed line represents the approximate detection limits for tin oxide.363
- Figure 5.1.35 – A plot of copper oxide versus zinc oxide for the translucent copper-green and turquoise samples from Eriswell. The dashed line represents the approximate detection limits for zinc oxide.363
- Figure 5.1.36 – BSE micrograph showing translucent copper-green sample ERL104:G290:1721, a *Mosaic?* bead. Several large angular inclusions of copper oxide are visible, which are likely to represent relicts of the colourant. These are immediately surrounded by numerous acicular calcium silicate crystals, corresponding to the mineral wollastonite (CaSiO_3). The bright white crystals visible in the surrounding soda-lime silicate glass matrix are lead-tin oxide. The black area to the top-left is a void.365
- Figure 35.1.37 – BSE micrograph showing translucent copper-green sample ERL104:G290:1721, a *Mosaic?* bead. A bright copper-rich area of soda-lime-silica glass is visible containing numerous dark grey acicular calcium silicate crystals, corresponding to the mineral wollastonite (CaSiO_3). The sparse bright white flecks in the surrounding soda-lime-silica glass are lead-tin oxide crystals.365
- Figure 5.1.38 – BSE micrograph showing translucent copper-green sample ERL104:G362:1961 & 1969, a *Traffic Light Twisted Trail* bead. A small sub-angular sodium-aluminium-silicate inclusion (black) corresponding to the mineral nepheline ($\text{Na}_3\text{KAl}_4\text{Si}_4\text{O}_{16}$) is visible containing a crystal of lead-tin oxide in its centre. The sparse bright white crystals in the surrounding soda-lime-silica glass matrix are lead-tin oxide. The darker grey patches are rich in calcium, and are likely to represent devitrification products.367
- Figure 5.1.39 – BSE micrograph showing translucent copper-green sample ERL046:G38:1048, a *YellowGreen* bead. A small irregular sodium aluminium silicate sulphate inclusion (black) corresponding to the mineral lazurite ($\text{Na}_3\text{Ca}(\text{Al}_3\text{Si}_3\text{O}_{12})\text{S}$) is visible associated with crystals of lead-tin oxide (white).367
- Figure 5.1.40 – Average colourant and colourant-related element concentrations for the translucent copper-green and turquoise samples from Eriswell, showing the different base glass types identified. Note the logarithmic scale.369
- Figure 5.1.41 – A plot of copper versus arsenic for the translucent copper-green and turquoise samples from Eriswell.369
- Figure 5.1.42 – A plot of copper versus silver for the translucent copper-green and turquoise samples from Eriswell.370
- Figure 5.1.43 – A plot of silica versus iron oxide for the ‘dark’ samples from Eriswell, showing the different base glass types identified.371
- Figure 5.1.44 – A plot of tin oxide versus lead oxide for the ‘dark’ samples from Eriswell, showing the different base glass types identified. The dashed lines represent the approximate detection limits for tin oxide and lead oxide.371
- Figure 5.1.45 – BSE micrograph showing ‘dark’ sample ERL104:G343:1671, a *Dark Globular* bead. An angular fragment of iron oxide (pale grey) can be seen in a soda-lime-silica glass matrix (dark grey). The glass at the boundary of this inclusion is slightly enriched in iron, and whilst this could just be resolved in the SEM it is not easy to see here.373
- Figure 5.1.46 – BSE micrograph showing ‘dark’ sample ERL104:G144:2559, a *Dark Globular* bead. A fragment of iron scale (pale grey) is visible in a soda-lime-silica glass matrix (dark grey).374

Figure 5.1.47 – BSE micrograph showing ‘dark’ sample ERL104:G242:2273, a <i>Miniature Dark</i> bead. Two inclusions of fayalitic slag (dark grey) in a high-lead soda-lime-silica glass matrix coloured by iron (pale grey) are visible. The slag particles consist of irregular wüstite grains (1), together with intergrowths of fayalite (2) and interstitial silicate glass (3). The slag has clearly begun to dissolve in the surrounding glass.	374
Figure 5.1.48 – BSE micrograph showing ‘dark’ sample ERL104:G290:1734, a <i>DarkPoly4</i> bead. An irregular inclusion consisting of grains of iron oxide corresponding to wüstite (FeO) is visible (pale grey) in a soda-lime-silica glass matrix (dark grey).	375
Figure 5.1.49 – Colourant and colourant-related elements for the ‘dark’ samples from Eriswell, showing the different base glass types identified. Note the logarithmic scale.	378
Figure 5.2.1 – A plot of tin oxide versus lead oxide for the white samples from Eriswell. Compare to Figure 5.2.2. The dashed lines represent the approximate detection limits for tin oxide and lead oxide.	381
Figure 5.2.2 – A plot of tin oxide versus lead oxide for the opaque white samples from Eriswell, showing the different base glass types identified. Compare to Figure 5.2.1. The dashed lines represent the approximate detection limits for tin oxide and lead oxide.	381
Figure 5.2.3 – A plot of tin oxide versus antimony oxide for the white samples from Eriswell. Compare to Figure 5.2.4. The dashed lines represent approximate detection limits for tin oxide and antimony oxide.	382
Figure 5.2.4 – A plot of tin oxide versus antimony oxide for the opaque white samples from Eriswell, showing the different base glass types identified. Compare to Figure 5.2.4. The dashed lines represent approximate detection limits for tin oxide and antimony oxide.	382
Figure 5.2.5 – BSE micrograph showing opaque white sample ERL104:G193:1312, a <i>Cylindrical Round</i> bead. Bright white crystals of cassiterite (tin oxide), heterogeneously dispersed in a lead-rich soda-lime-silica glass matrix (grey), act as the opacifying agent.	383
Figure 5.2.6 – BSE micrograph showing opaque white sample ERL104:G237:1151, a <i>Cylindrical Round</i> bead. Bright white crystals of cassiterite (tin oxide), heterogeneously dispersed in a lead-rich soda-lime-silica glass matrix (grey), act as the opacifying agent. Several voids (black) and bubbles are also visible.	383
Figure 5.2.7 – BSE micrograph showing opaque white sample ERL104:G107:1128, a <i>Koch34</i> bead. Bright white crystals of cassiterite (tin oxide), heterogeneously dispersed in a lead-rich soda-lime-silica glass matrix (grey), act as the opacifying agent. Several large bubbles can also be seen.	384
Figure 5.2.8 – BSE micrograph showing opaque white sample ERL104:G195:1352, a <i>Koch34</i> bead. Bright white crystals of cassiterite (tin oxide), heterogeneously dispersed in a lead-rich soda-lime-silica glass matrix (grey), act as the opacifying agent. Numerous bubbles are also visible.	384
Figure 5.2.9 – BSE micrograph showing opaque white sample ERL104:G367:3625, a <i>White Cylindrical, pentagonal</i> bead. A heterogeneous dispersion of tiny bubbles of varying size act as the opacifying agent.	385
Figure 5.2.10 – BSE micrograph showing opaque white sample ERL104:G367:3619, a <i>WhitePoly3</i> bead. A heterogeneous dispersion of tiny bubbles of varying size act as the opacifying agent.	385
Figure 5.2.11 – BSE micrograph showing sample ERL114:G422:1454, a <i>BlueGreen Spiral</i> bead. A heterogeneous dispersion of tiny bubbles of varying size act as the opacifying agent in the opaque white glass at the top of the image. The grey soda-lime-silica glass at the bottom of the image represents translucent cobalt-blue applied decoration. The large bright elongated inclusion is a fragment of iron oxide scale, probably pulled from the mandrel, which has begun to partially dissolve in the surrounding glass matrix.	387
Figure 5.2.12 – BSE micrograph showing opaque white sample ERL114:G450:1164, a <i>WhitePoly2</i> bead. A sparse dispersion of tiny bubbles of varying size act as the opacifying agent. Small hollow crystals of calcium silicate (pale grey), corresponding to wollastonite (CaSiO ₃) are visible throughout the glass matrix.	387
Figure 5.2.13 – A plot of reduced (*) alumina and iron oxide in the opaque white samples from Eriswell. Compare to Figure 5.2.14.	389

Figure 5.2.14 – A plot of reduced (*) alumina and iron oxide in the opaque white samples from Eriswell, showing the different base glass types identified. Compare to Figure 5.2.13.	389
Figure 5.2.15 – Average colourant and colourant-related elements for the opaque white samples from Eriswell, showing the different base glass types identified. Note the logarithmic scale.	391
Figure 5.2.16 – A plot of indium versus tin for the opaque white samples from Eriswell. Note the logarithmic scale.	391
Figure 5.2.17 – A plot of soda versus lead oxide for the opaque yellow and opaque green samples from Eriswell.	393
Figure 5.2.18 – A plot of lime versus lead oxide for the opaque yellow and opaque green samples from Eriswell.	394
Figure 5.2.19 – A plot of silica versus lead oxide for the opaque yellow and opaque green samples from Eriswell.	394
Figure 5.2.20 – A plot of tin oxide versus lead oxide for the opaque yellow and opaque green samples from Eriswell. Compare to Figure 5.2.21. The dashed line represents the approximate detection limits for tin oxide.	395
Figure 5.2.21 – A plot of tin oxide versus lead oxide for the opaque yellow and opaque green samples from Eriswell, showing the different base glass types identified. Compare to Figure 5.2.20. The dashed line represents the approximate detection limits for tin oxide.	395
Figure 5.2.22 – BSE micrograph showing sample ERL104:G144:2598, a <i>Traffic Light Twisted Trail</i> bead. Three different colours of soda-lime-silica glass are visible: opaque red (left), opaque yellow (centre) and translucent green (right). The opaque yellow glass appears brighter due to the higher concentration of lead in this glass. Bright white crystals of lead-tin oxide are visible heterogeneously dispersed in both the opaque yellow and translucent green colours, but are much sparser in the latter. A number of large bubbles (black) are also visible.	397
Figure 5.2.23 – BSE micrograph showing sample ERL104:G281:1797, a <i>Koch34</i> bead. The darker grey soda-lime-silica glass is opaque red, coloured and opacified by nanoparticles of metallic copper. The pale grey soda-lime-silica glass is opaque yellow, coloured and opacified by a dispersion of lead-tin oxide crystals (white). The opaque yellow glass appears brighter in the image due to the higher concentration of lead present. Several bubbles are also visible.	398
Figure 5.2.24 – BSE micrograph showing opaque yellow sample ERL046:G18:1787, a <i>Norfolk Melon related?</i> bead. Several irregular crystals of lead-tin oxide (white) are visible heterogeneously dispersed in a lead-rich soda-lime-silica glass matrix (grey). The pale grey streaks result from variations in the lead content, which results from poor mixing of the batch.	398
Figure 5.2.25 – BSE micrograph showing opaque yellow sample ERL104:G195:1356, a <i>Segmented Globular</i> bead. A large sub-angular inclusion rich in lead and tin is visible, containing an abundance of lead-tin oxide crystals (white) in a lead-rich soda-lime-silica glass matrix (grey). The glass is opacified by a heterogeneous dispersion of lead-tin oxide crystals (white).	399
Figure 5.2.26 – BSE micrograph showing an enlargement of the sub-angular aggregate of lead-tin oxide crystals (white) in opaque yellow sample ERL104:G195:1356, shown in Figure 5.2.25. Within this aggregate, small particles of sodium aluminium silicate corresponding to the mineral nepheline ($\text{Na}_3\text{KAl}_4\text{Si}_4\text{O}_{16}$) can be seen (black).	399
Figure 5.2.27 – BSE micrograph showing opaque yellow sample ERL104:G367:3627, a <i>Norfolk Melon related?</i> bead. A large irregular region rich in lead and tin, containing a dense dispersion of lead-tin oxide crystals (white), is visible within a lead-rich soda-lime-silica glass matrix (grey). Large particles of sodium aluminium silicate, corresponding to the mineral nepheline ($\text{Na}_3\text{KAl}_4\text{Si}_4\text{O}_{16}$), are clearly visible (black).	400
Figure 5.2.28 – BSE micrograph showing opaque green sample ERL104:G242:3321, a <i>Green Constricted Segmented</i> bead. A very sparse and heterogeneous dispersion of lead-tin oxide crystals (white) can be seen, together with several diamond-shaped crystals of tin oxide rich in calcium and silicon (pale grey). Also visible are a number of irregular aggregates of sodium calcium silicate (dark grey) associated with lead-tin oxide (white flecks). The brighter streaks in the soda-lime-silica glass matrix reflect variations in the lead content, resulting from poor mixing of the batch.	402

- Figure 5.2.29 – BSE micrograph showing opaque green sample ERL104:G242:2273/11, a *Green Constricted Segmented* bead. A sparse, heterogeneous dispersion of lead-tin oxide crystals (white) is visible. Some of these are associated with several large aggregates of sodium calcium silicate (dark grey).....402
- Figure 5.2.30 – BSE micrograph showing opaque yellow sample ERL104:G242:2217, a *Yellow Globular, opaque* bead. Numerous lead-tin oxide crystals (white) are visible heterogeneously dispersed in a lead-rich soda-lime-silica glass matrix (grey). Several small sodium aluminium silicate inclusions (black), corresponding to the mineral nepheline ($\text{Na}_3\text{KAl}_4\text{Si}_4\text{O}_{16}$), can be seen associated with some of these opacifying crystals. A number of bubbles are also visible.....403
- Figure 5.2.31 – BSE micrograph showing opaque yellow sample ERL046:G03:1303, a *Norfolk YellowRed* bead. Several lead-tin oxide crystals (white) are visible heterogeneously dispersed in a lead-rich soda-lime-silica glass matrix (grey). An agglomerate of sodium aluminium silicate inclusions (black), corresponding to the mineral nepheline ($\text{Na}_3\text{KAl}_4\text{Si}_4\text{O}_{16}$), can be seen associated with some of these opacifying crystals. Several cracks in the glass are also visible to the bottom-right.403
- Figure 5.2.32 – BSE micrograph showing opaque yellow sample ERL114:G422:1453, a *Norfolk Melon* bead. Numerous lead-tin oxide crystals (white) are visible heterogeneously dispersed in a lead-rich soda-lime-silica glass matrix (grey). Two sodium aluminium silicate inclusions (black), corresponding to the mineral lazurite ($\text{Na}_3\text{Ca}(\text{Al}_3\text{Si}_3\text{O}_{12})\text{S}$), are visible associated with lead-tin oxide crystals.406
- Figure 5.2.33 – BSE micrograph showing opaque yellow sample ERL104:G242:2161, a *RedPoly2* bead. A heterogeneous dispersion of lead-tin oxide crystals (white) is visible in a lead-rich soda-lime-silica glass matrix (grey). Numerous acicular calcium silicate crystals (dark grey), corresponding to wollastonite (CaSiO_3), can be seen. Several particles of sodium aluminium silicate, corresponding to the mineral nepheline ($\text{Na}_3\text{KAl}_4\text{Si}_4\text{O}_{16}$), are also visible (black). Some of these are associated with a small aggregate of lead-tin oxide crystals (white) and lead-silicate (very pale grey) towards the top of the image. The porous areas to the top-left and top-right of the image are weathered glass.406
- Figure 5.2.34 – BSE micrograph showing opaque green sample ERL104:G352:2812, a *Green Globular* bead. Crystals of lead-tin oxide (white) are visible heterogeneously dispersed in a lead-rich soda-lime-silica glass matrix (grey). The bright grain towards the centre of the image is rich in lead and silica, and is surrounded by numerous acicular calcium silicate crystals (dark grey). The glass matrix appears brighter in the areas immediately surrounding this due to the higher concentrations of lead in these regions.407
- Figure 5.2.35 – BSE micrograph showing opaque green sample ERL104:G367:3646, a *Green Globular* bead. A sparse and heterogeneous dispersion of lead-tin oxide crystals (white) are visible in a lead-rich soda-lime-silica glass matrix (grey). The brighter streaks in the glass are slightly higher in lead, and result from poor mixing of the batch. Several small sodium aluminium silicate inclusions (black), corresponding to the mineral (nepheline, $\text{Na}_3\text{KAl}_4\text{Si}_4\text{O}_{16}$) can also be seen, together with several acicular and euhedral crystals of calcium silicate (dark grey). The large irregular inclusion towards the top of the image is likely to reflect part of the refractory ceramic in which the glass was melted, and contains several grains of silica (darker grey).....407
- Figure 5.2.36 – BSE micrograph showing opaque yellow sample ERL104:G242:2206, a *Yellow Globular, opaque* bead. A heterogeneous dispersion of lead-tin oxide crystals (white) is visible heterogeneously dispersed in a lead-rich soda-lime-silica glass matrix (grey). The brighter areas of the glass matrix are lightly richer in lead. A sub-angular silica grain is visible (dark grey) towards the centre of the image, surrounded by several small bubbles.408
- Figure 5.2.37 – BSE micrograph showing opaque green sample ERL104:G144:2604, a *Green Melon, ribbed* bead. A sparse dispersion of lead-tin oxide crystals (white) is visible heterogeneously dispersed in a lead-rich soda-lime-silica glass matrix (pale grey). Numerous acicular crystals of calcium silicate (grey), corresponding to the mineral wollastonite (CaSiO_3), can also be seen dispersed throughout the glass. The dark grey inclusions are silica grains.408

- Figure 5.2.38 – BSE micrograph showing opaque green sample ERL104:G144:2604, a *Green Melon, ribbed* bead. Crystals of lead-tin oxide (white) are visible dispersed in a lead-rich soda-lime-silica glass matrix (pale grey), together with numerous acicular crystals of calcium silicate (grey) corresponding to the mineral wollastonite (CaSiO_3). The large inclusion towards the centre of the image (dark grey) is rich in silica, magnesia, iron and lime. This may reflect a relict of the crucible in which the glass was melted.409
- Figure 5.2.39 – Average colourant and colourant-related elements for the opaque yellow samples from Eriswell, showing the different base glass types identified. Note the logarithmic scale.410
- Figure 5.2.40 – Average colourant and colourant-related elements for the opaque green samples from Eriswell, showing the different base glass types identified. Note the logarithmic scale.410
- Figure 5.2.41 – A plot of indium versus tin for the opaque yellow and opaque green lead-tin oxide opacified samples from Eriswell.411
- Figure 5.2.42 – BSE micrograph showing opaque red sample ERL104:G367:3653, a *Traffic Light Other* bead. A dispersion of tiny metallic copper particles (white) is visible dispersed in a soda-lime-silica glass matrix (grey). Note that visible copper particles are too large to contribute to the colour; colour is instead produced by much smaller metallic copper nanoparticles which are well below the resolution of the SEM.412
- Figure 5.2.43 – A plot of copper oxide versus tin oxide for the opaque red samples from Eriswell, showing the different base glass types identified. The dashed line represents the approximate detection limits for tin oxide.416
- Figure 5.2.44 – A plot of tin oxide versus lead oxide for the opaque red samples from Eriswell, compared to the opaque yellow samples (Figure 5.2.20). The dashed lines represent the approximate detection limits for tin oxide and lead oxide.416
- Figure 5.2.45 – A plot of tin oxide versus lead oxide for the opaque red glasses compared to the opaque and translucent green glasses from Eriswell (Figures 5.1.37). The dashed lines represent the approximate detection limits for tin oxide and lead oxide.417
- Figure 5.2.46 – A plot of tin oxide versus lead oxide for the opaque red samples from Eriswell, showing the different base glass types identified. The dashed lines represent the approximate detection limits for tin oxide and lead oxide.417
- Figure 5.2.47 – A plot of copper oxide versus zinc oxide for the opaque red glasses from Eriswell, showing the different base glass types identified. The dashed line represents the approximate detection limits for zinc oxide.418
- Figure 5.2.48 – A plot of lime versus iron oxide for selected fayalitic and kirschsteinitic slag inclusions in the opaque red samples from Eriswell. Data are taken from area analyses of slag inclusions (Table 5.2.4).426
- Figure 5.2.49 – BSE micrograph of sample ERL104:G242:2158, a *Traffic Light Twisted Trail* bead, showing fayalitic slag inclusions in an opaque red glass matrix coloured by metallic copper nanoparticles. The slag primarily consists of irregular grains of wüstite (1), together with fayalite (2), hercynite (3), leucite (4) and interstitial glass (5). The ‘feathery’ phases (6) are fayalitic intergrowths containing elevated levels of sodium and calcium. Large bright metallic copper particles are visible surrounding the slag (7), together with sparse crystals of lead-tin oxide (8) and tin oxide (9). The dark acicular crystals are calcium silicate, corresponding to the mineral wollastonite (CaSiO_3) (10).432
- Figure 5.2.50 – BSE micrograph of sample ERL104:G242:2207, a *Red Globular* bead, showing inclusions of fayalitic slag in an opaque red glass matrix coloured by metallic copper nanoparticles. Several metallic copper particles (1) can be seen surrounding these inclusions. The slag particles primarily consist of solid phases of fayalite (2) and fayalitic intergrowths (3), interstitial glass (4) and dendritic iron oxide (5). An angular inclusion rich in iron and copper (6), and sparse lead-tin oxide crystals are also visible (7). The black areas (8) represent voids.432

- Figure 5.2.51 – BSE micrograph of sample ERL104:G362:1961&1969, a *Traffic Light Twisted Trail* bead, showing fayalitic slag inclusions in an opaque red glass matrix coloured by metallic copper nanoparticles. The main phase of the slag primarily consists of fayalite with containing slightly elevated levels of sodium and calcium (1), fayalitic intergrowths (2) and irregular dendrites or grains of wüstite (3). The black phases (4) represent interstitial glass. The dark grey areas surrounding the slag (5) are soda-lime-silica glass containing elevated levels of iron. Several irregular calcium silicate crystals, corresponding to the mineral wollastonite (CaSiO_3) (6), and bubbles (7) are also visible.433
- Figure 5.2.52 – BSE micrograph of sample ERL046:G38:1046, a *Red Cylindrical* bead, showing a fayalitic slag inclusion in an opaque red glass matrix coloured by metallic copper nanoparticles. Several bright metallic copper particles can be seen surrounding this inclusion (1). The slag primarily consists of solid phases of fayalite (2) and interstitial glass (3), with fayalitic intergrowths at the periphery (4). Several minor iron oxide phases (5) and sparsely distributed lead-tin oxide crystals (6) can also be seen. A few bubbles are also present (7).....433
- Figure 5.2.53 – BSE micrograph of sample ERL046:G03:1271, a *RedPoly6* bead, showing two large fayalitic slag inclusions in an opaque red glass matrix coloured by metallic copper nanoparticles. The slag primarily consists of fayalite (1) and fayalitic intergrowths (2) containing elevated levels of sodium. Irregular grains and dendrites of wüstite (3) and phases of interstitial glass (4) are also visible. The black phases (5) are sodium aluminium silicate rich in iron and phosphate. Fragments of iron oxide scale (6), around which several large metallic copper particles (7) have precipitated, can also be seen. A small number of acicular calcium silicate crystals (8), occasional bright lead-tin oxide crystals (9) and several large bubbles (10) are also present.434
- Figure 5.2.54 – BSE micrograph of sample ERL046:G38:1053, a *Traffic Light Twisted Trail* bead, showing a fayalitic slag inclusion in an opaque red glass matrix coloured by metallic copper nanoparticles. The main phase of the slag corresponds to fayalite (1). Numerous grains and dendrites of wüstite (2) are also visible, together with interstitial glass (3). A large particle of iron oxide (4) can be seen. Within the glass matrix, itself numerous acicular calcium silicate crystals, corresponding to the mineral wollastonite (CaSiO_3) (5) are present, together with sparse crystals of lead-tin oxide (6). Several bubbles (7) are also present.434
- Figure 5.2.55 – BSE micrograph of sample ERL046:G38:1063, a *RedPoly6* bead, showing fayalitic slag inclusions in an opaque red glass matrix coloured by metallic copper nanoparticles. The slag primarily consists of fayalite (1), fayalitic intergrowths (2), and calcic fayalite (3), together with interstitial glass (4). Wüstite is also present as coarse grains and dendrites (5). Several large crystals of tin oxide (6), lead-tin oxide (7) and metallic copper (8) are visible. Irregular calcium silicate crystals, corresponding to the mineral wollastonite (CaSiO_3) (9) can also be seen within the glass matrix.435
- Figure 5.2.56 – BSE micrograph of sample ERL104:G242:2196, a *Traffic Light Streaked* bead, showing fayalitic slag inclusions in an opaque red glass matrix coloured by metallic copper nanoparticles. Several large particles of metallic copper (1) are visible immediately surrounding the slag. The slag primarily consists of fayalite (2) and fayalitic intergrowths (3), together with interstitial glass (4) and irregular grains or dendrites of wüstite (5). A small number of lead-tin oxide crystals (6) and several small bubbles are also visible.435
- Figure 5.2.57 – BSE micrograph of sample ERL104:G268:3257, a *Traffic Light Imitation* bead, showing complex fayalitic slag inclusions in an opaque red glass matrix coloured by metallic copper nanoparticles. The main phase of the slag corresponds to fayalite (1). Fayalitic intergrowths (2) and irregular grains or dendrites of wüstite (3) are also present, together with interstitial glass (4). The black phases correspond to leucite (5), but other black areas represent bubbles or voids (6). Sparse lead-tin oxide crystals (7), tin oxide crystals (8) and nepheline inclusions (9) can also be seen. The glass immediately surrounding the slag appears darker due to the elevated levels of iron in these regions. Large copper oxide particles are also present here, but are difficult to resolve in the BSE micrograph.436

- Figure 5.2.58 – BSE micrograph of sample ERL046:G43:1726, a *RedPoly5* bead, showing fayalitic slag inclusions in an opaque red glass matrix coloured by metallic copper nanoparticles. Several metallic copper particles (1) are visible surrounding these slag particles, due to their larger sizes in these regions. The slag primarily consists of fayalite (2), fayalite enriched in sodium (3), interstitial glass (4) and irregular grains of wüstite (5). A large fragment of iron oxide scale is also present (6). Several crystals of lead-tin oxide (7) and calcium silicate, corresponding to the mineral wollastonite (CaSiO_3) (8) can be seen. The black areas represent voids and bubbles (9).436
- Figure 5.2.59 – BSE micrograph of sample ERL114:G422:1420, a *Norfolk YellowRed* bead, showing a fayalitic slag inclusion in an opaque red glass matrix coloured by metallic copper nanoparticles. Several metallic copper particles (1) can be seen surrounding the slag, due to their larger size in these regions. The slag primarily consists of fayalite (2) and ‘feathery’ fayalitic intergrowths (3) containing elevated levels of sodium and calcium. Interstitial glass (4) and wüstite rims (5) are also present. The glass contains several acicular calcium silicate crystals, corresponding to the mineral wollastonite (CaSiO_3) (6), and a nepheline inclusion (7) associated with bright white lead-tin oxide crystals. The glass immediately surrounding the slag sometimes appears darker (8) due to elevated levels of iron and calcium in these regions.437
- Figure 5.2.60 – BSE micrograph of sample ERL104:G107:1141, a *Koch34* bead, showing a fayalitic slag inclusion in an opaque red glass matrix coloured by metallic copper nanoparticles. Several metallic copper particles (1) are visible immediately surrounding the slag. The slag primarily consists of irregular grains of wüstite (2) and fayalitic intergrowths (3) enriched in sodium and aluminium, together with interstitial glass (4). Within the glass matrix several dark grey acicular crystals of calcium silicate, corresponding to the mineral wollastonite (CaSiO_3) (5) can also be seen.437
- Figure 5.2.61 – BSE micrograph of sample ERL104:G315:2346, a *Traffic Light Twisted Trail* bead, showing fayalitic slag inclusions in an opaque red glass matrix coloured by metallic copper nanoparticles. Several metallic copper particles (1) are visible immediately surrounding the slag inclusions due to their larger sizes in these regions. The slag primarily consists of calcic fayalite enriched in sodium (2) and fayalitic intergrowths (3), together with irregular grains of wüstite (4). A large agglomerate of metallic copper (5) is visible, containing approximately 4% silver oxide. A number of lead-tin oxide crystals (6) and several large bubbles (7) can also be seen. Numerous acicular calcium silicate crystals, corresponding to the mineral wollastonite (CaSiO_3) (8) are present. The glass immediately surrounding the slag sometimes appears darker (9) due to the elevated levels of iron and calcium in these regions.438
- Figure 5.2.62 – BSE micrograph of sample ERL104:G193:1311, a *Koch34* bead, showing a lump of an iron-copper alloy in an opaque red glass matrix coloured by metallic copper nanoparticles. The core of this inclusion (darker grey) is metallic iron, whereas the rim (paler grey) is metallic copper containing approximately 3% iron.438
- Figure 5.2.63 – BSE micrograph of sample ERL104:G281:1795, a *Red Globular* bead, showing a large kirschsteinitic slag inclusion in an opaque red glass matrix coloured by metallic copper nanoparticles. The main phase of the slag corresponds to kirschsteinite (1). Interstitial glass (2), a number of dendritic magnetite crystals (3), and zones of bright white copper particles surrounding the inclusion (4) are also present. The black areas (5) represent voids.440
- Figure 5.2.64 – BSE micrograph of sample ERL104:G268:3260, a *Candy Variant* bead, showing opaque yellow (left), opaque red (right) and translucent green-tinted (bottom) glass. The opaque yellow and red glasses (pale grey and grey respectively) appear brighter than the translucent green glass (black) due to the higher concentration of lead in these colours. The opaque yellow glass is both coloured and opacified by crystals of lead-tin oxide (white). The opaque red glass contains a high density of angular kirschsteinitic slag inclusions (grey) and large bubbles, but colour and opacity are primarily caused by nanoparticles of metallic copper which are too small to be resolved in the SEM.440

- Figure 5.2.65 – BSE micrograph of sample ERL104:G268:3260, a *Candy Variant* bead, showing a high density of kirschsteinitic slag inclusions in an opaque red glass matrix coloured by metallic copper nanoparticles. The main phase of the slag corresponds to kirschsteinite (1). Interstitial glass (2) and dendritic crystals of magnetite (3) are present. A number of bubbles (4) and a large nepheline inclusion (5) containing bright white crystals of lead-tin oxide are also visible.....441
- Figure 5.2.66 – BSE micrograph of sample ERL104:G268:3260, a *Candy Variant* bead, showing kirschsteinitic slag inclusions in an opaque red glass matrix coloured by copper nanoparticles. The main phase of the slag (grey) corresponds to kirschsteinite. Dendrites of magnetite (pale grey) and interstitial glass (dark grey) can also be seen. The sparse bright white particles in the surrounding soda-lime silica glass are crystals of lead-tin oxide.....441
- Figure 5.2.67 – BSE micrograph of sample ERL104:G268:3260, a *Candy Variant* bead, showing an opaque red glass matrix coloured and opacified by metallic copper nanoparticles. A large sodium aluminium silicate inclusion (black), corresponding to the mineral nepheline ($\text{Na}_3\text{KAl}_4\text{Si}_4\text{O}_{16}$), is visible. This is associated with numerous lead-tin oxide crystals (white) which vary in shape from euhedral to acicular. The pale grey area in the centre of the inclusion is soda-lime-silica glass containing a higher concentration of lead. Also visible are particles of kirschsteinitic slag (bottom-right and top-left) and a large bubble.443
- Figure 5.2.68 – BSE micrograph of sample ERL104:G262:1261, a *Koch34* bead, showing a high-lead opaque red glass matrix coloured by metallic copper nanoparticles. The large bright white inclusion towards the centre of the image is a bubble filled with lead oxide. An irregularly shaped lump of iron oxide is also visible (large dark grey inclusion). Several crystals of lead-tin oxide (bright white grains) and tin oxide (pale grey ‘feathery’ crystals) are present heterogeneously dispersed throughout the glass, together with numerous angular sodium calcium lead tin silicate inclusions (dark grey). Several bubbles and a small number of acicular calcium silicate crystals, corresponding to the mineral wollastonite (CaSiO_3) are also visible.....447
- Figure 5.2.69 – BSE micrograph of sample ERL104:G262:1261, a *Koch34* bead, showing a high-lead opaque red glass matrix coloured by metallic copper nanoparticles. Several crystals of lead-tin oxide (bright white grains) and tin oxide (pale grey ‘feathery’ crystals) are visible heterogeneously dispersed throughout the glass, together with numerous angular sodium calcium lead tin silicate inclusions (dark grey). The darker grey glass to the bottom-left of the image is an opaque white glass, opacified by crystals of tin oxide.....447
- Figure 5.2.70 – BSE micrograph of sample ERL104:G262:1287, a *Cylindrical Round* bead, showing an opaque red glass matrix coloured by metallic copper nanoparticles. Several opaque blue streaks are visible, which appear brighter in the image due to the higher concentration of lead in these regions. Numerous lead-tin oxide crystals and several tin oxide crystals are also visible (bright white), together with several large bubbles.....450
- Figure 5.2.71 – BSE micrograph of sample ERL104:G262:1287, a *Cylindrical Round* bead, showing an opaque red glass matrix coloured by metallic copper nanoparticles. Several opaque blue streaks are visible, which appear brighter in the image due to the higher concentration of lead in these regions. A few sparse crystals of lead-tin oxide can be seen in these streaks (bright white). An iron-rich inclusion of fayalitic composition is also present, containing numerous dendrites of iron oxide.....450
- Figure 5.2.72 – Average colourant and colourant-related elements for the opaque red samples from Eriswell, showing the different base glass types identified. Note the logarithmic scale.451
- Figure 5.2.73 – A plot of copper versus silver for the opaque red samples from Eriswell, showing the different base glass types identified. Note the logarithmic scale.452
- Figure 5.2.74 – A plot of indium versus tin for the opaque red samples from Eriswell, showing the different base glass types identified.453
- Figure 5.2.75 – BSE micrograph showing opaque orange sample ERL104:G266:1575, a *Orange* bead. A heterogeneous dispersion of tiny cuprite crystals can be seen (white) dispersed in a soda-lime-silica glass (grey). These impart both colour and opacity to the glass. Note that some areas are devoid of cuprite crystals, as a result of poor mixing of the batch.454

- Figure 5.2.76 – BSE micrograph showing opaque orange sample ERL104:G107:1105, a *Orange* bead. A heterogeneous dispersion of tiny cuprite crystals can be seen (white) dispersed in a soda-lime-silica glass (grey), sometimes forming as irregular agglomerates. These impart both colour and opacity to the glass.455
- Figure 5.2.77 – BSE micrograph showing opaque orange sample ERL104:G193:1294, a *Orange* bead. A heterogeneous dispersion of tiny cuprite crystals can be seen (white) dispersed in a soda-lime-silica glass (grey). These impart both colour and opacity to the glass. Three large lumps of cuprite are also visible (white). Streaks in the glass result from variations in the concentration of cuprite crystals, as a result of poor mixing of the batch.455
- Figure 5.2.78 – A plot of potash versus copper oxide for the opaque orange samples from Eriswell, showing the different base glass types identified and indicating the possibility of two different compositional groups.457
- Figure 5.2.79 – A plot of magnesia versus potash for the opaque orange samples from Eriswell, showing the different base glass types identified.457
- Figure 5.2.80 – A plot of magnesia versus phosphate for the opaque orange samples from Eriswell, showing the different base glass types identified.458
- Figure 5.2.81 – A plot of potash versus phosphate for the opaque orange samples from Eriswell, showing the different base glass types identified.458
- Figure 5.2.82 – Colourant and colourant-related element concentrations for opaque orange ‘Saxon II (high MgO, MnO)’ sample ERL104:G266:1575 from Eriswell, compared to the average concentrations of these components for opaque red glass. Note the logarithmic scale.460
- Figure 5.2.83 – BSE micrograph showing opaque greyish-blue sample ERL104:G353:3073, a *Cylindrical Round* bead. Several sparse crystals of tin oxide (white), which produce opacity, are visible heterogeneously dispersed throughout the soda-lime-silica glass matrix (grey).462
- Figure 5.2.84 – BSE micrograph showing opaque blue sample ERL104:G242:2200, a *Blue Globular, opaque* bead. A heterogeneous dispersion of tiny bubbles is visible (black) dispersed throughout a soda-lime-silica glass matrix (grey), which produce opacity.462
- Figure 5.2.85 – BSE micrograph showing opaque blue sample ERL046:G05:1436, a *Blue Globular, opaque* bead. A heterogeneous dispersion of tiny bubbles is visible (black) dispersed throughout a soda-lime-silica glass matrix (grey), which produce opacity. A large angular grain of silica can also be seen (dark grey inclusion towards the top-left of the image).463
- Figure 5.2.86 – A plot of tin oxide versus antimony oxide for the opaque blue samples from Eriswell, compared to the opaque white samples (see Figure 5.2.3). The dashed lines represent the approximate detection limits for tin oxide and antimony oxide.463
- Figure 5.2.87 – Colourant and colourant-related element concentrations for opaque cobalt-blue ‘Saxon II (high MgO, low MnO)’ sample ERL104:G237:1153 from Eriswell, compared to the average concentrations of these components for translucent blue glass. Note the logarithmic scale.464
- Figure 5.2.88 – BSE micrograph showing opaque turquoise sample ERL104:G112:1023, a *Blue Biconical, opaque* bead. A heterogeneous dispersion of tin oxide crystals is visible (white) dispersed throughout a soda-lime-silica glass matrix (grey), which produce opacity. A number of bubbles (black) can also be seen.466
- Figure 5.2.89 – BSE micrograph showing sample ERL104:G290:1734, a *DarkPoly4* bead. An opaque turquoise glass opacified by a heterogeneous dispersion of calcium antimonate crystals (white) dispersed throughout a soda-lime-silica glass matrix (grey) is visible. Several bubbles can also be seen. The glass devoid of opacifying crystals to the bottom-right of the image is a ‘dark’ glass.466
- Figure 5.2.90 – BSE micrograph showing opaque blue-green sample ERL046:G03:1289, a *Blue Melon, opaque* bead. A lead-rich soda-lime-silica glass matrix can be seen (pale grey). Apart from a few bubbles of considerably variable size and a two very small crystals of tin oxide (bright white), this glass is largely devoid of inclusions.468

- Figure 5.2.91 – BSE micrograph showing opaque blue-green sample ERL046:G03:1289, a *Blue Melon, opaque* bead. Towards the centre of the image a copper oxide inclusion (pale grey) is visible, containing trace levels of zinc and silver. Slightly above this inclusion, a small particle of metallic silver (bright white) can be seen. Variations in the shades of grey in this glass reflect slight differences in the lead content of the glass, due to uneven mixing of the batch. Black areas represent bubbles and voids. ...468
- Figure 5.2.92 – Colourant and colourant-related element concentrations for opaque blue-green sample ERL046:G03:1289 from Eriswell, compared to the average concentrations of these components for translucent green glass. All samples are of the ‘Roman’ type. Note the logarithmic scale.470
- Figure 5.3.1 – A plot of copper versus silver in the copper-based glass colours from Eriswell (LA-ICP-MS data). Note the logarithmic scale.476
- Figure 5.3.2 – A plot of copper versus zinc in the copper-based glass colours from Eriswell (LA-ICP-MS data)477
- Figure 5.3.3 – A plot of indium versus tin in selected glass colours from Eriswell (LA-ICP-MS data). Note the logarithmic scale.480
- Figure 5.3.4 – A plot of tin oxide versus lead oxide in the tin-containing glass colours from Eriswell. The dashed lines represent the approximate detection limits for tin oxide and lead oxide.482
- Figure 6.0.1 - A plot of soda versus lime for late Anglo-Saxon (8th-9th centuries) glass from Hamwic (Hunter and Heyworth 1998), Jarrow (Brill 1999; 2006; Freestone and Hughes 2006) and Wearmouth (Brill 2006) compared to the different base glass types identified at Eriswell.487
- Figure 6.0.2 - A plot of silica versus lime for late Anglo-Saxon (8th-9th centuries) glass from Hamwic (Hunter and Heyworth 1998), Jarrow (Brill 1999; 2006; Freestone and Hughes 2006) and Wearmouth (Brill 2006) compared to the different base glass types identified at Eriswell.487
- Figure 7.1.1 – BSE micrograph showing an opaque yellow sample from Bergh Apton, a probable *Yellow Globular, opaque* bead from grave 34Hvii. Numerous lead-tin oxide crystals (white) are visible heterogeneously dispersed throughout a lead-rich soda-lime-silica glass matrix (grey). Several small sodium aluminium silicate inclusions (black) corresponding to the mineral nepheline ($\text{Na}_3\text{KAl}_4\text{Si}_4\text{O}_{16}$) can be seen associated with some of these opacifying crystals.493
- Figure 7.1.2 – BSE micrograph showing an opaque white samples from Bergh Apton, a possible *White Cylindrical, pentagonal?* bead from grave 56Aiii. Bright white crystals of cassiterite (tin oxide), heterogeneously dispersed in a lead-rich soda-lime-silica glass matrix (grey), act as the opacifying agent. Several voids (black) and bubbles are also visible.493
- Figure 7.1.3 – BSE micrograph showing opaque white bead with translucent blue decoration from Bergh Apton, grave 62C. A dispersion of tiny bubbles of varying size, heterogeneously dispersed throughout a soda-lime-silica glass matrix (grey), act as the opacifying agent. The bubble-free glass to the bottom-right of the image is translucent blue.494
- Figure 7.1.4 – BSE micrograph of an opaque red sample from an unidentified bead from Spong Hill, grave 5/6c, showing fayalitic slag inclusions in an opaque red soda-lime-silica glass matrix coloured by copper nanoparticles. Numerous large bubbles are also visible.494
- Figure 7.1.5 – BSE micrograph of an undefined opaque white bead with green crossing trails and opaque red spots from Spong Hill, grave 42/3, showing a large fayalitic slag inclusion in an opaque red soda-lime-silica glass matrix coloured by copper nanoparticles. The slag has begun to significantly interact with the surrounding glass matrix, as evidenced by numerous bubbles filled with glass within its structure. A large number of iron rich dendrites are visible.495

Figure 7.1.6 – BSE micrograph of an opaque red cylindrical bead with opaque white decoration from Bergh Apton, unknown context, showing fayalitic slag inclusions in an opaque red lead-rich soda-lime-silica glass matrix (pale grey) coloured by copper nanoparticles. Several crystals of lead-tin oxide are visible within the glass matrix (bright white), and a sub-angular silica grain near the centre of the image (black). The glass matrix immediately surrounding the slag inclusions appears darker because it is lower in lead and higher in iron in these regions. Several bubbles are also visible.495

VOLUME II

Figure C.1 – Glass beads sampled from Grave 03, cemetery ERL 046, Eriswell.	681
Figure C.2 – Glass beads sampled from Grave 05, cemetery ERL 046, Eriswell.	681
Figure C.3 – Glass beads sampled from Grave 05, cemetery ERL 046, Eriswell.	682
Figure C.4 – Glass beads sampled from Grave 08, cemetery ERL 046, Eriswell.	682
Figure C.5 – Glass beads sampled from Grave 15, cemetery ERL 046, Eriswell.	683
Figure C.6 – Glass beads sampled from Grave 18, cemetery ERL 046, Eriswell.	683
Figure C.7 – Glass beads sampled from Grave 24, cemetery ERL 046, Eriswell.	684
Figure C.8 – Glass beads sampled from Grave 25, cemetery ERL 046, Eriswell.	684
Figure C.9 – Glass beads sampled from Grave 38, cemetery ERL 046, Eriswell.	685
Figure C.10 – Glass beads sampled from Grave 38, cemetery ERL 046, Eriswell.	685
Figure C.11 – Glass beads sampled from Grave 42, cemetery ERL 046, Eriswell.	686
Figure C.12 – Glass beads sampled from Grave 43, cemetery ERL 046, Eriswell.	686
Figure C.13 – Glass beads sampled from Grave 44, cemetery ERL 046, Eriswell.	687
Figure C.14 – Glass beads sampled from Grave 49, cemetery ERL 046, Eriswell.	687
Figure C.15 – Glass beads sampled from Grave 107, cemetery ERL 104, Eriswell.	688
Figure C.16 – Glass beads sampled from Grave 107, cemetery ERL 104, Eriswell.	688
Figure C.17 – Glass beads sampled from Grave 109, cemetery ERL 104, Eriswell.	689
Figure C.18 – Glass beads sampled from Grave 112, cemetery ERL 104, Eriswell.	689
Figure C.19 – Glass beads sampled from Grave 116, cemetery ERL 104, Eriswell.	690
Figure C.20 – Glass beads sampled from Grave 132, cemetery ERL 104, Eriswell.	690
Figure C.21 – Glass beads sampled from Grave 144, cemetery ERL 104, Eriswell.	691
Figure C.22 – Glass beads sampled from Grave 144, cemetery ERL 104, Eriswell.	691
Figure C.23 – Glass beads sampled from Grave 148, cemetery ERL 104, Eriswell.	692
Figure C.24 – Glass beads sampled from Grave 155, cemetery ERL 104, Eriswell.	692
Figure C.25 – Glass beads sampled from Grave 166, cemetery ERL 104, Eriswell.	693
Figure C.26 – Glass beads sampled from Grave 172, cemetery ERL 104, Eriswell.	693
Figure C.27 – Glass beads sampled from Grave 176, cemetery ERL 104, Eriswell.	694
Figure C.28 – Glass beads sampled from Grave 182, cemetery ERL 104, Eriswell.	694
Figure C.29 – Glass beads sampled from Grave 189, cemetery ERL 104, Eriswell.	695
Figure C.30 – Glass beads sampled from Grave 193, cemetery ERL 104, Eriswell.	695
Figure C.31 – Glass beads sampled from Grave 195, cemetery ERL 104, Eriswell.	696
Figure C.32 – Glass beads sampled from Grave 202, cemetery ERL 104, Eriswell.	696
Figure C.33 – Glass beads sampled from Grave 202, cemetery ERL 104, Eriswell.	697
Figure C.34 – Glass beads sampled from Grave 205, cemetery ERL 104, Eriswell.	697
Figure C.35 – Glass beads sampled from Grave 210, cemetery ERL 104, Eriswell.	698
Figure C.36 – Glass beads sampled from Grave 213, cemetery ERL 104, Eriswell.	698
Figure C.37 – Glass beads sampled from Grave 218, cemetery ERL 104, Eriswell.	699
Figure C.38 – Glass beads sampled from Grave 232, cemetery ERL 104, Eriswell.	699
Figure C.39 – Glass beads sampled from Grave 237, cemetery ERL 104, Eriswell.	700
Figure C.40 – Glass beads sampled from Grave 242, cemetery ERL 104, Eriswell.	700
Figure C.41 – Glass beads sampled from Grave 242, cemetery ERL 104, Eriswell.	701
Figure C.42 – Glass beads sampled from Grave 242, cemetery ERL 104, Eriswell.	701
Figure C.43 – Glass beads sampled from Grave 242, cemetery ERL 104, Eriswell.	702
Figure C.44 – Glass beads sampled from Grave 242, cemetery ERL 104, Eriswell.	702
Figure C.45 – Glass beads sampled from Grave 242, cemetery ERL 104, Eriswell.	703
Figure C.46 – Glass beads sampled from Grave 242, cemetery ERL 104, Eriswell.	703
Figure C.47 – Glass beads sampled from Grave 243, cemetery ERL 104, Eriswell.	704

Figure F.45 – Digitised x-radiograph of glass beads from Grave 281, cemetery ERL 104, Eriswell.	768
Figure F.46 – Digitised x-radiograph of glass beads from Grave 290, cemetery ERL 104, Eriswell.	768
Figure F.47 – Digitised x-radiograph of glass beads from Grave 305, cemetery ERL 104, Eriswell.	769
Figure F.48 – Digitised x-radiograph of glass beads from Grave 309, cemetery ERL 104, Eriswell.	769
Figure F.49 – Digitised x-radiograph of glass beads from Grave 315, cemetery ERL 104, Eriswell.	770
Figure F.50 – Digitised x-radiograph of glass beads from Grave 336, cemetery ERL 104, Eriswell.	770
Figure F.51 – Digitised x-radiograph of glass beads from Grave 343, cemetery ERL 104, Eriswell.	771
Figure F.52 – Digitised x-radiograph of glass beads from Grave 344, cemetery ERL 104, Eriswell.	771
Figure F.53 – Digitised x-radiograph of glass beads from Grave 350, cemetery ERL 104, Eriswell.	772
Figure F.54 – Digitised x-radiograph of glass beads from Grave 352, cemetery ERL 104, Eriswell.	772
Figure F.55 – Digitised x-radiograph of glass beads from Grave 353, cemetery ERL 104, Eriswell.	773
Figure F.56 – Digitised x-radiograph of glass beads from Grave 362, cemetery ERL 104, Eriswell.	773
Figure F.57 – Digitised x-radiograph of glass beads from Grave 363, cemetery ERL 104, Eriswell.	774
Figure F.58 – Digitised x-radiograph of glass beads from Grave 367, cemetery ERL 104, Eriswell.	774
Figure F.59 – Digitised x-radiograph of glass beads from Grave 367, cemetery ERL 104, Eriswell.	775
Figure F.60 – Digitised x-radiograph of glass beads from Grave 413, cemetery ERL 104, Eriswell.	775
Figure F.61 – Digitised x-radiograph of glass beads from Grave 414, cemetery ERL 104, Eriswell.	776
Figure F.62 – Digitised x-radiograph of glass beads from Grave 422, cemetery ERL 104, Eriswell.	776
Figure F.63 – Digitised x-radiograph of glass beads from Grave 447, cemetery ERL 104, Eriswell.	777
Figure F.64 – Digitised x-radiograph of glass beads from Grave 450, cemetery ERL 104, Eriswell.	777
Figure L.1 – BSE image showing the locations of the spot analyses shown in Table L.1.	867
Figure L.2 – BSE image showing the locations of the spot analyses shown in Table L.2.	867

LIST OF TABLES

VOLUME I

Table 2.2.1 – SEM-EDS area analyses of Early Byzantine glass tesserae (Caesarea, Israel) acquired from polished samples.	54
Table 2.2.2 – SEM-EDS area analyses of Early Byzantine glass tesserae (Caesarea, Israel) acquired from polished samples, compared to those acquired from flakes obtained using the DIAM technique.	58
Table 2.2.3 – SEM-EDS area analyses of Early Byzantine glass tesserae (Caesarea, Israel) acquired from polished samples, compared to those acquired directly from the tesserae by ESEM-EDS.	64
Table 2.3.1 – Elements and element oxides measured by SEM-EDS in the present study.	70
Table 2.3.2 – SEM-EDS area analyses of Corning A and B glass standards.	76
Table 2.3.3 – Elements measured by LA-ICP-MS in the present study.	80
Table 2.3.4 – Elemental MUQ (mud from Queensland) values used for normalisation of the LA-ICP-MS data (after Kamber <i>et al.</i> 2005).	86
Table 3.2.1 – X-radiographs of the opaque white beads from Eriswell, showing the method of opacification and those beads which are likely to contain opaque red glass at their core.	103
Table 3.2.2 – X-radiographs of the opaque red beads coated with opaque blue glass from Eriswell, showing the method of opacification and those beads which contain opaque red glass at their core.	107
Table 4.1.1 – A worked example of the re-summing (normalisation) process for opaque red sample ERL114:G413:1495, showing how iron and alumina values are assumed.	122
Table 4.2.1 – Average compositions for the different base glass types identified at Eriswell.	135
Table 4.4.1 – Average compositions for the five different sub-groups of ‘Saxon I’ and ‘Saxon II’ glass identified at Eriswell.	185
Table 4.4.2 – Hypothetical glass compositions for a mixture of 10% ash-rich glass (after Freestone <i>et al.</i> 2008) with ‘Saxon I (natron)’ glass, and of 10% beech ash (after Jackson <i>et al.</i> 2005) with ‘Saxon II (natron)’ glass, compared to the mean composition of ‘Saxon II (high MgO, MnO)’ glass.	199
Table 4.10.1 – Comparisons between the composition of bead body and applied decoration on the Koch* bead types from Eriswell.	302
Table 5.1.1 – SEM-EDS area analyses of two different samples from the translucent blue glass decoration on bead ERL046:G38:1036, highlighting marked differences in the concentration of potash.	346
Table 5.1.2 – Selected SEM-EDS spot analyses of aluminium-rich inclusions observed in several translucent copper-green samples from Eriswell.	368
Table 5.1.3 – Selected SEM-EDS area and spot analyses of the fayalitic slag inclusions in ‘dark’ sample ERL104:G242:2273/16, showing the bulk composition of the slag and the composition of the different phases identified.	376
Table 5.2.1 – Selected SEM-EDS spot analyses of the aluminium-rich inclusions observed in several opaque yellow samples from Eriswell.	404
Table 5.2.2 – Selected SEM-EDS spot analyses of the aluminium-rich inclusions observed in several opaque green samples from Eriswell.	405
Table 5.2.3 – Selected SEM-EDS spot analyses of the aluminium-rich inclusions observed in several of the opaque red samples from Eriswell.	420
Table 5.2.4 – Selected SEM-EDS area analyses of the fayalitic and kirschsteinitic slag inclusions in several of the opaque red samples from Eriswell, highlighting the compositional differences between the two slag types.	424
Table 5.2.5 – Selected SEM-EDS spot analyses of the phases within the fayalitic slag inclusions observed in several of the opaque red samples from Eriswell.	427
Table 5.2.6 – Selected SEM-EDS spot analyses of the phases within the kirschsteinitic slag inclusions observed in several of the opaque red samples from Eriswell.	442
Table 5.2.7 – Selected SEM-EDS spot analyses of the sodium calcium lead-tin silicate crystals observed in opaque red sample ERL104:G262:1261.	448

VOLUME II

Table A.1. – The Eriswell glass bead catalogue.....	551
Table B1 – The distribution of the bead types A-J at Eriswell. * denotes bead sub-types that have been grouped together.....	670
Table B2 – The distribution of bead types K-Z at Eriswell. * denotes bead sub-types that have been grouped together.....	675
Table G.1 – Raw SEM-EDS data for the glass beads from Eriswell, ordered numerically by grave and small finds number.....	779
Table G.2 – Reduced SEM-EDS data for the glass beads from Eriswell, ordered numerically by grave and small finds number. Red numbers represent assumed values.....	805
Table G.3 – Raw LA-ICP-MS sediment-related element (SRE) data for the glass beads from Eriswell, ordered numerically by grave and small finds number.....	831
Table G.4 – Raw LA-ICP-MS rare earth element (REE) data for the glass beads from Eriswell, ordered numerically by grave and small finds number.....	835
Table G.5 – Raw LA-ICP-MS colourant and colourant-related element data for the glass beads from Eriswell, ordered numerically by grave and small finds number.....	839
Table H.1 – Raw SEM-EDS data for the glass beads from Spong Hill, ordered numerically by grave number.....	844
Table H.2 – Reduced SEM-EDS data for the glass beads from Spong Hill, ordered numerically by grave. Red numbers represent assumed values.....	849
Table I.1 – Raw SEM-EDS data for the glass beads from Bergh Apton, ordered numerically by grave number.....	855
Table I.2 – Reduced SEM-EDS data for the glass beads from Bergh Apton, ordered numerically by grave. Red numbers represent assumed values.....	857
Table J.1 – Raw SEM-EDS data for the glass beads from Morning Thorpe, ordered numerically by grave number.....	860
Table J.2 – Reduced SEM-EDS data for the glass beads from Morning Thorpe, ordered numerically by grave. Red numbers represent assumed values.....	861
Table K.1 – The composition of the different bead types analysed, showing the number of beads analysed, the number of beads excavated and their typical composition. * denotes bead sub-types that have been grouped together.....	863
Table L.1 – EDS pot analyses of the cobalt-rich phases in the cobalt-rich mineral inclusion in translucent blue sample ERL104:G263:1411 from Eriswell. For spectrum locations refer to Figure L.1.....	868
Table L.2 – EDS pot analyses of the cobalt-deficient phases in the cobalt-rich mineral inclusion in translucent blue sample ERL104:G263:1411 from Eriswell. For spectrum locations refer to Figure L.2.....	868

ACKNOWLEDGEMENTS

It is with great pleasure that I am able to thank the following people for their time and support over the past three years. Without their hard work, encouragement and guidance this project would not have been started, let alone completed.

First and foremost, I would like to thank my supervisors: Prof. John Hines, Prof. Ian Freestone and Dr. Panagiota (Yiota) Manti. John sustained and encouraged me throughout the project, especially in the final stages. His guidance, particularly in the archaeological aspects of the project, as well as his thorough proof-reading, is greatly appreciated. I am indebted to Ian, who could not have been a more inspirational supervisor, and without whom I would not have gained the analytical skills and experience necessary to complete the project in the years leading up to it. He also provided me with the Corning glass standards, cobalt wire and contemporary Early Byzantine material from Caesarea, Israel, for analysis. I am particularly grateful for his continued support and advice upon his leaving Cardiff. I am also grateful to Yiota for taking over from Ian as my second supervisor in the summer of 2011, and for her advice and support during the latter stages of the project.

This project would not have been possible without funding from the Ministry of Defence and Defence estates (United States Forces), through Suffolk County Council Archaeological Service (SCCAS) as a research partner. I am also grateful for financial assistance from Cardiff University Postgraduate Quality Committee, the Sir Cyril Fox Fund and Suffolk County Council, which enabled me to travel to Bury St. Edmunds, Norwich and London to collect and sample the beads analysed as part of this project. I also thank the *Association Internationale pour l'Histoire du Verre* (AIHV), Katholieke Univeriteit Leuven, Cardiff University Postgraduate Quality Committee, and the *British Association for the History of Glass* (AHG), for providing me with financial support to attend conferences in Piran (Slovenia), Leuven (Belgium), Brussels (Belgium) and York (UK) respectively, which were beneficial to my work.

There are a number of people in addition to those aforementioned whom I thank for providing me with access to materials and information. Jo Caruth, Senior Project Officer of Suffolk County Council Archaeological Service (SCCAS), provided me with access to the Eriswell bead assemblage and background material relating to the Eriswell cemetery complex and the beads themselves. She also kindly showed me around RAF Lakenheath and the surrounding countryside. Dr. Birte Brugmann meticulously examined and catalogued the Eriswell bead assemblage; without such a comprehensive and thorough typology, selection of a comprehensive range of beads for analysis would have been far more difficult and the full potential of the analytical data would certainly not have been realised. The results of this study are a credit to her hard work. Also thanks to Dr. Tim Pestell, Curator at Norwich Castle Museum, who kindly provided permission to sample a selection of early Anglo-Saxon glass beads from Spong Hill, Bergh Apton and Morning Thorpe in Norfolk for inclusion in the present study.

Numerous people assisted me with the technical aspects of the project. Particular thanks go to Phil Parkes, Cardiff University, for producing the reference standards spectra and maintaining the SEM, and for putting up with the path I wore to his office door whilst undertaking compositional analysis. I also thank Iain MacDonald, Cardiff University, for the time he spent training me to analyse glass by LA-ICP-MS, and for calibrating the equipment and the resulting data. Thanks to all of the undergraduate and masters Conservation students at Cardiff University, past and present, who helped to clean many of the Eriswell beads as part of their studies for photography prior to analysis: Melanie Keable, Marie Jordan, Helen Butler, Rebecca Lumsden, Jenny Matthiason and Ciarán Lavelle. I am grateful to John Morgan, formerly of Cardiff University but now retired, for the technical assistance he provided during digital photography of the beads. I also thank Sue Virgo, Cardiff University, for ordering the materials necessary for sample preparation on my behalf.

Thanks to all of those who provided me with specialist advice and support. Dr. Tim Young, Cardiff University, gave some particularly insightful comments regarding the identification of the metallurgical slag in the opaque red glass. Dr. Sonia O'Connor, University of Bradford, provided me with very useful information regarding wet-plate x-radiography; in particular the acquisition of high-quality

digital x-ray scans. I thank Dr. Andrew Meek, Department of Scientific Research, British Museum, for providing me with access to his scientific report on beads from the Ringlemere Anglo-Saxon cemetery. Thanks also to Dr. Sarah Paynter, English Heritage, for looking for the samples of Anglo-Saxon beads from Mucking and Edix Hill analysed by Cath Mortimer in the 1990's, which unfortunately could not be located, and for providing me with useful articles and references relating to the composition of metallurgical slag.

Finally, thanks to all of those who provided me with moral support, particularly my mother, who waded through this thesis correcting my bad grammar. Also thanks to my father and brother. Further thanks go to my friends, colleagues and housemates in Cardiff over the years, who put up with me at my worst (usually first thing in the morning), and put me up in London, Bath and Cardiff after I moved back to North Devon in the summer of 2012. In particular: Angharad Evans, Johnny Horn, Richard James, the 'Green' clan (Seann, Matt and Jessica), Melanie Keable, Helen Sivey, Jennifer Jones, Iain Bennett, Julia Best, Garth Wood, Jihyun Kwon, Emily Yates, Kate Hudson-McAulay, Morwenna Perrott, Joe Lewis, Alice Forward, Matt Nicholas, James Rodliff, Andrew Kelly, Neil Atherton, David Pearson, Susan Stratton, Lara Hogg, Robin Hawkins and Ellen Keld, in addition to the Conservation students previously mentioned.

It is to all of these people that I dedicate this thesis.

LIST OF ABBREVIATIONS

AD	Anno Domini
BC	Before Christ
b.d.	below detection
BEI	backscattered electron imaging
BSE	backscattered electron
<i>c.</i>	<i>circa</i>
<i>cf.</i>	<i>confer</i> , compare
cm	centimetres
cps	counts per second
DIAM	technique so-called for the removal of samples using diamond-coated files
EDS	energy-dispersive x-ray spectrometry
EPMA	electron probe microanalysis
ERL	Eriswell (as in ERL 104)
ESEM-EDS	environmental scanning electron microscopy with energy-dispersive x-ray spectrometry
G	grave (as in G242)
HIMT	High Iron, Manganese and Titanium
Hz	Hertz
ICP-MS	inductively coupled plasma mass spectrometry
ICPS	inductively coupled plasma spectroscopy
km	kilometres
kV	kilovolts / kilovoltage
LA-ICP-MS	laser ablation inductively coupled plasma mass spectrometry
mJ	millijoules
mm	millimetres
MoD	Ministry of Defence
MUQ	mud of Queensland
n	number (as in $n = 1$)
NIST	National Institute of Standards and Technology
n.a.	not analysed

no.	number
NMAS	Norfolk Museums and Archaeology Service
op.	opaque
PIGE	particle-induced gamma-ray emission
PIXE	particle-induced x-ray emission
ppm	parts per million
r^2	correlation coefficient
RA	relative accuracy
REE	rare earth elements
RSD	relative standard deviation
SCCAS	Suffolk County Council Archaeological Service
SD	standard deviation
SEI	secondary electron image
SEM	scanning electron microscope
SEM-EDS	scanning electron microscopy with energy-dispersive x-ray spectrometry
SF	small finds
SRE	sediment-related elements
SRM	standard reference materials
tr.	translucent
UCC	upper continental crust
μm	micron
USAF	United States Air Force
USF	United States Forces
UV	ultraviolet
vs.	versus
wt %	weight percent
XRF	x-ray fluorescence
%	percent, calculated by weight when used to indicate proportions of chemical compounds in text
*	indicates reduced or base glass composition normalised to 100% (<i>e.g.</i> Na_2O^*). When used in conjunction with bead types (<i>e.g.</i> <i>WhitePoly*</i>), it denotes when sub-types of bead are grouped together (<i>e.g.</i> <i>WhitePoly 1</i> , <i>WhitePoly2</i> , etc.)

For element oxide abbreviations refer to Chapter 2, Table 2.3.1.

For element abbreviations refer to Chapter 2, Table 2.3.3.

CHRONOLOGY

The early Anglo-Saxon period is assumed to encompass the period following the withdrawal of Rome from Britain until the mid-7th century (*i.e. c.* AD 411-650). The mid Anglo-Saxon period is assumed to encompass the mid-7th to mid-9th centuries (*i.e. c.* AD 651-850). The late Anglo-Saxon period is of little relevance to this study, but encompasses the centuries following the mid-9th century (*i.e. c.* AD 851-1100).

Brugmann's bead chronology is as follows (Brugmann 2004: 70):

- Phase A1 *c.* AD 450-530
- Phase A2 *c.* AD 480-580
- Phase A2b *c.* AD 530-580
- Phase B1 *c.* AD 555-600
- Phase B2 *c.* AD 580-650
- Phase C *c.* AD 650-700

All dates should be assumed as AD unless otherwise stated.

CHAPTER ONE

1. Introduction

Our understanding of the materials and technology available for the production of artefacts yielded by the furnished graves of the early Anglo-Saxon period (5th-7th centuries AD) in England is riddled with gaps and ambiguities (Thomas 2011: 407). A lack of workshop evidence and historical sources has meant that it is difficult to corroborate the material culture left behind by these early peoples (Thomas 2011: 407). This is particularly the case with glass.

The excavation of the early Anglo-Saxon cemetery complex at RAF Lakenheath (Eriswell) in Suffolk has produced a broad range of artefacts spanning the 5th-7th centuries AD. This has provided an opportunity to bridge some of the gaps in our knowledge of early medieval glass in England; a comprehensive approach to material and technical analyses was purposefully included in the post-excavation research design for this site, for which this project forms an important part. The diverse range of bead types within the Eriswell assemblage, of which over 1000 are glass, offers the potential to take the study of early Anglo-Saxon glass further than before. Glass beads can provide an important source of information about chronology, economy, society and culture, especially through inter-comparisons between site assemblages (Hirst 2000: 121). However, little is known about the production of glass beads in the early Anglo-Saxon period, as they have mostly only been studied in terms of their stylistic attributes (*e.g.* Henderson 1990; 2011; Mortimer 1996a; 1996b).

There were undoubtedly trade links between Anglo-Saxon England and the wider world, whether direct or indirect; for example, amber was probably imported from the Baltic region, whereas amethyst may well have come from India via the Eastern Mediterranean (Huggett 1988: 66; Welch 1999: 2). However, it remains unclear as to what extent Anglo-Saxon glass beads were imported from the Continent or further afield, or to what extent they were locally produced. It also remains unclear as to

whether there was a break in the production of, or trade in glass following the collapse of the Roman Empire (*e.g.* Jackson 1996; Sanderson *et al.* 1984; Velde 1990), and the degree to which scrap Roman material was recycled where ‘fresh’ glass was not available (Welch 1999: 5). It is not yet known whether there were workshops specialising in the production of certain types of bead, or centres which specialised in the production of particular colours of glass, which may have been traded in their unworked form (Henderson 1999a: 81).

It is not until the mid-Saxon period in the 8th and 9th centuries that we begin to see tangible evidence for glass-working in the archaeological record, particularly in the manufacture of windows at monastic sites such as Monkwearmouth, Jarrow, Barking and Glastonbury (Bayley 2000b: 138-139; 2000c; Heyworth 1992: 169-171; Hinton 2011: 429; Thomas 2011: 412). However, the lack of archaeological evidence for glass production in Britain and Europe prior to this means that much less is known about the organisation of the glass industry during the early medieval period (Bimson and Freestone 2000: 133; Freestone and Hughes 2006: 152; Guido and Welch 2000: 115; Leahy 2011: 457; Thomas 2011: 407). Archaeological and stylistic evidence largely suggests that most craft production during the early Anglo-Saxon period was undertaken at a domestic level within largely self-sufficient rural communities, but that non-utilitarian goods were produced by a limited number of specialist itinerant craftsmen (Thomas 2011: 408-409). Metalworking in the 5th and 6th centuries in particular is widely thought to have been undertaken by itinerant craftsmen. Chemical analysis offers the potential to provide further insights into the production and distribution of early glass, and how this varied with space and time. This can complement traditional art-historical studies.

There are several studies that have focused upon the technology and composition of early Anglo-Saxon glass beads, but these are typically incorporated into site reports with little integration (Guido and Welch 2000: 115; Welch 1999: 2). Such studies have previously focused upon analysis of beads, mostly by non-destructive qualitative or semi-quantitative x-ray fluorescence (XRF), from Buckland (Dover) (Bayley 1987), Finglesham (Wilthew 2006) and Ringlemere (Meek 2010) in Kent, Great Chesterford (Heyworth 1994) and Mucking (Mortimer 1996b; Mortimer and Heyworth 2009) in Essex, Edix Hill (Barrington A) (Mortimer 1996a; Mortimer

1998) in Cambridgeshire, Empingham II (Heyworth 1996b) in Rutland, Portway (Andover) (Bayley 1985) and Alton (Wilthew 1988) in Hampshire, Apple Down (Chichester) (Henderson 1990) in West Sussex, Butler's Field (Lechlade) (Henderson 2011) in Gloucestershire, Beckford (Heyworth 1996a) in Worcestershire, and Sewerby (Biek *et al.* 1985) in Yorkshire.

The vast majority of these studies are very selective and have as yet failed to place the technology and composition of Anglo-Saxon glass into the wider context of contemporary glass manufacture within or outside of Britain. These studies have generally failed to establish any meaningful compositional groupings or to attribute beads to possible production zones due to the typical use of non-destructive surface analysis techniques (*e.g.* x-ray fluorescence, XRF), which usually only produce quantitative or semi-quantitative data, together with a lack of material available for analysis; the scientific examination of complete assemblages has never been attempted. Furthermore, these studies have not achieved their full potential because they are usually based upon poorly understood typologies, resulting in inadequate sampling strategies (Caruth and Anderson 2005: 41). The majority have only really succeeded in identifying the nature of the raw materials, colourants and opacifiers used.

There are larger quantities of data available for Merovingian (5th-7th century) glass beads from contemporary Continental cemeteries. This includes material from Endingen, Eichstetten, Groß-Gerau, Greisheim, Koblenz (Saffig and Miesenheim) and Krefeld-Gellep in Germany, and Schleithem in Switzerland; mostly analysed by Martin Heck, Peter Hoffmann and co-workers (*e.g.* Heck 2000; Heck and Hoffmann 2000; 2002; Hoffmann 1994; Hoffmann *et al.* 1999; 2000). Heck (2000) semi-quantitatively analysed 1403 opaque Merovingian glass beads from these sites using non-destructive XRF as part of his thesis; 29 of these beads were also analysed quantitatively using electron-probe microanalysis (EPMA). More recently, quantitative analysis of Merovingian glass beads has been undertaken by PIXE (Particle-Induced X-ray Emission) and PIGE (Particle-Induced Gamma-ray Emission); 216 beads from Bossut-Gottechain in Belgium have been analysed by Mathis *et al.* (2010) using this technique, although the results have not yet been fully published.

In the light of newly published typologies for early Anglo-Saxon glass beads in England, representative scientific sampling strategies can now be established and chemical composition can be linked to closely dated bead types of known manufacturing series. Improvements in the capabilities of analytical techniques and our understanding of early glass in recent decades also means that it is now possible to accurately and reliably characterise the chemical make-up of these beads. In turn, it sometimes proves possible to relate individual glass types and raw materials to specific production zones, particularly through the analysis of elements present at trace levels. Eriswell, Suffolk, presents an excellent candidate for such a study because of the wide range of bead types represented, for which there is particularly detailed information on chronology and typology.

The present study reports upon the analysis of a range of the glass beads from Eriswell. Major element data for 537 different samples of glass from a total of 380 individual beads from the site were obtained by energy-dispersive x-ray spectrometry in the scanning electron microscope (SEM-EDS). Trace element data were obtained for 75 of these samples, taken from a total of 65 individual beads, using laser ablation inductively coupled plasma mass spectrometry (LA-ICP-MS). In addition, major element data are reported for 103 different samples of glass from a maximum of 85 individual beads from Spong Hill, Bergh Apton and Morning Thorpe in Norfolk (the fragmentary nature of many of these beads means that exact numbers are uncertain here).

A number of analytical techniques were tested in order to justify the methods of analysis chosen (Chapter 2). The beads were then interpreted in terms of their technology (Chapter 3) and chemical composition; the different glass types used were established and compared (Chapter 4). Detailed comparisons were made between the compositions of the beads and their purported typological and chronological attributions, as well as the contexts from which they were recovered. The compositional data were compared to published data for glass from the preceding Roman period, as well as contemporary glass from elsewhere in Britain, Europe and the Eastern Mediterranean, in order to place the beads into the wider context of glass production and use during the Roman and early medieval periods. The colourants and opacifiers used were established and compared in terms of their

visual attributes and chemical composition (Chapter 5). Later Anglo-Saxon glass is also briefly touched upon (Chapter 6). Finally, the results were synthesised in an attempt to reconstruct how the beadmaking industry may have been organised in England during the early Anglo-Saxon period (Chapter 7).

1.1. Historical Context

The rapid decline of Roman Britain was the result of a combination of repeated raids and civil wars, political turmoil and increased taxation which, when combined, led to economic collapse and cultural breakdown (Fleming 2011: 24; Walton Rogers 2007: 5; Welch 1992: 101). Roman rule in Britain is thought to have come to an end in or around AD 410 (Walton Rogers 2007: 5; Welch 1992: 101). In the course of the 5th century, new groups of Germanic peoples made their way across the Channel and settled in eastern and southern England (Fleming 2011: 30; Lucy 2000: 1-4; Scull 1995: 71). This brought about a number of radical changes in the ways in which people lived and buried their dead. Archaeological and historical interpretations of this period rely heavily upon later historical accounts: primarily Gildas' 6th century *De Excidio Britonum* which dramatically recounts the decline of Roman Britain, and Bede's early 8th century *Historia Ecclesiastica* which describes the origins of these immigrants and their descendants (Brugmann 2011: 31; Scull 1995: 71).

Bede's account of the *adventus Saxonum* (the coming of the Saxons) famously describes three main cultural groups of people: the Angles were said to come from 'Angulus' (Angeln, southern Denmark), the Saxons descended from Old Saxony and the Jutes descended from Jutland (mainland Denmark) (Fleming 2011: 61; Lucy 2000: 156-157; Owen-Crocker 2004: 13; Walton Rogers 2007: 7). The Angles primarily populated the northern reaches of England and East Anglia, the Saxons the east, south and west, and the Jutes Kent, the Isle of Wight and the adjacent southern coast (Fleming 2011: 61; Hills 2011: 10; Owen-Crocker 2004: 13; Walton Rogers 2007: 7). This has come to form the foundations for many Anglo-Saxon studies.

However, the reliability of Bede's account is a subject of some debate. New identities were formed and many smaller territories were amalgamated into the 8th century kingdoms described by Bede (Hills 2011: 10). It is likely that his description of an 'invasion' was biased by the circumstances of the period in which he was writing (Fleming 2011: 92; Lucy 2000: 175; Scull 1995: 71); his account is politically manipulated in such a way as to substantiate royal lineages and reinforce

the ancestry of the contemporary ruling elite (Fleming 2011: 92; Scull 1995: 71; Welch 1992: 9).

There is in fact no reliable documentary evidence relating to the 5th and 6th century societies from which these kingdoms emerged (Scull 2011: 849); a period commonly termed the 'Migration Period'. As such, the nature of life in Britain following the withdrawal of Rome, including the scale of the migration, is hotly debated. Theories range from models of continuity from the Late Roman into the Anglo-Saxon period involving the acculturation of the indigenous Romano-British population and minimal population movement, to the large-scale immigration and settlement of warrior bands who displaced or eradicated the Romano-British population altogether.

Nevertheless, the settlement of particular ethnic groups of people as described by Bede is reflected by regional variations in the material culture they left behind; particularly female dress (Fleming 2011: 48; Hills 2011: 10; Owen-Crocker 2004: 13; Welch 1992: 11). However, it is clear that there were other groups of people involved which are not mentioned by Bede, such as the Franks and Frisians (Brugmann 2011: 33; Fleming 2011: 61; Owen-Crocker 2004: 13-14), and that his account masks a complex hierarchy of regional and social identities (Dickinson 2011: 230-231; Hills 2011: 10; Scull 1995: 73). The cessation of Romano-British material expression is generally considered to have been a result of social, political and economic collapse, as opposed to the invasion and settlement of these new Germanic peoples (Hills 2011: 9; Scull 1995: 72). The landscape, material culture and burial practices of 5th century Britain paint a picture of a mixture of continuity, peaceful co-existence, hostility and amalgamation; the culture of the native Romano-British people was probably incorporated into that of the Anglo-Saxons, as opposed to being wiped out completely (Brugmann 1997: 110-112; Fleming 2011: 50-52; Lucy 2000: 170-171; Owen-Crocker 2004: 21; Walton Rogers 2007: 232; West 1998: 261).

The Germanic 'invasion' is likely to have been a protracted process of small-scale migrations which took place gradually over a period of many decades, rather than a sudden event as implied by Bede (Brugmann 2011: 33; Fleming 2011: 40; Owen-Crocker 2004: 14; Scull 1995: 73; Walton Rogers 2007: 7; Welch 1999: 3). There is

little archaeological evidence to suggest that these immigrants consisted of groups of Germanic warriors; they are more likely to have been small farming families who settled as regional groups or tribes until, by the late 5th century, they had colonised most of southern and eastern England (Fleming 2011: 40; Owen-Crocker 2004: 21; Walton Rogers 2007: 7).

Whilst the general sequence of events leading to the formation of Anglo-Saxon England is known, the chronology is still inexact; a reliance upon historical sources means that past chronologies have assumed that Late Roman material cannot post-date AD 410 and insular Anglo-Saxon products cannot pre-date the *adventus Saxonum* in approximately AD 450. However, recent chronological studies have pushed this latter date back somewhat (Brugmann 2011: 40).

Burials are the primary source of archaeological evidence available for Anglo-Saxon England (Hills 2011: 4-7; Scull 1995: 72; 2011: 851; Williams 2011: 250). They frequently contain a range of grave goods typical of pagan burial; the dead were often buried fully clothed, accompanied by artefacts which may have included costume accessories, weapons, vessels or offerings (Fleming 2011: 45-46; Lucy 2000: 1). This is in stark contrast to the east-west orientated unfurnished Christian burials typical of the Late Roman period (Fleming 2011: 45-46; Lucy 2000: 1). However, patterns in material expression and dress are far from simple to interpret (Hills 2011: 6-7), and there is still some debate as to when and why mortuary rituals changed in relation to migration and the conversion to Christianity (Dickinson 2011: 229). This is complicated by the regional and local variability between cemeteries, as well as their internal diversity (Williams 2011: 240).

The early Anglo-Saxons of the Migration Period retained a large part of their Germanic identity which, although influenced by later social, political and economic changes, largely paralleled that of Continental Germanic tribes (Owen-Crocker 2004: 15). The grave goods with which they were buried reflect new ways of asserting gender identity, age, social status and wealth (Fleming 2011: 68; Hills 2011: 4; Scull 1995: 74; Owen-Crocker 2004: 23; Scull 2011: 851; Williams 2011: 250). In the course of the 6th century, regional fashions developed which appear to have reflected not only status, but also affiliations with particular groups of people (*e.g.* Anglian,

Saxon, Jutish) (Dickinson 2011: 230; Fleming 2011: 77; Owen-Crocker 2004: 24; 2011: 104-105; Williams 2011: 250). However, there are many Germanic grave goods which do not have Continental parallels, exhibiting distinctive insular characteristics (Dickinson 2011: 230; Fleming 2011: 48-50; Scull 1995: 76). Nevertheless, this material culture clearly expresses Germanic *influences*, suggesting that regional identity was expressed within a broader network of affiliation with the Continent (Scull 1995: 79).

The Anglo-Saxon community was well-established in England by the late 6th century, by which time a new social elite and kingdoms were rapidly emerging (Owen-Crocker 2004: 23; Welch 2011: 269); for example, Norfolk, Suffolk and areas of Cambridge were eventually consolidated into one kingdom (West 1998: 317). Through this territorial organisation, production, trade and exchange could presumably be more easily controlled (Scull 2011: 853). These new rulers claimed Continental Germanic ancestry, as evidenced by historical sources (Scull 2011: 849). They were integrated into extensive aristocratic networks of trade and gift exchange, providing them with access to exotic artefacts produced as far away as the Eastern Mediterranean (Fleming 2011: 117-118; Welch 1992: 117). This is evidenced by the prestigious grave goods from sites such as Sutton Hoo, Suffolk (Hinton 2005: 58-60; Lucy 2000: 5). These new contacts and the ability to control exchange may have helped to secure or accelerate the formation of a social or political hierarchy (Scull 2011: 853).

Christianity was also introduced, beginning with St. Augustine's mission to Kent in AD 597, and gradually spread throughout Anglo-Saxon England in the course of the 7th century (Fleming 2011: 132; Lucy 2000: 4; Owen-Crocker 2004: 25; 2011: 106; Welch 2011: 267); this period is commonly but misleadingly termed the 'Final Phase'. This coincided with an overall decline in the use of grave goods and the emergence of new burial practices, including barrow burial (Dickinson 2011: 231; Hinton 2005: 57-58; Welch 2011: 269). There appears to have been a dramatic 'transition' in costume, with regional variations in Anglo-Saxon dress giving way to a more uniform style (Geake 2002: 146; Hines 2003: 92; Hinton 2005: 57-58; Lucy 2000: 25; Owen-Crocker 2011: 100; Welch 2011: 266-267). These new styles appear to have been influenced by Continental Frankish tastes (Welch 2011: 267).

There appears to have been an increasing social divide, consistent with the evolution of territorial lordship and the emergence of broader regional identities and settlement hierarchy (Fleming 2011: 75; Lucy 2000: 183; Scull 1995: 78; 2011: 849); high-status 'royal' graves (*e.g.* Sutton Hoo) presumably reflect the emergence of aristocracies and their attempts to legitimise their status (Hinton 2005: 57; Lucy 2000: 4-5; Scull 2011: 849; Welch 2011: 269). More prestigious grave goods, including jewellery made of precious stones, cowrie shell and gold began to appear (Fleming 2011: 69-70; Lucy 2000: 25; Owen-Crocker 2004: 143; 2011: 100; Walton Rogers 2007: 128; Welch 1992: 117; 1999: 2). Fewer women appear to have worn jewellery and those that did typically appear to have worn valuable sets showing considerably less regional variation (Dickinson 2011: 231; Fleming 2011: 146; Hinton 2005: 57-58; Lucy 2000: 85; Owen-Crocker 2004: 129; 2011: 100; Walton Rogers 2007: 241).

The paucity of grave goods in the 7th century is traditionally attributed to the spread of Christianity. However, factors other than religion, such as changing social attitudes towards material wealth, or the economic or political climate, may also have influenced the deposition of artefacts in graves (Hinton 2005: 74; Lucy 2000: 183-184; Owen-Crocker 2004: 129); for example, it is possible that the introduction of a formal taxation system may have resulted in the decline in grave goods (Lucy 2000: 184). It is clear that furnished burial in Anglo-Saxon England continued well beyond St. Augustine's mission to Kent in AD 597, and probably well after the Council of Whitby in AD 664 (Hines *et al.*, in press). It is thought that Kent may have controlled the supply of goods (or even technological expertise) between Anglo-Saxon England and the Merovingian Continent, or access to materials, establishing political dominance in the south and east of England (Huggett 1988: 66; Scull 2011: 853; Thomas 2011: 410-411; Welch 1992: 117; 1999: 10). Certain object types, including glass vessels, amethyst beads and wheel-thrown pottery, are predominantly concentrated in Kent, whereas outside of Kent such goods are more uncommon, except within wealthier 'elite' burials (Huggett 1988: 91; Welch 1992: 117).

Whatever the reason(s), furnished burial gradually declined, so that by the late 7th century nearly all burials in England were unfurnished (Evison 2000: 78; Lucy 2000:

5; Owen-Crocker 2004: 25-26; West 1998: 319); Hines *et al.* (in press) suggest that it probably ended in the 660's or 670's AD. Earlier Anglo-Saxon cemeteries and settlements were largely abandoned (Dickinson 2011: 231; West 1998: 271). This broadly coincided with the emergence of *wics* or *emporia* (trading centres) in the late 7th and 8th centuries (Fleming 2011: 189-190; Scull 2011: 849; Walton Rogers 2007: 7; Welch 1992: 118; Welch 1999: 10), which are interpreted as special-purpose elite foundations in which manufacture, trade, surplus and revenue could be easily controlled (Welch 1992: 119; Scull 2011: 859; Thomas 2011: 413).

1.2. Archaeological Context

East Anglia is particularly rich in early Anglo-Saxon archaeology, and consists of the modern-day counties of Norfolk and Suffolk, shown in Figure 1.2.1. The principal sites discussed in the present study are all in East Anglia, and are shown in Figure 1.2.2.



Figure 1.2.1 – Map of Britain showing the location of East Anglia, currently the modern-day counties of Norfolk and Suffolk (map adapted from that of 1995 county boundaries © Ordnance Survey).

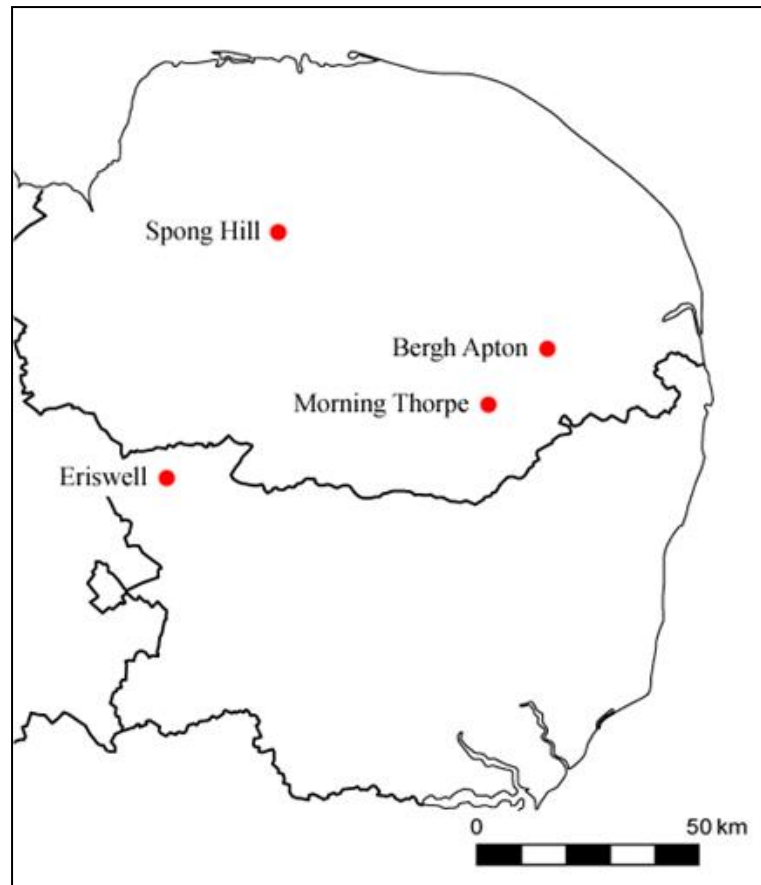


Figure 1.2.2 – Map of East Anglia showing the location of the principal archaeological sites discussed in this thesis.

1.2.1. RAF Lakenheath (Eriswell), Suffolk

The Anglo-Saxon cemetery complex at RAF Lakenheath was excavated between 1997 and 2002 by Suffolk County Council Archaeological Service (SCCAS) ahead of redevelopment of the site. The excavations were funded by the Ministry of Defence (MoD), Defence Estates (USF). The site has been occupied by the USAF since 1948 and lies on the western fringes of Suffolk within the Breckland area on the edge of the fenland to the west. The landscape is open, consisting primarily of large fields interspersed with patches of woodland, heath and marsh. There is also a natural rising spring at Caudle Head Mere on the northern boundary of the parish of Eriswell (Caruth and Anderson 2005: 1-2).

The site is situated within a rich archaeological landscape, consisting of a variety of sites, dating back as far as the Mesolithic period, which have been the subject of investigation for many years. A number of nearby Roman settlement sites, including one around Caudle Head Mere, appear to have been occupied up until the 5th century (Caruth and Anderson 2005: 5). There is extensive settlement evidence within the site stretching from the Late Iron Age to mid-Saxon periods; the land beyond this appears to have been farmed as far back as the prehistoric period (Caruth and Anderson 2005: 17).

The known Anglo-Saxon burial sites in the area are situated along the main river valleys and their tributaries, which are roughly reflected by the distribution of contemporary settlement sites (Caruth and Anderson 2005: 5). The earliest Anglo-Saxon sites in Suffolk are almost always located on lighter soils to the east of the county and the gravel terraces of the river valleys to the west (West 1998: 266). Past settlement has been concentrated in the northwest of Suffolk, along fen edge and the river valleys of the Lark, Black Bourn and the Kennett (West 1998: 261). At Eriswell, the first excavations of early Anglo-Saxon burials were undertaken in 1959 (Caruth and Anderson 2005: 5).

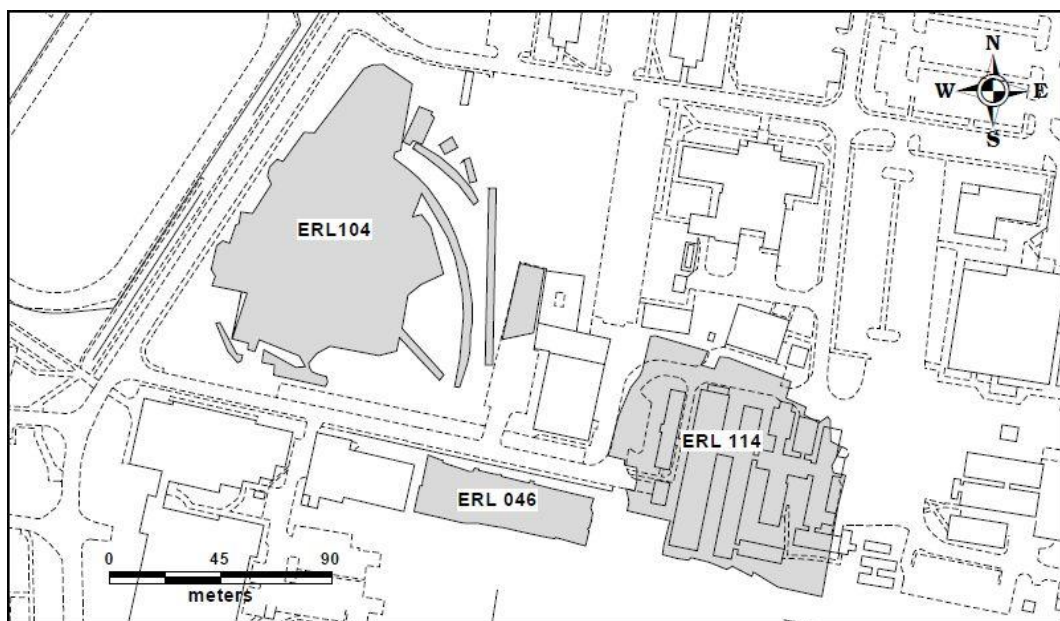


Figure 1.2.3 – Location of the excavation areas showing the three cemeteries at Eriswell: ERL 046, ERL 104 and ERL 114 (Caruth and Anderson 2005: 1).

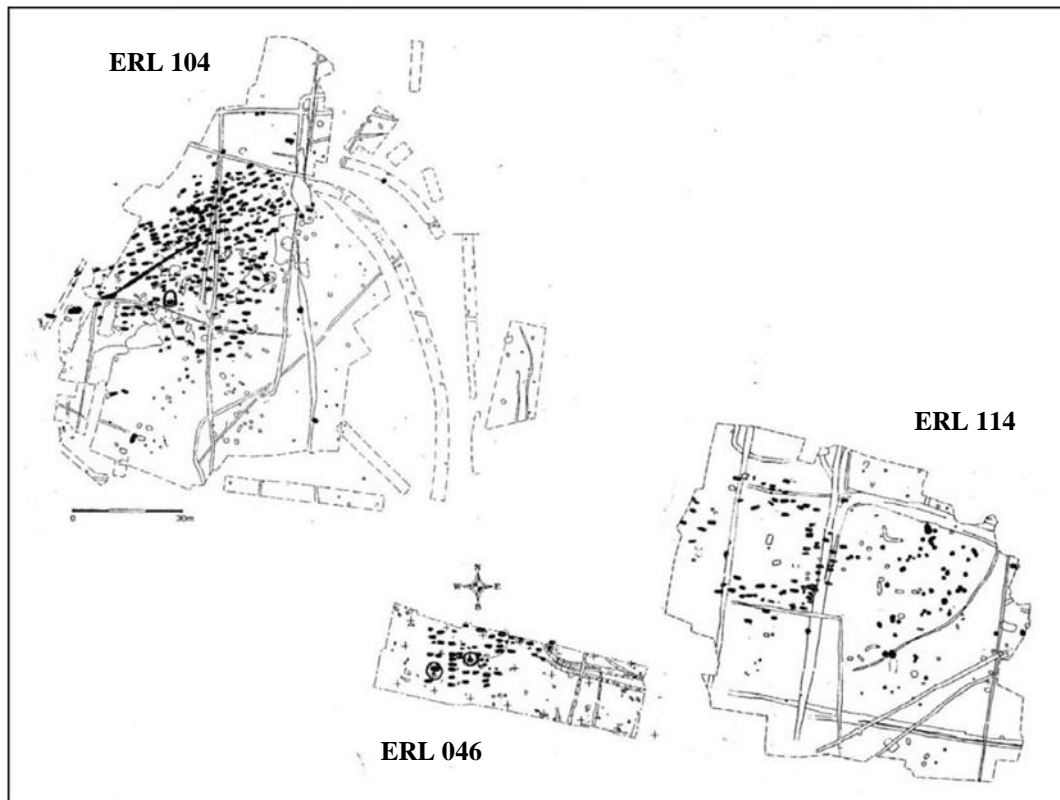


Figure 1.2.4 – Phase plan for the three cemeteries at Eriswell. Early Anglo-Saxon features (including graves) are highlighted in black (Caruth and Anderson 2005: 30).

The Eriswell site is exceptional in that the number of burials found places it amongst the largest inhumation cemeteries of the early Anglo-Saxon period in England. It comprises of a group of three cemeteries (ERL 046, ERL 104 and ERL 114), each individual in their own right, but all neighbouring one another (Figures 1.2.3 and 1.2.4) (Caruth and Anderson 2005: 17). A total of 424 inhumations and 17 cremations have been so far identified and it is likely that more remain yet to be discovered (Caruth and Anderson 2005: 11). Several isolated earlier burials have also been discovered scattered throughout the complex, dating to the Bronze Age and Roman periods (Caruth and Anderson 2005: 5; 22). There is also a small group of burials nearly dating to the late 7th or 8th centuries. As well as the cemeteries, a number of 6th century ‘sunken featured buildings’ were discovered nearby, including ten which overly the Roman settlement around Caudle Head (Caruth and Anderson 2005: 5).

The Anglo-Saxon cemeteries appear to have been in use from the late 5th through to the early or mid-7th centuries, meaning that they span a comprehensive period of Anglo-Saxon history (Caruth and Anderson 2005: 27). The vast majority of burials were supine and extended, or slightly flexed, orientated east-west (Caruth and Anderson 2005: 8). Many of these contained grave goods including swords, spears, knives, glass and amber beads, brooches, vessels and girdle hangers.

The largest cemetery, ERL 104, was previously unknown and was discovered in 1997 ahead of the construction of a dormitory complex over an existing baseball field (Caruth and Anderson 2005: 7). A total of 267 burials were discovered containing roughly equal numbers of men, women and children, although bone preservation varied as a result of the patchy combination of sandy and chalky soil (Caruth and Anderson 2005: 7-8). A small number of cremations, totalling 17, were also discovered (Caruth and Anderson 2005: 9). Whilst the northern, southern and eastern boundaries appear to have been excavated, there is evidence to suggest that there may be more burials to the west (Caruth and Anderson 2005: 9). The cemetery appears to have been situated in a natural sandy hollow surrounded by a chalk ridge on three sides; the majority of the burials were cut into the grey sandy soil in the centre of this, but some were also cut into the chalk (Caruth and Anderson 2005: 9). The horse and warrior burial from this cemetery is one of the most notable discoveries, consisting of a man buried with his horse (complete with bridle with gilded bronze fittings), sword, spear and shield, among other artefacts (Caruth 2000: 2).

Cemetery ERL 046 was excavated in 1999 ahead of building work, in an area where several burials had been previously discovered in the 1980's (Caruth and Anderson 2005: 9). A total of 59 graves were discovered, primarily to the west of the site (Caruth and Anderson 2005: 9). It is unclear as to whether the boundaries of this cemetery have been reached (except to the west), or as to whether it represents an extension of cemetery ERL 114; this seems unlikely (Caruth and Anderson 2005: 9). The majority of the graves were cut into a sandy soil, but several were also cut into chalk (Caruth and Anderson 2005: 9). In contrast to cemetery ERL 104 the majority of the burials are aligned in rows and the wealthier burials appear to have been deliberately grouped together (Caruth and Anderson 2005: 10).

Cemetery ERL 114 was excavated in 2001 ahead of the construction of a car park (Caruth and Anderson 2005: 10). This cemetery covers the burials excavated in the 1950's and is likely to represent an extension of these (cemetery ERL 008) (Caruth and Anderson 2005: 10). A total of 33 burials were excavated in the 1950's, and a further 65 in 2001 (Caruth and Anderson 2005: 10-11). The burials are likely to have been centred around two Bronze Age barrows, which may account for the high density of burials in this area of the site; a third probable Bronze Age burial was found to the north of the cemetery, as well as four pits containing Bronze Age pottery (Caruth and Anderson 2005: 11). The deliberate situation of a cemetery complex around a prehistoric barrow is a tradition also seen in northern Germany and Scandinavia (Brugmann 1997: 111).

The post-excavation analysis of the artefacts from the site, which includes the metalwork, potter and bone, is ongoing. It is due to be completed in 2015, with a report ready for publication.

1.2.1.1. The Beads

A total of 2576 beads were recovered from 102 graves at Eriswell (*e.g.* Figures 1.2.5 and 1.2.6), together with 77 pendants or pendant fragments. The majority of the beads are made of amber, but 1059 of the beads from Eriswell are glass. A small quantity of beads were made from other materials, including amethyst, chalk, jet, metal, cowrie shell, bone and rock crystal, but these bead types constitute less than 1% of the entire bead assemblage. The number of beads found in the individual inhumation graves varies from one through to 249 in Grave 242.



Figure 1.2.5 – Photograph of beads *in situ* in Grave 107, cemetery ERL 104, at Eriswell (© SCCAS).

The Eriswell beads were examined and catalogued first-hand by Birte Brugmann between 2001 and 2004 according to the typology for early Anglo-Saxon beads set out in Brugmann (2004) and Penn and Brugmann (2007). Those covered by these published typologies have been attributed to one of Brugmann's chronological phases: A, B, or C and the sub-phases therein (see this chapter, section 1.5). The glass, amethyst and cowrie shell beads excavated from ERL 104 were all examined as part of Brugmann's study of 5th-7th century Anglo-Saxon beads in England (Brugmann 2004).

Of the 1059 beads, 704 were attributed to Brugmann's type definitions; the remaining beads were attributed new type definitions created primarily on their colour and colour combinations by Birte Brugmann, and are therefore not represented in her published typologies. The type definitions are discussed in detail in Chapter 4, section 4.10, but the reader is invited to consult Brugmann (2004) and Penn and Brugmann (2007) for detailed descriptions of individual bead types. A full catalogue of the glass beads from Eriswell is presented in Appendix A, their

distribution at Eriswell (according to grave number) in Appendix B, and images of the glass beads sampled as part of the present study in Appendix C.



Figure 1.2.6 – Photograph of beads *in situ* in Grave 266, cemetery ERL 104, at Eriswell (© SCCAS).

1.2.2. Spong Hill, Bergh Apton and Morning Thorpe, Norfolk

An important part of this study is to compare the beads from Eriswell with those from other contemporary sites. For this purpose, Spong Hill in Norfolk was chosen, as it is only approximately 30 km northwest of Eriswell, as the crow flies. Furthermore, many of the bead types represented at Eriswell are also represented at Spong Hill, which offers better potential for comparison than bead assemblages from other sites. In addition, it was also possible to obtain a handful of samples from

broken beads from the nearby sites of Bergh Apton (approximately 50 km east-northeast of Eriswell) and Morning Thorpe (approximately 40 km east-northeast of Eriswell), also in Norfolk. Next to Eriswell, these three sites together have produced the largest body of material from Anglo-Saxon inhumation cemeteries in East Anglia (Penn and Brugmann 2007: 4). They are amongst the only substantial East Anglian early Anglo-Saxon inhumation cemeteries to have been well-excavated and published to date (Penn and Brugmann 2007: 11).

It should be noted that these cemeteries are biased towards southeast Norfolk, and may therefore not be representative of Norfolk as a whole (Penn and Brugmann 2007: 5). Furthermore, Spong Hill may have operated on a different infrastructure on a regional scale to Morning Thorpe and Bergh Apton (Penn and Brugmann 2007: 7). All three of these sites are situated on the slopes of river valleys, in areas of former Roman occupation (Penn and Brugmann 2007: 11). The cemeteries all appear to have had Bronze Age barrows at their focus (similar to cemetery ERL 114 at Eriswell), and the majority of inhumation graves are datable to the 6th century; the material culture here is similar to, but not exactly the same as that observed in contemporary cemeteries on the Continent and in Scandinavia (Penn and Brugmann 2007: 11). However, only Spong Hill has been fully excavated.

Spong Hill and Morning Thorpe were probably in use from approximately the mid-5th century onwards, whereas Bergh Apton was probably in use from approximately the late 5th century onwards (Penn and Brugmann 2007: 4). Spong Hill is particularly unusual in that it was such a huge cremation cemetery in the 5th century. Burial had ceased at Spong Hill by the mid-6th century and at Bergh Apton probably before the late 6th century. However, Morning Thorpe may have been in use until the late 6th century (Penn and Brugmann 2007: 4).

Spong Hill has been known as an archaeological site since at least the early 18th century, but systematic excavation did not begin until 1968, ceasing in 1981 (Penn and Brugmann 2004: 8). It lies on the southern part of a small ridge on the side of a valley through which the River Blackwater flows (Penn and Brugmann 2007: 8). The majority of the cemetery complex consists of approximately 2500 cremation burials, but a small cemetery containing 55 inhumation burials was discovered adjacent to

this (Penn and Brugmann 2007: 8). The graves are situated within the enclosure of a former Roman farmstead, with a small number of Anglo-Saxon buildings lying adjacent to it (Penn and Brugmann 2007: 8). Excavation of the inhumation graves appears to have been largely complete, but it is just possible that a small number of graves remain unexcavated.

The inhumation cemetery at Bergh Apton was discovered in 1973 as a result of gravel extraction (Penn and Brugmann 2007: 9). The site lies on top of a small hill to the north of the Well Beck river in Norfolk, 40 km southeast of Spong Hill (Penn and Brugmann 2007: 9). Rescue excavation was undertaken in 1973, during which 65 graves were excavated; this does not reflect the total number of burials present, some of which are likely to have been destroyed by quarrying (Penn and Brugmann 2007: 9). There is abundant evidence for prehistoric activity on the site and there are several other early cemeteries nearby, many of which are contemporary with Bergh Apton (Penn and Brugmann 2007: 9).

Morning Thorpe was discovered in 1974, again as a result of gravel extraction (Penn and Brugmann 2007: 9). The site is situated on a shallow slope adjacent to a branch of the River Tas, 10 km southeast of Bergh Apton and 35 km southeast of Spong Hill (Penn and Brugmann 2007: 9). Rescue excavation was undertaken in 1975, during which 320 inhumation burials and 9 cremations were discovered (Penn and Brugmann 2007: 9). This is unlikely to reflect the full extent of the burials present, as part of the northern area of the cemetery was destroyed by quarrying and the eastern extent of the cemetery was not established (Penn and Brugmann 2007: 9). There is also evidence for prehistoric and Roman activity at the site, as well as in neighbouring areas (Penn and Brugmann 2007: 10).

1.2.2.1. The Beads

At Spong Hill, 702 beads were recovered from the inhumation graves, of which 459 are glass. At Bergh Apton, 795 beads were recovered from the inhumation graves, of which 276 are glass. At Morning Thorpe, 2198 beads were recovered from the

inhumation graves, of which 1329 are glass (all bead totals from Brugmann 2004: Table 11).¹ Beads from cremations are not sampled as part of the present study as the majority have undergone significant alterations as a result of the high temperatures to which they were exposed in the funerary pyre, which hampers their identification.

As the beads from these cemeteries were bagged as groups according to grave, as opposed to individually by small finds (SF) number as is the case with the Eriswell assemblage, identification of the less diagnostic bead types (*e.g.* some monochrome beads) was not always possible. Identification of the beads analysed was undertaken by comparisons with published descriptions of the grave goods in the respective site reports for each site and by comparison with the online collections database for the Norfolk Museums and Archaeology Service (NMAS 2010). Beads which were too fragmentary to be identified are described as ‘fragments’. Beads which had lost their context, or were not covered by the typologies set out in Brugmann (2004) or Penn and Brugmann (2007), were described according to their descriptions as set out for each site in the online collections database for the Norfolk Museums and Archaeology Service (NMAS 2010).

The typological attribution of the beads analysed was undertaken by comparison with the chronological framework for Brugmann’s study on beads from Anglo-Saxon graves (Brugmann 2004: Table 11), for which beads from all three sites made up part of this national sample. The beads from these sites were particularly relevant to the chronological framework because they produced beads of Brugmann’s *Norfolk* types; so-called because of their main distribution (Penn and Brugmann 2007: 26). Chronological attributions for each of the bead types analysed are not bead-specific; they are instead based on the broad chronological attributions for the individual graves from which the beads were recovered, as set out in Brugmann (2004: Table 11). However, the beads from these sites have not been catalogued to the same extent as the Eriswell assemblage, so typological and chronological attributions are not available for all of the beads analysed as part of the present study.

¹ Only available online, from the Archaeology Data Service (ADS) website: http://archaeologydataservice.ac.uk/archives/view/brugmann_var_2003/downloads.cfm<bead_book_table_11.xls>

1.3. Glass Chemistry

Before we can begin to understand and interpret the composition of early glass, it is important to understand the basic physical and chemical properties of glass as a material. There is an abundance of information outlining the general structure of glass in published literature and textbooks covering the subject (*e.g.* see Davison 2003; Frank 1982; Freestone 2001, and references therein), so a detailed discussion is therefore not within the scope of the present study.

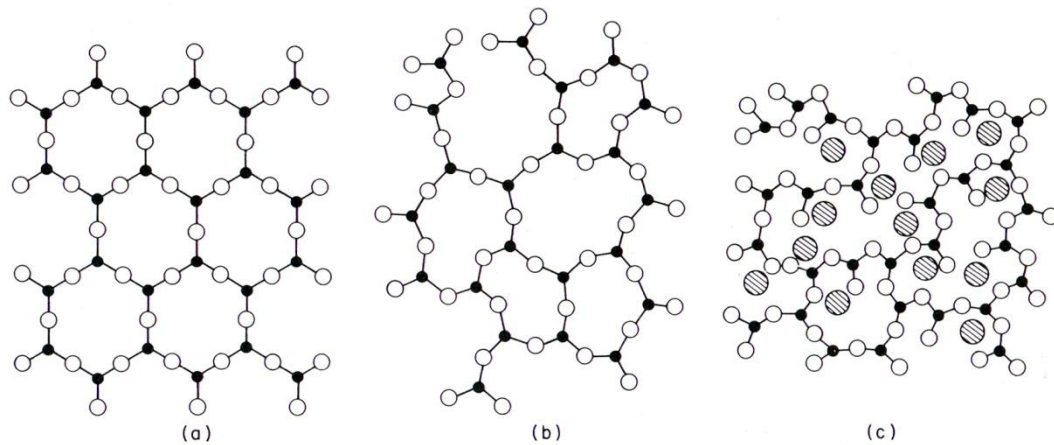


Figure 1.3.1 – Structure of a hypothetical two-dimensional crystalline compound, A_2O_3 ; (a) in crystalline form, (b) in vitreous form, (c) as a vitreous glass modified by the addition of network modifying ions (after Frank 1982: 9). Black circles represent atoms of ‘A’, white circles atoms of ‘O’ and shaded circles atoms of singly charged metallic ion ‘M’.

Glass is an amorphous substance which is typically made of silica (silicon dioxide, SiO_2) fused at high temperatures. All early glass is based on silica, which acts as the *network former* and is widely found in nature as quartz; this occurs as pebbles and as a major component in many sands (Freestone 2008: 83). Pure silica consists of a network of silicon atoms cross-linked by bridges of oxygen atoms (Davison 2003: 4; Frank 1982: 7). In its crystalline form, these atoms are regularly ordered with uniform bond lengths and angles (Figure 1.3.1, image a). However, in its vitreous (glassy) form, these atoms are irregularly ordered with variable bond lengths and angles (Figure 1.3.1, image b). This closely resembles the atomic structure of molten

silica (Davison 2003: 4; Frank 1982: 8-9), and for this reason glass is often referred to as a *supercooled liquid*.

The high temperatures required to melt pure quartz were not obtainable in preindustrial furnaces, so early glassmakers added fluxes to lower its melting point (Fiori and Vandini 2004: 151-152; Freestone 2008: 83; Henderson 1985: 271-272; Vallotto and Verità 2000: 63). These are known as *network modifiers*; they break some of the stronger oxygen bridges between silicon atoms, disrupting the continuity of the silica network (Figure 1.3.1, image c) and thus lowering its melting temperature (Davison 2003: 5; Frank 1982: 10). The flux used to produce glass throughout the majority of the 1st millennium AD in Europe and the Eastern Mediterranean was rich in soda (sodium oxide, Na₂O). However, fluxes rich in potash (potassium oxide, K₂O; typically from the 9th century onwards in northwestern Europe) and lead (lead oxide, PbO; typically from the 10th century onwards in northwestern Europe) were also used in some material or craftworking traditions. As well as the alkali oxides of sodium and/or potassium, the alkaline earth oxides lime (calcium oxide, CaO) and magnesia (magnesium oxide, MgO) can also act as network modifiers (Davison 2003: 5; Frank 1982: 10). However, these components are more typically known as *stabilisers*, as they render the glass more resistant to attack by water (Frank 1982: 10).

The different ingredients added to produce a glass make up what is known as the glass *batch*. Minor amounts of other components, including iron and alumina, were usually incorporated into the glass as impurities with the batch ingredients (Freestone 2008: 83). Additional ingredients, mostly consisting of metallic oxides, may have also been added to alter the properties of the batch (colour, opacity, etc.). A range of colours could be achieved by adding the right proportions of the right ingredients, together with appropriate control of the furnace atmosphere (Davison 2003: 6). The chemical composition of a glass is a reflection of the raw materials used in its production. This varies depending on the geographical region and the period in which the materials were sourced, which may consequently reflect variations and changes in the availability of raw materials or manufacturing technology through time and space.

1.4. Early Glass

The majority of early glass is of the *soda-lime-silica* compositional type. Two distinct sub-groups of soda-lime-silica glass have been identified by past studies: one of which contains magnesia and potash each at levels generally below 1.5%, the other conversely containing levels of these components each generally in excess of 1.5% (Brill 1970: 111; Freestone 2005: OO8.1.2; 2006: 202-203; Freestone *et al.* 2000: 69-70; 2008: 29; Jackson 1996: 290; Sayre 1965: 146; 150; Sayre and Smith 191: 1825-1826; Sayre and Smith 1967: 281-293; Shortland *et al.* 2006: 521). Whilst intermediate compositions do exist, this general division still applies. It is generally agreed that soda-lime-silica glass was produced using a two-component recipe (silica and soda; lime being introduced ‘unintentionally’ with the one of these ingredients, depending upon the soda source employed) (Freestone 2006: 207; Freestone *et al.* 2008: 29).

Low-magnesia, low-potash glass was produced using a fairly pure mineral source of soda such as natron (the evaporate *trona*, a hydrated sodium carbonate mineral), which in the past was (presumably) sourced from the Wadi Natrun between Cairo and Alexandria in Egypt, where it is deposited from a series of saline lakes (Brill 1988: 265; Foy and Nenna 2001: 22; Freestone 2005: OO8.1.1; 2006: 204; 2008: 84; Freestone and Gorin-Rosen 1999: 106; Freestone *et al.* 2008: 29; Henderson 1985: 273; 2000b: 148; 2000a: 26; Jackson 1996: 290; Nenna *et al.* 2000: 99; Shortland *et al.* 2006: 526-527; Vallotto and Verità 2000: 63; Verità 2001: 235; Wedepohl *et al.* 2011: 94). In contrast, high-magnesia, high-potash glass was produced using a soda-rich plant ash, obtained by calcining certain halophytic desert plants and seaweed (Brill 1988: 265; Brill 2006: 138; Foy and Nenna 2001: 24; Freestone 2006: 204; 2008: 83-84; Freestone *et al.* 2008: 29; Henderson 2000a: 26). These two glass types are generally termed *natron* and *plant-ash* glass respectively.

Natron glass was the principal glass type used in the Eastern Mediterranean and Europe during the Roman period, up until about the 9th century AD (Bimson and Freestone 2000: 133; Freestone *et al.* 2000: 257; 2008: 29; Henderson 2000a: 26). It was probably produced using a two-component recipe of natron and a quartz-rich

calcareous sand (Brill 1988: 265; Freestone 2006: 207; Freestone and Gorin-Rosen 1999: 111; Freestone *et al.* 2003a: 22-25; Vallotto and Verità 2002: 63). Plant-ash glass was used in the Eastern Mediterranean prior to the 7th century BC, and became commonplace once more from the 9th century AD onwards (Freestone *et al.* 2008: 29). It also continued to be used as a flux in the Middle East, east of the Euphrates, during the Sasanian period (3rd-7th centuries) (Freestone 2006: 204; Mirti *et al.* 2009: 1061). This glass type was probably produced using pure crushed quartz pebbles as a silica source, as plant ash is naturally rich in lime (Brill 1988: 265; Freestone 2006: 207; Freestone and Gorin-Rosen 1999: 111; Freestone *et al.* 2008: 30; Henderson *et al.* 2005: 666). Rarely, plant ash and calcareous sand were mixed to produce a glass containing lime from different sources, but this could lead to increased working temperatures and devitrification of the batch (Freestone *et al.* 2008: 30), as with the failed glass slab at Bet She'arim in Israel (Freestone 2006: 207; Freestone and Gorin-Rosen 1999). True plant ash glass is of little relevance to the period in question in the present study.

The origin of lime in natron glass has been widely debated and is still an ambiguous subject (*e.g.* Freestone 2006: 206-208; Freestone *et al.* 2003a: 22-25; Verità 1995: 292). It was either deliberately added as a separate ingredient, or introduced as fragments of shell or limestone naturally present in the glassmaking sand (Freestone 2005: OO8.1.4; 2006: 207; Freestone *et al.* 2003a: 22-25; Henderson 1985: 277; Jackson 1996: 290; Vallotto and Verità 2000: 65; Verità 1995: 292). Whilst some authors (*e.g.* Wedepohl and Baumann 2000: 132) argue that lime may have been added separately, it is more widely accepted that it was unintentionally added with the silica source through the use of a calcareous quartz sand containing the right proportion of marine shell (or limestone) to produce a stable glass (*e.g.* Brill 1988: 267; Freestone 2003: 111; 2005: OO8.1.4; 2006: 207; 2008: 90-91; Freestone *et al.* 2003a: 29; 2008: 30; Jackson 1996: 290; Verità 1995: 292).

Calcareous quartz sands of suitable composition for glassmaking were only available from a limited number of locations in the past; Pliny, writing in the 1st century AD, mentions the calcareous sands of the Belus River in Israel as being used for glassmaking (Brill 1988: 266; Freestone 2006: 207; 2008: 85-86; Freestone and Gorin-Rosen 1999: 110-111; Freestone *et al.* 2003a: 22-23). Indeed, sands from the

Levantine coast contain just the right amount of lime in the form of shell fragments, together with relatively few mineral impurities, to produce a high quality glass (Bimson and Freestone 2000: 133; Brill 1988: 267; Freestone 2006: 207; 2008: 86-87; Freestone *et al.* 2008: 30).

In recent decades the chemical analysis of Late Antique and early medieval glass has attracted considerable attention. At a very basic level, the theory is that glass objects produced in one production zone will have a chemical ‘fingerprint’ that allows them to be differentiated from glass objects produced in another production zone. This is only valid if glass was being made from its raw materials at a local or provincial level (‘dispersed’ production), whereby each workshop or perhaps group of workshops used local sand sources of a distinctive composition (*e.g.* Figure 1.4.1) (Freestone *et al.* 2002b: 257; 2008: 30). The dispersed model of production is based upon our understanding of the later medieval ‘forest’ glass industry in northern Europe, in which there were a large number of workshops producing glass from local sand (Freestone 2003: 111; 2005: OO8.1.1). However, this is unlikely to be the case for natron glass produced in the 1st millennium AD, which was probably mass-produced in a small number of institutions (‘centralised’ production), as will be seen (*e.g.* Figure 1.4.3).

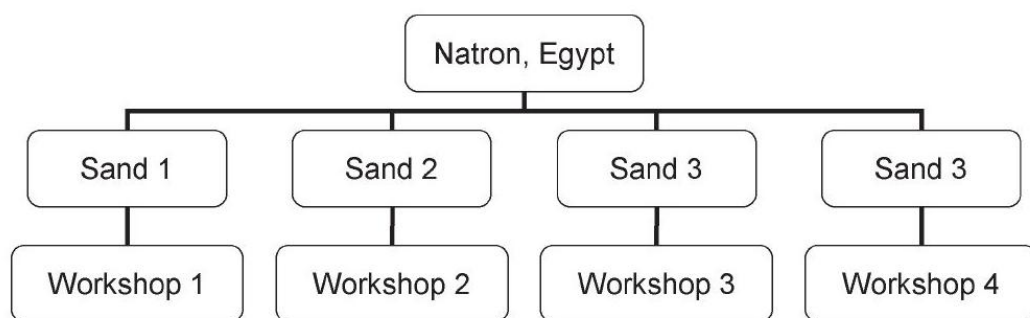


Figure 1.4.1 – The traditional division of production for natron-based glass (after Freestone *et al.* 2008: 30). Here natron is imported from Egypt to individual glass-making ‘workshops’, for example in Europe, which each exploit local sources of sand. Each of these therefore produces glass of a distinctive composition.

As such, correlations between typology and glass composition in early natron glass are unlikely, as many different glasshouses will have made objects from glass produced using very similar raw materials (Freestone *et al.* 2002b: 270; 2008: 30-31). The exceptions arise when different glasshouses obtain glass from different centralised workshops, or when there is a change in the location of centralised workshops over time.

In recent years, significant advances have been made in our understanding of natron glass produced in the Eastern Mediterranean region during the 1st millennium AD; a review of the production evidence here is essential in the study of the wider context of the glass industry in Britain and Europe during the early medieval period. It is first important to distinguish between *glass-making* and *glass-working*. Glass-making involves the production of glass from its primary raw materials (Brill 2006: 139; Henderson 1999a: 82), and usually took place in *primary* production centres which did not fabricate glass objects (Freestone 2005: OO8.1.3; Freestone *et al.* 2008: 31). Glass-working involves the re-melting of pre-made raw or recycled glass for the production of finished objects such as beads, and requires lower temperatures than glass-making (Brill 2006: 139; Henderson 1999a: 82); this usually took place in *secondary* production centres (Freestone 2005: OO8.1.3; Freestone *et al.* 2008: 31).

1.4.1. The Eastern Mediterranean

Natron glass was extensively produced in the Eastern Mediterranean during the Early Byzantine period (4th-7th centuries), but previous studies suggest that this was at more than a local level. It is now widely acknowledged that large quantities of natron glass were mass produced in temporary furnaces in a small number of primary production centres located throughout Egypt and Palestine (Freestone 2005: 197; Freestone *et al.* 2000: 66; 2002b: 258; 2008: 30). This large-scale production is suggested by the lack of compositional variability in natron glass (Fiori and Vandini 2004: 158; Foy *et al.* 2000: 51; Vallotto and Verità 2002: 63). Large primary *glass-making* furnaces have been identified in Egypt and Palestine, which mass-produced glass in large slabs from calcareous quartz-sand and imported natron (from Egypt) in

a single firing (Gorin-Rosen 2000; Freestone *et al.* 2000; Nenna *et al.* 2000: 99; 2005: 59-60; Picon and Vichy 2003: 27-28). A series of furnace floors have been excavated at Apollonia-Arsuf (Tal *et al.* 2004) and at Bet Eli'ezer (Figure 1.4.2) which testifies to this. The 8-ton glass slab at Bet She'arim in Israel is also a surviving example of such a process (Gorin-Rosen 2000: 55; Freestone 2006: 202; Freestone and Gorin-Rosen 1999: 105).



Figure 1.4.2 – A series of seventeen 8th-9th century furnace floors at Bet Eli'ezer, near Hadera, Israel (Foy and Nenna 2001: 37).

These enormous slabs were broken up and widely distributed as angular chunks or ingots (referred to as 'raw' glass), which were more easily transportable, to a larger number of secondary glass-working institutions (Brill 1988: 284; Foy *et al.* 2000: 51; Freestone 2005: 197; Freestone and Gorin-Rosen 1999: 108; Freestone *et al.* 2000: 66; 2002a: 167; 2008: 30; Gorin-Rosen 2000: 54; Nenna *et al.* 2000: 99). Here it was remelted, coloured if desired, and worked into finished objects such as vessels and beads (Freestone *et al.* 2008: 30). That the production of objects took place in separate workshops to those producing the raw glass is attested for by the absence of glassworking debris at these primary production sites. Furthermore, there is widespread evidence for a trade in raw glass chunks from shipwrecks and secondary glass-working sites (Foy and Jézégou 1997; Foy and Nenna 2001; Foy *et al.* 2000: 51-52; Gorin-Rosen 2000: 54).

As a result, a limited number of primary glass-making centres may have distributed glass to a multitude of secondary glass-working centres (Freestone 2005: OO8.1.3; Freestone *et al.* 2002b: 258-259; 2008: 31). If this were the case, secondary workshops could have produced a number of different glass objects of a similar compositional type regardless of their proximity to one another (Figure 1.4.3) (Freestone 2005: OO8.1.3; 2006: 202; Freestone *et al.* 2002b: 258-259; 2008: 31; 2008: 31). The composition of a glass object would therefore reflect the primary workshop(s) where the raw glass was manufactured, rather than the secondary workshop(s) where the objects were created (Freestone *et al.* 2002b: 258; 2008: 31). In principle, a secondary workshop could also have received raw glass from more than one primary production centre (*e.g.* ‘Workshop 3’ in Figure 1.4.3), and thus produced objects of more than one composition (Freestone 2005: OO8.1.3; Freestone *et al.* 2002b: 258-259; 2008: 31). Alternatively, different primary glass types may have been mixed together, so that the characteristic chemical signatures of the primary workshops that produced the original glass will have been lost.

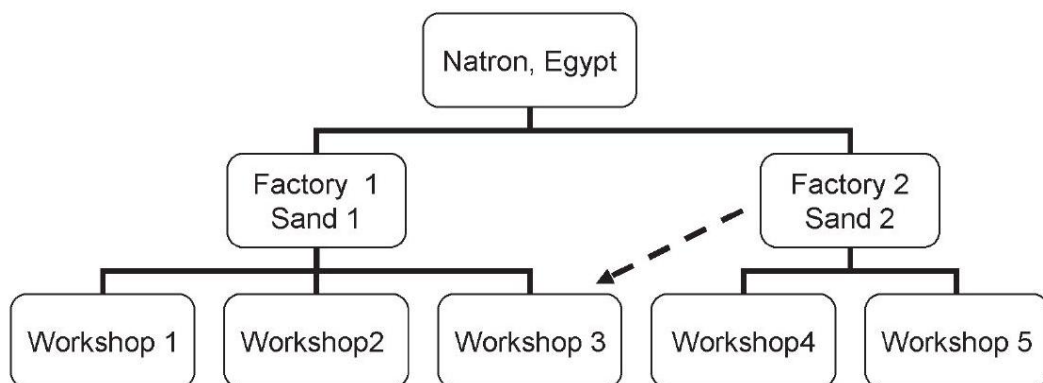


Figure 1.4.3 – Division of production for natron-based glass (after Freestone *et al.* 2008: 31). The primary glass-making ‘factories’ make glass from its primary raw materials (sand and natron). These produced glass of distinctive compositions relating to the source of sand used. The finished glass is broken up and distributed to a number of secondary glass-working ‘workshops’, for example in Europe. Each of these will have therefore produced objects of similar composition regardless of their proximity to one another. In principle, a workshop may be supplied by glass from more than one factory (*e.g.* Workshop 3).

There is evidence to suggest a similar system may have been operating during the Roman period (Degryse *et al.* 2008: 49; 2009: 568; Foy *et al.* 2000: 51; 2003; Freestone 2005: OO8.1.3; Nenna *et al.* 2000: 105); large primary glassmaking workshops have been identified from the Greco-Roman period (1st century BC to 3rd

century AD) in Egypt (Nenna *et al.* 1997: 84-86; 2000: 97; 2005: 59-60), although such institutions have yet to be found in the Levant (Degryse *et al.* 2009: 564; Freestone *et al.* 2008: 31; Jackson *et al.* 2009: 150). This view is also supported by the lack of compositional variability in Roman glass from region to region (*e.g.* Jackson 1992; 1996: 291; Nenna *et al.* 1997: 82), which is consistent with centralised production in a limited number of primary glassmaking institutions (Fiori and Vandini 2004: 158; Foy *et al.* 2000: 51; Vallotto and Verità 2002: 63).

Primary glass workshops would have been ideally situated in the Near East, as the raw materials necessary for glass production, such as natron, were readily available (Foy *et al.* 2000: 51; Freestone 2005: OO8.1.3; Freestone *et al.* 2008: 30). The sand from coastal areas of the Levant would have been very suitable for the manufacture of natron glass (Foy *et al.* 2000: 51; Freestone *et al.* 2008: 30-31); sand from the Palestinian coast was probably readily exploited for glassmaking as it contains just the right amount of shell to produce a stable glass (Bimson and Freestone 2000: 133; Brill 1988: 267; Freestone 2006: 206; Henderson 2000a: 43).

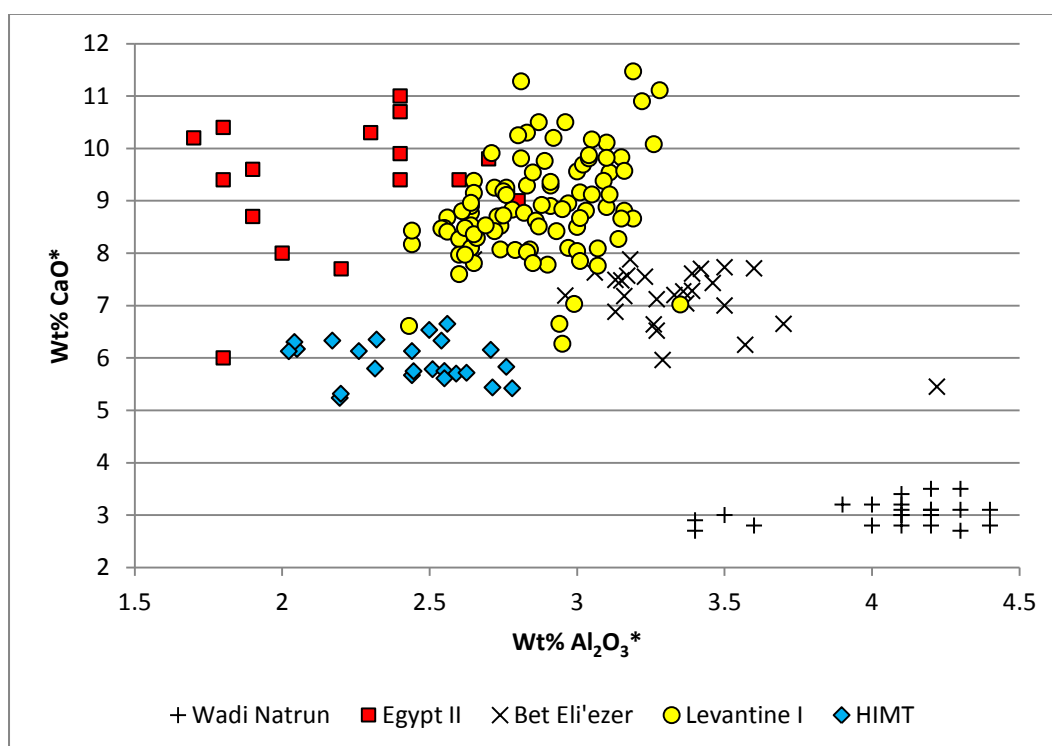


Figure 1.4.4 – A plot of alumina versus lime for the five major groups of natron glass produced in the Eastern Mediterranean between the 4th and 9th centuries AD (after Freestone *et al.* 2000; 2002a; 2002b; see text for details).

Previous work by Freestone and co-workers has identified five main compositional groups of natron glass in use in the Eastern Mediterranean between the 4th and 9th centuries AD (Figure 1.4.4) (Freestone *et al.* 2000; 2002a; 2002b). Whilst these glass types dominate Early Byzantine glass production in the Eastern Mediterranean, they are not exhaustive; other groups of primary glass are likely to be identified by future work (Freestone 2003: 112; see also this study). Natron consists almost entirely of soda, so variations in the composition of natron glasses predominantly reflects the composition of the different sand sources exploited, in the absence of added colourants and opacifiers (Freestone 2003: 111); for example, lime from calcium carbonate and alumina from feldspar (an aluminium-bearing silicate) and clay impurities naturally present in the sand. Lime and alumina are introduced from the sand in particularly high concentrations, so provide a good indication as to variations in the sand sources exploited (Freestone 2005: OO8.1.6; 2006: 208; Freestone *et al.* 2000: 71-72; 2002b: 265; 2008: 32). Each of the groups in Figure 1.4.4 therefore represents the product of a different primary glassmaking institution exploiting a slightly different source of calcareous sand.

The *Wadi Natrun* group is a low-lime, high-alumina glass first isolated by Gratuze and Barrandon (1990) in their study of 7th century Islamic glass weights, and is attributed to workshops near the Wadi Natrun, Egypt (Freestone *et al.* 2002a: 168; 2002b: 265). The *Egypt II* group, also isolated by Gratuze and Barrandon (1990), is a high-lime, low-alumina glass associated with 8th-9th century glass production, probably in Egypt where it has been recognised in glassworking debris (Freestone *et al.* 2002a: 168; 2002b: 265); it is later than the glass under investigation in the present study, so is unlikely to be of relevance.

The *Levantine* glass types (*Levantine I* and *Bet Eli'ezer*) are associated with Palestinian glass production. *Levantine I* glass consists of raw glass chunks from a number of Byzantine workshops in Israel, including Apollonia, Dor, and Bet She'an (Freestone *et al.* 2000: 72; 2002a: 168; 2002b: 265), together with Late Roman glass from Jalame (Brill 1988). This glass is assumed to have been made using sand sourced from the Palestinian coast, similar to that occurring at the mouth of the River Belus in the Bay of Haifa, Israel (Brill 1988: 266; Foy *et al.* 2003: 75; Freestone *et al.* 2000: 72; 2002a: 168; 2002b: 265; Freestone and Gorin-Rosen 1999: 110-111). It

appears to have been the most prevalent glass type used in the Levant between the 4th and 7th centuries (Foy *et al.* 2000: 54; Freestone 2003: 112; Freestone *et al.* 2002a: 168; 2002b: 265).

The *Bet Eli'ezer* group (sometimes termed *Levantine II*) is a product of the huge glassmaking furnaces discovered at Bet Eli'ezer, near Hadera in Israel (Freestone and Gorin-Rosen 1999: 105; Freestone *et al.* 2000: 77-78; 2002a: 168; 2002b: 265; Gorin-Rosen 2000: 52-54). This glass is of a slightly later date (early Islamic; 8th-9th centuries) than *Levantine I* glass and was produced from sand of a slightly different composition, sourced from elsewhere along the Palestinian coast. It appears to have displaced *Levantine I* glass in the 7th or 8th century (Freestone *et al.* 2002a: 168; 2002b: 265).

The final group, termed *HIMT* on account of its High levels of Iron, Manganese and Titanium, was first defined by Freestone (1994) in raw chunk glass from Carthage; this glass type was also isolated by Mirti *et al.* (1993) in glass from Aosta, Italy. The absence of *HIMT* glass in any quantity in northern Israel, where *Levantine I* glass dominated production, suggests that it was not produced on the Levantine coast (Freestone *et al.* 2002a: 172; 2002b: 269; Silvestri *et al.* 2005: 810); isotopic data supports an Egyptian origin (*e.g.* Freestone 2005: OO8.1.10; Freestone *et al.* 2005b: 155; 2009: 44; Leslie *et al.* 2006: 261). It was a widely distributed glass type that became common in the 4th century AD (Foster and Jackson 2009: 189; Freestone 2003: 112; Freestone *et al.* 2002a: 168; 2002b: 265; 2005b: 153-154; Freestone and Hughes 2006: 148; Foy *et al.* 2000: 54). It appears that both *Levantine I* and *HIMT* glass replaced the glass types typically used during the Imperial Roman period (1st-3rd centuries; see Chapter 4, section 4.3 for a summary); the reasons for this are unclear, but may relate to the widespread political and economic changes which took place at this time (Freestone *et al.* 2002a: 172).

It has been suggested that a trade in raw *Levantine I* and *HIMT* glass is likely to have dominated the 4th-7th centuries AD, when they were widely used in vessel production (Freestone 2003: 112; Freestone *et al.* 2002b: 270). However, the results of the present study suggest that the production of *HIMT* glass is in fact unlikely to have continued much beyond the late 4th or early 5th century and was in fact a relatively

short-lived glass type (see Chapter 4, section 4.5). This is in contrast to the current views of research, which suggests that *HIMT* or a variant of *HIMT* glass may have continued to be produced throughout the 5th century and possibly as late as the 8th century (Foy et al. 2000; 2003). Whilst there is abundant evidence for the distribution of raw natron glass in the form of chunks, the way in which they were traded, the extent to which they were traded and the range of different primary glass types produced in the past are not yet fully understood (Freestone *et al.* 2002b: 259).

By the 9th century there appears to have been a shortage in the supply of natron, which led to a change from natron to a soda-rich plant ash as a flux in the Eastern Mediterranean (Freestone 2006: 205; Freestone and Gorin-Rosen 1999: 116; Shortland *et al.* 2006: 523; Ubaldi and Verità 2003: 131; Wedepohl *et al.* 2011: 94-95). These apparent shortages in the supply of natron are likely to have resulted from political upheavals in the Near East between the 7th and 9th centuries (*e.g.* the Persian invasion (AD 619), which was closely followed by the Muslim conquest (AD 639-642), culminating in severe attacks on the Christian communities of northern Egypt in the 9th century (Shortland *et al.* 2006: 527-528). However, it has also been suggested that this may have been due to a wetter climate around this time, which could have affected the formation of natron (Picon and Vichy 2003: 30).

1.4.2. Britain and Northwestern Europe

There have been a number of studies in recent years which have focused upon the technology and origins of early medieval glass in Britain and northwestern Europe (*e.g.* Bimson and Freestone 2000; Brill 2006; Campbell and Lane 1993; Freestone and Hughes 2006; Freestone *et al.* 2008; Hunter and Heyworth 1998; Mirti *et al.* 2000; 2001; Sanderson *et al.* 1984; Wedepohl *et al.* 1997; 2011; Wolf *et al.* 2005; Velde 1990; Verità 1995). These have established that this glass is of the soda-lime-silica type produced in the 'Roman' tradition using a mineral source of soda (natron from Egypt) and a calcareous quartz-rich sand, similar to that produced in the Eastern Mediterranean at the same time (see this chapter, section 1.4.1).

To date the principal source of natron which is likely to have been exploited for glassmaking in the past is assumed to be the Wadi Natrun in Egypt (Bimson and Freestone 2000: 133; Brill 2006: 139; Freestone *et al.* 2008: 29; Nenna *et al.* 2000: 99; Shortland *et al.* 2006: 526-527; Wedepohl and Baumann 2000: 130); this source is testified for by an account in Pliny's *Naturalis Historiae* from the 1st century (Freestone 2008: 84). Whilst the possibility of a local northern European source of natron has been considered (*e.g.* Henderson 1985: 274; Heyworth 1992: 172), the climate does not favour its formation, which renders the Near East (particularly Egypt) the most likely source.

Impurities derived from the sand sources employed in the production of natron glass in northwestern Europe throughout the 1st millennium AD, up until the 9th century, are very constant, suggesting the use of a limited range of sand sources (Bimson and Freestone 2000: 133). Sands of suitable composition, matching those used in the production of this natron glass, are not found in northern Europe but are widely available in the Eastern Mediterranean (Bimson and Freestone 2000: 133). If early medieval craftsmen in Britain or northwestern Europe were producing glass from its raw materials, they would have had to have imported natron and sand for the purpose (Bimson and Freestone 2000: 133; Brill 2006: 139; Freestone and Hughes 2006: 152).

Sand would have had limited uses other than in glassmaking, so is unlikely to have profitable as a commodity (Bimson and Freestone 2000: 133). In addition, the archaeological evidence for the manufacture of glass from its raw materials in British and northwestern European workshops is limited (Bimson and Freestone 2000: 133; Freestone and Hughes 2006: 152; Heyworth 1992: 169). A trade in the raw materials used for glass-making to Europe is therefore very unlikely. However, it is notable that recent isotopic analysis of some Roman glass, which has a composition that would otherwise be consistent with Eastern Mediterranean production, suggests that the sands exploited instead have their origins in the Western Mediterranean (Degryse and Schneider 2008: 1997-1999; Degryse and Shortland 2009: 139; Degryse *et al.* 2009: 568; Leslie *et al.* 2006: 266), although archaeological evidence for such institutions operating in the west has yet to be identified.

There is very limited historical or archaeological evidence for glass production in the early medieval period in Britain and northwestern Europe. The historical accounts which do exist are usually later, referring to the glazing of ecclesiastical institutions from the mid-7th-8th centuries (Cramp 1970: 327-329; 1975: 89; 2006: 56; Sanderson *et al.* 1984: 53; Henderson 1999a: 82; Heyworth 1992: 169; Picon and Vichy 2003: 27; Welch 1999: 8); these are supported by glassworking evidence from Glastonbury Abbey in Somerset, Barking Abbey in Essex and Wearmouth/Jarrow in Northumbria (Bayley 2000b: 138-139; 2000c; Heyworth 1992: 170-171; Thomas 2011: 412). The glass furnaces at Glastonbury Abbey have recently been radiocarbon-dated to approximately AD 680, which provides the earliest most substantial archaeological evidence for a glass workshop in Anglo-Saxon England (AHG 2012: 15). Similarly, crucible fragments containing opaque pale yellow glass are known in England from probable 6th century contexts at Buckden, Cambridgeshire (Bayley 2000b: 138), and there is evidence for glass-working at 7th-9th century Hamwic, Southampton (Hunter and Heyworth 1998).

In the Celtic West, glass fragments have been recovered from sites such as Tintagel in Cornwall, Cadbury Castle in Somerset, and Dinas Powys in Wales (Heyworth 1992: 171). Vitreous enamels are sometimes found on Anglo-Saxon metalwork from the 6th-7th centuries and are commonplace on 'Celtic' metalwork from the 7th century and later (*e.g.* Brun and Pernot 1992; Stapleton *et al.* 1999; Youngs 1989). There is evidence for the production of opaque yellow beads, including crucible fragments, at the Early Christian (7th-9th century) sites of Dunmisk fort, County Tyrone (Henderson 1988b; Henderson and Ivens 1992), Dunadd in Argyll (Lane and Campbell 2000), and the Pictish monastery at Tarbat Ness in Portmahomack (Peake and Freestone, *in press*). Similar Early Christian glassworking waste has been recovered from Cathedral Hill and Scotch Street in Armagh, as well as Garranes fort and Movilla Abbey, all in Ireland (Heyworth 1992: 171). However, such evidence is not found to the same extent in Anglo-Saxon England; it is not until the late Anglo-Saxon and Viking periods that we begin to find conclusive evidence for glassworking in Britain and northwestern Europe, at sites such as Coppergate in York (Bayley 2000b: 139-140; Leahy 2011: 440-441).

On the Continent, glassworking waste associated with bead production in the 5th-6th centuries is also uncommon. Crucible fragments containing opaque yellow glass have been recovered from 6th-7th century contexts at Maastricht in The Netherlands (Sablerolles *et al.* 1997) and Schleithem in Switzerland (Heck *et al.* 2003). There is an apparent late 6th or 7th century beadmaking workshop at Rothulfuashem in The Netherlands, which includes bead types represented at Anglo-Saxon sites (Guido and Welch 2000: 115; Henderson 1999a: 85; Welch 1999: 7). There appears to have been a significant jewellery workshop operating at Helgö in Sweden during the 5th-6th centuries (Thomas 2011: 409). Further evidence for the production of beads comes from later sites including 9th century Ribe in Jutland (Andersen and Sode 2010; Sode 2004: 86-87), 8th century Åhus in Sweden (Callmer and Henderson 1991: 143-147) and 3rd-6th century Lundeberg in Denmark (Thomsen 1995: 20-22). Glass vessels also appear to have been produced in the 5th and 6th centuries at Maquenoise on the French-Belgian border (Heyworth 1992: 171).

There is clearly a distinct lack of direct archaeological evidence for glass-working in early Anglo-Saxon England and Merovingian Europe (Brugmann 2004: 2; Guido and Welch 2000: 115), and certainly no conclusive evidence for the manufacture of glass from its raw materials. In contrast, there is abundant workshop evidence in the Near East, where glass was mass produced in large tank furnaces for export, making a trade in raw glass from there far more likely (Brill 2006: 139; Freestone 2003: 111; Freestone and Hughes 2006: 152; Picon and Vichy 2003: 28). It therefore seems probable that glass-making was centralised in the Eastern Mediterranean, where natron and calcareous quartz-rich sand were readily available (Freestone *et al.* 2002a: 167). The archaeological evidence discussed earlier in this chapter (section 1.4.3) suggests that natron glass was manufactured in the Near East on a scale large enough to sustain a trade in raw glass. This raw glass is likely to have been far more viable as a commodity than the raw materials (sand and natron) themselves (Bimson and Freestone 2000: 133; Picon and Vichy 2003: 28).

Such a trade would account for the compositional homogeneity of natron glass and the apparent lack of archaeological evidence for glass-making in northwestern Europe (Freestone 2005: 195; Freestone and Hughes 2006: 152; Picon and Vichy 2003: 27). Whilst recent studies (*e.g.* Freestone 2003; Freestone and Hughes 2006;

Freestone *et al.* 2008; Picon and Vichy 2003) have suggested that the early medieval European glass industry may have depended upon a supply of 'raw' glass from the Eastern Mediterranean, the relationship between the Eastern Mediterranean and northern European glass industries in the early medieval period is still far from clear. Although it has been argued that natron was imported to Europe during the early medieval period and that local sources of sand were exploited (*e.g.* Wedepohl *et al.* 1997: 247; Wedepohl and Baumann 2000: 131-132), the centralised model is preferred.

At some point around the 8th or 9th centuries natron glass in northwestern Europe largely went out of use and was replaced by a glass rich in potash (K₂O), reflecting the use of the ashes of locally available inland plants or trees as a flux (Freestone and Gorin-Rosen 1999: 116; Freestone *et al.* 2008: 29; Henderson and Holand 1992: 37-38; Shortland *et al.* 2006: 523; Wedepohl 1997: 254; Wedepohl *et al.* 2011: 94-95); this probably stemmed in part from the demand for glass to glaze the major ecclesiastical establishments founded around this time (Heyworth 1992: 172). This coincided with a shift from the use of natron to plant ash, based on the ashes of halophytic marine plants, as a flux in glass in the Eastern Mediterranean, suggesting that natron was in short supply (Freestone and Gorin-Rosen 1999: 116; Shortland *et al.* 2006: 523; Ubaldi and Verità 2003: 131; Wedepohl *et al.* 2011: 94-95). This supports the view that the glass supplied to both northwestern Europe and the Eastern Mediterranean were dependent upon the same source(s) of natron (Freestone *et al.* 2008: 29).

A final consideration is the extent of recycling. In addition to raw glass, there is likely to have been a substantial reserve of cullet in the form of broken vessel glass of the natron type left over from the preceding Roman period (1st-4th centuries). It is possible that the early medieval glass industry in Britain and northwestern Europe was dependent upon a supply of this glass which, depending upon its availability and demand, is likely to have been repeatedly remelted and recycled for the production of objects (Bimson and Freestone 2000: 133; Brill 2006: 139-140; Freestone and Hughes 2006: 148; Freestone *et al.* 2008: 31; Heyworth 1992: 172-173; Hinton 2011: 428-429; Jackson 1996: 298-299; Thomas 2011: 406; Velde 1990: 116). It has been argued that vessel glass assemblages such as that from the mid-Saxon site at

Hamwic, Southampton, may represent a centre for such a trade in cullet (Hunter and Heyworth 1998).

Coloured Roman glass tesserae, which may have been used in beadmaking, have been found at various sites on the Continent including Ribe, Helgö, Paviken and Åhus (*e.g.* Callmer and Henderson 1991: 148-149; Evison 2000: 91; Henderson 2000a: 70-73; Lundström 1981: 17; Sode 2004: 87; Wedepohl 2001: 260), testifying to the re-use of Roman glass. Closer to home, tesserae have been found at the monastic sites of Jarrow, Beverley and Whitby, but in much smaller quantities (Cramp 2001: 71-72). These may have been imported, possibly from the Mediterranean (Hinton 2011: 429). However, tesserae are again rare on suspected beadmaking sites prior to the 8th and 9th centuries (Sablerolles 1999: 266-268).

Recycling would have had a number of advantages. As well as being economic, it would have negated the need for a supply of raw glass from elsewhere. It would have involved lower temperatures and would therefore have used less fuel than if glass were produced solely from its raw materials (Henderson 1985: 270). Furthermore, none of the technological knowledge required to make glass from its raw materials was required (Vallotto and Verità 2000: 63-64).

One of the main problems regarding the chemical classification of natron-type glasses relates to the potential re-use and mixing of glasses with different origins, because the compositional traits of primary glassmaking workshops are destroyed (Foy *et al.* 2003: 81; Freestone 2002b: 258; Henderson 1992: 175; Henderson 1993: 247; Henderson 1999a: 82; Jackson 1996: 299). Whilst recent work by Freestone *et al.* (2008: 40) suggests that most early Anglo-Saxon vessel glass is highly unlikely to have been produced from recycled Roman material, its use cannot be ruled out; production of window glass at the late 7th century monastic site of Jarrow, Northumbria, is likely to have included a significant amount of recycled Roman material (Freestone and Hughes 2006: 154). Recent analysis of Merovingian glass beads from Belgium also suggests a dependence upon recycled Roman material (Mathis *et al.* 2010: 2082).

1.5. Early Anglo-Saxon Beads and Bead Studies

Beads are the most numerous artefact-type recovered from early Anglo-Saxon contexts, particularly from female graves (Brugmann 2004: 1; Owen-Crocker 2004: 85; Welch 1999: 1-2). Whilst they are rarely found in male graves, large 'sword beads' are occasionally found in association with double-edged swords (Evison 2000: 48; Guido 1999: 24; Owen-Crocker 2004: 126; Welch 1999: 2). Anglo-Saxon beads may be made from a variety of materials; predominantly glass and amber, but also materials such as metal, shell, chalk, rock crystal, amethyst and jet (Brugmann 2004: 1; Walton Rogers 2007: 128; Welch 1999: 2). The way in which they were worn varied greatly between individuals and regions; some may have been worn as a mark of wealth, social status or identity (Owen-Crocker 2004: 317), and others as protective amulets (Meaney 1981: 205).

Early Anglo-Saxon bead strings were comprised of beads of various colours, shapes and materials; these beads may have been ordered randomly or sequentially (Owen-Crocker 2004: 87; Walton Rogers 2007: 193). They were typically worn in swags or festoons suspended between two brooches at the shoulders (Fleming 2011: 47; Lucy 2000: 25; Owen-Crocker 2004: 85; 2011: 98-100; Walton Rogers 2007: 193; Welch 1999: 1-2), but sometimes short loops of beads may have been suspended from just one brooch (Walton Rogers 2007: 193). They could also be worn as necklaces or bracelets, stitched to items of clothing or suspended from a belt (Guido 1999: 24; Owen-Crocker 2004: 85; Walton Rogers 2007: 193-195; Welch 1999: 2).

Glass was one of the most widely used materials for beads, owing to its durability, beauty and versatility (Brugmann 2004: 1; Lucy 2000: 41; Owen-Crocker 2004: 86). These beads often vary considerably in size, shape, colour decoration and technology, which lend them well to typological study (Brugmann 2004: 1; Lucy 2000: 41; Owen-Crocker 2004: 86). However, until recent years, their study had primarily been restricted to descriptions in site reports for individual cemeteries (Welch 1999: 2-3); by their nature these failed to place glass beads into more regional and national contexts. The potential of early Anglo-Saxon glass beads for

characterisation has been demonstrated in recent years with the publication of two major typologies, which have considerably advanced our current state of knowledge.

The first, Margaret Guido's *The Glass Beads of Anglo-Saxon England c. AD 400-700* (Guido 1999), is based upon visual examination of 5th to early 8th century beads from throughout Britain, Europe and Scandinavia, following on from her previous study of beads from the Prehistoric and Roman periods (Guido 1978). She attempts to establish approximate date ranges for Anglo-Saxon beads based on their shape, colour and decoration and through comparisons with more closely datable grave goods with which they may be associated, such as brooches. She also suggests whether specific bead types may be imports or insular products based upon their distributions. She divides her sample into monochrome and polychrome bead types, then attempts to characterise beads by colour and shape, together with decorative patterns and colour combinations. However, as Brugmann (2004: 27) notes, this means that beads which may have been produced as a series using the same techniques and decoration, but not necessarily in the same colours, are discussed out of context from one another. Guido's study was only partly successful, as the chronology of beads proved to be too complex to be based on visual attributes alone, and only very broad chronological groups could be established.

Typological studies have been considerably advanced since Guido's study with the development of specialist computer software; in particular *ProPer*, which was designed for beads from Continental row-grave cemeteries and enables the classification and statistical analysis of large numbers of beads (Brugmann 2004: 1-2; Hirst 2000: 121). The second and most recent major typological study, Birte Brugmann's *Glass Beads from Early Anglo-Saxon Graves* (Brugmann 2004), classifies beads by shape and colour according to the model produced by *ProPer*. Her study is based on a representative sample of 32231 beads from 1206 graves and 106 cemetery sites from across England. This was later extended by Penn and Brugmann (2007) through the examination of beads from four cemeteries in Norfolk; beads from three of these sites constitute part of the present study (see this chapter, section 1.2.2). Using distribution maps, Brugmann speculated as to which bead types are more likely to be insular products and which are more likely to be imports. She links particular stylistic characteristics of Anglo-Saxon glass beads to the definitions

already established for well-dated contemporary beads from the Continent using correspondence analysis.

Brugmann divided different bead types into three broad ‘Groups’ (also referred to as ‘phases’), within which are a number ‘Combination Groups’. These Groups were attributed absolute dates on the basis of correlations with well-dated Continental and Scandinavian glass bead sequences. Brugmann’s Phase A (containing sub-phases A1, A2 and A2b) corresponds to the so-called ‘Migration Period’ (c. AD 450-580), Phase B (containing sub-phases B1 and B2) to the transition period between the ‘Migration Period’ and the so-called ‘Final Phase’ (c. AD 555-650), and Phase C to the ‘Final Phase’ (c. AD 650-700) (see Chapter 4, section 4.8 for details). Phases A and B overlap in chronology, but phases B and C do not. She distinguishes between ‘Roman’ and ‘Germanic’ bead types, suggesting limited continuity between the Roman and Anglo-Saxon periods in spite of occasional Roman heirlooms. The chronological framework established by Hines *et al.* (in press) has attempted to further refine her chronology using typological study, correspondence analysis, Bayesian modelling and radiocarbon-dating to establish a multi-phase chronological series for Anglo-Saxon grave goods; this suggests that some of Brugmann’s dates, particularly for phase B2, may be considerably earlier than she suggests (see Chapter 4, section 4.8).

Whilst the distribution maps and typological comparisons produced by Guido (1999), Brugmann (2004) and Penn and Brugmann (2007) have proved useful indicators of possible production zones for specific bead types, they cannot be substantiated without archaeological evidence for beadmaking. The present study relies solely upon Brugmann’s typology and chronology as a basis in the interpretations of the chemical data for the Eriswell beads, primarily because this has formed the basis of the classification of the glass beads from the site. However, it should be noted that the chronology set out in Brugmann (2004) does not account for possible regional variations in bead fashion. It also assumes that the appearance of particular bead types on the Continent provides a *terminus post quem* for their introduction in England when, in theory at least, some bead types may have first appeared in England. Additionally, as Brugmann’s chronology does not account for other grave goods which may be present, it cannot be used to provide absolute dates

for individual graves, although recent work by Hines *et al.* (in press) has attempted to rectify this. However, the present study relies heavily upon Brugmann's typology and chronology, primarily because her study has formed the basis of the classification of the glass beads from the site. The interpretations in this thesis may therefore be subject to modification in the light of future developments in our understanding of early Anglo-Saxon bead chronology and typology.

1.6. Aims

The majority of studies on early medieval glass are either scientific or typological, with little crossover between the two. At present, it is unclear how glass-workers procured their glass following the withdrawal of Rome from northwestern Europe and prior to the production of ‘forest glass’ in the later medieval period. However, the wide range of glass colours, and thus raw materials, that were used in the production of early Anglo-Saxon glass beads lends them particularly well to chemical analysis. Whilst the general composition of the glass and the colourants employed are generally known, straightforward links between bead type, bead date and chemical composition have not yet been established. This study aims to establish the composition and affinities of typologically established groups of beads, the nature and sources of the raw materials used in their production and the extent of recycling.

There are three possibilities regarding the origins of natron glass in the early Anglo-Saxon period following the withdrawal of Rome, each of which would produce distinctive compositional patterns (Brill 2006: 139-140; Freestone 2003: 111; Freestone and Hughes 2006: 147-148; Freestone *et al.* 2008: 31):

- The glass may represent recycled material, mainly Roman.
- The glass may have been manufactured in Britain or Europe, using imported natron and local sand.
- The glass may have been manufactured in the Near East from its raw materials, where glass continued to be produced in the Roman tradition until the 9th century AD, and imported.

It is unlikely that just one of these models will apply; recycling of glass from a number of different sources is likely to have been practiced throughout the period in question, which will complicate the interpretation of any analyses. If recycled material was being used, an increase in the concentration of colourant elements, such as antimony or cobalt, may be expected due to the incidental incorporation of small quantities of old coloured and opaque glass into the melt. Furthermore, successive

re-melting of cullet may lead to an increase in iron, alumina and titanium as a result of contamination from the clay fabric of the melting pot, or the incorporation of iron scale from tools (Freestone 2003: 111).

If glass was produced in Britain and/or northwestern Europe using imported natron but local sand, each workshop would have produced glass of a distinct composition reflecting the different sand sources exploited. However, if glass was produced in centralised workshops in the Near East and imported as raw pre-made glass, the composition of the beads will be relatively uniform regardless of where they were produced; the composition of these beads could vary depending upon the number of different primary glassmaking institutions supplying the raw glass, or changes in the supply of this glass over time (Freestone 2003: 111).

The manufacture of the beads themselves can be treated as a separate issue. The variety of glass bead types produced by an individual craftsman or workshop would have depended on several factors: the availability of the necessary raw materials (*e.g.* raw glass, colourants, etc.), the skills of the craftsmen, the environment in which they were produced, and the demand for specific bead types (*i.e.* fashion) (Brugmann 2004: 17). There are four possibilities regarding the organisation of the beadmaking industry (Hoffmann *et al.* 2000: 93; Siegmann 2006: 1046):

- Beads may have been produced in fixed centralised workshops (possibly producing high quality or specialised bead types for widespread distribution), which may have been widely distributed by a number of intermediaries.
- Beads may have been produced in fixed regional workshops, for either widespread distribution or use on a more regional level.
- Beads may have been produced in fixed local workshops, for use by individual communities.
- Beads may have been produced in temporary local workshops by peripatetic craftsmen.

Again, any combination of these models is possible. However, if the glass or raw materials sustaining these workshops were obtained from a limited number of sources, it may not be possible to establish the extent to which any one or all of these models apply.

Compositional analysis provides the opportunity to address questions regarding the sources of the raw materials used in the production of early Anglo-Saxon glass, and the nature and quality of their supply, as well as its manufacture and distribution of the glass itself. Indications as to where the glass itself was being manufactured or sourced will allow an appraisal of the level of technological expertise possessed by these early craftsmen; *e.g.* whether they possessed the skills necessary to make glass from its raw materials. Changes in glass composition over time may reflect changes in the supply or demand of certain raw materials.

This study aims to characterise, at least in part, the material circumstances of daily life of early Anglo-Saxon communities in England, both economically and technologically. The accuracy of Brugmann's chronology and typology will be tested, and the current dating sequences attributed to specific bead types may consequently be enhanced and refined. This should provide a good foundation on which to attribute more precise dates to phases of use. The results can not only be compared to previous analyses of contemporary glass from elsewhere, but also analyses of glass from other periods, in order to identify possible links between these industries; for example, it has been suggested that beads and vessels were produced in separate workshops or regions to one another (Brugmann 2004: 17; Evison 2000: 49). Through comparisons with contemporary glass from the Near East and other British sites, as well as glass from the preceding Roman period, it may prove possible to place the Anglo-Saxon glass industry into the broader context of early medieval glass production.

The aims of the present study can be summarised as follows. From a purely scientific viewpoint, the following research questions are important:

- What raw materials (colourants, etc.) were used in the production of the glass?
- What base glass types are represented in the assemblage?
- How were different glass colours and bead types manufactured? How were the colours produced?
- Is there a link between glass composition and glass colour?
- Is there a relationship between glass composition and the degree of preservation?

By answering these basic questions, it is then possible to answer broader research questions relating to the organisation of the early Anglo-Saxon bead industry itself:

- Where were the raw materials (colourants, sand etc.) sourced?
- To what extent was glass being recycled?
- How does chemical composition relate to bead type? Do beads considered to be of the same manufacturing series have the same composition? Do beads of different manufacturing series have different compositions?
- Is there a link between bead composition and bead date? Were there changes in the compositions of beads over time?
- Is there any indication that more complex types of bead (*e.g.* reticella) or glass (*e.g.* opaque red) were specialist products?
- Where were different glass types, and/or the beads themselves, produced? To what extent were beads or different glass types produced locally and to what extent were they imported or traded?
- Is it possible to recognise workshop groupings from chemical composition based upon distribution patterns? Is there any indication that their location was fixed or temporary?
- Were any beads re-used or inherited?

- Were bead strings acquired as sets or composed over time? Were beads from the same grave assemblage produced by the same workshop, or by several workshops?
- How does the composition of the beads relate to other glass objects; *e.g.* vessels, windows, tesserae, etc.?
- Was glassworking closely related to other pyrotechnic industries, such as metalworking, perhaps determined by fuel sources (*e.g.* Brugmann 2004: 18; Henderson 2000a: 76)?

Comparison with contemporary material from elsewhere forms an important part of this study, as it will allow the beads to be placed into the wider context of glass production during the early medieval period. However, the majority of published analyses available for Anglo-Saxon and Merovingian glass beads mentioned in the introduction (Chapter 1) are generally not suitable for comparison; these data are mostly qualitative or semi-quantitative due to the use of non-destructive surface analysis techniques such as x-ray fluorescence (XRF), which are particularly prone to the influences of weathering (see Chapter 3, section 3.3).

Where quantitative data are available (*e.g.* Henderson 1990; 2011; Mortimer 1998; Mortimer and Heyworth 2009), these are often either reported to only one decimal place, lack analytical comparability (possibly as a result of analytical differences between laboratories), or do not report certain diagnostic elements (particularly antimony; primarily because the detection limits of the equipment were not sufficiently low). This makes meaningful comparisons difficult. More recent quantitative data obtained for Merovingian beads by PIXE/PIGE (*e.g.* Mathis *et al.* 2010) are not fully compatible with data obtained using the scientific techniques in the present study (SEM-EDS). Glass beads were selected from the nearby sites of Spong Hill, Bergh Apton and Morning Thorpe in Norfolk for comparison in the present study (see this chapter, section 1.2.2).

CHAPTER TWO

2. Materials and Methods

The chemical analysis of glass provides information about its composition which can be used to investigate the technology of its manufacture and origins, as well as to date it and investigate corrosion phenomena for conservation purposes. In order to be able to characterise a glass, it is usually necessary to analyse for a large number of elements. It is then possible to compare its composition with previously identified glass groups produced in different workshops at different times, with a hope of establishing provenance and/or date. The concentrations of light elements (*i.e.* those which have a relatively low atomic number in the periodic table; *e.g.* sodium, which has a low atomic number (11) relative to lead (82)) in a glass can be crucial in this process, but these elements are not usually measurable by non-destructive surface analysis techniques such as x-ray fluorescence (XRF) (*e.g.* Pollard *et al.* 2007: 106).

The analysis of early glass in the scanning electron microscope (SEM) has been well-demonstrated by a vast number of previous studies (*e.g.* Brill and Moll 1963; Freestone *et al.* 2000; Freestone *et al.* 2008; Verità *et al.* 1994). Scanning electron microscopy with energy dispersive x-ray analysis (SEM-EDS) was used to determine the relative quantities of the major and minor elements in the glasses (a total of 20 element oxides), and laser ablation inductively coupled plasma mass spectrometry (LA-ICP-MS) to determine the elements present at trace levels (a total of 44 elements). Major elements are deemed to be those which occur at levels above 1.0% and minor elements are those which occur at 0.1-1.0%. Trace elements are those which occur at levels below 0.1%, or 1000 ppm (ppm = parts per million).

2.1. Samples Analysed

2.1.1. RAF Lakenheath (Eriswell), Suffolk

The Eriswell bead assemblage was thoroughly examined and catalogued by Birte Brugmann in 2001. This includes, but is not limited to, brief descriptions of bead material, manufacturing technique, size (bead length and diameter, perforation diameter), shape (including number of segments), weight (for amber beads only), colour, translucency and descriptions of decorative techniques. The determination of glass colour was carried out in daylight, and kept relatively vague for simplicity (Brugmann 2004: 24). This database has been adapted by the author to include only the beads of glass, and further information including bead type and phase (established by Brugmann, after the typology and chronologies specified in Brugmann (2004) and Penn and Brugmann (2007)). This database is shown in Appendix A. The distribution of these bead types at Eriswell is shown in Appendix B, according to grave number (*i.e.* context).

For a detailed definition of individual bead types the reader is invited to consult Brugmann (2004) and Penn and Brugmann (2007). The type definitions for beads not covered by these typologies are mostly based upon the colour of the beads, with additional definitions according to shape for monochrome beads (*e.g.* *Red Melon*, *Green Globular*, etc.), and decorative designs for polychrome beads (*e.g.* *RedPoly1*, *RedPoly2*, *WhitePoly1*, *WhitePoly2*, etc.). In the present study, bead type attributions are always presented in *italics*. Images of the beads sampled are presented in Appendix C, sequentially ordered by grave and small finds number for ease of reference (this should be cross-referenced with the bead database in Appendix A for detailed description of these beads).

Beads from the Eriswell assemblage were chosen for analysis based on a number of criteria. The majority were selected based on their type attributions and colour, so as to be representative of the range of different beads and glass colours present. In addition, beads were chosen based upon the phases to which they had been attributed

by Brugmann, ensuring that a representative range from each of the phases represented was selected.

The blue-green vessel glass fragments recovered from Eriswell were also included in the sample set for comparative purposes. Broken beads were preferentially selected over intact ones where possible to avoid unnecessary damage to complete examples. Badly decayed beads were included within the sampling programme because it is sometimes possible to obtain reliable analytical information from them, and their state of preservation may reflect their composition. Furthermore, the exclusion of heavily decayed beads from the sampling strategy biases the dataset.

Following analysis of the initial sample set, additional beads were selected for analysis based on the identification of types which were compositionally unusual (*e.g.* opaque orange and opaque red colours, described in Chapter 5, section 5.2), or beads which had been under-represented by the initial sample set. The final sample set consisted of 380 individual beads, from which a total of 537 different samples were obtained.

2.1.2. Spong Hill, Bergh Apton and Morning Thorpe, Norfolk

The analysis of material from contemporary sites is an important part of the project, as it allows the Eriswell beads to be placed into the wider context of glass bead production and use in early Anglo-Saxon England. A request was submitted to Dr. Tim Pestell, curator of The Castle Museum in Norwich, for permission to sample a selection of glass beads from the Anglo-Saxon cemetery complex at Spong Hill, Norfolk (Appendix D). This site was chosen because it shares many similarities with that at Eriswell, including the presence of similar bead types, and because the two sites are relatively close to one another. The initial proposal was to analyse a representative selection of beads which spanned as many different bead types, glass colours and grave assemblages from Spong Hill as possible. Broken beads were identified where possible, but beads from cremations were excluded due to the

unknown effects of the high temperatures of cremation on the composition of the glass.

Whilst the initial request was refused on the grounds that semi-destructive analysis was not viable, permission was granted to take samples from broken beads. The majority of these were sampled, together with smaller bead fragments which had no context. In addition, permission was also granted to take any loose fragments of glass from the bead assemblages of the nearby sites of Bergh Apton and Morning Thorpe in Norfolk, which were also held at the museum. Unfortunately, in the majority of cases the poor condition of the beads meant that it was difficult to identify specific bead types using Brugmann's typology.

In total, it was possible to obtain 70 samples (from 55 individual beads at most) from Spong Hill, 13 samples (from 11 individual beads at most) from Morning Thorpe and 20 samples (from 19 individual beads at most) from Bergh Apton. As some of the fragments from which samples were taken are likely to have come from the same bead, as became evident during compositional analysis, the number of individual beads represented by these sites may be lower than stated here. A small number of the beads and bead fragments analysed had lost their context; whilst this meant that they could be sacrificed for analysis, they could not be attributed to a specific grave.

2.2. Methods Tested

In order to obtain reliable quantitative data it is usually necessary to take a sample; non-destructive surface analysis techniques often only provide qualitative or semi-quantitative data. Sampling is an undesirable part of analysis as it inevitably damages the object through the removal of material. Steps are usually taken to either avoid it altogether or minimise the extent of the damage caused where possible. Whilst permission to undertake destructive analysis on the glass beads from Eriswell had been granted, it was in the best interests of all parties involved to avoid, or at the very least minimise, the damage caused by sampling. This has a number of potential advantages:

- The beads are preserved for posterity, and will be retained intact for future research and display.
- Time and materials are potentially saved through not having to obtain or prepare samples for analysis.

As such, a number of non-destructive and semi-destructive analysis techniques were tested in order to determine the reliability of the results obtained, with a view to establishing viable alternatives to taking samples for quantitative SEM-EDS analysis. These tests were undertaken on number of highly coloured, mostly opaque, Early Byzantine (6th-7th centuries AD) mosaic glass tesserae from Caesarea (Israel) provided for analysis by Ian Freestone. The tesserae consisted of a wide range of both opaque and translucent colours. Samples were taken from a representative range of these, mounted in resin and polished in the standard way (see this chapter, section 2.3.1.1). They were analysed for major and minor elements using SEM-EDS (see this chapter, section 2.3.1.2 for details), in order to provide a reliable analytical dataset with which to compare the results of the methods tested. The results are presented in Table 2.2.1.

Table 2.2.1 – SEM-EDS area analyses of Early Byzantine glass tesserae (Caesarea, Israel) acquired from polished samples.

Sample	Colour ¹	Oxide (wt%) ²																		
		Na ₂ O	MgO	Al ₂ O ₃	SiO ₂	P ₂ O ₅	SO ₃	Cl	K ₂ O	CaO	TiO ₂	MnO	Fe ₂ O ₃	CoO	CuO	ZnO	SnO ₂	Sb ₂ O ₃	BaO	PbO
CES P1 C	Op. pale blue	16.58	0.56	2.34	64.10	0.14	0.61	0.53	0.73	7.47	b.d.	1.02	0.75	b.d.	0.44	b.d.	b.d.	4.49	b.d.	b.d.
CES P1 D	Op. pale green	14.93	0.37	2.34	61.49	b.d.	0.42	0.80	0.67	7.35	b.d.	b.d.	0.65	b.d.	1.04	b.d.	0.29	0.81	b.d.	8.58
CES P1 E (1)	Tr. dark green	15.18	0.47	2.19	60.8	b.d.	0.41	0.71	0.71	7.41	0.10	0.22	1.17	b.d.	3.75	b.d.	0.52	0.37	b.d.	5.92
CES P1 E (2)	Op. yellow	15.02	0.29	2.37	61.50	0.11	1.02	0.46	0.69	7.50	b.d.	b.d.	0.71	b.d.	0.35	b.d.	b.d.	0.92	b.d.	8.39
CES P1 F	Op. pale blue	14.99	0.65	2.96	66.15	0.87	0.19	0.78	0.87	10.68	b.d.	0.27	0.43	b.d.	0.32	b.d.	0.35	0.42	0.10	b.d.
Bull A1	Op. blue	14.46	0.78	2.82	68.81	0.33	0.10	0.87	1.00	8.63	0.16	0.61	0.95	b.d.	0.39	b.d.	b.d.	b.d.	b.d.	b.d.
Bull A2 (1)	Tr. turquoise	14.14	0.75	2.76	68.21	0.24	0.19	0.88	1.00	8.57	b.d.	0.38	0.53	b.d.	1.73	b.d.	b.d.	b.d.	0.13	b.d.
Bull A2 (2)	Op. pale blue	14.12	0.64	2.96	66.70	1.66	b.d.	0.52	0.86	10.07	b.d.	0.43	0.65	0.10	0.19	0.37	b.d.	b.d.	0.28	b.d.
Bull A3	Tr. blue	18.32	1.13	2.40	64.09	0.20	0.50	0.86	0.80	8.06	0.16	1.31	1.10	b.d.	0.43	b.d.	b.d.	b.d.	0.13	0.39
Bull DB (1)	Tr. 'colourless'	18.78	0.91	2.17	64.99	b.d.	0.45	0.98	0.64	7.59	0.15	1.54	0.82	b.d.	0.45	b.d.	b.d.	b.d.	0.13	b.d.
Bull DB (2)	Tr. 'colourless'	19.49	1.04	2.37	63.41	b.d.	0.46	0.90	0.76	7.47	b.d.	2.15	0.96	b.d.	0.46	b.d.	b.d.	b.d.	b.d.	b.d.
Bull DB (3)	Tr. blue	13.97	0.78	2.79	68.66	0.24	0.16	0.86	1.06	8.53	0.14	0.46	1.24	b.d.	0.56	b.d.	b.d.	b.d.	b.d.	b.d.
Bull F (1)	Op. green	13.51	0.58	2.37	57.66	b.d.	0.32	0.88	0.74	7.67	b.d.	0.35	0.34	b.d.	0.96	b.d.	1.54	b.d.	0.11	12.53
Bull F (2)	Tr. turquoise	13.17	0.66	2.67	64.64	0.10	0.16	0.84	1.01	8.06	0.13	0.56	0.50	b.d.	1.66	b.d.	0.73	b.d.	b.d.	4.98
Bull H (1)	Tr. blue	14.30	0.74	2.78	68.84	0.19	b.d.	0.85	1.07	8.49	b.d.	0.49	1.16	b.d.	0.67	b.d.	b.d.	b.d.	0.11	b.d.
Bull H (2)	Op. dark green	13.15	0.69	2.62	64.47	0.22	0.19	0.83	1.04	8.17	0.10	0.65	0.52	b.d.	1.50	b.d.	0.69	b.d.	b.d.	5.11
Bull H (3)	Op. pale green	13.19	0.70	2.30	55.59	0.13	0.16	1.06	0.75	7.93	b.d.	0.41	0.51	b.d.	1.24	b.d.	1.08	b.d.	b.d.	14.97
Bull H (4)	Tr. 'colourless'	18.46	1.05	2.17	64.50	0.12	0.46	0.96	0.73	8.00	0.16	1.84	0.90	b.d.	0.49	b.d.	b.d.	b.d.	b.d.	b.d.
Bull I	Tr. 'colourless'	16.04	0.55	3.11	68.32	b.d.	0.3	0.92	0.98	8.44	b.d.	b.d.	0.50	b.d.	0.35	b.d.	b.d.	b.d.	0.19	b.d.
Bull J	Tr. 'colourless'	19.58	1.08	2.40	63.97	b.d.	0.52	0.84	0.69	7.44	0.19	2.11	1.02	b.d.	0.36	b.d.	b.d.	b.d.	b.d.	b.d.
Bull K	Tr. 'colourless'	19.31	1.03	2.42	63.37	0.10	0.47	0.88	0.75	7.50	0.17	2.09	1.03	b.d.	0.53	b.d.	b.d.	b.d.	0.11	b.d.
Bull L1	Tr. 'colourless'	19.30	1.05	2.52	63.37	0.17	0.45	0.88	0.73	7.70	0.13	1.94	1.03	b.d.	0.46	b.d.	b.d.	b.d.	b.d.	b.d.
Bull L2	Tr. turquoise	14.65	0.75	2.78	68.70	0.23	b.d.	0.91	1.03	8.37	0.15	0.42	0.59	b.d.	1.43	0.11	b.d.	b.d.	b.d.	b.d.
Bull M (1)	Tr. turquoise	14.02	0.68	2.69	68.22	0.20	0.13	0.90	1.04	8.68	b.d.	0.41	0.58	b.d.	1.97	b.d.	0.26	b.d.	b.d.	b.d.
Bull M (2)	Op. pale green	12.83	0.67	2.51	62.33	0.16	0.18	0.84	0.99	7.89	b.d.	0.44	0.53	b.d.	1.01	b.d.	1.00	b.d.	b.d.	8.43
Bull M (3)	Op. dark green	13.70	0.59	2.20	54.89	0.18	b.d.	0.69	0.75	7.54	0.14	0.51	0.76	b.d.	1.14	b.d.	1.59	0.45	0.15	14.44
Bull (yellow)	Op. yellow	12.14	0.64	2.34	58.31	0.12	0.16	0.81	0.89	7.15	0.10	0.50	0.58	b.d.	0.54	0.12	1.54	b.d.	b.d.	14.21

¹Op. = opaque; Tr. = translucent.

²Results normalised to 100%. b.d. = below detection. The results are an average of three analyses. Detection limits were thought to be about 0.2% for most elements, although this is marginally higher for lead and tin at about 0.25-0.3%, and approximately 0.4% for antimony.

The results of the methods tested (the DIAM technique and environmental scanning electron microscopy; see below) are compared to those obtained by SEM-EDS of polished samples in Tables 2.2.2 and 2.2.3 (in this chapter, sections 2.2.1 and 2.2.2 respectively). Figures 2.2.1-2.2.6 and 2.2.8-2.2.13 show a series of graphs comparing some of the major elements obtained by these methods; if the results acquired match those for polished samples analysed using SEM-EDS exactly, all of the data points should fall along the diagonal line which intersects the axes at zero (note that these are *not* trendlines). Theoretically the deviation of the data points from the diagonal line is roughly proportional to the accuracy of the results (*i.e.* the further a data point is from the line, the more inaccurate the data obtained by the technique in question).

2.2.1. The DIAM Technique

The DIAM technique is a quasi non-destructive microsampling technique discussed by Bronk and Freestone (2001), who adapted it for the sampling of glass by SEM-EDS. It involves the use of diamond-coated files to remove small amounts of material from glass objects for compositional analysis. These files are approximately 6cm in length and are available in a variety of shapes (Bronk and Freestone 2001: 518). The general principle of the technique is to flake off minute particles of glass by filing for analysis, for which the coarser grades of file are most appropriate. Depending upon the topography of the glass surface, the size of the damaged area (a 'scratch') ranges from 3-10mm² (Bronk and Freestone 2001: 519).

2.2.1.1. Sample Preparation and Analytical Procedure

A small number of tesserae from the Caesarea assemblage were selected at random for sampling. Files with a triangular cross-section, as recommended by Bronk and Freestone (2001: 518), were chosen for the removal of material as this shape provides the best control over the extent of the area sampled.

It was first necessary to use the file to abrade away a small area of the surface of each tessera in order to remove weathered glass, as this is of altered composition (see Chapter 3, section 3.3). The extent of 'damage' is as a result dependent upon the thickness of weathered layer requiring removal (Bronk and Freestone 2001: 519), which varied between tesserae from thin iridescent layers to thick crusts. The resulting glass flakes were discarded. Using a clean file, the same area was then abraded again, and the resulting particles caught on a clean sheet of paper placed beneath. Files were cleaned between use by placing them in an ultrasonic bath of tap water for a few minutes and allowing them to dry on paper towelling. The best flakes removed (those which were largest and therefore most representative) were selected and placed on to adhesive carbon discs mounted on aluminium stubs. As many flakes from each tesserae as possible were placed on an individual stub so as to be more representative, allowing multiple analyses to be obtained from a number of different flakes. This allowed an average to be taken from analyses obtained from different flakes, reducing the likelihood of errors relating to the possible heterogeneity of the glass.

The samples were coated with a thin layer of carbon to prevent charging during analysis (*e.g.* Pollard *et al.* 2007: 111), and analysed under a high vacuum using SEM-EDS under the same conditions as for polished samples (see this chapter, section 2.3.1.2). The stage was adjusted to provide a 35mm working distance in the chamber, as for polished samples. Three analyses were obtained from each sample and an average taken from these to improve reliability. The SEM was calibrated against metallic cobalt wire, a small piece of which was attached to one of the stubs, to correct for instrumental drift.

2.2.1.2. Evaluation of Method and Results

In practice, the DIAM technique was less easy than anticipated. Glass is a very hard material, and it was very difficult to obtain large enough flakes for analysis; most of the material removed was fine and powdery. The majority of useful flakes were obtained from corners and edges, which were much easier to remove material from

than a flat surface. As a result, if this technique were to be used for the sampling of beads, the majority of which are spherical, the removal of material is likely to pose more of a problem. Furthermore, considerable force and pressure was necessary in order to successfully remove material by rasping; this would risk breakage given the fragility of many of the Eriswell beads.

The small size of the tesserae (similar to that of many of the beads), together with the small size of the files, meant that removing flakes of glass was particularly strenuous on the fingers, especially when taking into account the force required to remove usable flakes. It proved more controllable and far easier to rasp the tesserae along the file, as opposed to the file over the tessera, but it was difficult to hold such small objects steady without risking excessive damage to either the tesserae or the fingertips. This made it difficult to control the sample area; a means of holding the object steady (such as a small vice) would be necessary for maximum control, but would put the object at serious risk of breakage. Nevertheless, the extent of damage caused by the technique was minimal and relatively little sample preparation was necessary. However, the strain on the fingers, whilst bearable for a relatively small sample set of 20 or 30 beads, is not for an assemblage as large as that from Eriswell.

Several problems also surfaced during analysis. Because of the irregular nature and topography of the flakes, it was impossible to uniformly and evenly coat them with carbon. The coating was very flaky, and as a result localised areas of charging were numerous. This meant that it was impossible to obtain any useful images of the microstructure of the glasses using backscattered electron imaging. This was particularly problematic in the identification of opacifying crystals in opaque samples, as spot analysis was not possible. Furthermore, the nature of the flakes taken meant that they had a very irregular topography and varied in orientation, and it proved difficult to locate a relatively flat surface suitable for area analysis; this is necessary to avoid x-ray signals being deflected away from the detector (Pollard *et al.* 2007: 113). This affected element oxide totals; in many cases the total of measured oxides varied considerably from 100 wt%, but this was corrected by normalising the results to 100%.

Table 2.2.2 – SEM-EDS area analyses of Early Byzantine glass tesserae (Caesarea, Israel) acquired from polished samples, compared to those acquired from flakes obtained using the DIAM technique.

Sample	Description ¹	Oxide (wt%) ²																		
		Na ₂ O	MgO	Al ₂ O ₃	SiO ₂	P ₂ O ₅	SO ₃	Cl	K ₂ O	CaO	TiO ₂	MnO	Fe ₂ O ₃	CoO	CuO	ZnO	SnO ₂	Sb ₂ O ₃	BaO	PbO
CES P1 D	Polished	14.93	0.37	2.34	61.49	b.d.	0.42	0.80	0.67	7.35	b.d.	b.d.	0.65	b.d.	1.04	b.d.	b.d.	0.81	b.d.	8.58
	DIAM	18.54	0.60	2.65	60.17	0.22	0.51	0.77	0.55	5.97	b.d.	b.d.	0.58	b.d.	0.73	b.d.	b.d.	0.47	0.13	7.79
	SD	2.55	0.16	0.22	0.93	-	0.06	0.02	0.08	0.98	-	-	0.05	-	0.22	-	-	0.24	-	0.56
CES P1 E (1)	Polished	15.18	0.47	2.19	60.80	b.d.	0.41	0.71	0.71	7.41	0.10	0.22	1.17	b.d.	3.75	b.d.	0.52	0.37	b.d.	5.92
	DIAM	17.35	0.56	2.33	60.40	0.17	0.40	0.67	0.60	6.69	b.d.	0.14	1.03	b.d.	3.46	b.d.	0.36	b.d.	b.d.	5.54
	SD	1.53	0.06	0.10	0.28	-	0.01	0.03	0.08	0.51	-	0.06	0.10	-	0.21	-	0.11	-	-	0.27
CES P1 E (2)	Polished	15.02	0.29	2.37	61.50	0.11	1.02	0.46	0.69	7.50	b.d.	b.d.	0.71	b.d.	0.35	b.d.	b.d.	0.92	b.d.	8.39
	DIAM	14.28	0.43	2.43	57.27	b.d.	1.00	0.85	0.63	6.69	b.d.	b.d.	0.87	b.d.	0.30	b.d.	0.42	2.40	b.d.	12.47
	SD	0.52	0.10	0.04	2.99	-	0.01	0.28	0.04	0.57	-	-	0.11	-	0.04	-	-	1.05	-	2.88
Bull H (1)	Polished	14.30	0.74	2.78	68.84	0.19	b.d.	0.85	1.07	8.49	b.d.	0.49	1.16	b.d.	0.67	b.d.	b.d.	b.d.	0.11	b.d.
	DIAM	15.83	0.81	2.96	68.29	0.22	0.18	0.83	0.96	7.82	0.12	0.50	1.05	b.d.	0.23	b.d.	b.d.	b.d.	b.d.	b.d.
	SD	1.08	0.05	0.13	0.39	0.02	-	0.01	0.08	0.47	-	0.01	0.08	-	0.31	-	-	-	-	-
Bull L1	Polished	19.30	1.05	2.52	63.37	0.17	0.45	0.88	0.73	7.70	0.13	1.94	1.03	b.d.	0.46	b.d.	b.d.	b.d.	b.d.	b.d.
	DIAM	18.00	0.93	2.38	63.74	0.17	0.58	0.91	0.80	8.34	0.16	2.48	1.25	b.d.	0.25	b.d.	b.d.	b.d.	b.d.	b.d.
	SD	0.92	0.08	0.10	0.26	0.00	0.09	0.02	0.05	0.45	0.02	0.38	0.16	-	0.15	-	-	-	-	-
Bull yellow	Polished	12.14	0.64	2.34	58.31	0.12	0.16	0.81	0.89	7.15	0.10	0.50	0.58	b.d.	0.54	0.12	1.54	b.d.	b.d.	14.21
	DIAM	12.15	0.62	2.36	58.46	0.17	b.d.	0.89	0.82	7.46	b.d.	0.46	0.44	b.d.	0.42	b.d.	1.16	b.d.	b.d.	15.00
	SD	0.01	0.01	0.01	0.11	0.04	-	0.06	0.05	0.22	-	0.03	0.10	-	0.08	-	0.27	-	-	0.56

¹Polished = results acquired from polished samples (taken from Table 2.2.1). DIAM = results acquired from flakes obtained using the DIAM technique (see text for details). SD = standard deviation.

²Results normalised to 100%. b.d. = below detection. The results are an average of three analyses. Detection limits were thought to be about 0.2% for most elements, although this is marginally higher for lead and tin at about 0.25-0.3%, and approximately 0.4% for antimony.

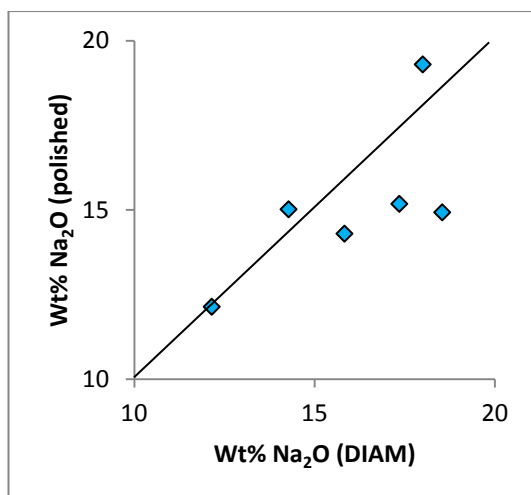


Figure 2.2.1 – A plot of soda (DIAM) versus soda (SEM-EDS) for Early Byzantine tesserae from Caesarea (Israel).

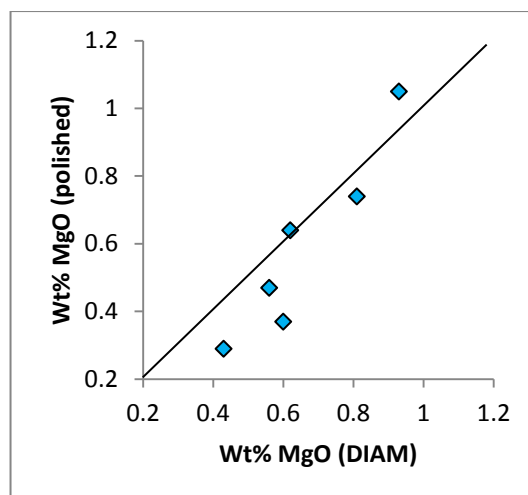


Figure 2.2.2 – A plot of magnesia (DIAM) versus magnesia (SEM-EDS) for Early Byzantine tesserae from Caesarea (Israel).

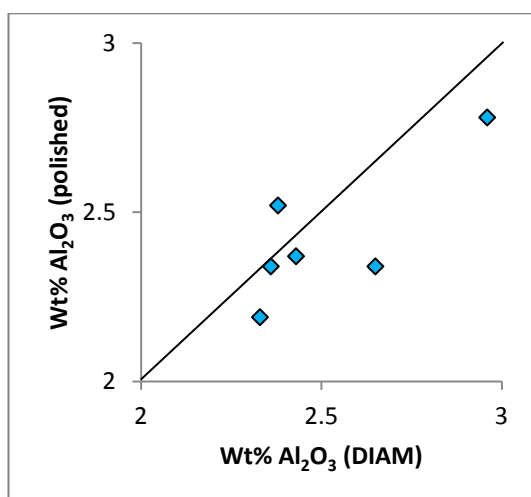


Figure 2.2.3 – A plot of alumina (DIAM) versus alumina (SEM-EDS) for Early Byzantine tesserae from Caesarea (Israel).

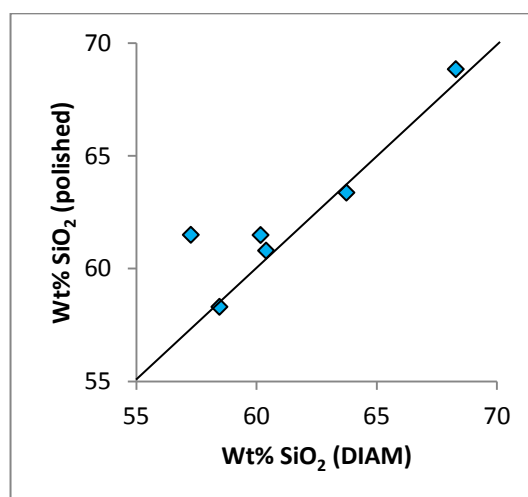


Figure 2.2.4 – A plot of silica (DIAM) versus silica (SEM-EDS) for Early Byzantine tesserae from Caesarea (Israel).

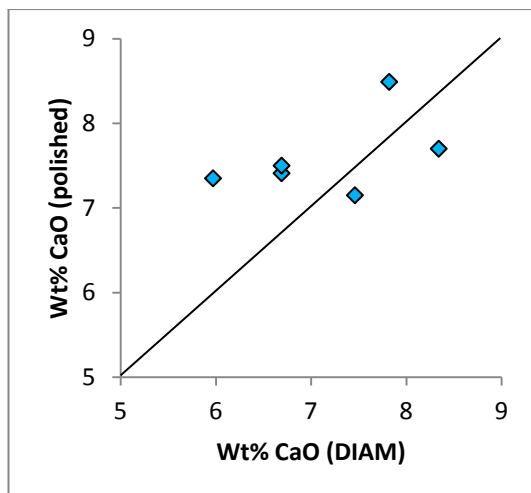


Figure 2.2.5 – A plot of lime (DIAM) versus soda (SEM-EDS) for Early Byzantine tesserae from Caesarea (Israel).

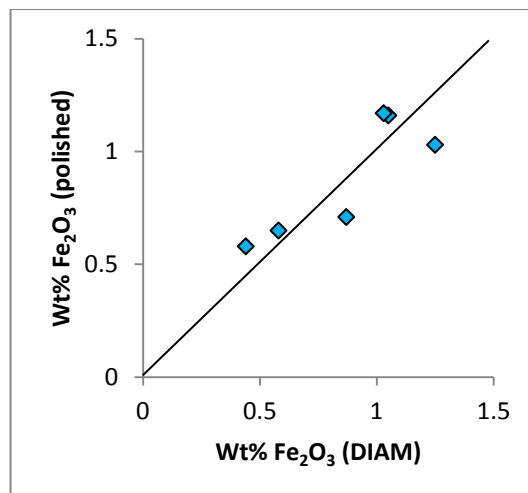


Figure 2.2.6 – A plot of iron oxide (DIAM) versus soda (SEM-EDS) for Early Byzantine tesserae from Caesarea (Israel).

In spite of the aforementioned problems, some fairly reliable quantitative analyses were obtained (Table 2.2.2). The majority of the results obtained match those obtained from polished samples relatively closely (Figures 2.2.1-2.2.6). However, the results for lime (Figure 2.2.5) and soda (Figure 2.2.1) are more variable. CaO is approximately 1% lower than was detected in the polished samples, but Na₂O is around 3% higher. This is quite unusual; if weathering products had inadvertently been incorporated into samples obtained using the DIAM technique one would expect soda levels to be lower than that detected in polished samples, but this is clearly not the case. It is possible that variations in lime and soda result from the heterogeneity of the glass, but it cannot be ruled out that this results from inconsistency in the accuracy or reproducibility of results (*i.e.* precision). This may have resulted, for example, from variations in the orientation of the flakes analysed.

2.2.2. Environmental Scanning Electron Microscopy (ESEM)

Within Cardiff University analysis of archaeological objects is usually only undertaken in the SEM under an environmental vacuum when a sample cannot be taken, or when only a semi-quantitative compositional analysis will suffice (*e.g.* for materials identification). Environmental scanning electron microscopy with energy-dispersive x-ray analysis (here termed ESEM-EDS) differs from conventional scanning electron microscopy (SEM-EDS) in that the specimen chamber is filled with gas, as opposed to being under a vacuum (Carlton *et al.* 2004a: 167). The presence of gas in the chamber prevents the sample from charging, thereby eliminating the need for a conductive coating (in this case carbon) on non-conductive samples, and amplifies secondary electrons for image generation (Carlton *et al.* 2004a: 167). However, the use of ESEM results in electron scatter and a much larger electron beam size than high-vacuum SEM-EDS, because of the interaction of the beam with gas molecules (Carlton *et al.* 2004a: 167). This is a problem for quantitative EDS analysis, as the larger beam size makes the analyses far more unreliable due to the problems of focussing the beam on the area of interest; this generates x-ray signals many microns from the target area (an ‘electron skirt’) (Carlton *et al.* 2004a: 167).

Given the problems with precision and accuracy in comparison to results obtained by SEM-EDS under high vacuum, analyses are generally assumed to be semi-quantitative. However, the extent of the reliability of results obtained by ESEM-EDS is unclear. Many correction methods have been proposed to account for electron beam scatter, but relatively few have been thoroughly tested (Carlton *et al.* 2004a: 167). Previous work has demonstrated that it is possible to achieve quantitative analyses with good accuracy and precision using ESEM, but suggests that in order to do this it is necessary to reduce surface charging effects and to use samples larger than the ‘electron skirt’ in order to reduce its influence (Carlton *et al.* 2004a; 2004b). Through the analysis of several of the tesserae from Caesarea by ESEM-EDS, it was hoped that the reliability of analyses obtained using ESEM-EDS could be gauged.

2.2.2.1. Sample Preparation and Analytical Procedure

As long as the object will fit within the chamber of the SEM, as is the case with glass tesserae and beads, samples do not need to be taken. Whilst it is not essential that the surface of the object is polished flat for analysis, it is preferable that the surface is as level as possible to avoid x-ray signals being deflected away from the detector (Pollard *et al.* 2007: 113). The outer surface of the glass must be removed prior to analysis in order to ensure that any weathered, or otherwise contaminated, glass is removed. The problems encountered in the reliability of analyses acquired by non-destructive surface analysis of glass beads, in which weathered glass is not removed, is particularly well illustrated in Martin Heck's thesis, which focused on the compositional analysis of Merovingian glass beads by non-destructive x-ray fluorescence (XRF) (Heck 2000; Heck and Hoffmann 2000: 343-350; Heck and Hoffmann 2002: 72).



Figure 2.2.7 – A photograph showing fragments of Early Byzantine glass tesserae from Caesarea, Israel, mounted on the SEM stage (approximately 6cm in diameter) for analysis by environmental scanning electron microscopy (ESEM-EDS).

Weathered glass can be carefully removed by polishing part of the outer surface of the object using fine grade (4000 grit) silicon carbide grinding papers, with water as a lubricant. Whilst this can be done manually on a bench, it was in fact easiest to use a polishing machine at the slowest speed setting (50 rpm), holding the object with tweezers or the fingers. The use of a small amount of abrasive diamond paste applied using a cotton swab was also tested, but proved ineffective. However, the use of pastes such as this should be avoided as the residue can be difficult to remove.

As a result, ESEM-EDS has an element of destructiveness, leaving a relatively inconspicuous 'polished' area on the surface of the object. In the present study, the fresh glass exposed after the acquisition of samples for polishing were analysed where possible, negating the removal of weathered glass. As the environment within the chamber is gaseous, the samples did not need to be carbon-coated. Each sample was securely adhered to the stage of the SEM using carbon putty, ensuring that they were as level as possible and at the object surfaces at approximately equal height relative to one another (Figure 2.2.7). The stage was adjusted to provide a 35mm working distance in the chamber, as for the polished samples. Three analyses were obtained from each sample and an average taken from these to improve reliability. The SEM was calibrated against metallic cobalt wire, a small fragment of which was attached to the stage using carbon putty, to correct for instrumental drift.

2.2.2.2. Evaluation of Method and Results

Whilst the need for taking and preparing samples is avoided in ESEM-EDS, a certain degree of surface preparation is necessary in order to remove weathered glass prior to analysis. This can prove fairly difficult, and risk damage to the object. The size and location of the area from which weathered glass was removed was fairly easily controlled. Furthermore, it is possible to analyse polychrome decoration, for example in the form of spots or trails, which could not otherwise be sampled. However, it is not possible to examine the internal microstructure of the glass due to the non-destructive nature of the technique.

Table 2.2.3 – SEM-EDS area analyses of Early Byzantine glass tesserae (Caesarea, Israel) acquired from polished samples, compared to those acquired directly from the tesserae by ESEM-EDS.

Sample	Description ¹	Oxide (wt%) ²																		
		Na ₂ O	MgO	Al ₂ O ₃	SiO ₂	P ₂ O ₅	SO ₃	Cl	K ₂ O	CaO	TiO ₂	MnO	Fe ₂ O ₃	CoO	CuO	ZnO	SnO ₂	Sb ₂ O ₃	BaO	PbO
CES P1 D	Polished	14.93	0.37	2.34	61.49	b.d.	0.42	0.80	0.67	7.35	b.d.	b.d.	0.65	b.d.	1.04	b.d.	0.29	0.81	b.d.	8.58
	ESEM	15.07	0.42	2.44	60.89	b.d.	0.68	0.87	0.73	7.17	0.10	b.d.	0.78	b.d.	0.60	b.d.	0.58	1.18	0.19	8.45
	SD	0.10	0.04	0.07	0.42	-	0.18	0.05	0.04	0.13	-	-	0.09	-	0.31	-	0.21	0.26	-	0.09
CES P1 E (1)	Polished	15.18	0.47	2.19	60.80	b.d.	0.41	0.71	0.71	7.41	0.10	0.22	1.17	b.d.	3.75	b.d.	0.52	0.37	b.d.	5.92
	ESEM	13.96	0.50	2.31	58.80	b.d.	0.60	0.73	0.85	7.70	0.15	b.d.	1.31	b.d.	3.46	0.11	1.30	2.24	0.11	5.74
	SD	0.86	0.02	0.08	1.41	-	0.13	0.01	0.10	0.21	0.04	-	0.10	-	0.21	-	0.55	1.32	-	0.13
CES P1 F	Polished	14.99	0.65	2.96	66.15	0.87	0.19	0.78	0.87	10.68	b.d.	0.27	0.43	b.d.	0.32	b.d.	0.35	0.42	0.10	b.d.
	ESEM	15.02	0.81	3.31	65.32	1.24	0.18	0.80	0.88	10.70	0.16	0.27	0.43	0.14	b.d.	b.d.	b.d.	0.48	b.d.	b.d.
	SD	0.02	0.11	0.25	0.59	0.26	0.01	0.01	0.01	0.01	-	0.00	0.00	-	-	-	-	0.04	-	-
Bull A1	Polished	14.46	0.78	2.82	68.81	0.33	0.10	0.87	1.00	8.63	0.16	0.61	0.95	b.d.	0.39	b.d.	b.d.	b.d.	b.d.	b.d.
	ESEM	15.19	0.64	3.02	69.12	0.54	0.24	0.83	0.92	8.86	b.d.	0.58	0.76	b.d.	b.d.	0.11	b.d.	b.d.	0.14	b.d.
	SD	0.52	0.10	0.14	0.22	0.15	0.10	0.03	0.06	0.16	-	0.02	0.13	-	-	0.04	-	-	-	-
Bull A2 (1)	Polished	14.14	0.75	2.76	68.21	0.24	0.19	0.88	1.00	8.57	b.d.	0.38	0.53	b.d.	1.73	b.d.	b.d.	b.d.	0.13	b.d.
	ESEM	13.97	0.75	3.23	68.52	b.d.	b.d.	0.83	1.07	9.05	b.d.	0.60	0.57	b.d.	1.75	0.16	b.d.	b.d.	b.d.	b.d.
	SD	0.12	0.00	0.33	0.22	-	-	0.04	0.05	0.34	-	0.16	0.03	-	0.01	-	-	-	-	-
Bull A2 (2)	Polished	14.12	0.64	2.96	66.70	1.66	b.d.	0.52	0.86	10.07	b.d.	0.43	0.65	0.10	0.19	0.37	b.d.	b.d.	0.28	b.d.
	ESEM	14.93	1.11	2.94	68.22	0.44	0.30	1.32	0.97	8.61	b.d.	0.57	0.80	b.d.	b.d.	0.10	b.d.	b.d.	b.d.	b.d.
	SD	0.57	0.33	0.01	1.07	0.86	-	0.57	0.08	1.03	-	0.10	0.11	-	-	0.19	-	-	-	-
Bull F (1)	Polished	13.51	0.58	2.37	57.66	b.d.	0.32	0.88	0.74	7.67	b.d.	0.35	0.34	b.d.	0.96	b.d.	1.54	b.d.	0.11	12.53
	ESEM	12.91	0.61	2.60	55.58	0.28	b.d.	0.91	0.85	7.74	0.14	0.48	0.64	b.d.	0.19	b.d.	1.78	b.d.	b.d.	16.12
	SD	0.42	0.02	0.16	1.47	-	-	0.02	0.08	0.05	-	0.09	0.21	-	0.54	-	0.17	-	-	2.54

Table 2.2.3 - (continued).

Sample	Description ¹	Oxide (wt%) ²																		
		Na ₂ O	MgO	Al ₂ O ₃	SiO ₂	P ₂ O ₅	SO ₃	Cl	K ₂ O	CaO	TiO ₂	MnO	Fe ₂ O ₃	CoO	CuO	ZnO	SnO ₂	Sb ₂ O ₃	BaO	PbO
Bull H (1)	Polished	14.30	0.74	2.78	68.84	0.19	b.d.	0.85	1.07	8.49	b.d.	0.49	1.16	b.d.	0.67	b.d.	b.d.	b.d.	0.11	b.d.
	ESEM	15.23	0.83	2.81	69.35	0.14	b.d.	0.84	0.94	8.19	b.d.	0.48	1.18	b.d.	0.10	0.11	b.d.	b.d.	0.10	0.32
	SD	0.66	0.06	0.02	0.36	0.04	-	0.01	0.09	0.21	-	0.01	0.01	-	0.40	-	-	-	0.01	-
Bull H (2)	Polished	13.15	0.69	2.62	64.47	0.22	0.19	0.83	1.04	8.17	0.10	0.65	0.52	b.d.	1.50	b.d.	0.69	b.d.	b.d.	5.11
	ESEM	13.39	0.70	2.68	66.20	0.04	b.d.	0.84	1.13	8.40	0.28	0.70	0.63	b.d.	1.27	b.d.	0.55	b.d.	b.d.	4.71
	SD	0.17	0.01	0.04	1.22	0.13	-	0.01	0.06	0.16	0.13	0.04	0.08	-	0.16	-	0.10	-	-	0.28
Bull H (3)	Polished	13.19	0.70	2.30	55.59	0.13	0.16	1.06	0.75	7.93	b.d.	0.41	0.51	b.d.	1.24	b.d.	1.08	b.d.	b.d.	14.97
	ESEM	11.21	0.71	2.31	53.91	0.13	0.94	1.15	0.78	8.69	b.d.	0.45	0.60	b.d.	0.98	b.d.	1.24	b.d.	b.d.	17.58
	SD	1.40	0.01	0.01	1.19	0.00	0.55	0.06	0.02	0.54	-	0.03	0.06	-	0.18	-	0.11	-	-	1.85
Bull H (4)	Polished	18.46	1.05	2.17	64.50	0.12	0.46	0.96	0.73	8.00	0.16	1.84	0.90	b.d.	0.49	b.d.	b.d.	b.d.	b.d.	b.d.
	ESEM	19.33	1.22	2.19	64.85	0.18	0.40	0.94	0.72	7.74	0.10	1.70	0.85	b.d.	b.d.	b.d.	b.d.	b.d.	b.d.	b.d.
	SD	0.62	0.12	0.01	0.25	0.04	0.04	0.01	0.01	0.18	0.04	0.10	0.04	-	-	-	-	-	-	-
Bull L1	Polished	19.30	1.05	2.52	63.37	0.17	0.45	0.88	0.73	7.70	0.13	1.94	1.03	b.d.	0.46	b.d.	b.d.	b.d.	b.d.	b.d.
	ESEM	19.48	1.05	2.76	63.28	0.02	0.36	0.94	0.76	8.29	0.24	2.26	1.12	b.d.	b.d.	b.d.	b.d.	b.d.	b.d.	b.d.
	SD	0.13	0.00	0.17	0.06	0.11	0.06	0.04	0.02	0.42	0.08	0.23	0.06	-	-	-	-	-	-	-

¹Polished = results acquired from polished samples (taken from Table 2.2.1). ESEM = results acquired using environmental scanning electron microscopy (see text for details). SD = standard deviation.

²Results normalised to 100%. b.d. = below detection. The results are an average of three analyses. Detection limits were thought to be about 0.2% for most elements, although this is marginally higher for lead and tin at about 0.25-0.3%, and approximately 0.4% for antimony.

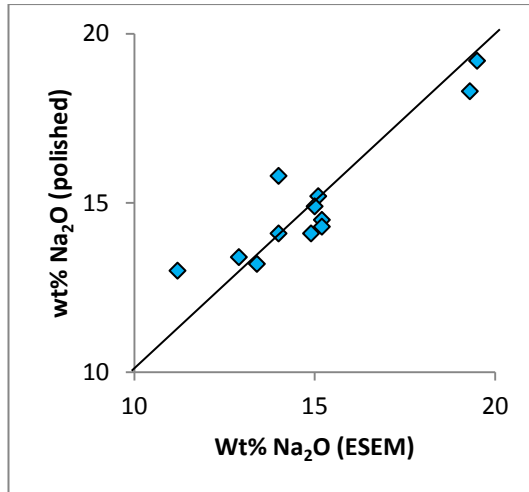


Figure 2.2.8 – A plot of soda (ESEM-EDS) versus soda (SEM-EDS) for Early Byzantine tesserae from Caesarea (Israel).

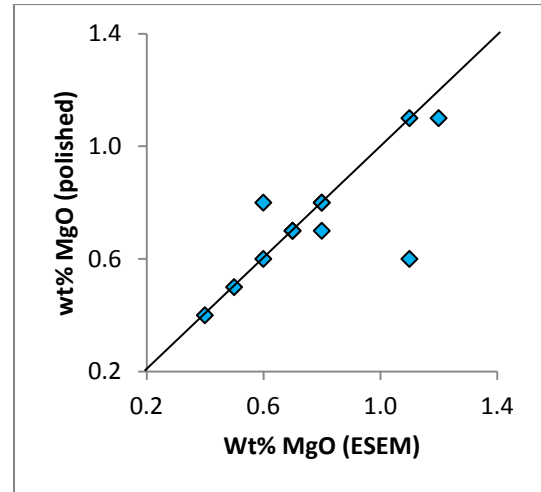


Figure 2.2.9 – A plot of magnesia (ESEM-EDS) versus soda (SEM-EDS) for Early Byzantine tesserae from Caesarea (Israel).

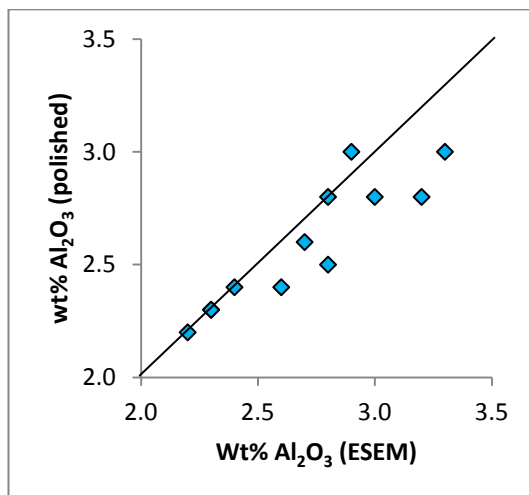


Figure 2.2.10 – A plot of alumina (ESEM-EDS) versus soda (SEM-EDS) for Early Byzantine tesserae from Caesarea (Israel).

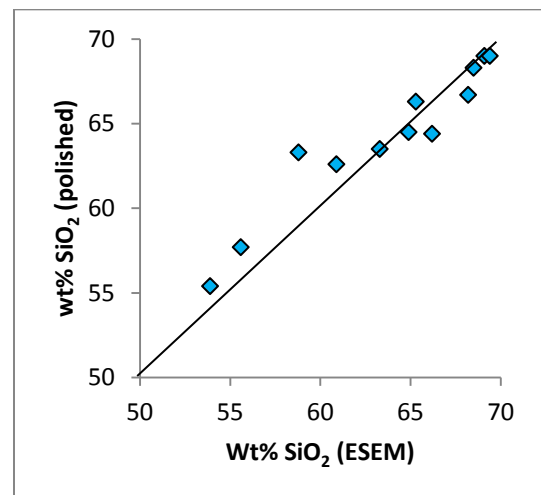


Figure 2.2.11 – A plot of silica (ESEM-EDS) versus soda (SEM-EDS) for Early Byzantine tesserae from Caesarea (Israel).

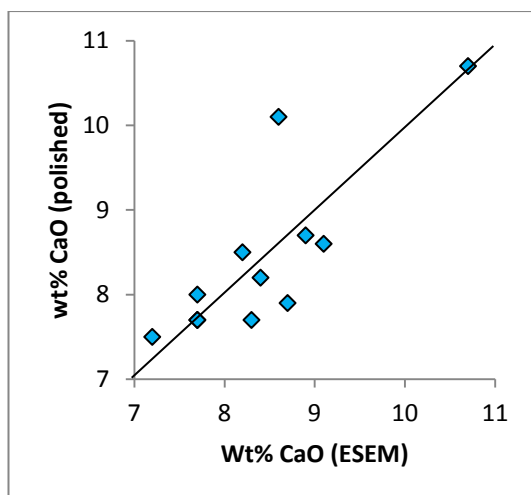


Figure 2.2.12 – A plot of lime (ESEM-EDS) versus soda (SEM-EDS) for Early Byzantine tesserae from Caesarea (Israel).

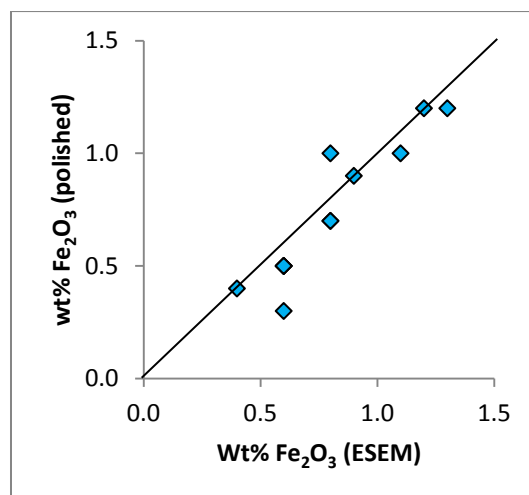


Figure 2.2.13 – A plot of iron oxide (ESEM-EDS) versus soda (SEM-EDS) for Early Byzantine tesserae from Caesarea (Israel).

Some fairly reliable quantitative analyses were obtained (Table 2.2.3), which appear to be slightly more reliable than those obtained using the DIAM technique (Table 2.2.2). The majority of the results match those obtained from polished samples quite closely (Figures 2.2.8-2.2.13), although there is some variability, particularly for lime (Figure 2.2.12) and alumina (Figure 2.2.10). As many of the samples are opaque and relatively heterogeneous, some variability may be expected; this may have resulted from the scattering of electrons by the presence of gas in the chamber.

2.2.3. Summary

Both the DIAM technique and ESEM-EDS produced relatively promising results, although the reproducibility of the analyses is reduced. Nevertheless, accuracy and precision are still reasonably good providing an average of several analyses is taken from each sample. Bronk and Freestone (2001: 525) recommend that up to ten analyses are obtained from different flakes of glass in order to reduce errors for the DIAM technique. However, this will significantly increase the time required for analysis. Whilst most of the results prove promising, there appears to be considerable variation in the levels of some components (most notably soda and lime) in some

samples, particularly if they are present in minor amounts. The variation observed does not appear to be consistent and, whilst it is possible that an average taken from more analyses may correct for this, it is more likely that the results obtained by these techniques are not consistently reliable.

The theory behind the method of sampling for the DIAM technique is sound, but in practice it is difficult to implement, time consuming, labour intensive and places those objects which are particularly small or fragile at risk of excessive damage. Whilst the corroded surface layer of glass also needs to be removed prior to ESEM-EDS analysis, this proved relatively straightforward. Furthermore, the examination of decorative trails and spots which are otherwise inaccessible for sampling is possible using this technique. However, all of the tests were undertaken on monochrome tesserae, and the ‘electron skirt’ phenomenon (*e.g.* Carlton *et al.* 2004a; 2004b) may prove more of a problem in the analysis of polychrome samples when x-ray signals generated by adjacent glass colours may be compromise the analyses.

Finally, it was not possible to examine the microstructure of the glasses using either the DIAM technique or ESEM, which means that opacifying compounds and other inclusions could not be confidently identified. Much can be learnt from the technology of early glass from its microstructure, as has been evidenced by previous studies of early medieval glass beads (*e.g.* Mortimer 1996a; 1996b; Mortimer and Heyworth 2009; Heck 2000; Heck and Hoffmann 2002), so the analysis of polished samples by SEM-EDS is therefore preferable over non-destructive analysis. It must also be stressed that quantitative analysis by SEM-EDS under a high vacuum will always produce better results than under an environmental vacuum (Newbury 2002: 576). The use of techniques in which the accuracy, precision or reliability of the data obtained is questionable, as is the case here, will compromise the results of the project. The analysis of polished resin-mounted samples by SEM-EDS will therefore provide the most reliable data, and can potentially provide much more technological information through facilitating the examination of the internal microstructure of the glass.

2.3. Analytical Techniques Employed

Major elements were analysed for by energy-dispersive x-ray analysis in the scanning electron microscope (SEM-EDS) and trace elements by laser ablation inductively coupled plasma mass spectrometry (LA-ICP-MS).

2.3.1. Scanning Electron Microscopy (SEM)

Scanning electron microscopy with energy-dispersive x-ray analysis (SEM-EDS) has become one of the standard methods for the analysis of early glass. The advantages of the technique include speed of analysis, the need for relatively small samples which are not destroyed, the ability to analyse different phases and inclusions within a glass, and the high degree of accuracy that can be obtained. However, in the characterisation of ancient glasses, SEM-EDS has a number of limitations in that the detection limits of the equipment are often too high to be able to accurately determine the concentration of elements present at trace levels; these can be particularly valuable in the characterisation of early glass. It is therefore necessary to complement major element analysis with trace element analysis (*e.g.* LA-ICP-MS, see this chapter, section 2.3.2).

The imaging capabilities of the SEM (see this chapter, section 2.3.1.2) allow the internal microstructure of samples to be clearly observed. This is useful for differentiating between weathered and unweathered glass, as well as the identification of inclusions. It also means that the area(s) of a glass subjected to analysis can be selected so as to avoid heterogeneous regions which may produce spurious results. Furthermore, whilst the sampling process is semi-destructive, the samples are not destroyed and can be re-analysed in the future.

A detailed discussion of the principles of scanning electron microscopy and energy-dispersive x-ray analysis is not within the scope of this study, but the reader is referred to any good textbook on the subject (*e.g.* Pollard *et al.* 2007; Goldstein *et al.*

2003) or to Freestone (1985). A list of the elements and element oxides determined by SEM-EDS in the present study is given in Table 2.3.1.

Table 2.3.1 – Elements and element oxides measured by SEM-EDS in the present study.

<i>Element</i>	<i>Element oxide</i>	<i>Formula</i>	<i>Element</i>	<i>Element oxide</i>	<i>Formula</i>
Sodium	Soda	Na ₂ O	Iron	Iron oxide	Fe ₂ O ₃
Magnesium	Magnesia	MgO	Cobalt	Cobalt oxide	CoO
Aluminium	Alumina	Al ₂ O ₃	Nickel	Nickel oxide	NiO
Silicon	Silica	SiO ₂	Copper	Copper oxide	CuO
Phosphorous	Phosphate	P ₂ O ₅	Zinc	Zinc oxide	ZnO
Sulphur	Sulphate	SO ₃	Arsenic	Arsenic oxide	As ₂ O ₃
Chlorine	-	Cl	Tin	Tin oxide	SnO ₂
Potassium	Potash	K ₂ O	Antimony	Antimony oxide	Sb ₂ O ₃
Calcium	Lime	CaO	Barium	Barium oxide	BaO
Titanium	Titanium oxide	TiO ₂	Lead	Lead oxide	PbO
Manganese	Manganese oxide	MnO			

2.3.1.1. Sample Preparation

Samples of 1-3mm in size were removed from each of the beads. Several methods are employed for the removal of samples: samples can be removed from many glass objects by scoring an edge with a tungsten carbide stylus and breaking away a small fragment with a pair of snub-nosed pliers. Alternatively, a small sample can be cut away with a rotary diamond wheel. Breaking away a fragment is preferred, due to the excessive loss of material as fine powder when using a diamond wheel. However, the scoring method is not practical for beads. Instead, the best method for sample removal proved to be pressure flaking using a tungsten carbide stylus; the bead was placed on its side and a small amount of pressure applied to the inner edge of the bead (just inside the perforation) using the tip of the stylus to remove a small flake of glass. Each bead was held inside a large transparent polythene bag to prevent the sample from being lost. Decorative trails and spots could also be sampled using this method as the glass frequently contained surface pits; the tip of the stylus

was placed within the pit, and a small amount of pressure applied to remove a flake in a similar way.

Whilst this method of sampling is not easily controlled and can very occasionally cause breakage, the majority of the beads were fairly resilient and the damage caused was nonetheless far less extensive than that caused by traditional methods of sampling; if done carefully, this did not place the beads at much greater risk of breakage.

The samples were mounted in epoxy resin blocks of 3cm in diameter as follows. Traditionally, each sample is adhered to the plastic base of a mould using Araldite™ 5-minute epoxy resin prior to setting in resin. However, due to the small nature of the samples, this was not practical as the samples would not stand on end; this would risk their loss during the polishing process. A new method was devised for the mounting of such small samples. The plastic base of the mould was covered with double-sided tape, and each sample adhered to this using tweezers. The sample number, colour and location on the plastic base were noted on a plan so that each could be identified. To avoid the samples being dislodged when resin was poured into the mould, a small spot of Araldite™ 5-minute epoxy was dabbed next to each sample using a needle or cocktail stick to secure them in place; their adhesion to the double-sided tape in this way fixed them in place (Figures 2.3.1 and 2.3.2).



Figure 2.3.1 – A photograph showing glass samples from Eriswell mounted on 3cm resin block mould bases using double-sided tape and Araldite™ 5-minute epoxy resin.

A soda-lime-silica glass standard was included in each block (either Corning A or Corning B, which were alternated between blocks). A small piece of cobalt wire was also included to calibrate the SEM between analyses, by correcting instrumental drift. The glass standard was orientated perpendicularly to the edge of the sample block to provide a ‘north point’, by which the orientation of the sample block in the SEM could be gauged (Figure 2.3.3).



Figure 2.3.2 – A photograph showing glass samples from Eriswell mounted on a 3cm resin block mould base using double-sided tape and Araldite™ 5-minute epoxy resin. Note the larger dark blue glass standard (Corning A) at the top of the image, which is orientated so as to provide a ‘north point’.

The mould was then filled with a slow-setting epoxy resin (EpoFix™), and any bubbles dislodged using a needle underneath a light microscope. It was allowed to set before the block was removed from the mould. Each resin block was polished flat (Figure 2.3.3) to expose the glass samples using a series of graded silicon carbide polishing papers (up to 4000 grit), using water as a lubricant. Polishing provides a flat surface with a known x-ray take-off angle, so that standard correction procedures can be applied to the analytical data (Bronk and Freestone 2001: 517). Each block was photographed to allow each sample to be labelled for ease of identification during SEM analysis, prior to vacuum-coating with a thin layer of carbon to prevent

charging during analysis. The labelled photographs of these sample blocks are shown in Appendix E.



Figure 2.3.3 – A photograph showing a polished sample block containing glass samples from Eriswell. Note the larger dark blue glass standard (Corning A) at the top of the image, which is orientated so as to provide a ‘north point’. Resin block is approximately 3cm in diameter.

2.3.1.2. Analytical Procedure

The sample blocks were placed in a holder and mounted in the SEM (Figure 2.3.4), thus ensuring that all samples were maintained at a standard angle and distance from the electron beam and sensor. Major and minor elements were analysed for by energy-dispersive x-ray analysis in a CamScan Maxim scanning electron microscope (SEM-EDS) at Cardiff University. An Oxford Instruments INCA energy-dispersive x-ray analyser was used, calibrated against pure elements, minerals and oxides. Operating conditions were a 20 kV accelerating potential and a 35° take-off angle, with a beam current adjusted to yield 4000 counts per second (cps) on metallic cobalt, for a counting live time of 200 seconds. Results were quantified using ZAF correction factors (atomic number [Z]; absorption [A]; fluorescence [F]). Prior to the analysis of each sample, the SEM was calibrated against cobalt wire to correct for

instrumental drift. The machine was left on for half an hour to warm up prior to beginning each session of analysis, which allowed the electron beam to stabilise.

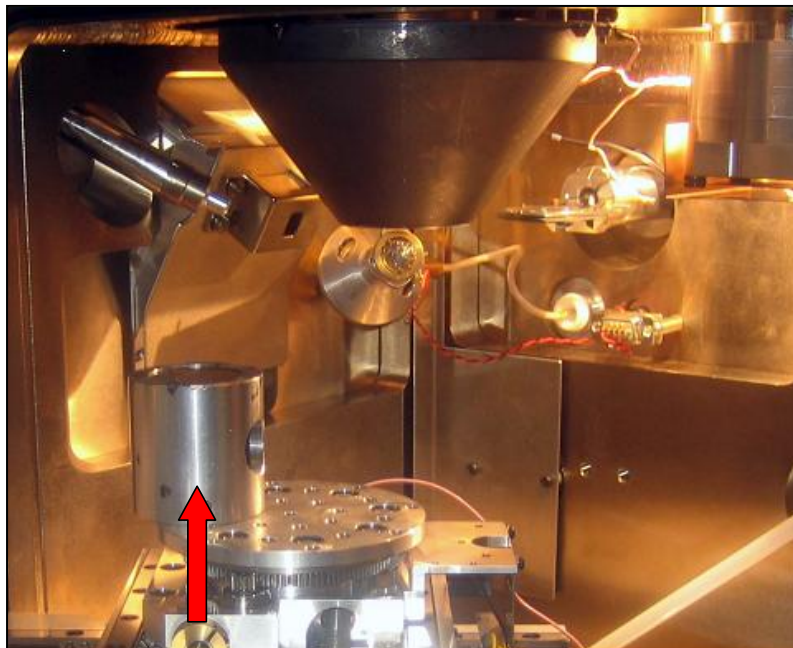


Figure 2.3.4 – A photograph showing a sample block mounted in the sample holder (shown by the red arrow) in the chamber of the scanning electron microscope ready for analysis.

As large an area of each sample as possible was analysed by rastering with a diffuse electron beam, avoiding any large inclusions or weathered glass, to ensure that the results were as representative as possible as lighter elements (*e.g.* sodium) have a tendency to migrate away from the beam. The errors associated with quantitative analysis may be reduced by taking repeat analyses; an average was therefore taken from a minimum of two analyses for translucent glasses, which were typically relatively homogeneous, and from a minimum of three analyses for opaque glasses, as these were typically much more heterogeneous in microstructure. The analyses, which totalled between 98% and 102%, were normalised to 100% to improve comparability. Any results which did not total $100 \pm 2\%$ were discarded and the sample re-analysed, following appropriate adjustments to the instrumental parameters where necessary.

Each of the glass samples was studied visually using backscattered electron imaging (BEI) and secondary electron imaging (SEI). Using BEI, the different components of the glasses can be distinguished by the atomic number of the elements present; elements with a higher atomic number, such as lead, appear brighter on the image than those with a lower atomic number, such as silicon (*e.g.* Mortimer 1996b: 2). This allowed a detailed examination of the microstructure of the samples analysed, including the identification of various inclusions such as opacifying compounds. These compositional differences sometimes appear quite large, but in many cases the brightness and contrast of these images have been altered to emphasise particular characteristics. Inclusions and opacifying crystals were identified by spot analysis; where inclusions were relatively large it was also possible to obtain analyses of their bulk composition.

Artificial glass standards Corning A and B, which are of known composition, were analysed to establish the precision and accuracy of the results (Table 2.3.2). Corning A and B were alternated in resin blocks and analysed three times at the beginning of each session of analysis, or after changing sample blocks in the SEM, and an average taken from these. If the results deviated unacceptably from the known values for these standards (Brill 1999: 539-544; Vicenzi *et al.* 2002), or the element oxide totals were outside 98-102%, the instrumental parameters were adjusted, or the SEM re-calibrated, until the results obtained from these standards were reliable. Detection limits were thought to be about 0.2% for most of the elements analysed, although this is marginally higher for lead, tin and antimony at about 0.25-0.3%. The values for CuO should be interpreted with some caution due to problems with contamination by copper during the carbon coating process. Whilst this is insignificant in the majority of cases, the presence of anything up to 0.3-0.4% CuO in some glasses (most notably opaque white, in which copper is typically absent) may reflect this.

Table 2.3.2 – SEM-EDS area analyses of Corning A and B glass standards.

Sample ¹	Oxide (wt%) ²																		
	Na ₂ O	MgO	Al ₂ O ₃	SiO ₂	P ₂ O ₅	SO ₃	Cl	K ₂ O	CaO	TiO ₂	MnO	Fe ₂ O ₃	CoO	CuO	ZnO	SnO ₂	Sb ₂ O ₃	BaO	PbO
Corning A (n = 24)																			
Minimum	13.65	2.48	0.88	66.26	0.09	0.14	0.07	2.88	4.77	0.75	0.99	1.03	0.12	1.21	b.d.	b.d.	1.31	0.38	b.d.
Maximum	14.79	2.72	1.06	67.36	0.24	0.27	0.12	3.03	5.19	0.93	1.11	1.17	0.23	1.64	0.11	0.43	1.97	0.62	b.d.
<i>Average</i>	14.21	2.58	0.93	66.75	0.17	0.20	0.10	2.97	5.00	0.85	1.05	1.10	0.18	1.34	b.d.	b.d.	1.70	0.48	b.d.
SD	0.26	0.05	0.05	0.30	0.04	0.04	0.02	0.04	0.08	0.05	0.03	0.03	0.03	0.12	-	-	0.18	0.07	0.07
Given composition	14.30	2.66	1.00	66.56	0.13	0.13	0.09	2.87	5.03	0.79	1.00	1.09	0.17	1.20	0.05	0.23	1.75	0.47	0.10
RSD	1.84	2.05	5.44	0.45	22.84	19.13	16.06	1.20	1.64	5.43	3.00	3.14	16.51	9.04	-	-	10.32	15.53	b.d.
RA	0.63	3.01	6.58	0.28	28.85	50.00	9.26	3.41	0.63	7.23	5.04	1.07	3.43	11.81	-	-	2.62	1.86	b.d.
Corning B (n = 21)																			
Minimum	16.57	0.95	4.05	61.05	0.80	0.57	0.15	0.99	8.37	0.03	0.16	0.30	b.d.	2.72	b.d.	b.d.	b.d.	b.d.	0.26
Maximum	17.28	1.11	4.21	62.38	0.97	0.72	0.21	1.11	8.85	0.16	0.29	0.41	0.11	3.29	0.34	0.32	0.84	0.18	0.58
<i>Average</i>	17.03	1.02	4.13	61.60	0.88	0.63	0.19	1.05	8.56	0.11	0.24	0.35	b.d.	2.92	0.21	b.d.	b.d.	b.d.	0.43
SD	0.19	0.04	0.04	0.35	0.05	0.04	0.02	0.03	0.10	0.04	0.03	0.03	-	0.12	0.06	-	-	-	0.08
Given composition	17.00	1.03	4.36	61.55	0.82	0.45	0.16	1.00	8.56	0.09	0.25	0.34	0.04	2.66	0.19	0.03	0.46	0.09	0.50
RSD	1.09	3.82	0.93	0.57	5.42	6.90	8.92	2.92	1.20	37.49	14.31	8.08	-	4.01	29.14	-	-	-	17.91
RA	0.17	1.39	5.31	0.08	7.08	39.05	17.86	4.81	0.05	16.93	4.00	2.94	-	9.94	9.52	-	-	-	14.00

¹Given compositions for Corning glass standards are taken from Brill (1999) and Vicenzi *et al.* (2002). SD = standard deviation; RSD = relative standard deviation; RA = relative accuracy.

²All results are normalised to 100%. b.d. = below detection. Detection limits were thought to be about 0.2% for most of the elements analysed, although this is marginally higher for lead and tin at about 0.25-0.3%, and approximately 0.4% for antimony.

The precision of repeat analyses is quantified using their standard deviation. The relative analytical precision is represented by the relative standard deviation (RSD) in Table 2.3.2. For major oxide components it was established as less than 4% for the majority of element oxides, but up to 10% for CuO and Sb₂O₃. For minor oxide components it was less than 20% for the majority of element oxides, but up to 30% for P₂O₅ and ZnO, and up to 40% for TiO₂. Precision is significantly reduced as the detection limits are reached (*i.e.* for elements in minor concentrations) due to an increase in analytical error (Freestone *et al.* 2002b: 260). The relative analytical accuracy is represented by the relative accuracy (RA) in Table 2.3.2. For major oxide components it was established as less than 5% for the majority of element oxides, but 12% for CuO. For minor oxide components it was less than 20% for the majority of element oxides, but nearly 30% for P₂O₅ and 50% for SO₃. As with precision, accuracy is significantly reduced as the detection limits are reached.

The oxides of nickel and arsenic were analysed for but not detected in any of the samples, so are not reported.

2.3.1.3. Presentation of Data

Data obtained by SEM-EDS are traditionally reported in tabular format in order of increasing atomic number as the elements appear in the Periodic Table. These are presented as element oxides in weight percent (wt %). The measured elemental data is calculated by stoichiometry, whereby wt % element concentrations are transformed into wt % oxides (based on their respective valencies) to account for oxygen in the glass, which cannot be accurately measured. All values were obtained to two decimal places. Traditionally, values below the detection limits of SEM-EDS are not reported, and are instead replaced with 'b.d.' (below detection) or 'n.d.' (not detected) (see Tables 2.2.1-2.2.3 and 2.3.1 for examples). However, this has proven far from satisfactory.

Detection limits are often assumed based on the analysis of glass standards (see this chapter, section 2.3.1.2). Whilst it is widely acknowledged that the reliability of

results decreases as the detection limits are approached, the detection limits depend upon the element in question, its concentration, and sometimes also its association with the other elements present. However, it has proven possible in the present study to establish meaningful compositional groups using elements in concentrations well below their assumed detection limits (*e.g.* lead and antimony). As such, it is best practice to report the *raw* values detected, alongside their uncertainty (Analytical Methods Committee 2001). Unfortunately negative values do occur, and it is not possible for an element to be present in amounts below absolute zero. However, “analytical results are not concentrations but error-prone estimates of concentrations”, so by removing them we are biasing the relative concentrations of the other elements present (Analytical Methods Committee 2001), especially as the results are typically normalised to 100% after doing so.

The raw data are therefore reported in Appendices F-I in the format in which they were obtained; that is with values ‘below detection’ still in place (note that this includes negative values), given that the *exact* detection limits for each element are unknown and vary between samples. This way, the results are not biased for future comparisons. Conversely, the results are discussed with assumed detection limits in place, so that negative values are not reproduced in graphs.

Correlations are either *positive* or *negative* (if the correlation is not described as either, it should be assumed as positive). Where appropriate, the coefficient of determination (denoted by r^2) is given to assess the *degree* of linearity between two variables for a particular set of data. This varies between 0 and 1, and cannot be negative. The closer the r^2 value is to 1, the stronger the correlation; an r^2 value close to 0 indicates that there is no linear correlation. This value represents the square of the coefficient of correlation (denoted by r), which is a measure of the *strength* of the linear relationship between two variables (*i.e.* x and y). This varies between -1 and 1, where -1 indicates an absolute negative correlation, +1 indicates an absolute positive correlation, and 0 indicates no linear correlation. In the present study, a correlation in which $r^2 = <0.29$ is not interpreted as statistically significant. When $r^2 = 0.30-0.49$ a correlation is interpreted as *weak* and described as ‘weak positive/negative’. When $r^2 = 0.50-0.69$ it is interpreted as *fair* and described as ‘positive/negative’, and when $r^2 = >0.70$ it is interpreted as *strong* and described as ‘strong positive/negative’.

2.3.2. Laser Ablation Inductively Coupled Plasma Mass Spectrometry (LA-ICP-MS)

It is usually possible to establish broad compositional groups of glass, which may relate to date or provenance for example, based on major element data obtained by techniques such as SEM-EDS. However, trace elements can be crucial in differentiating between glasses which have a very similar overall composition, but were produced in different workshops. From this, it is sometimes possible to identify the potential provenance of a glass, which can provide indications as to how it may have been traded.

Trace element analysis has become increasingly popular in recent years owing to the increased availability of and improvements in analytical equipment, together with the potential to differentiate between products of different workshops and production zones (Dussubieux *et al.* 2009: 152-153). Its application to the study of early glass has been demonstrated by a number of recent studies (*e.g.* Bertini *et al.* 2011; Dussubieux *et al.* 2008; 2009; Robertshaw *et al.* 2003; 2010a; 2010b; Shortland *et al.* 2007). As such, it is a complementary technique to SEM-EDS, which can be used to refine the groups established from the relative concentrations of major and minor elements. It is particularly important in provenance studies, as trace element patterns can be compared and matched to those of well-contextualised glasses (Dussubieux *et al.* 2009: 152).

ICP-MS coupled with laser ablation offers a number of advantages in the study of early glass, including ease of sample preparation, high sample throughput, high spatial resolution and excellent sensitivity (Dussubieux *et al.* 2009: 152-153; Popelka *et al.* 2005: 87). It allows the determination of a range of elements in trace concentrations from lithium through to uranium. It is often considered to be a quasi non-destructive analytical technique, but it does in fact involve the destruction of a sample on a microscopic scale. However, the nature of the technique means that samples do not need to be taken or prepared in any way, and that whole objects can be analysed providing size is not a limitation. The advantage of LA-ICP-MS over standard ICP-MS is that the dissolution of solid samples is negated. One of the

limitations of the technique is that the concentration of one of the major elements present is usually requires as an internal standard; this must be accurately determined by a technique such as SEM-EDS. A detailed discussion of the principles behind LA-ICP-MS and its operation is not within the scope of this study, but the reader is invited to consult Gratuze *et al.* (2001) or any good textbook on analytical chemistry (*e.g.* Pollard *et al.* 2007).

Table 2.3.3 – Elements measured by LA-ICP-MS in the present study.

<i>Element</i>	<i>Symbol</i>	<i>Element</i>	<i>Symbol</i>
Magnesium	Mg	Barium	Ba
Potassium	K	Lanthanum	La
Titanium	Ti	Cerium	Ce
Vanadium	V	Praesodymium	Pr
Chromium	Cr	Neodymium	Nd
Manganese	Mn	Samarium	Sm
Iron	Fe	Europium	Eu
Cobalt	Co	Gadolinium	Gd
Nickel	Ni	Terbium	Tb
Copper	Cu	Dysprosium	Dy
Zinc	Zn	Holmium	Ho
Gallium	Ga	Erbium	Er
Arsenic	As	Thulium	Tm
Rubidium	Rb	Ytterbium	Yb
Strontium	Sr	Lutetium	Lu
Yttrium	Y	Hafnium	Hf
Zirconium	Zr	Tantalum	Ta
Niobium	Nb	Tungsten	W
Silver	Ag	Gold	Au
Indium	In	Lead	Pb
Tin	Sn	Thorium	Th
Antimony	Sb	Uranium	U

Trace element data for a range of glass samples from Eriswell were obtained by LA-ICP-MS, to complement the results of SEM-EDS. Although the technique is micro-destructive, the small amount of material removed renders it essentially non-destructive. Using this technique, it was possible to establish the concentrations of a range of elements below the detection limits of SEM-EDS. More precise data for some of the minor elements in these glasses (particularly antimony, cobalt, lead and

tin) were also obtained using this technique. A list of the elements determined by LA-ICP-MS is presented in Table 2.3.3.

2.3.2.1. Sample Preparation

The advantage of laser ablation over conventional solution ICP-MS is that the need for sample preparation is avoided. Samples were analysed directly from the polished resin blocks prepared for SEM analysis, rather than from the beads themselves. The carbon coating was removed from these using acetone prior to analysis. Each block was mounted in the ablation cell and secured in place using Blu-Tack™, to prevent movement during analysis.

2.3.2.2. Analytical Procedure

LA-ICP-MS analysis was undertaken using a New Wave Research UP213 UV laser system coupled to a Thermo X-Series ICP-MS in the Department of Earth Science at Cardiff University, under the supervision of Iain McDonald. Laser ablation was carried out under helium, which was combined with argon as a carrier gas to transport the ablated material to the mass spectrometer. Laser ablation can be operated in several different analysis modes, including spot analysis of one area, or by scanning along a pre-defined line (Wagner *et al.* 2008: 419); the latter mode was chosen so that the results were more representative of the glass, owing to the heterogeneity of many of the samples. The laser beam moved at 6µm per second along pre-defined lines of approximately 400µm in length (Figure 2.3.5). A large laser spot size (100µm) was used to account for the heterogeneity of many of the samples analysed, and was operated at 0.35mJ and a frequency of 10Hz. One pre-ablation pass of the sample surface was undertaken prior to data acquisition to remove possible surface contamination. This was followed by two repeat analyses for each sample, from which an average was taken.

To obtain quantitative analyses, internal and external standards were used to establish calibration lines for each element. External standards included the National Institute of Standards and Technology (NIST) standard reference materials (SRM) 610 and 612, which are soda-lime-silica glasses doped with various concentrations of trace elements (Dussubieux *et al.* 2009: 153); these were used to correct for ablation yield variations and matrix differences. ^{44}CaO was used as an internal standard, the concentration of which was determined by SEM-EDS. Concentrations of trace elements were calibrated by Iain McDonald. Detection limits are assumed to be below 1 ppm for most of the elements analysed.

A range of different glass colours were analysed, but analysis was primarily focused upon the translucent blue glasses with a hope that this may provide some indication as to the nature of the cobalt colourant(s) employed in their production. Cobalt sources have particularly good potential in the characterisation and provenancing of early glass (see Chapter 5, section 5.1.3.1).

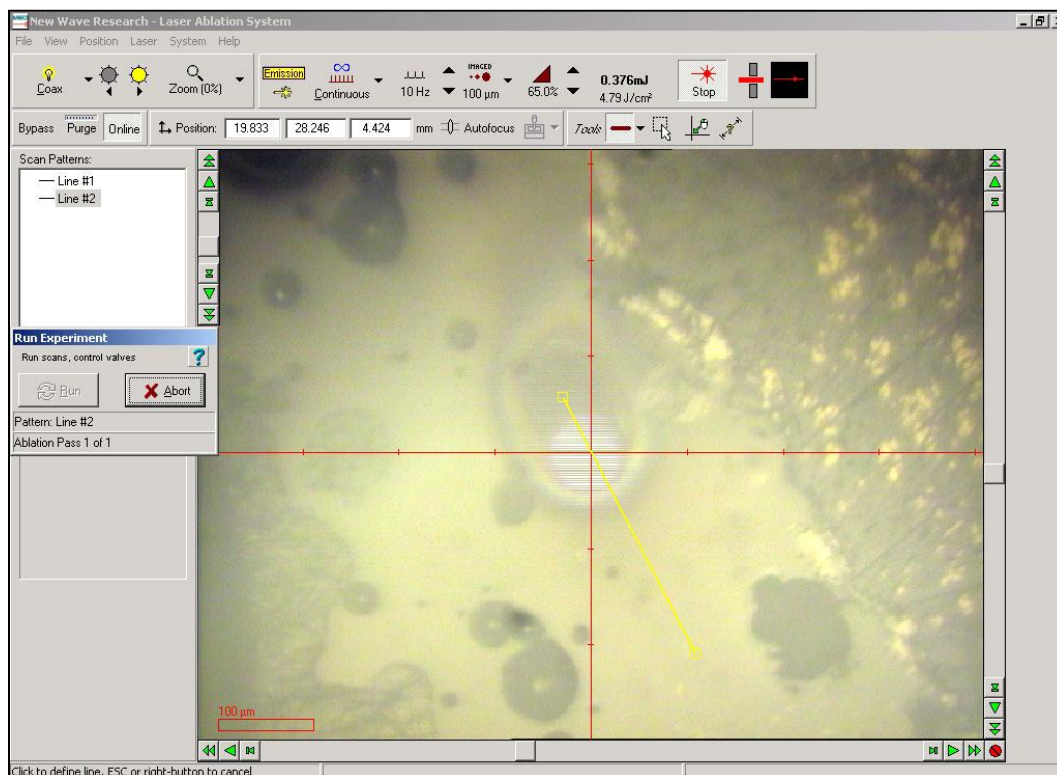


Figure 2.3.5 – A screenshot showing a laser ablation pass of a glass sample from Eriswell during LA-ICP-MS analysis. Note the heterogeneity of the sample.

2.3.2.3. Presentation of Data

As with SEM-EDS data, trace element data are presented in tabular format and usually organised according to the relative order of the elements in the periodic table. These elements are divided into groups to facilitate interpretation; each group of elements exhibits similar chemical properties and as a result behaves in a similar way geochemically (Henderson 1984). Elements may be divided into different groups in different ways to facilitate the interpretation and characterisation of a particular glass. The nature of these groups depends primarily upon the type of glass being analysed (*e.g. plant-ash* or *natron* glass) and the different elements that have been analysed for. In the present study, the trace elements have been divided into three main groups:

- Sediment-Related Elements (SRE).
- Rare Earth Elements (REE).
- Colourant and colourant-related elements.

Natural quartz sands are rarely pure, and commonly contain a host of additional minerals including feldspar, zircon, magnetite, pyroxene, etc. (Aerts *et al.* 2003: 664; Wedepohl *et al.* 1995: 78). These contribute a number of the so-called ‘sediment-related elements’ to the sand, along with rare earth elements, all of which accumulated in the Earth’s crust during its formation in the mantle (Wedepohl *et al.* 1995: 78). As such, the REE are effectively a sub-group of the SRE.

The SRE include the transition metals Ti, V, Cr, Y, Zr, Nb, Hf, Ta, W, together with Ga and the actinides Th and U. These are most likely to reflect the elements associated with sedimentary material such as alluvial deposits, and are introduced as contaminants with batch ingredients (*i.e.* the glassmaking sand). Rb, Sr and Ba are alkali and alkaline earth elements which generally relate to the alkali source used (mineral soda or plant ash), although they may also be introduced with the sand source (*e.g.* Sr from shell fragments in the sand). These elements are usually grouped separately when dealing with plant ash glasses because they are primarily introduced with the plant-ash. However, as the glasses in question in the present study are of the

natron type, these elements have been grouped with the SRE, as they are primarily likely to have been introduced as impurities with the glassmaking sand. Sr poses something of a problem because significant amounts can be introduced with both plant-ash and calcareous sand and it is very difficult to establish what proportion was introduced with either component (see Chapter 4, section 4.4.1). Iron and alumina are also SRE, but are typically present as major components so are reported as element oxides with the SEM-EDS data.

The REE comprise the lanthanides, which constitute a group of 14 elements in the periodic table from lanthanum through to lutetium. They are a sub-group of the SRE, but are treated separately because they are relatively stable and occur together in nature. Their chemical and physical properties are very similar, and they are often present at trace levels in many minerals, particularly silicates (Pollard *et al.* 2007: 211). The concentration of these elements therefore reflects the ultimate geological origin of the silica source (Kamber *et al.* 2005: 1047; Pollard *et al.* 2007: 211); that is, the rocks from which the glassmaking sand was formed. In most glasses the majority of the REE are introduced with the clay fraction of the sand, but relatively few are introduced with quartz. The relative concentrations of the REE are therefore a good indication as to the purity of the glassmaking sand used. Y is often included with the REE for discussion in many studies, due to its similar geochemical behaviour to the heavy lanthanides (Dy-Ho) (Degryse and Shortland 2009: 140). However, in the present study it is included with the SRE.

Finally, the colourant and colourant-related elements represent those components which contribute to the colour and/or opacity of the glasses analysed. Many of these were deliberately added to produce colour, but some were unintentionally incorporated as impurities with the colourants (*e.g.* zinc with copper or nickel with cobalt), or through the use of recycled material (*e.g.* antimony). These are usually metals which have been refined and so do not typically contribute to the concentrations of SRE or REE, unless of course they were added in their mineral form or had been contaminated with earth or clay, for example. Iron has been included here as, whilst small amounts are likely to have been unintentionally included with the glassmaking sand in the majority of cases, it sometimes contributes to the colour (see Chapter 5, section 5.1.1). Many of the colourant and colourant-

related elements were analysed for by SEM-EDS, but LA-ICP-MS can confirm the presence of deliberately added colourants at concentrations far below the detection limits of SEM (*e.g.* cobalt).

To enable comparisons between these elements, the data are usually *normalised* to the element concentrations of a chosen reference material, and their concentrations plotted on a logarithmic scale. This process involves dividing the concentration of each element by the concentration of the same element in the reference material. Each data point is plotted on a graph and traditionally joined together by a straight line to produce a 'pattern', which aids interpretation and comparison. The purpose of normalisation is to give smooth rather than jagged, saw-tooth trace element patterns, whereby major differences in the concentrations of different elements are 'smoothed' to aid interpretation.

There is no reference material used as standard for normalisation, but MUQ (average mud from Queensland) is often used as a substitute for the composition of the upper continental crust (UCC) (Kamber *et al.* 2005). This is chosen for the present study because it is close to the composition of sands formed by weathering. The colourant and colourant-related elements are not normalised in this way, as these reflect deliberate additions which are typically unaffected by geological processes. The MUQ values used for normalisation of the LA-ICP-MS data are shown in Table 2.3.4.

The raw trace element data obtained for the Eriswell glasses, each taken from an average of two analyses, are presented in Appendix G (note that these are *not* normalised to MUQ). In the presentation of data in bivariate graphs, correlations are described as either *positive* or *negative*. A correlation coefficient is provided where appropriate to indicate the strength of any correlations (see section 2.3.1.3 above for correlation coefficients).

Table 2.3.4 – Elemental MUQ (mud from Queensland) values used for normalisation of the LA-ICP-MS data (after Kamber *et al.* 2005).

<i>Element</i>	<i>MUQ (ppm)</i>	<i>Element</i>	<i>MUQ (ppm)</i>
Li	28.24	Ce	71.09
Be	1.92	Pr	8.46
Sc	16.49	Nd	32.91
Ti	6909.00	Sm	6.88
V	120.00	Eu	1.57
Cr	64.50	Gd	6.36
Co	22.39	Tb	0.99
Ni	31.57	Dy	5.89
Cu	32.36	Ho	1.22
Zn	73.47	Er	3.37
Ga	19.12	Tm	0.51
Rb	79.51	Yb	3.25
Sr	142.00	Lu	0.49
Y	31.85	Hf	5.32
Zr	199.00	Ta	1.12
Nb	15.33	W	1.60
Sn	2.77	Tl	0.42
Cs	5.38	Pb	20.44
Ba	396.00	Th	11.13
La	32.51	U	2.83

2.3.3. X-Radiography

The principles of x-radiography are not within the scope of the present study to discuss; the reader is invited to consult O'Connor and Brooks (2007) or Lang and Middleton (2007) and references therein for a detailed discussion of x-radiography and its application to materials in cultural heritage.

X-radiography is an imaging technique. It is usually routinely undertaken as part of post-excavation analysis in order to assist with the identification and interpretation of (mostly metal) objects, particularly their shape, technology and condition. It has a number of advantages; it is a rapid, non-destructive technique which is very cheap. Furthermore, it often allows the technological details and internal microstructure of objects to be revealed without any intervention, often highlighting features more clearly than can be seen by the eye (O'Connor and Brooks 2007: 30). X-radiographs

are essentially 2D representations of differences in radiographic opacity produced by 3D objects (O'Connor and Brooks 2007: 15).

Glass is rarely x-rayed, partly because the majority is translucent and partly because its original shape is rarely obscured by thick corrosion crusts (unlike metals). However, the x-radiography of opaque glass objects such as beads can provide insights into their internal structure and mode of construction. High-density glass will appear lighter in the x-radiograph (the lighter the shade, the denser the glass), primarily due to the presence of higher levels of lead (Freestone *et al.* 2005a: 72; O'Connor and Brooks 2007: 156-157). The contrast between high-lead and low-lead glasses can reveal the internal microstructure of polychrome glass objects particularly well (Freestone *et al.* 2005a: 72). Bubbles, striations, inclusions and stress-points may also be revealed, which can provide clues as to production and technology (Davison 2003: 230-231). However, the condition and thickness of a glass also affects the intensity of the x-ray image produced, and the superimposition of the 'front' and 'reverse' of an object on the same image can further complicate interpretation.

Variations in the kV adjusts the intensity of the x-rays; a lower kV will produce low-energy x-rays, which are more suitable for thin materials or those of low atomic number (*e.g.* low in lead) (O'Connor and Brooks 2007: 16). Variations in the exposure time adjusts the x-ray dose; this essentially adjusts the brightness of the image produced (O'Connor and Brooks 2007: 16). Test-runs were undertaken on a small batch of beads in order to establish the optimum parameters prior to x-radiography of the assemblage. Wet-plate x-radiographs were obtained at 90 kV for 2.5 minutes using a Faxitron 43805 x-ray machine at Cardiff University, using flexible plastic film cassettes. Lead intensifying screens were placed into the cassettes to reduce the effects of scattered x-rays, thereby producing a sharper image and reducing the exposure time (O'Connor and Brooks 2007: 41-43).

The majority of the opaque beads from Eriswell were x-rayed prior to cleaning and sampling. The only exclusions included those beads which were deemed too small to yield any useful information (mostly Brugmann's *Miniature Dark* types; 'dark' referring to beads which would otherwise have been termed 'black'), and those

beads which were heavily deteriorated (mostly opaque white; see Chapter 3, section 3.3). The translucent beads were also excluded for obvious reasons; *i.e.* their internal microstructure is visible by their very nature.

As many beads as possible were placed on individual x-ray cassettes so as to save time and resources. The developed films were scanned using a high-quality digital x-ray scanner. Digitised images were edited and enhanced using Adobe Photoshop, in which particular features could be highlighted by adjusting the image brightness and contrast (O'Connor and Brooks 2007: 76). The colours of the digitised x-radiographs were inverted to produce a 'positive' image; this can highlight particular features which are sometimes less obvious in the original 'negative' image (O'Connor and Brooks 2007: 75). The enhanced digitised x-radiographs for the Eriswell beads, sorted by grave and SF number, are shown in 'positive' and 'negative' format in Appendix F (not to scale).

CHAPTER THREE

3. Production Technology

3.1. Manufacturing Techniques

It was possible to produce a wide variety of different bead types by varying their shape, colour(s), and/or decoration, using only a limited range of manufacturing techniques (Brugmann 2004: 18). For example, red, yellow and green glass was used to produce beads of the *Traffic Light* type (for an explanation of bead type definitions, refer to Chapter 2, section 2.1.1. For detailed definitions of individual types, refer to Chapter 4, section 4.10), but the decorative motif and shape of these beads varies considerably (Brugmann 2004: 18). The manufacturing techniques used to shape and decorate glass beads during the early Anglo-Saxon period are generally known (*e.g.* see Brugmann 2004: 21; Guido 1978: 7), so will only be discussed briefly here.

The majority of the glass beads from the Anglo-Saxon period were produced by **winding** (Callmer 1977: 33); beads in parts of modern-day India and Turkey are still made in this way (Kock and Sode 1994; Küçükerman 1988; Sode 1995; Sode and Kock 2001). This involved winding a heated length of glass around a narrow metal rod (a *mandrel*); as a result, the structure of these beads (bubbles, striations and surface irregularities) is circumferential, running perpendicularly to the perforation (*e.g.* Figure 3.1.1) (Brugmann 2004: 21; Hirst 2000: 122). The bead was often shaped further using tools or by marvering, which can erase many of the visual indications of winding (Brugmann 2004: 21; Hirst 2000: 122; Sode 1995: 104).

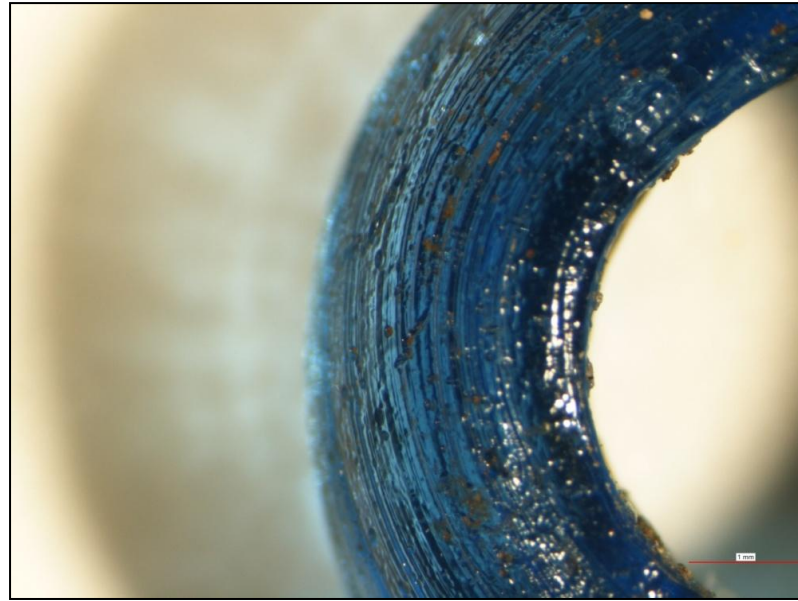


Figure 3.1.1 – Digital microscope image of translucent blue bead ERL046:G05:1438, a wound *Blue* bead, showing a ‘circumferential’ structure. Image is approximately 7mm across (image courtesy of Rebecca Lumsden).

A large number of Anglo-Saxon beads were produced by **drawing**. Drawn beads were produced by blowing molten glass into a bulb, then drawing it out into a tube using a rod (Brugmann 2004: 21; Guido 1978: 8; Hirst 2000: 122; Küçükerman 1995: 98). The thickness of the tube was determined by the speed at which the glass was drawn out (Küçükerman 1995: 98). It was then cut at the ends to create the bead, or crimped at intervals so that the tube could be broken into individual beads once the glass had cooled (Brugmann 2004: 21; Hirst 2000: 122). The resulting structure is longitudinal, with imperfections and striations running parallel to the perforation (Brugmann 2004: 21; Hirst 2000: 122). Most segmented beads (‘metal-in-glass’ types; *e.g.* Figure 3.1.4) were manufactured using this technique (Brugmann 2004: 21), although some were also produced by winding (Brugmann 2004: 21).

Glass beads could also be produced by **piercing**, whereby a drop of molten glass was pierced from one side using a tool (Brugmann 2004: 21). As a result, the pierced side (top) of the bead is concave; the other side (underside) is convex, or flat if the bead was pierced on a flat surface (Brugmann 2004: 21). Again, depending upon the extent to which the bead was reworked afterwards, there may be little visible

evidence for this method of manufacture (Brugmann 2004: 21). The only beads from Eriswell produced using this technique are of Brugmann's *Doughnut* type.

A limited number of Anglo-Saxon beads were produced by **folding**. Folded beads were made by folding a single piece of molten glass around a rod and fusing the two ends together, creating a seam down one side of the bead parallel with the perforation (Brugmann 2004: 21; Guido 1978: 8). **Mosaic** beads (see section 3.1.1 below) were produced using a similar technique, but using pre-made pieces of coloured rods which were fused together prior to being folded around a mandrel (Brugmann 2004: 21; Hirst 2000: 123-125; Sode 1995: 105); beads of this type are often described as *millefiori* ('a thousand flowers') as a result of the decorative effect produced. The so-called **Reticella** beads were also produced using a variation of both the folding and mosaic techniques. Here, twisted rods of multicoloured glass were folded around a pre-formed core of monochrome glass; the latter may have been produced by winding (see section 3.1.2.1 below). Only three beads of this type were recovered from Eriswell.

Several long cylindrical beads from Eriswell, similar to those produced by drawing, appear to have been produced by **coiling**. These are all of Brugmann's *Constricted Cylindrical, Variation* type. This technique appears to be a variation of winding, whereby glass is coiled along a length of wire and marvered flat to produce a long tube (Guido 1999: 50). The structure of the bead therefore appears 'twisted' or coiled. The ends may be either re-worked or cut.

The perforations of Anglo-Saxon glass beads are usually round in cross-section, reflecting the shape of the mandrel on which they were formed, but perforations of other shapes (*e.g.* square) are also sometimes found (Hirst 2000: 122). In some beads the perforation is parallel, whereby the diameter of the perforation is equal on both sides of the bead (Hirst 2000: 122). However, in many cases the perforation is tapered (*e.g.* Figure 3.2.3), whereby it is of a greater diameter on one side of the bead than the other (Hirst 2000: 122). This is particularly evident in the x-radiographs of the beads (see Appendix F). In the production of annular beads the mandrel would have been rotated to produce a larger perforation (Hirst 2000: 122), as with Brugmann's *Blue* beads; these are the most common bead type found at Eriswell.

Upon removal of the bead from the mandrel, it would have needed to be cooled slowly in a controlled way to avoid stresses building up which could cause the bead to crack or break (Sode 1995: 104). This process is known as annealing. It is unclear how this was undertaken in the Anglo-Saxon period, but traditional beadmakers in India use a small clay annealing pot into which the beads are knocked from the mandrel; when full this is covered to slow the rate of cooling (Sode 1995: 104).

3.1.1. Applied Decoration

It is often very difficult to establish exactly how decoration was applied, especially if a bead has been re-worked (Brugmann 2004: 22). The majority of polychrome beads from Eriswell were simply decorated by applying glass to the main body of the bead, either as trails or spots, or as a coating which covered the entire surface (Brugmann 2004: 21; Hirst 2000: 123). The applied decoration is sometimes left in relief above the surface, but could also be combed to produce different effects (*e.g.* Figure 3.1.2), or marvered flush with the bead surface (*e.g.* Figure 3.1.3) (Brugmann 2004: 21).

Alternatively, pre-formed rods of coloured glass may have been applied to a bead. These usually consisted of one or more glass rods of different colours which had been twisted together prior to application; either an 's' twist or a 'z' twist could be used, depending upon the direction of the twist (clockwise or anticlockwise) (Brugmann 2004: 21; Guido 1999: 65; Hirst 2000: 123). The application of alternating 's' and 'z' twisted rods, folded around a core of monochrome glass, created the herringbone pattern characteristic of the so-called **Reticella** decoration (*e.g.* Figures 3.2.7 and 3.2.8); these beads were re-worked and marvered into shape following application of these trails (rods) (Brugmann 2004: 21; Guido 1999: 65; Hirst 2000: 125; Sode 2004: 94). The production of beads such as this would probably have required considerable skill, which has led some authors to speculate that such beads were manufactured by a limited number of specialist workshops (Brugmann 2004: 17; Evison 1983: 92; Guido 1999: 65).



Figure 3.1.2 – Digital microscope image of ‘dark’ bead ERL104:G242:2142, a wound *DarkPoly2* bead, showing fine applied opaque white trails combed into a zigzag pattern. Image is approximately 6mm across (image courtesy of Helen Butler).



Figure 3.1.3 – Digital microscope image of opaque yellow bead ERL104:G195:1346, a wound *Koch34* bead, showing an applied opaque red circumferential narrow crossing trail marvered flush with the bead surface. Image is approximately 6mm across (image courtesy of Helen Butler).

Mosaic beads (also called *millefiori* beads; see above) are a more complicated type of polychrome bead made from pre-made sections of coloured glass rods, which were fused together and folded around a mandrel (Brugmann 2004: 21; Hirst 2000: 123-125; Sode 1995: 105). Depending on the cross-sections of the rods used, this decoration could consist of stripes, spirals and flower-like patterns (Brugmann 2004: 21). Modern Indian beadmakers make these beads by fusing sections of these coloured rods to a pre-formed core of molten glass on the end of a mandrel, so that the cross-section makes up the visible pattern (Sode 1995: 105). Only one bead of this type was recovered from Eriswell (sample ERL104:G290:1721, a *Mosaic?* bead), but it is so heavily fragmented that its attribution is uncertain.

3.1.2. 'Metal-in-Glass' Beads

The term 'metal-in-glass' is used here to describe beads composed of two layers of glass, typically containing a layer of foil between them. Brugmann (2004) terms them *Constricted Segmented* beads. These are traditionally called 'gold-in-glass' beads, as many are decorated using gold foil and have the appearance of gold-glass (*e.g.* Figure 3.1.4). In her typology, Brugmann (2004: 24) describes drawn beads which may contain a layer of metal foil as 'light', given that it is difficult to establish the presence or absence of such foil.

'Metal-in-glass' beads are a long-standing bead type which first appeared in the Ptolemaic period, when it is thought that they were produced as a substitute for metal beads (Boon 1977: 195; Hirst and Biek 1981: 140). The first known examples are probably no earlier than the 3rd century BC and were made from either coloured or colourless glass (Boon 1977: 195). They were produced throughout the Roman and Late Roman periods (Boon 1977: 196; Guido 1978: 93-94; Guido 1999: 78); first appearing in Roman Britain in the late 2nd century (Boon 1977: 200; Timby 1996: 48). 'Metal-in-glass' beads remained common in eastern and northern Europe in the 4th century, probably resulting from a continuation of earlier trade links (Boon 1977: 201); they are thought to have been manufactured in the Near East and exported to Europe at this time (Boon 1977: 201).

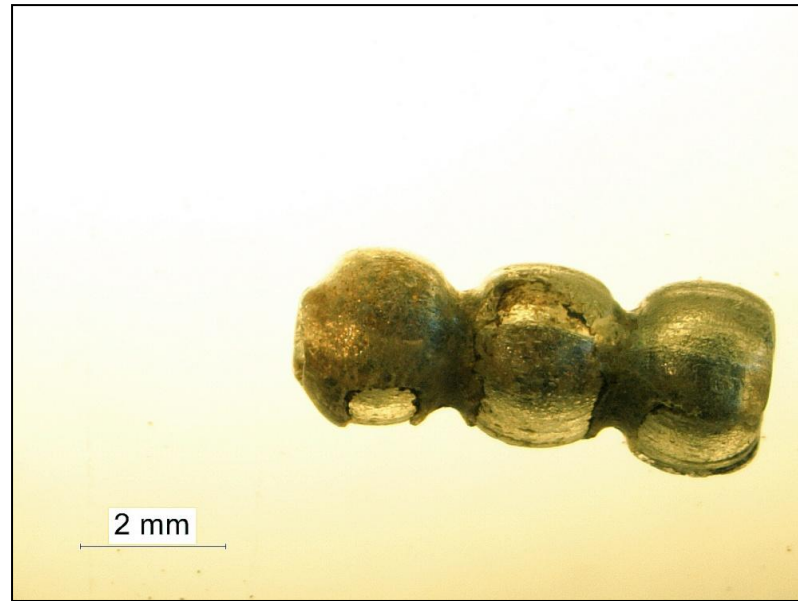


Figure 3.1.4 – Digital microscope image of ‘light’ bead ERL104:G172:3098, a drawn *Constricted Segmented* ‘metal-in-glass’ bead. A layer of metallic foil (probably gold) is visible, sandwiched between two layers of glass. Much of the outer layer of glass is missing, revealing the foil beneath (image courtesy of Jenny Mathiasson).

Beads of this type are most commonly found in late 5th and 6th century contexts in Anglo-Saxon cemeteries (Boon 1977: 202; Hirst 2000: 122; Timby 1996: 48); Boon (1977: 201) suggests that they were manufactured on the Continent during this time, as they had apparently become less common in the Eastern Mediterranean (Boon 1977: 201). Conversely, Callmer (1995: 49) suggests that they were probably produced in the Byzantine provinces of the Near East. It has also been suggested that some of these may represent Roman survivals (Brugmann 2004: 29-30; Guido 1978: 94). Their origins are therefore unclear. However, they seem to have disappeared from most of Europe by the 7th century, which Callmer (1995: 49) attributes to a disruption in their production in the Near East as a result of the Byzantino-Persian wars.

As ‘metal-in-glass’ beads were produced over such a long period, it is often difficult to distinguish between early and late examples; it is usually only minor variations in production technology and style that provide clues (Spaer 1993: 10). Previous studies have identified four different types of metal-in-glass bead in use during the Anglo-Saxon period (*e.g.* Bayley 1994; Bayley 2009: 413; Biek and Gillmore 1997; Biek *et al.* 1985; Hirst 2000: 122; Jönsson and Hunner 1995: 114; Sode 2004: 97):

- Beads coloured with a layer of metallic gold foil sandwiched between two layers of glass.
- Beads coloured by a layer of metallic silver foil sandwiched between two layers of glass.
- Beads in which there is no metal between the layers of glass. They instead use a poor quality inner tube, typically containing bubbles, in which light reflected from the interface between the two layers to give the appearance of a foil layer.
- Beads in which there is no metal between the layers of glass, but the outer layer of glass is tinted either amber or brown to produce a similar effect as a layer of gold foil.

The exact methods used to manufacture ‘metal-in-glass’ beads are still not fully understood, although there are several possible theories (*e.g.* see Jönsson and Hunner 1995). These beads were certainly produced by drawing (see above) (Brugmann 2004: 28; Guido 1978: 93; Jönsson and Hunner 1995: 114). The tube of glass was then cooled before applying metal (gold or silver) onto its surface (in those beads containing metal), covering this with a further layer of glass, and crimping it at regular intervals to produce globular segments (Bayley 1994: 1; Boon 1977: 193; Guido 1999: 78; Hirst 2000: 122; Jönsson and Hunner 1995: 113; Mortimer 1996b: 15; Spaer 1993: 10; Timby 1996: 48). This outer layer of glass is often very fragile and is frequently damaged, exposing the glass or foil beneath (*e.g.* Figure 3.1.4).

It has been suggested that the metal may have been applied by either dipping the glass tube into molten metal or by applying it as foil (Astrup and Anderson 1987); in the latter case an adhesive may have been used (Spaer 1993: 10). Examination of ‘metal-in glass’ beads from Mucking, Essex, by Bayley (1994) indicate that it is more likely to have been applied as foil, which was in some cases too narrow to completely cover the bead.

The resulting glass tube may have been threaded onto a thin length of wire and crimped to produce the segments (Bayley 1994: 1; Boon 1977: 193; Hirst and Biek

1981: 140). Alternatively, some studies have suggested that the tube of glass was rolled over corrugated moulds to produce the segments, for which there is evidence from early medieval Alexandria (Sode 2004: 97-978; Spaer 1993: 14). The latter interpretation is favoured in the present study for a number of reasons; the segments are generally very evenly spaced, in contrast to some other types of segmented bead. Furthermore, crimping by hand would have required the glass tube to have been kept pliable for much longer periods, risking failure or deformation of the beads.

The crimped lengths of glass were easily broken into single- or multiple-segment beads (Bayley 1994: 1). The ends of the beads were sometimes re-worked, but in many cases they were left jagged (Guido 1999: 78; Sode 2004: 97). Due to their fragility these beads are often found broken, so it is difficult to establish the original number of segments, or even whether the beads were broken before, during, or after burial (Timby 1996: 48). At Eriswell, these beads are typically no larger than 5 mm in diameter (*e.g.* Figure 3.1.4), but six beads have slightly larger diameters and are consequently listed as variants (Birte Brugmann, pers. comm.).

3.2. Manufacturing Techniques: New Insights

Most of the opaque beads from Eriswell were x-rayed, with the hope of gaining further insights into their technology and internal microstructure (see Chapter 2, section 2.3.3). The majority of the x-radiographs did not reveal any technological features that were not already apparent from visual examination. However, the contrast between high-density high-lead glass (which appears brighter in the radiographs) and low-density low-lead glass allowed the internal structure of some of the beads to be seen extremely well (*e.g.* Figure 3.2.1). This also gave some indication as to the lead content of the beads. The colourant technology of beads which were not analysed can sometimes consequently be deduced (*e.g.* opaque white glass; see section 3.2.2 below). In several of the beads very small crystals of opacifying agents could also be seen within the glass matrix, confirming their presence (*e.g.* Figure 3.2.2).



Figure 3.2.1 – Bead ERL104:G305:1871, a *Melon Associated* bead, showing an opaque yellow circumferential zigzag trail on a ‘dark’ bead body (left) and a positive x-radiograph of the bead (right). The opaque yellow glass appears darker in the image as it is denser, due to a much higher lead content.



Figure 3.2.2 – Bead ERL046:G15:1740, a *DarkPoly1* bead, showing an opaque white circumferential zigzag trail on a ‘dark’ bead body (left) and a positive x-radiograph of the bead (right). The dark flecks visible in the x-radiograph are particles of a crystalline opacifying agent (tin oxide) present in the opaque white decoration.

3.2.1. Iron Scale

A black layer was observed covering the inside of the perforation of many of the beads from Eriswell (*e.g.* Figure 3.2.3); a feature which is commonly observed in Anglo-Saxon beads (*e.g.* Hirst 2000: 125; Mortimer 1996a: 5; Mortimer 1996b: 7). It was possible to examine this deposit in the SEM in several of the samples taken, which confirmed the presence of an iron oxide layer approximately 70 μm in thickness (Figures 3.2.4-3.2.6). This is consistent with iron oxide scale pulled from an iron mandrel during the beadmaking process (Bayley 1995: 1203; Hirst 2000: 125; Mortimer 1996a: 5; Mortimer 1996b: 7). In many cases the glass had begun to interact with this iron oxide layer (*e.g.* Figure 3.2.6; note how the crystals of metallic copper in the glass are larger immediately adjacent to the iron scale, due to the powerful effects of iron as a reducing agent).

A number of factors determine how easily a glass bead was separated from the mandrel around which it was wound. These include the temperature of the glass, the extent to which the rod was pre-heated, the material from which the rod was made (in this case iron), the taper of the rod, and whether or not the bead was reheated (Tweddle 1986: 212). Furthermore, the composition of the glass (*e.g.* lead content) can affect the viscosity of the melt, which will also be a determining factor. The exact processes used to produce the Eriswell beads are unclear. It is likely that the mandrel was dipped into a 'releasing agent', such as sand or baked clay powder, to aid the removal of the finished bead (Tweddle 1986: 212; Sode 2004: 90). Sode (1995: 104; 2004: 90) describes how traditional glass beadmakers in India rub the tip of the mandrel in rock salt as a releasing agent; a chemical reaction takes place between the salt and the iron, which forms a black layer of iron oxide within the perforation similar to that observed in the beads from Eriswell. This enables the beads to be removed from the mandrel more easily. It is unclear whether Anglo-Saxon beadmakers used such a releasing agent, but it is clear that the mandrels used were, at least in the majority of cases, made from iron.

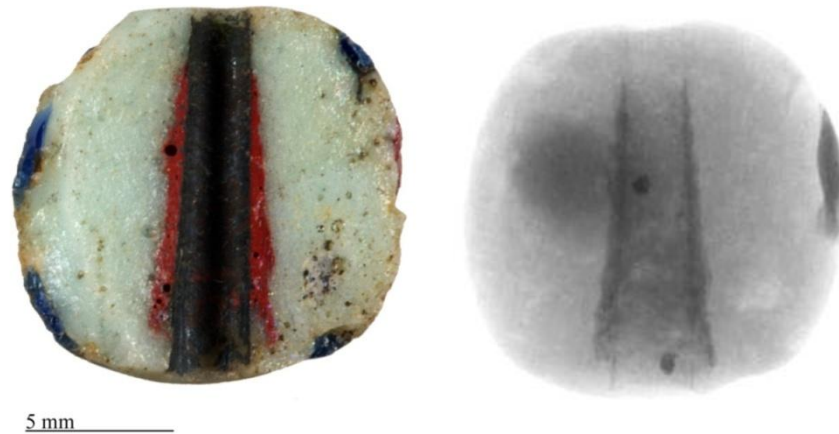


Figure 3.2.3 – A section through bead ERL104:G367:3619 (a *WhitePoly3* bead) showing a layer of opaque red glass at the core (left). A slight taper to the perforation can be seen, indicating the use of a tapered mandrel. The black layer visible within the perforation is oxidised iron scale pulled from the mandrel around which the bead was formed. Also shown is a positive x-radiograph of the same bead prior to sectioning (right); the red glass appears darker because it is denser, due to its higher lead content. Note the absence of any visible crystalline opacifying agent in the bead body; the more ‘mottled’ appearance on the x-radiograph results from opacification by bubbles.

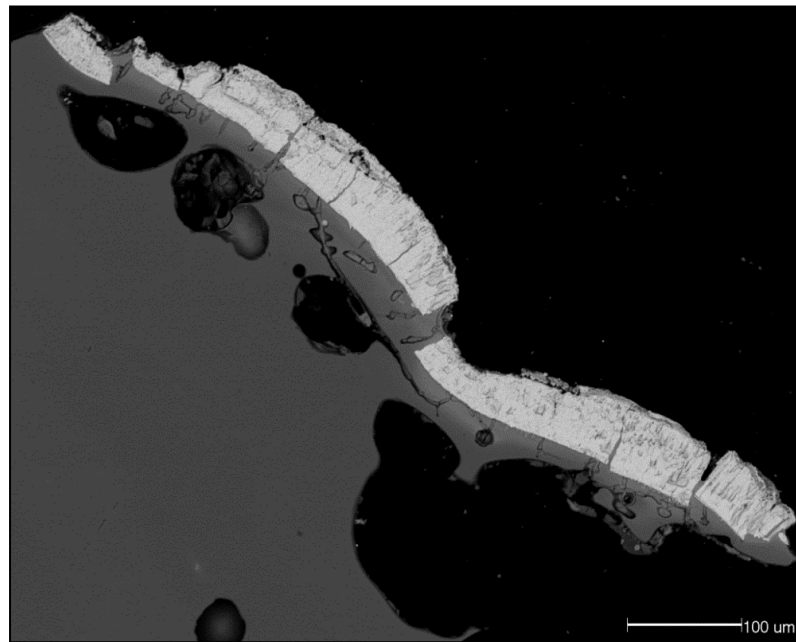


Figure 3.2.4 – BSE micrograph showing translucent blue-green tinted sample ERL104:G144:2595, a *Hourglass Variation* bead. A thick layer of iron oxide scale (pale grey) can be seen adhered to the surface of the soda-lime-silica glass matrix (dark grey). Several large voids and bubbles are also visible.

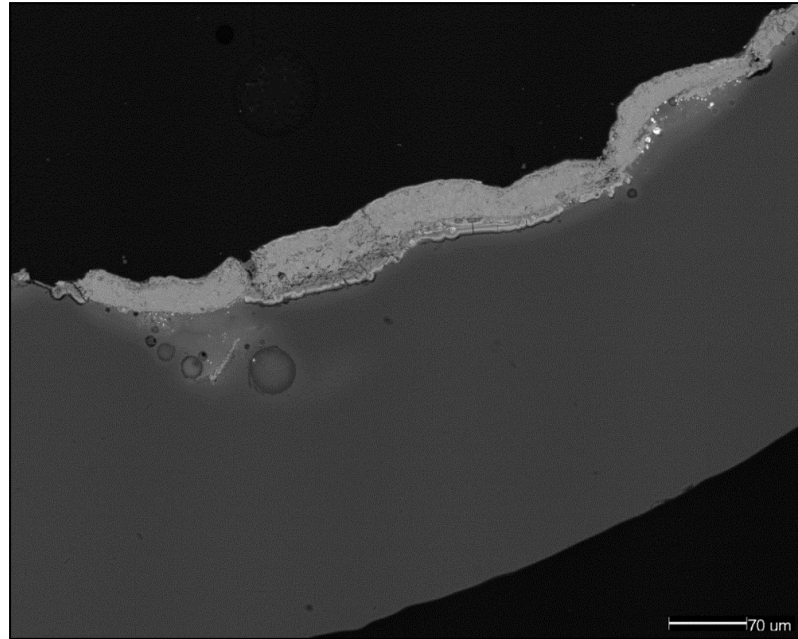


Figure 3.2.5 – BSE micrograph showing translucent green tinted sample ERL104:G263:1396, a *Cloak* bead. A thick layer of iron oxide scale (pale grey) can be seen adhered to the surface of the soda-lime-silica glass matrix (dark grey).

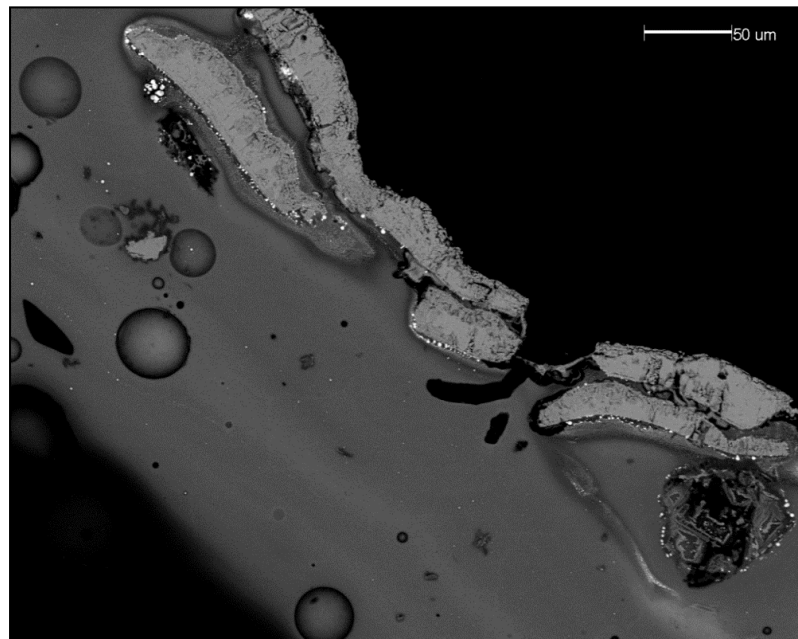


Figure 3.2.6 – BSE micrograph showing opaque red sample ERL046:G03:1271, a *RedPoly6* bead. Several thick layers of iron oxide scale (pale grey) can be seen adhered to the surface of the soda-lime-silica glass matrix (darker grey). Several fayalitic slag particles and large bubbles are also visible. The bright white particles immediately surrounding the iron scale are metallic copper; copper having been added as a colourant in this glass (see Chapter 5, section 5.2.3).

3.2.2. Opaque Red Glass Cores

A layer of opaque red glass was observed at the core of several of the beads from Eriswell. All of these beads are opaque white, and are restricted to a few specific types (primarily Brugmann's *WhitePoly** types; the asterisk denotes that this bead type includes sub-types). Red glass at the core of opaque white Anglo-Saxon beads is not unknown (*e.g.* Hirst 2000: 125; Hirst and Clark 2009: 505).

All of the beads from Eriswell containing red glass at their core are produced from recycled Roman material (see Chapter 4, section 4.3) and all are opacified by a dispersion of tiny bubbles (as opposed to tin oxide; see Chapter 5, section 5.2.1). The beads in question are primarily polychrome, consisting of opaque white glass decorated with either translucent blue glass, or a combination of translucent blue and opaque red glass; bead ERL104:G352:2805 (*White Globular*) is an exception because it is monochrome.

In the majority of these beads these red glass cores would never have been seen, so it is unlikely to have been a decorative feature. X-radiography shows beads exhibiting this feature particularly well, especially in cases where coloured glass cores cannot be identified by visual examination. Table 3.2.1 shows positive x-ray images for the opaque white beads from Eriswell, noting their type attribution, the method of opacification, and whether or not opaque red glass is present at their core. Queries (?) denote when the method of opacification has not been confirmed by compositional analysis, and when the presence of opaque red glass at the core has not been confirmed by visual examination or sectioning; these data have been established by examination of the x-rays alone. It must be stressed that considerable weathering of some of the bubble-opacified white beads has made their x-radiographs difficult to interpret. Furthermore, some opaque white beads, presumably bubble-opacified, were not x-rayed as they were in such poor condition (see this chapter, section 3.3).

Table 3.2.1 – X-radiographs of the opaque white beads from Eriswell, showing the method of opacification and those beads which are likely to contain opaque red glass at their core.






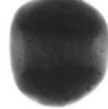













<i>Bead Type</i>	<i>Bead Number</i>	<i>X-ray¹</i>	<i>Opacifier²</i>	<i>Red core³</i>
<i>Cylindrical Round</i>	ERL104:G193:1312		Tin oxide	-
	ERL104:G237:1151		Tin oxide	-
	ERL104:G262:1258		Tin oxide?	-
	ERL104:G262:1282		Tin oxide	-
	ERL104:G273:3330a/07		Tin oxide	-
<i>Dot34</i>	ERL104:G109:1100		Tin oxide	-
<i>Koch34</i>	ERL104:G107:1128		Tin oxide	-
	ERL104:G107:1145		Tin oxide	-
	ERL104:G193:1295		Tin oxide	-
	ERL104:G195:1350		Tin oxide	-
	ERL104:G195:1352		Tin oxide	-
	ERL104:G195:1353		Tin oxide?	-
	ERL104:G195:1355		Tin oxide?	-
	ERL104:G237:1154		Tin oxide	-
	ERL104:G237:1158		Tin oxide?	-
	ERL104:G262:1286		Tin oxide	-
	ERL104:G281:1796		Tin oxide	-
	ERL104:G353:3070		Tin oxide	-
ERL104:G353:3072		Tin oxide?	-	

Table 3.2.1 – (continued).

<i>Bead Type</i>	<i>Bead number</i>	<i>X-ray</i> ¹	<i>Opacifier</i> ²	<i>Red core</i> ³
<i>Norfolk Blue White</i>	ERL046:G18:1788		Bubbles	-
	ERL104:G350:1506		Bubbles	-
<i>White Biconical</i>	ERL104:G353:3080		Tin oxide	-
<i>White Cylindrical, round</i>	ERL104:G262:1231		Tin oxide	-
	ERL104:G262:1283		Tin oxide	-
<i>White Cylindrical, pentagonal</i>	ERL104:G376:3625		Bubbles	-
<i>White Globular</i>	ERL046:G05:1461		Bubbles?	-
	ERL046:G05:1491		Bubbles	-
	ERL046:G05:1513		Bubbles?	-
	ERL046:G05:1516		Bubbles	-
	ERL046:G08:1597		Bubbles	-
	ERL104:G243:1370		Bubbles	-
	ERL104:G243:1383		Bubbles?	-
	ERL104:G352:2805		Bubbles?	Yes?
	ERL104:G352:2806		Bubbles?	-
	ERL104:G352:2808		Bubbles?	-
	ERL104:G352:2809		Bubbles?	-
	ERL104:G352:2814		Bubbles	-
	ERL104:G367:3640		Bubbles?	-
	ERL104:G107:1124		Tin oxide?	-
ERL104:G107:1137		Tin oxide	-	
ERL104:G107:1142		Tin Oxide	-	

Table 3.2.1 – (continued).

























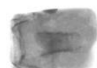

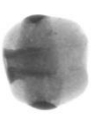


<i>Bead Type</i>	<i>Bead number</i>	<i>X-ray¹</i>	<i>Opacifier²</i>	<i>Red core³</i>
<i>White Globular</i>	ERL104:G242:2256/14		Tin oxide?	-
	ERL104:G273:3330a/08		Tin oxide?	-
	ERL104:G353:3071		Tin oxide?	-
<i>WhitePoly2</i>	ERL114:G450:1153		Bubbles?	-
	ERL114:G450:1164		Bubbles	-
	ERL104:G242:2176		Tin oxide?	-
	ERL104:G242:2244		Tin oxide	-
<i>WhitePoly3</i>	ERL046:G03:1322		Bubbles	-
	ERL104:G144:2563		Bubbles?	-
	ERL104:G148:2739		Bubbles	-
	ERL104:G242:2159		Bubbles	Yes
	ERL104:G362:1975		Bubbles?	Yes
	ERL104:G367:3619		Bubbles	Yes
	ERL104:G243:1373		Tin oxide	-
ERL104:G243:1379		Tin oxide?	-	
<i>WhitePoly4</i>	ERL104:G344:2834		Bubbles	Yes
	ERL104:G268:3255		Tin oxide	-
	ERL104:G268:3258		Tin oxide	-

Table 3.2.1 – (continued).





<i>Bead Type</i>	<i>Bead number</i>	<i>X-ray</i> ¹	<i>Opacifier</i> ²	<i>Red core</i> ³
<i>WhitePoly5</i>	ERL104:G166:3437		Bubbles	Yes?
	ERL046:G08:1595		Bubbles?	Yes?
<i>WhitePoly6</i>	ERL046:G08:1612		Bubbles	Yes?
	ERL046:G08:1614		Bubbles?	-
	ERL046:G38:1035		Bubbles?	Yes?
	ERL046:G38:1067		Bubbles	Yes?
<i>WhitePoly7</i>	ERL104:G144:2569		Bubbles	Yes?
	ERL104:G144:2606		Bubbles?	Yes?
<i>WhitePoly8</i>	ERL104:G367:3624		Bubbles	Yes
	ERL104:G242:2256/15		Bubbles?	-
<i>Undefined</i>	ERL104:G242:2264		Bubbles?	-

¹Digital x-rays are reproduced here as positive images. High-density glass (lead-rich) therefore appears darker in the image. For original negative images, refer to Appendix F. X-rays are not to scale.

²Where there is a query (?), this indicates that the method of opacification has been suggested from examination of the x-rays, and has not been confirmed by chemical analysis. Crystals of opacifier can sometimes be seen as darker flecks in the x-ray, which suggest opacification by tin oxide (opacification by antimony is also possible, but less likely). The lower-density beads (very pale grey) do not contain lead in any significant quantity, or visible opacifier crystals, and are therefore likely to be opacified by bubbles. However, chemical analysis is needed to confirm this.

³Where there is a query (?), this indicates that the presence of red glass at the core of the bead has been suggested from examination of the x-ray, and has not been confirmed by visual examination. The higher-density glass (darker grey) at the core of the beads suggests the presence of a lead-rich glass (probably opaque red). However, the beads need to be sectioned in order to confirm its presence and colour.

Table 3.2.2 – X-radiographs of the opaque red beads coated with opaque blue glass from Eriswell, showing the method of opacification and those beads which contain opaque red glass at their core.

<i>Bead Type</i>	<i>Bead number</i>	<i>X-ray</i> ¹	<i>Opacifier</i> ²	<i>Red core</i> ³
<i>RedPoly6</i>	ERL046:G03:1271		-	Yes
	ERL046:G38:1063		Bubbles	Yes
<i>Undefined</i>	ERL046:G38:1036		-	Yes
	ERL046:G03:1297		Bubbles?	Yes

¹Digital x-rays are reproduced here as positive images; see Table 3.2.1 for details. X-rays are not to scale.

²Opacifier refers to the blue glass coating only. Where there is a query (?), this indicates that the method of opacification has been suggested from examination of the x-rays. See Table 3.2.1 for details.

³The higher-density glass (darker grey) at the core of the beads suggests the presence of a lead-rich opaque red glass, which has been confirmed by visual examination in all cases.

Opaque red glass is only found at the core of bubble-opacified white beads; it is not observed in any of the tin oxide opacified types. Furthermore, not all of the bubble-opacified bead types in question contain red glass at their cores, suggesting that it was not a universal part of in their manufacture; *e.g.* beads ERL046:G03:1322 and ERL104:G148:2739 (both *WhitePoly3* beads). Hirst and Clark (2009: 505) suggest that this practice is peculiar to the 5th and 6th centuries, which is supported by their chronological attributes (see Chapter 4, sections 4.8-4.10). It has been suggested that opaque red glass was used to facilitate the removal of the bead from the mandrel (Hirst 2000: 125; Hirst and Clark 2009: 505); high-lead red glass of this type (see Chapter 5, section 5.2.3) would have had a lower melting point than the body of the bead, thus ensuring that the core remained soft once the bead itself had sufficiently solidified. This interpretation is supported by the fact that the bubble-opacified whites do not contain lead (see Chapter 5, section 5.2.1). In contrast, the tin oxide opacified whites contained sufficient lead to facilitate their removal from the mandrel.

Analysis of sample ERL104:G367:3624 (a *WhitePoly8* bead) indicates that the same batch of opaque red glass was used for both the core and the applied decoration. This

confirms that these beads were both formed and decorated in the same workshop, as opposed to being transported elsewhere for decorating. However, it seems unusual that opaque red glass was used; other glass types (*e.g.* opaque yellow; see Chapter 5, section 5.2.2) also contain high levels of lead and would presumably have also been suited to the purpose.

There are several possible reasons for this: it is possible that the craftsmen producing these beads did not have access to other high-lead glass colours, such as opaque yellow and green. This interpretation is supported by the absence of such colours as decoration on these beads. Opaque yellow and opaque green glasses are based on compounds of tin (see this Chapter 5, section 5.2.2) which, when considering that the opaque white beads in question are opacified by bubbles, may suggest that the beadmakers producing these beads may not have had access to a source of tin (see Chapter 4, section 4.9). However, it is likely that a material rich in both lead and tin was used to produce opaque red glass (see Chapter 5, section 5.3), so may not have been the case. Alternatively, more value may have been placed on other high-lead colours such as opaque yellow, particularly if they were more difficult or expensive to produce, or if the raw materials needed to produce them (*e.g.* tin) were less readily available.

Nevertheless, the use of opaque red glass for such a purpose suggests that it was a relatively readily available glass colour, which is unlikely to have been an expensive or particularly difficult colour to produce. However, opaque yellow glass seems to have been just as common (see Chapter 4, section 4.9). Whilst the addition of a small quantity of lead to the opaque white glass would have negated the need to apply red glass to the mandrel prior to forming these beads, the presence of lead would probably have clarified the glass (due to a decrease in viscosity), thus destroying the opacity. The opaque red glass at the centre of these beads may have held some special significance, possibly having a symbolic meaning. However, as this trait is restricted only to bubble-opacified glass, it is far more likely to have been undertaken for technological benefits. This technology is closely paralleled by opaque red beads coated with opaque or translucent blue glass (Table 3.2.2). However, further work is required in order to establish the precise nature of this practice.

3.2.3. 'Reticella' Beads

X-radiography of the *Reticella* beads produced very detailed images of their internal microstructures in a way which is not reflected in other bead types. These beads were produced by the application of alternating 's' and 'z' twisted rods consisting of two or more different colours of glass, folded around a core of monochrome glass, to create a herringbone pattern (see this chapter, section 3.1). The differences in lead content of the individual glass colours used to produce these beads means that the way in which these rods were twisted and applied is particularly clear. In both of the *Reticella* beads x-rayed (Figures 3.2.7 and 3.2.8), it can be seen that twisted canes of coloured glass were folded around a monochrome glass core, then marvered into shape. The 'hatched' appearance of the x-rays shows how these canes were twisted. The x-rays indicate that these twisted canes were round, and approximately 3-4mm in diameter. The glass core around which sections of these canes were folded was approximately 12mm in diameter (including the perforation), and a slightly tapered mandrel was used.

Two types of *Reticella* bead were identified at Eriswell: drum-shaped and biconical (Figures 3.2.7 and 3.2.8). The drum-shaped beads appear to be more common in early Anglo-Saxon contexts, but it is likely that both types have similar dates (Guido 1999: 66-67). They are common in the 6th century but may have continued to be produced into the 7th century (Guido 1999: 67).



Figure 3.2.7 – Bead ERL104:G305:1875, a *Reticella* bead (left) produced from three twisted trails of opaque red, opaque yellow and translucent glass arranged in a herringbone pattern. The high-lead opaque yellow glass appears darker in positive x-radiograph (right), and highlights the way in which the glass is twisted.

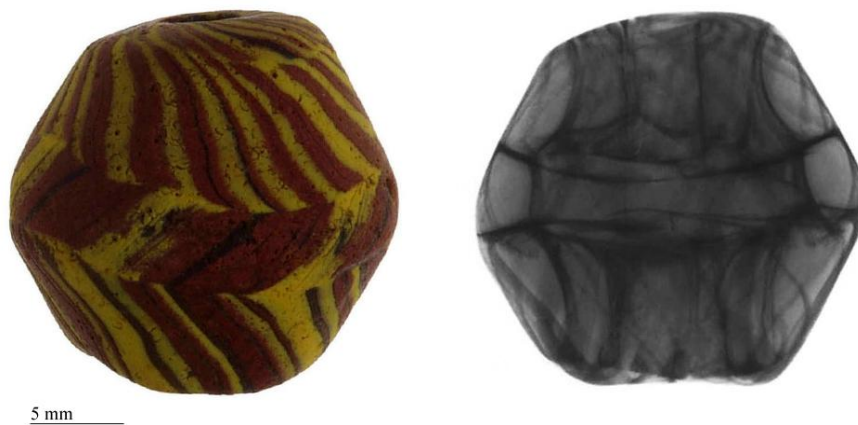


Figure 3.2.8 – Bead ERL104:G305:1876, a *Reticella* bead (left) produced from three twisted trails of opaque red, opaque yellow and translucent glass arranged in a herringbone pattern. The high-lead opaque yellow glass appears darker in positive x-radiograph (right), and highlights the way in which the glass is twisted.

3.3. Chemical Durability and Decay

A detailed discussion of the corrosion and decay mechanisms of soda-lime-silica glass is not within the scope of the present study, but information on the subject is widely available in published literature (*e.g.* Cox and Ford 1989; Cox and Ford 1993; Davison 2003; Freestone 2001).

Glass that has been in contact with soil and groundwater for long periods of time will often show signs of decay. The extent of deterioration of archaeological glass depends upon its chemical composition, its microstructure (inclusions, faults, etc.), the nature of the burial environment (acidity, moisture, etc.), and the length of time for which it has been buried. There are two main mechanisms by which glass deteriorates: de-alkalisation (ion exchange) and network dissolution (Freestone 2001: 617).

In the process of de-alkalisation, groundwater leaches alkali ions such as sodium (Na^+), calcium (Ca^{2+}), potassium (K^+) and magnesium (Mg^{2+}) from the glass surface, where they are replaced by hydrogen ions (H^+) from groundwater (Cox and Ford 1989: 3148; Cox and Ford 1993: 5641; Freestone 2001: 617; Watkinson *et al.* 2005: 69). This results in a hydrated silica-rich layer on the surface of the glass, often termed a 'gel' layer, which is weaker than the original glass network (Freestone 2001: 617). In the process of network dissolution, the alkali-rich solution which has been leached from the glass surface (*e.g.* sodium and potassium hydroxide) can locally attack and break down the silica network itself, although this is strongly dependent upon the pH of the attacking solution (Davison 2003: 175; Freestone 2001: 617; Watkinson *et al.* 2005: 69). This is not a problem unless the burial environment is very alkaline (above pH 9) or if the leaching solution is frequently renewed (Davison 2003:175), for example in the well-draining soil at Eriswell.

The composition of the glass is crucial in determining the rate of deterioration; pure soda-silicate glasses are water soluble, and lime is a necessary addition to render them stable (Freestone 2001: 617). Soda-lime-silica glass is usually somewhat more durable than plant ash glass (Davison 2003: 178; Freestone 2001: 619), but the

amount of silica present and the addition of colourant metal oxides can affect the rate of corrosion (Freestone 2001: 617).

De-alkalisation usually dominates in buried glass (Freestone 2001: 618). This initially results in an iridescent, often flaking layer (*e.g.* Figure 3.3.1) (Freestone 2001: 619; Watkinson *et al.* 2005: 69), which can obscure or alter the original colour of the glass and eventually cause the loss of the original surface (*e.g.* Figure 3.3.2). The thicker corrosion crusts that form usually have a laminated structure and are often very fragile (Cox and Ford 1989: 3147; Cox and Ford 1993: 5638-5639; Freestone 2001: 618).

The hydrated silica-rich later on soda-lime-silica glass is typically no more than a few microns thick (Davison 2003: 178; Freestone 2001: 619). However, in areas where the glass is particularly vesicular or has been damaged weathering may be promoted, resulting in the formation of pits and plugs (*e.g.* Figure 3.3.3) (Watkinson *et al.* 2005: 69). These weathering crusts are often enriched in components which have leached out of the glass (*e.g.* lead) or components which have leached in from the surrounding environment (*e.g.* manganese) (Freestone 2001: 619); as such, non-destructive surface analysis of glass is not always a reliable indicator of its original composition, even when the glass looks in good condition.

Several of the opaque white glass beads from Eriswell had suffered particularly badly from decay; these beads have typically crumbled beyond recognition. All of the beads in question are opacified by bubbles (see Chapter 5, section 5.2.1). It is not the composition of the glass which has resulted in its accelerated deterioration, but its microstructure. The method of opacification produces a porous glass (*e.g.* Figures 3.3.3 and 3.3.4), often with a pitted surface. This facilitates the passage of groundwater into the internal structure of the glass, promoting its decay. As a result of the presence of bubbles, a larger surface area of the glass is exposed and prone to attack by water. This ultimately causes fragility in these beads, resulting in cracks and fissures, further facilitating the ingress of groundwater (Davison 2003: 191).

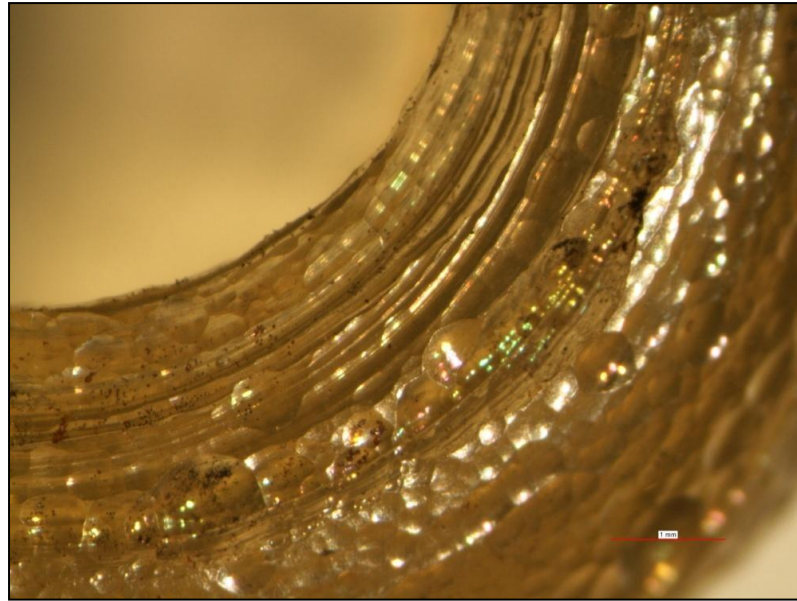


Figure 3.3.1 – Digital microscope image of bead ERL046:G03:1228, a wound *Green Globular* bead, showing a ‘circumferential’ structure. A filmy layer of patchy iridescent weathered glass is visible in places. Image is approximately 7mm across (image courtesy of Rebecca Lumsden).

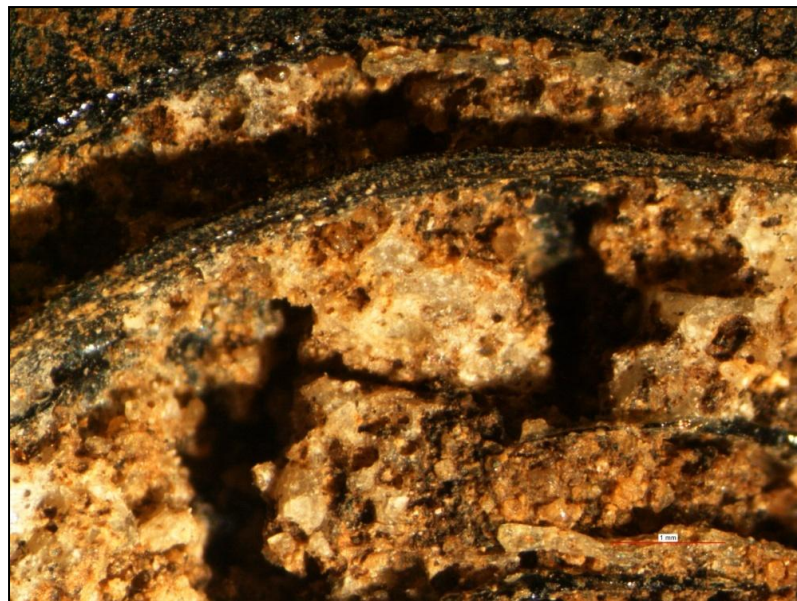


Figure 3.3.2 – Digital microscope image of bead ERL114:G414:1535, a wound *DarkPoly3* sword bead, showing opaque white applied decoration on a ‘dark’ bead body. The opaque white glass is opacified by bubbles and has suffered from considerable deterioration by groundwater as a result of its porosity. Image is approximately 7mm across (image courtesy of Rebecca Lumsden).

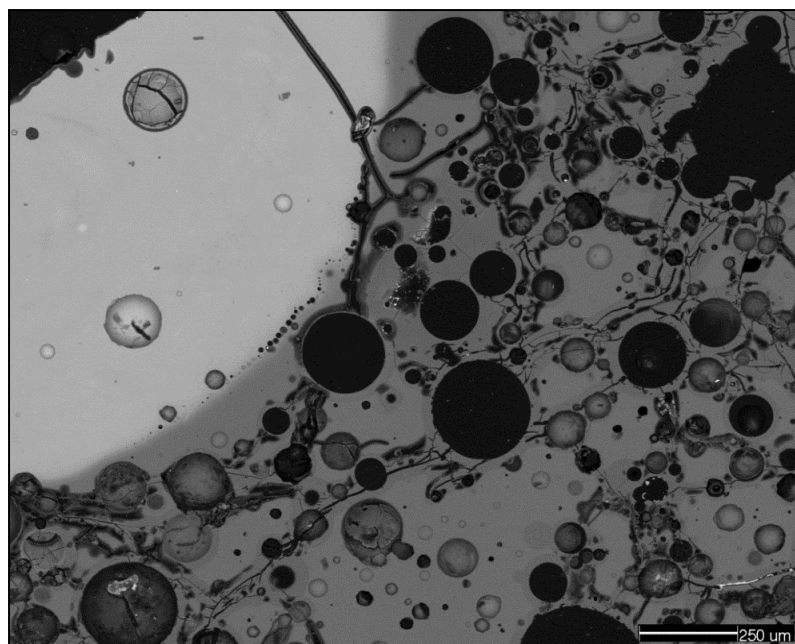


Figure 3.3.3 – BSE micrograph of an opaque white bead from Spong Hill (grave 5.6c), opacified by a dispersion of tiny bubbles in a soda-lime-silica glass matrix. This glass is heavily corroded; numerous cracks, fissures and pits are visible. The darker grey areas of glass adjacent to these cracks and fissures are depleted in alkali, which has been leached out of the glass by groundwater. Compare the condition of this glass with the adjacent translucent turquoise glass (pale grey glass towards the top-left of the image).

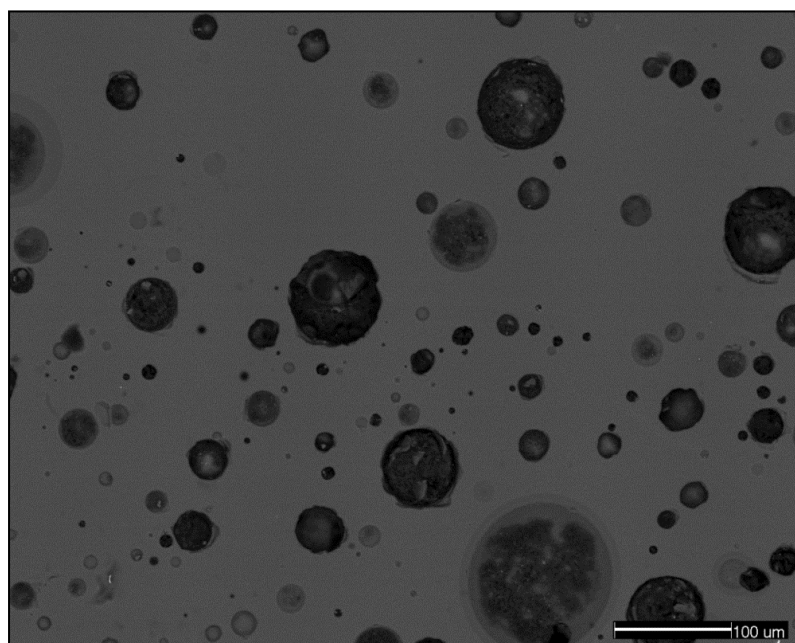


Figure 3.3.4 – BSE micrograph showing opaque white sample ERL104:G367:3619, a *WhitePoly3* bead. Numerous tiny bubbles are visible heterogeneously dispersed throughout the soda-lime-silica glass matrix. Surrounding several of these bubbles a thin layer of slightly darker grey glass can be seen, where the alkali components of the glass have been leached out by groundwater.

Upon excavation, these beads are allowed to dry and the hydrated corrosion layer shrinks as a result (Davison 2003: 175; Freestone 2001: 618). This contraction causes the weathered glass to crack and disintegrate (Davison 2003: 183; Shelby 1997: 175), which often results in considerable post-excavation deterioration (crumbling) and the loss of applied decoration. Apparently coherent glass may also undergo this transformation after excavation (Freestone 2001: 619). Even after drying, fluctuations in humidity within the storage environment can lead to further deterioration as leached layers continue to absorb and desorb moisture (Davison 2003: 183).

CHAPTER FOUR

4. Results: Glass Technology

Raw oxide, reduced oxide, and trace element data for the beads from Eriswell are presented in Appendix G. Raw oxide and reduced oxide data for the beads from Spong Hill are presented in Appendix H, for Bergh Apton in Appendix I, and for Morning Thorpe in Appendix J; glass from these latter sites is discussed in Chapter 7, section 7.1.

4.1. Base Glasses

By *reducing* the raw data, the composition of the glass prior to modifications by deliberate additives such as colourants and opacifiers can be obtained (*i.e.* the *base glass*). This is calculated by subtracting these deliberate additives (and where possible their associated impurities) from the data; it is therefore the sum of Na₂O, MgO, Al₂O₃, SiO₂, P₂O₅, SO₃, Cl, K₂O, CaO, TiO₂ and Fe₂O₃ re-summed (*normalised*) to 100% (Brill 1970: 122). Reduced data often allow much more reliable comparisons to be made between glasses than the raw data themselves (Brill 2006: 126), as they make it possible to establish whether a common base glass was used in the production of different glass colours before the complications of deliberate additives. In the present study, reduced element oxides are represented by the oxide abbreviation followed by an asterisk (*e.g.* Na₂O*).

It is unclear as to whether decolourants (antimony and manganese; see below, section 4.1.4.4) were added during the manufacture of the base glasses themselves or if they were later ‘secondary’ additions, as with colourants and opacifiers. Many studies exclude these components in the calculation of base glass compositions (*e.g.* Brill 1988: 258; Mirti *et al.* 1993: 236). However, in the present study both manganese and antimony have been included in the reduced data, as they can provide a strong indication as to the re-use of earlier Roman material (see this

chapter, section 4.3), or the addition of plant ash to the batch (see this chapter, section 4.4). Furthermore, their inclusion does not significantly depress the relative concentrations of the other components, as both antimony and manganese are present in relatively low concentrations ($\text{MnO}^* + \text{Sb}_2\text{O}_3^*$ is typically less than 3%).

Comparisons of the reduced compositions for highly coloured and opaque glasses is far more difficult than for 'colourless' and naturally coloured glass, as the concentrations of some base glass elements are often influenced through deliberate additions to the glass during the colouring process, or by contaminants introduced from the melting pot or furnace when the glass was molten. The concentration of elements present at minor or trace levels may therefore be considerably different to those present in the original base glass. Iron, for example, is typically thought to have been introduced with the glassmaking sand (*e.g.* see this chapter, section 4.1.1.3). However, in some glasses extra iron was deliberately introduced as a reducing agent (*e.g.* see Chapter 5, section 5.2.3) or colourant (*e.g.* see Chapter 5, section 5.1.5). This is clearly demonstrated by the high iron contents in certain glass colours relative to other colours (Figures 4.1.1 and 4.1.2). It is clear that some translucent blue glasses also contain slightly elevated levels of iron, which are likely to have been introduced as an impurity with the cobalt colourant (see Chapter 5, section 5.1.3).

The opaque yellow glasses are particularly difficult to compare, due to their extremely high levels of lead, which significantly depresses the concentrations of the other elements present (see Chapter 5, section 5.2.2). The corrosive action of lead (*e.g.* Biek and Bayley 1979: 16) poses a number of problems, as it has resulted in considerable contamination of the glass by elements introduced from the clay fabric of the melting pot; particularly iron and aluminium. Indeed, aluminium-rich feldspar inclusions were observed in the many of the samples (*e.g.* see Chapter 5, section 5.2.2), which are likely to have been introduced during the colouring process.

Figures 4.1.3-4.1.5 show the reduced (*) concentrations of iron and alumina for the high-lead samples from Eriswell, which demonstrates the problem of contamination. The samples containing the highest levels of lead typically contain the most elevated levels of iron and alumina; the low-lead opaque white, 'dark' and turquoise glasses

typically contain 2-3% Al_2O_3^* , whereas the high-lead yellow, red, green and ‘dark’ glasses typically contain higher levels, at 3-4% Al_2O_3^* (Figures 4.1.1, 4.1.3 and 4.1.4). In one opaque yellow sample as much as 6% Al_2O_3^* was detected (*e.g.* Figures 4.1.3 and 4.1.4). The positive correlation between lead and alumina (Figure 4.1.4; $r^2 = 0.59$) demonstrates that the degree of contamination by alumina (from the crucible) increases with the lead content of the glass.

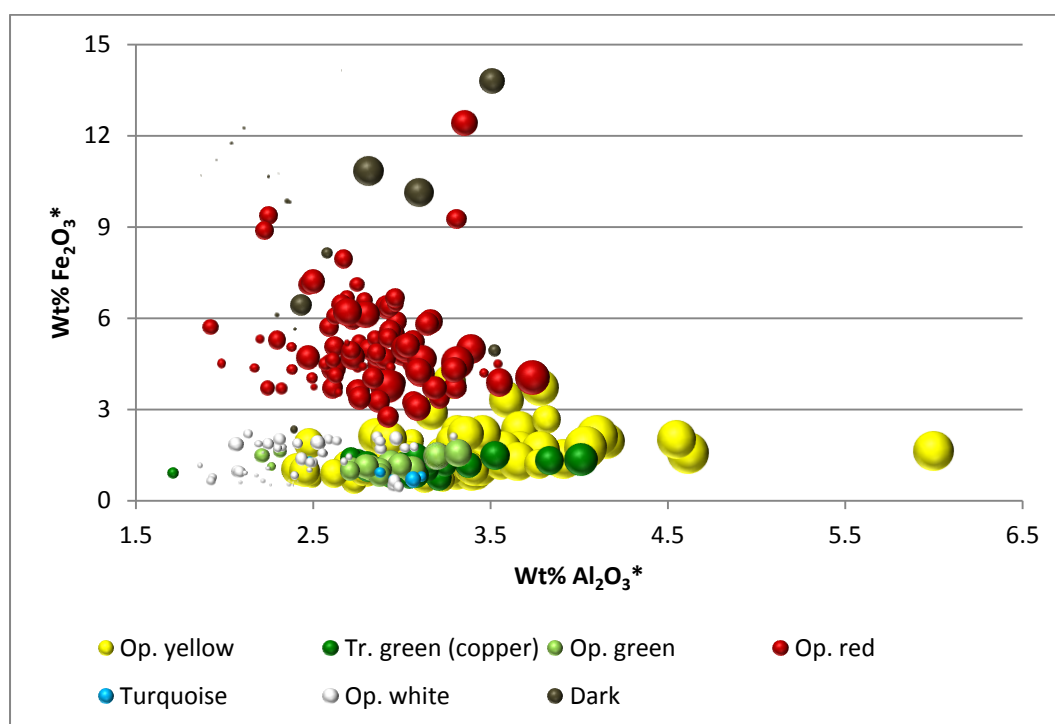


Figure 4.1.1 – A plot of alumina versus iron oxide for the high-lead yellow, green, red, white, turquoise and ‘dark’ samples from Eriswell. The size of the bubbles is proportional to the lead content (the larger the bubble, the higher the lead content), taken from the raw data (*i.e.* not reduced). Note that * indicates reduced glass composition in this and all subsequent graphs and tables.

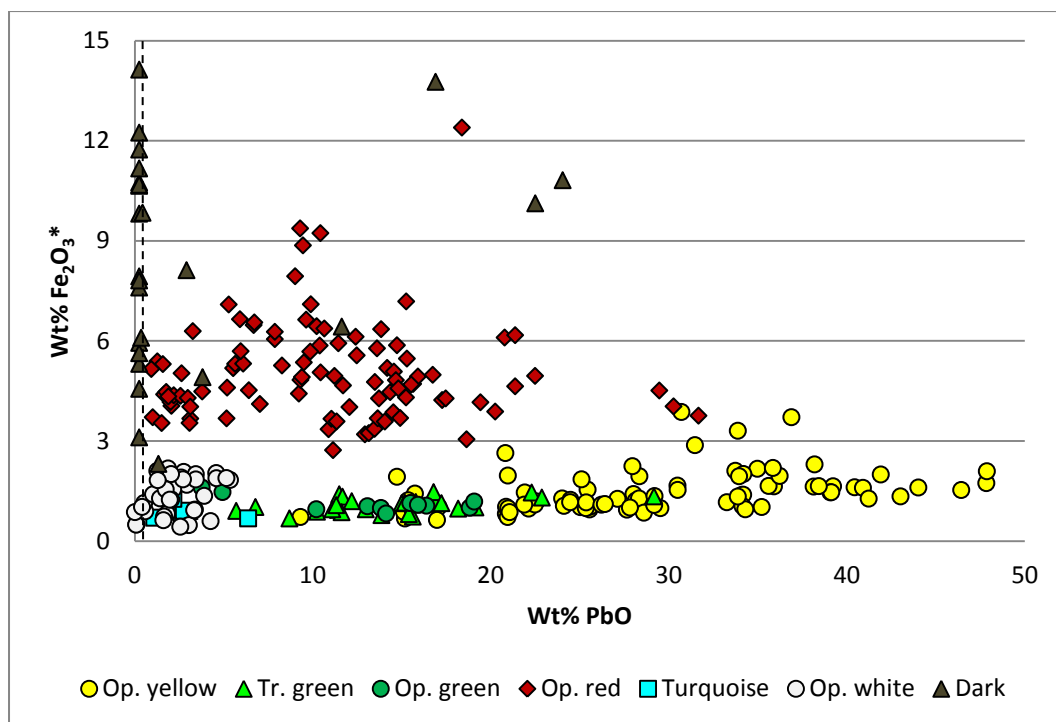


Figure 4.1.2 – A plot of raw (*i.e.* not reduced) lead oxide versus iron oxide for the high-lead yellow, green, red, white, turquoise and ‘dark’ samples from Eriswell. The dashed line represents the approximate detection limits for lead oxide.

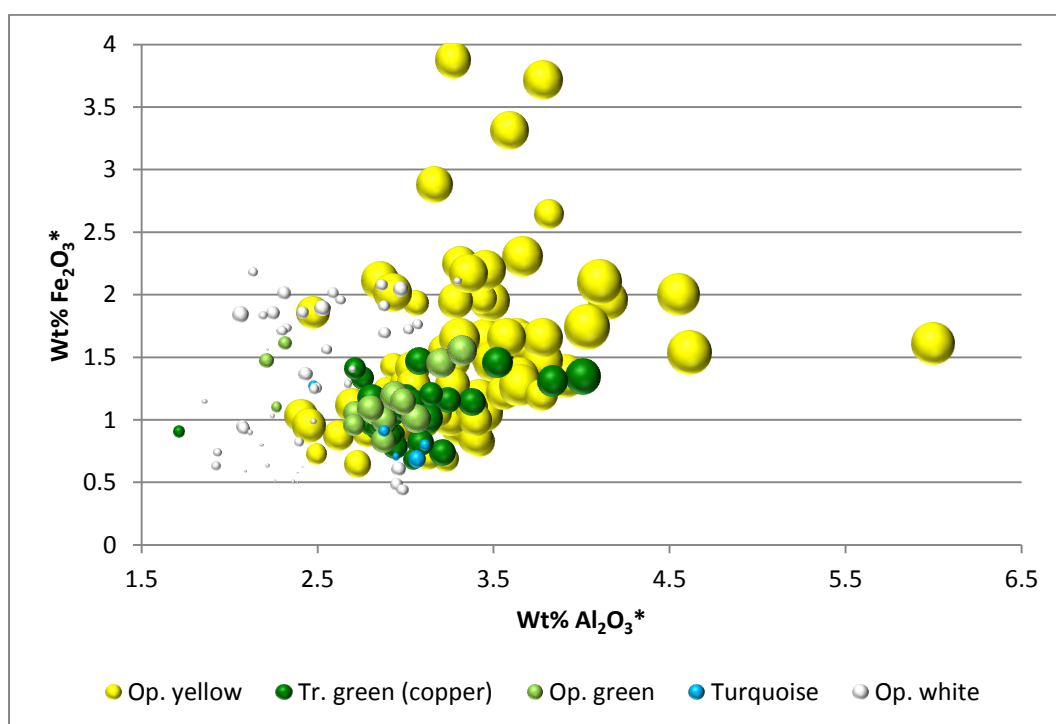


Figure 4.1.3 – A plot of alumina versus iron oxide for the high-lead yellow, green, white and turquoise samples from Eriswell. The size of the bubbles is proportional to the lead content (the larger the bubble, the higher the lead content), taken from the raw data (*i.e.* not reduced).

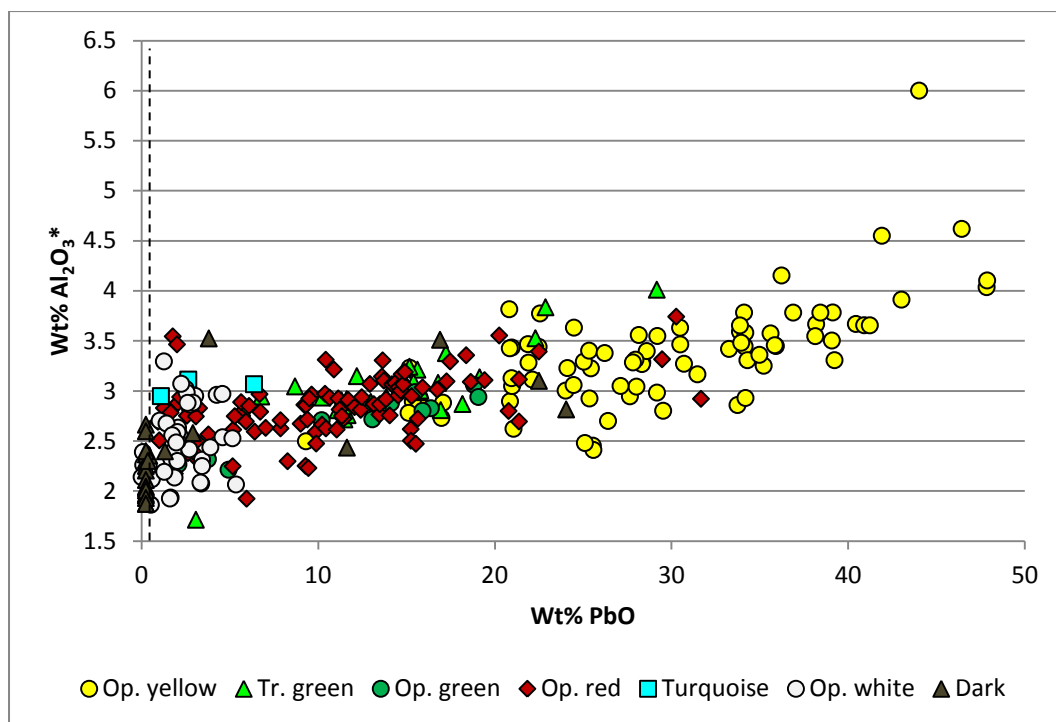


Figure 4.1.4 – A plot of raw (*i.e.* not reduced) lead oxide versus alumina for the high-lead yellow, green, red, white, turquoise and ‘dark’ glasses from Eriswell. The dashed line represents the approximate detection limits for lead oxide.

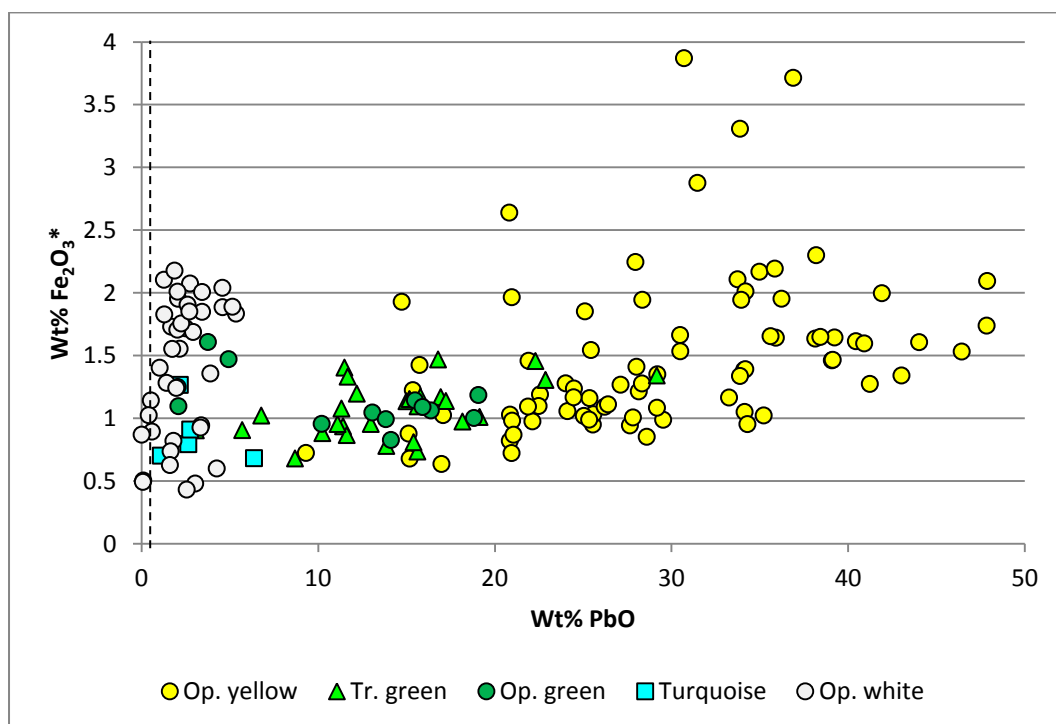


Figure 4.1.5 – A plot of raw (*i.e.* not reduced) lead oxide versus iron oxide for the high-lead yellow, green, white and turquoise glasses from Eriswell. The dashed line represents the approximate detection limits for lead oxide.

Iron is also elevated (to a lesser extent) in the high-lead colours, with opaque yellow and green glasses typically containing in excess of 1% Fe_2O_3^* (Figures 4.1.3 and 4.1.5). Many of the high-lead opaque yellow glasses contain in excess of 1.5% Fe_2O_3^* , sometimes up to as much as 3.9% Fe_2O_3^* . This can primarily be attributed to contamination from the crucible, as demonstrated by the weak positive correlation between lead and iron (Figure 4.1.5; $r^2 = 0.25$, when omitting the opaque white, opaque red and 'dark' glasses). In contrast, the majority of the samples from Eriswell in which lead is absent or near absent typically contain 0.3-1.5% Fe_2O_3^* and 1.6-2.7% Al_2O_3^* ; concentrations which are usually assumed to have been introduced with the glassmaking sand (see this chapter, section 4.1.1.3).

To account for contamination, average iron and alumina concentrations were taken from the translucent blue, pink-brown and uncoloured samples; this corresponded to 1.2% Fe_2O_3^* and 2.4% Al_2O_3^* . These values were *assumed* for the opaque red, opaque green, opaque yellow, translucent green and 'dark' glasses, following the initial reduction of their compositions, but only in those samples in which iron and/or alumina were above 1.3% and 2.5% respectively. They were then re-summed to 100%. A worked example of this process is shown in Table 4.1.1. As a result, where iron and alumina values had been assumed, the concentrations of these components could not be used for comparison.

Table 4.1.1 – A worked example of the re-summing (normalisation) process for opaque red sample ERL114:G413:1495, showing how iron and alumina values are assumed.

<i>Process</i>		<i>Oxide (wt %)</i>													
		<i>Na₂O</i>	<i>MgO</i>	<i>Al₂O₃</i>	<i>SiO₂</i>	<i>P₂O₅</i>	<i>SO₃</i>	<i>Cl</i>	<i>K₂O</i>	<i>CaO</i>	<i>TiO₂</i>	<i>MnO</i>	<i>Fe₂O₃</i>	<i>Sb₂O₃</i>	<i>Total</i>
1.	Subtract colourants and related elements	12.30	0.48	2.87	55.28	0.30	0.26	0.74	0.86	4.85	0.09	0.35	8.00	0.27	86.65
2.	Re-sum to 100%	14.20	0.55	3.31	63.80	0.35	0.30	0.85	0.99	5.60	0.10	0.40	9.23	0.31	100.00
3.	Assume average values for Al ₂ O ₃ (2.4%) and Fe ₂ O ₃ (1.2%)	14.20	0.55	2.40	63.80	0.35	0.30	0.85	0.99	5.60	0.10	0.40	1.20	0.31	91.05
4.	Re-sum to 100%	15.59	0.61	2.64	70.06	0.38	0.33	0.94	1.09	6.15	0.11	0.44	1.32	0.34	100.00

4.1.1. Raw Materials

The base glass types used in the manufacture of the majority of beads from Eriswell contain very similar levels of major oxide components. All are soda-lime-silica glasses typical of Anglo-Saxon glass (*e.g.* Biek *et al.* 1985; Bimson and Freestone 2000; Brill 2006; Freestone and Hughes 2006; Freestone *et al.* 2008; Henderson 1990; 1998; Hunter and Heyworth 1998; Mortimer and Heyworth 2009; Sanderson *et al.* 1984), containing 12-22% soda (Na_2O^*), 3-10% lime (CaO^*) and 62-73% silica (SiO_2^*).

4.1.1.1. Alkali

As previously mentioned (see Chapter 1, section 1.4), early soda-lime-silica glasses typically fall into two broad categories based on their respective contents of potash and magnesia. High-potash, high-magnesia glass typically contains in excess of 1.5% each of K_2O and MgO and was produced using soda-rich plant ash as a flux. In contrast, low-potash, low-magnesia glass typically contains less than 1.5% each of these components and was produced using a relatively pure form of evaporitic mineral soda (such as natron) as a flux.

In the Eriswell glasses, Na_2O^* is typically present in concentrations between 12-22%, and K_2O^* and MgO^* are both typically below 1.5% (Figure 4.1.6), indicating that were produced in the 'Roman' glassmaking tradition using a mixture of sand and natron (Aerts *et al.* 2003: 659; Brill 1988: 265; Freestone and Hughes 2006: 147; Freestone and Gorin-Rosen 1999: 110-111; Shortland *et al.* 2006: 523). Whilst several samples contain K_2O^* and MgO^* at concentrations above 1.5%, this is not high enough to suggest that they are mixed-alkali glasses (*e.g.* Brill 2006: 138; Henderson 1988a: 89; Henderson 1993: 251); the primary alkali source is again likely to have been natron. However, the strong correlation between potash and magnesia in those samples containing in excess of 1.2% MgO^* (Figure 4.1.6; $r^2 = 0.73$) suggests a plant-ash addition. The positive correlation between potash and

phosphate further suggests this (Figure 4.1.7; $r^2 = 0.64$, omitting samples containing less than 1.2% MgO^*), as will be seen (see this chapter, section 4.4).

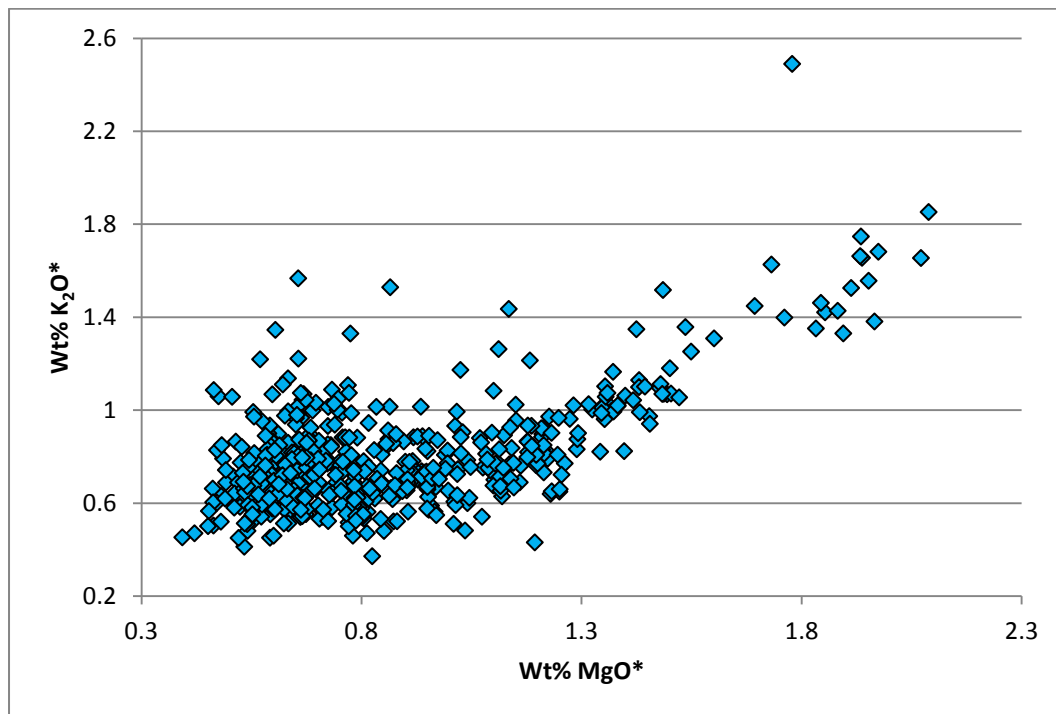


Figure 4.1.6 – A plot of magnesia versus potash in the base glasses from Eriswell.

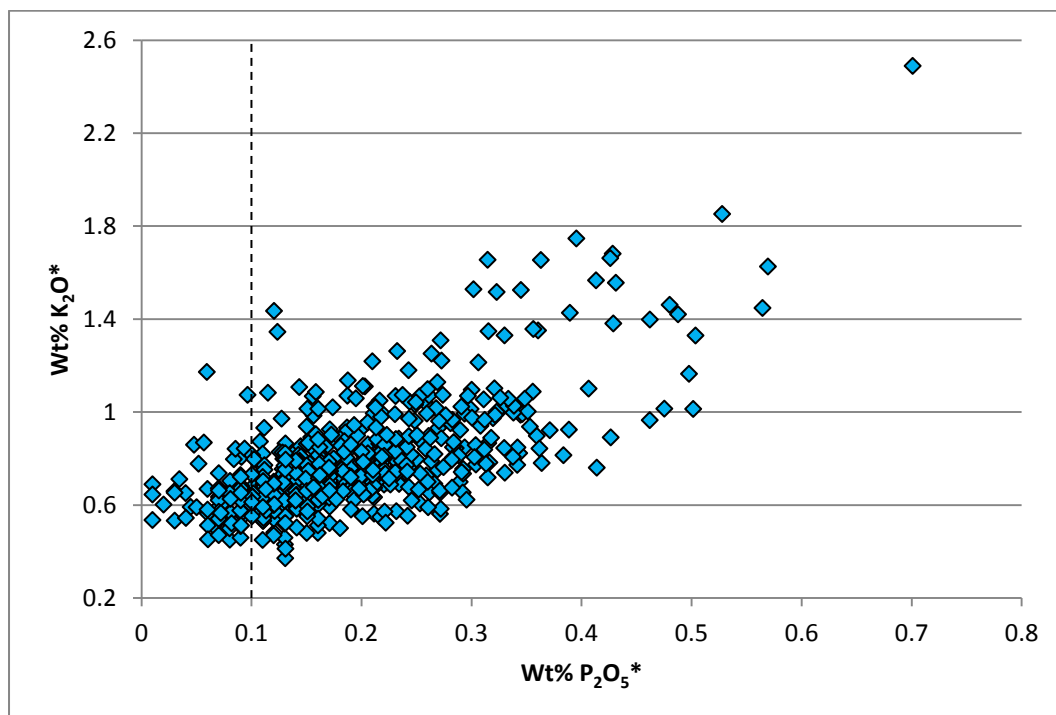


Figure 4.1.7 – A plot of phosphate versus potash in the base glasses from Eriswell. The dashed line represents the approximate detection limits for phosphate.

4.1.1.2. Silica

As previously mentioned (see Chapter 1, section 1.4), there are two possible sources of silica which may have been used for the production of early glass: crushed quartz (pebbles or quarried quartz) or quartz-rich sand (Freestone 2006: 205; Henderson *et al.* 2005: 665-666). It is generally assumed natron glass was produced using a calcareous quartz-rich sand, which introduced sufficient lime into the batch to render the glass stable (Freestone 2006: 205; Freestone *et al.* 2003a: 29; Henderson *et al.* 2005: 666; Verità 1995: 292). In contrast, low-lime sands or pure quartz pebbles are more likely to have been used in the production of plant-ash glass to prevent the glass from failing, as plant-ash is typically very rich in lime (Freestone 2006: 205-207; Freestone and Gorin-Rosen 1999: 105; Henderson *et al.* 2005: 666).

The use of pure quartz usually introduced relatively few impurities into the batch, whereas a number of mineral impurities (*e.g.* iron and alumina) were typically introduced with quartz-rich sand; *e.g.* alumina is introduced with mineral impurities such as feldspar and clay, and lime with shell or limestone naturally present in the sand (Arletti *et al.* 2008: 616; Freestone 2008: 83; Freestone and Hughes 2006: 151; Freestone *et al.* 2000: 72-73; Henderson *et al.* 2005: 670; Jackson 1996: 290-291; Verità 1995: 293). Alumina is disadvantageous to the glass batch as it increases the melting temperature, and is therefore assumed to be an unintentional addition (Jackson 1996: 291). Other common impurities typically include titanium, and occasionally also low levels potash and magnesia (Jackson 1996: 290-291; Verità 1995: 293).

The relative concentrations of these impurities vary from place to place, depending upon the geochemistry of the region from which the sand was sourced (Freestone *et al.* 2000: 71-72; Freestone and Hughes 2006: 151; Henderson 1985: 271; Vallotto and Verità 2000: 65-66). As such, the relative concentrations of these components can often be used as a chemical 'fingerprint', providing an indication as to the different sand source(s) exploited and sometimes its origins. All of the Eriswell glasses are likely to have been produced using a quartz-rich sand, which is primarily indicated by the high concentration of alumina present (in excess of 1.6% Al₂O₃*).

Iron is present at concentrations in excess of 0.3% Fe₂O₃*; the majority is usually introduced as an impurity with the glassmaking sand (*e.g.* Jackson 1996: 291), but small quantities were sometimes incidentally introduced with colourants such as cobalt (*e.g.* see Chapter 5, section 5.1.3) or through contamination from the fabric of the melting pot (see above). It may have also been deliberately added as a colourant (see Chapter 5, section 5.1.5) or a reducing agent (see Chapter 5, section 5.2.3), making the extent to which it was introduced with the silica source difficult to determine here.

In only one of the samples analysed as part of the present study, a bead from Spong Hill (Norfolk) discussed in section 4.1.1.3 below, is a pure silica source (*e.g.* quartz pebbles) likely to have been used. However, this is very unusual in natron glass.

4.1.1.3. Lime

As previously mentioned (see Chapter 1, section 4.1), lime in natron glass was either deliberately added as a separate component, or introduced as fragments of shell or limestone naturally present in the glassmaking sand (Freestone 2005: OO8.1.4; 2006: 207; Freestone *et al.* 2003a: 22-25; Henderson 1985: 277; Jackson 1996: 290; Vallotto and Verità 2000: 65). The origin of lime in natron glass has been widely debated and is still an ambiguous subject (*e.g.* Freestone 2006: 206-208; Freestone *et al.* 2003a: 22-25; see also Chapter 1, section 4.1). Whilst it is not possible to establish for certain whether lime was a deliberate addition in the Eriswell glasses, the author favours the view that it was probably ‘unintentionally’ added through the deliberate use of a calcareous quartz-rich sand. However, the composition of a translucent turquoise glass bead from Spong Hill (Norfolk) analysed as part of the present study suggests that lime was added as a separate ingredient on rare occasions.

The bead in question, a translucent turquoise biconical bead (coloured by copper; see Chapter 5, section 5.1.4) from grave 38/10a at Spong Hill, contains an unusually low concentration of alumina (0.6% Al₂O₃*) for a natron glass produced using a quartz-

rich sand; compare this to a minimum of 1.6% Al_2O_3^* in the other natron glasses analysed. The purity of the silica source used is further reflected by low concentrations of magnesia (0.7% MgO^*), potash (0.2% K_2O^*) and iron (0.4% Fe_2O_3^*). This is consistent with the use of pure silica, such as pebble quartz, as opposed to a quartz-rich sand. The low levels of potash and magnesia, together with the high concentration of soda present (18.9% Na_2O^*) are consistent with a natron alkali source. As such, the high concentration of lime (7.9% CaO^*) can only have been introduced as a separate ingredient, although it is not possible to determine whether this was in the form of shell or limestone without further analysis (*e.g.* for elemental strontium or strontium isotopes).

Elsewhere it has been noted that there is no evidence that natron glass was produced in the ancient world from pure quartz, and that none should be expected because their low lime content would have prevented its survival as it would have been susceptible to attack by groundwater (Freestone and Gorin-Rosen 1999: 115). Whilst this may be the case, the bead in question from Spong Hill survived because the glass contains a conscious, and probably separate, lime addition. However, this appears to be an isolated occurrence of such a glass, suggesting that the production of glass in this way was not common practice. It is not entirely clear why this is the case; the direct use of a calcareous quartz-rich sand would undoubtedly have been less labour-intensive than crushing quartz pebbles (Freestone 2006: 205). It may suggest production in a region in which such sands were not available, which may yet again open up the possibility of a trade in natron to Europe during the period; this is not within the scope of the present study to discuss, but as it is an isolated occurrence it cannot be used to argue for a widespread trade in natron.

Our understanding of early glass recipes is still far from clear; far more work is required in order to establish the extent to which lime was a deliberate or 'unintentional' addition. Previous studies have demonstrated the potential of strontium isotopes in establishing the form in which lime entered the batch in natron glass (marine shell or limestone) (*e.g.* Freestone *et al.* 2003a; Wedepohl and Baumann 2000), but these approaches cannot clarify whether or not it was a separate addition. In any case, these early craftsmen must have understood the amount of lime needed to produce a stable glass; excess lime would have led to failure of the batch

(*e.g.* Freestone and Gorin-Rosen 1999: 115). These early craftsmen clearly had an empirical knowledge of the importance of lime in glass production, and the identification of such a glass clearly demonstrates that lime was at the very least a conscious (if not a separate) addition.

4.1.1.4. Decolourants

Many uncoloured glasses are not truly colourless. They are often tinted to some degree, usually by low concentrations of impurities (most notably iron) which were unintentionally introduced into the glass with the batch ingredients (*e.g.* sand; see this chapter, section 4.1.1.3). This is discussed in detail in Chapter 5, section 5.1.1. These tints were often undesirable, so decolourants were added to counteract them, either during the primary production of the raw glass itself or the secondary remelting of this glass (Vallotto and Verità 2000: 63). The purpose of decolourisation was to remove any tints to produce a truly colourless glass. However, this was not always successful, as many of the glasses containing decolourants are tinted to some degree; it is therefore possible that they were added simply to reduce the *intensity* of these tints.

Two materials were used as decolourants in early glass: antimony and manganese (Biek and Bayley 1979: 6; Guido 1978: 9; Henderson 1985: 284; Jackson 1996: 291; 2005: 764; Sayre 1963: 265-266; Sayre 1965: 149; Wilthew 2006: 394). Under reducing conditions, these could counteract the undesirable tints caused by iron (Biek and Bayley 1979: 6; Schreurs and Brill 1984: 208). However, control of the redox conditions within the furnace, as well as the amount of decolourant added to the glass, was crucial in order to produce the desired effects. If the furnace atmosphere was oxidising antimony could instead cause opacity (Bayley 1999: 91; Heyworth 1996b: 51; Sayre 1963: 272; Sayre 1965: 149). Similarly, in oxidising conditions manganese could act as a colourant rather than a decolourant, producing a strong purple colour (Fiori and Vandini 2004: 189; Henderson 1985: 283; Schreurs and Brill 1984: 205; Weyl 1951: 123; see also Chapter 5, section 5.1.2).

Antimony is a more effective decolourant than manganese, and typically produces a very clear glass, but can also impart a slight yellow tint (Henderson 1985: 284; Henderson 2000a: 38; Sayre 1963: 280). It can also act as a clarifier by facilitating the removal of bubbles and gases from the melt, thereby increasing its brilliance (Bayley 1999: 91; Sayre 1963: 266; Weyl 1951: 118). Manganese oxide can be a somewhat less effective decolourant (Fiori and Vandini 2004: 190; Henderson 2000a: 38; Sayre 1963: 280), and can impart a pinkish tint to glass (Brill 1988: 276).

Antimony was used as a decolourant as early as the 7th century BC and continued in use throughout the Early Roman period (Fiori and Vandini 2004: 190; Guido 1978: 10; Sayre 1963: 270-272; Sayre and Smith 1967: 300-301). It is generally accepted that it was gradually replaced by manganese, both as a decolourant and opacifier, between the 2nd and 4th centuries AD (*e.g.* Brill 2006: 139; Sayre 1963: 279; Sayre 1965: 150). Much 'colourless' Roman glass contains low concentrations of both antimony and manganese (*e.g.* see this chapter, section 4.3), which has been attributed to the recycling and mixing of earlier antimony-decoloured and later manganese-decoloured glass (*e.g.* Jackson 2005: 773; Foster and Jackson 2010: 3072). Whilst there appear to be exceptions where antimony was used to decolourise post-Roman glass, it is more typically decolourised by manganese (Henderson 1990: 157; Henderson and Warren 1983: 169; Heyworth 1996b: 51; Sayre 1963: 279; Sayre 1965: 150). Antimony detected in glass from post-Roman contexts is therefore usually interpreted as being indicative of the recycling of earlier Roman material (Bimson and Freestone 2000: 134; Freestone 1993: 741; Heyworth 1996b: 51; Ubaldi and Verità 2003: 127).

Unlike antimony, which at detectable levels is usually taken to indicate a deliberate addition, manganese may be either incidentally incorporated into glass as an impurity (for example through the addition of plant-ash; see this chapter, section 4.4) or deliberately added as a separate ingredient (see Chapter 5, section 5.3.5). There is an enormous amount of inconsistency in published studies regarding the levels at which manganese is assumed to represent a deliberate addition, but it is generally assumed that anything above 0.2% MnO* in natron glass is intentional (*e.g.* Freestone 2006: 209; Freestone *et al.* 2005b: 154; Sayre 1963: 265; Silvestri 2008: 1496). Indeed, it is rare for glassmaking sands to contain manganese at levels in

excess of 0.1% (Foy *et al.* 2003: 47) and manganese is therefore only thought to have been introduced as an impurity in concentrations up to approximately 0.15% (Brill 1988: 259). Only when plant ash has been used can manganese be reliably interpreted as an unintentional addition, as some plant ashes are manganese-rich (*e.g.* Jackson and Smedley 2004: 39; 2007: 126-127; Jackson *et al.* 2005: 789).

A plot of the oxides of manganese and antimony (Figure 4.1.8) shows that the vast majority of samples from Eriswell contain manganese, with only a handful containing antimony at detectable levels. None of the glasses containing more than 1.0% MnO* contain detectable antimony. However, a significant proportion of these glasses contain both antimony and manganese, which is a characteristic of some Roman glass (see this chapter, section 4.3). The high levels of antimony in several samples in Figure 4.1.9 also suggests the re-use of earlier Roman material; those samples containing Sb₂O₃* in excess of 1.0%, all of which are translucent cobalt-blue except for one (opaque turquoise sample ERL104:G290:1734, containing 3.2% Sb₂O₃* as an opacifier), are likely to have been coloured using recycled Roman antimony-opacified blue cullet (see Chapter 5, section 5.1.3).

The addition of antimony and manganese to the Eriswell glasses as decolourants does not always appear to have been tightly controlled, as implied by the broad scatters of data in Figures 4.1.9 and 4.1.10. If they were controlled additions, a positive correlation would be expected with iron, unless antimony was added as an opacifier (this is likely to be the case with the majority of samples containing in excess of 1.0% Sb₂O₃* in Figure 4.1.9; see above). It is likely that the variable concentrations of antimony and manganese (when present as decolourants) relate to the nature of the different base glass types used; the addition of manganese in particular may have been carefully controlled in some cases (*e.g.* see this chapter, sections 4.4 and 4.5).

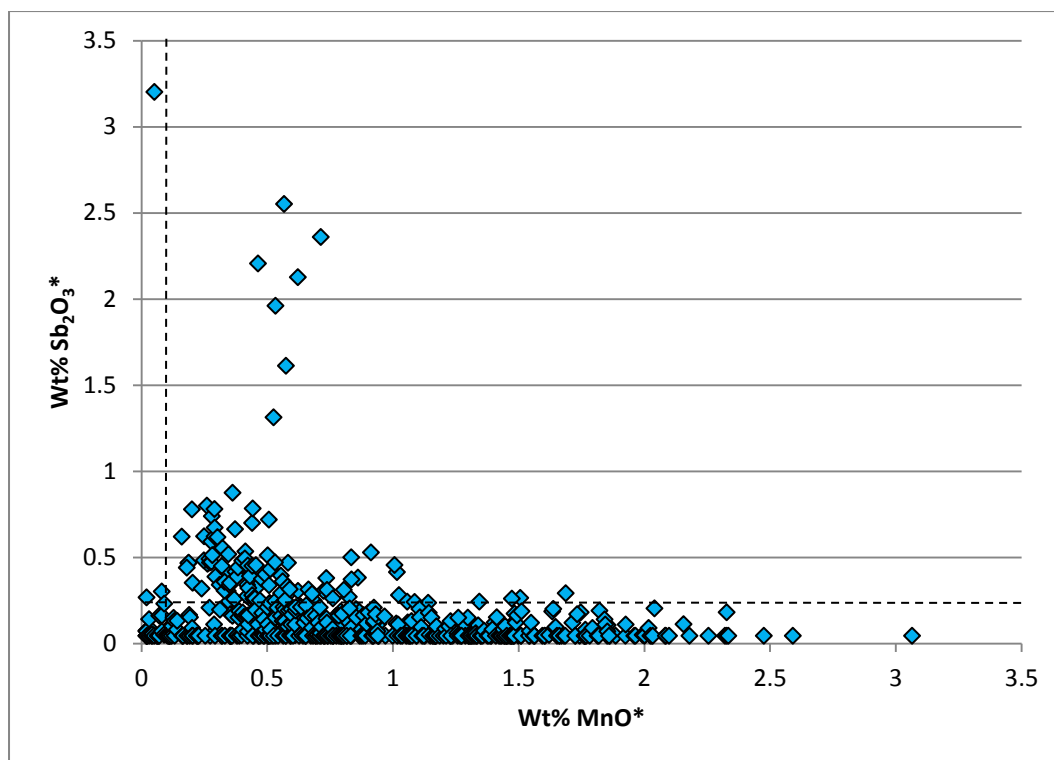


Figure 4.1.8 – A plot of manganese oxide versus antimony oxide for the reduced glasses from Eriswell. High-lead samples affected by contamination have been omitted (see text for details). The dashed lines represent the approximate detection limits for antimony oxide and manganese oxide.

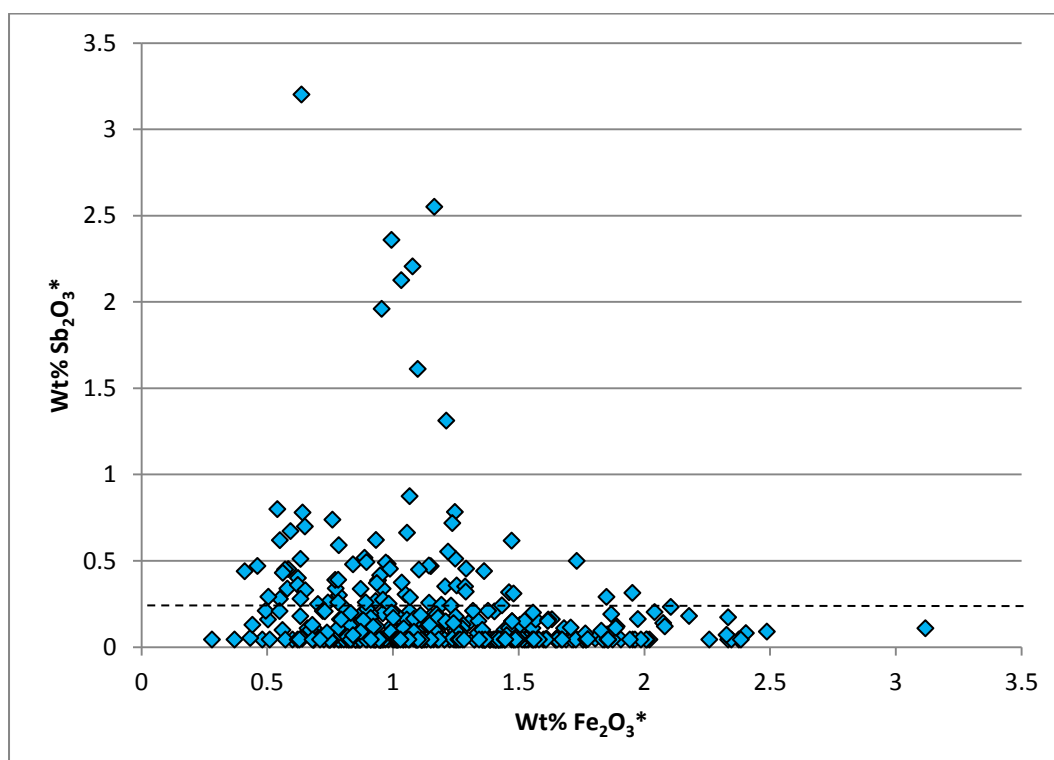


Figure 4.1.9 – A plot of iron oxide versus antimony oxide for the reduced glasses from Eriswell. High-lead samples affected by contamination have been omitted (see text for details). The dashed line represents the detection limits antimony oxide.

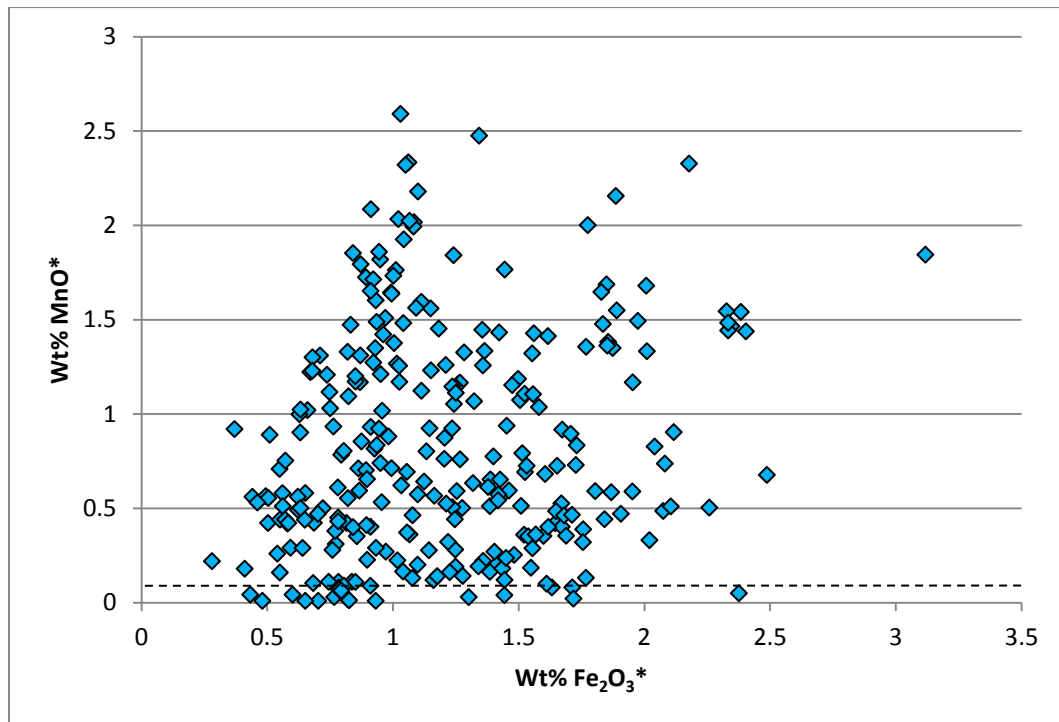


Figure 4.1.10 – A plot of iron oxide versus manganese oxide for the reduced glasses from Eriswell. High-lead samples affected by contamination have been omitted (see text for details). The dashed line represents the approximate detection limits for manganese oxide.

4.2. The Compositional Groups

Six different types of base glass have been identified at Eriswell using a number of different variables. With the exception of the ‘A2b Blue’ group, the names ascribed to these groups generally correspond to the names ascribed to these glass types in published literature. The number of different samples and individual beads analysed are specified for each group; sample numbers exceed bead numbers due to the sampling of a number of different glass colours from polychrome bead types. The groups are as follows:

- The ‘**Roman**’ group corresponds to published analyses of Roman blue-green tinted glass (*e.g.* Foster and Jackson 2009; Jackson 1992; Jackson 1996; Jackson 2005). Its composition suggests that it is likely to represent recycled material. It comprises 244 samples taken from a total of 155 beads.
- The ‘**Saxon I**’ group broadly corresponds to the ‘Period I natron’ group established by Freestone *et al.* (2008) for Anglo-Saxon vessel glass. It comprises 147 samples taken from a total of 144 beads.
- The ‘**Saxon II**’ group corresponds to the high MgO ‘Saxon II’ groups established by Freestone *et al.* (2008) for Anglo-Saxon vessel glass. It comprises 101 samples taken from a total of 68 beads. This is a complex group, some of which is likely to represent natron-type glass to which small quantities of plant ash have been added (see this chapter, section 4.4). Several samples from this group also correspond closely to Foy *et al.*’s ‘Group 2.1’ (Foy *et al.* 2003).
- The ‘**HIMT**’ group was first defined by Freestone (1994) and is so called on account of its **H**igh levels of **I**ron, **M**anganese, **T**itanium and **m**agnesia. It comprises a small group of 20 samples taken from a total of 16 beads.
- The ‘**Levantine I**’ group corresponds to Late Roman and Early Byzantine glass produced using sand sourced from the Palestinian coast (Brill 1988: 266; Freestone *et al.* 2000). It is a small group comprising 16 samples taken from a total of 13 beads
- The ‘**A2b Blue**’ group is a new glass group established in this study. It comprises a small assemblage of translucent cobalt-blue beads, primarily

attributed to Brugmann's phase A2b (Brugmann 2004; Penn and Brugmann 2007). It is a very small group consisting of 11 samples taken from a total of 11 beads.

A re-evaluation of the five 'Period II natron' samples analysed by Freestone *et al.* (2008) suggests that their cobalt-blue samples (samples 150 and 151; the globular beakers from Broomfield) correspond to 'Saxon I (blue)' glass in the present study (see this chapter, section 4.4). The olive-green claw beaker from Taplow (sample 79) appears to have been produced from 'Levantine I' glass (see this chapter, section 4.6). The remaining two 'Period II natron' glasses, including the green tinted palm cup from Faversham (sample 93) and the blue-green tinted globular beaker from Wye Down (sample 148), are likely to have been produced from recycled 'Roman' glass; as antimony was not analysed for in these latter two samples this cannot be confirmed, but the high levels of silica (approximately 69% SiO₂* in each) are well outside of the range typical for 'Saxon' glass and well within the range typical for 'Roman' glass (*e.g.* Figures 4.2.5 and 4.2.6). Furthermore, the low levels of manganese detected (approximately 0.3% MnO*), together with the 'natural' blue-green and green tints of these glasses, is consistent with the use of Roman blue-green tinted glass (see this chapter, section 4.3).

Average reduced compositions of the different base glass types at Eriswell are presented in Table 4.2.1, and the compositional differences between these groups are demonstrated by a series of bivariate plots in Figures 4.2.1-4.2.10.

Table 4.2.1 – Average compositions for the different base glass types identified at Eriswell.

<i>Composition</i> ¹	<i>Oxide (wt %)</i> ²													<i>Total</i>
	<i>Na₂O*</i>	<i>MgO*</i>	<i>Al₂O₃*</i>	<i>SiO₂*</i>	<i>P₂O₅*</i>	<i>SO₃*</i>	<i>Cl*</i>	<i>K₂O*</i>	<i>CaO*</i>	<i>TiO₂*</i>	<i>MnO*</i>	<i>Fe₂O₃*</i>	<i>Sb₂O₃*</i>	
Roman (n = 82)	17.6	0.6	2.3	68.4	0.2	0.4	1.1	0.7	6.6	0.1	0.6	0.9	0.5	100.0
SD	1.2	0.1	0.2	1.2	0.1	0.1	0.1	0.1	0.7	0.0	0.3	0.4	0.6	
Saxon I (n = 134)	18.9	0.9	2.3	65.5	0.1	0.5	1.0	0.7	7.6	0.2	1.0	1.3	b.d.	100.0
SD	1.0	0.2	0.2	1.0	0.1	0.1	0.1	0.1	0.7	0.1	0.5	0.4	-	
Saxon II (n = 54)	18.1	1.4	2.5	64.9	0.3	0.5	0.9	1.1	7.6	0.2	1.0	1.5	b.d.	100.0
SD	1.5	0.3	0.3	1.4	0.1	0.1	0.2	0.3	0.9	0.0	0.7	0.5	-	
HIMT (n = 6)	18.4	0.9	2.4	66.4	0.1	0.4	1.0	0.6	6.1	0.3	1.9	1.5	b.d.	100.0
SD	0.5	0.1	0.2	1.1	0.0	0.0	0.1	0.2	0.5	0.1	0.5	0.2	-	
Levantine I (n = 11)	15.2	0.7	3.1	69.6	0.2	0.2	1.0	0.7	8.3	0.1	0.1	0.8	b.d.	100.0
SD	0.8	0.2	0.2	1.1	0.1	0.1	0.0	0.1	0.7	0.0	0.1	0.3	-	
A2b Blue (n = 11)	19.8	0.7	2.2	68.4	0.1	0.5	1.1	0.6	5.6	0.1	0.1	0.8	b.d.	100.0
SD	0.7	0.1	0.1	0.9	0.0	0.1	0.1	0.1	0.4	0.0	0.1	0.0	-	

¹Averages taken only from samples for which the values for alumina and iron have *not* been assumed. SD = standard deviation.

²Area analyses normalised to 100%. b.d. = below detection. See Chapter 2, section 2.3.1 for details.

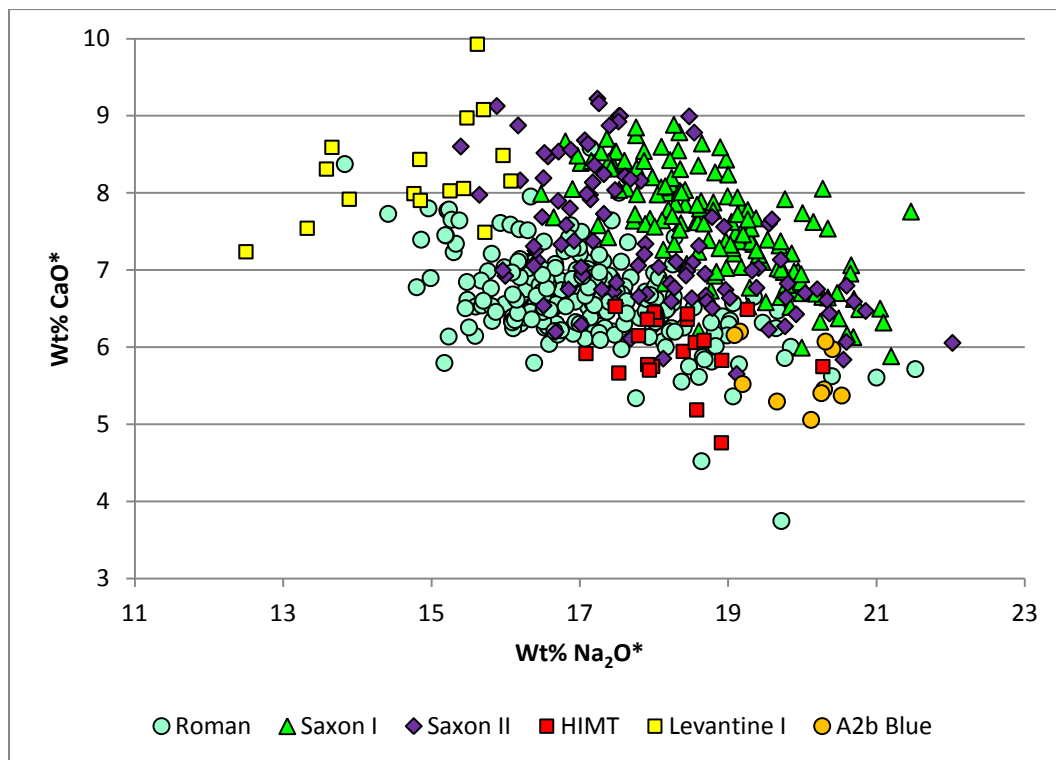


Figure 4.2.1 – A plot of soda versus lime for the different base glass types identified at Eriswell.

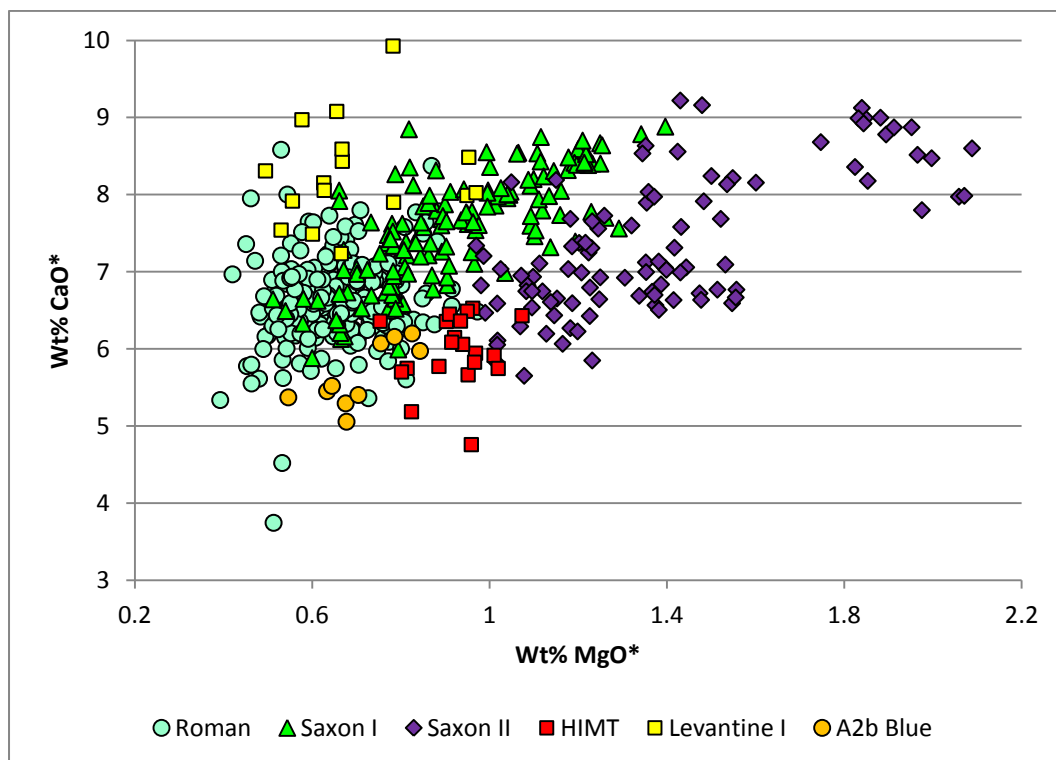


Figure 4.2.2 – A plot of magnesia versus lime for the different base glass types identified at Eriswell.

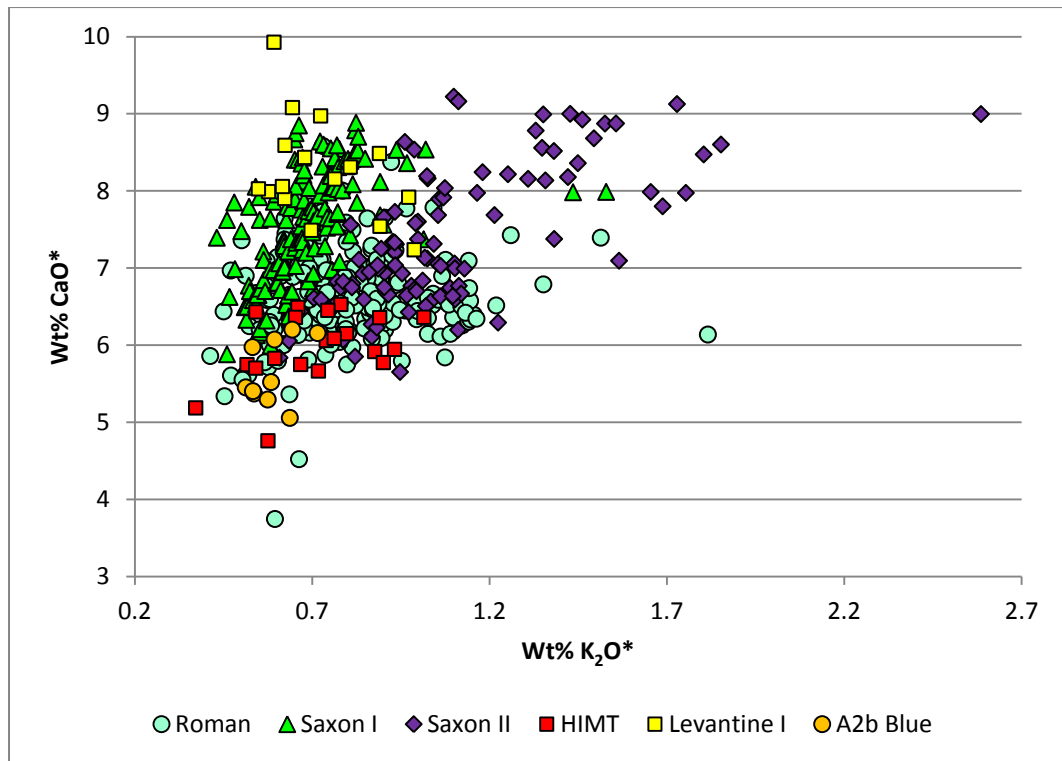


Figure 4.2.3 – A plot of potash versus lime for the different base glass types identified at Eriswell.

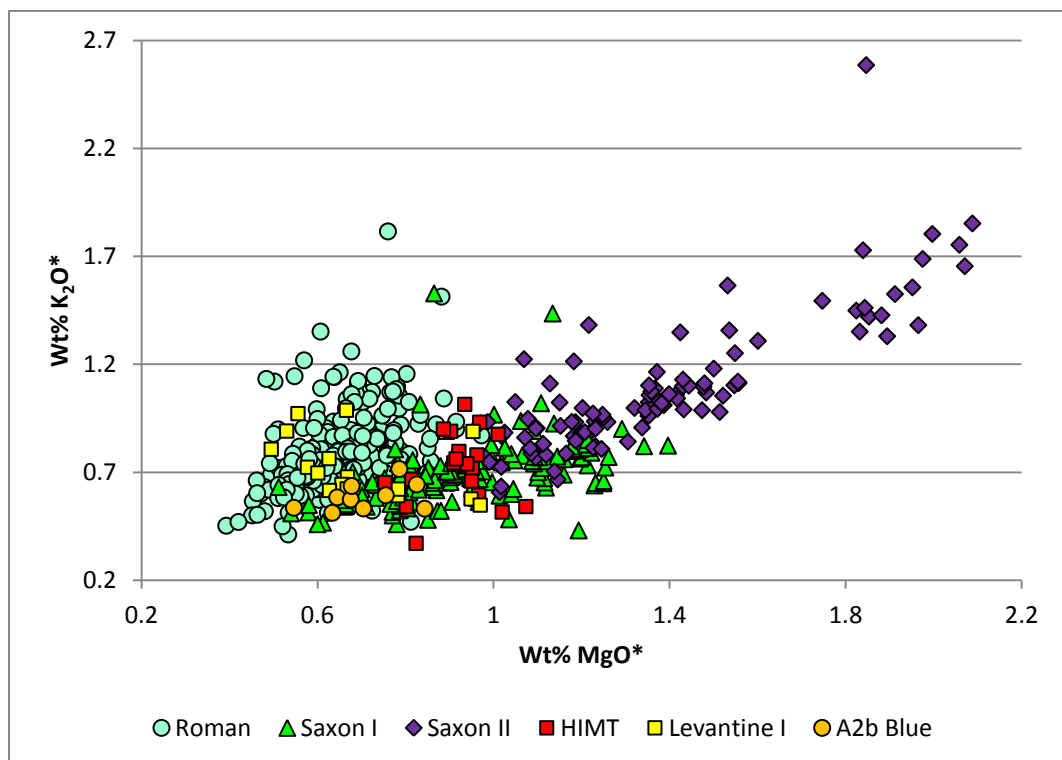


Figure 4.2.4 – A plot of magnesia versus potash for the different base glass types identified at Eriswell.

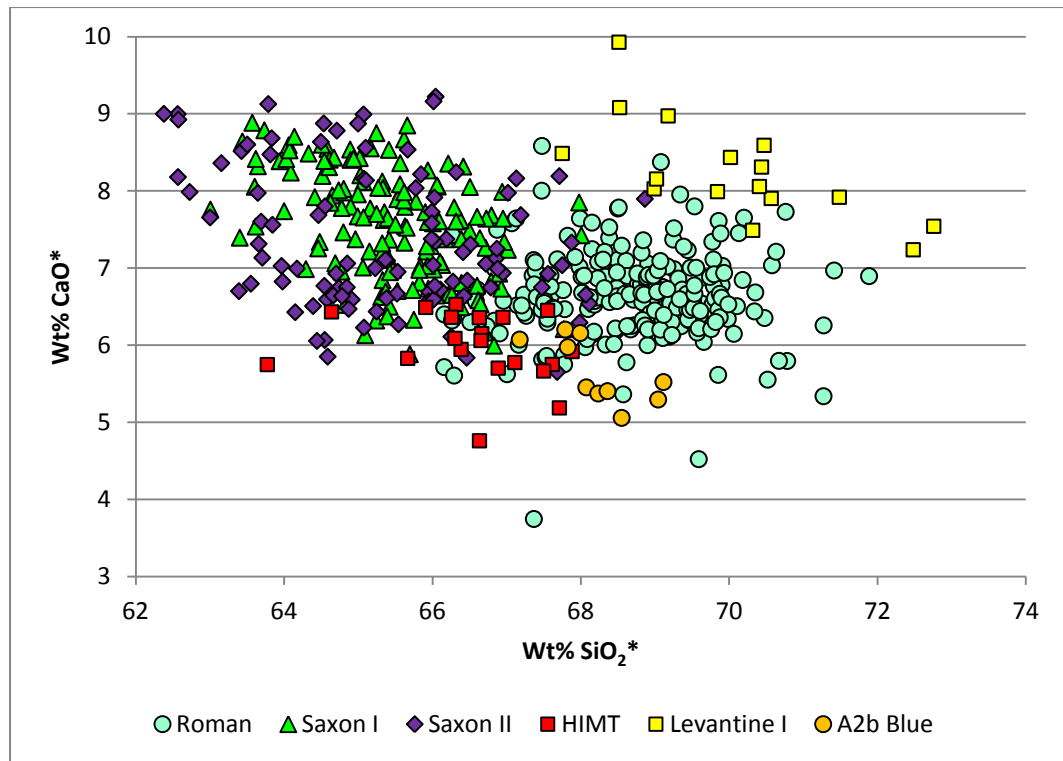


Figure 4.2.5 – A plot of silica versus lime for the different base glass types identified at Eriswell.

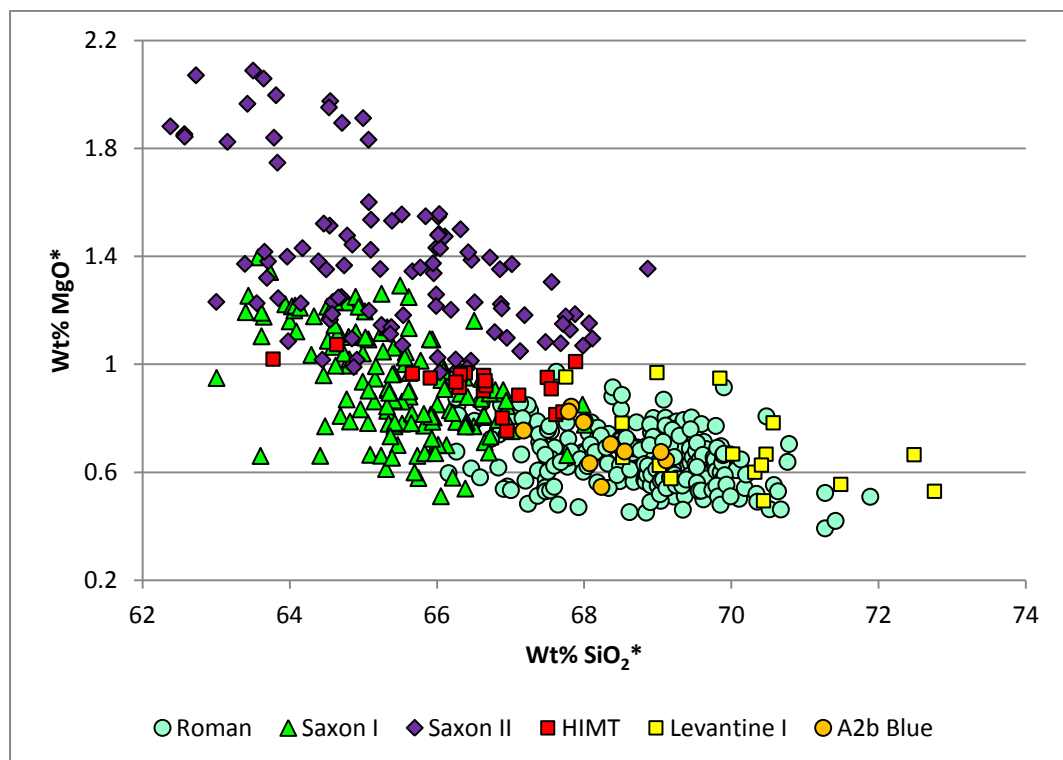


Figure 4.2.6 – A plot of silica versus magnesia for the different base glass types identified at Eriswell.

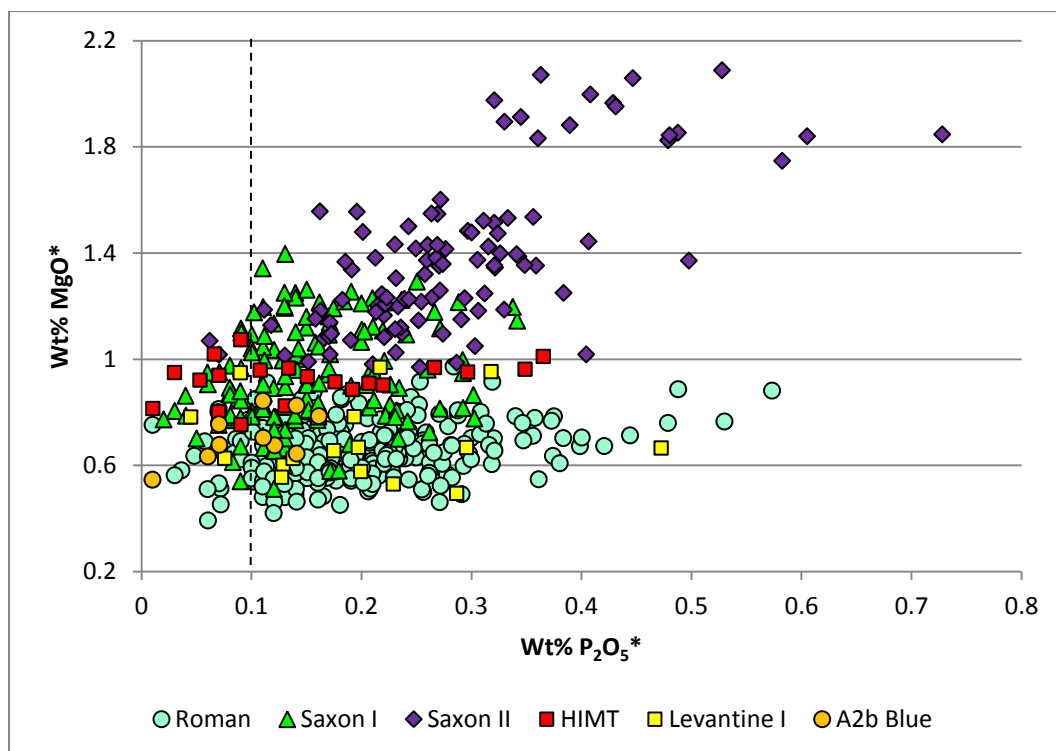


Figure 4.2.7 – A plot of phosphate versus magnesia for the different base glass types identified at Eriswell. The dashed line represents the approximate detection limits for phosphate.

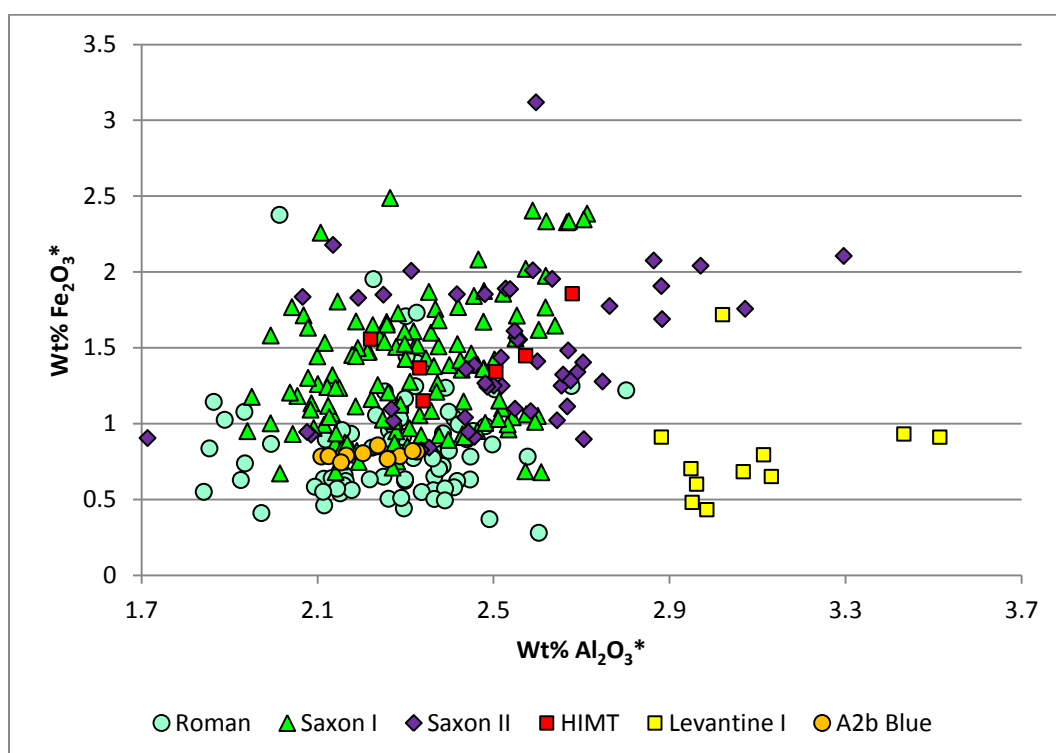


Figure 4.2.8 – A plot of alumina versus iron oxide for the different base glass types identified at Eriswell, omitting those samples which are likely to have been affected by iron and alumina contamination (see text for details).

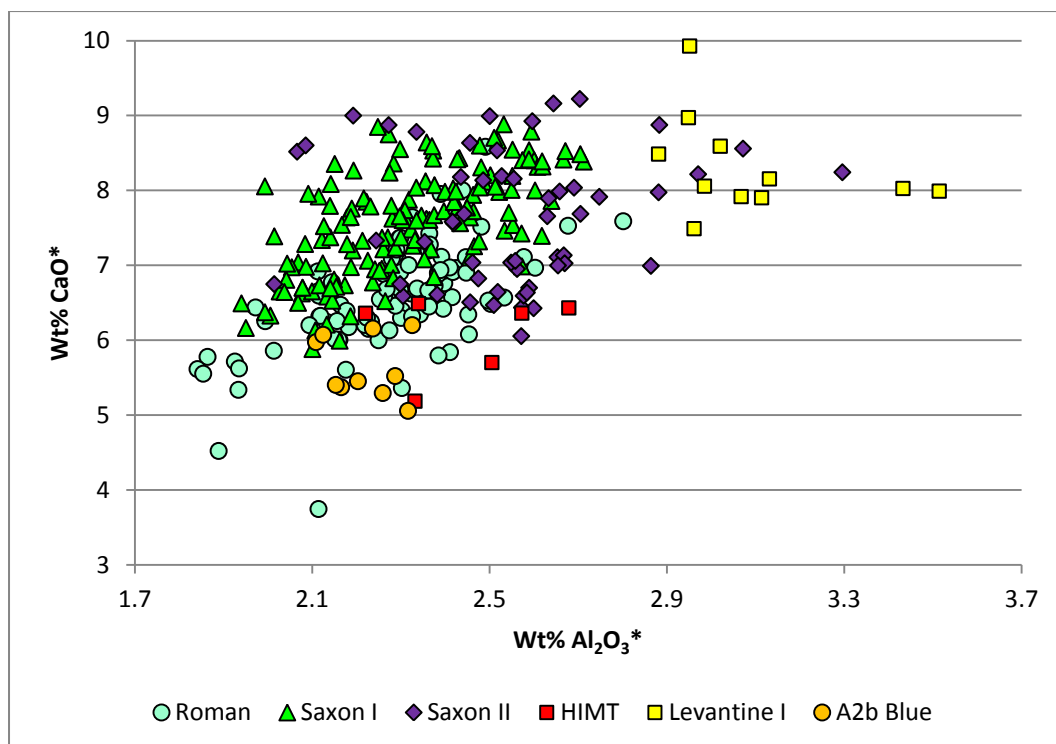


Figure 4.2.9 – A plot of alumina versus lime for the different base glass types identified at Eriswell, omitting those samples which are likely to have been affected by alumina contamination (see text for details).

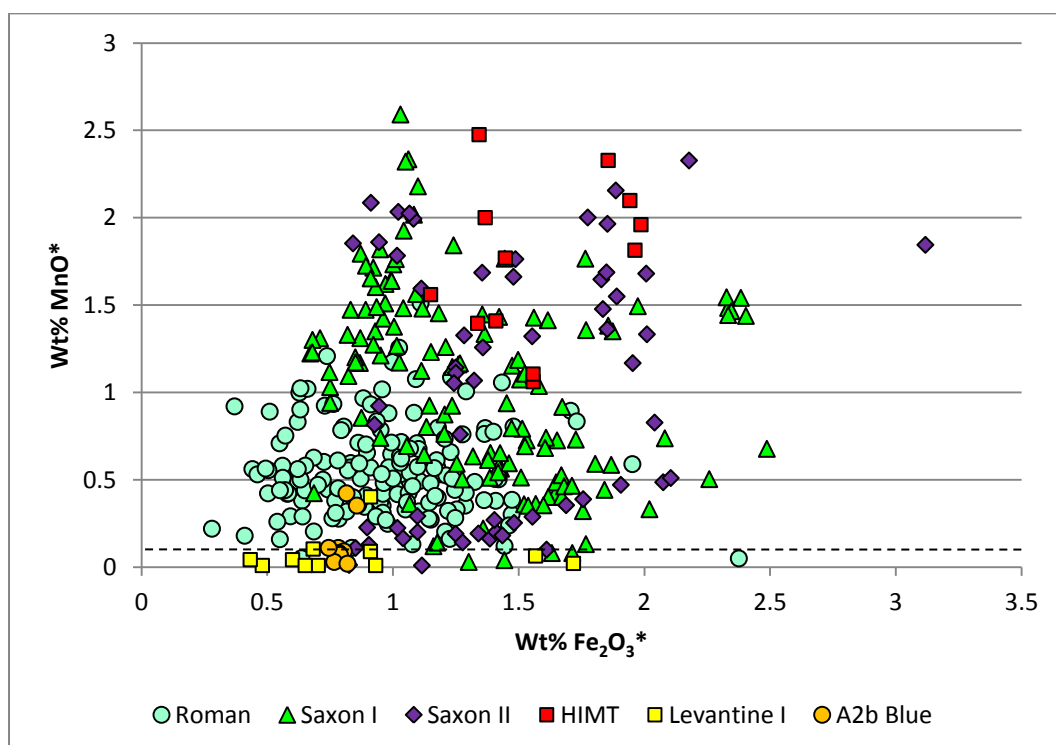


Figure 4.2.10 – A plot of iron oxide versus manganese oxide for the different base glass types identified at Eriswell, omitting those samples which are likely to have been affected by iron and alumina contamination (see text for details). The dashed line represents the approximate detection limits for manganese oxide.

Relative proportions of the oxides of iron, alumina and titanium are often strong indicators of different glass compositions as they reflect the use of different glassmaking sands (corresponding to impurities such as feldspar and clay) (Freestone *et al.* 2002b: 265). However, these components cannot be used as reliable compositional indicators in many of the glasses which contain lead in the present study, due to problems of contamination (see this chapter, section 4.1). However, a plot of alumina versus iron oxide (Figure 4.2.8) and alumina versus lime (Figure 4.2.9) for those samples which have been relatively unaffected by contamination is possible; this includes translucent 'light' and naturally coloured (uncoloured) glass, translucent pink-brown glass, translucent blue, glass translucent turquoise glass, some opaque white glasses, opaque blue glass, opaque turquoise glass and opaque orange glass. Iron oxide is clearly elevated in some of the cobalt-blue glasses, suggesting some contamination from iron impurities in the cobalt colourant (see Chapter 5, section 5.1.3); Figures 4.2.8-4.2.10 should therefore be interpreted with some caution.

The base glass types were grouped primarily according to their composition, but typology, chronology and colour were used to refine the final groups. However, the boundaries for many of these groups are not clear-cut, so the attribution of certain samples to one or the other group is in some cases subjective. In scientific studies of early glass, iron and alumina are usually among the first components to be examined in the distinction between different base glass types, as these components reflect variations in the composition of the sand source used. However, due to the problems of contamination discussed earlier, these components cannot be reliably compared in the present study. An attempt will therefore be made here to broadly explain how the three primary groups ('Roman', 'Saxon I' and 'Saxon II') were arrived at.

A plot of soda versus lime for the Eriswell glasses revealed two broad negative correlations, demonstrating two different ratios of soda to lime (Figure 4.2.11; compare to Figure 4.2.1). The Eriswell dataset was therefore simply divided into two groups according to their concentrations of soda and lime; 'high soda-lime' glasses (where $\text{Na}_2\text{O}^* + \text{CaO}^*$ is greater than 25%) and 'low soda-lime' glasses (where $\text{Na}_2\text{O}^* + \text{CaO}^*$ is less than 25%). The compositional distinction between these two groups was largely confirmed by a plot of silica versus lime: 'high soda-lime'

glasses typically contain $>67\%$ SiO_2^* , whereas 'low soda-lime' glasses typically contain $<67\%$ SiO_2^* (Figure 4.2.12; compare to Figure 4.2.5). These two groups were respectively sub-divided into 'high-magnesia' ($>1.0\%$ MgO^*) and 'low-magnesia' ($<1.0\%$ MgO^*) glasses (Figure 4.2.13; compare to Figure 4.2.2). The 'low soda-lime (low MgO)' group represents the foundation for the 'Roman' compositional group, the 'high soda-lime (low MgO)' group the foundation for the 'Saxon I' group, and the 'low soda-lime (high MgO)' and 'high soda-lime (high MgO)' groups the foundation for the 'Saxon II' group.

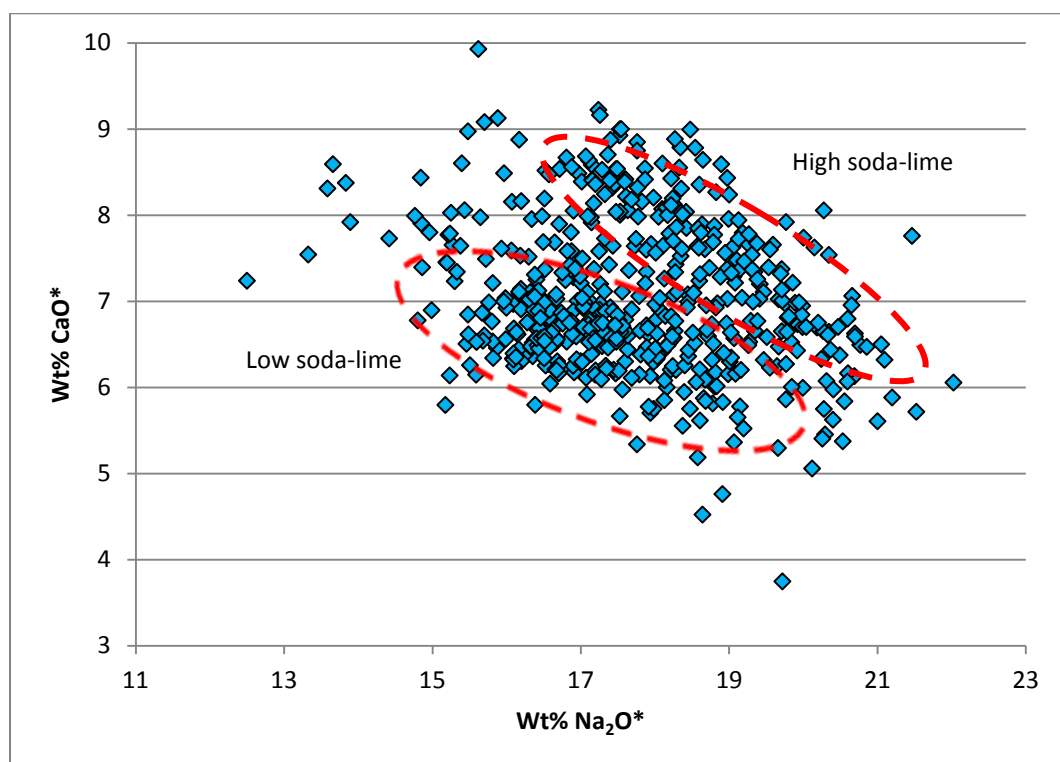


Figure 4.2.11 – A plot of soda versus lime for the different base glass types identified at Eriswell, showing the 'low-soda-lime' and 'high soda-lime' samples. Compare to Figure 4.2.1.

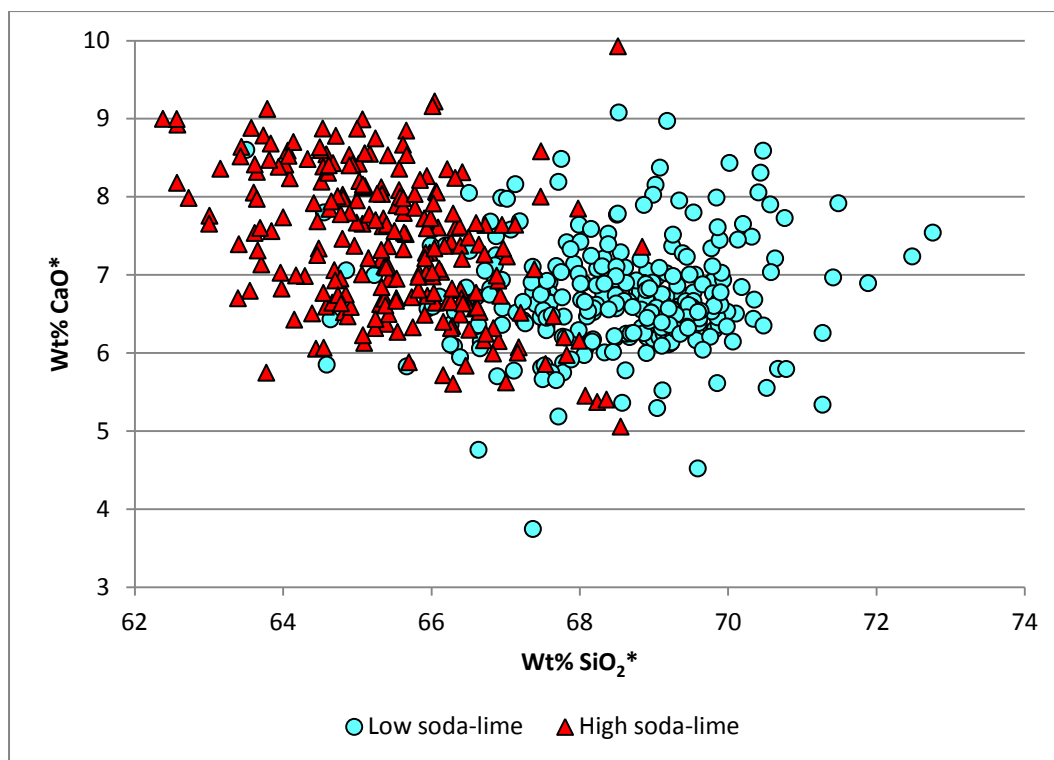


Figure 4.2.12 – A plot of silica versus lime for the different base glass types identified at Eriswell, showing the ‘low-soda-lime’ and ‘high soda-lime’ samples. Compare to Figure 4.2.5.

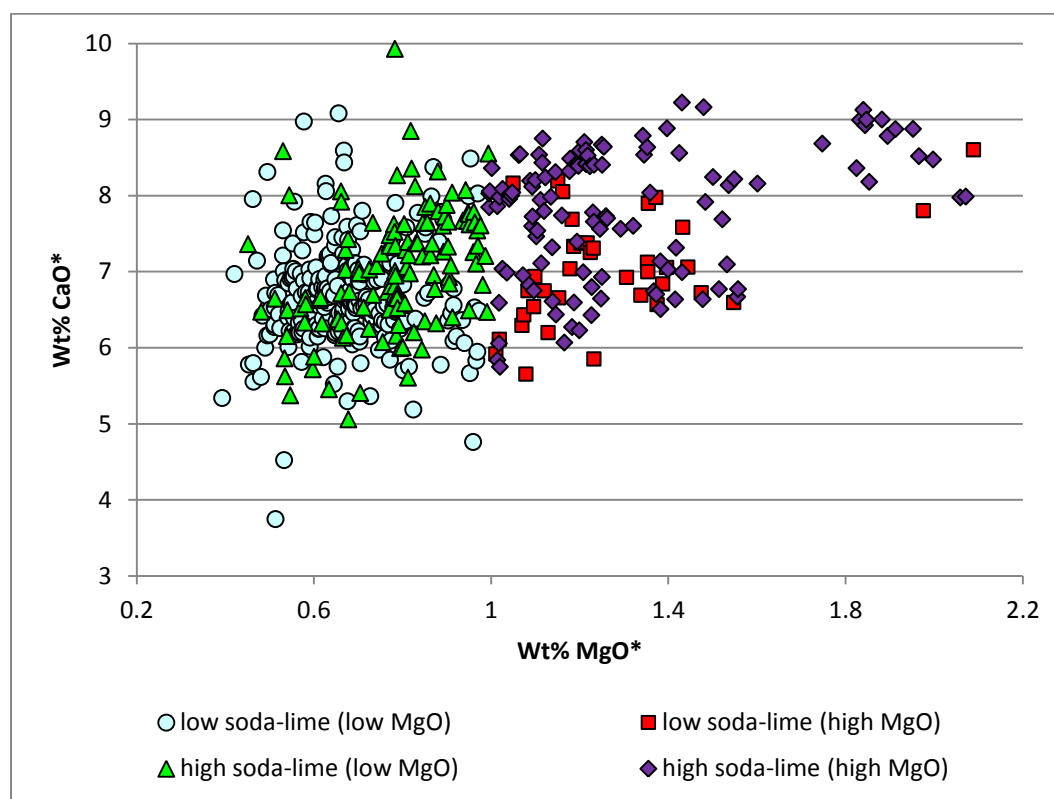


Figure 4.2.13 – A plot of magnesia versus lime for the different base glass types identified at Eriswell, showing high-magnesia and low-magnesia samples in the ‘low-soda-lime’ and ‘high soda-lime’ glasses respectively. Compare to Figure 4.2.2.

These groups were further refined by minor compositional differences; for example, samples containing antimony at detectable levels could be fairly confidently attributed to the ‘Roman’ group. The ‘Saxon’ groups were further refined and subdivided by a plot of manganese versus magnesia (see this chapter, section 4.4; in particular Figure 4.4.7). The final groups were arrived at using Brugmann’s typological and chronological attributions, together with the colour of the glass, as a guide. Beads attributed to phase A proved more likely to be of the ‘Saxon I’ type, whereas those attributed to phase B proved more likely to be of the ‘Saxon II’ type (see this chapter, section 4.2.8). Translucent samples proved more likely to be of the ‘Saxon I’ type and opaque samples of the ‘Saxon II’ type (see this chapter, section 4.2.9).

Overall, ‘Saxon I’ and ‘Saxon II’ glass is characterised by a lower concentration of silica relative to ‘Roman’ glass (typically <67% SiO₂* vs. typically >67% SiO₂*; Figures 4.2.5 and 4.2.6), together with different ratios of soda to lime (Figure 4.2.1). ‘Saxon II’ glass is further distinguished by elevated magnesia, which is strongly correlated with potash (Figure 4.2.4; $r^2 = 0.70$). The ‘Saxon I’ and ‘Saxon II’ glasses can only really be distinguished from one another based on their different proportions of magnesia to lime (Figure 4.2.2), which is reflected in a plot of lime versus potash (Figure 4.2.3).

The ‘HIMT’, ‘Levantine I’ and ‘A2b Blue’ groups were borne out by a number of components which do not match the compositions of *typical* ‘Roman’ or ‘Saxon’ type glasses (see this chapter, sections 4.5-4.7). The ‘HIMT’ and ‘Levantine I’ glasses are distinct glass types which are well-established in published literature (*e.g.* Freestone *et al.* 2000; 2002b; Freestone 2006). ‘HIMT’ glass can be primarily distinguished from other glass types based on its elevated levels of titanium (0.2-0.5% TiO₂*), CaO* at concentrations typically below 6.5% (*e.g.* Figures 4.2.1-4.2.3 and 4.2.5), MnO* in excess of 1.0% (*e.g.* Figure 4.2.10) and MgO* typically above 0.8% (*e.g.* Figure 4.2.2). However, this glass has a number of very close compositional similarities to ‘Saxon’ glass and is particularly difficult to distinguish from it; often the low levels of lime are of the few discriminating elements here, as titanium is sometimes introduced in high concentrations through contamination from the melting pot.

‘Levantine I’ glass is another very distinctive glass type (see this chapter, section 4.6), which is particularly characterised by low concentrations of Na_2O^* (typically well below 16%; *e.g.* Figure 4.2.1) in combination with high CaO^* (typically well above 7.5%; *e.g.* Figures 4.2.1 and 4.2.5) and Al_2O_3^* (typically above 2.9%; *e.g.* Figures 4.2.8 and 4.2.9) relative to other glass types. Manganese is also absent or near absent in this glass type (*e.g.* Figure 4.2.10). Its composition is otherwise fairly similar to ‘Roman’ glass; K_2O^* and MgO^* are both at concentrations below 1.0% (*e.g.* Figure 4.2.3) and silica is similarly elevated (typically above 67% SiO_2^* ; Figures 4.2.5 and 4.2.6).

‘A2b Blue’ glass also has a number of compositional similarities to ‘Roman’ and ‘Levantine I’ glass. Its only real distinguishing major elements are soda and lime; with Na_2O^* on the high side (typically above 18.5%; Figure 4.2.1) and CaO^* on the low side (typically less than 6.0%; *e.g.* Figures 4.2.3, 4.2.5 and 4.2.9). The absence of antimony and the near absence of manganese in ‘A2b Blue’ glass (*e.g.* Figure 4.2.10) are also distinguishing features of this glass type. As the name suggests, ‘A2b Blue’ glass is exclusively translucent blue.

In order to confirm the different base glass types established at Eriswell, cluster analysis was undertaken (Figure 4.2.14). Hierarchical clustering was performed with the SPSS software package, using Ward’s method with squared Euclidian distance as a measure of dissimilarity. Each element was standardised to a range of 0-1. The concentrations of all of the elements used to calculate the composition of the base glasses (Na_2O^* , MgO^* , Al_2O_3^* , SiO_2^* , P_2O_5^* , SO_3^* , Cl^* , K_2O^* , CaO^* , TiO_2^* , MnO^* , Fe_2O_3^* and Sb_2O_3^*) were employed to establish the clusters. Given the scale of the dataset, it was not feasible to include all samples in the cluster analysis as the diagram obtained is far too large to reproduce; it should be stressed that cluster analysis was undertaken to *confirm* the compositional groups, not to *establish* them.

A small number of samples were selected largely at random from each of the compositional groups established to provide an indication as to the reliability of these groups. 10 samples were selected from the smallest groups (‘HIMT’, ‘Levantine I’ and ‘A2b Blue’), and 20 samples from the largest groups (‘Saxon I’, ‘Saxon II’ and ‘Roman’; this includes the sub-groups established for ‘Saxon I’ and

‘Saxon II’ glasses later in this chapter, section 4.4). Samples in which the concentrations of iron and alumina had been assumed (due to contamination or deliberate iron additions) were avoided where possible to reduce any potential bias in the clusters produced. However, even when samples for which the concentrations of iron and alumina *have* been assumed are processed, the clusters produced (not reproduced here) are consistent with the compositional groups identified in Table 4.2.1 and Figures 4.2.1-4.2.10.

Figure 4.2.14 shows that the compositional groups identified at Eriswell are reflected very well by cluster analysis. The ‘Saxon I (natron)’, ‘Saxon II’ and ‘HIMT’ glasses all cluster relatively well as individual groups. The ‘Levantine I’, ‘A2b Blue’ and the ‘Saxon I (blue)’ glasses also cluster relatively well as individual groups, and cluster analysis again suggests that these three glass types were produced using similar raw materials. Whilst a handful of samples cluster in different groups to which they have been attributed, this is likely to have resulted from the compositional overlap between the different base glass types identified. The Eriswell glasses broadly cluster into two groups, indicated by the first two branches on the dendrogram (Figure 4.2.14); these are likely to broadly reflect the production zones of these different glass types.

‘Levantine I’ glass can be fairly confidently attributed to production in workshops using sand sourced from the Palestinian coast (*e.g.* Foster and Jackson 2009: 193; Foy *et al.* 2000: 54; Freestone 2003: 112; Freestone *et al.* 2000: 72; 2002b: 265; see this chapter, section 4.6). It is generally assumed that most ‘Roman’ blue-green tinted glass was produced from sand sourced from a similar region (*e.g.* Aerts *et al.* 2003: 659-660; Foster and Jackson 2010: 3075; see this chapter, section 4.3). ‘Roman’, ‘Levantine I’ and ‘A2b Blue’ glass can therefore probably be attributed to production from *Palestinian* sand, in workshops operating in the same region.

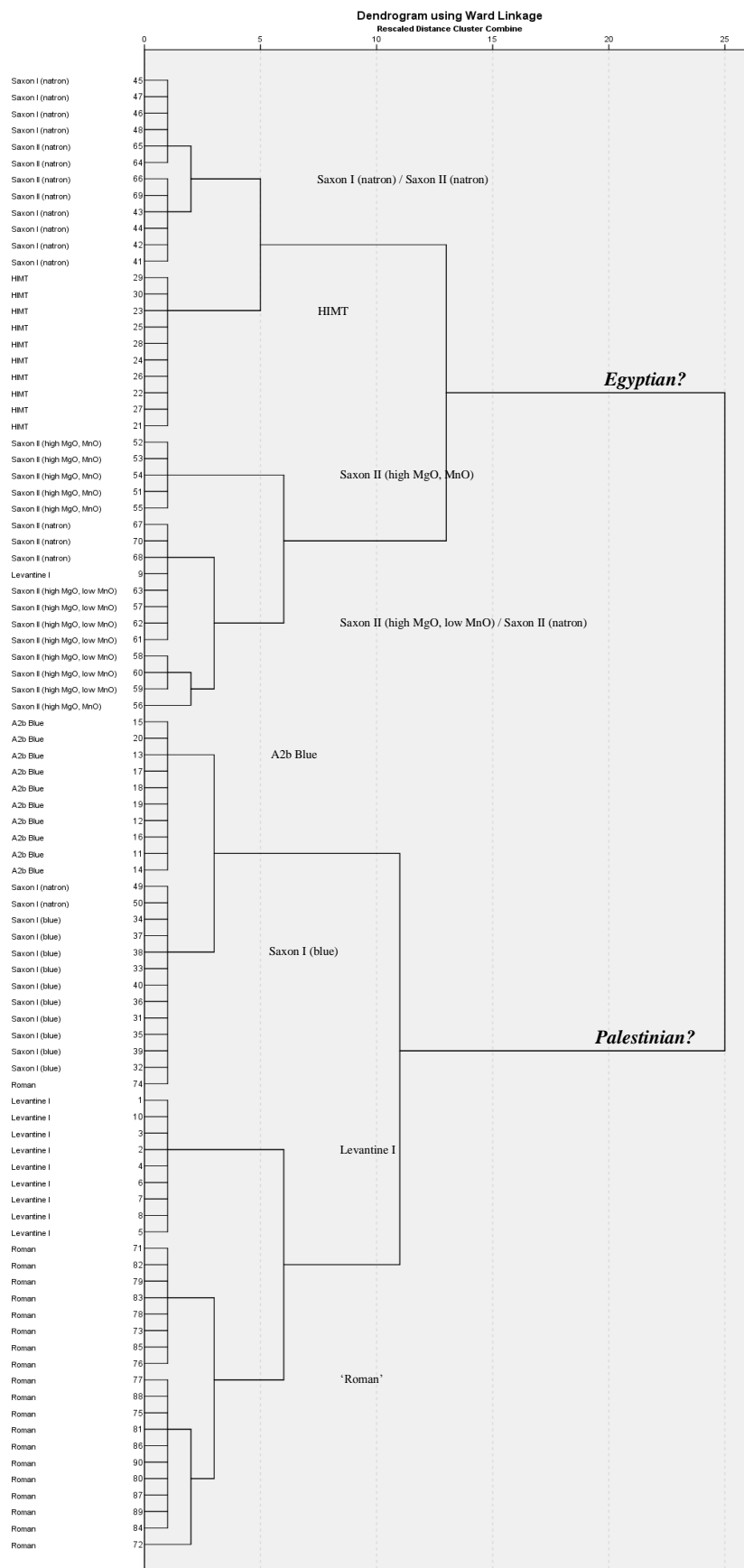


Figure 4.2.14 – Dendrogram for selected samples from Eriswell using Ward’s method, showing the grouping of the different base glass types identified.

In contrast, ‘HIMT’ glass is generally assumed to have been produced in Egyptian workshops (*e.g.* Foy *et al.* 2003: 47, Freestone *et al.* 2005b: 155; Leslie *et al.* 2006: 261; see this chapter, section 4.5). It has been suggested that ‘Saxon I (natron)’ glass was produced using sand sourced from a similar region (Freestone *et al.* 2008: 36), probably between the Nile and southern Israel (see this chapter, section 4.4). ‘Saxon I (natron)’, ‘Saxon II’ and ‘HIMT’ glass can therefore probably be attributed to production from *Egyptian* sand. The picture is less clear with ‘Saxon I (blue)’ glass; cluster analysis suggests that it is more similar to glass types assumed to have been produced using Palestinian coastal sand. However, it has a number of very close similarities to ‘Saxon I (natron)’ glass (see this chapter, section 4.4), which suggests that it is more likely to have been produced using sand sourced from between the Nile and southern Israel.

The characteristics of each of the compositional groups identified will be discussed in detail on an individual basis throughout the remainder of this chapter (sections 4.3-4.7), with reference to Figures 4.2.1-4.2.10 and 4.2.14.

4.2.1. Trace Element Analyses

A consequence of the use of glass produced in a few primary glassmaking institutions in the Near East is that the concentrations of major and minor element oxides are very similar (*e.g.* Table 4.2.1 and Figures 4.2.1-4.2.10); this makes compositional distinctions more difficult. However, trace element analysis offers the potential to further differentiate between these glass types (see Chapter 2, section 2.3.2). Whilst it has been noted that high-lead samples may have suffered from (sometimes considerable) contamination from the clay fabric of the melting pot; such contamination it is not accounted for in the interpretation of the trace element data, as it is unclear as to the extent to which it may have influenced the results.

4.2.1.1. Rare Earth Elements (REE)

Figure 4.2.15 shows average rare earth element (REE) concentrations for the six glass types identified in section 4.2, normalised to the average continental crust (MUQ). REE are useful for the characterisation of glass sources because they behave as a coherent geochemical group in nature; they are unlikely to be significantly modified by minor variations in the composition of sand sourced from the same stretch of coast, or by deliberately added colourants and opacifiers (Freestone 2003: 114). The majority of REE are usually introduced with the silt and clay fraction of sand (*i.e.* heavy minerals), which means that their concentrations are good indicators of the purity of the glassmaking sand used, especially as quartz is low in REE (Degryse and Shortland 2009: 140; Freestone *et al.* 2002b: 264).

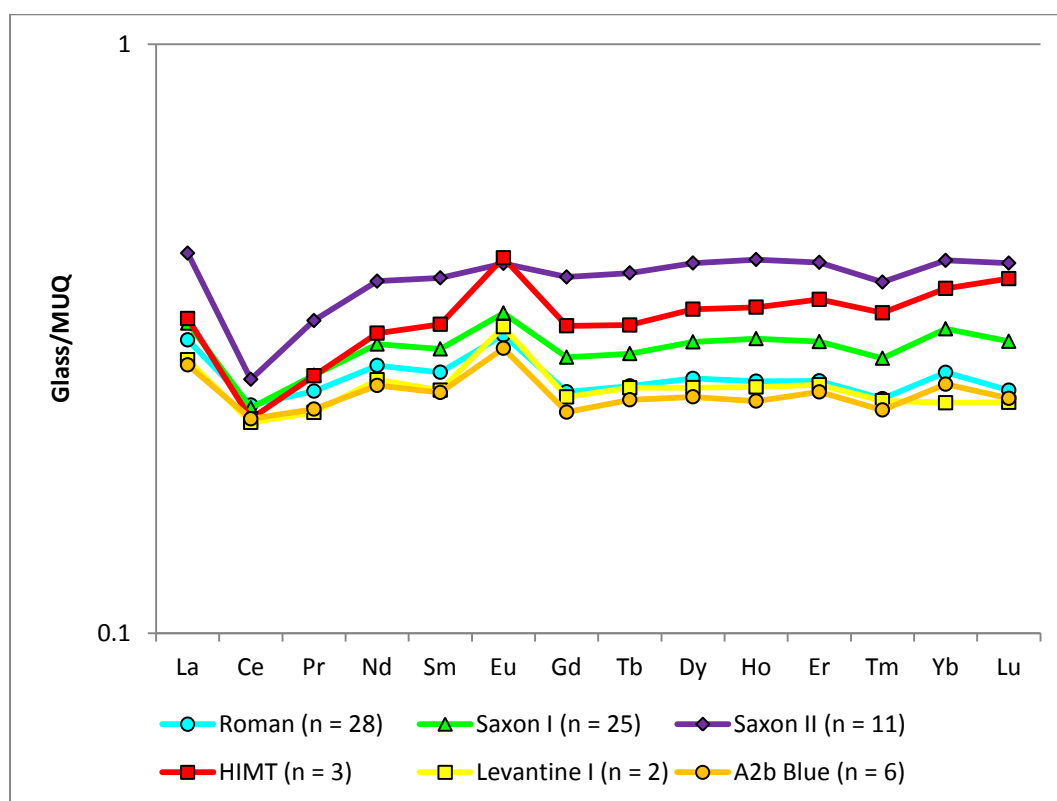


Figure 4.2.15 – Average rare earth element concentrations for the different base glass types identified at Eriswell, normalised to the weathered continental crust (see Chapter 2, section 2.3.2.3). Note the logarithmic scale.

The anomalies (*i.e.* peaks in the pattern, which may be either positive or negative) observed for Ce and Eu are not unusual, and relate to the variable oxidation states of these two elements, which affects the way in which they are deposited in rock-forming processes (Henderson 1984: 9; Pollard *et al.* 2007: 211). The slight variation in the concentration of Eu visible in ‘Saxon II’ glass type may relate to a slightly different plagioclase content in the sand used in the production of this glass (Degryse and Shortland 2009: 140). All of the REE positively correlate with one another and with the majority of SRE, indicating that they were probably introduced through a common ingredient (*i.e.* primarily the glassmaking sand). They do not correlate with soda or lime, indicating that they were not introduced with the alkali source or the lime component of the sand.

Figure 4.2.15 shows that ‘Roman’, ‘Levantine I’ and ‘A2b Blue’ glass have very similar REE patterns, suggesting that the glassmaking sands used in their production are likely to have their origins in the same, or at least a very similar, region. This supports the results of cluster analysis (Figure 4.2.14). ‘HIMT’ glass clearly has a slightly different origin; with the exception of Ce, the averaged REE element concentrations are higher than those seen in ‘Roman’, ‘Levantine I’ and ‘A2b Blue’ glass. This suggests the use of a less pure, different glassmaking sand, richer in heavy minerals (Freestone *et al.* 2002b: 264).

‘Saxon I’ glass, which also contains slightly elevated concentrations of REE relative to ‘Roman’, ‘Levantine I’ and ‘A2b Blue’ glass, is likely to have been made using a glassmaking sand purer than that used to produce ‘HIMT’ glass but less pure than that used to produce the ‘Levantine I’ glass (as well as ‘Roman’ and ‘A2b Blue’ glass). However, the REE pattern for ‘Saxon II’ glass is considerably elevated relative to the other glass types (Figure 4.2.15). This reflects the use of very different raw materials, and may result from the addition of small amounts of plant ash to several of these samples (see this chapter, section 4.4).

On balance, the similar REE patterns observed in the glass types represented in Figure 4.2.15 (with the notable exception of ‘Saxon II’ glass) suggest that the raw materials used in the production of the majority of these glass types are likely to have a broadly similar geographical origin. This is likely to be in the Near East,

where the sands along the Levantine and Egyptian coastlines have broadly similar compositions, as they are derived from Nile sediment which moved up the Palestinian coast with Mediterranean currents and longshore drift (Freestone 2006: 206; Freestone and Dell'Acqua 2005: 68; Freestone *et al.* 2008: 36; Leslie *et al.* 2006: 262). Glass produced from sand sourced from the Palestinian and Egyptian coastlines therefore exhibits very similar REE patterns, as might be observed in Figure 4.2.15. Slight differences in these patterns will therefore result from slight variations in the geochemistry of the sand, corresponding to the particular area of the Levantine coast from which the sand was sourced.

4.2.1.2. Sediment-Related Elements (SRE)

The sediment-related elements (SRE) relate to sediments which were naturally present as contaminants, in the batch materials; primarily the glassmaking sand. Their concentration is usually determined by the amount of heavy minerals in the sand, which varies from region to region, meaning that they have good potential for provenancing glass (Degryse and Shortland 2009: 140). Figure 4.2.16 shows the SRE concentrations for the different base glass types identified at Eriswell, normalised to the average continental crust (MUQ). This shows that the majority are broadly similar, again suggesting a common geological origin for the raw materials used to produce the raw glass (as suggested by the REE data), although there are some notable differences between glass types.

In all of the glass types, the majority of SRE strongly correlate with one another, and also with the REE, suggesting that they were probably introduced through a common ingredient (such as the glassmaking sand). Whilst variations in the concentrations of the SRE between glass types suggest that they are likely to have been produced in different workshops using slightly different glassmaking sands, the similarities suggest that they were produced in the same broad geographical region. Slight variations in the SRE are also likely to have resulted from variations in the relative proportions of the raw materials used in the manufacture of these glass types, the use of different tools in the preparation of raw materials, and the different additives

employed (colourants, opacifiers, etc.). ‘HIMT’ glass is a notable exception, and is likely to have been produced from a relatively impure quartz-rich sand, rich in heavy minerals and clays; this would account for the particularly elevated levels of Cr, Zr, Ba and Hf. The concentrations of Ti, V, Nb, Ta, W and Th are also elevated, suggesting the use of a very different sand source to the other glass types.

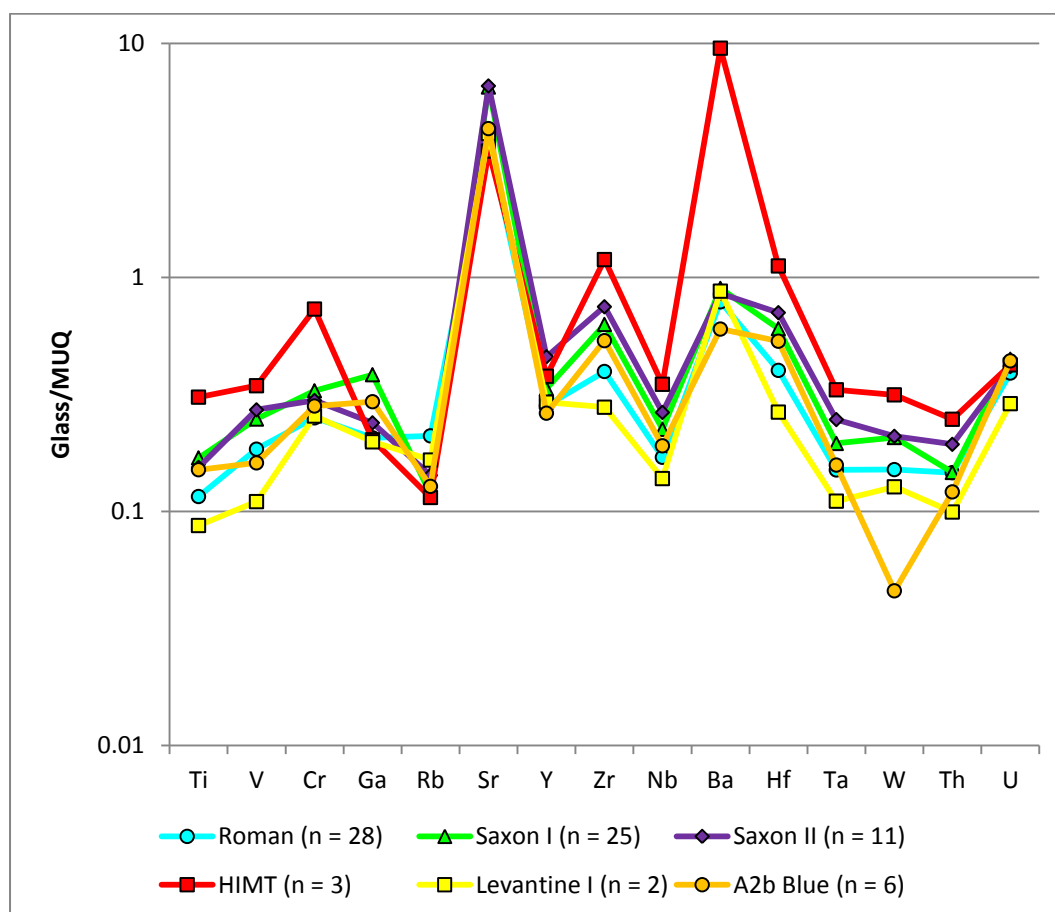


Figure 4.2.16 – Average sediment-related element concentrations for the different base glass types identified at Eriswell, normalised to the weathered continental crust (see Chapter 2, section 2.3.2.3). Note the logarithmic scale.

‘Levantine I’ glass generally contains slightly lower SRE levels than the other glass types, but the similarities with the SRE pattern for ‘Roman’ glass suggests that these two glass types are likely to have been produced using very similar raw materials (Figure 4.2.14). ‘A2b Blue’ glass contains marginally elevated levels of SRE relative to ‘Roman’ and ‘Levantine I’ glass, with Zr and Hf being particularly elevated. This suggests the use of a slightly different sand source, but it was probably produced in a

very similar region. The lower level of W in 'A2b Blue' glass is probably borne out by the general absence of manganese in this glass. However, when accounting for the logarithmic scale this difference is unlikely to be significant. 'Saxon I' and 'Saxon II' glass have very similar SRE patterns, although Ga is slightly elevated in 'Saxon I' glass. Both of these glass types were probably produced in a very similar region to one another, but in different workshops to 'Roman', 'Levantine I' and 'A2b Blue' glass.

A plot of Zr versus Hf shows a very marked positive correlation (Figure 4.2.17; $r^2 = 0.99$); this is because they both occur in the mineral zircon, which is a constituent of sand (Degryse and Shortland 2009: 140; Vallotto and Verità 2000: 68). Zr and Hf behave almost identically in nature, so variations in their ratio reflect regional differences in sand sources rather than local variations. The strong linear correlation suggests that the sand used to produce all of the glasses analysed is likely to have its origins in the same region; most likely the Eastern Mediterranean. These two elements also provide a particularly good indication of the concentration of heavy minerals in the silica source (Aerts *et al.* 2003: 664; Degryse and Shortland 2009: 140; Freestone *et al.* 2000: 73-74; Vallotto and Verità 2000: 68); the lower their concentration, the purer the silica source (Cagno *et al.* 2012: 1546). It can be seen that 'Levantine I' and 'Roman' glass was produced using a comparatively very pure silica source to the other glass types. 'A2b Blue' glass was also produced using a fairly pure silica source. In contrast, the glassmaking sand used in the production of 'Saxon I' and 'Saxon II' glasses was less pure.

'HIMT' glass was produced using the least pure sand, which is reflected by the high levels of Ti (Figure 4.2.18) and Fe which characterise this glass type (*e.g.* see Table 4.2.1), as well as the highest levels of Zr and Hf (Figure 4.2.17). This trend is generally reflected in the REE and SRE patterns for this glass type (Figures 4.2.15 and 4.2.16). That Zr was introduced with the sand is confirmed by the positive correlation between Ti and Zr (Figure 4.2.18; $r^2 = 0.72$). The generally lower levels of Zr and Ti in the other glass types suggest the use of a much purer sand source than for 'HIMT' glass.

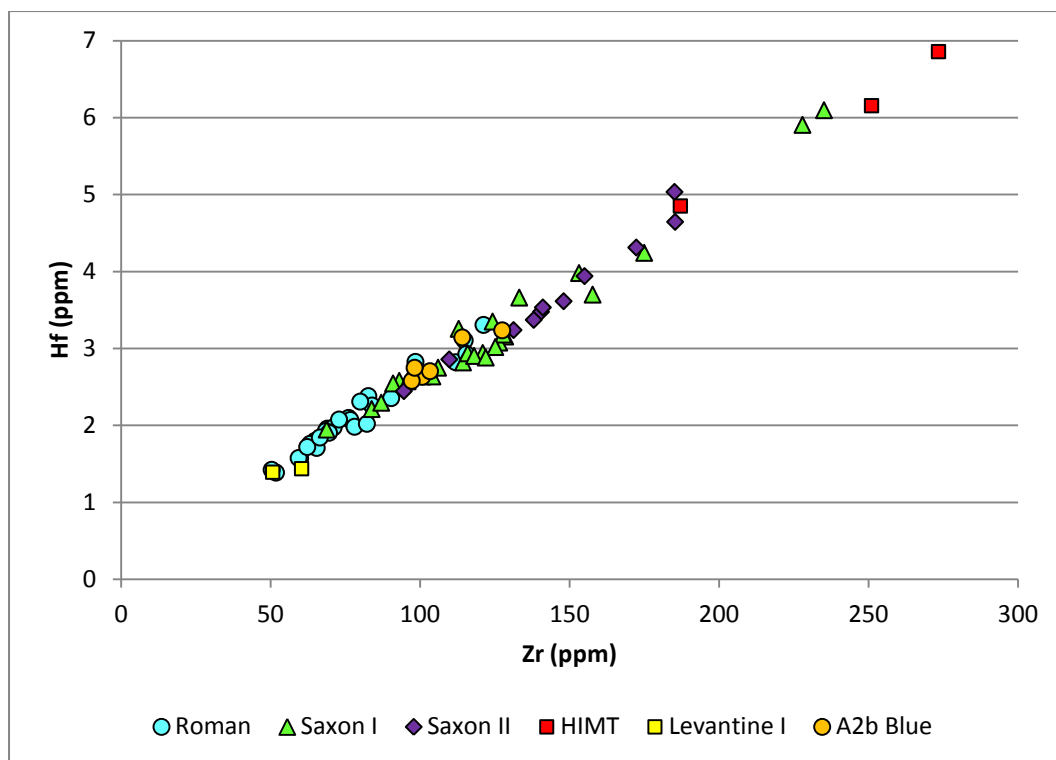


Figure 4.2.17 – A plot of zirconium versus hafnium for the different base glass types identified at Eriswell.

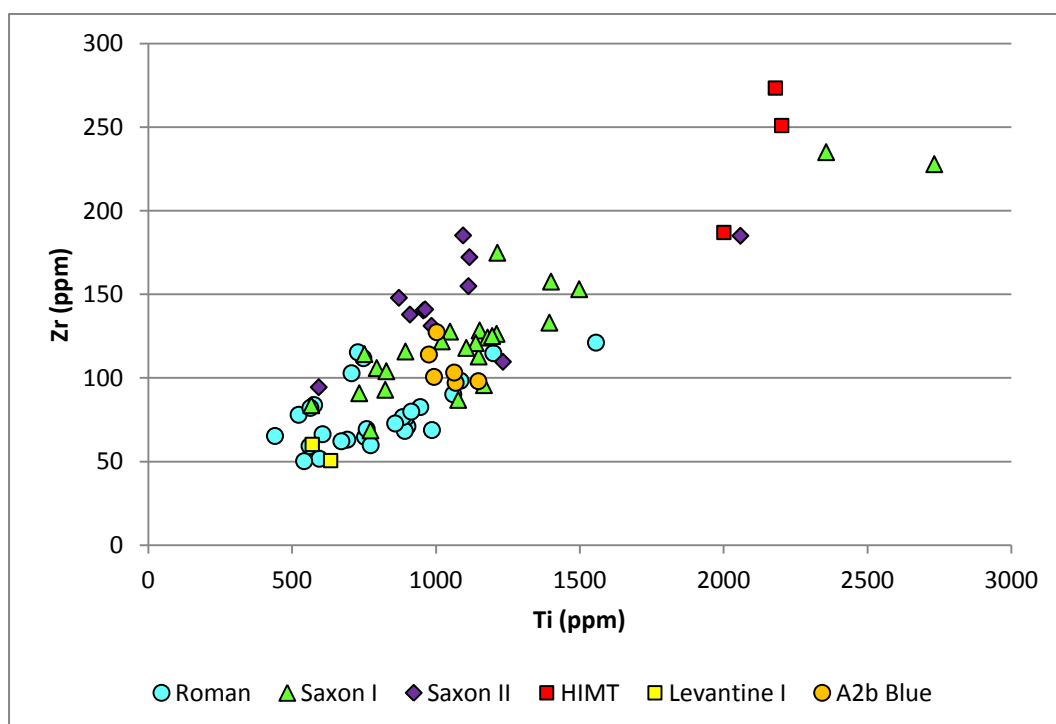


Figure 4.2.18 – A plot of titanium versus zirconium for the different base glass types identified at Eriswell.

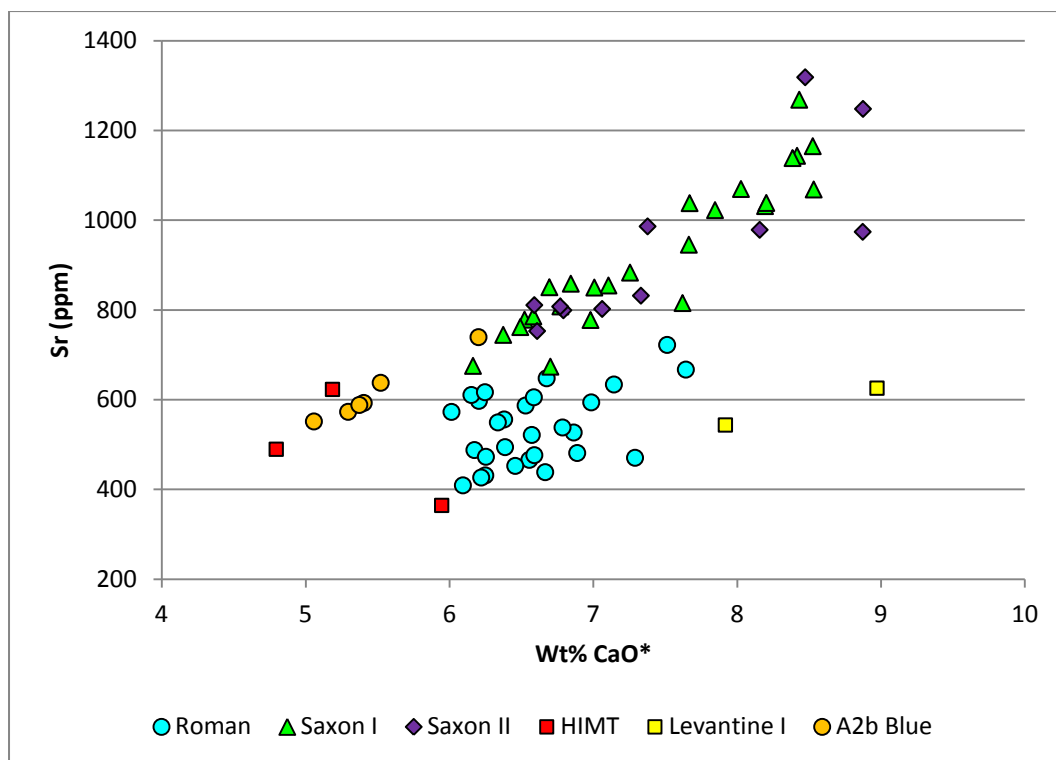


Figure 4.2.19 – A plot of lime versus strontium for the different base glass types identified at Eriswell.

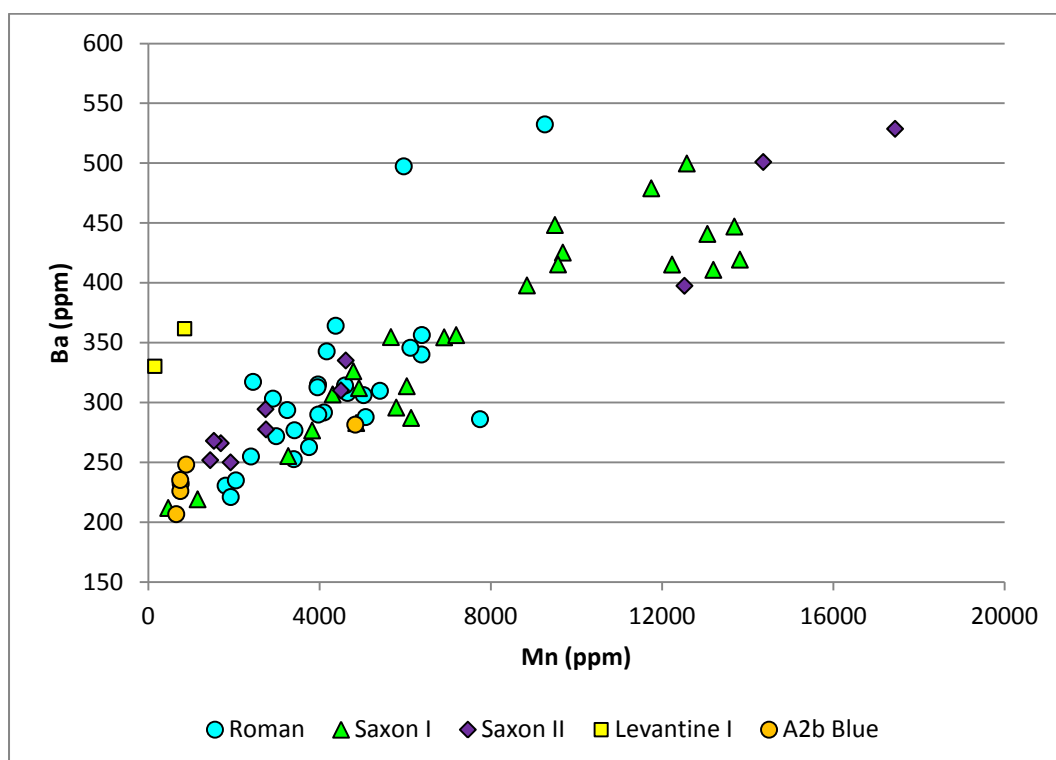


Figure 4.2.20 – A plot of manganese versus barium for the different base glass types identified at Eriswell. 'HIMT' samples have been excluded due to Ba contents in excess of 2500 ppm.

The strong positive correlation ($r^2 = 0.86$) between lime (CaO^*) and Sr in ‘Saxon I’, ‘Saxon II’ and ‘A2b Blue’ glass is likely to have resulted, at least in part, from the use of a sand containing calcite with a constant ratio of Sr to Ca (Figure 4.2.19). Glass produced using coastal sand from the Palestinian coast typically contains Sr at levels of approximately 400 ppm, due to the presence of a high quantity of calcite in the form of shell (which is relatively rich in Sr) (Paynter 2006:1038; Silvestri 2008: 1498; Silvestri *et al.* 2008: 338). In contrast, glass produced from inland sand contains lower concentrations of Sr (approximately 150 ppm), as the calcite is typically present in the form of limestone (which is relatively low in Sr) (Paynter 2006: 1038; Silvestri 2008: 1498; Silvestri *et al.* 2008: 338). The high levels of Sr in the Eriswell glasses (typically above 400 ppm, *e.g.* Figure 4.2.19) suggest the use of coastal sand (as opposed to inland sand). However, in many of the ‘Saxon’ samples, Sr is considerably elevated, and is likely to have been introduced from a number of different sources (*e.g.* small quantities of plant ash, feldspar, etc.; see this chapter, section 4.4.1).

The ‘Roman’ and ‘Levantine I’ glass types do not fit the same pattern as the other glass types (Figure 4.2.19), as Sr and Ca are not so markedly correlated with one another; there may be a slight positive correlation in ‘Levantine I’ glass, but the analysis of only two samples here limits the ability to speculate as to whether this is real. This suggests the use of a slightly different glassmaking sand in ‘Roman’ and ‘Levantine I’ glass; *i.e.* one which contains calcite with a different ratio of Sr to Ca.

Ba may also have been introduced as an impurity with the sand. However, it seems far more likely that the majority was introduced with a manganese-rich mineral, as Ba is strongly correlated with Mn (Figure 4.2.20; $r^2 = 0.75$). This is consistent with the addition of *wad*; the mining name given to ores composed mainly of manganese oxides or hydroxides (Silvestri 2008: 1499), which may have been deliberately added as a decolourant. In ‘HIMT’ glass Ba does not appear to be correlated with Mn, and the excessive amounts present (approximately 2500 ppm) are instead likely to have been introduced as an impurity with a different component, such as alkali feldspars in the glassmaking sand (Silvestri 2008: 1498).

4.2.1.3. Colourant and Colourant-Related Elements

The colourant and colourant-related elements are discussed in detail in Chapter 5, which deals with colourants and opacifiers on a colour-by-colour basis. Previous studies (*e.g.* Freestone *et al.* 2002b; Freestone 2006; Freestone and Hughes 2006) have demonstrated the potential of colourant elements present at trace levels as indicators of recycling in colourless and naturally coloured glasses. However, as the majority of the glasses analysed by LA-ICP-MS were deliberately coloured in some way, it is not possible to speculate as to the extent of recycling here as the elements in question were often deliberately added. Nevertheless, a plot of the decolourants employed (Mn versus Sb) illustrates the differences between the different compositional groups of glass identified (Figure 4.2.21).

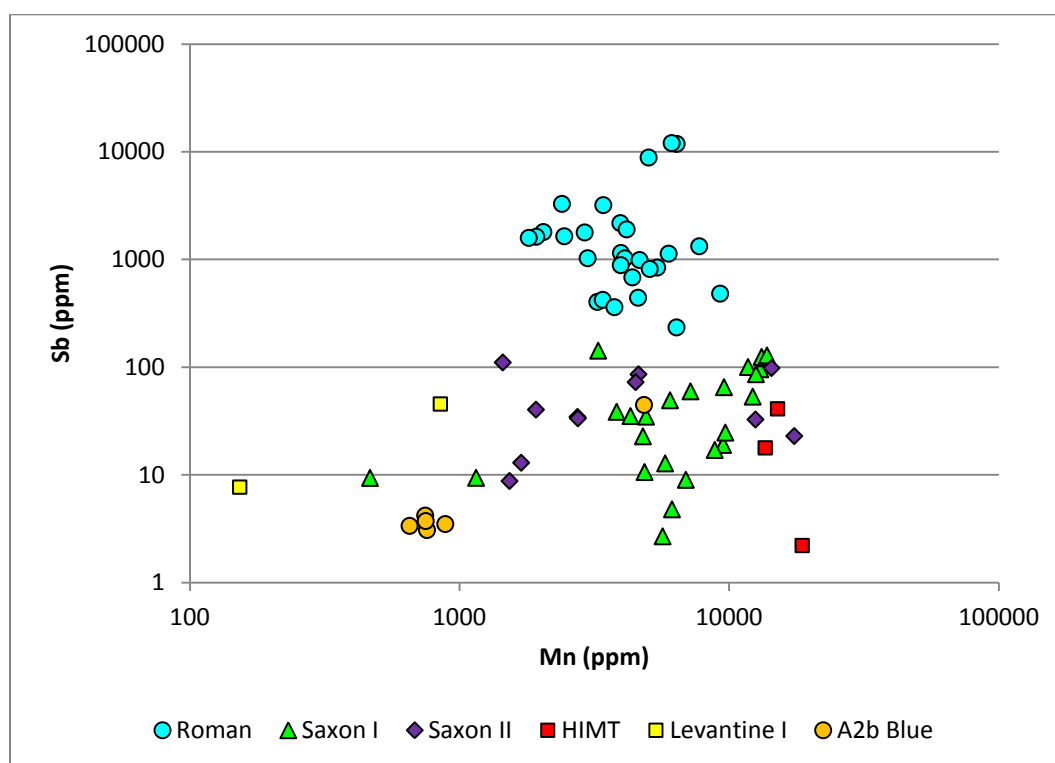


Figure 4.2.21 – A plot of manganese versus antimony for the different base glass types identified at Eriswell. Note the logarithmic scale.

Mn and Sb are usually assumed to have been deliberately added to glass to decolourise it (see this chapter, section 4.1.1.4). Furthermore, the presence of Sb in

glass from post-Roman contexts is usually taken as an indication of recycling (see this chapter, sections 4.1.4 and 4.3). Whilst 'Roman' glass contains similar levels of Mn to several of the other glass types identified, it is also characterised by elevated levels of Sb, suggesting that it represents recycled Roman material (see this chapter, section 4.3). It is not possible to easily differentiate between the other glass types identified using the relative concentrations of decolourants; 'HIMT' glass contains the highest levels of Mn and 'Levantine I' glass the lowest. The tight cluster of many of the 'A2b Blue' samples also suggests that the beads in question here may have been produced from the same batch (see this chapter, section 4.7).

4.3. 'Roman' Glass

'Roman' glass is one of the best represented base glass types identified at Eriswell, comprising 244 samples from a total of 155 beads. It consists primarily of opaque colours including yellow, opaque red and opaque white. Translucent blue, translucent copper green and translucent blue-green tinted glasses also make up a significant proportion of this group (see this chapter, section 4.9). It is compositionally very similar to glass in use during the preceding Roman period and is therefore likely to represent recycled material. The only antimony opacified sample, an opaque turquoise glass (ERL104:G290:1734, *DarkPoly4*; see Chapter 5, section 5.2.6), has also been assigned to this group, but represents a compositional outlier on account of its particularly low lime content (corresponding to 3.8% CaO*).

In order to confirm that the 'Roman' glass from Eriswell has its origins in the Roman period, a detailed comparison with earlier Roman glass is necessary. Three primary compositional types of Roman glass have been identified in British assemblages by previous studies. These include:

- Glass containing antimony as a decolourant (typically above 0.4%), where manganese is absent or near-absent. This corresponds to Jackson's 'Group 1' (Jackson 2005; Foster and Jackson 2010) and is termed '**Roman antimony-decolourised**' glass in the present study.
- Glass containing manganese (typically above 0.8%) as a decolourant, where antimony is usually completely absent. This corresponds to Jackson's 'Group 2b' (Jackson 2005; Foster and Jackson 2010) and is termed '**Roman manganese-decolourised**' glass in the present study.
- Glass containing both antimony and manganese (approximately 0.4% of each on average), corresponding closely to Roman blue-green glass typical of the Imperial period (Foster and Jackson 2009; Jackson 1992; Jackson *et al.* 1991). This is termed '**Roman blue-green**' glass in the present study.

Roman antimony-decolourised glass appears to have been a fairly widespread glass type; it usually appears 'colourless' or has a slight yellow tint. It was commonly used from the 1st-3rd centuries AD (Jackson 2005: 772-773), but does not appear to have been produced after the 4th century (Foster and Jackson 2010: 3074). Roman blue-green glass is one of the commonest types of Roman glass and is typically characterised by roughly equal quantities of both antimony and manganese (Jackson *et al.* 1991: 299). It is so-called on account of its typical blue-green tint. Again it represents a long-lived glass type, being produced from the 1st-3rd centuries AD (Foster and Jackson 2009: 189; Jackson 2005: 772-773; Jackson *et al.* 1991).

Roman manganese-decolourised glass appears to have been in use during the 4th century in Britain, but may have been in use for longer periods elsewhere in Western Europe (Foster and Jackson 2010: 3074). It is far less common than Roman antimony-decolourised and Roman blue-green glass (Foster and Jackson 2010: 3071; Jackson 2005: 768). Roman manganese-decolourised glass should not be confused with 'HIMT' glass; the latter was also in use during the 4th century, but contains manganese in conjunction with elevated levels of the oxides of iron, magnesia and titanium (see this chapter, section 4.5). It instead has a composition similar to Roman blue-green glass, except in that manganese is elevated and antimony absent or near-absent (Foster and Jackson 2010: 3071).

As antimony had largely been replaced by manganese as a decolourant in northwestern Europe by the 4th century AD (*e.g.* Brill 2006: 139; Sayre 1963: 279; Sayre 1965: 150), its presence is one of the best compositional indicators for the recycling of Roman glass in later periods. Figure 4.3.1 shows a plot of manganese versus antimony in the 'Roman' samples from Eriswell. The majority of these clearly contain antimony at levels close to, or below, the detection limits of SEM-EDS (approximately 0.3%). However, Sb_2O_3^* is more typically present at detectable levels in samples containing less than 0.8% MnO^* than in those containing MnO^* in excess of this.

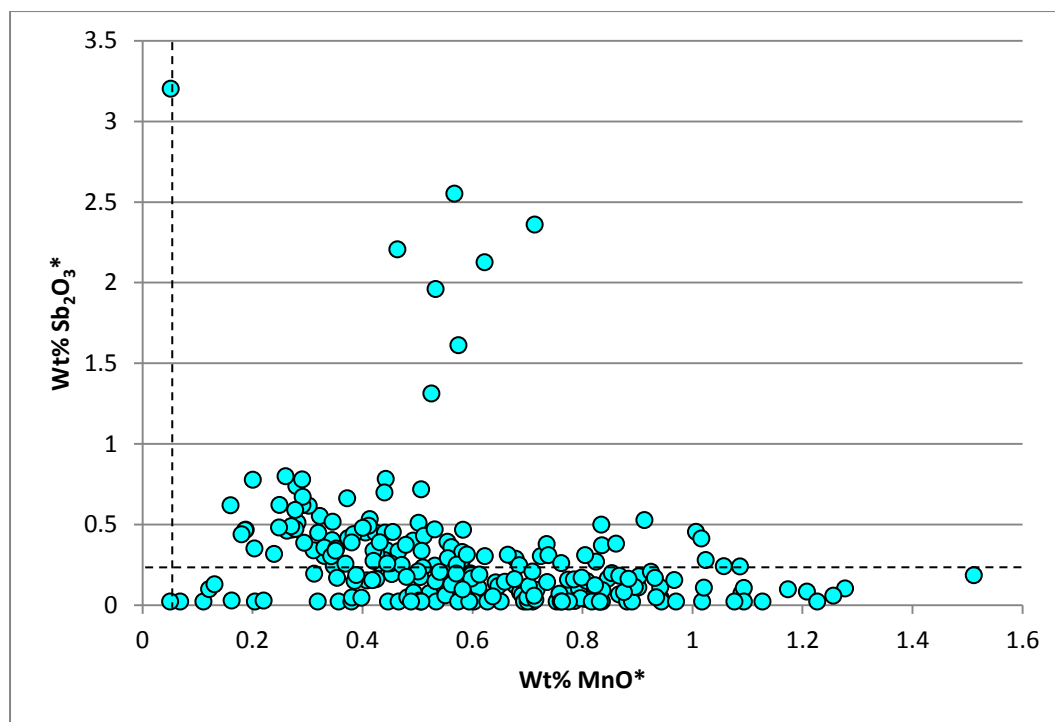


Figure 4.3.1 – A plot of manganese oxide versus antimony oxide in ‘Roman’ glass from Eriswell. The dashed lines represent the approximate detection limits for manganese oxide and antimony oxide.

The majority of samples containing less than approximately 0.8% MnO* are less likely to represent recycled Roman manganese-decolourised glass, which rarely contains manganese at concentrations below this; the detection of antimony in the majority of these samples supports this interpretation. These samples are also unlikely to represent the re-use of antimony-decolourised glass in which manganese is usually near absent (*i.e.* below 0.2% MnO*) (Foster and Jackson 2010: 3070). The few samples which contain less than 0.2% MnO* do not contain antimony at detectable levels, suggesting that they are unlikely to reflect Roman antimony-decolourised glass. The majority of samples are therefore likely to reflect recycled Roman blue-green glass, in which low concentrations of both antimony and manganese are typically present (*e.g.* Figure 4.3.1). However, those samples containing manganese in excess of 0.8% could conceivably represent Roman manganese-decolourised glass; this interpretation is supported by the general absence of detectable antimony in these samples.

The ‘Roman’ samples can be distinguished from the other base glass types identified at Eriswell by comparing a number of other major components (Figures 4.2.1-

4.2.10). Figures 4.3.2-4.3.4 reproduce the plots of soda versus lime, magnesia versus lime, and silica versus magnesia respectively for the six base glass types previously mentioned (see this chapter, section 4.2); bivariate graphs for these elements have been selected here as they are the best compositional discriminators for the different base glass types identified (*e.g.* compare Figures 4.2.1-4.2.10). The size of the ‘bubbles’ on these graphs are proportional to the antimony content of the individual samples; the larger the bubble, the higher the antimony content. Seven samples containing in excess of 1% Sb_2O_3^* have been excluded so that the size of these ‘bubbles’ does not obscure the other data points. With only one exception (‘A2b Blue’ sample ERL104:G202:2731b/5, containing 0.3% Sb_2O_3^*), which is likely to be borne out by the fact that the detection limits for antimony (approximately 0.3%) have been reached, all of the samples containing in excess of 0.3% Sb_2O_3^* correspond to the ‘Roman’ compositional group (Figures 4.3.2-4.3.4). This strongly suggests that this group represents recycled Roman material.

Figures 4.3.5-4.3.13 compare published data for the three major types of Roman glass mentioned above to the different base glass types identified at Eriswell. ‘Roman’ glass from Eriswell is particularly distinguished by a relatively high silica content (66-72% SiO_2^* ; *e.g.* Figure 4.2.6), different ratio of lime to soda (*e.g.* Figure 4.2.1) and low levels of magnesia (less than 1% MgO^* ; *e.g.* Figure 4.2.2) relative to the majority of the other glass types. However, as most of the published data for Roman glass were obtained by inductively coupled plasma spectroscopy (ICPS), silica was not analysed for as it was lost by dissolution during sample preparation (*e.g.* Jackson *et al.* 2003: 438); the silica contents for much of the published data for Roman glass (particularly Roman blue-green glass) from Britain therefore cannot be compared to the Eriswell assemblage (*e.g.* Figure 4.3.7).

The data for Roman blue-green glass (Figures 4.3.5-4.3.7) are taken from Basinghall Street (Freestone *et al.*, in press), Mancetter (Jackson 1992; 1994; Jackson *et al.* 1991), Leicester (Jackson 1992; 1994; Jackson *et al.* 1991), Fishergate (Jackson 1992; 1996), Deansway (Jackson 1992) and Coppergate (Jackson 1992). The data for Roman antimony-decolourised glass (4.3.8-4.3.10) are taken from Basinghall Street (Freestone *et al.*, in press), Coppergate (Jackson 1992; 2005), Colchester (Heyworth *et al.* 1990), Lincoln (Mortimer and Baxter 1996), Binchester (Paynter 2006), and a

dataset of 243 vessel glass fragments from various sites across Britain (Baxter *et al.* 2005). The data for Roman manganese-decolourised glass (Figure 4.3.11-4.3.13) are taken from Basinghall Street (Freestone *et al.*, in press), Mancetter (Jackson 1992; 2005), Coppergate (Jackson 1992; 2005), a small assemblage from a number of other British sites (Foster and Jackson 2010), and the *Iulia Felix* Roman shipwreck (northern Italy) (Silvestri *et al.* 2008). The majority of this glass dates predominantly to the 1st-4th centuries AD, with the exception of Roman manganese-decolourised glass which mostly dates to the 3rd-4th centuries AD.

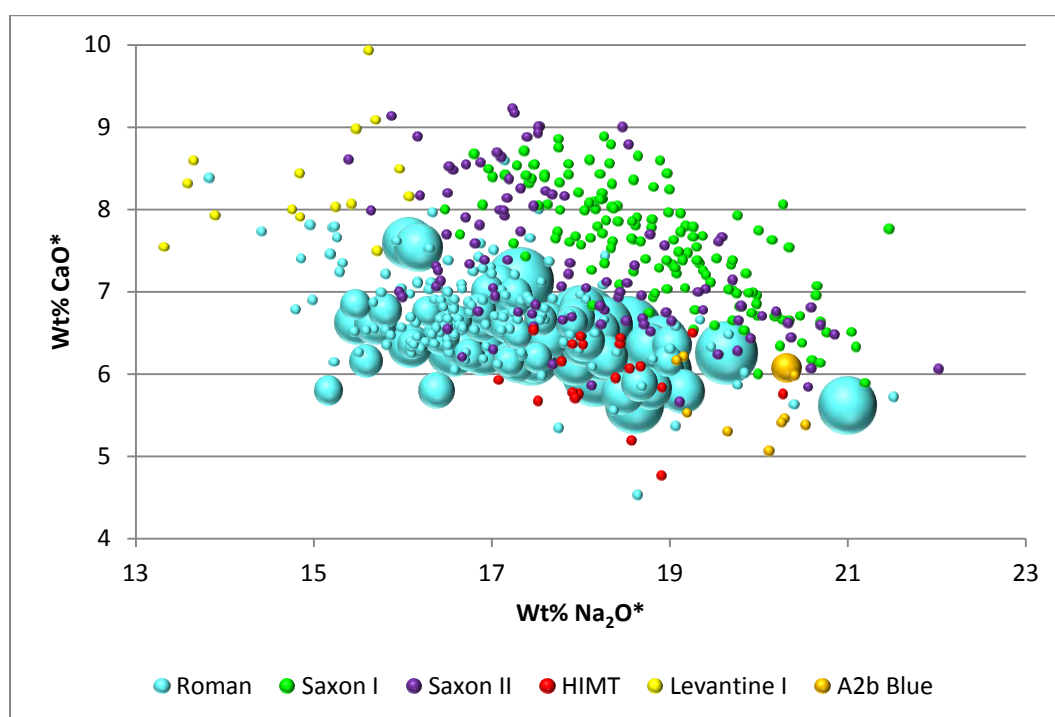


Figure 4.3.2 – A plot of soda versus lime for the different base glass types identified at Eriswell. The size of the bubbles is proportional to the antimony content (the larger the bubble, the higher the antimony content). The smallest bubbles represent samples containing <0.3% Sb_2O_3^* . The 7 samples containing >1.0% Sb_2O_3^* (all ‘Roman’) have been omitted due to the excessive size of the bubbles produced. Compare to Figure 4.2.1.

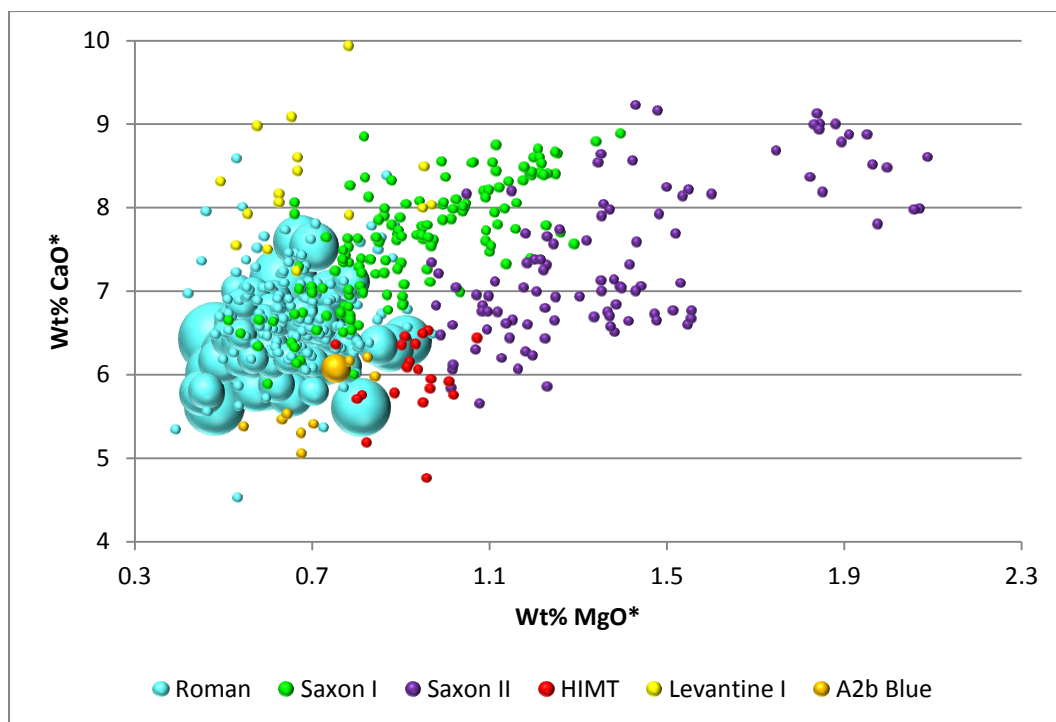


Figure 4.3.3 – A plot of magnesia versus lime for the different base glass types identified at Eriswell. The size of the bubbles is proportional to the antimony content (the larger the bubble, the higher the antimony content). The smallest bubbles represent samples containing $<0.3\%$ Sb_2O_3^* . The 7 samples containing $>1.0\%$ Sb_2O_3^* (all ‘Roman’) have been omitted due to the excessive size of the bubbles produced. Compare to Figure 4.2.2.

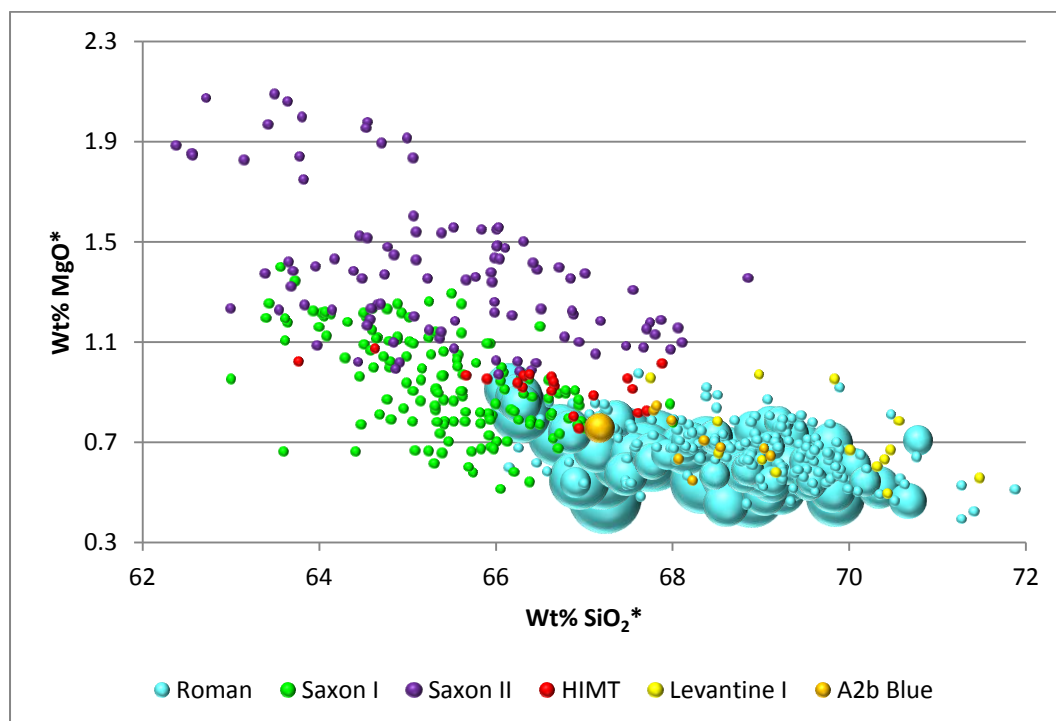


Figure 4.3.4 – A plot of silica versus magnesia for the different base glass types identified at Eriswell. The size of the bubbles is proportional to the antimony content (the larger the bubble, the higher the antimony content). The smallest bubbles represent samples containing $<0.3\%$ Sb_2O_3^* . The 7 samples containing $>1.0\%$ Sb_2O_3^* (all ‘Roman’) have been omitted due to the excessive size of the bubbles produced. Compare to Figure 4.2.6.

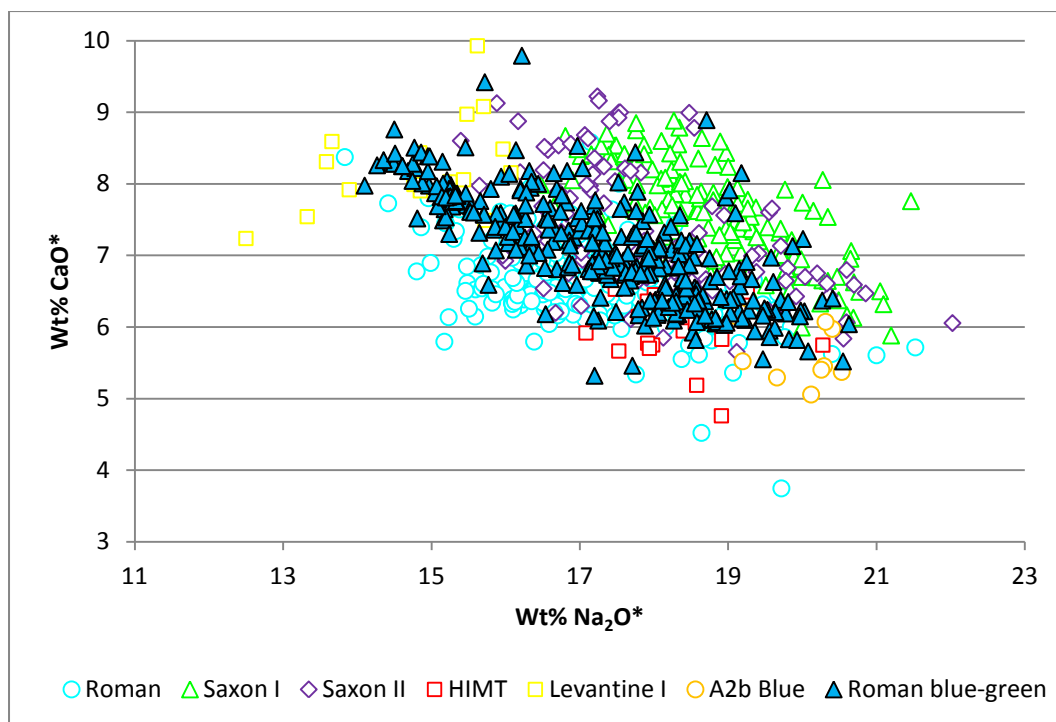


Figure 4.3.5 – A plot of soda versus lime for published Roman blue-green glass from (see text for details) compared to the different base glass types identified at Eriswell. Compare to Figure 4.2.1.

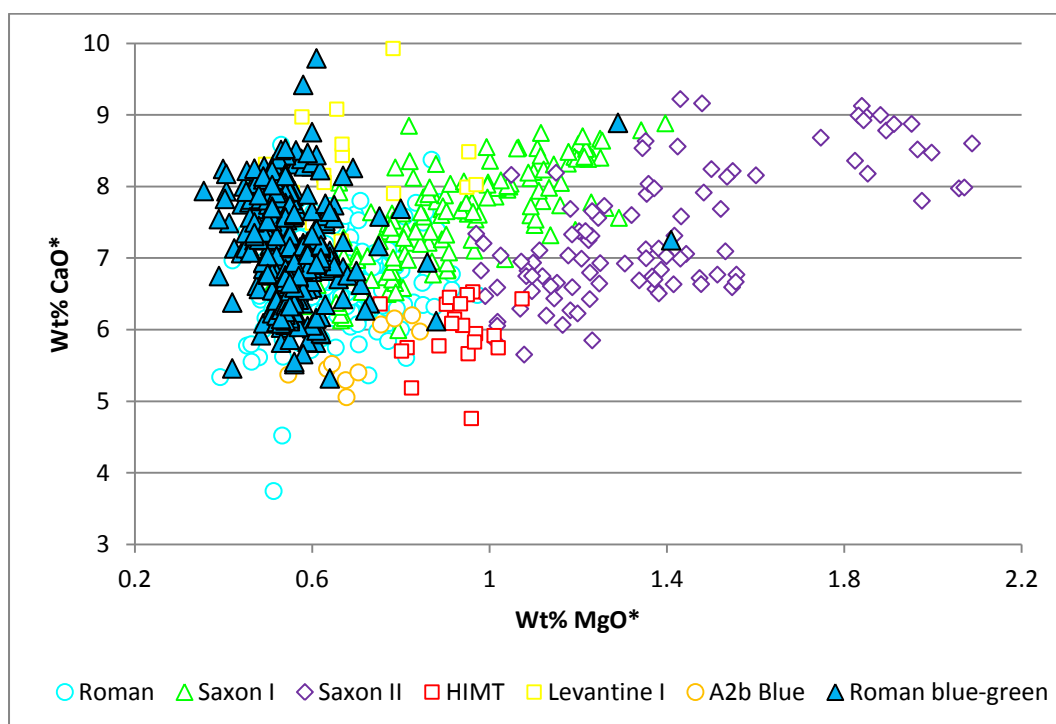


Figure 4.3.6 – A plot of magnesia versus lime for published Roman blue-green glass (see text for details) compared to the different base glass types identified at Eriswell. Compare to Figure 4.2.2.

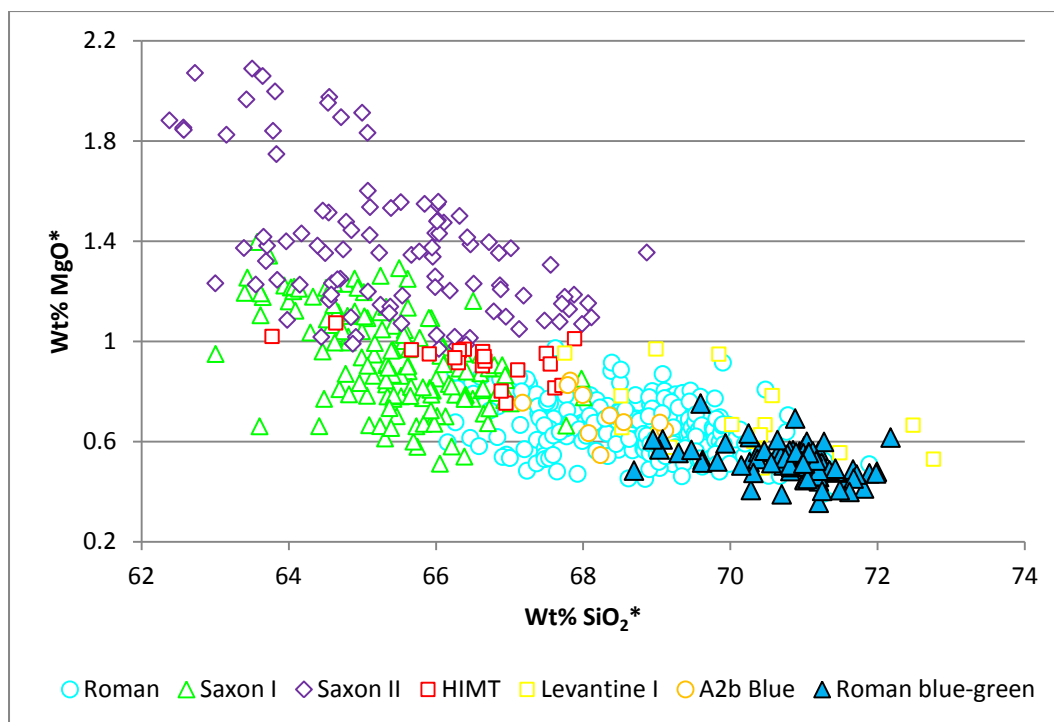


Figure 4.3.7 – A plot of silica versus magnesia for Roman blue-green glass from Basinghall Street (see text for details) compared to the different base glass types identified at Eriswell. Compare to Figure 4.2.6.

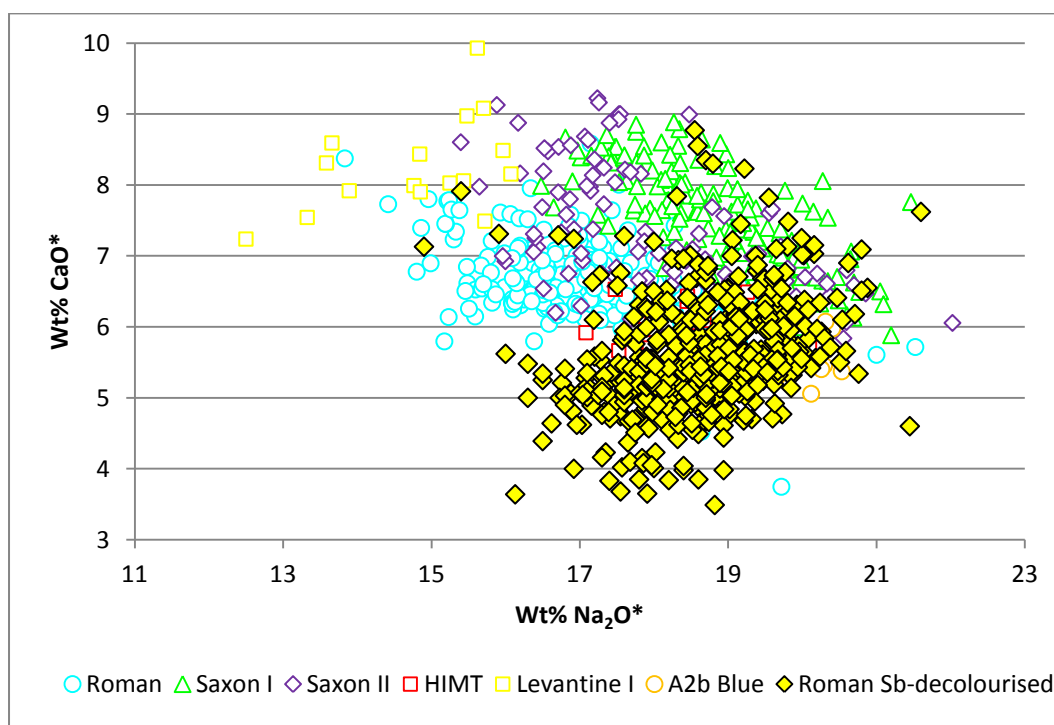


Figure 4.3.8 – A plot of soda versus lime for published Roman antimony-decolourised glass (see text for details) compared to the different base glass types identified at Eriswell. Compare to Figure 4.2.1.

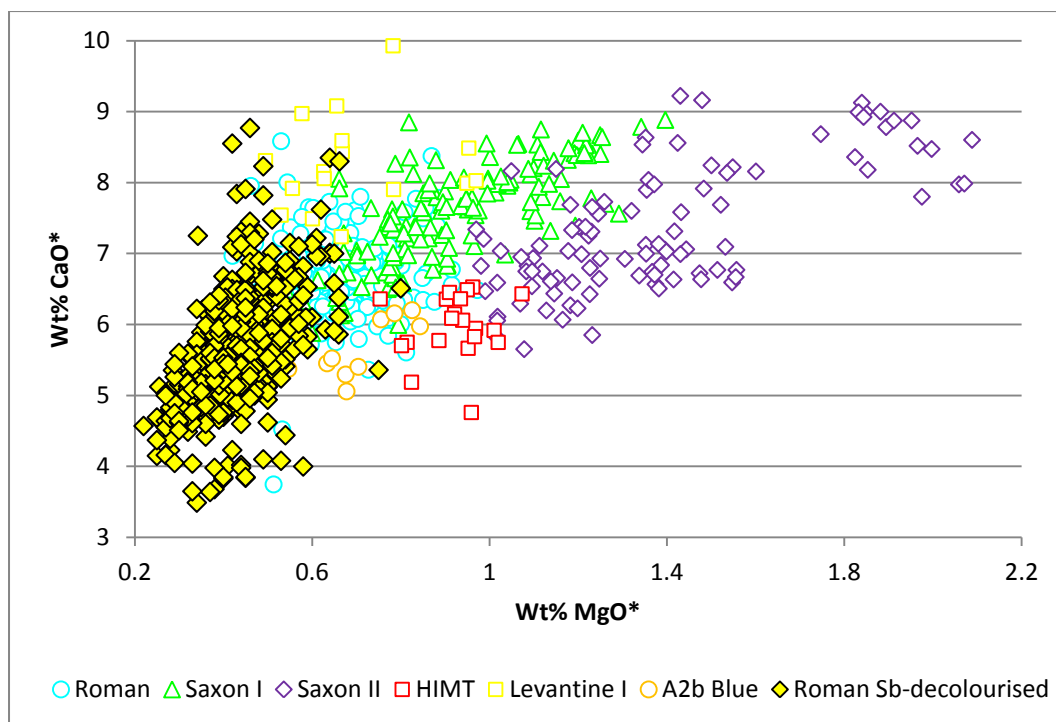


Figure 4.3.9 – A plot of magnesia versus lime for published Roman antimony-decolourised glass (see text for details) compared to the different base glass types identified at Eriswell. Compare to Figure 4.2.2.

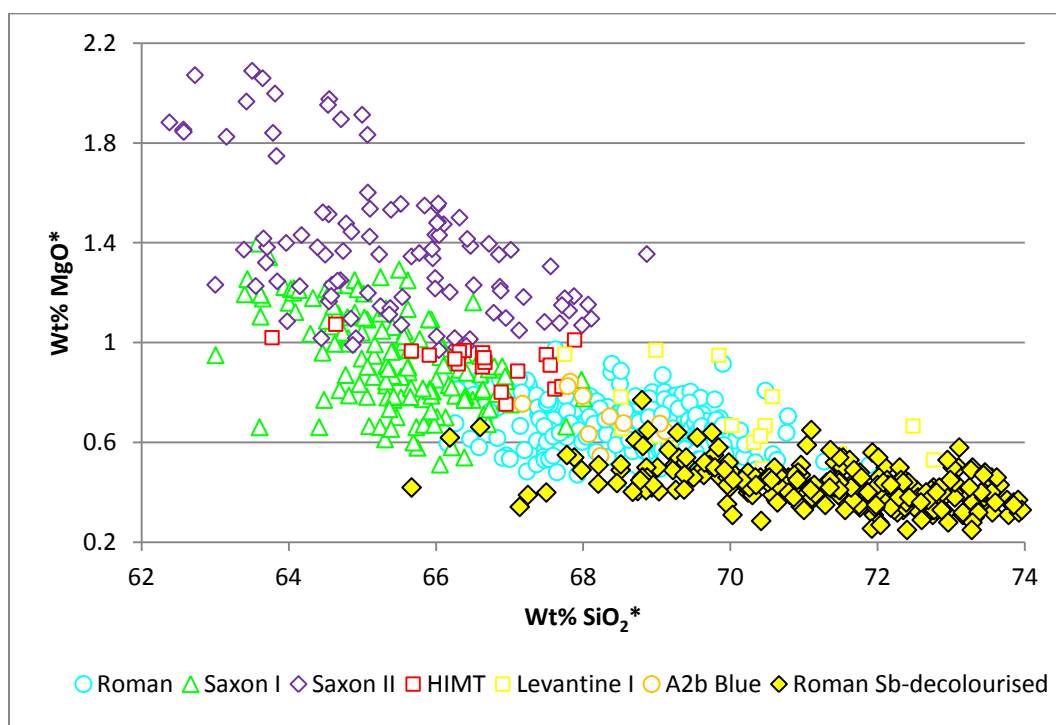


Figure 4.3.10 – A plot of silica versus magnesia for published Roman antimony-decolourised glass (see text for details) compared to the different base glass types identified at Eriswell. Compare to Figure 4.2.6.

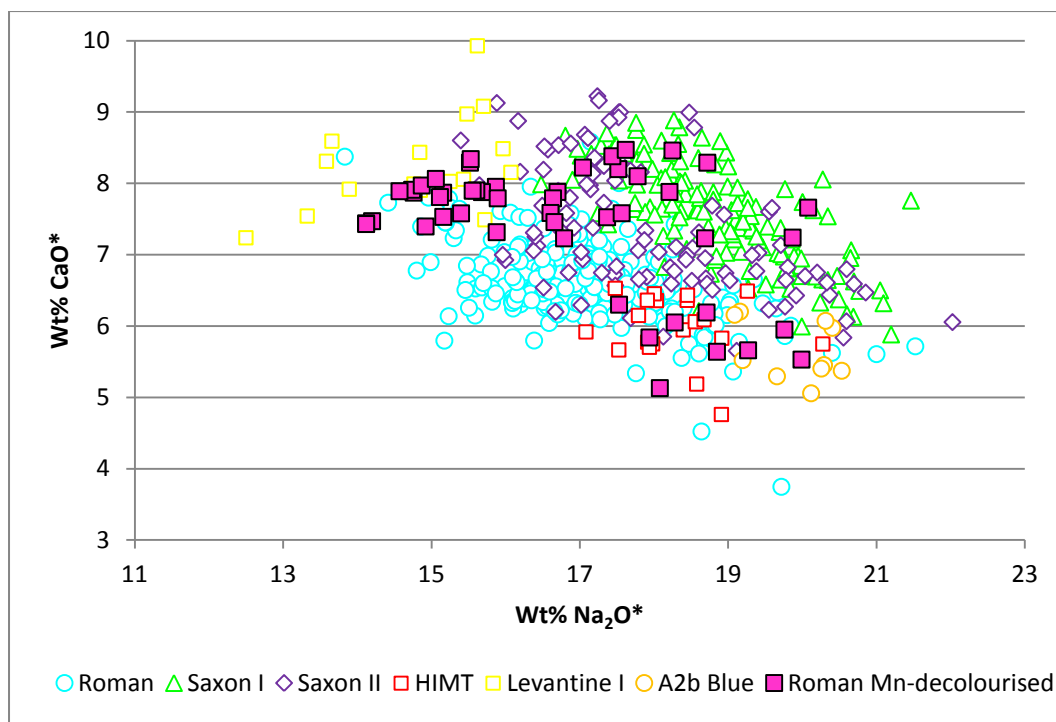


Figure 4.3.11 – A plot of soda versus lime for published Roman manganese-decolourised glass (see text for details) compared to the different base glass types identified at Eriswell. Compare to Figure 4.2.1.

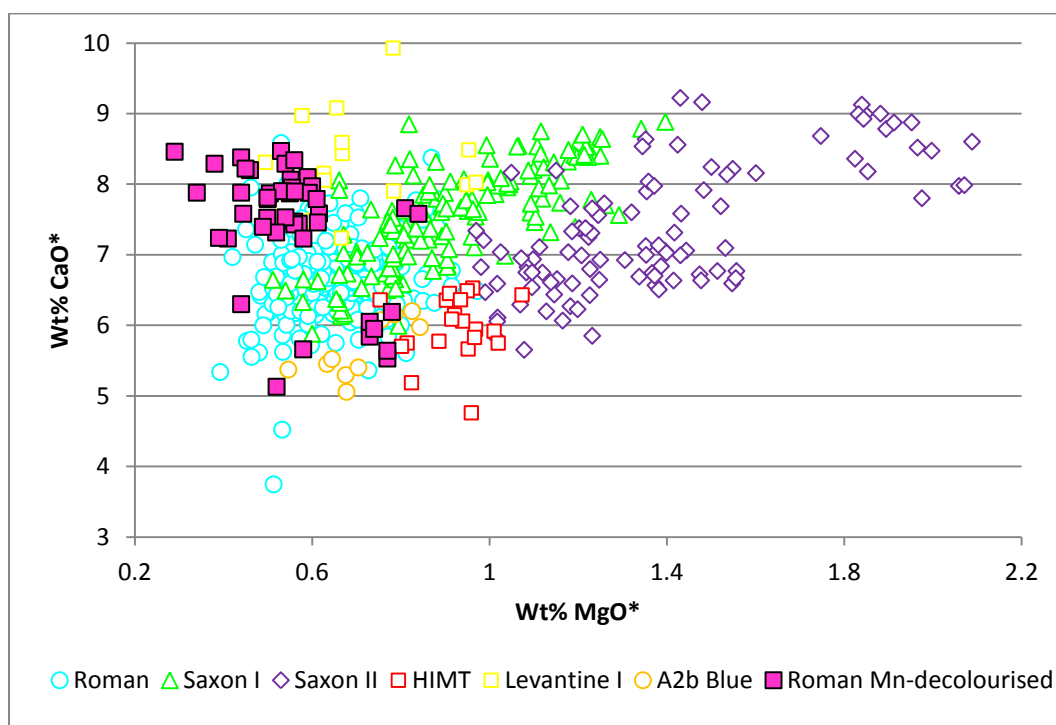


Figure 4.3.12 – A plot of magnesia versus lime for published Roman manganese-decolourised glass (see text for details) compared to the different base glass types identified at Eriswell. Compare to Figure 4.2.2.

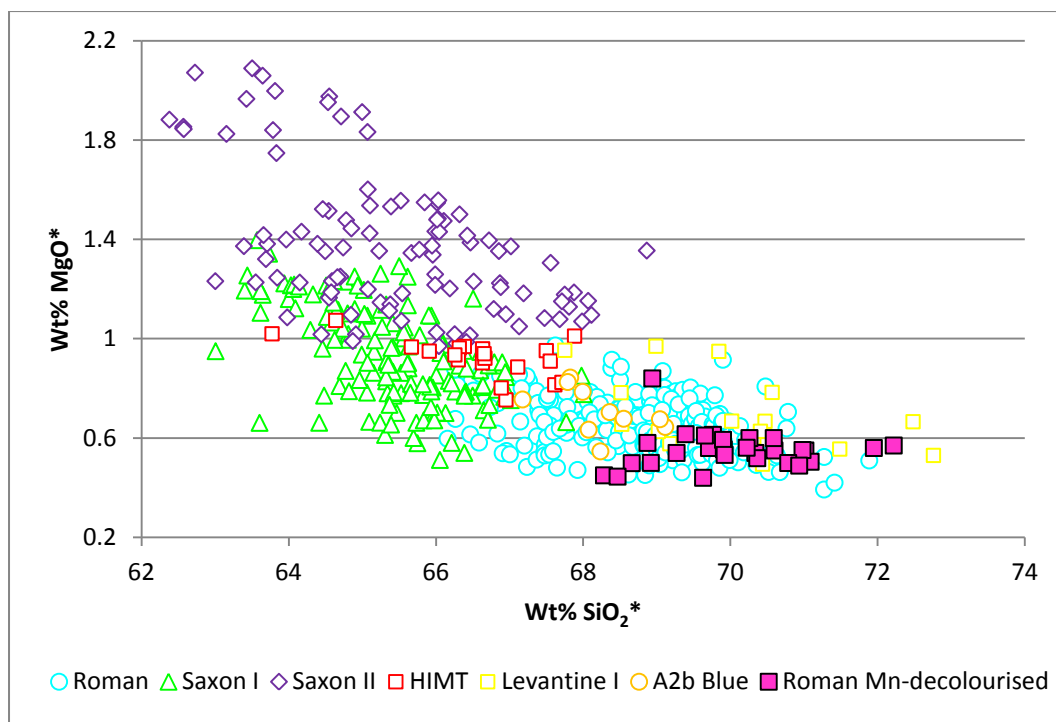


Figure 4.3.13 – A plot of silica versus lime for published Roman manganese-decolourised glass (see text for details) compared to the different base glass types identified at Eriswell. Compare to Figure 4.2.6.

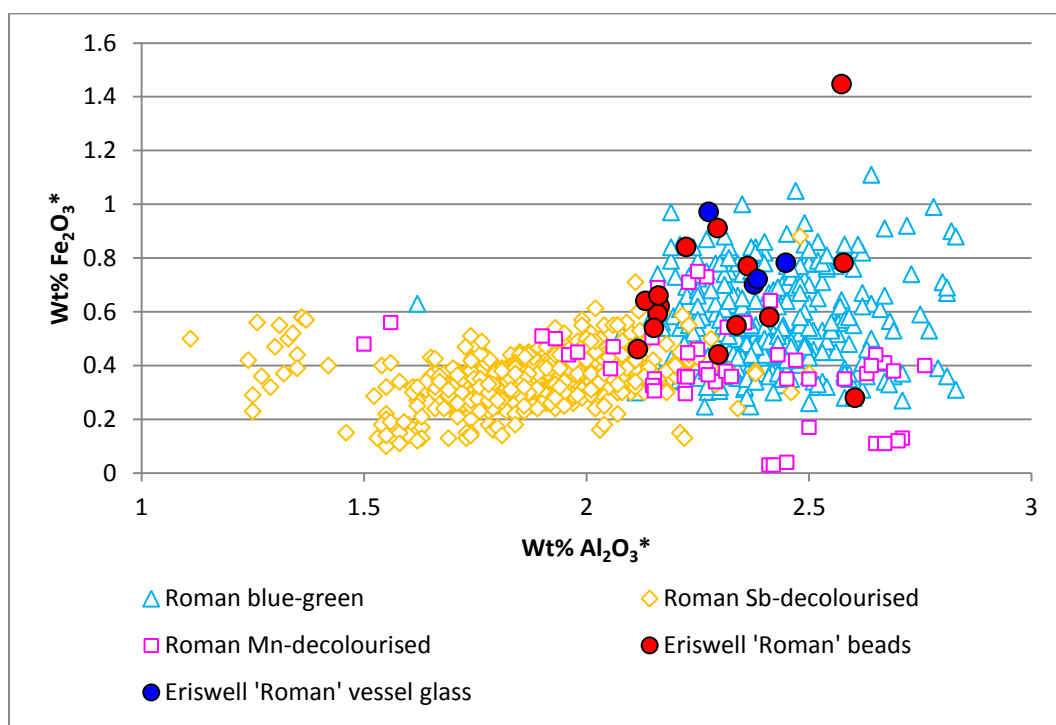


Figure 4.3.14 – A plot of alumina versus iron oxide for the lightly tinted 'Roman' beads and vessel glass fragments from Eriswell, compared to published data for Roman blue-green, antimony-decolourised and manganese-decolourised glass (see text for details).

Figures 4.3.5-4.3.13 clearly demonstrate that the composition of the 'Roman' glass from Eriswell is very similar to glass from the preceding Roman period. The magnesia and potash contents are low (typically below 1.0% each of MgO* and K₂O*), consistent with all of the earlier Roman types. However, Roman blue-green glass in particular has a number of very close similarities to 'Roman' glass from Eriswell; most notably a similar negative correlation between soda and lime (Figure 4.3.5; $r^2 = 0.48$ in Roman blue-green glass *cf.* $r^2 = 0.26$ in the Eriswell 'Roman' samples), together with similar levels of both magnesia (Figure 4.3.6; averaging 0.6% in Roman blue-green glass *cf.* 0.7% MgO* in the Eriswell 'Roman' samples) and potash (0.7% in Roman blue-green glass *cf.* 0.8% K₂O* in the Eriswell 'Roman' samples).

Whilst silica appears comparatively elevated in Roman blue-green glass (averaging 70.9% *cf.* 68.7% SiO₂*, Figure 4.3.7), silica was not analysed for in the majority of published Roman blue-green glass analyses, so only data from Basinghall Street (Freestone *et al.*, in press) are available for comparison here. This difference may therefore relate more to the compositional characteristics of the Basinghall Street assemblage than Roman blue-green glass as a whole; glass from this assemblage contains slightly less soda (averaging 15.5% *cf.* 17.9% Na₂O*) and more lime (averaging 7.7% *cf.* 6.9% CaO*) relative to 'typical' Roman blue-green glass, suggesting that this is likely to be the case.

In contrast, Roman antimony-decoloured glass is different from the Eriswell 'Roman' samples. It generally contains slightly less lime and slightly elevated soda in comparison to the majority of 'Roman' samples from Eriswell (averaging 18.6% *cf.* 17.1% Na₂O*; Figure 4.3.8). It also contains marginally less magnesia (averaging 0.4% *cf.* 0.7% MgO*; Figure 4.3.9) and elevated silica relative to the 'Roman' glass from Eriswell (averaging 70.6% *cf.* 68.7% SiO₂*; Figure 4.3.10). This supports the view that the majority of the 'Roman' glass from Eriswell does not represent recycled Roman antimony-decoloured glass.

A handful of samples contain manganese at levels which are not typically found in Roman blue-green glass; typically in excess of 1.0% MnO*. As antimony was not generally detected in these samples, they could conceivably represent recycled

Roman manganese-decolourised glass. Published data available for Roman manganese-decolourised glass are lacking, but those available bear a number of close similarities to the 'Roman' glass from Eriswell (Figures 4.3.11-4.3.13). The concentrations of lime (Figure 4.3.11) and magnesia (Figure 4.3.12) are considerably variable in Roman manganese-decolourised glass, but the 'Roman' glass from Eriswell falls within the typical range. The levels of silica are also comparable to the Eriswell 'Roman' samples (Figure 4.3.13). However, it remains unclear as to whether these 'high-manganese' samples do represent Roman manganese-decolourised glass, or Roman blue-green glass, perhaps to which manganese or a manganese-rich glass has been added. The apparent absence of antimony would appear to favour the former interpretation, but further work by trace element analysis is necessary in order to confirm this.

Iron and alumina are particularly discriminating elements in Roman glass (*e.g.* Foster and Jackson 2010: 3071-3074; Jackson *et al.* 1991: 299), but the extent of contamination by iron and alumina from the crucible fabric in the coloured 'Roman' samples from Eriswell limits the ability to compare these two components. However, Figure 4.3.13 compares the iron and alumina concentrations of the uncoloured 'Roman' samples from Eriswell, most of which have a blue-green tint, to published data for Roman glass. This shows that they correspond very closely to Roman blue-green glass. Roman antimony-decolourised glass typically contains lower levels of alumina and iron, and whilst Roman manganese-decolourised glass contains similar levels of alumina it typically contains lower levels of iron. Furthermore, the blue-green tint of the Eriswell 'Roman' samples supports the view that they represent recycled Roman blue-green glass.

The presence of blue-green vessel glass fragments in the Eriswell assemblage (hollow rim fragments were sometimes used as beads; see Henricson 1995: 15) demonstrates that early Anglo-Saxon communities almost certainly had access to a supply of Roman blue-green cullet. Parallels for the re-use of rim fragments from Roman and early medieval glass vessels are known from many other Anglo-Saxon sites in England, as well as Merovingian Germany and Scandinavia (Henricson 1995: 13-17). The blue-green beads from Eriswell are of a similar composition

(Figure 4.3.13) and are likely to reflect beads directly manufactured from earlier Roman blue-green glass, or beads curated from the preceding Roman period.

The exact locations of the primary glass-making workshop(s) in which Roman glass was produced have yet to be ascertained (Freestone *et al.* 2008: 31; Jackson *et al.* 2009: 150) and are not within the scope of the present study to discuss, but the general consensus is that many (particularly those producing blue-green tinted glass) were probably located somewhere in the Eastern Mediterranean (*e.g.* Aerts *et al.* 2003: 659-660; Degryse and Shortland 2009: 139; Degryse *et al.* 2009: 568; Freestone 2006: 206; 2008: 95-96; Nenna *et al.* 2000: 105; Picon and Vichy 2003: 17-18). Whilst the ratio of lime to alumina in Roman blue-green glass does not match that of 'Levantine I' glass (*e.g.* Freestone 2006: 211; Freestone *et al.* 2000: 73; Leslie *et al.* 2006: 264), the present data suggest that the 'Roman' glass from Eriswell is likely to have been produced in a similar geographic region (*i.e.* the Eastern Mediterranean), as has been suggested by previous studies (*e.g.* Nenna *et al.* 1997: 85-86; 2000: 105; Picon and Vichy 2003: 17-18). This view appears to be supported by trace element data (see section 4.3.1 below). However, recent work has suggested that some Roman glass may have also been produced in the western Mediterranean (*e.g.* Degryse and Schneider 2008: 1997-1999; Degryse and Shortland 2009: 139; Degryse *et al.* 2009: 568; Leslie *et al.* 2006: 266).

The detection of antimony in beads from other Anglo-Saxon cemeteries, including Ringlemere (Meek 2010), Mucking (Mortimer 1996b: 3-5; Mortimer and Heyworth 2009: 407), Edix Hill (Mortimer 1996a: 6), Portway (Bayley 1985: 85), Buckland (Bayley 1987: 186), Spong Hill (this study), Morning Thorpe (this study) and Bergh Apton (this study), supports the view that Roman glass is likely to have been widely recycled in the production of opaque and coloured beads. Biek *et al.* (1985: 85) identified the presence of significant amounts of antimony in solution in opaque white bubble-opacified beads at Sewerby, East Yorkshire; based on the results of the present study these beads are likely to have been produced from recycled Roman glass (see Chapter 5, section 5.2.1).

The dilution effects of high concentrations of lead and colourant elements typically seen in other glass colours are likely to have depressed antimony below the detection

limits of SEM-EDS, hence its apparent prevalence in opaque white bubble-opacified glass (which do not contain added colourants or opacifying agents) in the *raw* data. In addition, it is likely that many Merovingian beads on the Continent were produced from recycled Roman glass, as has been suggested by recent work (Mathis *et al.* 2010: 2082). A re-evaluation of that data in Freestone *et al.* (2008) (see this chapter, section 4.2) also suggests that recycled Roman glass is likely to have been used to produce vessels as well as beads.

On balance, the data suggest that the majority of ‘Roman’ glass from Eriswell is likely to represent recycled Roman blue-green cullet, which was commonly used in the production of vessels during the preceding Roman period. A small proportion of the ‘Roman’ samples are also likely to represent recycled Roman manganese-decolourised cullet. However, it seems that Roman antimony-decolourised cullet was not recycled to produce beads. This is likely to represent a relatively large-scale and/or widespread recycling practice.

4.3.1. Trace Element Analyses

Trace elements for 28 of the 'Roman' glasses from Eriswell were obtained by LA-ICP-MS.

4.3.1.1. Rare Earth Elements (REE)

The REE patterns for the 'Roman' samples analysed are relatively flat and form a fairly homogeneous group (Figure 4.3.15), suggesting that they were produced using similar raw materials and using a similar glassmaking recipe. Whilst there is some slight variation between samples, this may reflect natural variation in the raw materials or recipes used, as they are not significant enough to constitute different geochemical groups. Figure 4.3.15 suggests that these variations may relate to the colouration process; the opaque red glasses in particular contain elevated REE concentrations, which is likely to have resulted from the addition of metallurgical slag during the colouring process (see Chapter 5, section 5.2.3).

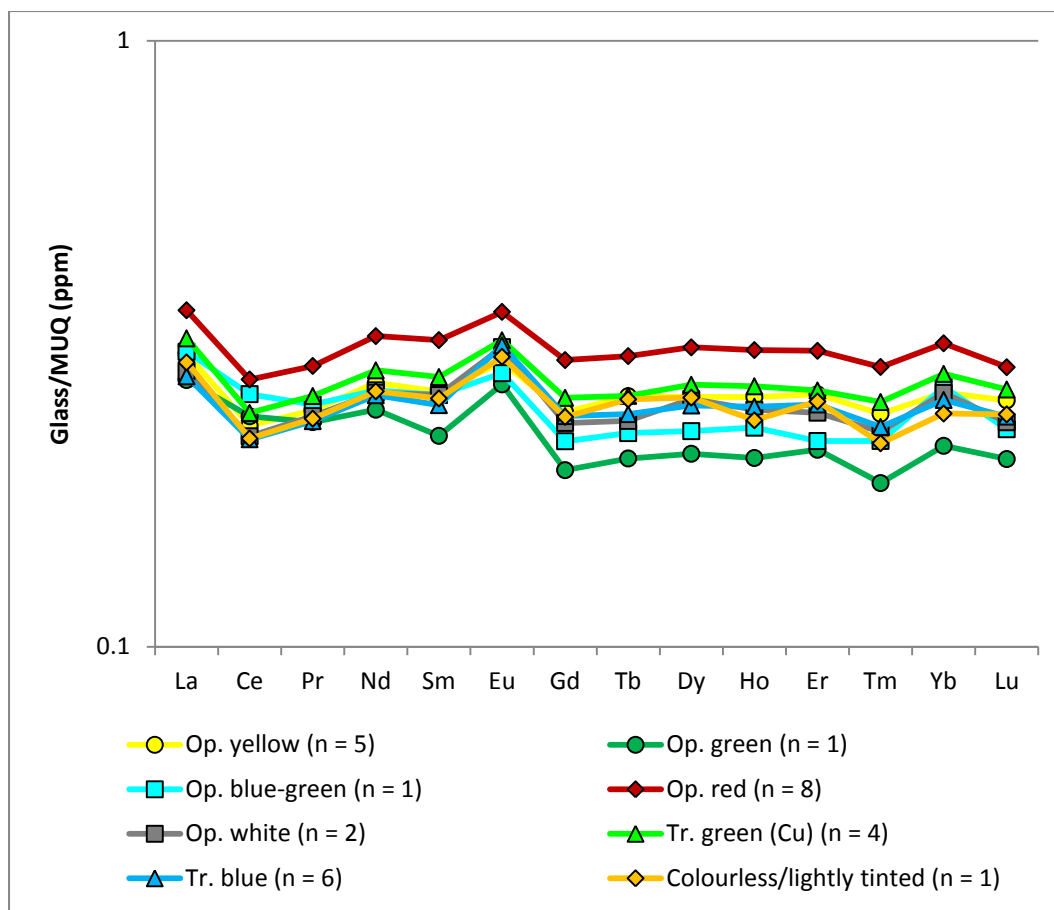


Figure 4.3.15 – Average rare earth element concentrations for ‘Roman’ glass from Eriswell, by colour, normalised to the weathered continental crust (see Chapter 2, section 2.3.2.3). Note the logarithmic scale.

The REE patterns for ‘Roman’ glass are similar to those for ‘Levantine I’ and ‘A2b Blue’ glass (Figures 4.2.11 and 4.3.16); all of these exhibit lower REE concentrations than ‘Saxon’ and ‘HIMT’ glass because purer raw glassmaking sands were used in their production. ‘Roman’ glass is likely to have a very similar geochemical origin to ‘Levantine I’ and ‘A2b Blue’ glass; ‘Levantine I’ glass can be fairly confidently attributed to Palestinian production (see this chapter, section 4.6).

4.3.1.2. Sediment-Related Elements (SRE)

SRE are introduced as impurities with the batch ingredients and are associated with sedimentary material such as silt and clay. They may be introduced through contamination from the crucible fabric or impurities in the glassmaking sand. Figure 4.3.16 shows that the SRE patterns for the ‘Roman’ samples analysed are very consistent. As with the REE, some slight variation between samples is also likely to have resulted from slight variations in the proportions of the raw materials used in the production of these glasses; the opaque red glasses again generally contain slightly elevated SRE concentrations (Figure 4.3.16), which is likely to have resulted from the addition of metallurgical slag to the batch (see Chapter 5, section 5.2.3).

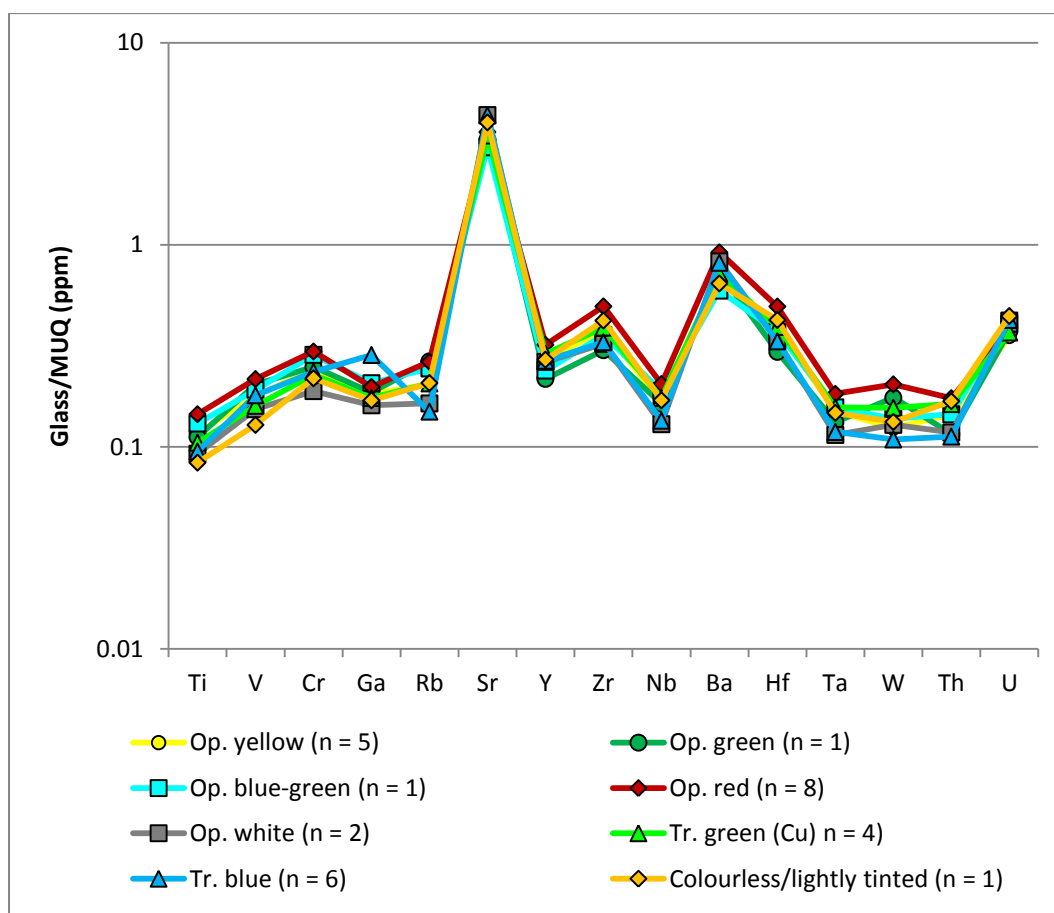


Figure 4.3.16 – Average sediment-related element concentrations for ‘Roman’ glass from Eriswell, by colour, normalised to the weathered continental crust (see Chapter 2, section 2.3.2.3). Note the logarithmic scale.

W varies slightly between samples, and Ga is elevated in the translucent blue samples; the latter may have resulted from the addition of a cobalt mineral as a colourant (see Chapter 5, section 5.1.3). In a plot of Zr versus Hf (Figure 4.2.13), the 'Roman' glasses appear to have been manufactured using a relatively pure quartz sand, similar to that used to produce 'Levantine I' and 'A2b Blue' glass.

The strong similarities in the SRE patterns between 'Roman' and 'Levantine I' glass is notable (Figure 4.2.12) and suggests that very similar batch materials were used in the production of both glass types. A plot of CaO* versus Sr (Figure 4.2.14) in the 'Roman' samples suggests the use of a glassmaking sand with a calcite component containing a different ratio of Sr to Ca than in the majority of the other glass types, with the notable exception of 'Levantine I' glass. This again supports the suggestion that 'Roman' and 'Levantine I' glass are likely to have been produced using similar glassmaking sands.

4.4. 'Saxon' Glass

The glass types discussed in the following section have been termed 'Saxon', but not as a reflection of their primary origins. In an ideal scenario, this glass would be named according to the primary origins of the raw glass itself (*e.g. Levantine, Egyptian, etc.*); however, this is not possible here as it remains unclear as to exactly where it was produced (see below). Whilst some primary glass types may also be named according to colour (*e.g. blue-green*; see this chapter, section 4.3) or compositional characteristics (*e.g. HIMT*; see this chapter, section 4.5), this is not possible here, as 'Saxon' glass in the present study is typically highly coloured; although compositional characteristics are sometimes used to distinguish between different types of 'Saxon' glass (*e.g. 'high MgO, MnO'*), as will be seen. The reason the term 'Saxon' has been chosen in the present study is because it is allusive to the period in which the glass was used and is memorable to the reader. The sub-divisions into 'Saxon I' and 'Saxon II' relate to the terminology adopted by Freestone *et al.* (2008) in their study of these glass types, based upon Evison's (now redundant; see Hines *et al.*, in press) chronology for Anglo-Saxon vessel glass (see below).

The 'Saxon I' and 'Saxon II' glass types are compositionally similar to one another in many respects, so are discussed here together to avoid repetition. Both types of glass constitute a significant proportion of the Eriswell assemblage. Both types can be distinguished from the other glass types identified by the concentrations of a number of different components (see this chapter, section 4.2); most notably their relatively low concentrations of SiO₂*, which typically fall below 67% (*e.g. Figure 4.2.5*).

The 'Saxon I' group corresponds closely to the low-MgO samples from the 'Period I' and 'Period II' groups defined by Freestone *et al.* (2008) for early Anglo-Saxon vessel glass from England. It comprises 147 samples taken from a total of 144 beads. The majority of these are translucent monochrome beads, in either translucent blue or 'naturally' tinted glass ('light', green and yellow tints). Translucent pink-brown and 'dark' glass also makes up a significant proportion of this compositional type. One opaque yellow, two opaque green and two opaque white samples are also

included here; see this chapter, section 4.9. ‘Saxon I’ glass is characterised by K_2O^* at levels typically below 1.0%, with variable levels of MgO^* up to 1.5% (*e.g.* Figure 4.2.4). However, they are particularly distinguished from ‘Saxon II’ glass by a different ratio of magnesia to lime (*e.g.* Figure 4.2.2), which is reflected in a plot of potash versus lime (Figure 4.2.3).

The ‘Saxon II’ group corresponds closely to the high-MgO samples in the ‘Period II’ group defined by Freestone *et al.* (2008). It comprises 101 samples taken from a total of 68 beads. The glass is predominantly opaque; mostly red, white, orange and yellow, but also includes a small number of translucent blue, ‘dark’ and naturally tinted glasses. Two opaque blue, one opaque green, one translucent green and one translucent turquoise samples are also included here; see this chapter, section 4.9. The majority of ‘Saxon II’ glasses are distinguishable by their generally elevated, but variable, levels of potash and magnesia relative to the other glass types identified (*e.g.* Figure 4.2.4); MgO^* is present at concentrations up to 2.1% and K_2O^* up to 2.6%.

The MgO^* and K_2O^* levels present in the ‘Saxon II’ glass from Eriswell are not high enough to class them as mixed-alkali glasses, in which one would expect to see potash at similar levels to soda (Brill 2006: 138). MgO^* and K_2O^* are strongly correlated in ‘Saxon II’ glass (Figure 4.4.1; $r^2 = 0.70$), but barely correlated in ‘Saxon I’ glass (Figure 4.4.1; $r^2 = 0.22$), suggesting that these two components are likely to have been introduced together in the former. Elevated levels of magnesia are not uncommon in glass beads from the Anglo-Saxon period; it has been suggested that the high levels of magnesia (up to 1.4% MgO) detected in several beads from the early Anglo-Saxon cemetery at Lechlade, Gloucestershire (Henderson 2011), may have resulted from a mineralogical impurity in the raw materials. However, magnesia may also be introduced with plant ash. Phosphate is not present at levels exceeding 0.3% in the ‘Saxon I’ samples, and is not correlated with potash (Figure 4.4.2), suggesting no such plant ash addition here. A plot of magnesia versus alumina shows that these two components are positively correlated in ‘Saxon I’ glass (Figure 4.4.3; $r^2 = 0.64$), suggesting that it is likely to have been introduced as a mineral impurity in the sand (alumina being introduced as an impurity with the sand; see this chapter, section 4.1.1.3). Furthermore, potash and

alumina are weakly correlated in ‘Saxon I’ glass (Figure 4.4.4; $r^2 = 0.30$, when omitting anomalies containing K_2O^* above 1.0%), suggesting that some potash was also introduced with a mineral impurity in the sand.

Potash and magnesia, together with alumina, are therefore likely to have been introduced together with the glassmaking sand in ‘Saxon I’ glass. This interpretation is borne out by the fact that alumina is not usually present in plant ash in the concentrations seen here (*e.g.* Jackson *et al.* 2005: 789). Lime is weakly correlated with alumina (Figure 4.2.9; $r^2 = 0.42$), magnesia (Figure 4.2.2; $r^2 = 0.56$) and potash (Figure 4.2.3; $r^2 = 0.37$, when omitting anomalies containing K_2O^* above 1.0%) in ‘Saxon I’ glass. It therefore seems likely that sand used to produce ‘Saxon I’ glass was rich in minerals derived from igneous rocks, such as feldspar (*e.g.* Degryse *et al.* 2006: 497), which would account for the positive correlations between alumina, potash and magnesia, as well as the particularly elevated levels of magnesia (Tal *et al.* 2004: 64). This would also account for the unusually elevated levels of strontium detected by trace element analysis in this glass type (see section 4.4.1 below). A similar correlation between alumina and magnesia is seen in ‘HIMT’ glass (Figure 4.4.5), suggesting the use of a sand containing similar mineral impurities in both of these glass types. It is likely that ‘Saxon I’ glass is closely related to ‘HIMT’ glass, perhaps even produced in neighbouring workshops (Freestone *et al.* 2008: 34; see also this chapter, section 4.5).

In contrast, alumina is not correlated with lime (Figure 4.2.9), magnesia (Figure 4.4.3) or potash (Figure 4.4.4) in the majority of ‘Saxon II’ samples, but lime is weakly correlated with magnesia (Figure 4.2.2; $r^2 = 0.46$) and potash (Figure 4.2.3; $r^2 = 0.45$). As such, the introduction of potash and magnesia, taken together with the strong positive correlation between these two components (Figure 4.4.1; $r^2 = 0.70$), cannot be explained by a mineral impurity in the glassmaking sand. However, up to 0.7% $P_2O_5^*$ (averaging 0.3% $P_2O_5^*$) is present in the ‘Saxon II’ samples, which is positively correlated with both magnesia (Figure 4.2.7; $r^2 = 0.47$) and potash (Figure 4.4.2; $r^2 = 0.55$). Slightly elevated levels of magnesia, potash and lime, together with low concentrations of phosphate were therefore, at least in part, probably introduced with a plant ash addition in several of the ‘Saxon II’ samples, as will be seen.

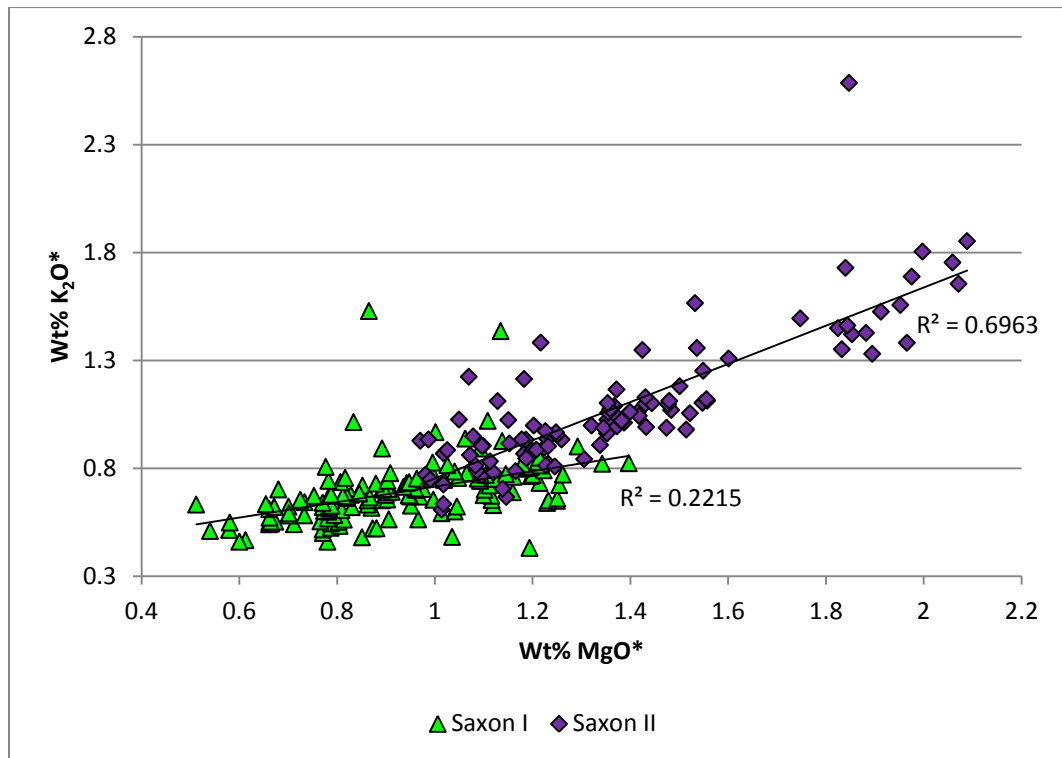


Figure 4.4.1 – A plot of magnesia versus potash for ‘Saxon I’ and ‘Saxon II’ glass from Eriswell.

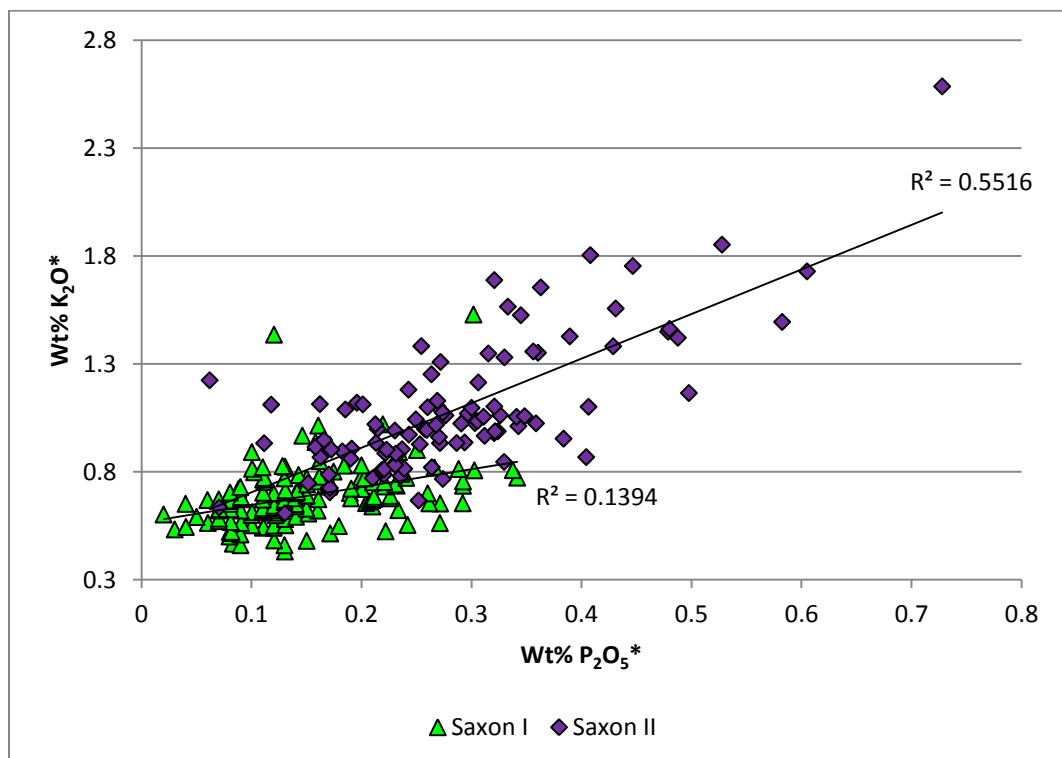


Figure 4.4.2 – A plot of phosphate versus potash for ‘Saxon I’ and ‘Saxon II’ glass from Eriswell.

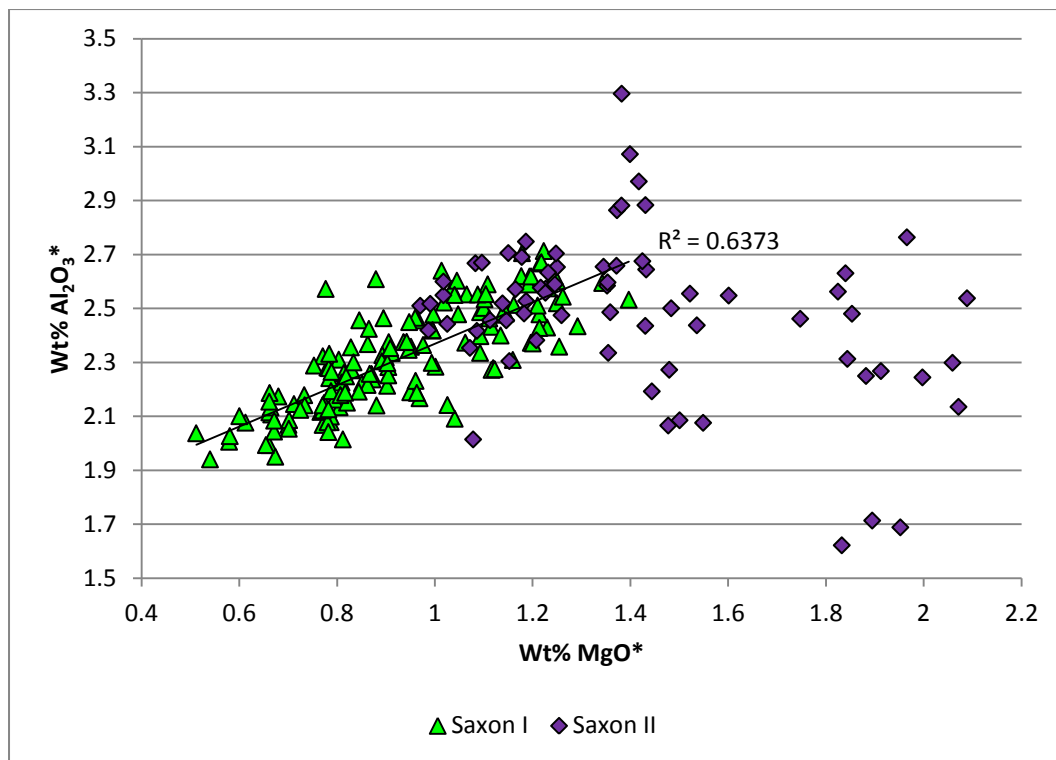


Figure 4.4.3 – A plot of magnesia versus alumina for ‘Saxon I’ and ‘Saxon II’ glass from Eriswell, omitting samples which are likely to have suffered from contamination by alumina (see this chapter, section 4.1 for details).

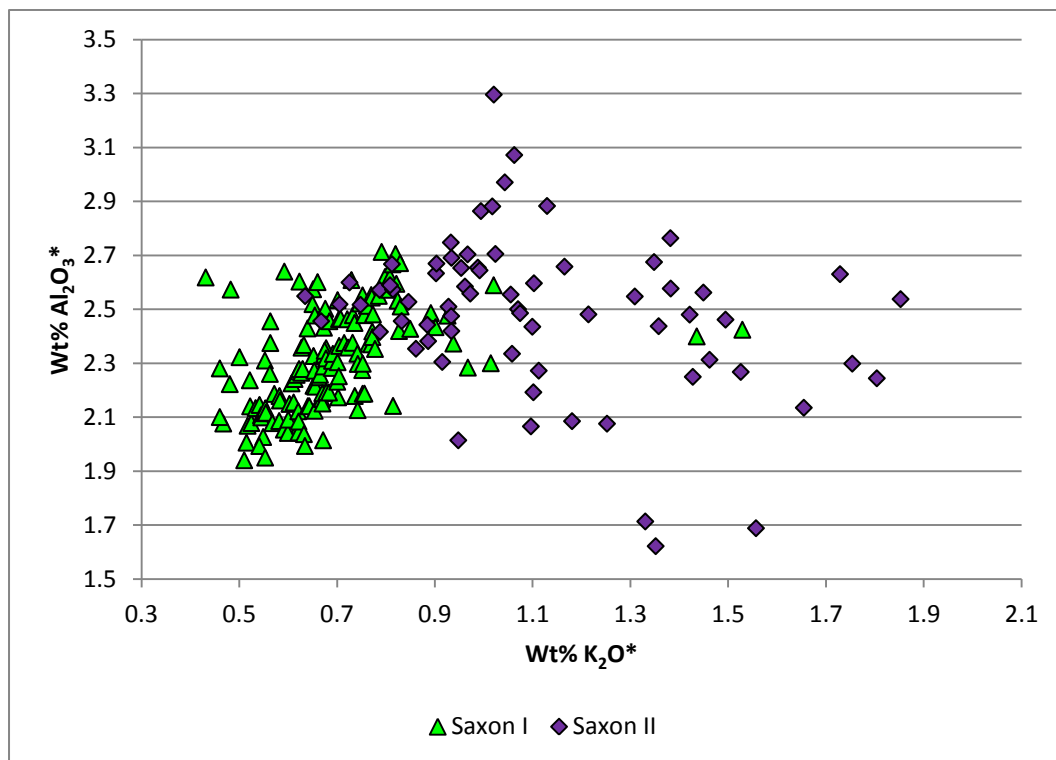


Figure 4.4.4 – A plot of potash versus alumina for ‘Saxon I’ and ‘Saxon II’ glass from Eriswell, omitting samples which are likely to have suffered from contamination by alumina (see this chapter, section 4.1 for details).

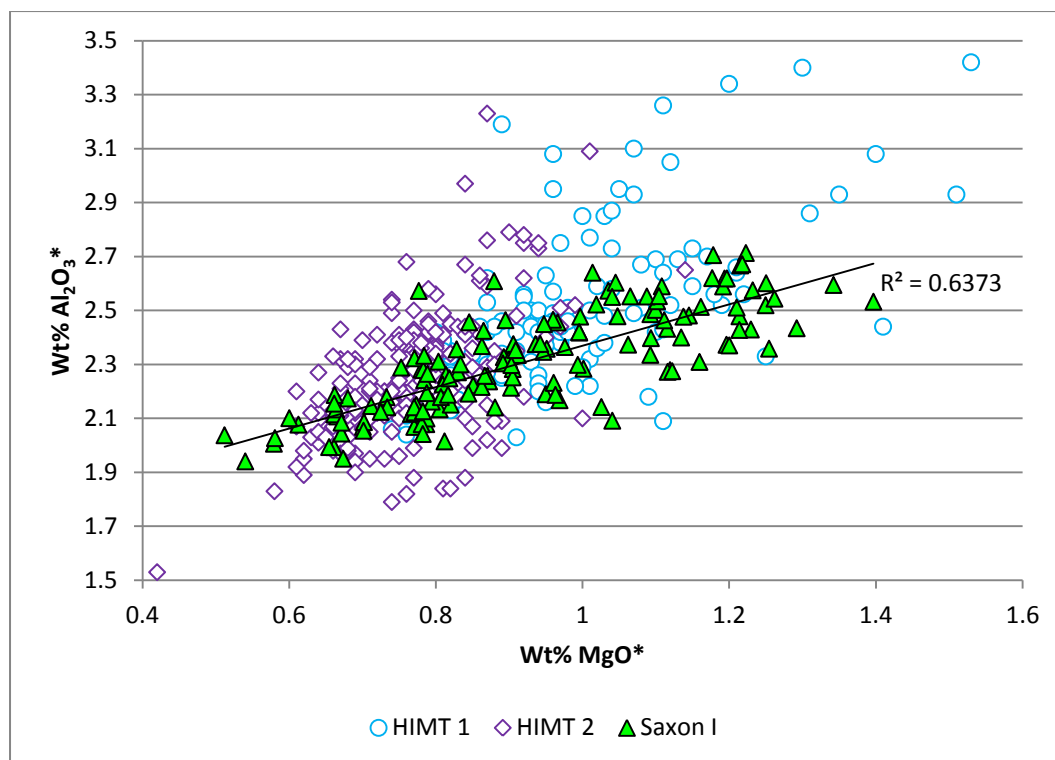


Figure 4.4.5 – A plot of magnesia versus alumina for ‘Saxon I’ glass from Eriswell, compared to published data for Late Roman ‘HIMT 1’ and ‘HIMT 2’ glass from Britain (after Foster and Jackson 2009). Samples which are likely to have been affected by alumina contamination have been omitted (see this chapter, section 4.1 for details).

Freestone *et al.* (2008) were able to clearly distinguish between their early Anglo-Saxon ‘Period I’ and ‘Period II’ vessel glass, and devised a series of sub-groups based on the relative concentrations of manganese and magnesia (Figure 4.4.6). Analysis of the Eriswell bead assemblage has allowed these groups to be somewhat expanded upon. Figure 4.4.7 shows a plot of manganese versus magnesia for the ‘Saxon I’ and ‘Saxon II’ glasses from Eriswell; it has been possible to sub-divide the data into five groups, which have a number of similarities to those in Figure 4.4.6:

- The ‘**Saxon I (blue)**’ group corresponds very approximately to the ‘Period II natron’ glasses identified by Freestone *et al.* (2008). A re-evaluation of Freestone *et al.*’s ‘Period II natron’ group suggests that only their two translucent blue samples (samples 150 and 151; globular beakers from Broomfield) correspond to ‘Saxon I (blue)’ glass consistent with the Eriswell data; the remaining samples are unlikely to represent ‘Saxon I (blue)’ glass (see this chapter, section 4.2). This group is termed ‘Saxon I’ as the majority

of these beads fall into Brugmann's phase A (*i.e.* prior to *c.* AD 580; see this chapter, section 4.8); Freestone *et al.*'s 'Period II' group is instead attributed to Evison's Period II (*i.e.* post *c.* AD 550) (Freestone *et al.* 2008: 31). The difference in name therefore relate to differences in chronological attribution rather than composition.

- The '**Saxon I (natron)**' group corresponds to the 'Period I natron' group defined by Freestone *et al.* (2008).
- The '**Saxon II (natron)**' was not identified in Anglo-Saxon vessel glass by Freestone *et al.* (2008). Whilst this group has a number of very close compositional similarities to 'Saxon I (natron)' glass, the different ratios of lime to both magnesia and potash (*e.g.* Figure 4.4.10) suggest that it is different. It corresponds to Foy *et al.*'s 'Group 2.1' (Foy *et al.* 2003).
- The '**Saxon II (high MgO, low MnO)**' group corresponds to the 'Period II high MgO, low MnO' group defined by Freestone *et al.* (2008).
- The '**Saxon II (high MgO, MnO)**' group corresponds to the 'Period II high MgO, MnO' group defined by Freestone *et al.* (2008).

The average compositions of these groups from Eriswell are shown in Table 4.4.1.

Table 4.4.1 – Average compositions for the five different sub-groups of ‘Saxon I’ and ‘Saxon II’ glass identified at Eriswell.

<i>Composition</i> ¹	<i>Oxide (wt %)</i> ²													<i>Total</i>
	<i>Na₂O*</i>	<i>MgO*</i>	<i>Al₂O₃*</i>	<i>SiO₂*</i>	<i>P₂O₅*</i>	<i>SO₃*</i>	<i>Cl*</i>	<i>K₂O*</i>	<i>CaO*</i>	<i>TiO₂*</i>	<i>MnO*</i>	<i>Fe₂O₃*</i>	<i>Sb₂O₃*</i>	
Saxon I (blue) (n = 66)	19.3	0.8	2.3	65.9	0.1	0.5	1.0	0.7	7.2	0.2	0.6	1.5	b.d.	100.0
SD	1.0	0.1	0.2	0.9	0.1	0.1	0.1	0.2	0.6	0.1	0.3	0.3	-	
Saxon I (natron) (n = 68)	18.5	1.0	2.4	65.0	0.2	0.5	0.9	0.7	8.0	0.2	1.5	1.2	b.d.	100.0
SD	1.0	0.2	0.2	0.9	0.1	0.1	0.1	0.1	0.6	0.0	0.3	0.5	-	
Saxon II (natron) (n = 27)	17.8	1.3	2.5	65.2	0.3	0.4	0.8	1.0	7.4	0.2	1.5	1.5	b.d.	100.0
SD	1.3	0.2	0.2	1.1	0.1	0.1	0.1	0.2	0.7	0.0	0.3	0.5	-	
Saxon II (high MgO, low MnO) (n = 27)	18.7	1.4	2.5	65.4	0.2	0.5	0.9	1.0	7.5	0.2	0.3	1.4	b.d.	100.0
SD	1.5	0.3	0.4	1.4	0.1	0.1	0.1	0.2	0.9	0.1	0.2	0.4	-	
Saxon II (high MgO, MnO) (n = 7)	16.8	2.0	2.3	63.1	0.4	0.5	0.7	1.5	8.6	0.2	2.0	1.8	b.d.	100.0
SD	0.9	0.1	0.3	0.8	0.1	0.2	0.3	0.2	0.4	0.0	0.2	0.4	-	

¹Averages taken only from samples for which the values for alumina and iron have *not* been assumed. SD = standard deviation.

²Area analyses normalised to 100%. b.d. = below detection. See Chapter 2, section 2.3.1 for details.

Figures 4.4.6 and 4.4.7 demonstrate that the groups established in the ‘Saxon I’ and ‘Saxon II’ glasses at Eriswell on a plot of manganese versus magnesia closely reflect those of Freestone *et al.* (2008: 37). The ‘Saxon I’ glasses typically contain low levels of MgO* (below 1.3%), and can be relatively easily divided into two groups according to their manganese contents. ‘Saxon I (blue)’ glass is so-called because the majority of the samples are translucent blue (see this chapter, section 4.9); trace element analysis suggests that the samples which are not blue are likely to be products of a different workshop (see section 4.4.1 below). It contains less than 1.2% MnO*, whereas the ‘Saxon I (natron)’ group contain in excess of 1.0% MnO*. The compositional overlap here is borne out by the attribution of translucent blue samples containing 1.0-1.2% MnO* *and* <0.9% MgO* to the ‘Saxon I (blue)’ group; translucent blue samples of the ‘Saxon I (natron)’ type conversely contain in excess of 1.0% of *both* MnO* and MgO*.

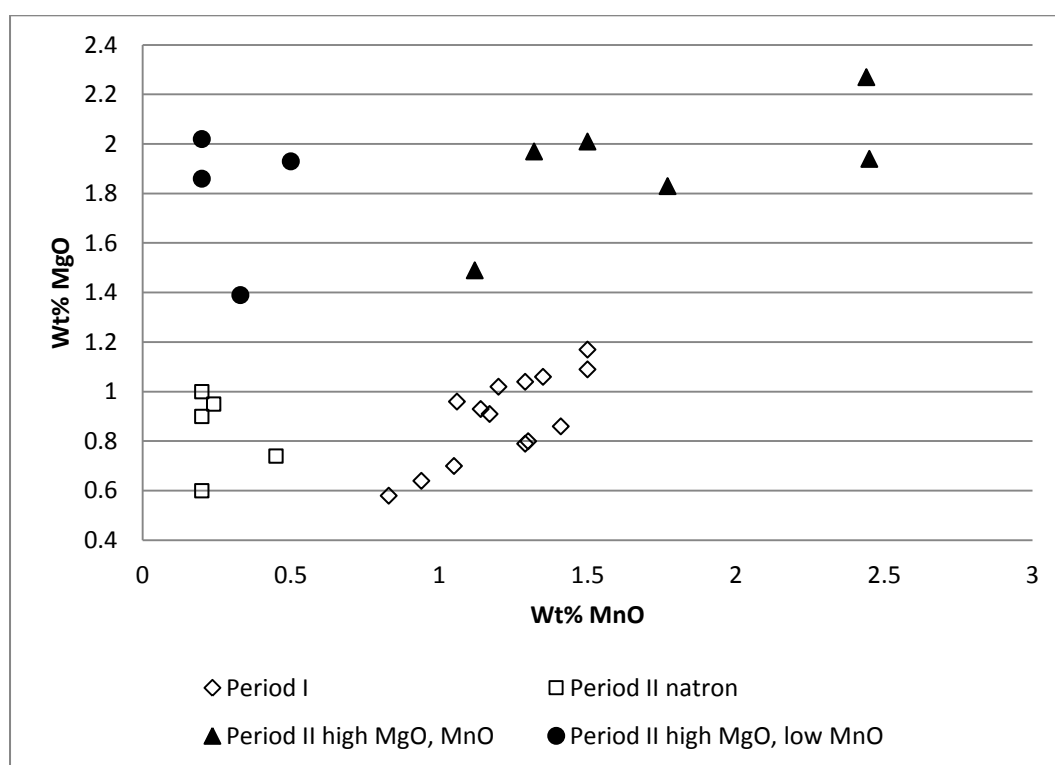


Figure 4.4.6 – A plot of manganese oxide versus magnesia for early Anglo-Saxon vessel glass (after Freestone *et al.* 2008).

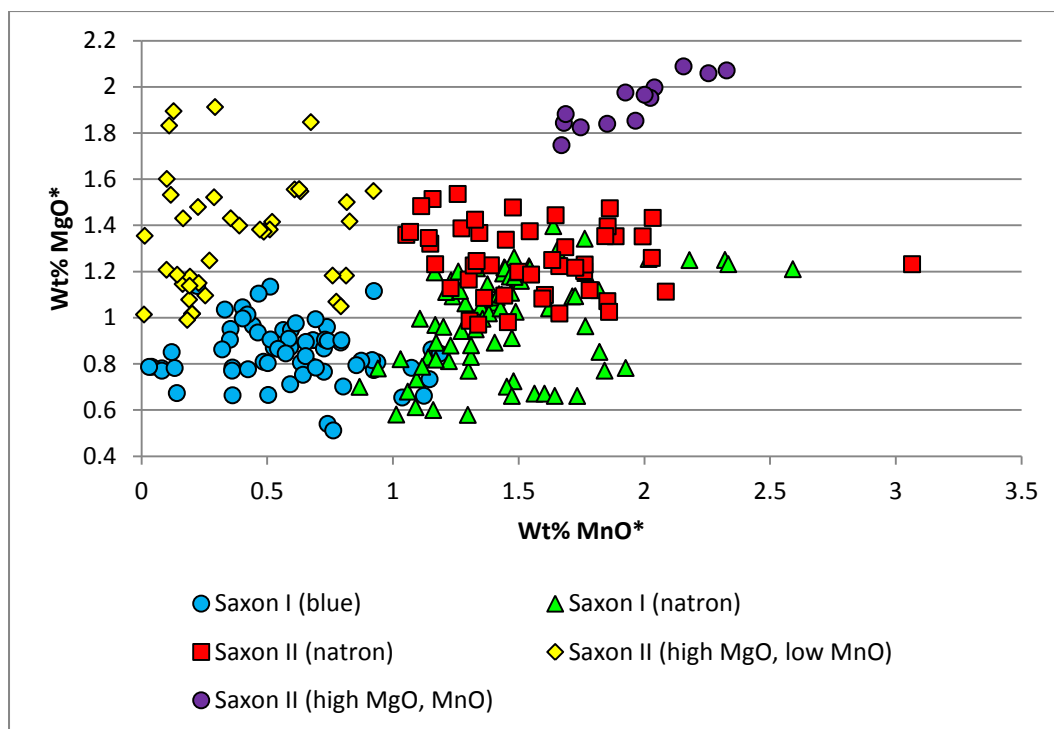


Figure 4.4.7 – A plot of manganese oxide versus magnesia for the ‘Saxon I’ and ‘Saxon II’ glass types from Eriswell.

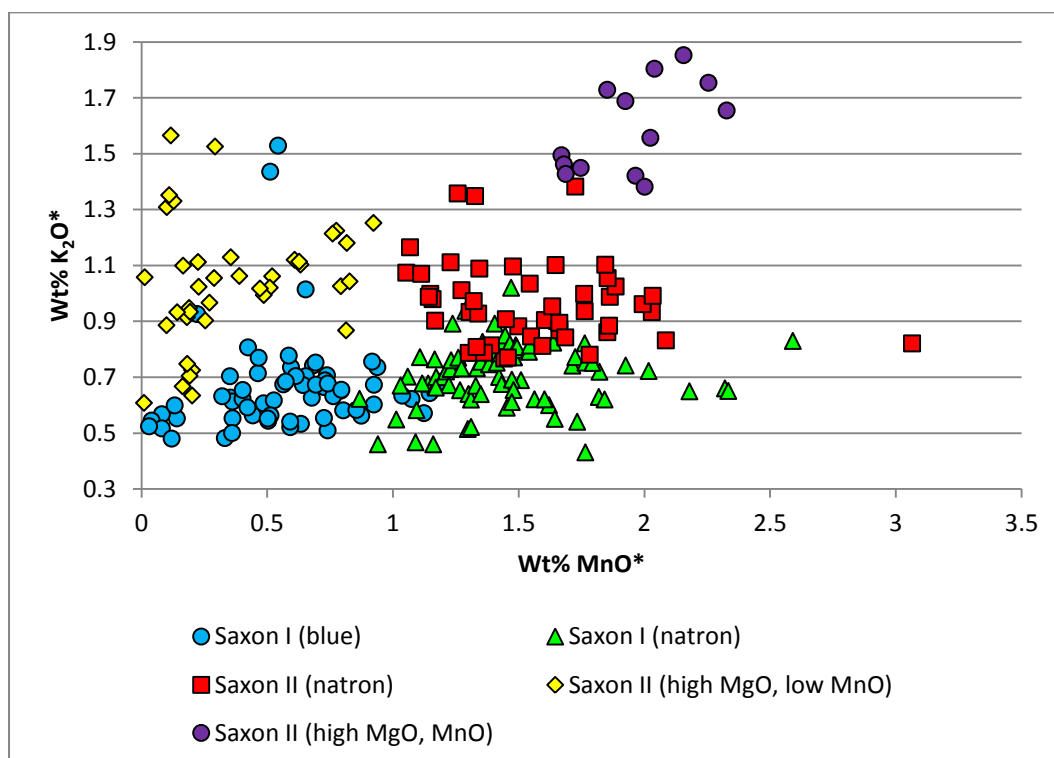


Figure 4.4.8 – A plot of manganese oxide versus potash for the ‘Saxon I’ and ‘Saxon II’ glass types from Eriswell. Opaque red sample ERL104:G193:1311 has been omitted due to its extraordinarily high concentration of potash (2.6% K₂O*).

‘Saxon II’ glasses typically contains high levels of MgO* (above 0.9%), and can also be relatively simply divided according to their manganese contents (Figure 4.4.7). The ‘Saxon II (high MgO, low MnO)’ group contains less than 1.0% MnO*; the compositional overlap between this group and ‘Saxon I (blue)’ glass results from the attribution of Brugmann’s phase B2 beads to the former type and her phase A translucent blue beads to the latter. Conversely, ‘Saxon II (natron)’ glass contains in excess of 1.0% MnO*, and overlaps considerably with ‘Saxon I (natron)’ glass. However, these two types differ according to the distinctions between ‘Saxon I’ and ‘Saxon II’ glass outlined above. Lastly, the ‘Saxon II (high MgO, MnO)’ group contains very high levels of both MnO* and MgO* (above 1.5% of each).

The five ‘Saxon’ glass types identified are similarly differentiated in a plot of manganese versus potash, although potash is far more variable than magnesia (Figure 4.4.8 *cf.* Figure 4.4.7). As mentioned above, ‘Saxon I’ glass is likely to have been produced from a relatively impure glassmaking sand rich in heavy minerals (*e.g.* feldspars), with which elevated levels of magnesia were introduced. The positive correlation between magnesia and alumina in the ‘Saxon I’ glass types is clearly demonstrated in Figure 4.4.9. However, whilst similar raw materials are likely to have been used in the production of ‘Saxon I (blue)’ and ‘Saxon I (natron)’ glass, the plot of manganese versus magnesia (Figure 4.4.7) suggests that the batch ingredients were slightly different. ‘Saxon I (blue)’ glass is generally much poorer in manganese than ‘Saxon I (natron)’ glass (Figures 4.4.7 and 4.4.8).

Whilst the weak positive correlation between manganese and magnesia (Figure 4.4.7; $r^2 = 0.46$ when omitting samples), and between manganese and alumina (Figure 4.4.11; $r^2 = 0.28$ when omitting samples containing $>1.7\%$ MnO* and translucent pink-brown samples) in ‘Saxon I (natron)’ glass would otherwise suggest that manganese was introduced as an impurity with the glassmaking sand, manganese-rich sands are unlikely to have been suitable for glass production (Foy *et al.* 2003: 47). These correlations can only be explained by the controlled addition of the correct amount of manganese to the batch (Ian Freestone, pers. comm.; Wedepohl *et al.* 2003: 57). The glassmakers must have known the approximate concentration of iron in ‘Saxon I (natron)’ glass, which was probably estimated based on the colour of test melts; this would have resulted in a positive correlation

between iron and manganese (Ian Freestone, pers. comm.; Wedepohl *et al.* 2003: 57). Such a correlation is not observed in ‘Saxon I (natron)’ glass from Eriswell due to the introduction of iron from a number of sources (*e.g.* contamination from the crucible fabric, the use of iron-rich colourants, etc.; see this chapter, section 4.1). However, like iron, alumina and magnesia are primarily introduced as impurities with the glassmaking sand here; manganese is therefore correlated with these components.

The controlled addition of high concentrations of manganese to ‘Saxon I (blue)’ glass would not have been crucial to the production of this glass as it is almost exclusively translucent blue (see this chapter, section 4.9); the tint produced from any iron impurity would therefore have been masked by the intensity of the cobalt colourant. ‘Saxon I (blue)’ and ‘Saxon I (natron)’ glass are therefore likely to have been produced using very similar, perhaps even identical, glassmaking sands, as evidenced by the similar correlations between magnesia and both alumina and lime (Figures 4.4.9 and 4.4.10). Manganese is likely to have been added to ‘Saxon I (natron)’ glass during the primary production of the glass itself. In contrast, cobalt was probably added to ‘Saxon I (blue)’ glass during the primary production of the glass itself; manganese here may have been either added in lower and much less controlled quantities, or introduced as an impurity with the colourant.

‘Saxon I (natron)’ glass corresponds closely to early medieval glass from elsewhere in Europe, as noted by Freestone *et al.* (2008: 34-36). This includes 5th-7th century Merovingian glass from Vicq (Yvelines, northern France) (Velde 1990), 5th-7th century Frankish glass from Krefeld-Gellep (Germany) (Wedepohl *et al.* 1997) and 5th-8th century glass from Grado and Vicenza (northern Italy) (Silvestri *et al.* 2005: Group A2/1). This glass type was clearly widely traded during the early medieval period, probably in its raw form. Figures 4.4.12 and 4.4.13 demonstrate the compositional similarities between these glass types. The positive correlation between manganese and magnesia in ‘Saxon I (natron)’ glass is particularly reflected in the Merovingian glass from Vicq (Figure 4.4.13; $r^2 = 0.83$).

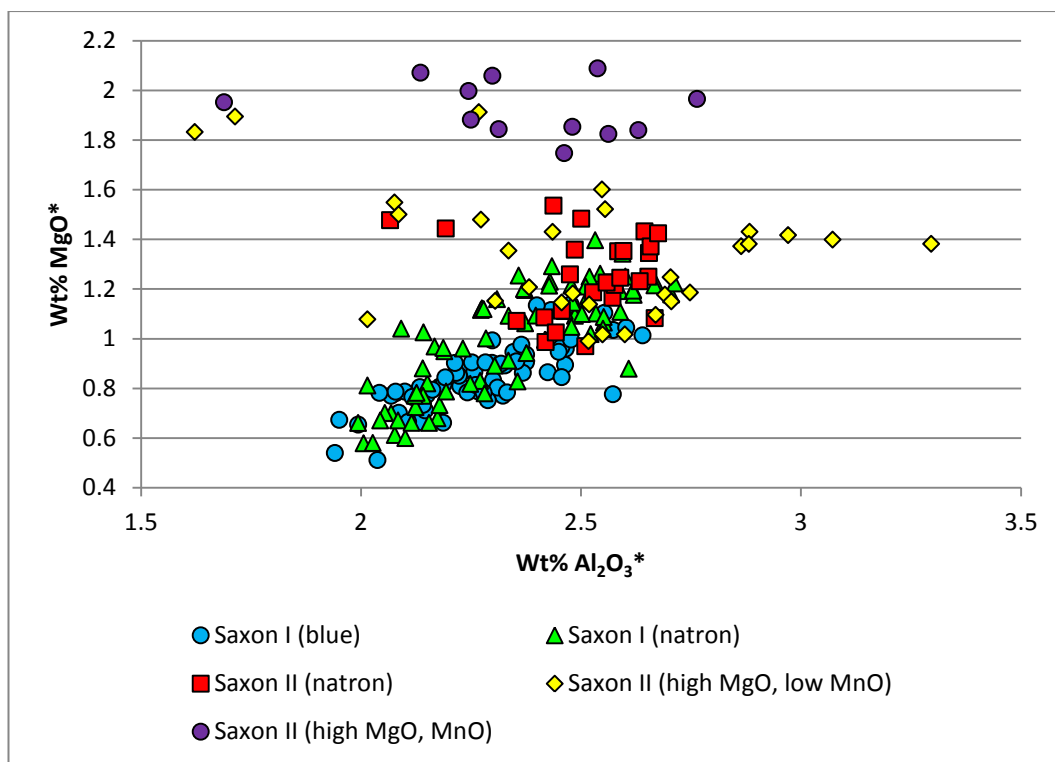


Figure 4.4.9 – A plot of alumina versus magnesia for the ‘Saxon I’ and ‘Saxon II’ glass types from Eriswell. Samples which are likely to have suffered from contamination by alumina have been omitted (see this chapter, section 4.1 for details).

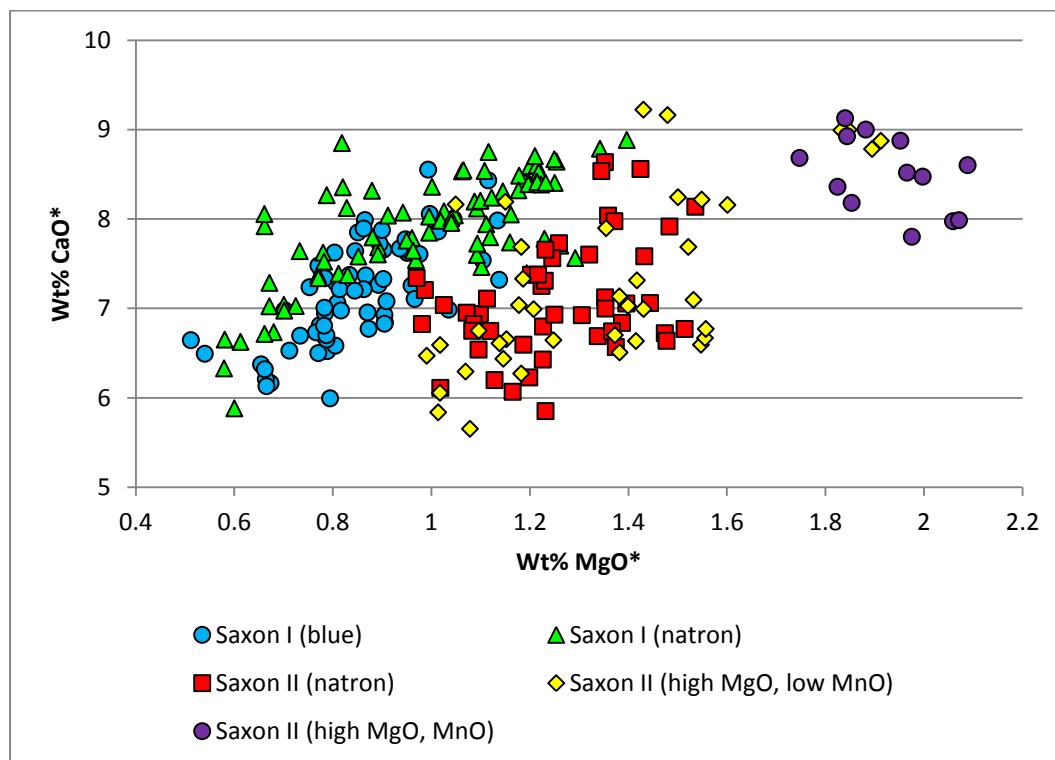


Figure 4.4.10 – A plot of magnesia versus lime for the ‘Saxon I’ and ‘Saxon II’ glass types from Eriswell.

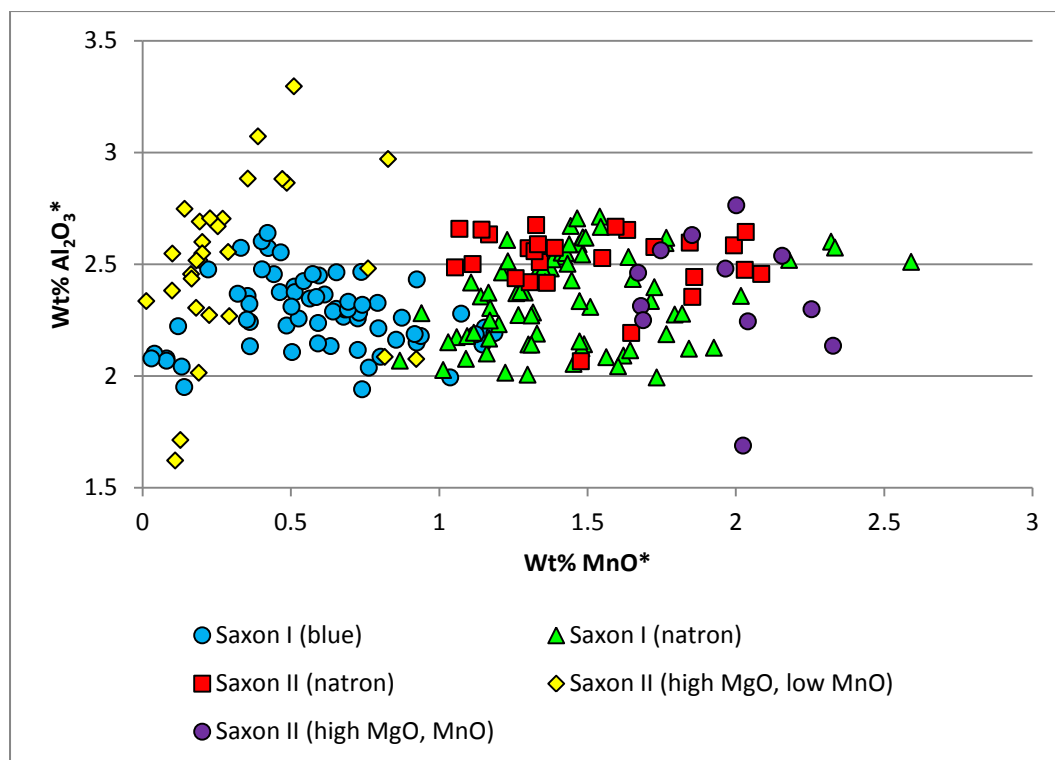


Figure 4.4.11 – A plot of manganese oxide versus alumina for the ‘Saxon I’ and ‘Saxon II’ glass types from Eriswell. Samples which are likely to have suffered from contamination by alumina have been omitted (see this chapter, section 4.1 for details).

The ‘Saxon II (natron)’ group corresponds closely to Foy *et al.*’s ‘Group 2.1’ (Foy *et al.* 2003). Foster and Jackson (2010: 193) suggest that this group is in fact a type of ‘HIMT’ glass (see this chapter, section 4.5), corresponding closely to their ‘HIMT 1’ group. However, the CaO* content of ‘HIMT’ glass is typically below 6.5% (*e.g.* Freestone 2003: 112), whereas in Foy *et al.*’s ‘Group 2.1’ CaO* is more typically present at concentrations well in excess of this. Whilst their attribution highlights the close similarities between these two types of glass, Foy *et al.*’s ‘Group 2.1’ (and consequently ‘Saxon II (natron)’ glass) is interpreted as a distinct type from ‘HIMT’ glass in the present study, although it may represent a continuum of the ‘HIMT’ tradition. It is just conceivable that the ‘Saxon II (natron)’ samples containing CaO* below 6.5%, which in some cases also contain elevated levels of TiO₂* (0.2-0.6%) typical of ‘HIMT’ glass, are in fact ‘HIMT’ glass. However, these are coincidentally almost all high-lead opaque yellow glasses which, considering the likelihood of contamination (particularly by iron) in this glass colour (see this chapter, section 4.1), suggests that low concentrations of titanium are more likely to have been introduced as a contaminant from the melting pot.

The similarities between Foy *et al.*'s 'Group 2.1' and 'Saxon II (natron)' glass are demonstrated in Figures 4.4.14 and 4.4.15, together with similar 5th-8th century glass from Grado and Vicenza (northern Italy) (Silvestri *et al.* 2005: Group A2/2) and mid-6th to early 7th century Celtic vessel glass from Longbury Bank, Dyfed (Wales) (Campbell and Lane 1993) which are also of the same type. There is a weak positive correlation between potash and magnesia in both the 'Saxon II (low MgO, high MnO)' glass (Figure 4.4.16; $r^2 = 0.36$), which is more pronounced in Foy *et al.*'s Group 2.1 (Figure 4.4.16; $r^2 = 0.61$). However, the levels of potash, magnesia and phosphate are too low to suggest a plant ash addition. Manganese is not correlated with magnesia (*e.g.* Figure 4.4.7) or potash (*e.g.* Figure 4.4.8), suggesting that it is likely to have been a separate, deliberate addition. It is also possible that the marginally elevated levels of magnesia and potash relative to 'Saxon I' glass (*e.g.* Figure 4.4.16) were introduced with a mineral impurity in the glassmaking sand, as the levels of phosphate are too low to suggest a plant ash addition.

The 'Saxon II (high MgO, MnO)' glasses form a relatively tight compositional group, containing by far the highest levels of potash and magnesia (*e.g.* Figures 4.4.7-4.4.10 and 4.4.16). As noted by Freestone *et al.* (2008: 37), potash and magnesia at these concentrations are not typically found in natron glass. Furthermore, these two components are weakly correlated with one another (Figure 4.4.16; $r^2 = 0.41$). Manganese is weakly correlated with potash (Figure 4.4.8; $r^2 = 0.34$) and strongly correlated with magnesia (Figure 4.4.7; $r^2 = 0.80$). In contrast to the 'Saxon I' glasses, none of these components are correlated with alumina (*e.g.* Figures 4.4.9 and 4.4.11), suggesting that they are unlikely to have been introduced as impurities with the glassmaking sand. However, potash and magnesia are correlated with phosphate (*e.g.* Figures 4.4.17 and 4.4.18); P₂O₅* is present at concentrations between 0.3 and 0.6%, which strongly suggests a plant ash addition. The generally elevated levels of lime (7.8-9.1% CaO*) and strontium (see section 4.4.1 below) in this glass type (*e.g.* Figure 4.4.10) also suggest a natron base glass produced using calcareous quartz sand was adulterated with small quantities of plant ash; plant ash being rich in both lime and strontium (*e.g.* Henderson *et al.* 2005: 666).

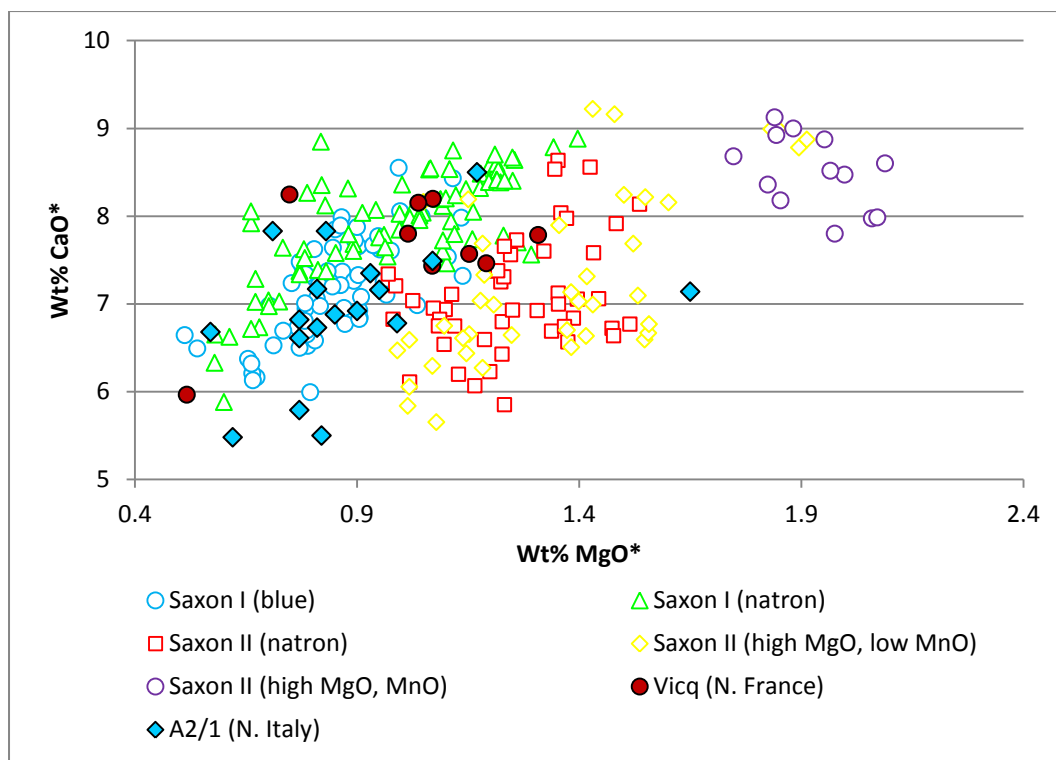


Figure 4.4.12 – A plot of magnesia versus lime for Merovingian (5th-7th century) glass from Vicq (Yvelines, N. France) (Velde 1990: 110) and 5th-8th century glass from Italy (Silvestri *et al.* 2005: Group A2/1), compared to the ‘Saxon I’ and ‘Saxon II’ glass types from Eriswell.

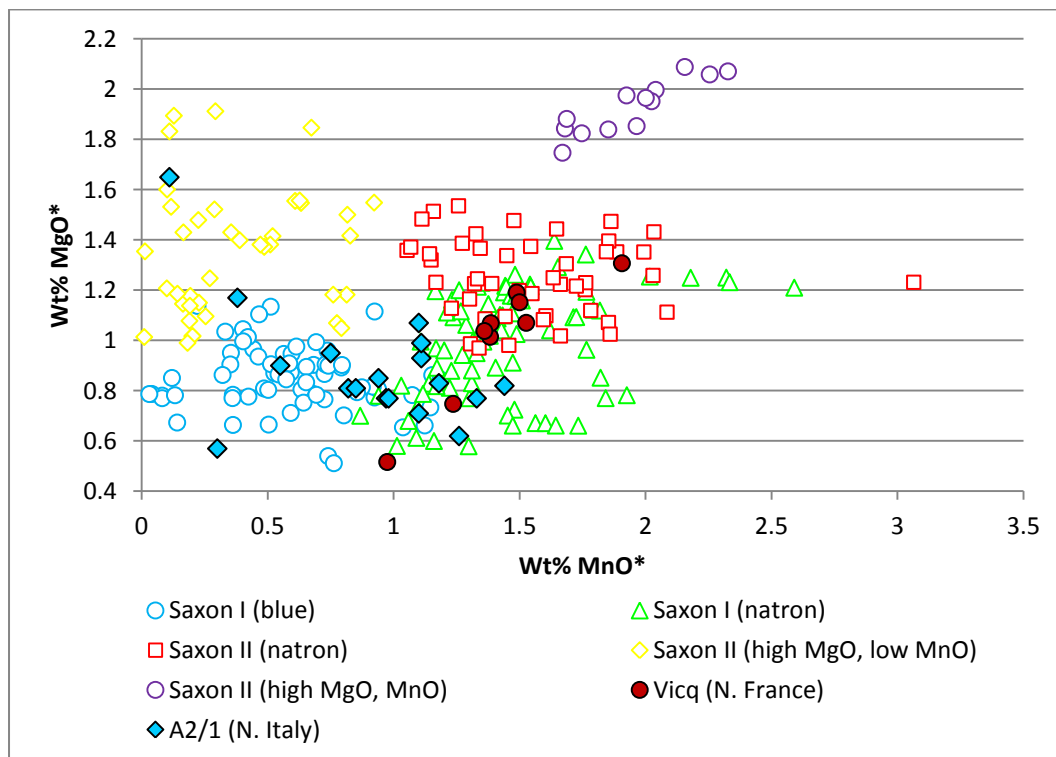


Figure 4.4.13 – A plot of manganese oxide versus magnesia for Merovingian (5th-7th century) glass from Vicq (Yvelines, N. France) (Velde 1990: 110) and 5th-8th century glass from Italy (Silvestri *et al.* 2005: Group A2/1), compared to the ‘Saxon I’ and ‘Saxon II’ glass types from Eriswell.

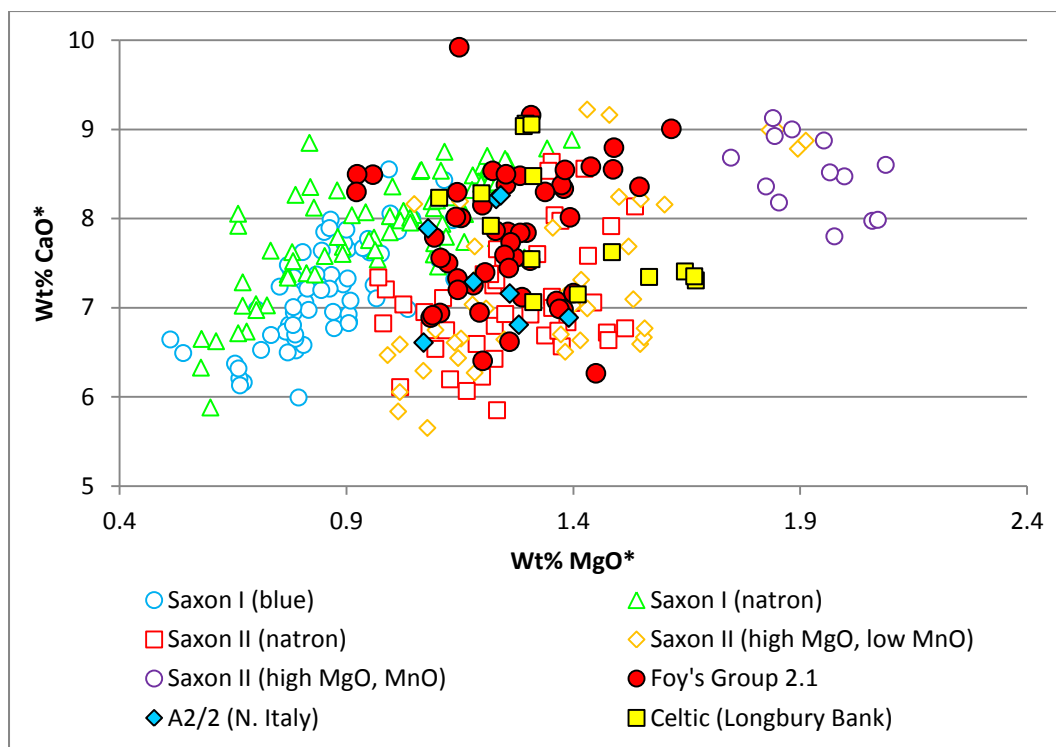


Figure 4.4.14 – A plot of magnesia versus lime for Foy *et al.*'s 'Group 2.1' (Foy *et al.* 2003: 84), 5th-8th century glass from Italy (Silvestri *et al.* 2005: Group A2/2) and mid-6th to early 7th century Celtic vessel glass from Wales (Campbell and Lane 1993: 48), compared to 'Saxon I' and 'Saxon II' glass types from Eriswell.

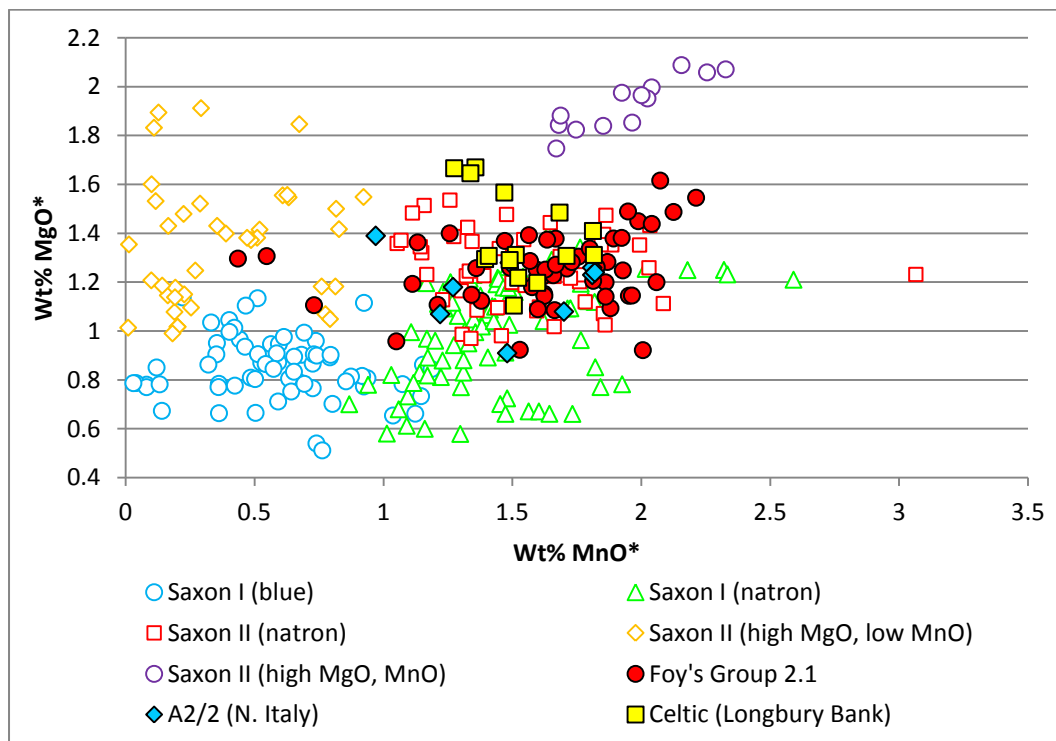


Figure 4.4.15 – A plot of manganese oxide versus magnesia for Foy *et al.*'s 'Group 2.1' (Foy *et al.* 2003: 84), 5th-8th century glass from Italy (Silvestri *et al.* 2005: Group A2/2) and mid-6th to early 7th century Celtic vessel glass from Wales (Campbell and Lane 1993: 48), compared to the 'Saxon I' and 'Saxon II' glass types from Eriswell.

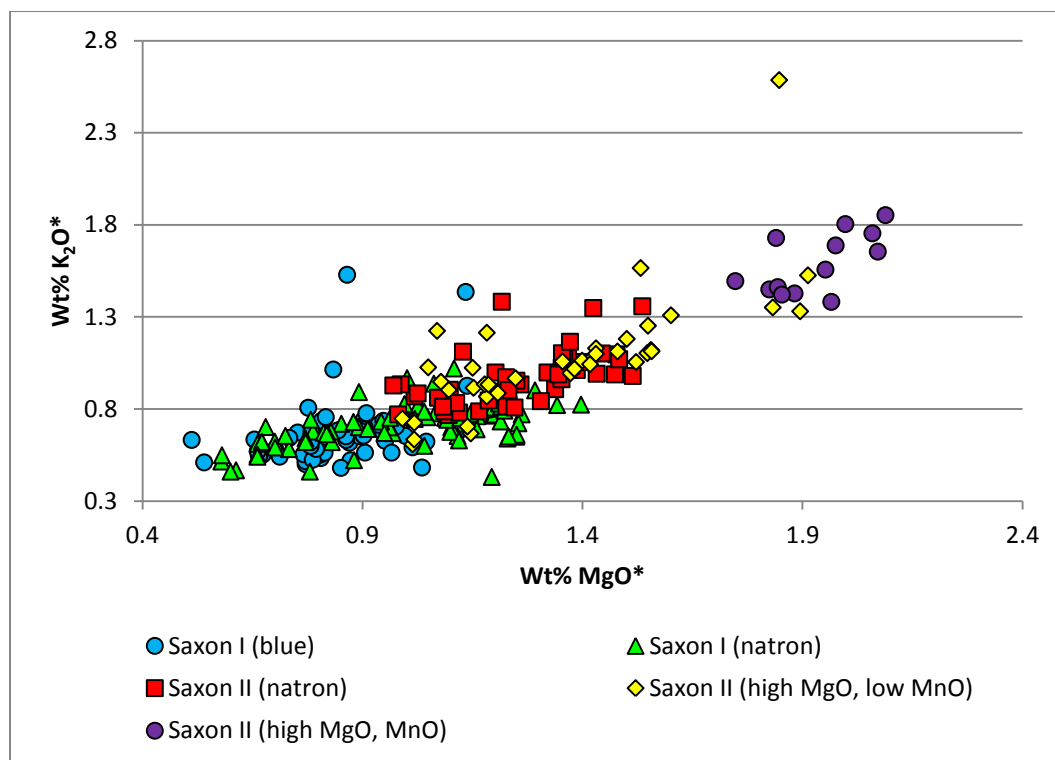


Figure 4.4.16 – A plot of magnesia versus potash for the ‘Saxon I’ and ‘Saxon II’ glass types from Eriswell.

Freestone *et al.* 2008: 37-38 suggest that some Anglo-Saxon vessel glass was produced from a mixture of plant ash glass and natron glass. Mixed-alkali glass has been identified in a dark green early Anglo-Saxon (6th century) bead from Apple Down, Chichester (Henderson 1990; Henderson 1999a: 87) and there is evidence to suggest that the early Anglo-Saxon Rainham Horn was produced using a soda-rich plant ash glass (Freestone *et al.* 2008: 38). However, it is widely accepted that plant ash glass did not generally come into use in the Western world until after the 8th or 9th centuries AD, when it replaced glass of the natron type (Freestone *et al.* 2008: 37). The question therefore arises as to the nature of this ash addition and whether it was deliberate or incidental.

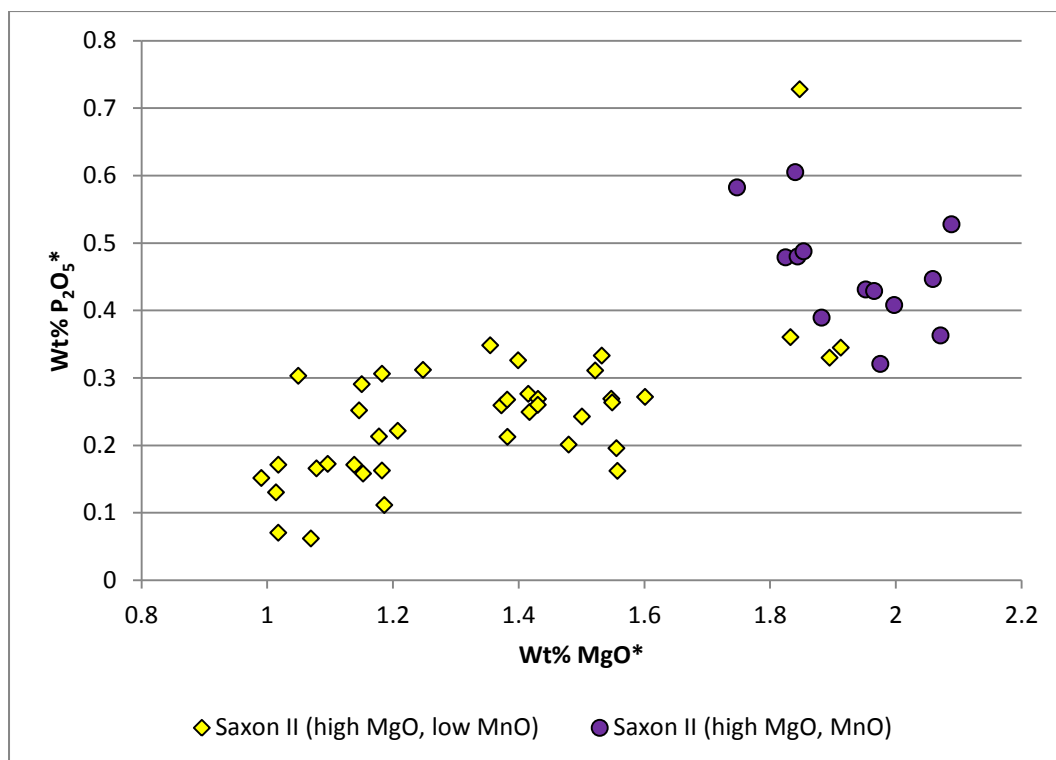


Figure 4.4.17 – A plot of magnesia versus phosphate for ‘Saxon II (high MgO, low MnO)’ and ‘Saxon II (high MnO, MnO)’ glass from Eriswell.

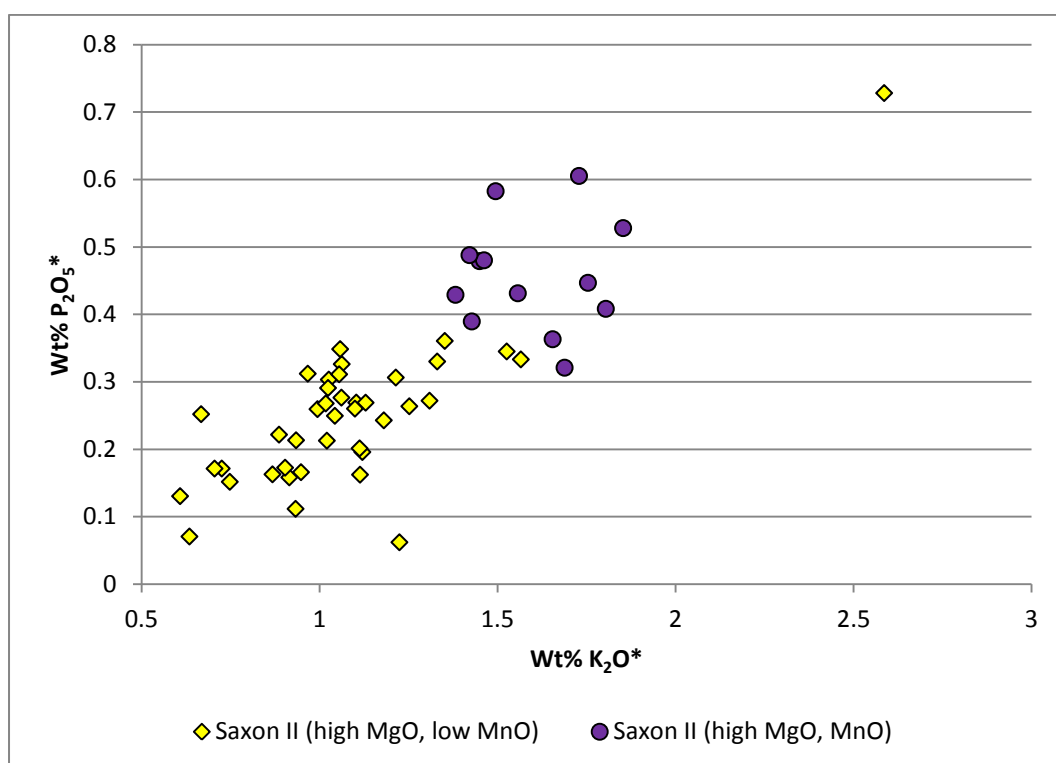


Figure 4.4.18 – A plot of potash versus phosphate for ‘Saxon II (high MgO, low MnO)’ and ‘Saxon II (high MnO, MnO)’ glass from Eriswell.

As previously mentioned (see Chapter 1, section 1.4), the production of plant ash and natron glass requires the use of different silica sources; plant ash is rich in lime and natron is poor in lime. The manufacture of natron glass thus necessitates the use of a calcareous quartz-rich sand or a deliberate lime addition to produce a stable glass. Trace element data suggests that the silica source used in ‘Saxon II (high MgO, MnO)’ glass is broadly similar to that used to produce the other natron-based ‘Saxon I’ and ‘Saxon II’ glasses at Eriswell; *i.e.* calcareous quartz-rich sand (see section 4.4.1 below).

This is consistent with the findings of Freestone *et al.* (2008: 39); they concluded that small quantities of an ash-rich material were added to a natron base glass in the production of ‘Saxon II (high MgO, MnO)’ glass. Whilst previous studies have demonstrated that small but considerable amounts of ash can sometimes be introduced through contamination from the wood used to fuel the furnace, as a result of poor separation between the glass and fuel (*e.g.* Tal *et al.* 2008a: 72; Tal *et al.* 2008b: 91), the levels of potash and magnesia observed in ‘Saxon II (high MgO, MnO)’ glass seem far too high to have been incidentally introduced in such a way. Furthermore, if this were the case, intermediate compositions between ‘Saxon II (high MgO, MnO)’ glass and ‘Saxon I (natron)’ or ‘Saxon II (natron)’ glass would be expected. This is clearly not the case, as demonstrated by the distinct cut-off point at approximately 1.6-1.8% MgO* in Figure 4.4.16. It is therefore likely that plant ash was a conscious addition.

The question now arises as to the nature of this ash-rich component. Freestone *et al.* (2008: 39) suggest that it is unlikely to have been a soda-rich ash; it is instead more similar to potassium-rich wood-ash used in later medieval northern European glassmaking (Wedepohl 2000: 255-256). The present data support this interpretation. Freestone *et al.* (2008: 39) calculated the composition of such an ash-rich material (Table 4.4.2, row 1), which they suggest was added to ‘Saxon I (natron)’ glass to produce ‘Saxon II (high MgO, MnO)’ glass. Table 4.4.2 shows that a hypothetical glass produced from a mixture of 10% of this ash-rich material (after Freestone *et al.* 2008) and 90% ‘Saxon I (natron)’ glass (Eriswell data) closely matches the composition of ‘Saxon II (high MgO, MnO)’ glass (Table 4.4.2, row 2 *cf.* row 3), although lime is slightly on the high side. This parallels the results of Freestone *et al.*

(2008: 46). However, silica is elevated in their hypothetical ash-rich material relative to potassium-rich wood ash, which has led them to suggest that the ash was added in the form of a rudimentary ash-rich 'glass', *i.e.* a mixture of plant ash and silica, as opposed to plant ash alone (Freestone *et al.* 2008: 39).

In the light of the identification of 'Saxon II (natron)' glass at Eriswell, an alternative can now be suggested. Previous work on the composition of potassium-rich plant ash has demonstrated that beech ash, for example, is usually richer in manganese than the ashes of oak or bracken, although the composition of wood-ash is notoriously variable (*e.g.* Jackson and Smedley 2004: 39; 2007: 126-127; Jackson *et al.* 2005: 789). Note that the composition of beech ash was selected here due to the particularly elevated levels of manganese in published analyses of this ash type, which correspond well with the elevated levels of MnO in 'Saxon II (high MgO, MnO)' glass; this should *not* be taken to suggest the exclusive use of beech ash as opposed to ash types from other plants (*e.g.* oak, bracken). The approximate composition of beech ash (after Jackson *et al.* (2005: 789) is shown in Table 4.4.2, row 4. The composition of a hypothetical glass produced from a mixture of 10% of this beech ash and 90% 'Saxon II (natron)' glass (Eriswell data) is shown in Table 4.4.2, row 5.

The similarities between the compositions of the resulting hypothetical glass and 'Saxon II (high MgO, MnO)' glass are striking (Table 4.4.2, row 5 *cf.* row 6). Only phosphate, potash and lime are enriched significantly beyond the norm in the hypothetical glass. However, this is not unexpected, as the levels of phosphate in wood-ash can be extremely variable; for example, oak ash has been shown to contain as little as 3% P₂O₅ (Jackson *et al.* 2005: 786). The presence of insoluble compounds, such as potassium calcium sulphate, in most wood ash can also result in depleted levels of potash and lime in the final glass relative to the composition of the ash used (Jackson *et al.* 2005: 790). Furthermore, elements such as silica and iron in the final glass may be introduced through contamination from the melting pot (see this chapter, section 4.1), which may account for the comparatively depleted concentrations of these two components in the hypothetical glass. The slight compositional differences observed are therefore not to be unexpected, especially as wood ash is notoriously variable in composition; for example, composition can vary

depending upon the part of the plant employed or the environment in which it grew (soil, climate, etc.) (Jackson *et al.* 2005: 791; Jackson and Smedley 2008: 127).

Table 4.4.2 – Hypothetical glass compositions for a mixture of 10% ash-rich glass (after Freestone *et al.* 2008) with ‘Saxon I (natron)’ glass, and of 10% beech ash (after Jackson *et al.* 2005) with ‘Saxon II (natron)’ glass, compared to the mean composition of ‘Saxon II (high MgO, MnO)’ glass.

Description	Oxide (wt %)									
	Na ₂ O	MgO	Al ₂ O ₃	SiO ₂	P ₂ O ₅	SO ₃	K ₂ O	CaO	MnO	Fe ₂ O ₃
1. Ash-rich material (Freestone <i>et al.</i> 2008)	1.0	10.0	1.0	35.0	3.0	-	10.0	30.0	5.0	5.0
2. Hypothetical (90% ‘Saxon I (natron)’ + 10% ash-rich material)	16.9	1.9	2.2	62.7	0.4	0.4	1.6	10.2	1.9	1.6
3. Saxon II (high MgO, MnO) (n = 7)	16.8	2.0	2.3	63.1	0.4	0.5	1.5	8.6	2.0	1.8
.....										
4. Beech ash (after Jackson <i>et al.</i> 2005)	0.6	6.4	0.9	16.7	14.1	1.1	18.5	28.8	5.7	0.9
5. Hypothetical (90% ‘Saxon II (natron)’ + 10% beech ash)	16.3	1.9	2.4	61.1	1.8	0.5	2.9	9.8	2.0	1.4
6. Saxon II (high MgO, MnO) (n = 7)	16.8	2.0	2.3	63.1	0.4	0.5	1.5	8.6	2.0	1.8

It is not possible to ascertain the type of ash employed in the production of ‘Saxon II (high MgO, MnO)’ glass, as it is difficult to distinguish between ashes from different potassium-rich plant species (Jackson *et al.* 2005: 793; Jackson and Smedley 2008: 126-127). Nevertheless, the calculations in Table 4.4.2 suggest up to 10% or more wood ash was added to ‘Saxon II (natron)’ glass to produce ‘Saxon II (high MgO, MnO)’ glass. The potassium-rich nature of this ash addition suggests that this practice probably took place in northwestern Europe, where woodland trees and plants were widely available for burning (Freestone *et al.* 2008: 41; Jackson and Smedley 2008: 118; Wedepohl 2000: 255-256). Freestone *et al.* (2008: 42) suggest that the apparent rarity of ‘Saxon II (high MgO, MnO)’ glass outside of Britain may indicate that this practice was exclusive to Anglo-Saxon workshops. However, there is no typological evidence to support this view; beads produced from this glass type in the present study are instead more consistent with Continental production,

whereas purportedly ‘Anglo-Saxon’ beads are primarily produced from recycled Roman material (see this chapter, section 4.10.2). This glass type may have been a precursor to the production of so-called ‘forest glass’, which replaced natron glass in Britain and northern Europe from the 8th or 9th centuries AD (*e.g.* Wedepohl 2000: 255; Wedepohl *et al.* 2011: 93). It is just possible that fuel ash from a glassmaking furnace elsewhere (*e.g.* in the Near East) was used, but this is less likely as glass of the ‘Saxon II (high MgO, MnO)’ composition has yet to be identified in the Eastern Mediterranean.

Whilst it cannot be ruled out that a rudimentary ash-rich glass such as that calculated by Freestone *et al.* (2008) (Table 4.4.2, row 1) was employed, it is unlikely for a number of reasons. It has now been demonstrated that pure plant ash could just as conceivably have been used. Furthermore, the production of a rudimentary ash-rich glass would have required a supply of a relatively pure source of silica (probably quartz pebbles, which would then had to have been crushed); this would have been far more labour intensive than the direct addition of plant ash to a molten natron base glass. The consistency in the composition of ‘Saxon II (high MgO, MnO)’ glass, particularly the ratio of manganese to magnesia (*e.g.* Figure 4.4.7), suggests that this glass was adulterated with ash in a limited number of workshops, perhaps only one; wood-ash is notoriously variable in composition (Freestone *et al.* 2008: 41), so if this practice was undertaken by a number of different workshops, the consistency observed would not be expected.

The reasons for the addition of small quantities of ash to natron-type glass are unclear, but the most likely explanation is that it was undertaken to extend the supply of glass due to difficulties in obtaining natron (Freestone *et al.* 2008: 41). The amount of ash which could have been added would have been limited by the lime-rich nature of the natron base glass; the addition of much more than approximately 10% ash would have introduced excessive amounts of lime which would risk failure of the batch (*e.g.* Freestone and Gorin-Rosen 1999: 115). The attribution of glass of this type to Brugmann’s phases B2 and C (*i.e.* after *c.* AD 580; see this chapter, section 4.8) and Evison’s Period II (*i.e.* after *c.* AD 550; Freestone *et al.* 2008) suggests that this practice is unlikely to pre-date the mid-6th century.

The addition of plant ash is also suggested in several of the ‘Saxon II (high MgO, low MnO)’ samples by the positive correlation between potash and magnesia (Figure 4.4.16; $r^2 = 0.54$). Four samples contain potash and magnesia at similar levels to ‘Saxon II (high MgO, MnO)’ glass, suggesting a considerable plant ash addition here (Figure 4.4.16). However, $P_2O_5^*$ is typically present at concentrations below 0.3% in the majority of samples of this compositional type, which are too low to confirm a plant ash addition. On the other hand, phosphate is weakly correlated with both magnesia ($r^2 = 0.41$, Figure 4.4.17) and more strongly with potash ($r^2 = 0.66$, Figure 4.4.18), so a plant ash addition cannot be ruled out.

As ‘Saxon I (blue)’ glass is almost exclusively translucent blue (see this chapter, section 4.9), the majority of ‘Saxon II (high MgO, low MnO)’ samples are unlikely to represent ‘Saxon I (blue)’ glass to which plant ash has been added. It is just possible that the blue ‘Saxon II (high MgO, low MnO)’ samples represent ‘Saxon I (blue)’ glass to which a small quantity of plant ash has been added; translucent blue sample ERL104:G281:1799 contains elevated levels of magnesia (1.6% MgO*) and potash (1.3% K_2O^*) relative to ‘Saxon I (blue)’ glass, suggesting a considerable plant-ash addition. This bead is also unusual in that it is of the *Blue* bead type typical of phase A ‘Saxon I (blue)’ beads, but has been attributed to phase B2, suggesting that it is later. However, other colours cannot be accounted for in this way.

It is very difficult to make sense of the ‘Saxon II (high MgO, low MnO)’ group due to its extremely variable composition. However, these samples are unlikely to represent products of the same workshop. They may also represent the products of mixing glass of different compositions, possibly as a result of recycling glass obtained from a number of different sources. Further work is required to establish the nature of this glass.

The origins of ‘Saxon’ glass are not entirely clear. Freestone *et al.* (2008: 32) state that ‘Saxon I’ glass is similar to contemporary natron glass produced in the Eastern Mediterranean. Figure 4.4.19 shows a plot of lime versus alumina for five major groups of natron glass produced in the Eastern Mediterranean from the 4th -9th centuries AD, each of which represents a product of a different workshop in a slightly different location (Freestone 2006; Freestone *et al.* 2000; 2002a; 2002b; see

also Chapter 1, section 1.4.1). It is clear that the composition of ‘Saxon I’ and ‘Saxon II’ glass is consistent with several of these groups, particularly ‘HIMT’ glass. Whilst ‘Saxon I’ glass has a different ratio of magnesia to lime than ‘HIMT’ glass (*e.g.* Figure 4.2.2), suggesting that it is different, previous work (*e.g.* Freestone *et al.* 2008: 36) suggests that ‘Saxon I (natron)’ glass is likely to have a similar origin to ‘HIMT’ glass. This is likely to have been between the Nile and southern Israel (Foy *et al.* 2003: 75; Freestone *et al.* 2008: 36), which is supported by isotopic analysis (Freestone *et al.* 2005b: 155-156; 2009: 44; see also this chapter, section 4.5).

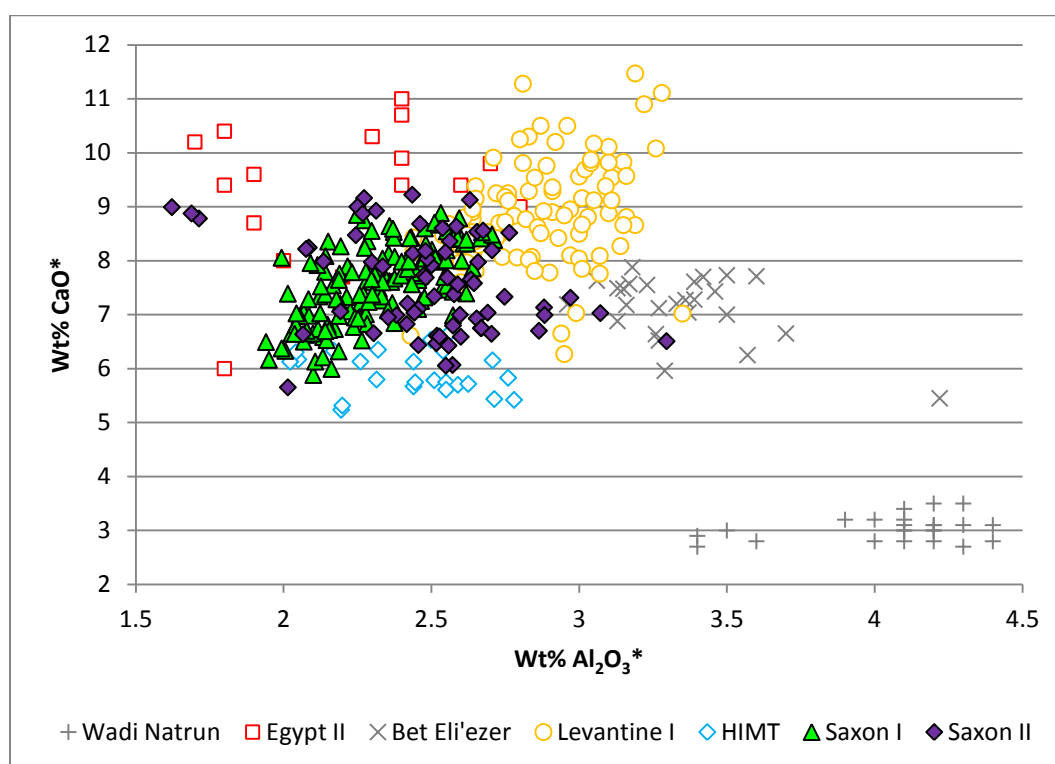


Figure 4.4.19 – A plot of alumina versus lime for ‘Saxon I’ and ‘Saxon II’ glass from Eriswell, compared to the five major groups of natron glass produced in the Eastern Mediterranean between the 4th and 9th centuries AD (see text for details). Samples which are likely to have been affected by alumina contamination have been omitted (see this chapter, section 4.1).

‘Saxon I (blue)’ glass has not been identified as a distinct type in published literature, with the exception of two cobalt-blue globular beakers from Broomfield (Bimson and Freestone 2000; Freestone *et al.* 2008). However, two fragments of deep blue vessel glass from Maroni Petrera in Cyprus attributed to the ‘HIMT’ type by Freestone *et al.* (2002b: samples 6830-7 and 6830-8), are in fact consistent with

‘Saxon I (blue)’ glass; their elevated levels of lime relative to ‘HIMT’ glass (6.9 and 7.6% CaO* *cf.* <6.5% CaO*) supports this view. Unfortunately, without supporting trace element analyses it is not possible to confirm that the same cobalt sources were exploited as in ‘Saxon I (blue)’ glass. Nevertheless, the similarities suggest that ‘Saxon I (blue)’ glass is likely to have been widely traded in its raw form, and was probably pre-coloured with cobalt in the Eastern Mediterranean. The author is unaware of further published analyses of cobalt-blue glass of this type.

It is likely that ‘Saxon II (natron)’ glass has its origins in the same production zone as Foy *et al.*’s ‘Group 2.1’ (Foy *et al.* 2003), attributed to the mid-6th to 7th centuries. Glass of this composition has been discovered in Egypt, Tunisia and France (Foy *et al.* 2003: 47). ‘Saxon II (natron)’ glass has also been identified from 5th-7th century contexts throughout Italy (Mirti *et al.* 2000; Silvestri *et al.* 2005; 2011), so was clearly widely distributed. Foy *et al.* (2003: 75) suggest that the workshops producing this glass type are likely to have neighboured those producing ‘HIMT’ glass, but that an Egyptian origin is unlikely. Production in the Sinai or southern Israel region is therefore a possibility.

Interestingly, the mid-6th to early 7th century Celtic vessel glass from Longbury Bank, Dyfed (southwest Wales) is of the ‘Saxon II (natron)’ type (Campbell and Lane 1993: 40-49). At the very least, this indicates that the workshops producing Celtic vessels and Anglo-Saxon beads from ‘Saxon II (natron)’ glass at this time procured their glass from the same source(s). These particular vessels are all assumed to have been Continental imports (Campbell and Lane 1993: 40-45) as they have parallels in Bordeaux, suggesting that they are likely to have their origins in western France (Campbell 2000: 42). Foy *et al.* (2003: 55-56) have identified raw glass chunks of this type in Bordeaux imported from the Eastern Mediterranean, which supports the view that these vessels were probably produced in this region. Curiously, no Anglo-Saxon vessels of the ‘Saxon II (natron)’ compositional type have been identified to date; the author is unaware of any analyses which may suggest that Anglo-Saxon vessels were produced from it. However, given the dearth of Anglo-Saxon vessel glass analyses, negative evidence such as this should be interpreted with caution.

4.4.1. Trace Element Analyses

Trace elements for 25 'Saxon I' glasses and 11 'Saxon II' glasses were obtained by LA-ICP-MS.

4.4.1.1. Rare Earth Elements (REE)

The 'Saxon I' glasses analysed are mainly translucent blue, with one dark sample. The REE patterns are all relatively flat and form a very coherent group (Figures 4.4.20-4.4.22). This suggests that 'Saxon I (blue)' and 'Saxon I (natron)' glass is likely to have a similar origin and that the sand sources used are likely to have been sourced from very similar or neighbouring regions. This consistent with the SEM-EDS data, which suggest a similar sand source for both glass types (see above). Whilst there is some slight variation in the REE concentrations between samples (Figures 4.4.21 and 4.4.22), these are not significant enough to suggest a different geochemical origin for any of the samples. The slight negative Ce and positive Eu anomalies in the samples relate to the variable oxidation states of these elements, which affects the way in which they are deposited in rock-forming processes.

In contrast to 'Saxon I' glass, 'Saxon II' glass does not form a coherent group (Figure 4.4.20). The REE concentrations are markedly varied between samples, with most having a significant negative Ce anomaly (Figures 4.4.23-4.4.25). Whilst some slight variation *may* have resulted from the colouring process, the variations in REE concentrations observed here are more likely to have resulted from the raw materials used to produce the base glass (*i.e.* the glassmaking sand); note that the same variation is not observed in highly coloured glass of the 'Roman' type (see this chapter, section 4.3.1).

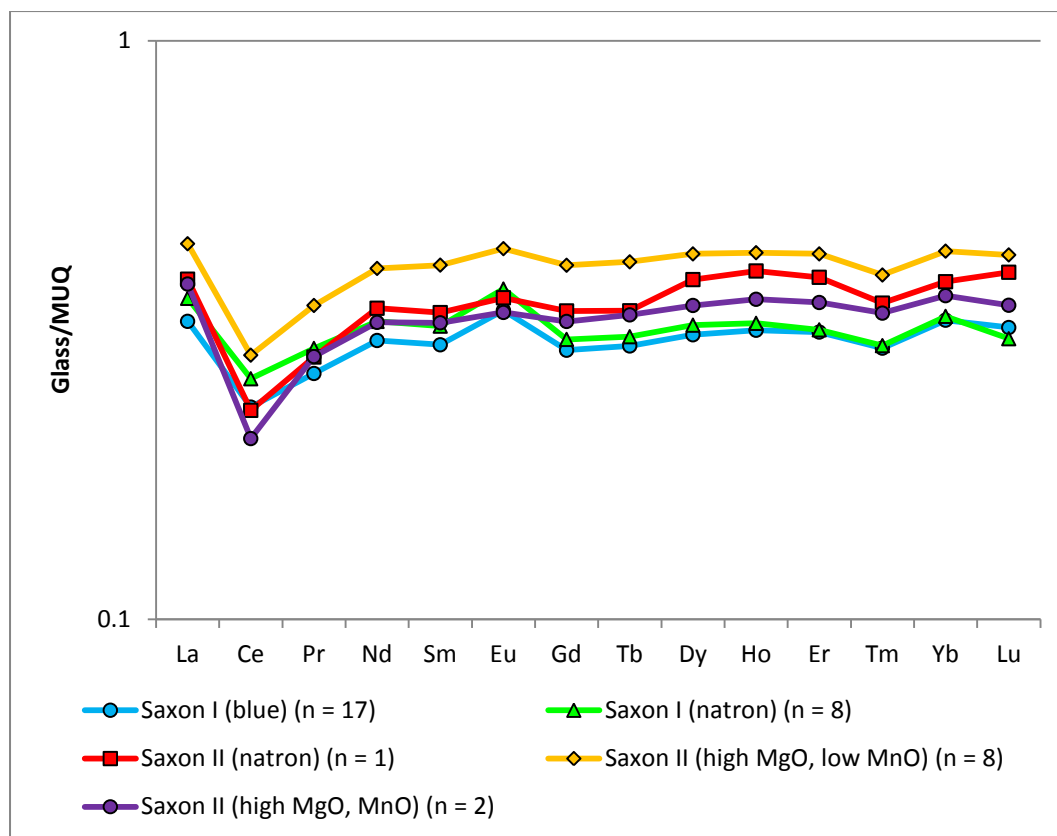


Figure 4.4.20 – Average rare earth elements concentrations for ‘Saxon I’ and 11 ‘Saxon II’ glass from Eriswell, normalised to the weathered continental crust (see Chapter 2, section 2.3.2.3). Note the logarithmic scale.

The REE patterns for the majority of ‘Saxon II’ samples are very similar in shape (Figures 4.4.23-4.4.25). Only one ‘Saxon II (natron)’ sample was analysed (Figure 4.4.23), so this glass type is poorly represented here. However, its REE pattern has a number of similarities to that of ‘Saxon I’ and ‘Saxon II (high MgO, MnO)’ glass, falling between the two (Figure 4.4.20). The close similarities between the REE patterns of ‘Saxon II (natron)’ and ‘Saxon II (high MgO, MnO)’ glass in particular (Figure 4.4.20; also compare Figures 4.4.23 and 4.4.24) supports the view that ‘Saxon II (high MgO, MnO)’ glass is likely to represent ‘Saxon II (natron)’ glass adulterated with plant ash. If an plant ash was added to ‘Saxon I (natron)’ glass to produce ‘Saxon II (high MgO, MnO)’ glass, as suggested by Freestone *et al.* (2008: 39), the REE pattern would be expected to be more similar to ‘Saxon I (natron)’ glass; this is clearly not the case (Figure 4.4.20; also compare to Figures 4.4.21 and 4.4.22). The Ce anomaly is considerably more negative and the Eu anomaly less positive in ‘Saxon II (natron)’ and ‘Saxon II (high MgO, MnO)’ glass when

compared to ‘Saxon I’ glass, suggesting that neither of these types are derived from ‘Saxon I (natron)’ glass.

The considerable variation in the concentrations of REE between the two ‘Saxon II (high MgO, MnO)’ samples (Figure 4.4.24) may have resulted from the incorporation of some REE with the plant ash component; *e.g.* through the incidental incorporation of some soil. However, the alumina content of the opaque orange sample is much lower (1.7% Al₂O₃*) to that observed in the opaque red sample (2.2% Al₂O₃*). It is therefore likely that the depleted concentrations of REE in the opaque orange sample result from the use of a slightly purer, perhaps refined, silica source.

The picture is far more complex with regard to the ‘Saxon II (high MgO, low MnO)’ samples. They contain considerably elevated REE concentrations on average relative to the other glass types (Figure 4.4.20), which may suggest the use of a much less pure silica source. However, the REE patterns vary considerably between samples (Figure 4.4.25); these patterns are generally much flatter and the REE concentrations much lower in the translucent blue and opaque green samples than in other colours. Furthermore, the Ce anomaly is less negative in these particular colours. They instead more closely reflect the REE patterns of ‘Saxon I (blue)’ glass (Figure 4.4.21). This supports the view that some of these samples are likely to represent ‘Saxon I (blue)’ glass which has been adulterated with small quantities of plant ash.

The picture is less clear regarding the opaque green sample (ERL104:G273:3330a/09, *Green Constricted Segmented*), in which the REE pattern does not match any of the other samples analysed (Figure 4.4.25). It probably represents a glass type produced using a slightly different silica source, similar to that used to produce ‘Saxon I (blue)’ glass. However, it contains 1.9% MgO* and 1.5% K₂O*, suggesting a considerable plant ash addition. Two *Green Constricted Segmented* beads (ERL104:G242:3321 and ERL104:G242:2273/11) attributed to the ‘Saxon I (blue)’ type, which were not analysed for trace elements, are likely be of related production. These samples are the only anomalies in the ‘Saxon I (blue)’ group, which otherwise consists exclusively of translucent blue glass.

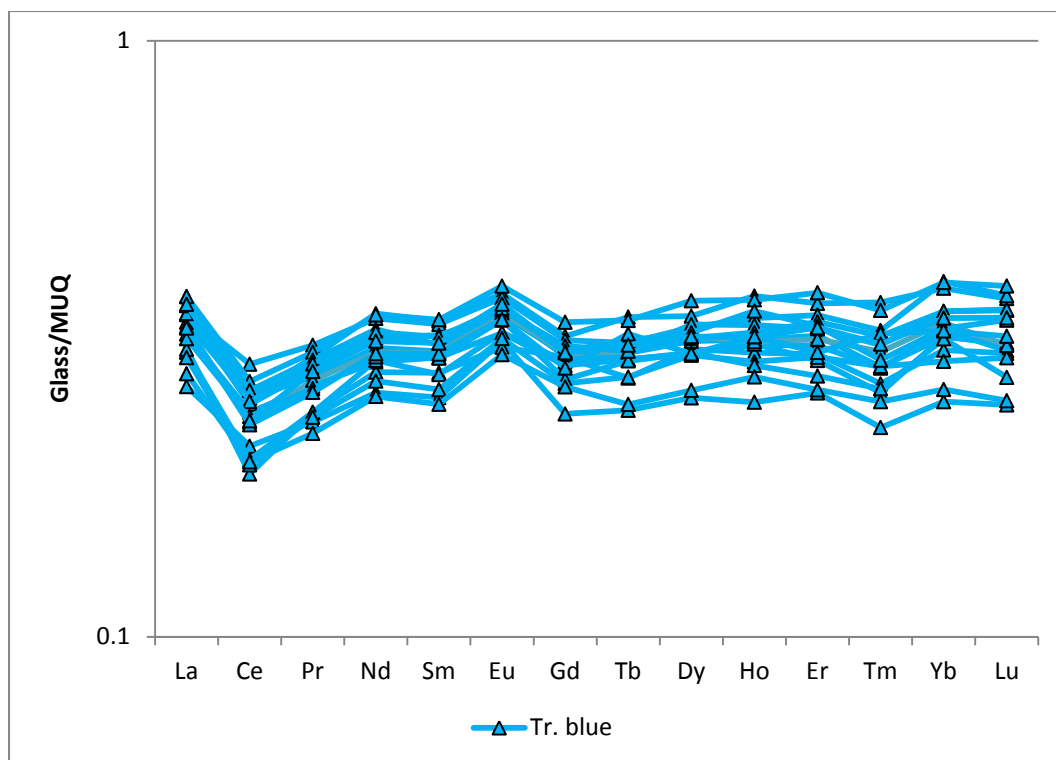


Figure 4.4.21 – Rare earth element concentrations for ‘Saxon I (blue)’ glass from Eriswell, by colour, normalised to the weathered continental crust (see Chapter 2, section 2.3.2.3). Note the logarithmic scale.

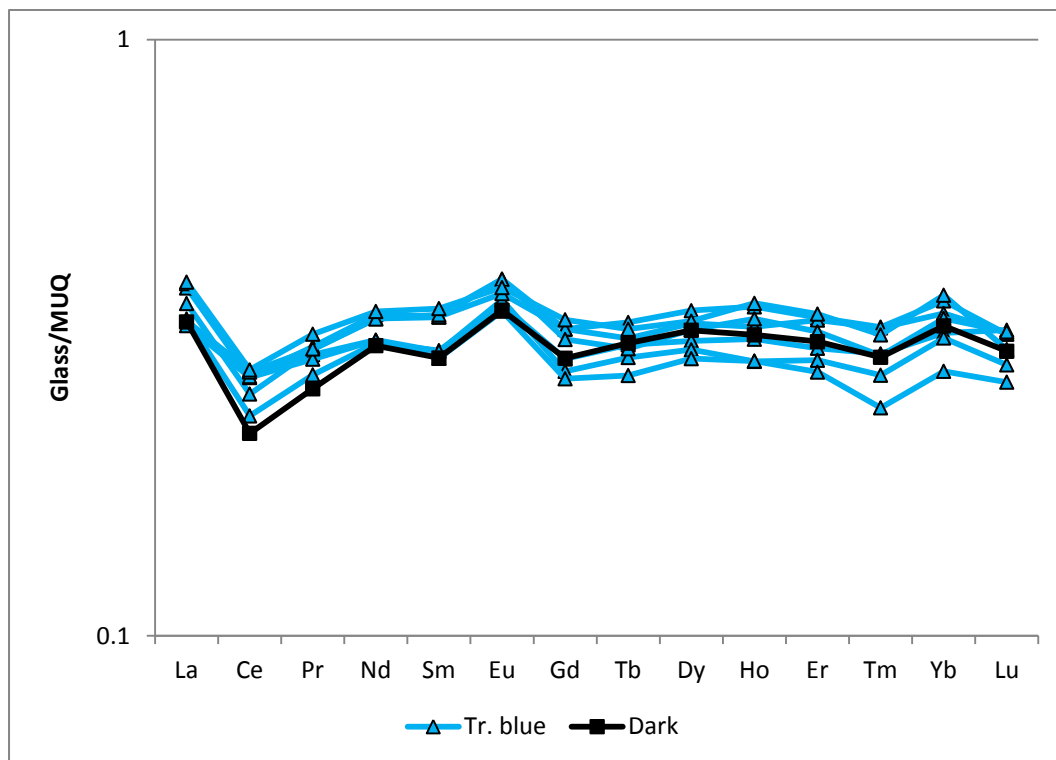


Figure 4.4.22 – Rare earth element concentrations for ‘Saxon I (natron)’ glass from Eriswell, by colour, normalised to the weathered continental crust (see Chapter 2, section 2.3.2.3). Note the logarithmic scale.

The remaining ‘Saxon II (high MgO, low MnO)’ samples have REE patterns very similar to the ‘Saxon II (natron)’ and ‘Saxon II (high MgO, MnO)’ samples (Figure 4.4.25; compare to Figures 4.4.23 and 4.4.24). Furthermore, the Ce anomaly is far more negative than that seen in the ‘Saxon I’ glass types (Figure 4.4.20), supporting the view that the majority of this glass type is not a variation of ‘Saxon I (blue)’ glass; it is instead likely to be more closely related to ‘Saxon II (natron)’ glass. Trace element analysis supports the view that the majority of ‘Saxon II (high MgO, low MnO)’ samples are unlikely to be products of just one workshop; further work is necessary to establish the origins of this glass.

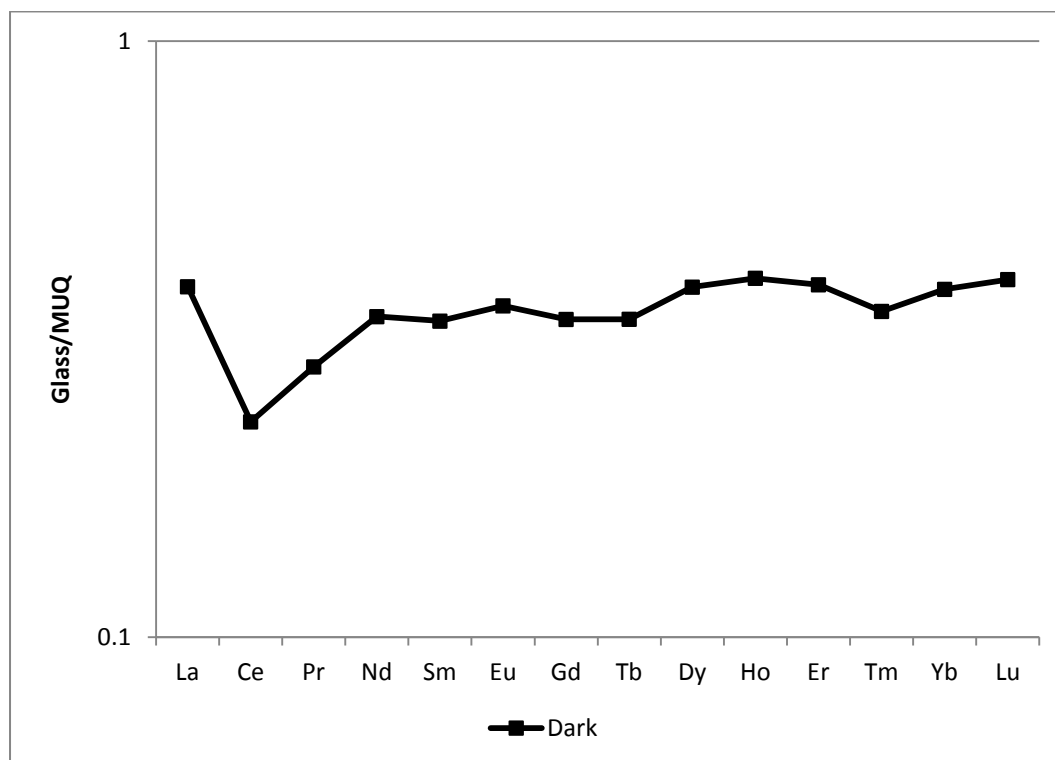


Figure 4.4.23 – Rare earth element concentrations for ‘Saxon II (natron)’ glass from Eriswell, by colour, normalised to the weathered continental crust (see Chapter 2, section 2.3.2.3). Note the logarithmic scale.

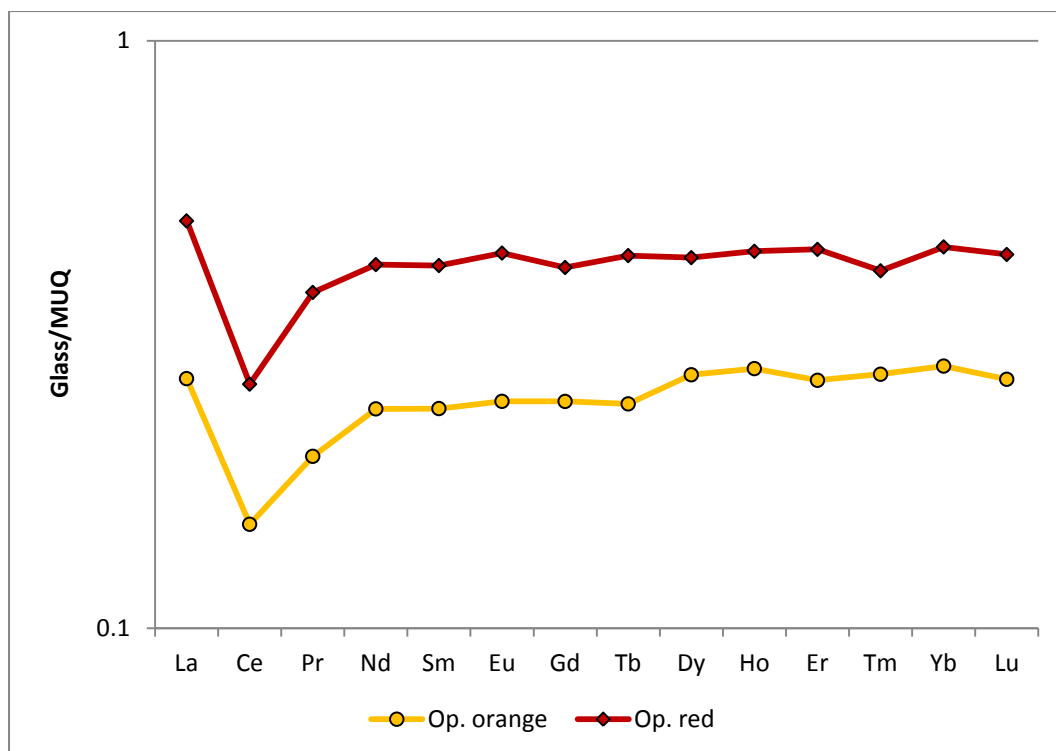


Figure 4.4.24 – Rare earth element concentrations for ‘Saxon II (high MgO, MnO)’ glass from Eriswell, by colour, normalised to the weathered continental crust (see Chapter 2, section 2.3.2.3). Note the logarithmic scale.

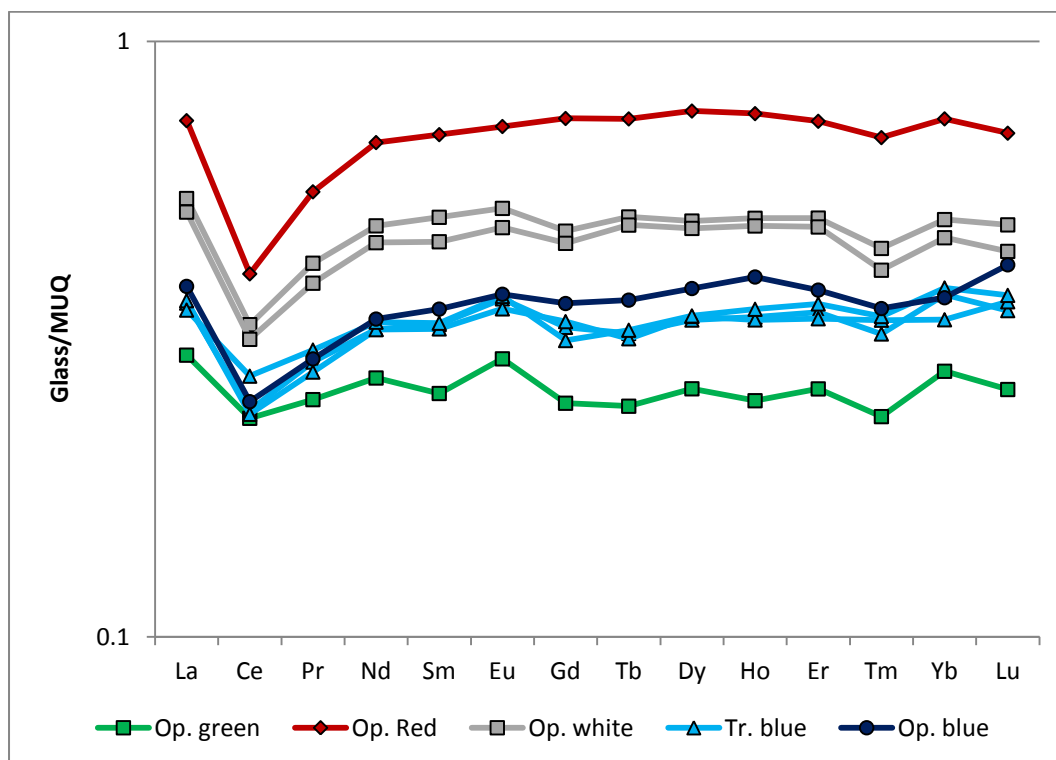


Figure 4.4.25 – Rare earth element concentrations for ‘Saxon II (high MgO, low MnO)’ glass from Eriswell, by colour, normalised to the weathered continental crust (see Chapter 2, section 2.3.2.3). Note the logarithmic scale.

4.4.1.2. Sediment-Related Elements (SRE)

The SRE patterns of the ‘Saxon’ glass types analysed are broadly similar (Figure 4.4.26), confirming that they are likely to be of related production. However, the concentrations of some of the SRE vary slightly between glass types, suggesting that they were not manufactured in exactly the same place from exactly the same raw materials.

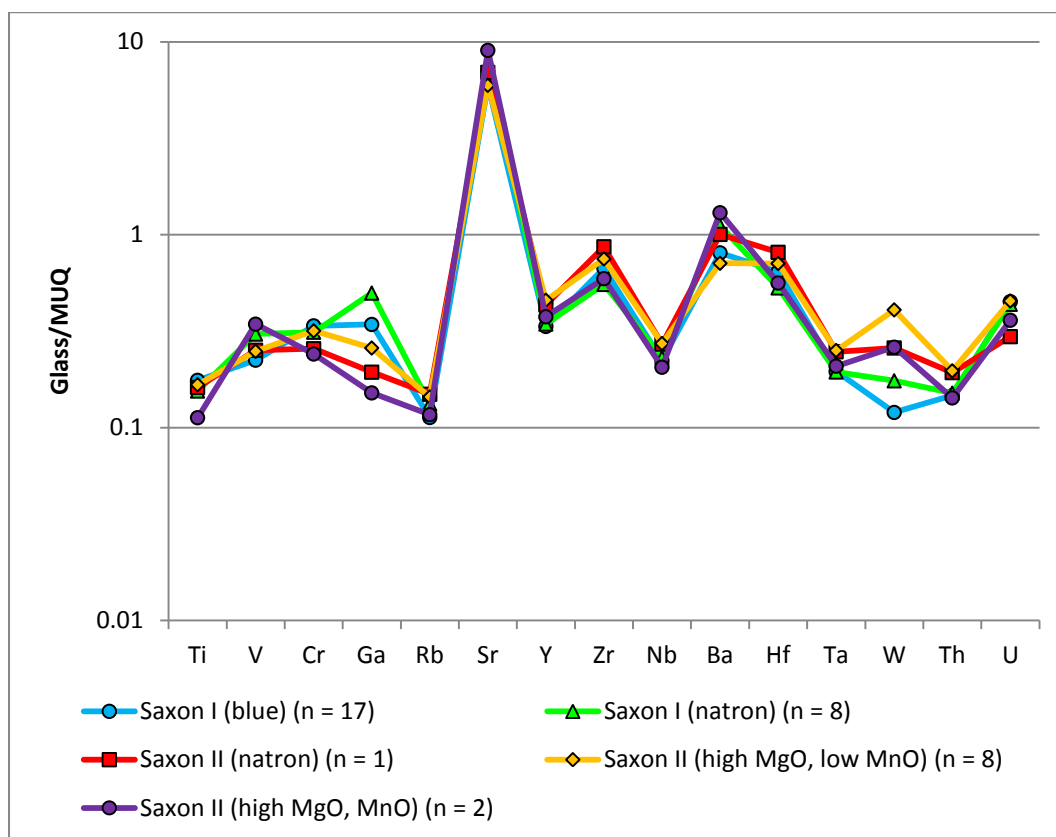


Figure 4.4.26 – Average sediment-related element concentrations for ‘Saxon I’ and ‘Saxon II’ glass from Eriswell, normalised to the weathered continental crust (see Chapter 2, section 2.3.2.3). Note the logarithmic scale.

The SRE patterns of the ‘Saxon I (blue)’ samples are very similar (Figure 4.4.27). Whilst there is some slight variation between samples, particularly in the concentrations of Ti, V, Cr, Ga, Zr, Hf and W, these are not significant enough to constitute different geochemical groups. The SRE patterns of the ‘Saxon I (natron)’ samples are also very homogeneous (Figure 4.4.28), which again confirms that the

batch materials used to produce them are likely to have been very similar. The average concentrations of Ga, Ba and W are slightly elevated in ‘Saxon I (blue)’ glass relative to ‘Saxon I (natron)’ glass (Figure 4.4.26), but this is likely to be caused by the natural variation of the raw materials used (*e.g.* the sand or cobalt minerals employed) rather than any major differences in technology. This is in line with major element and REE data, which suggest a similar origin for both ‘Saxon I (blue)’ and ‘Saxon I (natron)’ glass (see above).

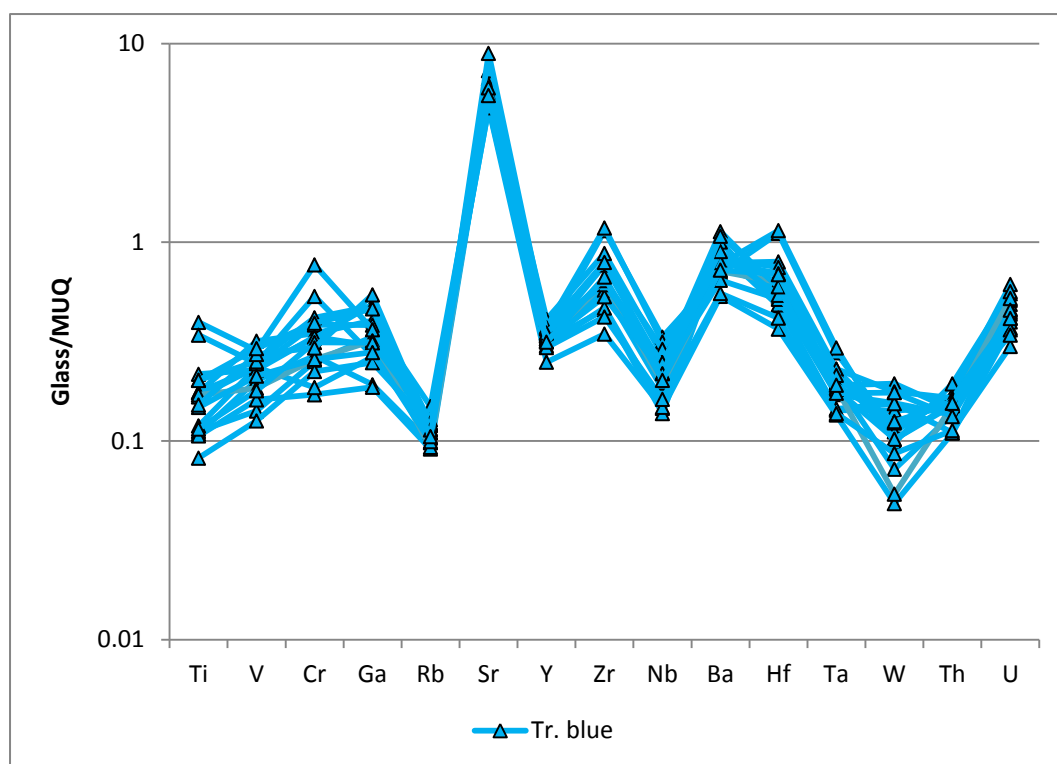


Figure 4.4.27 – Sediment-related element concentrations for ‘Saxon I (blue)’ glass from Eriswell, by colour, normalised to the weathered continental crust (see Chapter 2, section 2.3.2.3). Note the logarithmic scale.

The ‘dark’ ‘Saxon I (natron)’ sample (ERL114:G429:1566, *Miniature Dark*) has a slightly different SRE pattern, in that it contains comparatively depleted levels of V, Cr, Ga and U (Figure 4.4.28); this is more typical of the ‘dark’ ‘Saxon II (natron)’ sample (ERL104:G305:1813, *Dark Globular*; Figure 4.4.29). However, the elevated levels of Zr, Hf, Ta, W and Th, taken together with the slightly depleted levels of V and Cr in the ‘Saxon II (natron)’ sample indicate that this sample was likely to

have been produced from slightly different raw materials. The ‘Saxon II (natron)’ sample is particularly similar to ‘Saxon II (high MgO, MnO)’ glass (Figure 4.4.26).

The SRE patterns of the ‘Saxon II (high MgO, MnO)’ samples are very different to one another, probably as a result of the addition of small quantities of plant ash to the batch (see above). This is likely to have resulted in the elevated levels of Ba and Sr in this glass type relative to the other ‘Saxon I’ and ‘Saxon II’ glasses (Figure 4.4.26). Furthermore, they have elevated levels of V and depleted concentrations of Ti, Cr and Ga on average, suggesting the use of a slightly purer silica source. The opaque orange sample (ERL104:G266:1575, *Orange*) generally contains the lowest levels of SRE (Figure 4.4.30), which is reflected by its REE concentrations (*e.g.* Figure 4.4.24) and low alumina content (1.7% Al₂O₃*).

As demonstrated by the REE patterns, the ‘Saxon II (high MgO, low MnO)’ samples do not form a homogeneous group (Figure 4.4.31), but it is likely that these samples were produced from similar raw materials. The translucent blue samples probably reflect ‘Saxon I (blue)’ glass to which a small quantity of plant ash was added; this may account for the variability seen here. The opaque red sample generally contains elevated levels of most SRE, together with considerably elevated levels of REE (*e.g.* Figure 4.4.25); this may result from the addition of metallurgical slag in the colouring process (see Chapter 5, section 5.2.3). The opaque green sample (ERL104:G273:3330a/09, *Green Constricted Cylindrical*), as also suggested by its REE pattern (Figure 4.4.25), is probably different; it contains slightly lower concentrations of Y, Zr, Nb and Th, but considerably elevated levels of W. This strongly suggests the use of a different glassmaking sand, but this appears to be an isolated example.

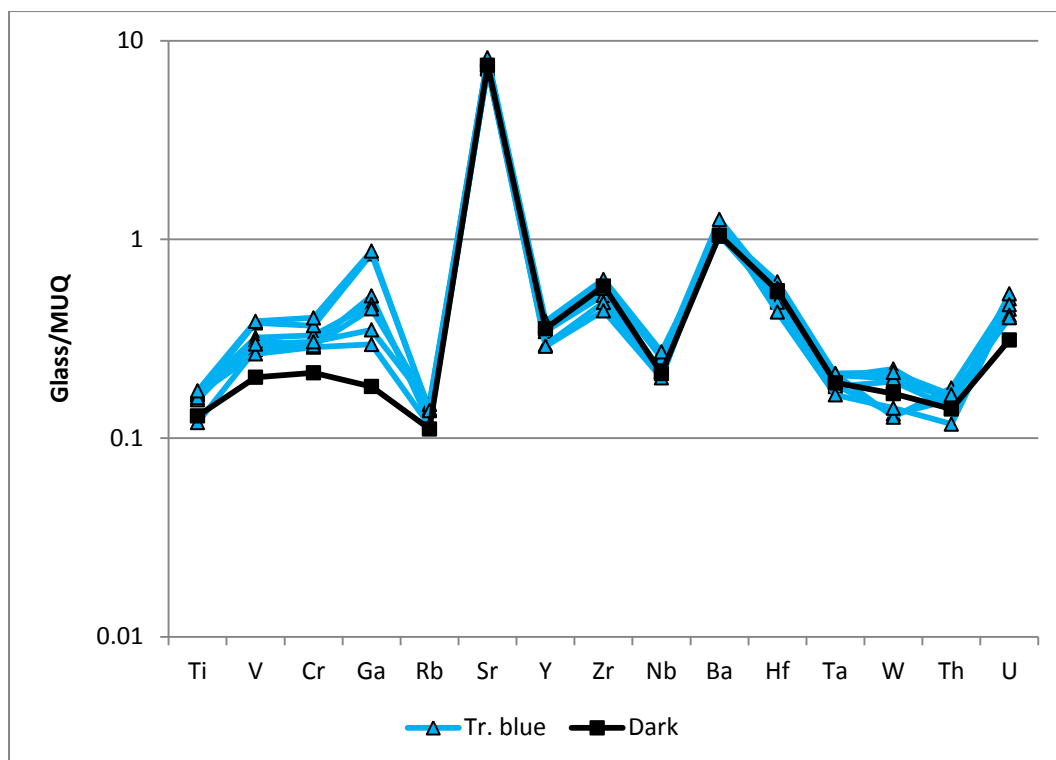


Figure 4.4.28 – Sediment-related element concentrations for ‘Saxon I (natron)’ glass from Eriswell, by colour, normalised to the weathered continental crust (see Chapter 2, section 2.3.2.3). Note the logarithmic scale.

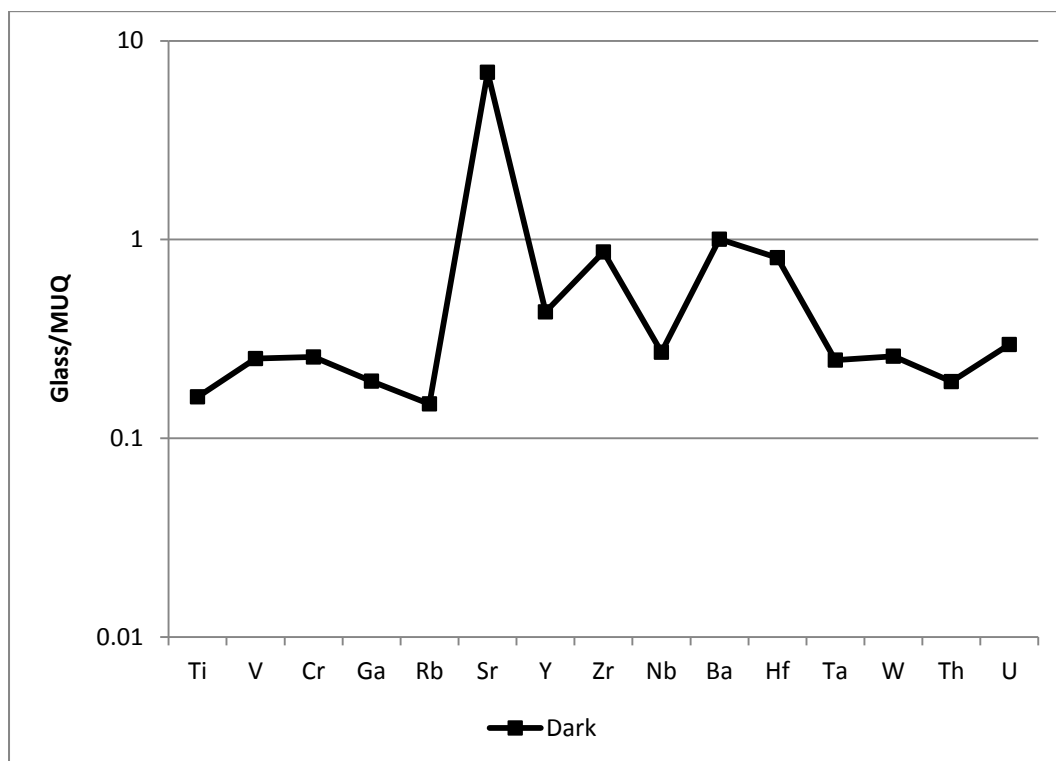


Figure 4.4.29 – Sediment-related element concentrations for ‘Saxon II (natron)’ glass from Eriswell, by colour, normalised to the weathered continental crust (see Chapter 2, section 2.3.2.3). Note the logarithmic scale.

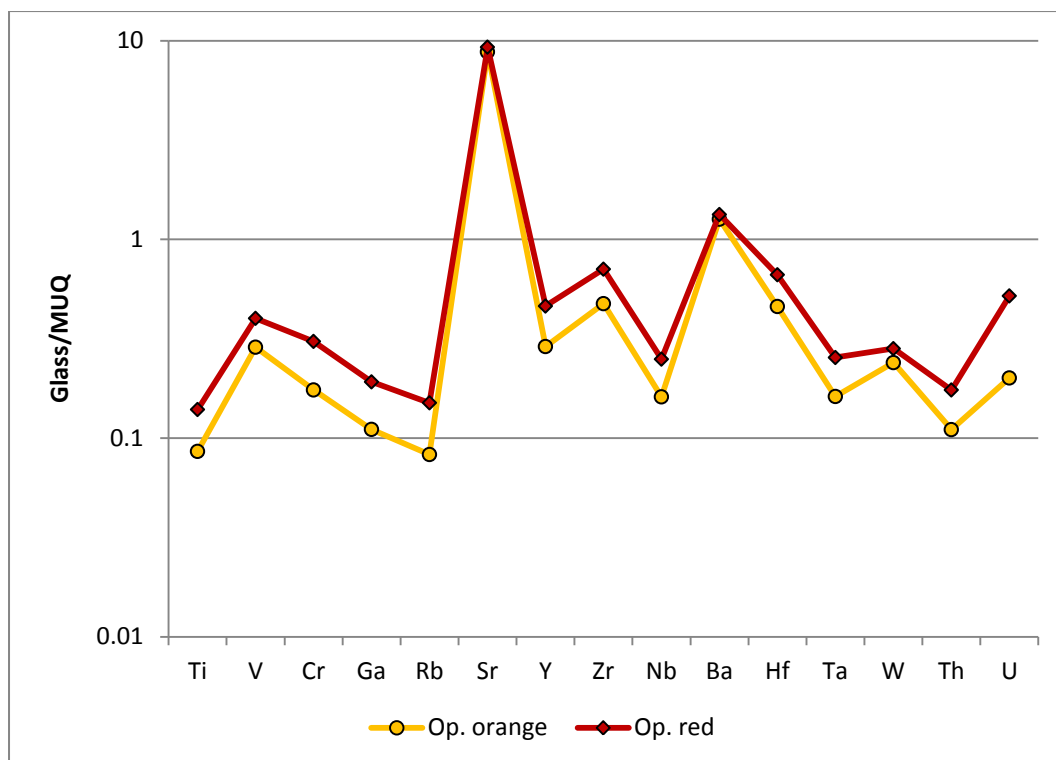


Figure 4.4.30 – Sediment-related element concentrations for ‘Saxon II (high MgO, MnO)’ glass from Eriswell, by colour, normalised to the weathered continental crust (see Chapter 2, section 2.3.2.3). Note the logarithmic scale.

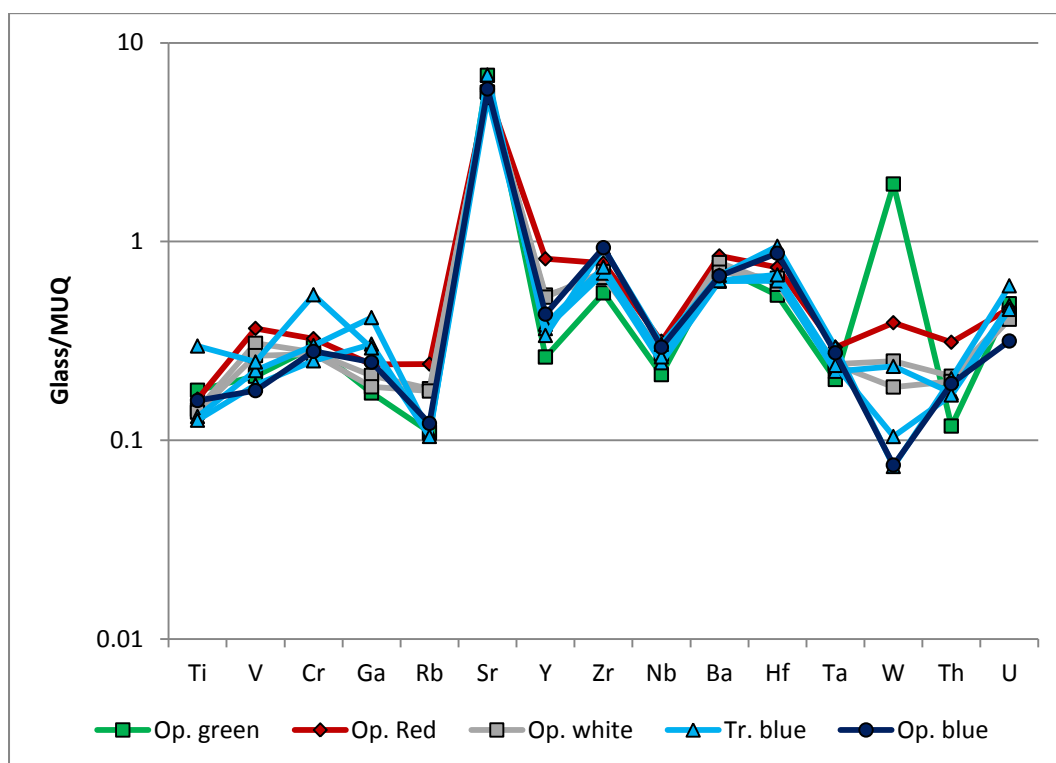


Figure 4.4.31 – Sediment-related element concentrations for ‘Saxon II (high MgO, low MnO)’ glass from Eriswell, by colour, normalised to the weathered continental crust (see Chapter 2, section 2.3.2.3). Note the logarithmic scale.

Sr varies considerably in all of the ‘Saxon’ glass types and may be introduced via a number of different sources. The strong positive correlations between CaO* and Sr in both the ‘Saxon I’ (Figure 4.4.32; $r^2 = 0.87$) and ‘Saxon II’ glasses (Figure 4.4.32; $r^2 = 0.69$) suggests that strontium was introduced in the form of a lime-rich component with a constant ratio of Ca to Sr. In natron glass, high levels of Sr are usually introduced with shell fragments in the glassmaking sand, whereas in plant-ash glass high levels are instead introduced with the ash component (Freestone *et al.* 2003a: 27; 2009: 35; Henderson *et al.* 2005: 670). Plant ash was not used in the production of ‘Saxon I (blue)’, ‘Saxon I (natron)’ and ‘Saxon II (natron)’ glass, but the levels of Sr observed are much higher than the 400-600 ppm Sr typically introduced with marine shell in the glassmaking sand (*e.g.* Degryse *et al.* 2006: 497; Freestone *et al.* 2008: 39; 2009: 35); compare this with up to 1300 ppm Sr here (*e.g.* Figure 4.4.32).

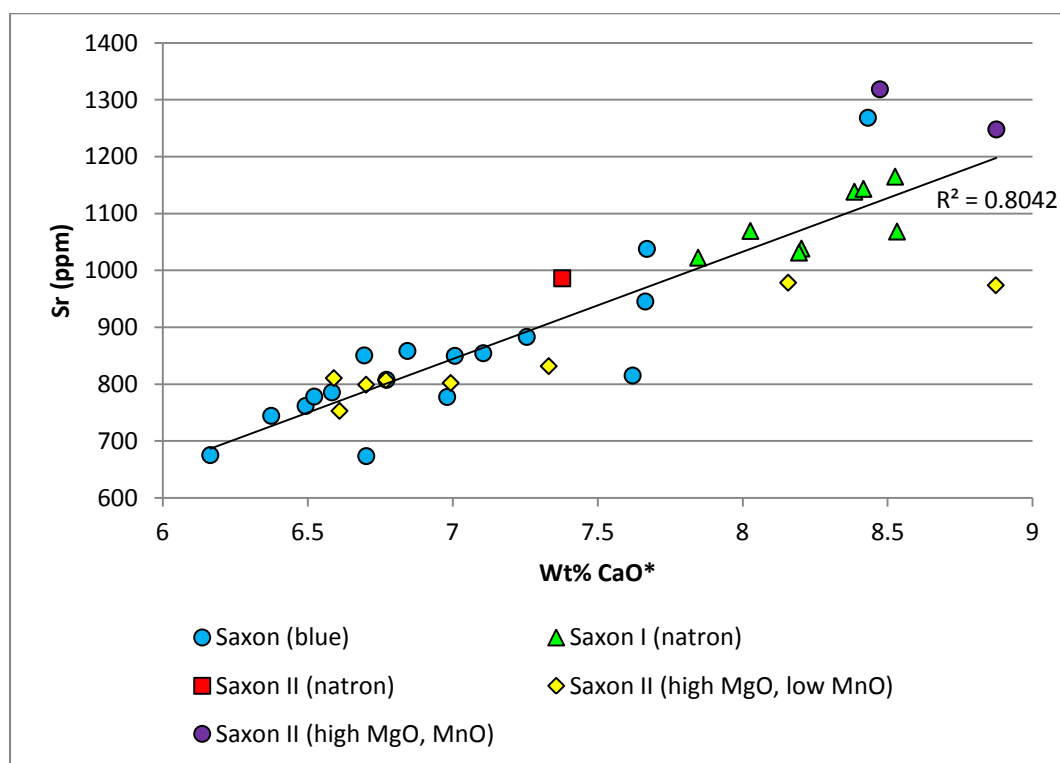


Figure 4.4.32 – A plot of lime versus strontium for the ‘Saxon I’ and ‘Saxon II’ samples from Eriswell.

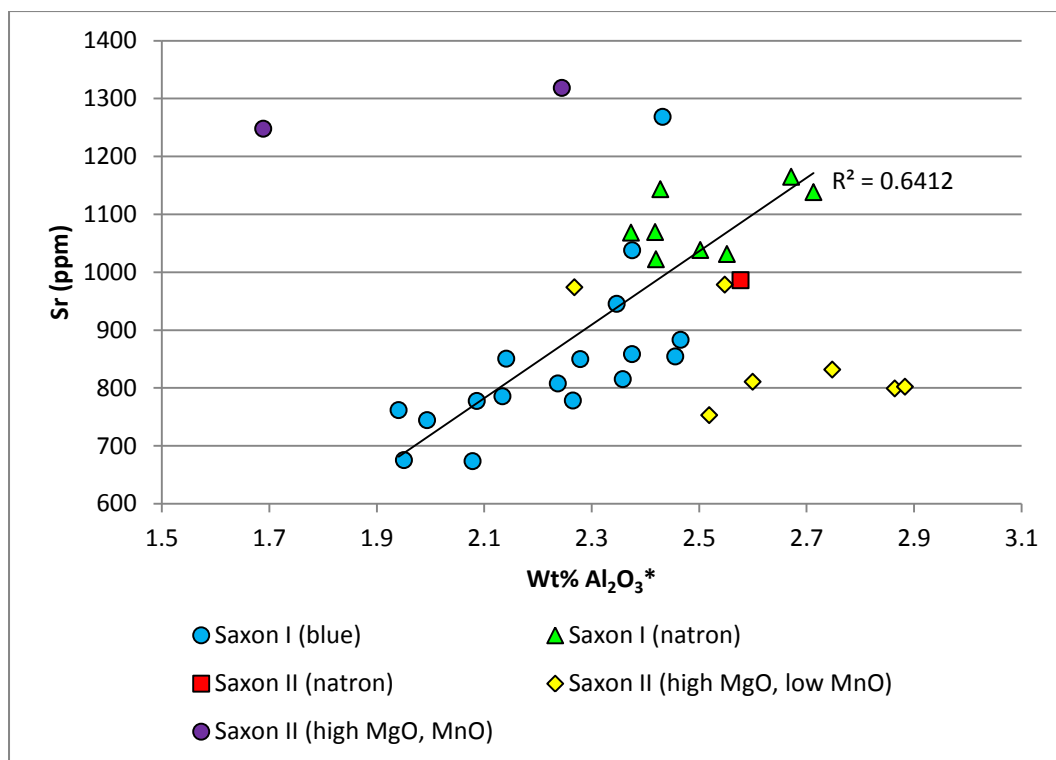


Figure 4.4.33 – A plot of alumina versus strontium for the ‘Saxon I’ and ‘Saxon II’ samples from Eriswell.

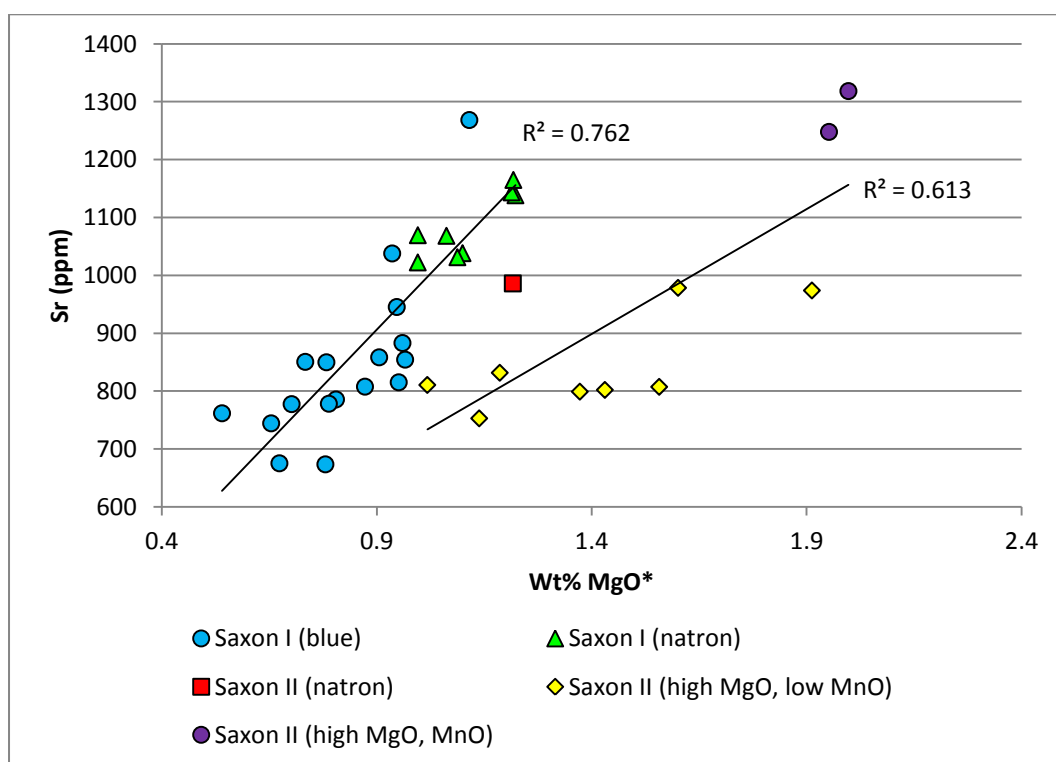


Figure 4.4.34 – A plot of magnesia versus strontium for the ‘Saxon I’ and ‘Saxon II’ samples from Eriswell.

Figure 4.4.33 shows a plot of Al_2O_3^* versus Sr for the ‘Saxon I’ and ‘Saxon II’ glasses. It is clear that alumina and Sr are positively correlated in the ‘Saxon I’ glasses ($r^2 = 0.64$), but negatively correlated in the ‘Saxon II’ glasses ($r^2 = 0.63$). This suggests that Sr is likely to have been primarily introduced in the form of a mineral impurity in the sand in ‘Saxon I’ glass (*e.g.* feldspar) (Degryse *et al.* 2006: 497; Freestone *et al.* 2003a: 27; Henderson *et al.* 2005: 670). This interpretation is consistent with the SEM-EDS data (see above), which indicate that low concentrations of magnesia and potash are also likely to have been introduced with a mineral impurity in the sand. A plot of MgO^* versus Sr reveals two different positive correlations (Figure 4.4.34), which are also reflected in a plot of K_2O^* versus Sr (Figure 4.4.35). This appears to confirm the introduction of Sr from at least two different sources in these two glass types.

It seems likely that a significant amount of Sr was introduced to ‘Saxon I’ glass as a mineral impurity in the glassmaking sand. In contrast, Sr in the majority of ‘Saxon II’ samples is likely to have been primarily introduced with a plant ash addition. A plot of P_2O_5^* (which is usually indicative of a plant ash addition) versus Sr supports this interpretation; here, a strong positive correlation (Figure 4.4.36; $r^2 = 0.73$) is observed between these two components in the ‘Saxon II’ glass types, suggesting that significant amounts of strontium were introduced with the plant ash component (particularly in ‘Saxon II (high MgO, MnO)’ glass). In contrast, no such correlation is observed in the ‘Saxon I (blue)’ glasses (Figure 4.4.36; $r^2 = 0.03$), although a positive correlation is observed in the ‘Saxon I (natron)’ glasses (Figure 4.4.36; $r^2 = 0.62$). Whilst high concentrations of Sr are also likely to have been introduced with marine shell fragments naturally present in the glassmaking sand, it is not possible to ascertain the extent of this as Sr was introduced from so many different sources.

A limited number of trace elements were sought by Freestone *et al.* (2008) in their study of early Anglo-Saxon vessel glass, and a comparison here is worthwhile. Figures 4.4.37-4.4.39 show the trace element patterns for the glass types identified by Freestone *et al.* (2008), compared to those identified at Eriswell. The average trace element patterns for the Eriswell samples are in very close agreement with those of Freestone *et al.* (2008).

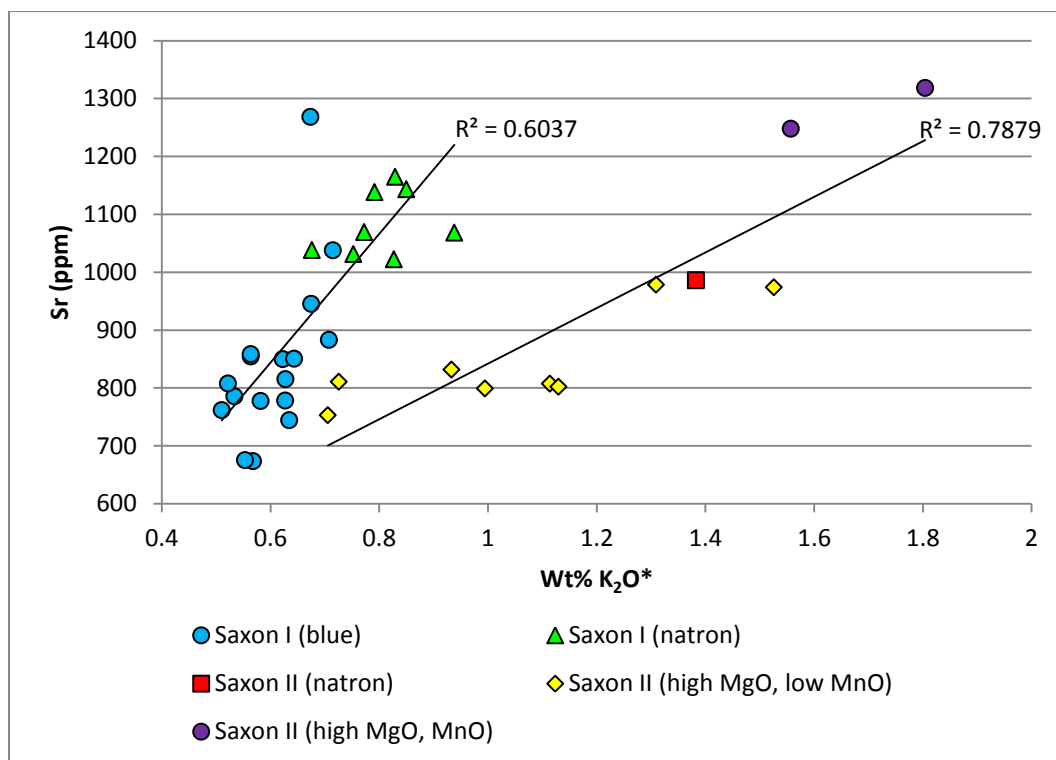


Figure 4.4.35 – A plot of potash versus strontium for the ‘Saxon I’ and ‘Saxon II’ samples from Eriswell.

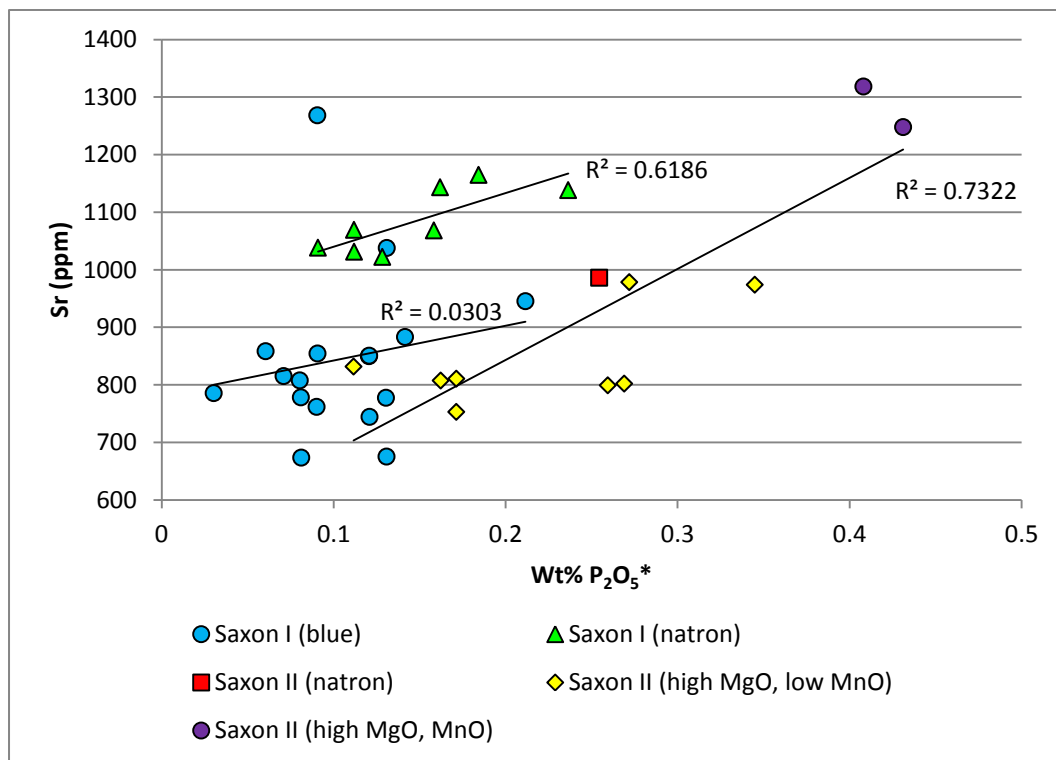


Figure 4.4.36 – A plot of phosphate versus strontium for the ‘Saxon I’ and ‘Saxon II’ samples from Eriswell.

The trace element patterns for Freestone *et al.*'s 'Period I' and 'Period II high MgO, MnO' glass are closely paralleled by those for the 'Saxon I (natron)' and 'Saxon II (high MgO, MnO)' glasses from Eriswell (Figures 4.4.37 and 4.4.38); these two glass types are therefore likely to have been produced using similar raw materials with a similar geochemical origin. Freestone *et al.*'s 'Period II high MgO, low MnO' glass is closely paralleled by the 'Saxon II (high MgO, low MnO)' glass from Eriswell (Figure 4.4.39), again suggesting very similar production zones for these two glass types; note the less marked peak for Ba here. No glass of the 'Saxon I (blue)' or 'Saxon II (natron)' types were analysed for trace elements by Freestone *et al.* (2008), but similarities in the trace element patterns in Figures 4.4.37-4.4.39 suggest a similar production zone to their 'Period I' and 'Period II' glasses, as expected. This demonstrates that the Anglo-Saxon bead and vessel glass industries obtained their glass from common sources. Whilst it is not possible to confirm that beads were produced in the same workshops as glass vessels from these data, the similarities observed make this possibility far more likely.

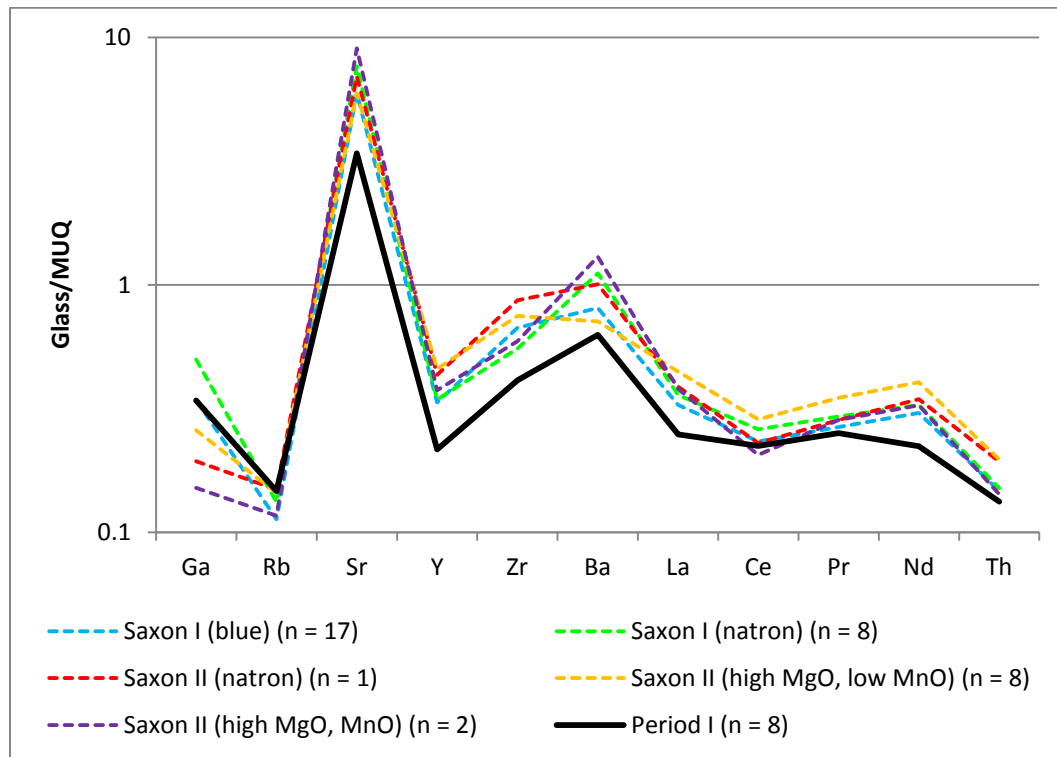


Figure 4.4.37 – Average concentrations of selected trace elements for 'Saxon I' and 'Saxon II' glass from Eriswell (dashed lines), compared to those for early Anglo-Saxon 'Period I' vessel glass (after Freestone *et al.* 2008).

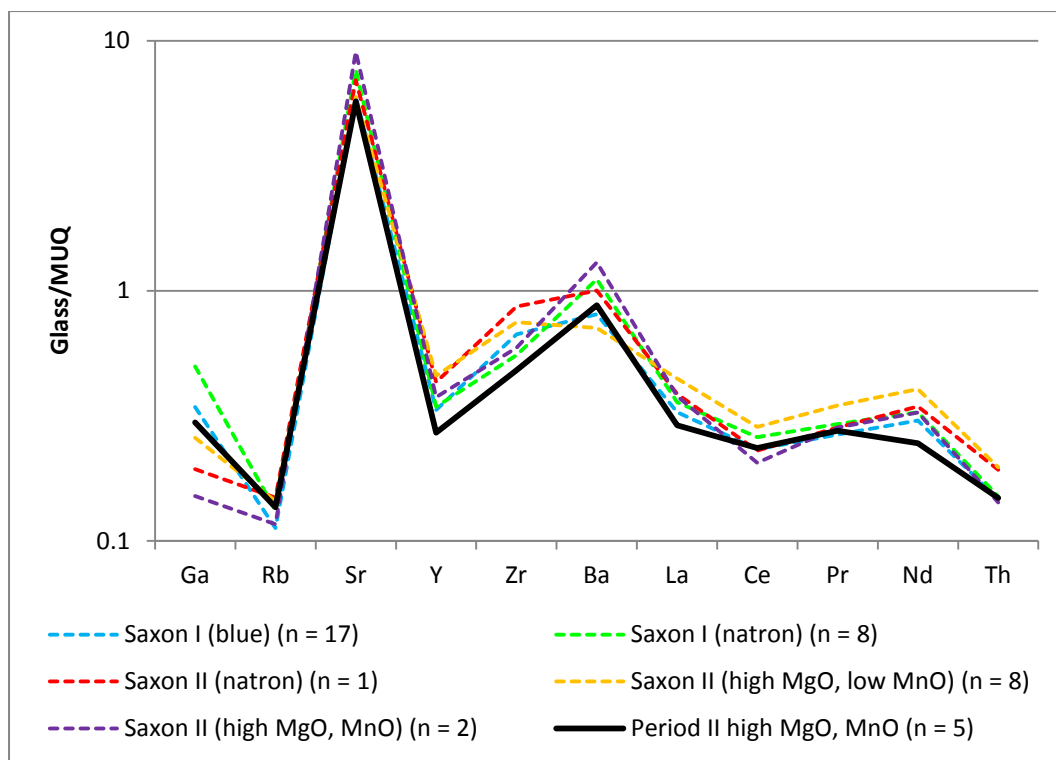


Figure 4.4.38 – Average concentrations of selected trace elements for ‘Saxon I’ and ‘Saxon II’ glass from Eriswell (dashed lines), compared to those for early Anglo-Saxon ‘Period II high MgO, MnO’ vessel glass (after Freestone *et al.* 2008).

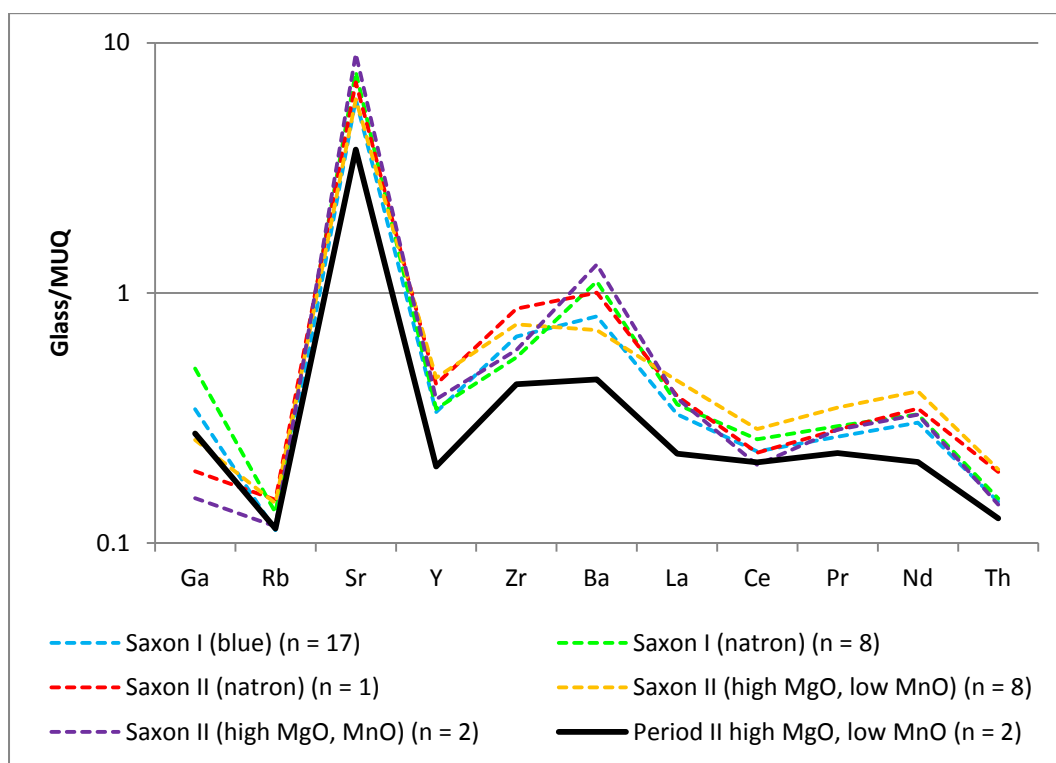


Figure 4.4.39 – Average concentrations of selected trace elements for ‘Saxon I’ and ‘Saxon II’ glass from Eriswell (dashed lines), compared to those for early Anglo-Saxon ‘Period II high MgO, low MnO’ vessel glass (after Freestone *et al.* 2008).

4.5. 'HIMT' Glass

'HIMT' glass is one of the most poorly represented glass types at Eriswell, consisting of 20 samples taken from a total of 16 beads. These are predominantly opaque red, opaque yellow and naturally coloured (mostly green tints). One opaque white bubble-opacified sample is also present (see this chapter, section 4.9). 'HIMT' glass was first defined by Freestone (1994) on account of its **H**igh levels of **I**ron, **M**anganese and **T**itanium, all of which are positively correlated and inter-correlated with one another (Foster and Jackson 2009: 189; Freestone 2003: 112; Freestone *et al.* 2002a: 168; 2002b: 265; 2005b: 153-154). It was also identified as a distinct glass type by Mirti *et al.* (1993: 236) and corresponds to Foy *et al.*'s 'Group 1' (Foy *et al.* 2000: 54; Foy *et al.* 2003: 45). 'HIMT' glass from Eriswell is characterised by both Fe_2O_3^* and MnO^* in excess of approximately 1.0%, and TiO_2^* in excess of 0.2%. It is also distinguished by elevated levels of soda (typically 17-19% Na_2O^* ; *e.g.* Figure 4.2.1) and magnesia (in excess of 0.7% MgO^* ; *e.g.* Figure 4.2.2), together with lower lime (less than 6.5% CaO^*) and silica (typically 64-68% SiO_2^*) relative to 'Roman' glass (*e.g.* Figure 4.2.5).

It is difficult to distinguish 'HIMT' glass from 'Saxon' glass as both glass types are generally characterised by very similar concentrations of major and minor elements (*e.g.* Table 4.2.1). Elevated levels of titanium are sometimes one of the only distinguishing components. However, a significant proportion of the samples from Eriswell containing in excess of 0.2% TiO_2^* are opaque yellow, but their compositions is otherwise not typical of 'HIMT' glass, suggesting that there is likely to have been some contamination by titanium from the crucible fabric (*e.g.* see this chapter, section 4.1). Furthermore, 'HIMT' glass may contain as little as 0.1% TiO_2^* (Foster and Jackson 2009: 189), which renders compositional distinctions based solely upon titanium invalid.

Uncoloured 'HIMT' glass typically has yellow-green to olive tint, in contrast to the more common blue-green tint of much Roman glass (Freestone *et al.* 2005b: 153). These different tints are generally attributed to an iron impurity from the glassmaking sand (see Chapter 5, section 5.1.1); iron is particularly elevated in

‘HIMT’ glass, suggesting the use of a relatively impure sand (Foster and Jackson 2009: 189). Manganese is likely to have been intentionally added to this glass type as a decolourant (Freestone *et al.* 2005b: 154); the strong correlations between manganese and iron, alumina, titanium and magnesia characteristic of this glass are likely to have resulted from the controlled addition of manganese, which was probably estimated based upon the colour of test melts (*e.g.* Wedepohl *et al.* 2003: 57; see this chapter, section 4.4 for a more detailed discussion). It has been tentatively suggested that ‘HIMT’ glass was produced by mixing two different compositional types of *primary* (*i.e.* not recycled) chunk glass produced from neighbouring, but geochemically distinctive sand deposits (Freestone 2005: OO8.1.10; Freestone *et al.* 2005b: 154-155); one of these is likely to have been produced from an inland sand source and the other from a coastal sand source. It is therefore possible that manganese was introduced in the form of a pre-made manganese-decolourised glass. However, the production technology of ‘HIMT’ glass remains far from clear.

The natural colour of ‘HIMT’ glass indicates that it is highly reduced, and demonstrates that the addition of manganese was not successful in removing the tint produced by the iron impurity. It has therefore been suggested that manganese was not added to oxidise the iron, but to oxidise a sulphur impurity; this would otherwise have combined with iron to precipitate iron sulphide under highly reducing conditions, turning the glass black (Freestone *et al.* 2005b: 156). Most of the ‘HIMT’ glass at Eriswell has been highly coloured in some way, so the colour produced by the iron impurity would not have posed much of a problem. However, ‘HIMT’ glass appears to have been deliberately selected for its colour in the production of the translucent green decoration on a handful of *Traffic Light* beads (*e.g.* beads ERL104:G242:2145 and ERL104:G242:2158).

‘HIMT’ glass was first produced in the Near East at some point during the 4th century AD, possibly as early as *c.* AD 330 (Foster and Jackson 2009: 192). It was widely traded throughout the Eastern Mediterranean and further afield (Foster and Jackson 2009: 194-195; Freestone 2003: 112; Freestone *et al.* 2005b: 153; Freestone and Hughes 2006: 148; Foy *et al.* 2000: 54); it has been identified throughout Britain (*e.g.* Freestone *et al.* 2005b; Foster and Jackson 2009) and Europe (*e.g.* Arletti *et al.*

2005; Foy *et al.* 2003; Freestone *et al.* 2002a; Mirti *et al.* 1993; Verità 1995), at Cyprus (Freestone *et al.* 2002b), Carthage (Freestone 1994; Foy *et al.* 2003) and Egypt (Foy *et al.* 2003; Freestone *et al.* 2002a). Furthermore, it appears to have been the most common ‘naturally’ coloured glass type in use in Britain during the 4th century AD (Foster and Jackson 2009: 194). Figure 4.5.1 shows a plot of lime versus alumina for ‘HIMT’ glass from Eriswell, compared to the five broad categories of glass in use between the 4th and 9th centuries AD in the Near East identified by Freestone and co-workers (*e.g.* Freestone *et al.* 2000: 82; Freestone *et al.* 2002b: 265-266; Freestone 2006: 208; see Chapter 1, section 1.4.1). This demonstrates that the ‘HIMT’ samples from Eriswell are in close agreement with ‘HIMT’ glass from Eastern Mediterranean contexts.

Foster and Jackson (2009: 189) have recently identified two possible sub-groups of Late Romano-British ‘HIMT’ glass, dubbed ‘HIMT 1’ and ‘HIMT 2’ glass respectively. Whilst both groups are broadly similar, ‘HIMT 1’ glass is characterised primarily by approximately twice the concentration of iron, manganese and titanium relative to ‘HIMT 2’ glass (corresponding to approximately 1.4%, 1.7% and 0.3% *cf.* 0.7% 0.9% and 0.1%) (Foster and Jackson 2009: 189). Figures 4.5.2-4.5.4 show plots of magnesia versus manganese, alumina versus iron and iron versus manganese respectively for the low-lead ‘HIMT’ samples from Eriswell, compared to ‘HIMT 1’ and ‘HIMT 2’ glass from Late Roman Britain (Foster and Jackson 2009). The majority of the ‘HIMT’ samples from Eriswell fall clearly into the ‘HIMT 1’ group. Whilst two samples may be attributed to the ‘HIMT 2’ group, considering the spread of data they could conceivably be of the ‘HIMT 1’ type.

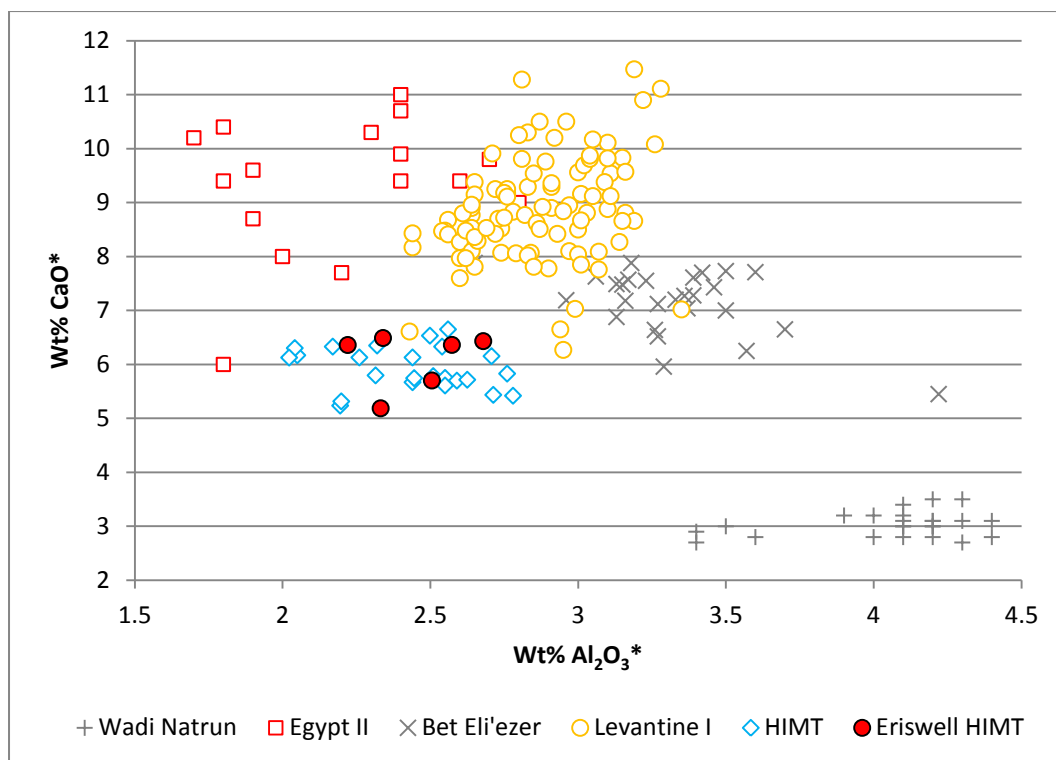


Figure 4.5.1 – A plot of alumina versus lime for ‘HIMT’ glass from Eriswell, compared to the five major groups of natron glass produced in the Eastern Mediterranean between the 4th and 9th centuries AD (see text for details). Samples which are likely to have been affected by alumina contamination have been omitted (see this chapter, section 4.1 for details).

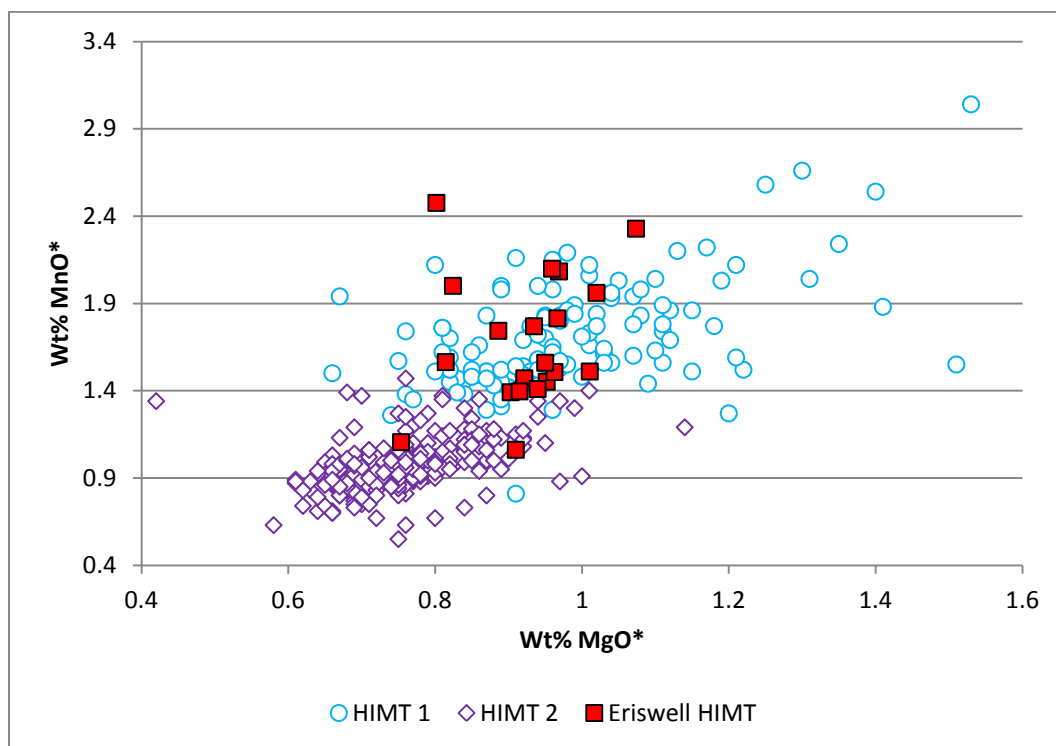


Figure 4.5.2 – A plot of magnesia versus manganese oxide for ‘HIMT’ glass from Eriswell, compared to published data for Late Roman ‘HIMT 1’ and ‘HIMT 2’ glass from Britain (after Foster and Jackson 2009).

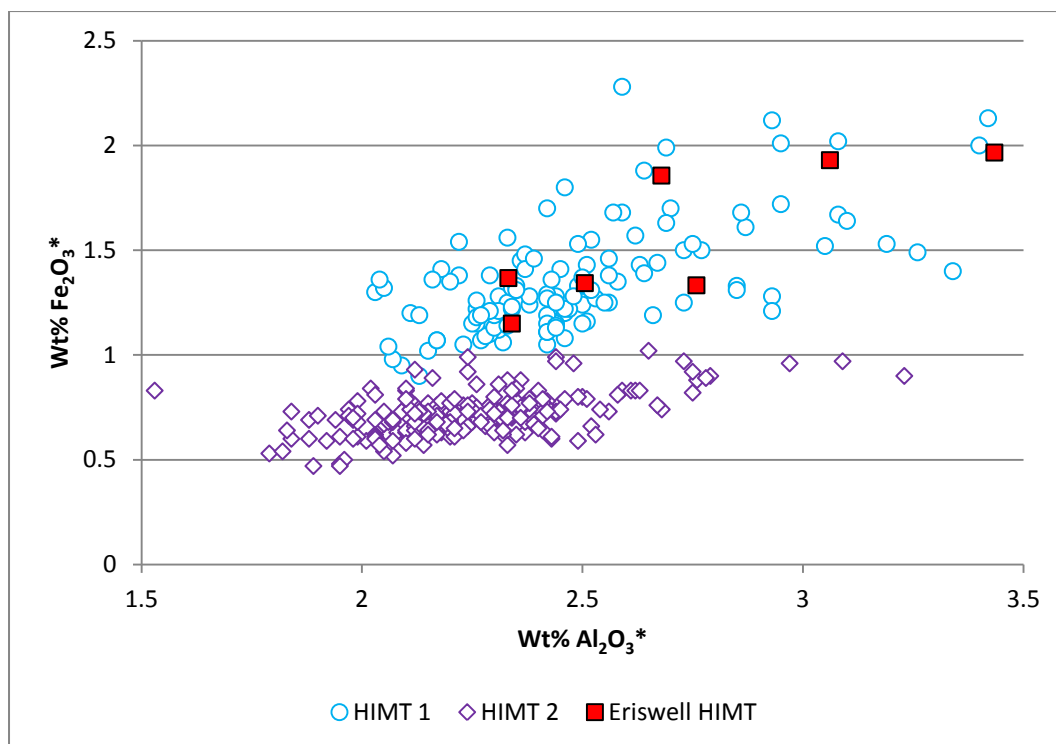


Figure 4.5.3 – A plot of alumina versus iron oxide for ‘HIMT’ glass from Eriswell, compared to published data for Late Roman ‘HIMT 1’ and ‘HIMT 2’ glass from Britain (after Foster and Jackson 2009). Samples which are likely to have been affected by iron and alumina contamination have been omitted (see this chapter, section 4.1 for details).

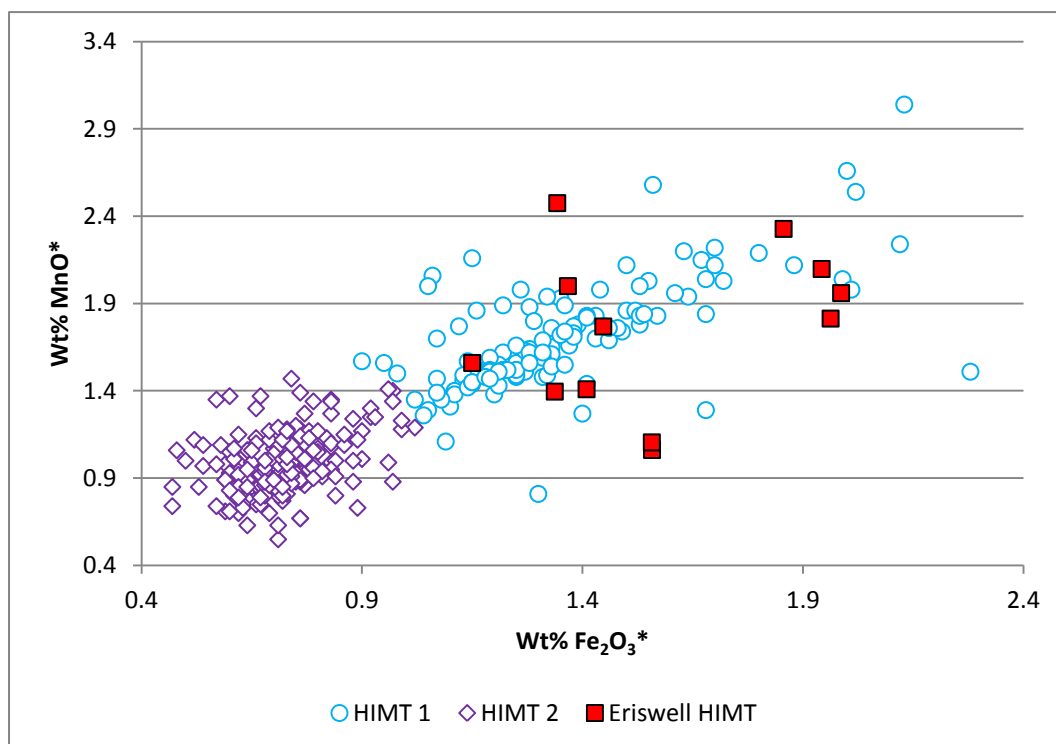


Figure 4.5.4 – A plot of iron oxide versus manganese oxide for ‘HIMT’ glass from Eriswell, compared to published data for Late Roman ‘HIMT 1’ and ‘HIMT 2’ glass from Britain (after Foster and Jackson 2009). Samples which are likely to have been affected by iron contamination have been omitted (see this chapter, section 4.1 for details).

The exact origins of 'HIMT' glass are unclear, but it has been suggested that production in Egypt is likely on account of the elevated titanium levels, which also characterise Egyptian glass (Foy *et al.* 2003: 47). Furthermore, 'HIMT' glass is more commonly found in Egypt than Israel, so is unlikely to have been produced in Palestinian workshops; production is more likely to have taken place in the southern regions of the Levant where natron was probably more readily available (Freestone *et al.* 2002a: 172-173; 2005b: 156). Trace element and isotopic data support this view, and suggest production probably took place somewhere between the Nile Delta and southern Israel (*e.g.* Freestone 2005: OO8.1.10; Freestone *et al.* 2005b: 155; 2009: 44; Leslie *et al.* 2006: 261). Whilst this does not prove an Egyptian origin, it makes it more likely.

Foster and Jackson (2009: 189-190) suggest that 'HIMT' glass continued to be produced until the late 1st Millennium AD. This interpretation may be borne out by the attribution of both Foy *et al.*'s 'Group 1' (5th century) and 'Group 2' (mid-6th to late 8th centuries) (Foy *et al.* 2000; 2003) to the 'HIMT' glass type. However, in the present study Foy *et al.*'s 'Group 2' is recognised as a distinct type (possibly even a variant) to 'HIMT' glass, instead corresponding to 'Saxon I' glass (see this chapter, section 4.4); nevertheless, it is likely that both 'HIMT' and 'Saxon I' glass share a similar origin, possibly having been produced in neighbouring workshops.

It is not possible to gauge the extent to which 'HIMT' glass may have been recycled from its composition, due to the highly coloured nature of this glass at Eriswell. However, typological evidence (see this chapter, section 4.10) indicates that 'HIMT' glass was typically used to produce bead types more typically produced from recycled 'Roman' glass. It is also commonly found in association with recycled 'Roman' glass on several polychrome beads. On balance, it is therefore more likely to represent the use of recycled material from the preceding Roman period than a supply of raw glass from the Near East, although Roman blue-green glass appears to have been preferred for recycling (see this chapter, section 4.3). This interpretation is supported by the poor representation of 'HIMT' glass at Eriswell relative to other raw glass types (*e.g.* 'Saxon I' glass). It is therefore unlikely that 'HIMT' glass continued to be produced into the early Anglo-Saxon period following the withdrawal of Rome from Britain. Production is likely to have ceased in the late 4th

or early 5th centuries; it appears to have been replaced by ‘Saxon I’ glass, which has a number of very close similarities to ‘HIMT’ glass (*e.g.* Foster and Jackson 2009: 193; Silvestri *et al.* 2005: 810), but is compositionally distinct (see this chapter, section 4.4). The similarities between ‘HIMT’ and ‘Saxon’ glass (*e.g.* Table 4.2.1 and Figure 4.2.14) suggest a similar origin for both glass types.

A re-evaluation of the available evidence suggests that production of ‘HIMT’ glass is unlikely to have continued into the late 5th or 6th centuries; there is no evidence for a trade in raw ‘HIMT’ glass after the withdrawal of the Roman Empire from Britain. No examples of ‘HIMT’ glass were identified by Freestone *et al.* (2008) in Anglo-Saxon vessel glass, suggesting that it is unlikely to have been available as a raw glass type. However, analysis of ‘HIMT’ glass from well-dated contexts on the Continent and particularly from the Near East is necessary in order to confirm and/or establish the longevity of this glass type.

4.5.1. Trace Element Analyses

Trace elements for three of the ‘HIMT’ samples from Eriswell were obtained by LA-ICP-MS, all of which were obtained from different colours on the same polychrome bead (ERL104:G268:3260, *Candy Variant*).

4.5.1.1. Rare Earth Elements (REE)

Figure 4.5.5 shows the REE patterns for the three ‘HIMT’ samples analysed by LA-ICP-MS. The opaque yellow and translucent green samples in particular have very similar concentrations of REE, indicating a common origin for this glass, as might be expected for samples taken from the same bead. However, whilst the REE pattern for the opaque red sample is similar in shape to the other colours, the REE in this glass are notably depleted. This almost certainly reflects the addition of a significant quantity of metallurgical slag to this glass as part of the colouring process (see Chapter 5, section 5.2.3). All of the samples analysed have significant negative Ce

and positive Eu anomalies, relating to the variable oxidation states of these elements which affects the way in which they are deposited in rock-forming processes.

The elevated levels of REE in ‘HIMT’ glass relative to the other glass types (Figure 4.2.15) suggest that ‘HIMT’ glass was produced from a relatively impure glassmaking sand. However, the broad similarities in the REE patterns between ‘Saxon I’ and ‘HIMT’ glass (Figure 4.2.15) suggests a similar origin for both glass types; this is also supported by the results of SEM-EDS (see this chapter, section 4.4 and above).

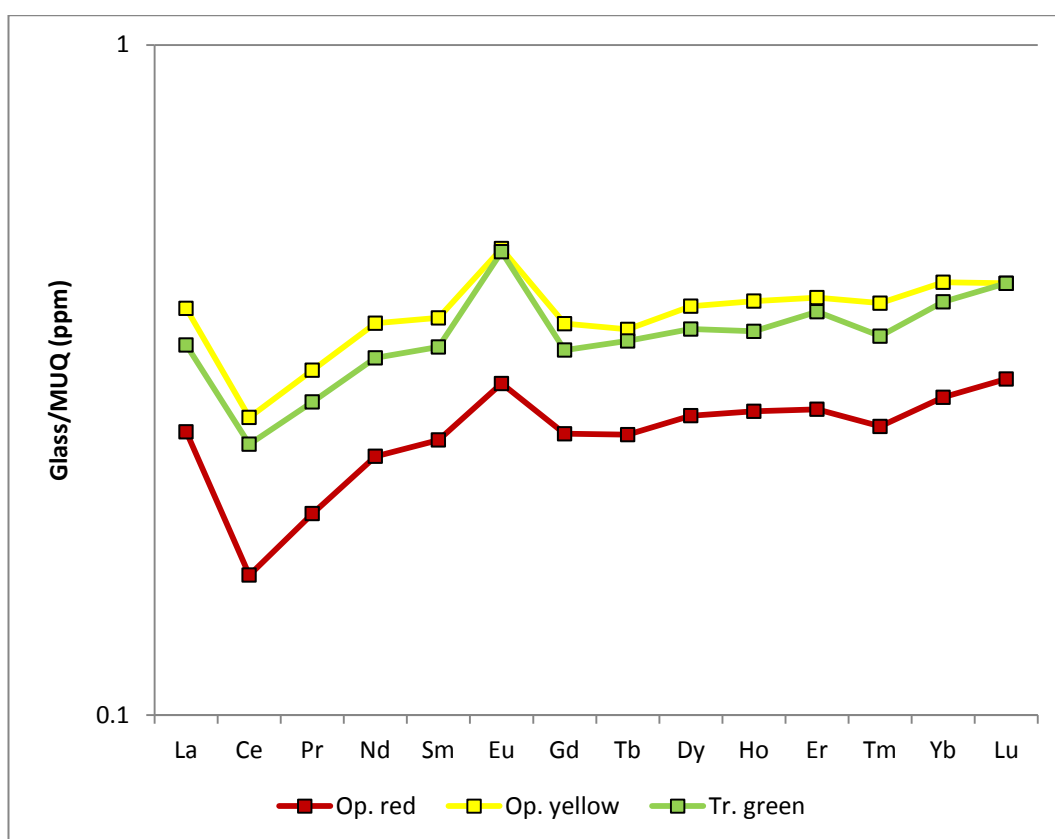


Figure 4.5.5 – Rare earth element concentrations for ‘HIMT’ glass from Eriswell, by colour, normalised to the weathered continental crust (see Chapter 2, section 2.3.2.3). All samples are from bead ERL104:G268:3260 (*Candy Variant*). Note the logarithmic scale.

4.5.1.2. Sediment-Related Elements (SRE)

The SRE patterns for the three ‘HIMT’ glasses analysed are shown in Figure 4.5.6. As expected, all are broadly similar, indicating that they were produced using similar

raw materials and a similar glassmaking recipe; probably from the same batch of glass. Slight variations are likely to have primarily resulted from the different additives employed in the production of the different colours. The opaque red sample generally contains slightly lower concentrations of SRE which, like the REE (see section 4.5.1.1. above), is likely to have resulted from the addition of a considerable amount of metallurgical slag as an internal reducing agent during the colouring process (see Chapter 5, section 5.2.3).

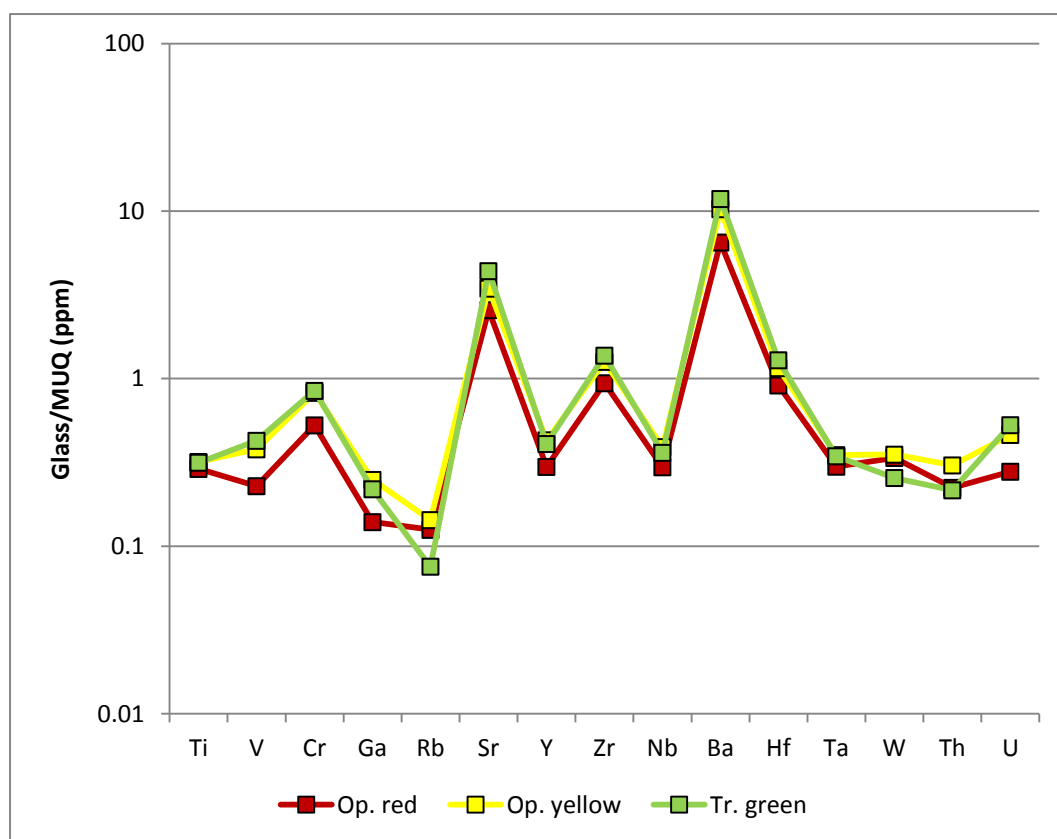


Figure 4.5.6 – Sediment-related element concentrations for ‘HIMT’ glass from Eriswell, by colour, normalised to the weathered continental crust (see Chapter 2, section 2.3.2.3). All samples are from bead ERL104:G268:3260 (*Candy Variant*). Note the logarithmic scale.

The ‘HIMT’ glass from Eriswell contains considerably elevated levels of most SRE relative to the other glass types (Figure 4.2.16); particularly Ti, Cr, Zr, Ba and Hf (see also Figure 4.2.17 and 4.2.18). Elevated levels of Ti, Ba, Cr, and Zr and Hf are typical of ‘HIMT’ glass (*e.g.* Foster and Jackson 2009: 192; Foy *et al.* 2000: 54; 2003: 83; Freestone *et al.* 2002b: 264) and relate to the use of an impure

glassmaking sand rich in heavy minerals and clays; barium is particularly elevated, corresponding to nearly 4000 ppm Ba. The ‘HIMT’ samples from Eriswell are in relatively close agreement with ‘HIMT 1’ glass from Late Roman Britain (Foster and Jackson 2009), as demonstrated by a plot of Sr versus CaO* (Figure 4.5.7). Whilst the ‘HIMT’ samples from Eriswell do not cluster tightly as a group here, this is likely to reflect the modification of these glasses with added colourants and opacifiers.

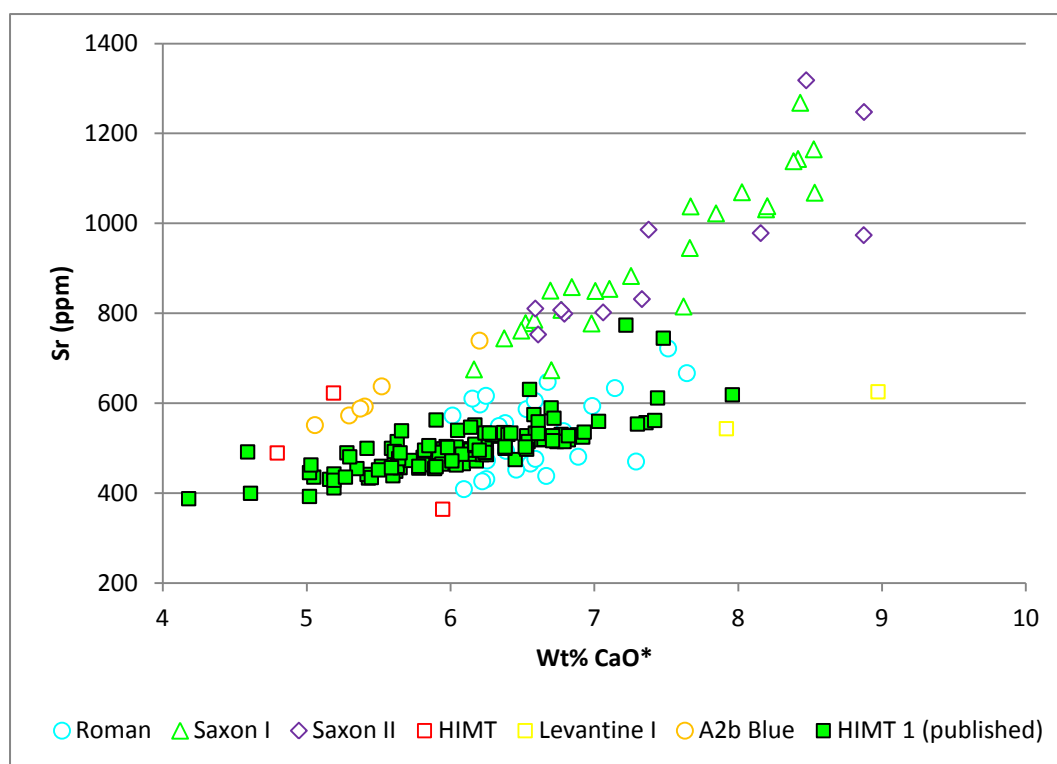


Figure 4.5.7 – A plot of lime versus strontium for 123 published ‘HIMT 1’ glass samples (after Foster and Jackson 2009), compared to the different base glass types identified at Eriswell.

4.6. 'Levantine I' Glass

'Levantine I' glass constitutes a very small proportion of the Eriswell assemblage, consisting of 16 samples from a total of 13 beads. These are mostly opaque orange, opaque red, tin oxide opacified white and translucent turquoise (see this chapter, section 4.9). 'Levantine I' glass is particularly distinguishable from the other glass types at Eriswell on account of its lower concentrations of soda (typically 13-16% Na₂O*; *e.g.* Figure 4.2.1), and particularly elevated levels of both silica (typically 68-73% SiO₂*; *e.g.* Figure 4.2.5) and alumina (typically well in excess of 2.9% Al₂O₃*; *e.g.* Figures 4.2.8 and 4.2.9).

'Levantine I' glass is typical of glass produced in Israel during the Early Byzantine period (4th-7th centuries AD) (Foster and Jackson 2009: 193; Foy *et al.* 2000: 54; Freestone 2003: 112; Freestone *et al.* 2000: 72; 2002a: 168; 2002b: 265), and corresponds closely to Foy *et al.*'s 'Group 3.1' (Foy *et al.* 2003: 42; 75). It can be relatively confidently attributed to Near Eastern workshops, as it was produced using quartz-rich sands sourced from the Palestinian coast (Foy *et al.* 2000: 54; Freestone 2003: 112; Freestone *et al.* 2000: 72; 2002a: 168; 2002b: 265). Raw glass chunks from a number of Israeli sites, including Dor, Bet Shean and Apollonia (Freestone *et al.* 2000: 72; 2002a: 168; 2002b: 265), together with Late Roman glass from Jalame (Brill 1998), are of the 'Levantine I' composition. The glass from Jalame in particular is assumed to have been produced from the famous glassmaking sands from the mouth of the River Belus in the Bay of Haifa, Israel (Brill 1988: 266; Freestone *et al.* 2000: 72; 2002a: 168; 2002b: 265), which are particularly high in alumina (Foy *et al.* 2003: 75).

Figure 4.6.1 shows a plot of the 'Levantine I' glass from Eriswell compared to the five major groups of natron-based glass produced in the Near East between the 4th and 9th centuries AD as identified by Freestone and co-workers, each of which represents a product of a different workshop in a slightly different location (*e.g.* Freestone *et al.* 2000: 82; Freestone *et al.* 2002b: 265-266; Freestone 2006: 208; see also Chapter 1, section 1.4.1). The 'Levantine I' glass from Eriswell corresponds closely to contemporary glass of this type from the Near East. Whilst the high levels

of alumina in several of the Eriswell samples appear to correspond more closely to ‘Levantine II’ (Bet Eli’ezer) glass, their composition is otherwise consistent with ‘Levantine I’ glass (Table 4.2.1); it is likely that extra alumina was introduced through contamination from the melting pot (see this chapter, section 4.1).

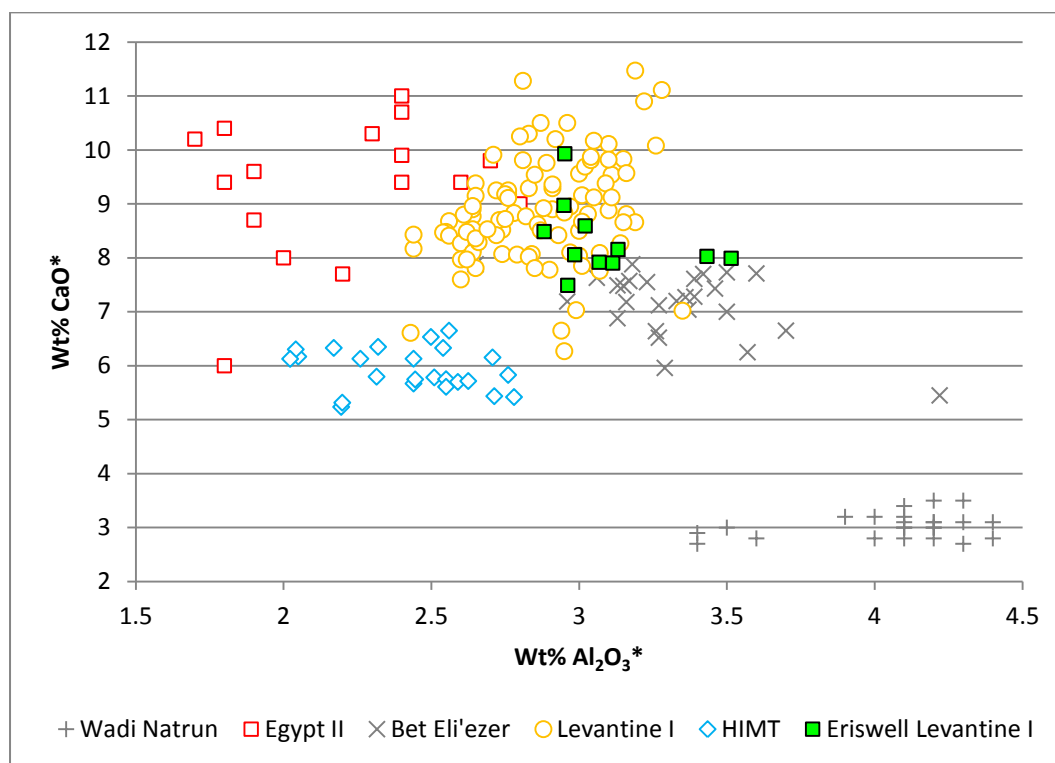


Figure 4.6.1 – A plot of alumina versus lime for ‘Levantine I’ glass from Eriswell, compared to the five major groups of natron glass produced in the Eastern Mediterranean between the 4th and 9th centuries AD (see text for details). Samples which are likely to have been affected by alumina contamination have been omitted (see this chapter, section 4.2 for details).

It is likely the ‘Levantine I’ glass from Eriswell reflects the use of a supply of raw glass imported (either directly or indirectly) from primary glassmaking workshops in the Near East. However, the small quantity of ‘Levantine I’ glass identified at Eriswell suggests that this glass type was probably not traded in significant quantities. Furthermore, the attribution of nearly all of the ‘Levantine I’ beads to Brugmann’s phase B2 (see this chapter, section 4.8) suggests that it was not used in Anglo-Saxon contexts until the 6th century. This supports the view that it is unlikely to represent recycled material from the preceding Roman period; if this were the case one would expect to see it in earlier beads, which were widely produced from

recycled material. It is therefore possible that there was a break in the production, supply and/or use of 'Levantine I' glass between approximately the early 5th and 6th centuries.

Whilst 'Levantine I' glass has been identified alongside 'HIMT' glass in Romano-British glass assemblages from the 4th century AD (Foster and Jackson 2009: 193), it seems to have been relatively uncommon outside of the Near East in comparison to 'HIMT' glass (see this chapter, section 4.5); the reasons for this are not entirely clear (Foster and Jackson 2009: 195). It has been suggested that this may relate to a preference for the colour of yellow-green tinted 'HIMT' glass over blue-green tinted 'Levantine I' glass, or to the lower melting temperatures of 'HIMT' glass as a result of its comparatively higher soda content (Foster and Jackson 2009: 194-195; Freestone *et al.* 2002a: 173). However, unlike the 'HIMT' samples from Eriswell (see this chapter, section 4.5), there is no evidence to suggest that the 'Levantine I' samples represent recycled material. The author favours the view that, whilst both 'Levantine I' and 'HIMT' glass were first produced in the 4th century, the production of 'HIMT' glass ceased no later than the early 5th century. In contrast, 'Levantine I' glass was clearly produced for a much longer period, possibly until the 7th century. Consequently, 'Levantine I' glass is far more common than 'HIMT' glass in the Near East.

4.6.1. Trace Element Analyses

Trace elements for two of the 'Levantine I' samples from Eriswell were obtained by LA-ICP-MS, both of which are translucent turquoise. As such, detailed comparisons are not possible here.

4.6.1.1. Rare Earth Elements (REE)

The REE patterns for both of the 'Levantine I' samples are broadly similar and relatively flat (Figure 4.6.2), suggesting the use of a similar glassmaking sand in the

production of both samples. Whilst there are slight variations in the REE patterns between samples, particularly from Gd through to Lu (the heavy REE), these are likely to have resulted from natural variations in the raw materials used in their production. There is a very slightly negative Ce anomaly and a strongly positive Eu anomaly in both samples.

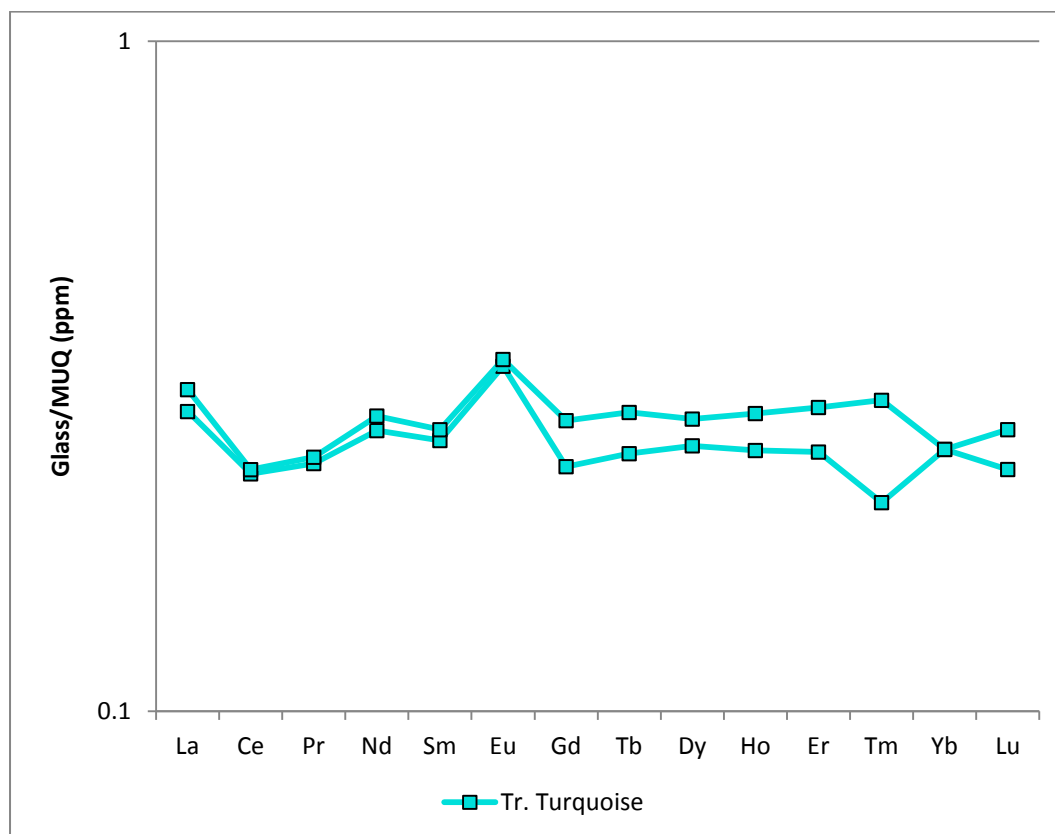


Figure 4.6.2 – Rare earth element concentrations for ‘Levantine I’ glass from Eriswell, by colour, normalised to the weathered continental crust (see Chapter, 2, section 2.3.2.3). Note the logarithmic scale.

As ‘Levantine I’ glass is assumed to have been produced using sand sourced from the Palestinian coast, a comparison with trace element data for Early Byzantine ‘Levantine’ glass from there is worthwhile. Figure 4.6.3 shows average REE data for raw uncoloured ‘Levantine I’ and ‘Levantine II’ glass from Apollonia-Arsuf and Bet Eli’ezer in Israel (unpublished data courtesy of Ian Freestone), compared ‘Levantine I’ glass from Eriswell. Whilst the concentrations of REE in ‘Levantine I’ glass from

Eriswell are elevated relative to those in ‘Levantine’ glass from Israel, there are a number of close similarities.

The shapes of the patterns are very similar, particularly for the light REE elements (La to Gd). However, there is slightly more variation in the concentrations of the heavy REE (Tb to Lu), most notably Tb and Ho. Whilst the Eriswell samples contain elevated levels of REE relative to ‘Levantine’ glass from Israel, suggesting the use of slightly different raw materials, this may difference may also be borne out by analytical differences between laboratories or the variability of the raw materials used; it should also be stressed that the ‘Levantine’ glass from Eriswell is intentionally coloured and may have been remelted a number of times, whereas that from Apollonia-Arsuf and Bet Eli’ezer represents raw uncoloured glass.

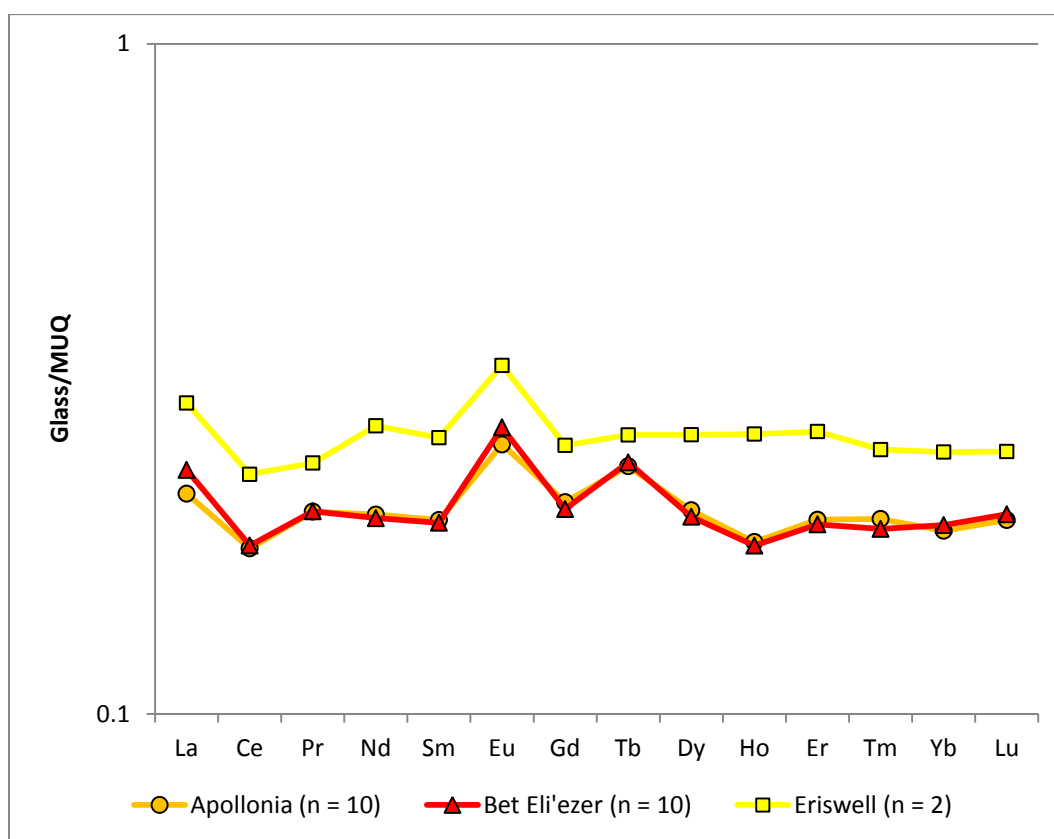


Figure 4.6.3 – Average rare earth element concentrations for ‘Levantine I’ glass from Eriswell, compared to ‘Levantine’ glass from Apollonia-Arsuf and Bet Eli’ezer in Israel (unpublished LA-ICP-MS data courtesy of Ian Freestone). Data are normalised to the weathered continental crust (see Chapter 2, section 2.3.2.3). Note the logarithmic scale.

4.6.1.2. Sediment-Related Elements (SRE)

The SRE patterns for the ‘Levantine I’ samples from Eriswell are very similar for all elements except W (Figure 4.6.4), indicating that both samples were produced from very similar raw materials and using a similar glassmaking recipe. The differences in W observed are likely to reflect variations in the levels of Mn present, as W and Mn are generally positively correlated in the majority of samples from Eriswell, so are likely to have been introduced together; sample ERL104:G193:1295 (*Koch34*) contains 850 ppm Mn and 0.34 ppm W, whereas sample ERL104:G281:1796 (*Koch34*) contains 150 ppm Mn but only 0.07 ppm W.

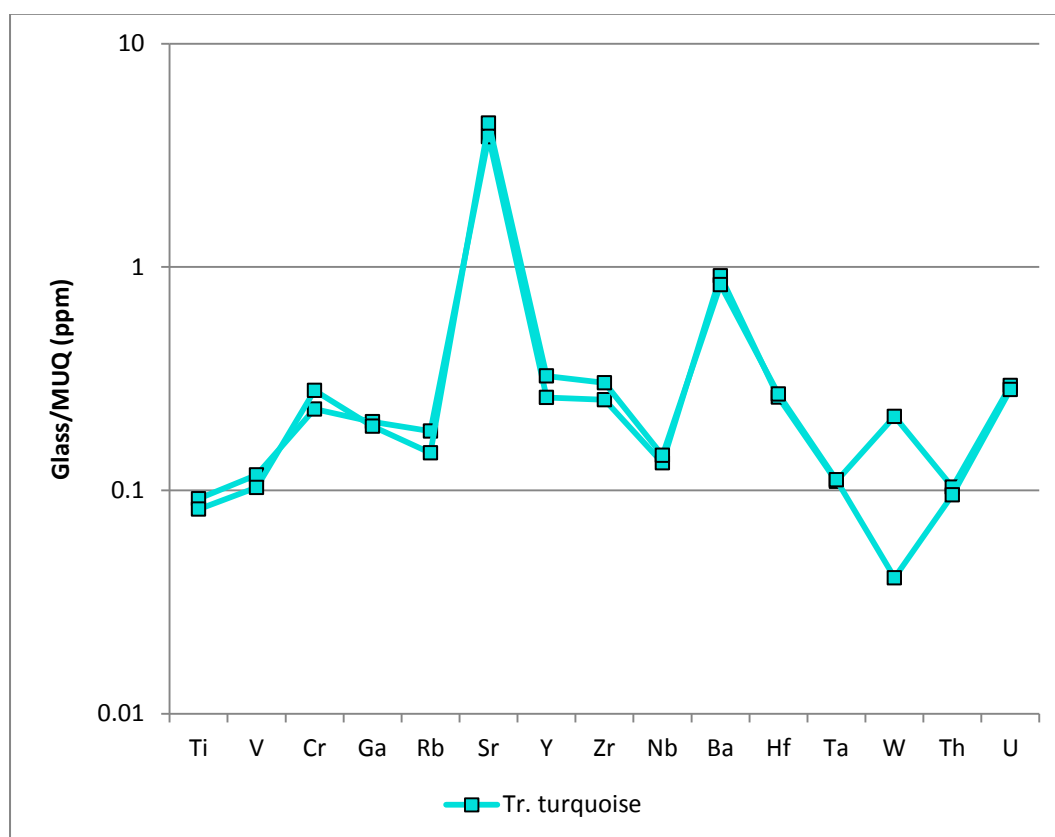


Figure 4.6.4 – Sediment-related element concentrations for ‘Levantine I’ glass from Eriswell, by colour, normalised to the weathered continental crust (see Chapter, 2, section 2.3.2.3). Note the logarithmic scale.

The purity of the sand used to produce ‘Levantine I’ glass relative to the other glass types identified at Eriswell is particularly well represented in plots of Zr versus Hf

(Figure 4.2.17) and Ti versus Zr (Figure 4.2.18). These components are present as impurities in the glassmaking sand and are therefore a good reflection of the concentration of heavy minerals present (Degryse and Shortland 2009: 140; Freestone *et al.* 2000: 73-74; Vallotto and Verità 2000: 68). The low concentrations of these components indicate the use of a very pure quartz-rich sand, consistent with that found along the Palestinian coast.

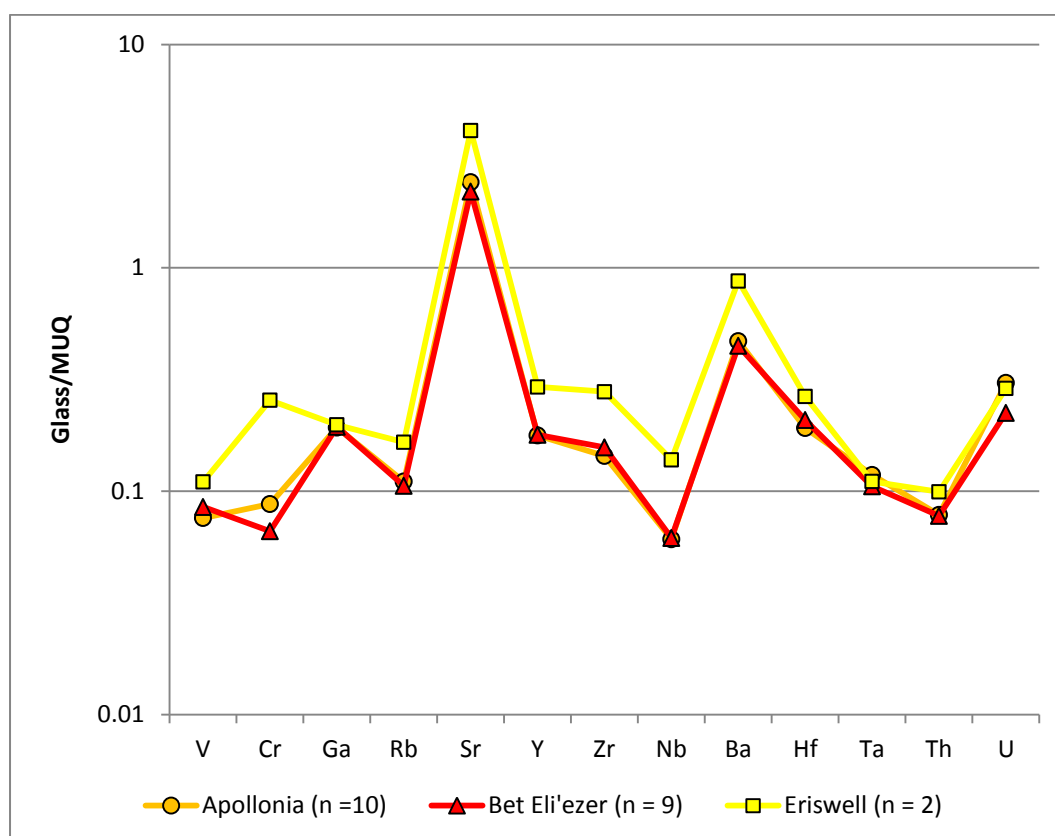


Figure 4.6.5 – Average concentrations of selected sediment-related elements for ‘Levantine I’ glass from Eriswell, compared to ‘Levantine’ glass from Apollonia-Arsuf and Bet Eli’ezer in Israel (unpublished LA-ICP-MS data courtesy of Ian Freestone). Data are normalised to the weathered continental crust (see Chapter 2, section 2.3.2.3). Note the logarithmic scale.

The SRE patterns for the ‘Levantine’ glasses from Apollonia-Arsuf and Bet Eli’ezer in Israel are very similar to those from Eriswell (Figure 4.6.5), although the majority of SRE in the Eriswell samples are slightly elevated by comparison. As with the REE, this may be borne out by the fact that the Eriswell samples have been deliberately remelted and coloured, or reflect natural variations in the purity of the raw materials used, or analytical differences between laboratories.

Figure 4.6.6 shows a plot of CaO* versus Sr from published glass data for ‘Levantine I’ glass from 4th century Britain (from Foster and Jackson 2009), compared to the different glass types identified at Eriswell (Figure 4.2.19). These data correspond very closely to the ‘Levantine I’ samples from Eriswell, indicating the use of a sand containing a very similar ratio of Ca to Sr. This further supports the view that the ‘Levantine I’ samples from Eriswell share a common origin with contemporary ‘Levantine I’ glass produced in the Near East.

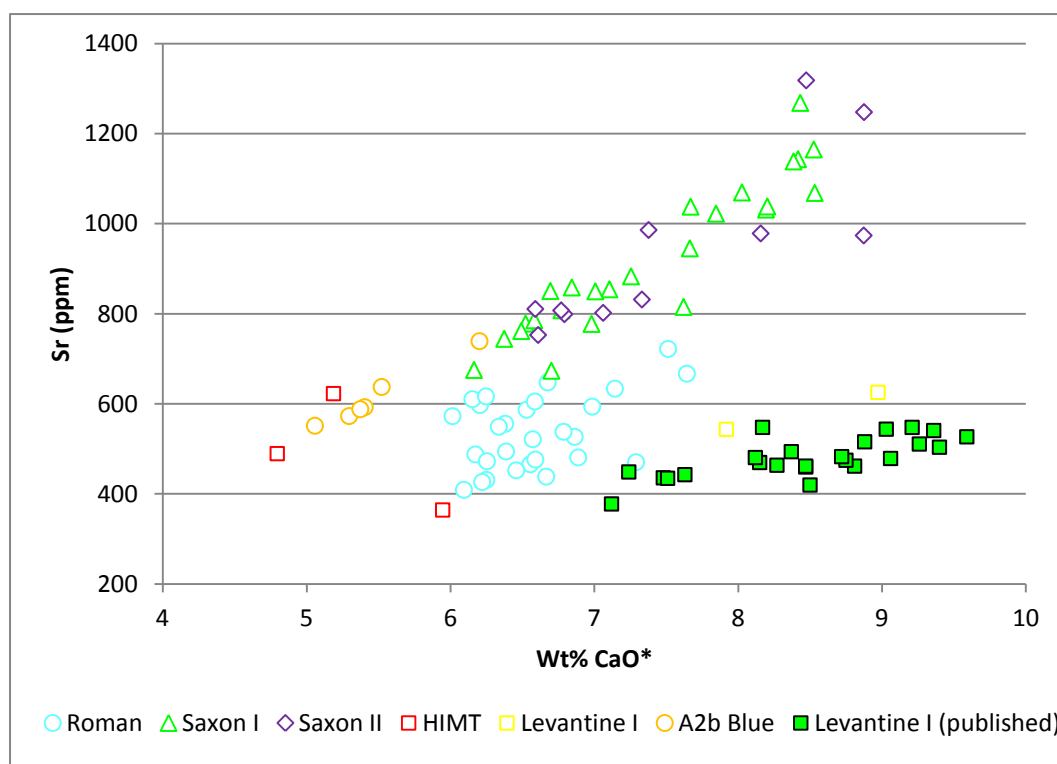


Figure 4.6.6 – A plot of lime versus strontium for 24 published 4th century ‘Levantine I’ glass samples from Britain (after Foster and Jackson 2009), compared to the different base glass types identified at Eriswell.

4.7. 'A2b Blue' Glass

'A2b Blue' glass is the smallest compositional group identified at Eriswell, consisting of only 11 translucent blue monochrome beads primarily of Brugmann's *Melon* and *Melon Variation?* types (see this chapter, section 4.10). It represents what is thought to be a previously unknown glass type, so-called because all of the beads are translucent blue (see this chapter, section 4.9) and the majority have been attributed to Brugmann's phase A2b (see this chapter, section 4.8). Their composition is very consistent, so it seems likely that the majority were produced from the same batch of glass, possibly in the same workshop. Small quantities have also been identified at Spong Hill, Bergh Apton and Morning Thorpe in Norfolk (see Chapter 7, section 7.1), suggesting that it was probably a widely used type, even if it was not particularly common

'A2b Blue' glass has a number of very close similarities to 'Roman' glass, particularly on account of its similarly elevated levels of silica (approximately 68% SiO₂*; *e.g.* Figures 4.2.5 and 4.2.6), although sodium is slightly on the high side relative to 'Roman' glass (19.8% Na₂O* *cf.* 17.6%; *e.g.* Figure 4.2.1). However, no antimony was detected by major or trace element analysis (see section 4.7.1 below), indicating that it does not represent recycled material. However, it is likely that the glassmaking sand was sourced from a very similar region to that used in the production of 'Roman' glass; this was probably in the Near East (see this chapter, section 4.3).

The composition of 'A2b Blue' glass also has a number of close similarities to 'Levantine I' glass; trace element analysis (*e.g.* Figure 4.2.15) suggests that 'A2b Blue' and 'Levantine I' glass may have been produced from very similar sand sources, so these two glass types may be of related production. However, the lime and alumina levels of 'A2b Blue' glass are far too low to suggest that is a variation of 'Levantine' glass (Figure 4.7.1); they are more consistent with 'HIMT' glass, although the levels of iron, titanium, magnesia and manganese in 'A2b Blue' glass are otherwise far too low to suggest that it is related to 'HIMT' glass.

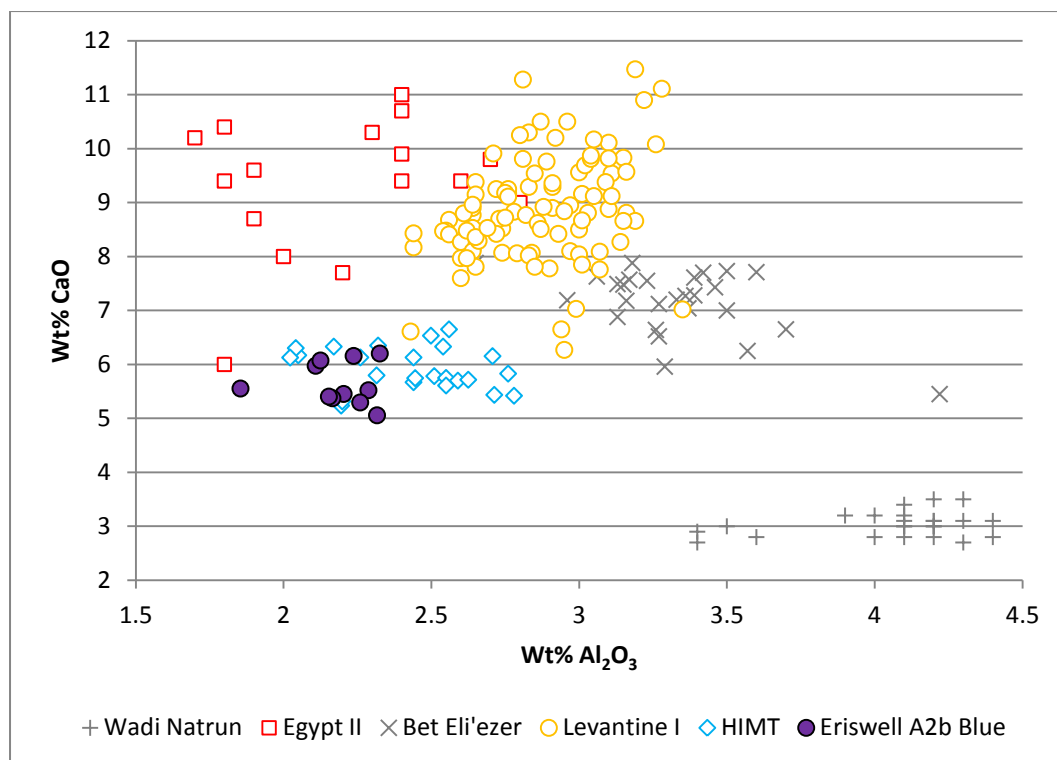


Figure 4.7.1 – A plot of alumina versus lime for ‘A2b Blue’ glass from Eriswell, compared to the five major groups of natron glass produced in the Eastern Mediterranean between the 4th and 9th centuries AD (see text for details).

‘A2b Blue’ glass therefore represents a distinct glass type, which is likely to have been produced in a similar region to ‘Roman’ and ‘Levantine I’ glass. ‘Levantine I’ glass in particular can be fairly confidently attributed to Palestinian workshops (see this chapter, section 4.6) and ‘Roman’ glass may also have its origins in this region (see this chapter, section 4.3). ‘A2b Blue’ glass is therefore consistent with Palestinian production. As this glass type is exclusively translucent blue, it is likely that it was pre-coloured in a similar manner to ‘Saxon I (blue)’ glass (see this chapter, sections 4.4 and 4.9); the colourant was probably added in the same workshops that produced the glass itself.

4.7.1. Trace Element Analyses

Trace element data for six of the ‘A2b Blue’ samples from Eriswell were obtained by LA-ICP-MS.

4.7.1.1. Rare Earth Elements (REE)

The REE patterns for the ‘A2b Blue’ glasses are very flat and very consistent (Figure 4.7.2), confirming that they were almost certainly produced in the same region using similar raw materials, possibly even in the same workshop from the same batch of glass. Very slight variations between samples are probably borne out by natural variations in the raw materials used (*e.g.* the glassmaking sand or cobalt mineral colourant). The REE concentrations are very similar to those of ‘Roman’ and ‘Levantine I’ glass (Figure 4.2.15), confirming that the raw materials used to produce all three of these glass types are likely to have a common geological origin.

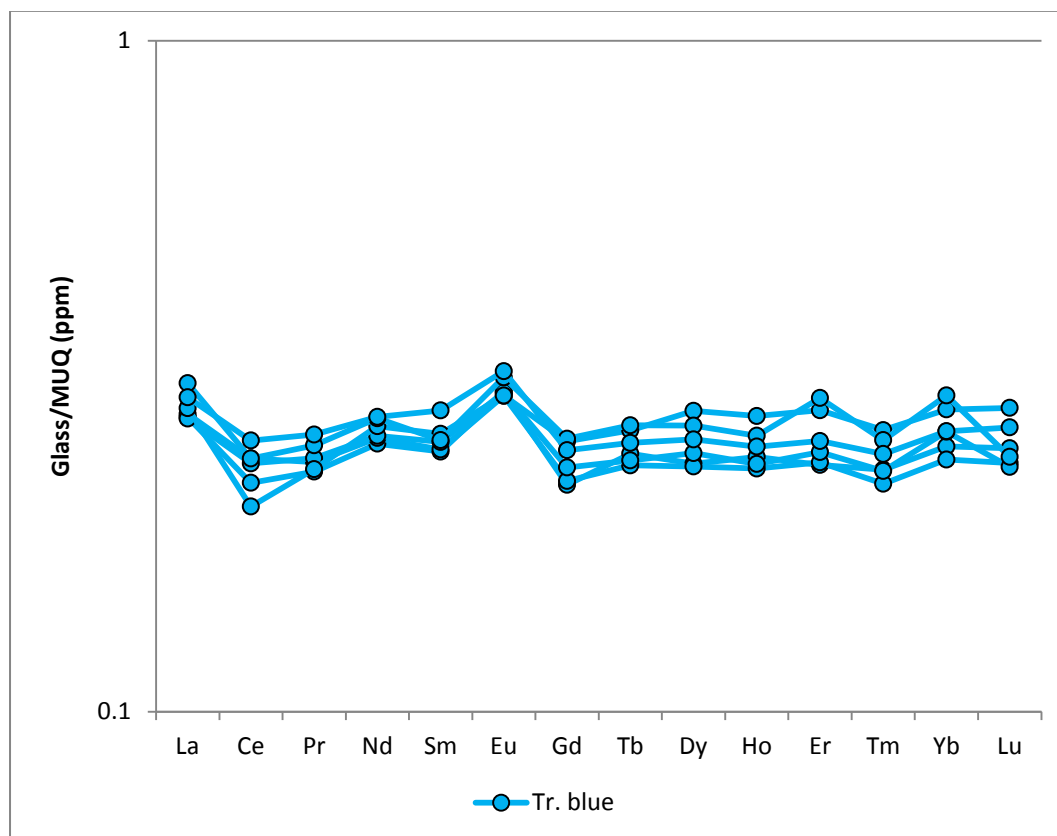


Figure 4.7.2 – Rare earth element concentrations for ‘A2b Blue’ glass from Eriswell, by colour, normalised to the weathered continental crust (see Chapter 2, section 2.3.2.3). Note the logarithmic scale.

4.7.1.2. Sediment-Related Elements (SRE)

The SRE patterns for the ‘A2b Blue’ samples, like the REE patterns, are very consistent (Figure 4.7.3), further confirming that the samples are likely to have a common origin. Slight variations between samples are again likely to be borne out by the natural variability of the raw materials used in their production. The difference in W relates to the Mn content of the samples (*e.g.* see this chapter, section 4.6.1); the majority contain less than 0.1 ppm W and less than 750 ppm Mn. However, sample ERL104:G305:1867 (*Melon*) contains nearly 0.2 ppm W and nearly 5000 ppm Mn; this sample is likely to have been produced from a different batch of glass by the same workshop. The similarities between ‘A2b Blue’, ‘Levantine I’ and ‘Roman’ glass are similarly reflected by the SRE patterns of these respective glass types (Figure 4.2.16).

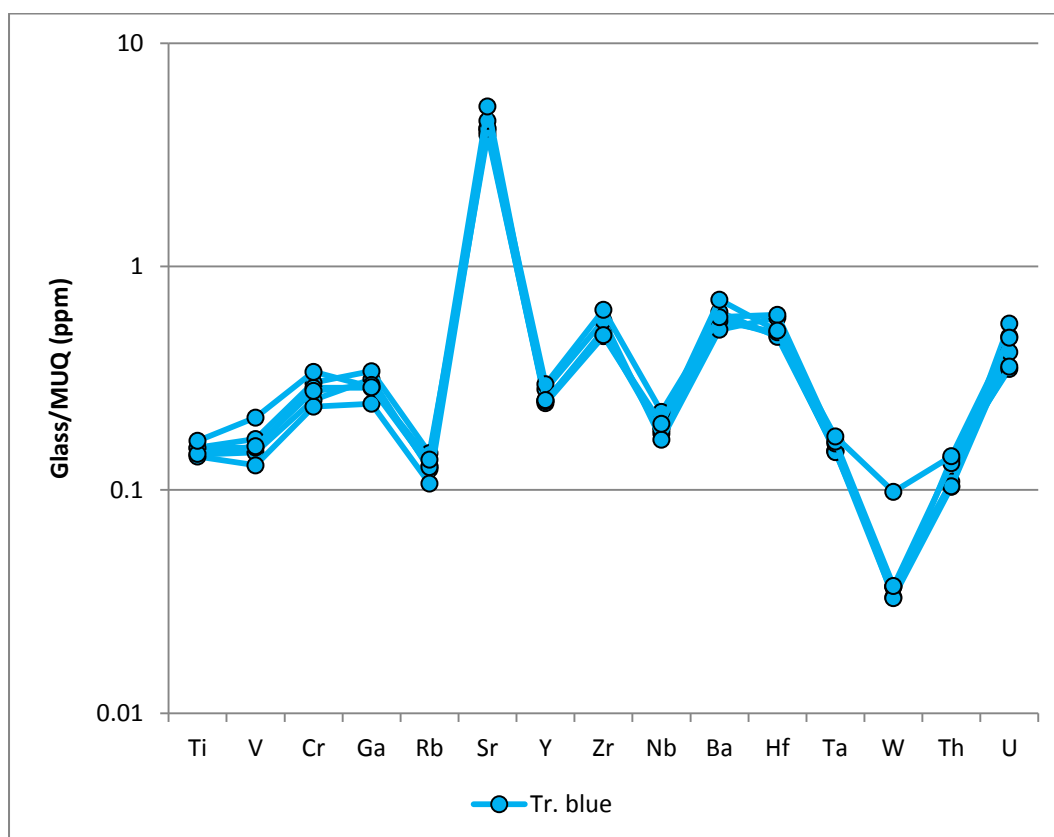


Figure 4.7.3 – Sediment-related element concentrations for ‘A2b Blue’ glass from Eriswell, by colour, normalised to the weathered continental crust (see Chapter 2, section 2.3.2.3). Note the logarithmic scale.

4.8. Relationship to Brugmann's Bead Chronology

An important part of this study is to establish the reliability of the chronological framework for early Anglo-Saxon beads in England established by Brugmann (2004). The beads from Eriswell were individually catalogued and dated in 2001 by Birte Brugmann (see Appendix A for type-phase attributions). However, only bead types covered by the bead typologies in Brugmann (2004) and Penn and Brugmann (2007) could be attributed to chronological phases.

Brugmann devised her chronological framework using correspondence analysis, comparing the associations and inter-associations of particular bead types with one another; *e.g.* *Constricted Segmented*, *Constricted Cylindrical* and *Reticella* beads appear to have been in use before *Koch20*, *Koch34* and *Orange* beads (Brugmann 2004: 44). Absolute dates were attributed to these phases on the basis of correlations with well-dates Continental and Scandinavian bead frameworks. The result was a series of overlapping Groups or phases (A-C), divided into a number Combination Groups (*i.e.* sub-phases), relating to Anglo-Saxon bead fashions between the 5th and 7th centuries (Brugmann 2004: 70; see also Chapter 1, section 1.5):

- Phase A1 *c.* AD 450-530
- Phase A2 *c.* AD 480-580
- Phase A2b *c.* AD 530-580

- Phase B1 *c.* AD 555-600
- Phase B2 *c.* AD 580-650

- Phase C *c.* AD 650-700

Phase A mostly comprises translucent monochrome or insular polychrome bead types, and includes beads from contexts known as the 'Early Phase' in Anglo-Saxon chronology (Brugmann 2004: 70). Phase B marks an increase in imported polychrome beads, and includes beads from both 'Anglian' and 'Saxon' contexts which fall between the 'Early Phase' and 'Final Phase' (Brugmann 2004: 70-71).

Lastly, phase C marks an abrupt change in bead fashion, and includes beads attributed to the ‘Final Phase’ in Anglo-Saxon chronology; this may begin somewhat earlier than *c.* AD 650, but continues until the end of furnished burial practice (Brugmann 2004: 70).

The dates of these phases are approximate for a number of reasons: it is not clear as to the extent to which regional bead fashions were affected by cultural and/or economic influences, which may have influenced the supply and use of particular bead types in England (Brugmann 2004: 70). Furthermore, the Continental bead frameworks upon which Brugmann’s phases are based vary between individual studies depending upon the way in which the evidence is arranged and interpreted; again this may be borne out by regional variations in the supply and use of particular bead types (Brugmann 2004: 44).

Brugmann’s chronology also assumes a *terminus post quem* for less common bead types from their associations with more closely datable bead types (Brugmann 2004: 70), when they may in fact be earlier than suggested by these associations. In addition, by basing her phases on Continental and Scandinavian frameworks, Brugmann assumes that purportedly ‘Continental’ bead types first appeared on the Continent *before* they did in England; if the types in question were first produced in England, they may not have appeared on the Continent until slightly later.

In the light of the chronology report by Hines *et al.* (in press), which involved typological study, correspondence analysis, Bayesian modelling and radiocarbon-dating to establish a multi-phase chronological series for Anglo-Saxon grave goods, the dates attributed to Brugmann’s chronology have been revised as a series of estimated calendrical dates (in ranges of probability):

(95% probability):

- Phase B1 commenced in *cal AD 470-545*, ending in *cal AD 555-630*
- Phase B2 commenced in *cal AD 510-540*, ending in *cal AD 610-650*
- Phase C commenced in *cal AD 610-650*, ending in *cal AD 660-685*

(68% probability):

- Phase B1 commenced in *cal AD 510-540*, ending in *cal AD 565-610*
- Phase B2 commenced in *cal AD 515-535*, ending in *cal AD 620-645*
- Phase C commenced in *cal AD 620-645*, ending in *cal AD 665-680*

The data collection and modelling undertaken by Hines *et al.* (in press) provides little information about beads attributed to Brugmann's phase A, as this was beyond the scope of their study (Hines *et al.*, in press). However, when phase A was constrained to end when phase B2 begins (as assumed by Brugmann), their results suggest that phase A2 ended in *cal AD 510-540* (95% probability) or *cal AD 515-535* (68% probability). When phase A is not constrained to end when phase B2 begins, their results suggest that phase A2 ended in *cal AD 545-650* (95% probability) or *cal AD 550-595* (68% probability); this model suggests that it is 99% probable that phase A2 ended after phase B2 began (Hines *et al.*, in press). Their results suggest that phase B1 may be restricted to a few years in the second quarter of the 6th century, and that phase C is likely to have begun before *c.* AD 650; possibly within the second quarter of the 7th century (Hines *et al.*, in press).

The aim of the present section is to establish the relationship between the six main base glass types discussed in sections 4.2-4.7 and the chronologies outlined by Brugmann (2004) and Hines *et al.* (in press), with a view to establishing the approximate dates for which these glass types were in use. Of the base glass types identified at Eriswell, five have been identified in previous studies so can be broadly dated independently of these chronologies:

- **'Roman'** glass, which is likely to largely represent recycled Roman blue-green glass produced during the 1st-3rd centuries (Foster and Jackson 2009: 189; Jackson 2005: 772-773). Date attributions for recycled glass of this type are not possible.
- **'Saxon I'** glass, defined by Freestone *et al.* (2008), corresponds to Evison's 'Period I' (*c.* AD 400-550) for Anglo-Saxon vessel glass (Evison 2000; 2008). 'Saxon I (natron)' glass has been identified in 5th-7th century contexts from France (Velde 1990), Germany (Wedepohl *et al.* 1997) and Italy

(Silvestri *et al.* 2005). It is therefore likely to have been first produced around the early 5th century, but appears to have largely gone out of use by the late 6th century.

- **‘Saxon II’** glass, defined by Freestone *et al.* (2008), corresponds to Evison’s ‘Period II’ (c. AD 550-700) for Anglo-Saxon vessel glass (Evison 2000; 2008). Glass of the ‘Saxon II (natron)’ type has been identified in France (Foy *et al.* 2003), Italy (Foy *et al.* 2003; Mirti *et al.* 2000; Silvestri *et al.* 2005), Wales (Campbell and Lane 1993), Egypt and Tunisia (Foy *et al.* 2003). It is generally attributed to the mid-6th to 7th centuries.
- **‘HIMT’** glass was first produced in the Late Roman period, at some point in the 4th century AD (Foster and Jackson 2009: 192; Freestone *et al.* 2005b: 153). It is unclear as to when this glass type ceased to be produced, but on balance the ‘HIMT’ glass from Eriswell is highly likely to represent recycled material from the preceding Late Roman period (see this chapter, section 4.5).
- **‘Levantine I’** glass was produced between the 4th and 7th centuries, using sand sourced from the Palestinian coast (*e.g.* Freestone *et al.* 2000). It has been identified at a number of sites in northern Israel (Brill 1988; Freestone *et al.* 2000) and throughout Europe (Foster and Jackson 2009; Foy *et al.* 2003; Silvestri *et al.* 2005).
- **‘A2b Blue’** glass has not been identified before, so production dates for this glass type are not available in published literature.

Figure 4.8.1 shows the *number of individual beads* produced using the different base glass types identified at Eriswell, relating to the chronological phases to which those beads have been attributed. It should be stressed that the number of beads is considerably influenced by the selection of beads during the sampling process (see Chapter 2, section 2.1). Several of the polychrome beads analysed pose something of a problem here, as different base glass types were sometimes used in the production of the different glass colours present. As a result, more than one compositional group of glass may be represented by the same bead. The glass types used in the production of applied decoration on polychrome beads are therefore presented separately to those used for the bead bodies to account for this (Figure 4.8.2); a polychrome bead

decorated with more than one glass colour may therefore be represented by more than one sample.

The data suggest that beads produced from the 'Roman', 'Saxon I' and 'HIMT' glass types were almost exclusively products of Brugmann's phase A (c. AD 450-580). In contrast, beads produced from the 'Saxon II' and 'Levantine I' glass types appear to be almost exclusively products of Brugmann's phases B-C (c. AD 555-700). Phase A2b represents a transition period between phases A and B (c. AD 530-580), and is particularly characterised by the use of 'A2b Blue' glass. The present data suggest that beads from this phase correspond more closely to beads from phase B2 (c. AD 580-650) than phase A2 (c. AD 480-580). This is consistent with the modelling of the currencies of phase B2 bead types in England established by Hines *et al.* (in press); their results suggest that phase B2 probably began before the end of phase A (99% probable). Phase B2 is therefore likely to have commenced earlier than suggested by Brugmann, overlapping with phase A2b (and possibly also phase A2) in a similar manner to phase B1.

It is not possible to distinguish between beads attributed to Brugmann's phases A1 and A2 on compositional grounds. 'Roman' 'Saxon I' and 'HIMT' glass were all used to produce beads of this date; 'Roman' and 'HIMT' glass is likely to represent recycled material from the preceding Roman period, so compositional indications of date are not possible here. Whilst 'Saxon I (blue)' glass was used to produce beads attributed to both phases A1 and A2, 'Saxon I (natron)' glass appears to be more typical of phase A2 and may therefore be a slightly later introduction. That 'Saxon I (blue)' and 'HIMT' glass were probably used contemporaneously with 'Roman' glass is attested for by the use of these glass types as decoration on polychrome beads of the 'Roman' compositional type. 'Saxon I (natron)' glass is not found in association with recycled 'Roman' or 'HIMT' glass. It is not possible to distinguish between beads attributed to Brugmann's phases B and C on compositional grounds; this suggests that there may be an overlap between phases B and C. However, the results of Hines *et al.* (in press) support Brugmann's view that phase C began when phase B2 ended. None of the 'later' 'Saxon II', 'Levantine I' and 'A2b Blue' glass types are found in association with 'Roman' or 'HIMT' glass on the same beads.

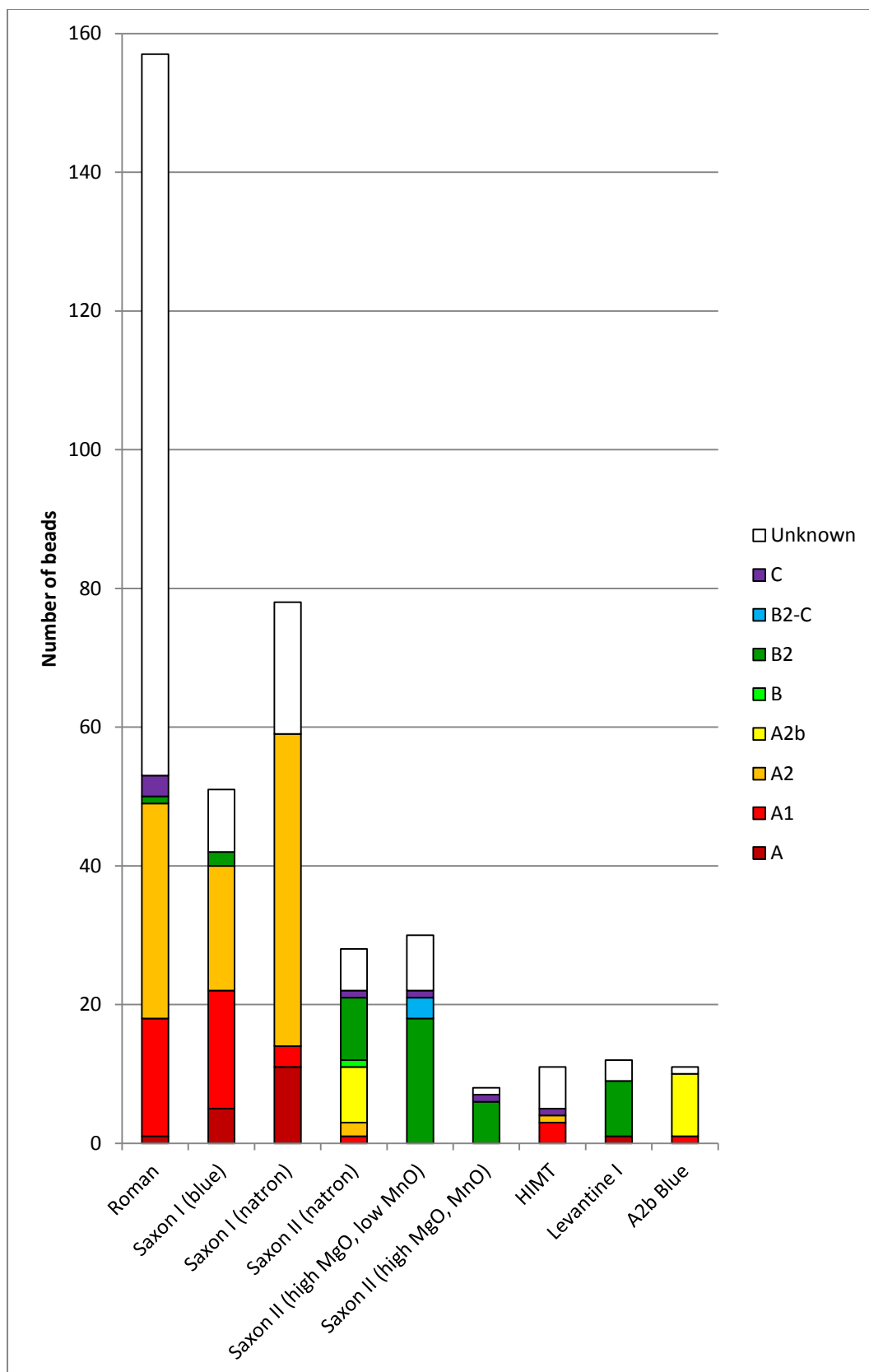


Figure 4.8.1 – Stacked histogram showing the relationship between the base glass types used for the bodies of the beads from Eriswell and Brugmann’s chronological attributions.

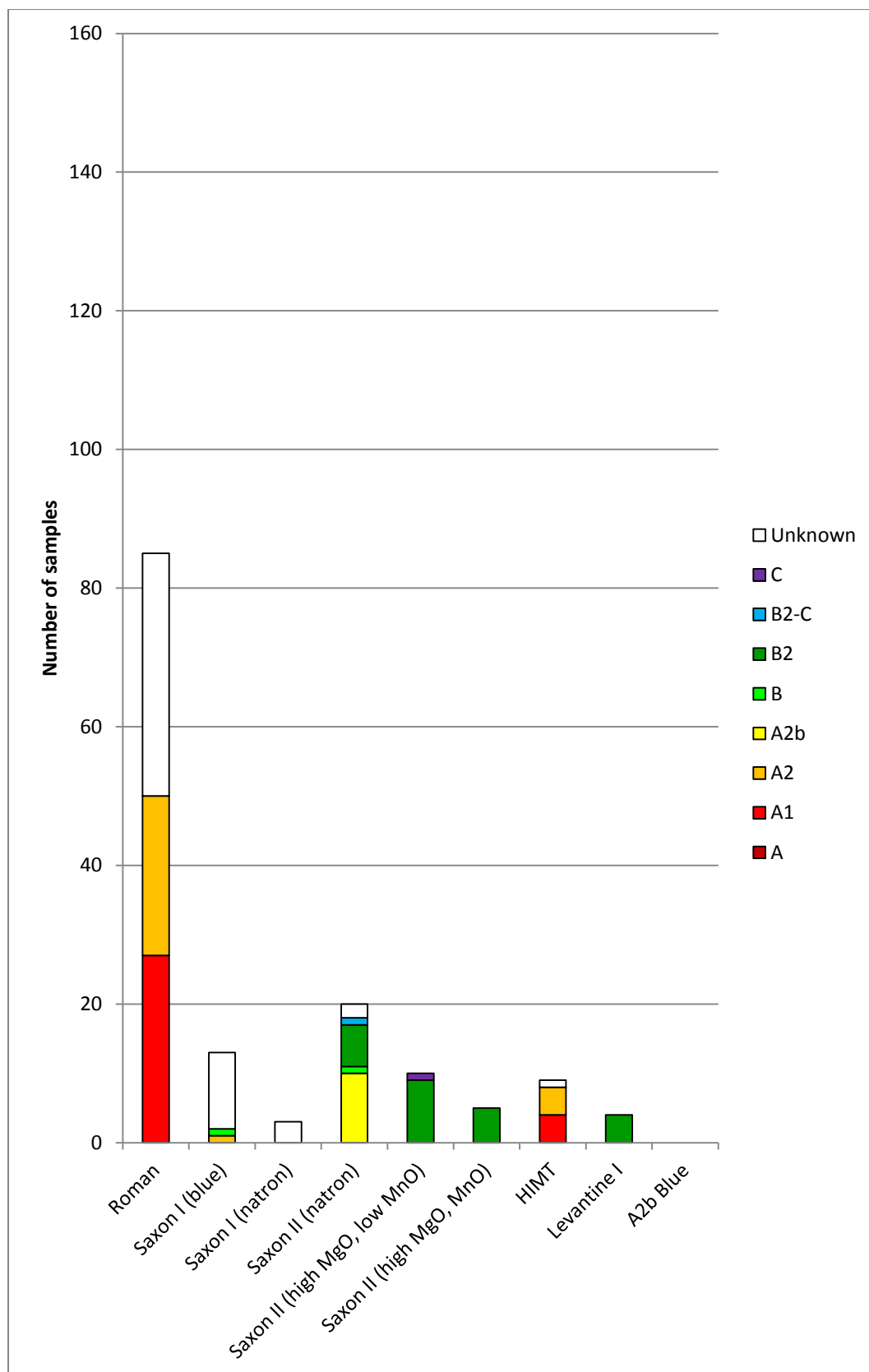


Figure 4.8.2 – Stacked histogram showing the relationship between the base glass types used for the decoration on polychrome beads from Eriswell and Brugmann's chronological attributions.

‘Saxon II (natron)’ glass appears to have been introduced in the transition period between Brugmann’s phases A and B, as a large proportion of the beads produced from it are attributed to Brugmann’s phase A2b. It is therefore likely that it was introduced roughly contemporaneously with ‘A2b Blue’ glass; probably whilst ‘Saxon I’ glass was still in use, but before ‘Saxon II (high MgO, low MnO)’, ‘Saxon II (high MgO, MnO)’ and ‘Levantine I’ glass. The similarities between ‘Saxon II (natron)’ glass and Foy *et al.*’s ‘Group 2.1’ (which is attributed to the mid-6th to 7th centuries; see this chapter, section 4.4) suggest that it is unlikely to pre-date the mid-6th century (*i.e.* the approximate overlap between phases A2 and A2b). Furthermore, Celtic vessel glass from Longbury Bank (southwest Wales), also of the ‘Saxon II (natron)’ type, is typologically dated to between the mid-6th and early 7th centuries (Campbell and Lane 1993: 40-45), supporting this date attribution.

Both ‘Saxon II (high MgO, low MnO)’ glass and ‘Saxon II (high MgO, MnO)’ glass are probably the latest glass types represented at Eriswell. This is suggested by the deliberate addition of small quantities of plant ash to the batch; true plant ash glass does not appear to have been produced in northwestern Europe until the 8th or 9th centuries (see this chapter, section 4.4). Compositional analysis of Anglo-Saxon vessel glass by Freestone *et al.* (2008) suggests that these glass types did not come into use until at least the mid-6th century.

It has been suggested that the adulteration of natron glass with small quantities of plant ash was very restricted in time and/or place, as mid-Saxon glass from the late 7th, 8th and 9th centuries does not appear to have been adulterated in this way (Freestone *et al.* 2008: 41; see also Chapter 6). However, it is likely that these ash-rich glasses were peculiar to Continental workshops, as characteristically ‘Anglo-Saxon’ beads do not appear to have been produced from them (see this chapter, section 4.10); a comparison with later Anglo-Saxon glass from English sites is therefore not valid. Whilst these glass types have yet to be identified in Europe, it is just possible that they represent precursors to true plant ash glass.

‘Levantine I’ glass has been identified in Late Roman vessel glass from Britain (Foster and Jackson 2009), but in Anglo-Saxon contexts it is peculiar to beads attributed to Brugmann’s phase B2 (Figures 4.8.1 and 4.8.2). This suggests that it

was not used to produce beads until the 6th century. The exact date of its reintroduction is unclear, but its general association with ‘Saxon II (high MgO, MnO)’ glass (*e.g.* see this chapter, section 4.10, Table 4.10.1) suggests that it is unlikely to have been introduced prior to the mid-6th century. There is no chronological evidence to suggest that ‘Levantine I’ glass continued to be used into Brugmann’s phase C (*i.e.* after the early or mid-7th century).

Overall, the results of the present study are in close agreement with Brugmann’s chronological attributions. Using this as a basis, approximate dates can be proposed for the introduction and cessation of the different base glass types identified. These are shown in Figure 4.8.3. Adjustments which account for the revised dates for Brugmann’s chronology proposed by Hines *et al.* (in press) are presented in Figure 4.8.4; uncertainty in the date ranges here are represented by dashes. The chronology proposed by Hines *et al.* (in press) is difficult to account for because the date estimates for the end of phase A are imprecise; this may produce more of an overlap in the use of different glass types than is the case. This uncertainty is reflected by the cut-off point at 500 AD in Figure 4.8.4.

The main consequences of the revised chronology proposed by Hines *et al.* (in press) are that ‘Saxon II’, ‘Levantine I’ and ‘A2b Blue’ glass are more likely to have been introduced a few decades earlier than assumed using Brugmann’s chronology (Figure 4.8.3 *cf.* Figure 4.8.4). On the basis of their chronology, ‘Saxon II (high MgO, low MnO)’ and ‘Saxon II (high MgO, MnO)’ glass may have potentially been introduced as early as the first few decades of the 6th century. The picture is less clear with regard to ‘Levantine I’ glass, but this glass type is unlikely to have been introduced earlier than the 6th century. The evidence at present supports the view that it was introduced around the early 6th century or later, and continued to be used into the early 7th century.

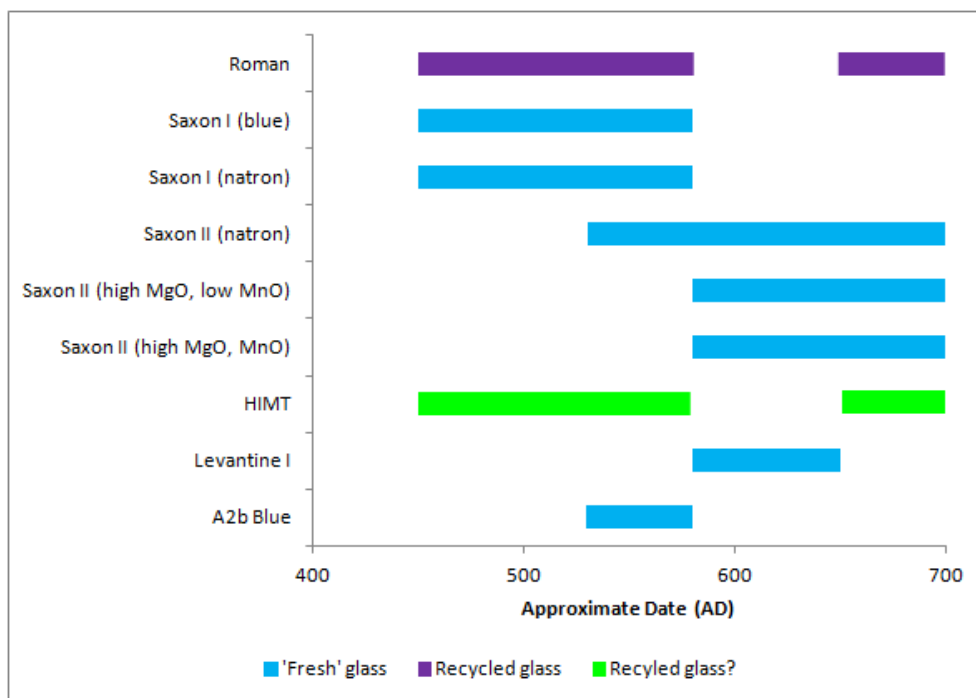


Figure 4.8.3 – An approximate chronology for the base glass types identified at Eriswell, based solely upon Brugmann's chronology (see text for details). Note that 'HIMT' glass is likely to reflect recycled material from the preceding 4th century, but this cannot be confirmed at present.

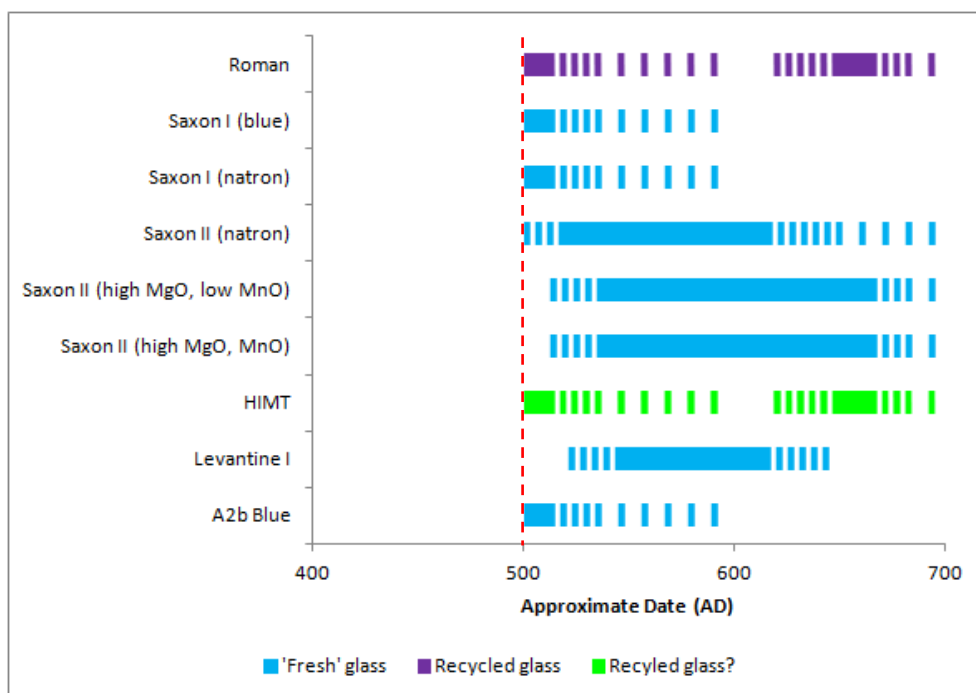


Figure 4.8.4 – An approximate chronology for the base glass types identified at Eriswell in use after the 5th century AD, based upon the chronology proposed by Hines *et al.* (in press). The dashed areas reflect uncertainties in the date ranges provided by the radiocarbon dates and the use of certain glass types; the more widely spaced dashes reflect greater uncertainty. There are considerable uncertainties relating to the end of phase A, meaning that it is not entirely clear when glass types in use during this period ceased to be used; this uncertainty is indicated by the red dashed line. Note that 'HIMT' glass is likely to reflect recycled material from the preceding 4th century, but this cannot be confirmed at present.

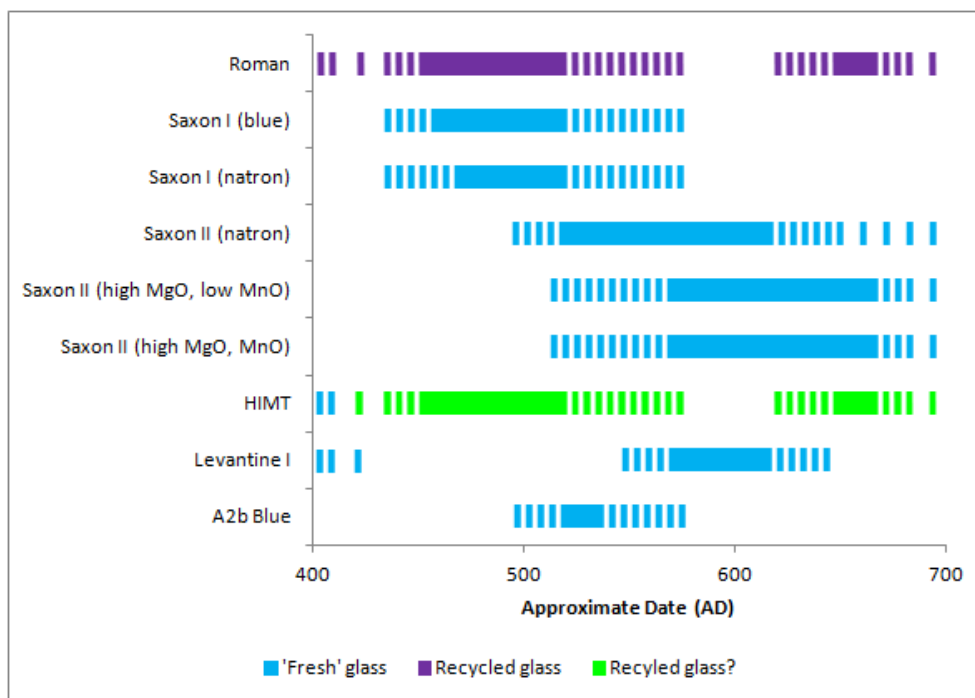


Figure 4.8.5 – An approximate chronology for the base glass types identified at Eriswell, based upon subjective judgements made from Brugmann's chronology (Figure 4.8.3), Hines *et al.*'s chronology (Figure 4.8.4), the compositional characteristics of the glass and published data (see text for details). The dashed areas reflect uncertainties in the use of certain glass types; the more widely spaced dashes reflect greater uncertainty. Note that 'HIMT' glass is likely to reflect recycled material from the preceding 4th century, but this cannot be confirmed at present.

An approximate chronology for these glass types has been synthesised based upon the chronologies proposed by Brugmann (2004) and Hines *et al.* (in press) (Figures 4.8.3 and 4.8.4), together with subjective judgements based upon the approximate dates attributed to the glass types recognised in published literature and their compositional attributes. The resulting chronology is presented in Figure 4.8.5. An attempt has been made here to factor the results of previous work on post-Roman glass in Britain, which has identified 'HIMT' and 'Levantine I' glass in 4th and 5th century contexts (Foster and Jackson 2009). It has been suggested that production of Roman blue-green glass may have continued into the 4th century, but it is also possible that it represents recycled material at this time (Foster and Jackson 2009: 194); on balance the latter interpretation seems more likely. However, it is unclear as to whether the practice of recycling 'Roman' blue-green tinted glass was a continuation of a Late Roman practice; if not, the break is unlikely to have lasted any more than a few decades at the most. It is also unclear as to when the production of raw 'HIMT' glass ceased, and when it first began to be recycled.

Whilst the dates attributed to the glass types in Figure 4.8.5 should be considered approximate at best, the general sequence in which they were introduced is likely to be fairly reliable. It is clear that the majority of the 'earlier' glass types ('Roman', 'Saxon I' and 'HIMT') appear to have largely gone out of use by the late 6th century. The majority of the 'later' glass types ('Saxon II', 'Levantine I' and 'A2b Blue') appear to have been introduced at some point in the 6th century. 'Saxon II (natron)' and 'A2b Blue' glass are likely to have been introduced prior to the 6th century, but could just have been introduced in the late 5th century.

Whilst 'A2b Blue' glass appears to have been a relatively short-lived glass type, unlikely to have been used into the 7th century, 'Saxon II (natron)' glass appears to have been a fairly long-lived glass type; it could conceivably have been used until the end of furnished burial practices in England. Indeed, 'Saxon II (natron)' glass is likely to have been used to produce 'Saxon II (high MgO, MnO)' glass (see this chapter, section 4.4). At some point in the 7th century, there appears to have been a re-introduction of the use of recycled Roman material ('Roman' and 'HIMT' glass), but in very small quantities; this is restricted to the production of *Doughnut* beads (see this chapter, section 4.10). However, here is a clear break in the use of these recycled glass types around the late 6th or early 7th century.

4.9. Relationship to Opacity and Colour of the Glass

It is clear from the division of the Eriswell glasses into different groups that some colours of glass are more typically produced from particular base glass types than others. Whilst the number of beads representing particular colours is biased by the sampling process (see Chapter 2, section 2.1), a number of trends are apparent. The discussion which follows is in the light of the results presented earlier in this chapter (section 4.8) regarding chronology, and those presented in Chapter 5 in which colourant technology is discussed in detail. Figure 4.9.1 shows data for translucent and opaque beads produced using the different base glass compositions identified at Eriswell. Figure 4.9.2 shows the same, but for applied decoration on polychrome beads (see this chapter, section 4.9 for details).

‘Roman’, ‘Saxon II’, ‘HIMT’ and ‘Levantine I’ glass was predominantly used to produce opaque beads, whereas ‘Saxon I’ and ‘A2b Blue’ glass was predominantly used to produce translucent beads (Figure 4.9.1). A significant proportion of ‘Roman’ glass was also used to produce translucent beads. This trend is broadly reflected by the decoration on polychrome beads (Figure 4.9.2), but there are a number of notable differences. When ‘Saxon II (high MgO, low MnO)’ glass is used as applied decoration, it is more frequently translucent than when it is used to produce bead bodies. Similarly, when ‘Levantine I’ glass is used for bead bodies it is more frequently opaque, but when used for decoration it is more frequently translucent. The majority of ‘Saxon I (natron)’ glass used for bead bodies is translucent, but the few samples used as decoration are opaque. These patterns may partly relate to translucent beads largely going out of fashion in the course of the 6th century (Brugmann 2004: 37); the ‘earlier’ beads (produced from ‘Saxon I’ and ‘A2b Blue’ glass) are more typically translucent, whereas the ‘later’ beads (produced from ‘Saxon II’ and ‘Levantine I’ glass) are more typically opaque. Beads made from ‘Roman’ and ‘HIMT’ glass are exceptions.

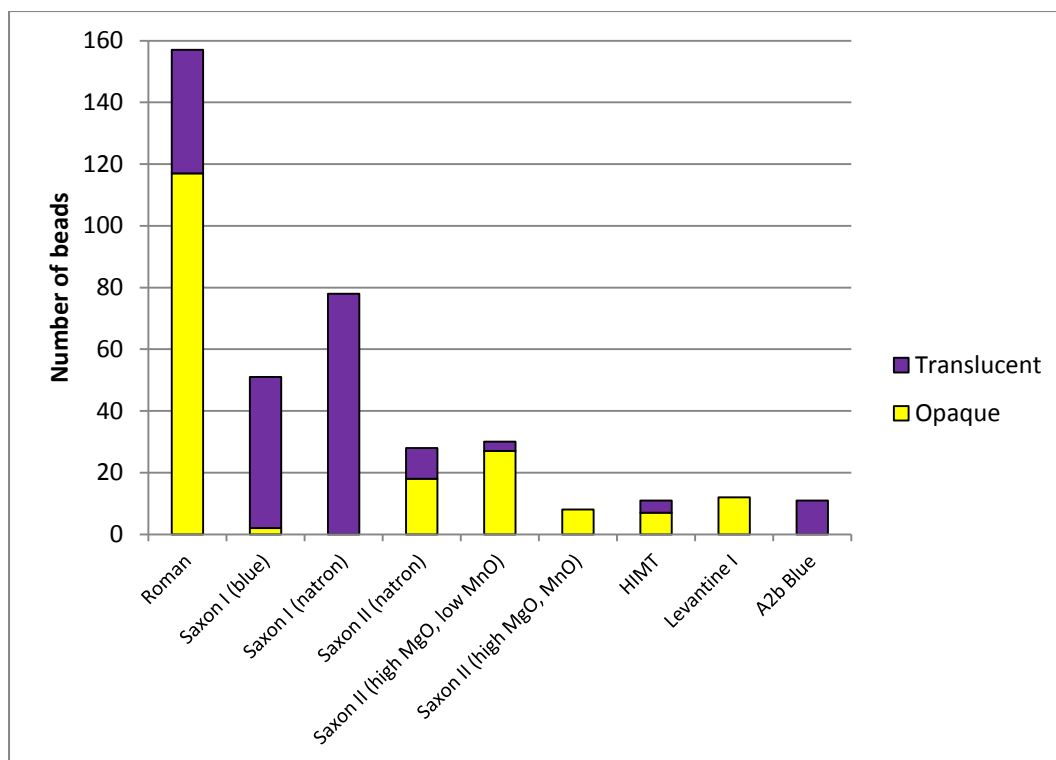


Figure 4.9.1 – Stacked histogram showing the relationship between the different base glass types used for the bodies of the beads from Eriswell and their translucency/opacity. Note that ‘dark’ glass is treated as translucent.

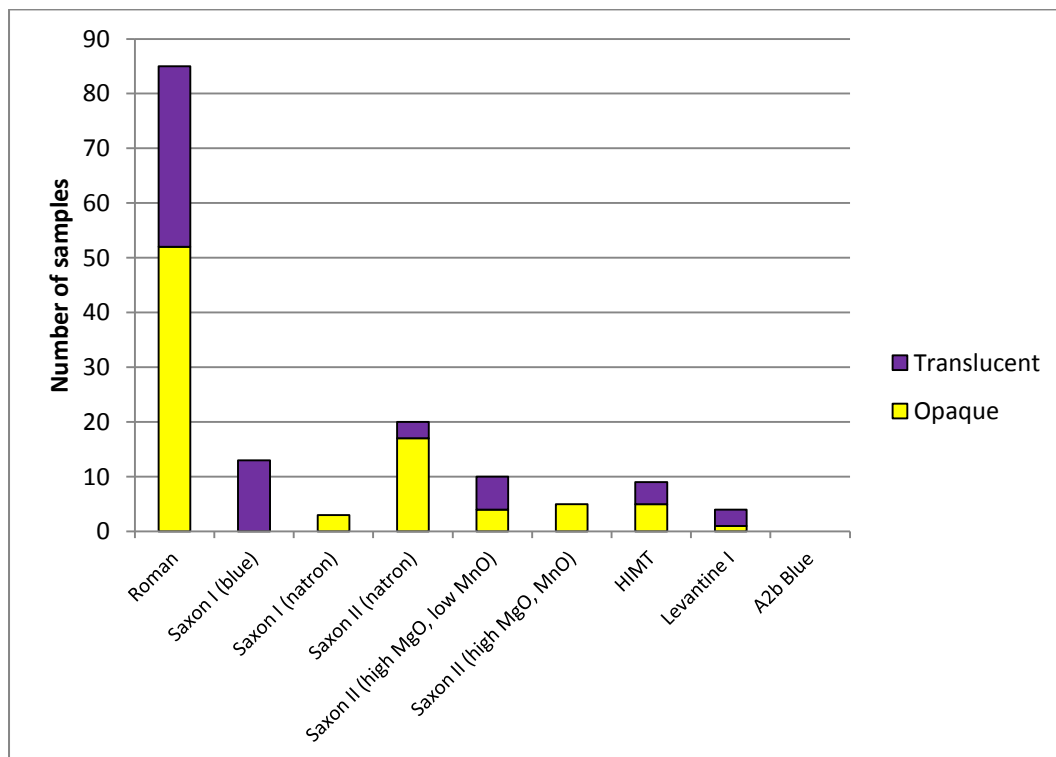


Figure 4.9.2 – Stacked histogram showing the relationship between the base glass types used for the decoration on polychrome beads from Eriswell and their translucency/opacity. Note that ‘dark’ glass is treated as translucent.

When these data are compared to Brugmann's chronology (see this chapter, section 4.8), it is clear that opaque beads attributed to phase A are almost entirely produced from 'Roman' or 'HIMT' glass, whereas translucent beads from these phases may be produced from 'Roman', 'Saxon I', 'HIMT' or 'A2b Blue' glass. The vast majority of beads attributed to Brugmann's phases B2 or C are opaque, typically produced from 'Saxon II' or 'Levantine I' glass, as translucent beads are comparatively much rarer in these later phases. Such trends are paralleled on the Continent; the majority of Merovingian beads produced after the mid-6th century are opaque, with translucent beads becoming far less common than they were in the 5th and early 6th centuries (Sablerolles 1999: 258).

Figure 4.9.3 shows data for the translucent glass beads from Eriswell, grouped by colour according to the different base glass types used. Figure 4.9.4 shows the same, but for translucent decoration on polychrome beads. Note that 'dark' glass is assumed to be translucent due to the absence of a crystalline opacifying agent (see Chapter 5, section 5.1.5). Figure 4.9.5 shows data for the opaque glass beads from Eriswell, grouped by colour according to the different base glass types used. Figure 4.9.6 shows the same, but for opaque decoration on polychrome beads. These graphs clearly show that some colours are far more frequently, sometimes exclusively, produced from certain base glass types.

'Saxon I (blue)' and 'A2b Blue' glass, as the names suggest, are almost exclusively translucent blue. The only exception is the presence of two opaque green samples attributed to the 'Saxon I (blue)' group. However, whilst the composition of these samples is consistent with 'Saxon I (blue)' glass, it is likely that they are products of a different workshop; both beads are of Brugmann's *Green Constricted Cylindrical* type, and trace element data for one such bead is not consistent with 'Saxon I (blue)' glass (see this chapter, section 4.4.1). Much translucent blue glass is also produced from 'Roman' and 'Saxon I (natron)' glass, and a small amount from 'Saxon II (high MgO, low MnO)' glass. Blue glass of the latter type could conceivably represent 'Saxon I (blue)' glass to which a small quantity of plant ash has been added (see this chapter, section 4.4).

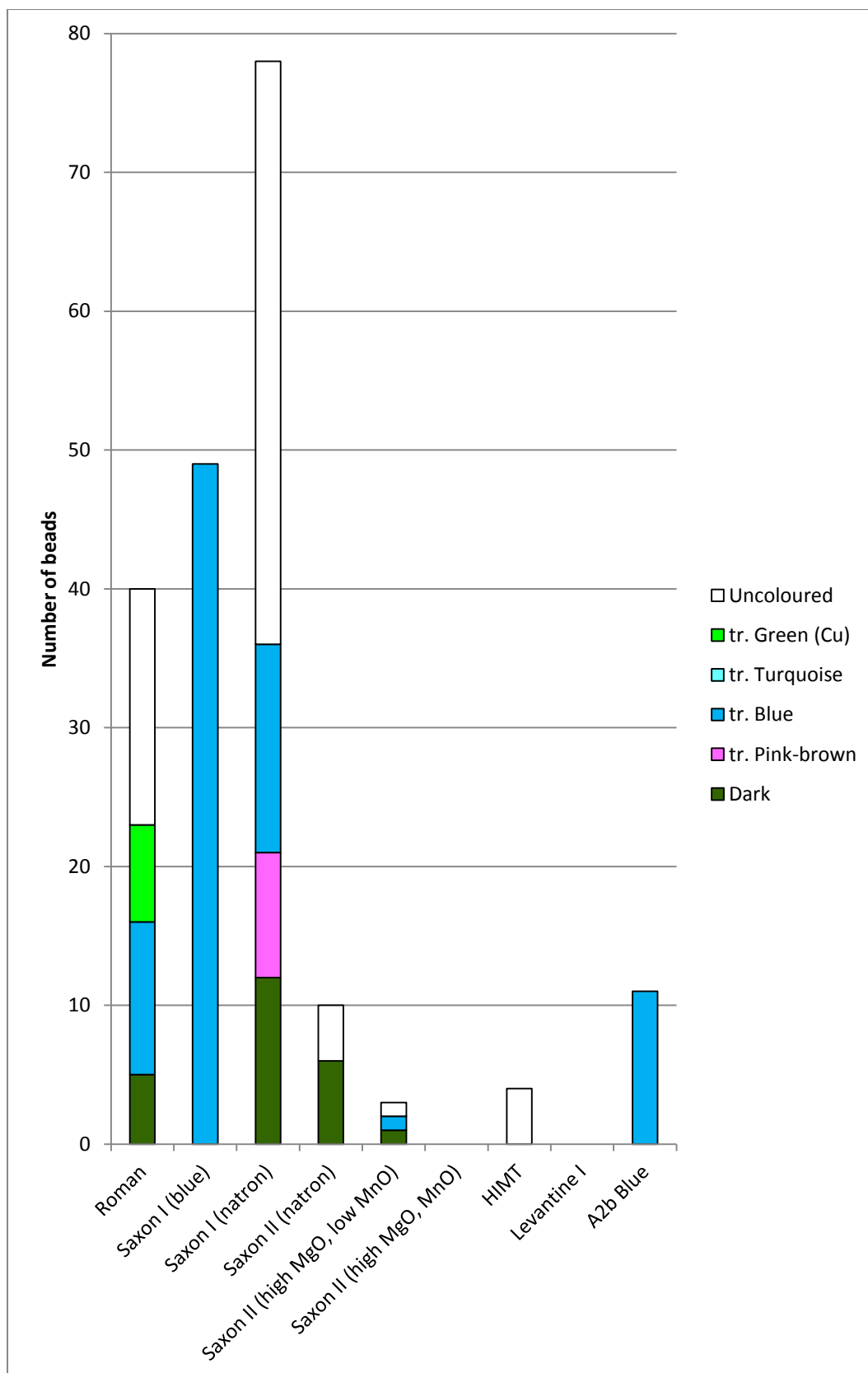


Figure 4.9.3 – Stacked histogram showing the relationship between the different base glass types used for the bodies of the translucent beads from Eriswell and their colour.

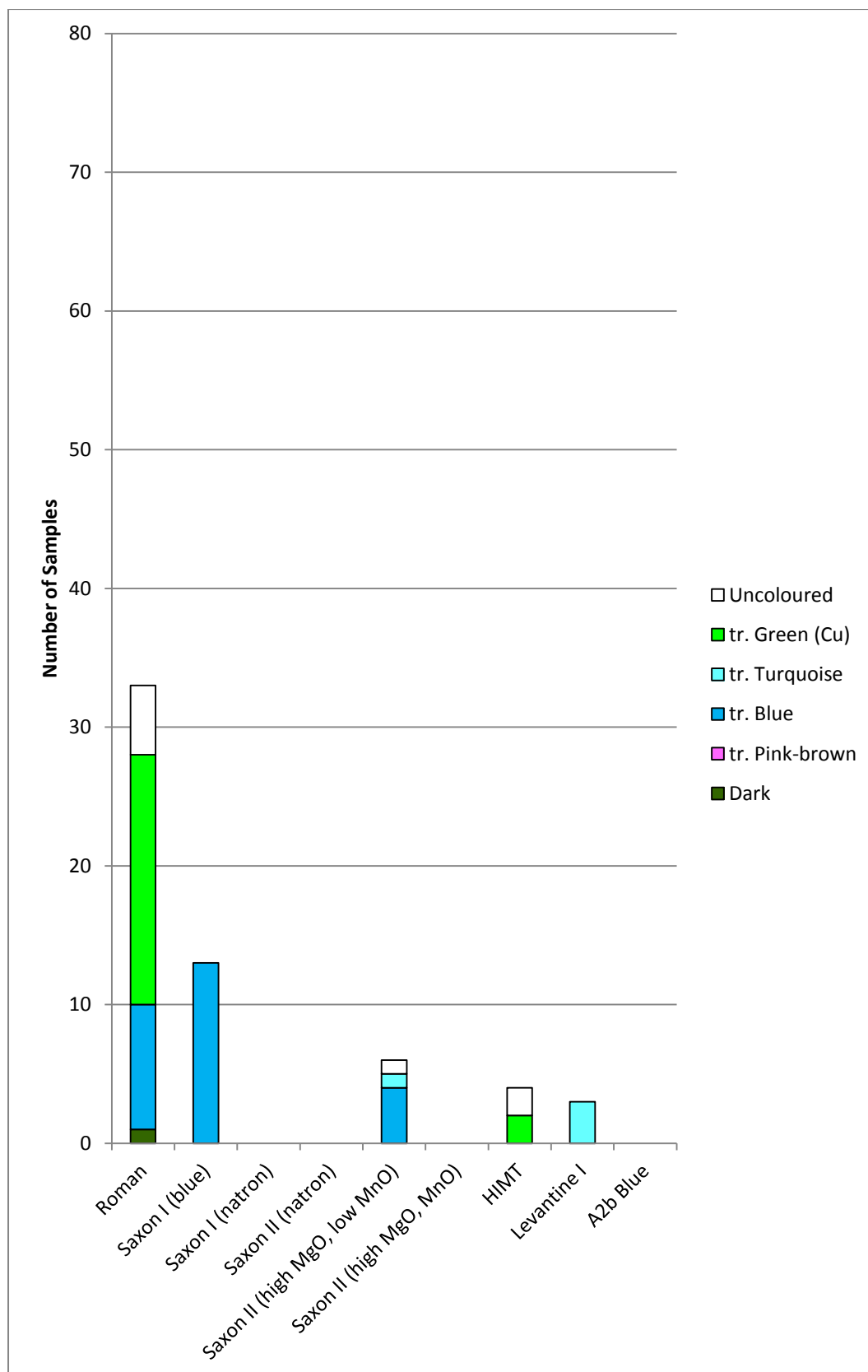


Figure 4.9.4 – Stacked histogram showing the relationship between the base glass types used for the translucent decoration on polychrome beads from Eriswell and its colour.

Translucent copper-green glass is exclusively produced using a 'Roman' base glass; although some copper-green applied decoration is produced using 'HIMT' glass. However, the majority of 'HIMT' glass is 'naturally' coloured (green tinted), so it is often difficult to distinguish between copper-green and iron-green without analysis (see Chapter 5, sections 5.1.1 and 5.1.4). Translucent pink-brown glass is exclusively of the 'Saxon I (natron)' type, as is the 'light' glass used to produce 'metal-in-glass' beads (see this chapter, section 4.10). These colours are unlikely to have been produced after the mid-6th century AD. 'Dark' glass does not appear to be peculiar to any particular glass type, and may be produced from 'Roman', 'Saxon I (natron)', 'Saxon II (natron)' and 'Saxon II (high MgO, low MnO)' glass. However, 'Dark' glass of the latter type appears to represent recycled opaque yellow glass (see Chapter 5, section 5.1.5).

The only translucent 'Levantine I' glass is turquoise in colour; all of which is present as applied decoration on otherwise opaque beads. One sample of 'Saxon II (high MgO, low MnO)' glass is also translucent turquoise, and one opaque turquoise bead is produced from 'Levantine I' glass. Considering the phases to which these glass types are attributed (see this chapter, section 4.8), turquoise glass does not seem to have been used in Anglo-Saxon beads until after the mid-6th century. Whilst one sample of 'Roman' glass is opaque turquoise, this is opacified by calcium antimonate and may represent a Roman survival, or the re-use of an opaque Roman glass (see Chapter 5, section 5.2.6).

The opaque glass colours are produced using a wider range of base glass types (Figures 4.9.5 and 4.9.6) than the translucent colours. Opaque white glass can be divided into two groups based upon the method of opacification; tin oxide or bubbles (see Chapter 5, section 5.2.1). The bubble-opacified types are exclusively produced from recycled 'Roman' glass, with the exception of one sample produced from 'HIMT' glass (also probably recycled); white bubble-opacified glass is rarely used as applied decoration. In contrast, white tin oxide opacified glass is produced from a wide range of glass types ('Roman', 'Saxon II' and 'Levantine I' glass) and is more readily used as applied decoration.

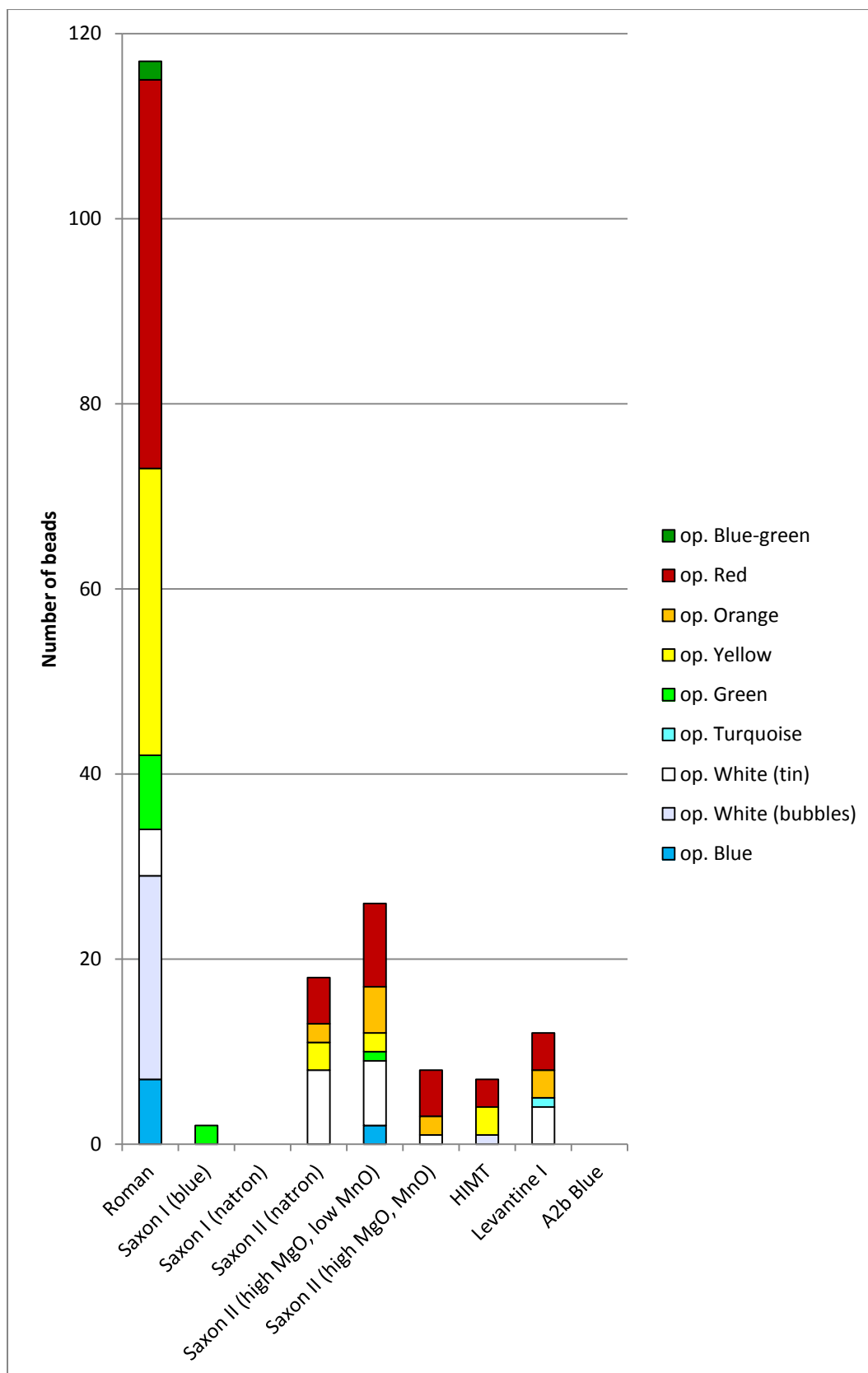


Figure 4.9.5 – Stacked histogram showing the relationship between the base glass types used for the bodies of the opaque beads from Eriswell and their colour.

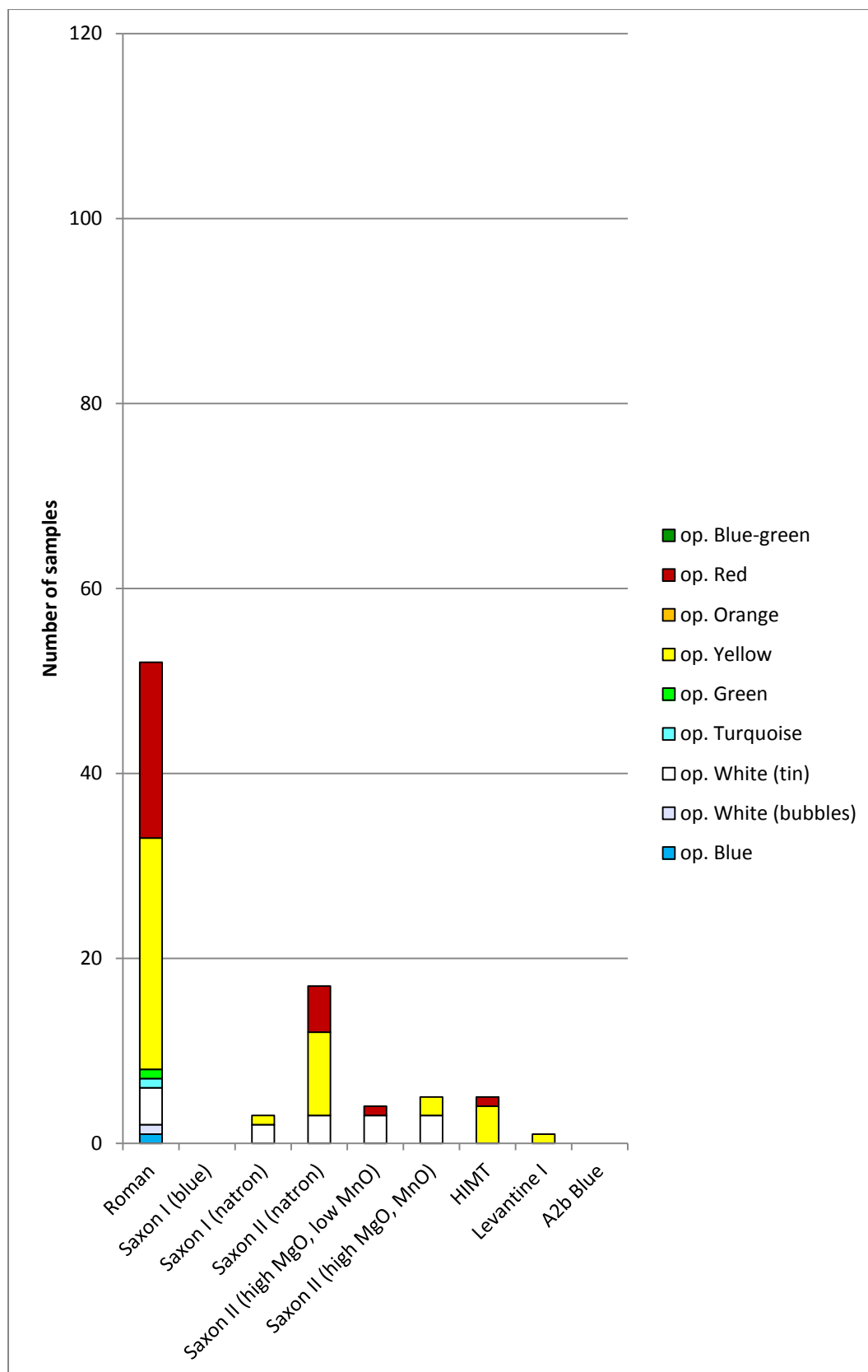


Figure 4.9.6 – Stacked histogram showing the relationship between the base glass types used for the opaque decoration on polychrome beads from Eriswell and its colour.

‘Roman’ and ‘HIMT’ glass appear to have been primarily used prior to approximately the mid-6th century, whereas ‘Saxon II’ and ‘Levantine I’ glass is more typical of beads produced after this date (see this chapter, section 4.8). Opacification by bubbles may therefore be a slightly earlier tradition than opacification by tin oxide.

These two methods of opacification (bubbles and tin oxide) may also reflect different production zones; beads produced from ‘Roman’ and ‘HIMT’ glass appear to be ‘Anglo-Saxon’ products (see this chapter, section 4.10). It is therefore possible that bubble-opacification was more of an insular Anglo-Saxon tradition, and tin oxide opacification more of a Continental tradition. Such differences may relate to the availability of tin as a raw material; British tin sources, which are primarily located in southwest England, would have been under Celtic control and therefore not easily exploitable by Anglo-Saxon craftsmen. There is now very convincing evidence relating to the geochemistry of radiocarbon-dated peat deposits on Dartmoor to suggest that there was a lull in the exploitation of tin in southwest England from c. AD 400-700 (Meharg *et al.* 2012: 725), although the scale (however small) of exploitation during this period remains unclear. However, this goes some way to supporting the view that bubble-opacification is likely to have been an Anglo-Saxon tradition.

This interpretation is borne out not only from typology and distribution patterns, but also because nearly all of the opaque white beads analysed from various sites across Merovingian Europe (approximately 100 beads) by Heck and co-workers (Heck 2000; Heck and Hoffmann 2000) contain in excess of 2% tin oxide. However, it cannot be ruled out that this trend results from the exclusion of weathered beads from their sample set; bubble-opacified glass is frequently heavily weathered (see Chapter 3, section 3.3).

Opaque blue glass from Eriswell corresponds closely to the technology of opaque white glass (see Chapter 5, section 5.2.5). All of the opaque blue glass produced from ‘Roman’ glass is opacified by bubbles, whereas that produced from the other glass types is opacified by tin oxide. As with the opaque white glass, this suggests

that bubble-opacified glass was probably primarily produced prior to approximately the mid-6th century and tin oxide opacified glass primarily after this date.

Opaque yellow glass from Eriswell is predominantly produced from ‘Roman’ glass, but small quantities are also produced from ‘Saxon II (natron)’, ‘Saxon II (high MgO, low MnO)’ and ‘HIMT’ glass. Similarly, opaque yellow glass used as applied decoration is typically produced from ‘Roman’ or ‘Saxon II (natron)’ glass, but small quantities were also produced from ‘Saxon II (high MgO, MnO)’, ‘HIMT’ and ‘Levantine I’ glass. It therefore seems likely that opaque yellow glass was produced throughout the early Anglo-Saxon period. Opaque green glass is similar in technology to opaque yellow glass (see Chapter 5, section 5.2.2), but appears to have only been produced from ‘Roman’ glass in any quantity. Two opaque green *Green Constricted Segmented* beads are attributed to the ‘Saxon I (blue)’ type, but these are in fact likely to represent products of a different workshop (see above). Figure 4.9.6 demonstrates that opaque green glass was rarely used as applied decoration. It therefore seems that opaque green glass was rarely produced after approximately the mid-6th century.

Opaque red glass is very common at Eriswell and is produced from a range of different base glass types, indicating that it was probably produced throughout the early Anglo-Saxon period. It is most commonly produced from ‘Roman’ glass, but a significant proportion is also produced from ‘Saxon II’, ‘HIMT’ and ‘Levantine I’ glass. It was also commonly used as applied decoration. Conversely, opaque orange glass clearly represents a late introduction, and is unlikely to have been produced prior to the mid-6th century; it is only produced from ‘Saxon II’ and ‘Levantine I’ glass. It does not feature in ‘earlier’ bead types, and is not found on polychrome beads; it is peculiar only to monochrome beads of Brugmann’s *Orange* type. Lastly, the opaque blue-green glass of the ‘Roman’ type is very uncommon. This is likely to represent a one-off product, as its colourant technology is extremely unusual (see Chapter 5, section 5.2.7).

Overall, ‘Roman’, ‘Saxon II’, ‘HIMT’ and ‘Levantine I’ glass appear to have been predominantly used to produce opaque colours. In contrast, ‘Saxon I’ and ‘A2b Blue’ glass was almost exclusively used in the production of translucent colours.

‘Saxon I (blue)’ and ‘A2b Blue’ glass are probably exclusively translucent blue. It is possible that these glass types were exported to a limited number of workshops which specialised only in the production of translucent blue glass beads. However, it is notable that a small but significant quantity of ‘Saxon I (blue)’ glass was applied as decoration in the production of opaque polychrome beads which, with the exception of one bead (ERL104:G109:1100, *Dot34*), were exclusively produced from ‘Roman’ glass. This suggests that blue glass was generally not coloured in the same workshops as those producing other glass colours; it is instead likely to have been imported ready-coloured.

If uncoloured ‘Saxon I (blue)’ and ‘A2b Blue’ glass was being coloured on a local or regional scale in northwestern Europe, one would expect to see other colours of glass produced from these base glass types. This would have also have necessitated a trade in cobalt, which would probably have had to have been imported, as it would have been a scarce and probably expensive colourant. It is just possible that there were workshops specialising in the colouring of blue glass (*e.g.* in northwestern Europe) prior to its distribution, but this is unlikely as it would have been far more cost-effective (*i.e.* fuel efficient) to add the colourant during the production of the primary glass itself.

On balance, it seems likely that the majority of translucent blue glass, particularly ‘Saxon I (blue)’ and ‘A2b Blue’ glass, was coloured in the primary workshops in which the glass itself was produced, which would have negated the need for cobalt by British or northwestern European workshops. This is most likely to have taken place in the Near East, in the large primary glassmaking institutions producing this glass from its raw materials. The export of ready-coloured glass would have meant that the production of translucent blue beads could take place on more of a national or regional (or even local) scale, without being dependent upon a source of cobalt.

The picture is far less clear with regard to ‘Saxon I (natron)’ glass. It was used to produce a limited range of colours, including translucent blue, translucent pink-brown and ‘dark’ glass, or left uncoloured; the majority of the uncoloured glass is represented by ‘metal-in-glass’ beads. Many of these colours would have required specialist raw materials; cobalt for translucent blue, manganese for translucent pink-

brown and gold or silver for the production of 'metal-in-glass' beads. It is therefore likely that at least some of these colours were produced and/or used by a limited number of specialist workshops. The presence of cobalt-blue glass of this type makes it tempting to assume that blue 'Saxon I (natron)' glass was also imported ready-coloured, but there is less evidence to support this view here.

It is likely that manganese was added as a decolourant in 'Saxon I (natron)' in the Near East, where this glass is likely to have been produced. This interpretation stems from the use of similar sand sources in both 'Saxon I (blue)' and 'Saxon I (natron)' glass (see this chapter, section 4.4); the addition of manganese appears to have been tightly controlled in 'Saxon I (natron)' glass, but was a more haphazard addition in 'Saxon I (blue)' glass. Its controlled addition as a decolourant would have been unnecessary in 'Saxon I (blue)' glass because undesirable tints would have been masked by the cobalt colourant. However, its addition to 'dark' 'Saxon I (natron)' glass is similarly unnecessary, and yet it was clearly added in controlled amounts. This suggests that 'dark' 'Saxon I (natron)' glass of this type was probably coloured in northwestern Europe, although it remains unclear as to where blue or pink-brown glass of this type was coloured.

In contrast to 'Saxon I' glass, 'Roman', 'Saxon II', 'HIMT' and 'Levantine I' glass was used to produce a range of different glass colours. It is likely that these glass types were all more widely distributed, probably being used by workshops working on more of a regional or local scale to produce a range of different, less specialised, glass colours. The raw materials necessary to produce these colours (lead, tin, copper) would probably have been far more easily obtainable and cheaper than those needed to produce blue (cobalt) and 'metal-in-glass' (gold or silver) beads. There is also evidence suggesting that some workshops operating in the 6th and 7th centuries are likely to have had access to more than one type of glass (see this chapter, section 4.10.3.3).

4.10. Relationship to Brugmann's Bead Typology

In the present study, the bead type definitions established by Brugmann (2004) and Penn and Brugmann (2007) are used to describe the beads analysed from Eriswell. The reader is invited to consult these studies for a detailed discussion of individual bead types, together with their distribution patterns. However, a number of beads from Eriswell are not covered by these typologies. The definitions of these types are primarily based upon colour and colour combinations, as established by Brugmann; monochrome beads are further defined by shape (*e.g. Brown Cylindrical, Red Melon*, etc.) and polychrome beads by decorative design (*e.g. WhitePoly1, WhitePoly2, RedPoly1, RedPoly2*, etc.) (Birte Brugmann, pers. comm.). Full type definitions for the beads discussed in this study are presented in *italics* in text, but abbreviated type definitions (see Brugmann 2004) are sometimes used in tables and figures.

The aim of the present section is to examine the associations between the composition and chronological and typological attributions of specific bead types, with a view to being able to date the more obscure types; *e.g.* monochrome beads which otherwise have limited stylistic features. A further aim is to examine the associations between the composition of purportedly 'Continental' and 'Anglo-Saxon' bead types, according to the distribution patterns set out in Brugmann (2004), with a view to establishing whether beads purportedly produced in different production zones can be compositionally differentiated.

Figure 4.10.1 shows the number of monochrome and polychrome bead types produced using the different base glass types identified at Eriswell. It is clear that 'Saxon I (blue), 'Saxon I (natron)' and 'A2b Blue' glass was used almost exclusively in the production of monochrome beads; these glass types are among the earliest (see this chapter, section 4.8). However, there is no clear trend with regard to the other glass types identified, which all appear to have been used to produce a roughly equal proportion of both monochrome and polychrome bead types. On the Continent the proportion of polychrome beads types appears to have increased relative to monochrome types towards the late 6th century and into the 7th century (Brugmann 2004: 37). Bead strings prior to this tended to be more heterogeneous, consisting of

beads of varying shapes and colour; typically green and blue (Brugmann 2004: 38). In early Anglo-Saxon England there is a general increase in the number of bead types which can be paralleled with Continental bead types towards the end of the 6th century (Brugmann 2004: 38).

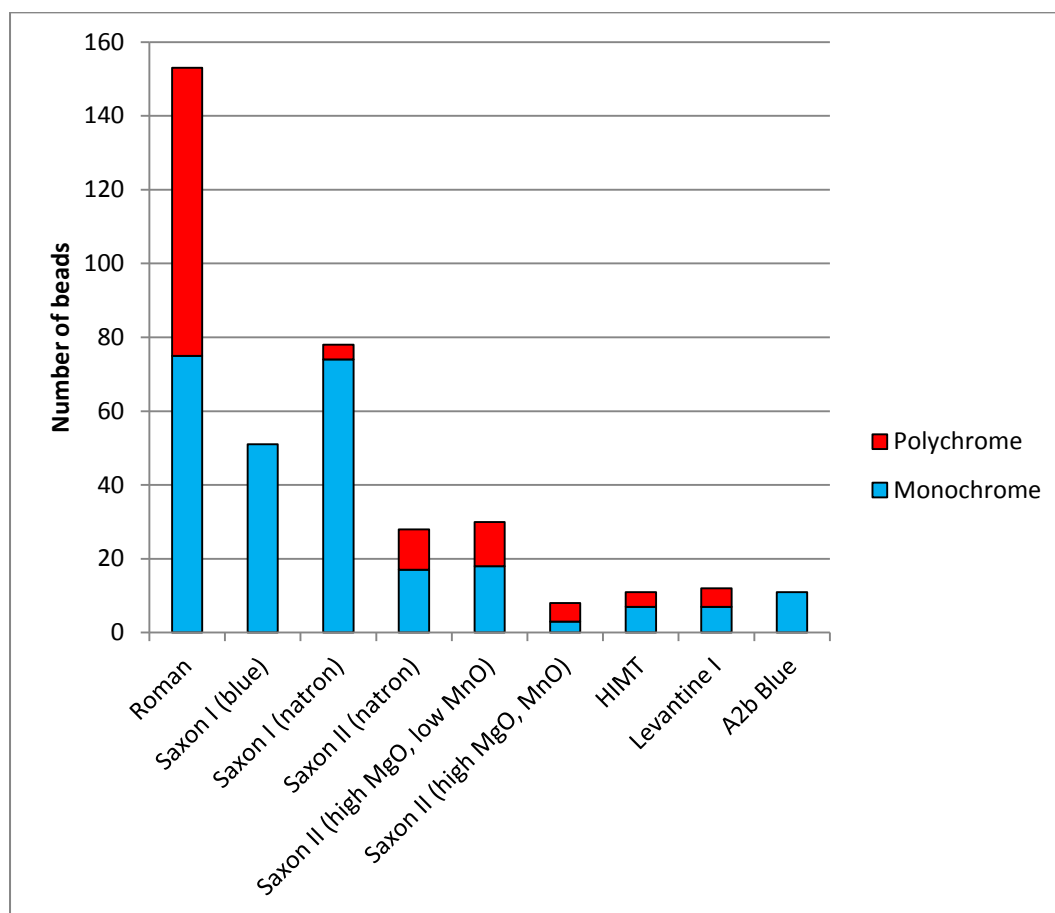


Figure 4.10.1 – Stacked histogram showing the relationship between the base glass types used for the bodies of the polychrome and monochrome beads from Eriswell.

4.10.1. Bead Type Chronology

Figures 4.10.2-4.10.5 show the different base glass types used to produce the bodies of the different bead types from Eriswell (*i.e.* the number of beads) and the applied decoration on the polychrome bead types respectively (see this chapter, section 4.8 for the separate treatment of polychrome decoration). These have been ordered by their phase attributions, and alphabetically within these divisions. The sub-types of ‘Saxon I’ and ‘Saxon II’ glass (see this chapter, section 4.4) are presented in separate histograms for simplicity; the inclusion of all glass groups and sub-groups in the same graph complicates interpretation somewhat. All of these graphs should be cross-referenced with this chapter, section 4.8 (particularly Figure 4.8.5).

Figures 4.10.2-4.10.5 show that the chronological attribution of individual bead types is in close agreement with their composition (see this chapter, section 4.8); beads attributed to Brugmann’s phase A are typically produced from the ‘earlier’ glass types (‘Roman’, ‘HIMT’, and ‘Saxon I’ glass), whereas beads attributed to Brugmann’s phases B and C are typically produced from the ‘later’ glass types (‘Saxon II’ and Levantine I’ glass).

Beads attributed to Brugmann’s phase A2b are produced from either ‘A2b Blue’ glass or ‘Saxon II (natron)’ glass, consistent with the apparent chronological crossover between these two glass types (*e.g.* see this chapter, section 4.8). Compositional distinctions between beads attributed to Brugmann’s phases A1 and A2 cannot be made; this may be because the chronological patterns for phase A1 and A2 beads are not clear cut (Brugmann 2004: 52). Additionally, compositional distinctions between beads attributed to Brugmann’s phases B and C are not possible.

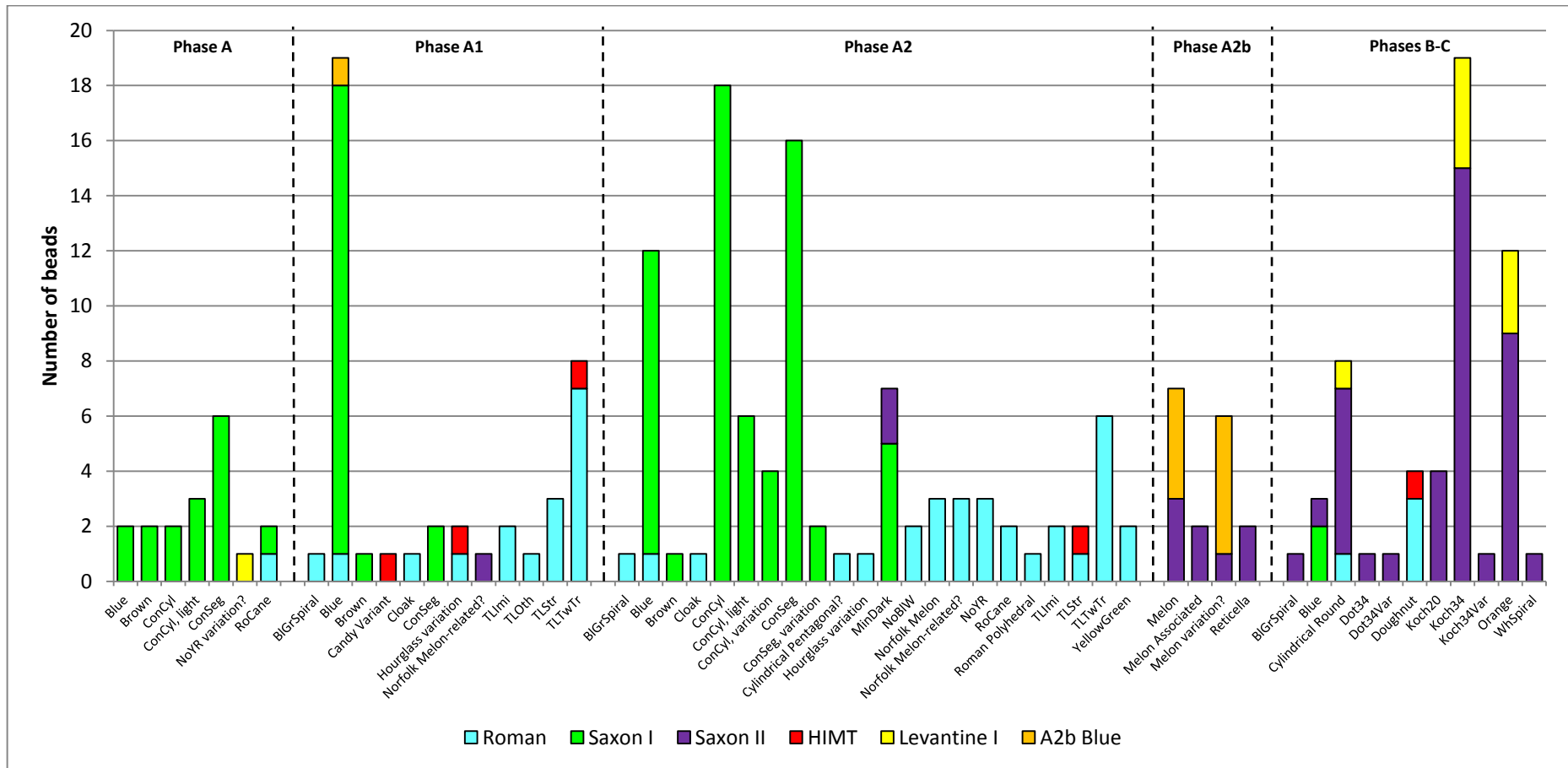


Figure 4.10.2 – Stacked histogram showing the base glass types used for the bodies of the different bead types from Eriswell, ordered by their phase attributions. These beads are covered by the typologies in Brugmann (2004) and Penn and Brugmann (2007).

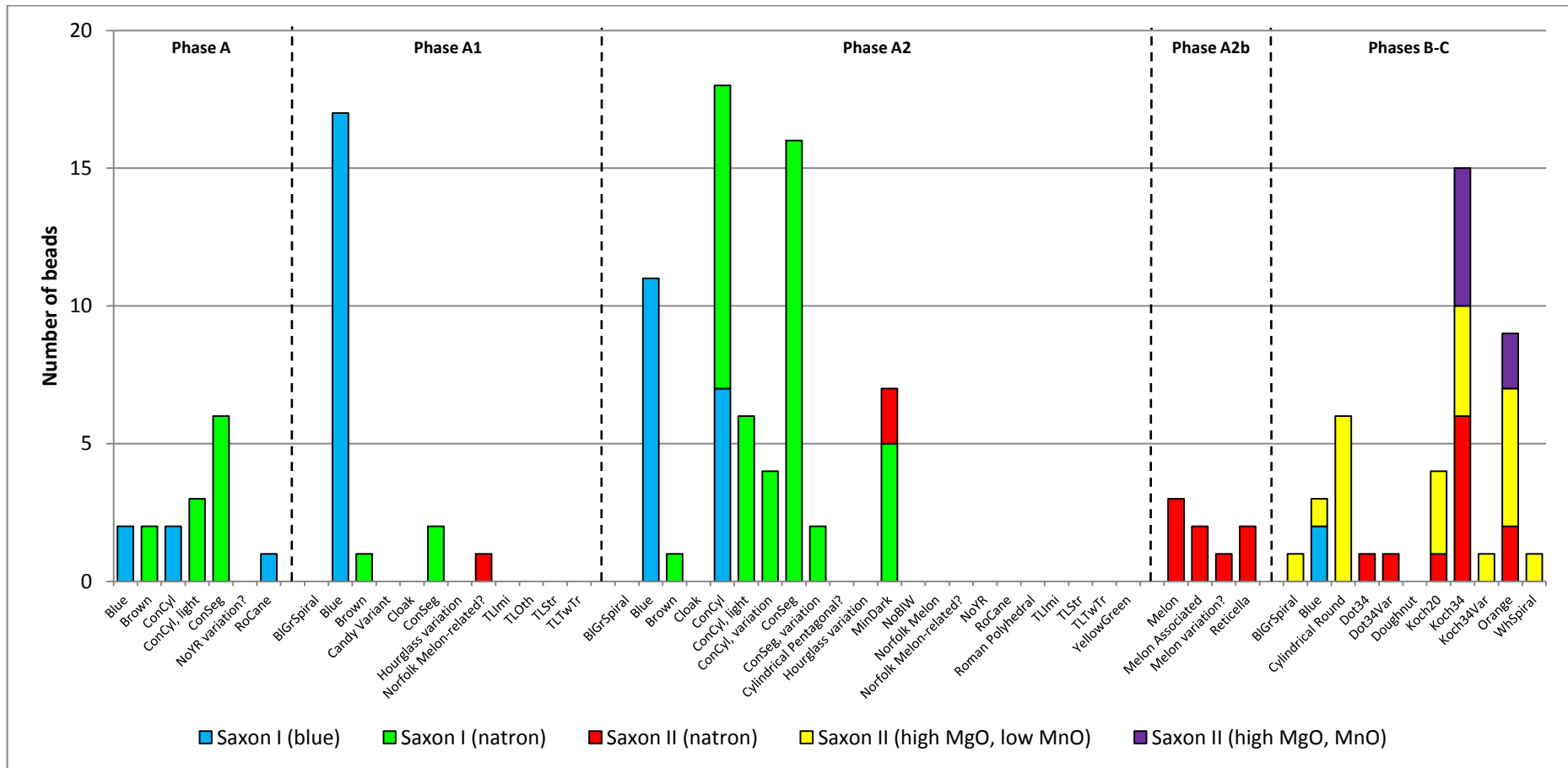


Figure 4.10.3 – Stacked histogram showing the ‘Saxon’ base glass types used for the bodies of the different bead types from Eriswell, ordered by their phase attributions. These beads are covered by the typologies in Brugmann (2004) and Penn and Brugmann (2007).

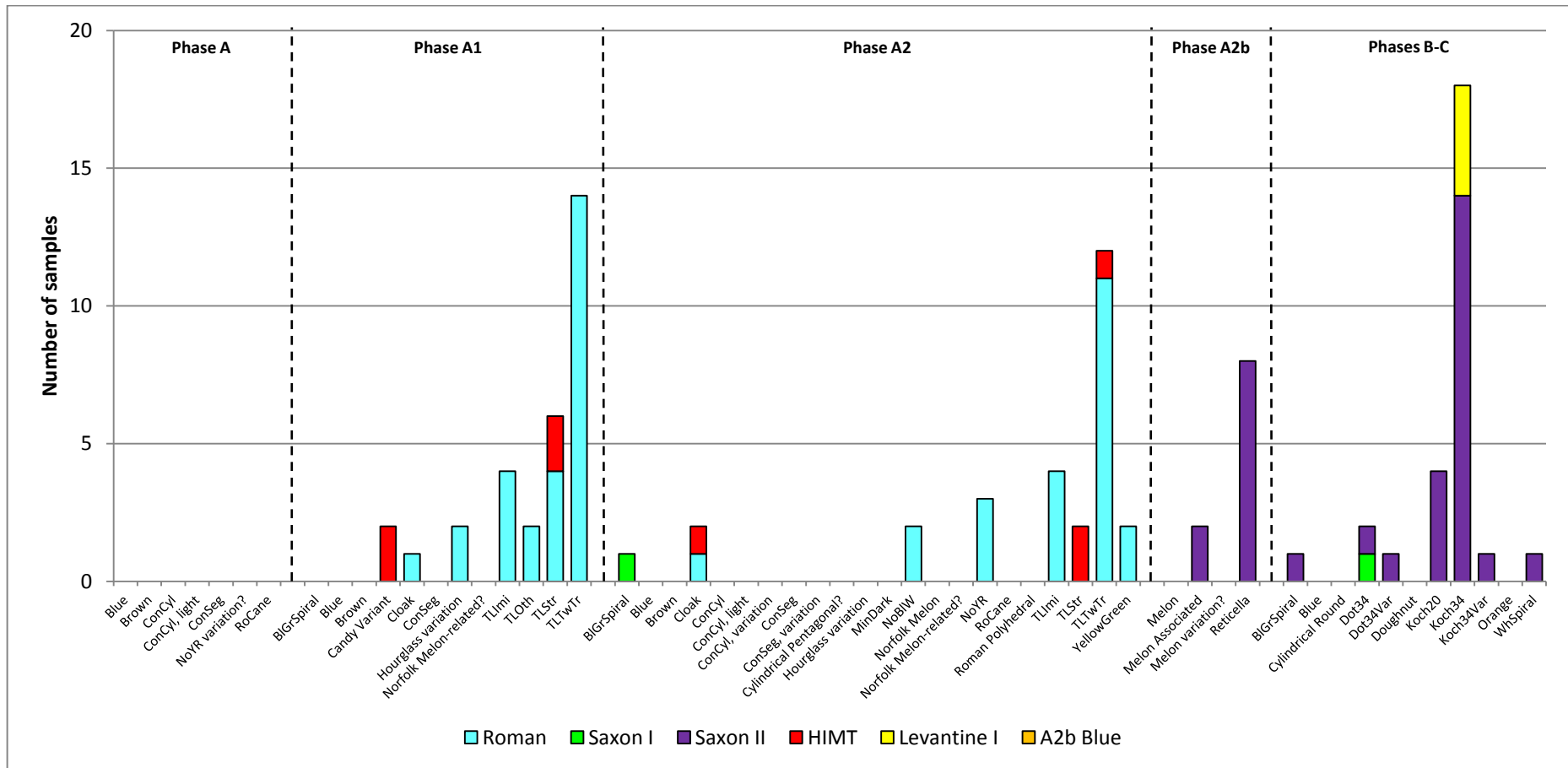


Figure 4.10.4 – Stacked histogram showing the base glass types used for the applied decoration on the different polychrome bead types from Eriswell, ordered by their phase attributions. These beads are covered by the typologies in Brugmann (2004) and Penn and Brugmann (2007).

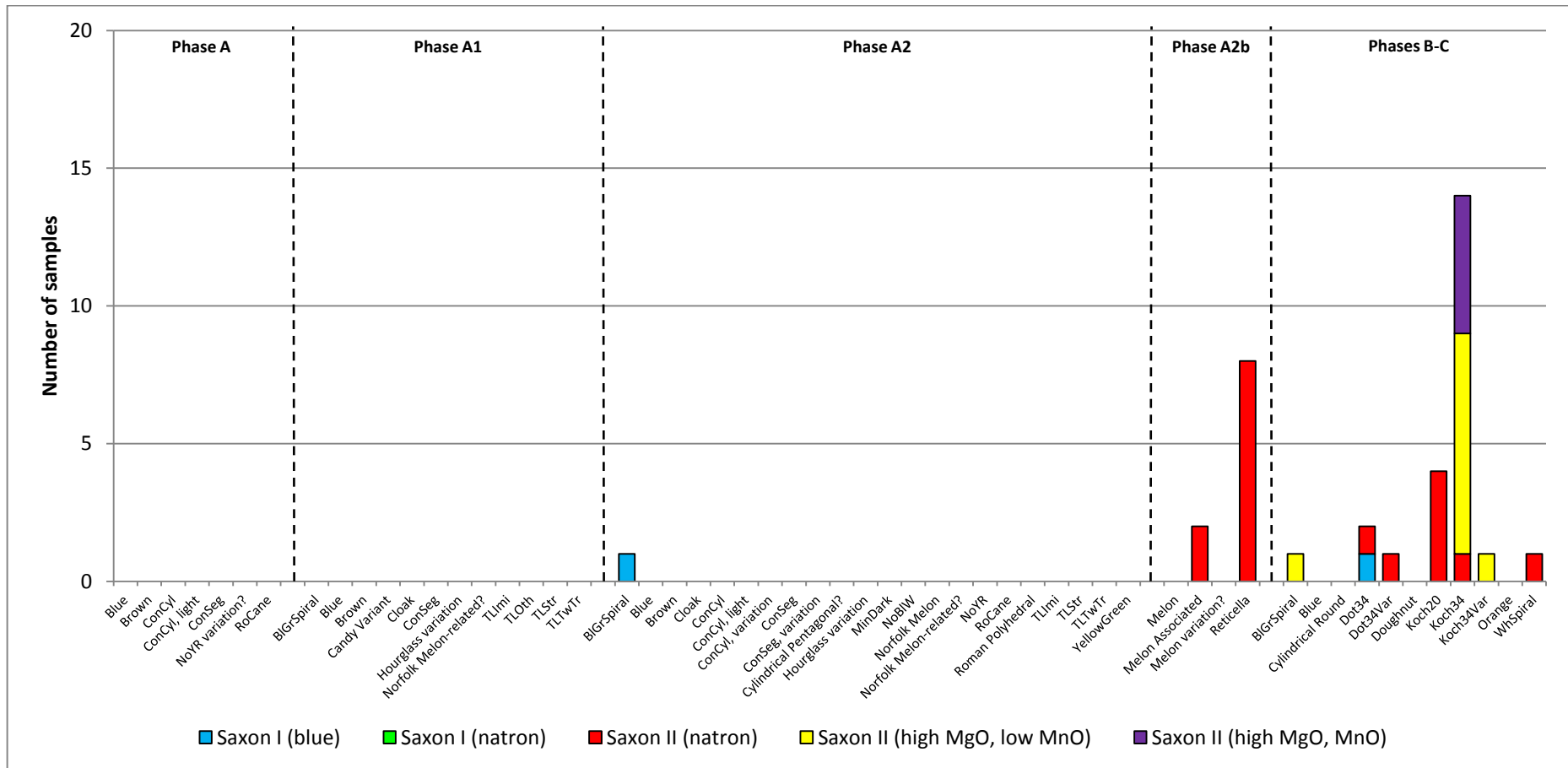


Figure 4.10.5 – Stacked histogram showing the ‘Saxon’ base glass types used for the applied decoration on the different polychrome bead types from Eriswell, ordered by their phase attributions. These beads are covered by the typologies in Brugmann (2004) and Penn and Brugmann (2007).

Figures 4.10.6-4.10.9 show data for the ‘undated’ bead types from Eriswell that are not covered by the typologies set out in Brugmann (2004) and Penn and Brugmann (2007). It is not within the scope of this study to discuss each of these bead types on a case-by-case basis, but by comparing their composition with the chronology established for the different base glass types (see this chapter, section 4.8) it is possible to attribute them approximately to one (or more) of Brugmann’s chronological phases.

Those bead types in Figures 4.10.6-4.10.9 produced from ‘Roman’, ‘Saxon I’ or ‘HIMT’ glass are more consistent with Brugmann’s phase A, whereas those beads produced from ‘Saxon II’, ‘Levantine I’ or ‘A2b Blue’ glass are more consistent with Brugmann’s phases B or C. It is clear that some bead types, including *Blue Biconical*, *Blue Globular*, *Red Globular* and *White Globular* beads, are produced from both ‘earlier’ and ‘later’ glass types. The bead types in question are almost exclusively opaque monochrome types, and their composition suggests that they are likely to have been produced over a much longer period of early Anglo-Saxon history than polychrome and translucent monochrome bead types, as might be expected.

From these data, it is possible to predict the composition of those beads which have not been analysed, as some bead types are typically (sometimes exclusively) produced from certain base glass types. This is summarised in Appendix K; here, the number of each individual bead type analysed as part of the present study is detailed, alongside the number of beads of that particular type recovered from Eriswell. This should be compared to the distribution of these bead types at Eriswell, as shown in Appendix B. An attempt has been made to establish the ‘typical’ composition of certain bead types. This is relatively straightforward for some types; *e.g.* the 26 *Constricted Segmented** and 9 *Brown** beads analysed are all produced exclusively from ‘Saxon I (natron)’ glass, so the remaining 154 *Constricted Segmented** and 4 *Brown** beads can be relatively confidently attributed to the ‘Saxon I (natron)’ type. However, there are a number of bead types which may be produced from more than one base glass type.

It is possible to gauge the 'typical' composition of these bead types, but the compositional attribution of those which have not been analysed is less certain; *e.g.* the *Constricted Cylindrical* beads analysed are produced from either 'Saxon I (blue)' glass (9 beads) or 'Saxon I (natron)' glass (11 beads). Whilst the remaining 32 *Constricted Cylindrical* beads can therefore be relatively confidently attributed to the 'Saxon I' glass type in general, it is impossible to determine the exact type of glass used without analysis. Similarly, a number of bead types analysed are represented in the present study by only one or two samples. It is therefore difficult to establish the 'typical' composition of these types, as they are unlikely to be representative; to do so on the basis of such a small sample set would be very misleading.

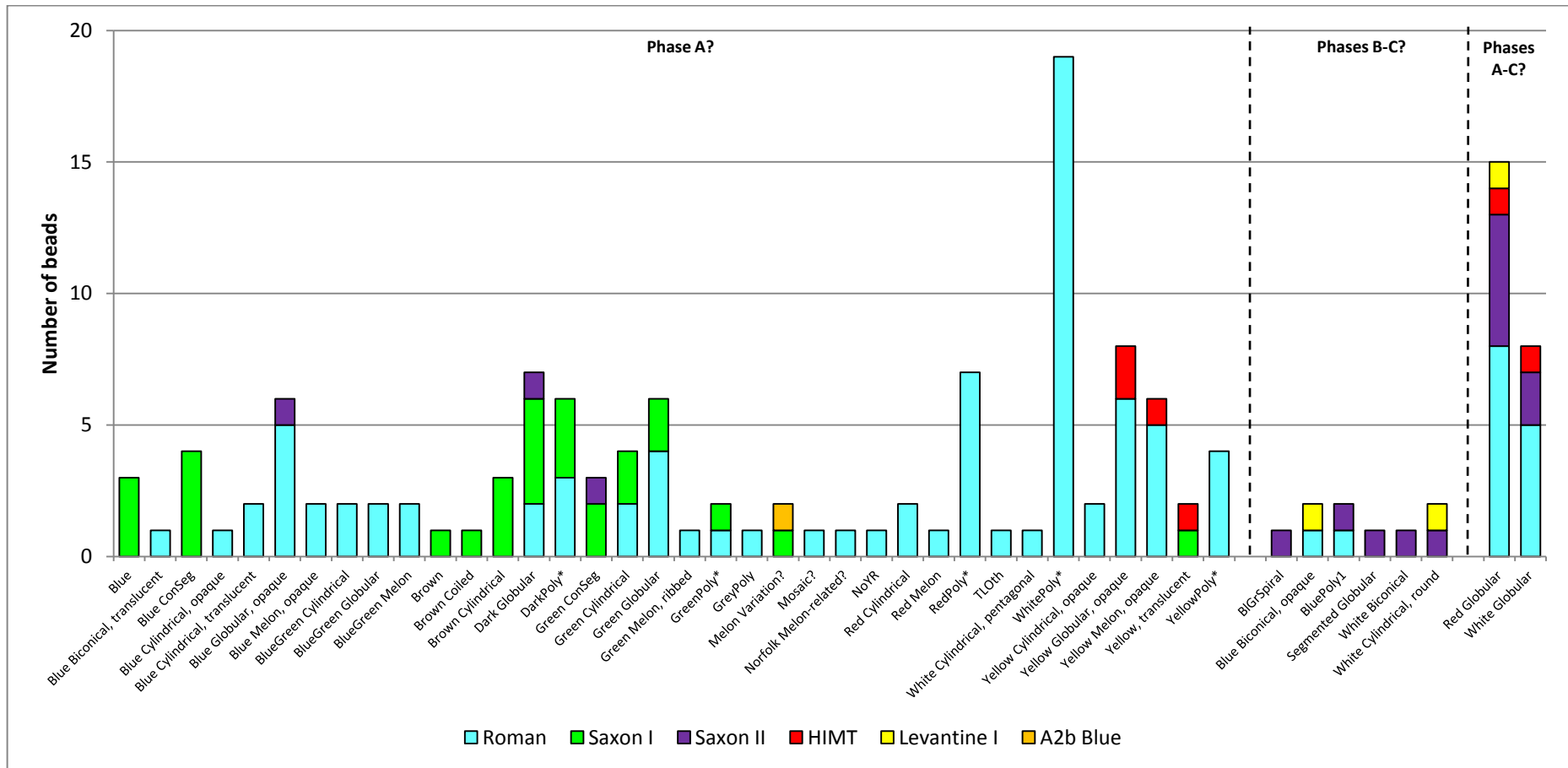


Figure 4.10.6 – Stacked histogram showing the base glass types used for the bodies of the different bead types from Eriswell, attributed to phases according to their compositional attributes. These beads are *not* covered by the typologies in Brugmann (2004) and Penn and Brugmann (2007). * denotes bead sub-types that have been grouped together.

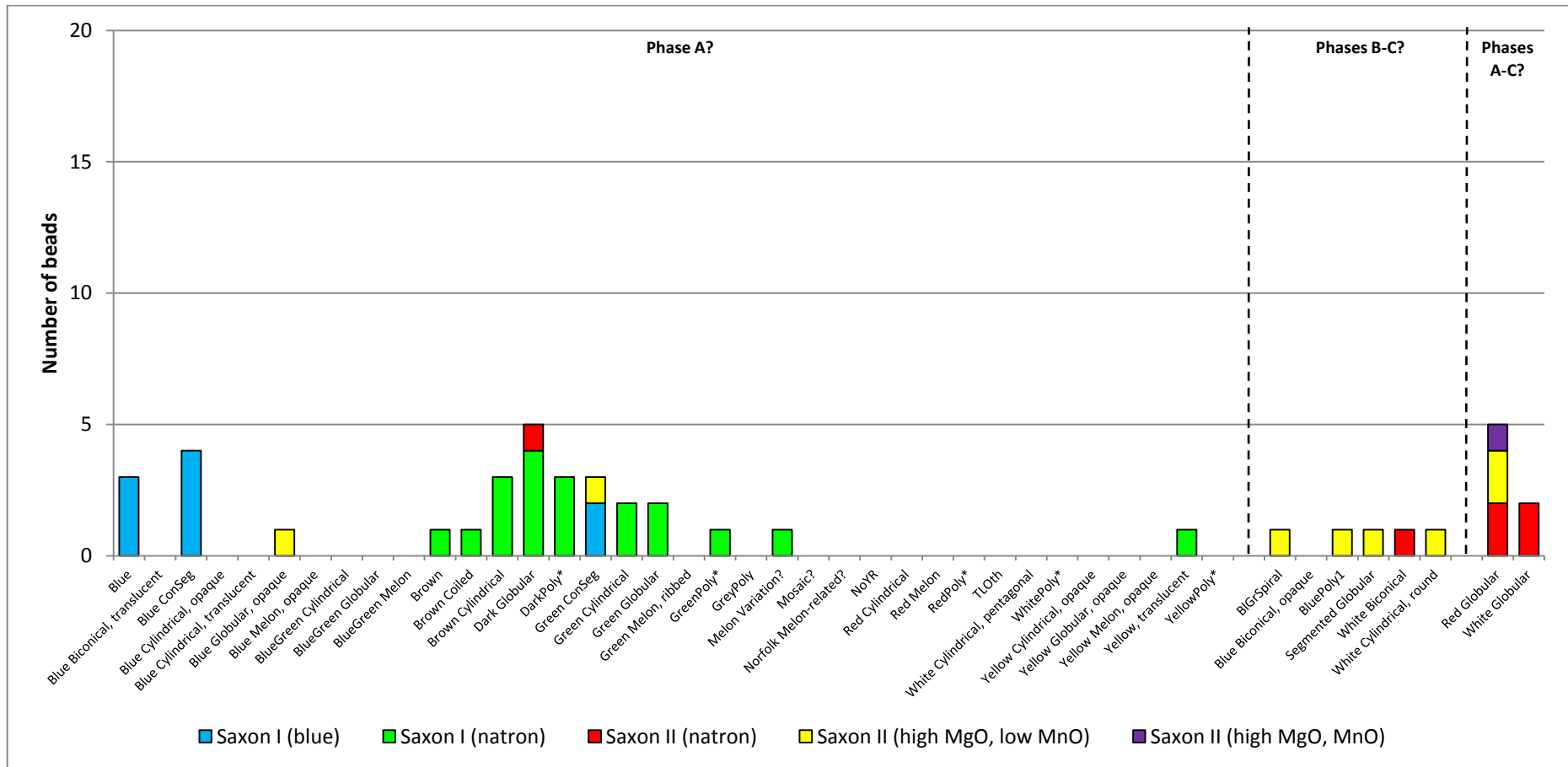


Figure 4.10.7 – Stacked histogram showing the ‘Saxon’ base glass types used for the bodies of the different bead types from Eriswell, attributed to phases according to their compositional attributes. These beads are *not* covered by the typologies in Brugmann (2004) and Penn and Brugmann (2007). * denotes bead sub-types that have been grouped together.

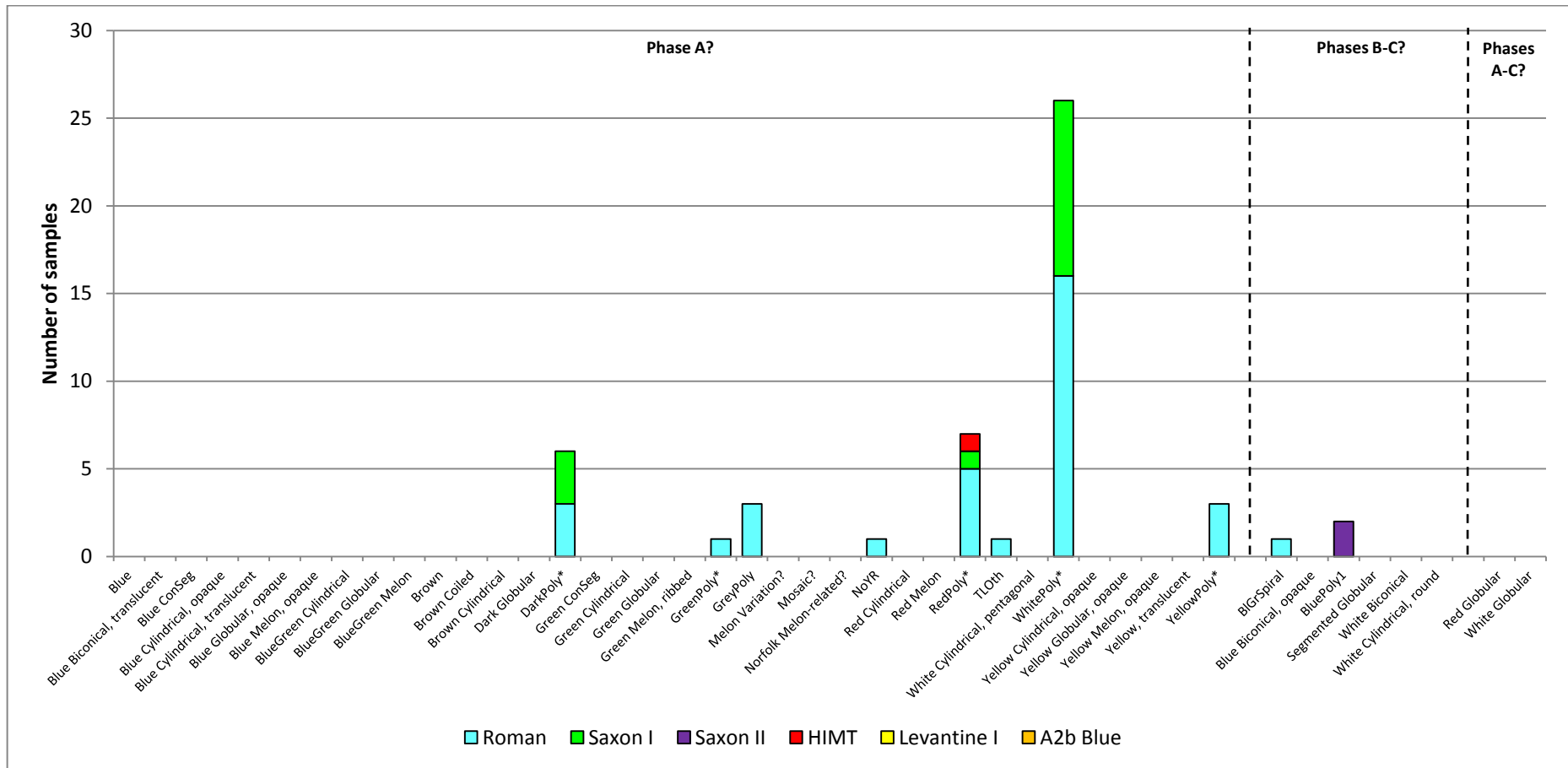


Figure 4.10.8 – Stacked histogram showing the base glass types used for the applied decoration on the different polychrome bead types from Eriswell, attributed to phases according to their compositional attributes. These beads are *not* covered by the typologies in Brugmann (2004) and Penn and Brugmann (2007). * denotes bead sub-types that have been grouped together.

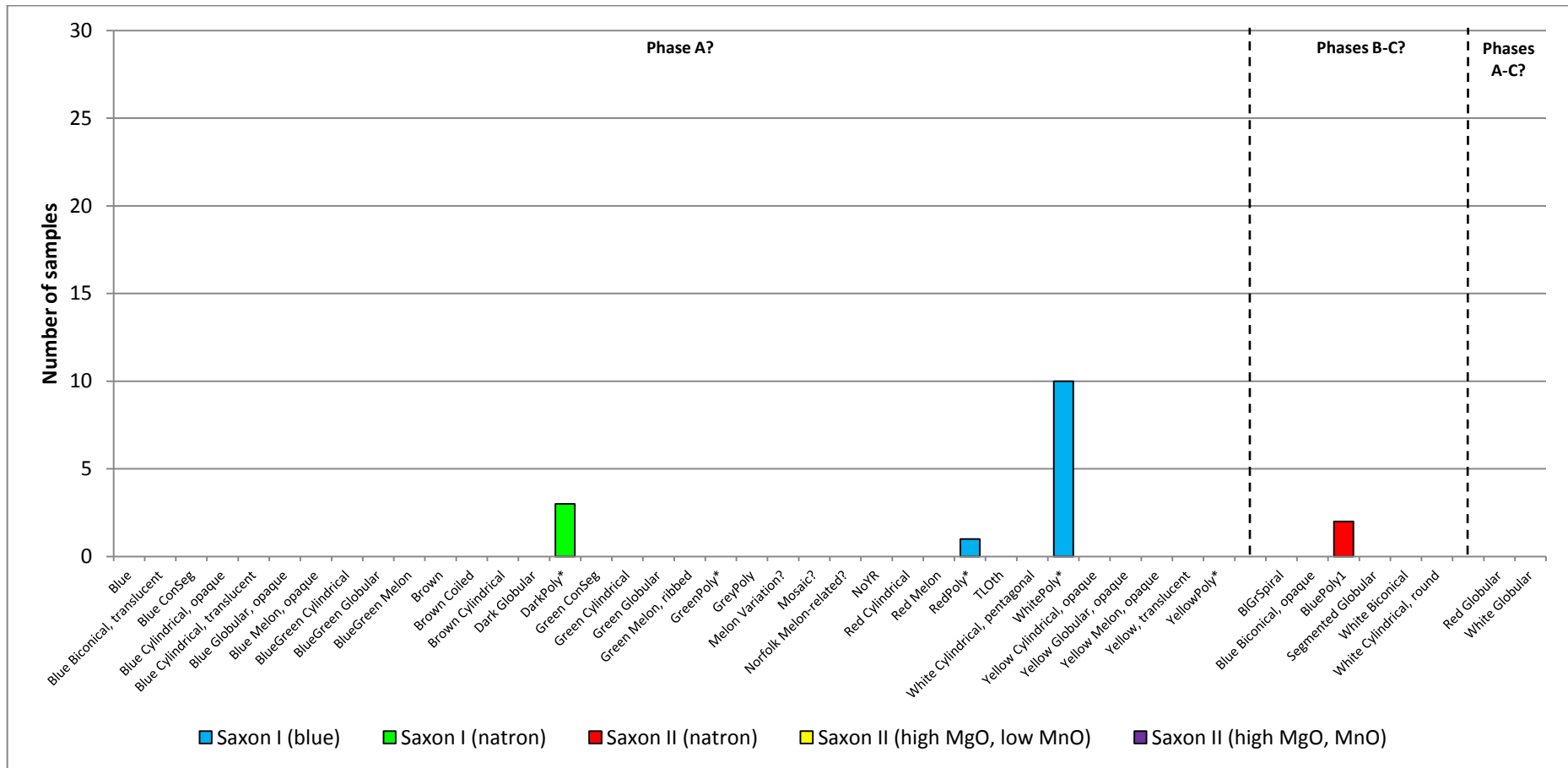


Figure 4.10.9 – Stacked histogram showing the ‘Saxon’ base glass types used for the applied decoration on the different polychrome bead types from Eriswell, attributed to phases according to their compositional attributes. These beads are *not* covered by the typologies in Brugmann (2004) and Penn and Brugmann (2007). * denotes bead subtypes that have been grouped together.

4.10.2. Bead Type Production Zones

Figures 4.10.10-4.10.13 show the different base glass types used to produce the bodies of the different bead types from Eriswell (*i.e.* the number of beads) and the applied decoration on the polychrome bead types respectively (see this chapter, section 4.8 for the separate treatment of polychrome decoration). These have been ordered by their distributions according to Brugmann (2004) and Penn and Brugmann (2007) (*i.e.* ‘Continental’ or ‘Anglo-Saxon’), and alphabetically within these divisions. The sub-types of ‘Saxon I’ and ‘Saxon II’ glass (see this chapter, section 4.4) are presented in separate histograms for simplicity; the inclusion of all glass groups and sub-groups in the same graph complicates interpretation somewhat.

As all of the glass types identified at Eriswell (including the recycled material) are likely to ultimately have their origins in the Near East, distinctions between different workshops are unexpected; their compositions will reflect the primary glassmaking institutions in which the raw glass itself was manufactured (*i.e.* the Near East), regardless of where the beads themselves were produced (see Chapter 1, section 1.4). However, distinct groups are unexpectedly apparent. The ‘Anglo-Saxon’ bead types are primarily produced from recycled ‘Roman’ or ‘HIMT’ glass. In contrast, the ‘Continental’ bead types are almost primarily from ‘Saxon I’, ‘Saxon II’, ‘A2b Blue’ and ‘Levantine I’ glass.

There are several ‘Continental’ bead types with a composition more consistent with ‘Anglo-Saxon’ production, and vice versa. The *Candy Variant* bead (ERL104:G268:3260) is assumed to be a ‘Continental’ type, but it is produced from ‘HIMT’ glass which is more consistent with ‘Anglo-Saxon’ production. However, this bead is unusual in a number of aspects (see section 4.10.3.2 below), so this cannot be confirmed. Furthermore, the ‘Continental’ *Roman* and *Mosaic?* bead types are typically produced from ‘Roman’ glass, again more typical of ‘Anglo-Saxon’ production; it cannot be ruled out that these beads may represent Roman survivals, as opposed to Anglo-Saxon beads produced from recycled ‘Roman’ glass.

The 'Anglo-Saxon' *BlueGreen Spiral* and *White Spiral* Bead types appear to be more consistent with 'Continental' production, but the presence of two *BlueGreen Spiral* beads produced from 'Roman' glass suggest that several examples are also consistent with 'Anglo-Saxon' production; it is therefore possible that this bead type was produced in both Anglo-Saxon and Continental workshops. *Blue* and *Brown* beads are commonly found in large numbers in both England and on the Continent; it has been suggested that *Blue* beads may have been manufactured in England in order to meet the large-scale demand for them (Brugmann 2004: 33; Hirst and Biek 1981: 142), and that *Brown* beads were may have been produced in the same workshops. Brugmann (2004: 33-34) attributes both bead types to 'Anglo-Saxon' production, but in the present study they have been treated separately as they are also found in large numbers on the Continent. Their composition is more consistent with 'Continental' production, suggesting that they are more likely to be imports. However, the identification of two *Blue* beads produced from 'Roman' glass suggests that isolated examples may have also been produced in England. There is evidence to suggest that a small amount of raw cobalt-blue glass may have reached England (see section 4.10.4 below), so the production of *Blue* beads in England cannot be ruled out.

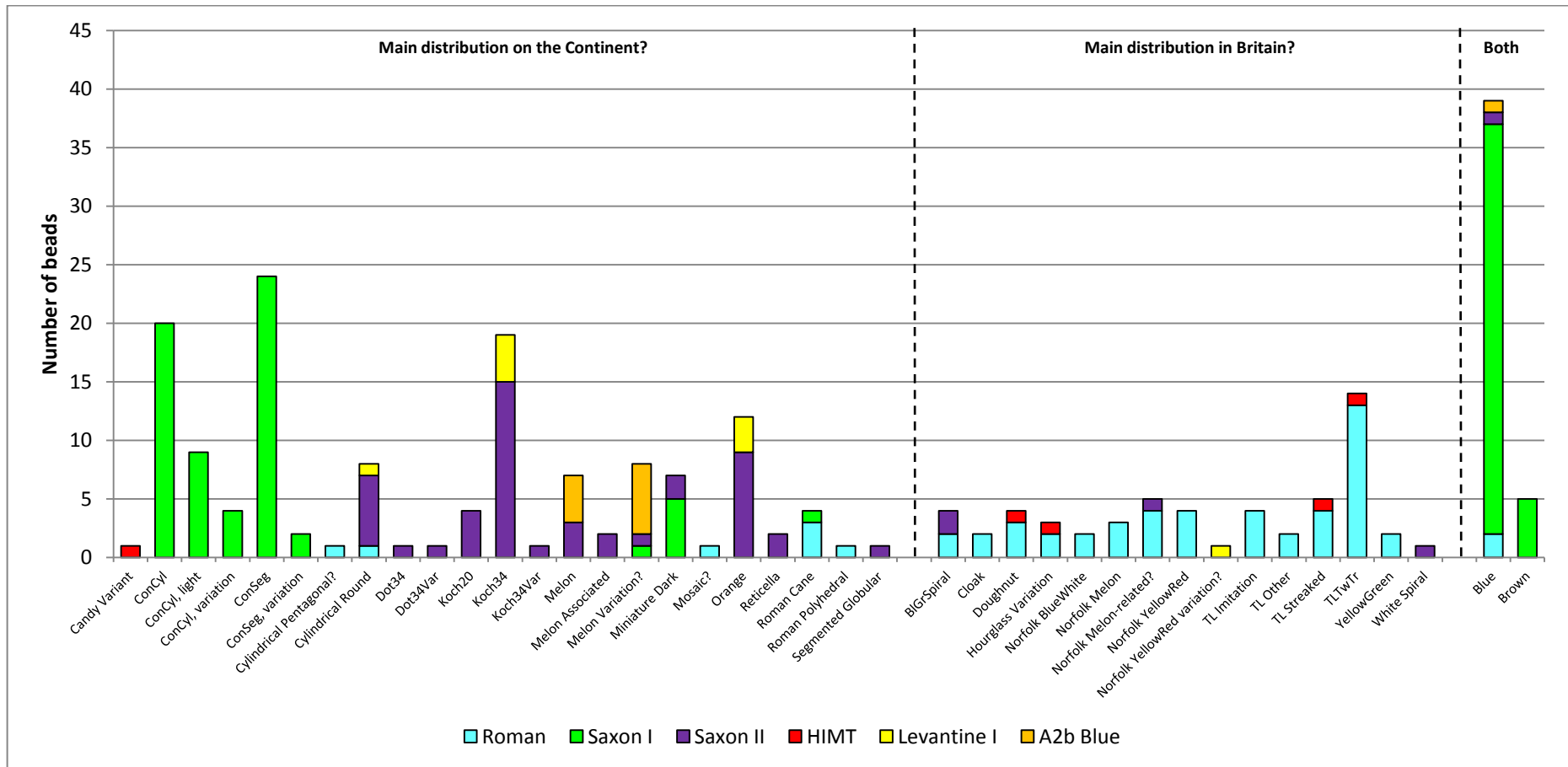


Figure 4.10.10 – Stacked histogram showing the base glass types used for the bodies of the different bead types from Eriswell, ordered by their main distribution. These beads are covered by the typologies in Brugmann (2004) and Penn and Brugmann (2007).

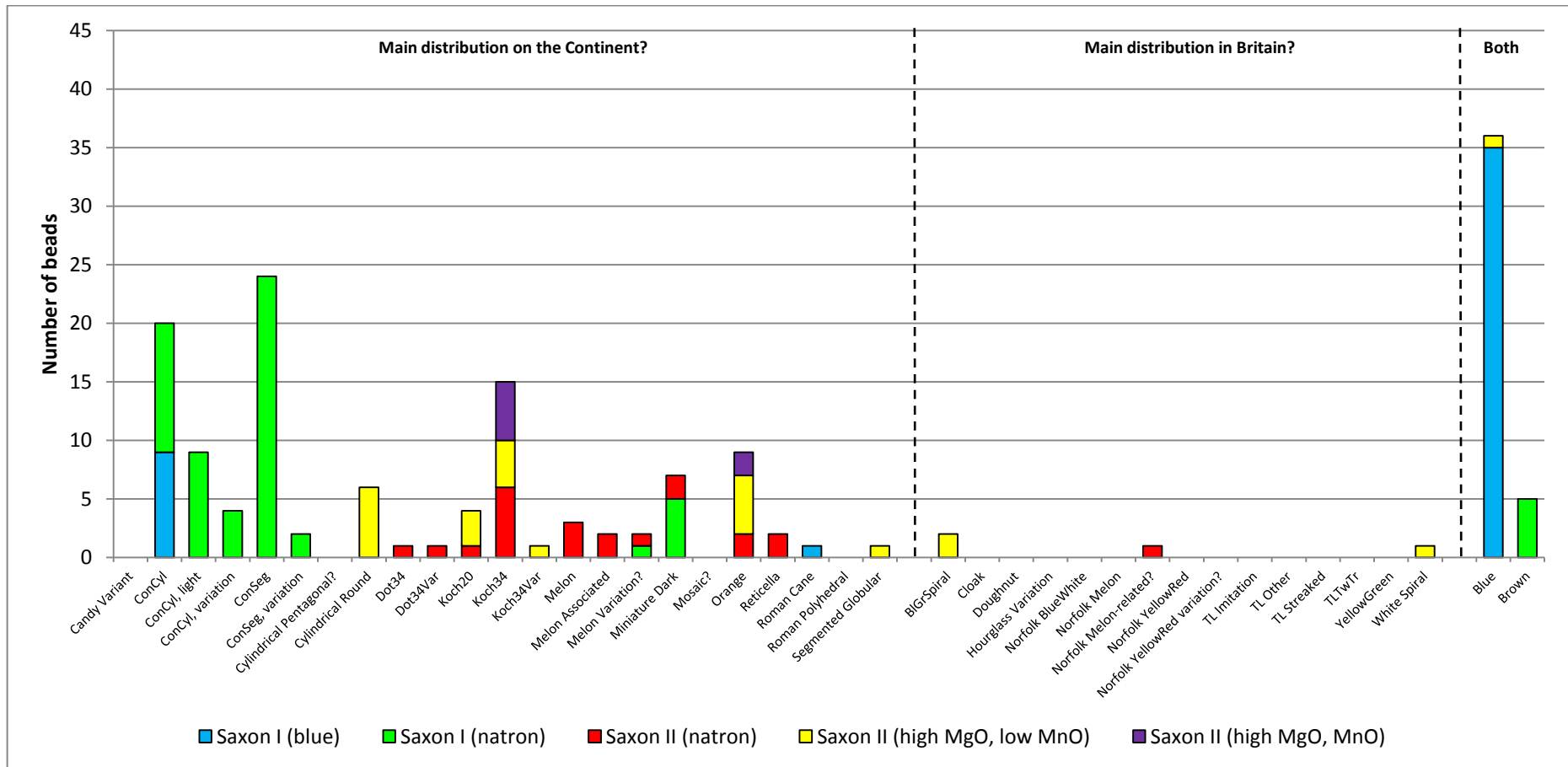


Figure 4.10.11 – Stacked histogram showing the 'Saxon' base glass types used for the bodies of the different bead types from Eriswell, ordered by their main distribution. These beads are covered by the typologies in Brugmann (2004) and Penn and Brugmann (2007).

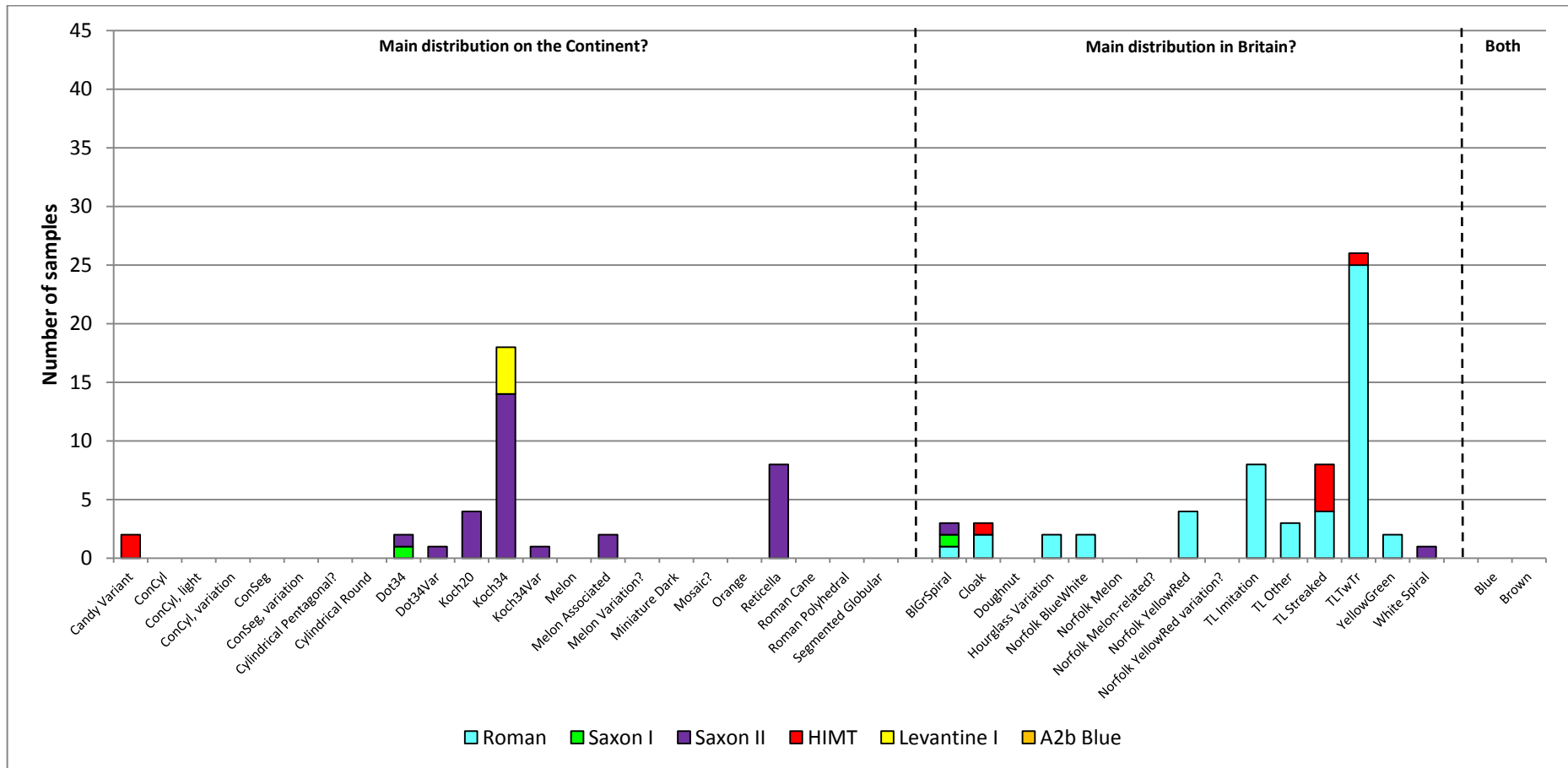


Figure 4.10.12 – Stacked histogram showing the base glass types used for applied decoration on the different polychrome bead types from Eriswell, ordered by their main distribution. These beads are covered by the typologies in Brugmann (2004) and Penn and Brugmann (2007).

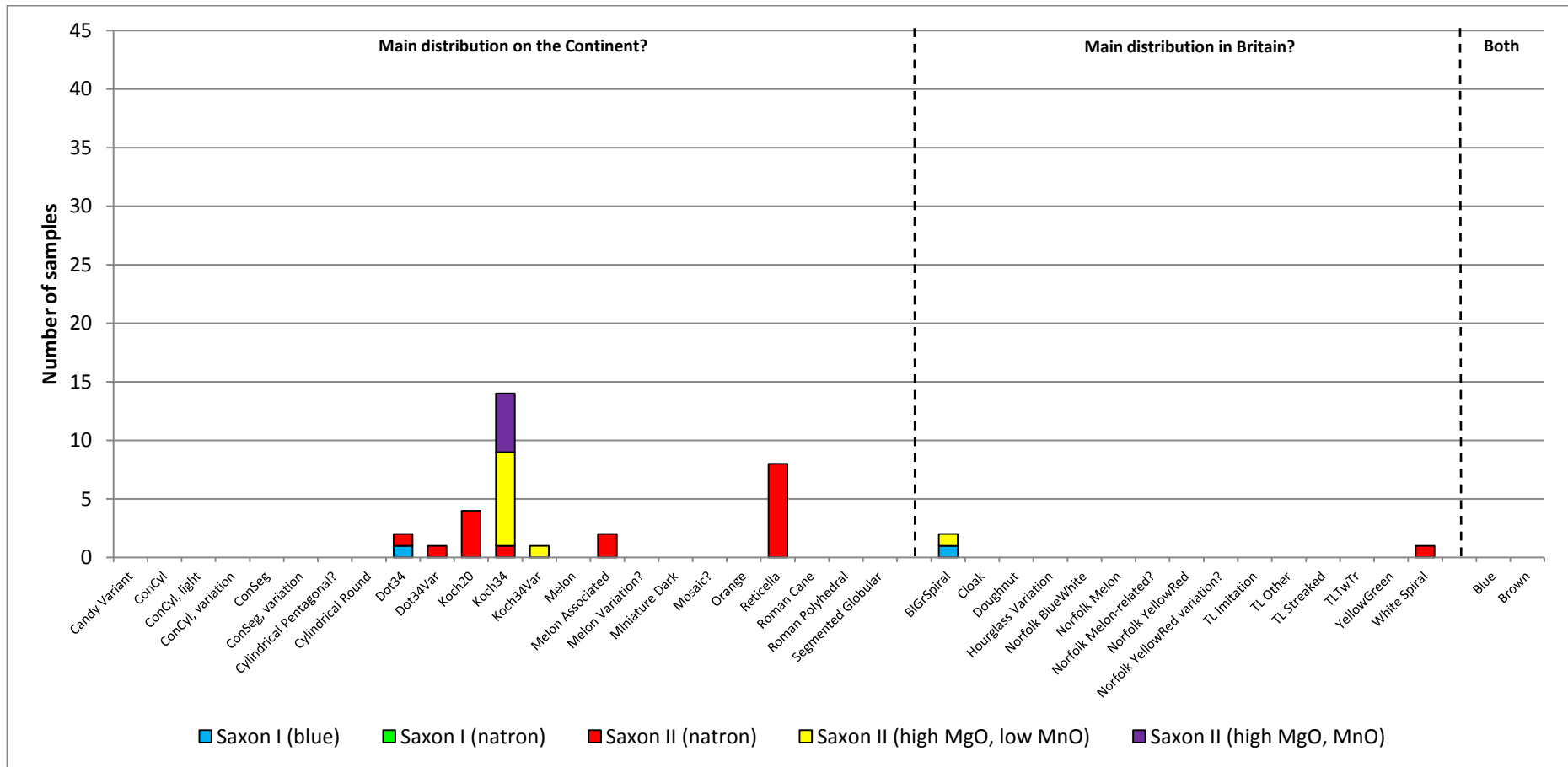


Figure 4.10.13 – Stacked histogram showing the ‘Saxon’ base glass types used for applied decoration on the different polychrome bead types from Eriswell, ordered by their main distribution. These beads are covered by the typologies in Brugmann (2004) and Penn and Brugmann (2007).

Figures 4.10.14-4.10.17 show data for the bead types not covered by the typologies in Brugmann (2004) or Penn and Brugmann (2007), ordered according to their *possible* production zones as established from examination their chemical composition. Beads produced from 'Roman' and 'HIMT' glass are generally more consistent with 'Anglo-Saxon' production, whereas those produced from other glass types are more consistent with 'Continental' production. In many cases, the compositional trends for certain bead types are to be expected; for example *Brown Coiled* and *Brown Cylindrical* beads are compositionally similar to 'Continental' *Brown* beads and are therefore likely to have a similar origin. Similarly, it is not unexpected that the majority of *Dark Globular* and *DarkPoly** beads are compositionally identical to 'Continental' *Miniature Dark* beads, which are all produced from 'dark' glass, again suggesting that they are of related production.

However, certain monochrome beads which do not have any distinctive stylistic features, including *White Globular* and *Red Globular* beads, have compositions which suggest that these types may have been produced in both 'Anglo-Saxon' and 'Continental' workshops. Interestingly, Guido (1999: 39; 44) suggests that *Yellow Melon, opaque* and *Green Melon, ribbed* beads may have been produced in Norfolk due to their concentration there, together with their general absence in Kent and on the Continent. Similarly, *Red Melon* beads have their main distribution in East Anglia (Guido 1999: 61). None of these bead types are discussed by Brugmann (2004), but their 'Roman' composition is indeed consistent with 'Anglo-Saxon' production.

The remaining beads are not well-represented types (typically represented by less than three beads at Eriswell); interpretations based on such a limited number of samples are difficult. However, the majority appear to have been produced primarily from 'Roman' glass, which is consistent with 'Anglo-Saxon' production (*e.g.* Figure 4.10.14).

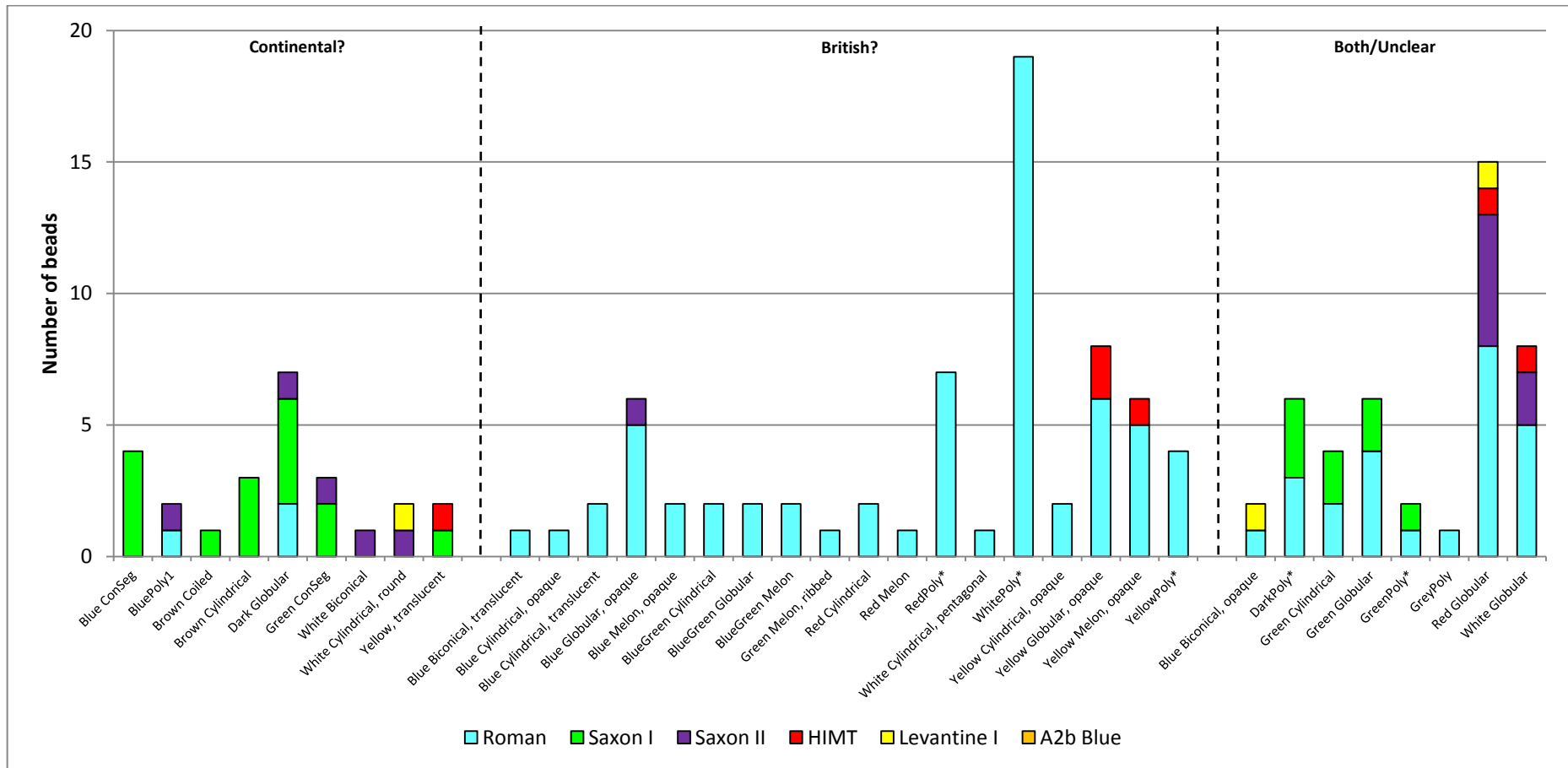


Figure 4.10.14 – Stacked histogram showing the base glass types used for the bodies of the different bead types from Eriswell, ordered by their possible production zones based upon their compositional attributes. These beads are *not* covered by the typologies in Brugmann (2004) and Penn and Brugmann (2007). * denotes bead sub-types that have been grouped together.

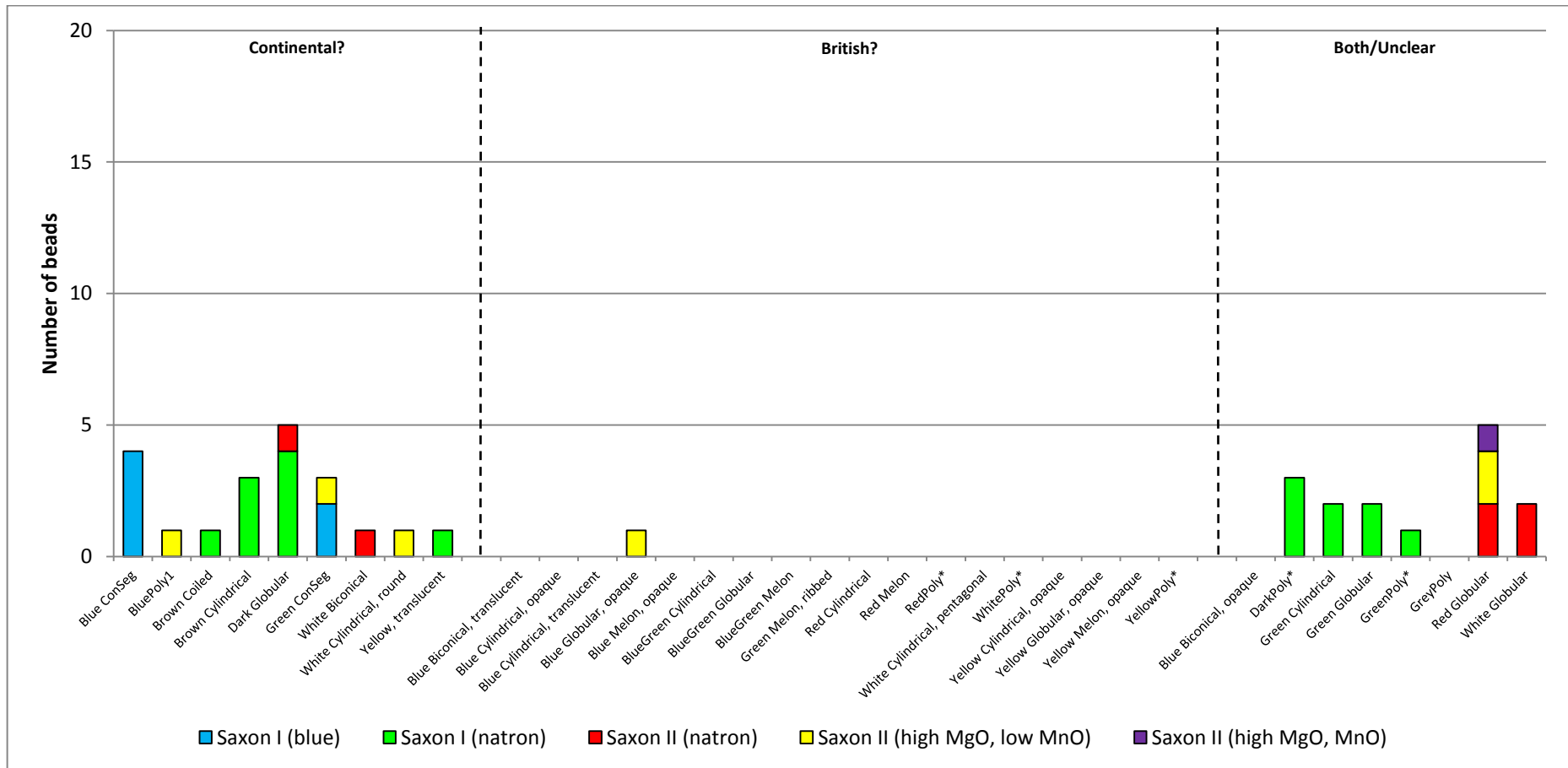


Figure 4.10.15 – Stacked histogram showing the ‘Saxon’ base glass types used for the bodies of the different bead types from Eriswell, ordered by their possible production zones based upon their compositional attributes. These beads are *not* covered by the typologies in Brugmann (2004) and Penn and Brugmann (2007). * denotes bead subtypes that have been grouped together.

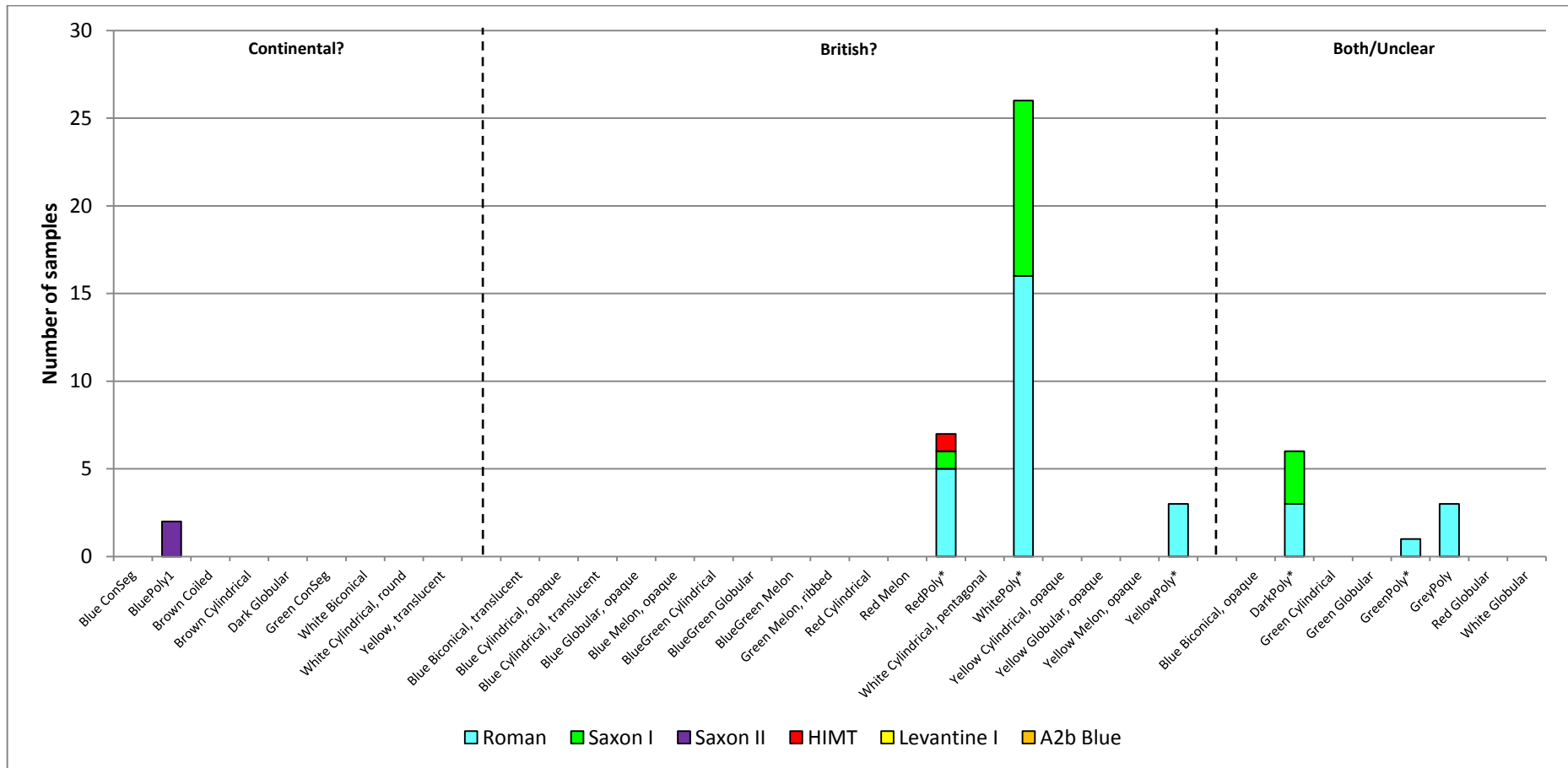


Figure 4.10.16 – Stacked histogram showing the base glass types used for applied decoration on the different polychrome bead types from Eriswell, ordered by their possible production zones based upon their compositional attributes. These beads are *not* covered by the typologies in Brugmann (2004) and Penn and Brugmann (2007). * denotes bead sub-types that have been grouped together.

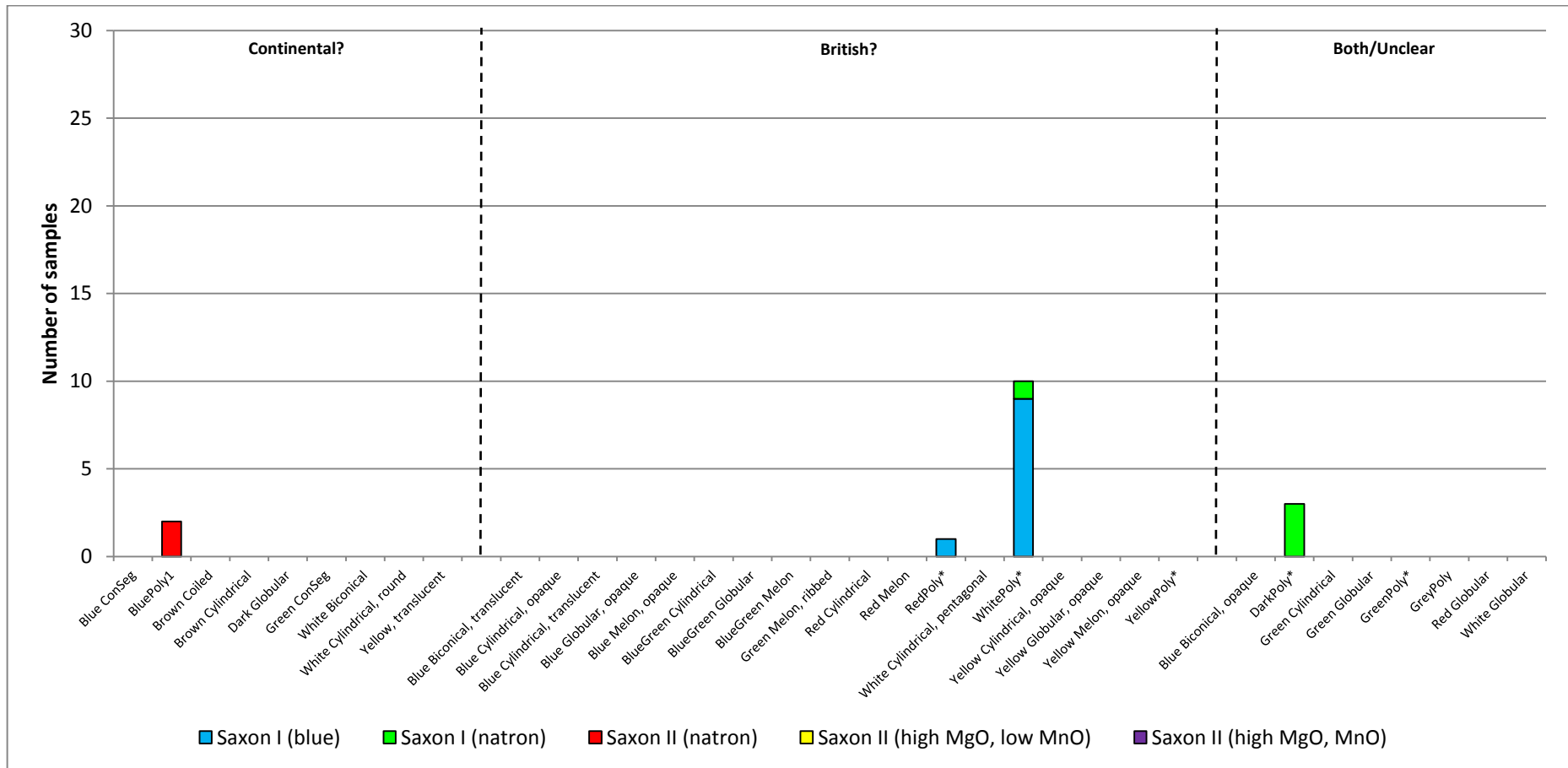


Figure 4.10.17 – Stacked histogram showing the ‘Saxon’ base glass types used for applied decoration on the different polychrome bead types from Eriswell, ordered by their possible production zones based upon their compositional attributes. These beads are *not* covered by the typologies in Brugmann (2004) and Penn and Brugmann (2007). * denotes bead sub-types that have been grouped together.

4.10.3. Individual Bead Type Definitions

An attempt is made here to discuss the main types from Eriswell represented by the typologies in Brugmann (2004) and Penn and Brugmann (2007). This discussion generally follows the order in which these bead types are discussed by Brugmann (2004). The reader is invited to consult Figures 4.10.2-4.10.17 for the composition of individual bead types.

4.10.3.1. 4th Century Types (Roman)

Roman beads were sometimes re-used in Anglo-Saxon bead strings. These beads are typically drawn or very long cylindrical types, often produced from blue glass but sometimes also green (Brugmann 2004: 29). Translucent cobalt-blue *Roman Cane* beads are cut at their perforated sides, and were sometimes used alongside characteristically Anglo-Saxon *Constricted Cylindrical* beads (see below), which although similar, are constricted at their perforated sides (Brugmann 2004: 29). Compositional data confirm that the *Roman Cane* beads from Eriswell are produced from 'Roman' glass and may represent Roman survivals. However, one of these beads (ERL046:G05:1411) is produced from 'Saxon I (blue)' glass, indicating that this type of bead was also produced in the early Anglo-Saxon period. Guido (1999: 49) suggests that these beads are likely to have been produced into the Anglo-Saxon period, and are found in large numbers in Belgium and the Netherlands. As such, it cannot be ruled out that *Roman Cane* beads produced from 'Roman' glass are in fact Anglo-Saxon beads produced using recycled Roman glass, as opposed to Roman survivals; the identification of a *Roman Cane* bead produced from 'Saxon I (blue)' glass suggests that this is also likely.

Roman Polyhedral beads are rare in Anglo-Saxon contexts (Brugmann 2004: 29), and may have been imported from central and eastern Europe prior to the end of the Roman period (Guido 1999: 50). Only one example was identified at Eriswell (ERL104:G242:2174). This bead is produced from 'Roman' glass and may therefore represent a Roman survival. *Miniature Dark* beads were also worn in the Late

Roman period (Brugmann 2004: 30), as were *Constricted Segmented* beads (Brugmann 2004: 28; Guido 1978: 93-94), but no 'Roman' examples were identified at Eriswell. Beads of these two types are therefore likely to represent Anglo-Saxon products (see section 4.10.3.2 below).

4.10.3.2. 5th-6th Century Types (Phases A1 and A2)

Miniature Dark beads are sometimes found in Late Roman contexts (see section 4.10.3.1 above), but were also commonly used in the early Anglo-Saxon period (Brugmann 2004: 30). The majority of *Miniature Dark* beads analysed from Eriswell are produced from 'Saxon I' glass, indicating that they are characteristically early medieval in date. The two produced from 'Saxon II (natron)' glass were probably produced from scrap opaque yellow glass (see Chapter 5, section 5.1.5), so represent a completely different technology. Guido (1999: 20) suggests that *Miniature Dark* beads may have been imported from the Rhineland.

One *Candy Variant* bead was recovered from Eriswell (bead ERL104:G268:3260), which is closely related to beads of Brugmann's *Candy* type. *Candy* beads are a 5th century early Germanic polychrome bead type (Brugmann 2004: 33). The opaque decoration on a translucent bead body which characterised this bead type is rare in Anglo-Saxon beads and resembles 'rock candy', which gives the type its name (Brugmann 2004: 33). The *Candy Variant* bead from Eriswell is not only stylistically unusual, but has a number of compositional characteristics which set it apart. It is produced from 'HIMT' glass, which is particularly distinguished by elevated levels of barium (see this chapter, section 4.5.1) corresponding to 0.4% BaO*; this was not detected in other 'HIMT' samples. Furthermore, the opaque red glass was produced using a very high concentration of kirschsteinitic slag; a slag type which is very rare in opaque red glass from Eriswell (see Chapter 5, section 5.2.3.1). Its unusual composition would support the view that this bead may be an import.

Blue beads are the commonest bead type represented at Eriswell. They were very common during the 5th and 6th centuries, but are rare from 7th and 8th century

contexts (Brugmann 2004: 40). They were also used in the contemporary Germanic Iron Age (c. 5th century AD), but Brugmann (2004: 32) states that *Blue* beads from this period are ‘brighter’ than Anglo-Saxon examples; this suggests that they may have been produced from a slightly different type of glass. They are numerous in Norway as well as on the Continent (John Hines, pers. comm.). The prominence of these beads in early Anglo-Saxon graves has led to speculation that they may have been manufactured in England in order to meet the large-scale demand for them (Brugmann 2004: 33; Hirst and Biek 1981: 142). However, they are also very common on the Continent. Guido (1999: 48) mentions a factory which produced *Blue* beads at Rothulfuashem in the Netherlands, dating to approximately AD 600. At Eriswell, their composition is consistent with ‘Continental’ production, but ‘Anglo-Saxon’ production cannot be ruled out (*e.g.* see section 4.10.4 below).

Blue beads were often combined with *Brown* beads on bead strings, which has led to speculation that both types were produced in the same workshops (Brugmann 2004: 34). Whilst their distribution patterns are similar, *Brown* beads appear to be a much shorter-lived type (Brugmann 2004: 34). However, *Blue* and *Brown* beads are produced from very different base glass types to one another, which is not consistent with associated production. The compositional data are consistent with ‘Continental’ production for *Blue* and *Brown* beads, but ‘Anglo-Saxon’ production is just possible if a supply of pre-coloured blue and/or pink-brown glass was reaching Britain (see this chapter, section 4.9).

The data suggest that the production of *Brown* beads may instead be related to the production of *Constricted Segmented*, some *Miniature Dark* beads and some *Constricted Cylindrical* beads; many of these beads are also produced from ‘Saxon I (natron)’ glass. *Blue* beads are produced from ‘Saxon I (blue)’ glass like some *Constricted Cylindrical* beads. However, they are unlikely to be of related production to *Constricted Cylindrical* beads, as the cobalt sources used to colour both bead types are different (see section 4.10.4 below). *Blue* beads are more likely to be of related production to *BlueGreen Spiral* and *WhitePoly** beads.

Blue beads are sometimes found associated with *Traffic Light* beads, which may suggest that the production of these two types is related (Brugmann 2004: 44-47).

Traffic Light beads, as the name suggests, are defined by the combination of red, yellow and green glass. They are characterised by the use of applied twisted trails as decoration, which is a technique not typically seen in bead fashions on the Continent or in Scandinavia, except in the later *Reticella* beads (Brugmann 2004: 24). It has been suggested that the use of twisted trails may have been derived from an earlier ‘Celtic’ beadmaking tradition (Brugmann 2004: 36).

Traffic Light beads are mainly distributed in East Anglia, suggesting that this is where the workshops producing them were located (Brugmann 2004: 34-35; Guido 1999: 62; Guido and Welch 2000: 116). Brugmann (2004: 34-35) has identified several sub-types of *Traffic Light* bead: *Traffic Light Twisted Trail* beads which are usually red with an applied green and yellow trail, *Traffic Light Streaked* beads in which these trails have melted into bichrome streaks, *Traffic Light Imitation* beads in which the decoration imitates twisted or streaked trails, and *Traffic Light Other* beads which have alternative patterns.

In all cases, the *Traffic Light* beads from Eriswell are produced from either ‘Roman’ or ‘HIMT’ glass (or a combination of the two), indicating that they were exclusively produced from recycled Roman glass. Assuming that they were produced in East Anglia, as seems very likely, this would suggest that Anglo-Saxon workshops were largely (if not solely) dependent upon Roman cullet as a source of glass. This may have been imported from the Continent, or may have been sourced locally; the latter interpretation seems far more likely, as this glass would probably have been widely available locally.

YellowGreen beads are very similar to *Traffic Light* beads. They are particularly common in East Anglia, but rare on the Continent, suggesting that they may also be insular Anglo-Saxon products (Guido 1999: 37; 40; Penn and Brugmann 2007: 28). At Eriswell they are all produced from ‘Roman’ glass, supporting the view that they are of related production to *Traffic Light* beads; they are therefore likely to be of ‘Anglo-Saxon’ production. Other apparently insular bead types include *Cloak* beads, which are characterised by an opaque red or yellow bead body almost entirely coated in translucent glass, although these do not appear to have been produced in large numbers; they are found evenly distributed throughout Anglo-Saxon England, but

are unknown outside of England (Brugmann 2004: 36). At Eriswell these beads are also made from either ‘Roman’ or ‘HIMT’ glass, consistent with the view that they were made in England.

Hourglass beads, which are characterised by opaque yellow decoration on translucent blue-green tinted glass and an hourglass-shaped body, have a similar distribution to *Traffic Light* beads (Brugmann 2004: 36). Brugmann (2004: 36) suggests that they may have been produced in the same workshops as *Traffic Light* beads, possibly from recycled Roman glass. This view is supported by compositional analysis; the *Hourglass Variation* beads from Eriswell are all produced from ‘Roman’ or ‘HIMT’ glass, consistent with ‘Anglo-Saxon’ production.

*Norfolk** beads appear to have succeeded *Traffic Light* beads, and refer to bead types predominantly from the cemeteries of Morning Thorpe and Bergh Apton (see Chapter 1, section 1.2.2). They are rarely found outside of Norfolk, suggesting that they are insular Anglo-Saxon products (Brugmann 2004: 36; Penn and Brugmann 2007: 26-28). Beads of this type include *Norfolk YellowRed* beads characterised by an irregular opaque red trail on an opaque yellow cylindrical body, and *Norfolk BlueWhite* beads characterised by an irregular trail of blue glass on an opaque white globular body (Brugmann 2004: 36-37; Penn and Brugmann 2007: 27). Additionally, small ribbed beads in opaque yellow or opaque green glass, termed *Norfolk Melon*, are included here (Penn and Brugmann 2007: 28). Again, at Eriswell *Norfolk** beads are almost exclusively produced from ‘Roman’ glass, similar to *Traffic Light* beads, consistent with ‘Anglo-Saxon’ production. The only exceptions are a *Norfolk Melon-related?* bead (ERL104:G367:3627) and a *Norfolk YellowRed-variation?* bead (ERL046:G05:1431). However, the tentative type attributions of these two beads (denoted by ‘?’) suggest that they may not be true *Norfolk** bead types.

BlueGreen Spiral beads are a distinctive bead type, characterised by an applied spiral trail of translucent blue-green glass on an opaque white body. They are widely distributed in small numbers in Anglo-Saxon graves, but a Continental origin has also been suggested (Brugmann 2004: 36; Guido 1999: 74). The compositional data for beads of this type from Eriswell is inconclusive. It is possible that those produced from ‘Roman’ glass are ‘Anglo-Saxon’ products, whereas those produced from

‘Saxon’ glass are imports, suggesting that they may have been produced in both England and abroad. As mentioned above, their production may be related to *Blue* beads.

‘Metal-in-glass’ beads, here termed *Constricted Segmented* beads, are predominantly distributed in southeast and mid-west England (particularly Kent) (Brugmann 2004: 30). On the Continent, they appear to have been worn broadly west of the Rhine between the 4th and 5th centuries AD (Brugmann 2004: 32). Stylistically these beads are very homogeneous and have a long-standing tradition of manufacture, but it remains unclear as to whether they were produced in Britain, Europe or the Near East (see Chapter 3, section 3.1.2).

All of the *Constricted Segmented* beads from Eriswell are produced from uncoloured ‘Saxon I (natron)’ glass, suggesting that they are likely to have been manufactured in just one or two specialist workshops. These beads are unlikely to have been produced in England; if this were the case, one would expect to find beads of this type produced from recycled Roman glass, or to see ‘Anglo-Saxon’ bead types produced from ‘Saxon I (natron)’ glass. This is clearly not the case. Their composition suggests that they may be related to *Brown*, some *Constricted Cylindrical* and some *Miniature Dark* beads; ‘Saxon I (natron)’ glass was also used to produce these bead types.

The manufacturing technique used to produce *Constricted Segmented* beads (drawing; see Chapter 3, section 3.1) is very similar to that used to produce *Constricted Cylindrical* beads. The distribution of both of these bead types is similar, but *Constricted Cylindrical* beads occur in much smaller numbers (Brugmann 2004: 37). It is not possible to speculate as to exactly where either bead type was produced as the raw glass has its origins in the Near East; Guido (1999: 50) suggests that *Constricted Segmented* beads may have been imported from northeastern France and the Low Countries.

Constricted Cylindrical beads are produced from both ‘Saxon I (blue)’ and ‘Saxon I (natron)’ glass, although there is some considerable compositional overlap between these two base glass types (see this chapter, section 4.4). This may suggest that

Constricted Cylindrical beads were produced by more than one workshop operating at around the same time, or it may be related to chronology (*i.e.* changes in glass sources over time). Alternatively, if pre-coloured cobalt-blue glass was widely distributed, these beads may have been produced in a larger number of smaller, more regional workshops. Trace element analysis suggests that they are unlikely to be related to *Blue* beads and are consequently far less likely to be ‘Anglo-Saxon’ products than *Blue* beads (see section 4.10.4 below).

4.10.3.3. 6th-7th Century Types (Phases A2b, B and C)

It should be stressed that the interpretations with regard to bead provenance (*i.e.* ‘Anglo-Saxon’ or ‘Continental’) for ‘later’ bead types are primarily based upon the composition of *Doughnut* beads; these are the only 7th century bead type represented at Eriswell which can be relatively confidently attributed to ‘Anglo-Saxon’ production (Brugmann 2004: 41). Similar bead types are known on the Continent but do not exactly match *Doughnut* beads from England (Brugmann 2004: 41). *Doughnut* beads are found evenly distributed throughout England and were produced by piercing (Brugmann 2004: 41; see also Chapter 3, section 3.1). They are primarily made from translucent blue-green glass; all of the beads of this type analysed from Eriswell are produced from either ‘Roman’ or ‘HIMT’ glass, consistent with their tint. Their composition is directly paralleled by earlier *Traffic Light* and *Norfolk* beads, and is consistent with ‘Anglo-Saxon’ production.

Doughnut beads are very low quality and crude in design, suggesting that the craftsmen producing them were less skilled than those producing the ‘Anglo-Saxon’ bead types which preceded them (*e.g.* *Traffic Light* beads). This view is supported by the method by which they are manufactured; *Doughnut* beads are pierced, which may imply that the craftsmen producing them did not have the tools, skill or knowledge necessary to produce wound or drawn beads. One of the most difficult processes in beadmaking appears to have been the removal of the bead from the mandrel (Brugmann 2004: 17), but this process is bypassed when producing pierced beads. Recent work by Hines *et al.* (in press) suggests that they were in use during a

very restricted period in the mid-7th century, consistent with Brugmann's attribution of this type to her phase C.

The remaining bead types attributed to Brugmann's phases A2b, B and C from Eriswell are not produced from 'Roman' or 'HIMT' glass; their composition is therefore consistent with 'Continental' production. By the late 6th century there is an increase in the number of Anglo-Saxon beads which can be paralleled with Continental beads (Brugmann 2004: 38); this appears to support the present view that the majority of 'later' beads types from Eriswell (with the exception of *Doughnut* beads) are consistent with 'Continental' production. However, recent work suggests that 'Roman' glass was also used by Continental workshops (Mathis *et al.* 2010: 2082), so the attribution of beads produced from recycled Roman glass to 'Anglo-Saxon' production is by no means clear-cut.

White Spiral beads are characterised by an applied trail of opaque white glass on a translucent blue-green body. They are often confused with 'earlier' *BlueGreen Spiral* beads (see section 4.10.1.2 above), so the extent of their distribution on the Continent is unclear (Brugmann 2004: 36; 80). Both Brugmann (2004: 36) and Guido (1999: 74) suggest that they may have been insular 'Anglo-Saxon' products. Only one bead (ERL104:G210:1569) of this type was analysed from Eriswell, which is not sufficient to draw any concrete conclusions. However, the use of 'Saxon II' glass here is more consistent with 'Continental' production. Hines *et al.* (in press) suggest that these beads were introduced roughly contemporaneously with *Doughnut* beads in Brugmann's phase C; they are therefore likely to be among the latest bead types at Eriswell.

Melon beads, which are either translucent blue or yellow-green in colour, are often associated with *Reticella* beads; both these bead types are assumed to be Continental imports (Brugmann 2004: 37). Both types are found in relatively small numbers and are evenly distributed throughout Anglo-Saxon England (Brugmann 2004: 37). Their use appears to have spanned the whole of the 6th century (Hines *et al.*, in press). *Reticella* beads are widely found in Merovingian graves on the Continent, but their origin is unknown (Evison 1983: 92). It has been suggested that reticella rods were manufactured in a limited number of workshops and traded (Evison 1983: 92).

However, Brugmann (2004: 38) suggests that the *Reticella* beads themselves are more likely to have been traded, on account of their complicated and therefore desirable decoration. *Melon Associated* beads are also often found associated with *Melon* and *Reticella* beads, but are instead characterised by an applied zigzag trail (in opaque yellow at Eriswell) on a ‘dark’ bead body (Brugmann 2004: 37). Guido (1999: 22) suggests that they are a Germanic bead type.

Several *Melon* and *Melon Variation?* beads were analysed from Eriswell, produced from either cobalt-blue or yellow-green tinted glass, although their type attributions are uncertain (denoted by ‘?’). These beads are produced from two different types of base glass; the translucent blue beads are produced from ‘A2b Blue’ glass, whereas the translucent yellow-green tinted beads are produced from ‘Saxon II (natron)’ glass. These two different colours of bead are likely to have been produced in the same workshops, as beads produced in both colours of glass are stylistically identical. This supports the view that raw ‘A2b Blue’ glass was imported ready-coloured; if it was not, one would expect to find beads produced from cobalt-blue ‘Saxon II (natron)’ glass.

Melon Associated and *Reticella* beads are also produced from ‘Saxon II (natron)’ glass. Whilst this does not necessarily confirm production in the same workshops(s), it does support the view that these bead types are contemporary with one another. As no ‘Anglo-Saxon’ bead types appear to have been produced using ‘Saxon II (natron)’ or ‘A2b Blue’ glass, ‘Continental’ production for all beads produced using these base glass types seems likely.

One *Mosaic?* bead (ERL104:G290:1721) was identified at Eriswell. *Mosaic* beads are again assumed to have been imported (Brugmann 2004: 38). However, all of the colours comprising this bead are produced from ‘Roman’ glass, which is more consistent with ‘Anglo-Saxon’ production, but the fragmentary nature of this bead means that its type attribution is dubious at best (denoted by ‘?’).

*Koch** bead types are based upon Ursula Koch’s typology for Merovingian beads from Schretzheim in Germany (Koch 1977: 207). Among the most numerous polychrome bead types from post-6th century Anglo-Saxon contexts include *Koch20*

and *Koch34* beads, all of which are also widely distributed on the Continent (Brugmann 2004: 39; Guido 1999: 63-64). Both bead types appear to have been popular throughout most of the 6th century, but whereas *Koch20* beads appear to have gone out of use around the turn of the 7th century, *Koch34* beads appear to have continued to be used into at least the first half of the 7th century (Hines *et al.*, in press). The numbers in which they are found suggests that they were probably made in a number of different workshops, and may have entered England via Kent and/or the Thames Estuary (Guido 1999: 63). At Eriswell, their compositional variability supports the view that they are unlikely to be products of just one workshop. *Koch20* beads are mainly distributed in Kent, whereas *Koch34* beads are distributed in both Kent and East Anglia (Brugmann 2004: 39-40). *Dot34* beads are likely to be related to *Koch34* beads and occur mainly in East Anglia, but the occasional occurrence of this bead type on the Continent has led Brugmann (2004: 40) to suggest that they are also imports. They appear to have been popular throughout most of the 6th century and into the early 7th century (Hines *et al.*, in press).

Koch20 beads are characterised by wide crossing trails and dots mostly in either white on red or yellow on red, some of which were produced in segmented form (Brugmann 2004: 39); at Eriswell all beads of this type consist of yellow decoration on red. *Koch34* beads are characterised by narrow crossing waves in a variety of colour combinations, mostly yellow on red, white on red or blue/turquoise on white (Brugmann 2004: 39). All of these colour combinations are represented by the Eriswell assemblage, but compositional distinctions between *Koch34* beads produced using different colour combinations were not apparent; as a result they have not been differentiated in the present study.

The *Koch** and *Dot** bead types from Eriswell (which includes *Koch20*, *Koch34*, *Dot34* beads and variants of these types) are produced from either ‘Saxon II’ or ‘Levantine I’ glass. The absence of any beads of these types produced from recycled Roman glass is consistent with ‘Continental’ production. The *Koch20* beads from Eriswell are made from ‘Saxon II (natron)’ glass, which is slightly earlier than ‘Saxon II (high MgO, low MnO)’, ‘Saxon II (high MgO, MnO)’ and ‘Levantine I’ glass (see this chapter, section 4.8, Figure 4.8.4); these latter glass types are more

typically used in the production of *Koch34*, supporting the view that *Koch20* beads were probably introduced slightly earlier than *Koch34* beads (Brugmann 2004: 58).

It is likely that the workshops producing *Koch** and *Dot** beads had access to a range of different glass types. Table 4.10.1 shows that whilst the base glass used in the production of the applied decoration on many *Koch** beads matches that of the bead body, on many others it does not. This demonstrates that the ‘Levantine I’ and ‘Saxon II (high MgO, MnO)’ base glass types were in use by the same beadmaking workshop(s). Similarly, the ‘Saxon II (natron)’ and ‘Saxon II (high MgO, low MnO)’ base glass types were in use by the same beadmaking workshop(s), but probably operating elsewhere.

The reasons for the use of more than one base glass type by the same workshop are not entirely clear. It is possible that some glass was imported ready-coloured, possibly from a workshop specialising in the production of particular colours of glass (*e.g.* turquoise); different colours of glass may therefore have been produced from different base glass types. Alternatively, some colours may have been made and kept ‘in stock’, so that glass reserved may have had a variety of different compositions.

As well as polychrome bead types, a large number of opaque monochrome beads appear to have been worn from the late 6th century onwards. These include *Cylindrical Round* and *Cylindrical Pentagonal* beads, which were produced from white, yellow, red and blue glass (Brugmann 2004: 40). They are distributed throughout Anglo-Saxon England, but are mainly found in Kent and East Anglia (Brugmann 2004: 40). Their use appears to be largely restricted to the 6th century (Hines *et al.*, in press). Similar beads were produced in segments of two or three, and are termed *Segmented Globular* by Brugmann (2004: 40). All of these bead types are thought to have been Continental imports (Brugmann 2004: 40; Guido 1999: 32); at Eriswell they are predominantly made from ‘Saxon II (high MgO, low MnO)’ glass, consistent with this view. However, the only *Cylindrical Pentagonal?* bead analysed (bead ERL046:G18:1786) is produced from ‘Roman’ glass, consistent with ‘Anglo-Saxon’ production. However, its type attribution is tentative (denoted by ‘?’).

Table 4.10.1 – Comparisons between the composition of bead body and applied decoration on the *Koch** bead types from Eriswell.

<i>Bead Number</i>	<i>Bead Type</i>	<i>Composition (body)</i>	<i>Composition (decoration)</i>
<i>Identical body / decoration composition</i>			
ERL104:G107:1125	Koch34	Levantine I	Levantine I
ERL104:G107:1141	Koch34	Saxon II (high MgO, MnO)	Saxon II (high MgO, MnO)
ERL104:G193:1295	Koch34	Levantine I	Levantine I
ERL104:G193:1311	Koch34	Saxon II (high MgO, low MnO)	Saxon II (high MgO, low MnO)
ERL104:G195:1345	Koch20	Saxon II (natron)	Saxon II (natron)
ERL104:G195:1350	Koch34	Saxon II (high MgO, low MnO)	Saxon II (high MgO, low MnO)
ERL104:G237:1154	Koch34	Saxon II (high MgO, low MnO)	Saxon II (high MgO, low MnO)
ERL104:G262:1259a/2	Koch34	Saxon II (high MgO, MnO)	Saxon II (high MgO, MnO)
ERL104:G262:1261	Koch34	Saxon II (high MgO, low MnO)	Saxon II (high MgO, low MnO)
ERL104:G262:1284	Koch34Var	Saxon II (high MgO, low MnO)	Saxon II (high MgO, low MnO)
ERL104:G262:1289	Koch34	Saxon II (natron)	Saxon II (natron)
ERL104:G273:3330a/01	Koch34	Saxon II (high MgO, MnO)	Saxon II (high MgO, MnO)
ERL104:G281:1796	Koch34	Levantine I	Levantine I
ERL104:G281:1797	Koch34	Saxon II (high MgO, MnO)	Saxon II (high MgO, MnO)
<i>Different body / decoration composition</i>			
ERL104:G107:1123	Koch34	Levantine I	Saxon II (high MgO, MnO)
ERL104:G107:1128	Koch34	Saxon II (natron)	Saxon II (high MgO, low MnO)
ERL104:G107:1145	Koch34	Saxon II (high MgO, MnO)	Levantine I
ERL104:G195:1346	Koch34	Saxon II (natron)	Saxon II (high MgO, low MnO)
ERL104:G262:1286	Koch34	Saxon II (natron)	Saxon II (high MgO, low MnO)
ERL104:G353:3066	Koch20	Saxon II (high MgO, low MnO)	Saxon II (natron)
ERL104:G353:3069	Koch20	Saxon II (high MgO, low MnO)	Saxon II (natron)
ERL104:G353:3070	Koch34	Saxon II (natron)	Saxon II (high MgO, low MnO)
ERL104:G353:3079	Koch20	Saxon II (high MgO, low MnO)	Saxon II (natron)

One *Cylindrical Round* bead (ERL104:G193:1312) was analysed from Eriswell, and is also produced from ‘Roman’ glass again consistent with ‘Anglo-Saxon’ production. However, this bead is unusual in that it is opacified by tin oxide, whereas opaque white glass of the ‘Roman’ composition from Eriswell is more typically opacified by bubbles (see this chapter, section 4.9 and also Chapter 5, section 5.2.1). It was previously suggested that opacification by bubbles is more consistent with ‘Anglo-Saxon’ bead production, whereas opacification by tin oxide is more consistent with ‘Continental’ production (see this chapter, section 4.9). Whilst a very tentative interpretation, this would suggest that beads of the ‘Roman’ composition opacified by tin oxide may be imports; indeed, previous work suggests that some ‘Continental’ bead types were produced from ‘Roman’ glass (Mathis *et al.* 2012: 2082). This complicates the picture somewhat, but the general trend remains that ‘Anglo-Saxon’ beads were typically produced from recycled Roman material.

Monochrome biconical bead types are thought to have been introduced at around the same time as the monochrome bead types mentioned above. Such beads include *Orange* beads, which are the only Anglo-Saxon bead type to have been produced from opaque orange glass (Brugmann 2004: 40; Guido 1999: 68-69; see also Chapter 5, section 5.2.4). *Orange* beads are mostly concentrated in Kent and are comparatively rare in other parts of Anglo-Saxon England (Brugmann 2004: 40; Guido 1999: 68). However, they have a much wider type and date range on the Continent, where they appear to have been produced into the 8th century (Brugmann 2004: 40; Guido 1999: 68). In England, these beads have been mostly dated to the 7th century (Brugmann 2004: 75; Evison 1987: 61-62; Guido 1999: 68) and are the latest bead type represented by Continental frameworks that is relevant to Anglo-Saxon England (Brugmann 2004: 58). They appear to have been in continuous use between the mid-6th mid-7th centuries, but do not appear in the latest furnished burials in England (Hines *et al.*, in press). They are assumed to be imports as they have a wide distribution on the Continent (Brugmann 2004: 75; Guido 1999: 68-69). At Eriswell they are produced from ‘Levantine I’ glass and ‘Saxon II’ glass, consistent with this view.

All of the graves containing *Orange* beads (G107, G116, G193, G262 and G266) contain two or more of these beads. However, only in G116 are all of the *Orange*

beads present produced from the *same* base glass type. The *Orange* beads recovered from the remaining graves are heterogeneous in composition; they are all produced from different base glass types to one another. However, in the light of the compositions of the *Koch** bead types (Table 4.10.1), this cannot be taken to suggest production in different workshops, as individual workshops operating at this time clearly had access to more than one type of base glass. It is just possible that the beads were acquired at slightly different times and/or from different workshops, but this is unclear at present.

4.10.4. Blue Glass Beads: Cobalt Sources

Impurities associated with cobalt minerals have the potential to discriminate between and provenance cobalt-blue glass. This is discussed in detail in Chapter 5, section 5.1.3.1, according to the different base glass types from which the cobalt-blue beads from Eriswell are made. However, the different cobalt sources used to colour the blue beads from Eriswell also bears a strong relationship to bead type. This is particularly well illustrated by a plot of cobalt versus nickel (Figure 4.10.18) and of lead versus iron (Figure 4.10.19 and 4.10.20). A number of different compositional groups corresponding closely to the different bead types represented at Eriswell are apparent. Whilst the levels of lead oxide which define several of the groups in Figures 4.10.19 and 4.10.20 are below the limits of detection for SEM-EDS (approximately 0.3%), these groups have been confirmed by LA-ICP-MS. However, it should be noted that iron is likely to have been introduced from a number of sources, as well as an impurity associated with the cobalt colourant (see this chapter, section 4.1).

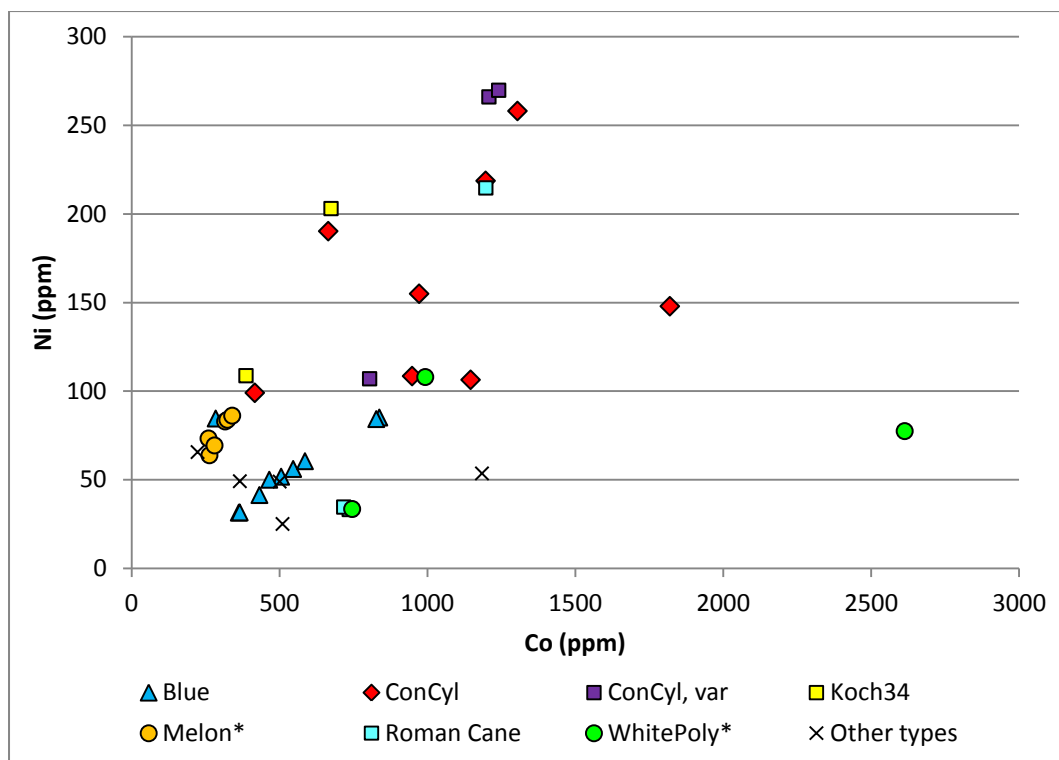


Figure 4.10.18 – A plot of cobalt versus nickel in the translucent cobalt-blue bead types from Eriswell (LA-ICP-MS data). * denotes bead sub-types that have been grouped together.

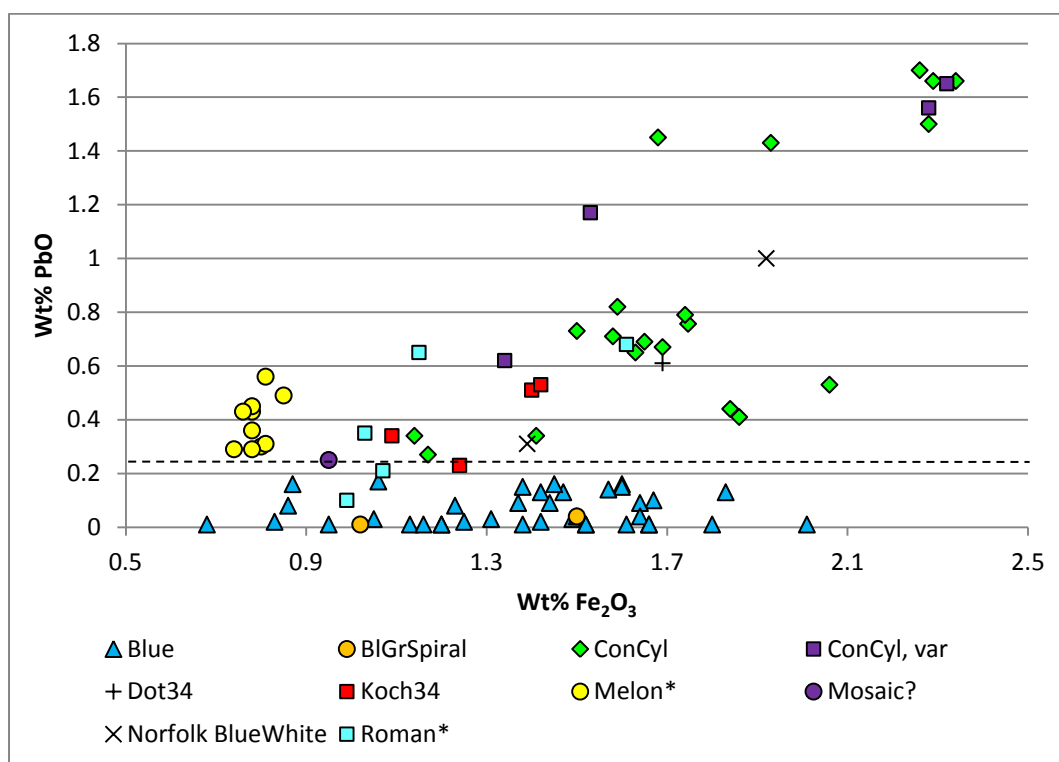


Figure 4.10.19 – A plot of iron oxide versus lead oxide in the translucent cobalt-blue bead types from Eriswell covered by the typologies in Brugmann (2004) and Penn and Brugmann (2007). The dashed line represents the approximate detection limits for lead oxide. * denotes bead sub-types that have been grouped together.

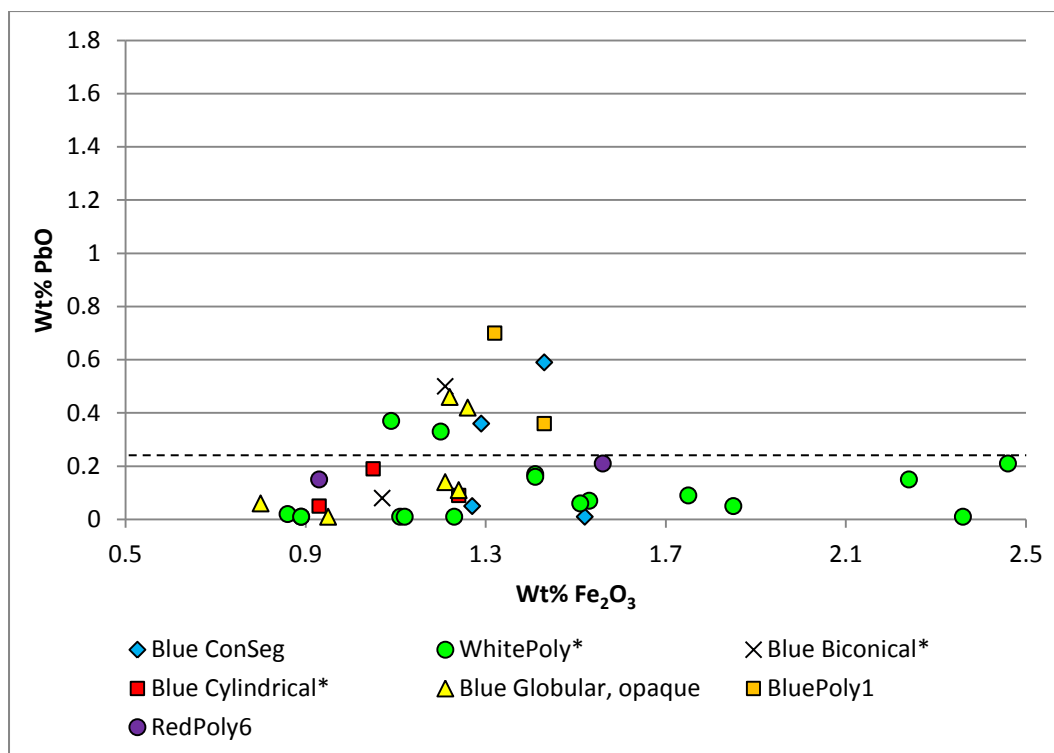


Figure 4.10.20 – A plot of iron oxide versus lead oxide in the translucent cobalt-blue bead types from Eriswell covered by the typologies in Brugmann (2004) and Penn and Brugmann (2007). The dashed line represents the approximate detection limits for lead oxide. * denotes bead sub-types that have been grouped together.

Blue beads form a relatively tight compositional group, containing PbO at concentrations below 0.2% (Figure 4.10.19). There is also a particularly strong correlation between cobalt and nickel in these beads (Figure 4.10.18), which strongly suggests that a common cobalt source was used to colour the glass in the majority of cases; the only *Blue* bead which does not fit this correlation (ERL104:G281:1799) has been attributed to Brugmann's phase B, suggesting that it is later. The composition of the blue decoration from the *BlueGreen Spiral* beads at Eriswell falls within the same range, and suggests that these beads may be of related production to *Blue* beads. This is also reflected in many of the *WhitePoly** bead types; the translucent blue decoration used in a large number of these beads is likely to be of the same 'Saxon I (blue)' type as that used to produce *Blue* beads (Figure 4.10.20 cf. Figure 4.10.19). *WhitePoly** beads do not appear to be a 'Continental' bead type; they are usually produced from 'Roman' glass which is more consistent with 'Anglo-Saxon' production (see section 4.10.2 above). These beads have not been attributed to a chronological phase by Brugmann, but the use of 'Saxon I (blue)'

glass to decorate many of them is consistent with Brugmann's phase A (see this chapter, section 4.8).

It is just possible that the decoration on the *WhitePoly** beads represents recycled 'Saxon I (blue)' glass, perhaps obtained from broken *Blue* beads or vessels; a handful of the translucent blue trails on *WhitePoly** beads are almost certainly produced from recycled 'Roman' glass (e.g. beads ERL046:G38:1067, ERL104:G268:3258 and ERL104:G268:3255). However, if this were the case, it is unusual that the glass used to produce *Constricted Cylindrical* beads was not recycled for such a purpose.

On balance, it therefore seems more likely that a small quantity of 'Saxon I (blue)' glass was reaching Britain, either in its raw unworked form or as scrap cullet. If this were the case, it is conceivable that *Blue* beads were being produced in England, as suggested by Brugmann (Brugmann 2004: 33). This would appear to be supported by analysis of two translucent blue globular beakers from Broomfield by Freestone *et al.* (2008: cat nos. 150 and 151), which are also of the 'Saxon I (blue)' composition; Evison (2008: 8) suggests that these beakers are very high status items which were also probably produced in England. Interestingly, it has been suggested that the production of vessels from cobalt-blue glass is an indicator of insular 'Anglo-Saxon' production; several vessels and fragments of cobalt-blue glass have been recovered from Faversham in Kent, which has been taken to suggest the production of blue glass objects may have taken place there (Stephens 2006: 15).

The globular beaker (Figure 4.10.21) from Wye Down, Kent, analysed by Freestone *et al.* (2008: cat no. 148) is probably produced from recycled 'Roman' glass (see this chapter, section 4.2); again 'Anglo-Saxon' production is implied as this vessel form is uncommon on the Continent (Evison 2008: 7). This particular vessel is unusual because it is produced from more than one colour of glass (Stephens 2006: 21; see also Figure 4.10.21); the applied decoration is translucent blue (Evison 2008: cat no. 148; Stephens 2006: Item 168) and although it was not chemically analysed by Freestone *et al.* (2008), it is possible that it is of the 'Saxon I (blue)' base glass type. If this is the case, it would support the view that a supply of raw translucent 'Saxon I (blue)' glass was reaching Britain, and consequently that *Blue* beads may have been

produced in Anglo-Saxon workshops. However, as previously mentioned (*e.g.* section 4.10.2), ‘Anglo-Saxon’ bead types are typically produced from recycled Roman material. As such, it cannot be confirmed that raw cobalt-blue glass ever reached Britain without further supporting evidence (*e.g.* the discovery of cobalt-blue glass chunks).



Figure 4.10.21 – A translucent blue-green globular beaker from Wye Down, Kent (Evison 2008: 141). Six turns of a translucent blue trail are applied to the neck and shoulder, and another six vertical loops to the lower half of the vessel (Evison 2008: cat no. 148).

A large number of *Constricted Cylindrical* beads from Eriswell were produced from ‘Saxon I (blue)’ glass, but in contrast to *Blue* beads they do not form a tight compositional group (Figures 4.10.18 and 4.10.19). Their elevated levels of PbO, in excess of 0.2% but anywhere up to 0.8%, suggests the use of a different cobalt source (perhaps even more than one); they are therefore highly unlikely to be of related manufacture to *Blue* beads. The *Constricted Cylindrical, Variant* beads, as the name suggests, are a coiled variation of *Constricted Cylindrical* beads. Their composition, similarly variable in PbO, suggests that they are likely to be of related production to *Constricted Cylindrical* beads.

The cobalt-blue *Melon** beads (this includes *Melon* and *Melon Variation?* beads) from Eriswell form a very tight compositional group (Figure 4.10.18 and 4.10.19). These are amongst the only beads to be produced from ‘A2b Blue’ glass, so are unlikely to be related to the other translucent blue bead types identified at Eriswell. It is likely that they were all produced in the same workshop, possibly even from the same batch of glass (see also this chapter, section 4.7).

It is difficult to draw conclusions as to which of the other bead types analysed may be of related production, either because they are represented by such broad spreads of data or because relatively few samples were analysed (*e.g.* Figure 4.10.20). However, the general trend suggests that different cobalt sources were used to colour different bead types. This suggests production of certain bead types at slightly different times, and/or in different workshops specialising in the production of certain types of bead.

The impurities associated with cobalt have allowed a distinction between *Constricted Segmented* and *Blue* beads to be made; both of these bead types were produced from ‘Saxon I (blue)’ glass coloured by cobalt from different sources. It also seems likely that *WhitePoly** are contemporary with *Blue* beads, possibly even of related production; this provides some of the only compositional evidence to suggest that *Blue* beads may have been produced in England. In contrast, there is no evidence to suggest that *Constricted Cylindrical* beads were made in England, or that the raw glass used to produce them ever reached Anglo-Saxon workshops. Trace element analysis of *Blue* beads from the Continent would be particularly worthwhile in order to confirm whether or not they were coloured using the same cobalt source(s) as *Blue* beads from England.

4.11. Relationship to Bead Context

4.11.1. The Chronology of the Burials at Eriswell

By identifying the bead type associations within the individual burials at Eriswell, it is possible to estimate their approximate dates based upon the base glass types represented (see this chapter, section 4.8), as well as to identify which base glass types may have been in use contemporaneously with one another. Figures 4.11.1-4.11.12 show the base glass types represented within the individual burials from cemeteries ERL 046, ERL 104 and ERL 114. These are organised by the chronological phases to which these graves have been attributed by Birte Brugmann, based upon the bead types and bead type combinations present. The composition of the bead bodies (*i.e.* the number of beads) and the decoration on polychrome beads are presented separately for each of the cemeteries (see this chapter, section 4.8 for details). The sub-types of ‘Saxon I’ and ‘Saxon II’ glass (see this chapter, section 4.4) are presented in separate histograms for simplicity; the inclusion of all glass groups and sub-groups in the same graph complicates interpretation somewhat. All of these figures should be cross-referenced with the results presented earlier in this chapter (section 4.8; particularly Figure 4.8.5).

Complete glass bead assemblages were analysed from G15 (1 bead), G18 (3 beads), G25 (3 beads), G42 (5 beads), G43 (3 beads), G109 (1 bead), G116 (2 beads), G132 (2 beads), G189 (1 bead), G205 (4 beads), G266 (5 beads), G290 (2 beads), G319 (2 beads) and G414 (1 bead). The data for the remaining graves reflect incomplete assemblages and are therefore biased by the sampling process (see Chapter 2, section 2.1.1). To avoid repetition and due to constraints of space, no attempt is made here to discuss graves on a case-by-case basis; the cemeteries will instead be discussed in general terms.

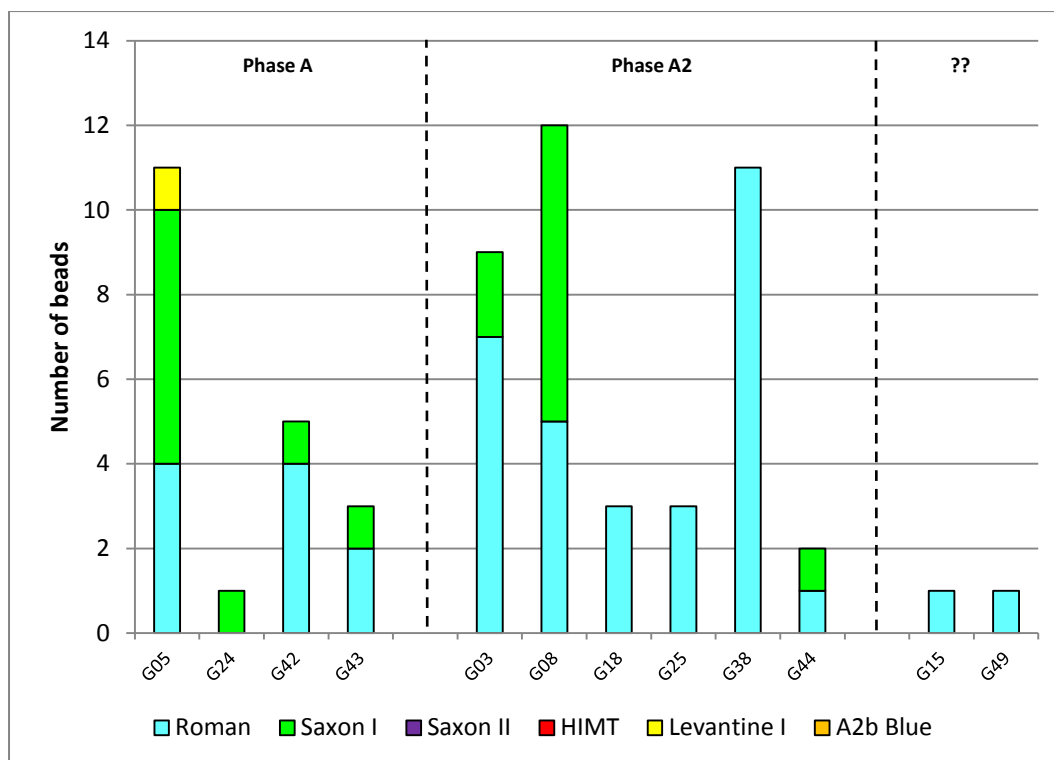


Figure 4.11.1 – Stacked histogram showing the relationship between the composition of bead bodies and grave number in cemetery ERL 046 at Eriswell.

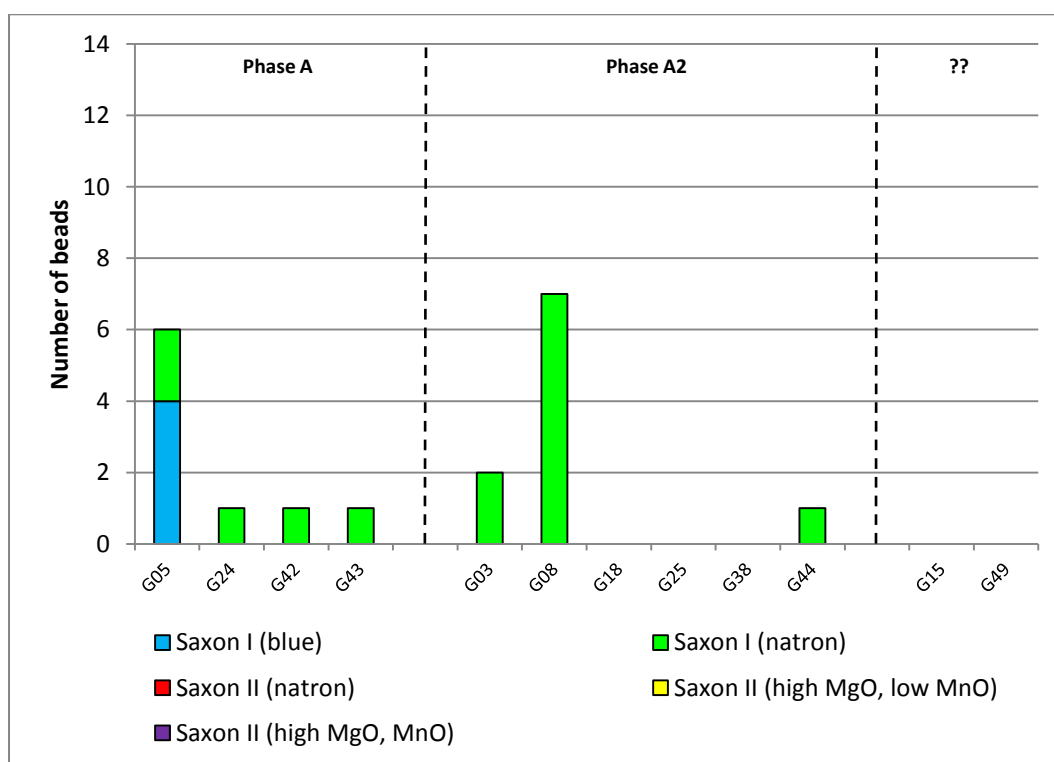


Figure 4.11.2 – Stacked histogram showing the relationship between the composition of 'Saxon' type bead bodies and grave number in cemetery ERL 046 at Eriswell.

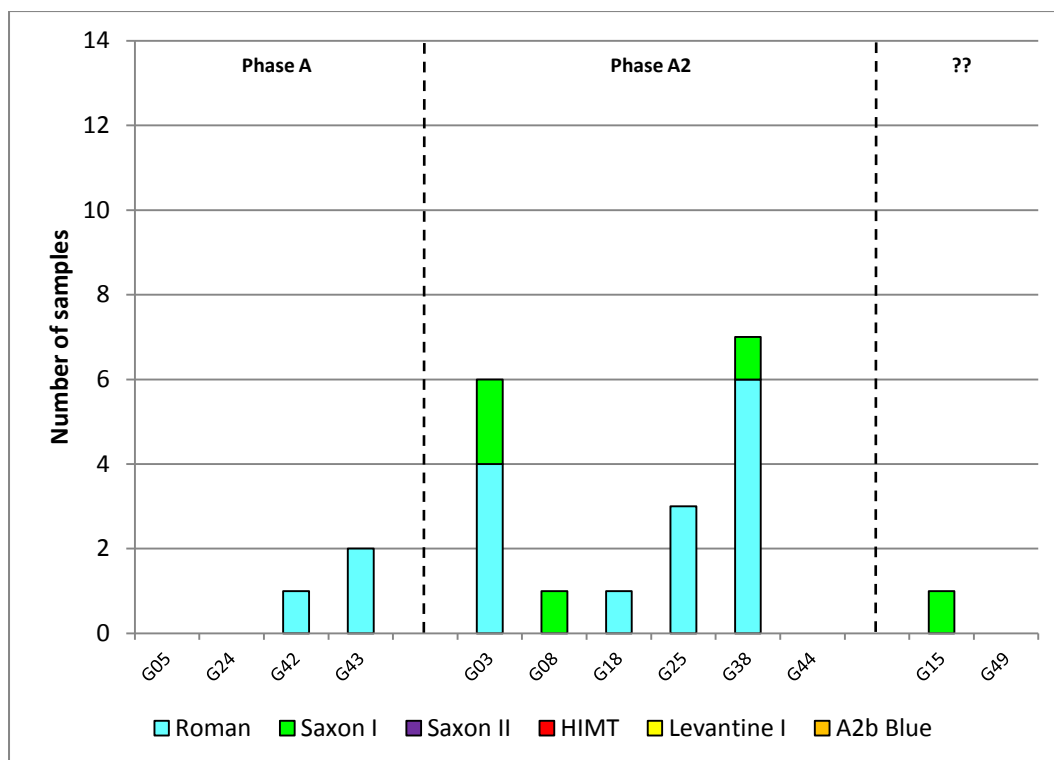


Figure 4.11.3 – Stacked histogram showing the relationship between the composition of applied decoration on polychrome beads and grave number in cemetery ERL 046 at Eriswell.

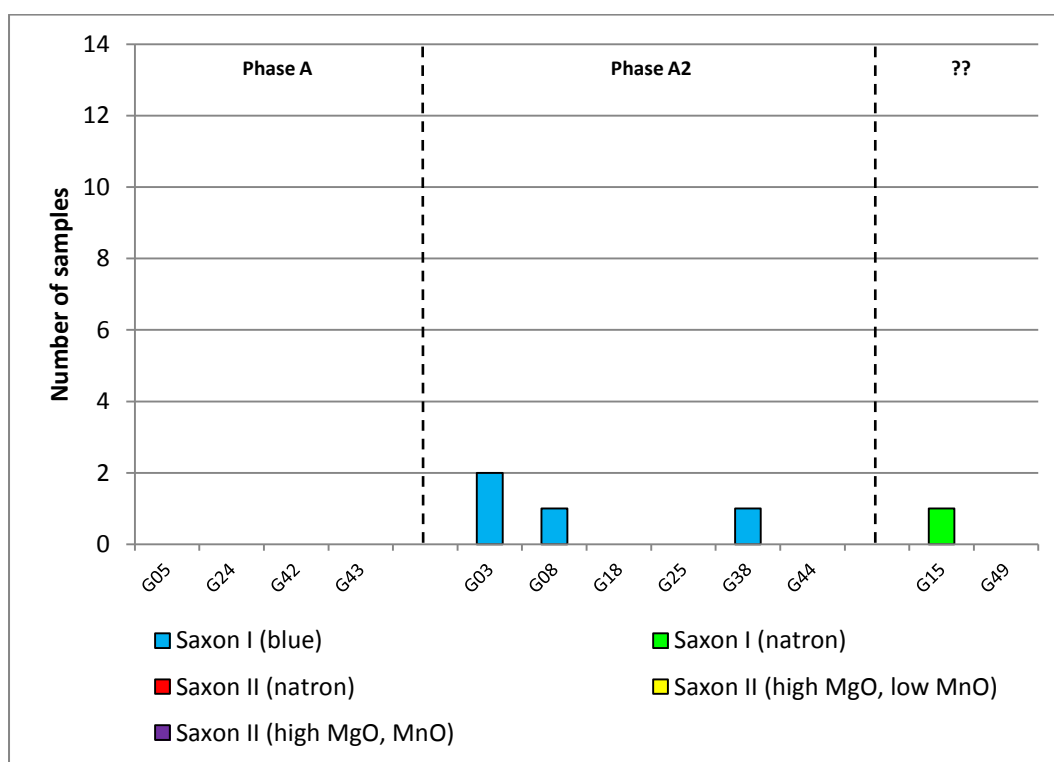


Figure 4.11.4 – Stacked histogram showing the relationship between the composition of 'Saxon' type applied decoration on polychrome beads and grave number in cemetery ERL 046 at Eriswell.

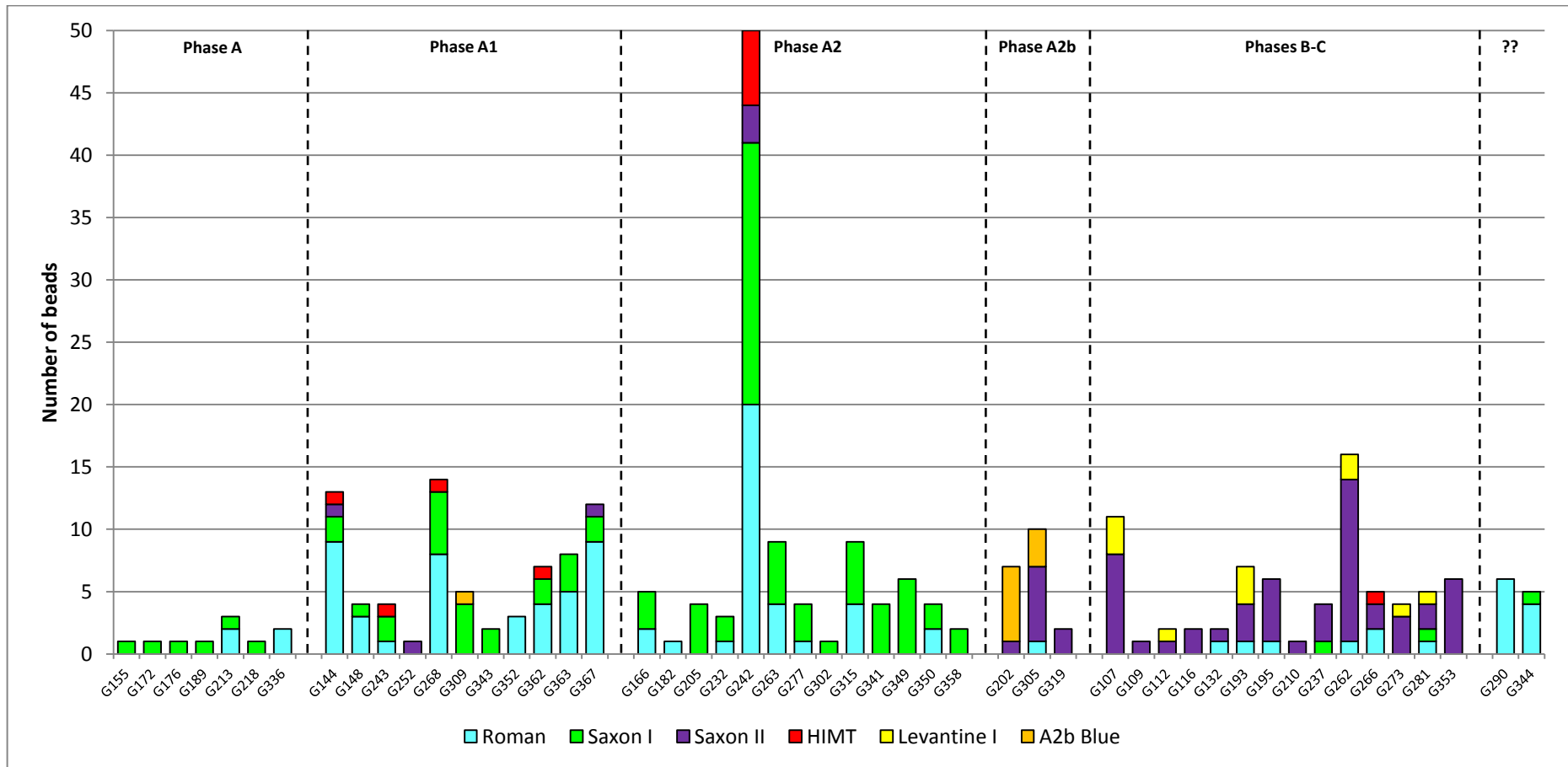


Figure 4.11.5 – Stacked histogram showing the relationship between the composition of bead bodies and grave number in cemetery ERL 104 at Eriswell.

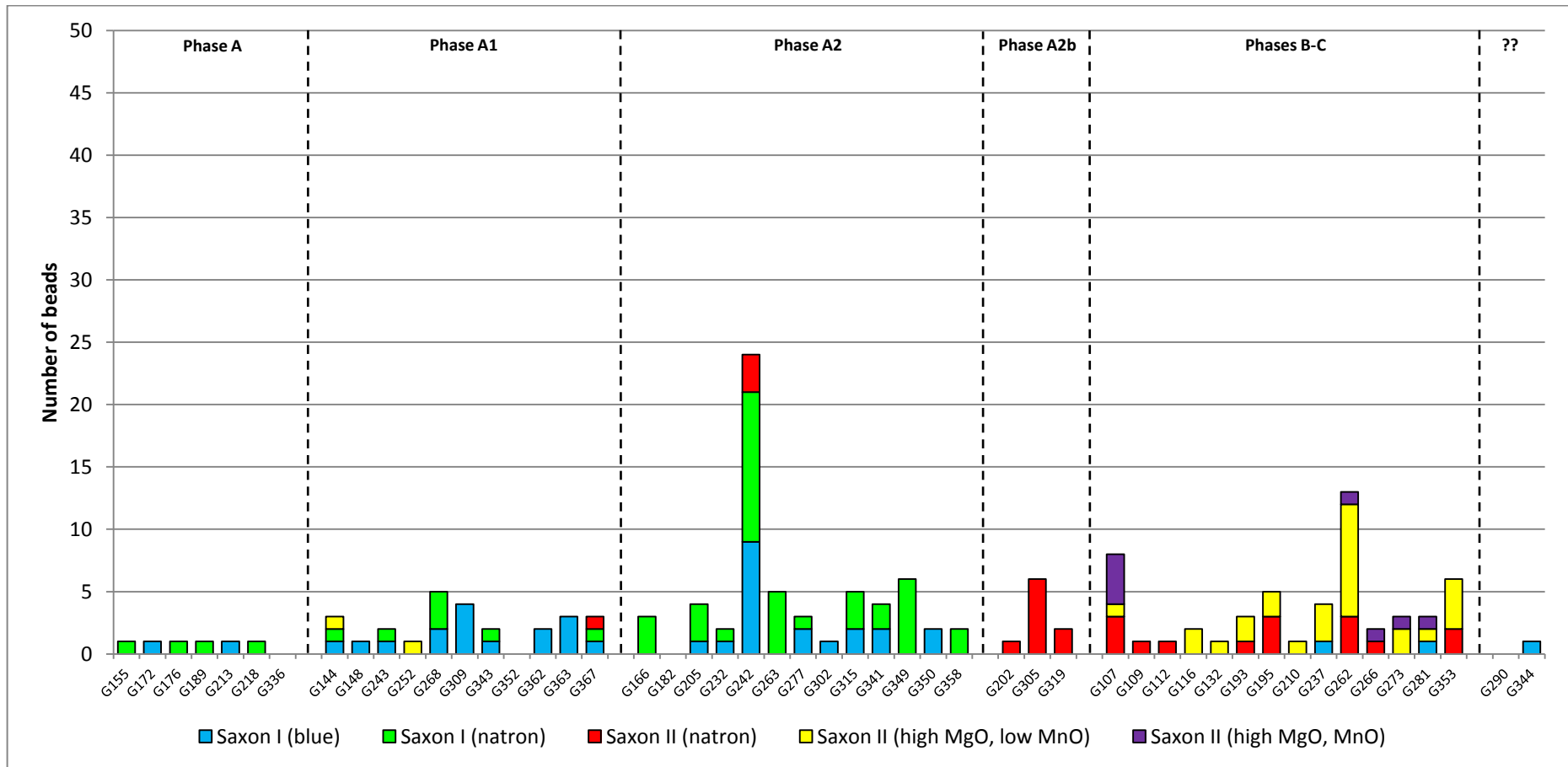


Figure 4.11.6 – Stacked histogram showing the relationship between the composition of ‘Saxon’ type bead bodies of and grave number in cemetery ERL 104 at Eriswell.

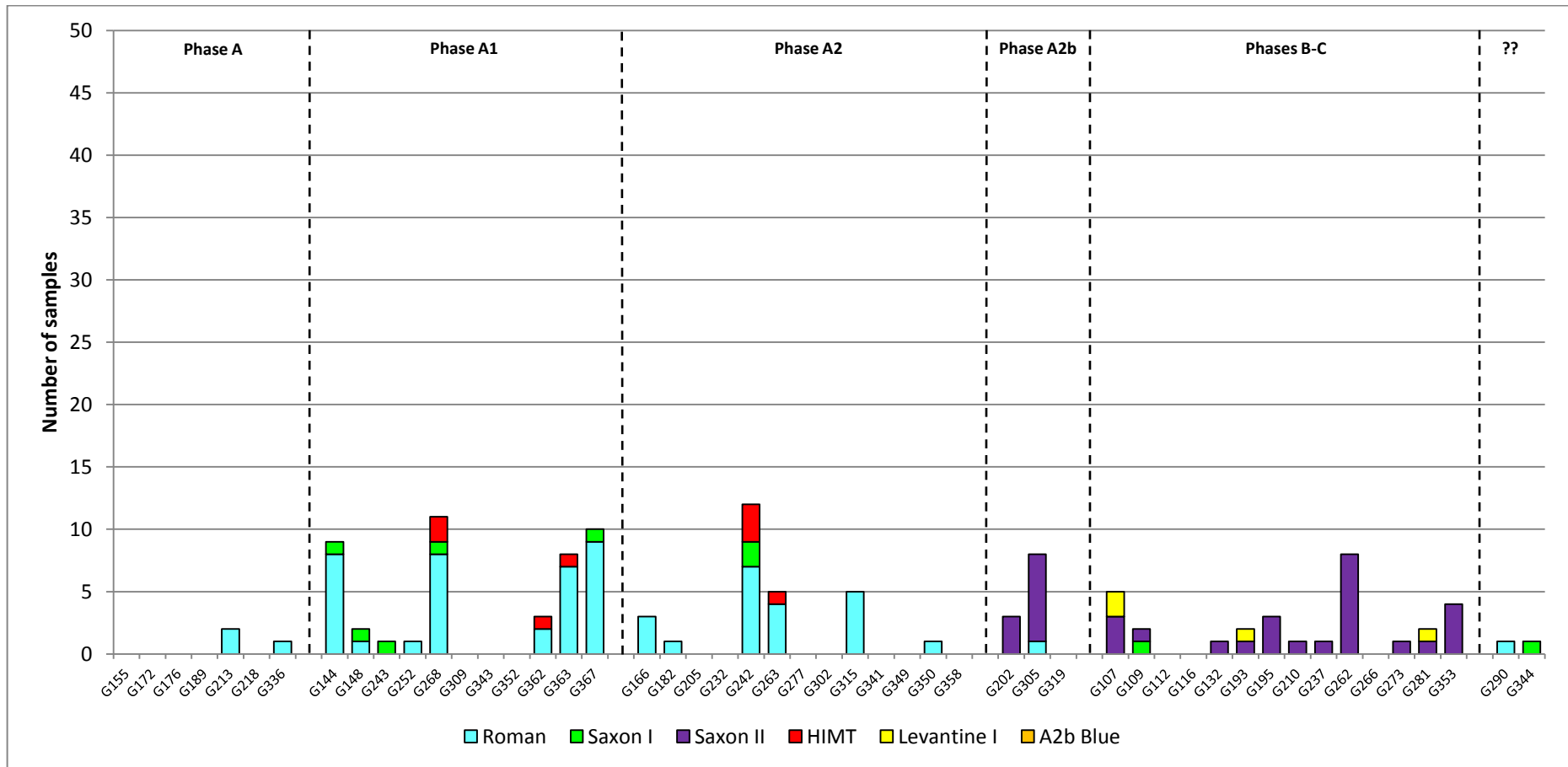


Figure 4.11.7 – Stacked histogram showing the relationship between the composition of applied decoration on polychrome beads and grave number in cemetery ERL 104 at Eriswell.

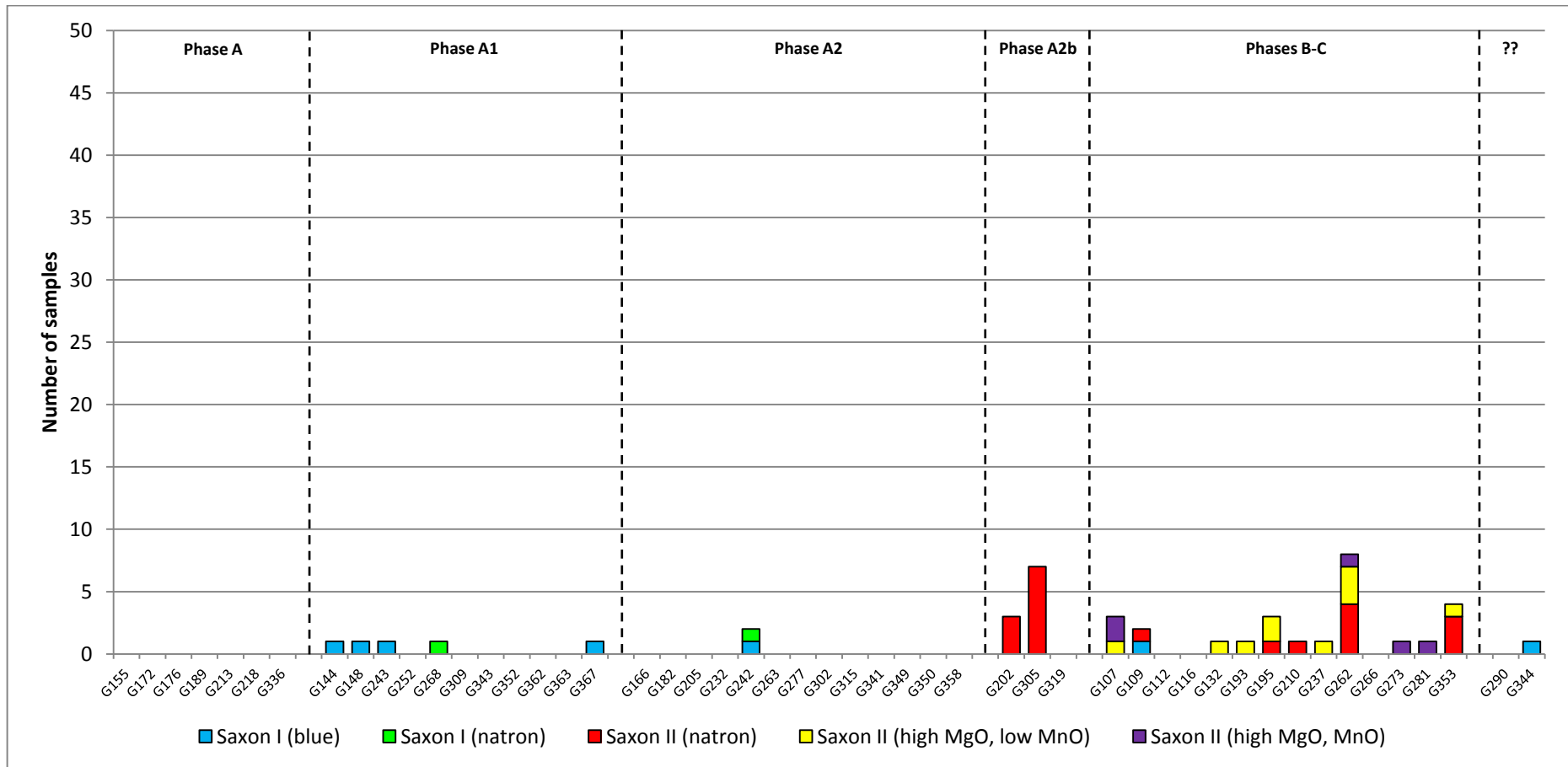


Figure 4.11.8 – Stacked histogram showing the relationship between the composition of ‘Saxon’ type applied decoration on polychrome beads and grave number in cemetery ERL 104 at Eriswell.

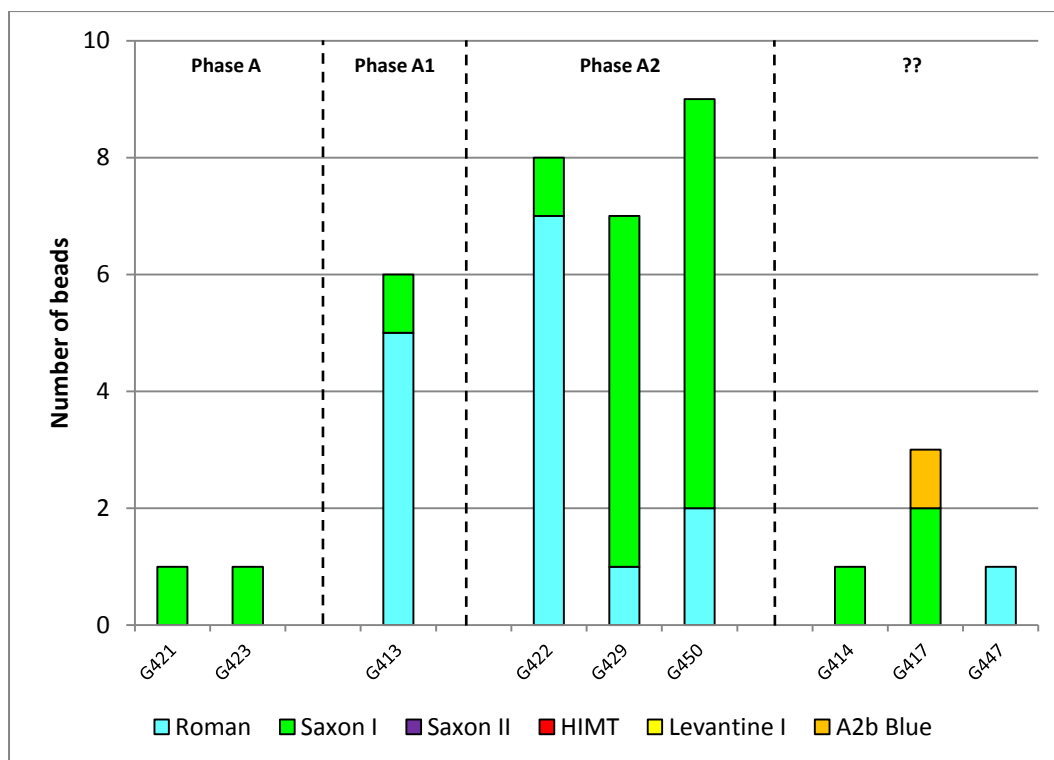


Figure 4.11.9 – Stacked histogram showing the relationship between the composition of bead body and grave number in cemetery ERL 114 at Eriswell.

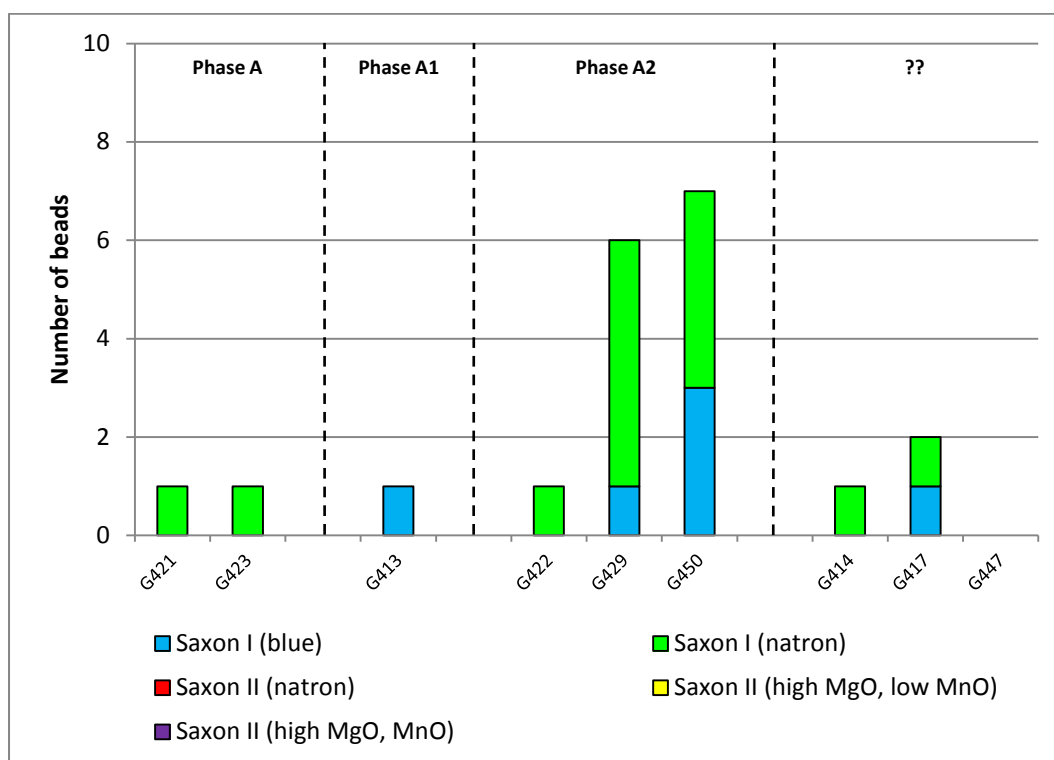


Figure 4.11.10 – Stacked histogram showing the relationship between the composition of 'Saxon' type bead bodies and grave number in cemetery ERL 114 at Eriswell.

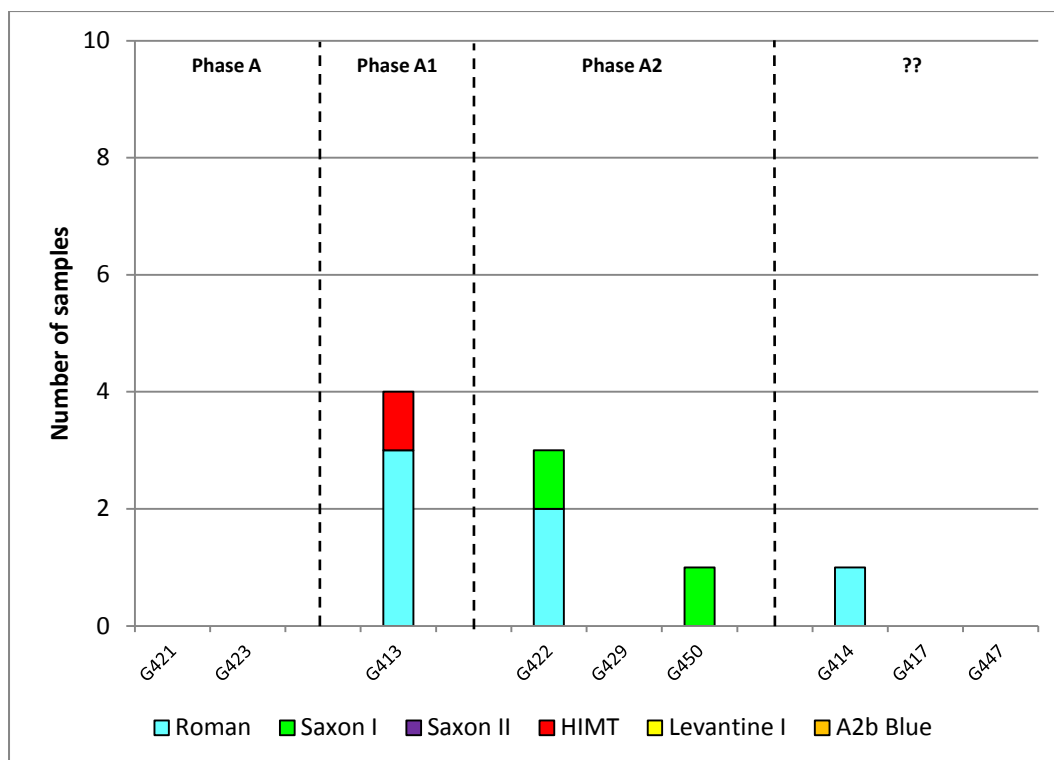


Figure 4.11.11 – Stacked histogram showing the relationship between the composition of applied decoration on polychrome beads and grave number in cemetery ERL 114 at Eriswell.

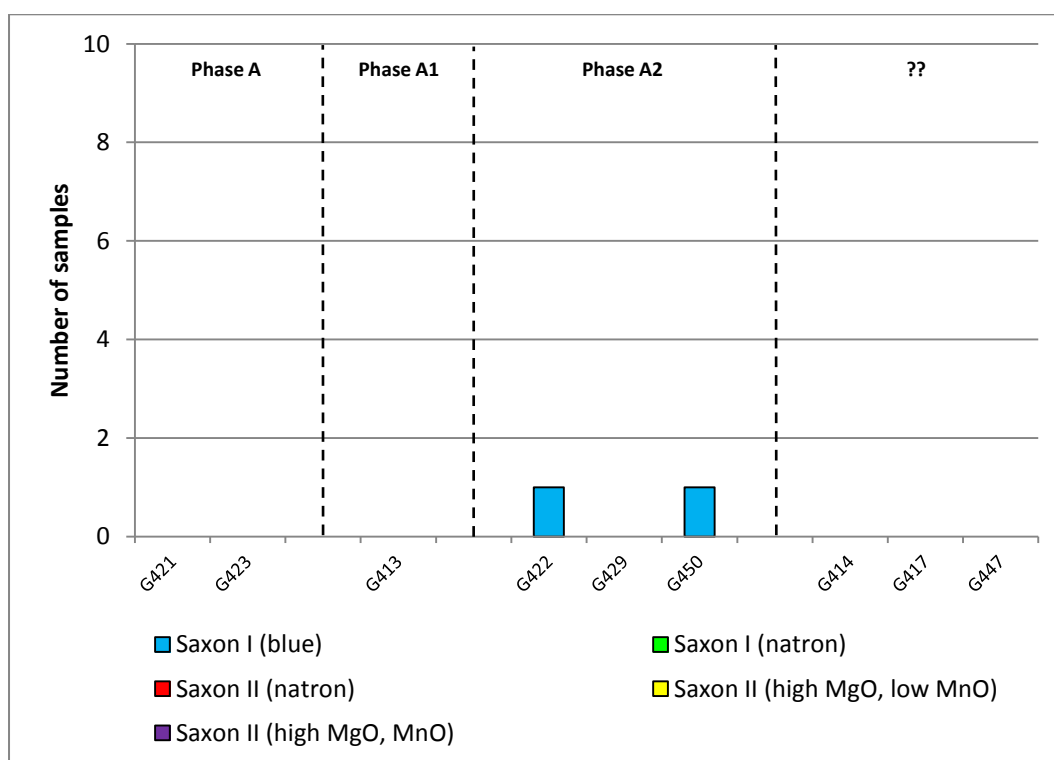


Figure 4.11.12 – Stacked histogram showing the relationship between the composition of 'Saxon' type applied decoration on polychrome beads and grave number in cemetery ERL 114 at Eriswell.

Figures 4.11.1-4.11.12 show that there is a very close agreement between Brugmann's chronological attributions for the individual graves from Eriswell and the base glass types represented by the beads within them (compare to this chapter, section 4.8). Beads produced from 'Saxon I', 'Roman' and 'HIMT' glass are generally associated together within the same graves, suggesting that these glass types were typically in use contemporaneously with one another. Similarly, beads produced from 'Saxon II' and 'Levantine I' glass are generally associated together within the same graves, again suggesting that these glass types were typically in use contemporaneously with one another. Beads produced from 'A2b Blue' glass are typically associated with beads produced from 'Saxon II (natron)' glass, supporting the view that these two glass types are likely to have been in use contemporaneously; this is consistent with the results presented earlier in this chapter (section 4.8; particularly Figure 4.8.5).

The general absence of 'later' base glass types from cemeteries ERL 046 (Figures 4.11.1-4.11.4) and ERL 114 (Figures 4.11.9-4.11.12) suggests that they are likely to have ceased operating before cemetery ERL 104 (Figures 4.11.5-4.11.8), although the identification of one 'Levantine I' sample in G05 (cemetery ERL 046; see Figure 4.11.1) suggests that this grave might be slightly later. The range of base glass types present suggests that the majority of the burials in cemeteries ERL 046 and ERL 114 are not later than the mid- or late 6th century AD.

In contrast, whilst cemetery ERL 104 appears to have been in use contemporaneously with cemeteries ERL 046 and ERL 114, it is likely to have continued to be used well into the 7th century AD, as evidenced by the presence of typically 'later' base glass types (see this chapter, section 4.8). This is in close agreement with Brugmann's phase attributions for the individual graves from this cemetery (Figures 4.11.5-4.11.8). It is possible to gauge an idea of which burials are likely to be later from the base glass types present. Graves containing beads produced from 'Saxon II (high MgO, MnO)' glass are likely to be among the latest (Figures 4.11.6 and 4.11.8); they are probably not earlier than the mid-6th century. To these can be added the majority of graves which contain beads produced from 'Saxon II (high MgO, low MnO)' glass. However, 'Saxon II (high MgO, low MnO)' glass is very complex (see this chapter, section 4.4), and it is conceivable that a

handful of these graves are marginally earlier than those containing beads produced from 'Saxon II (high MgO, MnO)' glass. Nevertheless, the majority of these graves are probably not earlier than the mid-6th century and are certainly no earlier the 6th century.

'Levantine I' glass is typically associated with 'later' glass types (*e.g.* Figures 4.11.5 and 4.11.7); the identification of a bead produced from 'Levantine I' glass in G112 suggests that this grave is therefore unlikely to pre-date the mid-6th century. 'Saxon II (natron)' glass appears to have been used over a relatively long period, probably spanning the late 5th or early 6th century through to the mid-7th century (see this chapter, section 4.8). However, it is clear from Figures 4.11.6 and 4.11.8 that beads produced from this glass type are more typically associated with beads produced from 'Saxon II (high MgO, MnO)' and 'Saxon II (high MgO, low MnO)' glass, suggesting that it was more commonly used to produce beads after the mid-6th century. The notable exceptions to this trend include G242 and G367 in which the majority of beads are produced from 'Saxon I', 'Roman' or 'HIMT' glass, and G202 and G305 in which the majority of beads are produced from 'A2b Blue' glass. It is therefore likely that all of these graves date to somewhere between the first and third quarters of the 6th century, in line with the introduction of 'Saxon II (natron)' glass. The remaining graves from cemetery ERL 104 generally contain significant numbers of beads produced from 'Saxon I' and/or 'Roman' glass, more typical of 'earlier' bead production; as such, these graves are likely to pre-date the mid-6th century.

It must be borne in mind that 'earlier' glass can be recycled at a later date, and 'earlier' beads re-used or inherited. However, there is little evidence to suggest that these were extensive practices. 'Roman', 'Saxon I' and 'HIMT' glass appear to have been far more commonly used to produce beads attributed to Brugmann's phase A, as these glass types are comparatively *much* scarcer in graves containing beads produced from 'later' 'Saxon II' and 'Levantine I' glass. The graves which have not been attributed to a chronological phase by Brugmann (denoted by '??' in Figures 4.11.1-4.11.12) all contain either 'Roman', 'Saxon I' or 'A2b Blue' glass; they are therefore consistent with Brugmann's phase A.

4.11.2. The Homogeneity of Bead Strings

By comparing the compositions of beads associated with one another in the individual graves at Eriswell, it is possible to comment upon the compositional homogeneity of the bead strings worn by particular individuals. This concept depends upon recognition of a ‘batch’: the production of a group of beads of a certain type (or even different types) from a single batch of glass (*i.e.* the same melt) in the same workshop, followed by their acquisition as a *set* by a particular individual. As such, the beads from a particular grave or string will have a very tight composition, reflecting the homogeneity of the batch from which they were produced (see Freestone *et al.* 2009: 132). However, if beads were produced by different workshops, or acquired over time, they will have slightly different compositions to one another, regardless of whether or not a common base glass type was used in their production. This is because they will have been produced from slightly different batches of glass (*i.e.* different melts). As such, it may be possible to gain insights into how beads were produced, distributed and acquired by certain workshops or individuals.

Figures 4.11.1-4.11.12 show that the majority of individual graves at Eriswell contain beads produced from a range of different base glass types. There are several possible explanations for this. Generally speaking those beads types produced from ‘Roman’ and ‘HIMT’ glass appear to be ‘Anglo-Saxon’ products, whereas those produced from other glass types appear to be ‘Continental’ imports (see this chapter, section 4.10). Many bead strings (particularly prior to the mid-6th century) clearly consist of a mixture of ‘Anglo-Saxon’ and ‘Continental’ bead types. This suggests that beads were obtained from a number of different sources, or possibly also traded and exchanged between individuals. Most individual bead strings are therefore more likely to have been composed over time rather than acquired as complete sets. Regardless of the reasons for the variability observed within many of the individual bead strings, in the majority of cases it is highly unlikely that the beads from individual graves represent the products of just one or two workshops operating at a single time and/or place.

It is highly likely that some beads types were obtained as small ‘sets’ by some individuals; for example, the *Melon* and *Melon Variation?* beads are exclusively produced from ‘A2b Blue glass’ (see this chapter, section 4.10), of which the majority are found in only two graves (G202 and G305; see Figure 4.11.5). Similarly, the two *Blue Melon, opaque* beads (ERL046:G03:1289 and ERL046:G03:1325) from G03 are clearly one-off products produced from the same batch of glass, as suggested by their unusual colourant technology (see Chapter 5, section 5.2.7). However, the evidence suggests that such ‘sets’ are likely to have consisted of just two or three beads for inclusion in a larger string. These ‘sets’ were probably bought, or perhaps even commissioned, by the same individual for inclusion in a string composed of other bead types. In some cases at least, beadmaking workshops therefore appear to have produced consignments of beads of a certain type from the same batch of glass, as might be expected. These beads may then have been split up and bought (or sold) individually as small ‘sets’ or individual beads.

However, some beads of the same type from individual bead strings were clearly not acquired as sets. The six *Blue* beads analysed from G242, which are all of the ‘Saxon I (blue)’ type, were not all produced from the same batch of glass. However, some of these appear to have been produced from the same batch of glass, and are again likely to have been acquired as small ‘sets’ of two or three beads. In contrast, the five *Blue* beads analysed from G309 were *all* produced from slightly different batches of ‘Saxon I (blue)’ glass, suggesting that they were not acquired as a set. The same pattern is reflected in *Blue* beads from other graves, including G315, G362, G363 and G367. Similarly, the six *Brown** beads from G242 do not appear to have been produced from the same batch of glass, even though they are all of the ‘Saxon I (natron)’ type. This suggests that beads of the *same* type on some strings may have been acquired at different times and/or from different workshops.

A similar pattern is observed with other common bead types at Eriswell. Three slightly different batches of ‘Saxon I (natron)’ glass appear to have been used to produce the five *Constricted Segmented* beads analysed from G242; this again suggests that they were acquired as small ‘sets’ of two or three beads over time.

Analysis of larger assemblages from individual graves may reveal that larger ‘sets’ than this were sometimes acquired.

This pattern becomes far more marked in bead strings worn after the mid-6th century. Out of the four *Orange* beads from G193, two were made from ‘Levantine I’ glass, one from ‘Saxon II (natron)’ glass and one from ‘Saxon II (high MgO, low MnO)’ glass, which strongly suggests that they were acquired at different times and/or from different workshops. However, as previously mentioned (see this chapter, section 4.10.3.3), some workshops producing beads at this time appear to have had access to more than one type of base glass. Nevertheless, these beads were certainly produced from different batches of glass, and therefore probably also at different times. It cannot be excluded that they were acquired as a ‘set’ assuming that they were produced in the same workshop utilising different glass types, but this seems highly unlikely.

It seems most likely that ‘Anglo-Saxon’ beads were acquired over time (sometimes as pairs or small ‘sets’), particularly prior to the mid-6th century, probably from the same workshop producing consignments of the same bead type from slightly different batches of glass at a local or regional level. However, the ‘Continental’ bead types from Eriswell were clearly widely traded. Many of these bead types, particularly after the mid-6th century, were probably produced by several different workshops over a period of time. Consignments of beads may have been imported to England from a number of these different workshops producing beads for the export market; this would result in the ultimate mixing of beads produced at different times by different workshops from different batches of glass. Whilst these beads may subsequently have been acquired as small ‘sets’ in England, the mixing of different types during their export and/or distribution would mean that such ‘sets’ may have a considerably variable composition; for example, Guido (1999: 64) suggests that exotic goods such as *Orange* beads may have reached Kent from a variety of trade routes rather than as a single package, which would account for the compositional variability observed in beads of this type from Eriswell.

4.11.2. The Distribution of Glass Types

Figure 4.11.13 shows the number of graves at Eriswell in which the different glass types identified are represented. Whilst this is again biased by the sampling process (see Chapter 2, section 2.1.2), a concerted effort was made to sample beads from as many different graves as possible; samples were analysed from beads from 71 out of the 78 graves in which glass beads were recovered at Eriswell. Figure 4.11.13 shows that 'Roman' and 'Saxon I' glass are by far the most widely distributed glass types at Eriswell, each being represented by beads from well over 30 graves. In contrast, the remaining glass types are each represented by beads from less than 15 graves. This indicates that beads produced from the 'earlier' glass types were generally much more widely distributed than those produced from the 'later' glass types. This is consistent with a fall in the number of beads deposited with the dead by the 7th century (Hines et al., in press).

The most poorly distributed glass types at Eriswell are 'Saxon II (high MgO, MnO)' and 'A2b Blue' glass; each of which are represented in no more than 5 graves. This is consistent with the view that they are likely to have been relatively short-lived glass types, probably used by a very limited number of workshops. 'HIMT' glass, which was more typically used in the production of 'earlier' beads, is not widely distributed; this is consistent with the view that it represents recycled material, which was either not widely available or not widely used for bead production. The poor distribution of 'Levantine I' glass suggests that it is unlikely to have been in use for an extended period; its availability is likely to have been restricted, both in quantity and in the number of workshops able to access it.

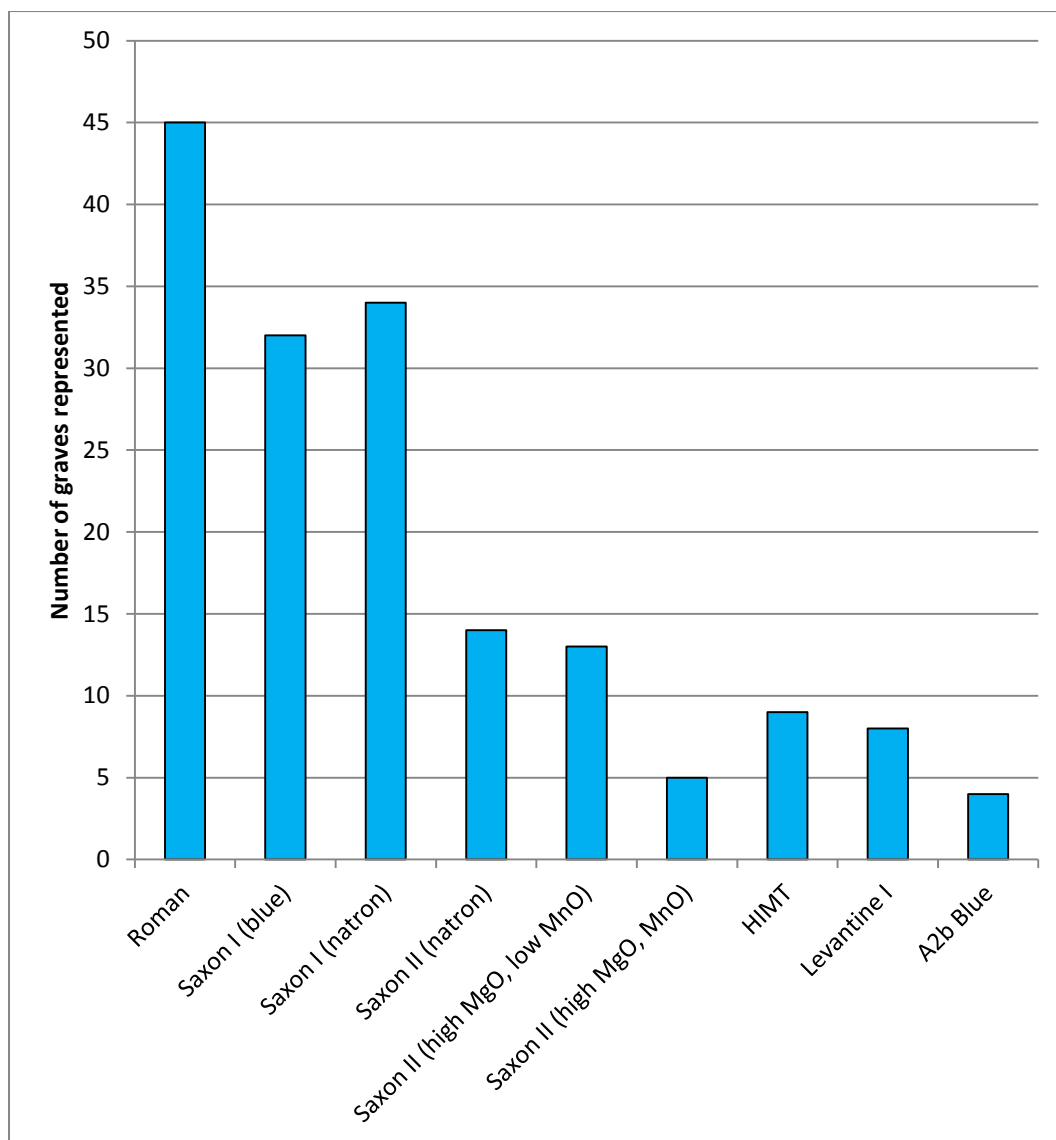


Figure 4.11.13 – The number of graves at Eriswell in which the different base glass types identified are represented.

CHAPTER FIVE

5. Results: Colourant Technology

Intentionally coloured glasses are those to which colouring materials have been deliberately added, whereas naturally coloured glasses are coloured by small quantities of impurities present in the raw materials. It is sometimes difficult or impossible to determine whether a glass has been deliberately coloured. There are a number of ways in which an intentionally coloured translucent or opaque glass may have been produced:

- The raw colourant and/or opacifying materials may have been added to a batch of glassmaking raw materials (sand and natron), which were melted together to produce a finished coloured glass.
- The raw colourant and/or opacifying materials may have been added to a ready-made base glass, possibly produced elsewhere, to colour or opacify it.
- The raw colourant and/or opacifying materials may have been preheated to produce pre-made pigments, which were then added to a ready-made base glass to colour or opacify it.

The production of Anglo-Saxon coloured glasses is not restricted to any one of these methods, and a combination may have been employed in the production of different colours; for example, it has been demonstrated that cobalt-blue glass is likely to have been coloured during the production of the raw glass itself (see Chapter 4, section 4.9). Once colourants, decolourants and/or opacifiers had been added as desired, the glass was ready to be shaped. This may have been undertaken in the same workshops that coloured the glass, or the glass may have been transported elsewhere to be shaped.

The interpretation of intentionally and naturally coloured glasses is often very complex as a number of factors, both internal and external, can affect its final appearance. This includes deliberate additives (colourants, decolourants and

opacifying agents), impurities associated with these additives or the raw materials used to produce the raw glass (*e.g.* sand), the furnace conditions (*e.g.* temperature, redox conditions and the duration of heating) and the composition of the glass itself (Bayley 1999: 89; Mirti *et al.* 2002: 221; Paynter and Kearns 2011: 5). The range of different glass colours represented in the Eriswell assemblage suggests that the early craftsmen that produced them exercised considerable control and understanding of the colourants and opacifiers they employed. The main elements used to alter the appearance of the glasses at Eriswell include manganese, antimony, iron, copper, cobalt and tin, but lead can also sometimes affect colour or opacity.

Brugmann (2004) uses only approximate colour definitions, as opposed to specific colour definitions (*e.g.* the Munsell Book of Colour) to describe the different colours present in Anglo-Saxon glass beads. This is because of difficulties in being able to use colour charts consistently under varying light conditions in different institutions (Brugmann 2004: 24). All beads which would have been otherwise described as black are termed ‘dark’ and all beads that would have been otherwise described as ‘metal-in-glass’ are termed ‘light’, as metal foil is not always present in the latter (Brugmann 2004: 24; see also Chapter 3, section 3.1.2). The broad colour descriptions used therefore account for subjective differences in the interpretation of the same colours by different individuals (see Brugmann 2004: 24).

Glasses containing crystalline opacifying agents (or bubbles) in sufficient quantity to cause *complete* opacity are classed as opaque (*i.e.* do not allow the passage of light) in the present study (see this chapter, section 5.2), whereas glasses containing these inclusions in insufficient quantity to cause complete opacity (*i.e.* semi-opaque) are classed as translucent (see this chapter, section 5.1). Note that ‘dark’ glass is deemed translucent here, as opacity is caused by the depth of colour rather than through the presence of a crystalline opacifying agent.

The primary crystalline opacifying agents used in early glass were based on antimony or tin, but copper can also cause opacity in its reduced state (cupric or cuprous). Antimony-based opacifiers are typically associated with glass produced until the 4th century AD. Tin-based opacifiers only became common after the 4th century AD, when they generally replaced those based on compounds of antimony

(Biek and Bayley 1979: 9; Rooksby 1962: 23; Sayre 1963: 281; Sayre 1965: 150; Tite *et al.* 2008: 68; Turner and Rooksby 1961: 2). They were extensively used throughout the rest of the 1st millennium AD. The subsequent switch from antimony to tin-based opacifiers in both northern Europe and the Eastern Mediterranean is likely to have resulted from a breakdown in the supply of antimony (Tite *et al.* 2008: 79). It is likely that the introduction of tin-based opacifiers in northern Europe was independent from their introduction in the Eastern Mediterranean (Tite *et al.* 2008: 80). However, whilst tin replaced antimony as an opacifier in the Eastern Mediterranean and northern Europe, antimony-based opacifiers appear to have continued to be used (or re-used) in some parts of the Western Mediterranean (Italy) until the 13th century AD (Uboldi and Verità 2003: 136; Tite *et al.* 2008: 68).

Many opaque glasses also contain lead, which not only lowers the melting point of the glass, but can also promote the solubility of opacifying agents and facilitate the controlled precipitation of crystals on cooling of the melt (Bayley 1995: 1198; Bayley and Wilthew 1986; Biek and Bayley 1979: 16-17).

Opacity can also result from the intensity of the colour, the thickness of the glass, surface abrasion, weathering phenomena and surface decay (Bayley 1999: 92; Biek *et al.* 1985: 79-80; see also Chapter 3, section 3.3). In addition, many of the samples from Eriswell contain relicts of raw materials which have not fully dissolved in the glass, and are almost certainly associated with the colouring and/or opacifying processes. These include fragments of refractory ceramic, metallic globules and scale which may have been incorporated through working and marvering, or as a result of incomplete melting of the batch materials (Brill 1988: 282-283; Brill and Moll 1963: 300), which can sometimes contribute to opacity. Their presence suggests that firing times were short or temperatures low, or both. Other crystalline components may include devitrification products (*e.g.* wollastonite, CaSiO_3) which formed as the glass cooled (Bayley 1999: 92; Brill and Moll 1963: 300; Brun and Pernot 1992: 245-247; Henderson 1985: 286), or reaction products which formed as a result of interactions between the glass and the crucible fabric, or between the raw materials themselves. These can also contribute to opacity, depending upon their size and density. It has been suggested that the formation of devitrification products may be promoted by high levels of lead within a glass (Brun and Pernot 1992: 247).

5.1. Translucent Glass

All of the translucent glasses from Eriswell are natron-based soda-lime-silica glasses to which different colouring agents and quantities of lead have been added. These colourants typically take the form of deliberately or unintentionally added transition metal ions dissolved in the glass; the intensity of the colour depends largely upon the type of ion present and its state of oxidation (Mirti *et al.* 2002: 221; Sanderson and Hutchings 1987: 99). Whilst these glasses are sometimes referred to as lead-soda-lime-silica glasses on account of the high lead contents (*e.g.* Henderson and Ivens 1992: 60; Henderson 2000b: 144), typically greater than 3% PbO, here they are referred to as soda-lime-silica glasses; lead was added during the colouring process rather than during the production of the raw glass itself, as evidenced by the absence of lead in uncoloured glass.

5.1.1. Uncoloured and Naturally Tinted Glass

It is generally assumed that most naturally tinted and uncoloured glasses were probably not deliberately coloured. The colour was instead caused by an undesirable iron impurity primarily introduced with the glassmaking sand (Bayley 1999: 90; Frederickx *et al.* 2004: 330; Henderson 1985: 283; Heyworth 1996b: 54; Jackson 2005: 763-764; Schreurs and Brill 1984: 207; Weyl 1951: 91). Iron may be present in glass in the ferric or ferrous state, depending upon the redox conditions within the melt (Brill 1988: 269; Schreurs and Brill 1984: 199; Silvestri *et al.* 2005: 811; Uboldi and Verità 2003: 132). Glass may have been tinted blue in strongly reducing conditions (ferrous iron), green in weaker reducing conditions (ferrous and ferric iron), and yellow-brown in oxidising conditions (ferric iron) (Bayley 1999: 89; Brill 1988: 269; Heyworth 1994: 79; Mirti *et al.* 2002: 221; Mortimer and Heyworth 2009: 409; Sanderson and Hutchings 1987: 105; Schreurs and Brill 1984: 199; Uboldi and Verità 2003: 132; Vallotto and Verità 2000: 71; Weyl 1951: 91). Iron in both the ferric and ferrous states can exist within the same glass, and a combination of colours could therefore be achieved depending upon the furnace atmosphere (Mirti *et al.* 1993: 230-231; Mirti *et al.* 2002: 221; Silvestri *et al.* 2005: 811). Olive

and strong yellow-amber tints could also form in reducing conditions by ferri-sulphide complexes; sulphur sometimes being introduced with organic material such as plant ash (Brill 1988: 272; Mirti *et al.* 1993: 231; Schreurs and Brill 1984: 207).

In highly coloured glasses the effects of iron did not pose a problem because they were masked by the deliberate addition of a colouring agent (Henderson 2000a: 34; Heyworth 1996b: 54). However, to produce colourless or near-colourless glass the raw materials selected needed to be relatively pure (*i.e.* low in iron) (Jackson 2005: 763-764). Alternatively, decolourising agents could be added to counteract (oxidise) the iron impurity (Mirti *et al.* 2002: 221; Schreurs and Brill 1984: 208). Antimony and manganese were two such materials used for decolourisation in the past; these are described in detail in Chapter 4, section 4.1.4. The colour of lightly tinted glass is further affected by the redox equilibrium between iron and any added decolourants, and is largely independent of the purity of the glassmaking sand or the quantity of added decolourant (Brill 1988: 275; Mirti *et al.* 1993: 231; Mirti *et al.* 2002: 221; Sanderson and Hutchings 1987: 105; Schreurs and Brill 1984: 204; Vallotto and Verità 2000: 71).

Samples of uncoloured and naturally tinted glass were obtained from 78 beads from Eriswell. A number of different tints ranging from yellow through to blue-green and green have been described by Birte Brugmann. The tints of these glasses have been established by eye under daylight, and are therefore subjective (Brugmann 2004: 24). Some tints were more difficult to identify, primarily because they were used as decoration on highly coloured glass or to produce visually complex patterns (*e.g.* *Reticella* beads), so can only be described as 'translucent'. Furthermore, glass described as 'translucent green' may be coloured by either copper or iron. The presence of copper is assumed to indicate a deliberate addition, discussed in section 5.1.4 below. The present section refers only to translucent green glasses coloured by iron, which is generally assumed to have been an unintentional addition.

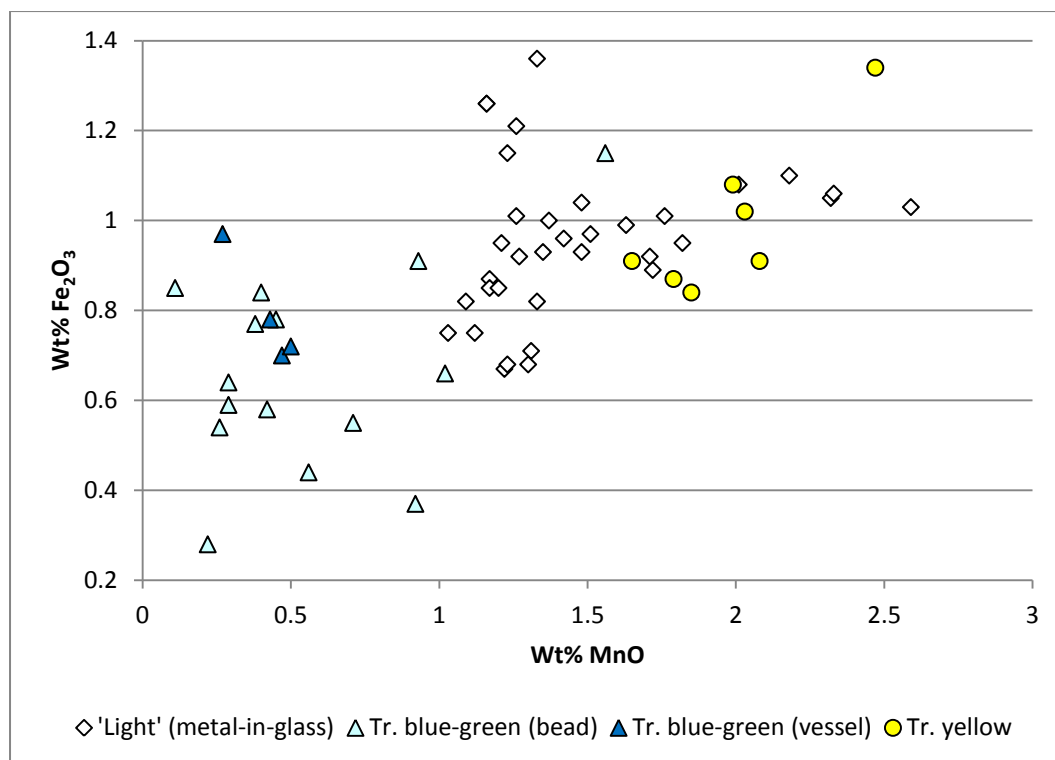


Figure 5.1.1 – A plot of iron oxide versus manganese oxide for the naturally coloured samples from Eriswell, showing 'light' ('metal-in-glass'), blue-green and yellow tints. Compare to Figure 5.1.2.

A plot of iron versus manganese (Figures 5.1.1 and 5.1.2) in the uncoloured and naturally tinted glasses analysed from Eriswell shows that the relative proportions of these two components strongly relate to the tint. 'HIMT' glass generally contains the most iron (typically in excess of 1.3% Fe_2O_3) and is the one of the most strongly tinted glasses, resulting from the use of an impure glassmaking sand. Comparison with Figure 5.1.3 shows that 'Roman' glass is predominantly blue-green tinted, 'Saxon I' and 'Saxon II' glass is predominantly 'light' or yellow tinted and 'HIMT' glass is predominantly green tinted. 'Roman' glass generally contains the least iron (typically less than 1% Fe_2O_3), reflecting the use of a relatively pure glassmaking sand; the presence of low levels (typically less than 1.0%; Figures 5.1.4 and 5.1.5) of both antimony and manganese, which are typical of Roman blue-green glass (see this chapter, section 4.3), are likely to contribute to decolourisation. It is not possible to distinguish between blue-green beads and vessel fragments (presumably Roman), supporting the view that these beads were probably produced from recycled blue-green tinted material.

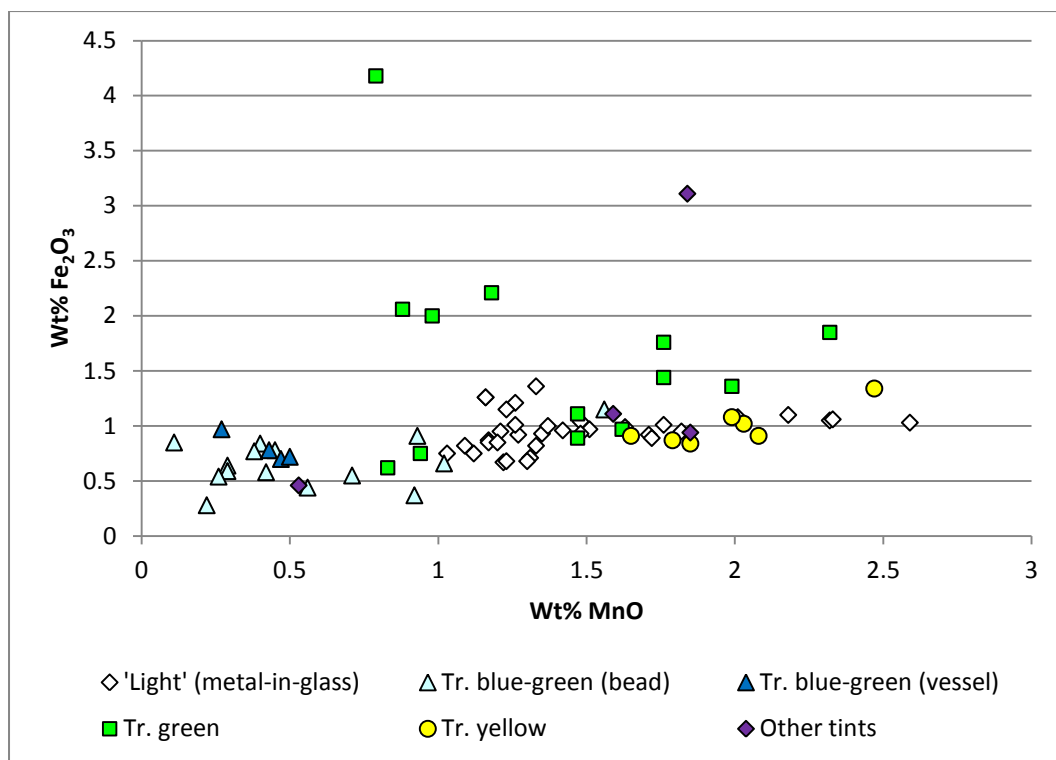


Figure 5.1.2 – A plot of iron oxide versus manganese oxide for the naturally coloured samples from Eriswell, showing the different tints identified. Compare to Figure 5.1.3.

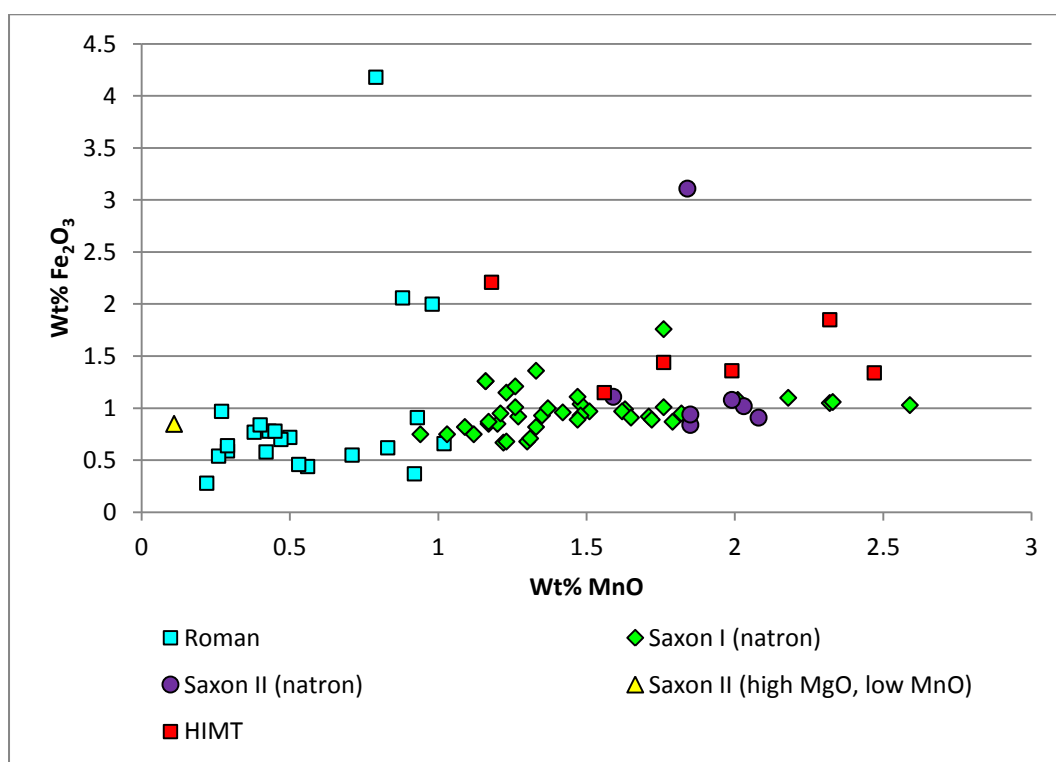


Figure 5.1.3 – A plot of iron oxide versus manganese oxide for the naturally coloured samples from Eriswell, showing the different base glass types identified. Compare to Figure 5.1.2.

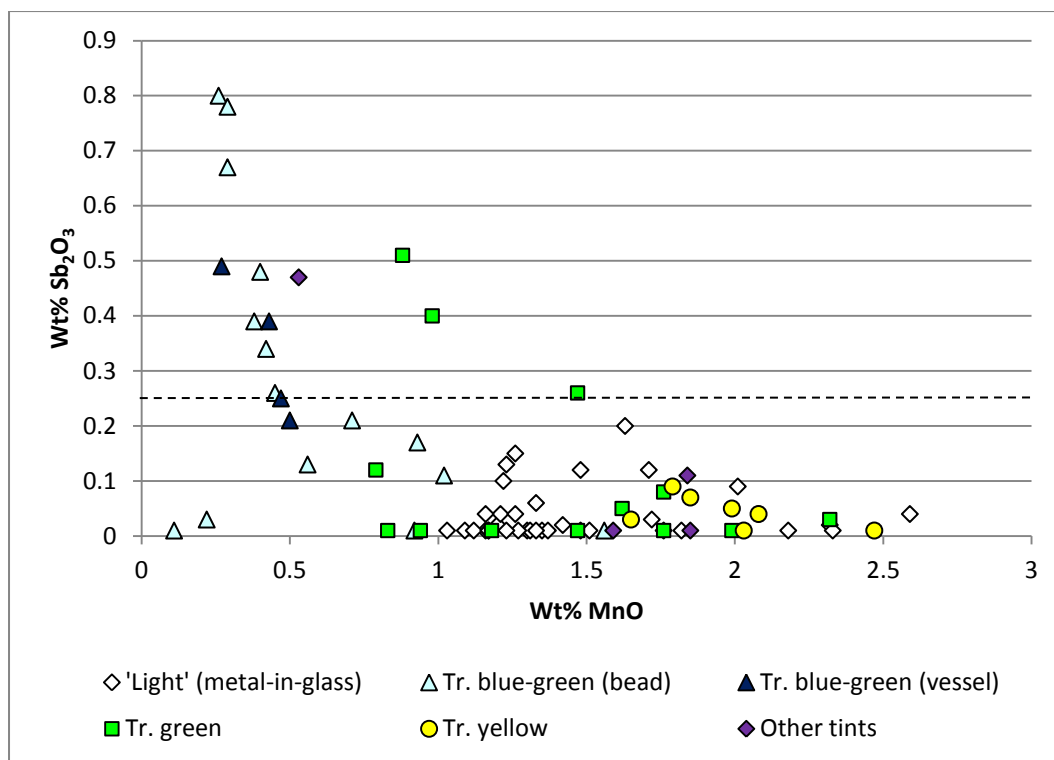


Figure 5.1.4 – A plot of antimony oxide versus manganese oxide in the naturally coloured samples from Eriswell, showing the different tints identified. Compare to Figure 5.1.5. The dashed line represents the approximate detection limits for antimony.

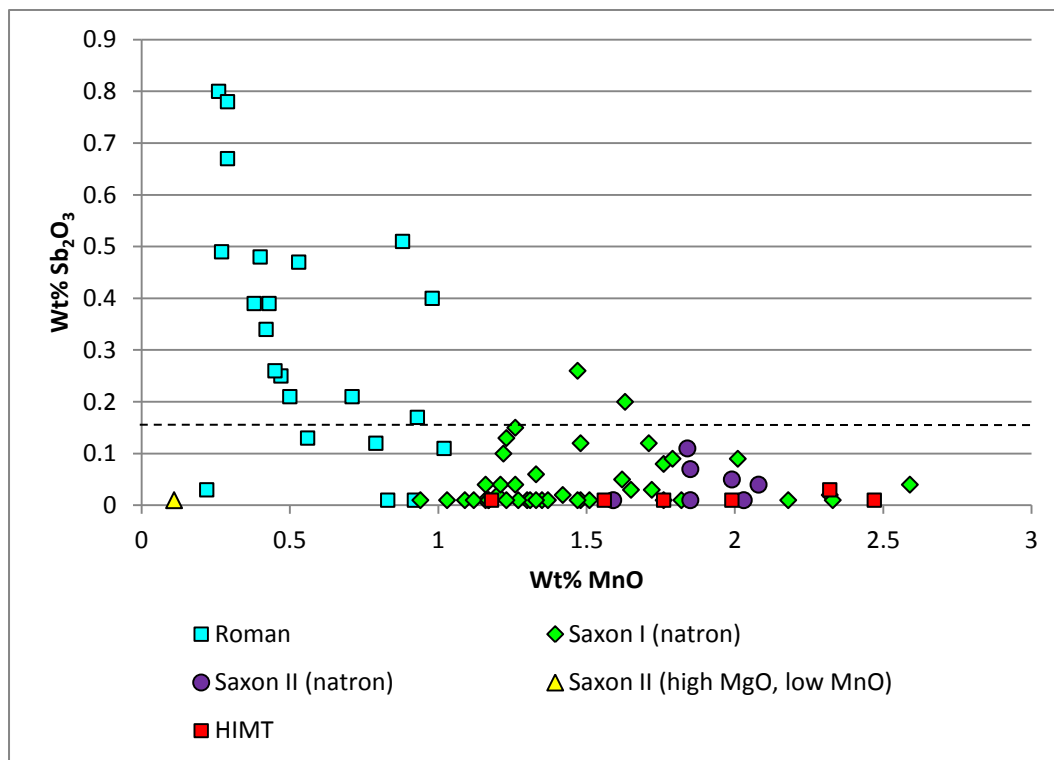


Figure 5.1.5 – A plot of antimony oxide versus manganese oxide in the naturally coloured samples from Eriswell, showing the different base glass types identified. Compare to Figure 5.1.4. The dashed line represents the approximate detection limits for antimony.

‘Saxon’ and HIMT’ glass types typically contain in excess of 1% MnO. Decolourants were clearly not always successful in completely eliminating the colour caused by iron impurities. The very weak positive correlation between iron and manganese (Figures 5.1.1-5.1.3; $r^2 = 0.37$ when excluding translucent green and ‘other’ tints) suggests that some control may have been exercised over the amount of manganese added to the batch (see also Chapter 4, section 4.4).

Several of the translucent green tinted samples contain particularly elevated levels of iron (Fe_2O_3 in excess of 3%) (Figure 5.1.2) which does not appear to relate to the base glass used (Figure 5.1.3). Furthermore, such high levels are unlikely to have resulted from contamination from the melting pot, as the samples in question so not contain lead (see Chapter 4, section 4.1). It is therefore likely that iron was deliberately added in these samples to produce the colour, or that impure (*i.e.* iron-rich) raw materials were deliberately selected for their production. Translucent green sample ERL104:G315:2346 contains 4.2% Fe_2O_3 , and comprises decoration on a *Traffic Light Twisted Trail* bead; this bead type typically consists of translucent green glass trails coloured instead by copper (see section 5.1.4 below), supporting the view that iron was sometimes deliberately added as a colourant. Similarly, the use of a strongly green tinted ‘HIMT’ glass for the applied decoration on bead ERL104:G363:1922 (*Traffic Light Streaked*) is likely to reflect the deliberate selection of a naturally coloured glass, as the remaining colours on this bead were produced from a ‘Roman’ base glass.

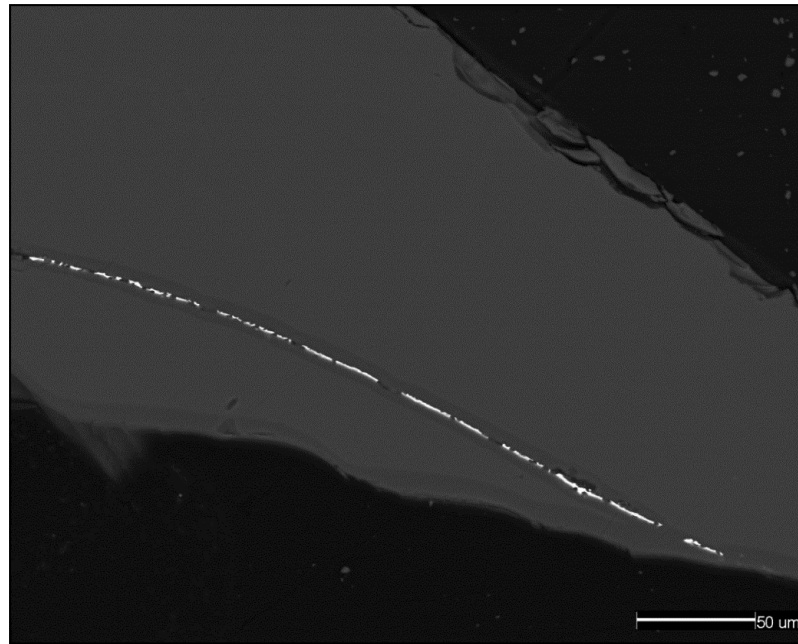


Figure 5.1.6 – BSE micrograph showing ‘light’ sample ERL104:G315:3244, a *Constricted Segmented* (‘metal-in-glass’) bead. A layer of gold foil (bright white) is visible sandwiched between two layers of soda-lime-silica glass (grey).

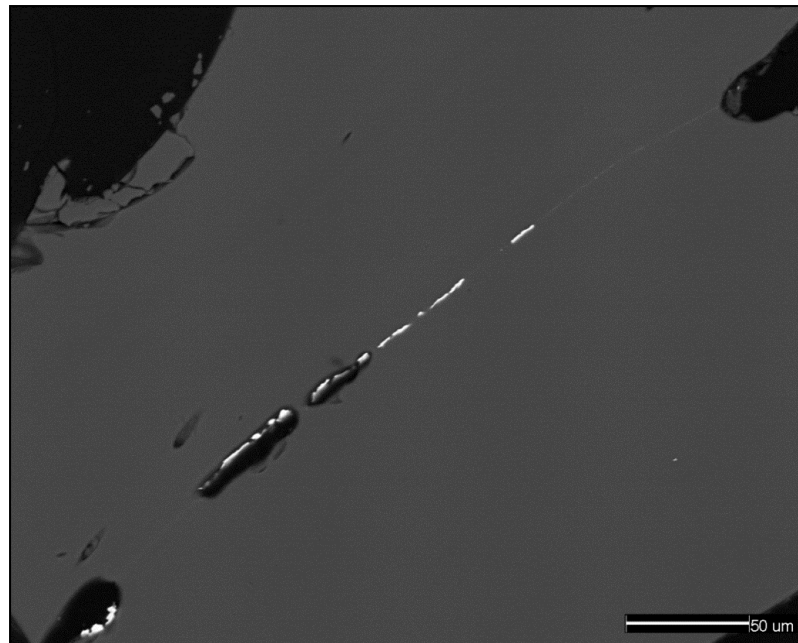


Figure 5.1.7 – BSE micrograph showing ‘light’ sample ERL104:G358:2762, a *Constricted Segmented* (‘metal-in-glass’) bead. A layer of silver foil (bright white) is visible sandwiched between two layers of soda-lime-silica glass (grey).

The metal-in-glass ('light') beads (Brugmann's *Constricted Segmented* and *Constricted Cylindrical, light* types) are all produced from 'Saxon I (natron)' glass and therefore form a relatively tight compositional group (see this chapter, section 4.10). The compositional homogeneity suggests that they may have been products of a limited number of specialist beadmaking workshops. The slight amber tint of many of these 'light' glasses is produced by low levels of iron present, corresponding to 0.4-1.4% Fe₂O₃. It was not possible to identify the type of metal foil (if present at all) used in the production of every *Constricted Segmented* bead analysed due to the small nature of the samples taken. Beads ERL104:G277:1600, ERL104:G315:3244, ERL046:G08:1550 and ERL046:G08:1584 all contained gold foil (Figure 5.1.6), whereas bead ERL104:G358:2762 contained silver foil (Figure 5.1.7). As all of these beads are of the same type, this suggests that they are likely to have been products of slightly different workshops using different types of foil, or of the same workshop operating at slightly different times, but all using the same type of 'Saxon I (natron)' glass. It is possible that some bead types (*e.g.* gold-foil beads) were more expensive to produce than others (*e.g.* silver-foil beads).

5.1.1.1. Trace Element Analyses

Only two naturally tinted glasses were analysed by LA-ICP-MS, so a detailed comparison between uncoloured glasses is not possible here. A plot of the translucent blue-green tinted 'Roman' sample with that of the translucent green tinted 'HIMT' sample analysed illustrates relatively little difference between the two tints (Figure 5.1.8). Both glasses contain relatively low levels of colouring elements; typically well below 100 ppm. The main differences are in manganese and antimony content, which relate to the base glass types used (see Chapter 4); antimony is considerably elevated in the 'Roman' glass (3300 ppm), whereas manganese is considerably elevated in the 'HIMT' glass (18670 ppm). Furthermore, the 'HIMT' green tinted glass contains far more iron than the 'Roman' blue-green tinted glass, reflecting the use of a much less pure glassmaking sand (see Chapter 4).

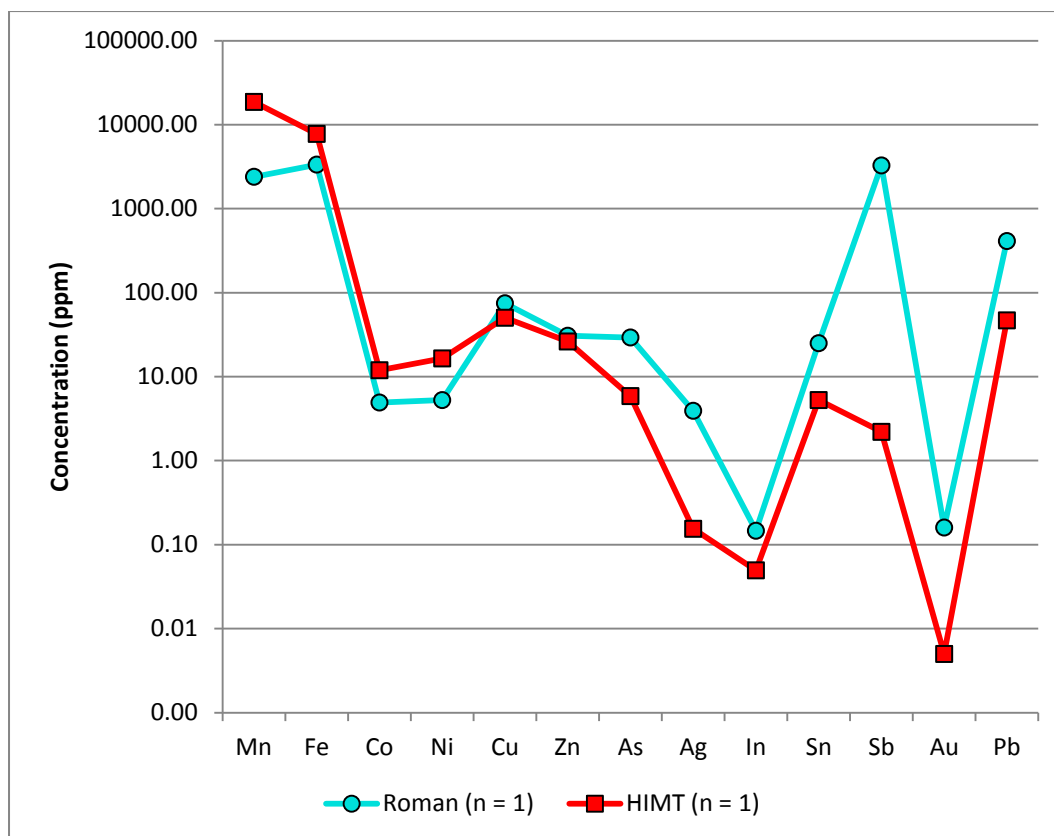


Figure 5.1.8 – Colourant and colourant-related element concentrations for translucent blue-green sample ERL104:G290:1721 and translucent green sample ERL104:G268:3260 from Eriswell. Note the logarithmic scale.

The slightly elevated levels of some colouring elements, including copper, arsenic, tin and lead in the ‘Roman’ blue-green tinted sample relative to the ‘HIMT’ sample are consistent with the use of recycled material (see Chapter 4, section 4.3).

5.1.2. Translucent Pink-Brown Glass

Samples of translucent pink-brown glass were obtained from nine beads from Eriswell, all of which are coloured by manganese at concentrations corresponding to 1.4-1.9% MnO. When in the divalent form (Mn^{2+}), manganese acts as a decolourant (Mirti *et al.* 1993: 231; Weyl 1951: 123; see Chapter 4, section 4.1.1.4). However, in the trivalent form (Mn^{3+}) it acts as a colourant, imparting a strong purple or pink-brown colour to glass (Fiori and Vandini 2004: 189; Henderson 1985: 283; Mirti *et al.* 1993: 231; Mirti *et al.* 2002: 221-222; Schreurs and Brill 1984: 205; Weyl 1951: 123), as is the case here. Figure 5.1.9 shows a plot of manganese versus iron in the translucent pink-brown glasses analysed, compared to those for the naturally tinted uncoloured glasses discussed in section 5.1.1 above. It is clear that the relative concentrations of these two components are consistent with those observed in uncoloured manganese-decoloured glass, indicating that careful control of the redox conditions within the furnace were necessary in order to produce the colour. The pink-brown glass was melted in an extremely oxidising atmosphere (Weyl 1951: 129), in contrast to the reducing atmosphere necessary for the production of manganese-decoloured glass.

All of the translucent pink-brown samples analysed are probably of the 'Saxon I (natron)' compositional type (see Chapter 4, section 4.9). However, a plot of manganese versus magnesia (Figure 5.1.10) shows that they form a relatively tight compositional group which does not correspond exactly with 'Saxon I (natron)' glass. This is consistent with a separate manganese addition, probably to a 'Saxon I (natron)' base glass. No samples of this glass colour were analysed for trace elements.

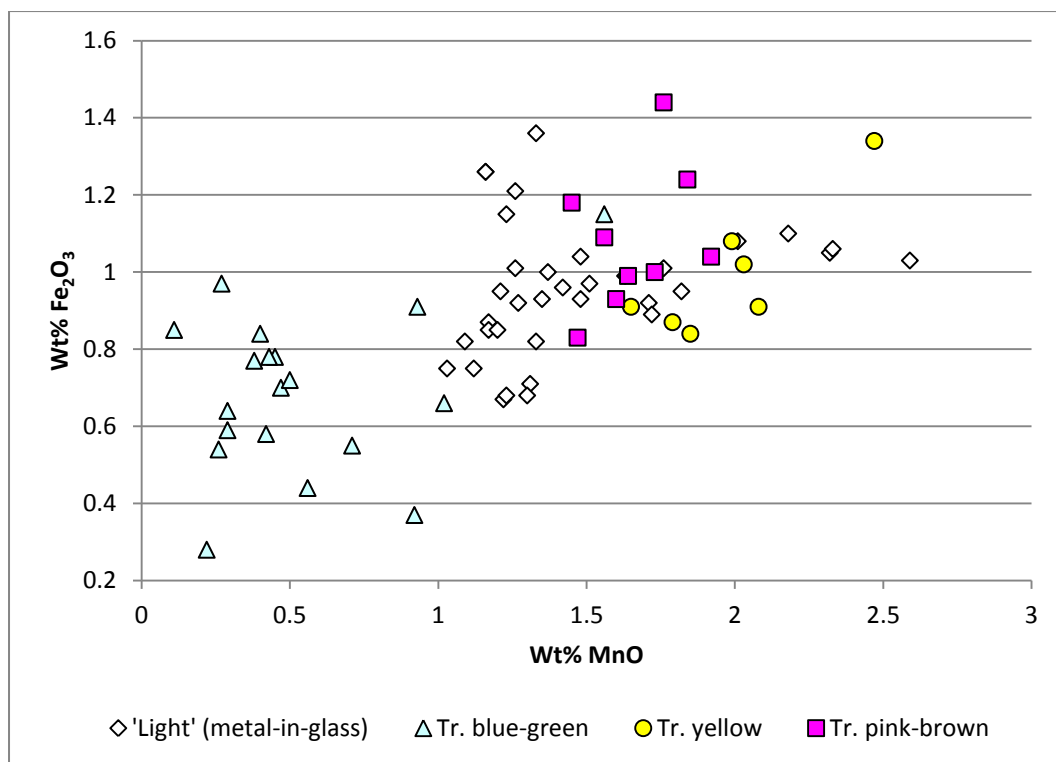


Figure 5.1.9 – A plot of iron oxide versus manganese oxide for the translucent pink-brown samples from Eriswell, compared to the naturally coloured samples (Figure 5.1.1).

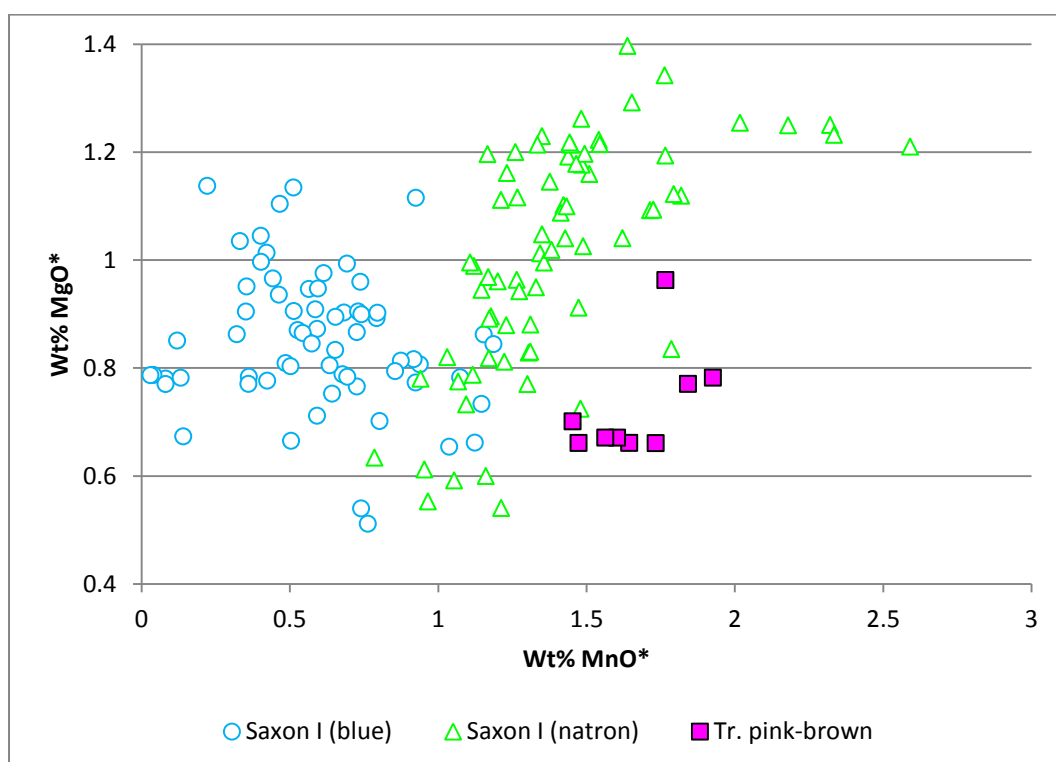


Figure 5.1.10 – A plot of manganese oxide versus magnesia for the translucent pink-brown samples from Eriswell, compared to 'Saxon I' glass (see Chapter 4, section 4.4).

5.1.3. Translucent Blue Glass

Samples of translucent blue glass were obtained from 113 beads from Eriswell. These are all coloured by cobalt in concentrations corresponding to anywhere up to 0.3% CoO. When present in the divalent form (Co^{2+}), cobalt can produce an intense blue colour at very low concentrations (Bayley 1995: 1196; Bayley 1999: 90; Biek and Bayley 1979: 8; Brill 2006: 134; Henderson 1985: 278; Sanderson and Hutchings 1987: 102; Vallotto and Verità 2000: 72; Weyl 1951: 170; Wilthew 2006: 390). Many different shades of blue can be produced through only slight variations in the amount added, together with variations in the thickness of the glass. Whilst early blue glass may sometimes be coloured by copper (Biek and Bayley 1979: 8; Brill 2006: 134; Frederickx *et al.* 2004: 333; Mirti *et al.* 20002: 222; Wilthew 2006: 390), CuO is typically present at levels below 0.8% in the blue samples analysed from Eriswell, indicating that copper is not the principal colouring agent here. Where cobalt was not detected, it could be present at concentrations below the detection limits of SEM-EDS (approximately 0.1% for CoO) (Bayley 2000a: 217; Henderson 1990: 157; Heyworth 1996b: 54; Mortimer 1998: 256; Mortimer and Heyworth 2009: 407-409).

Cobalt is usually accompanied by a number of impurities (see section 5.1.3.1 below). Whilst iron is likely to have been primarily introduced with the glassmaking sand used in the production of the base glass (*e.g.* see Chapter 4, section 4.1.1.3), the levels of iron observed in many of the blue glasses are elevated (0.7-2.5% Fe_2O_3) relative to uncoloured glass (typically up to 1.4% Fe_2O_3). It is probable that some iron was introduced as an impurity with the cobalt source; the identification of a cobalt inclusion rich in iron (see below) supports this view. However, the intensity of the cobalt colourant masks the colouring effects of iron (Bayley 1995: 1196; Bayley 1999: 90).

Several samples contain elevated levels of lead, corresponding to up to 1.7% PbO. This was probably introduced as an impurity with the cobalt colourant, as the levels of lead observed here are too low to suggest a deliberate addition; lead at these levels is unlikely to have had much of a technological benefit. As previously mentioned

(see Chapter 4, section 4.10.4), lead and iron bear a close relationship to the different bead types, suggesting the production of certain bead types in workshops using glass coloured using slightly different sources of cobalt. This trend is broadly reflected in the different base glass types identified (Figure 5.11), suggesting that different cobalt sources have been used to colour different types of glass. This suggests either that there were different workshops producing slightly different types of cobalt-blue glass, reflecting the exploitation of different cobalt sources, or that cobalt sources being exploited at slightly different times.

A handful of the translucent blue samples analysed contain high levels of antimony, corresponding in some cases to as much as 2.5% Sb_2O_3 (Figure 5.12). This is unlikely to reflect the use of a 'Roman' base glass containing antimony, as other colours produced from the same base glass contain less than approximately 0.8% Sb_2O_3 (*e.g.* see Chapter 4, section 4.3); seven of the translucent blue samples analysed contain antimony at levels in excess of this (Figure 5.1.12; the variation in manganese here relates to the base glass used). This is consistent with the addition of old antimony-opacified blue cullet as a colourant (Gratuze *et al.* 1995: 126; Henderson 2000b: 154), possibly in the form of tesserae from the preceding Roman period, as described by Theophilus (Freestone 1993: 743; Gratuze *et al.* 1995: 126; Hawthorne and Smith 1979: 59).

The samples containing in excess of 2.0% Sb_2O_3 are all of Brugmann's *Roman** type (one *Roman Polyhedral* and three *Roman Cane* beads). It is just possible that these represent re-used Roman beads, or Anglo-Saxon beads produced in the Roman tradition from recycled Roman glass (see Chapter 4, section 4.10.3.1). However, as all of these samples contain detectable manganese (Figure 5.1.12), they are unlikely to represent Roman antimony-decolourised glass. Furthermore, Roman blue-green glass does not typically contain in excess of 0.8% Sb_2O_3 (see Chapter 4, section 4.3). The results therefore suggest that they are more likely to be Anglo-Saxon products. Whether the antimony in the samples containing 0.5-1.0% Sb_2O_3 was introduced with a 'Roman' base glass or through the separate addition of opaque blue cullet is less certain.

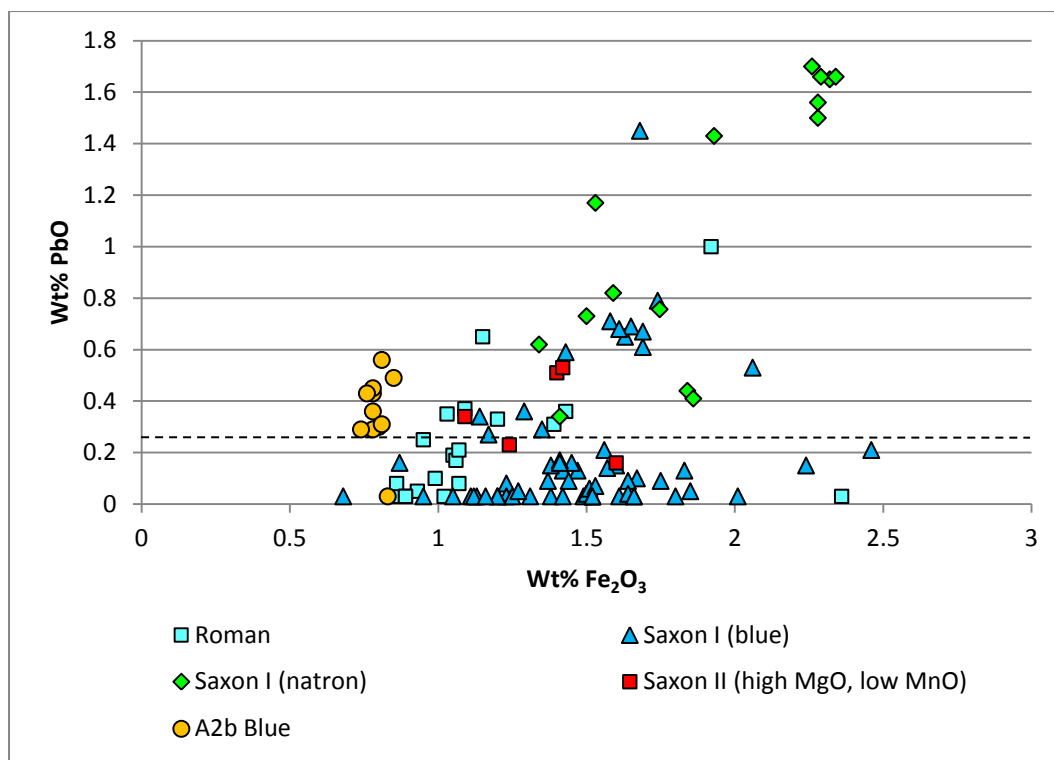


Figure 5.1.11 – A plot of iron oxide versus lead oxide for the translucent cobalt-blue samples from Eriswell, showing the different base glass types identified. The dashed line represents the approximate detection limits for lead.

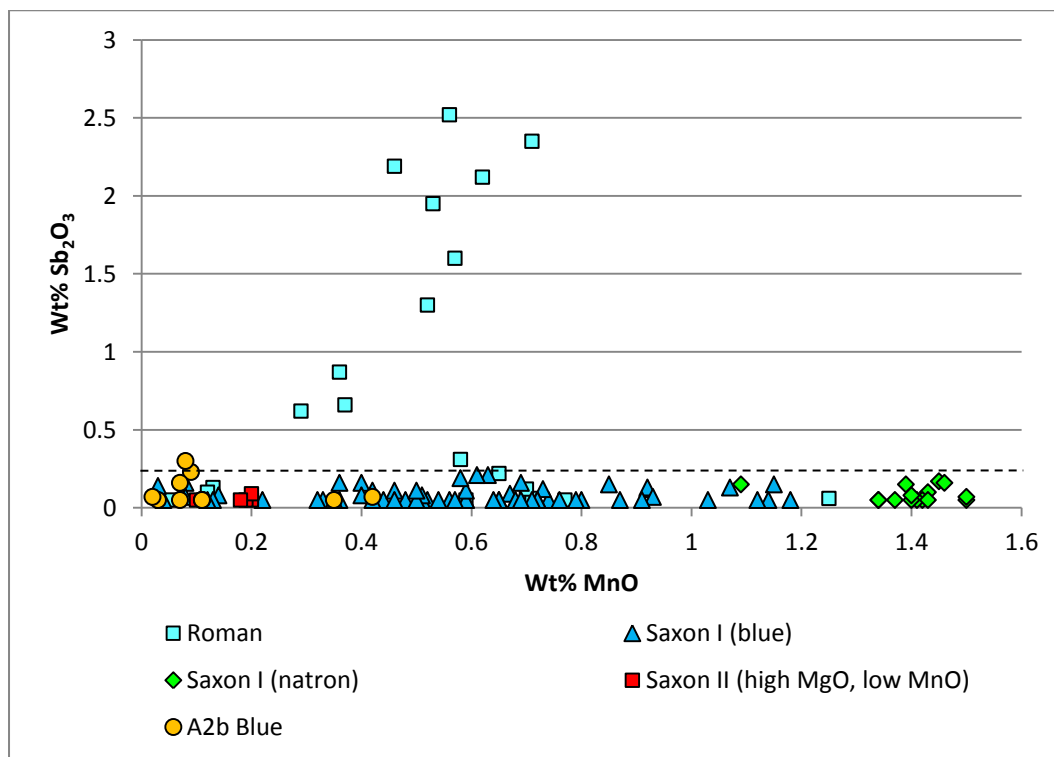


Figure 5.1.12 – A plot of antimony oxide versus manganese oxide in the translucent cobalt-blue samples from Eriswell, showing the different base glass types identified. The dashed line represents the approximate detection limits for antimony.

Glassworking debris from a number of early medieval sites suggests that fragments of coloured glass were sometimes imported for the production of beads; for example, coloured tesserae have been recovered from Ribe (Näsman 1979), Helgö (Lundström 1981) and Åhus (Callmer and Henderson 1991). However, the majority of blue glass from Eriswell does not contain detectable antimony (Figure 5.1.12), suggesting that colouration of blue glass using old opaque blue Roman cullet was a fairly restricted practice. The majority of translucent blue beads from Eriswell therefore appear to have been produced from a supply of fresh cobalt-blue glass, probably from the Near East (*e.g.* see Chapter 4, section 4.9).

A number of inclusions were observed in several of the translucent blue samples which are worthy of comment. A porous inclusion of calcium phosphate was observed in sample ERL114:G450:1590 (a *Constricted Cylindrical, variation* bead), which may represent a particle of bone ash (Figure 5.1.13). Bone ash has been identified as a deliberate addition as an opacifier in coloured glass cakes and tesserae from the Early Byzantine period (4th-8th centuries AD) (Marii and Rehren 2009: 297). However, as the sample in question here is translucent it appears to be an isolated example of such an occurrence. Furthermore, the phosphate levels in this sample are too low (0.2%) to suggest that bone ash was a deliberate addition; it is therefore likely to have been incidentally introduced to the batch.

A small fragment of what appears to be refractory ceramic (Figure 5.1.14) was observed in sample ERL046:G44:1015 (a *Constricted Cylindrical* bead). It is likely that this was pulled from the walls of the crucible in which the glass was melted, but that it was not heated for long enough or at high enough temperatures to fully dissolve it. The inclusion contains several partially dissolved silica grains surrounded by a number of silica-rich crystals also containing elevated levels of calcium, iron and alumina, consistent with clay ceramic. Immediately surrounding this is a large particle of metallic copper containing approximately 2.0% NiO; this is likely to have been introduced as an impurity with a nickel-rich cobalt source (see section 5.1.3.1 below).

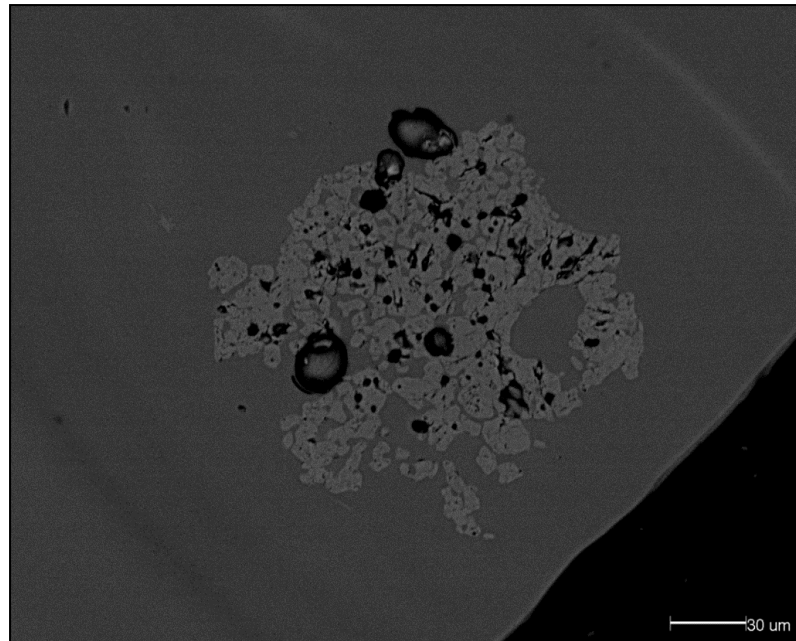


Figure 5.1.13 – BSE micrograph showing translucent blue sample ERL114:G450:1590, a *Constricted Cylindrical variation* bead. An irregular particle of calcium phosphate (pale grey) is visible within a soda-lime-silica glass matrix (grey). The black areas represent bubbles and voids.

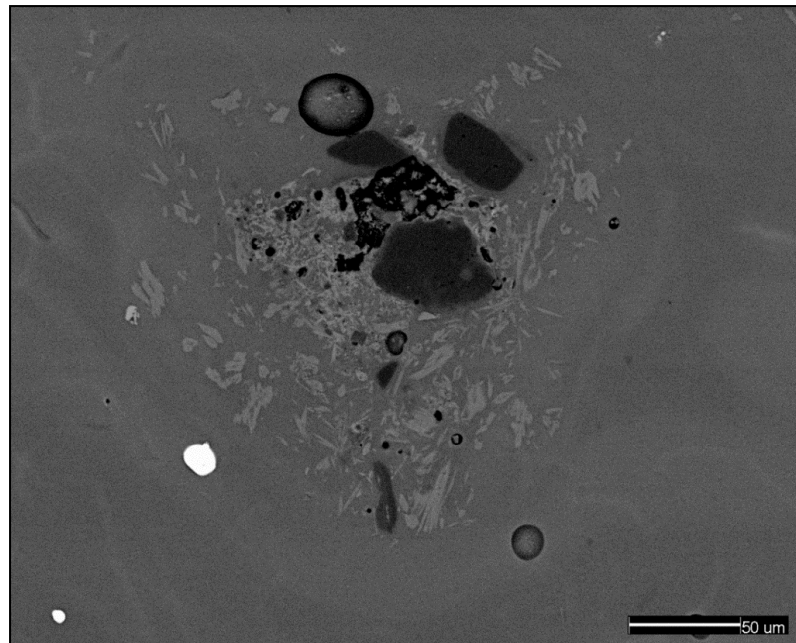


Figure 5.1.14 – BSE micrograph showing translucent blue sample ERL046:G44:1015, a *Constricted Cylindrical* bead. Three sub-angular grains of silica (dark grey) and numerous calcium-iron-aluminium-silicate crystals (pale grey) are visible in a soda-lime-silica glass matrix. The bright white particles are metallic copper, containing approximately 2% nickel.

Of particular interest was the identification of an inclusion rich in cobalt (up to 25% CoO) in sample ERL104:G263:1411 (a *Constricted Cylindrical* bead) (Figure 5.1.15). While this again appears to be an isolated example of such an occurrence, a similar inclusion has been identified in a blue glass bead from the early Anglo-Saxon cemetery at Ringlemere, Kent, containing up to approximately 27% CoO (Meek 2010: 29). However, the inclusion in the Eriswell bead contains a number of metallic and silicate phases and is far more complex in microstructure. A discussion and detailed spot analyses of this inclusion are presented in Appendix L. It is notable that many of the elements associated with this inclusion, such as nickel, are positively correlated with cobalt (see section 5.1.3.1 below), suggesting that a similar cobalt source is likely have been employed in a number of the other cobalt-blue glasses from Eriswell.

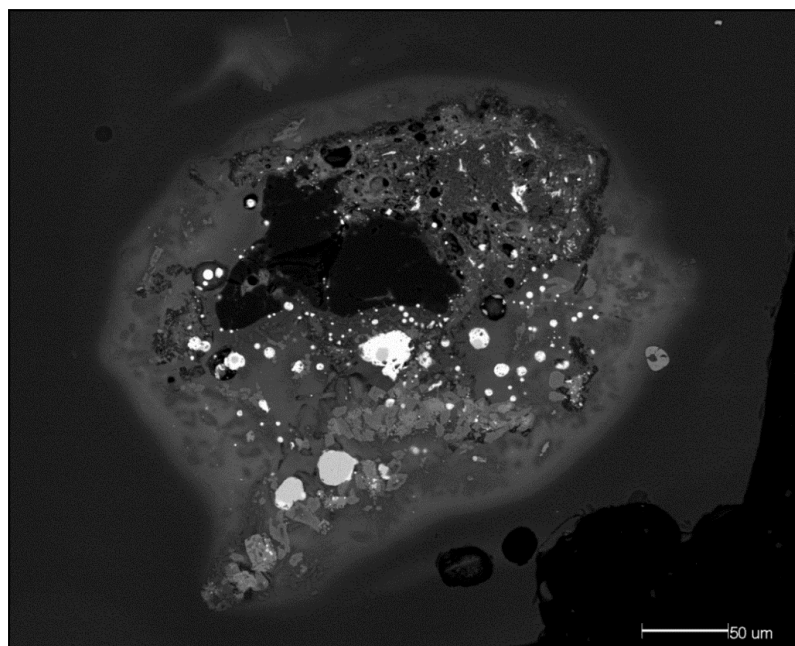


Figure 5.1.15 – BSE micrograph showing translucent blue sample ERL104:G263:1411, a *Constricted Cylindrical* bead. A complex cobalt-rich inclusion is visible within a soda-lime-silica glass matrix. For a detailed analysis of the individual phases present, refer to Appendix L.

Finally, it is of note that two samples of translucent blue glass were taken from different areas on bead ERL046:G38:1036 (*WhitePoly6?*). The blue spiral decoration on this bead is continuous, so the glass is certainly from the same batch. However, the levels of potash differ considerably (0.7 and 1.5% K₂O respectively). This is

unlikely to have resulted from poor mixing of the batch given the consistency in other elements between the samples (Table 5.1.1). It is more likely to represent heterogeneous potassium enrichment of the glass surface as a result of contamination from the furnace in which the bead was formed (*e.g.* Paynter 2008; Tal *et al.* 2008a; Tal *et al.* 2008b); at certain high temperatures potassium is vaporised from wood ash (*i.e.* the furnace fuel) and can enrich the glass (Tal *et al.* 2008a: 73; Tal *et al.* 2008b: 92).

Table 5.1.1 – SEM-EDS area analyses of two different samples from the translucent blue glass decoration on bead ERL046:G38:1036, highlighting marked differences in the concentration of potash.

Sample	Oxide (wt %) ¹												
	Na ₂ O	MgO	Al ₂ O ₃	SiO ₂	P ₂ O ₅	SO ₃	Cl	K ₂ O	CaO	TiO ₂	MnO	Fe ₂ O ₃	CuO
High K ₂ O	16.4	0.9	2.4	66.5	0.3	0.5	0.8	1.5	7.9	0.2	0.5	1.4	0.2
Low K ₂ O	17.6	0.8	2.4	66.5	0.2	0.5	0.8	0.7	7.6	0.2	0.6	1.4	0.2

¹Area analyses normalised to 100%. See Chapter 2, section 2.3.1 for details. The oxides of cobalt, zinc, arsenic, tin, antimony, barium and lead were analysed for but not detected.

5.1.3.1. Trace Element Analyses

In nature cobalt is typically found in conjunction with a variety of other impurities which are characteristic of the mineral source exploited. Such components include aluminium, iron, nickel, arsenic, copper, zinc, lead, manganese and antimony; the concentrations of which will vary according depending upon the cobalt source used (*e.g.* Hall and Yablonsky 1997: 373; Henderson 1985: 280; Henderson 2000a: 30-32; Towle *et al.* 2001: 23; Shortland 2012: 164); for example, cobalt minerals rich in manganese were sometimes used to colour Roman blue glasses (Henderson 2000a: 32; Sayre 1964: 7-8), and arsenical cobalt sources often contain zinc (Henderson 1985: 280). As such, many studies have attempted to characterise and provenance the cobalt sources used in the production of early blue glasses (*e.g.* Gratuze *et al.* 1995; Henderson 1985; Henderson 2000a; Meek 2010; Rehren 2001). Trace element analysis has great potential in this, as the majority of impurities introduced with

cobalt are below the detection limits of conventional SEM-EDS analysis. However, the characterisation of cobalt source(s) is notoriously difficult, especially as a single cobalt source may be quite variable in composition. The possible sources of cobalt used are discussed in this chapter, section 5.3.1.

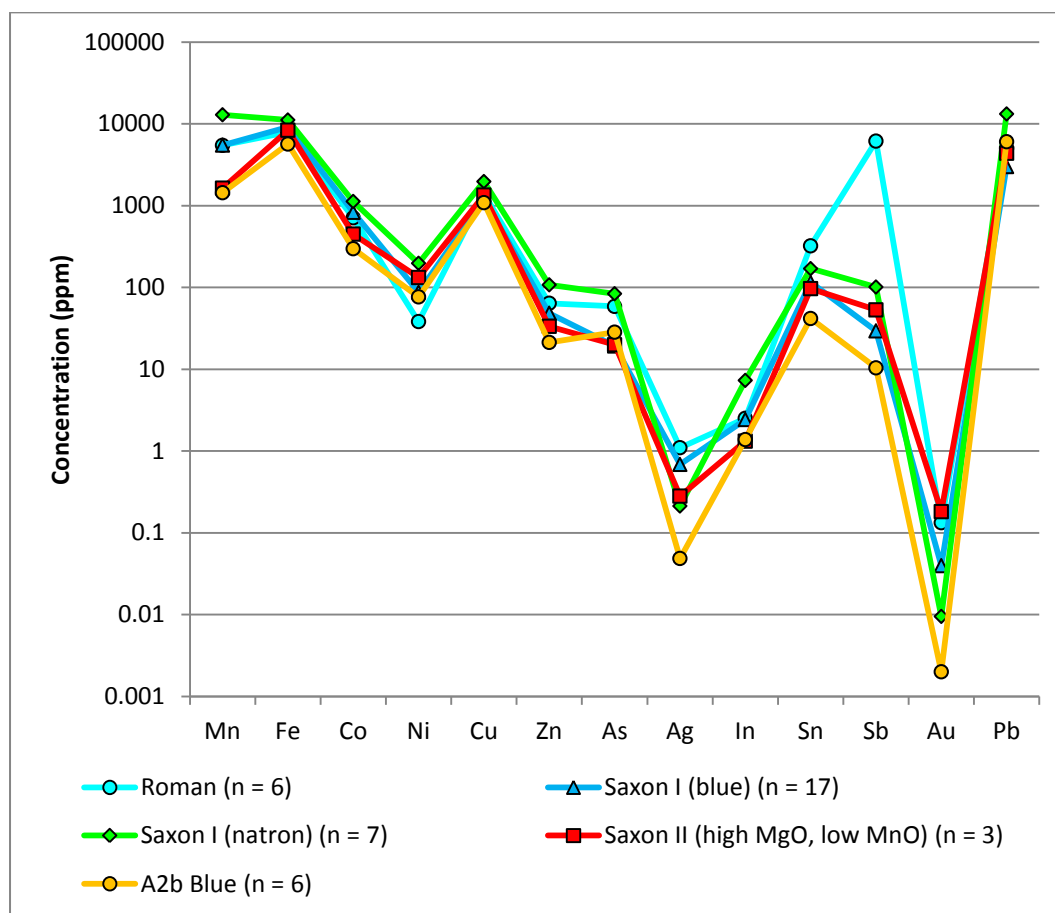


Figure 5.1.16 – Average colourant and colourant-related element concentrations for the translucent cobalt-blue samples from Eriswell, showing the different base glass types identified. Note the logarithmic scale.

The blue glasses from Eriswell were the primary focus of LA-ICP-MS analysis; 39 cobalt-blue samples were analysed. Most of these are produced from either a ‘Saxon I (blue)’ or a ‘Saxon I (natron)’ base glass, but samples produced from ‘Roman’, ‘Saxon II (high MgO, low MnO)’ and ‘A2b Blue’ glass were also analysed. No translucent blue glasses from Eriswell were produced from ‘Saxon II (natron)’, ‘Saxon II (high MgO, MnO)’, ‘HIMT’ or ‘Levantine I’ glass (see Chapter 4, section 4.9). Averaged colourant and colourant-related concentrations for each of the base

glass types identified are shown in Figure 5.1.16. There is relatively little difference in colourant technology between the different base glass types; variations in the levels of iron, manganese and antimony primarily result from the nature of the different base glasses used (see Chapter 4).

Trace element analysis confirmed the presence of cobalt as the colourant in all cases; Co is present at between 260-2620 ppm, averaging 750 ppm. It was clearly deliberately added as a colourant, as other glass colours typically contain Co at concentrations below 90 ppm. The glasses containing the lowest concentrations are consistently of the 'A2b Blue' type, whereas the 'Saxon II (high MgO, low MnO)' samples typically contain the highest levels. The amount of cobalt added consequently affected the depth of the colour produced. Figures 5.1.17-5.1.25 illustrate that the 'A2b Blue' group is very homogeneous, and that the majority of the samples of this type are likely to have been produced using a common cobalt source. This supports the view that the majority are likely to have been products of the same batch of glass (see Chapter 4, section 4.7). Copper is present at between 340-3730 ppm, averaging 1370 ppm, but these levels are too low to contribute to the colour, as cobalt is the stronger colourant here. It is likely that copper was introduced as an impurity with the cobalt colourant, as evidenced by the weak positive correlation between these two elements (Figure 5.1.17; $r^2 = 0.41$); this correlation is particularly strong in the 'Saxon I (blue)' samples (Figure 5.1.17; $r^2 = 0.72$).

Iron is present at concentrations between 4800-16480 ppm, averaging 8700 ppm. The elevated levels of iron observed in many of the blue glasses suggest that some was introduced as an impurity with the cobalt colourant; iron is positively correlated with cobalt (Figure 5.1.18; $r^2 = 0.63$), supporting this view. The correlation would probably have been stronger were it not for the introduction of additional iron as an impurity with the glassmaking sand (see Chapter 4, section 4.1.1.3). Analysis of the cobalt-rich inclusion in Figure 5.1.15 (see Appendix L) also suggests that the cobalt mineral employed was iron-rich.

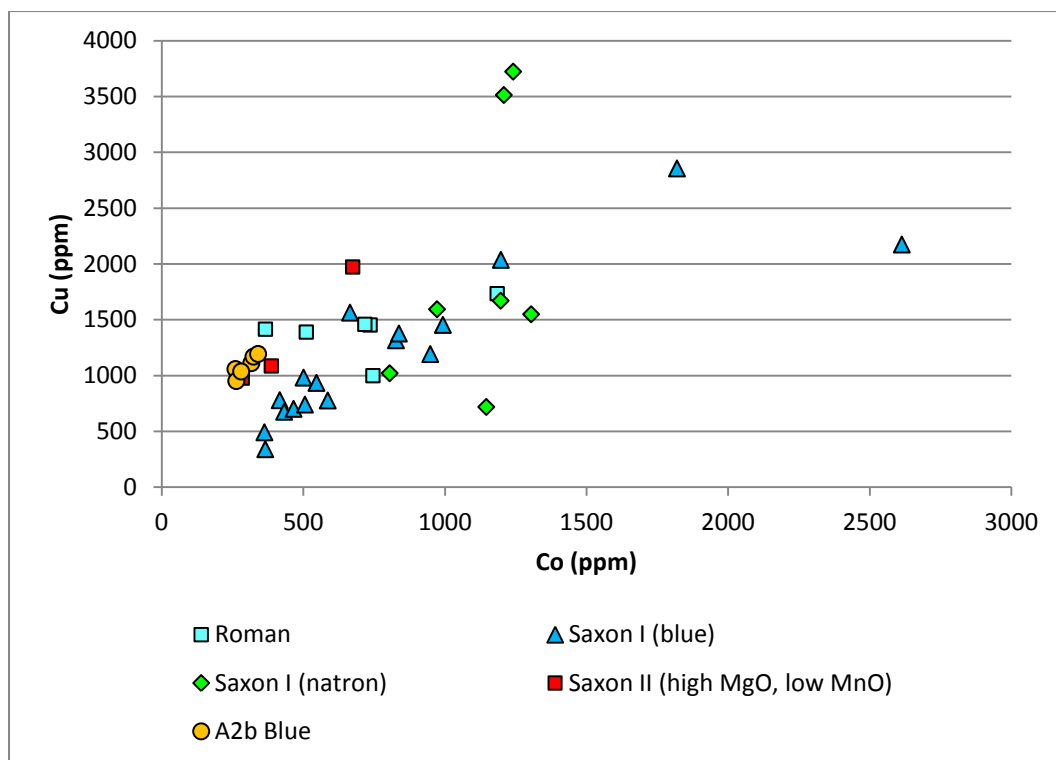


Figure 5.1.17 – A plot of cobalt versus copper for the translucent cobalt-blue samples from Eriswell, showing the different base glass types identified.

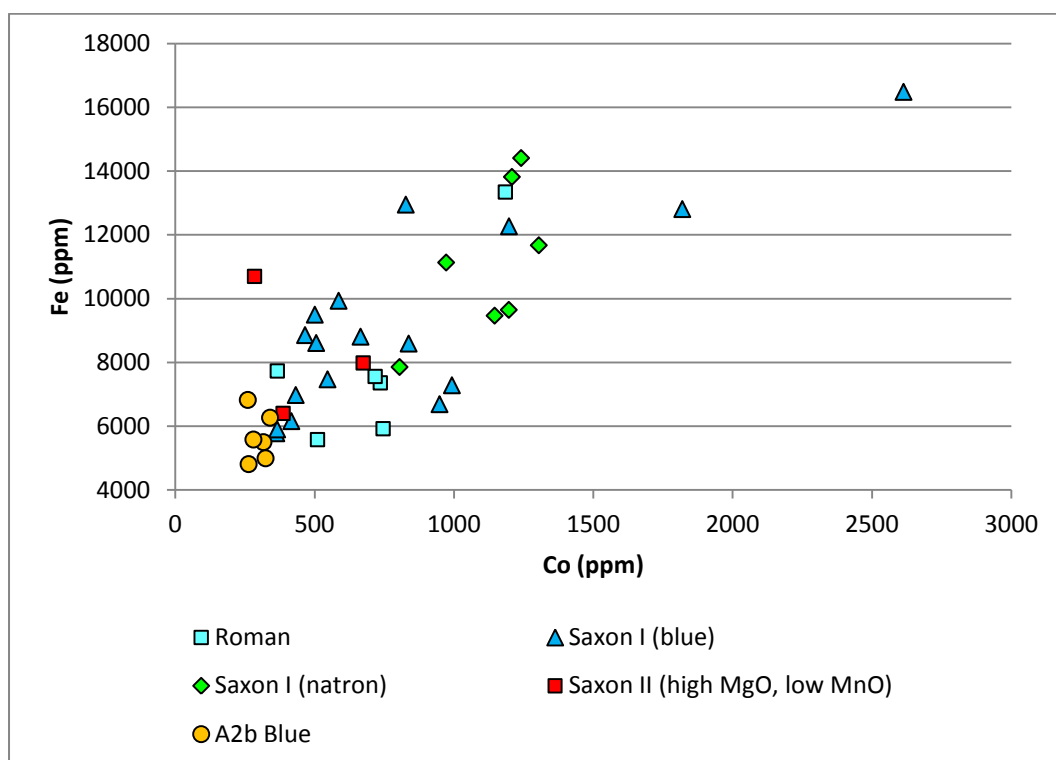


Figure 5.1.18 – A plot of cobalt versus iron for the translucent cobalt-blue samples from Eriswell, showing the different base glass types identified.

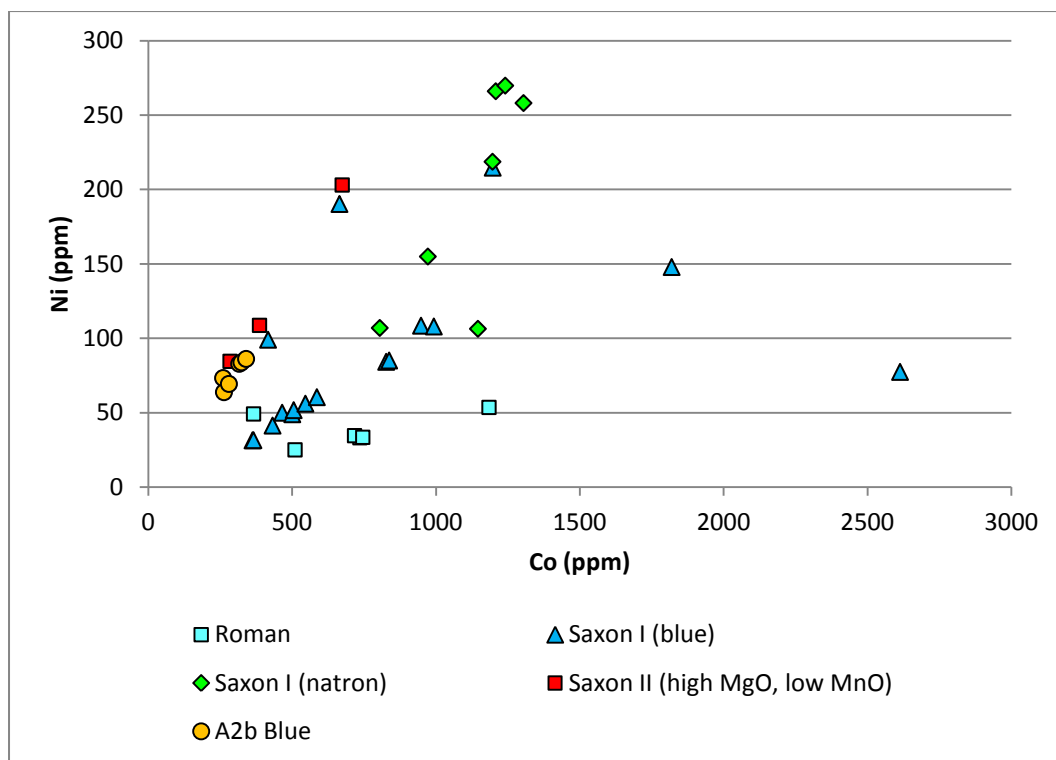


Figure 5.1.19 – A plot of cobalt versus nickel for the translucent cobalt-blue samples from Eriswell, showing the different base glass types identified.

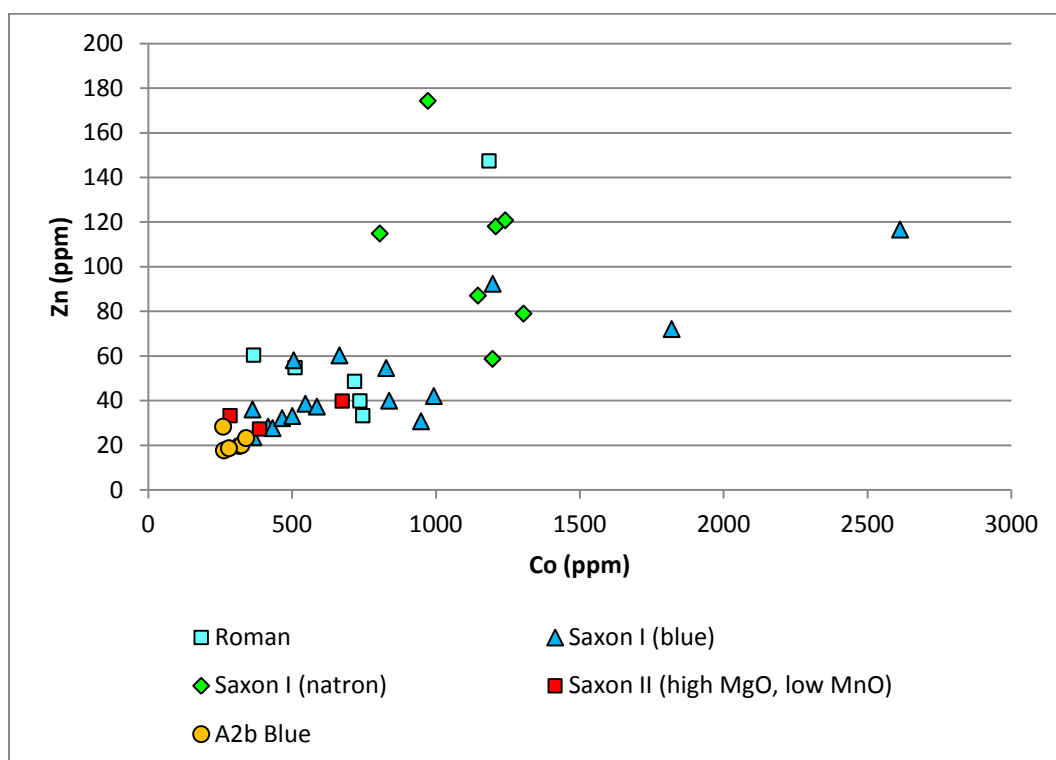


Figure 5.1.20 – A plot of cobalt versus zinc for the translucent cobalt-blue samples from Eriswell, showing the different base glass types identified.

Cobalt is positively correlated with many of the components detected in the cobalt inclusion discussed in Appendix L. A strong positive correlation is observed between cobalt and nickel in many of the ‘Saxon I (blue)’ samples (Figure 5.1.19; $r^2 = 0.66$ when omitting samples containing in excess of 1000 ppm Co and 110 ppm Ni) and ‘Saxon II (high MgO, low MnO)’ samples (Figure 5.1.19; $r^2 = 1.0$); nickel is often found as an impurity in conjunction with cobalt (Bayley 2000a: 218; Fiori and Vandini 2004: 187; Henderson 1985: 35). Zinc is also weakly positively correlated with cobalt (Figure 5.1.20; $r^2 = 0.43$); this is again particularly strong in ‘Saxon I (blue)’ glass (Figure 5.1.20; $r^2 = 0.72$).

No strong correlations are observed between cobalt and lead (Figure 5.1.21), or between cobalt and antimony (Figure 5.1.22). This may reflect the natural variability of these components in the cobalt sources employed; analysis of the cobalt inclusion discussed previously (Appendix L) suggests that lead was probably present in heterogeneous ‘pockets’. However, lead is present at concentrations up to 25000 ppm, and may reflect a ‘deliberate’ addition here; the lack of any correlation with cobalt may suggest that it was introduced separately from the cobalt colourant. A very weak positive correlation is observed between cobalt and indium (Figure 5.1.23; $r^2 = 0.29$), although indium is not present in excess of 15 ppm. A strong linear positive correlation is observed between tin and indium in glass colours other than blue (see Figure 5.3.3), confirming that indium was introduced as an impurity with the cobalt colourant.

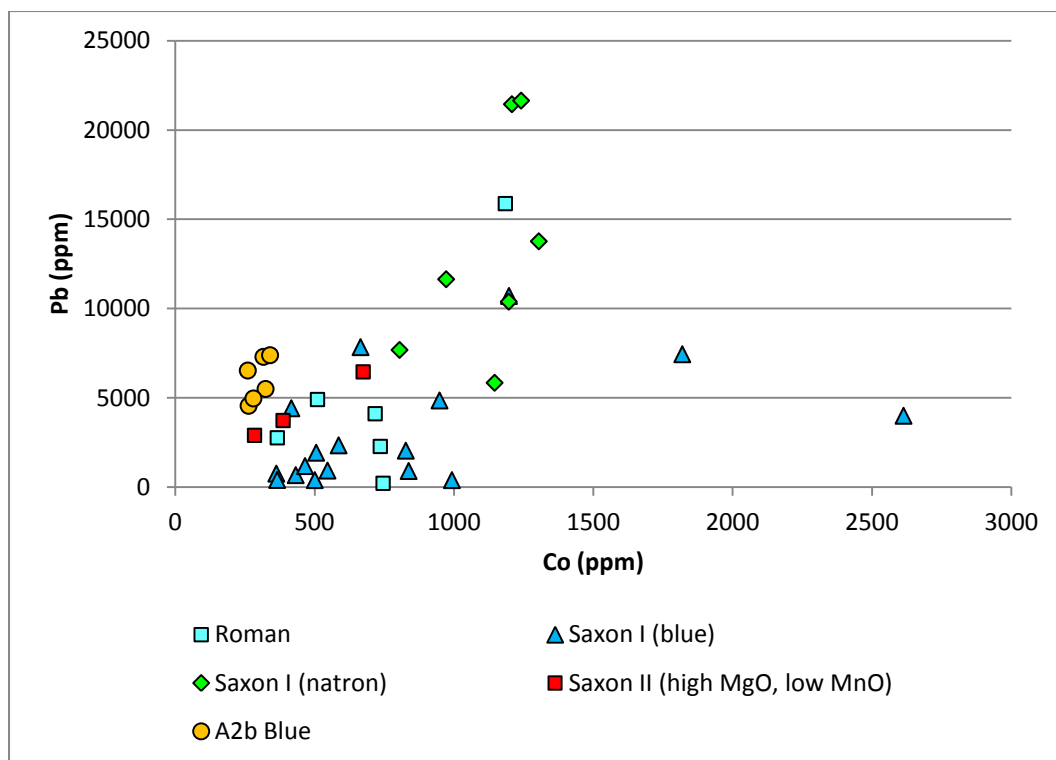


Figure 5.1.21 – A plot of cobalt versus lead for the translucent cobalt-blue samples from Eriswell, showing the different base glass types identified.

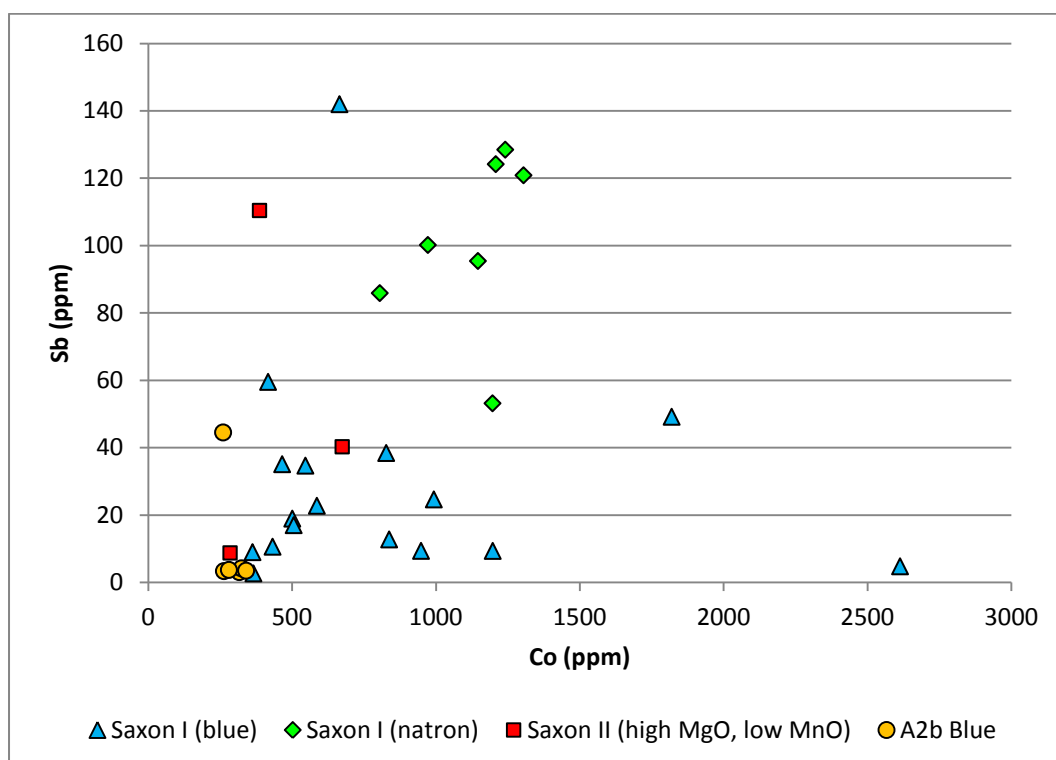


Figure 5.1.22 – A plot of cobalt versus antimony for the translucent cobalt-blue samples from Eriswell, showing the different base glass types identified. ‘Roman’ samples have been omitted due to the introduction of antimony with the base glass.

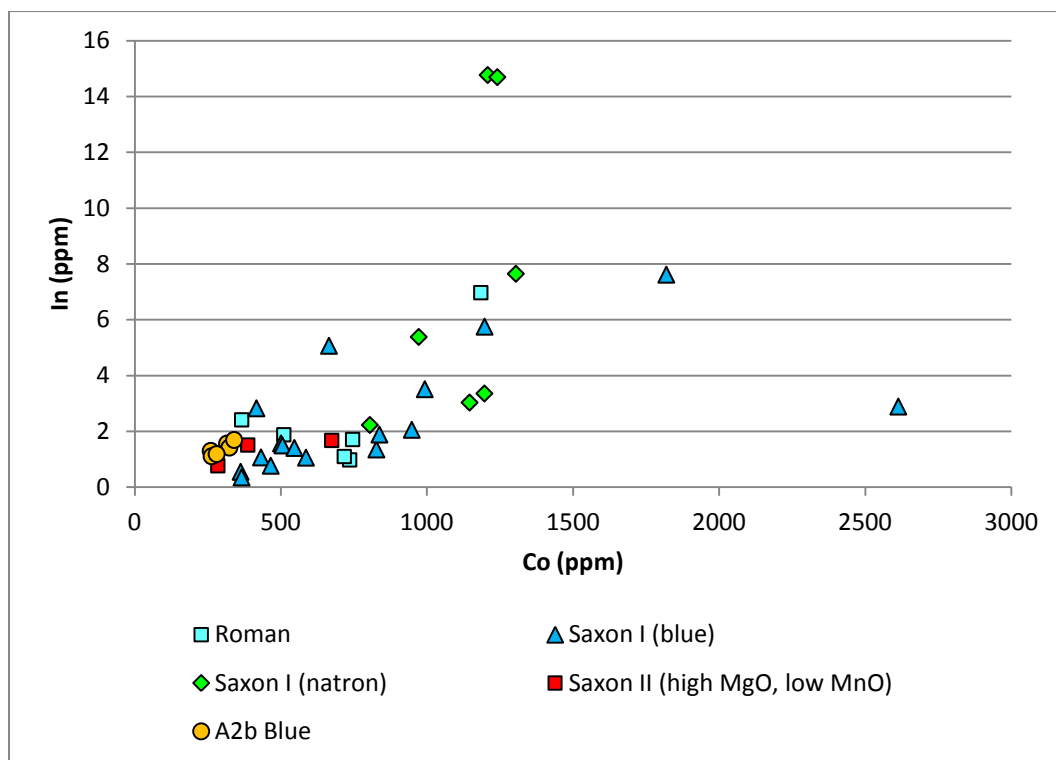


Figure 5.1.23 – A plot of cobalt versus indium for the translucent cobalt-blue samples from Eriswell, showing the different base glass types identified.

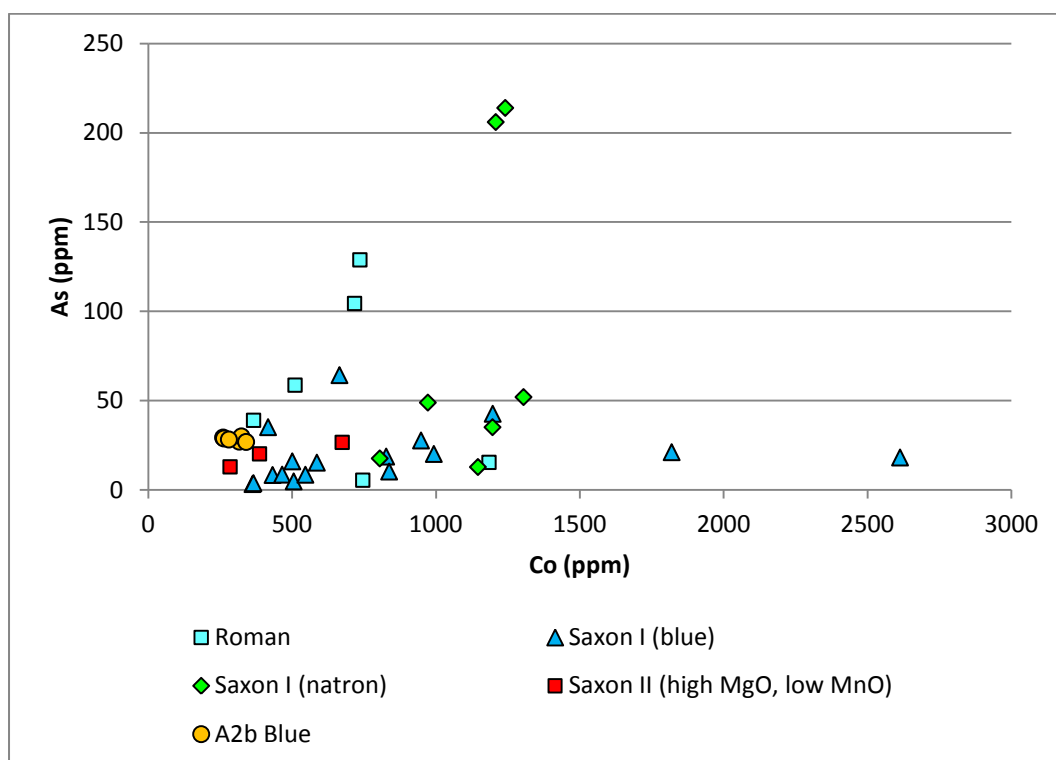


Figure 5.1.24 – A plot of cobalt versus arsenic for the translucent cobalt-blue samples from Eriswell, showing the different base glass types identified.

Two main types of cobalt ore have been identified in the past: one that is rich in arsenic and one that is rich in manganese (Hall and Yablonsky 1997: 373; Henderson 1985: 278-281). However, the concentration of arsenic is very variable in the samples analysed (Figure 5.1.24), so the use of an arsenical cobalt source cannot be confirmed. However, this may be borne out by the use of different temperatures and/or melting times in the production of these glasses, as arsenic is volatilised at high temperatures (Fiori and Vandini 2004: 186; Henderson 1990: 157; Shortland 2012: 165). Two of the 'Saxon I (natron)' samples (samples ERL104:G349:2980 and ERL114:G450:1590, both *Constricted Cylindrical, Variation* beads) contain particularly elevated levels of arsenic (approximately 210 ppm) and are also characterised by elevated levels of lead (approximately 21500 ppm). It is therefore possible that a cobalt source rich in arsenic was used in the production of some beads; up to 1.3% As_2O_3 was detected in analysis of the cobalt inclusion discussed in Appendix L (compare this to up to just 0.8% MnO), which would appear to support the view that the cobalt source employed probably contained some arsenic. It is difficult to comment upon the manganese content of the cobalt source, as the majority of manganese appears to have been introduced with the base glasses (see Chapter 4).

Overall, the data suggest that the cobalt source exploited in the majority of translucent blue glasses from Eriswell was primarily rich in iron, copper and sometimes lead as impurities at significant concentrations matching or exceeding those of cobalt itself (*e.g.* Figure 5.1.16). The cobalt colourant also appears to have contained smaller concentrations of zinc and nickel impurities, possibly with some antimony. Whilst it is not possible to establish the extent to which arsenic or manganese may have been introduced with cobalt, on balance the use of an arsenical cobalt source in at least some of the samples from Eriswell seems likely.

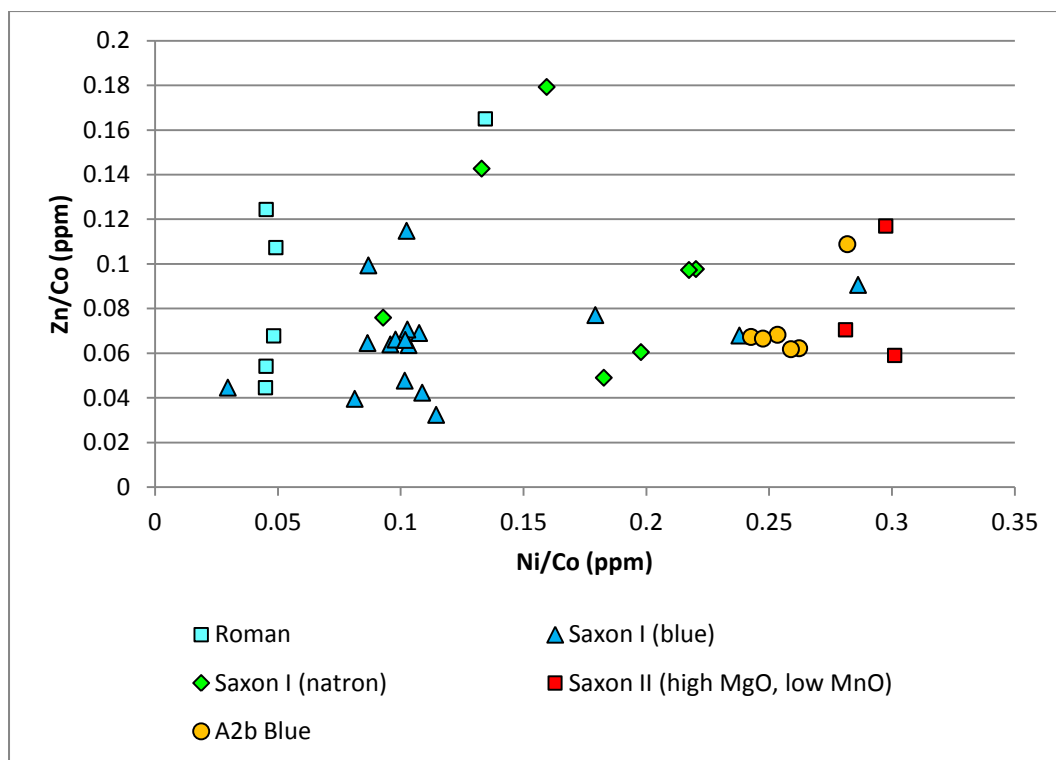


Figure 5.1.25 – A plot of the ratios of Ni/Co versus Zn/Co for the translucent cobalt-blue samples from Eriswell, showing the different base glass types identified.

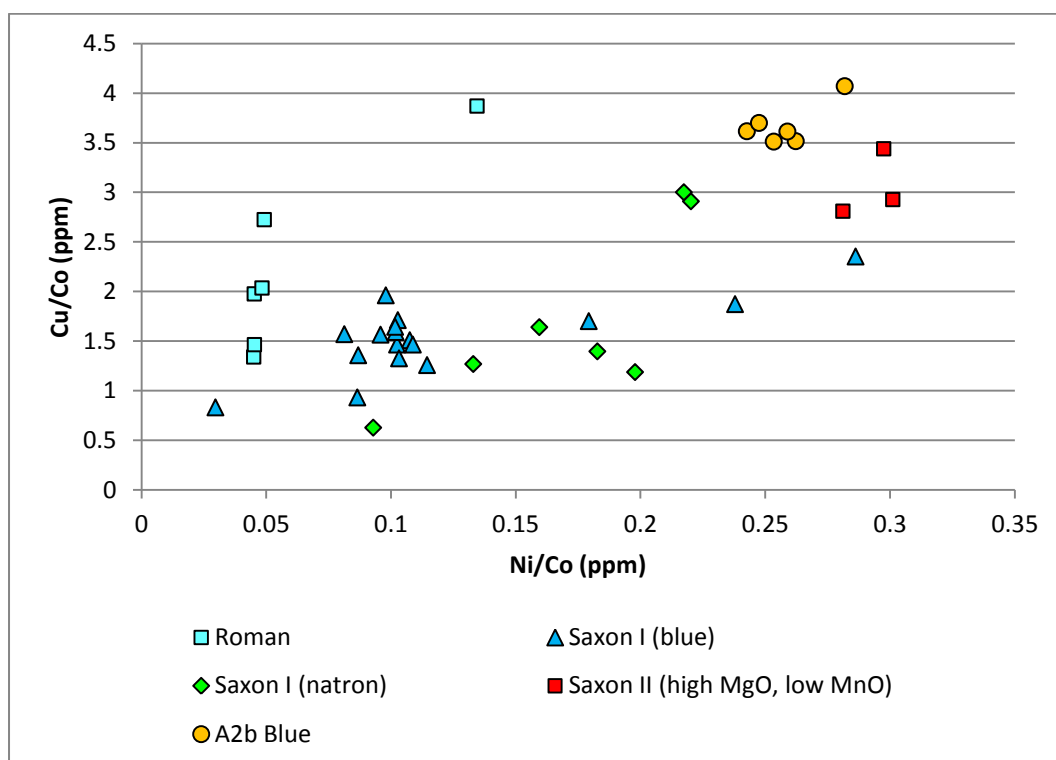


Figure 5.1.26 – A plot of the ratios of Ni/Co versus Cu/Co for the translucent cobalt-blue samples from Eriswell, showing the different base glass types identified.

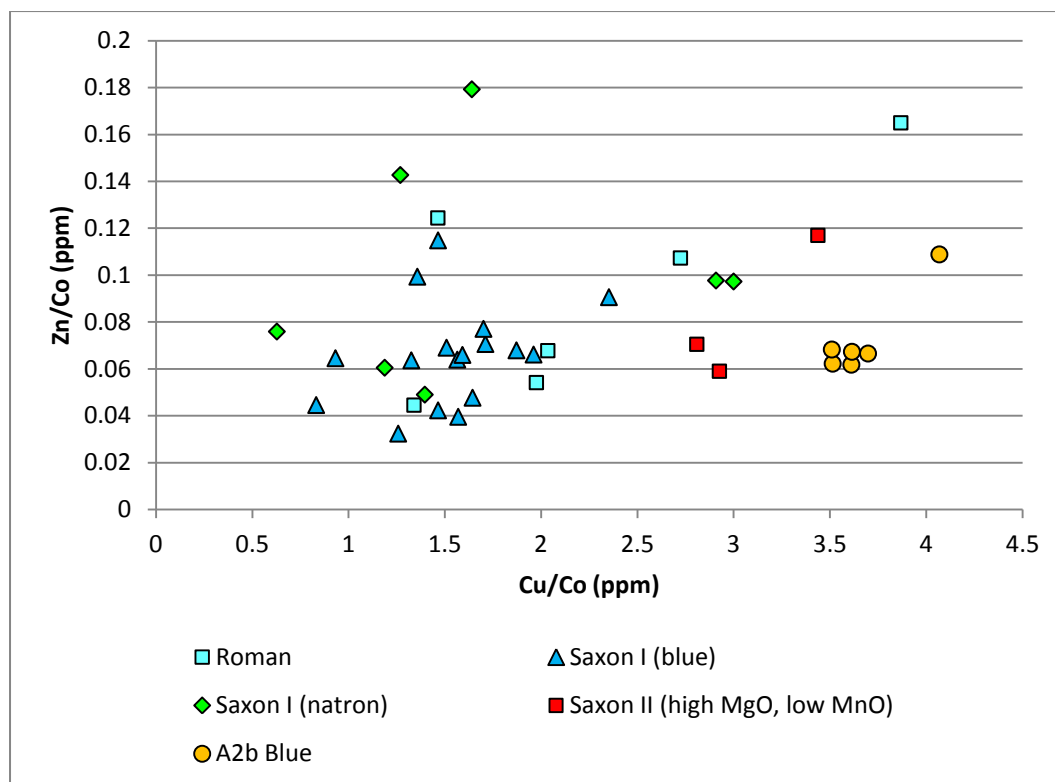


Figure 5.1.27 – A plot of the ratios of Cu/Co versus Zn/Co for the translucent cobalt-blue samples from Eriswell, showing the different base glass types identified.

It is clear from the strong correlations discussed above that copper, nickel and zinc are some of the only components associated with the cobalt colourant which are unlikely to have been introduced as impurities with other batch ingredients. They should therefore be good discriminators of the different cobalt sources used. Figures 5.1.25-5.1.27 compare the ratios of these components to cobalt. The ‘A2b Blue’ samples cluster very tightly as a group, as previously noted, indicating the use of a common cobalt source. The ‘Saxon II (high MgO, low MnO)’ samples also cluster relatively tightly as a group, in a similar region to the ‘A2b Blue’ samples; this suggests the use of a similar cobalt source in both of these glass types. In contrast, the ‘Roman’, ‘Saxon I (blue)’ and ‘Saxon I (natron)’ samples are much more variable. The ‘Saxon I (blue)’ samples cluster reasonably tightly as a group, although nickel is somewhat variable. In contrast, the nickel content of the ‘Roman’ samples is very consistent, but copper and zinc are somewhat variable. ‘Saxon I (natron)’ glass does not cluster tightly as a group.

5.1.4. Translucent Copper-Green and Turquoise Glass

Glass may be coloured green by either a deliberate copper addition or by an iron impurity; the latter has been discussed in section 5.1.1 above. The detection of 1-7% CuO in many of the translucent green glasses (here termed copper-green) indicates the deliberate addition of copper as a colourant. Similarly, a number of translucent turquoise samples are also coloured by approximately 2-5% CuO, again indicating a deliberate copper addition. Samples of translucent copper-green glass were obtained from 28 beads from Eriswell and samples of translucent turquoise glass from four beads.

The colour produced from the addition of copper to an uncoloured base glass is complex, as it depends on a number of factors. The redox conditions of the furnace determine the oxidation state of the copper (cupric or cuprous). In oxidising conditions cupric (Cu^{2+}) copper forms, producing shades of blue, green and turquoise, whereas in reducing conditions cuprous (Cu^+) or metallic copper (Cu^0) is more common, typically producing shades of red (Bayley 1999: 90; Cable and Smedley 1987; Henderson 2000a: 32; Turner and Rooksby 1959: 25-27; Weyl 1951: 155; Wilthew 2006: 389). It is cupric copper that is of interest here. Elevated levels of iron and manganese, which are commonly found in copper-green glasses (iron as an impurity from the glassmaking sand and manganese usually as a decolourant in the base glass), may have optimised the colour (Bimson and Freestone 2000: 132).

In copper-green glasses, it is the lead content that determines the colour; green is produced in a high-lead glass, whereas turquoise usually results in a low-lead alkali glass (Bayley and Wilthew 1986; Bayley 1987: 185; Bayley 1999: 90; Bayley 2000a: 218; Fiori and Vandini 2004: 188; Weyl 1951: 165; Wilthew 2006: 389). This is illustrated particularly well by a plot of CuO and PbO (Figure 5.1.28) in which it is clear that the turquoise glasses are typically low in lead (1-7% PbO), whereas the green glasses are typically high in lead (3-30% PbO). However, the distinction between these two colours is by no means clear-cut; a number of hues between green and turquoise may be produced depending upon the amount of lead present, as might be expected.

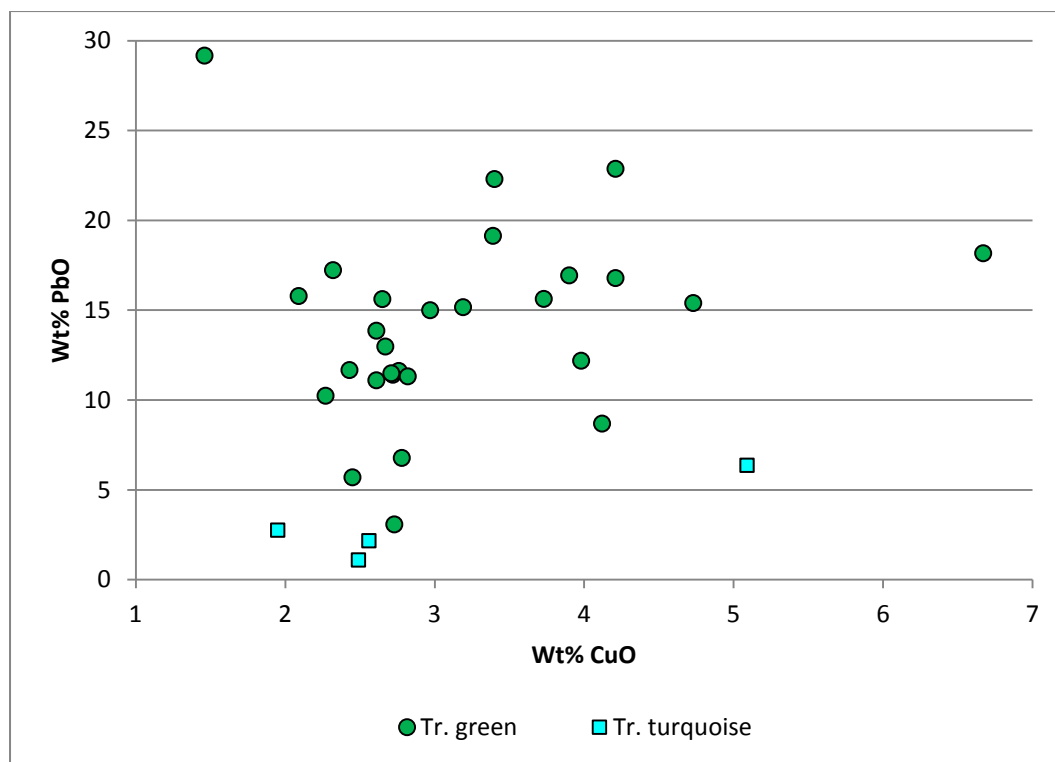


Figure 5.1.28 – A plot of copper oxide versus lead oxide for the translucent copper-green and turquoise glasses from Eriswell.

Several of the translucent copper-green glasses were poorly mixed, as indicated by streaks of glass richer in lead in many of the samples (Figure 5.1.29); this suggests low melting temperatures and/or short firing times. Furthermore, many of the copper-green glasses are not entirely translucent; sparse crystals of lead-tin oxide (PbSnO_3 , lead stannate), as is typically seen as an opacifying agent in opaque yellow glass (see this chapter, section 5.2.2), together with occasional crystals of tin oxide (SnO_2), were observed in the majority of the samples analysed (*e.g.* Figures 5.1.36-5.1.39). These are not sufficient to cause complete opacity, but have rendered several of the samples semi-opaque. The translucent copper-green glasses typically contain 0.1-1.5% SnO_2 , whereas the translucent turquoise glasses generally contain slightly less, at 0.1-0.7% SnO_2 (Figure 5.1.32). Lead was clearly intentionally added to produce the colour in the copper-green glasses, but it is less clear as to how tin was introduced.

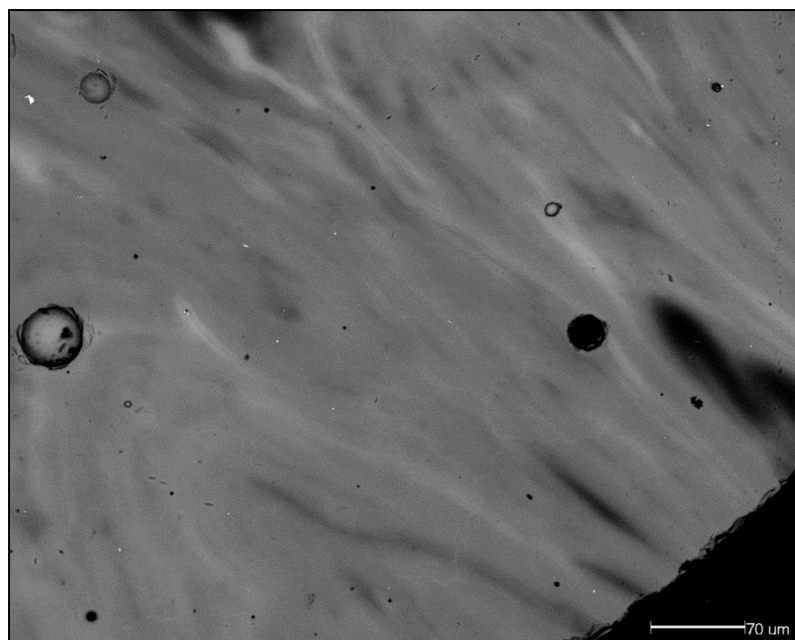


Figure 5.1.29 – BSE micrograph showing translucent copper-green sample ERL104:G242:2266, a *Green Cylindrical* bead. A lead-rich soda-lime-silica glass matrix is visible, relatively free of inclusions except for a few sparse bubbles and voids. The brighter areas of glass are richer in lead, and have resulted from poor mixing of the batch.

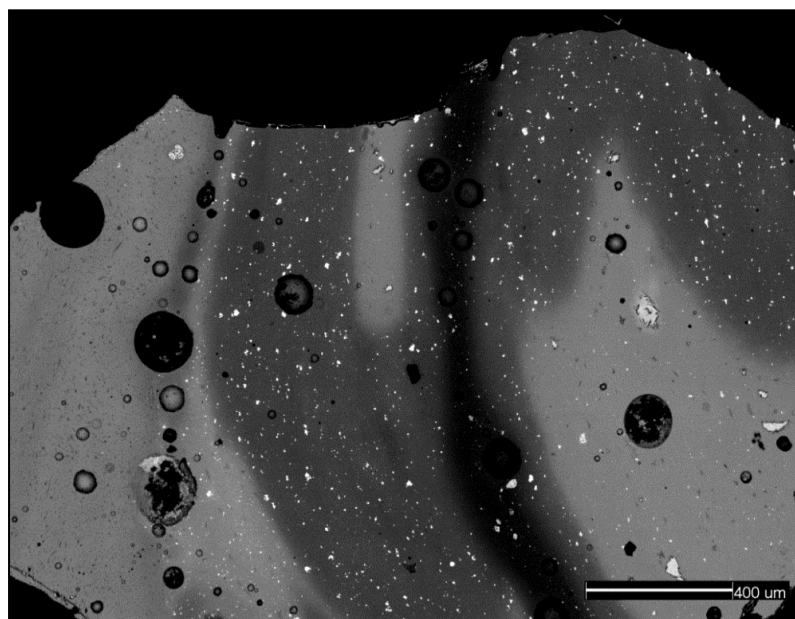


Figure 5.1.30 – BSE micrograph showing sample ERL104:G290:1721, a *Mosaic?* bead. Three different colours of soda-lime-silica glass can be seen. The pale grey glass to the left is a lead-rich opaque red glass, coloured and opacified by nanoparticles of metallic copper. The darker grey glass in the centre is opaque yellow, coloured and opacified by lead-tin oxide (white crystals). The pale grey glass to the right is a lead-rich translucent copper-green glass. The dark grey streak running down the centre of the sample is lower in lead, and has resulted from poor mixing of the batch. Numerous large bubbles and voids are visible, particularly in the red glass. Note how the three colours have mixed at their boundaries.

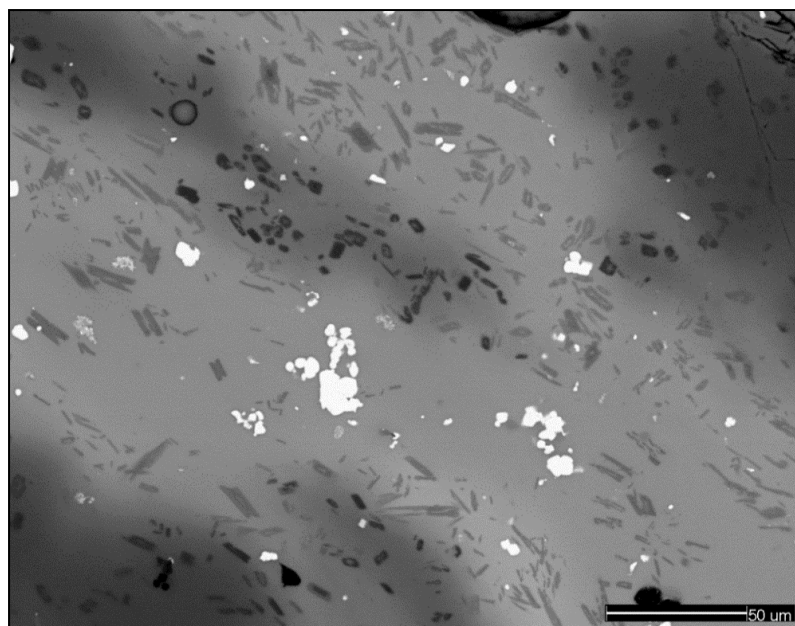


Figure 5.1.31 – BSE micrograph showing sample ERL104:G144:2567, a *Traffic Light Twisted Trail* bead. The pale grey glass is a lead-rich opaque yellow soda-lime-silica glass, opacified by lead-tin oxide (white crystals). Heavily inter-mixed with this is a translucent green glass (dark grey) containing slightly less lead. The dark grey crystals visible in both colours correspond to the mineral wollastonite (CaSiO₃).

The vast majority of these glasses form part of the decoration on beads, either as trails, twisted trails or streaks, usually in association with opaque yellow glass (Figures 5.1.30-5.1.31). Whilst it is just possible that some tin was introduced through contamination from adjacent opaque yellow glass, this is unlikely; the translucent copper-green glasses are typically poorly mixed and considerable mixing with opaque yellow glass would have been necessary in order to introduce the concentrations of tin detected. Furthermore, several of the samples analysed are not associated with opaque lead-tin yellow glass, suggesting that tin was not introduced as a contaminant.

Previous studies have suggested that tin may have been introduced as an impurity with the copper colourant, in the form of an alloy such as bronze (*e.g.* Sayre and Smith 1967: 307-309). However, there is no significant correlation between copper and tin (Figure 5.1.32; $r^2 = 0.28$ when omitting the sample containing 1.5% SnO₂), which suggests that this is unlikely to be the case. Tin instead appears to have been introduced with lead in the form of a material rich in both lead and tin, similar to that used in the production of opaque yellow glass (see this chapter, section 5.2.2). This

view is supported by the presence of tin as lead-tin oxide crystals, but also by the ratios of lead to tin, which closely match those observed in opaque lead-tin yellow glass (Figure 5.1.33). The levels of tin detected in the translucent copper-green samples analysed are too low and variable to confidently identify any correlation with lead, but this is likely to be borne out by the compositional variability of the lead-tin calx employed. However, it is notable that the levels of lead and tin detected closely match those detected in opaque green glass from Eriswell (Figure 5.1.34); this is also opacified by lead-tin oxide, albeit in lesser quantities than in opaque yellow glass (see this chapter, section 5.2.2).

It has also been suggested that the low levels of lead present in some glasses coloured by copper may have been introduced as an impurity with the copper colourant (Meek 2010: 7; Wilthew 2006: 389). The levels of lead observed in the Eriswell samples suggest that such an alloy would have consisted of approximately 50-95% PbO in the translucent copper-green glasses and 30-60% PbO in the translucent turquoise glasses. However, these levels of lead are well outside of the range typical for copper alloys, so this is clearly not the case.

On balance, it therefore seems likely that tin was introduced as an impurity with lead (*i.e.* as a lead-tin calx); lead being necessary to produce the colour in copper-green glass and tin probably representing an unnecessary by-product of this ingredient. Careful control of the furnace conditions would have ensured that the glass produced was (at least predominantly) translucent, rather than fully opaque. It is just possible that tin had some technological benefit, but there is as yet no evidence to support this.

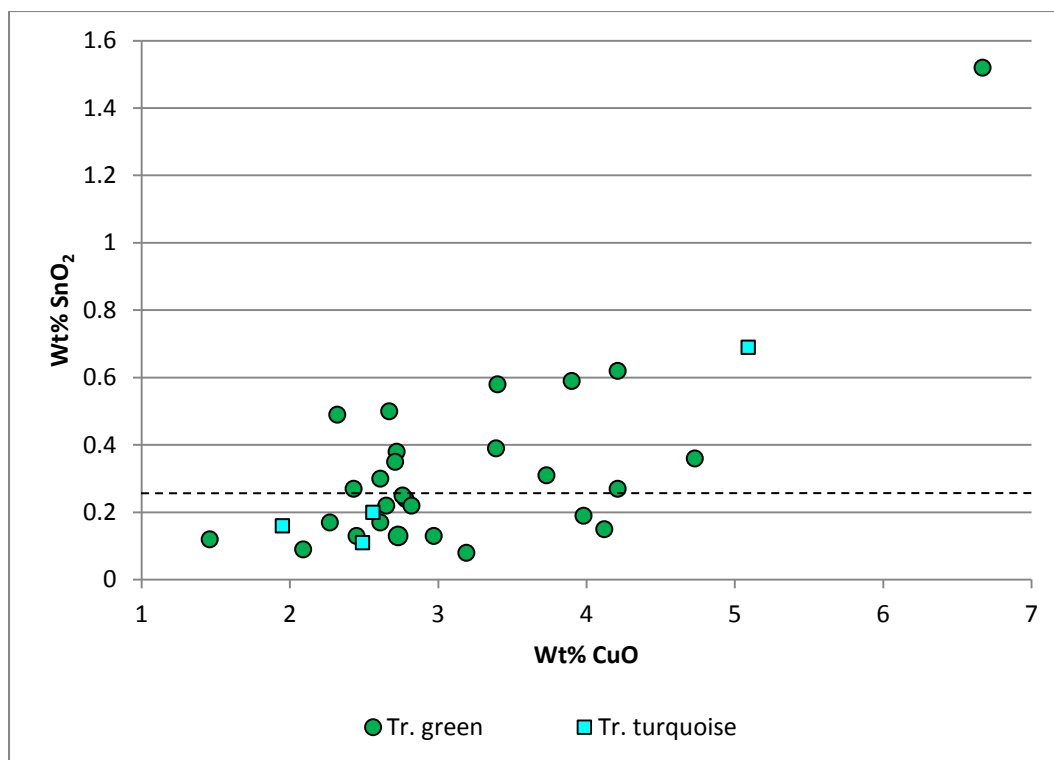


Figure 5.1.32 – A plot of copper oxide versus tin oxide for the translucent copper-green and turquoise samples from Eriswell. The dashed line represents the approximate detection limits for tin oxide.

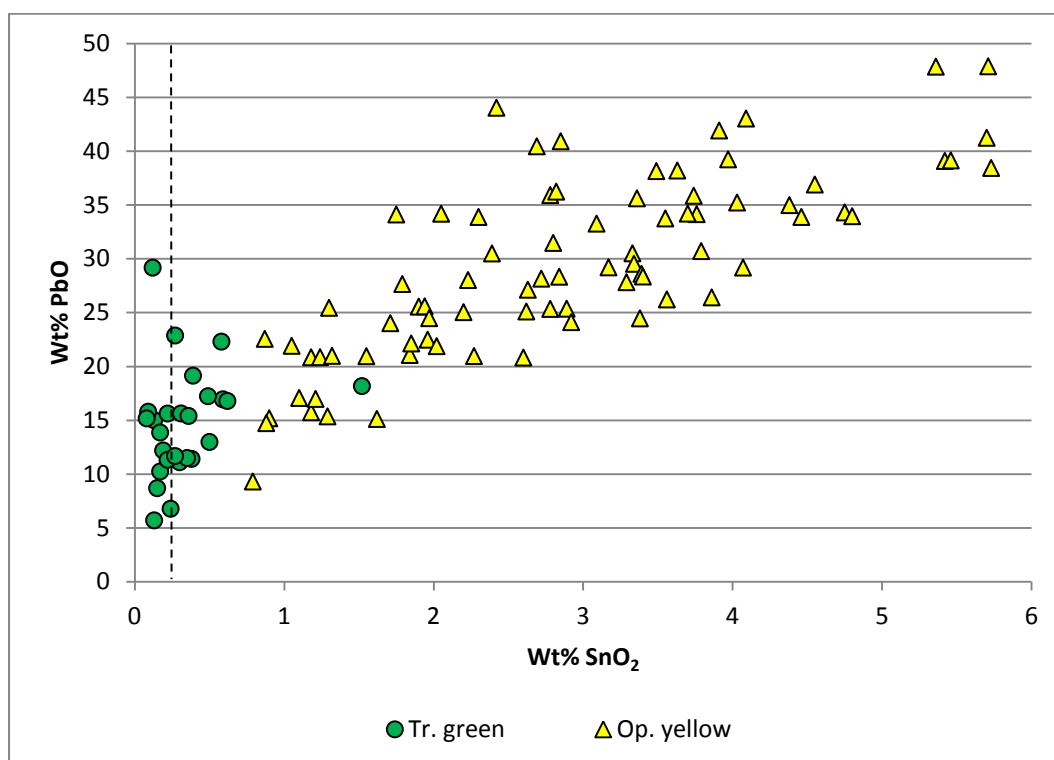


Figure 5.1.33 – A plot of tin oxide versus lead oxide for the translucent copper-green samples from Eriswell, compared to opaque yellow samples (see this chapter, section 5.2.2). The dashed line represents the approximate detection limits for tin oxide.

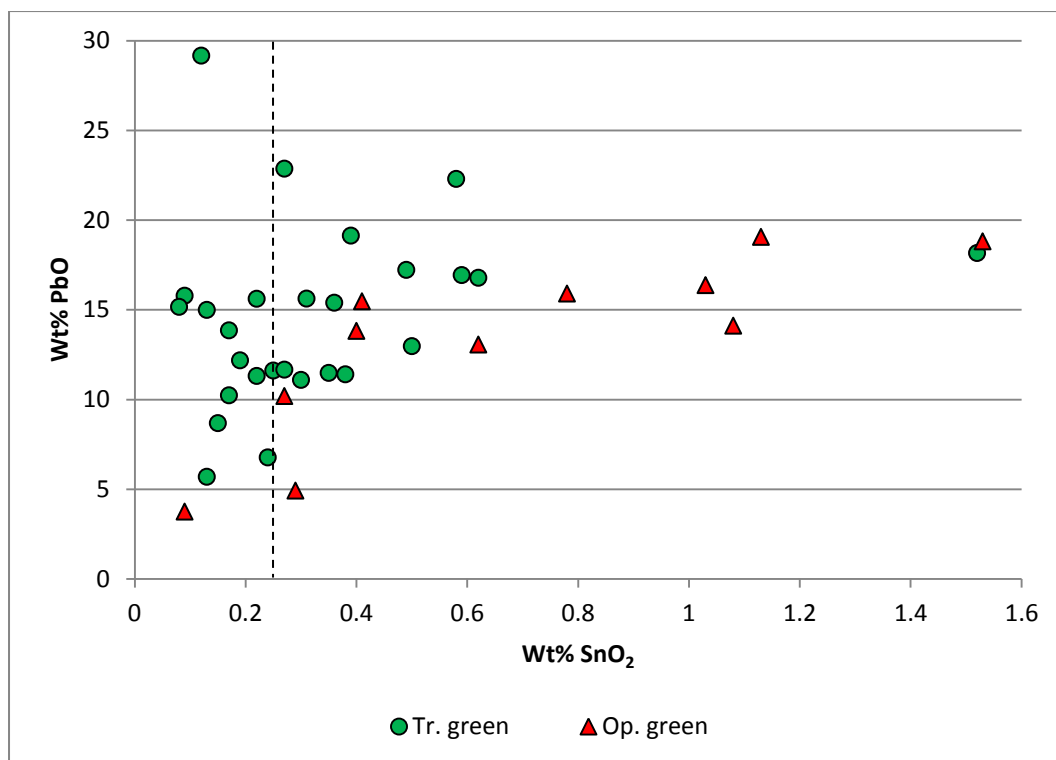


Figure 5.1.34 – A plot of tin oxide versus lead oxide for the translucent copper-green samples from Eriswell, compared to opaque copper-green samples (see this chapter, section 5.2.2). The dashed line represents the approximate detection limits for tin oxide.

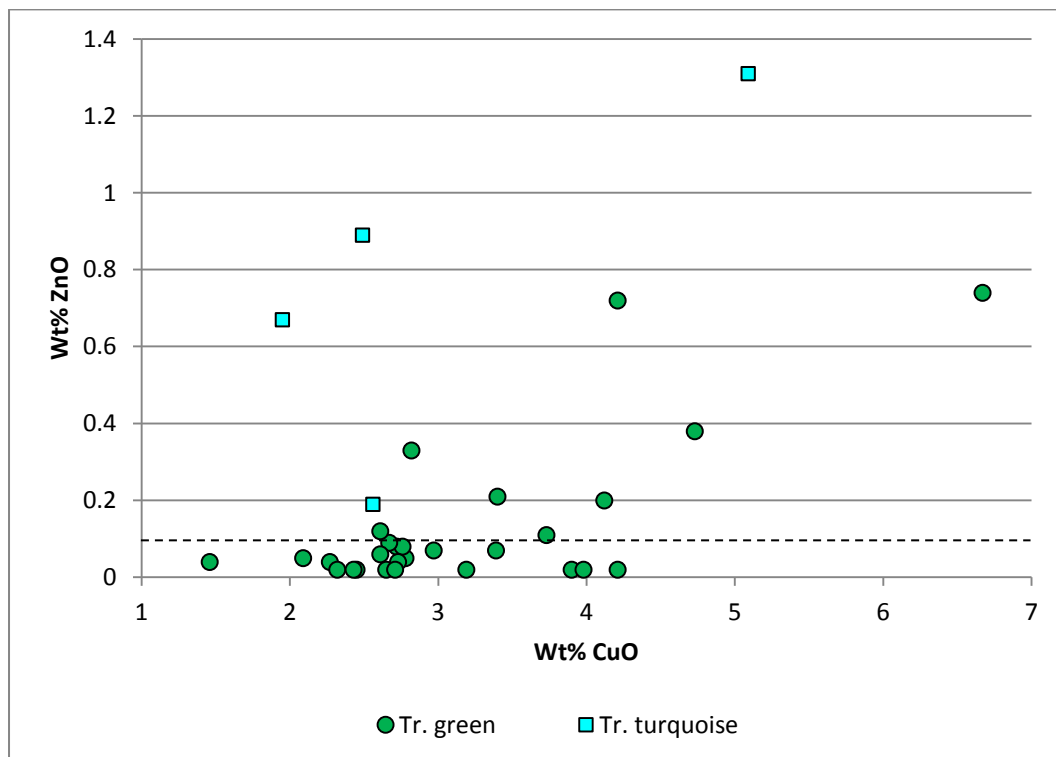


Figure 5.1.35 – A plot of copper oxide versus zinc oxide for the translucent copper-green and turquoise samples from Eriswell. The dashed line represents the approximate detection limits for zinc oxide.

The picture is less clear with regard to the translucent turquoise glasses. The small number of samples of this colour analysed limits the ability to speculate here. As lead is not necessary to produce the colour, tin is less likely to have been introduced in the form of a lead-tin calx. However, the data suggest that if it was introduced in the form of a copper alloy, such an alloy would have consisted of approximately 4-12% tin. This is well within the limits for bronze (Bayley 1998: 7). Furthermore, the presence of 0.6-1.3% ZnO, which is positively correlated with copper (Figure 5.1.35; $r^2 = 0.53$), in all but one of the translucent turquoise samples, is strongly indicative of the use of a copper alloy colourant. It is not unusual to find zinc in turquoise glasses from the early medieval period; this is usually interpreted as being indicative of the use of scrap copper alloy (*e.g.* brass) as a colourant (Bayley 2000a: 218; Henderson 1985: 282; Henderson 2000a: 33). In contrast, only two translucent copper-green samples contain in excess of 0.6% ZnO (Figure 5.1.35), suggesting that a zinc-rich copper alloy was not the primary colourant source here.

It is unclear how copper was treated prior to its addition as a colourant to produce the copper-green and turquoise glasses, but small grains and aggregates of copper oxide were observed in several samples. In sample ERL104:G290:1721 (a *Mosaic?* bead), several lumps of copper oxide (consisting of 90% elemental copper) were observed (Figure 5.1.36), some of which had clearly begun to dissolve (Figure 5.1.37). These are surrounded by acicular calcium silicate crystals which are likely to have formed as devitrification products upon cooling of the melt. The irregular angular shape of these copper-rich inclusions suggests that they are unlikely to have precipitated out of the melt, and may therefore represent relicts of the added colourant (*e.g.* copper scale or dross) which were not heated for long enough to fully dissolve in the glass. Spot analysis of these inclusions revealed no other metallic impurities, arguing against the use of a copper alloy; if this were the case traces of tin, zinc, lead or possibly even arsenic would be expected. This further supports the view that tin and lead were not introduced with copper, and suggests the use of a relatively pure copper colourant.

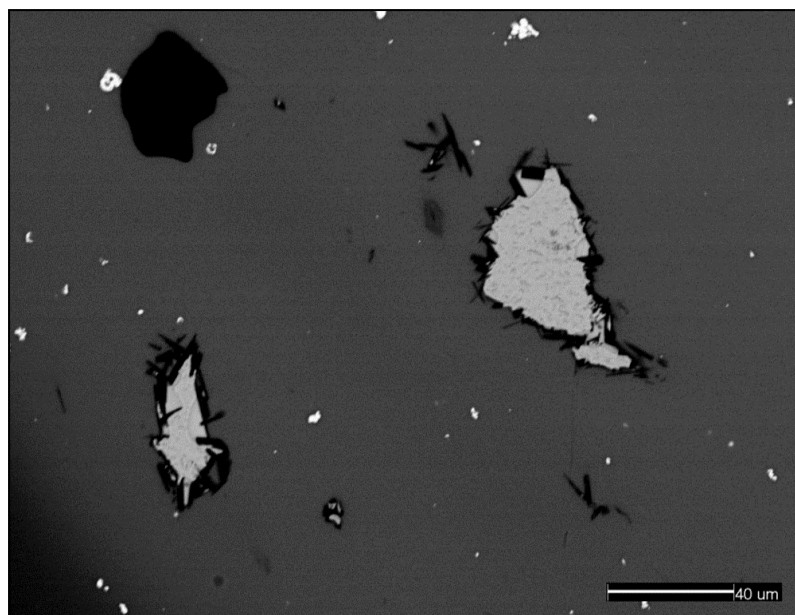


Figure 5.1.36 – BSE micrograph showing translucent copper-green sample ERL104:G290:1721, a *Mosaic?* bead. Several large angular inclusions of copper oxide are visible, which are likely to represent relicts of the colourant. These are immediately surrounded by numerous acicular calcium silicate crystals, corresponding to the mineral wollastonite (CaSiO₃). The bright white crystals visible in the surrounding soda-lime silicate glass matrix are lead-tin oxide. The black area to the top-left is a void.

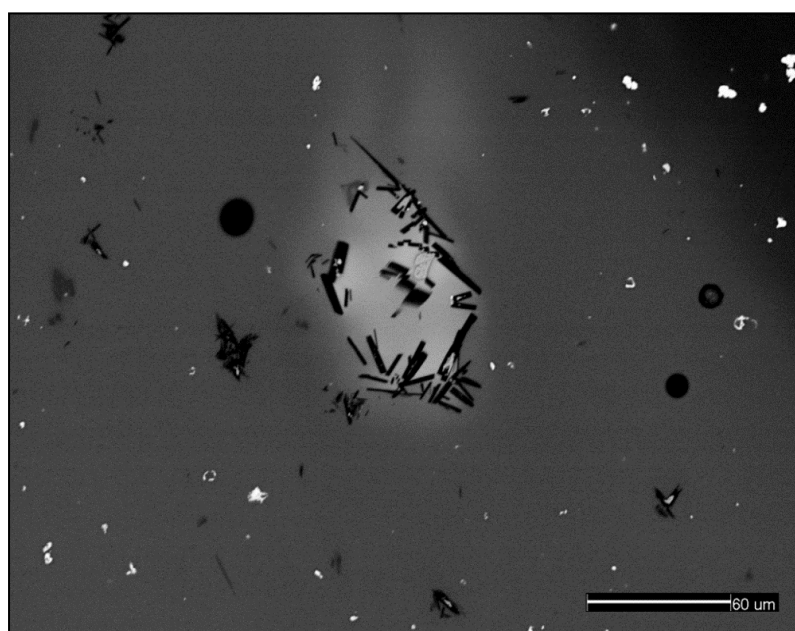


Figure 35.1.37 – BSE micrograph showing translucent copper-green sample ERL104:G290:1721, a *Mosaic?* bead. A bright copper-rich area of soda-lime-silica glass is visible containing numerous dark grey acicular calcium silicate crystals, corresponding to the mineral wollastonite (CaSiO₃). The sparse bright white flecks in the surrounding soda-lime-silica glass are lead-tin oxide crystals.

Sparse crystals of sodium aluminium silicate (Figure 5.1.38) and sodium aluminium silicate sulphate (Figure 5.1.39) were observed in several samples (Table 5.1.2). The former corresponds to the mineral nepheline ($\text{Na}_3\text{KAl}_4\text{Si}_4\text{O}_{16}$); the latter to the mineral lazurite ($\text{Na}_3\text{Ca}(\text{Al}_3\text{Si}_3\text{O}_{12})\text{S}$). Similar inclusions have been identified in Roman opaque yellow lead-antimonate opacified tesserae from Essex (Paynter and Kearns 2011: 16), which are interpreted as nosean ($\text{Na}_8(\text{Al}_6\text{Si}_6\text{O}_{24})\text{SO}_4$). However, the detection of calcium in the inclusions in the Eriswell samples suggests that they are lazurite. In addition, a similar inclusion, corresponding to the mineral leucite (KAlSi_2O_6), was observed in sample ERL046:G03:1279 (a *YellowGreen* bead).

In all cases, these inclusions are typically associated with crystals of lead-tin oxide (PbSnO_3 , lead stannate). They are likely to have formed from a reaction between the high soda content of the soda-lime-silica glass and the clay-ceramic material of a crucible (Heck *et al.* 2003: 38; Peake and Freestone 2012: 842204-10; Peake and Freestone, in press; Santagostino Barbone *et al.* 2008: 466). As the inclusions are typically associated with lead-tin oxide, they may have formed during the production of a lead-tin calx (see this chapter, section 5.2.2), which appears to have been introduced into the glass as a source of lead. This interpretation is borne out by the absence of similar feldspar inclusions in glasses which do not contain lead-tin oxide crystals (*e.g.* opaque white; see this chapter, section 5.2.1).

Acicular crystals of calcium silicate, corresponding to the mineral wollastonite (CaSiO_3), were also observed in a small number of samples (Figure 5.1.31). These are likely to have crystallised from the melt upon cooling, and seem to be peculiar to glasses containing high levels of lead.

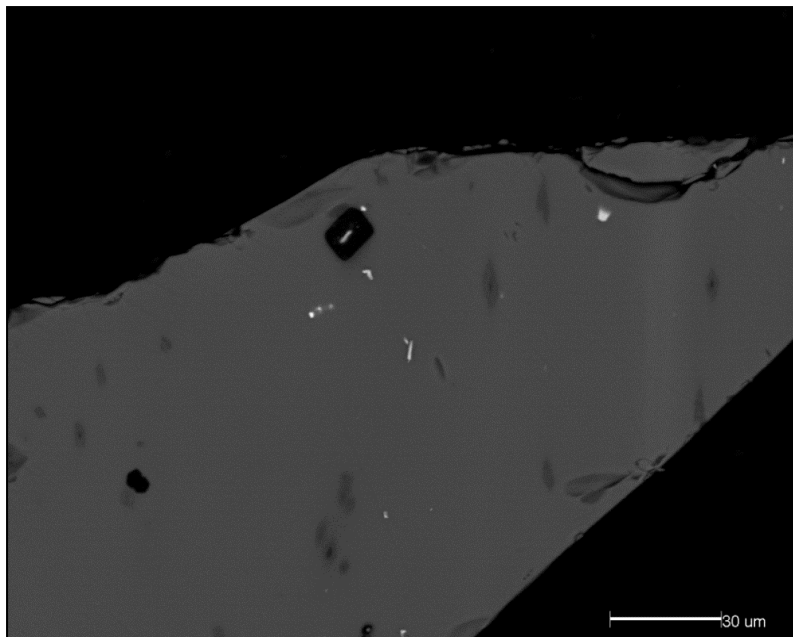


Figure 5.1.38 – BSE micrograph showing translucent copper-green sample ERL104:G362:1961&1969, a *Traffic Light Twisted Trail* bead. A small sub-angular sodium-aluminium-silicate inclusion (black) corresponding to the mineral nepheline ($\text{Na}_3\text{KAl}_4\text{Si}_4\text{O}_{16}$) is visible containing a crystal of lead-tin oxide in its centre. The sparse bright white crystals in the surrounding soda-lime-silica glass matrix are lead-tin oxide. The darker grey patches are rich in calcium, and are likely to represent devitrification products.

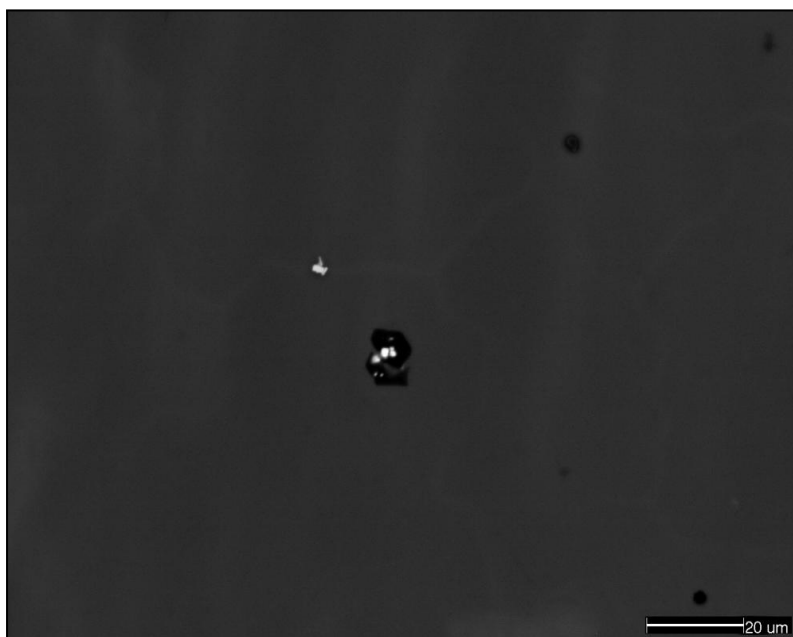


Figure 5.1.39 – BSE micrograph showing translucent copper-green sample ERL046:G38:1048, a *YellowGreen* bead. A small irregular sodium aluminium silicate sulphate inclusion (black) corresponding to the mineral lazurite ($\text{Na}_3\text{Ca}(\text{Al}_3\text{Si}_3\text{O}_{12})\text{S}$) is visible associated with crystals of lead-tin oxide (white).

Table 5.1.2 – Selected SEM-EDS spot analyses of aluminium-rich inclusions observed in several translucent copper-green samples from Eriswell.

Sample ¹	Oxide (wt %) ²									
	Na ₂ O	Al ₂ O ₃	SiO ₂	SO ₃	S	K ₂ O	CaO	Fe ₂ O ₃	SnO ₂	PbO
<i>Nepheline</i>	15.9	34.9	41.1	-	-	8.1	-	-	-	-
ERL104:G213:2474	17.5	33.1	44.1	b.d.	-	1.5	0.9	0.9	b.d.	0.7
ERL104:G362:1961&1969	18.4	31.3	41.7	b.d.	-	1.5	0.5	1.0	0.9	4.0
ERL104:G363:1916	18.3	34.2	42.1	b.d.	-	2.2	0.5	0.4	b.d.	1.4
<i>Lazurite</i>	18.7	30.7	36.2	(16.1)	6.4	-	11.3	-	-	-
ERL104:G367:3633	17.9	27.7	30.6	13.1	(5.3)	0.6	7.1	0.3	b.d.	0.8
ERL046:G38:1048	15.4	24.9	37.7	11.4	(4.6)	0.3	4.7	0.8	0.4	2.5
<i>Leucite</i>	-	23.4	55.1	-	-	21.6	-	-	-	-
ERL046:G03:1279	0.5	18.3	64.1	b.d.	-	16.0	b.d.	b.d.	b.d.	b.d.

¹Theoretical compositions for nepheline (Na₃KAl₄Si₄O₁₆), lazurite (Na₃Ca(Al₃Si₃O₁₂)S) and leucite (KAlSi₂O₆) are in *italics*.

²Spot analyses normalised to 100%. b.d. = below detection. See Chapter 2, section 2.3.1 for details. Values in brackets represent hypothetical S values.

5.1.4.1. Trace Element Analyses

Four translucent copper-green and two translucent turquoise glasses from Eriswell were analysed by LA-ICP-MS. The turquoise glasses contain elevated levels of nickel, zinc and arsenic (Figure 5.1.40); elevated levels of zinc were also detected in many of the turquoise glasses by SEM-EDS (Figure 5.1.35). Zinc varies from 6950-12660 ppm in the translucent turquoise glasses, in comparison to 20-440 ppm in the translucent green glasses. This suggests the use of different sources of copper as colourants; most likely an alloy of copper and zinc (*e.g.* brass) in the production of the turquoise glasses. Copper is strongly positively correlated with arsenic ($r^2 = 0.85$; Figure 5.1.41) and weakly correlated with silver (Figure 5.1.42; $r^2 = 0.32$) in both the green and turquoise glasses, suggesting that trace levels of these two components were also introduced with the copper colourant. Variations in the levels of antimony and manganese are likely to reflect the composition of the different base glass types used (see Chapter 4).

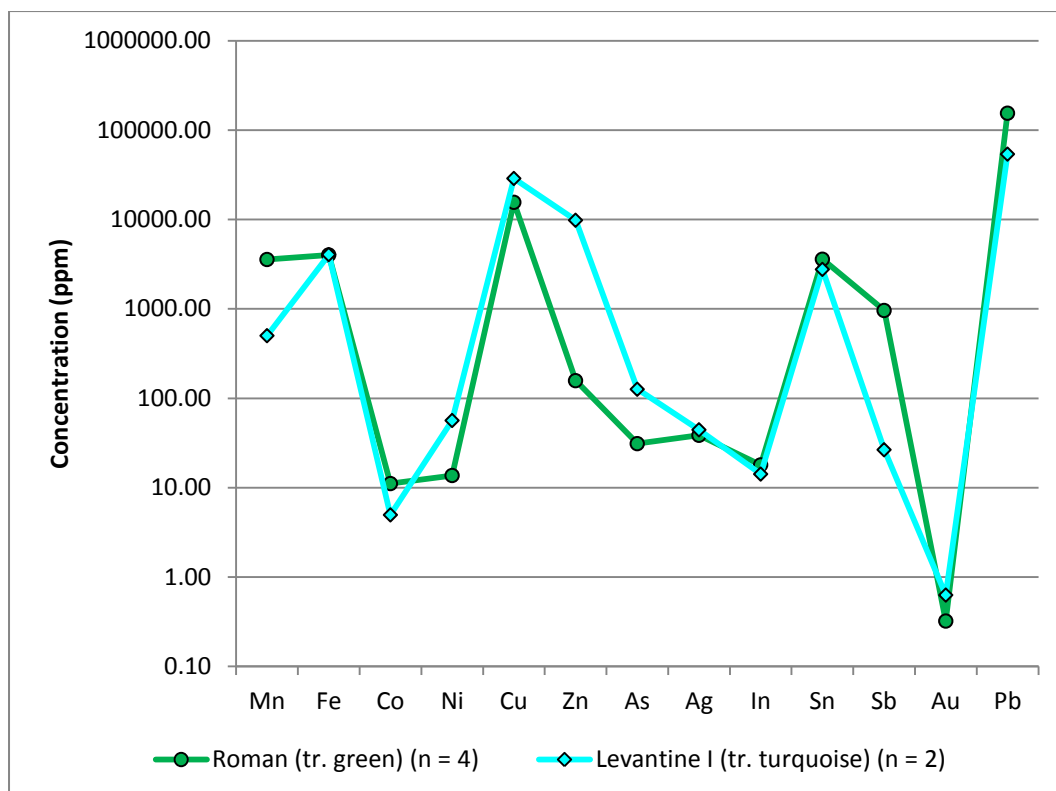


Figure 5.1.40 – Average colourant and colourant-related element concentrations for the translucent copper-green and turquoise samples from Eriswell, showing the different base glass types identified. Note the logarithmic scale.

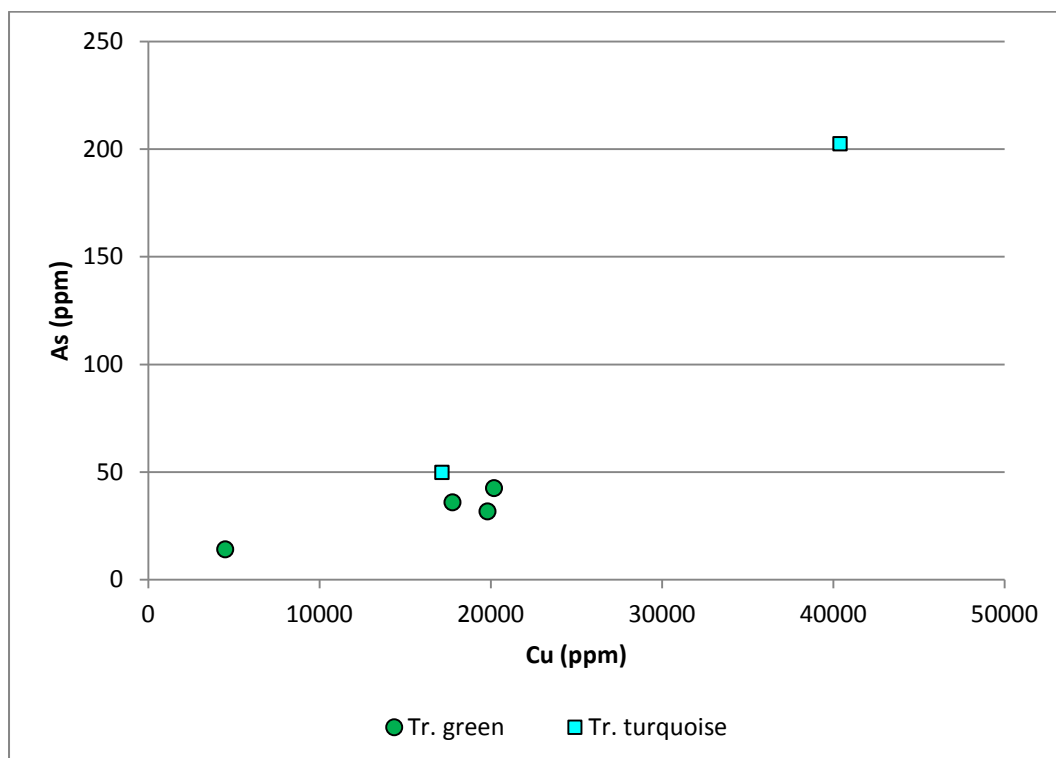


Figure 5.1.41 – A plot of copper versus arsenic for the translucent copper-green and turquoise samples from Eriswell.

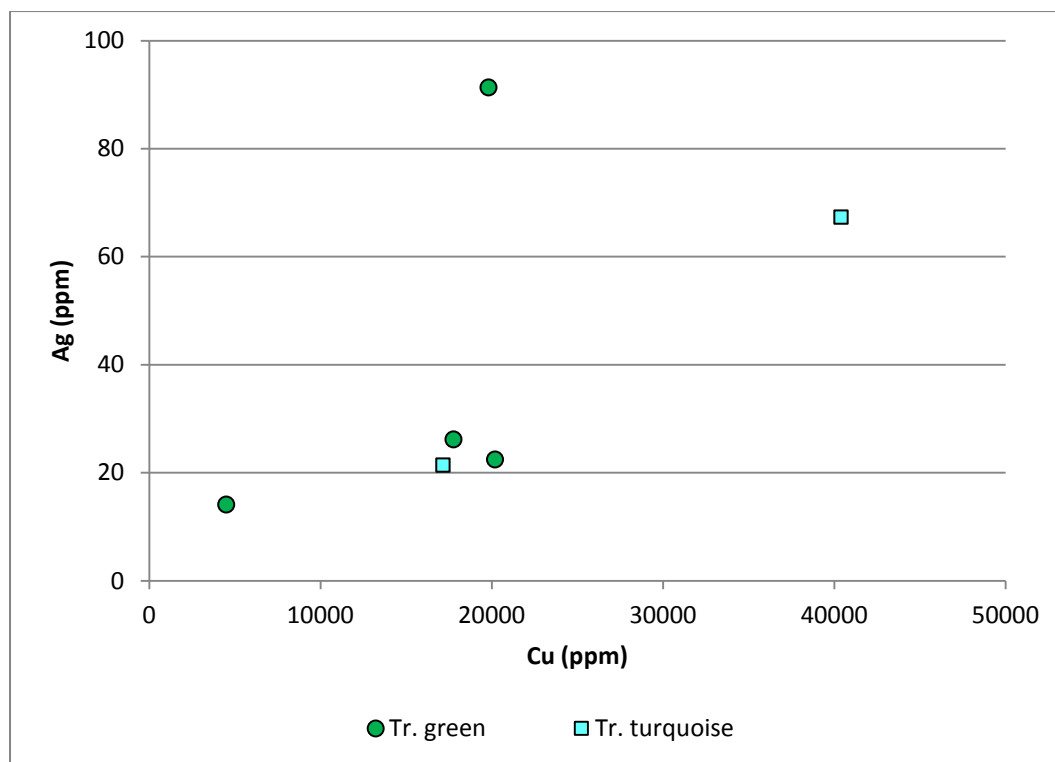


Figure 5.1.42 – A plot of copper versus silver for the translucent copper-green and turquoise samples from Eriswell.

5.1.5. 'Dark' Glass

Whilst 'dark' glass from Eriswell is visually opaque, it is described as translucent because it does not contain a crystalline opacifying agent; opacity is instead caused by the depth of colour (Guido 1999: 17). It has been suggested that glass of this colour may have been used as a substitute for jet (Guido 1999: 18). Samples of 'dark' glass were obtained from 25 beads from Eriswell. They are all coloured by high levels of iron (corresponding to 2-25% Fe_2O_3). This produces a translucent olive-green colour so deep that it prevents light from passing through, thereby making the glass appear black (Bayley 1995: 1196; Bayley 1999: 90; Henderson 1985: 283; Mortimer and Heyworth 2009: 409). The high levels of iron present have depressed the concentrations of many of the other major components, as demonstrated by the negative correlation between iron and silica in Figure 5.1.43.

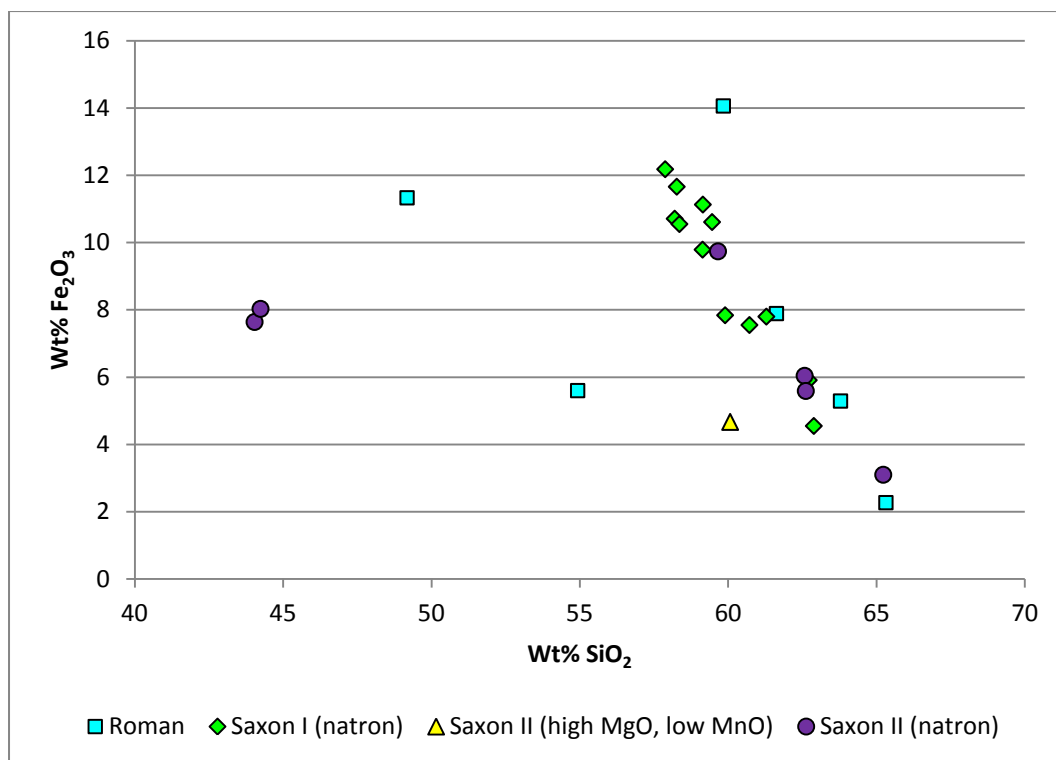


Figure 5.1.43 – A plot of silica versus iron oxide for the ‘dark’ samples from Eriswell, showing the different base glass types identified.

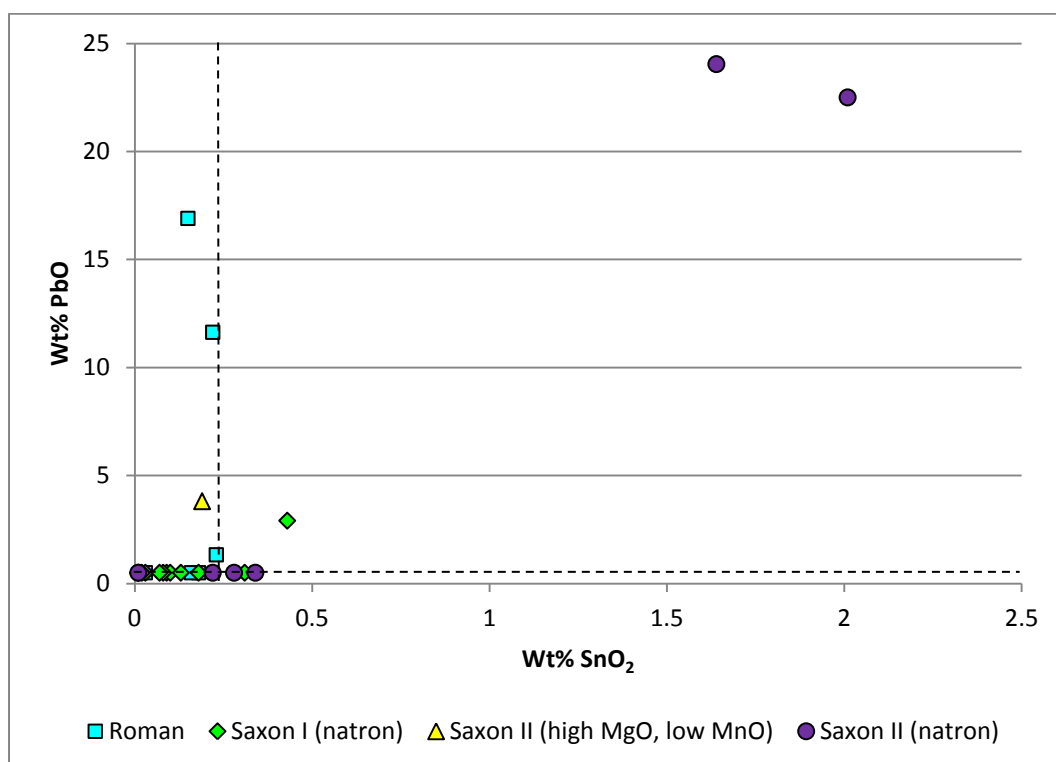


Figure 5.1.44 – A plot of tin oxide versus lead oxide for the ‘dark’ samples from Eriswell, showing the different base glass types identified. The dashed lines represent the approximate detection limits for tin oxide and lead oxide.

The manganese content is variable, but generally high (corresponding to 0.3-2.1% MnO); its concentration is likely to reflect the base glass types used (see Chapter 4). It is not correlated with iron, in contrast to the uncoloured glasses, which results from the deliberate addition of iron as a colourant to a manganese-decoloured base glass. The colour of the base glass used in the production of 'dark' glass was not important, as it would have been masked by intensity of the iron colourant and may have even facilitated the production of the colour. Lead is very variable in the 'dark' glasses analysed (Figure 5.1.44). The majority typically contain lead below the detection limits of SEM-EDS, but three samples contain 1-4% PbO and four samples contain in excess of 10% PbO. Lead is not necessary to produce the colour and is unlikely to have dramatically affected the working properties of the glass at concentrations below 4%. However, lead in excess of 10% will have reduced the melting temperature, allowing the glass to be worked for longer periods and at lower temperatures. The concentration of lead present does not appear to bear any relation to bead type, bead date or base glass composition (*e.g.* Figure 5.1.44), so it is unclear why it was added.

It has been suggested that 'dark' glass was sometimes produced by mixing together scrap glass of different colours (Heyworth 1994: 80; Mortimer and Heyworth 2009: 409). However, whilst two of the samples analysed contain CuO at concentrations in excess of 0.5% (sample ERL104:G262:1284, a *Koch34, variation* bead and sample ERL104:G213:2474, a *WhitePoly3* bead), copper was not detected in the majority of samples, suggesting that scrap copper-based colours (*i.e.* red, orange, turquoise and green) were probably not used in their production. Furthermore, blue glass is unlikely to have been used because the levels of cobalt identified by trace element analysis (see section 5.1.5.1 below) are too low to suggest its addition. However, two 'dark' glass samples from G242 (samples ERL104:G242:2273/28 and ERL104:G242:2273/16, both *Miniature Dark* beads) are compositionally distinct in that they were certainly produced using scrap glass of another colour.

The composition of the two beads in question closely reflects that of opaque yellow glass (see this chapter, section 5.2.2); particularly in the high lead and tin contents, corresponding to approximately 23% PbO and 2% SnO₂ respectively. It is likely that they were produced using scrap opaque yellow glass, or perhaps a failed opaque

yellow glass. The absence of lead-tin oxide crystals is likely to have resulted from the instability of this compound at high temperatures; these crystals are destroyed at temperatures in excess of 1000°C (Henderson 1985: 286). Interestingly, a ‘black’ glass bead of very similar composition was identified at Mucking (Essex), containing 22.6% PbO and 3.6% SnO₂ (Mortimer 1996b: 3-4; Mortimer and Heyworth 2009: 409). This suggests that the practice of producing ‘dark’ glass from old opaque yellow glass is not an isolated occurrence; it is just possible that this bead was a product of the same workshop as the two of similar composition from Eriswell.

It is unclear as to the form in which the iron colourant was added in the production of ‘dark’ glass, but the presence of various inclusions in several of the samples analysed suggests a number of possibilities. A large angular fragment of iron oxide was observed in sample ERL104:G343:1671 (*Dark Globular*), which is probably a relict of the raw colourant (Figure 5.1.45); it is too large and irregular to represent a fragment of iron scale pulled from the mandrel on which the bead was formed (see Chapter 3, section 3.2.1), such as that shown in Figure 5.1.46.

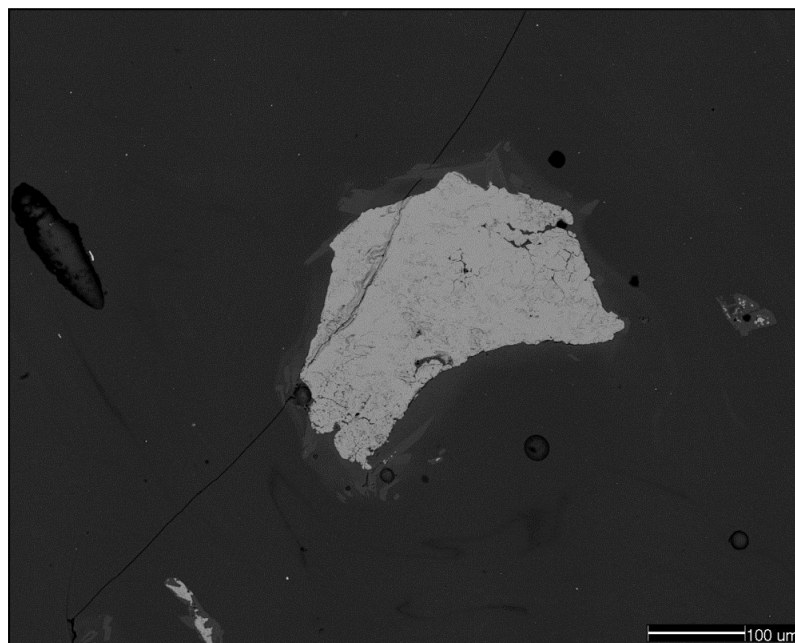


Figure 5.1.45 – BSE micrograph showing ‘dark’ sample ERL104:G343:1671, a *Dark Globular* bead.

An angular fragment of iron oxide (pale grey) can be seen in a soda-lime-silica glass matrix (dark grey). The glass at the boundary of this inclusion is slightly enriched in iron, and whilst this could just be resolved in the SEM it is not easy to see here.



Figure 5.1.46 – BSE micrograph showing ‘dark’ sample ERL104:G144:2559, a *Dark Globular* bead. A fragment of iron scale (pale grey) is visible in a soda-lime-silica glass matrix (dark grey).

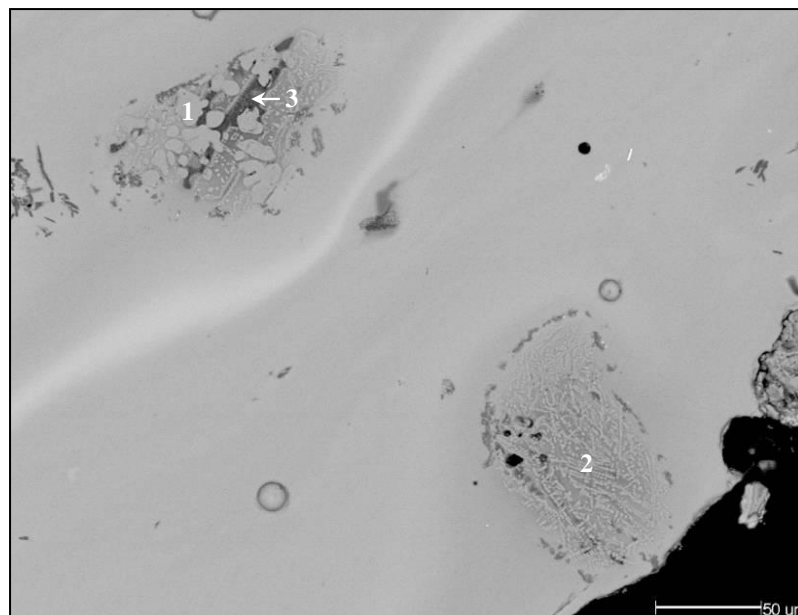


Figure 5.1.47 – BSE micrograph showing ‘dark’ sample ERL104:G242:2273, a *Miniature Dark* bead. Two inclusions of fayalitic slag (dark grey) in a high-lead soda-lime-silica glass matrix coloured by iron (pale grey) are visible. The slag particles consist of irregular wüstite grains (1), together with intergrowths of fayalite (2) and interstitial silicate glass (3). The slag has clearly begun to dissolve in the surrounding glass.

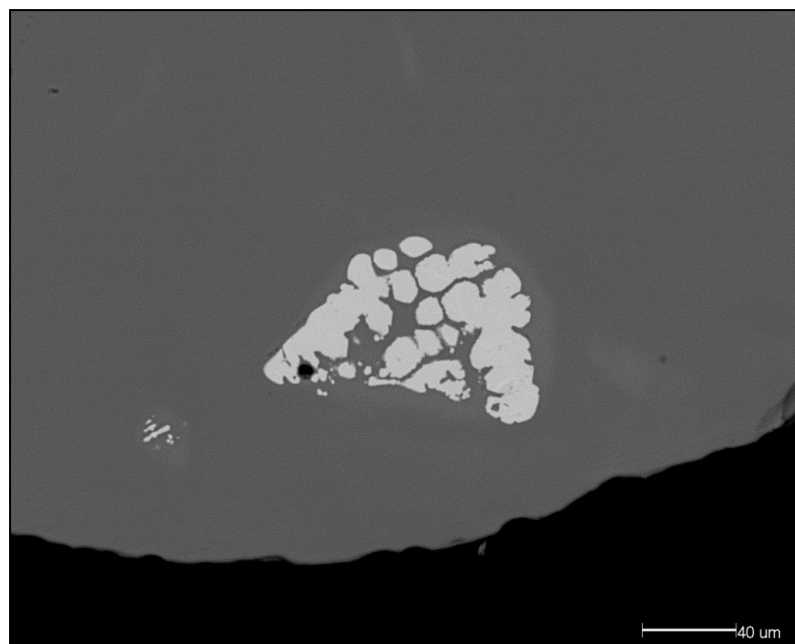


Figure 5.1.48 – BSE micrograph showing ‘dark’ sample ERL104:G290:1734, a *DarkPoly4* bead. An irregular inclusion consisting of grains of iron oxide corresponding to wüstite (FeO) is visible (pale grey) in a soda-lime-silica glass matrix (dark grey).

Furthermore, several particles of iron-rich slag were observed in sample ERL104:G242:2273/16 (a *Miniature Dark* bead), the main phase of which corresponds to the mineral fayalite (FeSiO_4) (Table 5.1.3). The slag has begun to dissolve in the surrounding glass matrix, making it difficult to resolve in the SEM (Figure 5.1.47), but was almost certainly added as a colourant. This dissolution has resulted in considerable contamination of the slag by elements from the surrounding soda-lime-silica glass (primarily soda and lead), as is evident from the bulk compositions (Table 5.1.3). This is also apparent from the analyses of the interstitial glassy phases of this slag, where soda and lead are particularly elevated, but also magnesia, potash, manganese and tin. No slag was observed in sample ERL104:G242:2273/28, which is of a very similar composition to sample ERL104:G242:2273/16, but this is likely to be borne out by the small nature of the samples taken or the complete dissolution of the slag in this glass. A similar inclusion was observed in sample ERL104:G290:1734, consisting of irregular grains of wüstite (FeO) (Figure 5.1.48), but it cannot be confirmed whether this reflects the addition of slag.

Table 5.1.3 – Selected SEM-EDS area and spot analyses of the fayalitic slag inclusions in ‘dark’ sample ERL104:G242:2273/16, showing the bulk composition of the slag and the composition of the different phases identified.

Sample ¹	Oxide (wt%) ²														
	Na ₂ O	MgO	Al ₂ O ₃	SiO ₂	P ₂ O ₅	SO ₃	K ₂ O	CaO	TiO ₂	MnO	Fe ₂ O ₃	FeO	SnO ₂	Sb ₂ O ₃	PbO
<i>Fayalite</i>	-	-	-	29.5	-	-	-	-	-	-	-	70.5	-	-	-
Bulk slag	7.4	0.4	4.8	19.6	0.8	0.3	0.3	1.5	0.2	1.1	57.5	(51.7)	b.d.	b.d.	4.5
	7.9	0.4	3.5	24.9	0.7	0.4	0.4	1.8	0.3	0.7	50.4	(45.4)	b.d.	b.d.	7.1
Main phase	b.d.	4.7	0.2	28.1	b.d.	b.d.	0.1	1.1	b.d.	0.5	64.9	(58.4)	b.d.	b.d.	b.d.
	11.6	0.9	3.1	39.1	0.8	0.1	0.5	2.3	b.d.	1.5	30.4	-	b.d.	b.d.	9.2
Interstitial glass	10.2	1.3	2.4	44.3	1.0	0.3	0.8	2.3	b.d.	2.2	28.9	-	b.d.	b.d.	6.5
	13.8	0.2	17.8	33.7	4.0	1.3	0.7	3.4	0.1	0.6	19.9	-	b.d.	b.d.	4.1
	12.7	0.3	16.9	33.4	3.6	1.2	0.8	3.2	0.2	0.7	21.9	-	b.d.	0.7	3.7
	9.1	0.4	5.3	39.6	0.8	0.8	0.8	2.8	0.2	0.7	25.1	-	0.7	0.7	12.6
	9.1	0.3	4.7	24.8	0.7	b.d.	0.4	1.4	0.2	0.7	50.6	-	b.d.	b.d.	6.2
	2.5	2.6	0.2	34.3	0.4	b.d.	b.d.	2.6	b.d.	3.8	51.9	-	b.d.	b.d.	1.8

¹Theoretical composition for fayalite (Fe₂SiO₄) is in *italics*. ‘Bulk slag’ represents the bulk composition of the slag inclusions; ‘Main phase’ the composition of the main phase of the slag; and ‘Interstitial glass’ the composition of the glassy phases of the slag.

²Area and spot analyses normalised to 100%. b.d. = below detection. See Chapter 2, section 2.3.1 for details. Values in brackets represent hypothetical FeO values. Chlorine and the oxides of cobalt, nickel, copper, zinc, arsenic and barium were analysed for but not detected.

There are a number of very close similarities in composition and microstructure of the slag in sample ERL104:G242:2273/16 to the fayalitic slag identified in many of the opaque red glasses from Eriswell (see this chapter, section 5.2.3.1), suggesting that the same type of slag (*i.e.* fayalitic) was used to produce both colours. It is just possible that these colours were produced in the same workshops. Of particular note is the absence of any copper or tin oxide particles surrounding the slag (Figure 5.1.47), which is so characteristic of the slag particles observed in the opaque red glasses.

5.1.5.1. Trace Element Analyses

Only two ‘dark’ glass samples (ERL104:G305:1813, a ‘Saxon II (natron)’ *Dark Globular* bead, and ERL114:G429:1566, a ‘Saxon I (natron)’ *Miniature Dark* bead) were analysed by LA-ICP-MS, so a detailed comparison of the colourant technology and colourant-related elements is not possible. However, it can be seen from Figure 5.1.49 that both samples are characterised by high levels of iron oxide and manganese, with slightly elevated levels of lead. The low concentrations of other colourant elements, such as cobalt and antimony, indicate that these components were not deliberately added. However, variations in the concentrations of components such as copper (roughly 100 and 370 ppm respectively) and tin (roughly 500 and 250 ppm respectively) may reflect the incorporation of some recycled material into the batch.



Figure 5.1.49 – Colourant and colourant-related elements for the ‘dark’ samples from Eriswell, showing the different base glass types identified. Note the logarithmic scale.

5.2. Opaque Glass

All of the opaque glasses from Eriswell are natron-based soda-lime-silica glasses, which have been modified through the addition of various colourants and opacifiers. As with translucent glasses (see section 5.1 above), lead was added during the colouring process rather than during the production of the raw glass itself. Semi-opaque glass has been discussed in section 5.1; the present section deals exclusively with fully opaque glass.

Opacity is caused by a dispersion of metals, metal compounds, bubbles, or a combination of these. When incident light hits a transparent glass containing a suspension of these particles (or bubbles), it is scattered and prevented from passing through (Weyl 1951: 369). The degree of opacity therefore depends upon the size, distribution and density of the inclusions present (Turner and Rooksby 1959: 17).

5.2.1. Opaque White Glass

Samples of opaque white glass were obtained from 64 beads from Eriswell. Two different opacifying agents were identified: tin oxide and bubbles. The differences between the two methods of opacification are clearly illustrated by a plot of lead versus tin (Figures 5.2.1 and 5.2.2) and antimony versus tin (Figures 5.2.3 and 5.2.4).

The samples opacified by tin contain 0.4-7.9% SnO₂, in conjunction with up to 5.4% PbO. Bright white crystals of tin oxide can be seen heterogeneously dispersed throughout the glass matrix in Figures 5.2.5-5.2.8, producing both opacity and colour (Bayley 1999: 91; Turner and Rooksby 1959: 25). These appear brighter in the BSE micrographs due to the higher atomic number of tin compared to the surrounding soda-lime-silica glass matrix. The crystals vary considerably in size and shape, often forming as large aggregates. The weak positive correlation (Figures 5.2.1 and 5.2.2; $r^2 = 0.33$) between lead and tin indicates that these two components may have been introduced together as a single ingredient. This is unsurprising, as it is difficult to

calcine metallic tin without the presence of lead (Freestone *et al.* 1990: 275; Kingery and Vandiver 1986: 116). Slight variations in the proportions of these two components, coupled with the heterogeneity of the glass, are likely to have resulted in the wide range of values observed for lead and tin. Several of the tin oxide opacified whites also contain numerous large bubbles (Figures 5.2.6-5.2.8). Whilst these would normally contribute something to the opacity, the primary opacifying agent here is tin oxide and their presence is unlikely to be intentional, instead reflecting short firing times and/or low melting temperatures.

Opacification resulting solely from bubbles is not unknown in opaque white glasses from the early Anglo-Saxon and preceding Roman periods (*e.g.* Bayley and Wilthew 1986; Biek *et al.* 1985: 85; Brill and Whitehouse 1988: 40; Mortimer 1996b: 4; Mortimer and Heyworth 2009: 409). The bubble-opacified glasses from Eriswell contain neither tin nor lead at detectable concentrations (Figure 5.2.1) and a dispersion of tiny bubbles is clearly visible throughout the glass matrix (Figures 5.2.9-5.2.11). It is unclear exactly how such a fine dispersion of bubbles was produced, but it is likely that careful control of the furnace conditions were necessary. Temperatures are likely to have been low and the glass was probably molten for a very short time, because the gases have not been given sufficient time to escape (Bayley 1995: 1195; Bayley 1999: 89).

Bubble-opacified glass is frequently heavily weathered, as the porous nature of the glass provided a mechanism by which groundwater could enter (see Chapter 3, section 3.3). Many of the bubble-opacified whites contain low levels of antimony, corresponding to up to 0.8% Sb_2O_3 (Figure 5.2.3). Antimony was used as an opacifier in glasses produced in the Roman period and earlier, but was generally replaced by tin oxide between the 2nd and 4th centuries AD (Biek and Bayley 1979: 9; Fiori and Vandini 2004: 191; Foster and Jackson 2005: 331; Turner and Rooksby 1961: 1-2). However, antimony is present in solution and reflects the use of a 'Roman' base glass (Figure 5.2.4; see also Chapter 4, section 4.3), as opposed to the deliberate addition of antimony for the purpose of opacification.

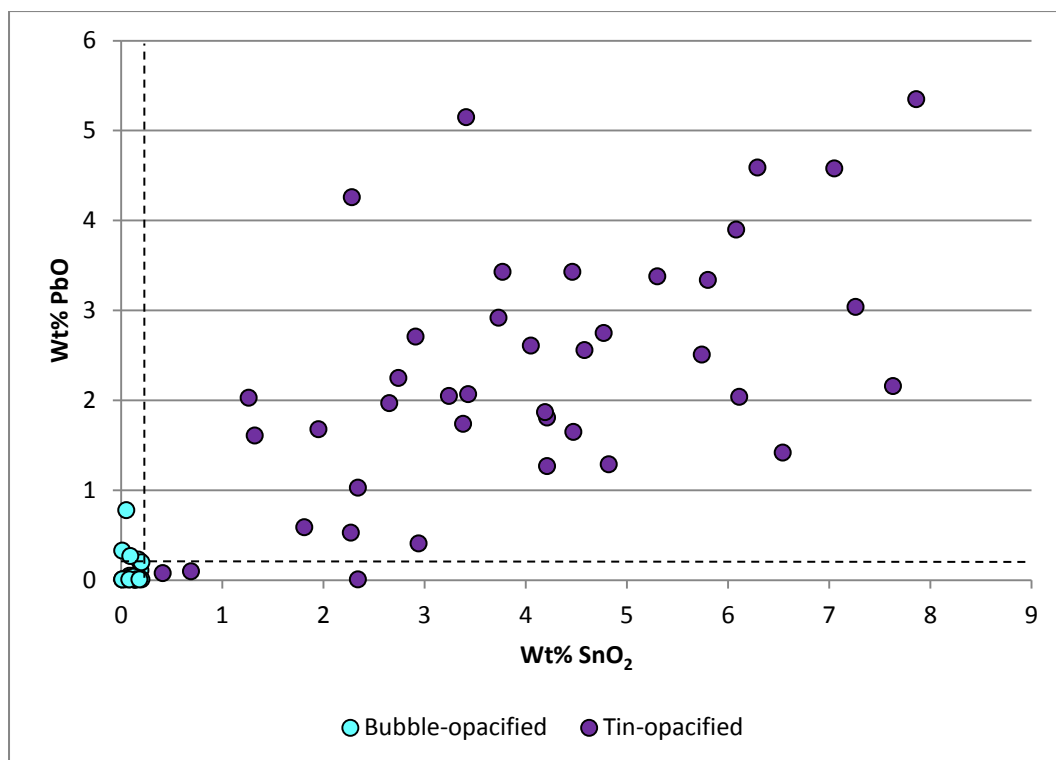


Figure 5.2.1 – A plot of tin oxide versus lead oxide for the white samples from Eriswell. Compare to Figure 5.2.2. The dashed lines represent the approximate detection limits for tin oxide and lead oxide.

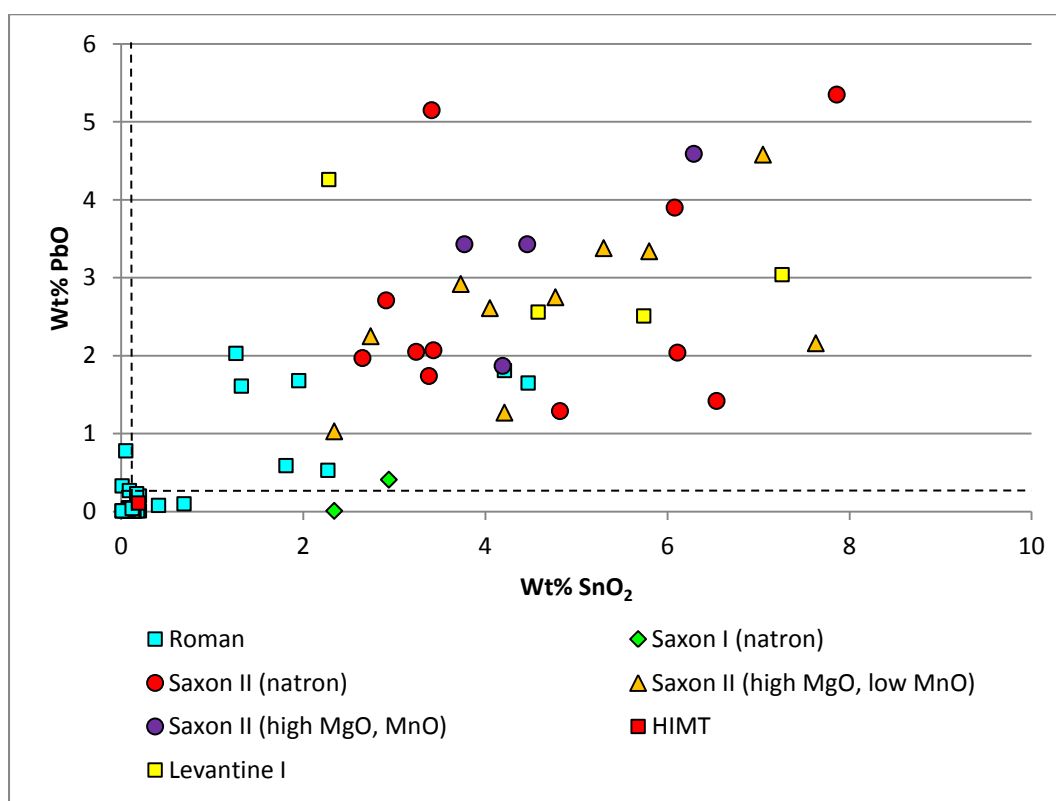


Figure 5.2.2 – A plot of tin oxide versus lead oxide for the opaque white samples from Eriswell, showing the different base glass types identified. Compare to Figure 5.2.1. The dashed lines represent the approximate detection limits for tin oxide and lead oxide.

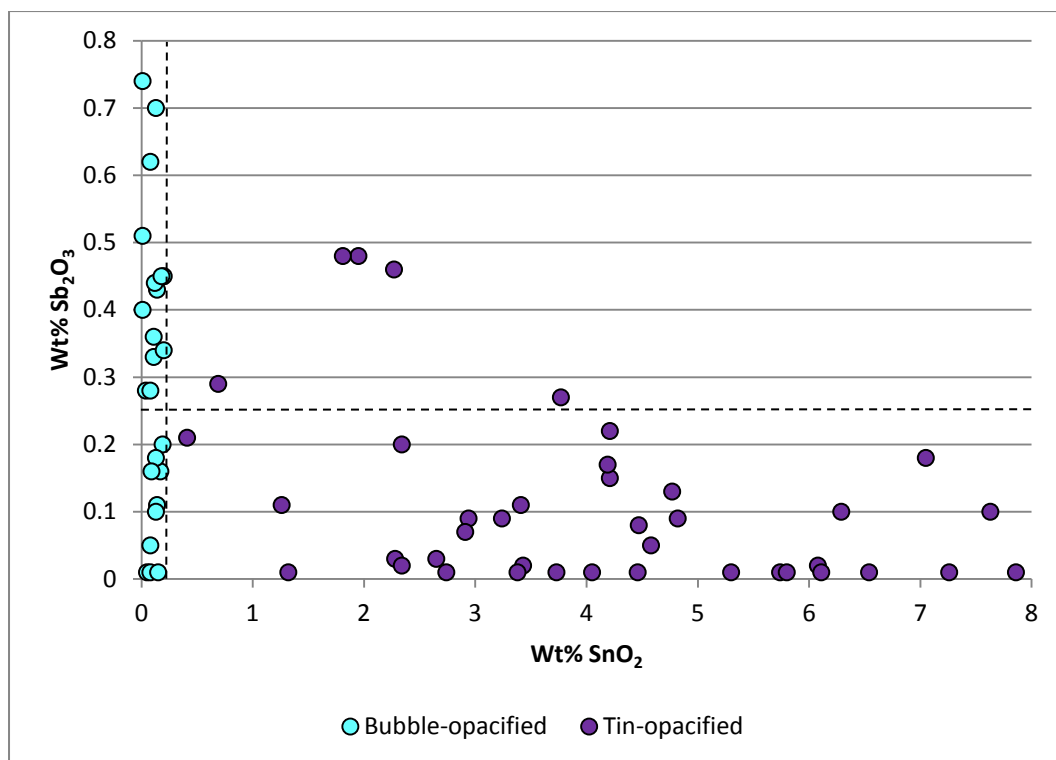


Figure 5.2.3 – A plot of tin oxide versus antimony oxide for the white samples from Eriswell. Compare to Figure 5.2.4. The dashed lines represent approximate detection limits for tin oxide and antimony oxide.

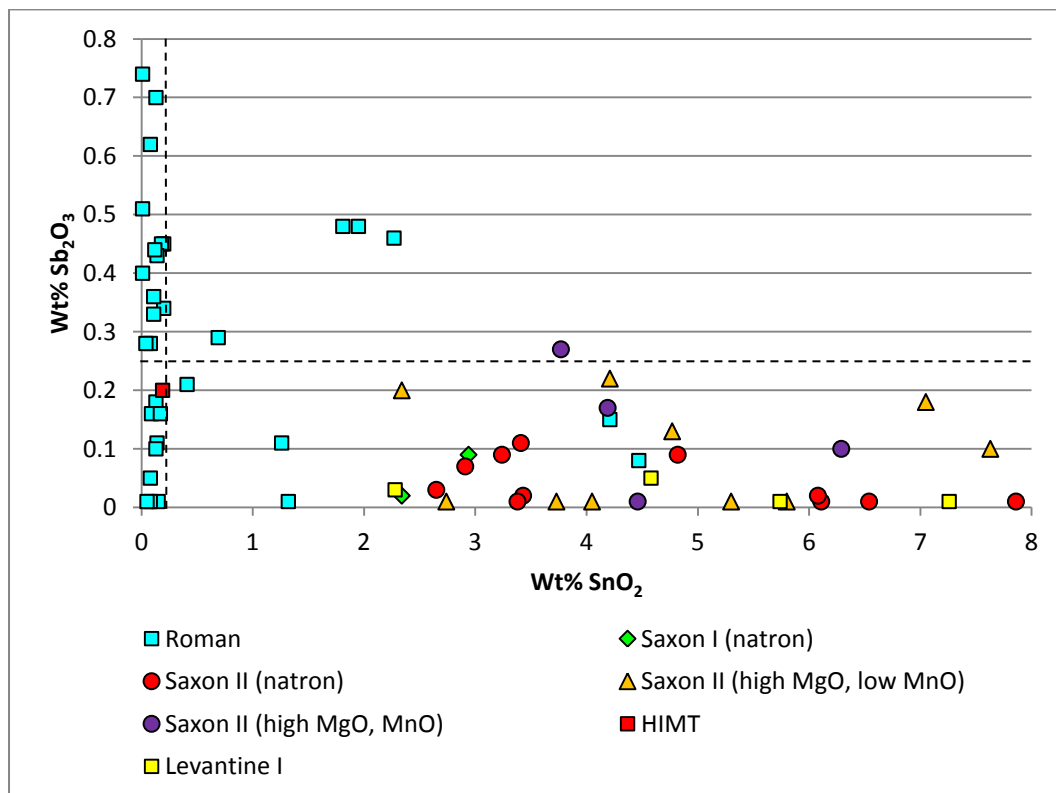


Figure 5.2.4 – A plot of tin oxide versus antimony oxide for the opaque white samples from Eriswell, showing the different base glass types identified. Compare to Figure 5.2.4. The dashed lines represent approximate detection limits for tin oxide and antimony oxide.

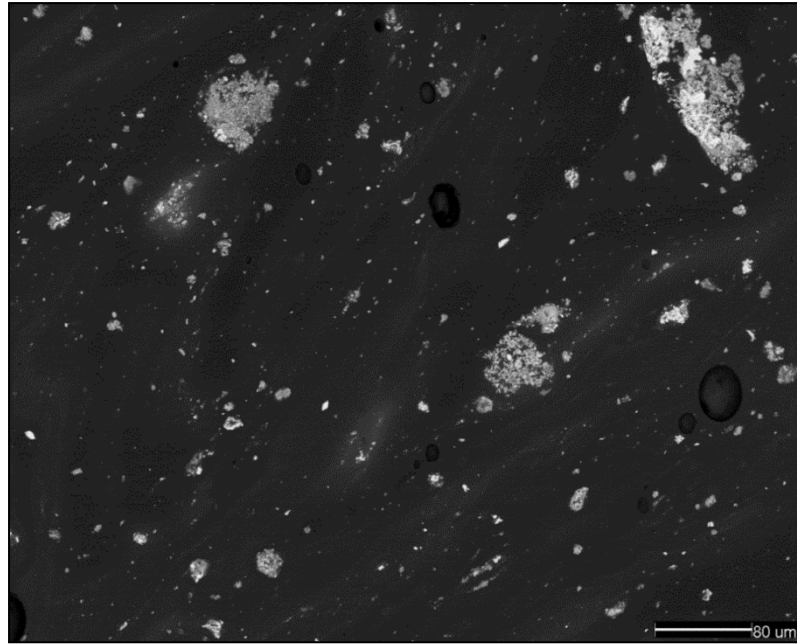


Figure 5.2.5 – BSE micrograph showing opaque white sample ERL104:G193:1312, a *Cylindrical Round* bead. Bright white crystals of cassiterite (tin oxide), heterogeneously dispersed in a lead-rich soda-lime-silica glass matrix (grey), act as the opacifying agent.

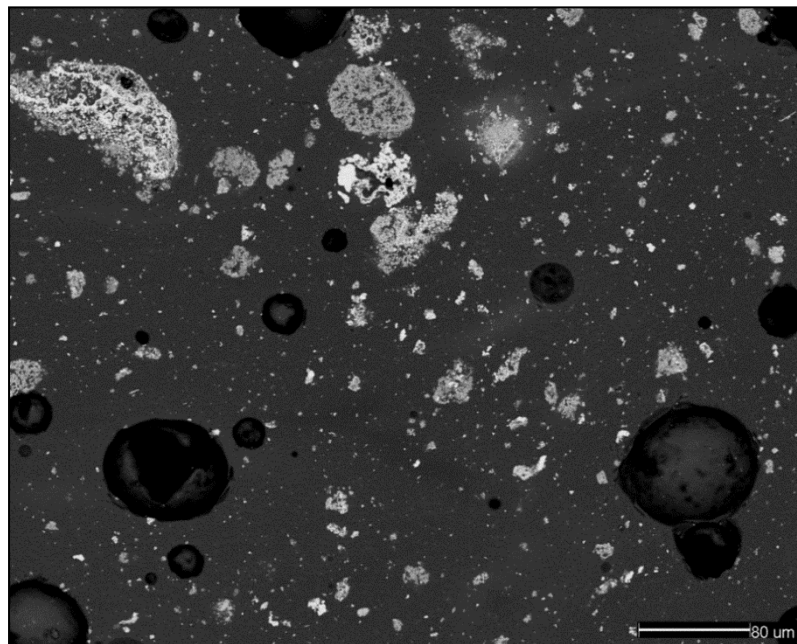


Figure 5.2.6 – BSE micrograph showing opaque white sample ERL104:G237:1151, a *Cylindrical Round* bead. Bright white crystals of cassiterite (tin oxide), heterogeneously dispersed in a lead-rich soda-lime-silica glass matrix (grey), act as the opacifying agent. Several voids (black) and bubbles are also visible.

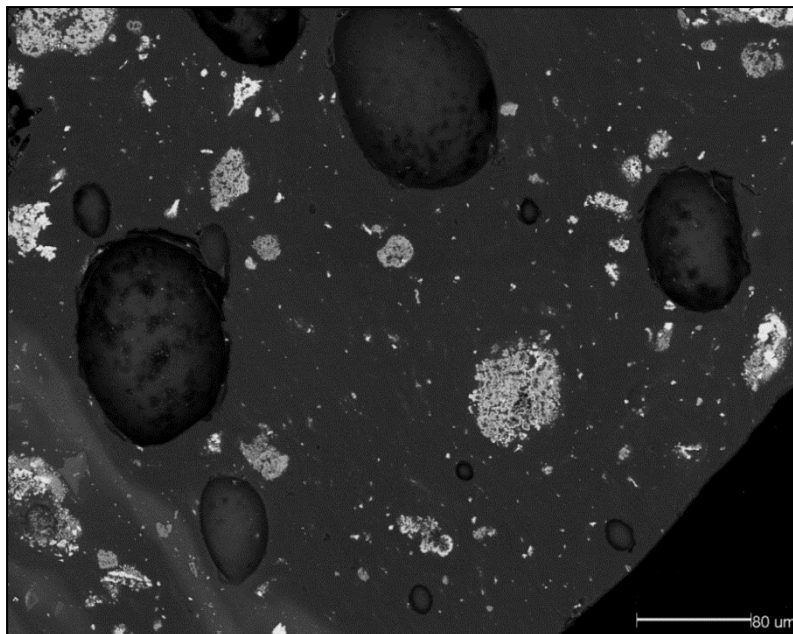


Figure 5.2.7 – BSE micrograph showing opaque white sample ERL104:G107:1128, a *Koch34* bead. Bright white crystals of cassiterite (tin oxide), heterogeneously dispersed in a lead-rich soda-lime-silica glass matrix (grey), act as the opacifying agent. Several large bubbles can also be seen.

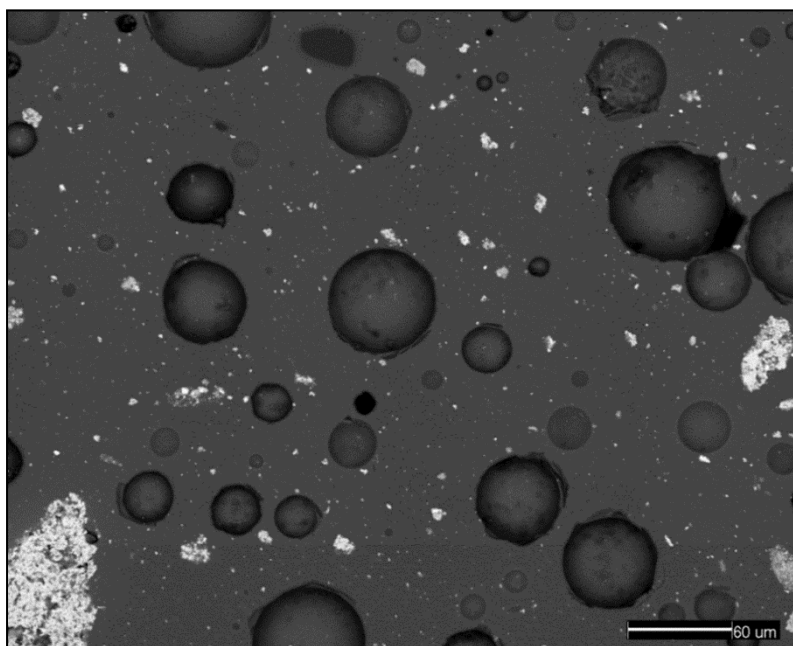


Figure 5.2.8 – BSE micrograph showing opaque white sample ERL104:G195:1352, a *Koch34* bead. Bright white crystals of cassiterite (tin oxide), heterogeneously dispersed in a lead-rich soda-lime-silica glass matrix (grey), act as the opacifying agent. Numerous bubbles are also visible.

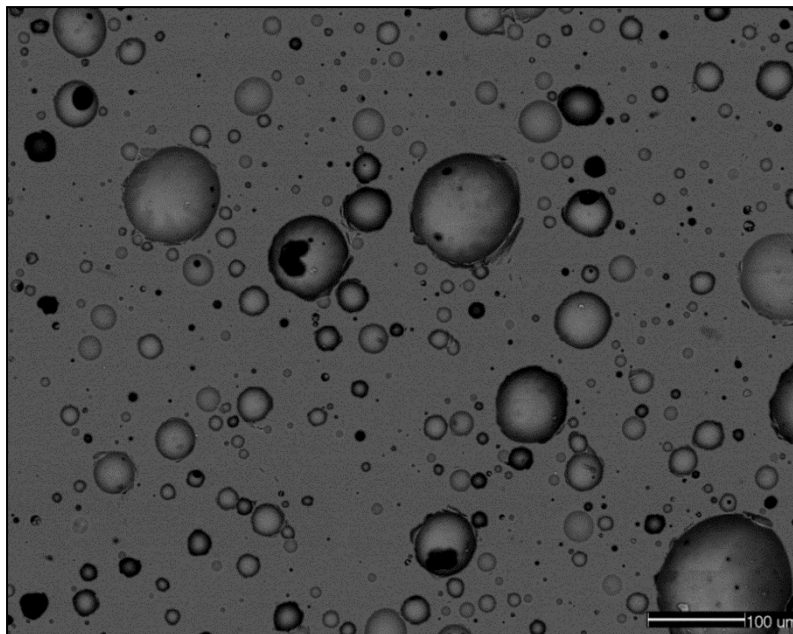


Figure 5.2.9 – BSE micrograph showing opaque white sample ERL104:G367:3625, a *White Cylindrical, pentagonal* bead. A heterogeneous dispersion of tiny bubbles of varying size act as the opacifying agent.

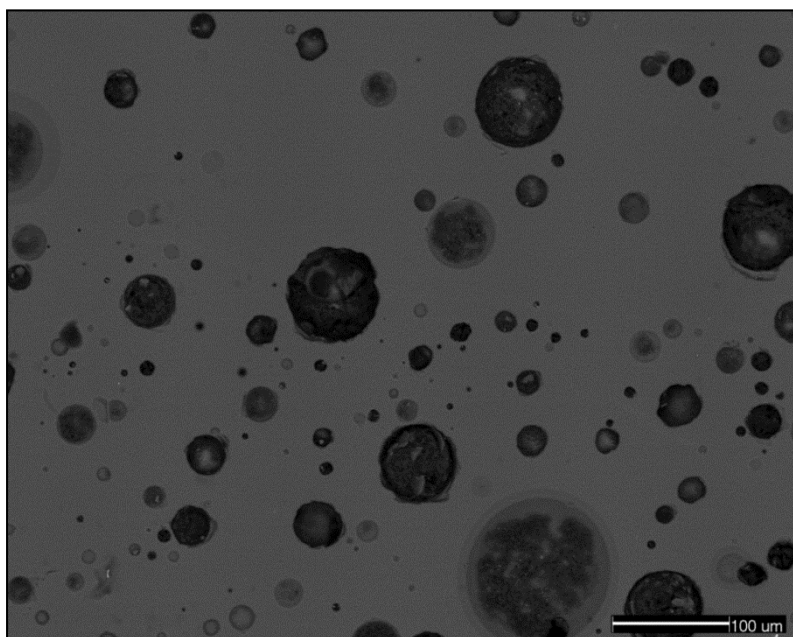


Figure 5.2.10 – BSE micrograph showing opaque white sample ERL104:G367:3619, a *White Poly3* bead. A heterogeneous dispersion of tiny bubbles of varying size act as the opacifying agent.

Low levels of antimony in solution have been identified in bubble-opacified white glasses from a number of other early Anglo-Saxon sites (*e.g.* Bayley 1985: 85; Mortimer 1996b: 4; Mortimer and Heyworth 2009: 407-410), suggesting that most (probably all) bubble-opacified white glass was produced using a 'Roman' base glass (see Chapter 4, section 4.9). Three of the tin oxide opacified samples (ERL046:G42:1142, ERL104:G243:1373 and ERL104:G315:2345) also contain up to approximately 0.5% Sb_2O_3 (Figure 5.2.3). The presence of both tin and antimony is not unknown in early medieval opaque white glass (*e.g.* Bayley and Wilthew 1986; Henderson 2002) and is again likely to reflect the use of a 'Roman' base glass (Figure 5.2.4).

The colour of the base glass used in the production of an opaque white glass opacified by tin oxide would not have been crucial because the opacifying agent is white; any undesirable tints will therefore be obscured by the opacifying crystals (Bayley 1999: 93). In contrast, the bubble-opacified whites do not contain a white opacifying agent, so are affected much more by the tint of the base glass. As such, in order to produce the whitest glass possible, the base glass needed to be as close to colourless as possible; this required the use of a relatively pure glassmaking sand and/or the selection of a base glass as close to colourless as possible. The low iron and alumina contents of the bubble-opacified whites reflects this; they typically contain 0.4-1.0% Fe_2O_3^* and 1.8-2.5% Al_2O_3^* (Figure 5.2.13). In contrast, the tin oxide opacified whites contain comparatively elevated levels of iron and alumina, typically corresponding to 0.4-2.0% Fe_2O_3^* and 1.9-3.3% Al_2O_3^* . However, bubble-opacified sample ERL104:G243:1370 (a *White Globular* bead) contains elevated levels of iron, corresponding to 1.6% Fe_2O_3^* (Figure 5.2.14), resulting from the use of 'HIMT' glass (see Chapter 4, section 4.5). This is unusual because this glass type is typically heavily tinted, usually olive or green.

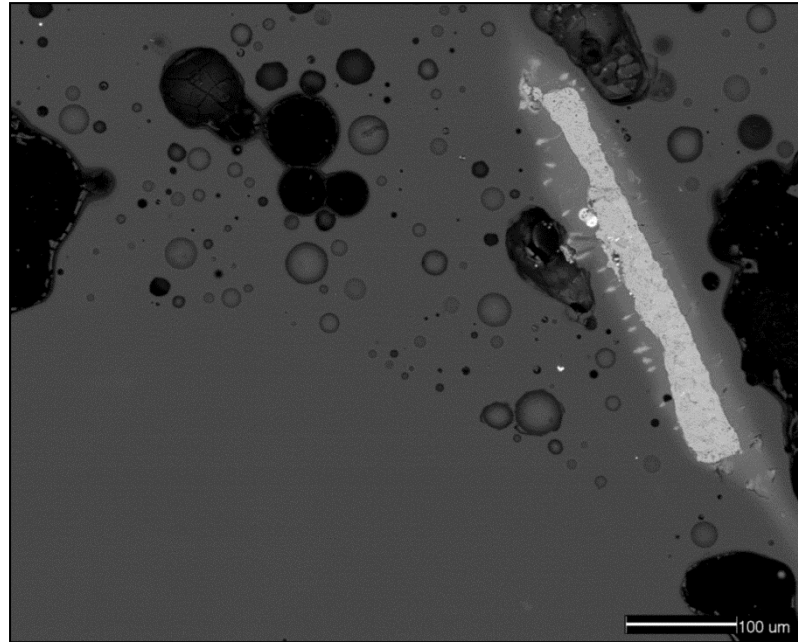


Figure 5.2.11 – BSE micrograph showing sample ERL114:G422:1454, a *BlueGreen Spiral* bead. A heterogeneous dispersion of tiny bubbles of varying size act as the opacifying agent in the opaque white glass at the top of the image. The grey soda-lime-silica glass at the bottom of the image represents translucent cobalt-blue applied decoration. The large bright elongated inclusion is a fragment of iron oxide scale, probably pulled from the mandrel, which has begun to partially dissolve in the surrounding glass matrix.

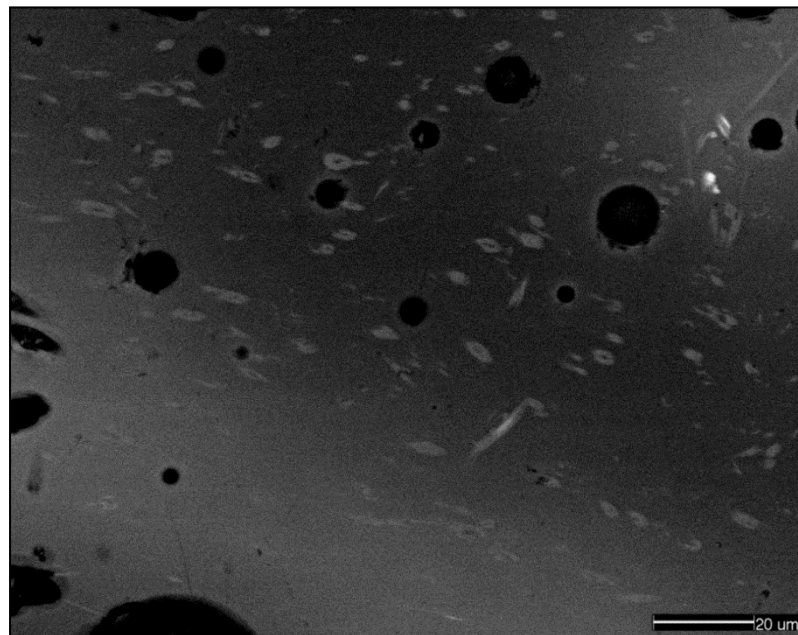


Figure 5.2.12 – BSE micrograph showing opaque white sample ERL114:G450:1164, a *WhitePoly2* bead. A sparse dispersion of tiny bubbles of varying size act as the opacifying agent. Small hollow crystals of calcium silicate (pale grey), corresponding to wollastonite (CaSiO_3) are visible throughout the glass matrix.

It is possible that a 'Roman' base glass was deliberately selected for the production of bubble-opacified white glass, as it was produced using relatively pure raw materials. However, it is more likely that the difference relates to the availability of particular base glass types to the workshops producing tin oxide and bubble-opacified glasses respectively. This may relate production zone, as the majority of bubble-opacified whites appear to be Anglo-Saxon products produced from recycled Roman material, whereas the majority of tin oxide opacified whites appear to be Continental products produced mostly from 'Saxon II' and 'Levantine I' glass (compare Figures 5.2.1-5.2.4; see also Chapter 4, sections 4.9 and 4.10). It is also notable that the opaque red glass sometimes observed at the core of opaque white beads is peculiar to the bubble-opacified types (see Chapter 3, section 3.2.2).

Inclusions of iron oxide were observed in several samples (*e.g.* Figure 5.2.11), which are likely to represent pieces of iron scale pulled from the mandrel around which the bead was formed (see Chapter 3, section 3.2.1). Small hollow crystals of calcium silicate corresponding to the mineral wollastonite (CaSiO_3) were also observed in a number of samples (Figure 5.2.12), and are likely to have formed as devitrification products upon cooling of the melt.

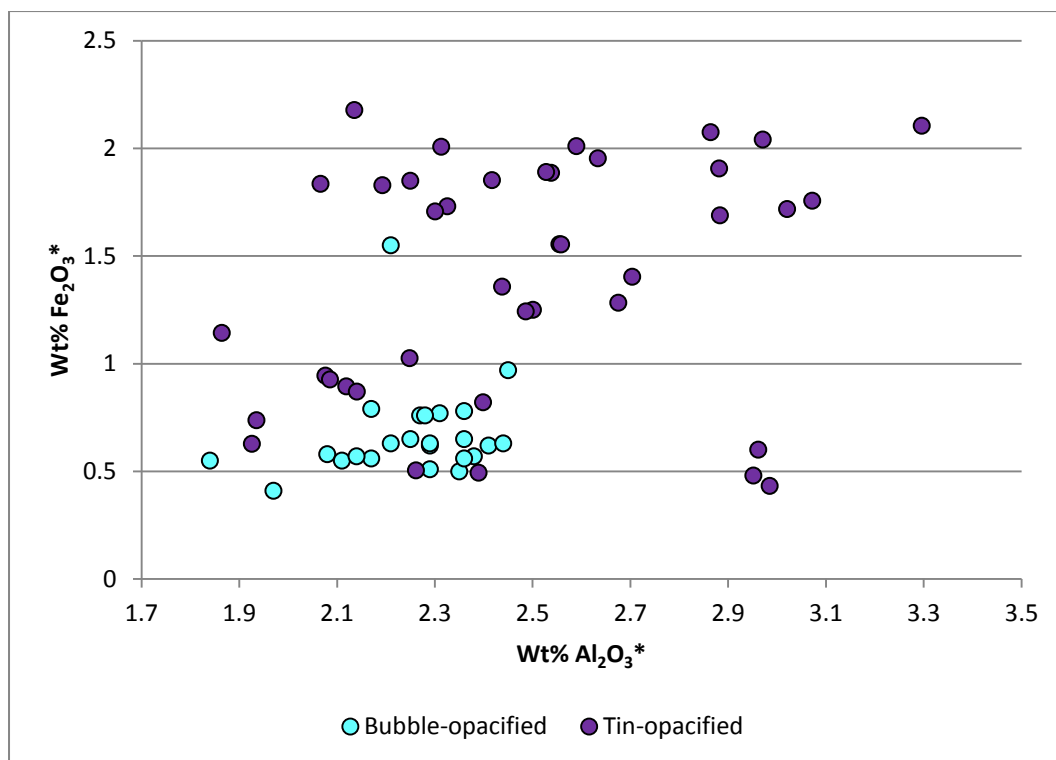


Figure 5.2.13 – A plot of reduced (*) alumina and iron oxide in the opaque white samples from Eriswell. Compare to Figure 5.2.14.

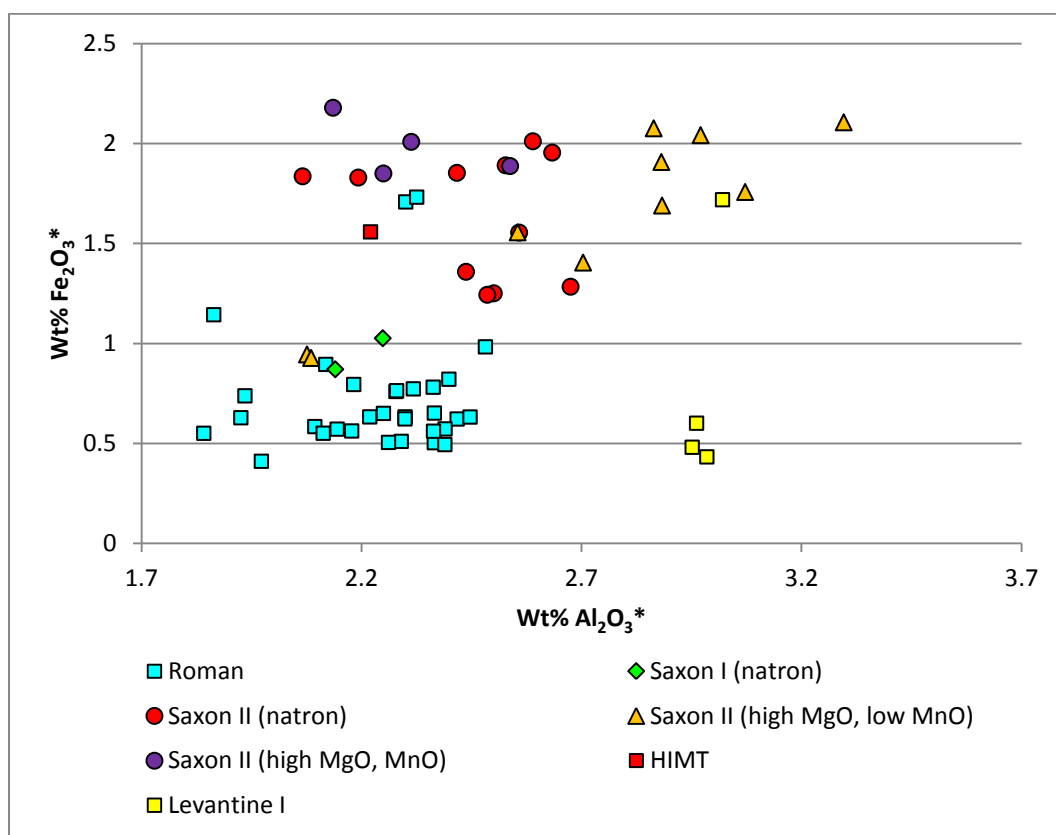


Figure 5.2.14 – A plot of reduced (*) alumina and iron oxide in the opaque white samples from Eriswell, showing the different base glass types identified. Compare to Figure 5.2.13.

5.2.1.1. Trace Element Analyses

Only four opaque white glasses were analysed by LA-ICP-MS; two of which are opacified by tin oxide and two by bubbles. Both of the tin oxide opacified samples are of the ‘Saxon II (high MgO, low MnO)’ compositional type whereas both of the bubble-opacified samples are of the ‘Roman’ compositional type. Average colourant and colourant-related elements for these are shown in Figure 5.2.15. The main differences observed between the two types are in the concentrations of lead, tin, antimony and iron; the former two components relate to the method of opacification (see section 5.2.1 above) and the latter two to the respective base glass types used (see Chapter 4).

The elevated levels of lead (averaging 2636 ppm Pb) and tin (averaging 94 ppm Sn) in the bubble-opacified samples suggests the use of recycled material, as might be expected in glass of the ‘Roman’ type; the concentrations of these components are too low to suggest a deliberate addition. Both the tin oxide and bubble-opacified samples contain elevated levels of copper (approximately 100 ppm Cu), which again suggests the introduction of some recycled material. Indium was introduced as an impurity with the tin component, as demonstrated by the elevated levels of In in the tin oxide opacified samples (Figure 5.2.15; 253 ppm In *cf.* 0.5 ppm In) and the absolute positive correlation between these two elements (Figure 5.2.16; $r^2 = 1.0$). This results from the geochemical vicinity of tin and indium; stannite is often an indium-bearing phase (Benzaazoua *et al.* 2002: 168).

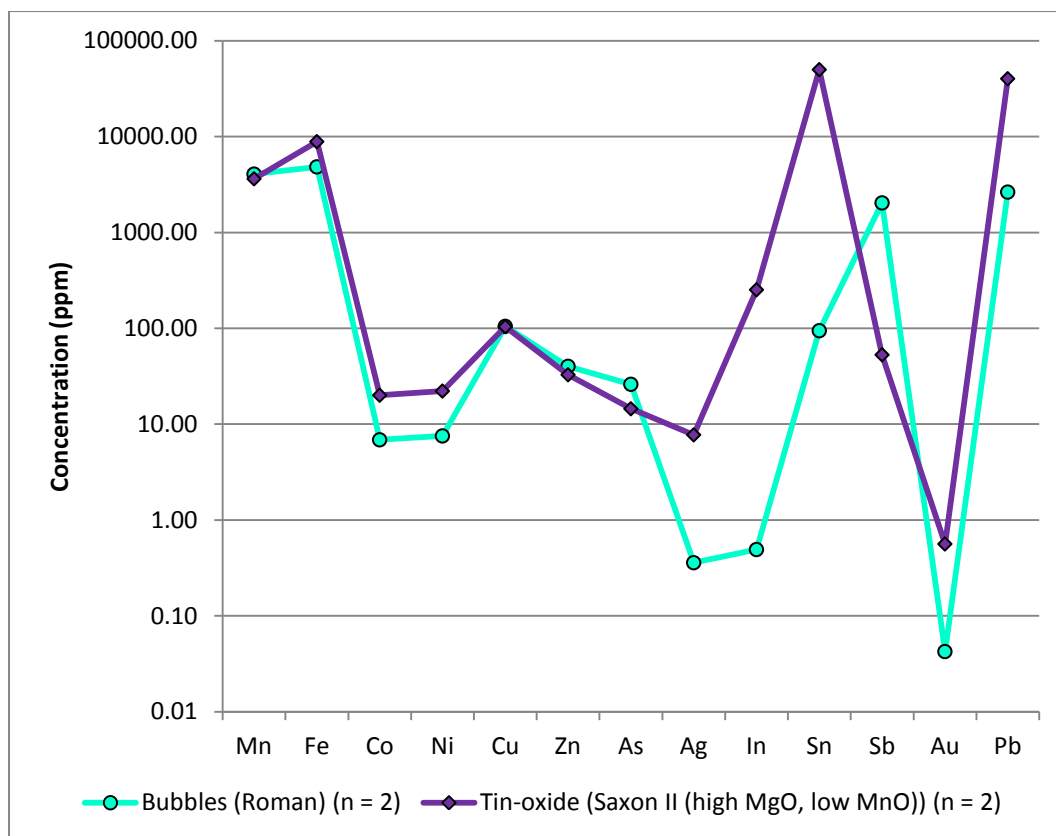


Figure 5.2.15 – Average colourant and colourant-related elements for the opaque white samples from Eriswell, showing the different base glass types identified. Note the logarithmic scale.

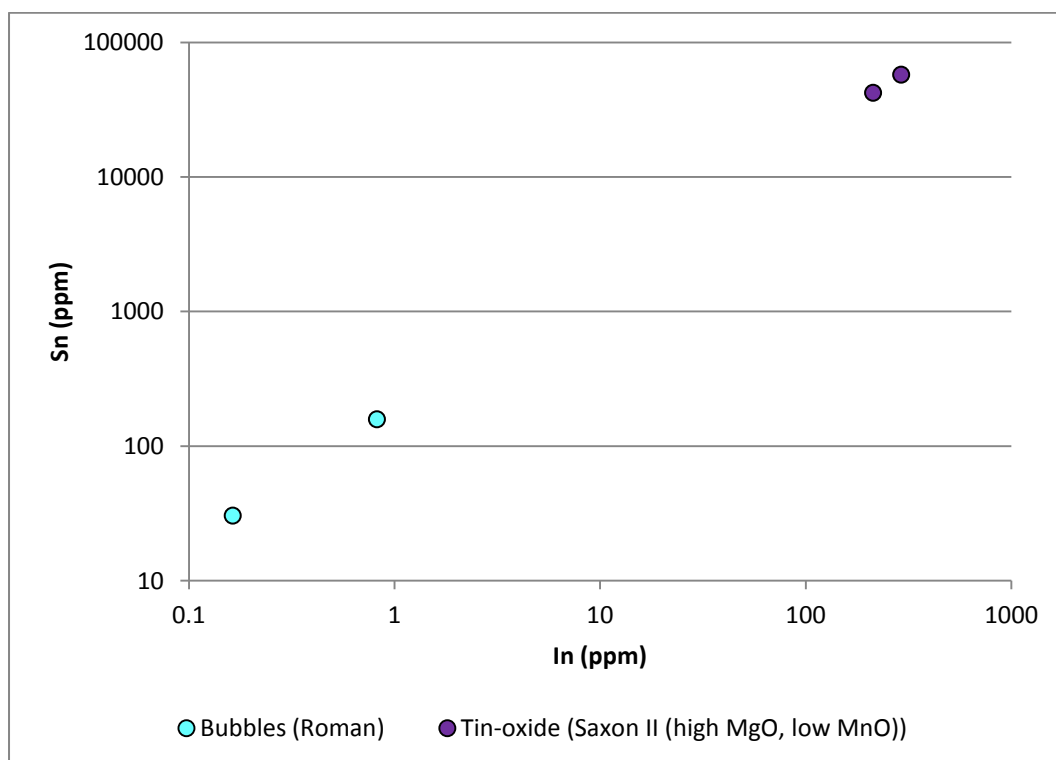


Figure 5.2.16 – A plot of indium versus tin for the opaque white samples from Eriswell. Note the logarithmic scale.

5.2.2. Opaque Yellow and Green Glass

Samples of opaque yellow glass were obtained from 81 beads from Eriswell and samples of opaque green glass from 12 beads. Early opaque yellow and opaque green glass is usually opacified by either lead-antimony oxide (lead antimonate, $\text{Pb}_2\text{Sb}_2\text{O}_7$) or lead-tin oxide (lead stannate, PbSnO_3) (Bayley 1999: 91; Rooksby 1962: 23-24; Tite *et al.* 2008: 70). Opaque yellow glass opacified by compounds of tin was first produced in northern Europe for a short period between the 2nd and 1st centuries BC, then again from the 4th century AD onwards (Henderson 1989a: 50-52; Henderson and Ivens 1992: 60; Henderson and Warren 1983; Tite *et al.* 2008: 67-68). However, during the Roman period it was typically opacified by compounds of antimony (Henderson 1999b; Tite *et al.* 2008: 68).

All of the samples analysed are opacified by crystals of lead-tin oxide (lead stannate, PbSnO_3) heterogeneously dispersed throughout the glass matrix (Figures 5.2.22-5.2.38). These crystals consist of approximately 30-35% SnO_2 and 60-65% PbO , as determined by spot analysis, corresponding to the cubic phase PbSnO_3 (Moretti and Hreglich 1984; Rooksby 1964: 21; Tite *et al.* 2008: 70). In the opaque yellow samples this compound also produces the colour, whereas in the opaque green samples the colour is produced through the addition of copper; this produces green in the presence of lead (see this chapter, section 5.1.4).

It is far more difficult to characterise the opaque yellow and opaque green glass from Eriswell than it is for other colours because of contaminants (particularly iron and alumina) introduced during its manufacture (see Chapter 4, section 4.1). The high levels of lead present have also dramatically depressed the relative quantities of major components including soda, lime and silica, as shown by the strong negative correlations between lead and these components (Figures 5.2.17, 5.2.18 and 5.2.19; $r^2 = 0.87, 0.75$ and 0.96 respectively). However, they are essentially mixtures of soda-lime-silica glass and an ingredient rich in the oxides of lead and tin, as demonstrated by the positive correlation between these two components (Figures 5.2.20 and 5.2.21; $r^2 = 0.72$).

The concentration of lead present in the opaque yellow samples is variable (9.3-47.9% PbO), but always exceeds the amount of tin (0.7-5.7% SnO₂). The ratio of PbO/SnO₂ in all cases is approximately 10. Whilst the levels of these components are also variable in the opaque green glasses, the concentrations present are typically much lower (2.1-19.1% PbO and up to 1.5% SnO₂); here the ratio of PbO/SnO₂ is closer to 20 in all of the base glass types identified, suggesting the use of a slightly different lead-tin calx (*i.e.* one produced using different quantities of lead and tin). This suggests that opaque green glass is not opaque yellow glass to which copper has been added.

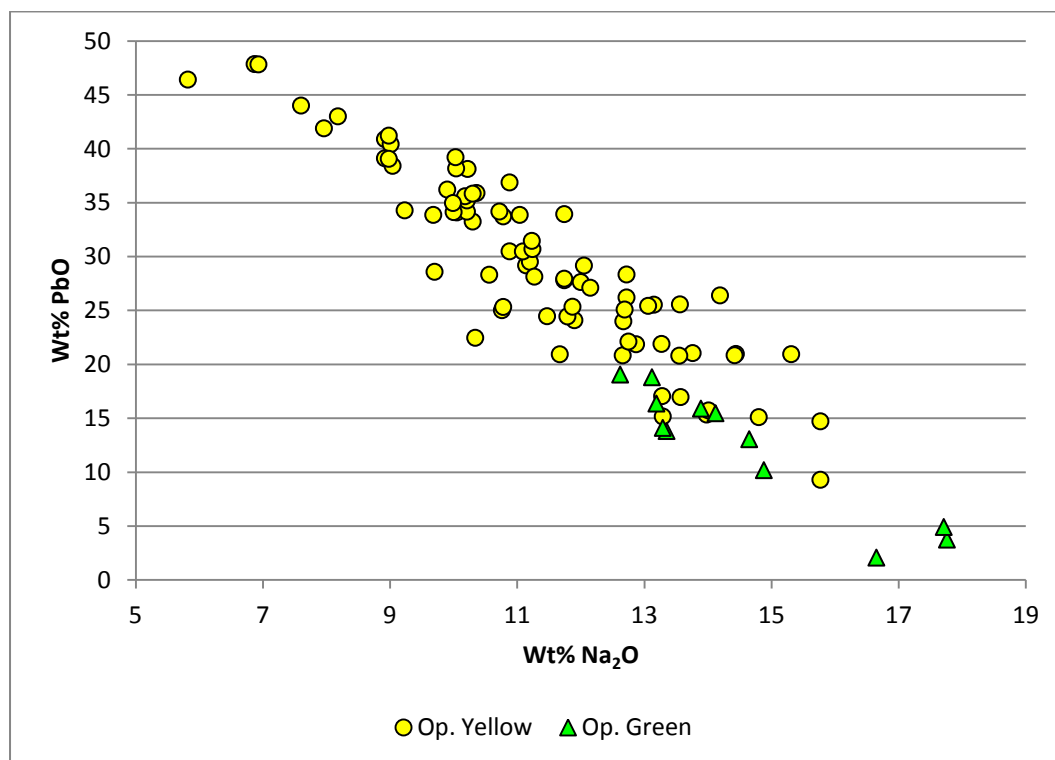


Figure 5.2.17 – A plot of soda versus lead oxide for the opaque yellow and opaque green samples from Eriswell.

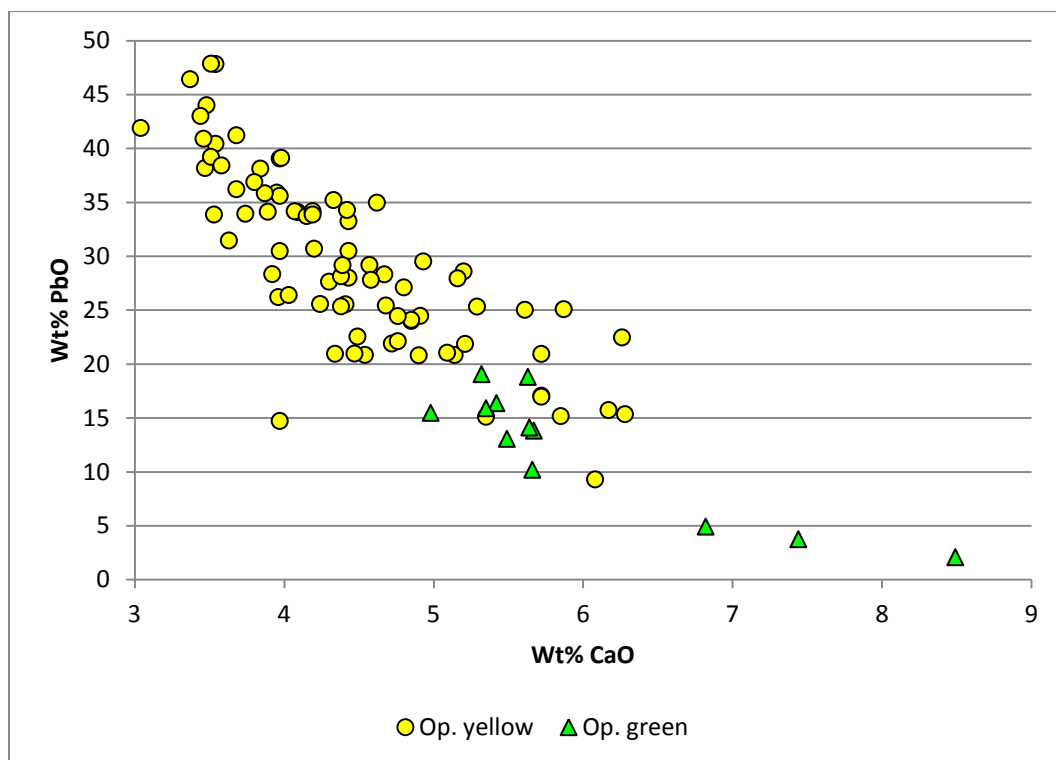


Figure 5.2.18 – A plot of lime versus lead oxide for the opaque yellow and opaque green samples from Eriswell.

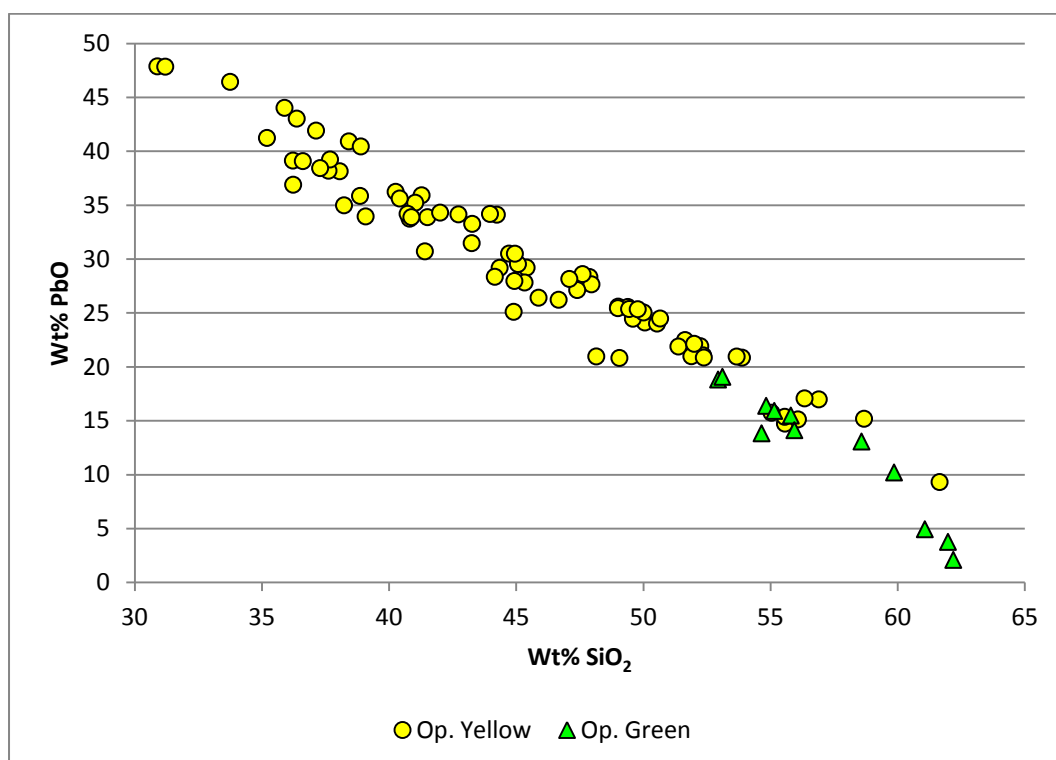


Figure 5.2.19 – A plot of silica versus lead oxide for the opaque yellow and opaque green samples from Eriswell.

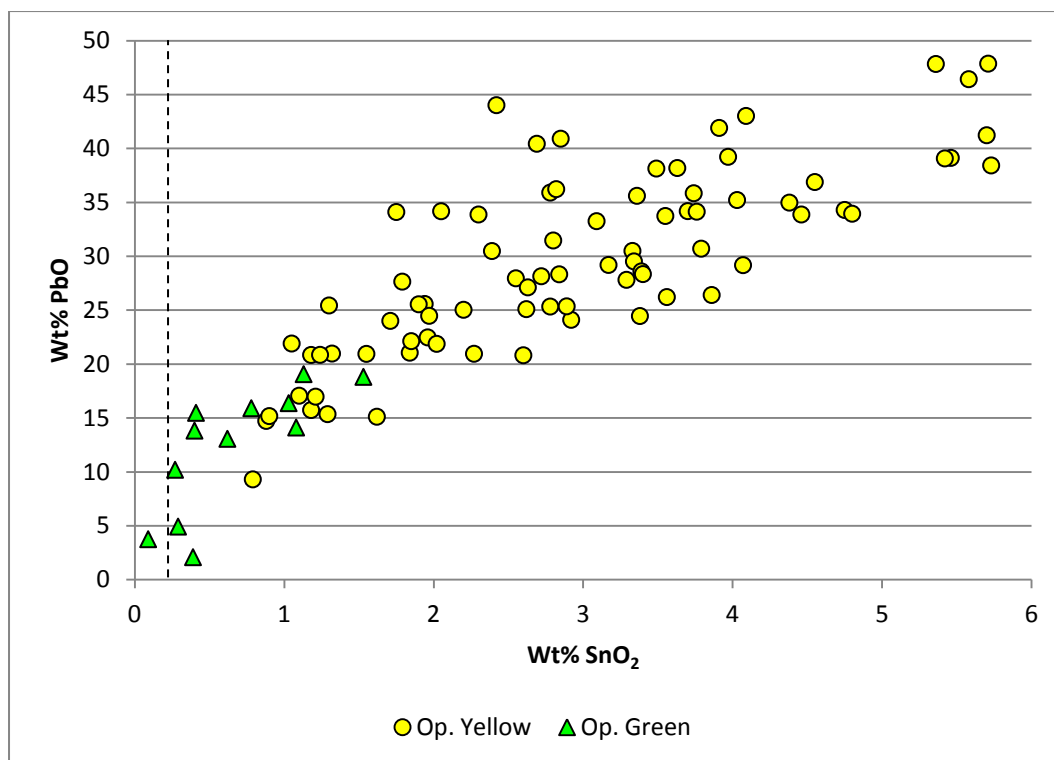


Figure 5.2.20 – A plot of tin oxide versus lead oxide for the opaque yellow and opaque green samples from Eriswell. Compare to Figure 5.2.21. The dashed line represents the approximate detection limits for tin oxide.

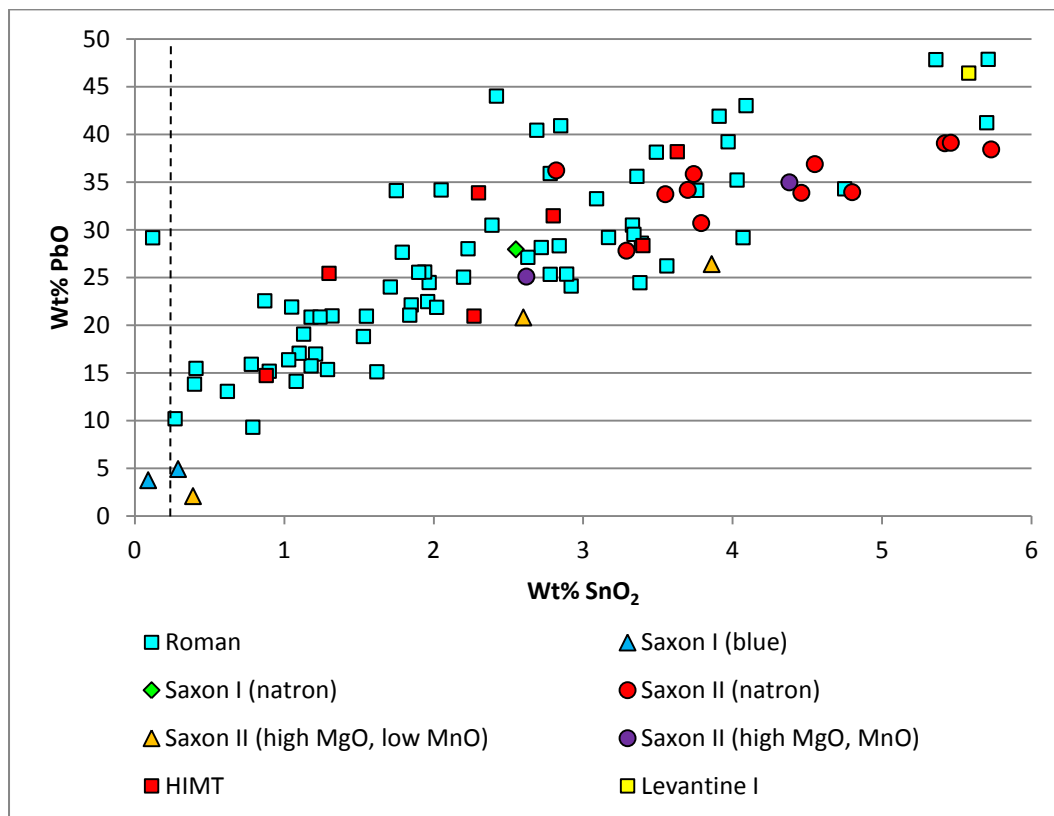


Figure 5.2.21 – A plot of tin oxide versus lead oxide for the opaque yellow and opaque green samples from Eriswell, showing the different base glass types identified. Compare to Figure 5.2.20. The dashed line represents the approximate detection limits for tin oxide.

Three of the opaque green samples contain low concentrations of tin (up to 0.4% SnO₂) and lead (2-5% PbO) (Figure 5.2.17-5.2.20), all of which are *Green Constricted Segmented* beads. However, the presence of a sparse dispersion of lead-tin oxide crystals was confirmed (*e.g.* Figures 5.2.28 and 5.2.29). There does not appear to be any clear relationship between the quantity of lead or tin added and the type of base glass used (Figure 5.2.21). However, opaque yellow samples produced from 'Saxon II' and 'Levantine I' glass generally contain elevated levels of lead and tin (>20% PbO and >2% SnO₂) relative to those produced from 'Roman' and 'HIMT' glass. Conversely, opaque green samples produced from 'Saxon I' and 'Saxon II' glass (all *Green Constricted Segmented* beads) contain less lead and tin than those produced from 'Roman' glass (Figures 5.2.20 and 5.2.21; <5% PbO and <0.4% SnO₂ *cf.* >10% PbO and >0.3% SnO₂).

Previous work suggests that opaque yellow glass is likely to have been produced through the addition of a pre-formed yellow pigment, contaminated with crucible material, to an otherwise uncoloured base glass (Heck *et al.* 2003: 41-42; Heck and Hoffmann 2000: 350-351). This pigment was produced through reaction of the lead-tin material with the crucible fabric, so that it became enriched primarily with silica, but also alumina and iron (Heck *et al.* 2003: 41-42; Heck and Hoffmann 2000: 350). The aggressive action of lead on silica would have rapidly led to the breakdown of a silica-rich crucible (Bayley and Eckstein 1997: 111; Heck and Hoffmann 2000: 350).

The resulting pigment consisted of crystals of lead-tin oxide in a lead-silica glass (Heck *et al.* 2003: 41). Silica is necessary in the transformation of otherwise *pale* yellow orthorhombic 'PbSnO₄' to *deep* yellow cubic 'PbSnO₃' (Rooksby 1964: 21). This lead-tin-silicate precursor was then crushed and mixed with a pre-made soda-lime-silica base glass (Heck *et al.* 2003: 42; Heck and Hoffmann 2000: 350). It is unlikely that it could be used directly in polychrome beadmaking as its softening temperature, viscosity and expansion coefficient were much lower than that of other colours (Peake and Freestone, in press).

The identification of a sub-angular agglomerate of lead-tin oxide in sample ERL104:G195:1356 (a *Segmented Globular* bead) is likely to represent a fragment of such a pre-formed lead-tin yellow pigment (Figures 5.2.25-5.2.26), supporting this

view. This is consistent with the findings of Heck *et al.* (2003) and Peake and Freestone (in press). The sub-angular nature of this aggregate is paralleled by those observed in opaque yellow glassworking waste from the early medieval (8th century AD) monastic site at Tarbat in Scotland (Peake and Freestone, in press), suggesting that it was a well-established and widespread technology. Similar agglomerates were observed in sample ERL104:G367:3627 (Figure 5.2.27). It appears that the hybrid soda-lime-silica base glass to which crushed lumps of this pre-formed pigment were added was not always heated for long enough to fully disperse it (Peake and Freestone, in press). It is likely that variations in the degree of contamination from the melting pot, together with the proportions of pigment added, account for the considerable variation in the composition of the opaque yellow glasses from Eriswell, rather than any major differences in technology.

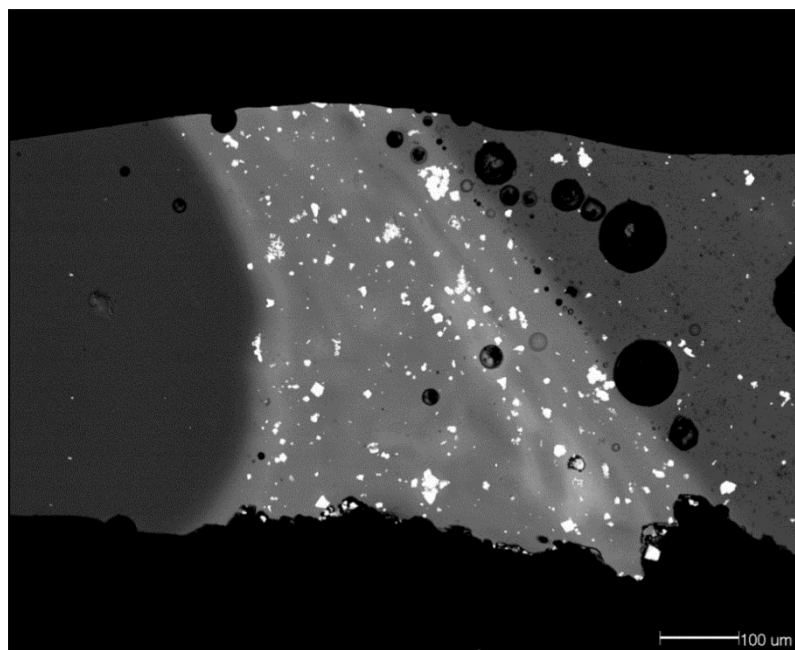


Figure 5.2.22 – BSE micrograph showing sample ERL104:G144:2598, a *Traffic Light Twisted Trail* bead. Three different colours of soda-lime-silica glass are visible: opaque red (left), opaque yellow (centre) and translucent green (right). The opaque yellow glass appears brighter due to the higher concentration of lead in this glass. Bright white crystals of lead-tin oxide are visible heterogeneously dispersed in both the opaque yellow and translucent green colours, but are much sparser in the latter. A number of large bubbles (black) are also visible.

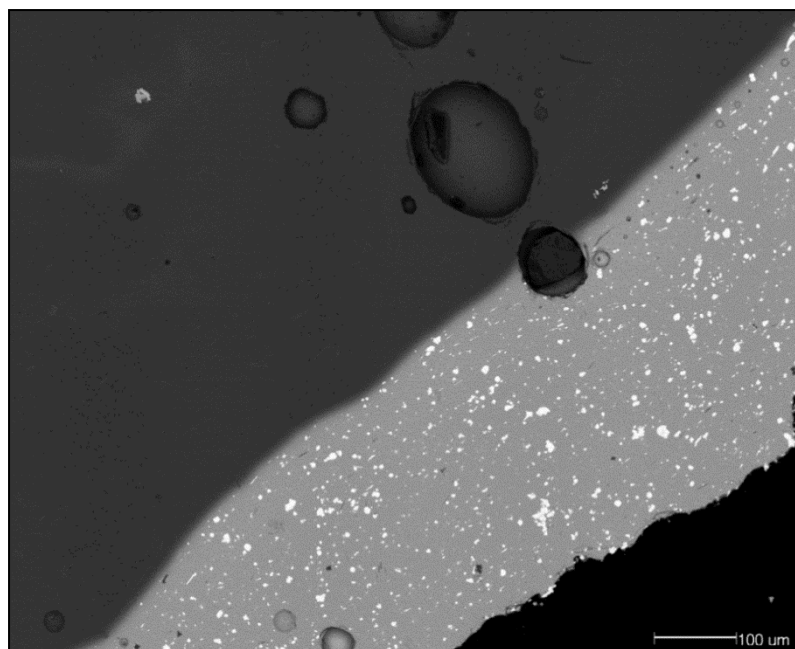


Figure 5.2.23 – BSE micrograph showing sample ERL104:G281:1797, a *Koch34* bead. The darker grey soda-lime-silica glass is opaque red, coloured and opacified by nanoparticles of metallic copper. The pale grey soda-lime-silica glass is opaque yellow, coloured and opacified by a dispersion of lead-tin oxide crystals (white). The opaque yellow glass appears brighter in the image due to the higher concentration of lead present. Several bubbles are also visible.

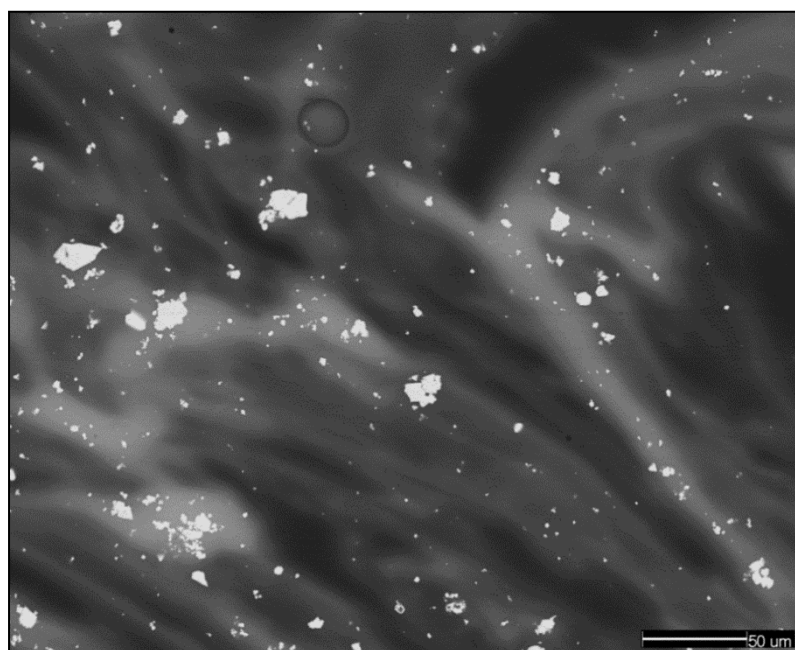


Figure 5.2.24 – BSE micrograph showing opaque yellow sample ERL046:G18:1787, a *Norfolk Melon related?* bead. Several irregular crystals of lead-tin oxide (white) are visible heterogeneously dispersed in a lead-rich soda-lime-silica glass matrix (grey). The pale grey streaks result from variations in the lead content, which results from poor mixing of the batch.

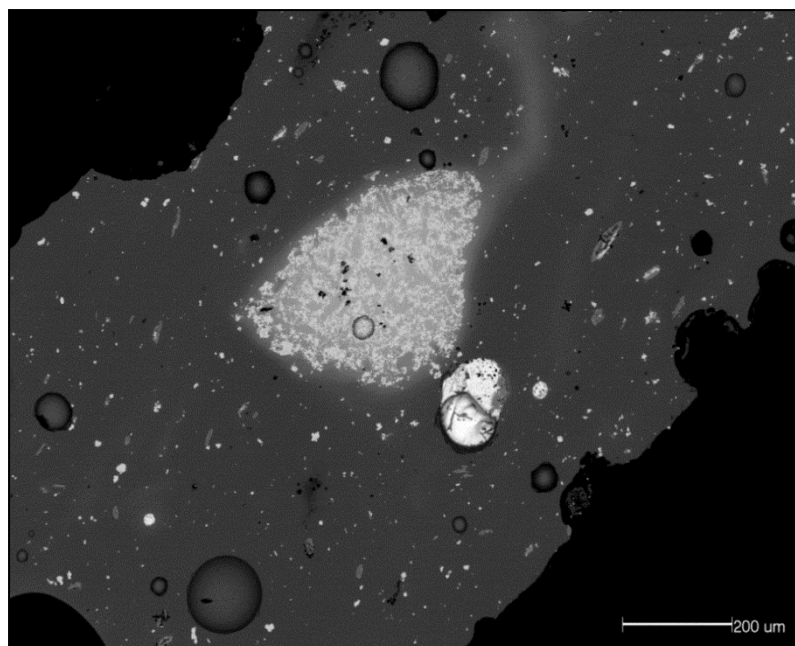


Figure 5.2.25 – BSE micrograph showing opaque yellow sample ERL104:G195:1356, a *Segmented Globular* bead. A large sub-angular inclusion rich in lead and tin is visible, containing an abundance of lead-tin oxide crystals (white) in a lead-rich soda-lime-silica glass matrix (grey). The glass is opacified by a heterogeneous dispersion of lead-tin oxide crystals (white).

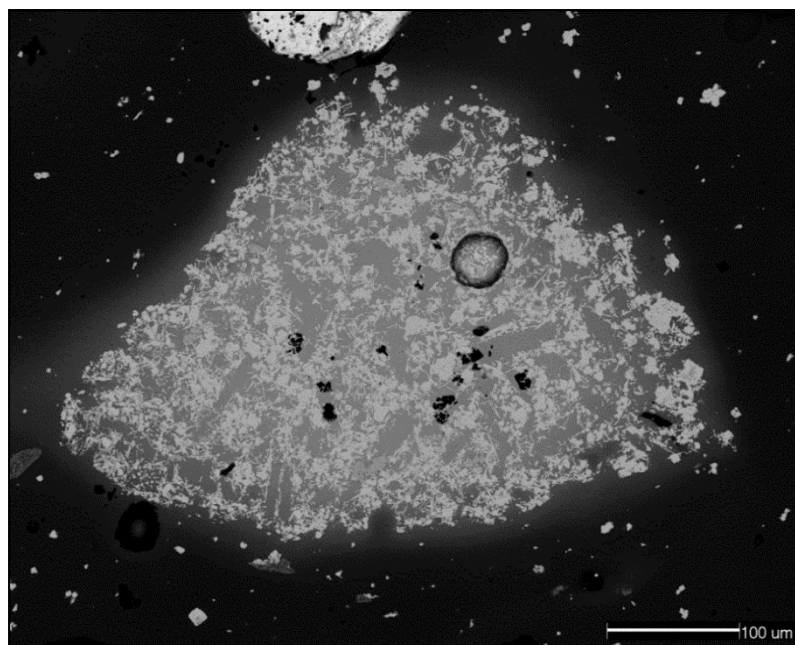


Figure 5.2.26 – BSE micrograph showing an enlargement of the sub-angular aggregate of lead-tin oxide crystals (white) in opaque yellow sample ERL104:G195:1356, shown in Figure 5.2.25. Within this aggregate, small particles of sodium aluminium silicate corresponding to the mineral nepheline ($\text{Na}_3\text{KAl}_4\text{Si}_4\text{O}_{16}$) can be seen (black).

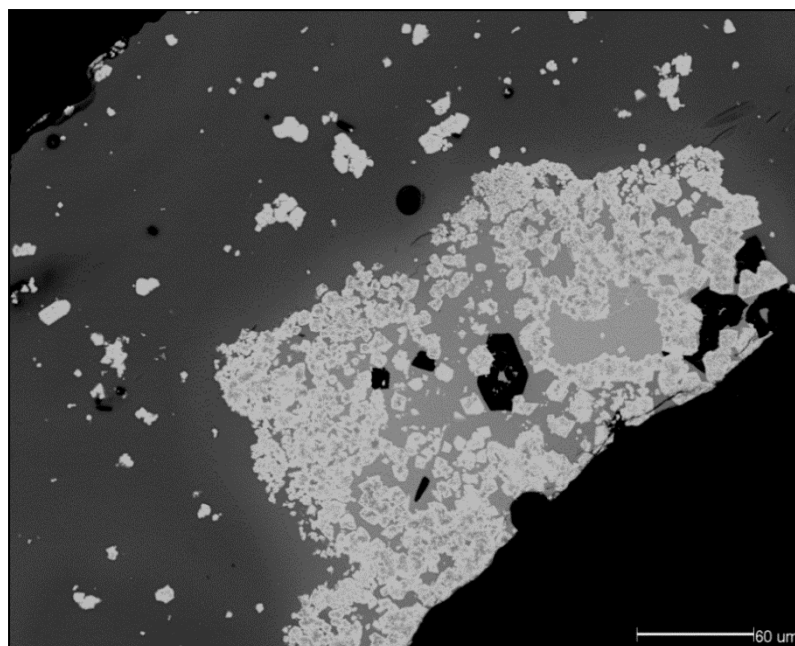


Figure 5.2.27 – BSE micrograph showing opaque yellow sample ERL104:G367:3627, a *Norfolk Melon related?* bead. A large irregular region rich in lead and tin, containing a dense dispersion of lead-tin oxide crystals (white), is visible within a lead-rich soda-lime-silica glass matrix (grey). Large particles of sodium aluminium silicate, corresponding to the mineral nepheline ($\text{Na}_3\text{KAl}_4\text{Si}_4\text{O}_{16}$), are clearly visible (black).

The duration of heating would have been kept to a minimum as lead-tin yellow is unstable and can readily lose its colour at high temperatures (above 900 °C), turning white as a result of the decomposition of lead-tin oxide to tin oxide (Bayley 1995: 1197; Bayley 1999: 91; Bayley 2000a: 218; Biek and Bayley 1979: 9; Henderson 1985: 285-286; Heyworth 1994: 80; Mortimer and Heyworth 2009: 411; Rooksby 1964: 25; Tite *et al.* 2008: 76; Turner and Rooksby 1959: 25; Wilthew 2006: 390). The temperature at which lead-tin oxide decomposes to tin oxide is considerably reduced with increasing silica content, so it would have been essential to mix the lead-tin yellow pigment into the molten glass as quickly and at as low a temperature as possible (Tite *et al.* 2008: 76). The addition of excess lead to the melt was necessary to reduce the viscosity and melting temperature of the glass, thereby aiding the mixing process and facilitating the dispersion of the pigment (Tite *et al.* 2008: 76).

Textural differences in the density of the opacifying crystals in the samples analysed (*e.g.* compare Figures 5.2.23 and 5.2.24) are likely to have resulted from slight variations in the local conditions of heating and cooling (Peake and Freestone, in

press). Many samples also have a heterogeneous and stratified microstructure (*e.g.* Figures 5.2.24, 5.2.28 and 5.2.35), which is likely to have resulted from the short heating times and/or low temperatures required to prevent the colour from failing. Diamond-shaped tin oxide crystals were observed in opaque green sample ERL104:G242:3321 (Figure 5.2.28), suggesting that in some cases the lead-tin oxide had started to decompose; similar crystals were noted in an early Anglo-Saxon opaque green glass bead from Mucking (Mortimer 1996b: 5; Mortimer and Heyworth 2009: 411).

No opaque white glass of the same composition as opaque yellow glass was found at Eriswell (see this chapter, section 5.2.1), suggesting that overheating is unlikely to have been a problem. However, ‘dark’ beads with a very similar composition to opaque yellow glass have been identified at Eriswell and elsewhere (see this chapter, section 5.1.5); this may represent the innovative re-use of an overheated (failed) opaque yellow glass.

Sodium aluminium silicate inclusions, corresponding to the mineral nepheline ($\text{Na}_3\text{KAl}_4\text{Si}_4\text{O}_{16}$; see Tables 5.2.1 and 5.2.2), were observed in many of the opaque yellow (Figures 5.2.26-5.2.27, 5.2.30-5.2.33) and green (Figure 5.2.35) samples, typically associated with crystals of lead-tin oxide. Similar inclusions were observed in many of the translucent green and opaque red samples from Eriswell, again typically associated with crystals of lead-tin oxide (see this chapter, sections 5.1.4 and 5.2.3). Comparable inclusions have been identified in opaque yellow Anglo-Saxon beads from elsewhere, including Edix Hill (Mortimer 1996a: 5; Mortimer 1998) and Mucking (Mortimer 1996b: 6; Mortimer and Heyworth 2009: 412), where they were interpreted as albite ($\text{NaAlSi}_3\text{O}_8$). However, the presence of low levels of potassium (Tables 5.2.1 and 5.2.2) are more consistent with nepheline ($\text{Na}_3\text{KAl}_4\text{Si}_4\text{O}_{16}$).

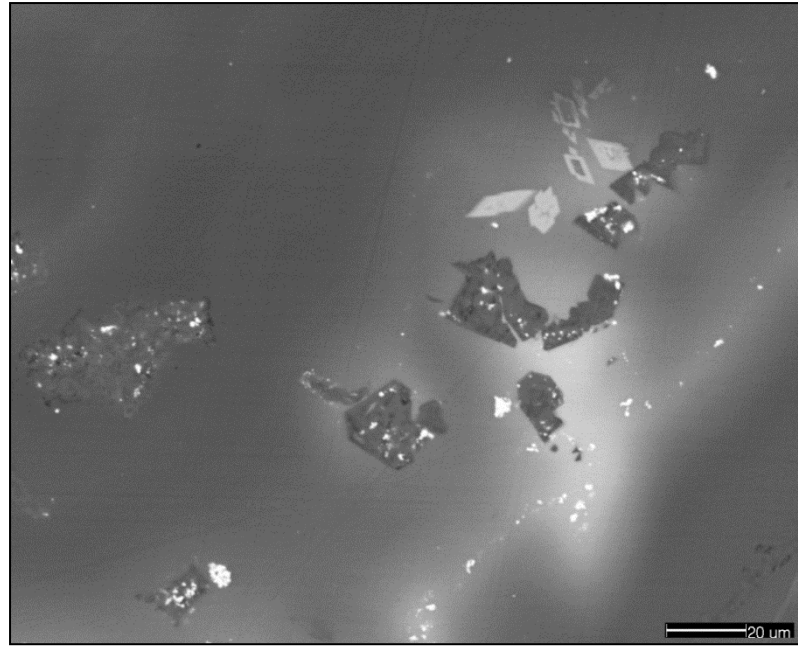


Figure 5.2.28 – BSE micrograph showing opaque green sample ERL104:G242:3321, a *Green Constricted Segmented* bead. A very sparse and heterogeneous dispersion of lead-tin oxide crystals (white) can be seen, together with several diamond-shaped crystals of tin oxide rich in calcium and silicon (pale grey). Also visible are a number of irregular aggregates of sodium calcium silicate (dark grey) associated with lead-tin oxide (white flecks). The brighter streaks in the soda-lime-silica glass matrix reflect variations in the lead content, resulting from poor mixing of the batch.

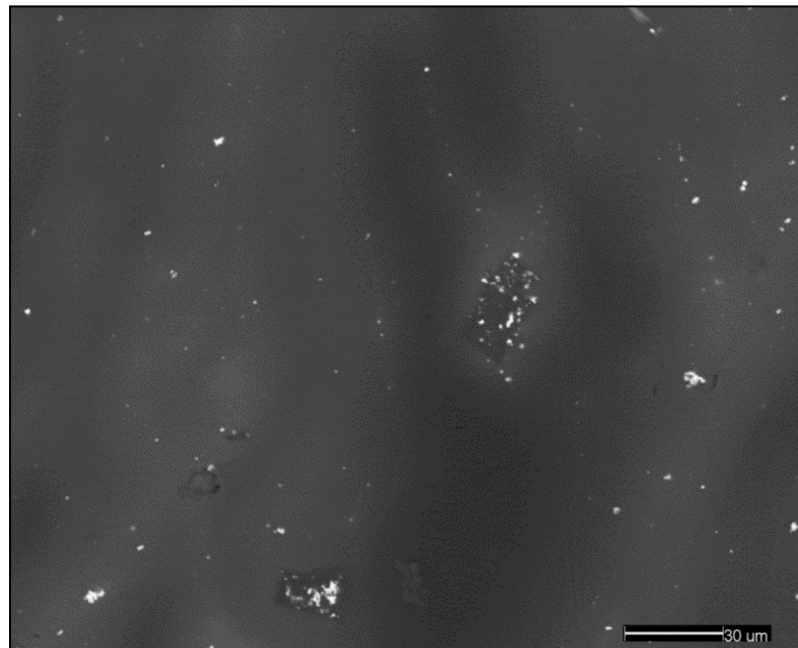


Figure 5.2.29 – BSE micrograph showing opaque green sample ERL104:G242:2273/11, a *Green Constricted Segmented* bead. A sparse, heterogeneous dispersion of lead-tin oxide crystals (white) is visible. Some of these are associated with several large aggregates of sodium calcium silicate (dark grey).

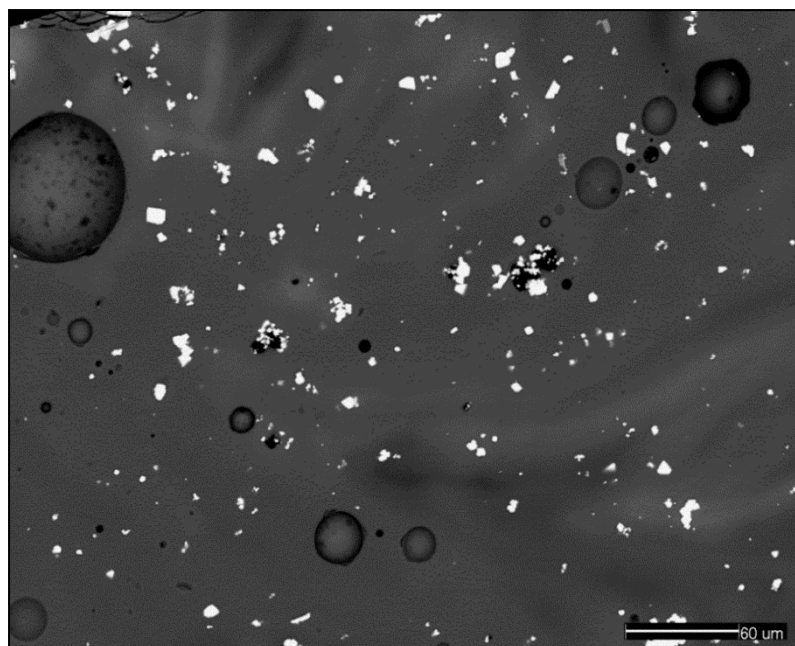


Figure 5.2.30 – BSE micrograph showing opaque yellow sample ERL104:G242:2217, a *Yellow Globular, opaque* bead. Numerous lead-tin oxide crystals (white) are visible heterogeneously dispersed in a lead-rich soda-lime-silica glass matrix (grey). Several small sodium aluminium silicate inclusions (black), corresponding to the mineral nepheline ($\text{Na}_3\text{KAl}_4\text{Si}_4\text{O}_{16}$), can be seen associated with some of these opacifying crystals. A number of bubbles are also visible.

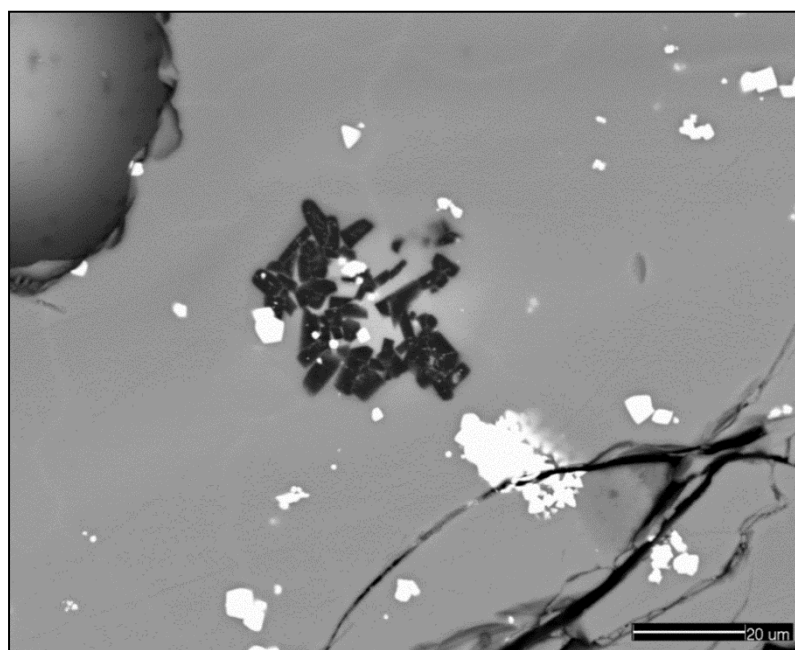


Figure 5.2.31 – BSE micrograph showing opaque yellow sample ERL046:G03:1303, a *Norfolk YellowRed* bead. Several lead-tin oxide crystals (white) are visible heterogeneously dispersed in a lead-rich soda-lime-silica glass matrix (grey). An agglomerate of sodium aluminium silicate inclusions (black), corresponding to the mineral nepheline ($\text{Na}_3\text{KAl}_4\text{Si}_4\text{O}_{16}$), can be seen associated with some of these opacifying crystals. Several cracks in the glass are also visible to the bottom-right.

Table 5.2.1 – Selected SEM-EDS spot analyses of the aluminium-rich inclusions observed in several opaque yellow samples from Eriswell.

Sample ¹	Oxide (wt %) ²									
	Na ₂ O	Al ₂ O ₃	SiO ₂	SO ₃	S	K ₂ O	CaO	Fe ₂ O ₃	SnO ₂	PbO
<i>Nepheline</i>	15.9	34.9	41.1	-	-	8.1	-	-	-	-
ERL046:G03:1303	18.3	33.3	41.5	b.d.	-	1.7	0.7	0.5	b.d.	3.0
ERL046:G49:1776/4	18.6	34.7	41.9	b.d.	-	1.8	0.2	0.6	b.d.	1.8
ERL104:G242:2161	18.1	33.9	41.0	b.d.	-	3.3	0.1	0.6	0.7	2.2
ERL104:G242:2180	17.4	32.3	42.8	b.d.	-	1.7	0.4	0.7	0.6	3.8
ERL104:G242:2213	16.5	34.2	40.7	b.d.	-	5.9	b.d.	0.4	b.d.	1.2
ERL104:G242:2206	18.3	33.1	42.7	b.d.	-	1.9	0.1	0.5	0.5	2.3
ERL104:G262:1261	17.9	34.7	41.3	b.d.	-	3.4	b.d.	0.6	b.d.	1.1
ERL104:G344:2837	17.8	34.0	41.3	b.d.	-	2.8	0.2	0.8	0.8	2.0
ERL104:G367:3627	17.2	34.5	41.4	b.d.	-	3.8	b.d.	0.6	b.d.	1.6
ERL104:G367:3633	16.3	32.7	40.5	b.d.	-	5.9	0.5	0.7	b.d.	2.0
ERL114:G422:1456	19.0	32.9	40.5	b.d.	-	2.2	0.6	0.2	b.d.	3.4
<i>Lazurite</i>	18.7	30.7	36.2	-	6.4	-	11.3	-	-	-
ERL104:G242:2153	18.2	26.1	32.9	10.5	(4.2)	0.2	3.3	0.3	1.9	6.1
ERL114:G422:1453	19.6	27.3	33.0	11.4	(4.6)	0.2	4.1	0.5	0.7	2.2
ERL114:G422:1456	16.2	25.5	36.4	11.7	(4.7)	0.2	4.4	0.6	0.5	4.2

¹Theoretical compositions for nepheline (Na₃KAl₄Si₄O₁₆) and lazurite (Na₃Ca(Al₃Si₃O₁₂)S) are in *italics*.

²Spot analyses normalised to 100%. b.d. = below detection. See Chapter 2, section 2.3.1 for details. Values in brackets represent hypothetical S values.

Sodium aluminium silicate sulphate inclusions were also observed in some samples (Figure 5.2.32), corresponding to the mineral lazurite (Na₃Ca(Al₃Si₃O₁₂)S; see Tables 5.2.1 and 5.2.2); similar inclusions were observed in many of the translucent green samples from Eriswell (see this chapter, section 5.1.4). Comparable inclusions have also been identified in Late Roman lead-antimonate opacified yellow glass, where they are interpreted as nosean (Na₈(Al₆Si₆O₂₄)SO₄) (*e.g.* Santagostino Barbone *et al.* 2008; Paynter and Kearns 2011: 16); in the Eriswell samples they are interpreted as lazurite (Na₃Ca(Al₃Si₃O₁₂)S), due to the presence of calcium (Tables 5.2.1 and 5.2.2). It has been suggested that sulphur may have been introduced through the use of sulphide-rich ores (Paynter and Kearns 2011: 16) or with a network former such as natron (Santagostino Barbone *et al.* 2008: 466); the latter seems unlikely as similar inclusions were not observed in any of the uncoloured samples. It is likely that the majority of these aluminous inclusions observed formed

as reaction products during the production of the lead-tin pigment or the glass itself in a crucible; the crucible fabric is likely to have been rich in potassium feldspar.

Table 5.2.2 – Selected SEM-EDS spot analyses of the aluminium-rich inclusions observed in several opaque green samples from Eriswell.

Sample ¹	Oxide (wt %) ²									
	Na ₂ O	Al ₂ O ₃	SiO ₂	SO ₃	S	K ₂ O	CaO	Fe ₂ O ₃	SnO ₂	PbO
<i>Nepheline</i>	15.9	34.9	41.1	-	-	8.1	-	-	-	-
ERL046:G05:1403	17.9	34.4	42.8	b.d.	-	1.6	0.7	0.3	b.d.	0.9
ERL104:G305:1820	17.0	32.2	46.6	b.d.	-	1.1	0.2	1.0	0.3	1.0
ERL104:G363:1910	19.9	33.9	41.2	b.d.	-	1.5	0.3	1.7	b.d.	0.8
ERL104:G367:3646	16.9	33.5	44.0	b.d.	-	1.7	0.7	0.5	b.d.	2.0
<i>Lazurite</i>	18.7	30.7	36.2	-	6.4	-	11.3	-	-	-
ERL046:G08:1611	16.2	28.8	33.9	13.5	(5.4)	b.d.	5.2	0.3	b.d.	1.0
ERL104:G305:1820	17.1	27.6	32.5	14.2	(5.7)	b.d.	6.3	0.3	b.d.	0.9

¹Theoretical compositions for nepheline (Na₃KAl₄Si₄O₁₆) and lazurite (Na₃Ca(Al₃Si₃O₁₂)S) are in *italics*.

²Spot analyses normalised to 100%. b.d. = below detection. See Chapter 2, section 2.3.1 for details. Values in brackets represent hypothetical S values.

Aggregates of sodium calcium silicate were observed in a small number of samples (Figures 5.2.28 and 5.2.29), which may again have formed from a reaction with the crucible fabric. Devitrification products corresponding to the mineral wollastonite (calcium silicate, CaSiO₃) were also observed in a number of samples (*e.g.* Figures 5.2.33 and 5.2.37). These are likely to have formed upon cooling of the melt, possibly promoted by the high levels of lead present (Brun and Pernot 1992: 247). In addition, inclusions of what are likely to be fragments of refractory ceramic were observed in opaque green samples ERL104:G367:3646 (Figure 5.2.35; a *Green Globular* bead) and ERL104:G144:2604 (Figure 5.2.38; a *Green Melon, ribbed* bead). A grain of silica in an opaque yellow sample (ERL104:G242:2206, a *Yellow Globular* bead) may represent a relict of the batch materials used to produce this glass (Figure 5.2.36).

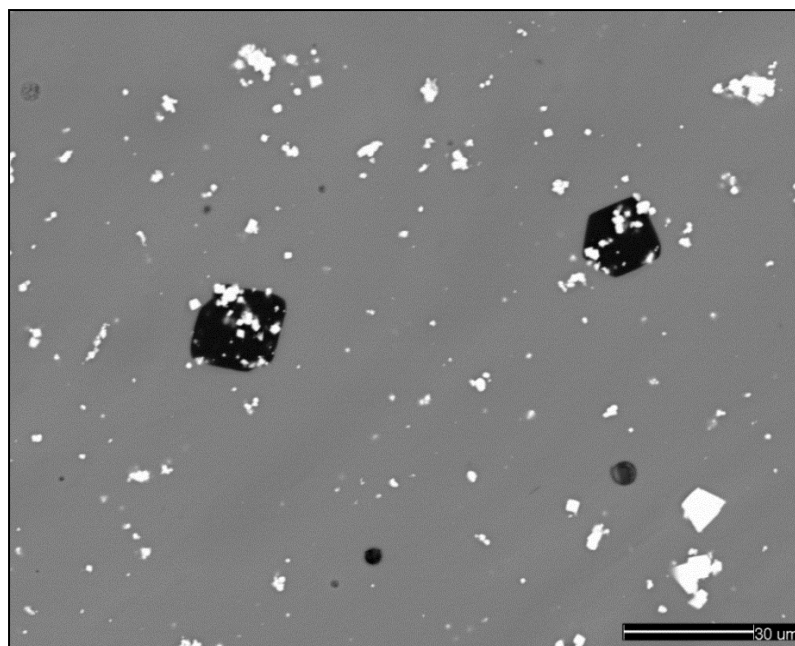


Figure 5.2.32 – BSE micrograph showing opaque yellow sample ERL114:G422:1453, a *Norfolk Melon* bead. Numerous lead-tin oxide crystals (white) are visible heterogeneously dispersed in a lead-rich soda-lime-silica glass matrix (grey). Two sodium aluminium silicate inclusions (black), corresponding to the mineral lazurite ($\text{Na}_3\text{Ca}(\text{Al}_3\text{Si}_3\text{O}_{12})\text{S}$), are visible associated with lead-tin oxide crystals.

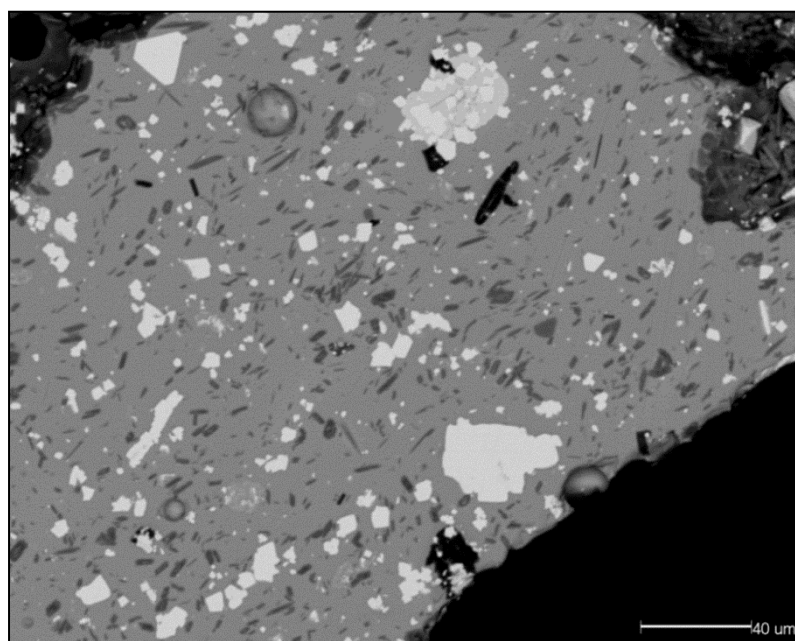


Figure 5.2.33 – BSE micrograph showing opaque yellow sample ERL104:G242:2161, a *RedPoly2* bead. A heterogeneous dispersion of lead-tin oxide crystals (white) is visible in a lead-rich soda-lime-silica glass matrix (grey). Numerous acicular calcium silicate crystals (dark grey), corresponding to wollastonite (CaSiO_3), can be seen. Several particles of sodium aluminium silicate, corresponding to the mineral nepheline ($\text{Na}_3\text{KAl}_4\text{Si}_4\text{O}_{16}$), are also visible (black). Some of these are associated with a small aggregate of lead-tin oxide crystals (white) and lead-silicate (very pale grey) towards the top of the image. The porous areas to the top-left and top-right of the image are weathered glass.

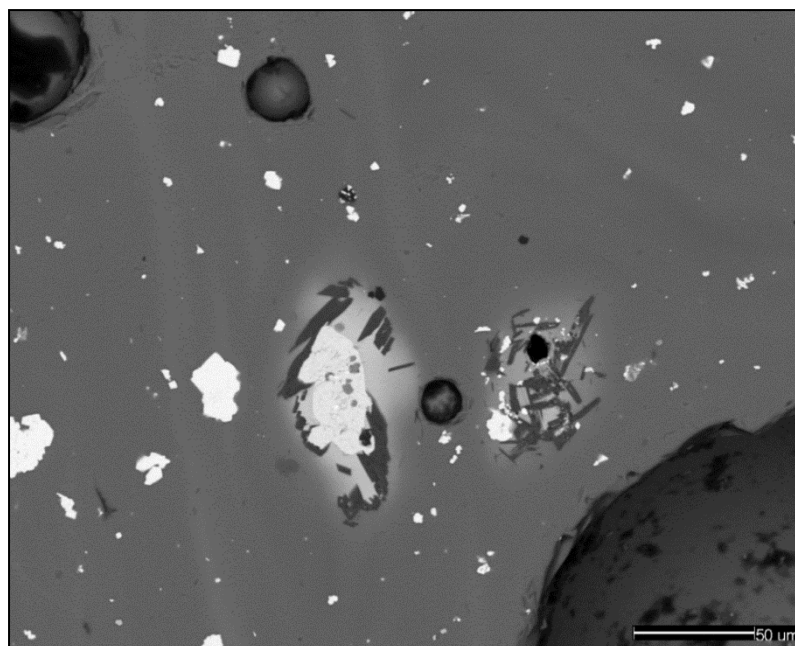


Figure 5.2.34 – BSE micrograph showing opaque green sample ERL104:G352:2812, a *Green Globular* bead. Crystals of lead-tin oxide (white) are visible heterogeneously dispersed in a lead-rich soda-lime-silica glass matrix (grey). The bright grain towards the centre of the image is rich in lead and silica, and is surrounded by numerous acicular calcium silicate crystals (dark grey). The glass matrix appears brighter in the areas immediately surrounding this due to the higher concentrations of lead in these regions.

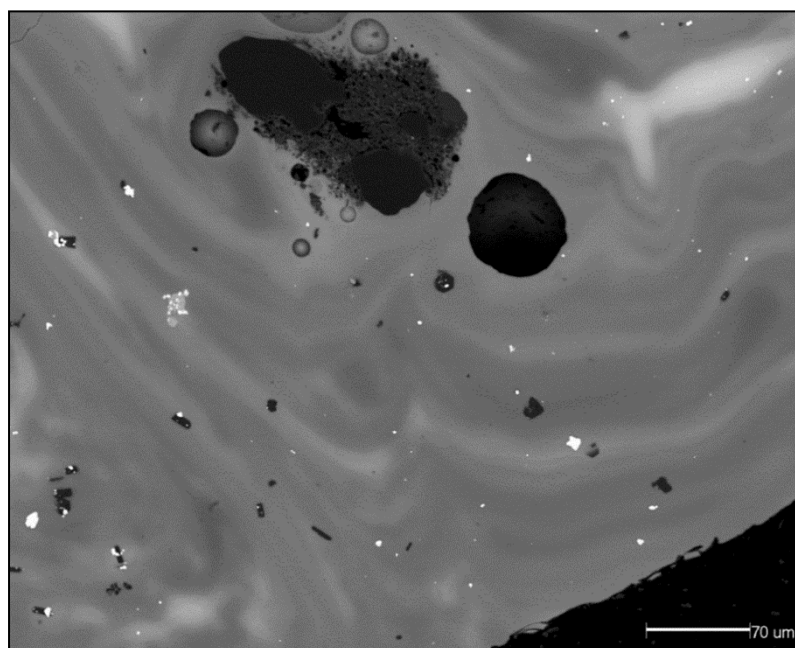


Figure 5.2.35 – BSE micrograph showing opaque green sample ERL104:G367:3646, a *Green Globular* bead. A sparse and heterogeneous dispersion of lead-tin oxide crystals (white) are visible in a lead-rich soda-lime-silica glass matrix (grey). The brighter streaks in the glass are slightly higher in lead, and result from poor mixing of the batch. Several small sodium aluminium silicate inclusions (black), corresponding to the mineral (nepheline, $\text{Na}_3\text{KAl}_4\text{Si}_4\text{O}_{16}$) can also be seen, together with several acicular and euhedral crystals of calcium silicate (dark grey). The large irregular inclusion towards the top of the image is likely to reflect part of the refractory ceramic in which the glass was melted, and contains several grains of silica (darker grey).

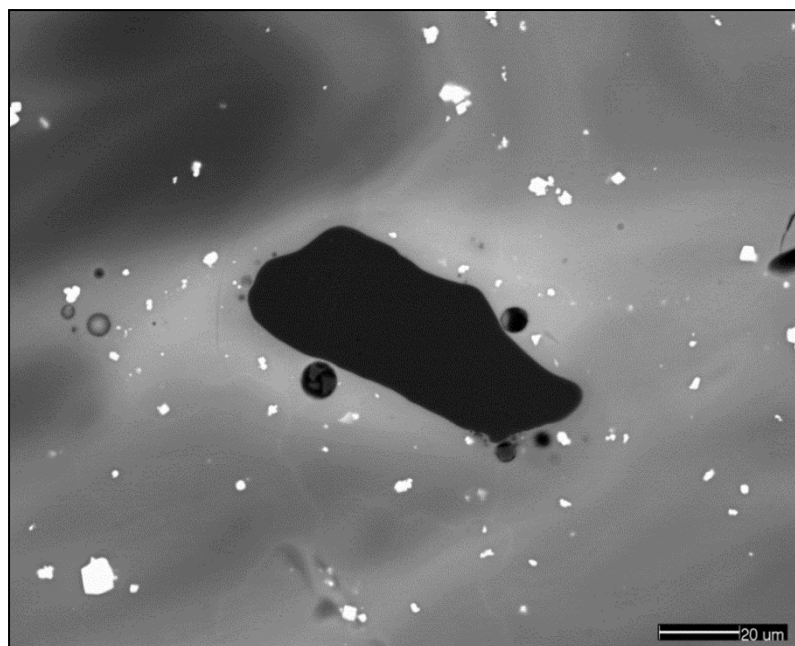


Figure 5.2.36 – BSE micrograph showing opaque yellow sample ERL104:G242:2206, a *Yellow Globular, opaque* bead. A heterogeneous dispersion of lead-tin oxide crystals (white) is visible heterogeneously dispersed in a lead-rich soda-lime-silica glass matrix (grey). The brighter areas of the glass matrix are lightly richer in lead. A sub-angular silica grain is visible (dark grey) towards the centre of the image, surrounded by several small bubbles.

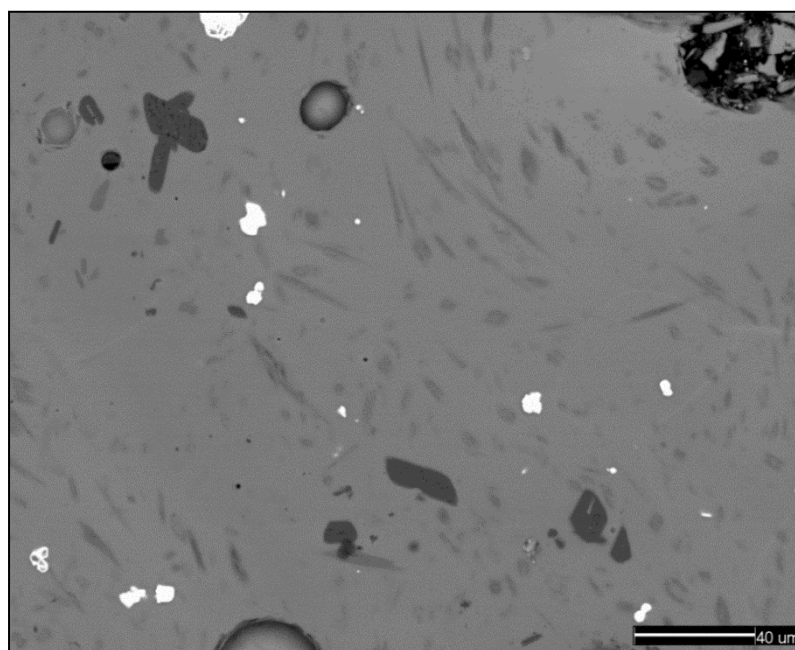


Figure 5.2.37 – BSE micrograph showing opaque green sample ERL104:G144:2604, a *Green Melon, ribbed* bead. A sparse dispersion of lead-tin oxide crystals (white) is visible heterogeneously dispersed in a lead-rich soda-lime-silica glass matrix (pale grey). Numerous acicular crystals of calcium silicate (grey), corresponding to the mineral wollastonite (CaSiO_3), can also be seen dispersed throughout the glass. The dark grey inclusions are silica grains.

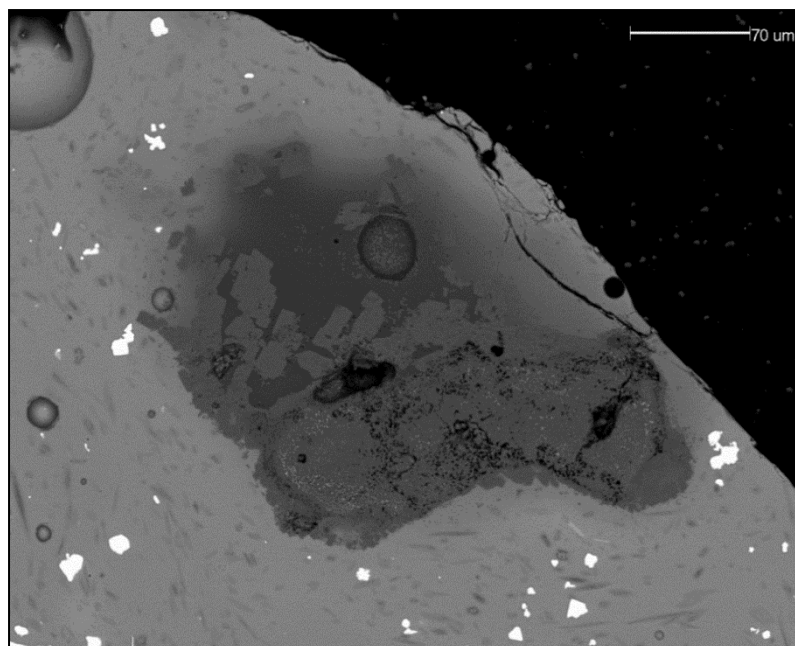


Figure 5.2.38 – BSE micrograph showing opaque green sample ERL104:G144:2604, a *Green Melon, ribbed* bead. Crystals of lead-tin oxide (white) are visible dispersed in a lead-rich soda-lime-silica glass matrix (pale grey), together with numerous acicular crystals of calcium silicate (grey) corresponding to the mineral wollastonite (CaSiO_3). The large inclusion towards the centre of the image (dark grey) is rich in silica, magnesia, iron and lime. This may reflect a relict of the crucible in which the glass was melted.

5.2.2.1. Trace Element Analyses

Five opaque yellow and two opaque green glasses from Eriswell were analysed by LA-ICP-MS. The colourant and colourant related elements for the opaque yellow samples are shown in Figure 5.2.39, and for the opaque green glasses in Figure 5.2.40. The results have not revealed much information that was not already apparent from major element analysis; all samples contain extremely high levels of lead and tin, and the opaque green glasses contain elevated levels of copper as a colourant in addition to this. The levels of manganese, antimony and iron generally reflect the composition of the respective base glass types used (see Chapter 4), but it is likely that some iron was also introduced as a contaminant from the fabric of the melting pot (see Chapter 4, section 4.2).

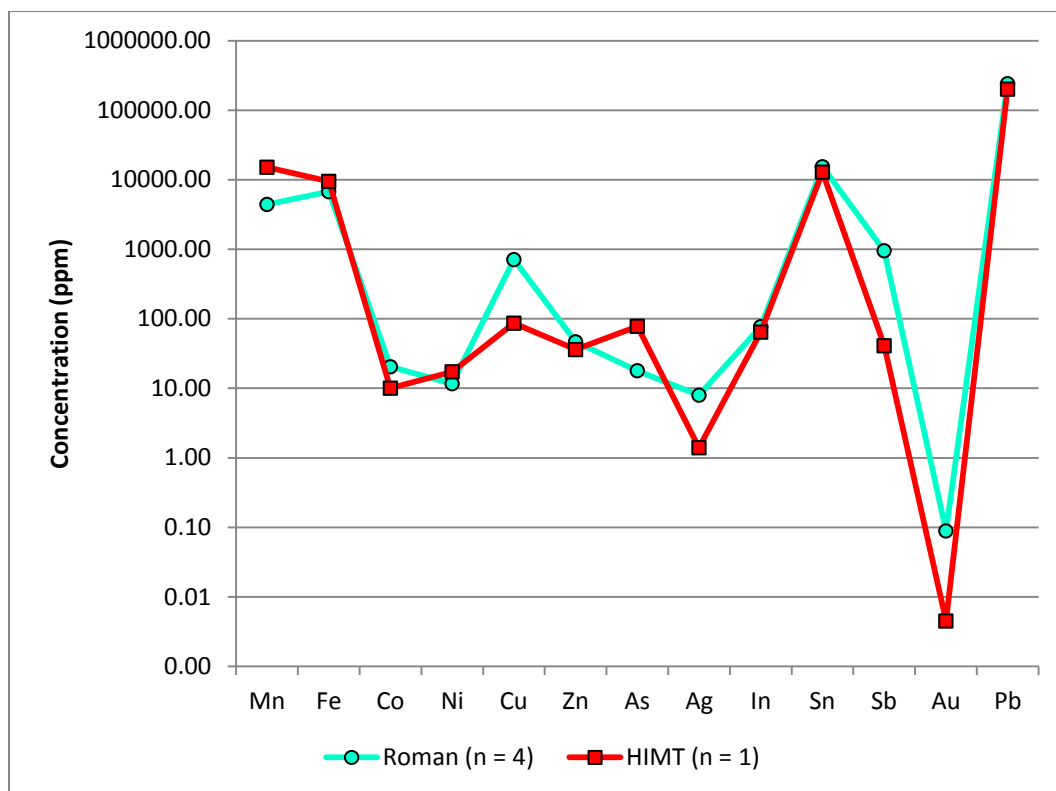


Figure 5.2.39 – Average colourant and colourant-related elements for the opaque yellow samples from Eriswell, showing the different base glass types identified. Note the logarithmic scale.

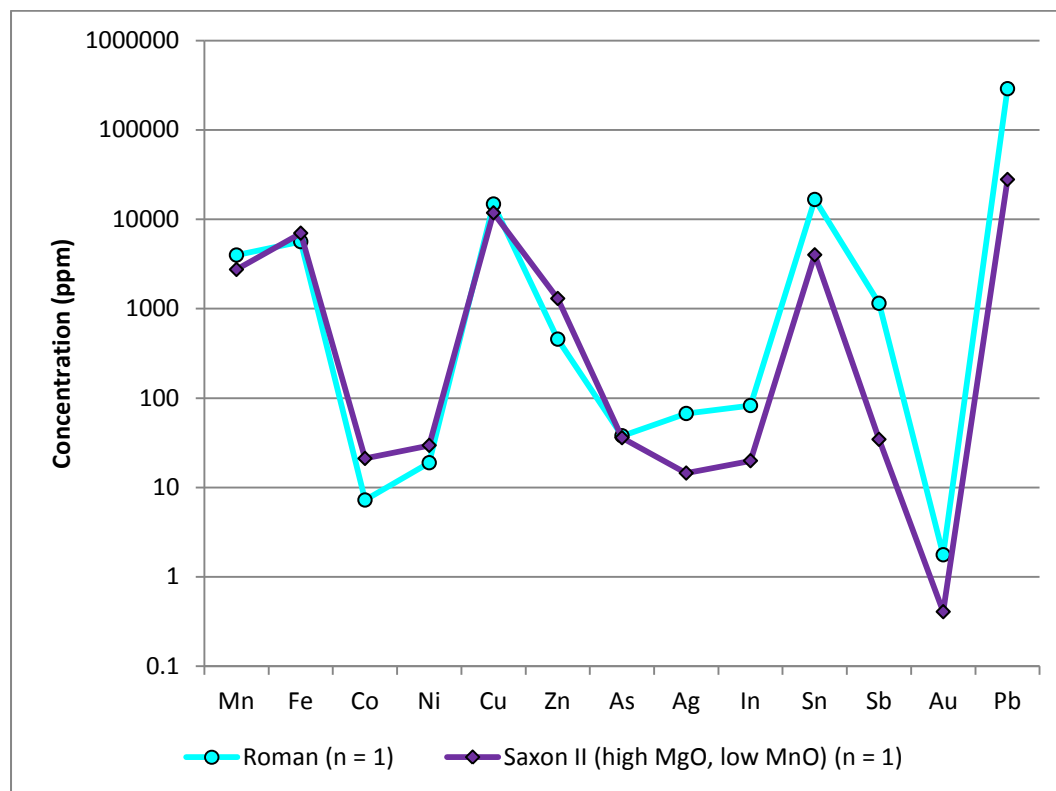


Figure 5.2.40 – Average colourant and colourant-related elements for the opaque green samples from Eriswell, showing the different base glass types identified. Note the logarithmic scale.

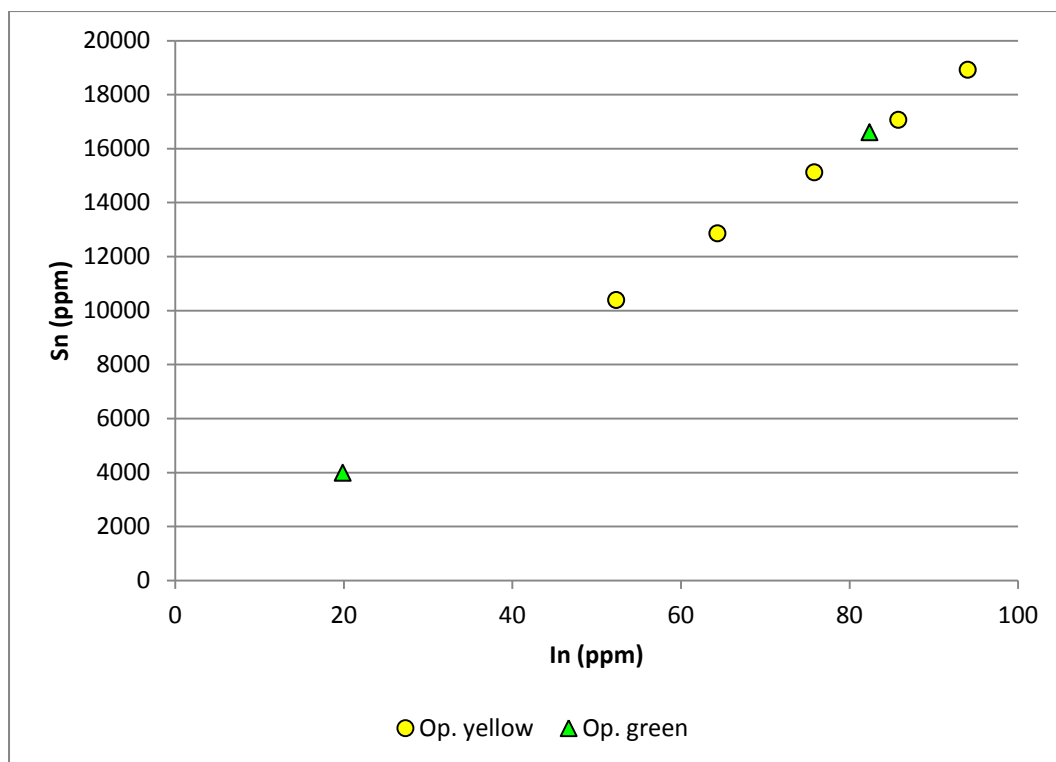


Figure 5.2.41 – A plot of indium versus tin for the opaque yellow and opaque green lead-tin oxide opacified samples from Eriswell.

Zinc is elevated in the opaque green samples (450-1300 ppm) relative to the opaque yellow samples (30-80 ppm), so is likely to have been introduced as an impurity with the copper colourant. The concentration of copper varies from 100-1200 ppm in the opaque yellow samples, which suggests that in some cases it was also introduced as an impurity, possibly through the use of recycled material. The absolute positive correlation between tin and indium ($r^2 = 1.0$; Figure 5.2.41) indicates that indium was introduced with as an impurity with tin (Benzaazoua *et al.* 2002: 168).

5.2.3. Opaque Red Glass

The opaque red glass from Eriswell is by far the most complex and variable glass colour present. Samples of opaque red glass were obtained from 96 beads from Eriswell; copper acts as both the colourant and the opacifying agent in all cases (Figure 5.2.42), and is present in concentrations corresponding to 0.8-4.2% CuO. All of the samples are very heterogeneous and in many cases contain a number of large bubbles (*e.g.* Figure 5.2.64); this indicates that a considerable amount of gas was released when the glass was molten, and that melting times were relatively short and/or temperatures low. Furthermore, the majority of samples contain angular particles of crushed metallurgical slag (Figures 5.2.49-5.2.61 and 5.2.63-5.2.66) which is likely to have been added as an internal reducing agent, as will be seen.

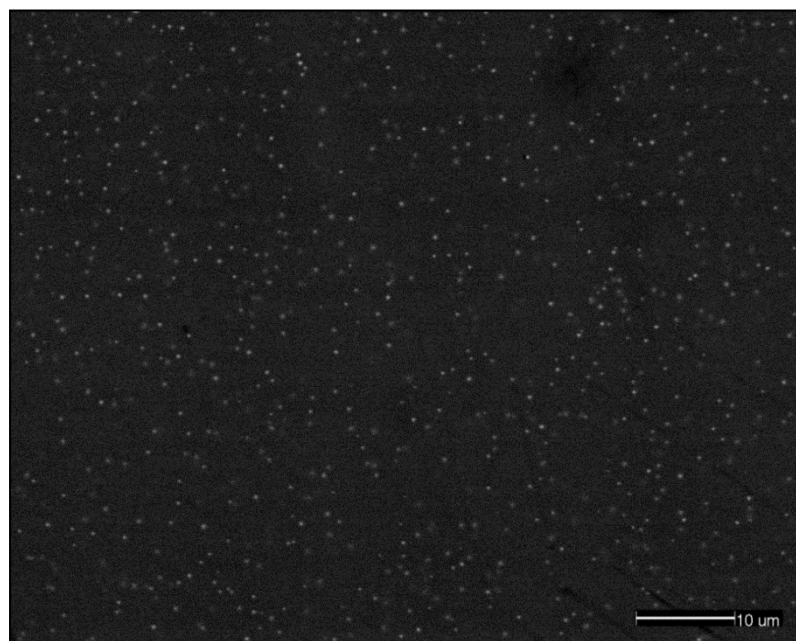


Figure 5.2.42 – BSE micrograph showing opaque red sample ERL104:G367:3653, a *Traffic Light Other* bead. A dispersion of tiny metallic copper particles (white) is visible dispersed in a soda-lime-silica glass matrix (grey). Note that visible copper particles are too large to contribute to the colour; colour is instead produced by much smaller metallic copper nanoparticles which are well below the resolution of the SEM.

Previous work has established that the majority of early opaque red glasses typically fall into one of two broad categories: high lead – high copper glasses containing around 20% or more PbO and 5-12% CuO, and low lead – low copper glasses

containing a few percent CuO and up to 15% PbO (Hughes 1972: 99; Freestone 1987; Henderson 1989a; Stapleton *et al.* 1999: 913). While there are exceptions, most generally fall into one or the other group. The high lead – high copper type is typically coloured by dendritic crystals of cuprite, which produce a bright ‘sealing wax’ red colour (Brun and Pernot 1992: 236; Hughes 1972: 99; Stapleton *et al.* 1999: 915). In contrast, the low lead – low copper type is coloured by particles of elemental copper, which produce a duller ‘liverish’ red colour (Hughes 1972: 104-105; Rooksby 1962: 23). The colourant particles are frequently below the resolution of routine SEM analysis, but direct observation using transmission electron microscopy (TEM) with electron diffraction confirms that the low lead – low copper reds are typically coloured by nanoparticles of metallic copper (Cu), whilst the high lead – high copper reds are coloured by cuprite (Cu₂O) (Brun *et al.* 1991; Barber *et al.* 2009: 124).

Whilst the production technology of both types of glass is still not fully understood, the requirement of a reducing environment (*i.e.* oxygen deficient) to facilitate the production of the colour, whether through the use of a reducing furnace atmosphere or an internal reductant (or both) is generally agreed (Freestone 1987; Brill and Cahill 1988: 18-19; Brun *et al.* 1991; Brun and Pernot 1992: 236; Cable and Smedley 1987; Henderson 1985: 281-282; Welham *et al.* 2000: 13-14).

In all of the opaque red samples analysed, copper is present in its elemental (metallic) form as minute particles, typically less than 1 µm in diameter, dispersed throughout the glass matrix. These precipitated out of the glass upon cooling and produce the deep red colour observed (Santagostino Barbone *et al.* 2008: 464). Whilst larger particles of metallic copper could just be resolved in the SEM in several of the samples, they are not easily seen in the BSE micrographs. However, it can be seen that they appear brighter around the slag inclusions due to their larger sizes in these regions (*e.g.* Figures 5.2.42, 5.2.49-5.2.50, 5.2.52-5.2.53, 5.2.56, 5.2.58-5.2.61 and 5.2.63). It should be noted that the visible copper particles are too large to contribute to the colour; this is instead produced by much smaller metallic copper nanoparticles which are below the resolution of the SEM.

The manganese and antimony contents of the opaque red samples are variable; MnO being present in concentrations of up to 2.1% and Sb₂O₃ up to 0.7%. Whilst the oxides of antimony can promote the reduction of copper (Brill and Cahill 1988: 19; Fiori 2011: 30), the concentrations of both antimony and manganese reflect the respective base glass types used (see Chapter 4).

The lead content is variable between samples, but the majority typically contain less than 20% PbO and can therefore be classed as low lead – low copper reds. Several contain higher levels (up to 32% PbO), but intermediate compositions between low lead – low copper and high lead – high copper reds such as this are not unknown (*e.g.* see Freestone 1987; Freestone *et al.* 1999). The addition of lead is thought to have helped to dissolve the copper to form a more homogeneous melt (Biek and Bayley 1979: 17; Brill 1970: 120; Hughes 1972: 99). However, lead is sometimes present in quantities as low as 0.9% PbO, suggesting that it is unlikely to have been a necessary ingredient. Tin was also detected in a number of the red samples analysed (anywhere up to 2.2% SnO₂), with sparse tin oxide crystals visible in several samples (*e.g.* Figures 5.2.49 and 5.2.55-5.2.57). However, crystals of lead-tin oxide (lead stannate, PbSnO₃) were more frequently encountered (*e.g.* Figures 5.2.49, 5.2.50, 5.2.52-5.2.58, 5.2.61 and 5.2.65-5.2.67); this is more typically seen as both a colourant and opacifying agent in opaque yellow glass (see this chapter, section 5.2.2).

Low concentrations of tin are frequently encountered in early opaque red glass, and it has been suggested that it may have been introduced as an impurity with the copper colourant in the form of an alloy such as bronze (Bayley 1987: 184; Bayley and Wilthew 1986; Brill 1970: 120; Brill and Cahill 1988; Brun and Pernot 1992: 239; Heck and Hoffmann 2000: 352; 2002: 74-75; Wilthew 2006: 391). High-tin bronzes typically contain up to a maximum of 25% tin (Schibille *et al.* 2012: 1487); the levels of tin in many of the Eriswell samples far exceeds this (in some cases they correspond to a bronze containing up to 80% tin). Furthermore, no correlation was observed between copper and tin (Figure 5.2.43), suggesting that the majority of tin is unlikely to have been introduced with copper. As opacity is caused by copper nanoparticles, tin was clearly not necessary to render the glass opaque.

The advantages of tin being used to improve the stability and reproducibility of red glasses coloured by copper have been noted by previous studies (*e.g.* Brill and Cahill 1988: 23; Shugar 2000: 382; Welham *et al.* 2000: 13-14); for example, in its absence ruby red colours do not always strike properly and turn ‘liverish’, but the reasons for this are unclear (Weyl 1951: 343). Tin can also act as a reducing agent, helping to deoxidise the glass (Mirti *et al.* 2002: 228; Shugar 2000: 382). It is just possible that tin had some technological benefits in the formation of the colour in the Eriswell reds, but it was not detected in all samples so was clearly not necessary to produce the colour. It has also been suggested that both tin and lead may have been introduced in the form of an alloy such as pewter (Fiori 2011: 32; Heck and Hoffmann 2002: 75; Mortimer 1996a: 11; Tite *et al.* 2008: 80) in its oxidised form; the colour of calcined scale or dross would have been pale yellow, which may have prompted glassworkers to use it as a colourant (Tite *et al.* 2008: 80).

On balance, it is far more likely that tin was introduced through the use of a material rich in both lead and tin, such as pewter. This interpretation is partly borne out by the typical presence of tin as crystals of lead-tin oxide (lead stannate, PbSnO_3 ; *e.g.* Figures 5.2.49-5.2.50, 5.2.52-5.2.58, 5.2.61 and 5.2.65-5.2.67) as opposed to tin oxide (cassiterite, SnO_2 ; *e.g.* Figures 5.2.49 and 5.2.55-5.2.57). As previously mentioned, lead-tin oxide is unstable at high temperatures, and was probably produced as a pre-formed pigment for the manufacture of opaque yellow glass (see this chapter, section 5.2.2).

The PbO/SnO_2 ratios of the opaque red glasses are broadly consistent with or higher than those for opaque yellow glass; the similarities are highlighted in Figures 5.2.44 and 5.2.45. Similarly, the lead and tin contents of the opaque red glasses are very similar to those observed in the opaque and translucent green glasses from Eriswell (Figure 5.2.45), in which tin also appears to have been introduced with lead in the form of a lead-tin calx (see this chapter, sections 5.1.4 and 5.2.2). The reasons for the addition of this lead-tin rich material are not entirely clear, but lead is frequently found in ancient copper-red glasses and offers a number of potential advantages (see section 5.3.4 below).

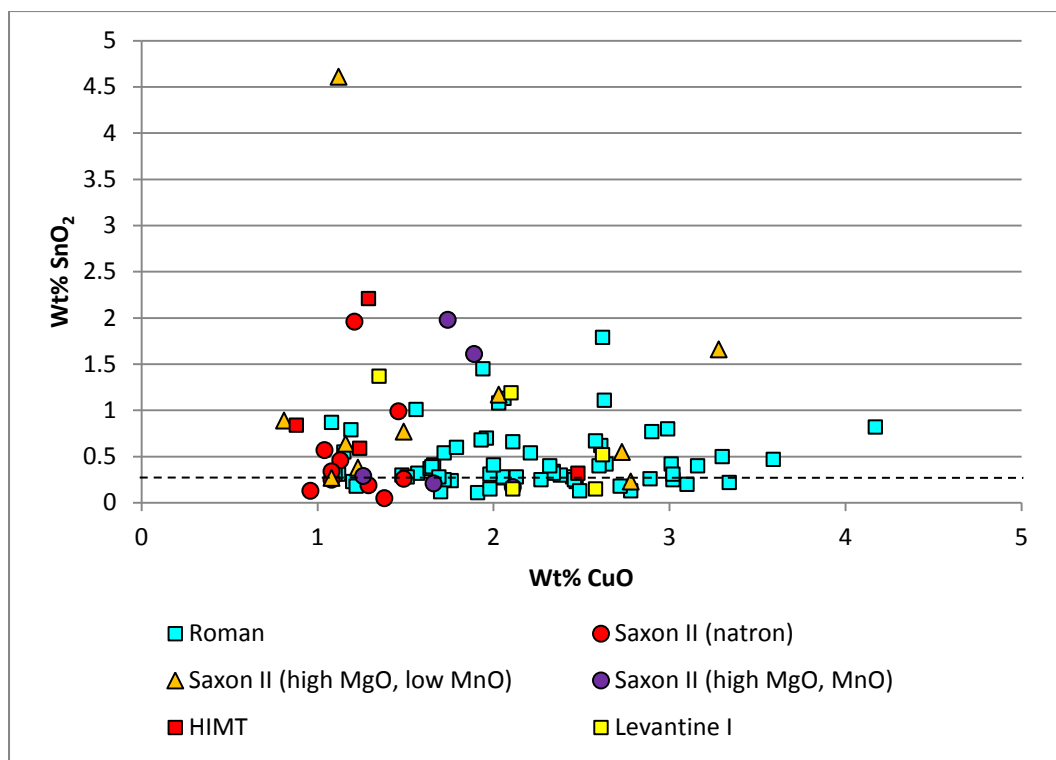


Figure 5.2.43 – A plot of copper oxide versus tin oxide for the opaque red samples from Eriswell, showing the different base glass types identified. The dashed line represents the approximate detection limits for tin oxide.

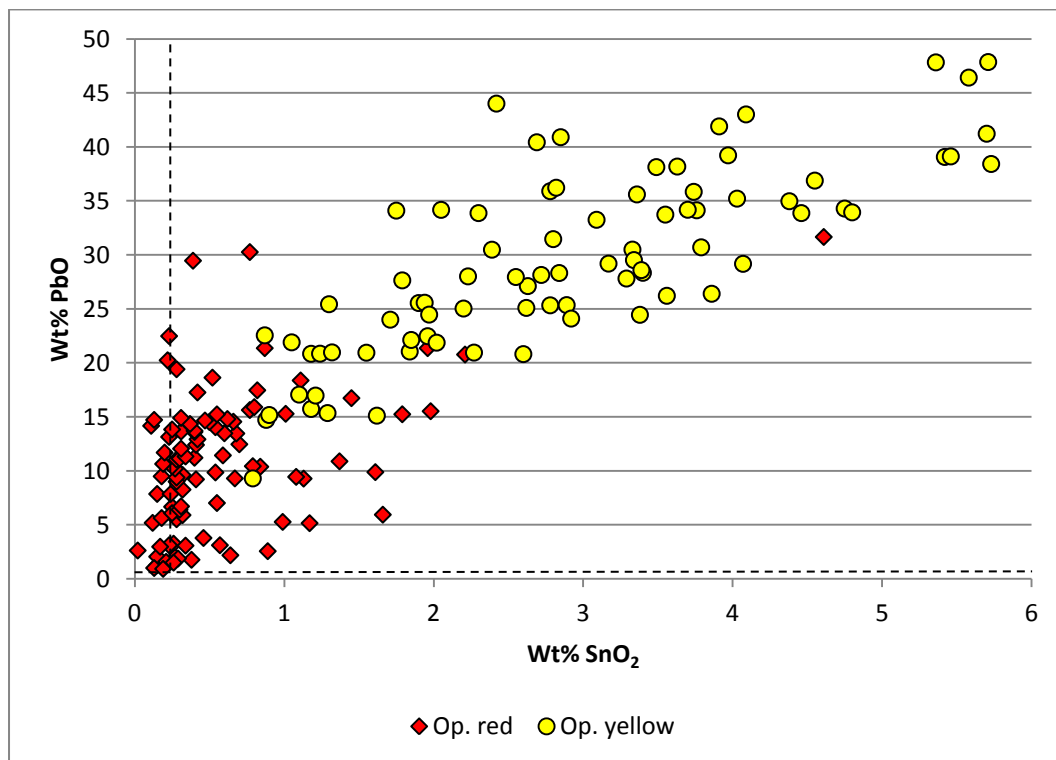


Figure 5.2.44 – A plot of tin oxide versus lead oxide for the opaque red samples from Eriswell, compared to the opaque yellow samples (Figure 5.2.20). The dashed lines represent the approximate detection limits for tin oxide and lead oxide.

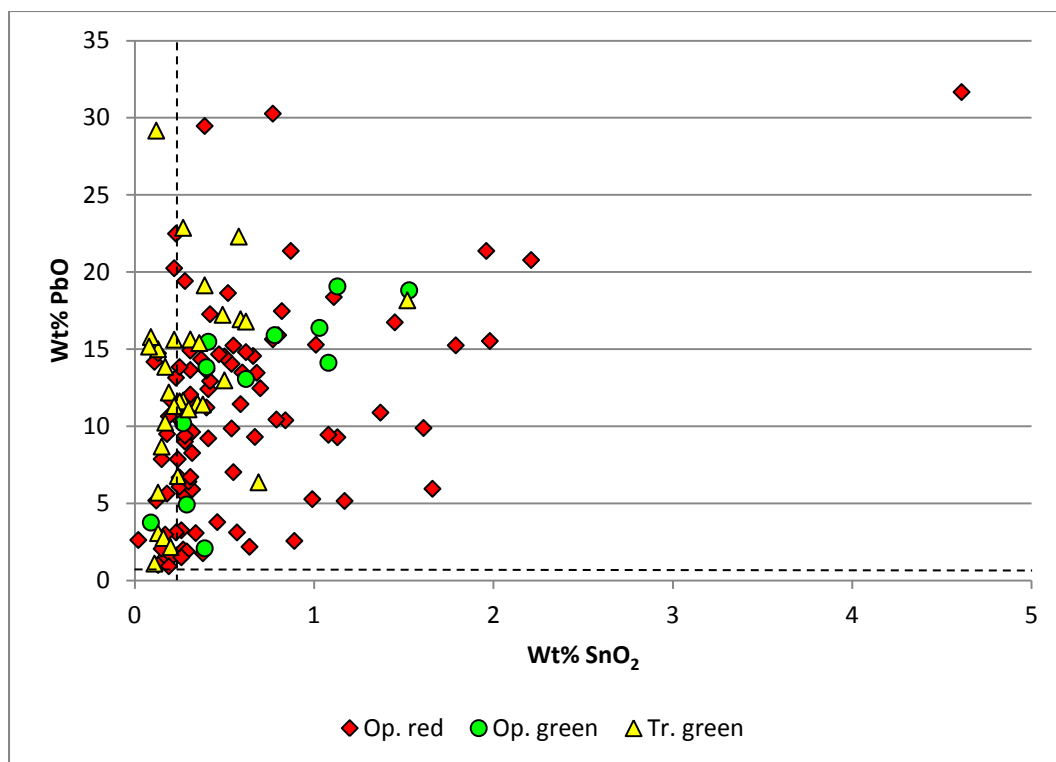


Figure 5.2.45 – A plot of tin oxide versus lead oxide for the opaque red glasses compared to the opaque and translucent green glasses from Eriswell (Figures 5.1.37). The dashed lines represent the approximate detection limits for tin oxide and lead oxide.

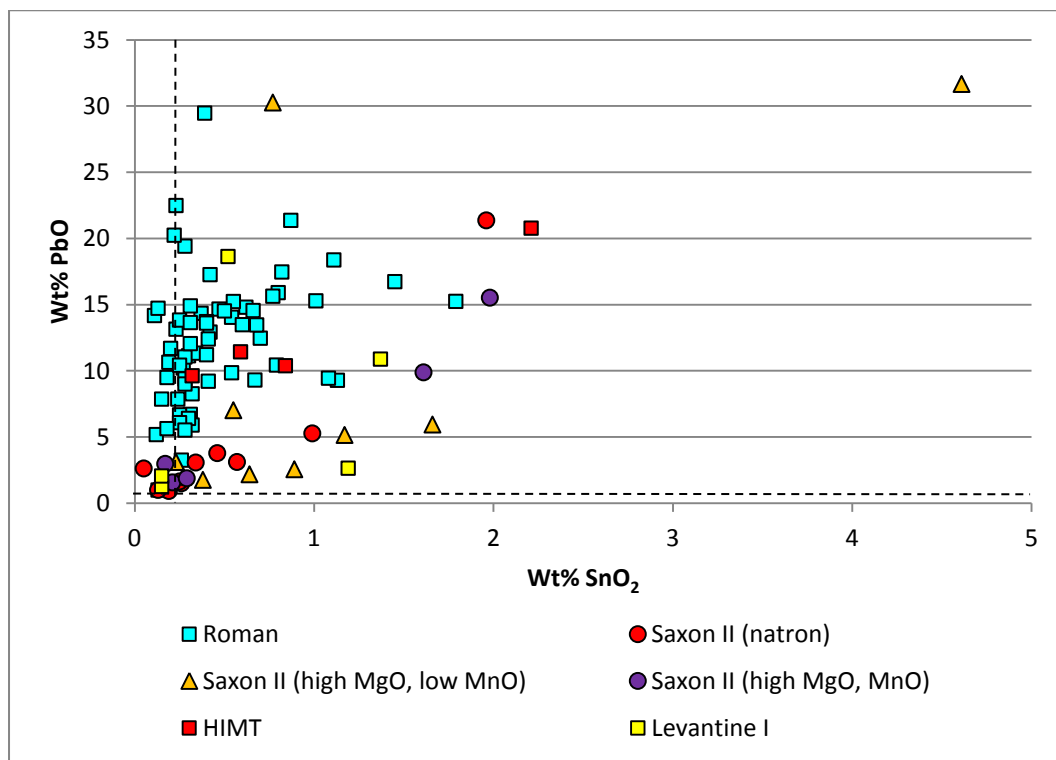


Figure 5.2.46 – A plot of tin oxide versus lead oxide for the opaque red samples from Eriswell, showing the different base glass types identified. The dashed lines represent the approximate detection limits for tin oxide and lead oxide.

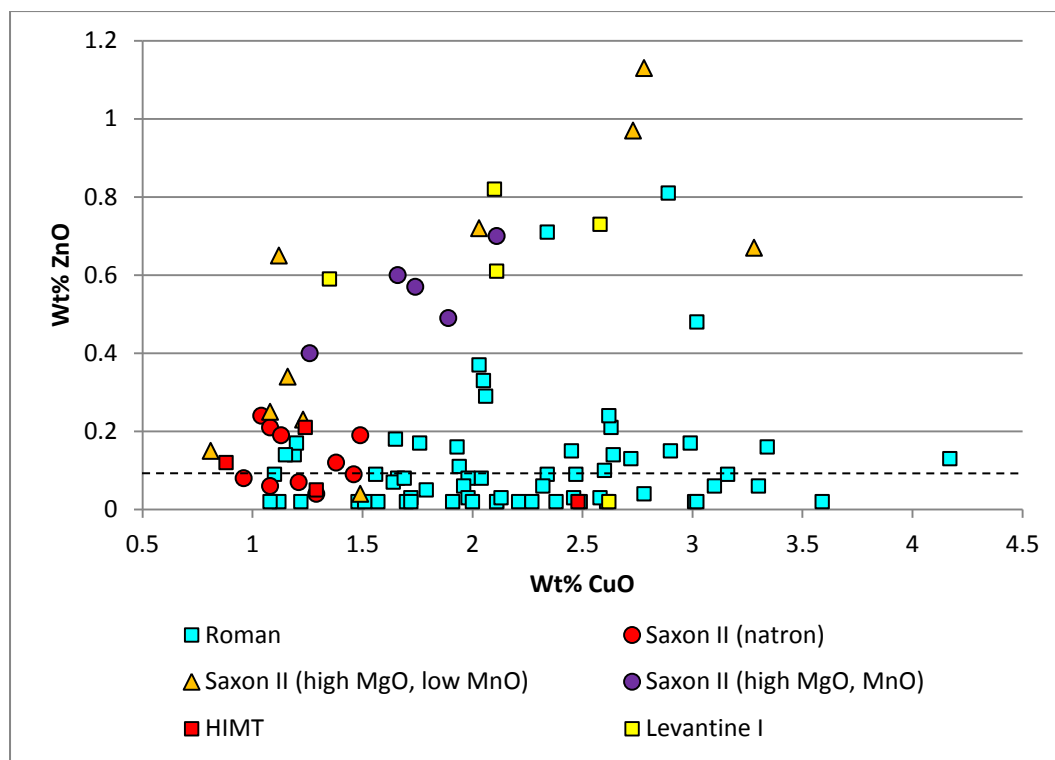


Figure 5.2.47 – A plot of copper oxide versus zinc oxide for the opaque red glasses from Eriswell, showing the different base glass types identified. The dashed line represents the approximate detection limits for zinc oxide.

Interestingly, the opaque red samples produced from the ‘Saxon II’ and several of the ‘Levantine I’ base glass types contain a different ratio of PbO/SnO_2 than those produced from the ‘Roman’ and ‘HIMT’ base glass types (Figure 5.2.46). This suggests the use of two slightly different lead-tin calxes. A similarly low ratio of PbO/SnO_2 is observed in the opaque green samples produced from ‘Saxon I’ and ‘Saxon II’ glass, relative to those produced from ‘Roman’ glass (Figure 5.2.21). The ‘later’ glass types (see Chapter 4, section 4.8) therefore appear to have been produced using a lead-tin calx containing a lower ratio of PbO/SnO_2 .

Zinc was also detected in a number of samples, but varying levels of zinc are not uncommon in early Anglo-Saxon opaque red glass (*e.g.* Bayley 1987: 184; Meek 2010: 9). The majority contain low levels of zinc (less than 0.4% ZnO), but several contain up to 1.1% ZnO. It has been suggested that this reflects the use of scrap copper alloy (*e.g.* brass) as a colourant (Bayley 1987: 184; Bayley 2000a: 218; Bayley and Wilthew 1986; Brill and Cahill 1988: 22; Fiori 2011: 30; Meek 2010: 7; Mortimer 1996a: 8), as zinc does not have any technological advantages. Variations

in zinc content may relate to chronological changes in manufacturing technology (*i.e.* the use of different copper alloys; see section 5.3.2 below); the majority of samples containing in excess of 0.3% ZnO are produced from a ‘later’ ‘Saxon II’ base glass type (Figure 5.2.47). Here zinc is positively correlated with copper (Figure 5.2.47; $r^2 = 0.60$), suggesting that it is likely to have been introduced in the form of an alloy.

All of the opaque red samples analysed are characterised by very high levels of iron, typically corresponding to 2-7% Fe₂O₃, but in some cases up to as much as 10% Fe₂O₃. This is paralleled by the composition of opaque red glass from elsewhere in early Anglo-Saxon England (*e.g.* Henderson 1990: 157; Mortimer 1996a: 8; Mortimer and Heyworth 2009: 411). Iron was introduced as an internal reducing agent in the form of crushed iron-rich metallurgical slag, which facilitated the precipitation of the metallic copper particles (*e.g.* Heck and Hoffmann 2000: 353; Mortimer 1996a: 8; Mortimer and Heyworth 2009: 411; Sayre and Smith 1967: 306). Isolated fragments of iron scale were also observed in several samples (*e.g.* Figures 5.2.53 and 5.2.58), but these are more likely to have been incidentally pulled from the mandrel on which the beads were manufactured (see Chapter 3, section 3.2.1).

The technical difficulties in producing opaque red glass have been widely acknowledged (Barber *et al.* 2009: 116; Brill and Cahill 1998: 18; Brun and Pernot 1992: 236-237; Hughes 1972: 99; Shugar 2000: 375), which has led to speculation that its production was a specialised industry restricted to just a few workshops (Brun and Pernot 1992: 237; Freestone *et al.* 1990; Shugar 2000: 375). Furthermore, experimental replication of opaque red glass has shown that even when a reducing furnace atmosphere is maintained, the homogeneous precipitation of copper nanoparticles may be difficult without the presence of such an internal reductant (Cable and Smedley 1987). However, opaque red glass is one of the most common colours at Eriswell, so it is possible that the reducing nature of the slag additive allowed production in a larger number of less specialised workshops; perhaps even on a local scale.

Table 5.2.3 – Selected SEM-EDS spot analyses of the aluminium-rich inclusions observed in several of the opaque red samples from Eriswell.

Sample ¹	Oxide (wt %) ²												
	Na ₂ O	Al ₂ O ₃	SiO ₂	SO ₃	S	K ₂ O	CaO	TiO ₂	Fe ₂ O ₃	FeO	CuO	SnO ₂	PbO
<i>Nepheline</i>	15.9	34.9	41.1	-	-	8.1	-	-	-	-	-	-	-
ERL104:G242:2145	17.8	33.9	42.7	b.d.	-	1.8	0.8	b.d.	0.9	-	0.2	0.4	0.8
ERL104:G242:2288	18.4	32.8	42.4	b.d.	-	1.6	0.7	b.d.	1.0	-	0.4	b.d.	1.9
ERL104:G263:1406	17.8	34.1	43.5	b.d.	-	1.6	0.7	b.d.	0.4	-	0.3	b.d.	1.0
ERL104:G268:3257	17.4	33.2	44.4	b.d.	-	1.7	0.4	b.d.	0.9	-	0.2	0.5	0.7
ERL104:G268:3260	18.6	33.6	41.5	b.d.	-	1.9	0.6	b.d.	1.4	-	b.d.	b.d.	1.2
ERL104:G268:3260	19.0	32.8	41.1	b.d.	-	2.0	0.7	b.d.	1.5	-	b.d.	0.3	2.0
ERL104:G305:1820	17.7	34.3	41.8	0.1	-	1.8	0.8	b.d.	1.2	-	b.d.	0.3	1.3
ERL104:G363:1922	17.7	29.0	37.7	0.1	-	2.1	1.1	b.d.	0.9	-	1.1	1.7	8.1
<i>Lazurite</i>	18.7	30.7	36.2	-	6.4	-	11.3	-	-	-	-	-	-
ERL104:G242:2145	16.1	28.6	37.9	10.0	(4.0)	0.4	3.8	b.d.	0.5	-	0.3	b.d.	1.1
ERL114:G413:1493	14.8	26.8	36.5	11.0	(4.4)	0.1	4.5	b.d.	0.7	-	0.2	2.0	3.8
ERL114:G413:1495	19.0	28.4	34.2	10.3	(4.1)	0.2	4.4	b.d.	1.1	-	b.d.	b.d.	b.d.
<i>Leucite</i>	-	23.4	55.1	-	-	21.6	-	-	-	-	-	-	-
ERL046:G03:1322	2.5	18.8	64.6	b.d.	-	13.5	b.d.	b.d.	0.2	-	b.d.	b.d.	b.d.
ERL046:G43:1721	4.4	18.9	63.6	0.2	-	10.9	b.d.	b.d.	0.2	-	b.d.	b.d.	b.d.

¹Theoretical compositions for nepheline (Na₃KAl₄Si₄O₁₆), lazurite (Na₃Ca(Al₃Si₃O₁₂)S) and leucite (KAlSi₂O₆) are in *italics*.

²Spot analyses normalised to 100%. b.d. = below detection. See Chapter 2, section 2.3.1 for details. Values in brackets represent hypothetical S and FeO values.

Sporadic sodium aluminium silicate and sodium aluminium silicate sulphate inclusions were also observed in many samples (*e.g.* Figures 5.2.57, 5.2.59, 5.2.65 and 5.2.67), typically ranging in size from 10-100 μm across. As with those identified in several of the translucent green (see this chapter, section 5.1.4), opaque yellow and opaque green glasses (see this chapter, section 5.2.2), these correspond to the minerals nepheline ($\text{Na}_3\text{KAl}_4\text{Si}_4\text{O}_{16}$) and lazurite ($\text{Na}_3\text{Ca}(\text{Al}_3\text{Si}_3\text{O}_{12})\text{S}$) respectively (Table 5.2.3) and are usually associated with crystals of lead-tin oxide (*e.g.* Figure 5.2.67). Similarly, particles of leucite (KAlSi_2O_6) were observed in two samples (Table 5.2.3). All of these products are all likely to have formed as a result of a reaction between the high sodium oxide content of a soda-lime-silica glass and the clay-ceramic material of a crucible.

By far the largest nepheline-lead-tin oxide inclusions were observed in sample ERL104:G268:3260 (a *Candy Variant* bead) (Figures 5.2.64 and 5.2.65). The association of nepheline with lead-tin oxide (*e.g.* Figure 5.2.67) suggests that this nepheline-lead-tin oxide material represents the dregs from a crucible used to make lead-tin yellow pigment for the production of opaque yellow glass, in the manner described by Heck *et al.* (2003; see also this chapter, section 5.2.2). In addition, a number of samples contain acicular crystals of calcium silicate, corresponding to the mineral wollastonite (CaSiO_3) (*e.g.* Figures 5.2.49, 5.2.51, 5.2.54, 5.2.55 and 5.2.58-5.2.61); this is likely to have formed as a devitrification product upon cooling of the melt.

5.2.3.1. Slag Additions

The slag inclusions in the opaque red glasses from Eriswell are discussed in detail in Peake and Freestone (2012). The author is particular grateful to Ian Freestone, who greatly assisted with the majority of the interpretations that follow in this section.

Previous studies have suggested the use of metallurgical by-products in the production of opaque red glass; for example, Stapleton *et al.* (1999: 919) have suggested that the red enamel used on early medieval metalwork may have been produced through the re-use of a raffination slag obtained from the recovery of silver

from recycled metalwork. Freestone *et al.* (2003b) have suggested that opaque red glass may have been coloured by the direct addition of copper-bearing metallurgical by-products, but the evidence is largely circumstantial. However, there is now abundant evidence for the addition of metallurgical slag in the production of opaque red glass in the early medieval period, not only from Eriswell, but also from Spong Hill and Bergh Apton in Norfolk (see Chapter 7, section 7.1), together with previously identified, apparently isolated, examples from Anglo-Saxon Mucking in Essex (Mortimer 1996b: 7; Mortimer and Heyworth 2009: 412) and Merovingian Eichstetten in Germany (Heck and Hoffmann 2002: 75-76). High iron levels have also been detected in early Anglo-Saxon opaque red glass beads from elsewhere in England (*e.g.* Bayley 1987; Meek 2010) and from Merovingian Europe (Heck and Hoffmann 2000: 353), suggesting the probable use of iron-rich slag.

Angular particles of iron-rich metallurgical slag are clearly visible in the BSE micrographs of the samples analysed (Figures 5.2.49-5.2.61 and 5.2.63-5.2.66), typically ranging in size from 10-200 μm across, but in some cases up to 400 μm across. The concentration of relatively large copper particles around many of these slag inclusions (*e.g.* Figures 5.2.49-5.2.50, 5.2.52-5.2.53, 5.2.56, 5.2.58-5.2.61 and 5.2.63) confirm that the slag served the function of reducing copper in the glass to the metallic state thus generating the red colouration, as has been suggested by Heck and Hoffmann (2002: 76). It was impossible to accurately quantify the number of slag particles present in the samples analysed due to the heterogeneity of the glasses analysed, together with the small nature of the samples taken. However, the few samples in which slag was not observed have compositions comparable to those which do contain visible slag inclusions (most notably their high iron contents), suggesting that slag *was* added during their production, but dissolved or was not observed due to the small size of the samples removed.

Whilst the apparent absence of slag in some samples probably relates to the sample size, its absence in some of the larger samples (*e.g.* Figures 5.2.22 and 5.2.23) cannot be explained so readily. This appears to relate to the lead content of the glass to which it was added. Lead acts as a flux, so glass containing high levels of PbO softens at lower temperatures than glass containing lower levels of PbO (Biek and Bayley 1979: 16). Slag particles are likely to have more readily retained their shape

in the samples containing high levels of lead (above approximately 7% PbO), which could be melted at lower temperatures. In contrast, the higher temperatures needed to melt a low-lead glass are likely to have led to the total or partial dissolution of the slag. The duration of heating would also have affected the extent of the dissolution of any slag particles, but this generally appears to have been kept to a minimum.

Whilst the slag particles observed are extremely complex and variable in microstructure, most are of the same compositional type. All are iron silicate slags, primarily consisting of varying amounts of olivine and iron oxide, together with a number of interstitial glassy phases. It has been possible to identify at least two different types of slag; the main phases of which correspond to fayalite (Fe_2SiO_4) or kirschsteinite (CaFeSiO_4) respectively (Table 5.2.4). The samples containing these two different types of slag cannot be differentiated from one another based on their bulk compositions. However, the differences between the fayalitic and kirschsteinitic slags are in both elemental composition (high versus low CaO and FeO; Figure 5.2.48) and in redox state. Textural differences between slag inclusions of the same type are likely to reflect differences in the heterogeneity of the slag exploited, together with variations in the manufacturing conditions (*e.g.* heating and cooling), rather than any major technological differences.

Iron-rich slags of the fayalitic variety are typical of both copper- and iron-smelting technologies throughout the ancient and medieval worlds (Bachmann 1982: 23; 31; Hauptmann 2007; Manasse *et al.* 2001: 951-955; Severin *et al.* 2011: 989), due to the powerful effect of iron as a flux (Severin *et al.* 2011: 989-990). Fayalite may also occur in iron-smithing slag, which is produced from a reaction between the iron scale on the artefact being worked and a quartz sand flux (Bachmann 1987: 30-31; Selskienė 2007: 26-27). Kirschsteinite may occur in both iron and copper-smelting slags (Bachmann 1982: 23-25; 30-33; Manasse *et al.* 2001: 951-958; Sharp and Mittwede 2011: 331-334), but in iron-smelting slag it typically occurs as calcium-rich rims on fayalite cores (Tim Young, pers. comm.). The presence of kirschsteinite is less likely in iron-smithing slag (Selskienė 2007: 26-27).

Table 5.2.4 – Selected SEM-EDS area analyses of the fayalitic and kirschsteinitic slag inclusions in several of the opaque red samples from Eriswell, highlighting the compositional differences between the two slag types.

<i>Sample</i> ¹	<i>Oxide (wt %)</i> ²													
	<i>Na₂O</i>	<i>MgO</i>	<i>Al₂O₃</i>	<i>SiO₂</i>	<i>P₂O₅</i>	<i>SO₃</i>	<i>K₂O</i>	<i>CaO</i>	<i>TiO₂</i>	<i>MnO</i>	<i>Fe₂O₃</i>	<i>FeO</i>	<i>CuO</i>	<i>PbO</i>
	<i>Fayalitic Slag</i>													
<i>Fayalite</i>	-	-	-	29.5	-	-	-	-	-	-	-	70.5	-	-
ERL046:G03:1271	2.9	0.2	5.1	19.0	1.2	b.d.	0.2	0.4	0.3	0.9	69.4	(62.5)	0.1	b.d.
ERL046:G03:1276	9.1	0.4	5.5	31.8	2.4	0.1	0.5	3.4	0.2	0.4	45.1	(40.6)	0.2	0.6
ERL046:G38:1046	2.3	0.3	3.6	31.2	0.2	0.2	0.4	2.7	b.d.	b.d.	59.2	(53.3)	b.d.	b.d.
ERL046:G38:1053	0.8	0.2	1.7	16.7	0.2	b.d.	0.1	1.0	0.1	b.d.	79.4	(71.5)	b.d.	b.d.
ERL046:G38:1063	5.7	0.3	5.8	33.4	1.7	b.d.	0.5	1.7	0.3	1.8	47.6	(42.8)	0.3	b.d.
ERL046:G43:1721	6.7	0.2	2.5	22.3	1.0	b.d.	0.3	1.2	b.d.	1.1	62.2	(56.0)	0.3	1.9
ERL046:G43:1726	1.6	0.2	3.0	23.0	1.1	b.d.	0.3	3.7	b.d.	1.5	65.3	(58.7)	0.3	b.d.
ERL104:G107:1141	6.7	0.3	3.6	17.0	0.6	0.1	0.6	1.2	0.2	1.0	65.5	(58.9)	0.7	1.9
ERL104:G148:2739	4.0	0.2	1.6	28.8	3.1	0.3	0.3	5.2	0.2	0.4	55.3	(49.7)	0.4	b.d.
ERL104:G242:2196	0.5	1.1	0.8	26.6	1.0	0.2	b.d.	2.1	0.1	0.3	67.0	(60.2)	b.d.	b.d.
ERL104:G242:2203	3.4	0.3	3.2	20.9	1.5	b.d.	1.1	2.5	b.d.	0.2	65.7	(59.1)	0.4	0.2
ERL104:G242:2207	5.1	0.4	5.2	32.2	2.1	b.d.	0.4	2.1	0.2	2.5	49.8	(44.8)	0.2	b.d.
ERL104:G242:2282	2.1	1.5	0.1	27.2	0.7	b.d.	b.d.	1.0	b.d.	0.4	65.8	(59.2)	0.3	0.6
ERL104:G242:2288	3.7	0.3	4.8	17.4	1.3	b.d.	0.3	2.0	0.2	0.2	68.5	(61.6)	0.3	0.5
ERL104:G268:3256	9.2	0.5	5.0	26.5	3.5	0.2	0.3	3.3	0.2	0.5	49.6	(44.6)	0.4	0.6
ERL104:G268:3257	1.6	1.0	1.9	27.6	1.6	b.d.	0.6	5.6	b.d.	0.2	59.4	(53.4)	0.4	b.d.
ERL104:G305:1820	9.9	0.6	5.1	28.4	2.5	b.d.	0.3	3.5	0.1	0.5	46.5	(41.8)	0.7	1.9
ERL104:G315:2346	6.7	0.3	0.9	32.6	0.5	b.d.	0.3	1.7	b.d.	0.1	55.6	(50.0)	0.4	0.3
ERL104:G362:1961	7.5	0.7	1.1	32.4	1.4	b.d.	b.d.	4.0	b.d.	0.6	50.7	(45.6)	0.3	1.1
ERL104:G362:1974	8.7	0.5	0.3	34.0	0.3	0.2	0.2	0.8	0.2	b.d.	53.8	(48.4)	0.5	0.5

Table 5.2.4 – (continued).

Sample ¹	Oxide (wt %) ²													
	Na ₂ O	MgO	Al ₂ O ₃	SiO ₂	P ₂ O ₅	SO ₃	K ₂ O	CaO	TiO ₂	MnO	Fe ₂ O ₃	FeO	CuO	PbO
ERL104:G363:1912	9.3	0.4	4.8	31.5	1.7	b.d.	0.3	3.4	0.3	0.9	44.6	(40.1)	0.8	2.0
ERL104:G367:3619	3.9	0.5	7.9	22.0	5.6	0.1	0.5	2.6	0.3	0.5	55.0	(49.5)	0.4	0.6
ERL114:G413:1495	4.9	0.3	1.0	19.9	0.5	b.d.	b.d.	2.8	b.d.	b.d.	68.3	(61.5)	0.6	0.9
ERL114:G413:1498	5.2	0.7	3.4	30.0	2.4	b.d.	0.3	2.2	0.1	0.7	53.8	(48.4)	0.4	0.3
ERL114:G422:1420	5.9	0.3	3.5	30.1	1.4	b.d.	0.4	0.5	0.3	1.4	55.3	(49.8)	0.2	0.2
<i>Kirschsteinitic Slag</i>														
<i>Kirschsteinite</i>	-	-	-	32.0	-	-	-	29.8	-	-	-	38.2	-	-
ERL104:G268:3260	0.7	0.8	0.9	28.0	2.2	0.2	b.d.	25.0	0.1	0.7	40.9	(36.8)	0.3	b.d.
ERL104:G268:3260	1.9	0.5	2.4	30.0	2.5	0.4	0.3	24.3	0.2	0.5	36.5	(32.8)	0.2	b.d.
ERL104:G268:3260	0.5	0.5	1.9	31.9	3.0	0.3	b.d.	26.0	0.2	0.4	33.4	(30.0)	0.7	1.1
ERL104:G281:1795	1.0	1.5	5.3	27.2	2.0	0.1	0.6	21.5	0.3	0.6	39.5	(35.6)	0.1	b.d.

¹Repeated sample numbers represent spot analyses of different areas of the same sample. Theoretical compositions for fayalite (Fe₂SiO₄) and kirschsteinite (CaFeSiO₄) are in *italics*.

²Area analyses normalised to 100%. b.d. = below detection. See Chapter 2, section 2.3.1 for details. Values in brackets represent hypothetical FeO values.

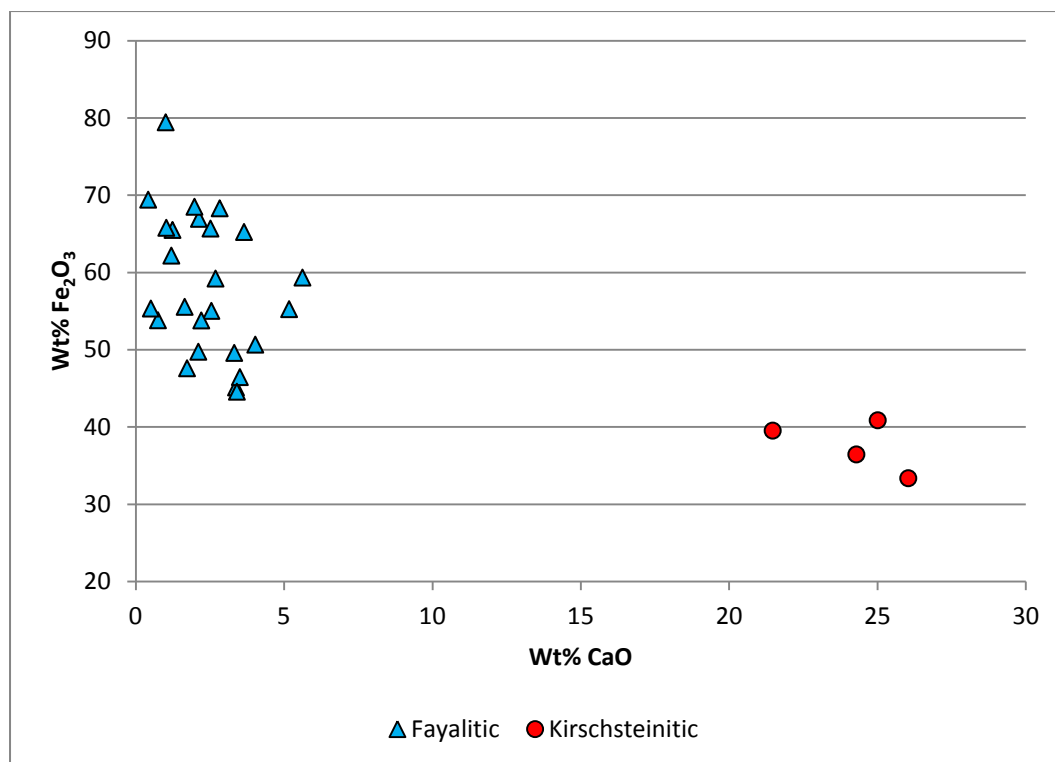


Figure 5.2.48 – A plot of lime versus iron oxide for selected fayalitic and kirschsteinitic slag inclusions in the opaque red samples from Eriswell. Data are taken from area analyses of slag inclusions (Table 5.2.4).

5.2.3.1.1. Fayalitic Slag

The main phase of the slag inclusions in the majority of samples corresponds to the mineral fayalite (Fe_2SiO_4), as confirmed by spot analysis of the individual phases (Table 5.2.5). Area analysis also shows a primarily fayalitic composition (Table 5.2.4). Wüstite (FeO) was identified as a major constituent of these slags, forming as large irregular grains and coarse dendrites (*e.g.* Figures 5.2.49, 5.2.51-5.2.54 and 5.2.56-5.2.61). Its presence was established by a combination of textural observations and by comparing the elemental oxygen concentrations (*i.e.* oxygen was analysed for instead of calculated by stoichiometry) between the iron phases in the kirschsteinitic and fayalitic slags.

Table 5.2.5 – Selected SEM-EDS spot analyses of the phases within the fayalitic slag inclusions observed in several of the opaque red samples from Eriswell.

Sample ¹	Oxide (wt %) ²														
	Na ₂ O	MgO	Al ₂ O ₃	SiO ₂	P ₂ O ₅	SO ₃	K ₂ O	CaO	TiO ₂	MnO	Fe ₂ O ₃	FeO	CuO	BaO	PbO
<i>Fayalite</i>	-	-	-	29.5	-	-	-	-	-	-	-	70.5	-	-	-
ERL046:G03:1271	b.d.	0.7	0.6	25.6	0.9	b.d.	b.d.	b.d.	b.d.	1.8	69.5	(62.6)	b.d.	b.d.	b.d.
ERL046:G03:1322	b.d.	0.5	b.d.	27.0	b.d.	b.d.	b.d.	0.5	b.d.	b.d.	71.7	(64.5)	b.d.	b.d.	b.d.
ERL046:G08:1593	b.d.	0.7	0.1	27.1	0.5	0.1	b.d.	1.8	b.d.	b.d.	69.0	(62.1)	b.d.	b.d.	b.d.
ERL046:G38:1046	b.d.	0.5	0.2	26.7	b.d.	b.d.	b.d.	0.6	b.d.	b.d.	71.3	(64.2)	b.d.	b.d.	b.d.
ERL046:G38:1053	b.d.	0.3	b.d.	26.6	0.3	b.d.	b.d.	0.7	b.d.	0.2	72.5	(65.2)	b.d.	b.d.	b.d.
ERL046:G38:1063	0.1	0.8	b.d.	27.0	0.7	b.d.	b.d.	0.3	b.d.	2.9	67.5	(60.8)	0.2	0.3	b.d.
ERL046:G43:1726	b.d.	0.3	b.d.	26.6	0.3	b.d.	b.d.	1.2	b.d.	2.5	69.0	(62.1)	b.d.	b.d.	b.d.
ERL104:G148:2739	b.d.	0.3	b.d.	27.1	0.2	b.d.	b.d.	0.8	b.d.	0.5	70.5	(63.5)	b.d.	b.d.	b.d.
ERL104:G242:2153	b.d.	2.0	0.1	26.3	0.4	b.d.	b.d.	0.9	b.d.	0.2	69.8	(62.8)	0.2	0.2	b.d.
ERL104:G242:2158	b.d.	b.d.	0.2	27.0	0.2	0.1	b.d.	1.6	b.d.	b.d.	70.2	(63.2)	b.d.	b.d.	b.d.
ERL104:G242:2196	b.d.	1.2	b.d.	27.1	0.4	0.1	b.d.	1.0	b.d.	0.4	69.7	(62.7)	0.1	b.d.	b.d.
ERL104:G242:2203	b.d.	1.0	0.2	26.9	0.2	b.d.	b.d.	1.2	b.d.	0.5	69.6	(62.7)	0.1	b.d.	b.d.
ERL104:G242:2207	b.d.	0.5	0.6	26.0	0.9	b.d.	b.d.	0.4	b.d.	2.7	68.8	(61.9)	b.d.	b.d.	b.d.
ERL104:G242:2282	b.d.	2.3	b.d.	27.3	0.3	b.d.	b.d.	0.7	b.d.	0.5	68.1	(61.2)	0.3	b.d.	b.d.
ERL104:G242:2288	b.d.	1.2	0.5	26.5	0.7	b.d.	b.d.	0.8	b.d.	0.3	69.6	(62.6)	0.2	b.d.	b.d.
ERL104:G268:3258	b.d.	0.7	0.3	26.0	0.3	b.d.	b.d.	0.2	b.d.	b.d.	71.7	(64.5)	b.d.	b.d.	b.d.
ERL114:G413:1498	b.d.	1.2	0.3	26.2	0.8	b.d.	b.d.	0.4	b.d.	1.1	69.5	(62.5)	b.d.	b.d.	b.d.
ERL114:G422:1420	b.d.	0.6	0.2	26.5	0.8	b.d.	b.d.	b.d.	b.d.	2.1	69.2	(62.2)	b.d.	b.d.	b.d.

Table 5.2.5 – (continued).

Sample ¹	Oxide (wt %) ²														
	Na ₂ O	MgO	Al ₂ O ₃	SiO ₂	P ₂ O ₅	SO ₃	K ₂ O	CaO	TiO ₂	MnO	Fe ₂ O ₃	FeO	CuO	BaO	PbO
<i>Hercynite</i>	-	-	58.7	-	-	-	-	-	-	-	-	41.3	-	-	-
ERL046:G03:1271	0.1	b.d.	42.7	0.8	0.5	b.d.	b.d.	b.d.	0.7	0.5	54.6	(49.1)	b.d.	b.d.	b.d.
ERL104:G148:2743	b.d.	0.1	47.6	0.6	b.d.	b.d.	b.d.	b.d.	0.4	0.7	49.6	(44.7)	0.2	b.d.	b.d.
ERL104:G242:2158	b.d.	b.d.	43.6	1.0	b.d.	b.d.	b.d.	0.2	0.8	0.2	53.5	(48.2)	b.d.	b.d.	b.d.
ERL104:G305:1820	b.d.	0.1	42.6	0.8	0.2	b.d.	b.d.	b.d.	0.9	0.6	54.5	(49.0)	b.d.	b.d.	b.d.
ERL104:G315:2345	0.2	b.d.	40.9	1.0	b.d.	b.d.	b.d.	b.d.	1.6	0.2	55.8	(50.2)	b.d.	b.d.	b.d.
<i>Leucite</i>	-	-	23.4	55.1	-	-	21.6	-	-	-	-	-	-	-	-
ERL046:G03:1303	5.1	b.d.	24.3	56.1	0.1	0.1	13.2	b.d.	b.d.	b.d.	0.3	-	b.d.	0.2	b.d.
ERL046:G43:1721	4.4	b.d.	18.9	63.6	0.2	0.2	10.9	b.d.	0.1	b.d.	0.2	-	b.d.	0.1	b.d.
ERL104:G242:2158	5.9	b.d.	23.3	53.6	0.3	b.d.	11.9	0.2	0.2	b.d.	4.1	-	0.2	0.2	b.d.
ERL104:G242:2196	2.8	b.d.	23.0	53.9	0.4	b.d.	15.8	0.3	b.d.	b.d.	3.0	-	0.1	b.d.	b.d.
<i>Nepheline</i>	15.9	-	34.9	41.1	-	-	8.1	-	-	-	-	-	-	-	-
ERL104:G148:2735	15.2	b.d.	23.0	42.4	3.7	0.6	0.7	3.3	b.d.	b.d.	9.9	-	0.5	b.d.	0.6
ERL104:G148:2743	18.4	0.2	33.9	42.3	0.1	b.d.	1.7	0.3	b.d.	b.d.	0.7	-	0.4	b.d.	2.2
ERL104:G315:2346	14.0	0.2	22.0	53.4	0.3	0.3	2.3	0.5	b.d.	b.d.	5.0	-	0.5	b.d.	0.9
<i>Interstitial Glass</i>															
ERL046:G03:1271	9.4	0.3	1.1	56.2	3.0	0.4	1.1	0.5	0.1	1.2	24.9	-	0.8	b.d.	0.5
ERL046:G03:1271	16.2	0.1	18.6	31.8	13.0	0.4	0.4	1.1	0.1	0.7	16.4	-	0.1	0.6	b.d.
ERL046:G03:1276	12.5	0.5	4.2	50.9	1.5	b.d.	0.9	3.1	0.1	0.4	23.4	-	b.d.	b.d.	2.2
ERL046:G03:1322	6.8	b.d.	7.6	48.1	1.4	0.1	0.8	6.6	0.5	b.d.	27.3	-	0.2	b.d.	0.3
ERL046:G03:1322	5.3	0.7	b.d.	45.8	0.1	b.d.	b.d.	11.5	b.d.	0.3	36.1	-	b.d.	b.d.	b.d.

Table 5.2.5 – (continued).

Sample ¹	Oxide (wt %) ²														
	Na ₂ O	MgO	Al ₂ O ₃	SiO ₂	P ₂ O ₅	SO ₃	K ₂ O	CaO	TiO ₂	MnO	Fe ₂ O ₃	FeO	CuO	BaO	PbO
ERL046:G05:1431	4.8	0.5	0.2	46.6	0.3	b.d.	b.d.	12.9	b.d.	0.1	32.9	-	0.1	b.d.	0.5
ERL046:G38:1046	3.5	b.d.	11.0	43.3	1.0	0.3	1.9	9.3	0.6	b.d.	29.1	-	b.d.	0.1	b.d.
ERL046:G38:1063	7.7	0.2	14.9	44.8	5.5	0.4	1.2	4.2	1.0	0.5	17.1	-	1.1	b.d.	1.8
ERL046:G43:1726	9.3	0.3	0.4	48.0	0.3	0.2	b.d.	5.9	b.d.	1.3	34.2	-	0.2	b.d.	b.d.
ERL046:G43:1726	11.3	b.d.	1.6	48.9	0.8	b.d.	0.2	4.3	b.d.	0.8	29.8	-	0.3	0.2	2.0
ERL104:G144:2599	7.5	3.6	0.5	43.4	0.4	b.d.	b.d.	6.8	b.d.	0.4	35.5	-	0.2	0.1	1.1
ERL104:G148:2739	5.5	0.1	0.2	44.3	0.4	0.1	0.7	1.6	b.d.	0.4	45.7	-	0.3	0.2	b.d.
ERL104:G182:3535	6.9	0.9	0.7	47.3	0.4	b.d.	b.d.	10.9	0.1	0.3	32.0	-	0.1	b.d.	b.d.
ERL104:G195:1346	9.5	2.0	0.1	50.2	0.1	0.1	b.d.	5.7	b.d.	b.d.	31.9	-	b.d.	b.d.	b.d.
ERL104:G242:2153	10.3	1.8	1.0	53.3	1.3	b.d.	0.4	2.8	b.d.	0.1	29.3	-	0.3	b.d.	b.d.
ERL104:G242:2154	10.4	0.4	0.7	52.4	0.6	0.3	0.6	3.5	b.d.	b.d.	28.7	-	0.3	0.1	1.0
ERL104:G242:2158	1.1	0.1	0.6	70.1	0.1	0.1	0.2	0.9	b.d.	0.1	26.0	-	0.1	b.d.	b.d.
ERL104:G242:2158	12.3	b.d.	5.2	47.5	1.2	0.3	0.6	3.9	0.1	0.3	23.3	-	0.2	0.8	3.2
ERL104:G242:2164	10.1	0.1	1.5	54.7	0.8	0.1	0.7	3.7	b.d.	b.d.	27.1	-	0.4	b.d.	b.d.
ERL104:G242:2207	8.1	0.3	2.8	55.6	0.7	0.2	0.9	1.5	b.d.	2.0	24.7	-	1.4	0.2	1.1
ERL104:G242:2207	8.8	b.d.	17.9	40.9	6.7	0.3	1.3	4.1	1.2	0.5	15.3	-	2.4	b.d.	0.5
ERL104:G242:2207	7.4	b.d.	17.8	39.3	6.2	0.4	1.2	7.7	1.1	0.8	18.7	-	0.1	b.d.	b.d.
ERL104:G268:3256	14.6	0.1	18.4	31.2	8.3	1.2	0.3	6.0	0.4	0.2	17.3	-	2.2	b.d.	b.d.
ERL104:G268:3258	6.1	0.8	0.4	43.8	0.2	b.d.	b.d.	7.8	b.d.	0.4	40.5	-	b.d.	0.1	0.8
ERL104:G268:3258	9.3	0.4	3.8	55.9	0.6	b.d.	1.2	0.9	b.d.	0.4	21.3	-	0.3	b.d.	5.5
ERL104:G305:1875	9.1	1.5	1.5	46.2	0.5	0.2	b.d.	8.8	0.3	1.1	30.8	-	b.d.	b.d.	0.3
ERL104:G315:2345	10.8	0.8	0.7	48.8	0.6	b.d.	b.d.	4.1	b.d.	b.d.	32.7	-	b.d.	0.2	1.1
ERL104:G315:2346	4.5	0.2	1.2	31.2	0.7	b.d.	0.4	0.9	0.1	0.1	56.5	-	3.1	b.d.	0.4
ERL104:G362:1961	9.3	1.0	0.4	45.2	0.4	b.d.	b.d.	5.6	0.1	0.6	37.0	-	b.d.	b.d.	b.d.

Table 5.2.5 – (continued).

Sample ¹	Oxide (wt %) ²														
	<i>Na₂O</i>	<i>MgO</i>	<i>Al₂O₃</i>	<i>SiO₂</i>	<i>P₂O₅</i>	<i>SO₃</i>	<i>K₂O</i>	<i>CaO</i>	<i>TiO₂</i>	<i>MnO</i>	<i>Fe₂O₃</i>	<i>FeO</i>	<i>CuO</i>	<i>BaO</i>	<i>PbO</i>
ERL104:G362:1961	8.9	0.4	1.2	39.7	1.7	b.d.	b.d.	4.1	0.1	0.5	38.0	-	1.6	b.d.	3.3
ERL104:G367:3619	7.2	2.4	0.6	44.2	0.7	b.d.	b.d.	9.2	b.d.	0.4	34.4	-	b.d.	0.2	b.d.
ERL104:G367:3619	6.6	1.2	2.4	55.4	1.8	0.2	1.0	1.0	b.d.	0.8	28.0	-	0.4	b.d.	0.4
ERL104:G367:3619	10.4	b.d.	8.3	26.7	12.3	0.5	0.6	12.1	b.d.	0.2	21.3	-	4.7	0.2	2.1
ERL114:G413:1495	9.7	0.7	3.5	45.3	1.3	0.5	0.4	8.6	0.1	0.3	22.6	-	1.0	b.d.	5.7
ERL114:G413:1498	8.6	0.9	1.9	48.0	1.5	0.1	0.4	4.1	b.d.	0.6	33.1	-	b.d.	b.d.	0.3
ERL114:G422:1420	10.1	0.2	14.9	45.4	4.5	0.1	1.1	1.1	0.4	0.8	20.8	-	0.4	b.d.	b.d.
ERL114:G422:1420	9.0	1.5	0.1	47.1	0.9	b.d.	b.d.	3.0	b.d.	2.3	35.4	-	0.2	0.1	b.d.
ERL114:G422:1420	9.8	0.6	0.4	47.6	1.1	b.d.	0.3	2.2	b.d.	1.2	35.8	-	b.d.	b.d.	b.d.

¹Repeated sample numbers represent spot analyses of different areas of the same sample. Theoretical compositions for fayalite (Fe₂SiO₄), hercynite (FeAl₂O₄), leucite (KAlSi₂O₆) and nepheline (Na₃KAl₄Si₄O₁₆) are in *italics*.

²Spot analyses normalised to 100%. b.d. = below detection. See Chapter 2, section 2.3.1 for details. Values in brackets represent hypothetical FeO values.

Many of the slag particles are characterised by fine feathery intergrowths of calcic-fayalite in a groundmass of glass (*e.g.* Figures 5.2.49-5.2.53, 5.2.55-5.2.57 and 5.2.59-5.2.61), compositionally falling between fayalite (Fe_2SiO_4) and kirschsteinite (CaFeSiO_4) (Sharp and Mittwede 2011: 331-333). A number of other minor phases were also identified, corresponding to either hercynite (FeAl_2O_4), leucite (KAlSi_2O_6) or nepheline ($\text{Na}_3\text{KAl}_4\text{Si}_4\text{O}_{16}$) (Table 5.2.5). Furthermore, complex silicate glass phases were present in many of these slag particles (*e.g.* Figures 5.2.49-5.2.60), typically consisting of the oxides of iron and silicon, together with variable amounts of soda, phosphate, lime and alumina (Table 5.2.5). However, their composition is very inconsistent, even within the same sample.

The complex and fine-grained microstructure of the slag inclusions meant that it was difficult to determine the composition of the interstitial glass. Whilst copper was not generally present in any significant quantity in the majority of these phases, some were found to contain high levels. In several samples (Table 5.2.5; *e.g.* samples ERL104:G268:3256, ERL104:G315:2346, ERL104:G362:1961 and ERL104:G367:3619) the CuO levels detected in the interstitial glass exceed the levels colouring the surrounding soda-lime-silica glass matrix. However, in many cases copper was not consistently present throughout the same slag particle (Table 5.2.5; *e.g.* samples ERL046:G03:1271, ERL104:G242:2207, ERL104:G362:1961 and ERL104:G367:3619). Furthermore, area analysis of the slag shows that copper is not present in a significant quantity (Table 5.2.4).

Magnesia and potash are not generally present in any significant quantity (Table 5.2.4), with the exception of a small number of potassium-rich phases corresponding to leucite (KAlSi_2O_6) in a limited number of slag inclusions (Table 5.2.5). The high soda levels typically present in the interstitial glass (Table 5.2.5) are unusual, and are not typically seen in fayalitic slag; they are likely to reflect considerable contamination from the surrounding soda-lime-silica glass. The high PbO content in the bulk analyses of some of these slag inclusions (Table 5.2.4, *e.g.* samples ERL046:G43:1721 and ERL104:G107:1141, ERL104:G305:1820, ERL104:G362:1961 and ERL104:G363:1912) also results from contamination from the surrounding glass; it is therefore possible that the concentration of copper was influenced by contamination from the surrounding copper-rich glass.

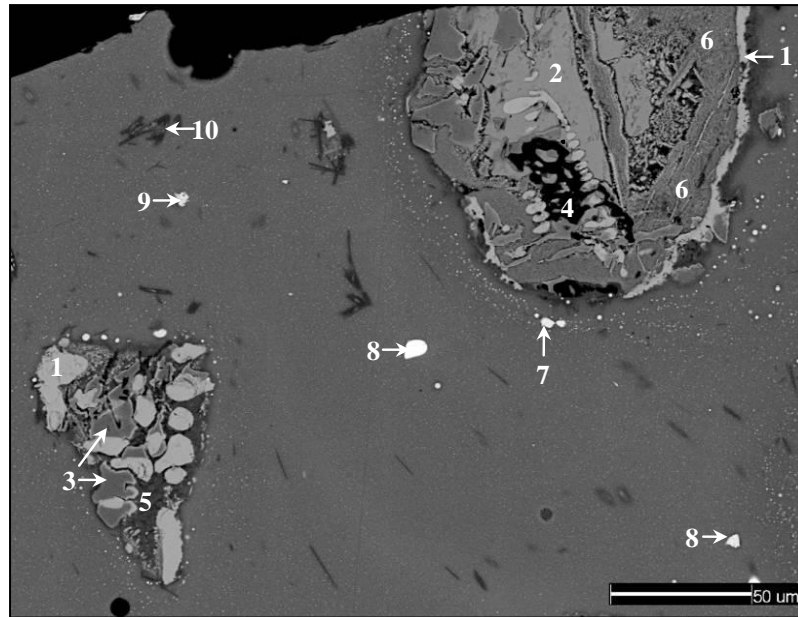


Figure 5.2.49 – BSE micrograph of sample ERL104:G242:2158, a *Traffic Light Twisted Trail* bead, showing fayalitic slag inclusions in an opaque red glass matrix coloured by metallic copper nanoparticles. The slag primarily consists of irregular grains of wüstite (1), together with fayalite (2), hercynite (3), leucite (4) and interstitial glass (5). The ‘feathery’ phases (6) are fayalitic intergrowths containing elevated levels of sodium and calcium. Large bright metallic copper particles are visible surrounding the slag (7), together with sparse crystals of lead-tin oxide (8) and tin oxide (9). The dark acicular crystals are calcium silicate, corresponding to the mineral wollastonite (CaSiO_3) (10).

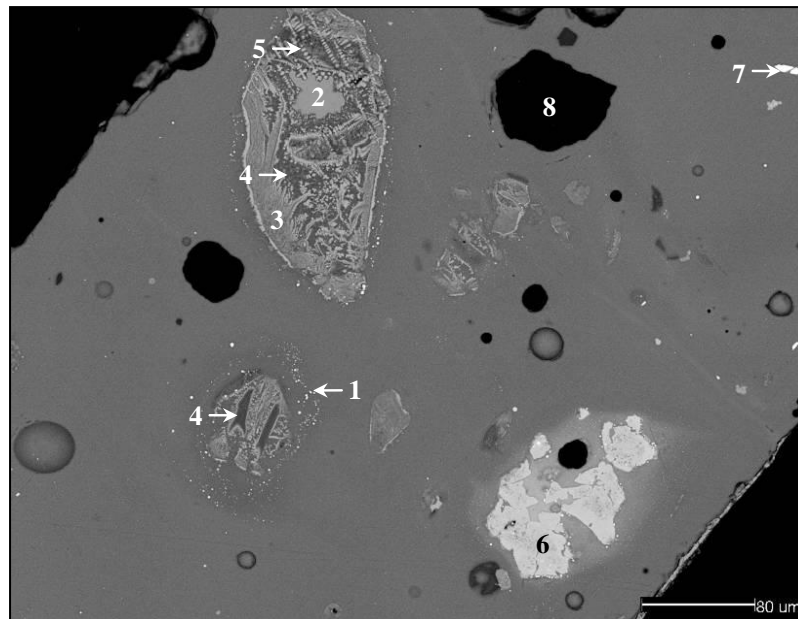


Figure 5.2.50 – BSE micrograph of sample ERL104:G242:2207, a *Red Globular* bead, showing inclusions of fayalitic slag in an opaque red glass matrix coloured by metallic copper nanoparticles. Several metallic copper particles (1) can be seen surrounding these inclusions. The slag particles primarily consist of solid phases of fayalite (2) and fayalitic intergrowths (3), interstitial glass (4) and dendritic iron oxide (5). An angular inclusion rich in iron and copper (6), and sparse lead-tin oxide crystals are also visible (7). The black areas (8) represent voids.

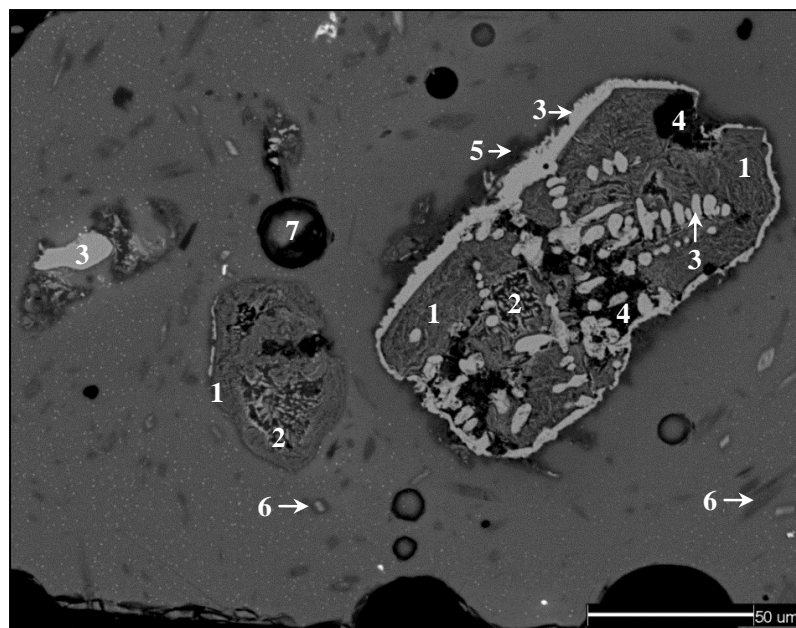


Figure 5.2.51 – BSE micrograph of sample ERL104:G362:1961 & 1969, a *Traffic Light Twisted Trail* bead, showing fayalitic slag inclusions in an opaque red glass matrix coloured by metallic copper nanoparticles. The main phase of the slag primarily consists of fayalite with containing slightly elevated levels of sodium and calcium (1), fayalitic intergrowths (2) and irregular dendrites or grains of wüstite (3). The black phases (4) represent interstitial glass. The dark grey areas surrounding the slag (5) are soda-lime-silica glass containing elevated levels of iron. Several irregular calcium silicate crystals, corresponding to the mineral wollastonite (CaSiO_3) (6), and bubbles (7) are also visible.

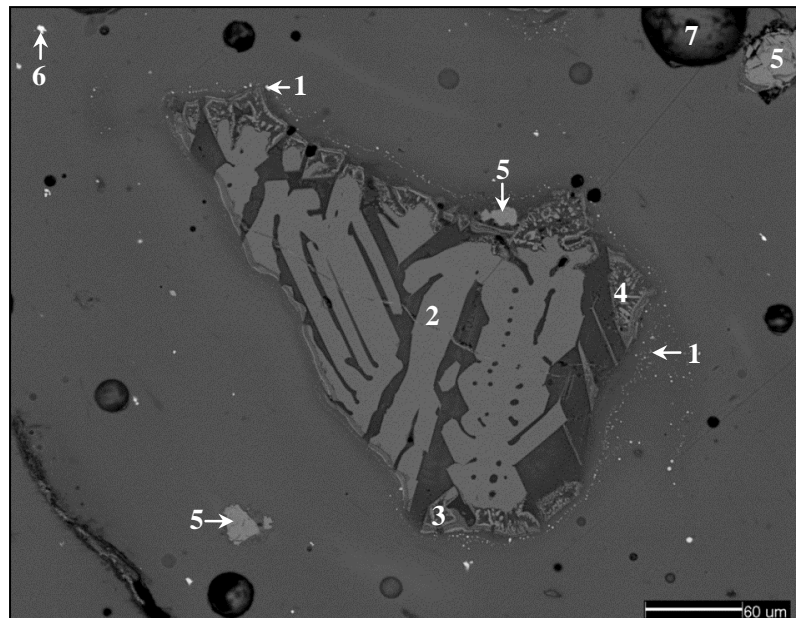


Figure 5.2.52 – BSE micrograph of sample ERL046:G38:1046, a *Red Cylindrical* bead, showing a fayalitic slag inclusion in an opaque red glass matrix coloured by metallic copper nanoparticles. Several bright metallic copper particles can be seen surrounding this inclusion (1). The slag primarily consists of solid phases of fayalite (2) and interstitial glass (3), with fayalitic intergrowths at the periphery (4). Several minor iron oxide phases (5) and sparsely distributed lead-tin oxide crystals (6) can also be seen. A few bubbles are also present (7).

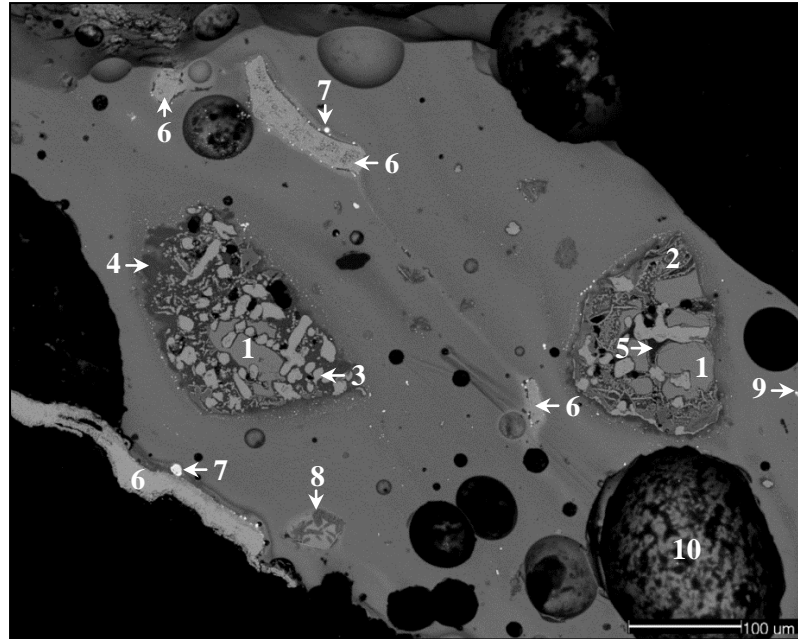


Figure 5.2.53 – BSE micrograph of sample ERL046:G03:1271, a *RedPoly6* bead, showing two large fayalitic slag inclusions in an opaque red glass matrix coloured by metallic copper nanoparticles. The slag primarily consists of fayalite (1) and fayalitic intergrowths (2) containing elevated levels of sodium. Irregular grains and dendrites of wüstite (3) and phases of interstitial glass (4) are also visible. The black phases (5) are sodium aluminium silicate rich in iron and phosphate. Fragments of iron oxide scale (6), around which several large metallic copper particles (7) have precipitated, can also be seen. A small number of acicular calcium silicate crystals (8), occasional bright lead-tin oxide crystals (9) and several large bubbles (10) are also present.

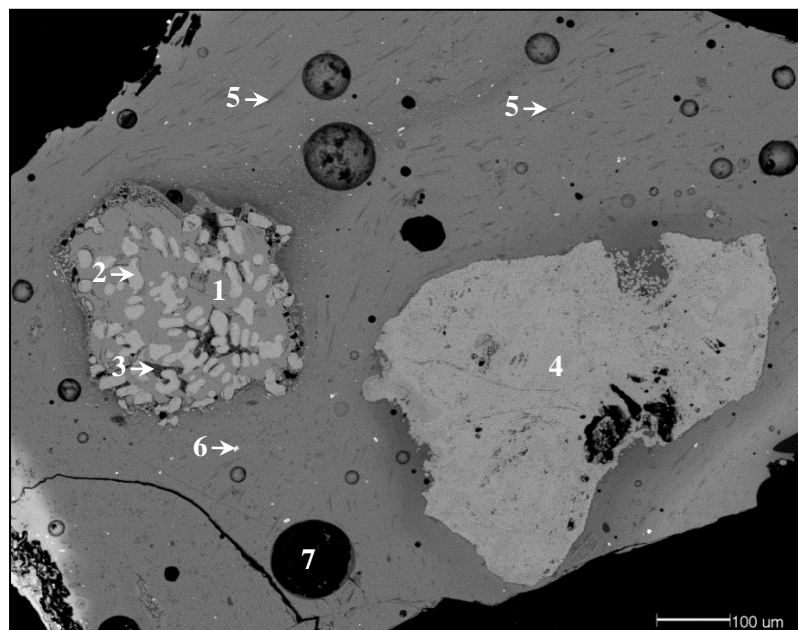


Figure 5.2.54 – BSE micrograph of sample ERL046:G38:1053, a *Traffic Light Twisted Trail* bead, showing a fayalitic slag inclusion in an opaque red glass matrix coloured by metallic copper nanoparticles. The main phase of the slag corresponds to fayalite (1). Numerous grains and dendrites of wüstite (2) are also visible, together with interstitial glass (3). A large particle of iron oxide (4) can be seen. Within the glass matrix, numerous acicular calcium silicate crystals, corresponding to the mineral wollastonite (CaSiO_3) (5) are present, together with sparse crystals of lead-tin oxide (6). Several bubbles (7) are also present.

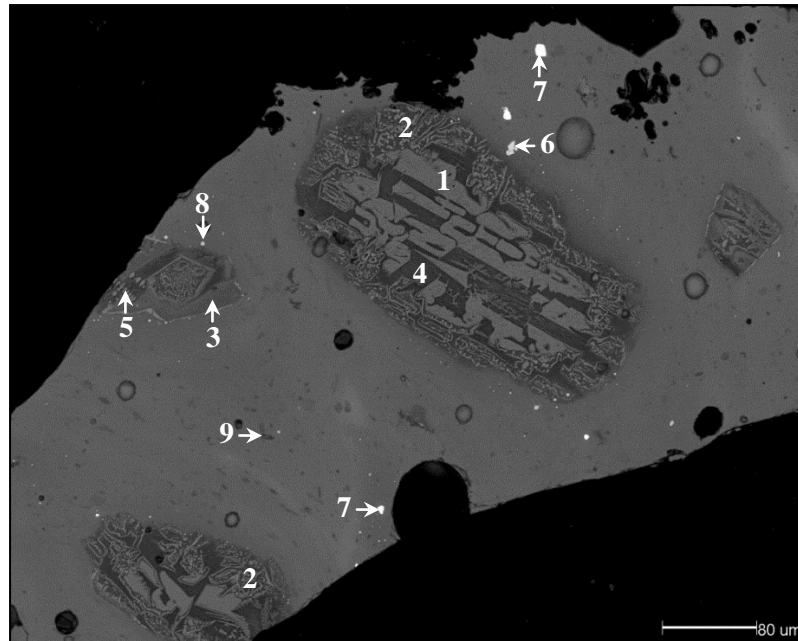


Figure 5.2.55 – BSE micrograph of sample ERL046:G38:1063, a *RedPoly6* bead, showing fayalitic slag inclusions in an opaque red glass matrix coloured by metallic copper nanoparticles. The slag primarily consists of fayalite (1), fayalitic intergrowths (2), and calcic fayalite (3), together with interstitial glass (4). Wüstite is also present as coarse grains and dendrites (5). Several large crystals of tin oxide (6), lead-tin oxide (7) and metallic copper (8) are visible. Irregular calcium silicate crystals, corresponding to the mineral wollastonite (CaSiO_3) (9) can also be seen within the glass matrix.

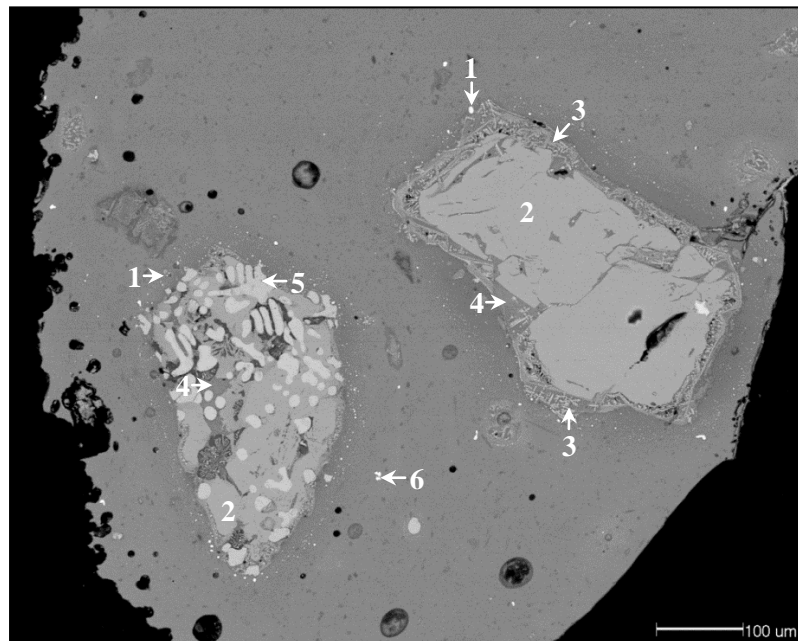


Figure 5.2.56 – BSE micrograph of sample ERL104:G242:2196, a *Traffic Light Streaked* bead, showing fayalitic slag inclusions in an opaque red glass matrix coloured by metallic copper nanoparticles. Several large particles of metallic copper (1) are visible immediately surrounding the slag. The slag primarily consists of fayalite (2) and fayalitic intergrowths (3), together with interstitial glass (4) and irregular grains or dendrites of wüstite (5). A small number of lead-tin oxide crystals (6) and several small bubbles are also visible.

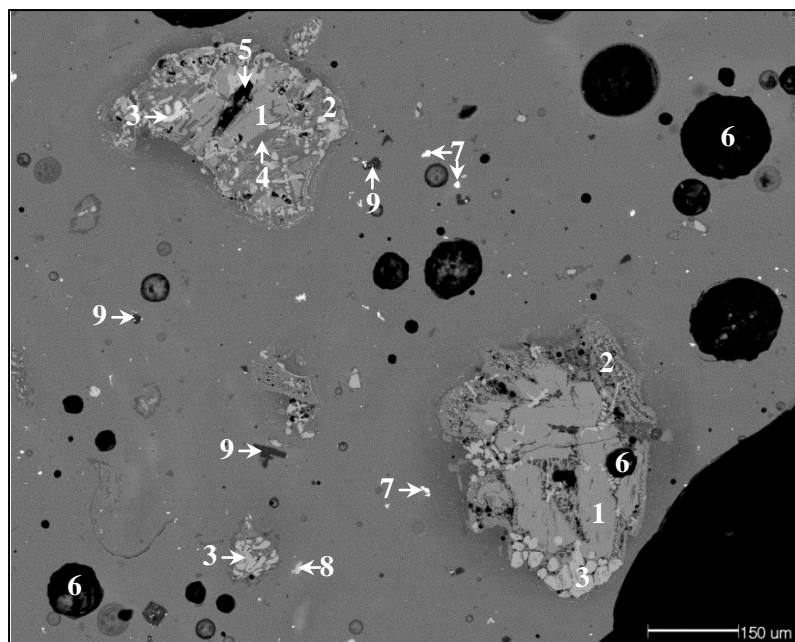


Figure 5.2.57 – BSE micrograph of sample ERL104:G268:3257, a *Traffic Light Imitation* bead, showing complex fayalitic slag inclusions in an opaque red glass matrix coloured by metallic copper nanoparticles. The main phase of the slag corresponds to fayalite (1). Fayalitic intergrowths (2) and irregular grains or dendrites of wüstite (3) are also present, together with interstitial glass (4). The black phases correspond to leucite (5), but other black areas represent bubbles or voids (6). Sparse lead-tin oxide crystals (7), tin oxide crystals (8) and nepheline inclusions (9) can also be seen. The glass immediately surrounding the slag appears darker due to the elevated levels of iron in these regions. Large copper oxide particles are also present here, but are difficult to resolve in the BSE micrograph.

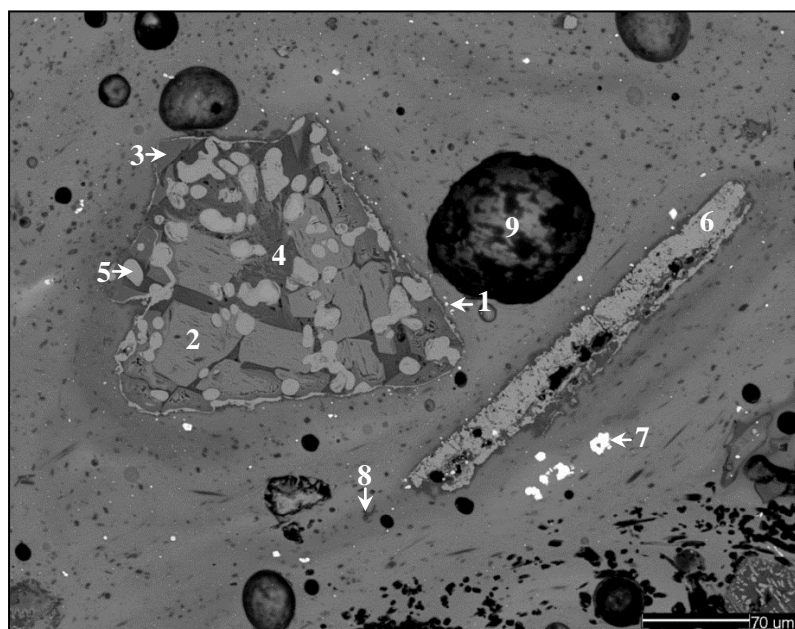


Figure 5.2.58 – BSE micrograph of sample ERL046:G43:1726, a *RedPoly5* bead, showing fayalitic slag inclusions in an opaque red glass matrix coloured by metallic copper nanoparticles. Several metallic copper particles (1) are visible surrounding these slag particles, due to their larger sizes in these regions. The slag primarily consists of fayalite (2), fayalite enriched in sodium (3), interstitial glass (4) and irregular grains of wüstite (5). A large fragment of iron oxide scale is also present (6). Several crystals of lead-tin oxide (7) and calcium silicate, corresponding to the mineral wollastonite (CaSiO_3) (8) can be seen. The black areas represent voids and bubbles (9).

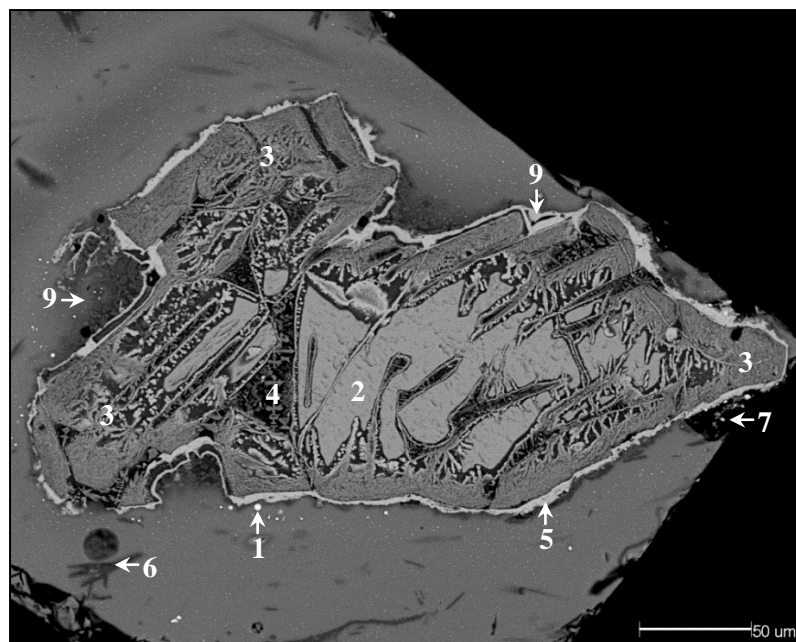


Figure 5.2.59 – BSE micrograph of sample ERL114:G422:1420, a *Norfolk YellowRed* bead, showing a fayalitic slag inclusion in an opaque red glass matrix coloured by metallic copper nanoparticles. Several metallic copper particles (1) can be seen surrounding the slag, due to their larger size in these regions. The slag primarily consists of fayalite (2) and ‘feathery’ fayalitic intergrowths (3) containing elevated levels of sodium and calcium. Interstitial glass (4) and wüstite rims (5) are also present. The glass contains several acicular calcium silicate crystals, corresponding to the mineral wollastonite (CaSiO_3) (6), and a nepheline inclusion (7) associated with bright white lead-tin oxide crystals. The glass immediately surrounding the slag sometimes appears darker (8) due to elevated levels of iron and calcium in these regions.

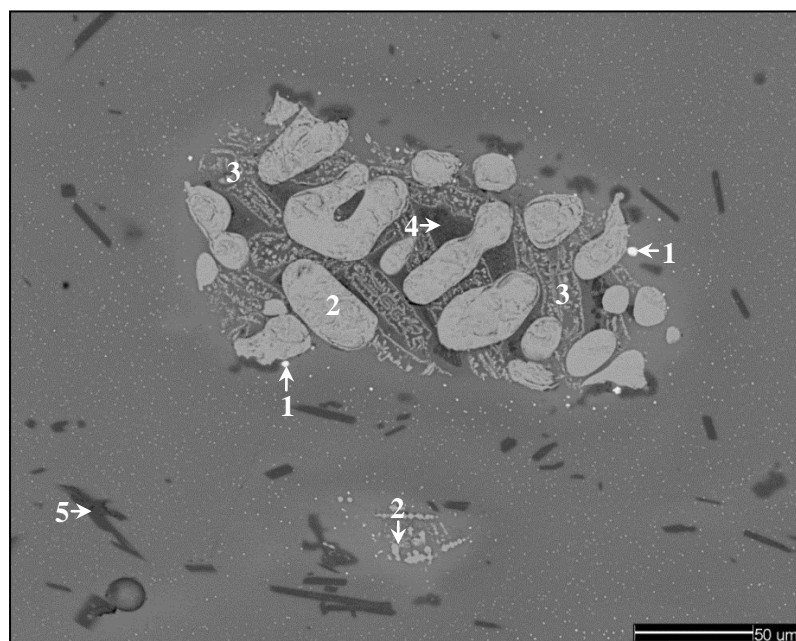


Figure 5.2.60 – BSE micrograph of sample ERL104:G107:1141, a *Koch34* bead, showing a fayalitic slag inclusion in an opaque red glass matrix coloured by metallic copper nanoparticles. Several metallic copper particles (1) are visible immediately surrounding the slag. The slag primarily consists of irregular grains of wüstite (2) and fayalitic intergrowths (3) enriched in sodium and aluminium, together with interstitial glass (4). Within the glass matrix several dark grey acicular crystals of calcium silicate, corresponding to the mineral wollastonite (CaSiO_3) (5) can also be seen.

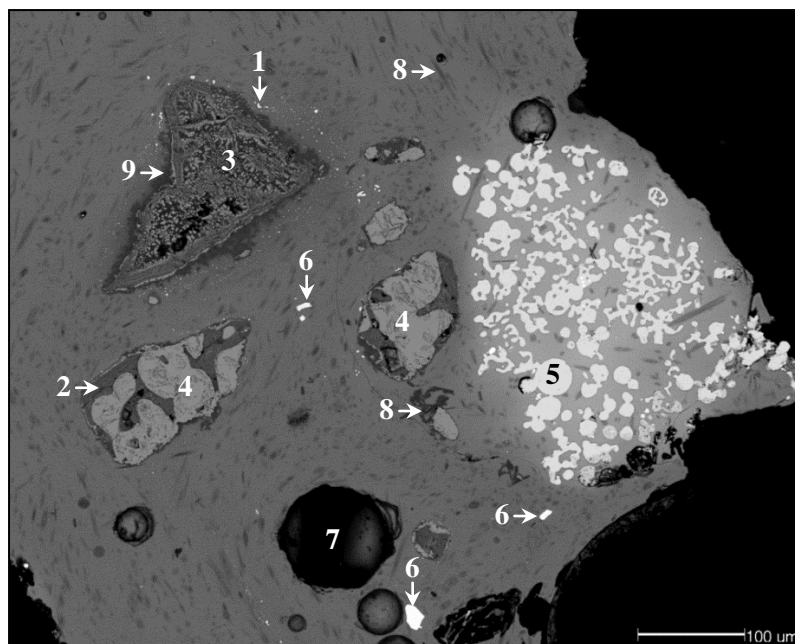


Figure 5.2.61 – BSE micrograph of sample ERL104:G315:2346, a *Traffic Light Twisted Trail* bead, showing fayalitic slag inclusions in an opaque red glass matrix coloured by metallic copper nanoparticles. Several metallic copper particles (1) are visible immediately surrounding the slag inclusions due to their larger sizes in these regions. The slag primarily consists of calcic fayalite enriched in sodium (2) and fayalitic intergrowths (3), together with irregular grains of wüstite (4). A large agglomerate of metallic copper (5) is visible, containing approximately 4% silver oxide. A number of lead-tin oxide crystals (6) and several large bubbles (7) can also be seen. Numerous acicular calcium silicate crystals, corresponding to the mineral wollastonite (CaSiO_3) (8) are present. The glass immediately surrounding the slag sometimes appears darker (9) due to the elevated levels of iron and calcium in these regions.

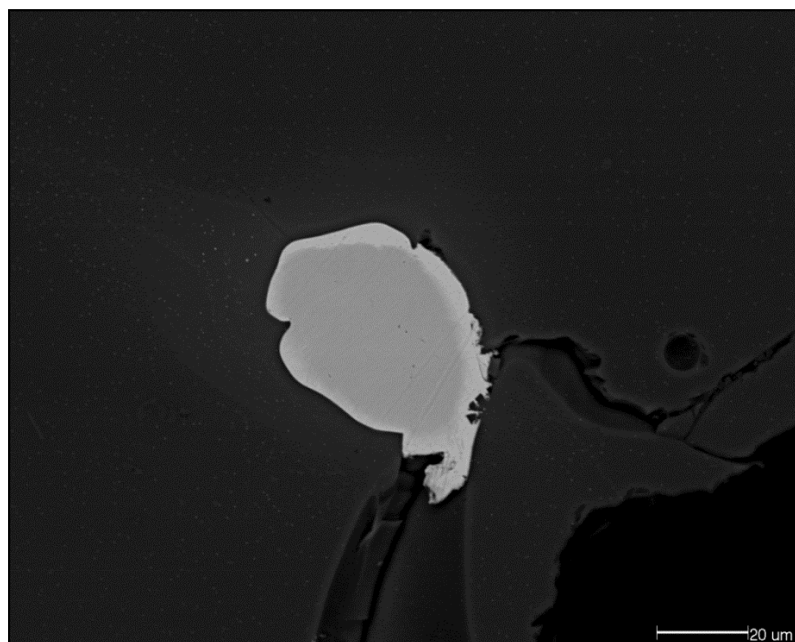


Figure 5.2.62 – BSE micrograph of sample ERL104:G193:1311, a *Koch34* bead, showing a lump of an iron-copper alloy in an opaque red glass matrix coloured by metallic copper nanoparticles. The core of this inclusion (darker grey) is metallic iron, whereas the rim (paler grey) is metallic copper containing approximately 3% iron.

Other notable features include a large copper-rich inclusion in sample ERL104:G242:2207 (Figure 5.2.50), containing 43.3% metallic copper and 50.2% iron oxide, together with minor amounts of alumina and tin oxide; this inclusion is not associated with fayalite so it cannot be confirmed that it was introduced with the slag. A grain of metallic copper-iron alloy was also observed in sample ERL104:G193:1311 (Figure 5.2.62), and an agglomerate of metallic copper particles in sample ERL104:G315:2346, which contain approximately 4% silver (Figure 5.2.61). However, again this is not associated with the slag.

5.2.3.1.2. Kirschsteinitic Slag

Samples ERL104:G281:1795 (a *Red Globular* bead) and ERL104:G268:3260 (a *Candy Variant* bead) are unusual in that they contain slag in which fayalite is absent (Figures 5.2.63-5.2.66). The main phase instead corresponds to kirschsteinite (CaFeSiO_4), an orthosilicate (olivine-type) mineral characterised by high amounts of the oxides of silicon, iron and calcium (Table 5.2.6). The form in which the iron oxides are present is different to those normally observed in the fayalitic slags. Fine dendritic crystals of magnetite (Fe_3O_4) (identified by spot analysis) are clearly visible (*e.g.* Figures 5.2.63, 5.2.65 and 5.2.66), in contrast to the irregular grains and coarse dendrites of wüstite (FeO) typically present in the fayalitic slags (*e.g.* Figures 5.2.49, 5.2.51-5.2.54 and 5.2.56-5.2.61). As with the identification of wüstite in the fayalitic slags, the presence of magnetite was confirmed by a combination of textural observations and by analysing for elemental oxygen.

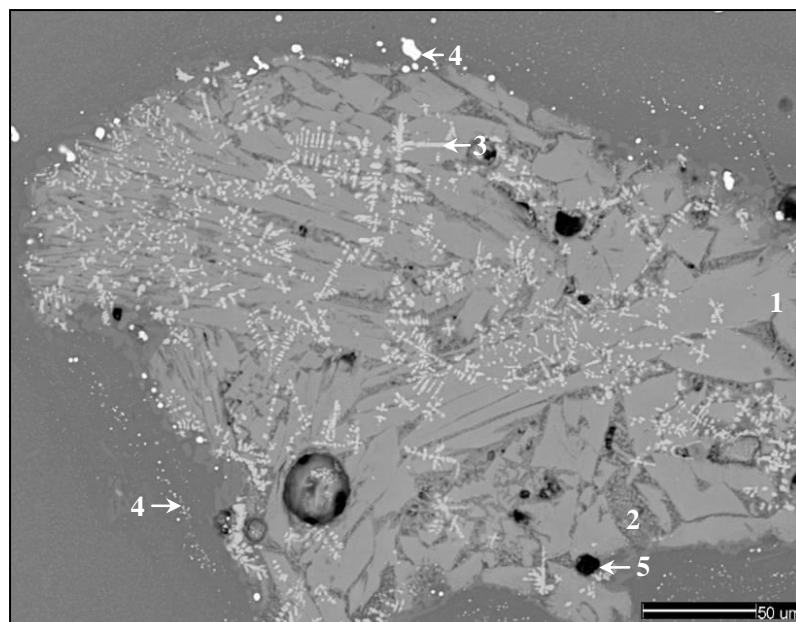


Figure 5.2.63 – BSE micrograph of sample ERL104:G281:1795, a *Red Globular* bead, showing a large kirschsteinitic slag inclusion in an opaque red glass matrix coloured by metallic copper nanoparticles. The main phase of the slag corresponds to kirschsteinite (1). Interstitial glass (2), a number of dendritic magnetite crystals (3), and zones of bright white copper particles surrounding the inclusion (4) are also present. The black areas (5) represent voids.

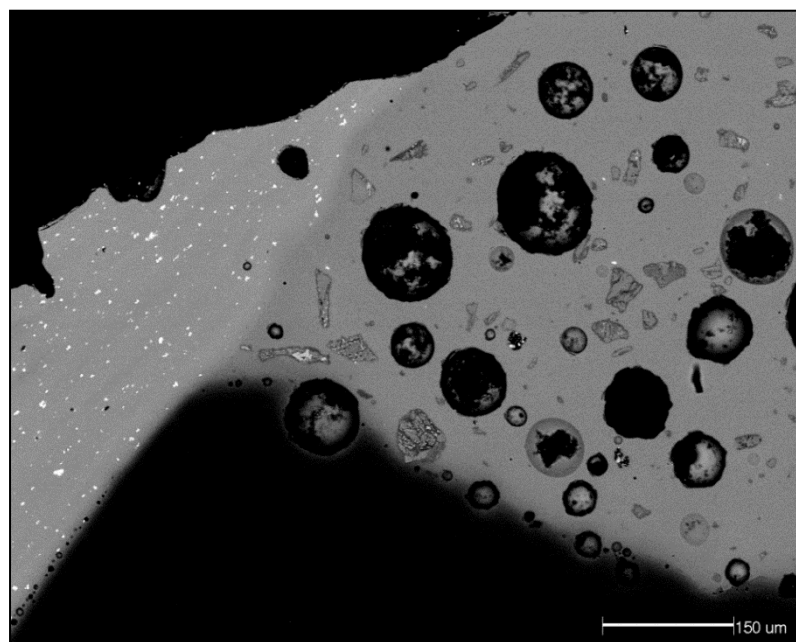


Figure 5.2.64 – BSE micrograph of sample ERL104:G268:3260, a *Candy Variant* bead, showing opaque yellow (left), opaque red (right) and translucent green-tinted (bottom) glass. The opaque yellow and red glasses (pale grey and grey respectively) appear brighter than the translucent green glass (black) due to the higher concentration of lead in these colours. The opaque yellow glass is both coloured and opacified by crystals of lead-tin oxide (white). The opaque red glass contains a high density of angular kirschsteinitic slag inclusions (grey) and large bubbles, but colour and opacity are primarily caused by nanoparticles of metallic copper which are too small to be resolved in the SEM.

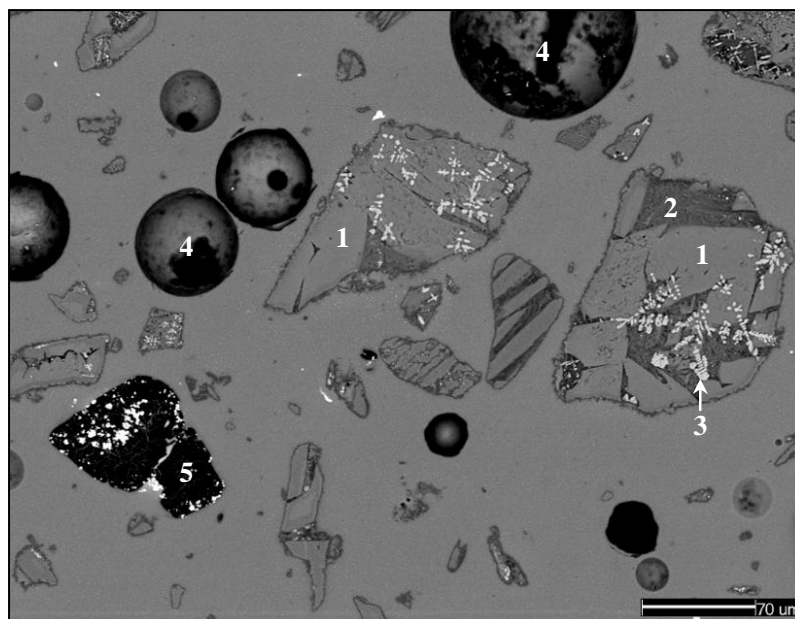


Figure 5.2.65 – BSE micrograph of sample ERL104:G268:3260, a *Candy Variant* bead, showing a high density of kirschsteinitic slag inclusions in an opaque red glass matrix coloured by metallic copper nanoparticles. The main phase of the slag corresponds to kirschsteinite (1). Interstitial glass (2) and dendritic crystals of magnetite (3) are present. A number of bubbles (4) and a large nepheline inclusion (5) containing bright white crystals of lead-tin oxide are also visible.

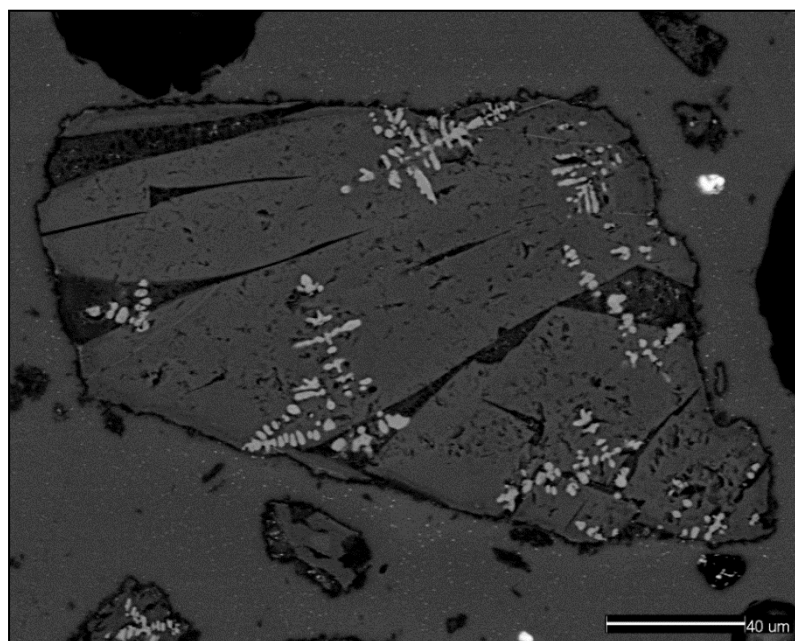


Figure 5.2.66 – BSE micrograph of sample ERL104:G268:3260, a *Candy Variant* bead, showing kirschsteinitic slag inclusions in an opaque red glass matrix coloured by copper nanoparticles. The main phase of the slag (grey) corresponds to kirschsteinite. Dendrites of magnetite (pale grey) and interstitial glass (dark grey) can also be seen. The sparse bright white particles in the surrounding soda-lime silica glass are crystals of lead-tin oxide.

Table 5.2.6 – Selected SEM-EDS spot analyses of the phases within the kirschsteinitic slag inclusions observed in several of the opaque red samples from Eriswell.

Sample ¹	Oxide (wt %) ²														
	Na ₂ O	MgO	Al ₂ O ₃	SiO ₂	P ₂ O ₅	SO ₃	K ₂ O	CaO	TiO ₂	MnO	Fe ₂ O ₃	FeO	CuO	BaO	PbO
<i>Kirschsteinite</i>	-	-	-	32.0	-	-	-	29.8	-	-	-	38.2	-	-	-
ERL104:G268:3260	0.1	1.2	b.d.	29.7	1.6	b.d.	b.d.	30.0	b.d.	0.7	35.7	(32.1)	b.d.	b.d.	0.2
ERL104:G268:3260	0.1	0.8	0.3	29.5	1.9	b.d.	b.d.	30.0	b.d.	0.7	37.5	(33.7)	0.2	b.d.	b.d.
ERL104:G268:3260	1.1	0.6	0.8	33.2	2.0	0.1	0.1	26.3	b.d.	0.7	34.6	(31.1)	b.d.	0.2	0.4
ERL104:G281:1795	0.1	3.2	0.1	29.9	1.7	b.d.	b.d.	28.9	b.d.	0.7	33.9	(30.5)	0.2	b.d.	b.d.
ERL104:G281:1795	0.2	3.0	0.2	29.9	1.9	b.d.	b.d.	28.5	b.d.	0.7	35.1	(31.6)	b.d.	b.d.	b.d.
<i>Interstitial Glass</i>															
ERL104:G268:3260	10.3	0.1	8.8	28.9	6.0	0.8	0.5	9.7	0.4	0.6	31.2	-	0.2	0.2	1.5
ERL104:G268:3260	6.2	0.2	5.8	38.1	4.2	1.2	0.3	26.0	0.3	0.4	13.9	-	2.7	0.2	0.6
ERL104:G268:3260	6.9	0.1	5.8	30.5	11.1	1.0	0.5	18.8	0.1	0.4	20.3	-	2.1	0.5	1.5
ERL104:G281:1795	1.6	1.3	6.6	42.5	1.0	b.d.	0.3	19.3	b.d.	0.4	25.9	-	0.2	0.1	b.d.
ERL104:G281:1795	0.4	0.6	21.5	25.4	3.6	0.2	1.6	19.5	0.9	0.4	25.8	-	0.1	0.2	b.d.
ERL104:G281:1795	4.0	0.4	12.9	37.3	2.4	0.2	2.0	14.2	0.6	0.3	25.2	-	0.4	b.d.	b.d.
ERL104:G281:1795	1.6	1.3	6.6	42.5	1.0	b.d.	0.3	19.3	b.d.	0.4	25.9	-	0.2	0.1	b.d.

¹Repeated sample numbers represent spot analyses of different areas of the same sample. Theoretical compositions for kirschsteinite (CaFeSiO₄) are in *italics*.

²Spot analyses normalised to 100%. b.d. = below detection. See Chapter 2, section 2.3.1 for details. Values in brackets represent hypothetical FeO values.

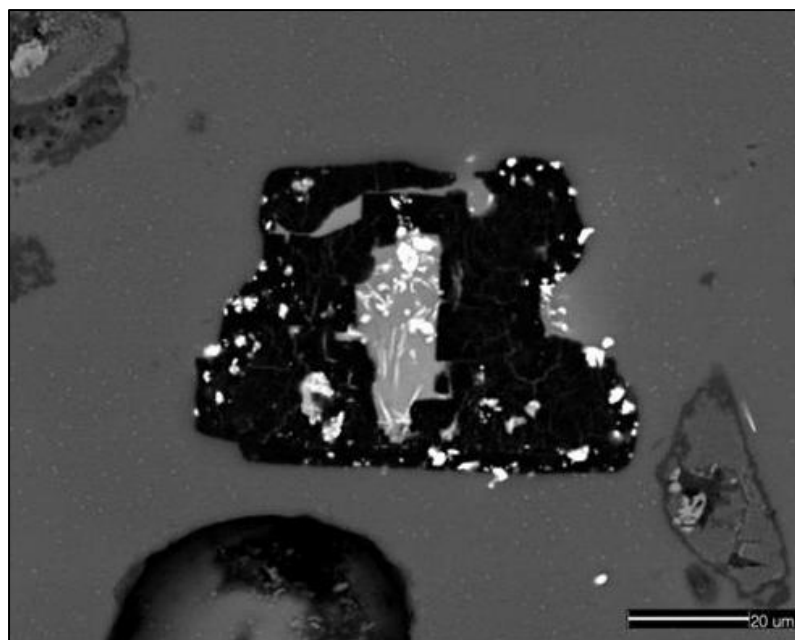


Figure 5.2.67 – BSE micrograph of sample ERL104:G268:3260, a *Candy Variant* bead, showing an opaque red glass matrix coloured and opacified by metallic copper nanoparticles. A large sodium aluminium silicate inclusion (black), corresponding to the mineral nepheline ($\text{Na}_3\text{KAl}_4\text{Si}_4\text{O}_{16}$), is visible. This is associated with numerous lead-tin oxide crystals (white) which vary in shape from euhedral to acicular. The pale grey area in the centre of the inclusion is soda-lime-silica glass containing a higher concentration of lead. Also visible are particles of kirschsteinitic slag (bottom-right and top-left) and a large bubble.

The interstitial glassy phases of this slag type are quite similar to those seen in the fayalitic variety, but differ in that they contain far more calcium (Table 5.2.4 and Figure 5.2.48) due to the calcic nature of the other phases present. Unlike the fayalitic slag, in which the range of different phases present is far more variable, the microstructure of the kirschsteinitic slag is far less variable. The only phases identified include kirschsteinite, magnetite and interstitial glass (Table 5.2.6); aluminium-rich phases were absent. Up to approximately 2.5% CuO was detected in the interstitial glassy phases in the slag in sample ERL104:G268:3260 (Table 5.2.6); considerably more than the 0.9% which colours the surrounding glass. However, similarly high levels of copper were not detected in the interstitial glass of the kirschsteinitic slag in sample ERL104:G281:1795 (Table 5.2.6). Furthermore, copper was not detected in any significant quantity in the area analyses of the slag inclusions in either sample (Table 5.2.4).

The particularly high content of slag inclusions in sample ERL104:G268:3260 (*e.g.* Figures 5.2.64 and 5.2.65, and see section 5.2.3 in this chapter) may indicate that this glass represents the material from the bottom of a crucible of red glass, where the slag particles had settled, and which was removed near the end of a round of colour making (see Peake and Freestone 2012). This bead is also characterised by the largest nepheline-lead-tin oxide inclusions (Figures 5.2.65 and 5.2.67).

5.2.3.1.3. Copper or Iron Smelting Slag?

It is unclear as to whether the fayalitic slags were formed as the result of iron or copper production. High copper concentrations were detected in the interstitial glasses of a number of the fayalitic slag inclusions, but the high levels of sodium suggest some contamination from the surrounding copper-rich soda-lime-silica glass (Table 5.2.5). The fayalitic slags are clearly more reducing than the kirschsteinitic types, as they contain wüstite rather than magnetite (*e.g.* Hauptmann 2007: 22). The higher iron contents (approximately 60% Fe₂O₃ as opposed to 40% Fe₂O₃; see Table 5.2.4 and Figure 5.2.48) are also more typical of iron-smelting slag, but could conceivably represent copper-smelting slag (Bachmann 1982: Table 1; Manasse *et al.* 2001: 952-958; Severin *et al.* 2011: 989).

Smelting copper under such highly reducing conditions is likely to have led to the precipitation of iron-copper alloy (Craddock and Meeks 1987), such as that observed in sample ERL104:G193:1311 (Figure 5.2.62), and while it is just possible that the large iron oxide – copper metal inclusion in sample ERL104:G242:2207 (Figure 5.2.50) also represents such an alloy phase, neither inclusion is directly associated with slag so this cannot be confirmed.

The detection of compositionally similar fayalitic slag additions in a high-lead ‘dark’ glass bead (see this chapter, section 5.1.5) supports this view. This glass contains no detectable copper (Table 5.1.3) and there are no copper particles surrounding the slag inclusions (Figure 5.1.49), as is typically seen in the red glasses. This strongly suggests that copper was added to the opaque red glasses separately from the

fayalitic slag. On balance it therefore seems more likely that the fayalitic slag was a by-product of iron-smelting.

Kirschsteinite in iron-smelting slag typically occurs as calcium-rich rims on fayalite cores, rather than as a homogeneous phase as observed here (Tim Young, pers. comm.). Furthermore, the presence of magnetite (Fe_3O_4) in the kirschsteinitic slags suggests that conditions were too oxidising to reduce iron to metal; wüstite (FeO) would be the stable iron oxide phase under such conditions (Severin *et al.* 2011: 989). On balance therefore, it would appear that the kirschsteinitic slags are likely to represent copper-smelting slag. This interpretation is borne out by the occurrence of approximately 2.5% CuO in the interstitial glass in slag from sample ERL104:G268:3260 (Table 5.2.6). Whilst it is possible that the slag fragments are contaminated by copper from the surrounding glass, the zones of metallic copper precipitation around the slag particles (*e.g.* Figure 5.2.63) indicate that conditions in the slag would probably have inhibited diffusion of copper by reducing it to metal.

Elsewhere it has been suggested that slag-like materials may have been added as a source of copper (*e.g.* Freestone *et al.* 2003b). The detection of copper in the interstitial glass of the kirschsteinitic slag in sample ERL104:G268:3260 (Table 5.2.6), together with the apparent derivation of this slag type from copper-smelting, raises the possibility that the slag may itself have served as a source of copper. However, the bulk copper contents of the slags are very low (Table 5.2.4), well below those of the glass, so this cannot be confirmed. Furthermore, the slag particles would have had to dissolve in the glass, and while it is clear that some interaction has occurred, they appear to have largely retained their angularity resulting from the crushing process (*e.g.* Figures 5.1.19 and 5.1.20). Assuming that the iron contents of the glasses originated from the slag, and that the average iron oxide content of slag is 50% and of glass is 5%, it is estimated that the glass typically contains about 10% dissolved slag. In order for the slag to have yielded a typical concentration of 2% CuO in the glass, it would have had to contain 20% copper. This is clearly not the case.

It would therefore appear that, in the majority of cases at least, the opaque red glasses were produced by adding copper (probably as oxide scale or dross from

copper alloy heated to high temperatures), a lead-tin by-product (*e.g.* lead-tin calx), and an iron-rich iron- or copper-smelting slag to a soda-lime-silica glass. Copper oxide scale is easily crushed and would have dissolved far more readily in the glass than metallic copper (Brill and Cahill 1988: 22). Red glasses rich in iron oxide occur in the Roman period but there are no reports of slag inclusions. It seems possible that this technology originated in early medieval Britain or Europe.

5.2.3.2. Anomalies

Several of the opaque red samples analysed have unusual microstructures or compositions. Sample ERL104:G262:1261 (a *Koch34* bead) contains 4.6% SnO₂, which is well above the levels of tin typically seen in the other opaque red samples analysed (anywhere up to 2.2% SnO₂). This sample also contains an unusually high concentration of lead, corresponding to 31.7% PbO. No slag was observed, but the presence of 3.8% Fe₂O₃* in the calculated base glass suggests that it was added. In contrast to the other opaque red sample, crystals of tin oxide are far more frequent in this glass (Figures 5.2.68 and 5.2.69). These were difficult to resolve in the SEM, but their density is similar to that observed in the adjacent tin oxide opacified white glass (Figure 5.2.69). Whilst these are sufficient to cause opacity, opacity is primarily caused by nanoparticles of metallic copper, which are below the resolution of the SEM.

Numerous angular crystals (Figures 5.2.68 and 5.2.69), primarily rich in soda, lime, lead, tin and silica, but also characterised by elevated levels of chlorine and iron (Table 5.2.7), were also observed in this sample. Nothing like this has been observed in opaque red glass before and they do not appear to correspond to any known mineral. They almost certainly crystallised out of solution upon cooling of the glass, as suggested by their angularity and compositional homogeneity, but it is unclear as to what they are or why they formed.

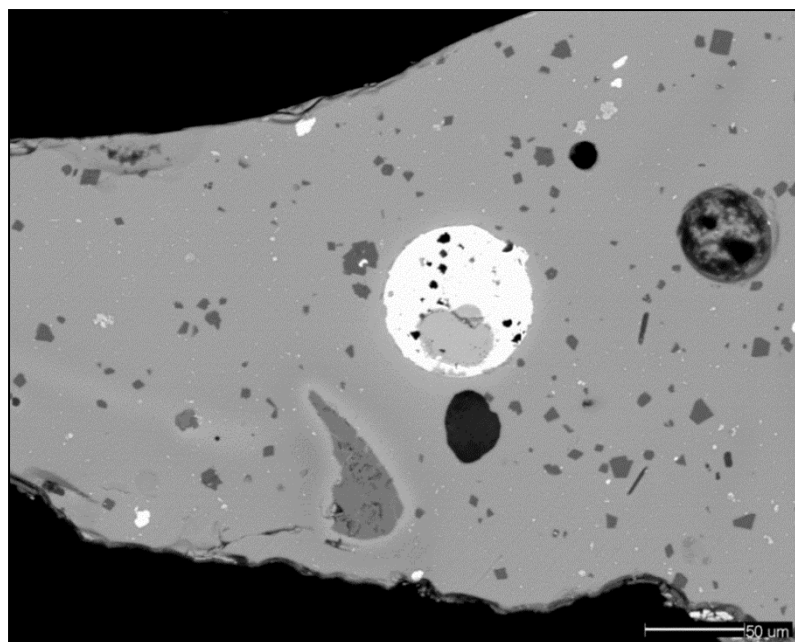


Figure 5.2.68 – BSE micrograph of sample ERL104:G262:1261, a *Koch34* bead, showing a high-lead opaque red glass matrix coloured by metallic copper nanoparticles. The large bright white inclusion towards the centre of the image is a bubble filled with lead oxide. An irregularly shaped lump of iron oxide is also visible (large dark grey inclusion). Several crystals of lead-tin oxide (bright white grains) and tin oxide (pale grey ‘feathery’ crystals) are present heterogeneously dispersed throughout the glass, together with numerous angular sodium calcium lead tin silicate inclusions (dark grey). Several bubbles and a small number of acicular calcium silicate crystals, corresponding to the mineral wollastonite (CaSiO_3) are also visible.

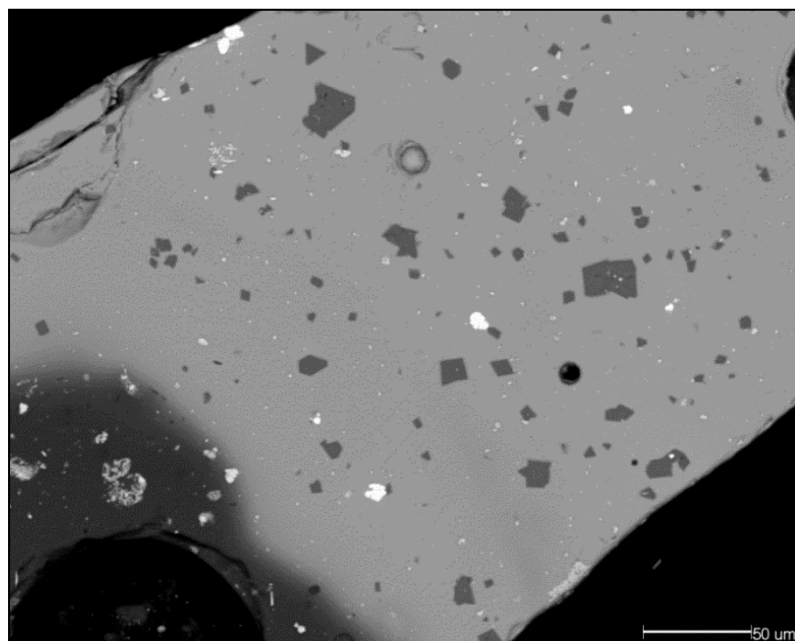


Figure 5.2.69 – BSE micrograph of sample ERL104:G262:1261, a *Koch34* bead, showing a high-lead opaque red glass matrix coloured by metallic copper nanoparticles. Several crystals of lead-tin oxide (bright white grains) and tin oxide (pale grey ‘feathery’ crystals) are visible heterogeneously dispersed throughout the glass, together with numerous angular sodium calcium lead tin silicate inclusions (dark grey). The darker grey glass to the bottom-left of the image is an opaque white glass, opacified by crystals of tin oxide.

Table 5.2.7 – Selected SEM-EDS spot analyses of the sodium calcium lead-tin silicate crystals observed in opaque red sample ERL104:G262:1261.

<i>Analysis Number</i>	<i>Oxide (wt %)¹</i>													
	<i>Na₂O</i>	<i>MgO</i>	<i>Al₂O₃</i>	<i>SiO₂</i>	<i>P₂O₅</i>	<i>SO₃</i>	<i>Cl</i>	<i>K₂O</i>	<i>CaO</i>	<i>TiO₂</i>	<i>Fe₂O₃</i>	<i>CuO</i>	<i>SnO₂</i>	<i>PbO</i>
<i>1</i>	10.8	0.2	0.2	48.5	0.2	b.d.	2.2	0.2	14.6	0.2	1.6	b.d.	12.4	9.7
<i>2</i>	11.6	0.3	0.2	47.0	0.1	0.3	2.1	0.2	14.6	b.d.	2.0	0.2	11.7	10.6
<i>3</i>	12.5	0.2	0.3	46.8	0.1	0.3	2.1	0.3	14.1	0.2	1.7	0.3	12.1	9.1
<i>4</i>	11.9	0.3	0.3	46.7	0.1	0.4	2.2	0.2	14.6	0.3	1.7	b.d.	12.0	9.3
<i>5</i>	12.3	0.2	0.4	46.7	b.d.	0.3	2.2	0.1	14.1	0.2	1.4	0.2	12.7	9.1
<i>6</i>	11.2	0.2	0.4	48.5	0.1	b.d.	2.2	0.2	14.6	0.1	1.8	0.2	11.9	9.4
<i>7</i>	12.1	0.3	0.3	47.2	0.2	b.d.	2.1	0.2	14.2	0.1	1.6	0.2	11.5	10.4
<i>8</i>	11.5	0.2	0.3	47.7	b.d.	0.4	2.1	0.2	14.1	0.2	1.5	0.3	12.5	9.4
<i>9</i>	10.1	0.2	0.4	48.2	0.2	0.2	2.2	0.2	14.4	0.2	1.5	0.2	12.4	10.2
<i>10</i>	11.0	0.2	0.4	47.2	b.d.	0.2	2.2	0.1	14.7	0.2	1.9	b.d.	11.7	10.4

¹Spot analyses normalised to 100%. b.d. = below detection. See Chapter 2, section 2.3.1 for details. The oxides of manganese, cobalt, nickel, zinc, arsenic, silver antimony and barium were analysed for but not detected.

Reheating glass to below its melting temperature to precipitate colloidal metal colourant particles can sometimes result in the precipitation of sodium chloride crystals (Barber and Freestone 1990: 41; Barber *et al.* 2009: 125); it is therefore possible that the crystals observed in this red sample were formed as a result of such reheating. Interestingly, the levels of lead and tin in this sample correspond closely to those of opaque yellow glass (*e.g.* Figure 5.2.44), which raises the possibility that this glass was produced from scrap opaque yellow glass. Some ‘dark’ glass appears to have been produced from scrap opaque yellow glass (see this chapter, section 5.1.5), suggesting that this is a strong possibility. The opaque red glass in question is likely to be an isolated occurrence, as x-radiography revealed that none of the other opaque red beads from the same grave are of the same high-lead composition.

In addition, samples ERL104:G262:1287 and ERL104:G262:1291 (both *Cylindrical Round* beads) differ from the other opaque red samples in that they contain blue streaks, which are clearly visible in the BSE micrographs (Figures 5.2.70 and 5.2.71). Their composition and context suggest that both beads were probably produced from the same melt. Whilst no slag was observed in either sample, the presence of approximately 4% Fe₂O₃, together with the identification of an agglomerate of iron oxide dendrites (Figure 5.2.71), suggest that slag was probably added. The blue streaks are of roughly the same composition as the adjacent red glass, but contain higher levels of lead (approximately 6% *cf.* 2% PbO) and tin (approximately 3% *cf.* 0.3% SnO₂); they are also characterised by sparse crystals of tin oxide and lead-tin oxide. It is possible that an old tin oxide opacified blue glass was used to produce these beads, but that the glass was not mixed and/or heated for long enough to homogenise the melt.

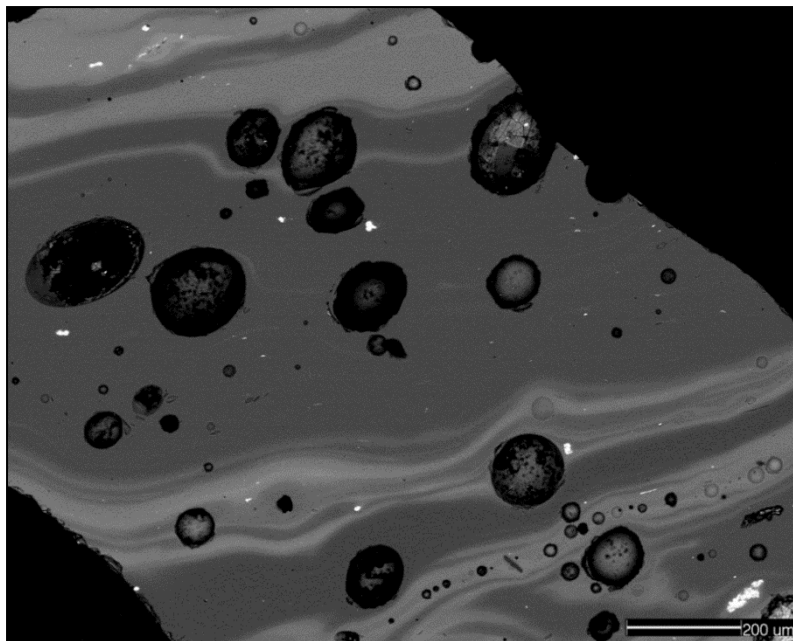


Figure 5.2.70 – BSE micrograph of sample ERL104:G262:1287, a *Cylindrical Round* bead, showing an opaque red glass matrix coloured by metallic copper nanoparticles. Several opaque blue streaks are visible, which appear brighter in the image due to the higher concentration of lead in these regions. Numerous lead-tin oxide crystals and several tin oxide crystals are also visible (bright white), together with several large bubbles.

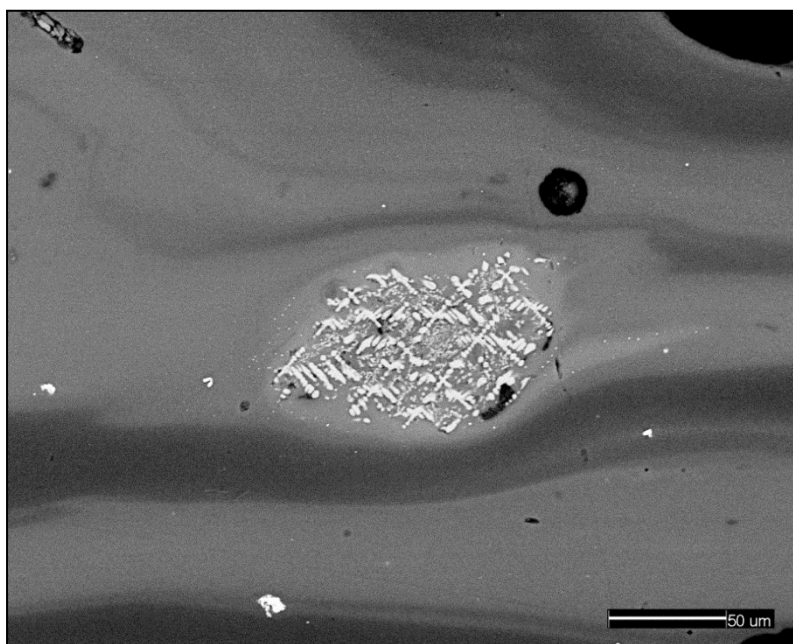


Figure 5.2.71 – BSE micrograph of sample ERL104:G262:1287, a *Cylindrical Round* bead, showing an opaque red glass matrix coloured by metallic copper nanoparticles. Several opaque blue streaks are visible, which appear brighter in the image due to the higher concentration of lead in these regions. A few sparse crystals of lead-tin oxide can be seen in these streaks (bright white). An iron-rich inclusion of fayalitic composition is also present, containing numerous dendrites of iron oxide.

5.2.3.3. Trace Element Analyses

11 of the opaque red samples were analysed by LA-ICP-MS. The average colourant and colourant-related elements for these are presented in Figure 5.2.72, which shows that there is relatively little difference in the colouring process between samples produced from different base glass types. Slight variations in the amounts of copper, tin, lead and iron are likely to relate to variations in the relative proportions of the raw materials added during the colouring process rather than differences in technology (see section 5.2.3 above), whereas variations in the concentrations of antimony and manganese relate to the composition of the relative base glass types used (see Chapter 4, section 4.2).

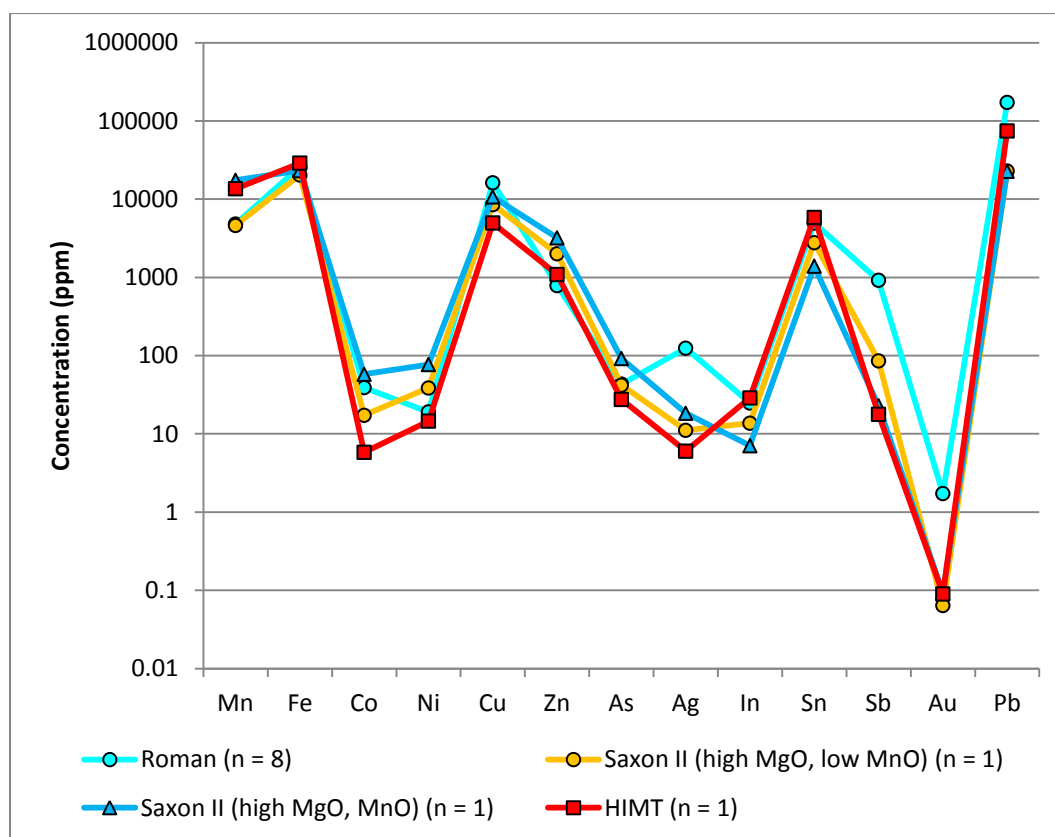


Figure 5.2.72 – Average colourant and colourant-related elements for the opaque red samples from Eriswell, showing the different base glass types identified. Note the logarithmic scale.

Spot analysis of some of the larger metallic copper particles by SEM-EDS in many samples revealed high levels of silver, which in most cases corresponded to

approximately 0.5-1.5% silver, but sometimes as much as 7.0% Ag (*e.g.* Figure 5.2.61); copper and silver often form a homogeneous solution when in the liquid state (Bayley and Eckstein 1997: 108-109). The presence of silver in these glasses was confirmed by trace element analysis; the samples analysed typically contain 50-400 ppm Ag, and is generally higher in the ‘Roman’ glasses (Figure 5.2.73). Whilst traces of silver are not unknown in early opaque red glasses (*e.g.* Brill 1976: 238; Hughes 1972: 99; Paynter and Kearns 2011: 11), the levels detected in some of the copper particles in the Eriswell reds seem very high. It is likely that silver precipitated out as a copper-silver alloy due to the extreme reducing conditions within the glass; when coupled with high melting temperatures, these conditions favour the formation of metallic silver (Weyl 1951: 405).

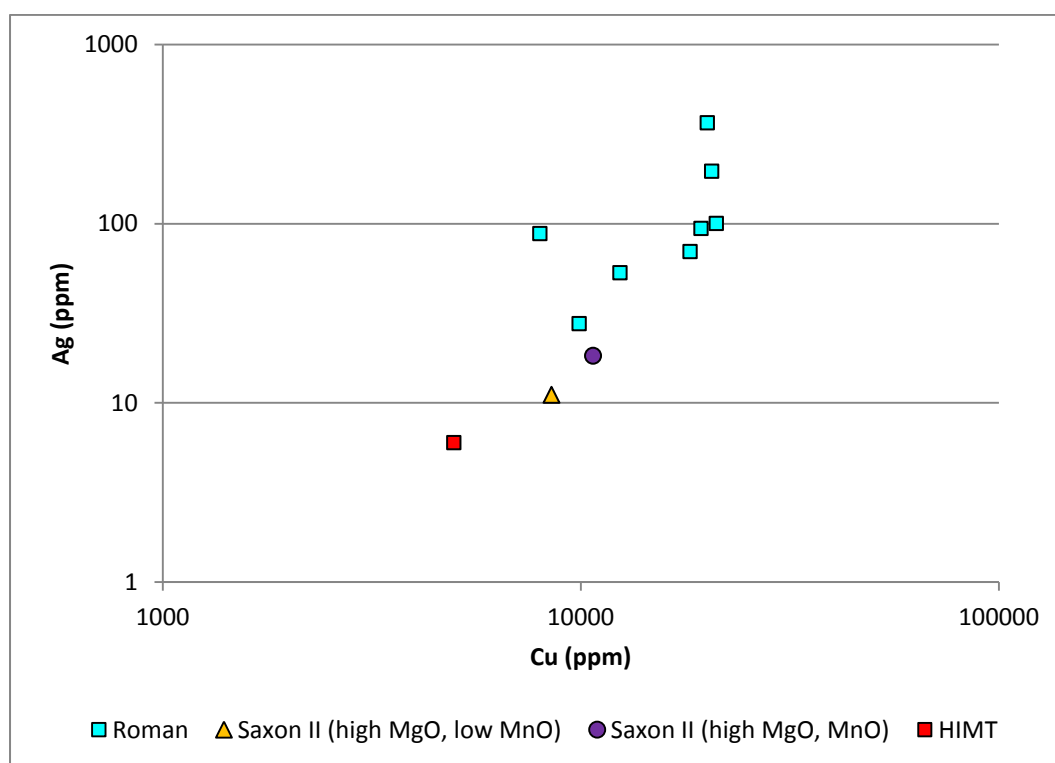


Figure 5.2.73 – A plot of copper versus silver for the opaque red samples from Eriswell, showing the different base glass types identified. Note the logarithmic scale.

No silver was detected in spot or area analysis of the any of the slag particles in the Eriswell reds, suggesting that it is unlikely to have been introduced with the slag additions. Furthermore, similar levels of silver were detected by LA-ICP-MS analysis in many of the green, turquoise and orange glasses (Figure 5.3.3), all of

which are coloured by copper, but none of which contain slag. Silver is therefore likely to have been introduced as an impurity with the copper colourant, as demonstrated by the weak positive correlation between copper and silver (Figure 5.2.73; $r^2 = 0.43$). An absolute positive correlation was also observed between tin and indium in the opaque reds (Figure 5.2.74; $r^2 = 1.0$), indicating that indium was introduced as an impurity with tin (Benzaazoua *et al.* 2002: 168).

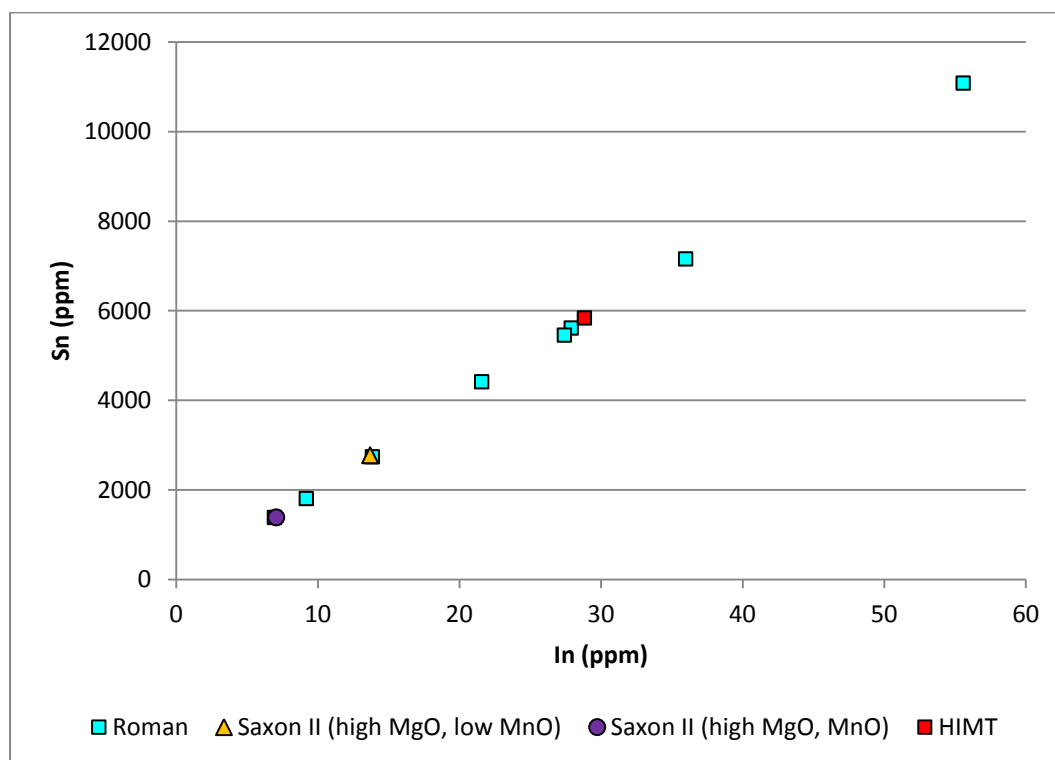


Figure 5.2.74 – A plot of indium versus tin for the opaque red samples from Eriswell, showing the different base glass types identified.

5.2.4. Opaque Orange Glass

Opaque orange glass is often overlooked in analytical studies because its technology is so closely related to that of opaque red glass; it is sometimes considered to be a variant of red glass (*e.g.* Brill 1970: 119; Brill and Cahill 1988: 23; Guido 1999: 68). Samples of this glass colour were obtained from 12 beads from Eriswell, all of which are of Brugmann's *Orange* type. They all contain copper at extraordinarily high levels, corresponding to 15-22% CuO; compare this to a maximum of 4.2% CuO in opaque red glass and a maximum of 6.7% CuO in other copper-based colours.

However, high levels of copper have been detected in opaque orange glass beads from other Anglo-Saxon sites (*e.g.* Bayley and Wilthew 1986; Mortimer and Heyworth 2009: 411; Wilthew 2006: 391) and contemporary Merovingian cemeteries in Europe (*e.g.* Heck and Hoffmann 2000: 344-347; Hoffmann *et al.* 2000: 97). Here, copper is present as a fine dispersion of coarse grains and dendrites of cuprite, Cu_2O (Heck and Hoffmann 2000: 354), which cause both colour and opacity in the glass (Figures 5.2.75-5.2.77).

Some early opaque red glasses (high lead – high copper ‘sealing wax’ reds) are coloured and opacified by cuprite (see this chapter, section 5.2.3), although no glass of this type was identified at Eriswell. In red glasses such as this, the cuprite crystals which produce the colour and opacity are usually much larger than those observed in the opaque orange samples; when cuprite crystals are large they impart a red colour, but when they are fine they impart more of a yellow or orange colour (Ahmed and Ashour 1981: 32; Barber *et al.* 2009: 124; Brill and Cahill 1988: 23-24; Brun and Pernot 1992: 239; Cable and Smedley 1987; Heck and Hoffmann 2000: 354; Welham *et al.* 2000: 13).

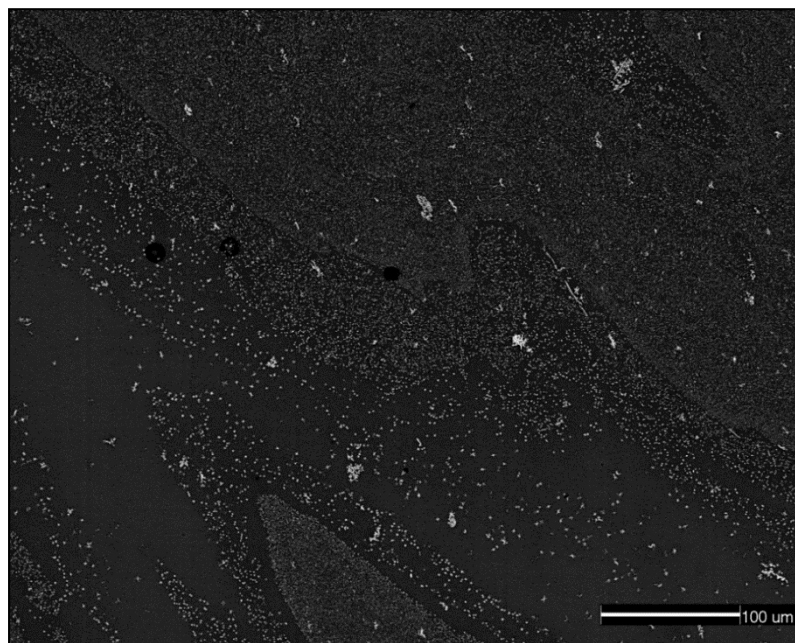


Figure 5.2.75 – BSE micrograph showing opaque orange sample ERL104:G266:1575, a *Orange* bead. A heterogeneous dispersion of tiny cuprite crystals can be seen (white) dispersed in a soda-lime-silica glass (grey). These impart both colour and opacity to the glass. Note that some areas are devoid of cuprite crystals, as a result of poor mixing of the batch.

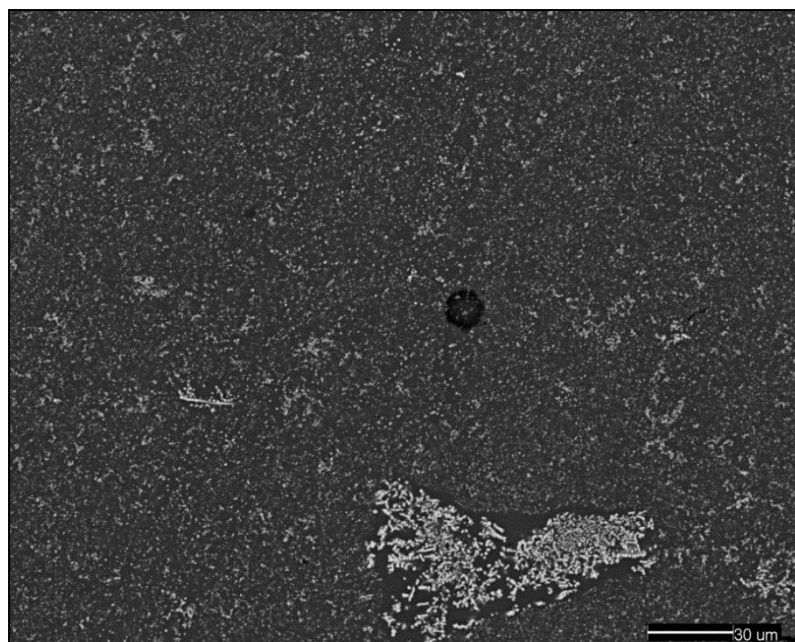


Figure 5.2.76 – BSE micrograph showing opaque orange sample ERL104:G107:1105, a *Orange* bead. A heterogeneous dispersion of tiny cuprite crystals can be seen (white) dispersed in a soda-lime-silica glass (grey), sometimes forming as irregular agglomerates. These impart both colour and opacity to the glass.

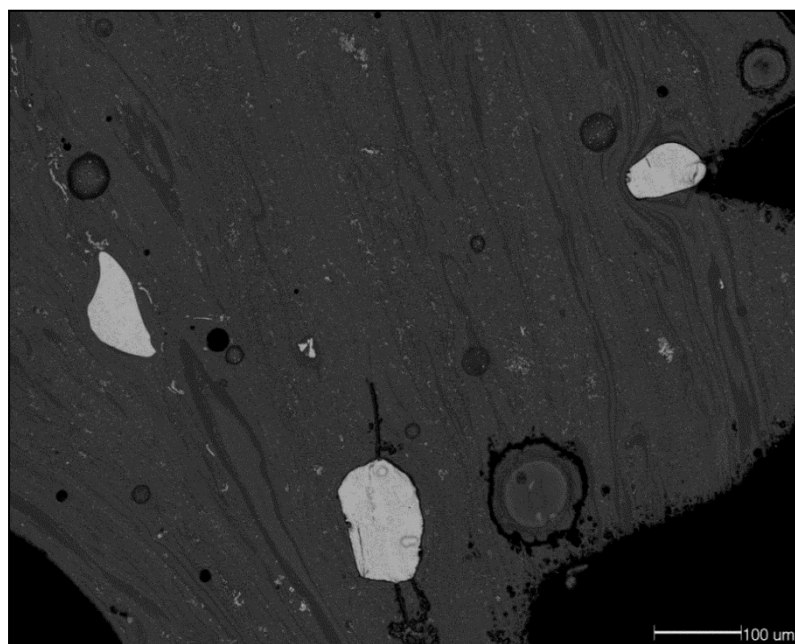


Figure 5.2.77 – BSE micrograph showing opaque orange sample ERL104:G193:1294, a *Orange* bead. A heterogeneous dispersion of tiny cuprite crystals can be seen (white) dispersed in a soda-lime-silica glass (grey). Three large lumps of cuprite are also visible (white). Streaks in the glass result from variations in the concentration of cuprite crystals, as a result of poor mixing of the batch.

As with opaque red glass, the formation of cuprite crystals in opaque orange glass requires a reducing environment. In the red glasses this was obtained through the deliberate addition of iron-rich metallurgical slag as an internal reducing agent (see this chapter, section 5.2.3); this is not the case in the opaque orange glasses. Some studies have suggested that the formation of cuprite may have been aided by the addition of an internal reducing agent such as charcoal or fuel ash (Cable and Smedley 1987; Freestone 1987; Schibille *et al.* 2012: 1490), but its use is often difficult to detect in glass because it is completely burnt away. If such materials were added as reducing agents, a positive correlation may be expected between potash, magnesia and phosphate as fuel ash is often enriched in these components (Paynter 2008; Tal *et al.* 2008a: 73; Tal *et al.* 2008b: 91). A plot of potash versus magnesia reveals a strong positive correlation (Figure 5.2.79; $r^2 = 0.82$); magnesia and phosphate are also positively correlated (Figure 5.2.80; $r^2 = 0.57$), as are potash and phosphate (Figure 5.2.81; $r^2 = 0.61$); this is more likely to relate to the composition of the base glasses used (Figure 5.2.79), to which small quantities of plant ash appear to have been added (see Chapter 4, section 4.4), rather than the colourant technology.

Orange glass can also be produced by rapid cooling and/or an increased concentration of copper relative to opaque red glass (Biek and Bayley 1979: 12); cuprite is more soluble in silicate glasses than metallic copper, so in order for it to precipitate very high concentrations are necessary, typically between 5-10% (Barber *et al.* 2009: 124). Welham *et al.* (2000: 14) suggest that an increase in the concentration of copper results in the precipitation of smaller cuprite crystals; these would be orange rather than red. The extraordinarily high levels of copper detected in the opaque orange samples from Eriswell are therefore likely to have been necessary in order to ensure the precipitation of small cuprite crystals.

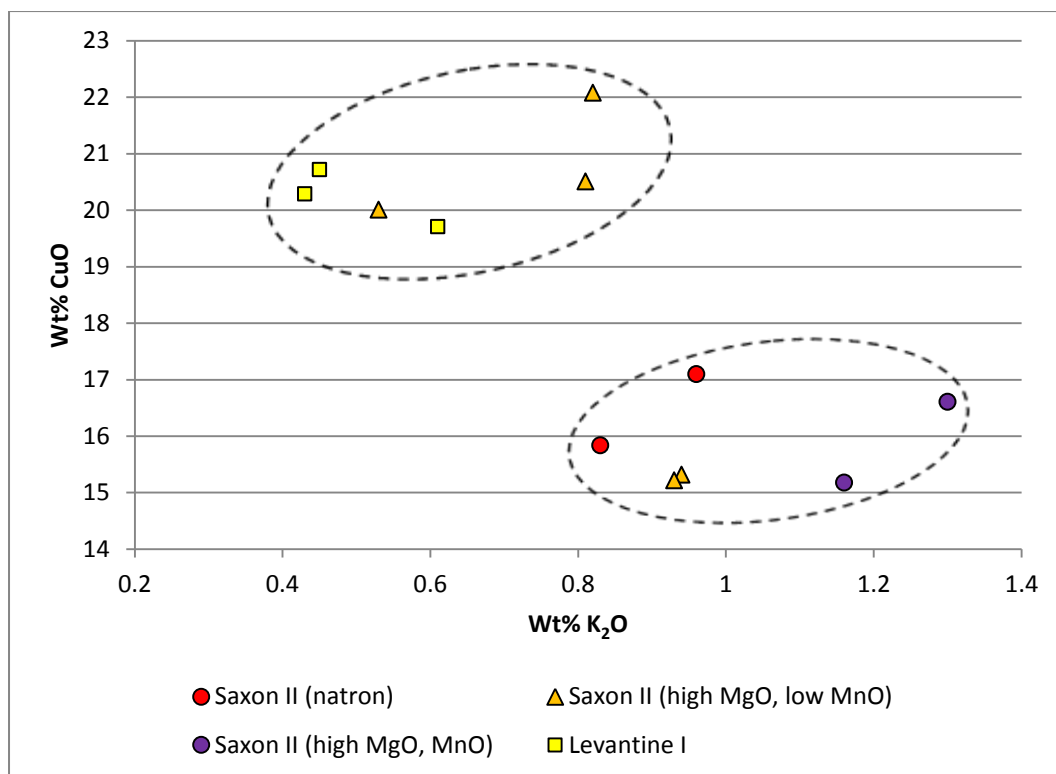


Figure 5.2.78 – A plot of potash versus copper oxide for the opaque orange samples from Eriswell, showing the different base glass types identified and indicating the possibility of two different compositional groups.

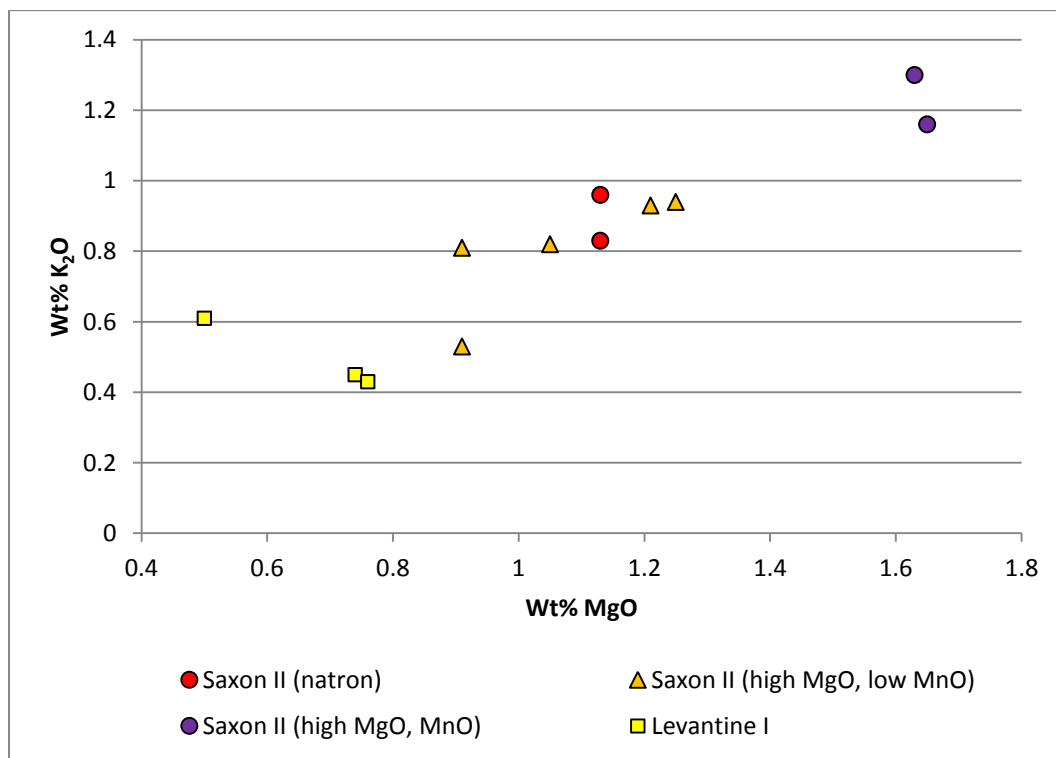


Figure 5.2.79 – A plot of magnesia versus potash for the opaque orange samples from Eriswell, showing the different base glass types identified.

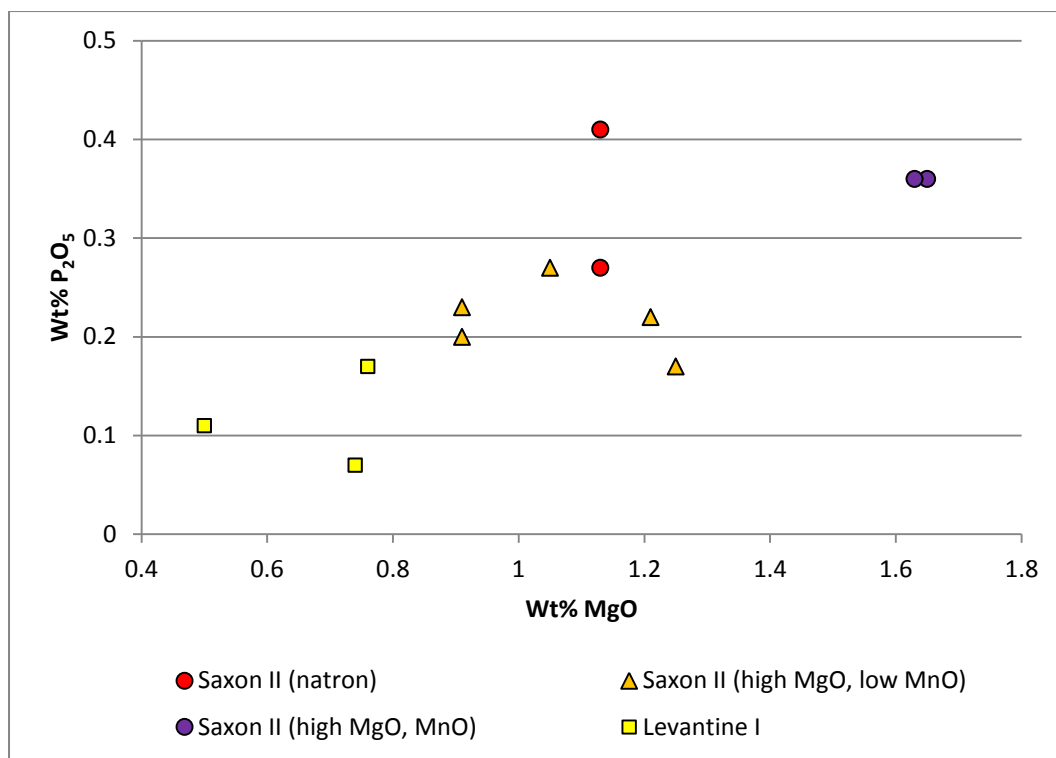


Figure 5.2.80 – A plot of magnesia versus phosphate for the opaque orange samples from Eriswell, showing the different base glass types identified.

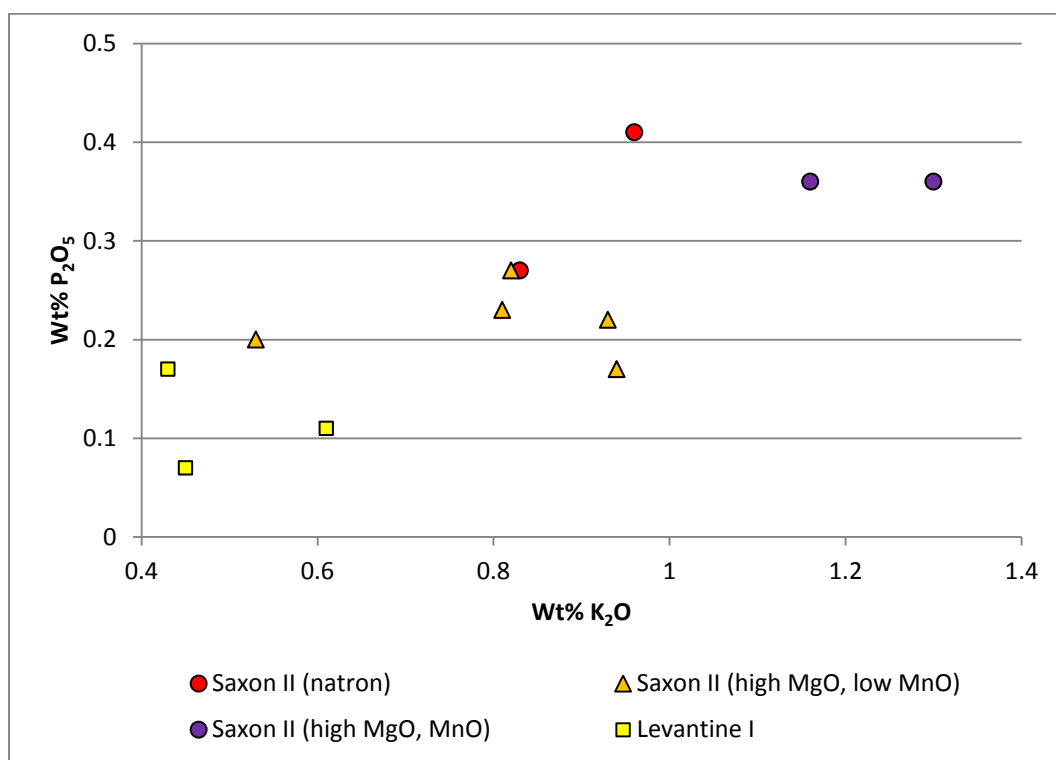


Figure 5.2.81 – A plot of potash versus phosphate for the opaque orange samples from Eriswell, showing the different base glass types identified.

In sample ERL104:G193:1294 several large inclusions of copper oxide were observed (Figure 5.2.77). The sub-angular nature of some of these suggests that they are unlikely to have precipitated out of solution, and are therefore likely to represent relicts of the raw copper colourant. The glass is unlikely to have been heated for long enough and/or at temperatures high enough to fully disperse them. Their presence is a strong indication that copper was added in its oxidised form, for example as scale or dross, which would have been easier to crush than metallic copper (Brill 2006: 134). The general absence of zinc, tin, and arsenic suggest that the copper source is likely to have been relatively pure.

It is possible to divide the opaque orange glasses from Eriswell into two groups based upon the levels of copper present; this is well illustrated by a plot of potash versus copper (Figure 5.2.78). One group contains 15-17% CuO, and the other 19-22% CuO. These groups do not appear to relate closely to the composition of the base glass types used or the chronological phases to which the beads have been attributed. However, in general the 'high-copper' samples are predominantly produced from 'Saxon II (high MgO, low MnO)' and 'Levantine I' glass attributed to Brugmann's phases B2-C and C, whereas the 'low-copper' samples are produced from 'Saxon II' glass attributed to Brugmann's phase B2 only (Figure 5.2.78). This suggests that the 'high-copper' group *may* be marginally later.

Visually, several beads are characterised by thin black or green bands running through the glass. The black bands are likely to be caused by areas of glass largely deficient in cuprite crystals, as can be seen in Figure 5.2.75. It is likely that uneven mixing of the batch (*e.g.* Santagostino Barbone *et al.* 2008; Brill and Cahill 1988: 18) or variations in the melting conditions hindered the formation of cuprite in these areas. The green streaks may have resulted from differences in the oxidation state of the copper colourant, also as a result of localised variations in the melting conditions. It has been suggested that orange beads may have originally been green, turning orange due to a reaction with the burial environment (Brugmann 2004: 40; Siegmund 1998: 61); however, unexposed 'fresh' glass beneath the surface of these beads would be green if this was the case, and all of the samples taken were orange throughout. Furthermore, the orange samples analysed have distinct (high-copper) compositions when compared to the green samples (see this chapter, section 5.2.2).

5.2.4.1. Trace Element Analyses

Only one opaque orange sample (ERL104:G266:1575, an *Orange* bead of ‘Saxon II (high MgO, MnO)’ composition) was analysed by LA-ICP-MS, so it is impossible to draw comparisons between samples of this colour. However, a comparison to opaque red glass from Eriswell is worthwhile, as this is also coloured by copper in the reduced state (albeit metallic copper as opposed to cuprite). The trace element patterns for the colourant and colourant-related elements (Figure 5.2.82) show that the opaque orange sample is quite distinct from opaque red glass. The orange sample is much lower in Pb (1720 ppm) and Sn (160 ppm) than the opaque red samples, suggesting that these components were not deliberately added and may instead have been introduced as impurities with the copper colourant.

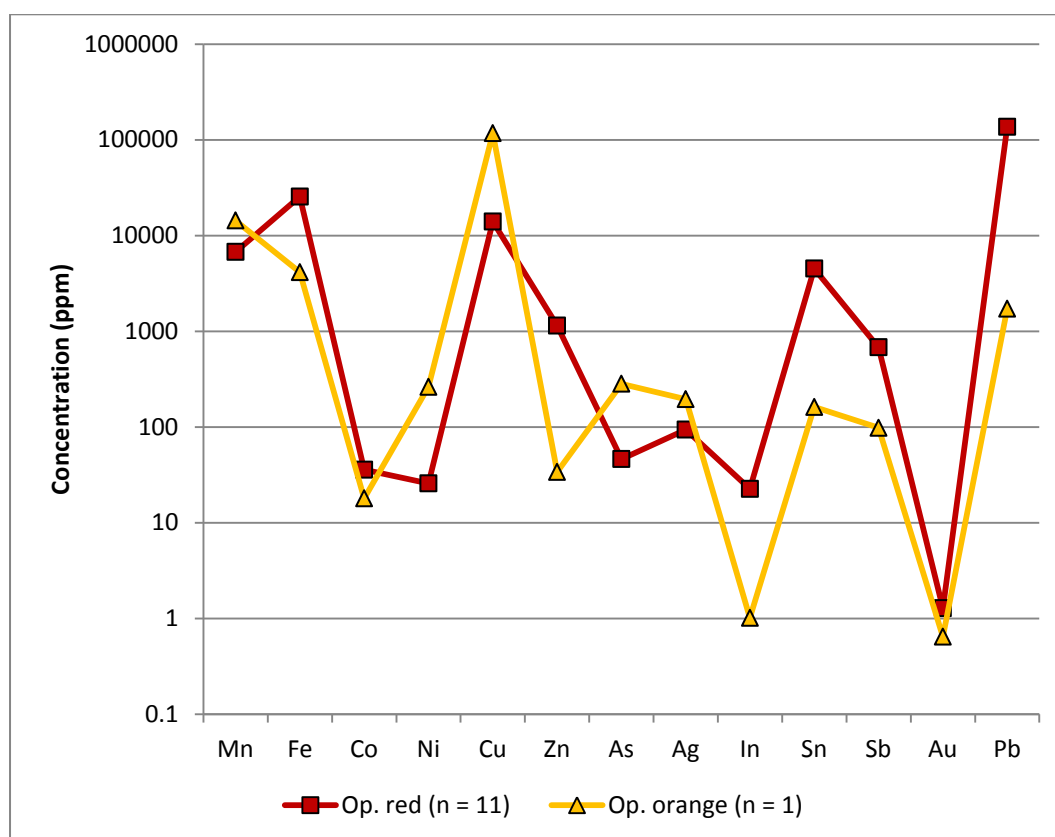


Figure 5.2.82 – Colourant and colourant-related element concentrations for opaque orange ‘Saxon II (high MgO, MnO)’ sample ERL104:G266:1575 from Eriswell, compared to the average concentrations of these components for opaque red glass. Note the logarithmic scale.

The concentrations of Ni (260 ppm), As (280 ppm) and Ag (200 ppm) are also elevated relative to opaque red glass, and are again likely to have entered as impurities with copper colourant. The elevated levels of many colourant-related impurities relative to opaque red glass are likely to be borne out by the addition of significantly more copper; on balance the lower levels of tin and zinc relative to opaque red glass suggest the use of a relatively pure source of copper.

5.2.5. Opaque Blue Glass

Samples of opaque blue glass were obtained from 10 beads from Eriswell. They are all coloured by low concentrations of cobalt, in the same manner as the translucent blue glasses (see this chapter, section 5.1.3). One sample of opaque greyish-blue glass was also obtained, but trace element analysis was not undertaken on this sample so the presence of cobalt could not be confirmed.

Opacity can be achieved by a variety of methods. Two opaque blue samples (ERL104:G237:1153, a *Blue Globular, opaque* bead and ERL104:G262:1244, a *BluePoly1* bead) and the opaque greyish-blue sample (ERL104:G353:3073, a *Cylindrical Round* bead) contain low concentrations of tin (0.4-0.7% SnO₂), present as crystals of tin oxide (Figure 5.2.83). Whilst these are sparse, they are evidently enough to cause opacity. All of these samples are produced using a ‘Saxon II (high MgO, low MnO)’ base glass. The remaining samples are opacified by a dispersion of tiny bubbles (Figures 5.2.84 and 5.2.85); they typically contain low levels of antimony (up to 0.8% Sb₂O₃) in solution, which results from the use of a ‘Roman’ base glass (see Chapter 4, section 4.3). It is just possible that some antimony was introduced through the addition of old Roman blue cullet as a colourant (see this chapter, section 5.1.3), but this cannot be confirmed.

The differences in opacity are strongly paralleled by opaque white glass from Eriswell (Figure 5.2.86; see also this chapter, section 5.2.1); particularly the exclusive use of a ‘Roman’ base glass to produce the bubble-opacified types. The opaque blue glasses are therefore essentially variations of opaque white glass coloured by cobalt.

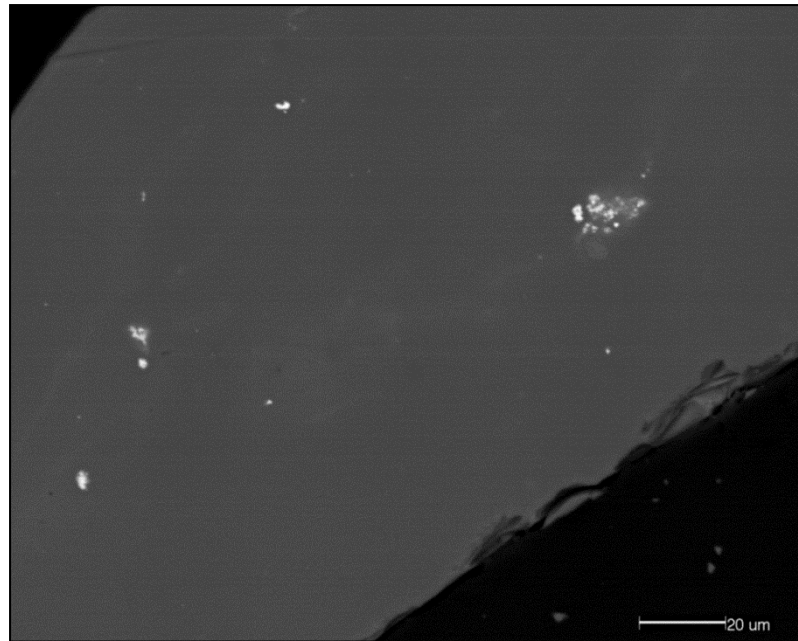


Figure 5.2.83 – BSE micrograph showing opaque greyish-blue sample ERL104:G353:3073, a *Cylindrical Round* bead. Several sparse crystals of tin oxide (white), which produce opacity, are visible heterogeneously dispersed throughout the soda-lime-silica glass matrix (grey).

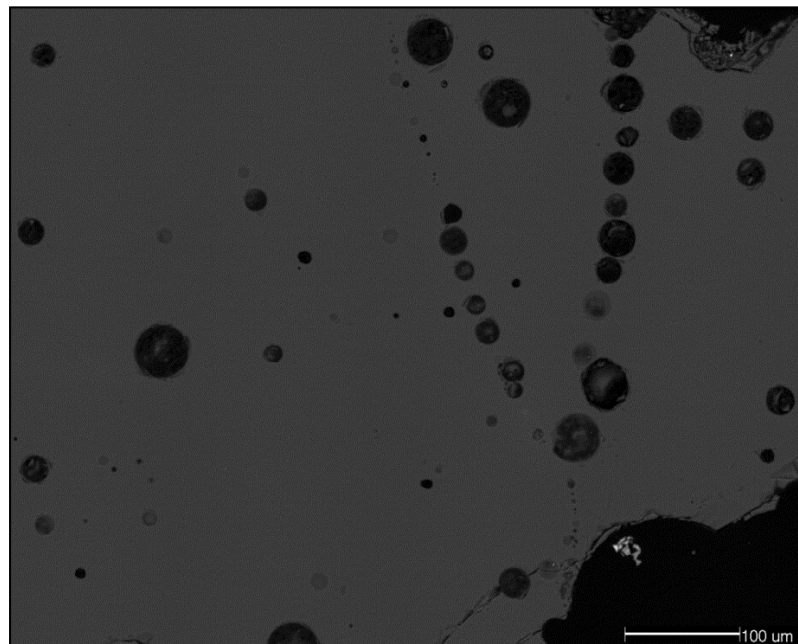


Figure 5.2.84 – BSE micrograph showing opaque blue sample ERL104:G242:2200, a *Blue Globular, opaque* bead. A heterogeneous dispersion of tiny bubbles is visible (black) dispersed throughout a soda-lime-silica glass matrix (grey), which produce opacity.

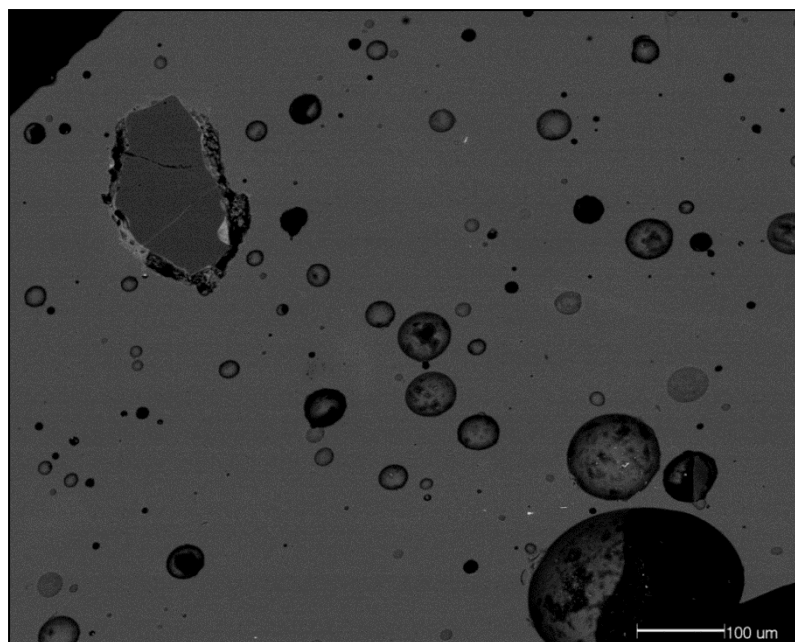


Figure 5.2.85 – BSE micrograph showing opaque blue sample ERL046:G05:1436, a *Blue Globular, opaque* bead. A heterogeneous dispersion of tiny bubbles is visible (black) dispersed throughout a soda-lime-silica glass matrix (grey), which produce opacity. A large angular grain of silica can also be seen (dark grey inclusion towards the top-left of the image).

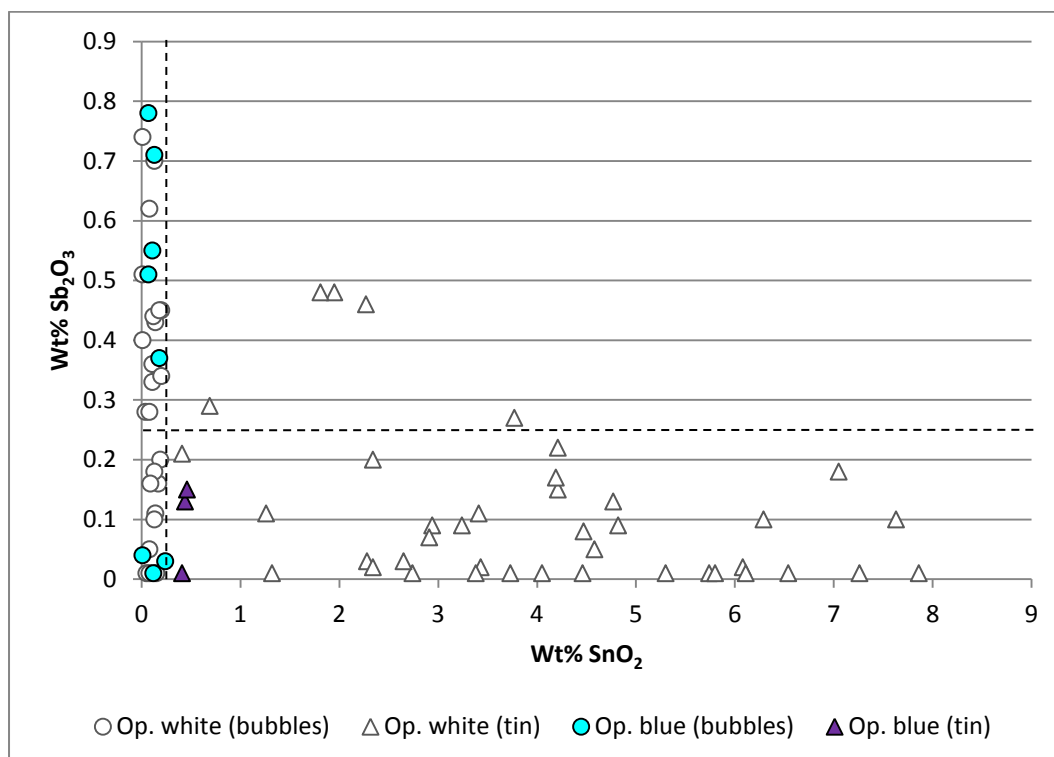


Figure 5.2.86 – A plot of tin oxide versus antimony oxide for the opaque blue samples from Eriswell, compared to the opaque white samples (see Figure 5.2.3). The dashed lines represent the approximate detection limits for tin oxide and antimony oxide.

5.2.5.1. Trace Element Analyses

Only one opaque blue sample from Eriswell (ERL104:G237:1153, a *Blue Globular* bead produced from ‘Saxon II (high MgO, low MnO)’ glass) was analysed by LA-ICP-MS, so it is not possible to draw comparisons between glasses of this colour; however, a comparison with translucent blue glass (see this chapter, section 5.1.3.1) is worthwhile. The colourant and colourant-related trace element patterns for the opaque and translucent blue glasses show that both colours are broadly very similar (Figure 5.2.87). Cobalt is the colourant in both glass types, corresponding to 220 ppm Co in the opaque blue sample. Variations in the levels of antimony present are likely to reflect the respective base glass types used (see Chapter 4), or possibly the use of old Roman blue cullet as a colourant, whereas variations in the levels of tin reflect the deliberate addition of tin as an opacifying agent in the opaque blue sample, as discussed above.

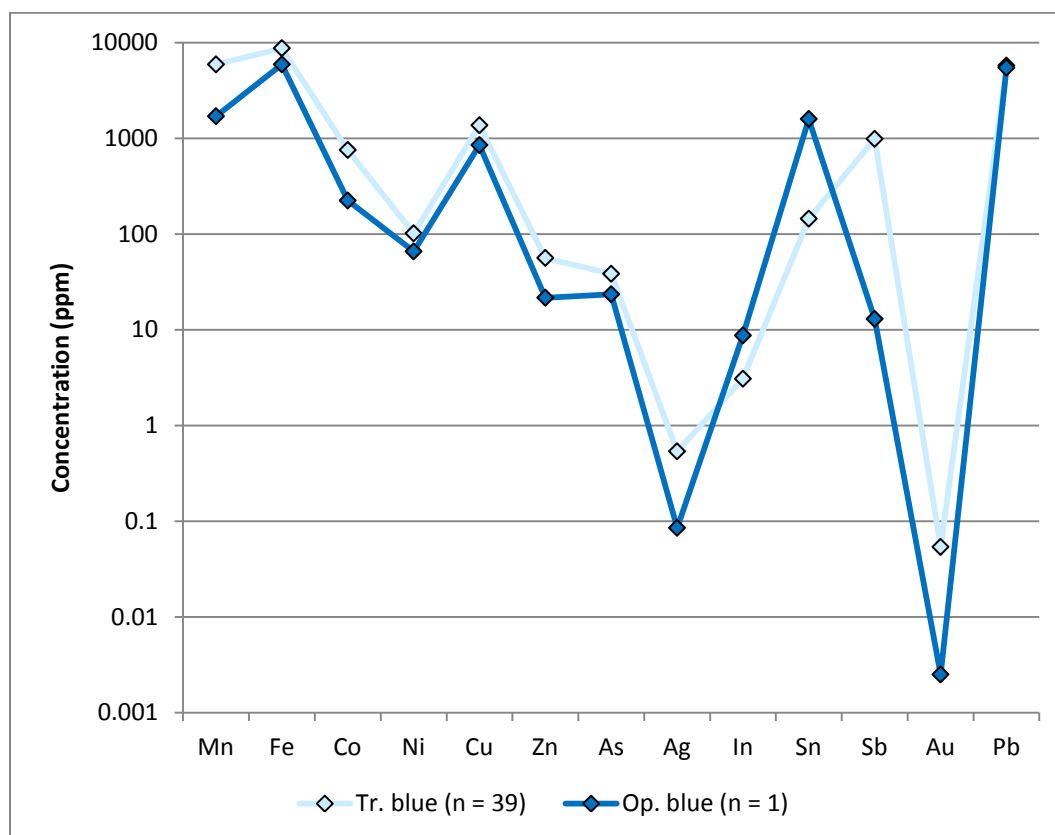


Figure 5.2.87 – Colourant and colourant-related element concentrations for opaque cobalt-blue ‘Saxon II (high MgO, low MnO)’ sample ERL104:G237:1153 from Eriswell, compared to the average concentrations of these components for translucent blue glass. Note the logarithmic scale.

5.2.6. Opaque Turquoise Glass

Samples of opaque turquoise glass were obtained from only two beads from Eriswell, due to the scarcity of this colour in the assemblage. As with the translucent turquoise samples (see this chapter, section 5.1.4), they are coloured by cupric copper, corresponding to approximately 2.5% CuO; this produces turquoise in a low-lead glass. Sample ERL104:G112:1023 (a *Blue Biconical, opaque* bead) contains a high level of zinc (0.8% ZnO), suggesting the use of scrap copper alloy (*e.g.* brass) as a colourant (Bayley 1987: 184; Bayley and Wilthew 1986; Brill and Whitehouse 1988: 40; Mortimer 1996a: 8). However, it is the nature of opacification which differentiates between the two samples analysed.

Sample ERL104:G112:1023 (a *Blue Biconical, opaque* bead) contains 1.2% SnO₂ and is opacified by tin oxide (Figure 5.2.88), but sample ERL104:G290:1734 (*DarkPoly4*) contains 3.1% Sb₂O₃ and is instead opacified by calcium antimonate (Ca₂Sb₂O₇ or CaSb₂O₆) (Figure 5.2.89). Tin oxide opacification has been discussed in detail elsewhere (see this chapter, section 5.2.1). Sample ERL104:G290:1734 represents the only sample opacified by compounds of antimony from the Eriswell assemblage. Experiments have shown that these crystals form in the glass through the reaction of antimony, which may have been added in the form of a compound such as stibnite (Sb₂S₃) or antimony oxide, with lime in the base glass (Foster and Jackson 2005: 328; Henderson 1985: 285; Mirti *et al.* 2002: 222; Rooksby 1962: 22). This sample contains the lowest level of lime in the assemblage (approximately 3.7% CaO), but extra antimony may have been added to compensate for this. The low ratio of CaO/Sb₂O₃ (approximately 1.2) usually favours the formation of CaSb₂O₆ over Ca₂Sb₂O₇ (Paynter and Kearns 2011: 39), but the presence of this compound cannot be confirmed here.

As tin had generally replaced antimony as an opacifying agent by the 5th century AD (Biek and Bayley 1979: 9; Bayley 1999: 91; Sayre 1963: 281; Sayre 1965: 150; Turner and Rooksby 1961: 2), bead ERL104:G290:1734 may be a Roman heirloom. The ‘dark’ glass body of this bead is also of the ‘Roman’ compositional type, supporting this view. Whilst it is just possible that it represents an Anglo-Saxon bead produced from recycled Roman material, the absence of typologically similar beads

from Anglo-Saxon contexts does not support this interpretation. No samples of opaque turquoise glass were analysed for trace elements.

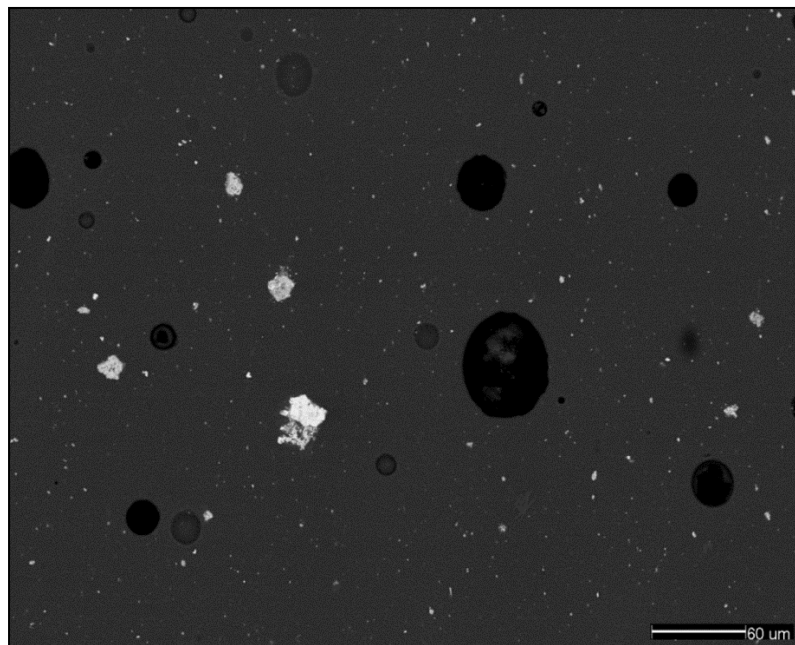


Figure 5.2.88 – BSE micrograph showing opaque turquoise sample ERL104:G112:1023, a *Blue Biconical, opaque* bead. A heterogeneous dispersion of tin oxide crystals is visible (white) dispersed throughout a soda-lime-silica glass matrix (grey), which produce opacity. A number of bubbles (black) can also be seen.

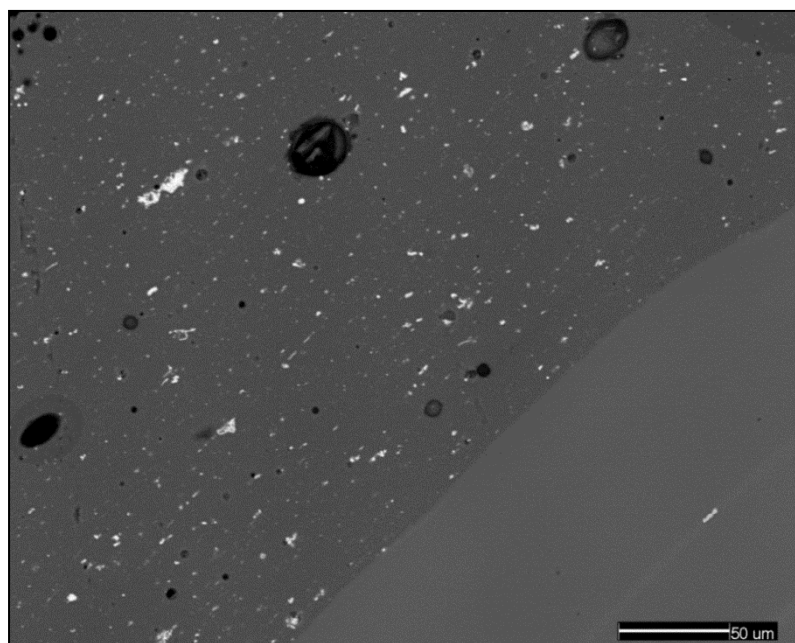


Figure 5.2.89 – BSE micrograph showing sample ERL104:G290:1734, a *DarkPoly4* bead. An opaque turquoise glass opacified by a heterogeneous dispersion of calcium antimonate crystals (white) dispersed throughout a soda-lime-silica glass matrix (grey) is visible. Several bubbles can also be seen. The glass devoid of opacifying crystals to the bottom-right of the image is a 'dark' glass.

5.2.7. Opaque Blue-Green Glass

Two samples of opaque blue-green glass (ERL046:G03:1289 and ERL046:G03:1325, both *Blue Melon, opaque* beads) were obtained from Eriswell. Both samples are of the 'Roman' compositional type containing low levels of antimony, corresponding to 0.2-0.4% Sb_2O_3 . They are very similar in composition to one another, and as they were recovered from the same grave they were almost certainly produced from the same batch of glass by the same workshop. The colour is produced by the addition of 4.2% CuO , which, produces green in the presence of lead (approximately 20% PbO here; see this chapter, section 5.1.4). A particle of copper oxide containing 0.7% zinc and 0.4% silver was identified in sample ERL046:G03:1289 (Figure 5.2.91); this may represent a relict of the colourant, and suggests that copper was probably added in its oxidised form (as scale or dross, etc.). Furthermore, the detection of zinc here suggests the use of a copper alloy such as brass, although zinc was not detected in area analysis of the glass itself.

These glasses are particularly unusual because both are heavily opaque, but no opacifying agent could be identified in the SEM (Figures 5.2.90 and 5.2.91). A few bubbles were present (Figure 5.2.90), but not in sufficient quantity to cause the level of opacity observed. However, trace element analysis revealed considerably elevated levels of silver in this glass (see section 5.2.7.1 below). Opacity can therefore only have been caused by a colloidal dispersion of metallic silver, too small to be observed in the SEM. This interpretation is supported by the identification of a large particle of silver, approximately 1-2 μm in diameter, in sample ERL046:G03:1289 (Figure 5.2.91). This suggests that the redox conditions within the glass would have favoured the precipitation of metallic silver.

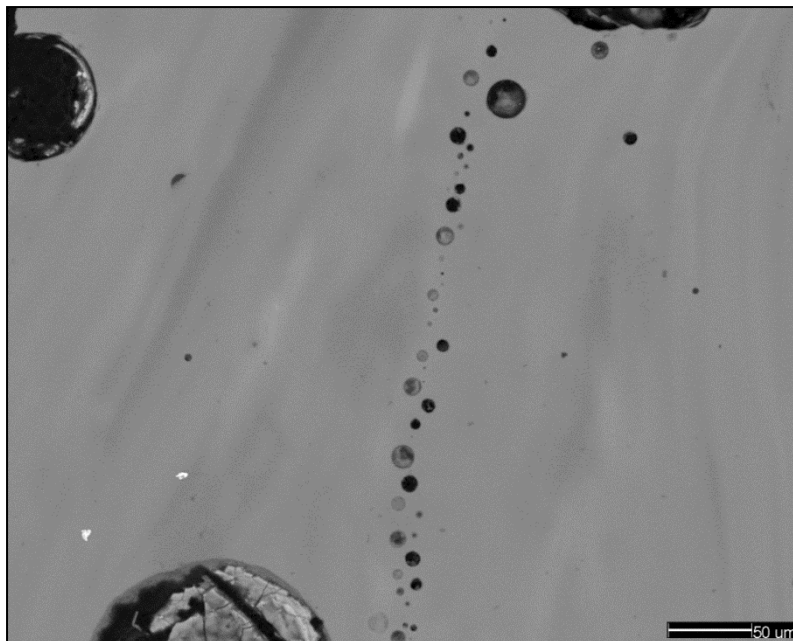


Figure 5.2.90 – BSE micrograph showing opaque blue-green sample ERL046:G03:1289, a *Blue Melon, opaque* bead. A lead-rich soda-lime-silica glass matrix can be seen (pale grey). Apart from a few bubbles of considerably variable size and a two very small crystals of tin oxide (bright white), this glass is largely devoid of inclusions.

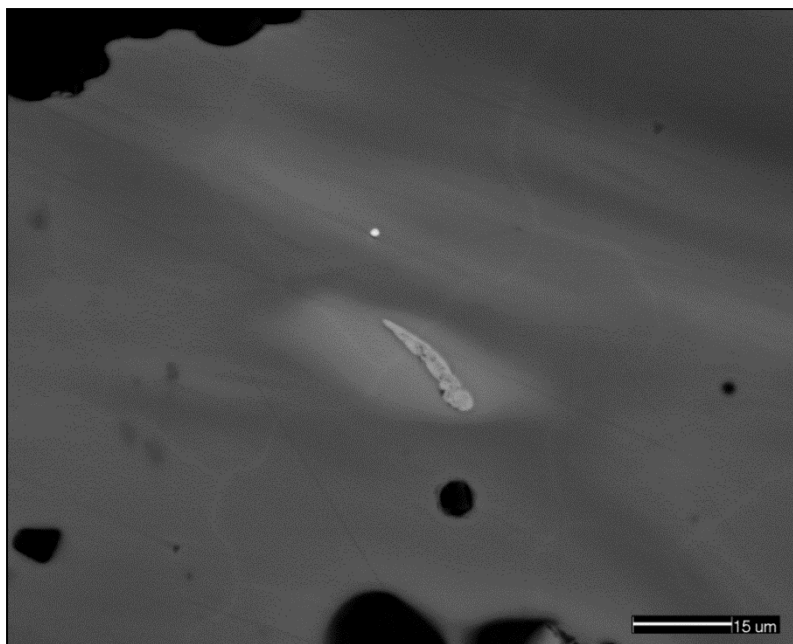


Figure 5.2.91 – BSE micrograph showing opaque blue-green sample ERL046:G03:1289, a *Blue Melon, opaque* bead. Towards the centre of the image a copper oxide inclusion (pale grey) is visible, containing trace levels of zinc and silver. Slightly above this inclusion, a small particle of metallic silver (bright white) can be seen. Variations in the shades of grey in this glass reflect slight differences in the lead content of the glass, due to uneven mixing of the batch. Black areas represent bubbles and voids.

The yellow colour produced by colloidal dispersions of metallic silver is well-recognised in the production of lustre glazes on ceramics from the 8th century AD onwards in the Islamic world (Brill 2006: 138). It is likely that this modified the typical green colour produced by copper in a high-lead glass, producing the blue-green colour observed; most dichroic glass coloured by gold or silver nanoparticles is bluish-grey or green in reflected light (Barber and Freestone 1990: 41; Brill 2006: 136). The deliberate use of recycled Roman cullet is likely to have favoured the reduction of metallic silver due to the presence of approximately 0.3% antimony, which was frequently used as a decolourant in Roman glass (Freestone *et al.* 2007: 272).

The technology of this glass is paralleled by that of glass from the preceding Roman period; for example, the production of dichroic glass such as that used to produce the Lycurgus Cup (Barber and Freestone 1990; Freestone *et al.* 2007). Two fragments of dichroic glass have also been recovered from the 7th century monastery at Jarrow in Northumbria (Brill 2006: 136). In all cases, colour is produced by minute metallic particles of gold-silver alloy containing low concentrations of copper (Barber and Freestone 1990: 41; Brill 2006: 136; Freestone *et al.* 2007: 272). However, only 2 ppm Au was detected in the opaque blue-green samples from Eriswell (see section 5.2.7.1 below), so opacity here is likely to be wholly caused by metallic silver. Furthermore, the samples analysed from Eriswell are not dichroic. Whether or not these beads represent a failed attempt at producing a dichroic glass is open to interpretation.

The technology of these beads demonstrates that the Anglo-Saxon craftsmen that produced them had considerable skill and expertise, especially considering the large number of variables which could lead to failure of the colour (Freestone *et al.* 2007: 275). As such, it may have been a very expensive colour to produce. Furthermore, this demonstrates the continuation of the use of nanotechnologies based upon silver into the early medieval period, following the collapse of the Roman Empire. Whilst it cannot be excluded that these beads were produced from a fragment of Roman glass which was already coloured in this way, even if this were the case considerable skill would have been required in order to retain this colour upon re-melting and cooling the glass.

5.2.7.1. Trace Element Analyses

‘Roman’ sample ERL046:G03:1289 (*Blue Melon, opaque*) was the only opaque blue-green glass analysed by LA-ICP-MS. The trace element pattern for the colourant and colourant-related elements for this sample match that for the ‘Roman’ translucent copper-green samples from Eriswell very closely (Figure 5.2.92), indicating that the colourant technologies are broadly similar. However, the opaque blue-green sample contains considerably elevated levels of silver, corresponding to 800 ppm Ag.

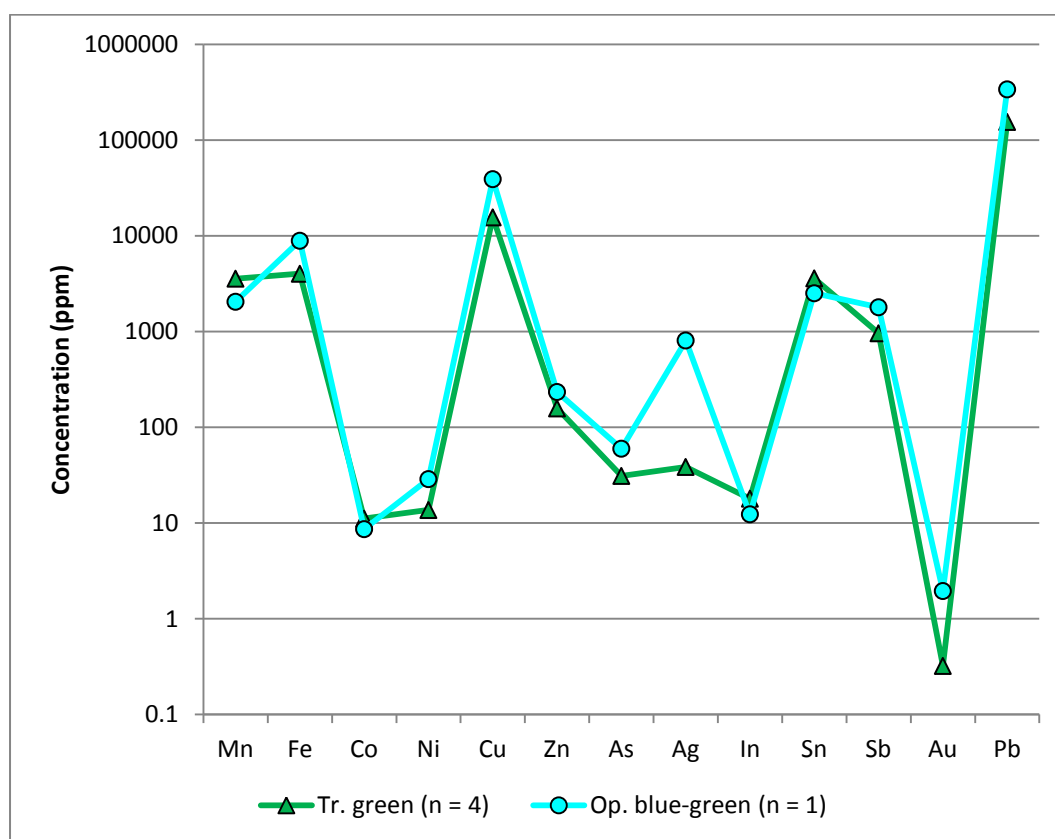


Figure 5.2.92 – Colourant and colourant-related element concentrations for opaque blue-green sample ERL046:G03:1289 from Eriswell, compared to the average concentrations of these components for translucent green glass. All samples are of the ‘Roman’ type. Note the logarithmic scale.

The concentration of silver is too high to suggest that it was incidentally introduced with copper as an impurity. Instead, it is likely to have been a deliberate addition to produce opacity, as described above. Whilst the presence of silver nanoparticles can

only be confirmed by further examination using transmission electron microscopy (TEM) (*e.g.* Barber and Freestone 1990; Barber *et al.* 2009; Brun *et al.* 1991; Frederickx *et al.* 2004; Freestone *et al.* 2007), the identification of a particle of metallic silver in sample ERL046:G03:1289 (Figure 5.2.91), when taken together with the lack of any visible opacifying agent and the detection of 800 ppm Ag, strongly argues for opacification by a colloidal dispersion of metallic silver.

5.3. Colourant Sources

The glassmakers producing coloured glasses would not have had a fundamental understanding of the chemistry of the additives they employed, but they clearly had the skill and knowledge necessary to produce a range of different colours. They were able to control the furnace atmosphere and redox conditions within the glass to an extent to which they could produce the colour they desired, relatively independently of the quantities of colourant materials and unintentional impurities introduced into the glass batch.

The naturally tinted (uncoloured) glasses are all unintentionally coloured by varying concentrations of an iron impurity, in combination with varying amounts of antimony and/or divalent manganese as decolourants, which produce different tints depending upon the redox conditions of the furnace atmosphere. A handful of translucent green glasses are coloured by high levels of iron in different states of oxidation (ferric to ferrous), which may have been deliberately added in a handful of cases. Iron is also a deliberate colourant in the 'dark' glasses, where it is present in very high concentrations. The pink-brown glasses are coloured by manganese in the trivalent state (Mn^{3+}), which required an oxidising furnace atmosphere to form. The blue glasses are all coloured by cobalt; copper was not identified as a colourant here but low concentrations appear to have been introduced as an impurity, together with iron, in the cobalt colourant.

The copper-green, turquoise, orange, red and opaque blue-green glasses are all coloured by copper, which produces a range of different colours depending upon its oxidation state: green or turquoise in oxidising conditions (cupric copper, Cu^{2+}) and red (metallic copper, Cu^0) or orange (cuprous copper, Cu^+) in reducing conditions. The concentration of lead in the glass further determined the colour produced by cupric copper: green results in a high-lead glass and turquoise in a low-lead glass. The opaque yellow glasses are both coloured and opacified by crystals of lead-tin oxide (lead stannate, PbSnO_3); this compound also produces the opacity in the opaque green glasses.

Compounds of tin were the primary crystalline opacifying agents observed in the opaque glasses from Eriswell. Opaque white glass does not contain a deliberate colourant, but is opacified either by tin oxide (cassiterite, SnO_2) or a dispersion of tiny bubbles. The opaque blue glasses are also opacified by either tin oxide or bubbles, but in the presence of a cobalt colourant. Opacity in the opaque turquoise glasses is caused by either tin oxide or calcium antimonate, in the presence of a cupric copper colourant; the calcium antimonate opacified glass may represent a Roman survival.

Opacity is caused by metallic copper nanoparticles in the opaque red glasses and by cuprite crystals in the opaque orange glasses; the copper also produces the colour in both cases (see above). Opacity in the two opaque blue-green samples analysed is probably caused by a colloidal dispersion of metallic silver in the presence of a cupric (Cu^{2+}) copper colourant, although further analysis is required to confirm this. While silver appears to have been introduced as an impurity with copper in all of the copper-based colours, it is comparatively elevated in opaque blue-green sample, suggesting a deliberate addition (Figure 5.3.1).

It has been suggested that most non-ferrous metalworking during the Anglo-Saxon period relied upon salvaged scrap (Leahy 2011: 451). This also appears to be the case for many of the colourants used to produce the coloured glasses from Eriswell, as will be seen.

5.3.1. Cobalt

Different cobalt ores are often associated with a number of impurities introduced at trace levels (*e.g.* indium; see Figure 5.3.3), lending them well to chemical characterisation. It is known that at least two main cobalt sources were exploited in antiquity: one that was rich in arsenic and one that was rich in manganese (Hall and Yablonsky 1997: 373; Henderson 1985: 278-281; Henderson 1990: 157; Henderson 2003: 240; Sayre 1963: 267). However, arsenic is very volatile, so its presence or absence is not always a reliable indicator of the use different cobalt sources (Fiori and Vandini 2004: 186; Henderson 1985: 36; Henderson 1990: 157; Shortland 2012:

165). Furthermore, manganese was often introduced as a decolourant in the base glass types used. There is still some disagreement as to where these different types of cobalt ore were obtained; some authors favour a Near Eastern or Iranian source, whereas others suggest that a European source is possible (Gratuze *et al.* 1995: 126).

Arsenical cobalt ores are typically low in manganese and rich in traces of copper, iron and zinc, whereas manganese-rich cobalt ores are usually low in copper and zinc (Hall and Yablonksy 1997: 373). Whilst it was not possible to accurately establish the extent to which manganese or arsenic were present in the cobalt colourants employed in the production of the blue samples from Eriswell, the presence of iron, copper, nickel and zinc as impurities (see this chapter, section 5.1.3.1) would appear to favour an arsenical cobalt source; copper is particularly strongly correlated with cobalt in the ‘Saxon I (blue)’ samples. The general detection of arsenic at higher concentrations than manganese in the cobalt inclusion in Appendix L supports this view. The association of cobalt with nickel, which are again positively correlated in many of the ‘Saxon I (blue)’ and ‘Saxon II (high MgO, low MnO)’ samples, is also consistent with this view; nickel is often found as an impurity in arsenical cobalt ores (Gratuze *et al.* 1995: 125; Kleinmann 1990: 334). Correlations between cobalt and zinc, as observed in the ‘Saxon I (blue)’ samples (see this chapter, section 5.1.3.1), may indicate the cobalt ore was extracted together with zinc blende (Gratuze *et al.* 1995: 125).

Arsenical cobalt sources are traditionally thought to have been sourced from the Middle East (Hall and Yablonksy 1997: 373; Henderson 2000a: 31; Kleinmann 1990: 334). This would support the view that ‘Saxon I (blue)’ glass may have been pre-coloured in the Near East, where the raw glass itself is likely to have been manufactured (see this chapter, section 4.9). Arsenic has also been found in cobalt ores, together with nickel, from the Blackforest (Henderson 1989b) and Erzgebirge (Ore Mountains) (Gratuze *et al.* 1995: 126) regions of Germany. However, cobalt mining does not appear to have taken place in these regions prior to the 12th century (Gratuze *et al.* 1995: 125), so they are unlikely to have been exploited for the production of blue glass in the early Anglo-Saxon period.

Cobalt is unlikely to have been as widely available as other colourants, which has led to suggestions that Anglo-Saxon blue glass may have been made at just one manufacturing centre (Wilthew 2006: 394). The Eriswell data support the view that cobalt-blue glass was coloured in a limited number of workshops; raw ‘Saxon I (blue)’ glass, ‘A2b Blue’ glass and possibly also translucent blue ‘Saxon I (natron)’ glass are likely to have been pre-coloured (see Chapter 4, section 4.9). There are also relatively clear correlations between the different cobalt sources used and bead type, suggesting that different bead types were produced in separate workshops or at slightly different times, using glass coloured by cobalt from slightly different sources (see Chapter 4, section 4.10.4). It is likely that some (or all) of these cobalt sources have their origins in the Near or Middle East. A European cobalt source cannot be ruled out, but on balance seems unlikely.

It is unclear as to how cobalt was prepared prior to its use as a colourant. Whilst it has been argued that the direct addition of a cobalt-rich ore to blue glass is unlikely (Fiori and Vandini 2004: 186; Henderson 1985: 279), the identification of an apparently unrefined cobalt-rich inclusion in bead ERL104:G263:1411 (see this chapter, section 5.1.3) suggests that cobalt is likely to have been directly added in its mineral form in at least some cases. If arsenical cobalt ores *were* used, it is possible that they were roasted prior to use, thus removing the majority of arsenic (Gratuze *et al.* 1995: 125), or that arsenic was lost during the melting of the glass itself.

In addition, a very limited quantity of translucent blue samples from Eriswell appear to have been coloured through the addition of old Roman antimony-opacified blue cullet, possibly in the form of tesserae (see this chapter, section 5.1.3); this practice may have taken place in either England or on the Continent, or both.

5.3.2. Copper

Scrap copper, as opposed to freshly smelted copper, is likely to have been used as a colourant in many of the coloured glasses from Eriswell. The data suggest that this scrap copper is likely to have been alloyed in many cases; for example with tin (*e.g.* bronze) or zinc (*e.g.* brass). It is likely that the supply of copper used in the

production of jewellery and glass was obtained as scrap metal from the preceding Roman period (Bayley *et al.* 2008: 50; Hinton 2011: 427; Leahy 2011: 451), as copper does not appear to have been exploited in England after the Roman period until the 12th century AD (Hinton 2011: 427). This view is supported by the presence of silver as an impurity in many of the glasses coloured by copper (*e.g.* Figure 5.3.1); high levels of silver were also detected during spot analysis of metallic copper particles in the opaque red glasses (see this chapter, section 5.2.3). The low-tin bronzes used during the Roman period often contain low levels of silver; some 4th century bronze coins have also been found to contain over 2% silver (Tylecote 1992: 70-71). Other bronze coins were plated with silver during the Roman period (Tylecote 1992: 70), so the use of scrap copper metal containing traces of silver, perhaps as decoration, is also feasible. It is not possible to speculate here as to the extent to which tin or lead may have been introduced through the use of copper alloys, as they appear to have been primarily introduced with a separate ingredient rich in both of these components.

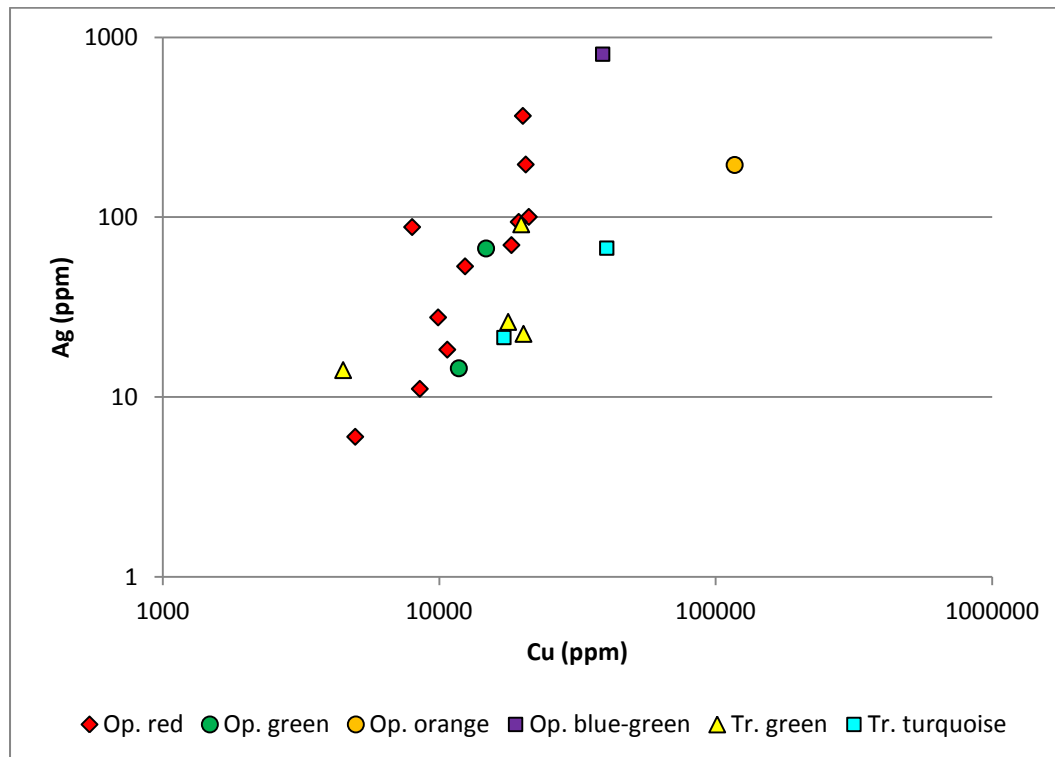


Figure 5.3.1 – A plot of copper versus silver in the copper-based glass colours from Eriswell (LA-ICP-MS data). Note the logarithmic scale.

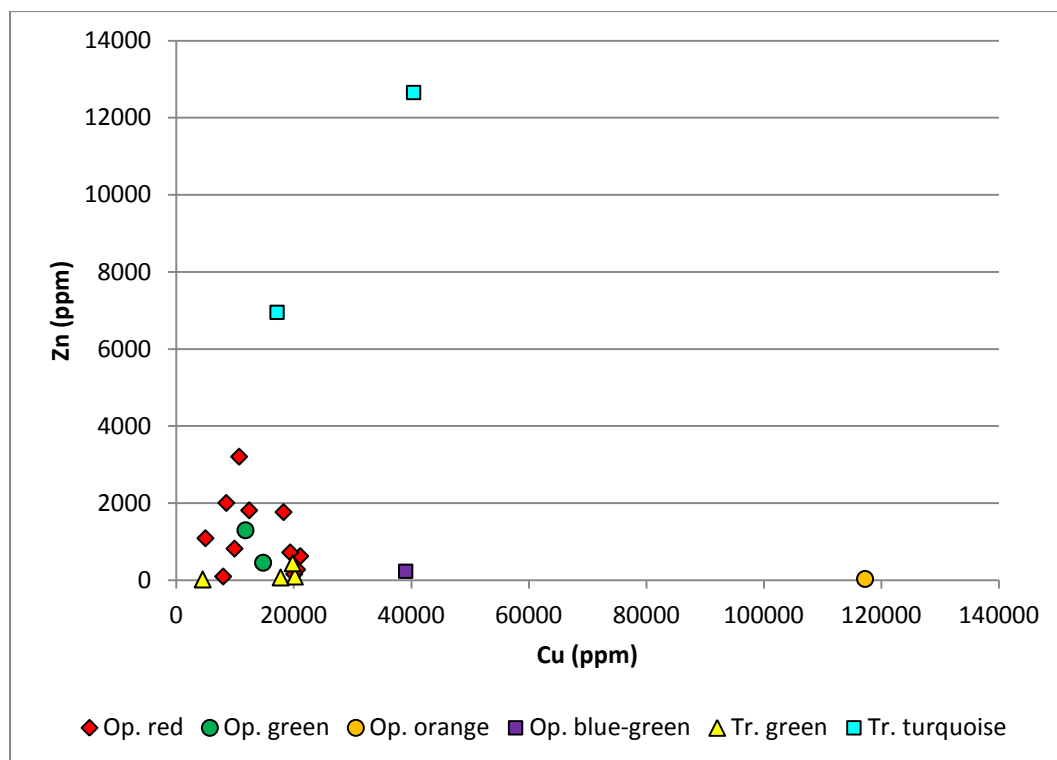


Figure 5.3.2 – A plot of copper versus zinc in the copper-based glass colours from Eriswell (LA-ICP-MS data).

On balance, it is likely that the source of copper in the majority of copper-based colours was sourced from scrap Roman material. Indeed, metalworking evidence from early Anglo-Saxon England is very rare; this appears to have been a period of recycling with little or no production of new metal (Bayley *et al.* 2008: 49-50). Furthermore, scrap copper alloy which was clearly scavenged from Roman sites has been found in Anglo-Saxon contexts (Hinton 2005: 35). The picture is less clear with regard to turquoise glass. The copper colourant used in the translucent turquoise samples appears to have contained particularly high levels of zinc (Figures 5.1.35 and 5.3.2), suggesting the use of an alloy such as brass in the production of this colour.

In other copper-based colours (red and green), the presence of zinc is primarily peculiar to ‘Saxon II’ glass (*e.g.* Figures 5.1.35 5.2.47), but it was also detected in a small number of ‘Roman’ samples suggesting that it may have been used earlier. The data for the majority of glasses containing in excess of 0.3% ZnO suggest that such a copper alloy would have typically contained approximately 10-30% zinc. Analyses of early brasses show that most contain 15-25% zinc, but may contain up to 28%

(Bayley *et al.* 2008: 47), which is broadly consistent with this. It is therefore likely that copper-zinc alloys were sourced from scrap Roman material.

5.3.3. Tin

Tin oxide was used to produce opacity in many of the opaque white and opaque blue samples from Eriswell. The main outcrops of tin in Europe are restricted to Spain, Brittany, Saxony and Britain, but it is virtually absent in Mediterranean regions (Salter 2009: 316). The tin deposits in Britain, predominantly situated in Devon and Cornwall, were the largest known to the ancient Western world (Meharg *et al.* 2012: 717). Spanish tin deposits were certainly exploited during Roman times, until the Spanish mines were exhausted in the 3rd century AD (Meharg *et al.* 2012: 717; 724; Tylecote 1992: 70). Whilst it has been assumed that British tin sources were not exploited until this time, recent evidence on the deposition of tin in radiocarbon-dated peat deposits from Dartmoor suggests that they are in fact likely to have been exploited throughout the Roman period, between *c.* AD 100-400 (Meharg *et al.* 2012: 724). These dates coincide well with the Roman occupation of Britain up until the 4th century (Meharg *et al.* 2012: 724) and also with the gradual introduction of tin as a substitute for antimony in glassmaking, which is thought to have taken place between the 2nd and 4th centuries AD (Turner and Rooksby 1961: 1-2; Turner and Rooksby 1963).

The tin sources exploited during the early Anglo-Saxon period remain unknown. British deposits of tin are all situated in areas which would have been under Celtic control during the early Anglo-Saxon period (Leahy 2003: 136) and would therefore not have been easily exploitable by Anglo-Saxon craftsmen. Indeed, scientific evidence suggests that there was a lull in tin exploitation in southwest Britain between the 5th and 7th centuries, as might be expected following the withdrawal of Rome, but that there was a resurgence in its extraction from approximately the 8th century onwards (Meharg *et al.* 2012: 725). The discovery of tin ingots suggests that tin may have been extracted by the native Britons between the 5th and 7th centuries (Hinton 2011: 428), but if so it is likely to have been a relatively small-scale industry; nevertheless this would probably have been a sufficient supply for the

production of opaque white glass. However, it is notable that Bede, writing in the 8th century, fails to mention tin as a natural asset of Britain in his *Ecclesiastical History*, but does include crops, trees, jet, silver, copper, lead and iron (Hinton 2011: 423).

It is likely that tin was also, or instead, obtained as scrap metal from the preceding Roman period; tin is found in small quantities on early Anglo-Saxon sites (Hinton 2005: 36), which may reflect such a practice. Furthermore, the lead-tin pigment used to produce opaque yellow glass may have been obtained from pewter (a lead-tin alloy), which could also have been used as a source of lead in the production of some colours (see section 5.3.4 below). It is notable that G242 and G243 at Eriswell contain both tin oxide and bubble-opacified white beads, suggesting that the two technologies may relate to different production zones; the use of ‘Roman’ glass to produce bubble-opacified glass is more consistent with ‘Anglo-Saxon’ production (see Chapter 4, section 4.10), which may support the view that local tin sources were unavailable. However, as bubble-opacified ‘Roman’ glass appears to be earlier, whereas tin oxide opacified ‘Saxon II’ and ‘Levantine I’ glass appear to be later, it is also possible that tin was not exploited in Britain (at least in any quantity) until the 6th century following the withdrawal of Rome.

Indium was introduced as an impurity with tin in all of the tin-containing glasses, with the exception of blue glass. Figure 5.3.3 shows an absolute linear positive correlation between tin and indium ($r^2 = 1.0$) in all colours, due to the introduction of indium with stannite; this correlation is not maintained in the cobalt-blue glasses due to the predominant introduction of tin as an impurity in the cobalt colourant.

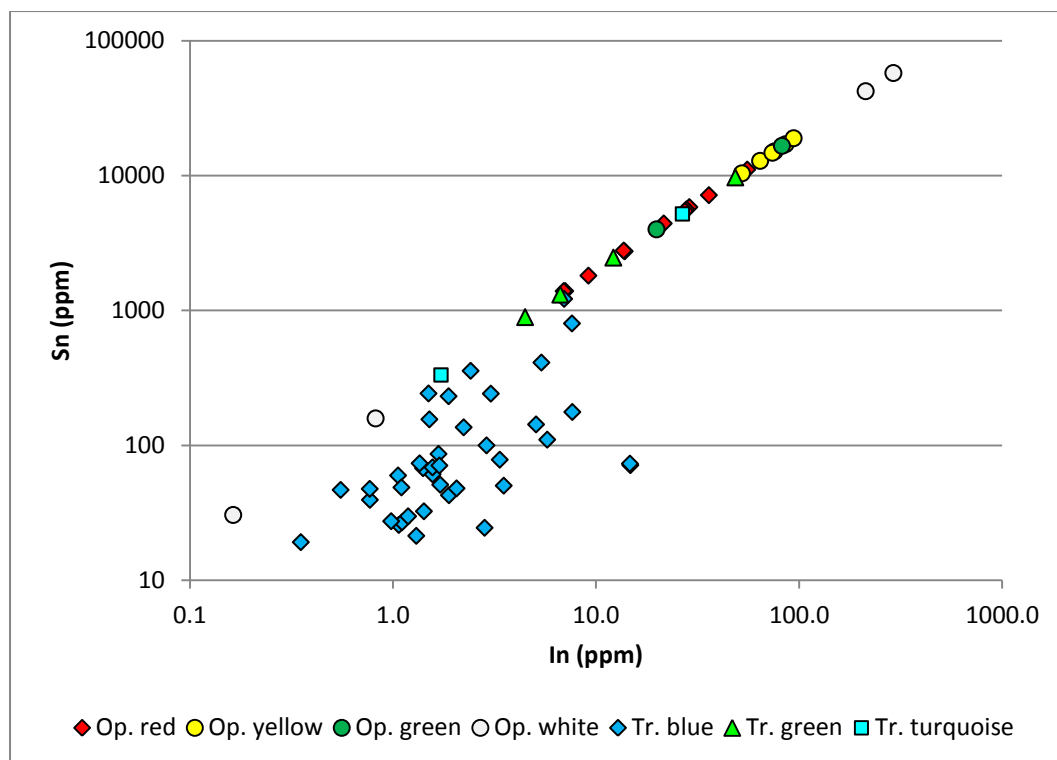


Figure 5.3.3 – A plot of indium versus tin in selected glass colours from Eriswell (LA-ICP-MS data). Note the logarithmic scale.

5.3.4. Lead

The benefits of lead as a flux are widely recognised; in the copper-green glasses its presence is required to produce the colour, but it also reduces the melting temperature of glass and consequently the labour and amount of fuel required to work it (*e.g.* Brill and Cahill 1988: 19-20; Cable and Smedley 1987; Freestone 1987, Freestone *et al.* 2003b). It may have been obtained as scrap from Roman sites during the early Anglo-Saxon period, where it would probably have been readily available (Hinton 2011: 428; Tylecote 1992: 89). It was principally used during the Roman period to produce pewter (an alloy of lead and tin) (Tylecote 1992: 92). Lead and tin were probably introduced together in tin oxide opacified white glass, as it is difficult to calcine metallic tin without lead (Freestone *et al.* 1990: 275; Kingery and Vandiver 1986: 116; see also this chapter, section 5.2.1). Similarly, in the production of opaque yellow glass, lead-tin oxide (lead stannate, PbSnO_3) is likely to have been added to a soda-lime-silica glass as a pre-formed pigment (see this chapter, section 5.2.2).

A similar lead-tin calx appears to have been used to produce opaque green glass (see this chapter, section 5.2.2), albeit in much lesser quantities; this suggests that it is not opaque yellow glass to which copper has been added. However, the present data suggest that a similar material, rich in both lead and tin, was used to produce other high-lead colours, including opaque red and translucent copper-green glass. Whilst tin could conceivably have had some technological benefit in the production of the colour in opaque red glass (see this chapter, section 5.2.3), this is not the case with translucent green glass. The quantities observed are too high to suggest that it was unintentionally introduced through the use of a copper alloy colourant or through accidental contamination from another tin-rich glass. It must therefore represent a 'deliberate' addition.

The ratios of lead and tin in the opaque red and translucent green glasses from Eriswell are similar to those detected in the opaque yellow and opaque green glasses (particularly the latter; *e.g.* Figure 5.3.4). This suggests that tin was introduced deliberately in the form of a material rich in both lead and tin, similar to lead-tin yellow pigment. It seems likely that this material was added as a source of lead. The reasons as to why lead does not appear to have been added as a separate ingredient are not entirely clear, but the most likely explanation is that it was only readily available as scrap pewter (a lead-tin alloy), perhaps Roman. It is also possible that lead could only be used in glass production if it was pre-mixed with silica, because melting temperature of lead is much lower than that of a soda-lime-silica base glass (Wedepohl *et al.* 1995: 65). Lead-tin yellow pigment contains silica from a reaction with the crucible in which it is produced (Heck *et al.* 2003: 37-38). As such, it would have had a higher melting temperature than metallic lead, more closely matching the soda-lime-silica glass to which it was added. By varying the amount added and carefully controlling the furnace conditions and/or cooling rate, it would have been possible to determine the extent to which tin crystallised out of solution as lead-tin oxide (*e.g.* in opaque yellow or green glass), or largely remained in solution (*e.g.* in translucent green and opaque red glass).

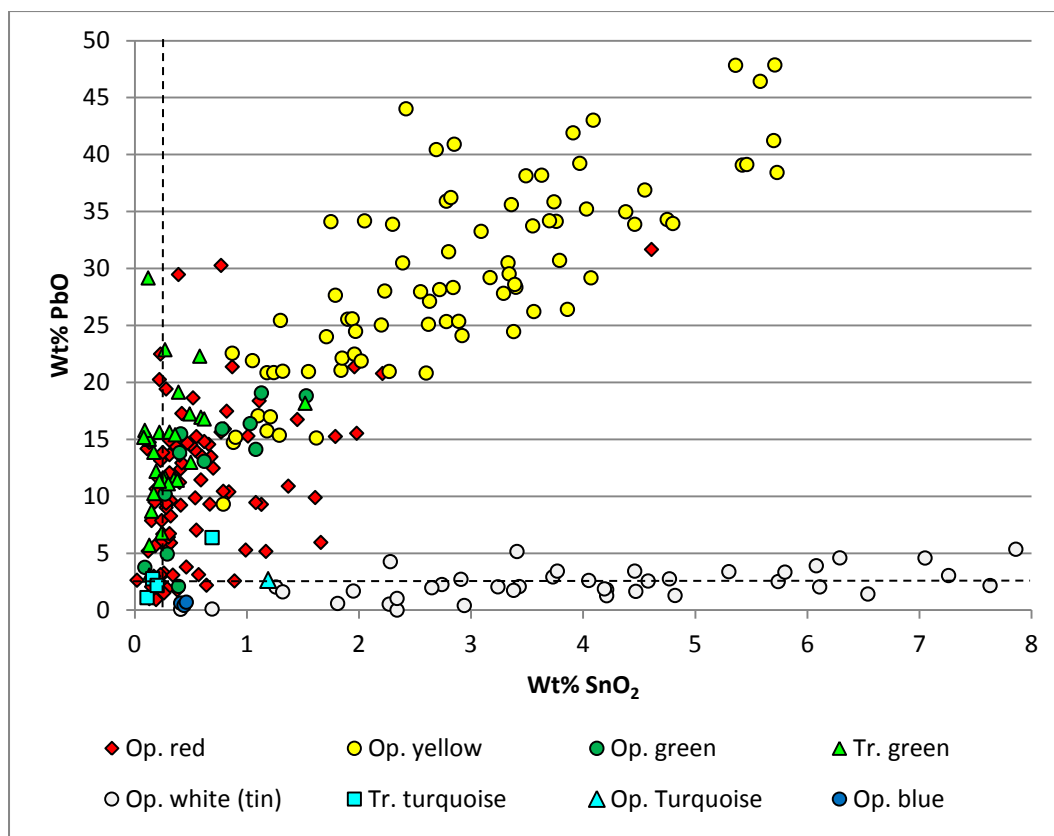


Figure 5.3.4 – A plot of tin oxide versus lead oxide in the tin-containing glass colours from Eriswell. The dashed lines represent the approximate detection limits for tin oxide and lead oxide.

Lead-tin yellow pigment may have been widely traded (*e.g.* Peake and Freestone, in press); it is therefore just possible that the lead-tin material used in the production of the glasses analysed from Eriswell was imported, although on balance this seems unlikely. Note that this is different to the lead-tin calx used to produce tin oxide opacified white, blue and turquoise glass (Figure 5.3.4). However, both lead and tin have been found in small quantities on early Anglo-Saxon sites (Hinton 2005: 36), so it cannot be excluded that lead-tin calx was locally produced from scrap material.

5.3.5. Manganese and Antimony

Manganese could be deliberately added as either a decolourant (see Chapter 4, section 4.1.4) or a colourant (see this chapter, section 5.1.2). Pyrolusite (MnO_2) is usually assumed to have been used as a source of manganese in early glassmaking (Brill 1988: 276; Freestone *et al.* 2005b: 156; Green and Hart 1987: 276; Henderson 1985: 283; Sayre 1963; Schreurs and Brill 1984: 208; Silvestri *et al.* 2005: 810; Silvestri *et al.* 2008: 336; Wedepohl *et al.* 2003: 57; Weyl 1951: 120), as it is one of the purest mineral forms of manganese (Jackson 2005: 764; Watkinson *et al.* 2005: 73). Manganese is also found in a number of other less pure minerals, but most of these would have required processing prior to use (Jackson 2005: 764). It is not possible to identify the sources of manganese from chemical analysis in the present study, as it is unclear as to whether (or how) mineral forms of manganese were processed prior to use (Jackson 2005: 764). However, the association of manganese with barium (*e.g.* Figure 4.2.20) suggests that the manganese oxide or hydroxide *wad* may have been used (Silvestri 2008: 1499). In addition, low concentrations of manganese may also be introduced with a plant-ash addition (see Chapter 4, section 4.4) or through the use of recycled manganese-bearing cullet (see Chapter 4, section 4.3).

Antimony is also found in several minerals (Biek and Bayley 1979: 9; Jackson 2005: 764), but is unlikely to have been sourced as a raw material in the early Anglo-Saxon period. It was instead unintentionally introduced to the batch through the use of old antimony-bearing Roman 'colourless' cullet (see Chapter 4, section 4.3), or through the addition of highly coloured antimony-opacified Roman cullet as a colourant (see this chapter, section 5.2.3).

5.3.6. Iron

Iron was required as a colourant in ‘dark’ glass (see this chapter, section 5.1.5) and as an internal reducing agent in opaque red glass (see this chapter, section 5.2.3). In the majority of cases, this appears to have been introduced in the form of fayalitic or kirschsteinitic metallurgical slag, but the addition of iron as scale or dross in some of the ‘dark’ glasses cannot be ruled out. The slag ultimately derived from the extraction of metals from their ores, which at present appears to have certainly included iron, and possibly also copper. Iron ores are widespread throughout Britain (Bayley *et al.* 2008: 44), so sourcing the raw materials from which the slag was derived is unlikely to have been a problem.

It is possible that these beads were produced in workshops which were located in close proximity to the copper- and iron-smelting industries respectively; there is likely to have been significant interaction between these two industries (see Peake and Freestone 2012). The local sourcing of slag for use in the production of opaque red glass would not have been a problem; for example, slag heaps have been discovered around the Anglo-Saxon cemetery at Cleatham, Lincolnshire (Leahy 2003: 96). Clearly at least two sources of slag were utilised (see this chapter, section 5.2.3.1), suggesting some experimentation. Alternatively, considering the extent of recycling of non-ferrous metals during the early Anglo-Saxon period (see section 5.3.2 above), the slag may have been sourced from historic (possibly Roman) metallurgical slag deposits. The composition of the slag is more consistent with smelting slag, which is less common on early Anglo-Saxon sites in England (Hinton 2005: 35), supporting this view.

CHAPTER SIX

6. Later Anglo-Saxon Glass

No mid-Saxon (8th-9th century) glass was analysed as part of the present study; furnished burial was generally no longer practiced by this time. However, a number of published analyses of glass of this date from England do exist, and a very brief comparison is therefore worthwhile. Window glass from the late 7th century monasteries at Wearmouth and Jarrow in Northumbria have been analysed by Brill (1999; 2006) and by Freestone and Hughes (2006). Furthermore, a large assemblage of 270 glass fragments from 8th-9th century Hamwic (Southampton) have been analysed by Hunter and Heyworth (1998).

These glasses are generally of the natron compositional type, containing low concentrations of both potash and magnesia, without an added ash component. This is reflected in contemporary glass from elsewhere in Europe (Freestone *et al.* 2008: 41), including the Crypta Balbi in Rome (Mirti *et al.* 2001) and San Vincenzo, Brescia and Cividale in Italy (Freestone and Dell'Acqua 2005). It is clear that old coloured Roman glass was being introduced into these glass batches, as evidenced by the presence of low concentrations of colourant elements detected, including antimony and lead (*e.g.* Brill 2006: 139-140; Freestone 2003: 113; Freestone and Hughes 2006: 150-151; Freestone *et al.* 2008: 41; Hunter and Heyworth 1998). This is likely to reflect an increasing dependence upon the recycling of old Roman material in the later Anglo-Saxon period (Freestone *et al.* 2008: 41).

Elevated levels of antimony have been detected in translucent glass from the mid-Saxon sites of Ribe (Jutland) and Åhus (Sweden) (Callmer and Henderson 1991: 148-149; Henderson 2000a: 72-73), which also suggest a dependence upon Roman cullet. This practice is further suggested by the increase in the presence of old Roman tesserae on known glassworking sites from this period (*e.g.* Ribe in Denmark) (Evison 2000: 91; Henderson 2000a: 70), presumably imported for the colouring of glass or for direct use in the production of coloured beads or enamels, in

a manner similar to that described by Theophilus (Freestone 1993: 743; Hawthorne and Smith 1979: 59). This view is supported by the presence of opacifying agents based on compounds of antimony (typically found in opaque Roman glass) in several of the opaque glass beads from Ribe (Henderson 2000a: 74) and Åhus (Callmer and Henderson 1991: 150-151).

A comparison of the glass analyses from Wearmouth/Jarrow and Hamwic (after Brill 2006; Freestone and Hughes 2006, and Hunter and Heyworth 1998) with the data from Eriswell shows that later Anglo-Saxon glass is broadly consistent with glass of the 'Roman' compositional type (Figures 6.0.1 and 6.0.2). This supports the view that the vast majority of later Anglo-Saxon glass is, at least in part, likely to be based upon the re-use of earlier Roman material (*e.g.* Freestone and Hughes 2006: 154). Whilst Freestone and Hughes argue that the Jarrow glass is essentially different from Roman colourless glass, their interpretation is based upon a comparison to both Roman blue-green *and* Roman antimony-decolourised glass; the latter has a different composition to the Jarrow glass, being lower in lime and alumina (see Chapter 4, section 4.3). When compared to Roman blue-green glass alone the similarities are far more striking (Figures 6.0.1 and 6.0.2). This trend is reflected at Eriswell; the predominant recycling of Roman blue-green glass, with recycled antimony-decolourised glass being absent or near-absent.

In spite of these similarities, later Anglo-Saxon glass has a number of differences which set it apart from earlier Roman glass; potash and iron oxide are both typically present at concentrations in excess of 1.0%, when they are typically present at concentrations below this in Roman glass. Furthermore, Alumina is often considerably elevated, being typically present at levels well in excess of 2.6%, when it is usually present at concentrations below this in Roman glass.

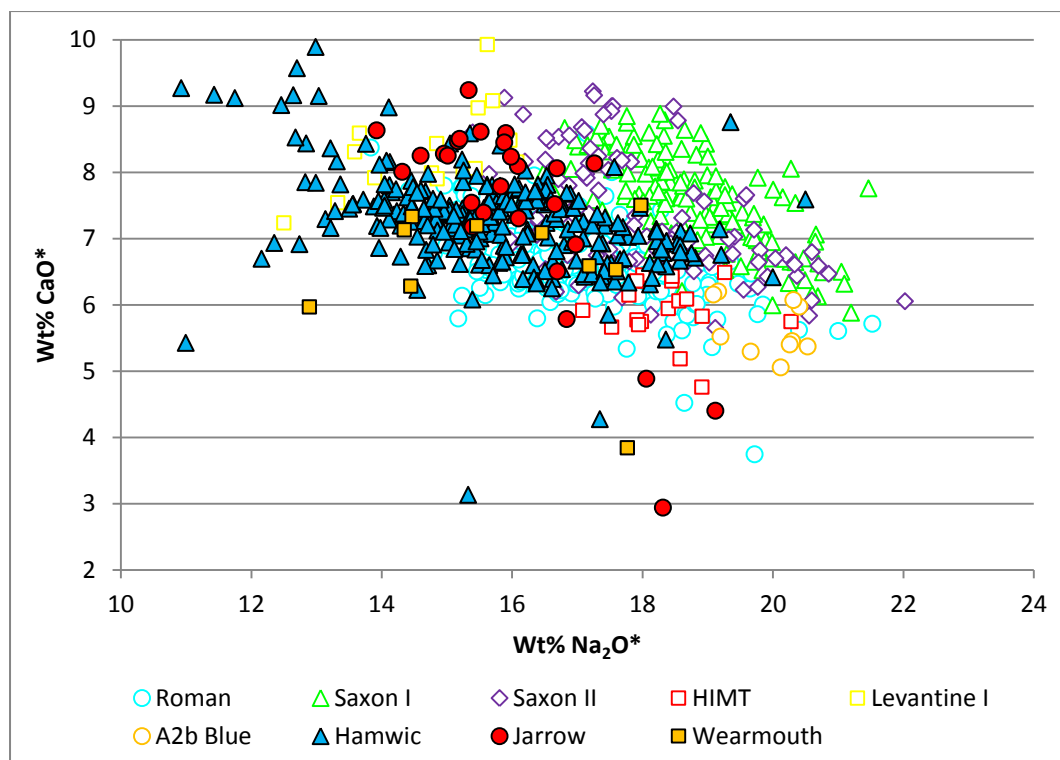


Figure 6.0.1 - A plot of soda versus lime for late Anglo-Saxon (8th-9th centuries) glass from Hamwic (Hunter and Heyworth 1998), Jarrow (Brill 1999; 2006; Freestone and Hughes 2006) and Wearmouth (Brill 2006) compared to the different base glass types identified at Eriswell.

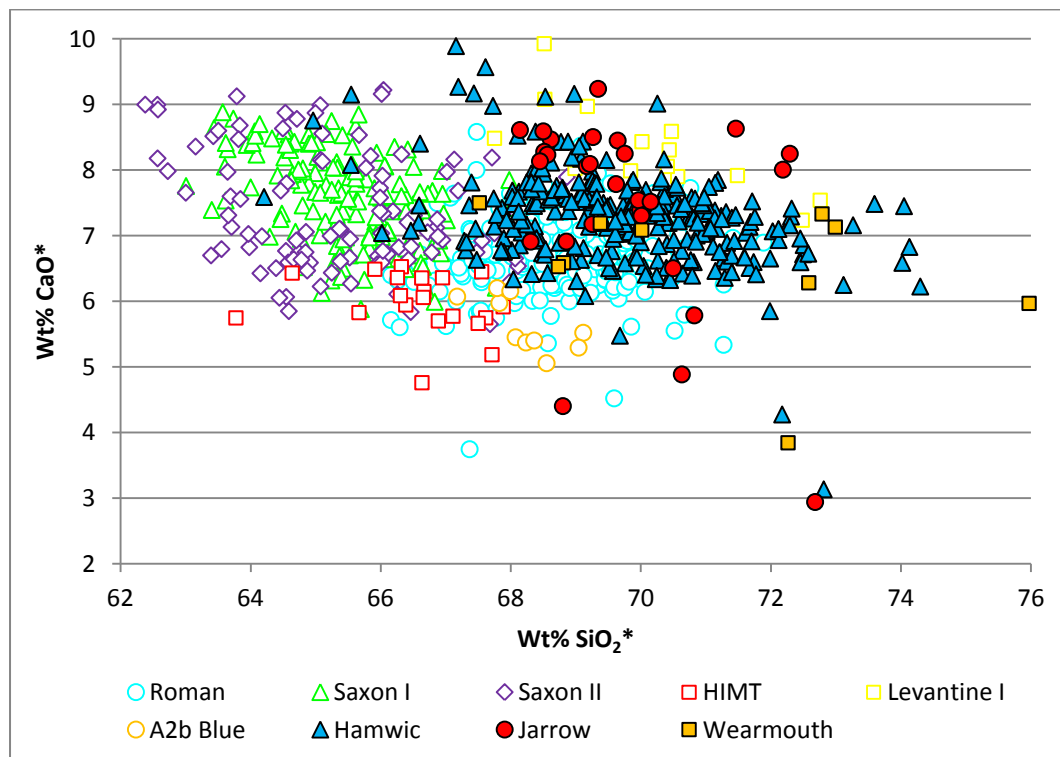


Figure 6.0.2 - A plot of silica versus lime for late Anglo-Saxon (8th-9th centuries) glass from Hamwic (Hunter and Heyworth 1998), Jarrow (Brill 1999; 2006; Freestone and Hughes 2006) and Wearmouth (Brill 2006) compared to the different base glass types identified at Eriswell.

This is consistent with recycled glass that has undergone a number of successive melting and re-melting cycles, becoming enriched in iron and alumina from the crucible (*e.g.* Freestone and Hughes 2006: 148; Jackson 1996: 291; see also Chapter 4, section 4.1), and potash from the furnace atmosphere or contamination by fuel ash (*e.g.* Paynter 2008; Tal *et al.* 2008a: 72; Tal *et al.* 2008b: 91). It is also possible that later Anglo-Saxon glass represents a mixture of glass from a number of different sources; for example, ‘HIMT’ glass may have been mixed into the batch (Freestone and Hughes 2006: 148). However, earlier ‘Saxon’ glass (*i.e.* ‘Saxon I’ and ‘Saxon II’ glass) does not appear to have been recycled, at least in any quantity, in the mid-Saxon period; note the different ratios of soda to lime in Figure 6.0.1 and the differences in silica content between ‘Roman’ and ‘Saxon’ glass in Figure 6.0.2.

The Eriswell data, together with that of Freestone *et al.* (2008), suggest that raw natron glass was in short supply by the 7th century. This is suggested by the adulteration of natron glass with small quantities of wood ash, probably to extend the supply of raw glass from the Near East (see Chapter 4, section 4.4). There appears to have been a reintroduction of recycled ‘Roman’ glass for bead production in England around the middle or end of the 7th century (*e.g.* *Doughnut* beads), after an apparent break in the use of ‘Roman’ glass for bead production in England from around the mid- or late 6th century (see Chapter 4, section 4.8). It therefore seems likely that the supply of raw natron glass from the Near East had all but dried up by the mid-7th century, which ultimately forced glassworkers to look for alternative sources of glass (Shortland *et al.* 2006: 523; Wedepohl *et al.* 2011: 94-95). It appears that they resorted to the use of earlier Roman material once more. The same trend is apparent in 7th and 8th century natron glass from Italy; the recycling of glass appears to have become far more widespread in the 8th century than in the preceding century (Mirti *et al.* 2001: 501; Uboldi and Verità 2003: 130).

The picture remains unclear as to why glassworkers did not continue to adulterate natron glass, including recycled Roman material, with small quantities of wood ash; it may have been for technical or aesthetic reasons. It is also unclear as to why earlier ‘Saxon’ glass does not appear to have been recycled; perhaps it was not as widely available as Roman glass, or perhaps its use has been masked by the homogenisation of a melt consisting primarily of Roman glass. In any case, by the 9th-10th centuries

the composition of glass was in a state of flux in both Europe and the Near East, ultimately culminating with the introduction of the medieval 'forest' glass tradition, which would come to dominate the glass industry in northern Europe for the next few centuries (Freestone *et al.* 2008: 41-42; Henderson 1993: 255-256; Wedepohl 1997: 254).

CHAPTER SEVEN

7. Discussion and Conclusions

7.1. Comparison with Contemporary Beads

The beads analysed from Spong Hill, Bergh Apton and Morning Thorpe in Norfolk have not been included in a chapter of their own because their specific typological and chronological attributions are uncertain; many are fragmented and could not be identified, and a large number are not covered by the typologies set out in Brugmann (2004) and Penn and Brugmann (2007). Detailed comparisons are therefore difficult and may even be misleading. The base glass compositions for the beads analysed from these sites were calculated in the same way as for the beads from Eriswell (see Chapter 4, section 4.2). All of the glass types identified are represented at Eriswell, with the exception of the translucent turquoise biconical bead from grave 38/10a at Spong Hill (discussed in Chapter 4, section 4.1.3). This confirms that the same glass types were used to produce the beads from these sites as used to produce those from Eriswell, regardless of bead type. The following base glass types were identified from the sites in question:

At Bergh Apton:

- ‘Roman’ glass.
- ‘Saxon I (blue)’ glass.
- ‘Saxon I (natron)’ glass.
- ‘Saxon II (natron)’ glass.
- ‘A2b Blue’ glass.

At Morning Thorpe:

- ‘Roman’ glass.
- ‘Saxon I (blue)’ glass.
- ‘Saxon I (natron)’ glass.
- ‘A2b Blue’ glass.

At Spong Hill:

- ‘Roman’ glass.
- ‘Saxon I (blue)’ glass.
- ‘Saxon I (natron)’ glass.
- ‘Saxon II (high MgO, low MnO)’ glass.
- ‘A2b Blue’ glass.

The phase attributions for the beads produced from these glass types are consistent with the chronology set out in Chapter 4, section 4.8; general phase attributions for the respective graves from which these beads were recovered were used here (after Brugmann 2004: Table 11) as opposed to phase attributions for specific bead types, since the typological attributions of many of the beads analysed were uncertain. The compositional data are consistent with the view that the cemeteries at all of these sites went out of use before those at Eriswell (See Chapter 1, section 1.2.2).

Other than the turquoise bead mentioned above there are, however, two outliers from Spong Hill which cannot be firmly attributed to a specific base glass type. The first is a probable *Dark Globular* bead from grave 26/1 containing very low levels of soda (13.0% Na₂O*) and high levels of lime (9.8% CaO*). The elevated levels of potash (2.8% K₂O*) and phosphate (0.5% P₂O₅*) suggest a plant ash addition, but the level of magnesia is too low (1.0% MgO*) to suggest that it is a soda-ash glass; it is instead more likely to be natron glass adulterated with potassium-rich plant-ash (see Chapter 4, section 4.4). The second is the translucent blue decoration from an opaque white globular bead, again from grave 26/1. This sample has a composition consistent with ‘Levantine I’ glass; in particular, high levels of alumina (3.0% Al₂O₃*) and lime (7.9% CaO*). However, the elevated level of manganese (1.0% MnO*) is not consistent with ‘Levantine I’ glass from Eriswell, which typically contains less than 0.1% MnO*. These two outliers are likely to be isolated occurrences, or to represent the mixing of glass types from two or more sources.

The colourants used in the samples analysed from all three of the Norfolk sites are also consistent with those identified in the samples from Eriswell (see Chapter 5 for details). The uncoloured samples are naturally coloured by an unintentional iron

impurity, the pink-brown samples are coloured by manganese, the blue samples are coloured by cobalt, the green, turquoise and red samples are coloured by copper, the 'dark' glasses are coloured by iron, and the yellow samples are both coloured and opacified by lead-tin oxide (lead stannate; Figure 7.1.1). The opaque white samples are opacified by either tin oxide (Figure 7.1.2) or a dispersion of tiny bubbles (Figure 7.1.3); as with the Eriswell samples, opacification by bubbles is peculiar to glass of the 'Roman' compositional type. Lastly, all of the opaque red samples are opacified by metallic copper nanoparticles; iron-rich fayalitic metallurgical slag was again added as an internal reducing agent (Figures 7.1.4-7.1.6). No opaque orange, opaque blue or opaque blue-green samples were analysed from these sites.

The composition of the bead types which could be identified using Brugmann's typology is generally consistent with those types represented at Eriswell; this includes *Constricted Cylindrical*, *Constricted Segmented*, *Brown* and *Blue* beads. The compositional similarities observed suggest that there were beadmaking workshops specialising in the production of specific types of bead, which were widely distributed (at least throughout East Anglia). The only apparent inconsistencies are a number of *Blue* beads produced from 'A2b Blue' glass from the Norfolk cemeteries, which is not consistent with *Blue* beads from Eriswell. This is likely to have resulted from typological misattribution (probably on the author's part), due to the very close similarities between *Blue* beads and blue *Melon Variation?* beads; the latter bead type is produced exclusively from 'A2b Blue' glass at Eriswell. It is therefore likely that these beads are in fact of the *Melon Variation?* type.

The bead types not represented at Eriswell all appear to have been produced from 'Roman' glass, and are likely to represent products of regional beadmaking workshops. The majority of these beads are not covered by the typologies in Brugmann (2004) or Penn and Brugmann (2007), supporting the view that they were not widely produced or distributed types, consistent with regional or local production.

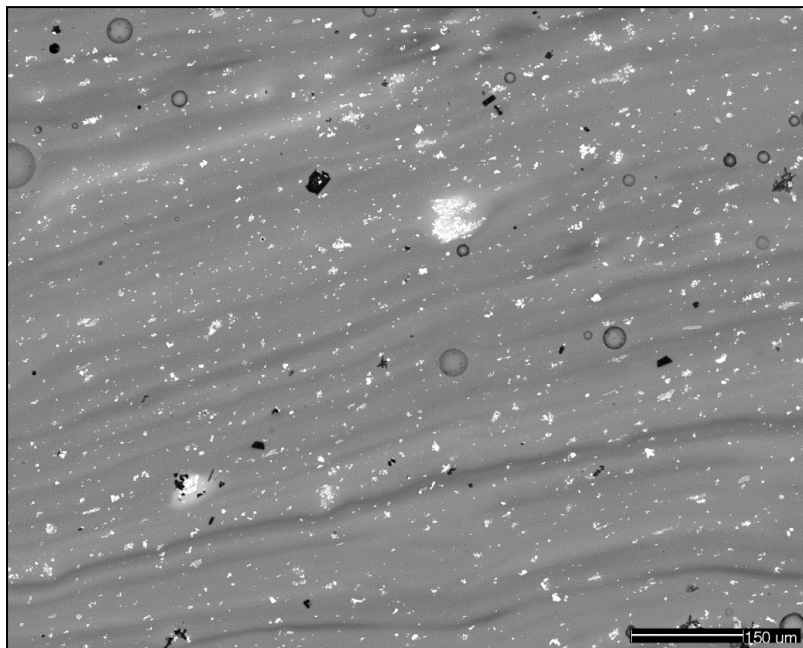


Figure 7.1.1 – BSE micrograph showing an opaque yellow sample from Bergh Apton, a probable *Yellow Globular, opaque* bead from grave 34Hvii. Numerous lead-tin oxide crystals (white) are visible heterogeneously dispersed throughout a lead-rich soda-lime-silica glass matrix (grey). Several small sodium aluminium silicate inclusions (black) corresponding to the mineral nepheline ($\text{Na}_3\text{KAl}_4\text{Si}_4\text{O}_{16}$) can be seen associated with some of these opacifying crystals.

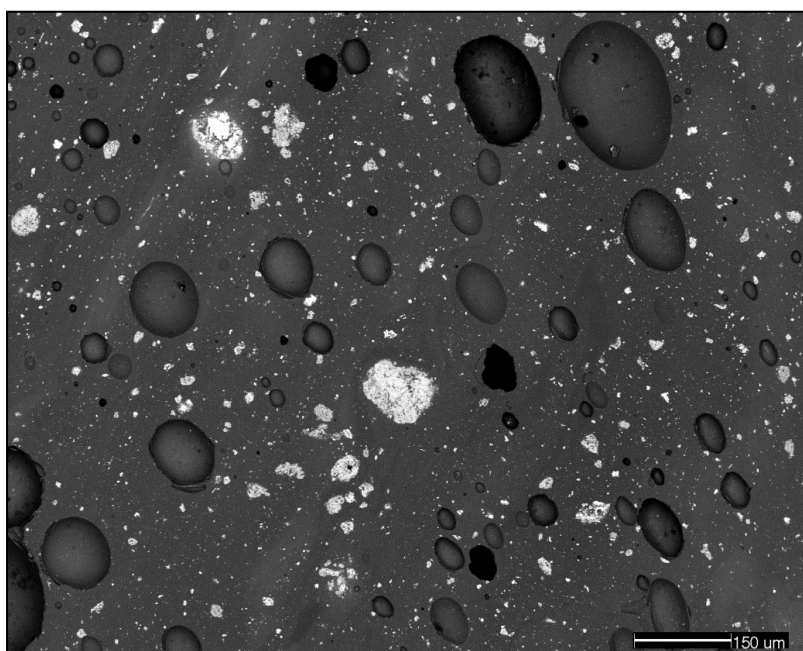


Figure 7.1.2 – BSE micrograph showing an opaque white samples from Bergh Apton, a possible *White Cylindrical, pentagonal?* bead from grave 56Aiii. Bright white crystals of cassiterite (tin oxide), heterogeneously dispersed in a lead-rich soda-lime-silica glass matrix (grey), act as the opacifying agent. Several voids (black) and bubbles are also visible.

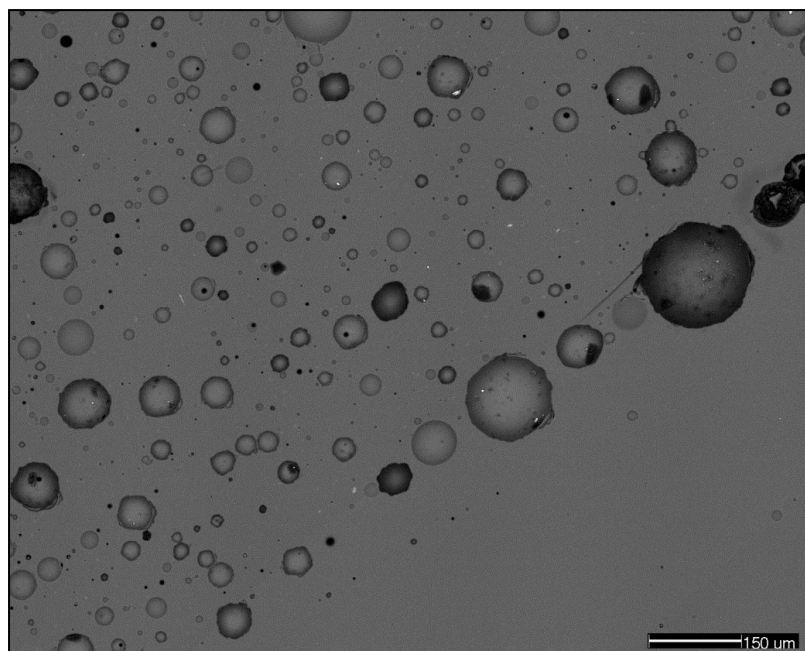


Figure 7.1.3 – BSE micrograph showing opaque white bead with translucent blue decoration from Bergh Apton, grave 62C. A dispersion of tiny bubbles of varying size, heterogeneously dispersed throughout a soda-lime-silica glass matrix (grey), act as the opacifying agent. The bubble-free glass to the bottom-right of the image is translucent blue.

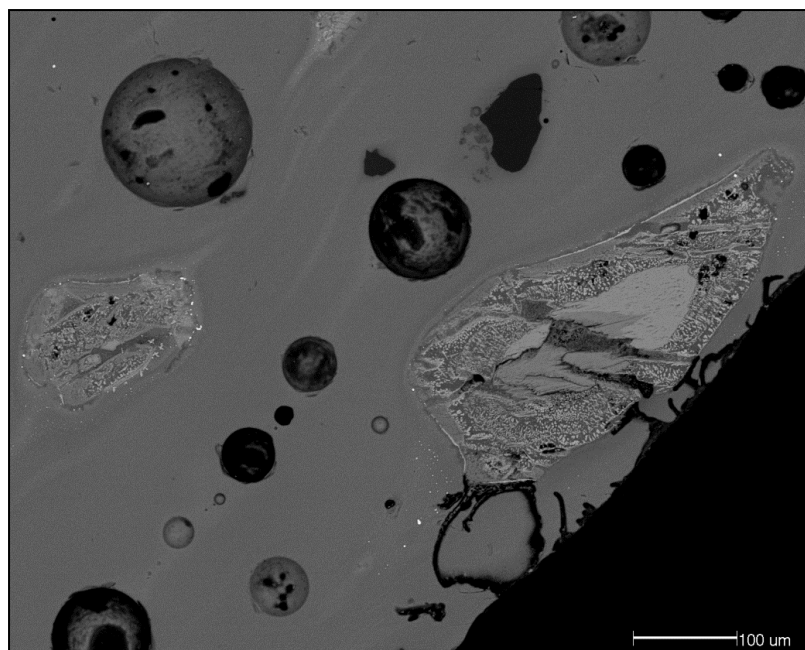


Figure 7.1.4 – BSE micrograph of an opaque red sample from an unidentified bead from Spong Hill, grave 5/6c, showing fayalitic slag inclusions in an opaque red soda-lime-silica glass matrix coloured by copper nanoparticles. Numerous large bubbles are also visible.

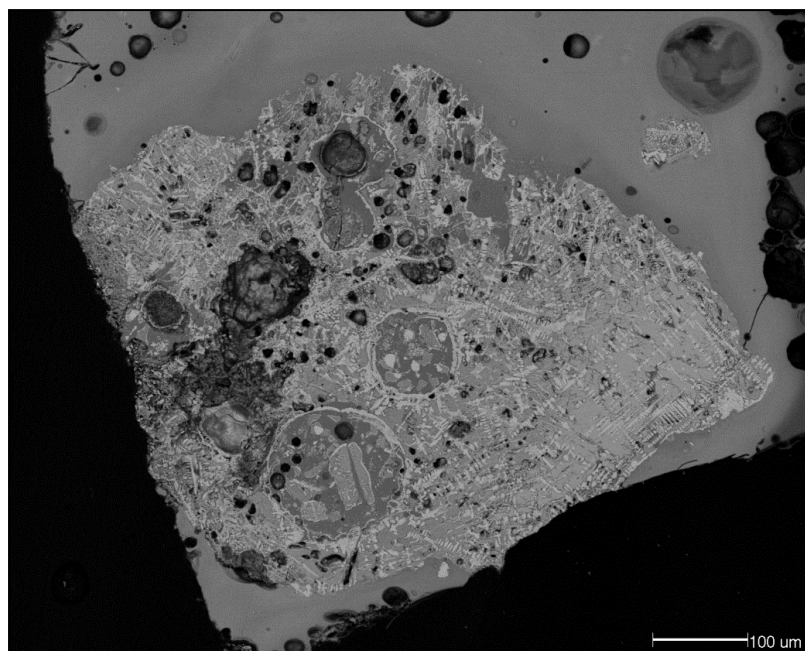


Figure 7.1.5 – BSE micrograph of an undefined opaque white bead with green crossing trails and opaque red spots from Spong Hill, grave 42/3, showing a large fayalitic slag inclusion in an opaque red soda-lime-silica glass matrix coloured by copper nanoparticles. The slag has begun to significantly interact with the surrounding glass matrix, as evidenced by numerous bubbles filled with glass within its structure. A large number of iron rich dendrites are visible.

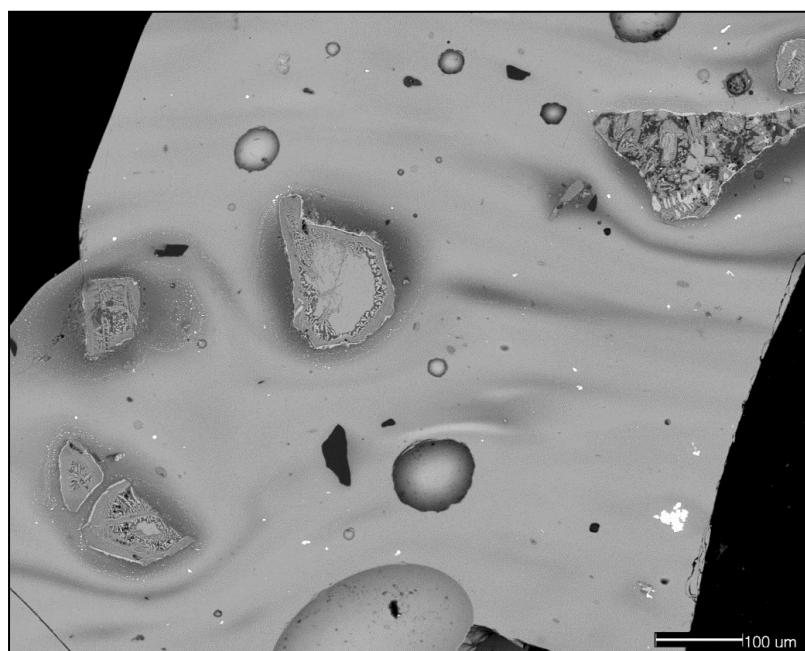


Figure 7.1.6 – BSE micrograph of an opaque red cylindrical bead with opaque white decoration from Bergh Apton, unknown context, showing fayalitic slag inclusions in an opaque red lead-rich soda-lime-silica glass matrix (pale grey) coloured by copper nanoparticles. Several crystals of lead-tin oxide are visible within the glass matrix (bright white), and a sub-angular silica grain near the centre of the image (black). The glass matrix immediately surrounding the slag inclusions appears darker because it is lower in lead and higher in iron in these regions. Several bubbles are also visible.

7.2. The Glass and its Raw Materials

7.2.1. Glass Types and Sources

All of the glass types identified in the present study are of the soda-lime silica compositional type, produced in the ‘Roman’ glassmaking tradition using a two-component recipe of calcareous quartz-rich sand and a relatively pure source of mineral soda (natron), probably from Egypt (the exception being a turquoise sample from Spong Hill which appears to have been produced from pure quartz with a separate lime addition; see Chapter 4, section 4.1.1.3). Natron glass of this type was the principal glass type used in Europe and the Eastern Mediterranean throughout the Roman period, up until approximately the 9th century AD. The results are therefore consistent with the results of previous scientific studies of Anglo-Saxon glass from England, as well as contemporary glass from elsewhere in Europe and the Near East.

A number of different base glass types have been identified in the beads from the sites studied; for the purpose of this study these have been termed ‘Roman’, ‘Saxon I’, ‘Saxon II’, ‘HIMT’, ‘Levantine I’ and ‘A2b Blue’ glass. With the exception of ‘A2b Blue’ glass, these glass types all correspond with those discussed in previous analytical studies of Roman and Anglo-Saxon glass from Britain (*e.g.* Foster and Jackson 2009; 2010; Freestone *et al.* 2000; 2008; and references therein). Whilst it has proven possible to distinguish between beads attributed to Brugmann’s phases A and B on compositional grounds, it has not proven possible to distinguish between beads attributed to Brugmann’s phases B and C. It was not possible to distinguish between beads attributed to Brugmann’s phases A1 and A2, although a handful of cobalt-blue beads attributed to Brugmann’s phase A2b were distinct; the remaining beads attributed to this latter phase are more consistent with beads attributed to Brugmann’s phases B and C. No beads from Brugmann’s phase B1 were available for analysis. The chronology of the different base glass types identified at Eriswell is presented in Chapter 4, Section 4.8 (particularly Figures 4.8.1 and 4.8.5).

The distribution of the glass types identified at Eriswell is summarised in Appendix K, which shows the typical composition of the different bead types analysed,

together with the number of beads analysed and the total recovered from the site. The contexts from which the different bead types were recovered are presented in Appendix B (compare to Appendix A). In addition to the 380 beads analysed as part of the present study, over 500 further beads can be *relatively* confidently attributed to a compositional type based upon these results; this accounts for the vast majority of the 1059 beads recovered from Eriswell.

The 'Roman' group represents recycled Roman blue-green tinted glass, which is characterised by low concentrations of both antimony and manganese as decolourants. This glass type was commonly used during the Imperial Roman Empire between the 1st and 3rd centuries. Small quantities of Roman manganese-decolourised glass also appears to have been used to produce a small number of beads, as suggested by the elevated levels of manganese in several of the 'Roman' samples. This glass type was probably in use during the 4th century, and is characterised by manganese at elevated levels but antimony at absent or near-absent levels. However, further work is necessary in order to establish the extent to which this glass was used. Roman antimony-decolourised glass, which was widely used between the 1st and 3rd centuries and is characterised by elevated antimony but manganese at absent or near-absent levels, was not identified in any samples. It is unclear where the 'Roman' glass from Eriswell was ultimately produced, but the trace element data is consistent with a Palestinian sand source; for this reason, the production of Roman blue-green tinted glass in Near Eastern workshops seems likely.

'HIMT' glass was first introduced at some point during the 4th century AD and was probably manufactured in Egypt (Foster and Jackson 2009; Foy *et al.* 2003; Freestone *et al.* 2005), although the workshops that produced it have yet to be found. The results of the present study suggest that it was probably a short-lived glass type which ceased to be produced in the late 4th or early 5th century, prior to the Anglo-Saxon migration. It is not represented in any significant quantity at Eriswell, and was not identified in beads from any of the other sites studied, suggesting that its production is unlikely to have continued into the Anglo-Saxon period. However, further work is necessary to confirm this. In Anglo-Saxon contexts it is likely to represent recycled Roman cullet, considering its association with bead types

typically produced from 'Roman' glass. Both 'Roman' and 'HIMT' glass were primarily in use prior to the mid-6th century, but there appears to have been a minor resurgence in their use in the decades around the mid-7th century.

'Levantine I' glass has been widely identified in published literature throughout Britain, Europe and the Eastern Mediterranean (*e.g.* Foster and Jackson 2009; Freestone *et al.* 2000; 2002a; 2002b). It can be fairly confidently attributed to production in Near Eastern workshops using sand sourced from the Palestinian coast. Whilst it was used in the 4th century in Britain (Forster and Jackson 2009), it is unlikely to represent recycled material from this period. It is not found in Anglo-Saxon beads from the 5th century, but appears to have come back into use sometime in the 6th century; it is not clear exactly when, but it is unlikely to have been much before the mid-6th century. It was probably not used much after the mid-7th century.

'Saxon I' glass was primarily used prior to approximately the mid-6th century, which is in close agreement with the results of Freestone *et al.* (2008) for early Anglo-Saxon vessel glass, based on the typology established by Evison (2000; 2008). It has been sub-divided into 'Saxon I (blue)' and 'Saxon I (natron)' glass in the present study. Both of these glass types are likely to have been produced using the same, or at least very similar, sources of sand, as indicated by the similar correlations and inter-correlations between major elements such as alumina, potash and magnesia. The compositional similarities between 'Saxon I' and 'HIMT' glass strongly suggest that 'Saxon I' glass was manufactured from its raw materials in Egypt or southern Israel; the workshops producing both of these glass types are likely to have neighboured one another. This glass type appears to have replaced 'HIMT' glass from the early 5th century onwards. 'Roman', 'Saxon I', and 'HIMT' glass are 'earlier' glass types in use during the 5th and 6th centuries, whereas 'Saxon II', 'Levantine I' glass are 'later' glass types in use during the 6th and 7th centuries; 'A2b Blue' glass appears to be peculiar to the 6th century.

The differences between 'Saxon I (blue)' and 'Saxon I (natron)' glass are not only in composition, but also in appearance. 'Saxon I (blue)' glass is almost exclusively translucent blue. In contrast, 'Saxon I (natron)' glass is observed in a much wider range of colours. 'Saxon I (blue)' glass has been previously identified in two

translucent blue Anglo-Saxon squat jars from Broomfield, Essex, by Freestone *et al.* (2008), but not as a distinctive pre-coloured glass type. Two translucent blue vessel glass fragments from Cyprus analysed by Freestone *et al.* (2002b) are also of the ‘Saxon I (blue)’ type, but are again not distinguished from uncoloured samples. The general absence of ‘Saxon I (blue)’ glass in published literature is likely to have resulted from the focus of many analytical studies on uncoloured rather than deliberately coloured glass. However, it is likely to have been widely distributed in its raw form as a pre-coloured glass type. As the raw glass itself was probably produced in the Near East, it is reasonable to assume that the cobalt colourant was added there.

Cobalt would have been a particularly rare and desirable colourant in Britain and Europe during the Anglo-Saxon period. Cobalt-bearing minerals would presumably have been mined, or at the very least sourced from surface deposits; they are commonly found as ores associated with various mineral impurities in ancient rock mineralisations (Henderson 2000a: 30). However, it is unclear as to how these ores were prepared prior to use. The ore may have been either crushed and added to the glass directly, or pre-treated in some way, perhaps by smelting or roasting to remove impurities. It is not entirely clear where cobalt was obtained, but as the majority of the blue glass appears to have been pre-coloured in the Near East, a European source seems unlikely. It was probably sourced somewhere in the Eastern Mediterranean, or perhaps the Middle East. Chunks of raw blue glass have been recovered from shipwrecks dating to the late 3rd century BC (Foy and Nenna 2001: 102; Foy *et al.* 2000: 52; Nenna *et al.* 2005: 60) and a trade in blue glass ingots has been attested for in the Near East during the Late Bronze Age (2nd millennium BC) (*e.g.* Nicholson *et al.* 1997). However, until now there has been limited evidence for a trade in such glass during the early medieval period.

‘Saxon I (natron)’ glass was a widespread glass type; it has been identified in contemporary vessel glass from Anglo-Saxon England (Freestone *et al.* 2008), northern France (Velde 1990), Germany (Wedepohl *et al.* 1997) and Italy (Silvestri *et al.* 2005). ‘Metal-in-glass’ beads and translucent pink-brown beads are exclusively of the ‘Saxon I (natron)’ type, but some cobalt-blue and ‘dark’ beads were also produced from it. It is unclear whether any of this glass was pre-coloured; its

exclusive use for pink-brown glass suggests that some of it may have been coloured elsewhere. Cobalt-blue glass of this type may also have been pre-coloured, considering the evidence for a trade in cobalt-blue ‘Saxon I (blue)’ glass. However, uncoloured ‘Saxon I (natron)’ glass was clearly reaching Europe; it was used to produce many uncoloured bead types and some glass vessels (*e.g.* Freestone *et al.* 2008). It is therefore conceivable that it was coloured in northwestern Europe, but on balance it is likely that at least some of it was pre-coloured, possibly in the Near East. Further work is necessary to establish the extent of this.

‘Saxon II’ glass was primarily in use from the 6th century, which is in close agreement with the results of Freestone *et al.* (2008) for early Anglo-Saxon vessel glass, based on the typology established by Evison (2000; 2008). It has been subdivided into ‘Saxon II (natron)’, ‘Saxon II (high MgO, low MnO)’ and ‘Saxon II (high MgO, MnO)’ glass in the present study. Of these, only the latter two types have been identified in contemporary Anglo-Saxon vessel glass (see Freestone *et al.* 2008). Whilst ‘Saxon II (natron)’ glass has not been identified in Anglo-Saxon vessel glass to date, it is perhaps curious that it has been identified in contemporary British vessel glass from Wales; presumably imported from western France (Campbell 2000: 42; Campbell and Lane 1993: 40-49). ‘Saxon II (natron)’ glass is likely to have neighboured those workshops producing ‘HIMT’ glass in Egypt, although it has been suggested that Egyptian production is unlikely (Foy *et al.* 2003: 75); production in southern Israel or the Sinai region therefore seems most likely. There is considerable evidence to suggest that it was widely distributed in its raw form, as it has been identified in significant quantities in Egypt, Tunisia, France (Foy *et al.* 2003) and Italy (Mirti *et al.* 2000; Silvestri *et al.* 2005; 2011), as well as Wales (Campbell and Lane 1993).

‘Saxon II (high MgO, MnO)’ glass has only been previously identified in early Anglo-Saxon vessel glass (Freestone *et al.* 2008); at present it is unknown elsewhere. The results of the present study suggest that it represents ‘Saxon II (natron)’ glass to which small quantities (approximately 10%) of plant ash, from inland plants and trees, was deliberately added. The potassium-rich nature of this ash addition is paralleled by later medieval ‘wood-ash’ or ‘forest’ glass, which replaced natron glass in Britain and northern Europe from around the 9th century onwards. It

is therefore likely that this ash component was added in northwestern Europe, where potassium-rich inland plants and trees were widely available. It is not entirely clear as to why natron glass was adulterated with ash, but it seems probable that it was to extend the supply of raw natron glass (Freestone *et al.* 2008: 41). This glass type may have been a precursor to true plant-ash glass, but it has not been identified in later Anglo-Saxon natron glass from the 8th and 9th centuries. Whilst negative evidence such as this should be interpreted with some caution, it suggests that the adulteration of natron glass with plant ash may have been a relatively short-lived practice. There is little evidence to suggest that glass of this type was ever used in Britain; it is therefore likely to have been a Continental initiative.

The majority of ‘Saxon II (high MgO, low MnO)’ glass is similarly likely to represent natron glass which has been adulterated with small quantities of plant ash; in some cases at least, this appears to have been rich in potassium. However, some of the samples attributed to this group may also represent unadulterated natron glass. This group is very much a hotchpotch; it has not been possible to make complete sense of it, but it is certainly not the product of just one primary glassmaking workshop. Further work is necessary to establish the nature of the ash additions and the composition of the original natron base glass to which they were added.

Lastly, ‘A2b Blue’ glass is a previously unknown glass type. Major and trace element data suggest that it is likely to have been produced in a similar region to ‘Roman’ and ‘Levantine I’ glass, probably in Near Eastern workshops using sand sourced from the Palestinian coast. Its composition is very tight (particularly at Eriswell) and it appears to be used to produce a very limited range of bead types (mostly *Melon* and *Melon Variation?* beads), suggesting that it may have been used by just one beadmaking workshop. Although this is the most poorly represented glass type at Eriswell, it has been identified in beads from Spong Hill, Bergh Apton and Morning Thorpe; this suggests that beads produced from it were relatively widely distributed (at least in East Anglia). As with ‘Saxon I (blue)’ glass, ‘A2b Blue’ glass is exclusively translucent blue, suggesting that it is likely to have been pre-coloured in the Near East. It was probably a relatively short-lived glass type, primarily used around the early or mid-6th century, but it is just possible that it was introduced as early as the latter decades of the 5th century.

7.2.2. Colourant Sources

Anglo-Saxon beadmaking workshops are likely to have sourced the majority of their colourants locally as scrap material (*e.g.* copper alloy, slag, etc.), probably from the preceding Roman period; however, it remains unclear as to how they procured their lead or tin.

In almost all of the glass colours containing lead in any significant quantity (red, green, yellow), lead appears to have been added in the form of a lead-tin calx, almost identical in composition to the lead-tin pigment used to produce opaque yellow glass. However, this material is of a different composition to that used in the production of tin oxide opacified white glass. Opaque white glasses opacified by bubbles appear to be earlier insular ‘Anglo-Saxon’ products, whereas those opacified by tin appear to be later ‘Continental’ products. For this reason, it seems likely that Anglo-Saxon beadmakers did not have access to local sources of tin (from southwest Britain) for the production of opaque white glass; this view is supported by recent work on historic tin exploitation by Meharg *et al.* (2012).

Anglo-Saxon workshops were clearly producing opaque yellow, green and red glass based (at least in part) on tin at the same time as they were producing opaque white glass opacified by bubbles. The extent to which lead-tin calx appears to have been used to produce these colours suggests that tin was relatively readily available, but its absence in opaque white glass suggests that it was not available in its pure form. It is therefore most likely that this lead-tin calx was obtained by calcining scrap material from the preceding Roman period (*e.g.* pewter; a lead-tin alloy). This lead-tin alloy appears to have been used as a ‘universal’ ingredient which could serve either as a colourant or opacifier, or simply as a source of lead, as dictated by careful control of the furnace atmosphere and/or the quantity added to the batch. For whatever reason, it was not used to produce opaque white glass; perhaps because it was not suitable, or because purer whites could be obtained through opacification by bubbles; lead would probably have acted as a fining agent if added to bubble-opacified glass, destroying the opacity. Experimental reproduction of these colours would be

worthwhile in order to establish whether it is possible to produce a good quality opaque white glass using oxidised pewter.

Cobalt-blue glass has already been discussed (see section 7.2.1 above). It is likely that this glass was coloured in the Near East, probably using cobalt sourced from there. In addition, old coloured Roman tesserae appear to have been used as colourants in a limited number of the samples analysed from Eriswell, all of which are translucent blue. There is no evidence to suggest that coloured glass tesserae were extensively recycled for use in beadmaking in England during the early Anglo-Saxon period. There is also limited evidence to suggest that such tesserae were remelted and used directly in beadmaking, without first being mixed into a pre-existing uncoloured soda-lime-silica glass. It is clear from the compositional data that blue tesserae were probably more highly prized as a colourant than other colours of tesserae; this again suggests that cobalt was not available locally as a colourant and supports the view that a supply of raw cobalt-blue glass is unlikely to have reached Britain.

7.3. The Trade in Glass

The results of the present study suggest that the Anglo-Saxon beadmaking industry was based almost entirely upon recycled Roman material. There is limited evidence to suggest that beads were curated from the preceding Roman period in any significant quantity; the vast majority of the beads analysed, including some of the characteristically *Roman* types, are certainly early medieval products. Comparison of the chemical composition of particular bead types to their distribution patterns suggests that characteristically ‘Anglo-Saxon’ beads were predominantly made from recycled ‘Roman’ blue-green tinted cullet, whereas characteristically ‘Continental’ beads were produced using a ‘fresh’ supply of raw glass imported from primary glassmaking workshops in the Eastern Mediterranean.

The source(s) of old Roman cullet remain unclear. It is likely to have been widely available in both Britain and northwestern Europe following the withdrawal of Rome in the early 5th century; fragments of Roman glass have been recovered from a number of early Anglo-Saxon sites (*e.g.* Evison 2000: 91), as well as Eriswell, which attest to this. It is more likely that it was locally sourced than imported. Raw unworked glass would presumably have been more expensive than old Roman cullet, as it would have been procured from further away and is likely to have been less readily available; cobalt is one of the rarer colourants, so raw pre-coloured cobalt-blue glass is likely to have been amongst the most desirable and expensive colours.

Prior to the 7th century, the use of raw ‘Saxon I’ glass appears to have been restricted to the production of specialist bead types and glass colours; for example ‘metal-in-glass’, *Blue* and *Brown* beads. It cannot be excluded that at least some of this glass may have been imported to England as raw unworked cullet, especially considering the trade links between England and the Continent, but this seems unlikely as there would probably have been enough old Roman cullet available locally to sustain the beadmaking industry in England at this time. The results of previous studies on later Anglo-Saxon glass (*e.g.* Freestone and Hughes 2006; Hunter and Heyworth 1998; see also Chapter 6) suggest that the glass industry in England is likely to have been based largely upon recycled Roman material well into the 8th and 9th centuries.

It has been suggested that the recycling of glass during the early medieval period was far less systematic and controlled than it was during the preceding Roman period (Jackson 1996: 298). The results of the present study suggest that this is unlikely to be the case, and that old Roman cullet was carefully selected and/or sorted (presumably by tint or colour) prior to its use in beadmaking; this interpretation stems from the apparent absence of recycled Roman antimony-decolourised glass in any of the assemblages analysed. It is unclear as to why Roman antimony-decolourised glass was not recycled; it is possible that it was mixed with manganese-decolourised glass in the recycling process, which would result in a glass containing both antimony and manganese similar to blue-green tinted glass (Jackson 2005: 772; Silvestri 2008: 1497). It is also possible that it was not as widely available as Roman blue-green cullet. However, these explanations are far from satisfactory.

There is limited evidence to suggest that different base glass types were mixed; for example, in the production of polychrome *Koch34* beads 'Levantine I' glass appears to have been used in conjunction with 'Saxon II (high MgO, MnO)' glass, and 'Saxon II (natron)' glass in conjunction with 'Saxon II (high MgO, low MnO)' glass. This suggests that different base glass types in use by the same workshop were kept separate, and implies the careful sorting of glass. There would probably have been no technological or colour-related benefits to this; any undesirable tints would have typically been masked by added colourants. It is just possible that certain colours were produced and kept 'in stock' by these workshops for later use.

Unfortunately, the distinction between 'Anglo-Saxon' beads produced using recycled Roman material and 'Continental' beads produced from raw natron glass is unlikely to be as straightforward as it appears in the present study; Roman material is also likely to have been widely recycled on the Continent. Some imported beads may therefore have a 'Roman' composition, which would otherwise be consistent with 'Anglo-Saxon' manufacture. Indeed, recent analysis of contemporary Merovingian glass beads from Belgium suggests that many 'Continental' bead types were also produced from recycled Roman glass (*e.g.* Mathis *et al.* 2010: 2082). However, the results of the present study suggest that such beads are unlikely to have reached England in any quantity.

The model favoured by the author is as follows: recycled Roman glass is likely to have been predominantly used to produce local and/or regional bead types in beadmaking workshops operating in both England and on the Continent. Each of these workshops would have had a relatively small catchment area, so these beads are unlikely to have been widely distributed (e.g. *Traffic Light* beads). In contrast, raw natron glass imported from the Near East is likely to have been used by a small number of much larger specialist beadmaking workshops (probably situated in northwestern Europe), producing more specialist bead types (e.g. ‘metal-in-glass’ beads). These workshops are likely to have had relatively large catchment areas, extending to England, so the resulting beads are likely to have been highly prized and widely distributed.

The distribution of old uncoloured Roman cullet is likely to have consisted of a network of many relatively small-scale trade routes (‘capillaries’), each covering relatively short distances, destined for local or regional beadmaking workshops. This cullet would probably have been widely available throughout Britain and Europe, and as such is unlikely to have been desirable as a commodity over large distances. In contrast, raw glass from the Near East is likely to have been far more desirable as a commodity (particularly cobalt-blue glass), and is therefore more likely to have been distributed via a much smaller number of relatively large trade routes (‘arteries’), destined for larger, more *specialist* beadmaking workshops. As Anglo-Saxon vessel glass was mostly produced from raw glass from the Near East (Freestone *et al.* 2008), it is likely that such workshops also specialised in the production of other high-quality glass objects, including vessels.

It remains unclear as to the extent to which either Roman cullet or raw unworked glass crossed the Channel into England; there is some evidence to suggest that small quantities of raw ‘Saxon I (blue)’ glass reached England, as it was sometimes used to decorate (presumably ‘Anglo-Saxon’) beads of ‘Roman’ composition.

7.4. Where Were the Beadmaking Workshops?

The manufacture of glass from its raw materials was a highly specialised activity undertaken by a few large primary glassmaking institutions located in the Near East. Here, the workshops had direct access to the raw materials necessary to produce glass: natron from Egypt and relatively pure calcareous glassmaking sand. As a result, the chemical composition of the beads analysed represents the primary origins of the raw glass itself, rather than the workshops in which they were produced. The widespread trade in this raw glass and the finished beads themselves makes it impossible to attribute individual bead types to specific production zones. Similarly, the compositional traits of the individual workshops that produced beads from recycled glass (mostly Roman) are destroyed as a result of the mixing and re-melting of material from a number of different sources.

Whilst it is likely that the beadmaking workshops operating in England and northwestern Europe coloured the majority of the glass themselves, detailed analysis of colourants (*e.g.* isotopic analysis) could conceivably offer the potential to elucidate the possible locations of these workshops. However, as it is likely that the majority of colourants were obtained from recycled materials or widely traded, any distinctive compositional traits are again likely to have been destroyed.

Secondary glass-*working* (*e.g.* beadmaking) is often much more difficult to detect in the archaeological record than primary glass-*making* for a number of reasons. Firstly, considering the scale of glass recycling in this period, it is likely that scrap glass, failed beads, spills and waste material from any beadmaking furnaces would have been collected and recycled. This view is supported by the identification of two 'dark' glass beads from Eriswell, together with one from Mucking (see Mortimer 1996b; Mortimer and Heyworth 2009), which appear to have been produced from scrap (perhaps failed) opaque yellow glass (see Chapter 5, section 5.1.5). Secondly, the beadmaking furnaces would have been smaller and more transient than the workshops producing the raw glass itself (Foy and Nenna 2001: 40); the lead-rich glass used for the production of the majority of early Anglo-Saxon glass beads would have melted at very low temperatures (500-700°C), which can be achieved in

a simple hearth or bonfire (Henderson 1999a: 85). This would not leave definite traces in the archaeological record. Thirdly, the identification of metallurgical slag in the majority of opaque red glass suggests considerable interaction between the glass and metalworking industries (see Peake and Freestone 2012). If this is the case, and glassworking was perhaps a 'secondary' activity to metalworking, such evidence may be obscured by that of other pyrotechnic industries.

Nevertheless, it can be stated with some confidence that there was a glass bead industry in England at least during the latter half of the 5th and first half of the 6th centuries, but it is unlikely to have left significant traces in the archaeological record. As such, distribution patterns currently provide the best source of information regarding possible production zones for individual bead types. Without direct evidence for early Anglo-Saxon beadmaking in England, in the form of workshop sites and/or glassworking waste, it may never be possible to elucidate the precise location(s) of such institutions.

7.5. The Question of Roman Continuity

In one sense the Anglo-Saxon glass industry can be viewed as a continuation of the Roman glass industry, in that similar raw materials were used in the production of the raw soda-lime-silica glass itself (calcareous sand and natron): the so-called 'Roman' glassmaking tradition. However, in another sense it is not a continuation; the primary decolourant employed in Anglo-Saxon glass is manganese, whereas in the preceding Roman period antimony was more typical. Similarly, the opacifiers used in the production of colours analysed, such as opaque white and opaque yellow, are based on compounds of tin; in the Roman period they were typically based upon compounds of antimony. The glass used to produce the beads from the sites studied is therefore distinctively early medieval. Even where Roman glass has been recycled, the nature of the colourants and opacifiers used generally suggests that Anglo-Saxon craftsmen coloured the majority of this glass themselves, using their own distinctive recipes

Whilst there is no evidence to suggest that there was any continuity in the glass industry from the preceding Roman period, there is also no evidence to suggest that new glass types were introduced to *Britain* following the withdrawal of Rome. A lack of continuity is supported by the apparent cessation in the use of several primary glass types prevalent in Britain during the Late Roman period; namely 'Levantine I' and 'HIMT' glass. As mentioned above (section 7.2.1), 'HIMT' glass is unlikely to have been produced into the Anglo-Saxon period for a number of reasons. Furthermore, according to Brugmann's chronology there is a clear break of a century or more in the use of 'Levantine I' glass between the Late Roman and early Anglo-Saxon period; it appears to have gone out of use in the late 4th or early 5th century and been re-introduced once more in the 6th century, but not in Britain.

The onset of the early Anglo-Saxon period is characterised by the introduction of a number of glass types which are not found in Roman contexts: 'Saxon I' glass, closely followed by 'A2b Blue' and 'Saxon II' glass. However, there is little evidence to suggest that these new glass types ever reached Britain in their raw unworked form; the Anglo-Saxon glass industry instead appears to have been solely

dependent upon the recycling of earlier Roman material, probably until the introduction of plant-ash glass in around the 8th or 9th centuries. On balance, the results of the present study suggest a break in glassworking between the Roman and Anglo-Saxon periods. Furthermore, it is likely that the collapse of Roman rule in Britain marked the end of a trade in natron glass to Britain from the Eastern Mediterranean for good.

7.6. The Rise and Fall of Anglo-Saxon Beadmaking

The beads worn by Anglo-Saxon women in the 5th and early 6th centuries exhibited a high degree of regional variation; distribution maps and typological attributions support the view that many of these earlier bead types were produced in England, but also suggest that a large number were imported from the Continent. This view is now supported by compositional analysis. It seems that largely self-sufficient secondary beadmaking workshops were set up on a local or regional level, relying almost entirely upon recycled Roman material for their glass and colourants; probably sourced locally. Anglo-Saxon England appears to have retained strong links with the Continent, where more specialist types of bead appear to have been produced in relatively centralised workshops; these sourced their raw glass either directly or indirectly from primary glassmaking workshops operating in the Near East. The finished beads were then exported to England, and probably elsewhere in northwestern Europe.

It is unclear exactly when the beadmaking workshops in England were set up following the arrival of the first immigrants. Did they bring these skills with them or did the craftsmen themselves arrive slightly later? What is relatively certain is that beadmaking workshops had been established in England by the late 5th century, and probably continued to produce beads at least into the early 6th century; possibly even up until the late 6th century. However, the beadmaking industry in England appears to have been relatively short lived when compared with that on the Continent, perhaps lasting only a century or so; 150 years at the most.

At some point in the latter half of the 6th century there appear to have been a number of radical changes, not only in the types and numbers of beads being worn, but also in the base glass types used. The recycling of material from the preceding Roman period appears to have suddenly stopped. The glass types which came to dominate were ultimately imported as raw glass from the Near East, but these probably never reached Britain.

Some of these new glass types appear to have been adulterated with small quantities of plant ash. This has been previously interpreted as the result of a shortage of natron glass (*e.g.* Freestone 2008: 41); the Anglo-Saxon glass industry was clearly dependent upon cullet from the preceding Roman period, which would gradually have diminished in quantity, meaning that alternative sources of glass would have had to have been found. Difficulties in obtaining natron in the Near East may have compromised the production of raw natron glass; the addition of small quantities of plant ash to much of the natron glass in use by the 7th century would appear to support the view that natron glass was in short supply, and that ash was added as an extender (Freestone *et al.* 2008: 41). However, this explanation is not entirely satisfactory.

Whether or not there was a shortage of Roman cullet in Britain by the 7th century is open to interpretation; the apparent reliance upon old Roman material in the mid-Saxon period (*e.g.* Freestone and Hughes 2006; Hunter and Heyworth 1998; see also Chapter 6) suggests that it was still widely available until at least the 8th century. If there was a shortage of Roman cullet, why is there an apparent resurgence in its use from the late 7th century onwards? Secondly, if ash was added as an extender due to shortages in the supply of natron glass, why is *adulterated* ‘Saxon II (high MgO, MnO)’ glass found in association with *unadulterated* ‘Levantine I’ glass on the same polychrome bead types? Why was plant ash added to some types of natron glass, but not to other types clearly in use at the same time and by the same workshops?

The answers to these questions are far from clear. What is apparent is that the glassmaking industry in *Britain* appears to have suddenly collapsed at some point in the latter half of the 6th century. The decline in the use of recycled Roman material to produce beads around this time partly attests to this. Such a rapid decline seems unlikely to have resulted from a sudden shortage of glass; if this were the case a more gradual decline might be expected. The rapid decrease in the number of characteristically ‘Anglo-Saxon’ bead types suggests that this decline was a result of more than just a shortage of material. *Doughnut* beads are the only purportedly ‘Anglo-Saxon’ bead type represented at Eriswell from the 7th century (the so-called ‘Final Phase’), and may therefore hold the key to explaining this.

Doughnut beads are of considerable interest here for a number of reasons. They are the *only* bead type from 7th century contexts at Eriswell which are consistently manufactured from recycled Roman material. They are remarkably evenly distributed throughout Anglo-Saxon England (Brugmann 2004: 41), but they are very low-quality when compared with other bead types in use at the same time, as well as bead types in use during the preceding centuries. They are not deliberately coloured, are often poorly shaped and are often filled with bubbles. Furthermore, they were produced by piercing, whereas the majority of other Anglo-Saxon beads are wound or drawn. Piercing would have required much less skill than winding or drawing; it would have negated the removal of the bead from the mandrel, which appears to have been one of the most difficult processes in the production of beads (Brugmann 2004: 17). On balance, it seems likely that *Doughnut* beads were produced in different workshops to the majority of other beads in use at the same time. The craftsmen producing them appear to have been very unskilled; they probably lacked the ability or knowledge necessary to colour their own glass, wind it around a mandrel or otherwise shape it by marvering. Their skill is arguably unlikely to have extended much beyond the ability to melt old cullet.

This suggests that the skills necessary to produce the brightly coloured wound monochrome and polychrome beads, such as the polychrome *Traffic Light* beads of the 5th and 6th centuries, were no longer available in Britain by the 7th century. The reasons for this are not entirely clear, but there is some evidence to support an apparent lack of skilled craftsmen at this time. Bede writes of the import of glaziers from Gaul by Benedict Biscop to glaze the windows of the monastery at Wearmouth, Northumbria, in *c.* AD 674, due to a lack of ‘*vitri factores*’ in Britain; this is traditionally interpreted as meaning a lack of ‘makers of glass’ (Cramp 1970: 327; 1975: 89; 2006: 56; Heyworth 1992: 169; Welch 1999: 8), but the literal translation is very misleading.

We know that these people were probably not making glass from its raw materials from the scientific analysis of window glass from the monastic sites of Wearmouth and Jarrow (Brill 2006; Freestone and Hughes 2006); this glass is of the natron type, ultimately produced from its raw materials in the Near East – not in Europe. Bede is therefore more likely to be referring to craftsmen who could *work* or *blow* glass

rather than *make* it from its raw materials, but this is not entirely clear from the literal translation of '*factores*' from Latin. In the mid-8th century, the Abbot of Wearmouth again requested the assistance of glassmakers to manufacture vessel glass, this time from Mainz, again due to a lack of skilled craftsmen locally (Cramp 1970: 329; Cramp 1975: 89; Heyworth 1992: 169).

These accounts do not specifically refer to beadmaking; the production of windows was undertaken by blowing glass, which was a more specialised industry requiring far more skill than beadmaking. Nevertheless, Bede's account suggests that it is just possible craftsmen skilled in beadmaking were also unavailable in England by the late 7th century. It is probable that such skills had been lacking in England for quite some time; certainly more than a generation or two. It is reasonable to assume that this coincided with the significant changes in beadmaking practices that apparently took place relatively rapidly at some point around in the late 6th century.

The reasons for such a lack of skill in England by the 7th century are far from clear. It appears to have coincided with other radical changes taking place at this time; the conversion to Christianity and the emergence of kingdoms (see Chapter 1, section 1.1). The emergence of a new ruling elite seems the most likely candidate for a disruption in the local or regional production and supply of beads. It is possible that social or political constraints were imposed upon access to raw materials and craft skills needed to produce the goods through which identity was expressed (Scull 2011: 857). Access to skilled craftsmen (and the resulting goods) may therefore have been tightly controlled, or even treated as a privilege.

Undoubtedly links with the Continent and Scandinavia rapidly developed following the collapse of insular beadmaking in England and the emergence of kingdoms. This is not to say that the number of 'Continental' bead types increased in England relative to the preceding 5th and 6th centuries; they may have *decreased*. Indeed, there was a significant drop in the number of beads deposited with the dead from the late 6th century onwards (Hines *et al.*, in press). However, 'Continental' bead types had clearly more dominant by the 7th century. Hines *et al.* (in press) state that the lowest frequency of furnished female burial in England occurred in the 580's and 590's, but gradually recovered in the early 7th century, rising sharply in the mid-7th

century. This is consistent with a sudden collapse in insular Anglo-Saxon beadmaking in the late 6th century, followed by a gradually increasing reliance on Continental imports in subsequent decades.

For whatever reason, the beadmaking industry in England appears to have begun to die out *prior* to the conversion to Christianity, beginning in AD 597; it is therefore unlikely that this new religion was the cause. It remains unclear as to what happened to the beadmakers or the knowledge they possessed. It is unlikely that they had become peripatetic; this would not account for the production of *Doughnut* beads from recycled Roman glass, when the majority of other bead types were produced using a fresh supply of glass from the East. Purported shortages of raw natron glass by the 7th century probably only affected Continental beadmaking workshops, considering that the beadmaking industry in England was never reliant upon a supply of raw glass from the Eastern Mediterranean.

It must not be forgotten that the beadmaking industry represents just one arm of a technology which also encompasses glass vessels, window glass and enamels. Beads must be studied in context together with other objects with which they are often associated (pendants, brooches, clasps, etc.). It is more likely than not that many other early Anglo-Saxon crafts were also based upon the recycling of earlier Roman material (*e.g.* metalworking). However, it is at present unclear as to whether these industries continued in England into the 7th century, or whether they succumbed to the same fate as the Anglo-Saxon beadmaking industry. In any case, the likelihood is that Anglo-Saxon England was never *directly* integrated into the Byzantine trade networks that were so extensive across Western Europe and the Celtic West between the 5th and 7th centuries.

7.7. Further Work

7.7.1. Glass Studies in General

This study represents the largest scientific study undertaken on early Anglo-Saxon glass beads to date. It would undoubtedly have failed to reach its full potential were it not for the attribution of these beads to a well-defined typology and chronology, which facilitated the selection of a representative range for analysis and the creation of meaningful compositional groups. Future scientific studies should be undertaken in the light of reliable chronological and typological attributions in order to maximise their output.

The analytical methods tested as part of this study, which included non-destructive and quasi non-destructive sampling and analysis techniques, demonstrate that even when the weathered surface of the glass has been removed quantitative results are not always reliable or comparable. Whilst it is often difficult to take samples, or obtain permission to do so, semi-destructive analysis of polished samples clearly provides the most reliable compositional data. Average values for iron and alumina had to be assumed for many of the samples analysed when calculating the composition of the base glasses, due to the extent of contamination from the melting pot in glasses containing lead, or the introduction of iron as part of the colouring process. Future studies focussing on coloured and opaque glass must consider this; iron and alumina are not necessarily reliable discriminators of different glass types.

It is also important that future studies analyse for a full suite of elements; antimony in particular is an important indicator for the recycling of earlier Roman glass. Data should be published to at least two decimal places, and the substitution of values below the detection limits of the equipment for 'b.d' (below detection) or 'n.d.' (not detected) should be avoided in order to maximise the comparability of this data in the future; it is far more useful to tabulate the raw data as it was originally obtained, but to note the detection limits as a footnote. This will prevent potentially diagnostic elements present at particularly low concentrations from being omitted; lead and

antimony have proven to be reliable discriminators in the present study even at concentrations well below their supposed detection limits.

There is now a serious need for the development of consistent, unambiguous and comprehensible terminology for different primary/base glass types, especially as more begin to come to light. At present, descriptions of different primary glass types are very inconsistent, being based upon provenance (*e.g. Levantine I, Bet Eli'ezer, Wadi Natrun, Egypt II, etc.*), colour (*e.g. Roman blue-green, A2b Blue, Saxon I (blue), etc.*), compositional characteristics (*e.g. HIMT*), chronology (*e.g. Period I, Saxon I, A2b Blue, etc.*), or simply using a series of sequential numbers and/or letters (*e.g. Group 1, Group 2, Group A, etc.*). However, these are *far* from satisfactory, as many are potentially ambiguous and misleading.

In an ideal scenario, different base glass types might be labelled according to their primary origins and perhaps also their chronological attributes. Unfortunately the primary origins of most glass types cannot be confirmed without supporting workshop evidence, and their chronology is typically imprecise. As such, there is a need to synthesise informative, transparent and comprehensive terminology for the known glass types in published literature, including those identified in the present study. Whilst a series of numbered groups is arguably one of the most unambiguous ways of doing this (*e.g. see the classification system adopted by Foy et al. 2003*), this is often very difficult to remember and consequently difficult to use, and implies a chronological sequence which may not exist. Terminology should be easy to remember and allusive to the different glass types referred to. However, once terminology has entered the public sphere it can continue to resonate for decades to come, even well after it has been superseded by more up-to-date classifications; such an undertaking will therefore be far from easy.

7.7.2. Anglo-Saxon Glass Bead Studies

All of the beads analysed as part of the present study were from East Anglia. Analysis of beads from elsewhere would therefore be very worthwhile, even if only to confirm the conclusions of the present study. It is clear that there are still huge gaps in the typology and chronology of the less common Anglo-Saxon bead types (e.g. *WhitePoly** beads). Bead typologies and distribution maps need to be established at more of a regional level in England, building on the work of Brugmann (2004) and Penn and Brugmann (2007), in order for meaningful compositional comparisons between insular bead types from other Anglo-Saxon sites to be made.

Whilst the organisation of the bead industry in the 5th and early 6th centuries appears relatively straightforward, the production and distribution of beads in the late 6th and 7th centuries remains far from clear. Natron glass adulterated with plant ash has yet to be identified in contemporary glass from Continental contexts. Further analysis of *Doughnut* beads is also worthwhile, as these appear to be one of a limited number of insular ‘Anglo-Saxon’ bead types produced during the 7th century. Major element analysis, complemented by trace element analysis (particularly to confirm the presence of antimony), has proven particularly informative, but requires a sample in order to maximise the reliability of the results.

Recent studies have demonstrated the potential of the analysis of radiogenic isotopes (particularly Sr, Nd and Pb) in early glass. Sr-Nd isotopic analysis is a relatively new technique used to provenance primary glass production; it is particularly useful for differentiating between European and Eastern Mediterranean glass sources (Degryse and Schneider 2008: 1997-1999; Degryse and Shortland 2009: 139; Degryse *et al.* 2010: 83-84; Freestone *et al.* 2009: 35-38). However, many of the characteristic isotopic signatures for Anglo-Saxon glass will have been lost due to the extent of recycling (e.g. Degryse *et al.* 2006; Freestone *et al.* 2009: 46; Leslie *et al.* 2006: 254) or the adulteration of natron glass with plant ash, so it is unclear as to how useful it would be. It could nevertheless prove useful in confirming a Near Eastern origin for several of the glass types identified in the present study. However, it is unlikely that

it will ever be possible to elucidate where the beads themselves were manufactured using compositional analysis.

Detailed analysis of colourants, many of which were presumably added in the secondary beadmaking workshops themselves, may have some potential. The potential of lead isotope analysis in the provenancing of ancient lead sources, particularly in the Near East, has been demonstrated by a number of recent studies (*e.g.* Shortland 2006; Shortland *et al.* 2000), but remains problematic due to an insufficient database of lead isotope signatures for comparison. Nevertheless, such analysis may provide clues as to the where the lead used in the production of certain colours of glass, including opaque yellow and red, was sourced. Cobalt is also frequently associated with a lead impurity, so lead isotope analysis may be of use in provenancing the cobalt sources exploited (*e.g.* Brill 1988: 288-289).

Even if it is not possible to reliably provenance the lead source(s), inter-comparisons of lead isotope signatures obtained from 'Anglo-Saxon' and 'Continental' bead types may provide the potential to distinguish 'regional' groups. However, as lead is likely to have been obtained as recycled material (*e.g.* pewter), lead isotope analysis may be of limited use as the characteristic isotope signatures might have been destroyed by the recycling process. Lead isotope analysis of cobalt-blue glass would be particularly worthwhile. Trace elements analysis has also shown considerable potential in differentiating between cobalt sources.

Trace element analysis, in combination with major element analysis, is likely to offer one way forward in the study of Anglo-Saxon and Merovingian glass beads. LA-ICP-MS is a particularly viable technique as it is micro-destructive, so damage is not usually visible. Although only a small assemblage of beads could be analysed for trace elements in the present study due to constraints of time and finance, it allowed the origins of the glass to be inferred and facilitated some extremely useful inter-comparisons between different glass types. It was also useful in the identification of 'Roman' glass, in which antimony is a distinguishing element at concentrations typically below the detection limits of SEM-EDS.

7.7.3. Near Eastern Glass

The present study has raised a number of questions relating to the wider context of glass production in the Eastern Mediterranean during the Early Byzantine period. At present, 'Saxon I (blue)', 'Saxon I (natron)' and 'A2b Blue' glass has not yet been conclusively identified in Near Eastern contexts. Future work should focus on cobalt-blue glass from this region, as the majority appears to have been pre-coloured there.

Furthermore, significant doubt has now been placed upon the longevity of 'HIMT' glass. It is known that this glass type was first introduced in the 4th century, but the results of the present study suggest that it is unlikely to have been produced much beyond the early 5th century; this is in contrast to previous suggestions that it may have been produced until the 6th or 7th centuries (Foster and Jackson 2009: 189-190). Further work is necessary in order to establish the extent to which 'HIMT' glass is present in 5th-7th century contexts, and whether glass that has been previously assumed to represent 'HIMT' glass is in fact one of the very similar (but compositionally distinct) 'Saxon' glass types discussed in the present study.

It would also be of interest to explore the possibility of a break in the production of 'Levantine I' glass in the Near East between the 5th and 6th centuries. It is unclear as to whether the absence of 'Levantine I' beads attributed to Brugmann's phase A stems simply from a break in the trade in this glass type, or from a break in its production altogether.

CHAPTER EIGHT

8. References

Aerts, A., Velde, B., Janssens, K. and Dijkman, W. (2003) 'Change in silica sources in Roman and post-Roman glass', *Spectrochimica Acta Part B*, 58, 659-667.

AHG (2012) 'Glastonbury Abbey excavations reveal Saxon glass industry', *Glass News*, 32, 15.

Ahmed, A. A. and Ashour G. M. (1981) 'Effect of heat treatment on the crystallisation of cuprous oxide in glass', *Glass Technology*, 22, 24-34.

Analytical Methods Committee (2001) *What should be done with results below the detection limit? Mentioning the unmentionable*, AMC Technical Brief No. 5. London: Royal Society of Chemistry.

Andersen, J. H. and Sode, T. (2010) 'The glass bead material', in M. Bencard (ed.), *Ribe Excavations 1970-76*, Volume 6, 17-128.

Arletti, R. Giordani, N., Tarpini, R. and Vezzalini, G. (2005) 'Archaeometrical analysis of glass of Western Emilia Romagna (Italy) from the imperial age', *Annales du 16^e Congrès de l'Association Internationale pour l'Histoire du Verre*, 80-84.

Arletti, R., Vezzalini, G., Biaggio Simona, S. and Maselli Scotti, F. (2008) 'Archaeometrical studies of Roman imperial age glass from Canton Ticino', *Archaeometry*, 50(4), 606-626.

Astrup, E. and Andersen, A. (1987) 'A study of metal foiled glass beads from the Viking period', *Acta Archaeologica*, 58, 222-228.

Bachmann, H.-G. (1982) *The Identification of Slags from Archaeological Sites*. London: Institute of Archaeology.

Barber, D. J. and Freestone, I. C. (1990) 'An investigation of the origin of the colour of the Lycurgus Cup by analytical transmission electron microscopy', *Archaeometry*, 32(1), 33-45.

Barber, D. J., Freestone, I. C. and Moulding, K. M. (2009) 'Ancient copper red glasses: investigation and analysis by microbeam techniques', in A. J. Shortland, I. C. Freestone and Th. Rehren (eds.), *From Mine to Microscope: Advances in the Study of Ancient Technology*, 115-127. Oxford: Oxbow Books.

Baxter, M. J., Cool, H. E. M. and Jackson, C. M. (2005) 'Further studies in the compositional variability of colourless Romano-British vessel glass', *Archaeometry*, 47(1), 47-68.

Bayley, J. (1985) 'Analysis of some of the Anglo-Saxon glass beads from Portway, Andover', in A. M. Cook and M. W. Dacre, *Excavations at Portway, Andover 1973-1975*, 84-87. Oxford: Oxford University Committee for Archaeology.

Bayley, J. (1987) 'Qualitative analyses of some of the beads', in V. I. Evison, *Dover: The Buckland Anglo-Saxon Cemetery*, 182-189. London: Historic Buildings & Monuments Commission for England.

Bayley, J. (1994) *Gold-in-Glass Beads from Mucking, Essex*, Ancient Monuments Laboratory Report 1/94. Unpublished Report, English Heritage.

Bayley, J. (1995) 'The analysis of glass beads', in K. Blockley, M. Blockley, P. Blockley, S. S. Frere, and S. Stow, *Excavations in the Marlowe Car Park and Surrounding Areas, Part II: The Finds*, 1194-1199; 1202-1205. Canterbury: Canterbury Archaeological Trust.

Bayley, J. (1998) 'The production of brass in antiquity with particular reference to Roman Britain', in P. T. Craddock (ed.), *2000 Years of Zinc and Brass*, 7-26. London: The British Museum.

Bayley, J. (1999) 'Appendix: notes on the composition of coloured glasses', in M. Guido, *The Glass Beads of Anglo-Saxon England c.AD 400-700: A Preliminary Visual Classification of the More Definitive and Diagnostic Types*, Report of the Research Committee of the Society of Antiquaries of London No. 58, 89-93. Woodbridge: The Boydell Press.

Bayley, J. (2000a) 'XRF analysis of the beads', in A. Lane and E. Campbell, *Dunadd: An Early Dalriadic Capital*, 217-218. Oxford: Oxbow Books.

Bayley, J. (2000b) 'Glassworking in early medieval England', in J. Price (ed.), *Glass in Britain and Ireland AD 350-1100*, 137-141. London: British Museum Press.

Bayley, J. (2000c) 'Saxon glass working at Glastonbury Abbey', in J. Price (ed.), *Glass in Britain and Ireland AD 350-1100*, 161-188. London: British Museum Press.

Bayley, J. (2009) 'Scientific examination of the 'gold-in-glass' type beads', in S. M. Hirst and D. Clark, *Excavations at Mucking: Volume 3, The Anglo-Saxon Cemeteries*, 413-414. London: Museum of London Archaeology.

Bayley, J. and Eckstein, K. (1997) 'Silver refining – production, recycling, assaying', in A. Sinclair, E. Slater and J. Gowlett (eds.), *Archaeological Sciences 1995*, 107-111. Oxford: Oxbow Monograph 64.

Bayley, J. and Wilthew, P. T. (1986) 'Qualitative and semi-quantitative analyses of glass beads', in J. S. Olin and M. J. Blackman (eds.), *Proceedings of the 24th International Archaeometry Symposium*, 55-62. Washington DC: Smithsonian Institution Press.

Bayley, J., Crossley, D. and Ponting, M. (2008) *Metals and Metalworking: A Research Framework for Archaeometallurgy*, The Historical Metallurgy Society Occasional Publication No. 6. London: The Historical Metallurgy Society.

Benzaazoua, M., Marion, P., Liouville-Bourgeois, L., Joussemet, R., Houot, R., Franco, A. and Pinto, A. (2002) 'Mineralogical distribution of some minor and trace elements during a laboratory flotation processing of Neves-Corvo ore (Portugal)', *International Journal of Mineral Processing*, 66, 163-181.

Bertini, M., Shortland, A., Milek, K. and Krupp, E. M. (2011) 'Investigation of Iron Age north-eastern Scottish glass beads using element analysis with LA-ICP-MS', *Journal of Archaeological Science*, 38, 2750-2766.

Biek, L. and Bayley, J. (1979) 'Glass and other vitreous materials', *World Archaeology*, 11(1), 1-25.

Biek, L., Bayley, J. and Gilmore, G. R. (1985) 'Scientific examination of the glass beads', in S. M. Hirst (ed.), *An Anglo-Saxon Inhumation Cemetery at Sewerby East Yorkshire*, York University Archaeological Publications, 4, 77-85. York: University of York.

Biek, L. and Gilmore, G. (1997) 'Non-invasive revelation of precious metal decoration in glass beads', in A. Sinclair, E. Slater, and J. Gowlett (eds.), *Archaeological Sciences 1995: Proceedings of a Conference on the Application of Scientific Techniques to the Study of Archaeology*, 38-42. Oxford: Oxbow Books.

Bimson, M. and Freestone, I. C. (2000) 'Analysis of some glass from Anglo-Saxon jewellery', in J. Price (ed.), *Glass in Britain and Ireland AD 350-1100*, British Museum Occasional Paper 127, 131-136. London: British Museum Press.

Boon, G. C. (1977) 'Gold-in-glass beads from the ancient world', *Britannia*, 8, 193-207.

Brill, R. H. (1970) 'The chemical interpretation of the texts', in A. L. Oppenheim, R. H. Brill, D. Barag and A. von Saldern (eds.), *Glass and Glassmaking in Ancient Mesopotamia: An Edition of the Cuneiform Texts Which Contain Instructions for Glassmakers With a Catalogue of Surviving Objects*, 105-128. Corning, New York: The Corning Museum of Glass Press.

Brill R. H. (1976) 'Scientific studies of the panel materials', in L. Ibrahim, R. Scranton and R. Brill (eds.), *The Panels of Opus Sectile in Glass. Kenchreai Eastern Port of Corinth, II*. 227-255. Leiden: The University of Chicago and Indiana University for the American School of Classical Studies at Athens.

Brill, R. H. (1988) 'Scientific investigations of the Jalame glass and related finds', in G. D. Weinberg (ed.), *Excavations at Jalame: Site of a Glass Factory in Late Roman Palestine*, 257-295. Columbia: University of Missouri Press.

Brill, R. H. (1999) *Chemical Analyses of Early Glasses: Volumes I and II*. New York: Corning Museum of Glass.

Brill, R. H. (2006) 'Chemical analyses of some glasses from Jarrow and Wearmouth', in R. Cramp (ed.), *Wearmouth and Jarrow Monastic Sites*, 126-147. Swindon: English Heritage.

Brill, R. H. and Cahill, N. D. (1988) 'A red opaque glass from Sardis and some thoughts on red opaques in general', *Journal of Glass Studies*, 30, 16-27.

Brill, R. H. and Moll, S. (1963) 'The electron beam probe microanalysis of ancient glass', in F. R. Matson and G. E. Rindone (eds.), *Advances in Glass Technology, Part 2*, 293-302. New York: Plenum Press.

Brill, R. H. and Whitehouse, D. (1988) 'The Thomas panel', *Journal of Glass Studies*, 30, 34-50.

Bronk, H. and Freestone, I. C. (2001) 'A quasi non-destructive microsampling technique for the analysis of intact glass objects by SEM/EDXA', *Archaeometry*, 43(4), 517-527.

Brugmann, B. (1997) 'Typology and dating', in K. Parfitt and B. Brugmann (eds.), *The Anglo-Saxon Cemetery on Mill Hill, Deal, Kent*, 31-93. London: The Society for Medieval Archaeology.

Brugmann, B. (2004) *Glass Beads from Early Anglo-Saxon Graves: A Study of the Provenance and Chronology of Glass Beads from Early Anglo-Saxon Graves, Based on Visual Examination*. Oxford: Oxbow Books.

Brugmann, B. (2011) 'Migration and endogenous change', in H. Hamerow, D. A. Hinton and S. Crawford (eds.), *The Oxford Handbook of Anglo-Saxon Archaeology*, 30-45. Oxford: Oxford University Press.

Brun, N., Mazerolles, L. and Pernot, M. (1991) 'Microstructure of opaque red glass containing copper', *Journal of Materials Science Letters*, 10, 1418-1420.

Brun, N. and Pernot, M. (1992) 'The opaque red glass of Celtic enamels from continental Europe', *Archaeometry*, 34(2), 235-252.

Cable, M. and Smedley, J. (1987) 'The replication of an opaque red glass from Nimrud', in M. Bimson and I. C. Freestone (eds.), *Early Vitreous Materials*, British Museum Occasional Paper 56, 151-164. London: British Museum.

Cagno, S., Favaretto, L., Mendera, M., Izmer, A., Vanhaecke, F. and Janssens, K. (2012) 'Evidence of early medieval soda ash glass in the archaeological site of San Genesio (Tuscany)', *Journal of Archaeological Science*, 39, 1540-1552.

Callmer J. (1977) *Trade beads and bead trade in Scandinavia c. 800–1000 A.D.*, Acta Archaeologica Lundensia Series in 4°, 11. Bonn: Lund.

Callmer, J. (1995) 'The influx of oriental beads into Europe during the 8th century A.D.', in M. Rasmussen, U. Lund Hansen, and U. Näsman (eds.), *Glass Beads: Cultural History, Technology, Experiment and Analogy*, Studies in Technology and Culture vol. 2, 49-54. Lejre: Historical-Archaeological Experimental Centre.

Callmer, J. and Henderson, J. (1991) 'Glassworking at Åhus, S. Sweden (eighth century AD)', *Laborativ Arkeologi* 5, 143-154. Stockholm: Stockholm University.

Campbell, E. and Lane, A. (1993) 'Excavations at Longbury Bank, Dyfed, and early medieval settlement in south Wales', *Medieval Archaeology*, 37, 15-77.

Campbell, E. (2000) 'A review of glass vessels in western Britain and Ireland AD 400-800', in J. Price (ed.), *Glass in Britain and Ireland AD 350-1100*, 33-46. London: British Museum Press.

Carlton, R. A., Lyman, C. E. and Roberts, J. E. (2004a) 'Accuracy and precision of quantitative energy-dispersive x-ray spectrometry in the environmental scanning electron microscope', *Scanning*, 26(4), 167-174.

Carlton, R. A., Lyman, C. E. and Roberts, J. E. (2004b) 'Charge Neutralisation in the SEM for quantitative x-ray Microanalysis', *Microscopy and Microanalysis*, 10, 753-763.

Caruth, J. and Anderson, S. (2005) *An Assessment of the Potential for Analysis and Publication for Archaeological Work Carried Out at RAF Lakenheath Between 1987 and June 2005, Volume I: The Anglo-Saxon Cemeteries ERL 104, ERL 046 and ERL 114*, SCCAS Report No. 2005/94. Unpublished Report, Suffolk County Council Archaeological Service.

Cox, G. A. and Ford, B. A. (1989) 'Corrosion of glass on the sea bed', *Journal of Materials Science*, 24, 3146-3153.

Cox, G. A. and Ford, B. A. (1993) 'The long-term corrosion of glass by groundwater', *Journal of Materials Science*, 28, 5637-5647.

Craddock, P. T. and Meeks, N. D. (1987) 'Iron in ancient copper', *Archaeometry*, 29(2), 187-204.

Cramp, R. (1970) 'Decorated window-glass and millefiori from Monkwearmouth', *The Antiquaries Journal*, 50, 327-335.

Cramp, R. (1975) 'Window glass from the monastic site of Jarrow: problems of Interpretation', *Journal of Glass Studies*, 17, 88-96.

Cramp, R. (2001) 'Window glass from the British Isles, 7th-10th century', in F. Dell'Acqua and R. Silva (eds.), *Il Colore Nel Medioevo: La Vetrata in Occidente dal IV All'XI Secolo*, 67-86. Lucca: Istituto Storico Lucchese.

Cramp, R. (2006) 'The Anglo-Saxon window glass', in R. Cramp (ed.), *Wearmouth and Jarrow Monastic Sites*, 56-80. Swindon: English Heritage.

Davison, S. (2003) *Conservation and Restoration of Glass*. Oxford: Butterworth-Heinemann.

Degryse, P., Freestone, I. C., Schneider, J. and Jennings, S. (2010) 'Technology and provenance of Levantine plant ash glass using Sr-Nd isotope analysis', in J. Drauschke and D. Keller (eds.), *Glass in Byzantium – Production, Usage, Analyses*, 83-91. Mainz: Romisch-Germanischen Zentralmuseum.

Degryse, P. and Schneider, J. (2008) 'Pliny the Elder and Sr-Nd isotopes: tracing the provenance of raw materials for Roman glass production', *Journal of Archaeological Science*, 35, 1993-2000.

Degryse, P., Schneider, J., Haack, U., Lauwers, V., Poblome, J., Waelkens, M. and Muechez, Ph. (2006) 'Evidence for glass 'recycling' using Pb and Sr isotopic ratios and Sr-mixing lines: the case of early Byzantine Sagalassos', *Journal of Archaeological Science*, 33, 494-501.

Degryse, P., Schneider, J., Lauwers, V. and Brems, D. (2008) 'Sr-Nd isotopic analysis of glass from Sagalassos (SW Turkey)', *Journal of Cultural Heritage*, 9, 47-49.

Degryse, P., Schneider, J., Lauwers, V., De Muynck, D., Vanhaecke, F., Waelkens, M. and Muchez, P. (2009) 'Sr and Nd isotopic evidence in the primary provenance determination of Roman glass from Sagalassos (SW Turkey)', *Annales du 17^e Congrès de l'Association Internationale pour l'Histoire du Verre*, 564-570.

Degryse, P. and Shortland, A. J. (2009) 'Trace elements in provenancing raw materials for Roman glass production', *Geologica Belgica*, 12(3-4), 135-143.

Dickinson, T. M. (2011) 'Overview: mortuary ritual', in H. Hamerow, D. A. Hinton and S. Crawford (eds.), *The Oxford Handbook of Anglo-Saxon Archaeology*, 221-237. Oxford: Oxford University Press.

Dussubieux, L., Kusimba, C. M., Gogte, V., Kusimba, S. B., Gratuze, B. and Oka, R. (2008) 'The trading of ancient glass beads: new analytical data from South Asian and East African soda-alumina glass beads', *Archaeometry*, 50(5), 797-821.

Dussubieux, L., Robertshaw, P. and Glascock, M. D. (2009) 'LA-ICP-MS analysis of African glass beads: laboratory inter-comparison with an emphasis on the impact of corrosion on data interpretation', *International Journal of Mass Spectrometry*, 284, 152-161.

Evison, V. I. (1983) 'Some distinctive glass vessels of the post-Roman period', *Journal of Glass Studies*, 25, 87-93.

Evison, V. (1987) *Dover: The Buckland Anglo-Saxon Cemetery*. London: Historic Monuments & Buildings Commission for England.

Evison, V. I. (2000) 'Glass vessels in England AD 400-1100', in J. Price (ed.), *Glass in Britain and Ireland AD 350-1100*, 47-104. London: British Museum Press.

Evison, V. I. (2008) *Catalogue of Anglo-Saxon Glass in the British Museum*. London: British Museum Press.

Fiori, C. (2011) 'Vetro musivo del VI secolo dagli scavi della Basilica di San Severo a Classe (Ravenna)', *Rivista della Stazione Sperimentale del Vetro*, 1-2011, 22-34.

Fiori, C. and Vandini, M. (2004) 'Chemical composition of glass and its raw materials: chronological and geographical development in the first millennium A.D.', in M. Beretta (ed.), *When Glass Matters: Studies in the History of Science and Art from Graeco-Roman Antiquity to Early Modern Era*, 151-194. Florence: Leo S. Olschki.

Fleming, R. (2011) *Britain After Rome: The Fall and Rise 400 to 1070*. London: Penguin Books Ltd.

Foster, H. E. and Jackson, C. M. (2005) '“A whiter shade of pale”? Chemical and experimental investigation of opaque white Roman glass gaming counters', *Glass Technology*, 46(5), 327-333.

Foster, H. E. and Jackson, C. M. (2009) 'The composition of 'naturally coloured' late Roman vessel glass from Britain and the implications for models of glass production and supply', *Journal of Archaeological Science*, 36, 189-204.

Foster, H. E. and Jackson, C. M. (2010) 'The composition of late Romano-British colourless vessel glass: glass production and consumption', *Journal of Archaeological Science*, 37, 3068-3080.

Foy, D. and Jézégou, M. P. (1997) 'Une épave charge de lingots et de vaisselle de verre: un témoin exceptionnel du commerce et de la technologie du verre en Méditerranée antique', *Verre*, 3, 65-70.

Foy, D. and Nenna, M.-D. (2001) *Tout Feu Tout Sable: Mille ans de Verre Antique dans le Midi de la France*. Marseille: Musées de Marseille / Éditions Édisud.

Foy, D., Picon, M., Vichy, M. and Thirion-Merle, V. (2003) 'Caractérisation des verres de la fin de l'Antiquité en Méditerranée occidentale: l'émergence de nouveaux courants commerciaux', in D. Foy and M.-D. Nenna (eds.), *Échanges et Commerce du Verre dans le Monde Antique*, 41-85. Montagnac: Editions Mionique Mergoil.

Foy, D., Vichy, M. and Picon, M. (2000) 'Lingots de verre en Méditerranée occidentale (III^e siècle av.J.-C. – VII^e siècle ap.J.-C.)', *Annales du 14^e Congrès de l'Association Internationale pour l'Histoire du Verre*, 51-57.

Frank, S. (1982) *Glass and Archaeology*. London: Academic Press.

Frederickx, P., De Ryck, I., Janssens, K., Schryvers, D., Petit, J.-P. and Döcking, H. (2004) 'EPMA and μ -SRXRF analysis and TEM-based microstructure characterization of a set of Roman glass fragments', *X-Ray Spectrometry*, 33, 326-333.

Freestone, I. C. (1985) 'Scanning electron microscopy and X-ray microanalysis', in P. Phillips (ed.), *The Archaeologist and the Laboratory*, Council for British Archaeology Research Report No. 58, 67-68. London: Council for British Archaeology.

Freestone, I. C. (1987) 'Composition and microstructure of early opaque red glass', in M. Bimson and I. C. Freestone (eds.), *Early Vitreous Materials*, British Museum Occasional Paper, 56, 173-191. London: British Museum.

Freestone, I. C. (1993) 'Theophilus and the composition of medieval glass', in P. B. Vandiver, J. R. Druzik, G. S. Wheeler, and I. C. Freestone (eds.), *Materials Issues in Art and Archaeology III*. Materials Research Society Symposium Proceedings, Volume 267, 739-746.

Freestone, I. C. (1994) 'Appendix: chemical analysis of 'raw' glass fragments', in H. Hurst, *Excavations at Carthage vol. II, 1: The Circular Harbour, North Side*, 290. Oxford: Oxford University Press for the British Academy.

Freestone, I. C. (2001) 'Post-depositional changes in archaeological ceramics and glasses', in D. R. Brothwell and A. M. Pollard (eds.), *Handbook of Archaeological Science*, 615-625. Chichester: John Wiley & Sons, Ltd.

Freestone, I. C. (2003) 'Primary glass sources in the mid-first millennium AD', *Annales du 15^e Congrès de l'Association Internationale pour l'Histoire du Verre*, 111-115.

Freestone, I. C. (2005) 'The provenance of glass through compositional analysis', in P. B. Vandiver, J. L. Mass and A. Murray (eds.), *Materials Issues in Art and Archaeology VII*, Materials Research Society Symposium Proceedings Vol. 852, OO8.1.1-OO8.1.14. Warrendale, Pennsylvania: Materials Research Society.

Freestone, I. C. (2006) 'Glass production in Late Antiquity and the early Islamic period: a geochemical perspective', in M. Maggetti and B. Messiga (eds.), *Geomaterials in Cultural Heritage*, Geological Society of London Special Publication, 257, 201-216. London: Geological Society.

Freestone, I. C. (2008) 'Pliny on Roman glassmaking', in M. Martín-Torres and Th. Rehren (eds.), *Archaeology, History & Science: Integrating Approaches to Ancient Materials*, 77-100. Walnut Creek, California: Left Coast Press, Inc.

Freestone, I. C., Ambers, J. C., Simpson, St J. and as-Sayyani, M. (2005a) 'A Roman mosaic glass bowl from the Wadi Dura in Yemen', *Journal of Glass Studies*, 47, 69-75.

Freestone, I. C., Bimson, M. and Buckton, D. (1990) 'Compositional categories of Byzantine glass tesserae', *Annales du 11^e Congrès de l'Association Internationale pour l'Histoire du Verre*, 271-280.

Freestone, I. C. and Dell'Acqua, F. (2005) 'Early medieval glass from Brescia, Cividale and Salerno, Italy: composition and affinities', in D. Ferrari (ed.), *Il vetro nell'Alto Medioevo. Atti delle VIII Giornate Nazionali di Studio*, 65-75. Imola, Bologna: La Mandragora Editrice

Freestone, I. C. and Gorin-Rosen, Y. (1999) 'The great glass slab at Bet She'arim, Israel: an Early Islamic glassmaking experiment?', *Journal of Glass Studies*, 41, 105-116.

Freestone, I. C., Gorin-Rosen, Y. and Hughes, M. J. (2000) 'Primary glass from Israel and the production of glass in Late Antiquity and the early Islamic period', in M.-D. Nenna (ed.), *La Route du Verre: Ateliers Primaires et Secondaires de Verriers du Second Millinaire av. J.-C. au Moyen-Age*, 65-83. Lyon: Travaux de la Maison de l'Orient Méditerranéen no. 33.

Freestone, I. C., Greenwood, R. and Gorin-Rosen, Y. (2002a) 'Byzantine and early Islamic glassmaking in the Eastern Mediterranean: production and distribution of primary glass', in G. Kordas (ed.), *Hyalos-Vitrum-Glass*, 167-174. Athens: Glasnet Publications.

Freestone, I. C. and Hughes, M. J. (2006) 'The origins of the Jarrow glass', in R. Cramp (ed.), *Wearmouth and Jarrow Monastic Sites*, 147-155. Swindon: English Heritage.

Freestone, I. C., Hughes, M. J. and Stapleton, C. P. (2008) 'The composition and production of Anglo-Saxon glass', in V. I. Evison, *Catalogue of Anglo-Saxon Glass in the British Museum*, 29-46. London: The British Museum.

Freestone I. C., Kunicki-Goldfinger, J. J., McDonald, I., Gutjahr, M. and Pike, A. (in press) 'Composition, technology and origin of glass from the workshop at Basinghall Street'. Museum of London.

Freestone, I. C., Leslie, K. A., Thirlwall, M. and Gorin-Rosen, Y. (2003a) 'Strontium isotopes in the investigation of early glass production: Byzantine and early Islamic glass from the Near East', *Archaeometry*, 45, 19-32.

Freestone, I., Meeks, N., Sax, M. and Higgitt, M. (2007) 'The Lycurgus Cup – A Roman nanotechnology', *Gold Bulletin*, 40(4), 270-277.

Freestone, I. C., Ponting, M. and Hughes, M. J. (2002b) 'The origins of Byzantine glass from Maroni Petrera, Cyprus', *Archaeometry*, 44(2), 257-272.

Freestone, I. C., Price, J. and Cartwright, C. R. (2009) 'The batch: its recognition and significance', *Annales du 17^e Congrès de l'Association Internationale pour l'Histoire du Verre*, 130-135.

Freestone, I. C., Stapleton, C. P. and Rigby, V. (2003b) 'The production of red glass and enamel in the late Iron Age, Roman and Byzantine periods', in C. Entwistle (ed.), *Through a Glass Brightly: Studies in Byzantine and Medieval Art and Archaeology Presented to David Buckton*, 142-154. Oxford: Oxbow Books.

Freestone, I. C., Wolf, S. and Thirlwall, M. (2005b) 'The production of HIMT glass: elemental and isotopic evidence', *Annales du 16^e Congrès de l'Association Internationale pour l'Histoire du Verre*, 153-157.

Freestone, I. C., Wolf, S. and Thirlwall, M. (2009) 'Isotopic composition of glass from the Levant and south-east Mediterranean region', in P. Degryse, J. Henderson and G. Hodgins (eds.), *Studies in Archaeological Sciences: Isotopes in Vitreous Materials*, 31-52. Leuven: Leuven University Press.

Geake, H. (2002) 'Persistent problems in the study of Conversion-Period burials in England', in S. Lucy and A. Reynolds (eds.), *Burial in Early Medieval England and Wales*, The Society for Medieval Archaeology Monograph Series No. 17, 144-155. London: the Society for Medieval Archaeology.

Goldstein, J. I., Joy, D. C., Lefshin, E., Lyman, C. E., Michael, J. R., Newbury, D. E. and Sawyer, L. C. (2003) *Scanning Electron Microscopy and X-Ray Microanalysis*. New York: Kluwer Academic.

Gorin-Rosen Y. (2000) 'The ancient glass industry in Israel: summary of finds and new discoveries', in M.-D. Nenna (ed.), *La Route du Verre: Ateliers Primaires et Secondaires de Verriers du Second Millinaire av. J.-C. au Moyen-Age*, 49-64. Lyon: Travaux de la Maison de l'Orient Méditerranéen no. 33.

Gratuze, B. and Barrandon, J.-N. (1990) 'Islamic glass weights and stamps: analysis using nuclear techniques', *Archaeometry*, 32, 155-162.

Gratuze, B., Blet-Lemarquand, M. and Barrandon, J.-N. (2001) 'Mass spectrometry with laser sampling: a new tool to characterize archaeological materials', *Journal of Radioanalytical and Nuclear Chemistry*, 247(3), 645-656.

Gratuze, B., Soulier, I., Barrandon, J.-N. and Foy, D. (1995) 'The origin of cobalt blue pigments in French glass from the thirteenth to the eighteenth centuries', in D. R. Hook and D. R. M. Gaimster (eds.), *Trade and Discovery: The Scientific Study of Artefacts from Post-Medieval Europe and Beyond*, British Museum Occasional Paper 109, 123-133. London: The British Museum.

Green, L. R. and Hart, F. A. (1987) 'Colour and chemical composition in ancient glass: an examination of some Roman and Wealden glass by means of ultraviolet-visible-infra-red spectrometry and electron microprobe analysis', *Journal of Archaeological Science*, 14, 271-282.

Guido, M. (1978) *The Glass Beads of the Prehistoric and Roman Periods in Britain and Ireland*. London: The Society of Antiquaries of London.

Guido, M. (1999) *The Glass Beads of Anglo-Saxon England c. AD 400-700: A Preliminary Visual Classification of the More Definitive and Diagnostic Types*, Report of the Research Committee of the Society of Antiquaries of London No. 58. Woodbridge: The Boydell Press.

Guido, M. and Welch, M. (2000) 'Indirect evidence for glass bead manufacture in early Anglo-Saxon England', in J. Price (ed.), *Glass in Britain and Ireland AD 350-1100*, 115-119. London: British Museum Press.

Hall, M. and Yablonsky, L. (1997) 'Chemical analyses of glass beads found in two Sarmatian burials', *Archaeometry*, 39(2), 369-377.

Hawthorne, J. G. and Smith, C. S. (1979) *Theophilus: On Divers Arts*. New York: Dover Publications, Inc.

Hauptmann, A. (2007) *The Archaeometallurgy of Copper: Evidence from Faynan, Jordan*. Berlin: Springer.

Heck, M. (2000) *Chemisch-Analytische Untersuchungen an Fruhmittelalterlichen Glasperlen*, Unpublished PhD Thesis, Technical University Darmstadt. Available from: <http://elib.tu-darmstadt.de/diss/000065/>

Heck, M. and Hoffmann, P. (2000) 'Coloured opaque glass beads of the Merovingians', *Archaeometry*, 42(2), 341-357.

Heck, M. and Hoffmann, P. (2002) 'Analysis of early medieval glass beads: the raw materials to produce green, orange and brown colours', *Mikrochimica Acta*, 139, 71-76.

Heck, M., Rehren, T. and Hoffmann, P. (2003) 'The production of lead-tin yellow at Merovingian Schleithem (Switzerland)', *Archaeometry*, 45(1), 33-44.

Henderson, J. (1985) 'The raw materials of early glass production', *Oxford Journal of Archaeology*, 4(3), 267-291.

Henderson, J. (1988a) 'Electron probe microanalysis of mixed-alkali glasses', *Archaeometry*, 30(1), 77-91.

Henderson, J. (1988b) 'The nature of the Early Christian glass industry in Ireland: some evidence from Dunmisk Fort, Co. Tyrone', *Ulster Journal of Archaeology*, 51, 115-26.

Henderson, J. (1989a) 'The scientific analysis of ancient glass and its archaeological interpretation', in J. Henderson (ed.), *Scientific Analysis in Archaeology and its Interpretation*, 30-62. Oxford: Oxford University Committee for Archaeology.

Henderson, J. (1989b) 'The use of colorants in mixed-alkali and soda-lime-silica prehistoric glass', in Y. Maniatis (ed.), *Archaeometry: Proceedings of the 25th International Symposium*, 217-229. Amsterdam: Elsevier.

Henderson, J. (1990) 'The scientific investigation of the glass beads from the Apple Down Anglo-Saxon cemetery', in A. Down, and M. Welch, (eds.), *Chichester Excavations VII, Apple Down and the Marshes*, 156-168. Chichester: Chichester District Council.

Henderson, J. (1993) 'Aspects of early medieval glass production in Britain', *Annales du 12^e Congrès de l'Association Internationale pour l'Histoire du Verre*, 247-259.

Henderson, J. (1999a) 'Technological aspects of Anglo-Saxon glass beads', in M. Guido, *The Glass Beads of Anglo-Saxon England c.AD 400-700: A Preliminary Visual Classification of the More Definitive and Diagnostic Types*, Report of the Research Committee of the Society of Antiquaries of London No. 58, 81-88. Woodbridge: The Boydell Press.

Henderson, J. (1999b) 'Scientific analysis of the glass and the glass-bearing artefacts: technique, raw materials used and archaeological interpretation', in J. C. Besteman, J. M. Bos, D. A. Gerrets, H. A. Heidinga and J. De Koning (eds.), *The Excavations at Wijnaldum: Reports on Frisia in Roman and Medieval Times, Volume 1*, 287-297. Rotterdam: A. A. Balkema.

Henderson, J. (2000a) *The Science and Archaeology of Materials: An Investigation of Inorganic Materials*. London: Routledge.

Henderson, J. (2000b) 'The production technology of Irish early Christian glass with specific reference to beads and enamels', in J. Price (ed.), *Glass in Britain and Ireland AD 350-1100*, 143-159. London: British Museum Press.

Henderson, J. (2002) 'An archaeological and scientific study of 47 glass beads', in D. Freke, *Excavations on St Patrick's Isle, Peel, Isle of Man, 1982-88: Prehistoric, Viking, Medieval and Later*, 349-362. Liverpool: Liverpool University Press.

Henderson, J. (2011) 'The scientific analysis of selected glass beads', in A. Boyle, D. Jennings, D. Miles and S. Palmer, *The Anglo-Saxon Cemetery at Butler's Field, Lechlade, Gloucestershire. Volume 2: The Anglo-Saxon Grave Goods, Specialist Reports, Phasing and Discussion*, Thames Valley Landscapes Monograph No. 33, 115-117. Oxford: Oxford University School of Archaeology.

Henderson, J., Evans, J. A., Sloane, H. J., Leng, M. J. and Doherty, C. (2005) 'The use of oxygen, strontium and lead isotopes to provenance ancient glasses in the Middle East', *Journal of Archaeological Science*, 32, 665-673.

Henderson, J. and Ivens, R. (1992) 'Dunmisk and glass-making in Early Christian Ireland', *Antiquity*, 66, 52-64.

Henderson, J. and Warren, S. E. (1983) 'Analysis of Prehistoric lead glass', in A. Aspinall and S. E. Warren (eds.), *Proceedings of the 22nd International Symposium on Archaeometry, Bradford*, 168-180.

Henderson, P. (1984) 'General geochemical properties and abundances of the rare earth elements', in P. Henderson (ed.), *Rare Earth Element Geochemistry: Developments in Geochemistry 2*, 1-32. Amsterdam: Elsevier.

Henricson, L. G. (1995) 'Broken glass beakers re-used as glass beads', in M. Rasmussen, U. Lund Hansen and U. Näsman (eds.), *Glass Beads: Cultural History, Technology, Experiment and Analogy*, Studies in Technology and Culture vol. 2, 13-17. Lejre: Historical-Archaeological Experimental Centre.

Heyworth, M. (1992) 'Evidence for early medieval glass production in north-east Europe', in S. Jennings and A. Vince (eds.), *Medieval Europe 1992: Technology and Innovation, Pre-Printed Papers, Volume 3*, 169-174. York: Medieval Europe.

Heyworth, M. P. (1994) 'Examination and analysis of the glass beads', in V. I. Evison (ed.) *An Anglo-Saxon Cemetery at Great Chesterford, Essex*, 77-80. York: Council for British Archaeology.

Heyworth, M. P. (1996a) 'Examination and analysis of glass beads', in V. I. Evison, and P. Hill (eds.), *Two Anglo-Saxon Cemeteries at Beckford, Hereford and Worcester*, 66-70. York: Council for British Archaeology.

Heyworth, M. P. (1996b) 'Examination and analysis of glass beads from Empingham II', in J. R. Timby, *The Anglo-Saxon Cemetery at Empingham II, Rutland*, 50-55. Oxford: Oxbow Books.

Heyworth, M. P., Baxter, M. J. and Cool, H. E. M. (1990) *Compositional Analysis of Roman Glass from Colchester, Essex*, Ancient Monuments Laboratory Report 53/1990. Unpublished Report, English Heritage.

Hills, C. (2011) 'Overview: Anglo-Saxon identity', in H. Hamerow, D. A. Hinton and S. Crawford (eds.), *The Oxford Handbook of Anglo-Saxon Archaeology*, 3-11. Oxford: Oxford University Press.

Hines, J. (2003) 'Society, community and identity', in T. Charles-Edwards (ed.), *After Rome*, 61-102. Oxford: oxford University Press.

Hines, J. A., Bayliss, A. L., Højlund Nielsen, K. and Scull, C. (eds.) (in press) *Anglo-Saxon Graves and Grave Goods of the Sixth and Seventh Centuries AD: A Chronological Framework*, SMA Monograph. Leeds: Society for Medieval Archaeology.

Hinton, D. A. (2005) *Gold and Gilt, Pots and Pins: Possessions and People in Medieval Britain*. Oxford: Oxford University Press.

Hinton, D. A. (2011) 'Raw materials: sources and demand', in H. Hamerow, D. A. Hinton and S. Crawford (eds.), *The Oxford Handbook of Anglo-Saxon Archaeology*, 423-439. Oxford: Oxford University Press.

Hirst, S. M. (2000) 'An approach to the study of Anglo-Saxon glass beads', in J. Price (ed.), *Glass in Britain and Ireland AD 350-1100*, 121-129. London: British Museum Press.

Hirst, S. M. and Biek, L. (1981) 'Investigation of a glass bead assemblage from an Anglo-Saxon cemetery near York', *Revue d'Archéométrie: Actes du XX Symposium International d'Archéométrie, Supplément 1981*, 3, 139-146. Rennes: Loic Langouet.

Hirst, S. M. and Clark, D. (2009) *Excavations at Mucking: Volume 3, The Anglo-Saxon Cemeteries*. London: Museum of London Archaeology.

Hoffmann, P. (1994) 'Analytical determination of colouring elements and of their compounds in glass beads from graveyards of the Merovingian time', *Fresenius Journal of Analytical Chemistry*, 349, 320-333.

Hoffmann, P., Bichlmeier, S., Heck, M., Theune, C. and Callmer, J. (1999) 'Glasmatrix der perlen Merowingerzeitlicher frauengräber von Eichstetten und Endingen', *Archäologisches Korrespondenzblatt*, 29, 395-406.

Hoffmann, P., Bichlmeier, S., Heck, M., Theune, C. and Callmer, J. (2000) 'Chemical composition of glass beads of the Merovingian period from graveyards in the Black Forest, Germany', *X-Ray Spectrometry*, 29, 92-100.

Huggett, J. (1988) 'Imported grave goods and the early Anglo-Saxon economy', *Medieval Archaeology*, 32, 63-96.

Hughes, M. J. (1972) 'A technical study of opaque red glass of the Iron Age in Britain', *Proceedings of the Prehistoric Society*, 38, 98-107.

Hunter, J. and Heyworth, M. (1998) *The Hamwic Glass*. York: Council for British Archaeology.

Jackson, C. M. (1992) *A Compositional Analysis of Roman and Early Post-Roman Glass and Glassworking Waste from Selected British Sites*, Unpublished PhD Thesis, University of Bradford.

Jackson, C. M. (1994) 'Appendix A1', in M. J. Baxter, *Exploratory Multivariate Data Analysis in Archaeology*, 228-231. Edinburgh: Edinburgh University Press.

Jackson, C. M. (1996) 'From Roman to early medieval glasses: many happy returns or a new birth?', *Annales du 13^e Congrès de l'Association Internationale pour l'Histoire du Verre*, 289-301.

Jackson, C. M. (2005) 'Making colourless glass in the Roman period', *Archaeometry*, 47(4), 763-780.

Jackson, C. M., Booth, C. A. and Smedley, J. W. (2005) 'Glass by design? Raw materials, recipes and compositional data', *Archaeometry*, 47(4), 781-795.

Jackson, C. M., Hunter, J. R., Warren, S. E. and Cool H.E. M. (1991) 'The analysis of blue-green glass and glassy waste from two Romano-British glass-working sites', in E. Pernicka and G. A. Wagner (eds.), *Archaeometry '90*, 295-305. Basel: Birkhäuser Verlag.

Jackson, C. M., Joyner, L., Booth, C. A., Day, P. M., Wager, E. C. W. and Kilikoglou, V. (2003) 'Roman glass-making at Coppergate, York? Analytical evidence for the nature of production', *Archaeometry*, 45(3), 435-456.

Jackson, C. M., Price, J. and Lemke, C. (2009) 'Glass production in the 1st century AD: insights into glass technology', *Annales du 17^e Congrès de l'Association Internationale pour l'Histoire du Verre*, 150-155.

Jackson, C. M. and Smedley, J. W. (2004) 'Medieval and post-medieval glass technology: melting characteristics of some glasses melted from vegetable ash and sand mixtures', *Glass Technology*, 45(1), 36-42.

Jackson, C. M. and Smedley, J. W. (2008) 'Theophilus and the use of beech ash as a glassmaking alkali', in M. Martín-Torres and Th. Rehren (eds.), *Archaeology, History & Science: Integrating Approaches to Ancient Materials*, 117-130. Walnut Creek, California: Left Coast Press, Inc.

Jönsson, M. and Hunner, P. (1995) 'Gold-foil beads', in M. Rasmussen, U. Lund Hansen and U. Näsman (eds.), *Glass Beads: Cultural History, Technology, Experiment and Analogy*, Studies in Technology and Culture vol. 2, 113-116. Lejre: Historical-Archaeological Experimental Centre.

Kamber, B. S., Greig, A. and Collerson, K. D. (2005) 'A new estimate for the composition of weathered young upper continental crust from alluvial sediments, Queensland, Australia'. *Geochimica et Cosmochimica Acta*, 69, 1041-1058.

Kingery, W. D. and Vandiver, P. B. (1986) *Ceramic Masterpieces – Art, Structure and Technology*. New York: Free Press (Macmillan).

Kleinmann, B. (1990) 'Cobalt pigments in the early Islamic glazes and the reconstruction of the way of their manufacture', in E. Penicka and G. Wagner (eds.), *Archaeometry '90*, 327-336. Basel: Birkhäuser Verlag.

Koch, U. (1977) *Das Reihengräberfeld bei Schretzheim*, Germanische Denkmäler der Völkerwanderungszeit, Serie A 13. Berlin: Mann.

Kock, J. and Sode, T. (1994) *Glass, Glassbeads and Glassmakers in Northern India*. Vanlose, Denmark: THOT Print.

Küçükerman, Ö. (1988) *Glass Beads. Anatolian Glass Bead Making: The Final Traces of Three Millennia of Glass Making in the Mediterranean Region*. Istanbul: Turkish Touring and Automobile Association.

Lane, A. and Campbell, E. (2000) *Dunadd: An Early Dalriadic Capital*, 212-217. Oxford: Oxbow Books.

Lang, J. and Middleton, A. (2005) *Radiography of Cultural Material*. Oxford: Elsevier Butterworth-Heinemann.

Leahy, K. (2003) *Anglo-Saxon Crafts*. Stroud: Tempus Publishing.

Leahy, K. (2011) 'Anglo-Saxon crafts', in H. Hamerow, D. A. Hinton and S. Crawford (eds.), *The Oxford Handbook of Anglo-Saxon Archaeology*, 440-459. Oxford: Oxford University Press.

Leslie, K. A., Freestone, I. C., Lowry, D. and Thirlwall, M. (2006) 'The provenance and technology of Near Eastern glass: oxygen isotopes by laser fluorination as a complement to strontium', *Archaeometry*, 48(2), 253-270.

Lucy, S. (2000) *The Anglo-Saxon Way of Death: Burial Rites in Early England*. Stroud: Sutton Publishing Ltd.

Lundström, A. (1981) 'Survey of glass from Helgö', in A. Lundström and H. Clarke (eds.), *Excavations at Helgö VII: Glass-Iron-Clay*. Stockholm: Kungl. Vitterhets Historie och Antikvitets Akademien.

Manasse, A., Mellini, M. and Viti, C. (2001) 'The copper slags of the Capatolli Valley, Campiglia Marittima, Italy', *European Journal of Mineralogy*, 13, 949-960.

Marii, F. and Rehren, Th. (2009) 'Archaeological coloured glass cakes and tesserae from the Petra church', *Annales du 17^e Congrès de l'Association Internationale pour l'Histoire du Verre*, 295-300.

Mathis, F., Othmane, G., Vrielynck, O., Calvo del Castillo, H., Chêne, G., Dupuis, T. and Strivay, D. (2010) 'Combined PIXE/PIGE and IBIL with external beam applied to the analysis of Merovingian glass beads', *Nuclear Instruments and Methods in Physics Research B*, 268, 2078-2082.

Meaney, A. (1981) *Anglo-Saxon Amulets and Curing Stones*, British Archaeological Reports, British Series, 96. Oxford: British Archaeology Reports (B.A.R.).

Meek, A. (2010) *The Scientific Investigation of Glass from Ringlemere Anglo-Saxon Cemetery*, Department of Conservation and Scientific Research Project number 7389. Unpublished Report, British Museum.

Meharg, A. A., Edwards, K. J., Schofield, J. E., Raab, A., Feldmann, J., Moran, A., Bryant, C. L., Thornton, B. and Dawson J. J. C. (2012) 'First comprehensive peat depositional records for tin, lead and copper associated with the antiquity of Europe's largest cassiterite deposits', *Journal of Archaeological Science*, 39, 717-727.

Mirti, P., Casoli, A. and Appolonia, L. (1993) 'Scientific analysis of Roman glass from *Augusta Praetoria*', *Archaeometry*, 35(2), 225-240.

Mirti, P., Davit, P., Gulmini, M. and Saguì, L. (2001) 'Glass fragments from the Crypta Balbi in Rome: the composition of eighth-century fragments', *Archaeometry*, 43(4), 491-502.

Mirti, P., Davit, P. and Gulmini, M. (2002) 'Colourants and opacifiers in seventh and eighth century glass investigated by spectroscopic techniques', *Analytical and Bioanalytical Chemistry*, 372, 221-229.

Mirti, P., Lepora, A. and Saguì, L. (2000) 'Scientific analysis of seventh-century glass fragments from the Crypta Balbi in Rome', *Archaeometry*, 42(2), 359-374.

Mirti, P., Pace, M., Malandrino, M. and Ponzi, M. N. (2009) 'Sasanian glass from Veh Ardašīr: new evidences by ICP-MS analysis', *Journal of Archaeological Science*, 36, 1061-1069.

Moretti, C. and Hreglich, S. (1984) 'Opacification and colouring of glass by the use of 'anime'', *Glass Technology*, 25, 277-282.

Mortimer, C. (1996a) *Compositional and Structural Analysis of Glass Beads from Barrington Anglo-Saxon Cemetery, Cambridgeshire*, Ancient Monuments Laboratory Report 76/96. Unpublished Report, English Heritage.

Mortimer, C. (1996b) *Compositional and Structural Analysis of Glass Beads from Mucking Anglo-Saxon Cemeteries, Essex*, Ancient Monuments Laboratory Report 60/96. Unpublished Report, English Heritage.

Mortimer, C. (1998) 'Glass beads: a technological examination', in T. Malim and J. Hines (eds.), *The Anglo-Saxon Cemetery at Edix Hill (Barrington, A), Cambridgeshire*, CBA Research Report 112, 256-258. York: Council for British Archaeology.

Mortimer, C. and Baxter, M. J. (1996) *Analysis of Samples of Colourless Roman Vessel Glass from Lincoln*, Ancient Monuments Laboratory Report 44/96. Unpublished Report, English Heritage.

Mortimer, C. and Heyworth, M. P. (2009) 'Compositional and structural analysis of glass beads', in S. M. Hirst and D. Clark, *Excavations at Mucking: Volume 3, The Anglo-Saxon Cemeteries*, 403-413. London: Museum of London Archaeology.

Näsman, U. (1979) 'Wikingerzeitliches handwerk in Ribe', in M. Bencard (ed.), *Acta Archaeologica*, 49, 113-138.

Nenna, M.-D., Picon, M., Thirion-Merle, V. and Vichy, M. (2005) 'Ateliers primaires du Wadi Natrun: nouvelles découvertes', *Annales du 16^e Congrès de l'Association Internationale pour l'Histoire du Verre*, 59-63.

Nenna, M.-D., Picon, M. and Vichy, M. (2000) 'Ateliers primaires et secondaires en Égypte à l'èpoque Gréco-Romaine', in M.-D. Nenna (ed.), *La Route du Verre: Ateliers Primaires et Secondaires de Verriers du Second Millinaire av. J.-C. au Moyen-Age*, 97-112. Lyon: Travaux de la Maison de l'Orient Méditerranéen no. 33.

Nenna, M.-D., Vichy, M. and Picon, M. (1997) 'L'atelier de verrier de Lyon, du I^{er} siècle après J.-C., et l'origine des verres "Romains"', *Revue d'Archéométrie*, 21, 81-87.

Newbury, D. E. (2002) 'X-ray microanalysis in the variable pressure (environmental) scanning electron microscope', *Journal of Research of the National Institute of Standards and Technology*, 107(6), 567-603.

NMAS (2010) *Collections Online for All* [Online], Norfolk Museums & Archaeology Service [Accessed 6th March 2012]. Available from: <http://www.culturalmodes.norfolk.gov.uk/projects/nmaspub5.asp>

O'Connor, S. and Brooks, M. M. (2007) *X-Radiography of Textiles, Dress and Related Objects*. Oxford: Butterworth-Heinemann.

Owen-Crocker, G. (2004) *Dress in Anglo-Saxon England*. Woodbridge: The Boydell Press.

Owen-Crocker, G. R. (2011) 'Dress and identity', in H. Hamerow, D. A. Hinton and S. Crawford (eds.), *The Oxford Handbook of Anglo-Saxon Archaeology*, 91-116. Oxford: Oxford University Press.

Paynter, S. (2006) 'Analyses of colourless Roman glass from Binchester, County Durham', *Journal of Archaeological Science*, 33, 1037-1057.

Paynter, S. (2008) 'Experiments in the reconstruction of Roman wood-fired glassworking furnaces: waste products and their formation processes', *Journal of Glass Studies*, 50, 271-290.

Paynter, S. and Kearns, T. (2011) *West Clacton Reservoir, Great Bentley, Essex. Analysis of Glass Tesserae: Technology Report*, Research Department Report Series No. 44-2011. Unpublished Report, English Heritage.

Peake, J. R. N. and Freestone, I. C. (in press) 'Opaque yellow glass production in the early medieval period: new evidence', *Neighbours and Successors of Rome: Traditions of Glass Production and Use in Europe and the Middle East in the Later First Millennium AD*. Association for the History of Glass.

Peake, J. R. N. and Freestone, I. C. (2012) 'Cross-craft interactions between metal and glass working: slag additions to early Anglo-Saxon red glass', *Proceedings of SPIE Volume 8422: Integrated Approaches to the Study of Historical Glass*, 842204-1 – 842204-12.

Penn, K. and Brugmann, B. (2007) *Aspects of Anglo-Saxon Inhumation Burial: Morning Thorpe, Spong Hill, Bergh Apton and Westgarth Gardens*. Dereham: Norfolk Museums and Archaeology Service.

Picon, M. and Vichy, M. (2003) 'D'Orient en Occident: l'origine du verre à l'époque romaine et durant le haut Moyen Âge', in D. Foy and M.-D. Nenna (eds.), *Échanges et Commerce du verre dans le Monde Antique*, 17-31. Montagnac: Editions Mionique Mergoil.

Pollard, A. M., Batt, C., Stern, B. and Young, S. M. M. (2007) *Analytical Chemistry in Archaeology*. Cambridge: Cambridge University Press.

Popelka, R. S., Glascock, M. D., Robertshaw, P. and Wood, M. (2005) 'Laser ablation ICP-MS of African glass trade beads', in R. Speakman and H. Neff (eds.), *Laser Ablation ICP-MS in Archaeological Research*, 84-93. Albuquerque: University of New Mexico Press.

Rehren, Th. (2001) 'Aspects of the production of cobalt-blue glass in Egypt', *Archaeometry*, 43(4), 483-489.

Robertshaw, P., Benco, N., Wood, M., Dussubieux, L., Melchiorre, E. and Ettahiri, A. (2010a) 'Chemical analysis of glass beads from medieval Al-Basra (Morocco)', *Archaeometry*, 52(3), 355-379.

Robertshaw, P., Glascock, M. D., Wood, M., Popelka-Filcoff, R. S. (2003) 'Chemical analysis of ancient African glass beads: a very preliminary report', *Journal of African Archaeology*, 1, 139-146.

Robertshaw, P., Wood, M., Melchiorre, E., Popelka-Filcoff, R. S. and Glascock, M. D. (2010b) 'Southern African glass beads: chemistry, glass sources and patterns of trade', *Journal of Archaeological Science*, 37, 1898-1912.

Rooksby, H. P. (1962) 'Opacifiers in opal glasses through the ages', *GEC Journal of Science and Technology*, 29(1), 20-6.

Rooksby, H. P. (1964) 'A yellow cubic lead tin oxide opacifier in ancient glasses', *Physics and Chemistry of Glasses*, 5(1), 20-25.

Sablerolles, Y. (1999) 'Beads of glass, faience, amber, baked clay and metal, including production waste from glass and amber bead making', in J. C. Besteman, J. M. Bos, D. A. Gerrets, H. A. Heidinga and J. de Koning (eds.), *The Excavations at Wijnaldum: Reports on Frisia in Roman and Medieval Times, Volume 1*, 253-285. Rotterdam: A. A. Balkema.

Sablerolles, Y., Henderson, J. and Dijkman, W. (1997) 'Early medieval glass bead making in Maastricht (Jodenstraat 30), The Netherlands: an archaeological and scientific investigation', in U. von Freeden and A. Wiczorek (eds.), *Perlen: Archäologie, Techniken, Analysen*, 293-313. Bonn: Dr. Rudolf Habelt GmbH.

Salter, C. J. (2009) 'Early tin extraction in the south-west of England: a resource for Mediterranean metalworkers of late antiquity?', in M. M. Mango (ed.), *Byzantine Trade, 4th-12th Centuries: The Archaeology of Local, Regional and International Exchange. Papers of the Thirty-Eighth Spring Symposium of Byzantine Studies, St John's College, University of Oxford*, March 2004, 315-322. Farnham: Ashgate Publishing Limited.

Sanderson, D., Hunter, J. and Warren, S. (1984) 'Energy-dispersive x-ray fluorescence analysis of 1st millennium AD glass from Britain', *Journal of Archaeological Science*, 11, 53-69.

Sanderson, D. C. W. and Hutchings, J. B. (1987) 'The origins and measurement of colour in archaeological glasses', *Glass Technology*, 28(2), 99-105.

Santagostino Barbone, A., Gliozzo, E., D'Acapito, F., Memmi Turbanti, I., Turchiano, M. and Volpe, G. (2008) 'The *sectilia* panels of Faragola (Ascoli Satriano, Southern Italy): a multi-analytical study of the red, orange and yellow glass slabs', *Archaeometry*, 50(3), 451-473.

Sayre, E. V. (1963) 'The intentional use of antimony and manganese in ancient glasses', in F. R. Matson and G. E. Rindone (eds.), *VI International Congress on Glass: Advances in Glass Technology, Part 2*, 263-282. New York: Plenum Press.

Sayre, E. V. (1964) *Some Ancient Glass Specimens with Compositions of Particular Archaeological Significance*. New York: Brookhaven National Laboratory.

Sayre, E. V. (1965) 'Summary of the Brookhaven program of analysis of ancient glass', *Application of Science in the Examination of Works of Art*, 145-154. Boston: Museum of Fine Arts.

Sayre, E. V. and Smith, R. W. (1961) 'Compositional categories of ancient glass', *Science*, 133, 1824-1826.

Sayre, E. V. and Smith, R. W. (1967) 'Some materials of glass manufacturing in antiquity', in M. Levey (ed.), *Archaeological Chemistry: A Symposium*, 279-311. Philadelphia: University of Pennsylvania Press.

Schibille, N., Degryse, P., Corremans, M. and Specht, C. G. (2012) 'Chemical characterisation of glass mosaic tesserae from sixth-century Sagalassos (south-west Turkey): chronology and production techniques', *Journal of Archaeological Science*, 39, 1480-1492.

Schreurs, J. W. H. and Brill, R. H. (1984) 'Iron and sulphur related colours in ancient glasses', *Archaeometry*, 26(2), 199-209.

Scull, C. (1995) 'Approaches to material culture and social dynamics of the Migration Period in eastern England', in J. Bintliff and H. Hamerow (eds.), *Europe Between Late Antiquity and the Middle Ages: Recent Archaeological and Historical Research in Western and Southern Europe*, BAR International Series 617, 71-83. Oxford: Tempvs Reparatum.

Scull, C. (2011) 'Social transactions, gift exchange, and power in the archaeology of the fifth to seventh centuries', in H. Hamerow, D. A. Hinton and S. Crawford (eds.), *The Oxford Handbook of Anglo-Saxon Archaeology*, 848-864. Oxford: Oxford University Press.

Selskienė, A. (2007) 'Examination of smelting and smithing slags formed in bloomery iron-making process', *Chemija*, 18(2), 22-28.

Severin, T., Rehren, Th. and Schleicher, H. (2011) 'Early metal smelting in Aksum, Ethiopia: copper or iron?', *European Journal of Mineralogy*, 23, 981-992.

Sharp, W. E. and Mittwede, S. K. (2011) 'Medieval kirschsteinite-bearing iron slags of the Develi-Yahyali area (Kayseri), Turkey', *Proceedings of ICAM 2011*, 649-656.

Shelby, J. (1997) *Introduction to Glass Science and Technology*. Cambridge: The Royal Society of Chemistry.

Shortland, A. J. (2004) 'Evaporites of the Wadi Natrun: seasonal and annual variation and its implication for ancient exploitation', *Archaeometry*, 46(4), 497-516.

Shortland, A. J. (2006) 'Application of lead isotope analysis to a wide range of Late Bronze Age Egyptian materials', *Archaeometry*, 48(4), 657-669.

Shortland, A. J. (2012) *Lapis Lazuli from the Kiln: Glass and Glassmaking in the Late Bronze Age*, Studies in Archaeological Sciences 2. Leuven: Leuven University Press.

Shortland, A. J., Nicholson, P. T. and Jackson, C. M. (2000) 'Lead isotope analysis of eighteenth-dynasty Egyptian eyepaints and lead antimonate colourants', *Archaeometry*, 42(1), 153-157.

Shortland, A. J., Rogers, N. and Eremin, K. (2007) 'Trace element discriminants between Egyptian and Mesopotamian late Bronze Age glasses', *Journal of Archaeological Science*, 34, 781-789.

Shortland, A. J., Schachner, L., Freestone, I. C. and Tite, M. S. (2006) 'Natron as a flux in the early vitreous materials industry: sources, beginnings and reasons for decline', *Journal of Archaeological Science*, 33, 521-530.

Shugar, A. N. (2000) 'Byzantine opaque red glass tesserae from Beit Shean, Israel', *Archaeometry*, 42(2), 375-384.

Siegmann, M. (2006) *Bunte Pracht – Die Perlen der Frühmittelalterlichen Gräberfelder von Liebenau, Kreis Nienburg/Weser und Dörverden, Kreis Verden/Aller: Chronologie der Gräber, Entwicklung und Trageweise des Perlenschmucks, Technik der Perlen, Teil 5*. Wilkau-Haußlau: Beier und Beran.

Siegmund, F. (1998) *Merowingerzeit am Niederrhein: Die frühmittelalterlichen Funde aus dem Regierungsbezirk Düsseldorf und dem Kreis Heinsberg*, Rheinische Ausgrabungen 34. Köln: Rheinland-Verlag.

Silvestri, A. (2008) 'The coloured glass of *Iulia Felix*', *Journal of Archaeological Science*, 35, 1489-1501.

Silvestri, A., Molin, G. and Salviulo, G. (2005) 'Roman and medieval glass from the Italian area: bulk characterization and relationships with production technologies', *Archaeometry*, 47(4), 797-816.

Silvestri, A., Molin, G. and Salviulo, G. (2008) 'The colourless glass of *Iulia Felix*', *Journal of Archaeological Science*, 35, 331-341.

- Silvestri, A., Tonietto, S. and Molin, G. (2011) 'The palaeo-Christian glass mosaic of St. Prodocimus (Padova, Italy): archaeometric characterisation of 'gold' tesserae', *Journal of Archaeological Science*, 38, 3402-3414.
- Sode, T. (1995) 'Purdalpur, a Glass Bead-Making Village in Northern India', in M. Rasmussen, U. Lund Hansen, and U. Näsman (eds.), *Glass Beads: Cultural History, Technology, Experiment and Analogy*, Studies in Technology and Culture vol. 2, 103-107. Lejre: Historical-Archaeological Experimental Centre.
- Sode, T. (2004) 'Glass bead making technology', in M. Bencard, A. K. Rasmussen and H. B. Madsen (eds.), *Ribe Excavations 1970-76, Volume 5*, 83-102. Moesgård: Jutland Archaeological Society Publications.
- Sode, T. and Kock, J. (2001) 'Traditional raw glass production in Northern India: the final stage of an ancient technology', *Journal of Glass Studies*, 43, 155-169.
- Spaer, M. (1993) 'Gold-glass beads: a review of the evidence', *Beads*, 5, 9-25.
- Stapleton, C. P., Freestone, I. C. and Bowman, S. G. E. (1999) 'Composition and origin of early mediaeval opaque red enamel from Britain and Ireland', *Journal of Archaeological Science*, 26, 913-921.
- Stephens, W. (2006) *Early Medieval Glass Vessels found in Kent: A Catalogue of the Glass Vessels of European Migrants to Kent, from Approximately AD 450-700, in Museums, Archaeological Trusts and Societies, and Private Collections*, BAR Series 424. Oxford: Archaeopress.
- Tal, O., Jackson-Tal, R. E. and Freestone, I. C. (2004) 'New evidence of the production of raw glass at late Byzantine Apollonia-Arsuf, Israel', *Journal of Glass Studies*, 46, 51-66.
- Tal, O., Jackson-Tal, R. E. and Freestone, I. C. (2008a) 'A secondary glass workshop', in O. Tal and I. Taxel (eds.), *Ramla (South): An Early Islamic Industrial Site and Remains of Previous Periods*, Salvage Excavation Reports No. 5, 66-76. Tel Aviv, Israel: Tel Aviv University.
- Tal, O., Jackson-Tal, R. E. and Freestone, I. C. (2008b) 'Glass from a Late Byzantine secondary workshop at Ramla (South), Israel', *Journal of Glass Studies*, 50, 81-95.
- Thomas, G. (2011) 'Overview: craft production and technology', in H. Hamerow, D. A. Hinton and S. Crawford (eds.), *The Oxford Handbook of Anglo-Saxon Archaeology*, 405-422. Oxford: Oxford University Press.

Thomsen, P. (1995) 'The question of beadmaking in the late Roman Iron Age at Lundeberg, Denmark', in M. Rasmussen, U. Lund Hansen, and U. Näsman (eds.), *Glass Beads: Cultural History, Technology, Experiment and Analogy*, Studies in Technology and Culture vol. 2, 19-24. Lejre: Historical-Archaeological Experimental Centre.

Timby, J. R. (1996) *The Anglo-Saxon Cemetery at Empingham II, Rutland*. Oxford: Oxbow Books.

Tite, M., Pradell, T. and Shortland, A. (2008) 'Discovery, production and use of tin-based opacifiers in glasses, enamels and glazes from the late Iron Age onwards: a reassessment', *Archaeometry*, 50(1), 67-84.

Towle, A., Henderson, J., Bellintani, P. and Gambacurta, G. (2001) 'Frattesina and Adria: report of scientific analysis of early glass from the Veneto', *Padusa*, 37, 7-68.

Turner, W. E. S. and Rooksby, H. P. (1959) 'A study of the opalising agents in ancient opal glasses throughout three thousand four hundred years', *Glastechnische Berichte*, 32 K, 8, 17-28.

Turner, W. E. S. and Rooksby, H. P. (1961) 'Further historical studies based on x-ray diffraction methods of the reagents employed in making opal and opaque glasses', *Jahrbuch des Römisch-Germanischen Zentralmuseums*, 8, 1-6.

Tweddle, D. (ed.) (1986) *Finds from Parliament Street and Other Sites on the City Centre*, The Archaeology of York: The Small Finds vol. 17/4, 224-226. London: The Council for British Archaeology.

Tylecote, R. F. (1992) *A History of Early Metallurgy*. London: The Institute of Materials.

Uboldi, M. and Verità, M. (2003) 'Scientific analyses of glasses from late Antique and early medieval archaeological sites in northern Italy', *Journal of Glass Studies*, 45, 115-137.

Vallotto, M. and Verità, M. (2000) 'Glasses from Pompeii and Herculaneum and the sands of the rivers Belus and Volturno', in J. Renn and G. Castagnetti (eds.), *Homo Faber: Studies on Nature, Technology and Science at the Time of Pompeii*, 63-73. Rome: 'L'Erma' di Bretschneider.

Velde, B. (1990) 'Alumina and calcium oxide content of glass found in western and northern Europe, first to ninth centuries', *Oxford Journal of Archaeology*, 9(1), 105-117.

Verità, M. (1995) 'Le analisi dei vetri', in D. Foy (ed.), *La Verre de l'Antiquité Tardive et du haut Moyen Age*, 291-300. Musée Archéologique Départemental du Val d'Oise.

Verità, M. (2001) 'La composizione chimica di materiali vitrei in Italia tra IV e XI secolo D.C. attraverso le analisi di reperti archeologici ed architettonici', in F. Dell'Acqua and R. Silva (eds.), *Il Colore Nel Medioevo: La Vetrata in Occidente dal IV All'XI Secolo*, 233-245. Lucca: Istituto Storico Lucchese.

Verità, M., Basso, R., Wypyski, M. T. and Koestler, R. J. (1994) 'X-ray microanalysis of ancient glassy materials: a comparative study of wavelength dispersive and energy dispersive techniques', *Archaeometry*, 36, 241-252.

Vicenzi, E. P., Eggins, S., Logan, A. and Wysoczanski, R. (2002) 'Microbeam characterization of Corning archaeological reference glasses: new additions to the Smithsonian microbeam standard collection', *Journal of Research of the National Institute of Standards and Technology*, 107(6), 719-727.

Wagner, B., Nowak, A., Bulska, E., Kunicki-Goldfinger, J., Schalm, O. and Janssens, K. (2008) 'Complementary analysis of historical glass by scanning electron microscopy with energy dispersive X-ray spectroscopy and laser ablation inductively coupled plasma mass spectrometry', *Microchimica Acta*, 162, 415-424.

Walton Rogers, P. (2007) *Cloth and Clothing in Early Anglo-Saxon England, AD 450-700*, CBA Research Report 145. York: Council for British Archaeology.

Watkinson, D., Weber, L. and Anheuser, K. (2005) 'Staining of archaeological glass from manganese-rich environments', *Archaeometry*, 47(1), 69-82.

Wedepohl, K. H. (1997) 'Chemical composition of medieval glass from excavations in West Germany', *Glastechnische Berichte – Glass Science and Technology*, 70, 246-255.

Wedepohl, K. H. (2000) 'The change in composition of medieval glass types occurring in excavated fragments from Germany', *Annales du 14^e Congrès de l'Association Internationale pour l'Histoire du Verre*, 253-257.

Wedepohl, K. H. (2001) 'The Composition of glass from the Carolingian and post-Carolingian period in Central Europe', in F. Dell'Acqua R. and Silva (eds.), *Il Colore Nel Medioevo: La Vetrata in Occidente dal IV All'XI Secolo*, 257-270. Lucca: Istituto Storico Lucchese.

Wedepohl, K. H. and Baumann, A. (2000) 'The use of marine molluscan shells for Roman glass and local raw glass production in the Eifel Area (Western Germany)', *Die Naturwissenschaften*, 87(3), 129-132.

Wedepohl, K. H., Gaitzsch, W. and Follmann-Schulz, A. B. (2003) 'Glassmaking and glassworking in six Roman factories in the Hambach Forest, Germany', *Annales du 15^e Congrès de l'Association Internationale pour l'Histoire du Verre*, 56-61.

Wedepohl, K. H., Krueger, I. and Hartmann, G. (1995) 'Medieval lead glass from Northwestern Europe', *Journal of Glass Studies*, 37, 65-82.

Wedepohl, K. H., Pirling R. and Hartmann, G. (1997) 'Römische und Fränkische gläser aus dem gräberfeld von Krefeld-Gellep', *Bonner Jahrbücher*, 197, 177-189.

Wedepohl, K. H., Simon, K. and Kronz, A. (2011) 'Data on 61 chemical elements for the characterization of three major glass compositions in Late Antiquity and the Middle Ages', *Archaeometry*, 53(1), 81-102.

Welch, M. (1992) *Anglo-Saxon England*. London: B. T. Batsford Ltd.

Welch, M. (1999) 'Glass beads in early Anglo-Saxon contexts', in M. Guido, *The Glass Beads of Anglo-Saxon England c.AD 400-700: A Preliminary Visual Classification of the More Definitive and Diagnostic Types*, Report of the Research Committee of the Society of Antiquaries of London No. 58, 1-10. Woodbridge: The Boydell Press.

Welch, M. (2011) 'The mid Saxon 'Final Phase'', in H. Hamerow, D. A. Hinton and S. Crawford (eds.), *The Oxford Handbook of Anglo-Saxon Archaeology*, 266-287. Oxford: Oxford University Press.

Welham, K., Jackson, C. M. and Smedley, J. W. (2000) 'Colour formation in sealing wax red glass', *Annales du 14^e Congrès de l'Association Internationale pour l'Histoire du Verre*, 11-15.

West, S. (1998) *A Corpus of Anglo-Saxon Material from Suffolk*, East Anglian Archaeology 84. Ipswich: Suffolk County Council.

Weyl, W. A. (1951) *Coloured Glasses*. Sheffield: Society of Glass Technology.

Williams, H. (2011) 'Mortuary practices in early Anglo-Saxon England', in H. Hamerow, D. A. Hinton and S. Crawford (eds.), *The Oxford Handbook of Anglo-Saxon Archaeology*, 238-265. Oxford: Oxford University Press.

Wilthew, P. (1988) 'Examination and analysis of the glass beads', in V. I. Evison (ed.), *An Anglo-Saxon Cemetery at Alton, Hampshire*, 52-58. The Hampshire Field Club and Archaeological Society.

Wilthew, P. (2006) 'Examination and analysis of glass beads', in S. C. Hawkes and G. Grainger (eds.), *The Anglo-Saxon Cemetery at Finglesham, Kent*, Oxford University School of Archaeology Monograph No. 64, 383-394. Oxford: School of Archaeology, University of Oxford.

Youngs, S. (ed.) (1989) *'The Work of Angels': Masterpieces of Celtic Metalwork, 6th-9th Centuries AD*. London: British Museum Publications.